



# Principles of Naval Architecture

## Second Revision



Volume III • Motions in Waves  
and Controllability

Edward V. Lewis, Editor

Published by  
The Society of Naval Architects and Marine Engineers  
601 Pavonia Avenue  
Jersey City, NJ

2.313

Copyright © 1989 by The Society of Naval Architects and Marine Engineers.

It is understood and agreed that nothing expressed herein is intended or shall be construed to give any person, firm, or corporation any right, remedy, or claim against SNAME or any of its officers or members.

Library of Congress Catalog Card No. 88-60829  
ISBN No. 0-939773-02-3  
Printed in the United States of America  
First Printing, November, 1989



# Preface

The aim of this second revision (third edition) of the Society's successful *Principles of Naval Architecture* was to bring the subject matter up-to-date through revising or rewriting areas of greatest recent technical advances, which meant that some chapters would require many more changes than others. The basic objective of the book, however, remained unchanged: to provide a timely survey of the basic principles in the field of naval architecture for the use of both students and active professionals, making clear that research and engineering are continuing in almost all branches of the subject. References to available sources of additional details and to ongoing work to be followed in the future are included.

The preparation of this third edition was simplified by an earlier decision to incorporate a number of sections into the companion SNAME publication, *Ship Design and Construction*, which was revised in 1980. The topics of Load Lines, Tonnage Admeasurement and Launching seemed to be more appropriate for the latter book, and so Chapters V, VI, and XI became IV, V and XVII respectively, in *Ship Design and Construction*. This left eight chapters, instead of 11, for the revised *Principles of Naval Architecture*, which has since become nine in three volumes.

At the outset of work on the revision, the Control Committee decided that the increasing importance of high-speed computers demanded that their use be discussed in the individual chapters instead of in a separate appendix as before. It was also decided that throughout the book more attention should be given to the rapidly developing advanced marine vehicles.

In regard to units of measure, it was decided that the basic policy would be to use the International System of Units (S.I.). Since this is a transition period, conventional U.S. (or "English") units would be given in parentheses, where practical, throughout the book. This follows the practice adopted for the Society's companion volume, *Ship Design and Construction*. The U.S. Metric Conversion Act of 1975 (P.L. 94-168) declared a national policy of increasing the use of metric systems of measurement and established the U.S. Metric Board to coordinate voluntary conversion to S.I. The Maritime Administration, assisted by a SNAME ad hoc task group, developed a *Metric Practice Guide* to "help obtain uniform metric practice in the marine industry," and this guide was used here as a basic reference. Following this guide, ship displacement in metric tons (1000 kg) represents mass rather than weight. (In this book the familiar symbol,  $\Delta$ , is reserved for the displacement mass). When forces are considered, the corresponding unit is the kilonewton (kN), which applies, for example, to resistance and to displacement weight (symbol  $W$ , where  $W = \rho \Delta g$ ) or to buoyancy forces. When conventional or English units are used, displacement weight is in the familiar long ton unit

(Continued)

## PREFACE

(2240 lb), which numerically is  $1.015 \times$  metric ton. Power is usually in kilowatts ( $1 \text{ kW} = 1.34 \text{ hp}$ ). A conversion table also is included in the Nomenclature at the end of each volume

The first volume of the third edition of *Principles of Naval Architecture*, comprising Chapters I through IV, deals with the essentially static principles of naval architecture, leaving dynamic aspects to the remaining volumes. The second volume consists of Chapters V Resistance, VI Propulsion and VII Vibration, each of which has been extensively revised or rewritten.

Volume III contains the two final chapters, VIII Motions in Waves and IX Controllability. Because of important recent theoretical and experimental developments in these fields, it was necessary to rewrite most of both chapters and to add much new material. But the state-of-the-art continues to advance, and so extensive references to continuing work are included.

November 1989

Edward V. Lewis  
*Editor*

# Table of Contents

## Volume III

	Page		Page
Preface .....	iii	Acknowledgments.....	vi

### Chapter 8 (VIII) MOTIONS IN WAVES

ROBERT F. BECK, Professor, University of Michigan; WILLIAM E. CUMMINS,\*\* David Taylor Research Center; JOHN F. DALZELL, David Taylor Research Center; PHILIP MANDEL,\* and WILLIAM C. WEBSTER, Professor, University of California, Berkeley

1. Introduction .....	1	5. Derived Responses .....	109
2. Ocean Waves .....	3	6. Control of Ship Motions .....	126
3. Ship Responses to Regular Waves ....	41	7. Assessing Ship Seaway Performance	137
4. The Ship in a Seaway .....	84	8. Design Aspects.....	160
References .....	177		
Nomenclature .....	188		

### Chapter 9 (IX) CONTROLLABILITY

C. LINCOLN CRANE,\*\* Exxon Corporation; HARUZO EDA, Professor, Stevens Institute of Technology; ALEXANDER C. LANDSBURG, U.S. Maritime Administration

1. Introduction .....	191	9. Theoretical Prediction of Design Coefficient and Systems Identification .....	234
2. The Control Loop and Basic Equations of Motion .....	192	10. Accelerating, Stopping and Backing...	251
3. Motion Stability and Linear Equations.....	195	11. Automatic Control Systems .....	264
4. Analysis of Course Keeping— Controls-Fixed Stability .....	199	12. Effects of the Environment.....	268
5. Stability and Control .....	205	13. Vessel Waterway Interactions.....	279
6. Analysis of Turning Ability .....	209	14. Hydrodynamics of Control Surfaces...	291
7. Free Running Model Tests and Hydraulic Models .....	215	15. Maneuvering Trials and Performance Requirements .....	316
8. Nonlinear Equations of Motion and Captive Model Tests .....	217	16. Application to Design .....	327
References .....	408	17. Design of Rudder and Other Control Devices.....	364
Nomenclature .....	418		
General Symbols .....	421		
Index .....	424		

\* Now retired

\*\* Deceased

Note: The office affiliations given are those at the time of writing the chapters.

## Acknowledgments

In this Volume III, the Editor wishes to thank the authors of Chapter VIII, Robert F. Beck, John F. Dalzell, Philip Mandel and William C. Webster, for stepping in to complete the chapter on Motions in Waves after the untimely death of William E. Cummins. He also acknowledges the valuable assistance of SNAME T&R Panel H-7 (Seakeeping Characteristics) chaired by David D. Moran, in reviewing and commenting on early drafts of the chapter manuscript. Generous permission was granted by D. C. Murdey and his associates in the National Research Council of Canada for us to publish excerpts from their valuable reports on a series of model tests in calm water and in waves. Drafting services were provided by Keith L. MacPhee.

The Editor also wishes to express his appreciation for John Nachtsheim's valuable efforts in guiding the completion of Chapter IX on Controllability, and to Alexander Landsburg for joining in to assist the original two authors. All three authors wish to acknowledge their indebtedness to Philip Mandel, the author of the corresponding chapter in the preceding edition. Extensive use has been made of the original text and figures. The authors also wish to thank the members of Panel H-10 (Ship Controllability) who provided useful comments, especially Abraham Taplin. Completion of this chapter was greatly facilitated by Roderick A. Barr, who assisted in organizing the chapter in its early stages, by the excellent technical review and suggestions given by John A. Youngquist, and by the drafting services of Robinson de la Cruz.

The Control Committee provided essential guidance, as well as valuable assistance in the early stages. Members are:

John J. Nachtsheim, Chairman  
Thomas M. Buermann  
William A. Cleary, Jr.  
Richard B. Couch  
Jerome L. Goldman  
Jacques B. Hadler  
Ronald K. Kiss  
Donald P. Roseman  
Stanley G. Stiansen  
Charles Zeien

The Editor wishes to thank all of the Volume III authors for their fine work and full cooperation in making suggested revisions. Finally, he acknowledges the indispensable efforts of Trevor Lewis-Jones in doing detailed editing and preparing text and figures in proper format for publication.

November 1989

E. V. Lewis  
*Editor*

Robert F. Beck, William E. Cummins  
John F. Dalzell, Philip Mandel  
William C. Webster

# Motions in Waves

## Section 1

### Introduction<sup>1</sup>

**1.1 Ship motions at sea** have always been a problem for the naval architect. His or her responsibility has been to insure not only that the ship can safely ride out the roughest storms but that it can proceed on course under severe conditions with a minimum of delay, or carry out other specific missions successfully. However, the problem has changed through the years. Sailing vessels followed the prevailing winds—Columbus sailed west on the northeast trades and rode the prevailing westerlies farther north on his return voyages. The early clipper ships and the later grain racers from Australia to Europe made wide detours to take advantage of the trade winds. In so doing they made good time in spite of the extra distance travelled, but the important fact for the present purpose is that they seldom encountered head seas.

With the advent of steam, for the first time in the history of navigation, ships were able to move directly to windward. Hence, shipping water in heavy weather caused damage to superstructures, deck fittings and hatches to increase, and structural bottom damage near the bow appeared as a result of slamming. Structural improvements and easing of bottom lines forward relieved the latter situation, and for many years moderately powered cargo ships could use full engine power in almost any weather, even though speed was reduced by wind and sea. The same is true even today for giant, comparatively low-powered tankers and many dry-bulk carriers.

For many years the pilot charts issued by the U.S. Navy Oceanographic Office still showed special routes for “low-powered steamers” to avoid head winds and seas. It should be emphasized that the routes shown for the North Atlantic, for example, did not involve avoiding bad weather as such, for eastbound the routes for low and high-powered steamers were the same; but they did attempt to avoid the prevailing head winds

and head seas westbound that greatly reduced the speed of low-powered ships.

The situation is different for today’s modern fast passenger vessels and high-powered cargo ships. In really rough head seas, their available power is excessive and must be reduced voluntarily to avoid shipping of water forward or incurring structural damage to the bottom from slamming. Hence, maintaining schedule now depends as much on ship motions as on available power.

Similarly, high-powered naval vessels must often slow down in rough seas in order to reduce the motions that affect the performance of their particular mission or function—such as sonar search, landing of aircraft or helicopters and convoy escort duty. Furthermore, new and unusual high-performance craft—comparatively small in size—have appeared whose performance is even more drastically affected by ocean waves. These include high-speed planing craft, hydrofoil boats, catamarans and surface effect ships, most but not all being developed or considered for military uses.

A very different but related set of problems has arisen in the development of large floating structures and platforms that must be towed long distances and be accurately positioned in stormy seas for ocean-drilling and other purposes.

As seakeeping problems have thus become more serious, particularly for the design of higher-speed oceangoing vessels, rapid expansion began in the mid-1950s in the application of hydrodynamic theory, use of experimental model techniques and collection of full-scale empirical data. These important developments led to a better understanding of the problems and ways of dealing with them. Along with remarkable advances in oceanography and computer technology, they made it possible to predict in statistical terms many aspects of ship performance at sea. Furthermore, they could be applied to the seagoing problems involved in the design of the unusual new high-speed craft and floating platforms previously mentioned.

<sup>1</sup>This section written by the editor.

In view of the increasing importance of theoretical approaches to seakeeping problems, it is felt to be essential to cover in this chapter in a general way the basic hydrodynamic principles and mathematical techniques involved in predicting ship motions in both regular and irregular seas (Sections 2, 3 and 4). Some readers may wish to proceed directly to Sections 5-8, which discuss more practical aspects of ship motions and the problems of design for good seakeeping performance.

The understanding of ship motions at sea, and the ability to predict the behavior of any ship or marine structure in the design stage, begins with the study of the nature of the ocean waves that constitute the environment of the seagoing vessel. The outstanding characteristic of the open ocean is its irregularity, not only when storm winds are blowing but even under relatively calm conditions. Oceanographers have found that irregular seas can be described by statistical mathematics on the basis of the assumption that a large number of regular waves having different lengths, directions, and amplitudes are linearly superimposed. This powerful concept is discussed in Section 2 of this chapter, but it is important to understand that the characteristics of idealized regular waves, found in reality only in the laboratory, are also fundamental for the description and understanding of realistic irregular seas.

Consequently, in Section 2—after a brief discussion of the origin and propagation of ocean waves—the theory of regular gravity waves of simple form is presented. Mathematical models describing the complex irregular patterns actually observed at sea and encountered by a moving ship are then discussed in some detail. The essential feature of these models is the concept of a *spectrum*, defining the distribution of energy among the different hypothetical regular components having various frequencies (wave lengths) and directions. It is shown that various statistical characteristics of any seaway can be determined from such spectra. Sources of data on wave characteristics and spectra for various oceans of the world are presented.

It has been found that the irregular motions of a ship in a seaway can be described as the linear superposition of the responses of the ship to all the wave components of such a seaway. This principle of superposition, which was first applied to ships by St. Denis and Pierson (1953),<sup>2</sup> requires knowledge of both the sea components and the ship responses to them.

Hence, the vitally important linear theory of ship motions in simple, regular waves is next developed in Section 3. It begins with the simple case of pitch, heave and surge in head seas and then goes on to the general case of six degrees of freedom. The *equations of mo-*

*tion* are presented and the hydrodynamic forces evaluated on the basis of potential theory. The use of *strip theory* is then described as a convenient way to perform the integration for a slender body such as a ship.

Finally, practical data and experimental results for two cases are presented: the longitudinal motions of pitch-heave-surge alone, and the transverse motions of roll-sway-yaw.

In Section 4 the extension of the problem of ship motions to realistic irregular seas is considered in detail, the object being to show how modern techniques make it possible to predict motions of almost any type of craft or floating structure in any seaway in probability terms. It is shown that, knowing the wave spectrum and the characteristic response of a ship to the component waves of the irregular sea, a response spectrum can be determined. From it various statistical parameters of response can be obtained, just as wave characteristics are obtainable from wave spectra. Responses to long-crested seas are treated first, and then the more general case of short-crested seas. Particular attention is given to the short-term statistics of peaks, or maxima, of responses such as pitch, heave and roll; both motions and accelerations. Examples of typical calculations are included.

Section 5 considers the prediction of responses other than the simple motions of pitch, heave, roll, etc. These so-called *derived responses* include first the vertical motion (and velocity and acceleration) of any point in a ship as the result of the combined effect of all six modes, or degrees of freedom.

Consideration is given next to the relative motion of points in the ship and the water surface, which leads to methods of calculating probabilities of shipping water on deck, bow emergence and slamming. Non-linear effects come in here and are discussed, along with non-linear responses such as added resistance and power in waves. Finally, various wave-induced loads on a ship's hull structure are considered, some of which also involve non-linear effects.

Section 6 discusses the control of ship motions by means of various devices. Passive devices that do not require power or controls comprise bilge keels, anti-rolling tanks and moving weights. Five performance criteria for such devices are presented, and the influence of each is shown by calculations for a ship rolling in beam seas. Active devices, such as gyroscopes, controllable fins and controlled rudders are then discussed.

Section 7 deals with criteria and indexes of seakeeping performance. It is recognized that, in order for new designs to be evaluated and their acceptability determined, it is essential to establish standards of performance, just as in other chapters where criteria of stability, subdivision and strength are presented.

Various desirable features of ship behavior have been listed from time to time under the heading of *seakindliness*. These include easy motions, (i.e., low

<sup>2</sup>Complete references are listed at end of chapter.

accelerations), dry decks, absence of slamming and propeller racing, and easy steering. For naval ships important additional considerations include weapon system performance, landing of helicopters and sonar search effectiveness. This section considers in detail specific criteria by which to judge whether or not a ship can carry out a particular mission in a given sea condition, speed and heading. These criteria usually involve values of motion amplitude, velocity or acceleration at specific locations in the ship, or motions relative to the sea affecting shipping of water and slamming. Available prescribed values of acceptable performance are tabulated for different types of craft and various missions.

However, whether or not a ship can meet any of the criteria depends on factors such as sea condition, speed and heading. Therefore, a *Seakeeping Performance Index* (SPI) is needed that takes account of all the different sea conditions expected over a period of time and the speeds and headings attainable in each. It should measure the effectiveness of a ship in attaining its mission or missions in service. Two basic SPIs are described: A *Transit Speed* SPI and a *Mission Effectiveness* SPI. The first applies particularly to merchant ships whose mission is to deliver cargo and passengers safely and promptly, and is expressed as attainable average speed over one or more voyages without exceeding the applicable criteria. This SPI also applies to some functions of naval ships. The second SPI, Mission Effectiveness, applies particularly to naval ves-

sels, but also to Coast Guard cutters, fishing vessels on fishing grounds, oceanographic ships and floating platforms. For such ships the SPI defines the effectiveness of the ship in fulfilling specific missions or functions, usually in terms of the fraction of time that the ship can do so over a stated period. Methods of calculating these SPIs are given, along with specific examples.

Finally, having criteria and indexes of performance whereby predictions can be tested, the naval architect requires guidance as to choice of ship form, proportions, natural periods of rolling and pitching, freeboard forward and other characteristics favorable to good seagoing performance. In Section 8 the theoretical principles and experimental data developed in preceding sections are applied to providing such needed guidelines. Emphasis is on choosing the overall ship proportions and coefficients, since they must be established early in the design process and are shown to have more influence on performance than minor changes in full form. Consideration is also given to above-water form and freeboard, and to added power requirements in waves. Special design problems of high-performance craft are discussed.

Consideration is also given to design procedures that permit seakeeping considerations to be taken into account from the outset. It is shown that a choice among alternative designs can be made on the basis of economic considerations, for both commercial and naval vessels.

## Section 2

### Ocean Waves<sup>3</sup>

**2.1 Origin and Propagation of Ocean Waves.** As noted in Section 1, the outstanding visible characteristic of waves in the open ocean is their irregularity. Study of wave records confirms this irregularity of the sea, both in time and space. However, one is equally impressed by the fact that over a fairly wide area and often for a period of a half-hour or more the sea may maintain a characteristic appearance, because record analyses indicate it is very nearly statistically steady or *stationary*. At other times or places the sea condition will be quite different, and yet there will again be a characteristic appearance, with different but steady statistical parameters. Hence, for most problems of behavior of ships and floating structures at sea, attention can be focused on describing mathematically the surface waves as a random, or *stochastic*, process under short-term statistically stationary conditions. Analysis of wave records has also shown that

under such conditions they are approximately Gaussian in character, i.e., wave elevations read at random or at regular intervals of time have roughly a Gaussian, or normal, probability density function. This characteristic greatly simplifies the application of statistics, probability theory and Fourier analysis techniques to the development of suitable models.

The theory of seakeeping uses such mathematical models of ocean waves, which account for variability of waves in time and space, so long as conditions remain steady, permitting estimates of short-term ship performance for realistic environmental conditions over a relatively small area. These theories are based upon mathematical wave theory as well as on the laws of probability and statistics. The details of one model, particularly as they concern the naval architect, will be developed in this section.

However, for an overall understanding, as well as for solving some seakeeping problems, the variation in waves over long periods of time and over great distances cannot be overlooked. It is useful, therefore,

<sup>3</sup> By William E. Cummins, with paragraphs by John F. Dalzell.

to review the physical processes of storm wave generation and of wave propagation in a general way.

Storm waves are generated by the interaction of wind and the water surface. There are at least two physical processes involved, these being the friction between air and water and the local pressure fields associated with the wind blowing over the wave surface. Although a great deal of work has been done on the theory of wave generation by wind, as summarized by Korvin-Kroukovsky (1961) and Ursell (1956), no completely satisfactory mechanism has yet been devised to explain the transfer of energy from wind to sea. Nevertheless, it seems reasonable to assume that the total storm wave system is the result of many local interactions distributed over space and time. These events can be expected to be independent unless they are very close in both space and time. Each event will add a small local disturbance to the existing wave system.

Within the storm area, there will be wave interactions and wave-breaking processes that will affect and limit the growth and propagation of waves from the many local disturbances. Nevertheless, wave studies show that if wave amplitudes are small the principle of linear superposition governs the propagation and dispersion of the wave systems outside the generating area. Specifically, if  $\zeta_1(x, y, t)$  and  $\zeta_2(x, y, t)$  are two wave systems,  $\zeta_1(x, y, t) + \zeta_2(x, y, t)$  is also a wave system. This implies that one wave system can move through another wave system without modification. While this statement is not absolutely true, it is very nearly so, except when the sum is steep enough for wave breaking to occur.

A second important characteristic of water waves that affects the propagation of wave systems is that in deep water the phase velocity, or *celerity*, of a simple regular wave, such as can be generated in an experimental tank, is a function of wavelength. Longer waves travel faster than shorter waves. Study and analysis of ocean wave records has shown that any local system can be resolved into a sum of component regular waves of various lengths and directions, using Fourier Integral techniques. By an extension of the principle of superposition, the subsequent behavior of the sum of these component regular wave systems will determine the visible system of waves. Since these component waves have different celerities and directions, the propagating pattern will slowly change with time.

If the propagating wave system over a short period of time is the sum of a very large number of separate random contributions, all essentially independent, the surface elevation is

$$\zeta(x, y, t) = \sum_i \zeta_i(x, y, t) \quad (1)$$

and the laws of statistics yield some very useful conclusions. Since water is incompressible, the average

value of vertical displacement at any instant,  $t$ , in a regular component wave,  $\zeta_i$ , is zero (if it is assumed to be of sinusoidal form, as discussed subsequently), and therefore the average value for the wave system,  $\langle \zeta(x, y, t) \rangle$ , is also zero. However, the variance (or mean square deviation from the mean) of  $\zeta_i$ , which is the average value of  $\zeta_i^2$ , written  $\langle \zeta_i^2 \rangle$ , is a positive quantity that measures the severity of the sea. A fundamental theorem of statistics states that the variance of the sum of a set of independent random variables tends asymptotically to the sum of the variances of the component variables. Thus, for a very large (infinite) number of components, assumed to be independent,

$$\langle \zeta^2 \rangle = \sum \langle \zeta_i^2 \rangle \quad (2)$$

A final statistical conclusion is a consequence of the *central limit theorem* of statistics. In the case under discussion, this theorem implies that  $\zeta(x, y, t)$  will have a normal (or Gaussian) density function, even if the component variables  $\zeta_i(x, y, t)$  are not distributed normally. The importance of this result is that the density function of a normal random variable is known if its mean and variance are known. Therefore, if the variance of the surface elevation in the multi-component wave system can be estimated, its probability density as a random variable is known. Ochi (1986) deals with the analysis of non-Gaussian random processes.

These conclusions from the laws of statistics all depend upon the previously mentioned principle of superposition, which holds approximately but not absolutely for water waves, and on the assumption of independence of component waves. Therefore, the conclusions themselves are approximate and this should be remembered. However, it has been found that over the short term, deviations become significant only when the waves are very steep, and even then primarily in those characteristics that are strongly influenced by the crests.

It will be shown that the short-term descriptive model that has been described leads to a mathematical technique for describing the irregular sea at a given location and time, while conditions remain steady or *stationary*. Each sea condition can for short periods of time be as unique as a fingerprint, and yet, as with a fingerprint, it has order and pattern, as defined by its directional *spectrum*, to be explained subsequently (Section 2.6). However, since the wind velocities and directions are continually, albeit slowly, changing, the short-term mathematical description will also change. Hence, a broader model is also needed to cover large variations in time, involving wind effects on growth and decline of local wave systems, as well as propagation and dispersion.

Fig. 1(a) symbolizes a storm-wave generation area. It may be assumed that disturbances are being generated by the interaction of the wind and sea surface throughout the storm area from the time the wind



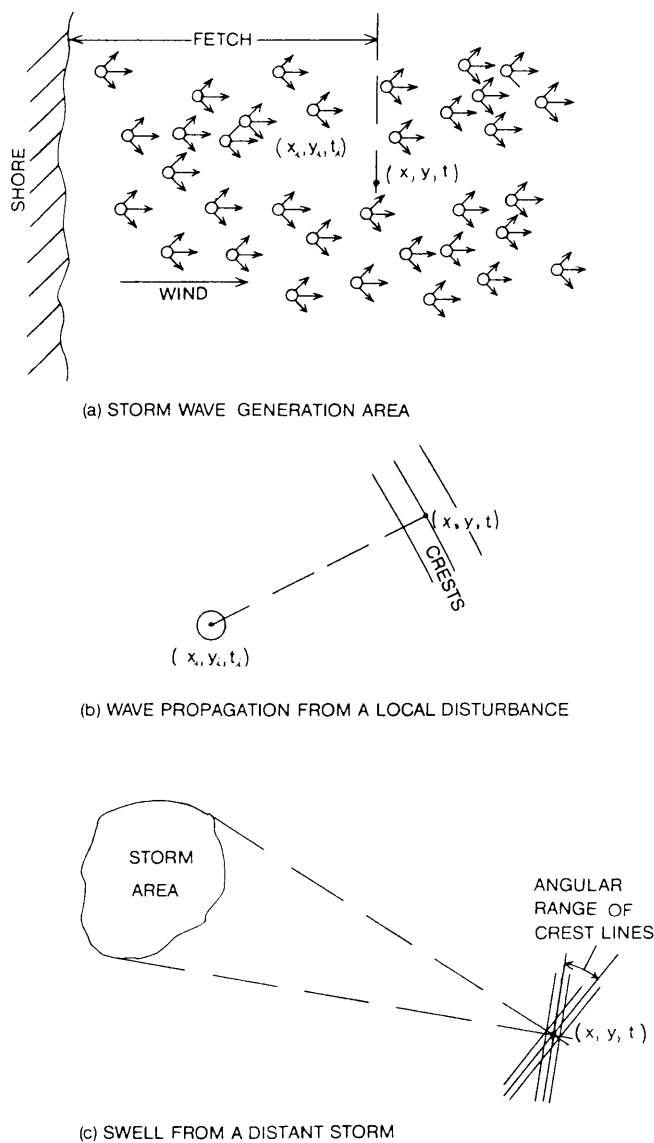


Fig. 1 Ocean wave generation and propagation

starts to blow over the region. Fig. 1(b) shows the effect at an observation point  $(x, y, t)$  of a disturbance at  $(x_i, y_i, t_i)$ . Since a specific disturbance creates a dispersive wave system originating with a local interaction between wind and sea, it has the form of radiating waves spreading from the point  $(x_i, y_i)$ . At any distant observation point it will appear to be a system of locally long-crested waves progressing from the direction of the point of origin. The original action (e.g., an impulsive displacement) is assumed to generate a band of frequencies, each corresponding to a different band of wavelengths. As different wavelengths advance at different celerities, the longest waves will reach the observation point first, and the observed average wavelength will decrease with increasing time,  $(t - t_i)$ . The total wave displacement,  $\zeta$ , at the observation point is

the sum of effects due all disturbances in the generation area that are upwind of a line through the observation point perpendicular to the wind direction. Because of angular dispersion, or *spreading*, the many wave systems will come from different directions, and the combined system will generally show *short-crestedness*.

If there is a boundary to windward of the generation area, a shore or the edge of the storm, the total wave systems at a series of observation points will differ in character as the points approach the boundary, as there will be fewer disturbances propagating over the observation point. This distance from the observation point to the boundary is called the *fetch*. Also, if the waves are observed at a fixed point, starting with the inception of the wind, the wave system will grow with time. The time interval between storm inception and observation is called *duration*. If wind speed is steady, while fetch and/or duration are increased, the sea condition eventually takes on a statistically stable structure which is called *fully developed*. Further increases in fetch and duration have no significant effect on the statistical characteristics of the wave pattern.

If the observation point is outside the storm area, Fig. 1(c), then it is seen that the arriving seas, now called *swells*, clearly have a more regular character, depending upon the distance and area of the storm. The crests of the various component wave trains become more nearly parallel as the observation point recedes from the storm area, with the result that actual waves become more and more *long-crested*, that is, the identifiable length of a wave crest becomes large compared with the spacing between crests. Distance or fetch has the effect of limiting the range of wavelengths (frequencies) reaching an observation point at a given time, i.e., the greater the distance, the narrower the bandwidth of frequencies. This filtering effect is due to the different celerities of the different component wavelengths. The lengths of waves in this band decrease with time, with the shortest identifiable components being greatly attenuated and perhaps arriving well after the storm has passed. These qualities of long-crestedness and limited bandwidth are responsible for the characteristic regular appearance of swell.

A complete long-term description can best be provided by specifying many spectra (short-term) for different points throughout the area under consideration, and at regular increments of time. Despite the lack of an entirely satisfactory theory of wave generation, oceanographers have devised semi-empirical methods of predicting the changing wave spectra by considering the effect of winds on the growth or decay of local wave systems. For example, Pierson, et al (1955) described a method of accomplishing this, making use of theoretical work of Phillips and Miles, as well as empirical data. See Section 2.9.

Since the short-term irregular wave patterns observed at sea will be described in terms of regular

component wave trains of different frequency and direction, it is important to consider next the characteristics of simple gravity waves.

**2.2 Theory of Simple Gravity Waves.** In the hydrodynamic theory of surface waves it is assumed that the crests are straight, infinitely long, parallel and equally spaced, and that wave heights are constant. The wave form advances in a direction perpendicular to the line of crests at a uniform velocity,  $V_c$ , usually referred to as *celerity* to emphasize that it is the wave form rather than the water particles that advances. Such simple waves are usually referred to as two-dimensional waves. It is assumed in wave theory that water has zero viscosity and is incompressible. It is convenient also to assume that, although waves are created by wind forces, atmospheric pressure on the water surface is constant after the wave train has been established.

The surface wave is the visible manifestation of pressure changes and water-particle motions affecting the entire body of fluid—theoretically to its full depth. The motion of particles under the idealized conditions can be characterized conveniently by a quantity known as the *velocity potential*  $\phi$  which is defined as a function whose negative derivative in any direction yields the velocity component of the fluid in the same direction. From this function all of the desired wave characteristics can be derived. Treatises on hydrodynamics give the velocity potential for a two-dimensional wave in any depth of water and express the resulting wave form by a Fourier series (Korvin-Kroukovsky, 1961; Lamb, 1924). If certain simplifications are introduced, which amount to assuming the waves to be of very small (theoretically infinitesimal) amplitudes, the so-called first-order theory reduces the wave to the first harmonic alone. (A more exact solution is discussed in Section 2.3). The simplified potential is as follows:

$$\phi = -\bar{\zeta} V_c \frac{\cosh k(z + h)}{\sinh kh} \cdot \sin k(x - V_c t) \quad (3)$$

The origin is taken at the still-water level directly over a hollow, Fig. 2;  $x$  is the horizontal coordinate, positive in the direction of wave propagation, and  $z$  is the vertical coordinate, positive upward. This positive upward convention is adopted for consistency with the work on ship motions to follow, although it differs from some references. Also

$\bar{\zeta}$  is surface wave amplitude (half-height from crest to trough)

$L_w$  is wave length

$h$  is depth of water

$k$  is the *wave number*,  $2\pi/L_w$

$V_c$  is wave velocity or *celerity*

$t$  is time

For the case of deep water (roughly  $h > L_w/2$ ) the ratio

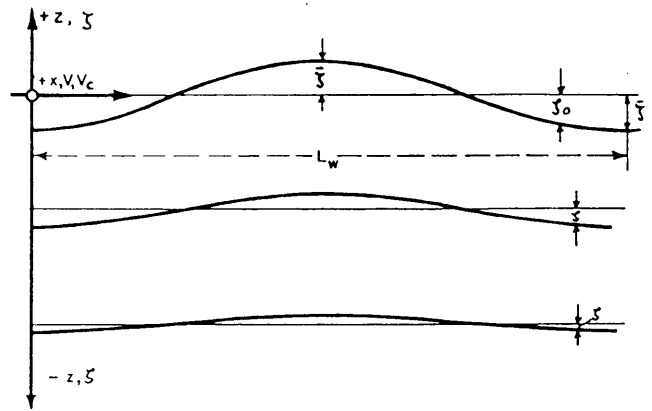


Fig. 2 Coordinates for waves

$$\frac{\cosh k(z + h)}{\sinh kh}$$

approaches  $e^{kz}$  and the expression for the velocity potential becomes

$$\phi = -\bar{\zeta} V_c e^{kz} \sin k(x - V_c t) \quad (4)$$

Hence, the horizontal and vertical components of water velocity at any point in deep water are given by

$$u = -\frac{\partial \phi}{\partial x} = k\bar{\zeta} V_c e^{kz} \cos k(x - V_c t) \quad (5)$$

and

$$w = -\frac{\partial \phi}{\partial z} = k\bar{\zeta} V_c e^{kz} \sin k(x - V_c t) \quad (6)$$

If the path of a particular particle be traced through a complete cycle, it will be found that in deep water all particles describe circular paths having radii that are  $\bar{\zeta}$  at the surface and decrease with depth in proportion to  $e^{kz}$ . Strictly,  $z$  should here be measured to the center of the circular path described by the particle. In shallow water the particles move in ellipses with a constant horizontal distance between foci and with vertical semi-axes varying with depth. At the bottom, the vertical semi-axis is zero, and the particles oscillate back and forth on straight lines.

To determine the foregoing velocities in any particular case, it is necessary to derive an expression for wave velocity  $V_c$ . Books by Milne-Thompson (1960) and Korvin-Kroukovsky (1961), show that the conditions of velocity and pressure at the surface of the wave require that

$$\frac{\partial^2 \phi}{\partial t^2} + g \frac{\partial \phi}{\partial z} = 0 \quad (7)$$

Inserting Equation (3) for the potential in (7), it can be shown that

$$V_c^2 = \frac{g}{k} \tanh kh \quad (8)$$

which defines the velocity of a wave in any depth of water. Then in very shallow water (roughly  $h < L_w/25$ )

$$V_c^2 = gh \quad (9)$$

and in deep water ( $h > L_w/2$ ),

$$V_c^2 = g/k = gL_w/2\pi \quad (10)$$

For many problems the most important aspect of waves is the distribution of pressure below the surface. It is convenient to compute the pressure relative to horizontal lines of constant pressure in still water. The elevation  $\zeta$  of lines of equal pressure in a wave relative to the still-water pressure lines, Fig. 2, is obtained from the expression

$$\zeta = \frac{1}{g} \frac{\partial \phi}{\partial t} \quad (11)$$

which is derived in hydrodynamics texts (Lamb, 1924) by means of Bernoulli's theorem for a gravity force acting on a body of fluid under uniform atmospheric pressure, assuming that wave height is small (strictly speaking, infinitesimal). Then for water of any depth

$$\zeta = \frac{k\bar{\zeta} V_c^2}{g} \frac{\cosh k(z+h)}{\sinh kh} \cos k(x - V_c t) \quad (12)$$

Since from Equation (8)  $kV_c^2/g = \tanh kh$ , this can be simplified to

$$\zeta = \bar{\zeta} \frac{\cosh(z+h)}{\cosh kh} \cos k(x - V_c t) \quad (13)$$

In deep water (large  $h$ ) the ratio  $\cosh k(z+h)/\cosh kh$  approaches  $e^{kz}$ , and

$$\zeta = \bar{\zeta} e^{kz} \cos k(x - V_c t) \quad (14)$$

These expressions show that contours of equal pressure at any depth are cosine curves which are functions of time when observed at a fixed point  $x_0$  or a function of distance  $x$  at a particular instant  $t_0$ . Since  $e^{kz}$  decreases as  $z$  decreases, the contours of equal pressure are attenuated with depth, approaching zero amplitude as  $z \rightarrow -\infty$ . These contours are the same as those generated by the orbital motions of individual particles.

To obtain the surface *wave profile*,  $z$  is taken equal to zero in Equation (13) or (14). Then

$$\zeta_0 = \bar{\zeta} \cos k(x - V_c t) \quad (15)$$

for both deep and shallow water.

A more convenient form for the equation of a simple harmonic wave can be obtained by using circular frequency  $\omega = 2\pi/T_w$ . The period  $T_w$  is the time required for the wave to travel one wave length, and hence the relationship between wave length and period in deep water can be derived from Equation (10).

$$T_w = \frac{L_w}{V_c} = \frac{L_w}{(gL_w/2\pi)^{1/2}} = \left( \frac{2\pi L_w}{g} \right)^{1/2} \quad (16)$$

Hence, circular frequency

$$\omega = \frac{2\pi}{T_w} = \left( \frac{2\pi}{L_w/g} \right)^{1/2} = (kg)^{1/2} = kV_c \quad (17)$$

and

$$\zeta_0 = \bar{\zeta} \cos(kx - \omega t) \quad (18)$$

When observed at a fixed point, with  $x = 0$

$$\zeta_0 = \bar{\zeta} \cos(-\omega t) = \bar{\zeta} \cos \omega t$$

Alternatively, if the wave profile is studied at  $t = 0$

$$\zeta_0 = \bar{\zeta} \cos kx$$

The slope of the wave surface is obtained by differentiation:

$$\frac{d\zeta_0}{dx} = k\bar{\zeta} \sin kx \quad (19)$$

The slope is maximum when  $kx = \pi/2$  and  $\sin kx = 1.0$ . Then

$$\text{Max } \frac{d\zeta_0}{dx} = k\bar{\zeta} = 2\pi \frac{\bar{\zeta}}{L_w} = \frac{\pi h_w}{L_w} \quad (20)$$

where  $h_w$  is the wave height from hollow to crest. This maximum slope occurs midway between a crest and a hollow.

The contours of constant pressure that have been derived in Equations (13) and (14) also indicate the increase or decrease in pressure relative to still water at any point in terms of depth or head. Hence, to obtain the pressure  $p$  at any point we need only multiply the head by density  $\rho g$ , or

$$p = \rho g(-z + \zeta)$$

In deep water, then, from Equations (11) and (14)

$$p = -\rho g z + \bar{\zeta} \rho g e^{kz} \cos(kx - \omega t)$$

As previously noted,  $z$  should be measured to the center of the circular path described by the particle at the point in question.

Evaluation of the equation for pressure in a deep-water wave under the crest, at  $2\bar{\zeta}$  below the original still-water level ( $z = -2\bar{\zeta}$ ), gives, for example

$$p = -\rho g(-2\bar{\zeta}) + \bar{\zeta} \rho g e^{2k\bar{\zeta}} = \rho \bar{\zeta} g(2 + e^{2k\bar{\zeta}})$$

and for  $k = 0.015$ , and  $\bar{\zeta} = 10$ , for example:

$$p = \rho \bar{\zeta} g(2.0 + 0.74) = \rho \bar{\zeta} g(2.74)$$

If the pressure were directly proportional to depth below the surface, it would be  $\rho \bar{\zeta} g(3.0)$  at this point. The difference represents the so-called *Smith effect* (Smith, 1883). Similarly, under the wave hollow at a depth of  $2\bar{\zeta}$  below still-water level ( $z = -2\bar{\zeta}$ ),

$$p = \rho \bar{\zeta} g(2.0 - 0.74) = \rho \bar{\zeta} g(1.26)$$

instead of  $\rho \bar{\zeta} g(1.0)$ . Thus under the crest the pressures

are decreased, and under the hollow the pressures are increased, by the Smith effect.

The *energy* in a train of regular waves consists of kinetic energy associated with the orbital motion of water particles and potential energy resulting from the change of water level in wave hollows and crests. The kinetic energy can be derived from the velocity potential. For one wave length  $L_w$  the kinetic energy per unit breadth of a wave of small height is given in books on hydrodynamics (Lamb, 1924; Korvin-Kroukovsky, 1961), as

$$\frac{1}{2} \int_0^{L_w} \phi \frac{\partial \phi}{\partial z} dx$$

This is evaluated for a simple cosine wave as

$$\frac{1}{4} \bar{\zeta}^2 \rho g L_w$$

The potential energy due to the elevation of water in one wave length is obtained by taking static moments about the still-water level. A unit increment of area is  $\bar{\zeta} dx$  and the lever arm is  $\zeta_0/2$ . Hence, integrating, potential energy is

$$\begin{aligned} & \int_0^{L_w} \rho g (\zeta_0/2) \bar{\zeta} dx \\ &= \frac{1}{2} \rho g \int_0^{L_w} \zeta_0^2 dx \end{aligned}$$

For a cosine wave,

$$\zeta_0 = \bar{\zeta} \cos k(x - V_c t)$$

and at  $t = 0$

$$\zeta_0 = \bar{\zeta} \cos kx$$

Hence, potential energy is

$$\frac{1}{4} \bar{\zeta}^2 \rho g L_w$$

These derivations show that wave energy is half kinetic and half potential when averaged over a wave length. Total energy is

$$\frac{1}{2} \rho g \bar{\zeta}^2 L_w$$

Or the average energy per unit area of surface,

$$\text{Ave. unit Energy} = \frac{1}{2} \rho g \bar{\zeta}^2 \quad (21)$$

Another useful property of waves, especially irregular waves to be discussed in Section 2.6, is the *variance*, or the mean-square value of surface elevation as a function of time. In general, the variance of a continuous function with zero mean is given by,

$$\langle \zeta(t)^2 \rangle = \lim_{T \rightarrow \infty} \frac{1}{T} \int_{-T/2}^{T/2} \zeta^2(t) dt \quad (22)$$

where the brackets  $\langle \rangle$  indicate mean value of.

In the case of a simple harmonic wave, as given by Equation (18) at  $x = 0$ ,  $T$  can be taken as the wave period, and it can be shown that

$$\langle \zeta(t)^2 \rangle = \frac{1}{2} \bar{\zeta}^2 \quad (23)$$

That is, the variance of wave elevation of a single cycle of a sine wave is equal to one-half the square of the amplitude. This theorem is also true for a finite number of complete cycles, or in the limit as  $T \rightarrow \infty$  in Equation (22).

For the work to follow, the two-dimensional regular wave can be considered to be a three-dimensional wave train with straight, infinitely long crests, i.e., a long-crested regular wave. Furthermore, with axes fixed in the earth the surface elevation of such waves traveling at any angle,  $\mu$ , to the  $x$ -axis can be described by the general equation,

$$\zeta(x, y, t) = \bar{\zeta} \cos [k(x \cos \mu + y \sin \mu) - \omega t + \epsilon] \quad (24)$$

where  $\epsilon$  is a phase angle. For the case  $\mu = 0$  this equation reduces to Equation (18), except for the phase angle, which is needed when more than one wave is present.

If a fixed point at the origin is considered ( $x = 0$ ,  $y = 0$ ), the equation becomes

$$\zeta(t) = \bar{\zeta} \cos (-\omega t + \epsilon) \quad (25)^4$$

*Wave Properties.* The following is a summary of the properties of two-dimensional harmonic waves and waves of finite height in deep water (any consistent units):

Wave number	$k = 2\pi/L_w = \omega^2/g$	
Surface profile	$\zeta_0 = \bar{\zeta} \cos k(x - V_c t)$	(15)

(first approximation)	$= \bar{\zeta} \cos (kx - \omega t)$	(18)
-----------------------	--------------------------------------	------

Velocity potential	$\phi = -\bar{\zeta} V_c e^{kz} \sin k(x - V_c t)$	(4)
--------------------	--	-----

Wave celerity	$V_c = \frac{L_w}{T} = \left( \frac{gL_w}{2\pi} \right)^{1/2} = \frac{gT_w}{2\pi} = \frac{g}{\omega}$	(10)
---------------	---	------

Wave length	$L_w = 2\pi \frac{V_c^2}{g} = \frac{gT_w^2}{2\pi}$	(16)
-------------	--	------

Wave period	$T_w = (2\pi L_w/g)^{1/2}$	(16)
-------------	----------------------------	------

Maximum wave slope (first approximation)	$k\bar{\zeta} = 2\pi \frac{\bar{\zeta}}{L_w} = \frac{\pi h_w}{L_w}$	(20)
--	---	------

Wave energy per unit area	$\frac{1}{2} \rho g \bar{\zeta}^2$	(21)
---------------------------	------------------------------------	------

Wave variance	$\langle \zeta^2 \rangle = \frac{1}{2} \bar{\zeta}^2$	(23)
---------------	---	------

*In feet-seconds units:*

Wave celerity	$V_c = 2.26 L_w^{1/2}$
---------------	------------------------

<sup>4</sup>  $\bar{\zeta}$  is often taken to represent the complex amplitude, in which case the imaginary part defines the phase angle and  $\epsilon$  is unnecessary.

Wave length	$L_w = 5.118 T_w^2 = 0.196 V_c^2$
Wave period	$T_w = 0.442 L_w^{1/2}$

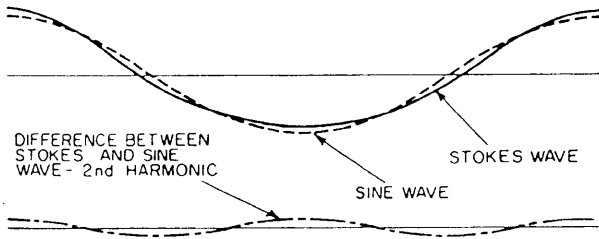


Fig. 3 Comparison of sine wave and Stokes wave

**2.3 Waves of Finite Height.** A hydrodynamic theory of waves of finite amplitude, i.e., not infinitesimal as previously assumed, was formulated by Stokes (1847) and others. It corresponds with the observed fact that actual waves have sharper crests and flatter hollows than the simple cosine wave assumed in the preceding section. The equation for velocity potential, which leads with approximations to the simple harmonic wave, yields a second-order wave profile when the approximations are not made. The solution can be extended with further refinements into a series expansion, and therefore, the wave form, in principle, can be expressed to any desired precision by taking a sufficient number of terms. Actually, for all practical purposes, the Stokes equation to the second order of approximation is satisfactory for ship problems. Expressed as a function of  $x$  at fixed time  $t = 0$ , in deep water, the surface profile is

$$\zeta_0 = \bar{\zeta} \cos kx + \pi \frac{\bar{\zeta}^2}{L_w} \cos 2kx \quad (26)$$

In other words, the simple cosine curve is modified by a harmonic which is half the length of the fundamental, Fig. 3. The velocity of the harmonic wave, however, must be the same as for the fundamental.

As wave height increases, the crest approaches a cusp, the double angle of which is  $2\pi/3$  radians or 120 deg, which corresponds to a limiting wave height from crest to trough of  $0.14L_w$  or approximately  $1/7 L_w$ . Real waves will break well before this height is reached.

Consideration of water-particle velocities in a wave of finite height reveals that the forward water velocity at a wave crest is greater than the backward velocity in the hollow. This difference in particle velocities, when averaged over wave length, leads to the mean velocity of water flow or *mass transport*

$$\bar{u} = k^2 \bar{\zeta}^2 V_c e^{2kz} \quad (27)$$

when  $z$  is the mean particle depth at which the velocity is sought. Hence, the particle motion is not exactly circular.

It can be seen from Equation (27) that the velocity

reduces rapidly with depth. Even at the surface the drift velocity is only of the order of 2 to 3 percent of wave velocity, although it may be a significant percentage of the water-particle velocities.

While the *Stokes wave*, with its sharpened crest and flattened trough, is a more accurate geometrical model of real regular waves, it suffers from a limitation that negates its value in treating storm seas and swell, and the principle of superposition does not apply. If two Stokes waves are added, the sum is not a valid wave form. This is easily seen by simply adding two identical waves, which is equivalent to multiplying Equation (26) for  $\zeta_0$  by 2. But for this to be a valid Stokes wave, the second term should have been multiplied by 4. It has become standard practice to accept the slight errors in wave shape of linear harmonic wave theory in order to achieve simplicity in treating the additive wave systems that are characteristic of both sea and swell. Errors in form become significant when waves become steep enough to approach breaking, and when the geometry of the wave crest is a factor in the treatment of a problem. But a correct mathematical analysis of nonlinear short-crested irregular waves implies a great increase in complexity (St. Denis, 1980).

**2.4 Trochoidal Waves.** From the early days of naval architecture it has been customary to make use of a *trochoidal* wave in some ship-design problems. It is a convenient form from the geometrical point of view, but it fails to meet certain requirements of classical hydrodynamics and cannot be derived from the velocity potential. Its profile is almost identical with the second-order Stokes wave. In deep water all particles within trochoidal waves follow circular orbits about fixed centers at a constant angular velocity. In any horizontal line of orbit centers, the radii are equal but the phase of adjacent particles varies successively. In any vertical line, all the particles have the same phase but the radii of their orbits decrease exponentially as the depth increases. Particles which, in still water, may be identified by the intersections of a rectangular grid, take the positions shown by the intersections of the distorted grid in Fig. 4 at some instant during the passage of a wave. Those which were originally in the same horizontal line lie on undulating surfaces, while those originally in the same vertical line lie along lines which sway from side to side, converging under the crests and diverging under the hollows. The orbit centers are somewhat above the still-water positions of the corresponding particles. The wave form travels to the left when the generating circles, with fixed centers, revolve counterclockwise.

The curve joining a series of particles originally in the same horizontal plane is the same as that which is generated by a point on the radius of a circle as the circle rolls along the underside of a horizontal straight line, as is evident from a comparison of Figs. 4 and 5. Such curves, whose limit is the cycloid, are called trochoids. They are also contours of equal pressure.

$R$  = RADIUS OF ROLLING CIRCLE.  
SEE FIG. 5

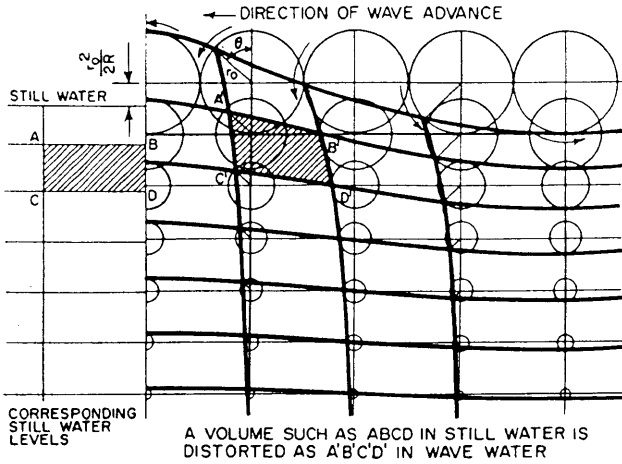


Fig. 4 Trochoidal wave motion

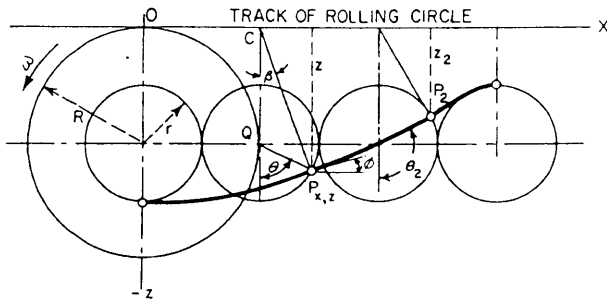


Fig. 5 Geometry of trochoid

If we call the orbit radius  $r$  and the amplitude  $\bar{\zeta}$ , then  $\bar{\zeta} = r$ . Quantities referring to the surface wave are denoted by subscript 0; thus  $\bar{\zeta} = r_0$ . If  $R$  is the radius of the rolling circle and  $L_w$  is the wave length from crest to crest,  $L_w = 2\pi R$ . To draw a trochoidal-wave surface, the selected wave length is divided by a convenient number of equally spaced points, and, with each as a center, a circle of diameter equal to the selected wave height is described. In these circles are drawn radii at successive angles which increase by the same fraction of 360 deg as the spacing of the circles in relation to wave length. The curve connecting the ends of those radii is the desired trochoid.

In Fig. 5, an ordinate  $z$  upward, and an angular velocity  $\omega$  counterclockwise, are considered positive. From an initial position, shown at the left, the large circle is assumed to be rolling steadily, counterclockwise, and after time  $t$  to have reached the position  $OCP$ , having turned through the angle  $\theta = \omega t$ . In this case  $\theta$  is positive since  $\omega$  is counterclockwise.

The parametric equations of the trochoid in Fig. 5 are

$$\begin{aligned} x &= R\theta + r \sin \theta = R\omega t + r \sin \omega t \\ z &= R + r \cos \theta = R + r \cos \omega t \end{aligned} \quad (28)$$

The radii of the circles in which the particles move decrease exponentially with depth; that is, as in the case of the harmonic wave

$$r = r_0 e^{kz}$$

where  $r_0$  is the radius of a particle at the surface, and  $z$  is measured to the center of the circle in which the particle moves.

The trochoidal wave is somewhat sharp in the crest and flat in the trough like a simple wave in a model tank, and like the Stokes wave, Fig. 3. Consequently, for equal water volumes the lines of orbit centers must be somewhat above the corresponding still-water levels in order that the amount of water in the crest will equal the amount removed in the hollow. It can be shown that this rise of orbit centers is  $r^2/2R$ , Fig. 4.

Although the trochoidal wave is reasonably realistic for waves up to about  $L/20$  in height, the limiting case of  $R = r$  gives an impossibly steep wave with very sharp cusps. Other characteristics of the trochoidal wave, such as velocity, period, pressure change with depth, are the same as for the simple harmonic wave previously discussed.

Obviously the pressure at any point on the surface of a wave is atmospheric. Furthermore, the sum of all the hydrodynamic and buoyant forces acting on a surface particle is perpendicular to the surface, as demonstrated by Froude with a little float carrying a pendulum. Although this statement can be proved on the basis of the theory of a simple harmonic wave, it is most easily demonstrated by means of trochoidal theory.

Following Froude's approach, it is convenient to deal with the inertial reactions to the water-pressure forces acting on the particle  $P$  in Fig. 6, although the latter could also be determined directly. As previously shown, the buoyancy and hydrodynamic pressure forces in the wave cause the particle to move in a circular path, and the equal and opposite reactions consist of gravity  $mg$  acting downward and a centrifugal reaction  $QF'$  resulting from orbital motion of the particle

$$mr\omega^2$$

It can be shown that in a trochoidal gravity wave  $\omega^2 = g/R$  and therefore the centrifugal reaction is

$$mg(r/R)$$

The resultant is  $PF$  in Fig. 6.

In triangles  $QCP$  and  $F'FP$ ,  $PF'$  is in line with  $QP$  and  $F'F$  is parallel to  $QC$ . Also

$$\frac{PF'}{FF'} = \left( mg \frac{r}{R} \right) / mg = \frac{r}{R} = \frac{QP}{QC}$$

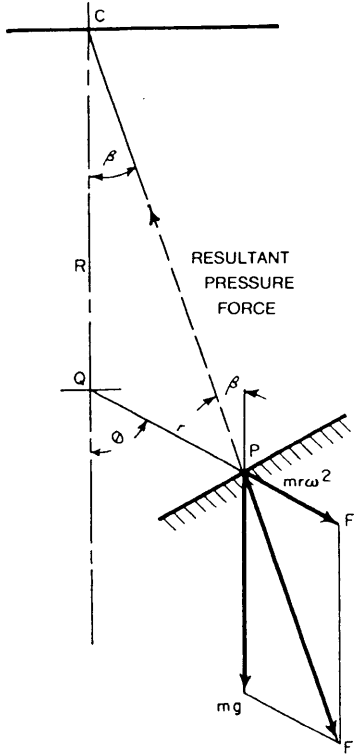


Fig. 6 Inertial reactions on water particle in trochoidal wave

Hence the two triangles are similar and  $PF$ , the resultant, is in line with  $CP$  and normal to the trochoidal surface. Any particle in the surface is acted upon, therefore, by a resultant pressure force which is normal to the surface. The net wave pressure force on the particle is equal and opposite to  $PF$ . Since no tangential force exists, the surface must be one of equal pressure.

**2.5 Compound Gravity Waves.** The highly idealized simple harmonic regular wave provides the hydrodynamic basis for short-term stochastic models of ocean waves, but its physical existence is for practical purposes limited to the laboratory. As described in Section 2.1, natural waves may usually be considered to be sums of many independent regular waves—or surface disturbances which can themselves be treated as sums of simple regular waves. Before treating these stochastic models, it is useful to consider several compound wave systems that exhibit important physical effects, even though they are just as idealized as the regular progressive wave.

(a) *Standing Waves.* Suppose we superimpose two regular waves of the same amplitude and period, but travelling in opposite directions. From Equation (18) the sum of surface elevations can be written

$$\zeta(x, t) = \bar{\zeta} [\cos(kx - \omega t) + \cos(kx + \omega t)] \quad (29)$$

$$= 2\bar{\zeta} \cos kx \cos \omega t$$

When  $t = 0$ ,  $T_w$ ,  $2T_w$ , . . . , the wave form is a cosine curve with crests at  $x = 0, L_w, 2L_w, \dots$ . When  $t = \frac{1}{2}T_w$ ,  $\frac{3}{2}T_w$ , . . . , the form is the negative of the first form, with troughs at  $x = 0, L_w, \dots$ . When  $t = \frac{1}{4}T_w$ ,  $\frac{3}{4}T_w$ , . . . , the surface is completely flat. At intermediate times, the surface has the same shape as at  $t = 0$ , but with amplitude  $2\bar{\zeta} \cos \omega t$ . Thus, the crests never move but decrease in place and become troughs after passing through zero. This is known as a *standing wave*. By adding the velocity potentials of the two component progressive waves, it can be shown that the particle velocity at  $x = 0$  is always vertical, and at  $x = L_w/4, 3L_w/4, \dots$  (the nodes), the velocity is always horizontal. Therefore, the wave form is the same as it would be if a wall were placed at  $x = 0$ , and, in fact, a standing wave is generated when a progressive regular wave is reflected from a vertical wall perpendicular to its direction of advance.

(b) *Wave Groups.* It is frequently observed that natural waves may appear to exist in packets or *groups*, with relatively calm patches between groups. In effect, the waves have an envelope that itself rises and falls with time and distance. This phenomenon is particularly characteristic of swell waves and is of importance in wave propagation.

An idealized wave group pattern can be simulated by a sum of two progressive waves of the same amplitude but with slightly different frequencies, moving in the same direction. Thus,

$$\begin{aligned} \zeta(x, t) &= \bar{\zeta} [\cos(k_1 x - \omega_1 t) + \cos(k_2 x - \omega_2 t)] \\ &= 2\bar{\zeta} \cos \frac{1}{2}[(k_1 + k_2)x - (\omega_1 + \omega_2)t] \\ &\quad \cos \frac{1}{2}[(k_1 - k_2)x - (\omega_1 - \omega_2)t] \end{aligned} \quad (30)$$

The first cosine factor in this equation has the form of a progressive regular wave with wave length

$$L_w = 2\pi / \frac{1}{2}(k_1 + k_2)$$

or,

$$\frac{1}{L_w} = \frac{1}{L_1} + \frac{1}{L_2}$$

Thus, the wavelength of this factor is the harmonic mean of the wavelengths of the two components. The factor is multiplied by another cosine factor with wavelength,

$$L_g = 2\pi / \frac{1}{2}(k_1 - k_2)$$

and period

$$T_g = 2\pi / \frac{1}{2}(\omega_1 - \omega_2)$$

Since  $k_1$  and  $k_2$  have been considered to be nearly equal, the wavelength of this factor is very large compared with the wavelength of the first cosine factor. Therefore, it behaves like an envelope slowly advancing. It has the velocity,

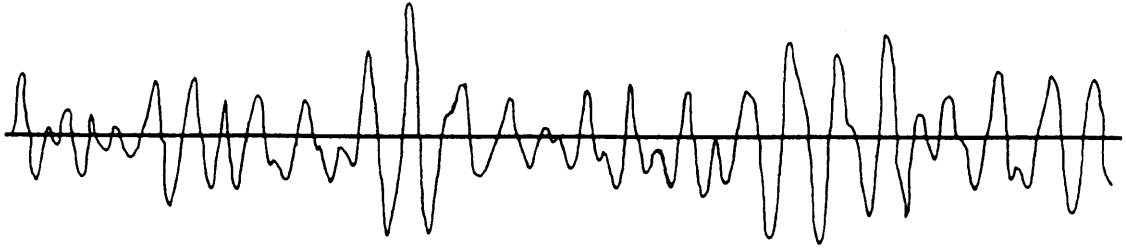


Fig. 7 Typical record of irregular sea taken at a fixed point

$$V_g = L_g / T_g = \frac{\delta \omega}{\delta k}$$

or, in the limit, as  $\delta \omega$ ,  $\delta k$  approach zero,

$$V_g = \frac{d\omega}{dk} = \frac{d(kV_c)}{dk} = V_c + k \frac{dV_c}{dk} \quad (31)$$

This is known as the *group velocity*. When the water is very deep its value approaches  $V_c/2$ , or one-half the celerity of the progressive waves under the envelope. If a particular wave crest is followed, starting at the rear of a group, it will move forward through the group, growing to a peak value, and then shrink and disappear as it approaches the leading boundary of the group. In the case of shallow water, the group velocity approaches  $V_c$ . In this case, individual waves maintain their identity within the group, which advances at wave celerity without change in wave form.

This model of groups is idealized, but group velocity and group behavior are important aspects of wave propagation. A wave group can be considered a concentration of wave energy, and group velocity is the velocity of advance of wave energy.

Studies of the statistical characteristics of wave groups under real conditions in the open ocean have been reported by Kimura (1980), Longuet-Higgins (1984) and others.

An important practical consequence of wave group behavior is that the time required for the wave energy of a given frequency to arrive (in deep water) at a specific location is twice that which would be estimated from wave celerity.

## 2.6 Waves in the Open Ocean.

(a) *A short-term model with constant amplitude components.* A conceptual model to describe ocean waves has been presented in Section 2.1. It is possible to give the short-term model more precise mathematical form at this point, one that has become extremely useful in the treatment of ship motions in natural environments. As previously explained, the wave system in the neighborhood of a particular place and time is assumed to be the sum of many regular waves, each progressing in its own direction and celerity. (The changing long-term situation is discussed in Section 2.9).

It is convenient to begin with the simple case of the wave pattern observed at a fixed point ( $x = 0$ ,  $y = 0$ ), neglecting consideration of the different directions,

$\mu$ , of wave components, Fig. 7. This is equivalent to assuming that all wave components travel in the same direction, with  $\mu = 0$ , resulting in a long-crested irregular wave observed at a fixed point. Later the effects of wave direction and moving point of observation will be considered. Following St. Denis and Pierson (1953), each of the large number of wave components is assumed to have a definite frequency and a random phase angle. The form for the equation of any component wave is as given in Equation (25),

$$\zeta_i(t) = \bar{\zeta}_i \cos(-\omega_i t + \epsilon_i) \quad (32)$$

where  $\bar{\zeta}_i$  is a component amplitude corresponding to wave frequency  $\omega_i$ , and  $\epsilon_i$  is the random phase angle.

The total wave system is then assumed to be a summation of many (theoretically an infinite number) of independent components,

$$\zeta(t) = \sum_i \bar{\zeta}_i \cos(-\omega_i t + \epsilon_i) \quad (33)$$

It has been found convenient to define these wave components in terms of a function known as a *variance spectrum*,  $S(\omega)$ . This function is also referred to as a *point spectrum*, since the wave is observed at a fixed point without consideration of the directions of component waves. At any particular wave frequency,  $\omega_i$ , the variance of all the wave components within a small finite frequency band,  $\delta \omega$ , centered upon  $\omega_i$  is given by

$$\langle \zeta_i(t)^2 \rangle \equiv S(\omega_i) \delta \omega \quad (34)$$

Finally, in the limit as  $\delta \omega \rightarrow 0$  this reduces to the variance of a single infinitesimal harmonic component.

It has been shown in Section 2.2 that for a simple, regular wave (one cycle or an infinite time)

$$\langle \zeta_i(t)^2 \rangle = \frac{1}{2} \bar{\zeta}_i^2 \quad (35)$$

Hence, if it is desired to visualize the amplitudes of the wave components, we can substitute Equation (35) in (34), so that

$$\frac{1}{2} \bar{\zeta}_i^2 = S(\omega_i) \delta \omega$$

and a component amplitude is

$$\bar{\zeta}_i = \sqrt{2 S(\omega_i) \delta \omega} \quad (36)$$

in the limit as  $\delta \omega$  approaches zero. Of course, it cannot be evaluated directly, but it can be approximated when



$\delta\omega$  is taken to be very small. See Fig. 8.

More important than the component amplitudes, however, is the total variance of the wave system, usually designated  $E$ , which is a good measure of the severity of the sea.

$$E \equiv \langle \zeta(t)^2 \rangle$$

The components on the right-hand side of (33) have been assumed to be independent random variables by virtue of their random phases. Since, as noted in Section 2.1, the variance of the sum of a large number of independent random variables approaches the sum of the variances of these variables, Equation (2) gives

$$E \equiv \langle \zeta(t)^2 \rangle = \sum_i \langle \zeta_i(t)^2 \rangle$$

or integrating Equation (34) and substituting,

$$E = \int_0^\infty S(\omega) d\omega \quad (37)$$

That is, the area under the spectrum is equal to the variance,  $E$ , of the wave system.

Referring to the typical plot of a variance spectrum at a point (Fig. 8), the areas of the elemental rectangles,  $S(\omega_i) \delta\omega$ , may be seen from (34) to define the variances of the wave components. Strictly speaking, the foregoing interpretation of the spectrum in terms of component waves is valid only for the limiting case  $\delta\omega \rightarrow 0$  and the number of components  $\rightarrow \infty$ .

By Equation (36) the elemental rectangles also define the amplitudes of the components in the limit. However, when a large number of components is assumed, say 15 or 20, a fair finite-sum model of a unidirectional (long-crested) sea is obtained. (A multi-directional, short-crested, sea requires many more). Since any particular rectangle represents the variance in that band of frequencies, a wave of the indicated finite amplitude would have the same variance as the infinite number of components within that band. Hence, the algebraic addition of these 15 or 20 component waves, shown at the bottom of Fig. 8, will give a pattern that has the same total variance and closely resembles the record from which the spectrum was obtained. It will also have many of the same statistical properties. However, we can never match the record exactly, no matter how many components are assumed, for although an artificial wave can be made to repeat itself, a real ocean wave record never does so. This is actually no handicap, for it is statistical information that we ultimately need for application to ship design.

It is of interest to plot five or more sine curves through several cycles and to add successive ordinates algebraically or to carry out the same procedure on an electronic computer. The resulting curve will demonstrate clearly that the sum of even a small number of regular sine waves is an irregular pattern, provided that the component waves are in random phase.

It should be emphasized that the component waves are not directly visible either at sea or in a wave record. However, the variance spectrum defining these components can be obtained from a wave record by applying the techniques of generalized harmonic analysis (Wiener, 1930, 1949), provided that the record is long enough (15 to 20 min) and that sea conditions remain steady. Such records have been obtained mainly by means of shipborne recorders aboard stationary vessels (such as weather ships). Airborne laser and radar scanning have also been used, and radar altimeters on spacecraft are under development (Pierson, 1974).

In the analysis procedure developed by Tukey (1949) and Rice (1945 and 1954) points are first read from the record at equal increments of time. Then the *autocorrelation function* of the data sample is obtained by evaluating the integral

$$\int_0^T \zeta(t) \cdot \zeta(t + \tau) dt$$

for discrete values of *time lag*,  $\tau$ . The raw point spectrum is then obtained by taking the *Fourier cosine transform* of the autocorrelation function. Some

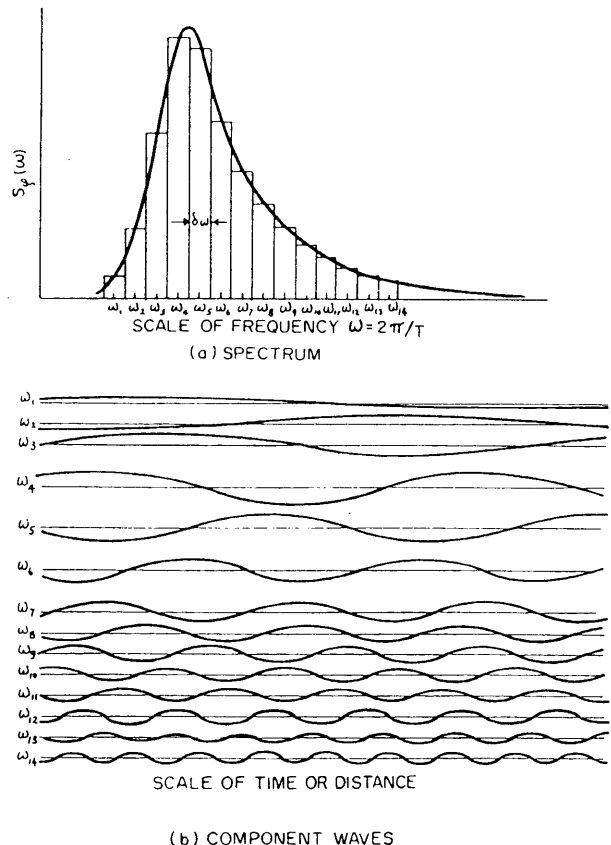


Fig. 8 Typical variance spectrum of waves, showing approximation by a finite sum of components

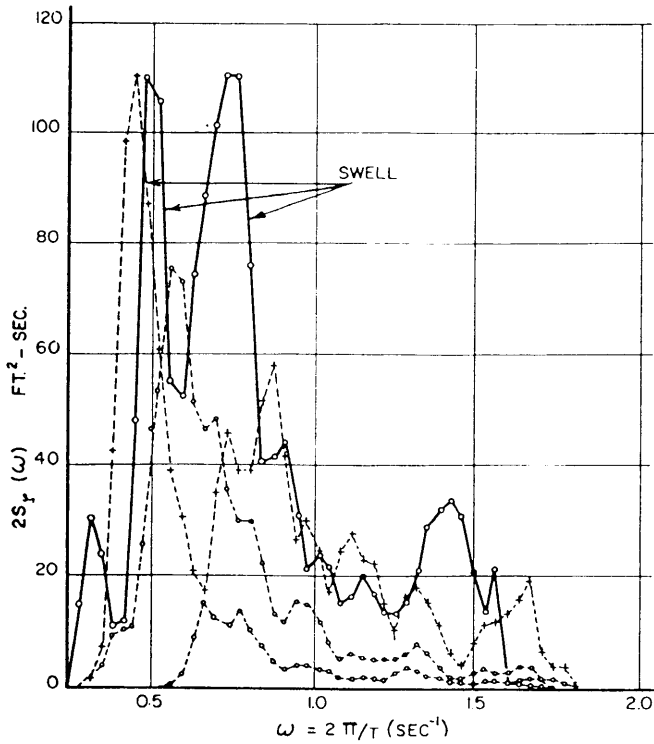


Fig. 9 Typical sea spectra, winds from 24 to 47 knots (Moskowitz, et al, 1962)

“smoothing” of the raw spectrum is desirable to improve the accuracy of the estimate, involving one of several *smoothing functions*. Finally, the theory provides a means of evaluating the accuracy, that is, defining the confidence bands of the spectral estimates, taking account of the sampling interval  $\delta t$ , the number of data points in the sample, and the number of lags. (The procedure is summarized by Korvin-Kroukovsky (1961), and discussed in detail by Bendat and Piersol (1971).

The foregoing operations can be readily carried out on a digital computer. However, in recent years, it has been found to be more expeditious to employ standard *Fast Fourier* programs, which also provide superior resolution (Bendat and Piersol, 1971). The effects of using different analysis methods on the same data are considered by Donelan and Pierson (1983). Many examples of point spectra have been derived from ocean wave records. Several of these are shown in Fig. 9.

It should be noted that some authors prefer to use a spectrum form based on wave period rather than frequency, since it is more consistent with wave observations and when plotted gives more emphasis to the important low frequencies and less to the less important high frequencies.

It has been shown in Section 2.2 that energy per unit surface area in a simple harmonic wave is proportional to the square of the amplitude, or, more specifically,

$$\text{Unit Energy} = \frac{1}{2} \rho g \bar{\zeta}^2 \quad (21)$$

Equations (34) and (35) show that the variance of the wave components within a band of frequencies,  $\delta\omega$ , is

$$\langle \zeta_i(t)^2 \rangle \equiv S(\omega_i) \delta\omega = \frac{1}{2} \bar{\zeta}^2 \quad (38)$$

which differs only by a factor of  $\rho g$  from the unit energy of Equation (21). Hence, the spectrum  $S(\omega)$ , which describes the allocation of the variance of a wave system among components can also be considered an allocation of Energy/ $\rho g$ . For this reason, it is sometimes called, somewhat loosely, the *energy spectrum*.

Note that if the sea were unidirectional, or long-crested, the point spectrum, together with the direction, would be a complete statistical definition of the seaway, assuming it to be a Gaussian random process, with zero mean. This condition is sometimes approximated in nature when the predominant waves are from a single distant storm.

Although the variance  $E$ , obtained from a point spectrum is a good measure of the severity of *any* sea, it will be shown that the seaway can be more completely characterized by considering the component wave directions by means of a *directional spectrum*. Coming now to this more general three-dimensional case, a single wave train is described by Equation (24). The general equation for the total wave system of components moving in different directions,  $\mu$ , is then

$$\zeta(x, y, t) = \sum_i \sum_j \bar{\zeta}_{ij} \cos [k_i(x \cos \mu_j + y \sin \mu_j) - \omega_i t + \epsilon_{ij}] \quad (39)$$

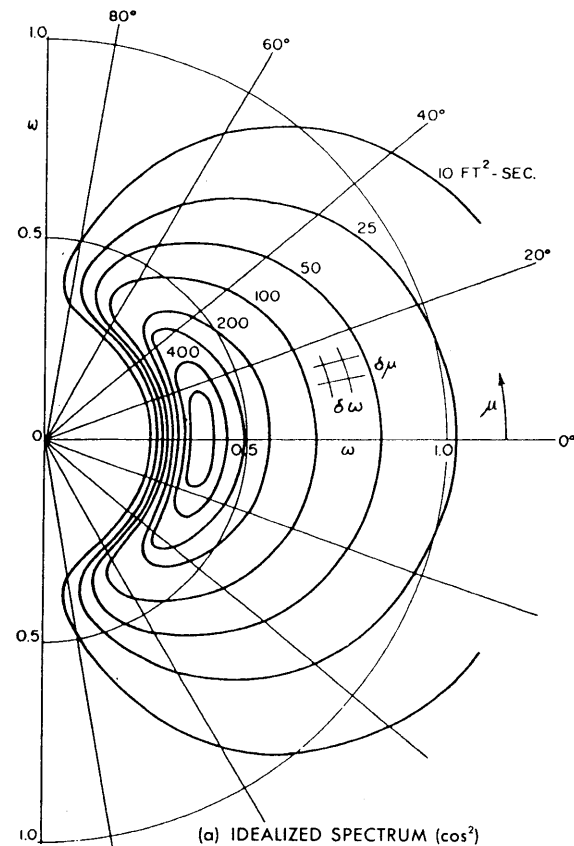
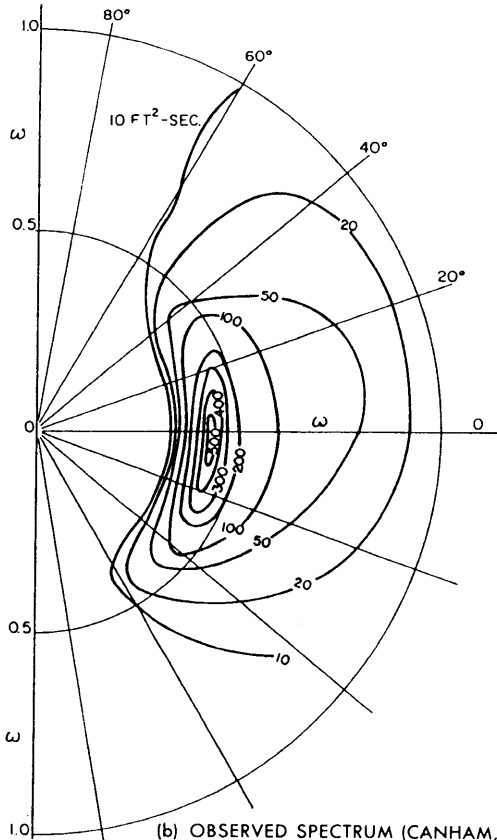
In a manner similar to the case of the point spectrum, the wave elevation may be considered at a point ( $x = 0$ ;  $y = 0$ ), but component wave direction,  $\mu$ , must still be accounted for. Hence,

$$\zeta(t) = \sum_i \sum_j \bar{\zeta}_{ij} \cos (-\omega_i t + \epsilon_{ij}) \quad (40)$$

and

$$\begin{aligned} \langle \zeta(t)^2 \rangle \equiv E &= \frac{1}{2} \sum_i \sum_j \bar{\zeta}_{ij}^2 \\ &= \int_0^\infty \int_0^{2\pi} S(\omega, \mu) d\mu d\omega \quad (41) \end{aligned}$$

where the variance  $E$ , as previously noted, is an important statistical parameter, and the components are defined by both frequency,  $\omega$ , and direction,  $\mu$ , with  $i$  and  $j$  referring to specific values of  $\omega$  and  $\mu$ , respectively, and the directional spectrum  $S(\omega, \mu)$  defines the allocation by frequency and direction of the variances of the components of the wave system. Each of the infinite number of wave components is assumed to have a definite frequency and direction, with random phase angle. The component amplitudes are defined for the incremental areas,  $\delta\omega\delta\mu$ , in the limit as  $\delta\omega$  and  $\delta\mu \rightarrow 0$ , when

(a) IDEALIZED SPECTRUM ( $\cos^2$ )

(b) OBSERVED SPECTRUM (CANHAM, ET AL 1962)

Fig. 10 Typical directional sea spectra

$$\bar{\zeta}_{ij} = \sqrt{2S(\omega_i, \mu_j)} \delta\omega \delta\mu \quad (42)$$

Thus,  $S(\omega, \mu)$  defines the sea state more completely than the point spectrum. See Fig. 10(a) which can be considered an idealized contour plot of a three-dimensional figure in which the axis perpendicular to the paper represents  $S(\omega, \mu)$ . A typical directional spectrum obtained from wave buoy records is shown in Fig. 10(b) (Canham, et al, 1962). An alternate form of plotting is given in Fig. 11. The latter can be considered to represent the long-crested irregular wave trains of different average directions that superimpose to form the short-crested sea in the limit as  $\delta\mu \rightarrow 0$ .

Integrating the directional spectrum, Equation (41), with respect to  $\mu$  leads to

$$\int_0^\infty S(\omega) d\omega = \frac{1}{2} \sum_i \bar{\zeta}_i^2 = E \quad (43)$$

where  $S(\omega)$  is the point spectrum previously discussed.

(b) *Generational Theory of Ocean Waves.* Another less simple stochastic model of ocean waves takes account of the process of generating a storm sea by assuming that the separate disturbances generated in the storm areas, as discussed in Section 2.1, are in the form of wave groups rather than simple trains of regular waves. These component systems superimpose on one another and propagate away from the generating area. The final result of this approach would be a mathematical model that differs from the simpler case in that Equation (39) requires another factor representing a wave component of fixed frequency,  $\bar{\omega}$ —a *carrier* in electronics terminology—and the substitution of  $(\omega_i - \bar{\omega})$  for  $\omega_i$  to account for the slow amplitude modulation.<sup>5</sup>

The examples of directional spectra shown in Figs. 10 and 11 apply equally to the present model and to the simpler one previously given, but in the present case the spectra will change slowly with time.

Both models are local, in the sense that they describe the statistical behavior of storm waves in the immediate neighborhood of a geographical point. However, the first model has the form of a stationary or statistically constant sea over all space and time. The second model readily allows for changes due to such effects as fetch and duration. In the first model, any realization based upon a discrete set of sine waves will have a random but constant phase between components of the same frequency but different directions, which is inconsistent with the second model. It should be noted that any realization based upon discrete sine waves, even if a large number of components is assumed, may lead to erroneous correlations among ship responses (phase between heave and pitch, for example). While the simple statistical parameters will

<sup>5</sup> (This model, conceived by Dr. W.E. Cummins, has not been developed in detail.—Ed.)

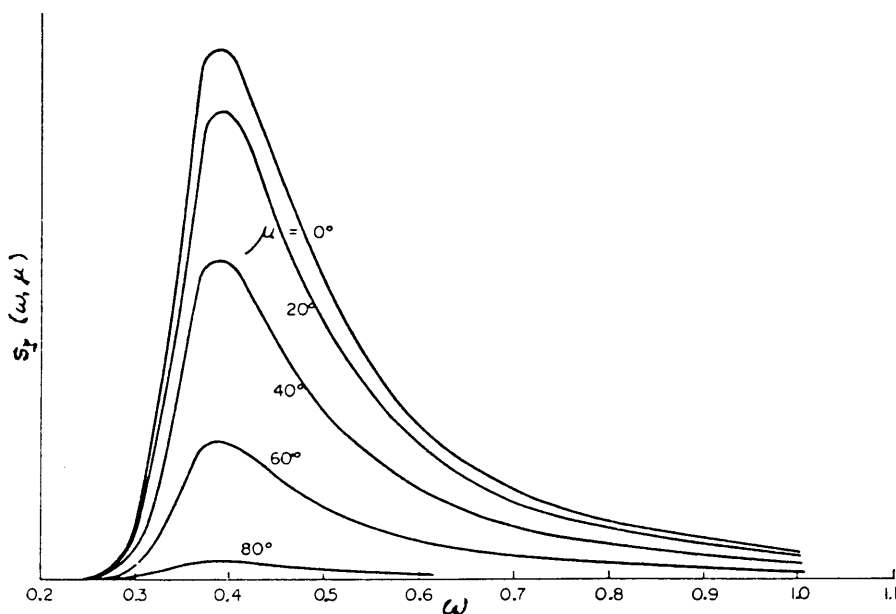


Fig. 11 Angular components of directional sea spectrum

generally be identical between the two models, more complex measures that involve two or more responses may behave quite differently. Further treatment of this question is beyond the scope of the discussion here, and in fact it is an area of controversy and continuing research. This second model is discussed, not just to provide a better understanding of the storm sea, but to lay a foundation for treating complex ship-wave interaction.

(c) *Characteristics of point spectra.* A typical record of waves observed at a fixed point is a continuous irregular function of time, such as Fig. 7, that never repeats itself exactly. The continuous line in Fig. 12 might represent a segment of such a record of length  $T$ . If it is assumed to be a zero-mean process, its variance is given mathematically by

$$\langle \zeta(t)^2 \rangle = \lim_{T \rightarrow \infty} \frac{1}{T} \int_{-T/2}^{T/2} \zeta^2(t) dt \quad (22)$$

Therefore, the variance can be approximated by taking measurements of a large number of closely spaced deviations from the mean line, squaring them and integrating numerically. But we have seen that the area under the point spectrum,  $E$ , is also equal to the variance of the process (Equation 37). Hence, if the spectrum is known, the variance can be easily obtained by integrating the spectrum. Alternatively, if one computes the variance directly from the wave record one obtains the area under the unknown spectrum, but not its shape.

A normal distribution is completely defined when the mean and variance are known. The mean here is zero,

and the variance has been shown to be  $E$ . The probability density function for  $\zeta(t)$  is then

$$p(\zeta) = \frac{1}{\sqrt{2\pi E}} \exp(-\zeta^2/2E) \quad (44)$$

the familiar bell-shaped curve shown in Fig. 13.

For most practical purposes, however, we are more interested in the statistics of visible or "apparent" properties of the wave record than in its Gaussian properties or its invisible component waves. Fortunately, the shape of the spectrum supplies a great deal of useful information about the visible characteristics of the ocean wave system to which it corresponds.

As mathematical functions, spectra are always non-negative (since they represent a squared quantity: the variance), but with a finite area,  $E$ . An infinite area would imply an infinite mean square surface displacement. Point spectra (Figs. 8 and 9) rise to one or more peaks or modes, and then vanish at very high frequencies. The modal frequency corresponding to the highest peak of a spectrum is designated  $\omega_m$ , and the corresponding period,  $2\pi/\omega_m$  is designated  $T_m$ . The frequency of greatest variance density is  $\omega_m$ , and it is frequently used as an identifying parameter, together with  $E$ , in analyses using sets of spectra. The period  $T_m$  is sometimes called the most probable period, but this is an erroneous concept, as the point spectrum is not in any sense a probability density function. While this parameter has intuitive significance, it should be used with caution in discussion of spectra derived from wave records. It can be shown to have poor sampling characteristics, since its precise value depends solely

upon the variation of  $S(\omega)$  in the immediate neighborhood of  $\omega_m$ , and the small errors that are inherent in the calculation from a specific wave record can result in large shifts in the position of the peak.

More meaningful frequency parameters can be obtained from the set of *moments*, which depend on spectrum shape

$$m_n = \int_0^\infty \omega^n S(\omega) d\omega \quad (45)$$

where  $n$  is an integer. In particular, the area,  $m_0$ , is the variance or  $E$ . These moments have better-behaved statistical sampling characteristics than  $T_m$ , as they depend upon *all* values of  $S(\omega)$ . The moments  $m_2$  and  $m_4$  have a dynamic significance that can be shown by differentiating Equation (33) with respect to time.

$$\begin{aligned} \dot{\zeta}(t) &= \sum -\omega_i \bar{\zeta}_i \sin[\omega_i t + \epsilon_i] \\ &= \sum -\omega_i \bar{\zeta}_i \cos\left[\omega_i t + \left(\epsilon_i - \frac{\pi}{2}\right)\right] \end{aligned} \quad (46)$$

By analogy with Equations (35) and (36), giving the component amplitude of wave elevation and its variance, the amplitude of component vertical velocity must be  $\omega_i \bar{\zeta}_i$  and the variance of component velocity

$$\langle (\omega_i \bar{\zeta}_i)^2 \rangle = \frac{1}{2} (\omega_i \bar{\zeta}_i)^2 = (\omega_i^2 S(\omega_i)) \delta\omega$$

Hence, the spectrum of velocity,  $\dot{\zeta}(t)$ , is seen to be  $\omega^2 S(\omega)$ . Similarly, the spectrum of acceleration,  $\ddot{\zeta}(t)$ , is  $\omega^4 S(\omega)$ . Therefore,

$$m_2 = \langle \dot{\zeta}(t)^2 \rangle \quad (47)$$

$$m_4 = \langle \ddot{\zeta}(t)^2 \rangle \quad (48)$$

There are a number of descriptive parameters that can be computed from the spectral moments, which are valuable for characterizing the visual appearance of the wave record. These include the zero-crossing period (average time interval between zero upcrossings), average peak-to-peak period, average slope, average wavelength, and average wave height (vertical distance, trough to crest). The quantities being averaged are illustrated in the sample time record shown in Fig. 12, except for wave slope which is not defined in a time record.

Average period of component waves,

$$\begin{aligned} T_{-1} &= \int_0^\infty T S(\omega) d\omega / \int_0^\infty S(\omega) d\omega \\ &= 2\pi m_{-1} / m_0 \end{aligned} \quad (49)$$

Period corresponding to average frequency of component waves,

$$\begin{aligned} T_1 &= 2\pi \left( \int_0^\infty \omega S(\omega) d\omega / m_0 \right)^{-1} \\ &= 2\pi m_0 / m_1 \end{aligned} \quad (50)$$

Average period between zero upcrossings of  $\zeta(t)$ , see Price and Bishop (1974),

$$T_z = 2\pi \sqrt{m_0 / m_2} \quad (51)$$

Average period between peaks (maxima) or hollows (minima),

$$T_c = 2\pi \sqrt{m_2 / m_4} \quad (52)$$

A statistical measure of the slope of the wave surface  $\zeta'$  is its variance,

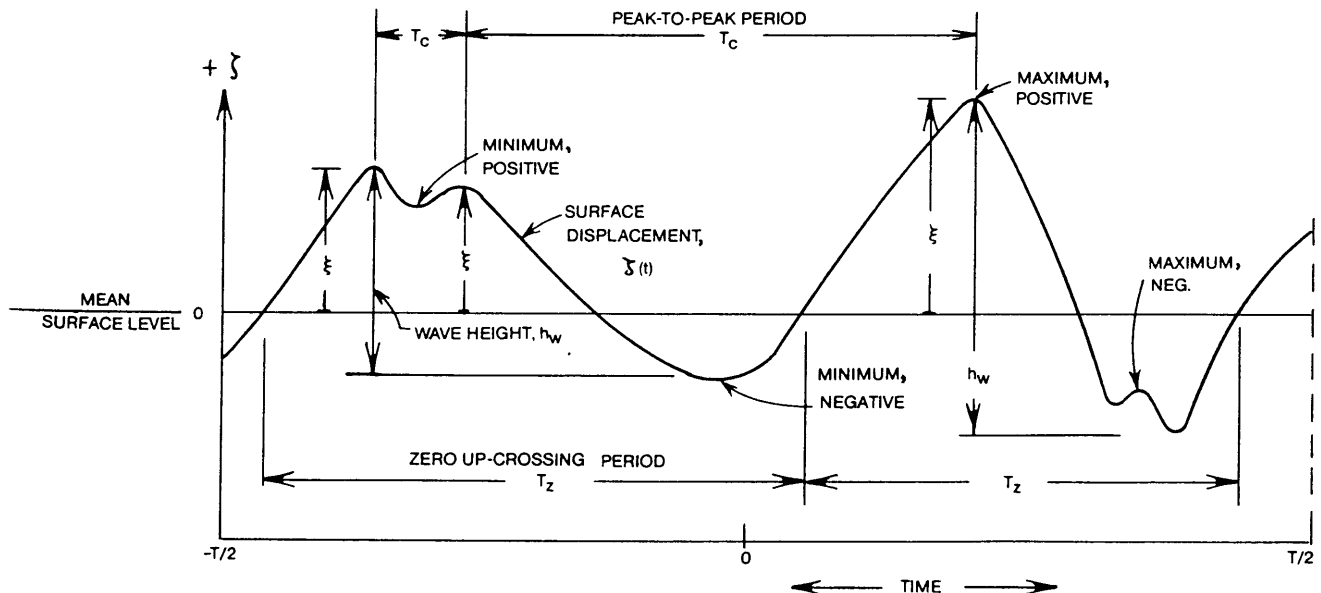


Fig. 12 Typical wave record at a fixed point, with definitions of terms

$$\langle (\zeta')^2 \rangle = m_4 / g^2 \quad (53)$$

where

$$(\zeta')^2 = \left( \frac{\partial \zeta}{\partial x} \right)^2 + \left( \frac{\partial \zeta}{\partial y} \right)^2$$

See Section 2.7 and Cummins and Bales (1980).

Average wave length between zero up-crossings (Price and Bishop, 1974),

$$\langle L_w \rangle = \frac{g}{2\pi} T_z T_c \quad (54)$$

In considering visual wave amplitudes and heights, we note first that, as a consequence of the zero-mean Gaussian assumption, the process is statistically symmetrical about the zero line. For example, in the long run the average positive deviation from zero is equal to the average negative deviation. More importantly, in the present context, the Gaussian property requires that the maxima and minima of a record also be statistically symmetrical.

In the wave and ship response processes of interest the qualitative behavior sketched in Fig. 12 is not uncommon; that is, small short-period oscillations sometimes ride on long-period oscillations. Thus the possibility arises that there can be more than one maximum in an excursion of the process above zero. This necessarily means that there can also be minima that are positive. Thus, in contrast to the usual "givens" about maxima and minima of sinusoids, we have the prospect of dealing with positive maxima, negative

maxima, negative minima, and positive minima, as illustrated in Fig. 12.

The maxima of the process are random variables,  $\xi$ , that are derivable from the process. The theory for the probability density of all maxima (or minima) of a stationary zero-mean Gaussian process was first worked out by Rice (1945), and extensively discussed by Cartwright, et al (1956). The most compact form of the result is obtained by normalizing the dimensional maxima by  $\sqrt{m_0} = \sqrt{E}$  (the root-mean-square value of the process):

$$\Xi = \xi / \sqrt{m_0}$$

Then the probability density of the non-dimensional maxima,  $\Xi$ , may be written (Cartwright, et al, 1956)

$$p(\Xi) = \frac{1}{\sqrt{2\pi}} \left\{ \epsilon \exp \left[ -(\Xi/\epsilon)^2 / 2 \right] + \Xi \sqrt{1 - \epsilon^2} \exp \left[ -\Xi^2 / 2 \right] \phi(\Xi \sqrt{1 - \epsilon^2} / \epsilon) \right\} \quad (55)$$

where the so-called *spectral broadness parameter*  $\epsilon$ , is

$$\epsilon = \sqrt{1 - \frac{m_2^2}{m_0 m_4}}$$

and the function,  $\phi(\Xi \sqrt{1 - \epsilon^2} / \epsilon)$ , is defined:

$$\phi(\Xi \sqrt{1 - \epsilon^2} / \epsilon) = \int_{-\infty}^{\Xi \sqrt{1 - \epsilon^2} / \epsilon} \exp \left[ -v^2 / 2 \right] dv.$$

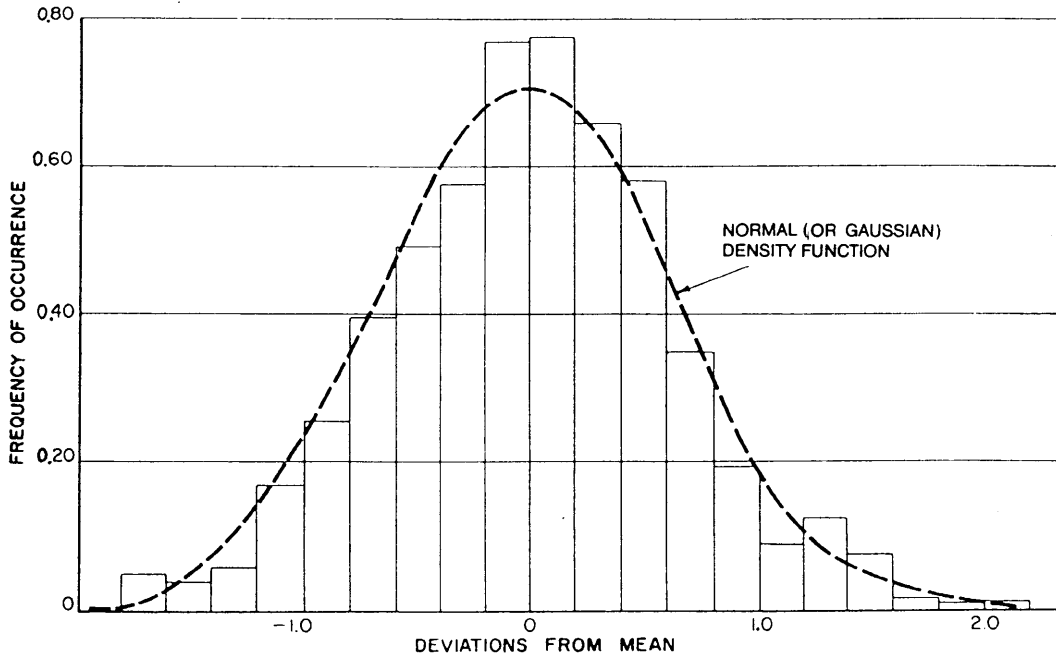


Fig. 13 Frequency of occurrence of deviations from mean value of points on a wave record

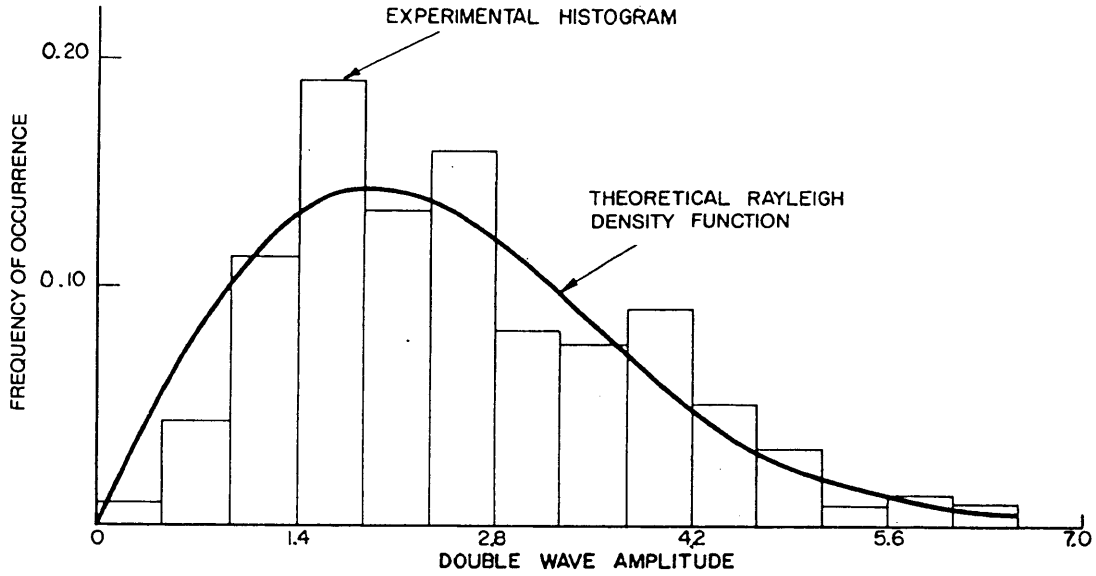


Fig. 14 Typical density function from Korvin-Kroukovsky (1961), of wave amplitudes in record of irregular waves in a model basin

where  $v$  is a dummy variable.

The most important thing to note about the result is that the probability density of maxima is completely defined (through  $\Xi$  and  $\epsilon$ ) by the first three even spectral moments,  $m_0$ ,  $m_2$ , and  $m_4$ . Once the spectrum is known, the moments can be worked out, and the probability function of the maxima is defined. Recalling Equations (51) and (52),  $\epsilon$  can be expressed as:

$$\epsilon = \sqrt{1 - (T_c/T_z)^2} \quad (56)$$

and it can be seen that this parameter is related to the ratio of the average period between peaks and the average period between zero up-crossings. When there are no multiple maxima in any excursions of the process above or below zero,  $T_c = T_z$ ,  $\epsilon = 0$ , and the spectrum is called *narrow band*. When  $\epsilon = 0$  is substituted into Equation (55) the result is:

$$p(\Xi) = \Xi \exp [-\Xi^2/2] \quad (57)$$

which is a non-dimensional form of the Rayleigh density function shown in Fig. 14. Conversely, when there are a very large number of maxima within each excursion of the process above or below zero,  $T_c \ll T_z$  and  $\epsilon \rightarrow 1$ ; the spectrum is considered *broad*.<sup>6</sup> Substitution of  $\epsilon = 1$  into Equation (55) yields a non-dimensional Gaussian density function:

$$p(\Xi) = \frac{1}{\sqrt{2\pi}} \exp [-\Xi^2/2] \quad (58)$$

Essentially, the probability density functions for the maxima of the process given by Equation (55) make a continuous transition from the Rayleigh to the Gaussian density functions, dependent upon the relative broadness of the spectrum.

Another measure of magnitude customarily used is the estimate of the average value of the  $1/n$ th highest maxima of the process. To illustrate the idea, if 1000 maxima were measured from a sample, the average of the  $1/10$ th highest would be obtained by first identifying the highest 100 maxima and then averaging them. The analogous estimate from the theory is illustrated by Fig. 15, which represents a probability density of maxima,  $p(\Xi)$ . The shaded area in the tail represents a probability  $(1/n)$  that a maximum will exceed  $\Xi_{1/n}$ . Mathematically this is written:

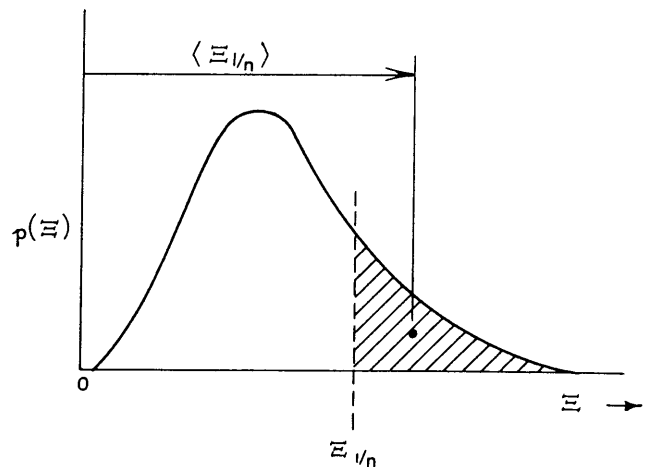


Fig. 15 Definition of  $\langle \Xi_{1/n} \rangle$  in relation to  $p(\Xi)$

<sup>6</sup> Note that a *white noise* spectrum of infinite broadness has an  $\epsilon$  of only  $\frac{2}{3}$ .

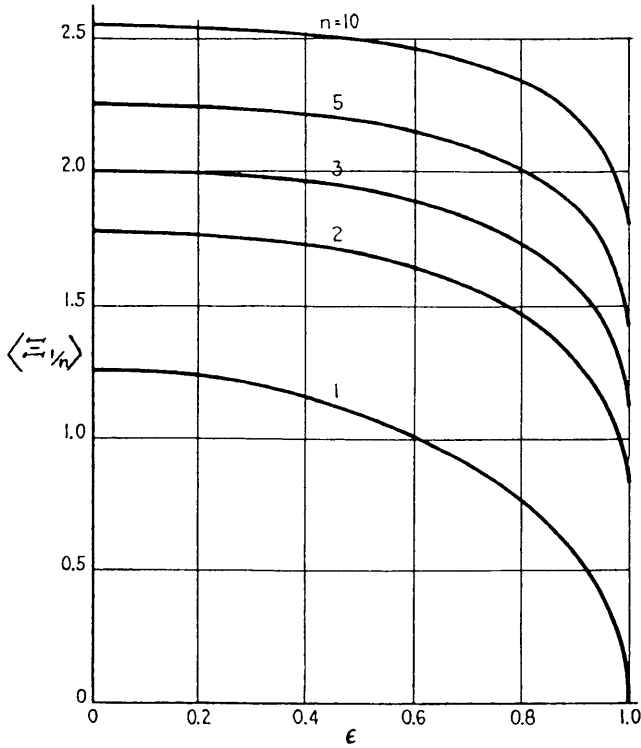


Fig. 16 Graphs of  $\langle \Xi_{1/n} \rangle$  the average of the  $1/n$ th highest maxima as a function of  $\epsilon$ , for  $n = 1, 2, 3, 5$ , and  $10$  (Korvin-Kroukovsky, 1961)

$$\text{Prob} [\Xi > \Xi_{1/n}] = \frac{1}{n} = \int_{\Xi_{1/n}}^{\infty} p(\Xi) d\Xi \quad (59)$$

Given an expression for  $p(\Xi)$  [Equations (55), (57), (58)], the value of  $\Xi_{1/n}$  may be worked out numerically from Equation (59). The statistical mean value of the values of  $\Xi$  above  $\Xi_{1/n}$  is then:

$$\langle \Xi_{1/n} \rangle = n \int_{\Xi_{1/n}}^{\infty} \Xi p(\Xi) d\Xi \quad (60)$$

which is the abscissa of the centroid of the shaded area in the figure, and the statistic desired.

Because the parameters in Equation (55) are non-dimensional, the process just outlined can be performed numerically once for all as a function of  $\Xi$  and  $\epsilon$ . The result is given in Fig. 16 (Cartwright, et al 1956). To illustrate practical use, if the spectral broadness parameter,  $\epsilon = 0.8$ , and the average of the  $1/5$  highest is desired,  $\langle \Xi_{1/5} \rangle \approx 2.0$ , and in this case the average of the  $1/5$  highest dimensional maxima is  $2.0\sqrt{m_0}$ .

The most common practical measure of wave (or response) magnitude is the *significant amplitude*. This is taken to be the average of the  $1/3$  highest maxima. Another common measure is the average of the tenth highest. It will be noted from Fig. 16 that for

broadness parameters,  $\epsilon$ , less than 0.5 or 0.6 the dependence of  $\langle \Xi_{1/3} \rangle$  and  $\langle \Xi_{1/10} \rangle$  on  $\epsilon$  is relatively small. In this range of  $\epsilon$  if the value of  $\langle \Xi_{1/n} \rangle$  is taken as that for the narrow-band case ( $\epsilon = 0$ ) the error committed is typically less than 10 percent. Fortunately, for most cases of interest (especially ship responses) the broadness parameter is less than 0.6. In the event a double amplitude is required (as wave height), the values for a narrow-band process are doubled.

Thus various statistical values of wave properties can be calculated from  $E = m_0$  by taking advantage of the fact that the peak-to-trough wave heights, as well as maxima, of a record follow approximately a Rayleigh density function. (See Fig. 14). For this purpose, from Equation (57), the probability density function of the wave height,  $h_w$  (Fig. 12), may be written

$$p(h_w) = \frac{h_w}{4E} \exp(-h_w^2/8E) \quad (61)$$

From this law, useful parameters are:

Average apparent wave height, crest to trough  $\langle 2\bar{\zeta} \rangle$  is,

$$\langle h_w \rangle = 2.5E^{1/2}$$

or average amplitude

$$\langle \bar{\zeta} \rangle = 1.25E^{1/2}$$

Similarly, the average of the  $1/3$  highest waves, or significant height:

$$\langle (h_w)_{1/3} \rangle = 4.0E^{1/2}$$

And the average of the  $1/10$  highest waves is

$$\langle (h_w)_{1/10} \rangle = 5.1E^{1/2}$$

As explained in Section 4, all of the above relations apply also to most ship responses to ocean waves. These measures are of a magnitude that would often be noticed in a relatively short observation of the process. There are occasions, however, when it is desired to estimate magnitudes of wave or response maxima that are unlikely to be exceeded very often; that is, to estimate extremes. The statistical theory of extreme values used in conjunction with the narrow-band assumption results in the estimates for the *expected highest* in a sample of  $N$  successive wave heights,

$$\begin{aligned} N = 100, & \quad 6.5E^{1/2} \\ N = 1000, & \quad 7.7E^{1/2} \\ N = 10,000, & \quad 8.9E^{1/2} \end{aligned}$$

However, if a large number of samples of the stated size are taken, 5 percent of them would be expected to have maximum heights as follows:

$$\begin{aligned} N = 100, & \quad 7.8E^{1/2} \\ N = 1000, & \quad 8.9E^{1/2} \end{aligned}$$

Since the heights given were arrived at by doubling the results for maxima, estimated values of the cor-



responding amplitudes may be obtained by halving the numbers given above.

(d) *Characteristics of directional spectra.* All of the parameters that have been defined for point spectra apply equally well for directional spectra, but additional parameters are needed to characterize the directional qualities. In most applications it is convenient to assume that  $S(\omega, \mu)$  is separable into two factors, one a function of frequency and one a function of direction:

$$S(\omega, \mu) = S(\omega) M(\mu) \quad (62)$$

where  $S(\omega)$  is the point spectrum and  $M(\mu)$  is called the *spreading function*. It is common practice to take

$$M(\mu) = \frac{1}{\mu_s} \cos^n \left( \frac{\mu_w}{\mu_s} \right) \frac{\pi}{2} \text{ for } -\mu_s \leq \mu_w \leq \mu_s$$

$$= 0 \text{ elsewhere}$$

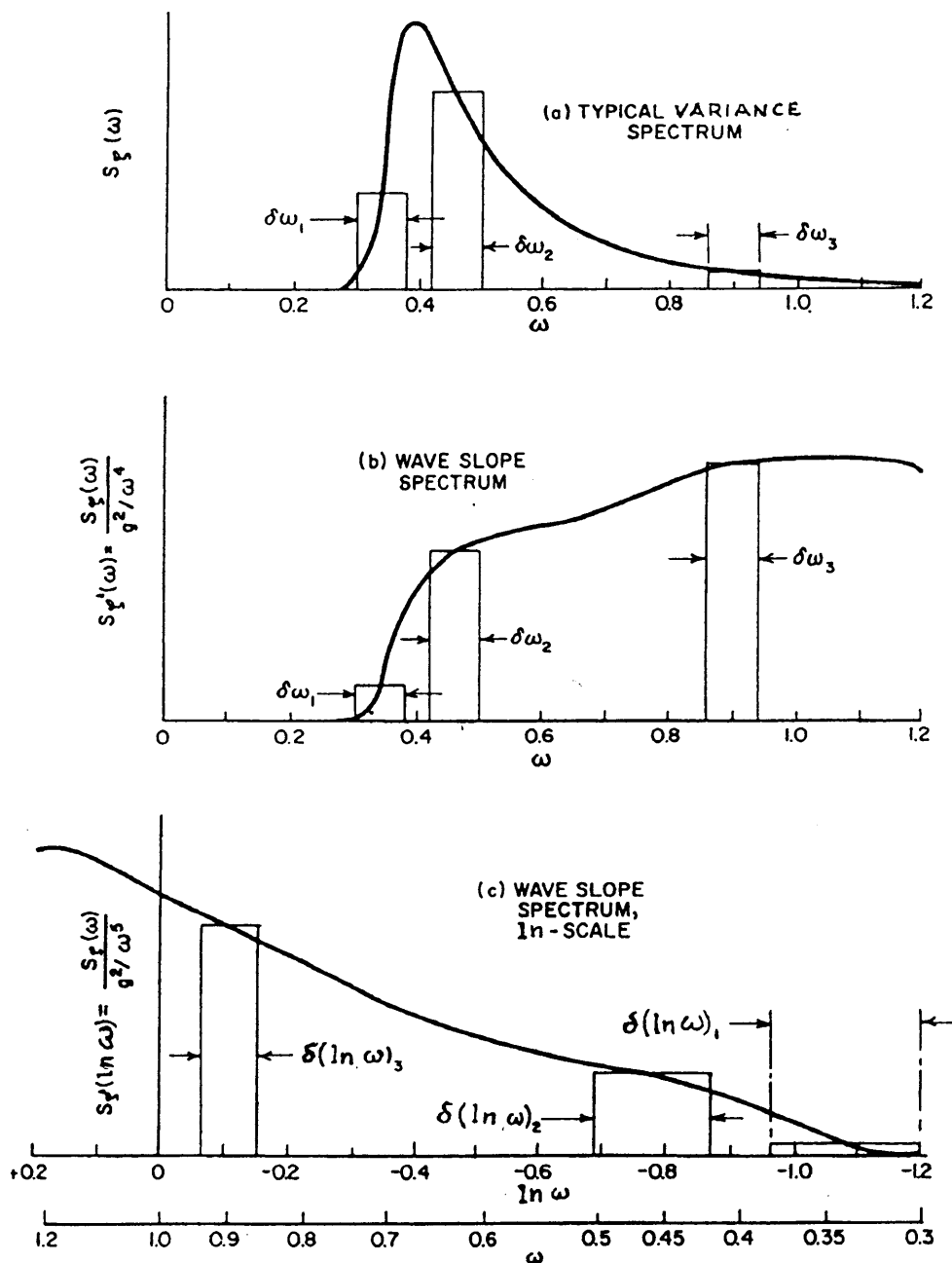


Fig. 17 Transformations of sea spectra

where  $\mu_r$  is the angle between a wave component and the dominant wave direction and  $\mu_s$  is the angular range of components on either side of the dominant wave direction. When  $n$  is taken as 2 and  $\mu_s$  as 90 deg, this is called a *cosine-squared* or  $\cos^2$  spreading function. Then

$$M(\mu) = \frac{2}{\pi} \cos^2 \mu \quad (63)$$

which is generally used pending availability of better data.

A two-dimensional spectrum is much more difficult to obtain at sea than a simple point spectrum, and only a few are presently available. One method involves a lengthy numerical autocorrelation analysis of stereophotographs (Chase, et al, 1960). Another method makes use of a buoy that records wave slopes as well as directions (Canham, et al, 1962). A third employs a fixed array of wave height recorders (Barber, 1963; Oakley, 1974). For further developments in directional spectra see Mitsuyasu (1975) and Hasselmann, et al (1976).

**2.7 Wave Slope and the Slope Spectrum.** Many marine systems (ships, platforms) are more sensitive to wave slope in certain modes of response than to wave height. Roll is an obvious example. But slope of a short-crested sea is a vector quantity since it has two perpendicular components,

$$\frac{\partial \zeta}{\partial x} \text{ and } \frac{\partial \zeta}{\partial y}$$

and must be treated somewhat differently from the scalars that have been discussed to this point. The magnitude of the slope,  $\zeta'$ , is never negative. It is easiest to discuss slope in terms of its components.

Starting with Equation (39),

$$\zeta(x, y, t) = \sum_i \sum_j \bar{\zeta}_{ij} \cos [k_i(x \cos \mu_j + y \sin \mu_j) - \omega_i t + \epsilon_{ij}] \quad (39)$$

Then

$$\frac{\partial \zeta}{\partial x} = - \sum_i \sum_j \bar{\zeta}_{ij} k_i \cos \mu_j \times \sin [k_i(x \cos \mu_j + y \sin \mu_j) - \omega_i t + \epsilon_{ij}]$$

The origin is a typical point, so let  $x, y$  be zero. Noting that  $k_i = \omega_i^2/g$ .

$$\frac{\partial \zeta}{\partial x} = \sum_i \sum_j (\bar{\zeta}_{ij} \omega_i^2 \cos \mu_j / g) \sin (\omega_i t - \epsilon_{ij}) \quad (64)$$

The coefficients in the summation for  $\partial \zeta / \partial x$  are those of the summation for  $\zeta$  multiplied by  $\omega_i^2 \cos \mu_j / g$ . Therefore, since the spectrum is proportional to the square of the coefficients,  $\partial \zeta / \partial x$  has the spectrum

$$S_x(\omega, \mu) = \omega^4 \cos^2 \mu S(\omega, \mu) / g^2 \quad (65a)$$

Similarly,

$$S_y(\omega, \mu) = \omega^4 \sin^2 \mu S(\omega, \mu) / g^2 \quad (65b)$$

Note that

$$S_{\zeta'}(\omega, \mu) = S_x + S_y = \omega^4 S(\omega, \mu) / g^2 \quad (65c)$$

The function  $S_{\zeta'}(\omega, \mu)$  cannot be considered the spectrum of the slope of a short-crested sea but it can be considered the density function of the mean-square absolute slope over the  $\omega, \mu$  plane, associated with the variance (or displacement) spectrum  $S(\omega, \mu)$ . If the wave spectrum is unidirectional (long-crested), say from the  $x$  direction,

$$S_{\zeta'}(\omega) = S_x(\omega) = \omega^4 S_{\zeta}(\omega) / g^2 \quad (66)$$

and  $S_{\zeta'}$  can be considered the point spectrum of the slope in the direction of the source of the wave system, or simply a *slope spectrum*. Note that it is equivalent also to the vertical acceleration spectrum, except for the factor  $1/g^2$ . A sample variance spectrum and the corresponding wave-slope spectrum are shown in Fig. 17(a) and (b). An interesting feature of the slope spectrum is that it is fairly uniform at the high frequencies beyond the peak of the variance spectrum. Thus, any marine system response mode that is primarily sensitive to wave slope may be insensitive to the location of the peak of the displacement spectrum (See Section 4). Note that the variance of wave slope is

$$\int S_{\zeta'}(\omega) d\omega = m_4 / g^2.$$

Slope is dimensionless, and for certain purposes it is desirable to have a dimensionless plot of the slope spectrum. This can be achieved by plotting it against the logarithm to base  $e$ ,  $\ln \omega$ . To make this transformation, we must first determine the increment on the  $\ln \omega$  scale,  $\delta(\ln \omega)$ , corresponding to  $\delta\omega$ .

$$\delta(\ln \omega) = \frac{d(\ln \omega)}{d\omega} \delta\omega = \frac{\delta\omega}{\omega}$$

Then, for an incremental area to be the same in both systems,

$$S_{\zeta'}(\ln \omega) = \frac{S_{\zeta'}(\omega)}{g^2 / \omega^4} = \omega \left( \frac{S(\omega)}{g^2 / \omega^4} \right) = \frac{\omega^5 S(\omega)}{g^2} \quad (67)$$

The transformed spectrum in log-slope form is shown in Fig. 17(c), where it will be noted that the range of general interest to us is negative in sign, and that short waves are to the left.

**2.8 Frequency-of-Encounter Spectrum.** Up to this point, the discussion of waves and wave spectra has been with respect to a fixed reference point. The time history of waves encountered by a moving point (a ship under way, for example) is significantly modified by the *Doppler Shift* in the component frequencies of the wave system. Suppose an  $x_0, y_0$  coordinate system,

fixed in relation to the earth, and a regular progressive wave of amplitude  $\bar{\zeta}$  and wave number,  $k$ , propagating in a direction  $\mu$  relative to the  $x_0$ -axis. In the fixed coordinate system the free surface of the wave field is described by (24):

$$\zeta(x_0, y_0, t) = \bar{\zeta} \cos [k(x_0 \cos \mu + y_0 \sin \mu) - \omega t + \epsilon] \quad (24)$$

Now suppose further that a ship proceeds in the direction of the  $x_0$ -axis at constant velocity  $U_0$ , and we wish to describe the wave field as would be observed from the moving ship. We assume a moving,  $x$ - $y$  coordinate system with origin in the ship and whose  $x$ -axis is aligned with the fixed  $x_0$ -axis. Since the location of the ship at any instant,  $t$ , is  $U_0 t$ , the relation between the two coordinate systems is:

$$x_0 = x + U_0 t$$

$$y_0 = y$$

Substituting in Equation (24) the expression for the wave field as seen from the moving ship becomes:

$$\zeta(x, y, t) = \bar{\zeta} \cos [kx \cos \mu + ky \sin \mu - (\omega - kU_0 \cos \mu)t + \epsilon] \quad (68)$$

The coefficient of  $t$  in Equation (68) defines a *frequency of encounter*,  $\omega_e$ , and noting that  $k = \omega^2/g$  for deep water:

$$\omega_e = \omega - \frac{\omega^2 U_0 \cos \mu}{g} \quad (69)$$

If attention is fixed upon the wave elevation at a single point relative to the ship, the moving coordinate positions,  $x$  and  $y$ , may be taken to be zero without loss of generality, and then, with Equation (69), the wave elevation that would be sensed at a point in the moving ship becomes:

$$\zeta_e(t; \mu, U_0, k) = \bar{\zeta} \cos [\epsilon - \omega_e t] \quad (70)$$

where the notation in the argument denotes that the function of time depends upon wave direction, ship speed, and wave number as parameters defining  $\omega_e$ .

In a short-crested sea, the wave field relative to fixed coordinates has been approximated as a superposition of many components having different wave numbers and directions, Equation (39). Transforming (39) to moving coordinates, the wave elevation sensed at a point in a ship moving in short-crested seas becomes:

$$\zeta_e(t; U_0) = \sum_i \sum_j \bar{\zeta}_{ij} \cos [\epsilon_{ij} - (\omega_e)_{ij} t] \quad (71)$$

The variance of this representation of the encountered waves is the same as that of waves defined with respect to fixed axes because only the point of observation has changed. Thus, writing the variance of the encountered waves as before:

$$\begin{aligned} \langle [\zeta_e(t; U_0)]^2 \rangle &= \frac{1}{2} \sum_i \sum_j \bar{\zeta}_{ij}^2 \\ &= E = \int_0^\infty \int_0^{2\pi} S(\omega_e, \mu) d\mu d\omega_e \end{aligned}$$

and we may identify the *spectrum of encounter* as before as a limit as  $\delta\omega_e$  and  $\delta\mu$  approach zero:

$$S[(\omega_e)_{ij}, \mu_j] = \frac{1}{2} \bar{\zeta}_{ij}^2 / \delta\omega_e \delta\mu \quad (72)$$

Noting that:

$$\delta\omega_e = \left(1 - \frac{2\omega U_0 \cos \mu}{g}\right) \delta\omega$$

we can write

$$S(\omega_e, \mu) = S(\omega, \mu) / [1 - (2\omega U_0 / g) \cos \mu] \quad (73)$$

Care must be taken in using this relation, for there may be three points in the  $\omega, \mu$  plane corresponding to any  $\omega_e, \mu$  when  $U_0 \cos \mu$  is negative. Also,  $S(\omega_e, \mu)$  will have a pole at the point corresponding to  $\omega = -g/2U_0 \cos \mu$  as  $\delta\omega_e \rightarrow 0$  for finite  $\delta\omega$ , unless  $S(\omega, \mu) = 0$  at this point.

While  $S(\omega_e, \mu)$  is the spectrum actually experienced

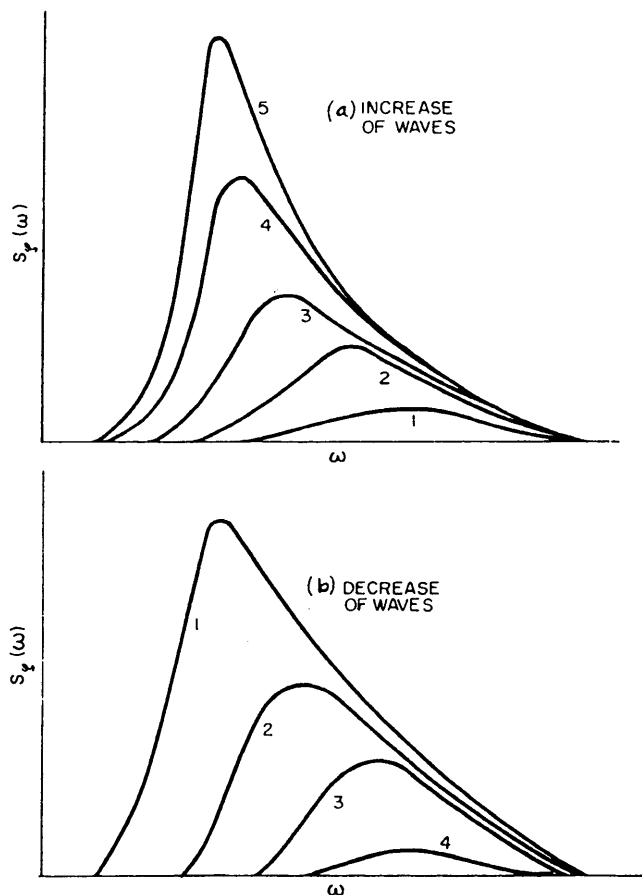


Fig. 18 Growth and decay of storm sea spectra (Iijima, 1957)

by a moving marine system, the complications can be avoided by keeping all calculations in the  $\omega, \mu$  plane. This can usually be done with little difficulty. Nevertheless, it is useful to be aware of the peculiarities that the *Doppler Shift* may produce in the encounter spectrum, and the complexities that they may lead to in the interpretation of the responses of a moving ship. These considerations will be discussed further in Section 4.

**2.9 Development and Decay of Spectra.** So far we have been considering primarily the short-term local description of the ocean under stationary conditions by means of point spectra, or better, by directional spectra. Attention will now be directed to the processes of changing wave patterns, as described by their spectra, in particular the manner in which the point spectrum in a wave generation area grows as the wind blows and how it decays after the wind has passed. Fig. 18 (Ijima, 1957) shows a case of wave growth as a function of wind duration. It can be seen that, at the high-frequency end, the spectrum quickly approaches an asymptotic curve. Further energy generated in these frequencies is dissipated by non-linear processes such as wave-breaking. The growth at lower frequencies is much slower, and the energy required for propagation at the high group velocities of these wave lengths may be more of a limiting factor to growth than wave-breaking. In any case, it can take many hours before the spectrum reaches its limiting form for high wind speeds.

It is believed that, for winds up to about 30 knots, waves frequently reach the fully-developed stage, beyond which there is little change in the spectrum area.

But fully developed seas corresponding to the greater wind velocities are found to be less frequent because these strong winds do not blow long enough. It should be noted that spectra, particularly for high winds, may also be limited by the *fetch* (distance over which the wind blows). As has been noted, fetch is determined by the size of the storm as well as by the presence of a shoreline to windward.

Winds affect the maintenance and decay of wave systems, as well as their generation. A wind that opposes an existing sea will damp it out, quickly or slowly, depending on wind velocity and direction. On the other hand, a wind continuing to blow steadily after developing a typical sea may maintain it essentially constant (in statistical terms) for many hours. Fig. 18 shows the decline of a spectrum as wind dies out and wave dispersion takes effect.

In the absence of wind, internal friction also results in a gradual decrease of wave amplitude. However, theory shows that this decay is very slow, particularly for wavelengths of, say, 100 ft or longer. This explains why swells from severe storms can travel for thousands of miles with little loss of energy if not damped out by an adverse wind. Consequently, new storms usually act on water already affected by previous storms. A typical condition would be a storm sea superimposed on a swell, each having a different average direction. Theoretically the spectrum of the combined disturbance is initially simply the sum of the spectra of the two separate wave trains, which gives rise to spectra with double peaks. Another important effect is the dispersion which occurs as a storm wave pattern leaves a generating area. Here, the wave energy

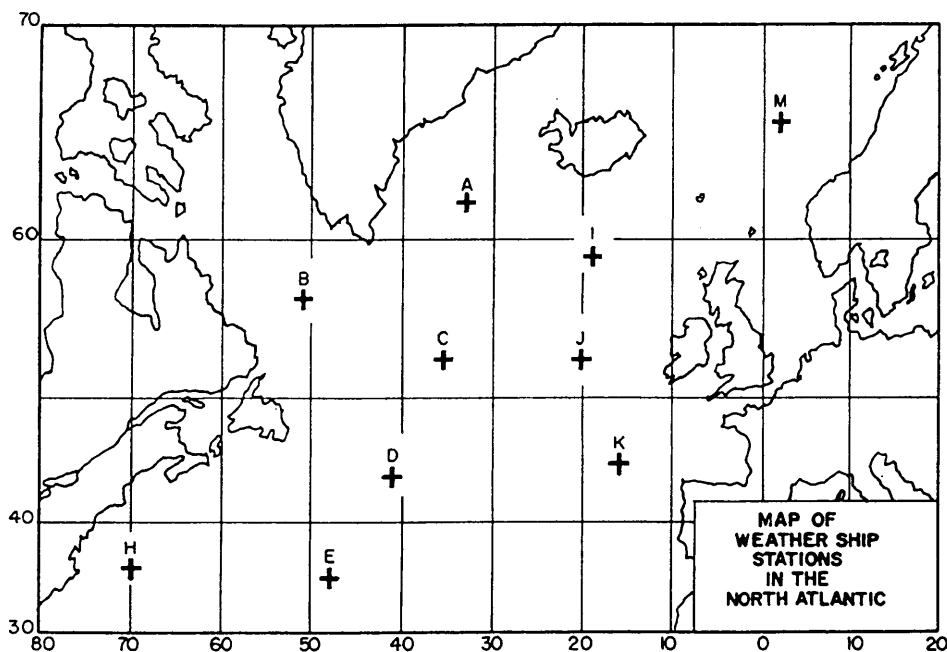


Fig. 19 Former weather ship locations in the North Atlantic, from Roll (1958)

Table 1—Typical Hindcast Directional Spectrum (Converted to Densities)

Time, Date - 9z, 8 Dec 66, Location - 58.579N / 18.175W WDDR - 280.565, WDSP - 56.386 (knots), White Caps - 28, USTR 2.936} (Friction Velocity knots)																Total Variance From Each Direction	Wave Directions (From)	MOTIONS IN WAVES
Wave Frequencies (hertz)	.308	.208	.158	.133	.117	.103	.092	.081	.072	.067	.061	.056	.050	.044	.039			
Spectral Densities	0.00	0.00	0.00	0.00	0.00	0.00	0.00	0.00	0.00	0.00	0.00	0.00	0.00	0.00	0.00	0.00	91.56	
	0.00	0.00	0.00	0.00	0.00	0.00	0.00	0.00	0.00	0.00	0.00	0.00	0.00	0.00	0.00	0.00	65.56	
	0.00	0.00	0.00	0.00	0.00	0.00	0.00	0.00	0.00	0.00	0.00	0.00	0.00	0.00	0.00	0.00	31.56	
	0.00	0.00	0.00	0.00	0.00	2.70	126.80	38.74	78.85	114.13	128.57	21.82	1.78	0.00	0.00	13.79	1.56	
	0.67	3.15	9.00	19.21	37.19	69.31	118.71	214.41	336.92	456.52	582.14	803.64	21.35	5.45	3.57	18.26	331.56	
	1.05	4.65	13.80	28.81	55.79	102.61	178.96	337.84	571.68	838.77	1201.79	1745.45	62.28	21.82	8.93	83.87	301.56	
	1.12	5.10	14.40	30.01	57.59	106.21	185.25	348.65	587.81	856.88	1208.93	1707.27	58.72	21.82	8.93	34.21	271.56	
	0.90	3.90	12.00	25.81	45.59	79.21	133.09	231.53	351.25	460.14	533.93	538.18	23.13	9.09	3.57	17.55	241.56	
	0.52	3.15	11.10	21.61	33.59	45.00	62.95	101.80	137.99	116.74	155.36	121.82	3.56	1.82	0.00	7.05	211.56	
	0.00	0.00	0.00	0.00	0.00	0.90	2.70	8.11	10.75	7.25	5.36	1.82	0.00	0.00	0.00	0.27	181.56	
	0.00	0.00	0.00	0.00	0.00	0.00	0.00	0.00	0.00	0.00	0.00	0.00	0.00	0.00	0.00	0.00	151.56	
	0.00	0.00	0.00	0.00	0.00	0.00	0.00	0.00	0.00	0.00	0.00	0.00	0.00	0.00	0.00	0.00	121.56	
Point Spectrum*																		
$S_1(f)$	4.27	19.94	60.29	125.45	229.75	405.94	808.45	1281.08	2075.27	2880.43	3816.07	4940.00	170.82	60.00	25.00	175.00	Total Variance (ft²)	
$S_2(\omega)$	0.68	3.17	9.60	19.97	36.57	64.61	128.67	203.89	330.29	458.44	607.35	786.23	27.19	9.55	3.98			
$S_3(\omega)$	0.06	0.29	0.89	1.85	3.40	6.00	11.95	18.94	30.68	42.59	56.42	73.04	2.53	0.89	0.37			

Significant Wave Height = 42.9 ft (13.1 m)

\* $S_1(f)$  in ft<sup>2</sup>-seconds,  $S_2(\omega)$  in ft<sup>2</sup>-seconds-radians<sup>-1</sup>,  $S_3(\omega)$  in meters<sup>2</sup>-seconds-radians<sup>-1</sup>

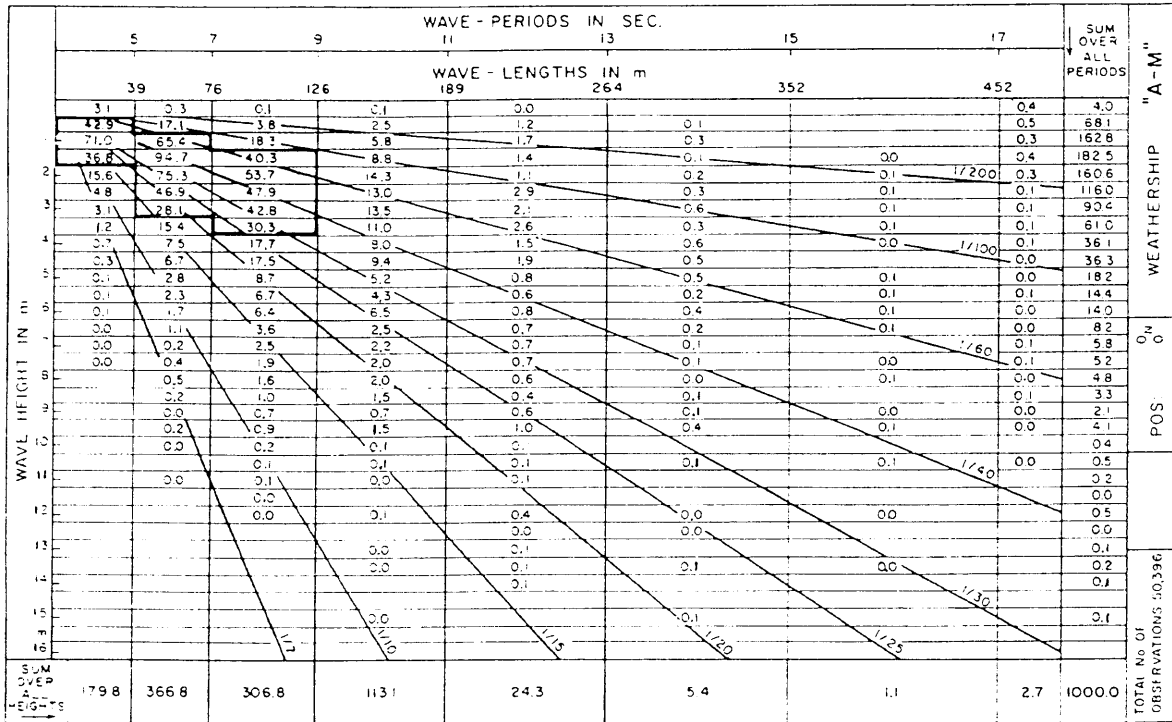


Fig. 20 Data on average wave characteristics and frequency of occurrence in the North Atlantic (Roll, 1958)

spreads over a widening arc.

As previously noted, semi-empirical, computer-based models for predicting the growth, decay and propagation of ocean wave spectra have been developed, for example, by Pierson et al (1955). Wave generation, decay and propagation are analyzed in time steps for a set of grid points extending over an entire ocean basin. The waves arriving at a grid point at a given time step, from all other grid points in the basin at preceding time steps, are estimated and combined with the waves currently being generated by local winds. These wave systems are then propagated in the appropriate directions to provide a basis for the calculation at the next time step. Local winds forecast by means of available meteorological data are used to estimate the locally generated seas. The procedure was further developed at the U.S. Navy's Fleet Numerical Oceanographic Center (FNOC) at Monterey, California, into the Spectral Ocean Wave Model (SOWM) (Pierson, 1982). The entire calculation is massive, requiring 1575 grid points in the Northern Hemisphere, with time steps every six hours.

The SOWM has been in regular use since 1974 for forecasting wave conditions in the North Atlantic and North Pacific Oceans. A sample of the resulting directional spectra for a particular grid point is shown in Table 1. Because of computer limitations, the resolution in both frequency and direction is not as sharp

as the engineer would desire. Nevertheless, such spectra provide far more information about the wave conditions expected at a given location at a given time than a point spectrum.

Comparisons of these forecasts with measurements are rather limited. However, there have been sufficient comparisons with point spectra from wave height measurements, at least, to justify such operational use as ship weather-routing, a routine function at FNOC. A further application of these wave forecasting techniques is discussed in Section 2.10.

**2.10 Ocean Wave Data.** As explained in Section 2.6, individual ocean wave conditions can be described adequately only by directional spectra. For a proper definition of a ship's operational environment, ship designers need many representative spectra for different trade routes, with probability measures of the conditions they represent. An adequate set of directional spectra derived from measurements in the open sea is not available, and will not be until greatly improved measurement techniques exist and are in routine use. Satellite-based systems, mentioned under (c) following, will undoubtedly be utilized in future. However, the U.S. Navy has essentially completed a hindcast wave climatology program that will go far toward satisfying the designer's needs for data on the oceans of the Northern Hemisphere. Some results from this effort are described under (d), to follow.

Table 2—Percentage Frequency of Occurrence of Wave Heights in One Meter Steps  
(Hogben and Lumb data)  
Ocean area (Numbers from Fig. 21)

Wave height, m	World wide (1-50)	North Atlantic Total	Northern North Atlantic (1, 2, 6, 7, 8)
0-1	30.88	25.43	19.03
1-2	41.39	41.21	36.29
2-3	17.35	19.43	22.96
3-4	6.31	7.92	11.57
4-5	2.46	3.47	5.64
5-6	0.57	0.83	1.37
6-7	0.54	0.84	1.46
7-8	0.25	0.42	0.78
8-9	0.14	0.24	0.46
9-10	0.116	0.22	0.42
10-11	0.002	0.004	0.009
11-12	0.0013	0.003	0.007

Table 3—Observed Percentage Frequency of Occurrence of Wave Heights and Periods (Hogben and Lumb data)  
Worldwide

Wave height, m	Wave Period $T_1$ , sec										Total
	2.5	6.5	8.5	10.5	12.5	14.5	16.5	18.5	20.5	Over 21	
0-1	24.0470	4.6416	0.9954	0.3316	0.1253	0.0440	0.0245	0.0147	0.1041	0.5480	30.8762
1-2	15.5208	17.0941	6.1091	1.7475	0.5498	0.1784	0.0626	0.0175	0.0194	0.0910	41.3902
2-3	1.3763	6.0543	6.0000	2.6736	0.8712	0.2668	0.0778	0.0188	0.0054	0.0057	17.3499
3-4	0.2008	1.2153	2.1165	1.6245	0.7848	0.2611	0.0817	0.0226	0.0026	0.0030	6.3129
4-5	0.0506	0.3278	0.6969	0.6998	0.4151	0.1726	0.0687	0.0196	0.0033	0.0020	2.4564
5-6	0.0187	0.0604	0.1469	0.1614	0.1063	0.0509	0.0180	0.0033	0.0012	0.0014	0.5685
6-7	0.0158	0.0587	0.1275	0.1551	0.1039	0.0490	0.0215	0.0039	0.0010	0.0011	0.5375
7-8	0.0032	0.0240	0.0622	0.0702	0.0501	0.0249	0.0120	0.0026	0.0008	0.0012	0.2512
8-9	0.0028	0.0102	0.0266	0.0380	0.0311	0.0169	0.0084	0.0018	0.0013	0.0011	0.1382
9-10	0.0013	0.0064	0.0182	0.0308	0.0247	0.0174	0.0093	0.0041	0.0022	0.0012	0.1156
10-11		0.0003	0.0002	0.0006	0.0006	0.0003	0.0001	0.0001			0.0022
11+		0.0001	0.0001	0.0004	0.0007			0.0001			0.0014
Totals	41.2373	29.4932	16.2996	7.5335	3.0636	1.0823	0.3846	0.1090	0.1414	0.6557	100.000

Table 4—Observed Percentage Frequency of Occurrence of Wave Heights and Periods (Hogben and Lumb data)  
North Atlantic

Wave height, m	Wave Period $T_1$ , sec										Total
	2.5	6.5	8.5	10.5	12.5	14.5	16.5	18.5	20.5	Over 21	
0-1	18.6846	4.5036	1.0144	0.3511	0.1381	0.0512	0.0341	0.0179	0.0976	0.5336	25.4262
1-2	14.4152	17.6097	6.4484	1.7936	0.5534	0.1852	0.0721	0.0218	0.0213	0.0913	41.2120
2-3	1.5051	6.9322	6.7253	2.9229	0.9292	0.2935	0.0825	0.0230	0.0064	0.0074	19.4275
3-4	0.2466	1.5878	2.7234	1.9934	0.9298	0.3039	0.0945	0.0299	0.0039	0.0032	7.9164
4-5	0.0666	0.4775	1.0347	0.9763	0.5518	0.2304	0.0907	0.0290	0.0058	0.0037	3.4665
5-6	0.0197	0.0868	0.2222	0.2434	0.1522	0.0701	0.0237	0.0048	0.0019	0.0018	0.8266
6-7	0.0191	0.0903	0.2038	0.2534	0.1622	0.0723	0.0271	0.0064	0.0017	0.0017	0.8380
7-8	0.0045	0.0384	0.0996	0.1212	0.0873	0.0425	0.0189	0.0037	0.0009	0.0017	0.4187
8-9	0.0023	0.0172	0.0450	0.0671	0.0570	0.0304	0.0155	0.0026	0.0014	0.0024	0.2409
9-10	0.0018	0.0110	0.0353	0.0602	0.0495	0.0315	0.0163	0.0080	0.0043	0.0024	0.2203
10-11		0.0003	0.0005	0.0010	0.0014	0.0005		0.0002			0.0039
11+		0.0003	0.0003	0.0008	0.0018	0.0001			0.0001		0.0034
Totals	34.9655	31.3551	18.5529	8.7844	3.6137	1.3116	0.4754	0.1473	0.1453	0.6492	100.000

Meanwhile, the designer's needs can be partially satisfied by point spectra that can be associated with wind speeds or Beaufort numbers. A small set of such spectra is available for a specific location, Weather Station

*India*, discussed in (b). But the largest collections of sea data are visual observations of height and period, some by trained observers on weather ships and some by officers of merchant ships making routine reports

Table 5—Observed Percentage Frequency of Occurrence of Wave Heights and Periods (Hogben and Lumb data)  
Northern North Atlantic

Wave height, m	Wave Period $T_1$ , sec									
	2.5	6.5	8.5	10.5	12.5	14.5	16.5	18.5	20.5	Over 21
0-1	13.7204	3.4934	0.8559	0.3301	0.1127	0.0438	0.0249	0.0172	0.0723	0.3584
1-2	11.4889	15.5036	6.4817	1.8618	0.5807	0.1883	0.0671	0.0254	0.0203	0.0763
2-3	1.5944	7.8562	8.0854	3.7270	1.1790	0.3713	0.1002	0.0321	0.0091	0.0082
3-4	0.3244	2.2487	4.0393	2.9762	1.3536	0.4477	0.1307	0.0428	0.0050	0.0040
4-5	0.1027	0.7838	1.6998	1.5882	0.9084	0.3574	0.1443	0.0433	0.0072	0.0049
5-6	0.0263	0.1456	0.3749	0.4038	0.2493	0.1200	0.0382	0.0067	0.0027	0.0027
6-7	0.0277	0.1477	0.3614	0.4472	0.2804	0.1301	0.0504	0.0113	0.0011	0.0032
7-8	0.0084	0.0714	0.1882	0.2199	0.1634	0.0785	0.0353	0.0069	0.0018	0.0034
8-9	0.0037	0.0325	0.0856	0.1252	0.1119	0.0558	0.0303	0.0045	0.0027	0.0033
9-10	0.0034	0.0204	0.0674	0.1173	0.0983	0.0550	0.0303	0.0173	0.0079	0.0047
10-11		0.0005	0.0012	0.0023	0.0031	0.0012		0.0005		
11+		0.0005	0.0007	0.0019	0.0035	0.0002			0.0005	
Totals	27.3003	30.3043	22.2415	11.8009	5.0143	1.8493	0.6517	0.2080	0.1306	0.4691
										100.000

Table 6—Annual Sea-State Occurrences in the Open Ocean, North Atlantic

Sea State Number	Significant Wave Height (m)		Significant Wave Height (ft)		Sustained Wind Speed (Knots)*		Percentage Probability of Sea State	Modal Wave Period (Sec)	
	Range	Mean	Range	Mean	Range	Mean		Range**	Most Probable***
0-1	0-0.1	0.05	0-0.3	0.15	0-6	3	0.70	—	—
2	0.1-0.5	0.3	0.3-1.6	1.0	7-10	8.5	6.80	3.3-12.8	7.5
3	0.5-1.25	0.88	1.6-4.1	2.9	11-16	13.5	23.70	5.0-14.8	7.5
4	1.25-2.5	1.88	4.1-8.2	6.2	17-21	19	27.80	6.1-15.2	8.8
5	2.5-4	3.25	8.2-13.1	10.7	22-27	24.5	20.64	8.3-15.5	9.7
6	4-6	5	13.1-19.7	16.4	28-47	37.5	13.15	9.8-16.2	12.4
7	6-9	7.5	19.7-29.5	24.6	48-55	51.5	6.05	11.8-18.5	15.0
8	9-14	11.5	29.5-45.9	37.7	56-63	59.5	1.11	14.2-18.6	16.4
> 8	> 14	> 14	> 45.9	45.9	> 63	> 63	0.05	18.0-23.7	20.0

\* Ambient wind sustained at 19.5 m above surface to generate fully-developed seas. To convert to another altitude,  $H_2$ , apply  $V_2 = V_1(H_2/19.5)^{1/7}$

\*\* Minimum is 5 percentile and maximum is 95 percentile for periods given wave height range.

\*\*\* Based on periods associated with central frequencies included in Hindcast Climatology.

Source: Lee and Bales (1984).

Table 7—Annual Sea State Occurrences in the Open Ocean, North Pacific

Sea State Number	Significant Wave Height (m)		Significant Wave Height (ft)		Sustained Wind Speed (Knots)*		Percentage Probability of Sea State	Modal Wave Period (Sec)	
	Range	Mean	Range	Mean	Range	Mean		Range**	Most Probable***
0-1	0-0.1	0.05	3-0.3	0.15	0-6	3	1.30	—	—
2	0.1-0.5	0.3	0.3-1.6	1.0	7-10	8.5	6.40	5.1-14.9	6.3
3	0.5-1.25	0.88	1.6-4.1	2.9	11-16	13.5	15.50	5.3-16.1	7.5
4	1.25-2.5	1.88	4.1-8.2	6.2	17-21	19	31.60	6.1-17.2	8.8
5	2.5-4	3.25	8.2-13.1	10.7	22-27	24.5	20.94	7.7-17.8	9.7
6	4-6	5	13.1-19.7	16.4	28-47	37.5	15.03	10.0-18.7	12.4
7	6-9	7.5	19.7-29.5	24.6	48-55	51.5	7.60	11.7-19.8	15.0
8	9-14	11.5	29.5-45.9	37.7	56-63	59.5	1.56	14.5-21.5	16.4
> 8	> 14	> 14	> 45.9	45.9	> 63	> 63	0.07	16.4-22.5	20.0

\* Ambient wind sustained at 19.5 m above surface to generate fully-developed seas. To convert to another altitude,  $H_2$ , apply  $V_2 = V_1(H_2/19.5)^{1/7}$

\*\* Minimum is 5 percentile and maximum is 95 percentile for periods given wave height range.

\*\*\* Based on periods associated with central frequencies included in Hindcast Climatology.

Source: Lee and Bales (1984).



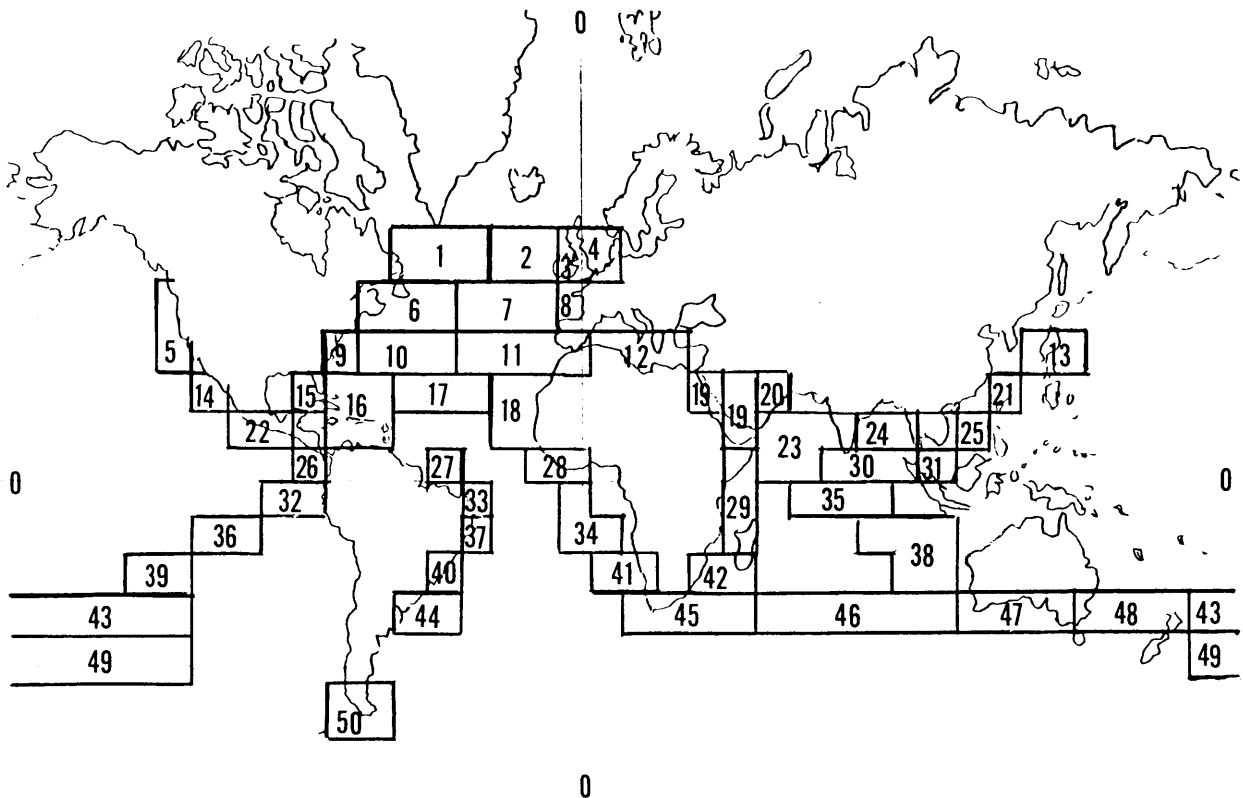


Fig. 21 Grouping of Marsden squares into areas (Hogben and Lumb, 1967)

to the Weather Service. These visual collections have provided the widest coverage of the world's oceans presently available. Although there are inevitable questions as to the meaning and accuracy of these visual estimates, they have provided the only available information about the wave conditions in certain ocean areas.

(a) *Visual estimates of wave conditions.* Visual estimates of height and period by trained observers aboard weather ships can be expected to be more consistent than those by officers reporting from so-called "ships of opportunity." The weather ships are at least of roughly the same size, a factor of importance, as the visual impression of the seaway is sensitive to the height of the observer above the water surface. Unfortunately, published weather ship data are limited to the North Atlantic. There are two collections available. In the first, Roll (1958) presents a statistical analysis of data collected during two years at the stations shown in Fig. 19 (Note that the weather ships have since been relocated). Results in terms of frequency of occurrence of waves of different average period and height are given in Fig. 20. These can well be considered as representative for the North Atlantic north of 30 deg latitude on account of the vessels' uniform distribution.

Because the data are limited to just two years and the variability of weather conditions from year to year

is significant. Roll's data suffer from the inherent statistical inaccuracies of small samples, even though the amount of data for those years may be large. This limitation is partially overcome by Walden's (1964) analysis of ten years of data, although it is limited to stations I and J. These stations both lie in a region that experiences very severe weather throughout the year (Cummins and Bales, 1980), and such statistics can hardly be considered representative of even the North Atlantic.

The most comprehensive collection currently available is that of Hogben and Lumb (1967), collected from log entries of some 500 British ships. These observations were taken during the period 1953 to 1961, and were taken on routes followed by British ships in all of the oceans of the world, Fig. 21. There are gaps, as there are important operational areas that rarely see ships of British flag, and some of the data are sparse. Nevertheless, this collection provides the most extensive coverage available. Yamanouchi and Ogawa (1970) and Research Panel (1980) provide additional data of the same nature obtained by Japanese ships in the North Pacific.

Tables 2 to 5 summarize the data presented by Hogben and Lumb—World-Wide, North Atlantic, and Northern North Atlantic. These tables, taken from Lofft and Price (1973), provide a valuable overview of over a million observations. The entries relating to the

Table 8—Available Noon Weather Ship Records at Station India 1954-67,  
from Hoffman and Miles (1976)

Group No.	Wind Speed, Knots	Winter (Dec-Feb)	Spring (Mar-May)	Summer (Jun-Aug)	Fall (Sept-Nov)	Total
I	0-10	27	48	85	38	198
II	11-21	90	117	138	91	436
III	22-33	112	83	57	102	354
IV	34-47	41	22	5	22	90
V	48-71	4	—	1	2	7
Total		274	270	286	255	1085

two North Atlantic areas are probably as good as the visual estimate technique permits, since the coverage in area and in numbers of seasons is large. The "World-Wide" statistics should be used with caution, as there are serious geographical gaps, and biases where there are no gaps. As all observations were weighted equally, those regions with many observations in effect received much more weight than those regions with few observations. While these tables are useful for gross estimates of conditions to be expected, a more refined estimate should be based upon the complete data (Hogben and Lumb, 1967), for the region in question (Research Panel 1980).

Such tabulated data on joint probabilities of wave heights and periods can also be presented graphically (See Fig. 14 in Chapter IV of Vol. I, for example).

The basic question remains as to the reliability of visual estimates and just how they relate to the parameters derived from the directional or point spectrum. For some years it was considered that the visually estimated wave height could be taken as the significant wave height,  $H_{1/3}$ , and the observed period was thought to be the zero-crossing period,  $T_z$ . These hypotheses were tested by Hogben and Lumb (1967), using simultaneous data from "trained" weather ship observers and wave recordings. The wave records were converted into point spectra, taking into account a high-frequency attenuation by the wave recorder. About 400 pairs of visual and measured data were available. Using linear regression, the following relationships were obtained:

$$H_{1/3} = 1.23 + 0.88H_v, \text{ m} \quad (74a)$$

$$T_z = 4.70 + 0.32 T_v, \text{ sec} \quad (74b)$$

where  $H_v$  and  $T_v$  are visually estimated height and period. While these are satisfactory fits within the range of the rather scattered data, they seem to be in error for small values of  $H_v$  and  $T_v$ . Nordenström (1969) re-analyzed the same data, assuming log-normal distributions for wave height and period measures. He derived "calibration" equations for such visual observations:

$$H_{1/3} = 1.68 H_v^{0.75} \quad (75a)$$

$$T_z = 0.82 T_v^{0.96} \quad (75b)$$

These curves fit the available data about as well as the preceding straight line fits, and at least do not lead to obvious error outside the range of data. They are recommended for use for deriving estimates of the spectral parameters  $H_{1/3}$  and  $T_z$  from visual estimates. This assumes that the calibration equations for trained weather ship observers are the same as those for merchant ship officers, and this assumption is suspect. However, there exists no other large body of data of measurements and observations that could provide better calibration.

Tables 6 and 7 (Lee and Bales, 1984) summarize U.S. Navy data on probabilities of different wind and wave conditions in two areas of open ocean, based on the so-called "hindcast climatology" discussed in item (d) to follow. The table for the North Atlantic is also a NATO standard.

Although many tabulations of wave data make use of significant wave height, it will be noted that these tables utilize a scale of "Sea State Numbers." The significant height ranges are those adopted by the World Meteorological Organization and are becoming more generally used by ship operators. However, other scales are also in use, including some based on the Beaufort scale, which was originally a wind-speed scale. Care must be exercised to ascertain what scale is intended when sea state numbers are given.

(b) *Point spectra from wave measurements.* Point spectra have been computed from wave records since shortly after the wave spectral model was invented. Any accurate wave trace of sufficient duration is usable for this purpose, and the *Tucker meter*, a ship-borne wave meter, has made it possible to obtain records in the open ocean (Tucker, 1956). While in such an instrument there is a frequency attenuation effect for the shorter wavelengths, the spectrum can be partially corrected for the error introduced. Certain of the British weather ships have been fitted with Tucker meters, and wave height records have been collected on a routine basis while on station, although these strip chart records have not been routinely used to

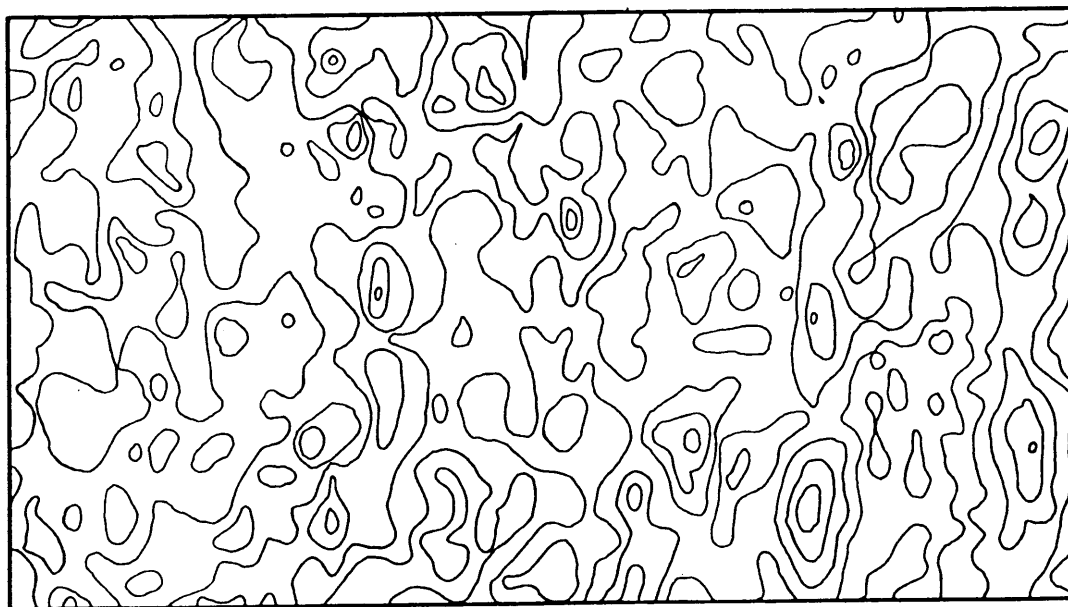


Fig. 22 Typical contour plot of the sea—from stereo photos

calculate the point spectra. Floating buoys with vertical accelerometers have also been used for source data.

The shipborne records attracted the attention of oceanographers Pierson and Moskowitz, who were interested in the wave generation process and fully-developed spectra in particular. 460 wave records were selected that appeared to represent the proper meteorological conditions, but it was discovered after spectra had been computed that even in this deliberately biased set only about one in seven could be considered to represent an "uncontaminated" fully-developed sea-way (Moskowitz, et al, 1962, 1963). While these spectra provide valuable information, the biases toward fully-developed seas in the selection process make the set unsuitable for general use. Wave conditions are more typically either rising or decaying, and are usually contaminated with swell from other storms.

The problem of obtaining a more representative set was addressed by Hoffman and Miles (1976) using the statistical technique of stratified sampling. Hoffman

reviewed a listing of the wave records obtained on three weather ships at Station *India* (I on Fig. 19) during the period 1954–1967. A total of 1085 records was available, roughly equally spread over the year. These were sorted into groups by wind speed and season (Table 8). A set of 334 records was then selected by a reasonably random process, so as to have approximately equal numbers in the various wind speed-season groups, except in the higher sea states (Table 9).

This collection of point spectra provides a very useful display of typical conditions to be expected in the severe weather region of Station *India*. The set is free from a bias toward fully-developed seas, and multimodal (double-peaked) spectra are frequent. While Tables 8 and 9 show the set to be biased toward more severe seas, there are sufficient data to restore the balance. Indeed, if it be assumed that the types of seas associated with a wind of given intensity are independent of location, the data can be used to predict ship behavior in any region for which there is knowledge

Table 9—Records at Station *India* Selected for Stratified Sample  
by Hoffman and Miles (1976)

Group No.	Wind Speed Knots	Winter	Spring	Summer	Fall	Total
I	0-10	21	22	25	21	89
II	11-21	19	21	22	19	81
III	22-33	22	22	23	19	86
IV	34-47	23	10	13*	11	57*
V	48-71	7*	—	2*	1	10*
Total		92	75	85	71	323

\* Includes some records selected for hours other than noon.

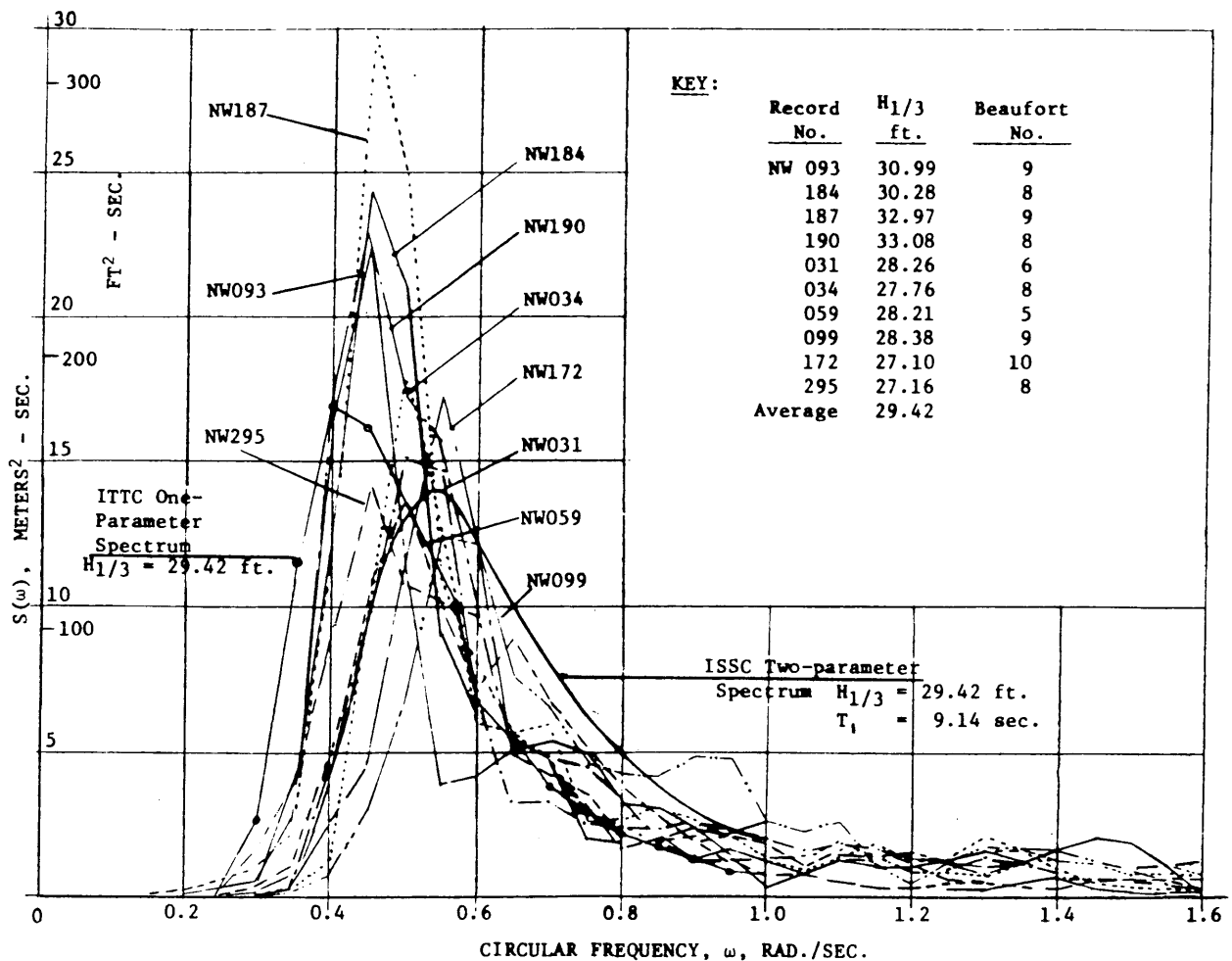


Fig. 23a Typical families of wave spectra significant wave height range of 7.6-10.7 m. (5-35 ft.)

of wind climatology. While this assumption cannot be taken as strictly true (swell patterns, storm durations, and fetch can be expected to have geographical variation independently of wind speed), it is still possible to generate an approximate wave climatology.

The variability of spectra having approximately the same area and hence the same average or significant wave height is interesting and important for ship design. Figs. 23 (a) and (b) show sets of such spectra from Hoffman and Miles (1976) for two ranges of  $H_{1/3}$ . If a particular ship response is sharply tuned to a natural frequency (as is the usual case with roll, Section 3) it would behave in quite different ways in the various seas shown in any one set. This suggests that height and period should be considered as separate variables in predicting seakeeping performance in a given environmental area.

(c) *Directional spectra.* As previously noted there does not exist a collection of directional spectra derived from wave pattern measurements comparable to the sets of point spectra described in the previous section. While such spectra are needed for both oceanographic

and engineering purposes, the vast amount of simultaneous wave pattern data required and the complexity of the analysis have made such a project prohibitively expensive for other than a few samples. In effect, an instantaneous contour map of the surface is needed, or, if directional ambiguities are to be eliminated, contour maps that are slightly displaced in time are required. An example of such a map is shown in Fig. 22. While such an analysis has been tried, using stereo pairs of photographs from an airplane (Chase, et al 1960) the sets of spectra are so limited as to be of little use for engineering purposes.

An alternative approach has been to fit a buoy with an inertial measurement system. The quantities recorded are wave slope in two perpendicular known compass directions, and surface displacement (by double integration of the measured vertical acceleration). From records of these quantities against time, it is possible to estimate the distribution of variance with respect to direction in any frequency band (Longuet-Higgins, Cartwright and Smith, 1963). If assumptions are made as to the nature of the spreading function,

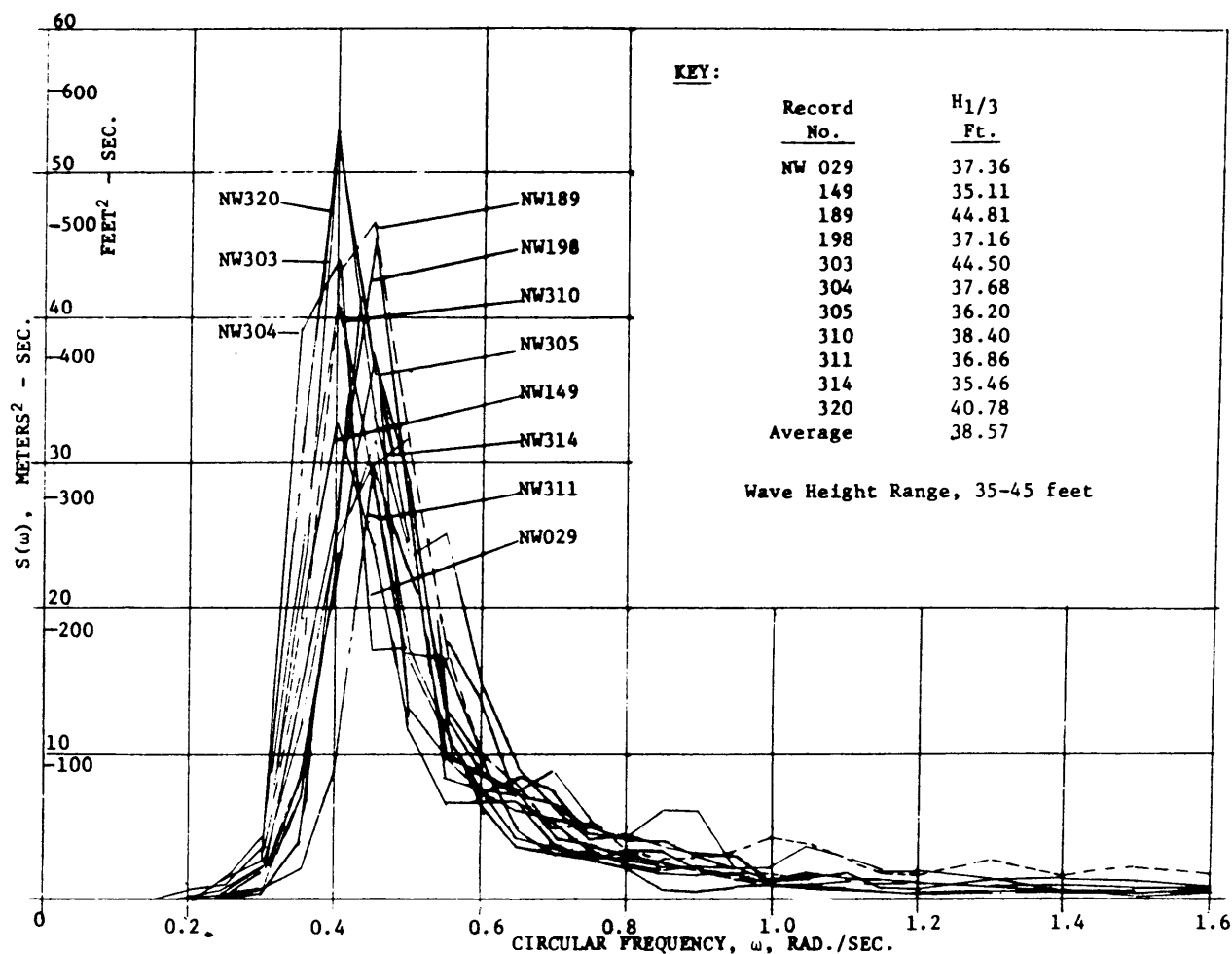


Fig. 23b Typical families of wave spectra significant wave height range of 10.7-13.7 m (35-45 ft) (Hoffman and Miles, 1976)

it is possible to generate a simplified directional spectrum estimate from these data. This technique has been used primarily for special situations such as full-scale trials, and no large collections are available for more general application.

However, new techniques are being developed for

obtaining directional spectra in the open ocean. For example, there are airborne instrument systems that are operable, and one of which is used from a satellite spacecraft (Jackson, et al, 1985). Also, estimated directional spectra, based on available wind data, have been obtained systematically in connection with the

Table 10—Relative Frequency of Occurrence of Significant Wave Heights within Sub-Regions of the North Atlantic, from Stratified Sample of Hindcasts in U.S.

Navy Wave Climatology							
Region \ Stratum	1	2	3	4	5	6	Sample Size
	0-1 m	1-2 m	2-3 m	3-5 m	5-8 m	> 8 m	
A	0.087	0.207	0.211	0.304	0.153	0.039	1133
B	.132	.226	.211	.254	.139	.038	1599
C	.441	.317	.137	.088	.015	.002	1007
D	.320	.296	.162	.156	.057	.009	2486
E	.270	.341	.188	.154	.042	.006	1300
Total A-E	.252	.278	.181	.190	.081	.018	7525
North Sea	.276	.347	.204	.141	.026	.007	427
G. of Mexico	.547	.352	.081	.020	0	0	298



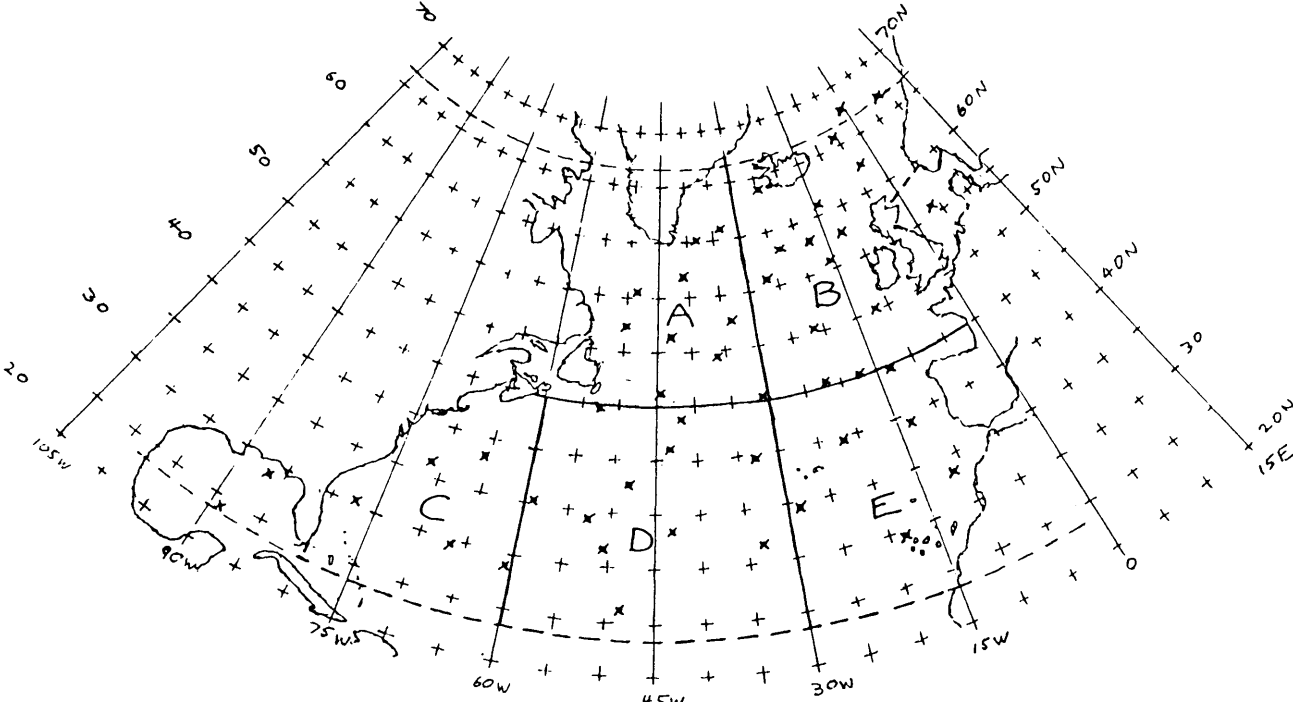


Fig. 24 Subregions for stratified sample of hindcasts of wave conditions in the North Atlantic. Locations included in sample are marked with an X, from Cummins and Bales (1980)

U.S. Navy's Hindcast Wave Climatology.

(d) *U.S. Navy hindcast wave climatology.* Since little wave data are available in spectral form, an alternative approach to meeting the needs of the ship designer is to calculate a set of spectra from the com-

prehensive wind data that have been reported and collected for years over the world's important trade routes. Accordingly, the U.S. Navy undertook to make use of the forecasting tool SOWM (described in Section 2.9), in conjunction with observed rather than forecast wind data, to *hindcast* conditions for the entire Northern Hemisphere over a twenty-year period.

Since these spectra are based upon previously recorded, rather than forecast, meteorological data, they presumably should be somewhat more accurate than the routine forecasts. It should be noted, however, that the primary need of the ship designer is unbiased statistical sets of spectra, typical of region and season. Precise accuracy of the spectra for a given location and time is not essential so long as the discrepancies between the hindcast and actual spectra are relatively unbiased. An added feature of this approach is that it provides estimated directional as well as point spectra.

From the large quantity of calculated directional wave spectra stored on magnetic tape in the format of Table 1, a *wave climatology* has been generated, organized for the ship designer (Cummins and Bales, 1980; Bales, et al, 1982; Bales, 1984). Stratified samples of hindcast spectra were prepared for both the North Atlantic and the North Pacific. Each of these sets includes approximately 2000 spectra, divided into six strata (by significant wave height), randomly distributed by season and location. Fig. 24 shows the North Atlantic divided into 5 sub-regions, A to E. Fig. 25 shows the relative weights (i.e., frequencies of occur-

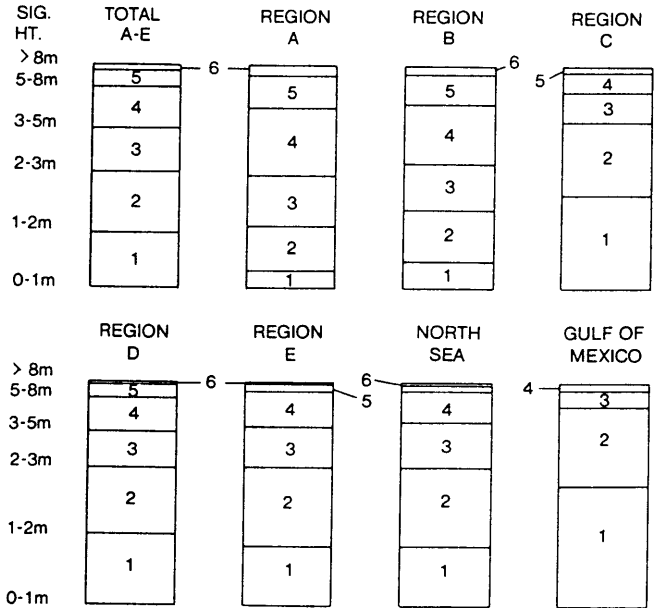


Fig. 25 Relative frequency of occurrence of significant wave heights within strata of sub-regions of the North Atlantic (U.S. Navy hindcast wave climatology, Cummins and Bales, 1980)

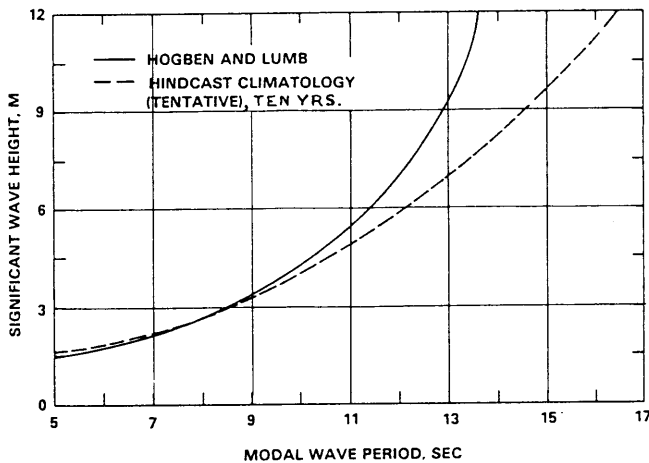


Fig. 26 Comparison of most probable modal periods for North Atlantic during winter, from Cummins and Bales (1980)

rence) of the six strata for the five regions, while numerical values are given in Table 10.

It should not be expected that statistics derived from hindcasts will be identical (or even very similar) to those from other sources. The hindcasts are free from geographical and observer biases, although wind data are more plentiful in some areas than in others. But they substitute the inaccuracies of the pressure field-wind-wave propagation model, with its computational limitations. Comparisons with recorded data are at least as good for hindcasts as for visual estimates. The two elements of the hindcasts that are absent from all other data sets are information on the directional aspects, which, though approximate, can be critical for ship design, and a valid measure of probability of occurrence associated with each hindcast.

The wave climatology also includes a wealth of statistical data on parameters describing the collected wave spectra, as for example, the significant wave heights and modal periods, that can be used to generate Bretschneider point spectra, as discussed in Section 2.11(b). Other data include primary wave direction, wave *persistence* (duration), and corresponding wind speed and direction (U.S. Navy 1983, 1985), (Bales, et al 1981) and (Lee, et al 1985).

Cummins and Bales (1980) review a ten-year span of results in the North Atlantic. Conclusions of general interest follow. There is a band across the North Atlantic from Ireland to Newfoundland that experiences severe sea conditions (over 3 m average significant wave height) for over six months of the year. Several times a year storms may be expected in this region with significant wave heights exceeding 10 m. Modal wave periods exceed values that would be estimated from observed data such as found in Hogben and Lumb (1967), particularly for the more severe seas. Fig. 26 compares the most probable modal period for a given significant wave height, as obtained from Hogben and

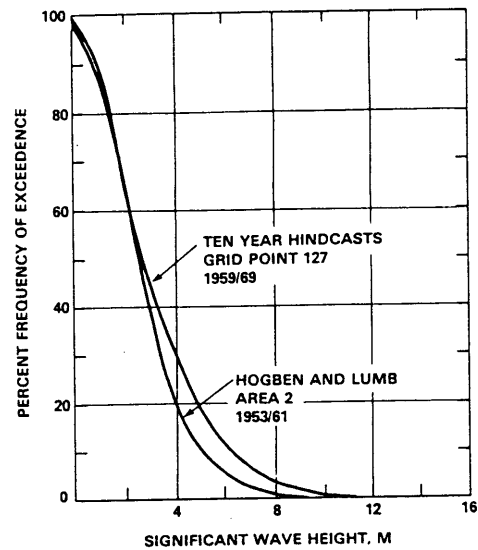


Fig. 27 Comparison of hindcast and observed wave height occurrences, from Cummins and Bales (1980). Location of Grid Point 127 is shown in Fig. 28

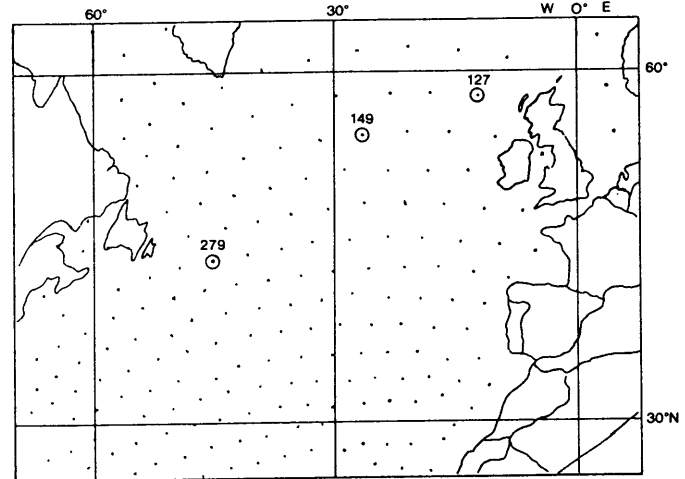


Fig. 28 Location of three grid points (279, 149, 127) in North Atlantic (Cummins, et al, 1981)

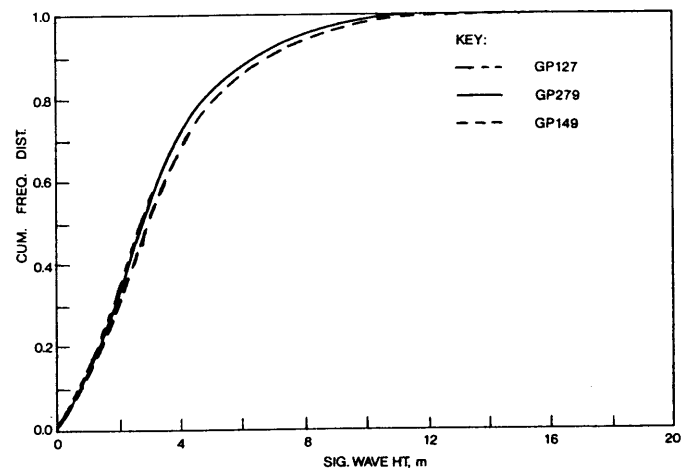


Fig. 29 Cumulative frequency distributions of significant wave height for three grid points in North Atlantic, 1959 to 1969. (Cummins, et al, 1981)

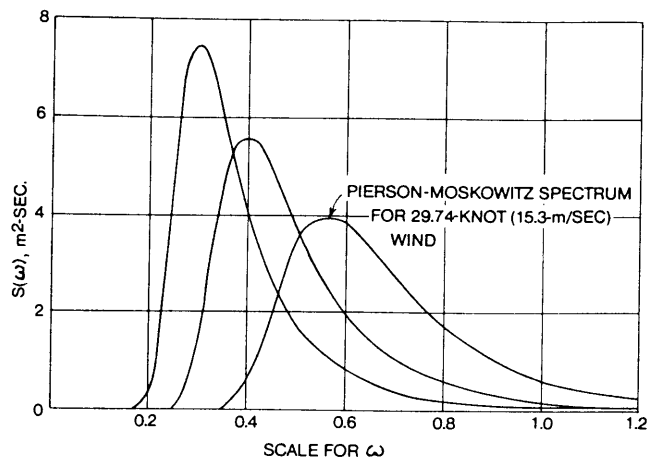


Fig. 30 Various Bretschneider spectra for 5-m significant wave height

Lumb, with the hindcast data. The frequency of occurrence of high waves also exceeds Hogben and Lumb estimates, as shown in Fig. 27. (The location of grid point 127 is shown in Fig. 28). These differences are significant and should eventually be resolved as more observed and measured data become available. Meanwhile, for design purposes the hindcast climatology seems to differ on the safe side.

Cummins, Bales and Gentile (1981) examined hindcasts over a ten-year period at three locations in the severe North Atlantic weather zone, one on each side of the basin and one in the center, Fig. 28. While there are differences that can be associated with geographical location (relation of prevailing wind to land masses, for example) the similarities are even more striking. Fig. 29 shows the almost identical cumulative distributions of significant wave height. Therefore, a climatology based on any one of these locations would not be greatly in error for the entire zone, except for slight displacement of the seasons.

The directional parameters of the climatology and their inter-relations were examined, although assumptions made in the mathematical forecasting model permit only general conclusions to be drawn until better data on directionality become available. A typical pattern begins to emerge, that is, severe sea states (above 5 m or 16 ft significant wave height) tend to be quite uniform in their spectral structure, while moderate seas (less than 2 m or 6 ft) vary greatly. The spectra of severe seas are usually unimodal, nearly symmetric about the dominant direction, and have a spreading function near  $\cos^2$  over  $\pm 90$  deg from the dominant direction. Moderate sea states vary from near unidirectional to a locally generated wind sea superimposed on one or more identifiable swells from random directions. Thus, the spectral structure is likely to be far more complex than that of the severe storm seas. See Fig. 29.

Bales, Cummins and Comstock (1982) are primarily

concerned with estimates of the performance of various ships in sets of the hindcast sea states. However, this reference includes a comparison between the Station *India* wave data and hindcasts for the same dates at a nearby grid point. A similar comparison is available in Chen, Chen and Hoffman (1979). Both of these evaluations conclude that point spectra derived from the hindcasts are reasonably consistent with weather ship measurements.

**2.11 Idealized Spectral Families.** The variation in form of both directional and point spectra is great, even for spectra with nearly identical significant wave heights. Designing for this multiplicity of environmental conditions introduces some difficult logical questions. While these questions can be treated, an attractive alternative is provided by certain idealized families of spectra that have been devised for special purposes. The spectra in these families are identified by a small number of parameters, permitting an analysis of the variations of some ship operational quality with respect to variation of a particular sea parameter. Where a probability of occurrence can be assigned to members of the family, these families are particularly useful for design. But even when such probability measures are not available, a design based upon acceptable performance over the entire set should be a successful design. The following discussion of particular families of point spectra will review limitations that can affect their use in design of ships and floating structures.

(a) *The Pierson-Moskowitz Spectrum.* This spectral form, which depends upon a single parameter, was developed primarily for oceanographic use, and in fact is a basic element in the forecasting of storm waves. It is intended to represent the point spectrum of a fully-developed sea, that is, fetch and duration are great, and there is no contaminating swell from other generating areas. As previously mentioned, from 460 available point spectra Moskowitz, et al (1962, 1963) chose 54 spectra that met the appropriate weather criteria. The winds for the chosen spectra had to be of reasonable duration, to be less at the beginning and end of the wave record than the mean, and to be within  $\pm 45$  deg of the mean wind direction throughout the record. Since forward speed affects the records the ship making the wave measurements by means of a Tucker wave recorder had to have a speed less than 2 knots. Spectra containing noticeable swell were eliminated by inspection.

These selected spectra were grouped into a family of five wind speeds: 20, 25, 30, 35, and 40 knots. Using this spectral family, along with the similarity theory of S. A. Kitaigorodskii, Pierson and Moskowitz (1964) arrived at the following analytical formulation for ideal sea spectra representing fully-developed seas,

$$S(\omega) = \frac{\alpha g^2}{\omega^5} \exp[-\beta(g/V_w)^4] \quad (76)$$

where



$S(\omega)$  = spectral ordinate in  $\text{cm}^2\text{-sec}$   
 $\omega$  = frequency in radians/sec  
 $\alpha = 8.10 \times 10^{-3}$   
 $\beta = 0.74$   
 $g$  = acceleration of gravity in  $\text{cm/sec}^2$   
 $V_w$  = wind speed in  $\text{cm/sec}$  (19.5 m above the surface)

It is clear that the only parameter is the wind speed.

This spectral family is inappropriate for general design use. While its oceanographic importance is great, it should be recognized as an asymptotic form, reached after an extended period of steady wind, with no contamination from an underlying swell. While it might seem an appropriate model for extreme storm conditions, fully-developed seas for very high winds are known to be rare, as the duration and fetch are seldom sufficient for spectral stability to be reached.

(b) *The Bretschneider Spectrum.* This spectrum is a two-parameter family that permits period and wave height to be assigned separately (Bretschneider, 1952, 1957). It has the form,

$$S(\omega) = \frac{A}{\omega^5} \exp[-B/\omega^4] \quad (77)$$

where the two parameters  $A$  and  $B$  depend upon the modal frequency,  $\omega_m$ , and the variance,  $E$ . The modal (peak) frequency is

$$\omega_m = \left[ \frac{4}{5} B \right]^{1/4} \quad (78)$$

and

$$E = A/4B \quad (79)$$

A family of these spectra for fixed significant wave height of 5 m is shown in Fig. 30. This family was designed to represent rising and falling seas as well as fully-developed seas. While it must be considered

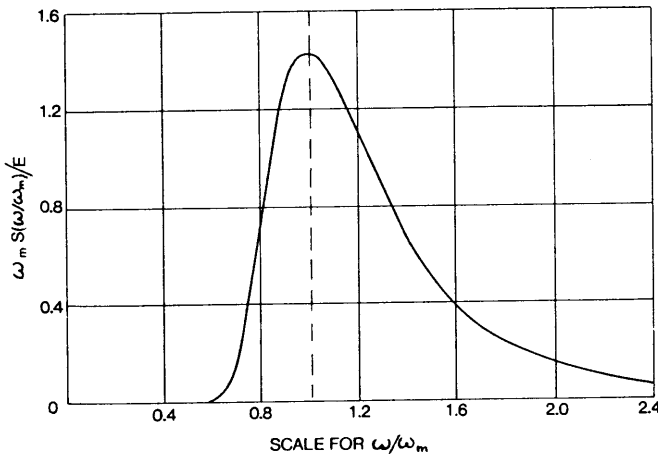


Fig. 31 Normalized Bretschneider spectrum

approximate, at best, it has proven to be of great value for engineering purposes. A Pierson-Moskowitz spectrum family is obtained when

$$\frac{A}{B/\omega^4} = \frac{\alpha g^2}{\beta (g/V_w)^4}$$

Useful forms of the Bretschneider spectrum can be obtained by normalizing frequency with respect to the modal value,  $\omega_m$ . Then,

$$\frac{\omega_m S(\omega/\omega_m)}{E} = 5 (\omega_m/\omega)^5 \exp[-1.25(\omega_m/\omega)^4] \quad (80)$$

The two parameters are seen to be  $\omega_m$  and  $E$ . See Fig. 31, which is identical for all the members of the family.

It is often more convenient to substitute  $H_{1/3}$  for  $E$ . With a narrow-band spectrum,<sup>7</sup>  $H_{1/3} = 4\sqrt{E}$ . Then

$$\frac{\omega_m S(\omega/\omega_m)}{H_{1/3}^2} = 0.312 (\omega_m/\omega)^5 \exp[-1.25(\omega_m/\omega)^4] \quad (81)$$

The parameters  $\omega_m$  and  $H_{1/3}$  can be directly related to the extensive data available on observed wave heights and periods, as discussed later.

The moments of the Bretschneider family are

$$m_{-1} = 0.8572 E/\omega_m \quad (82a)$$

$$m_1 = 1.294 E \omega_m \quad (82b)$$

$$m_2 = 1.982 E \omega_m^2 \quad (82c)$$

The fourth moment diverges, which implies that the mean crest-to-crest frequency and the mean-square slope are infinite. This is a complication in treating certain problems analytically. However, the integrand is asymptotic to  $\text{Constant}/\omega$  for large  $\omega$ ; so the integral for  $m_4$  diverges very slowly. In problems involving  $m_4$ , the spectrum should be truncated at some reasonable value (St. Denis, 1980). If  $\omega$  does not exceed  $5\omega_m$ , corresponding to a wavelength  $1/25$ th of the modal wavelength,  $m_4 = 7.049 E \omega_m^4$ .

From the moments, the various period parameters can be calculated:

$$T_{-1} = 0.857 T_m = 5.385/\omega_m \quad (83a)$$

$$T_1 = 0.773 T_m \quad (83b)$$

$$T_z = 0.710 T_m \quad (83c)$$

The 15th International Towing Tank Conference (ITTC, 1978) recommended the use of a form of the Bretschneider spectrum (for average conditions, not fully developed seas) when more specifically appropriate spectral forms are not known. This is Equation (77), with

<sup>7</sup> But with a Bretschneider spectrum, where  $\epsilon = 1$ , St. Denis (1980) points out that  $H_{1/3} = 3\sqrt{E} = \frac{3}{2}\sqrt{A/B}$ .

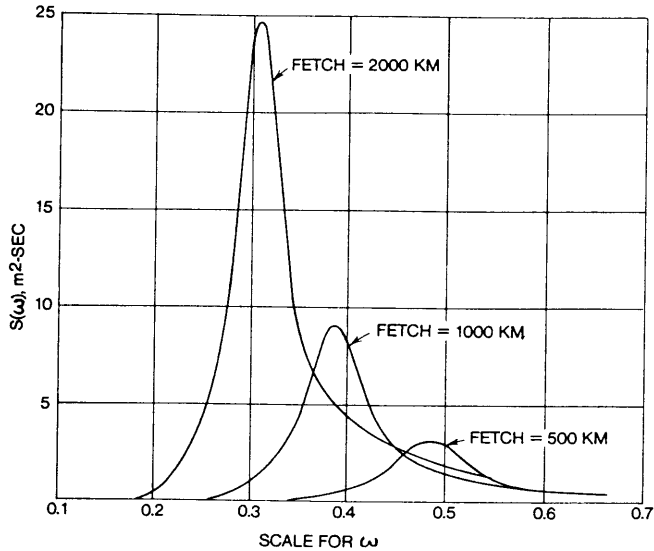


Fig. 32 JONSWAP spectra for various fetches, with wind speed of 20m/sec

$$A = 173 H_{1/3}^2 / T_1^4$$

$$B = 691 / T_1^4 \text{ in sec}^{-4}$$

Note that the spectrum will be in  $\text{m}^2\text{-sec}$  or  $\text{ft}^2\text{-sec}$ , depending on whether  $H_{1/3}$  is in m or ft. Here the parameters are  $T_1$  and  $H_{1/3}$ . The ITTC further recommended a directional spectrum that combines the above spectrum and a spreading function,

$$S(\omega, \mu) = \kappa S(\omega) \cos^n \mu \quad (84)$$

with  $-\pi/2 < \mu < \pi/2$ . In this modification  $\mu$  is the angle between the predominant wave direction and a wave component. The values of  $n = 2$  and  $\kappa = 2/\pi$  are suggested for use until more definitive data become available.

The Bretschneider spectral form has no associated probability measure that would assign a probability (frequency of occurrence) for spectra defined by the pair  $\omega_m$  (or  $T_1$ ) and  $H_{1/3}$ . It is common practice to estimate such probabilities from tables of visually-observed height and period. In order to obtain the spectra, use is made of Equation (75a), which relates observed height,  $H_v$ , to  $H_{1/3}$ :

$$H_{1/3} = 1.68 H_v^{0.75} \quad (85)$$

and Equations (75b) and (83c), which relate observed period,  $T_v$ , to  $T_z$  and  $\omega_m$ :

$$\omega_m = \frac{2\pi}{T_m} = \frac{2\pi}{T_z/0.71} = \frac{5.44}{T_v^{0.96}} \quad (86)$$

Tables 3, 4, and 5 or similar tables derived from specific area-season tabulations in Hogben and Lumb (1967) can be considered as defining a two-parameter Bret-

schneider spectral family, with probability measures for each member.

The basic assumption in such a procedure is that any seaway can be adequately represented by a Bretschneider spectral form, or at least that errors in form introduce no bias in the corresponding measures of ship performance when using sets of Bretschneider spectra. But the errors in form in particular cases may be considerable. Point spectra from wave records (such as Figs. 9 and 23) show that multi-modal spectra are common, and no single-modal Bretschneider form can match the shape of such a spectrum very well. A more subtle error may be present in the fit of the spectrum of a swell from a distant storm that is sufficiently dominant to hide the effects of any local disturbance. This is also a fairly common condition. In such a case, the effect of distance from the wave source is to limit the band width of the waves reaching the observation point. In effect, the high-frequency tail is reduced or eliminated. The Bretschneider form will be a poor fit, as it has a well-defined tail, proportioned to the modal value of the spectrum. This could lead to a prediction of a high-frequency response much greater than that which would actually occur (St. Denis, 1980a).

Accepting the fact that some of the spectra corresponding to a particular pair  $H_v, T_v$  may deviate from the corresponding Bretschneider form, the latter may still provide a good measure of ship performance if the deviations collectively do not introduce a large bias. Comparisons have been made between calculated ship performance in observed spectra and "matching" Bretschneider spectra (Ochi and Bales, 1977). While there were the expected differences in performance for specific pairs, these differences tended to disappear through statistical averaging when sets of pairs were compared. This study is reassuring for those who have made use of this very powerful tool. However, in any particular problem the possibility of bias should always be considered. An example where bias might be present is a search for extreme conditions, i.e., those that would induce extreme ship rolling or hull bending moment. It is probable that such conditions are more likely to occur in a narrow-band swell rather than in the wider band of a Bretschneider spectrum. In this case, average response is not desired. Rather, a measure is needed of seas within a period-height cell that induces large responses.

(c) *The JONSWAP Spectrum.* The ideal spectral forms described in the preceding sub-sections are intended to represent open-ocean wave conditions. However, there are many regions of engineering importance where there are geographical boundaries that limit the fetch in the generating area. The North Sea is such a region. Extensive oceanographic measurements have been made there under the Joint North Sea Wave Project (JONSWAP) (Hasselmann, 1973, and Ewing, 1975). Wave measurements were made at a

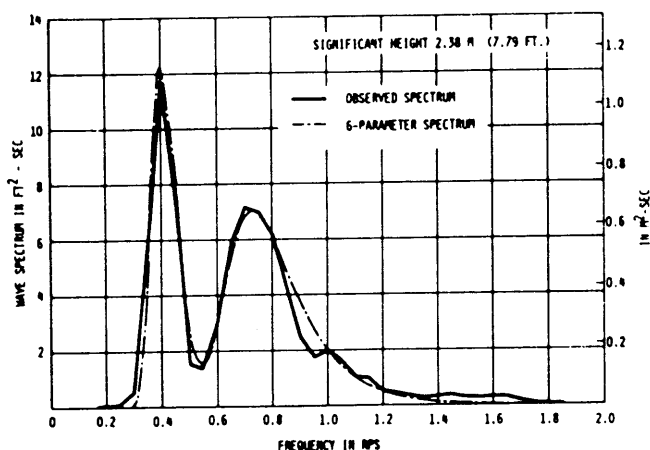


Fig. 33 Comparison of measured and six-parameter spectrum, significant wave height 2.38 m (7.8 ft), from Ochi and Hubble (1976)

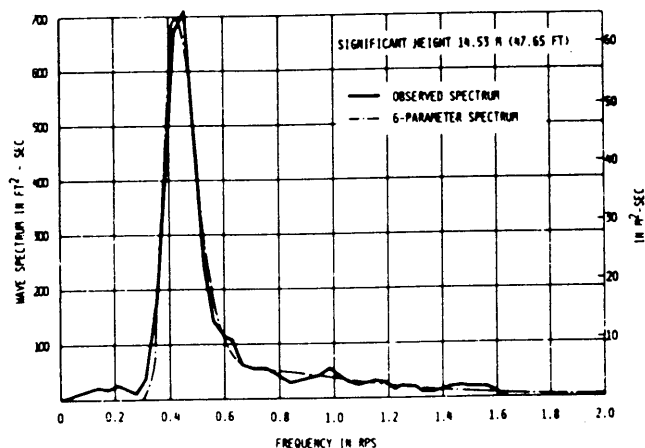


Fig. 34 Comparison of measured and six-parameter spectrum, significant wave height 14.5 m (47.7 ft), from Ochi and Hubble (1976)

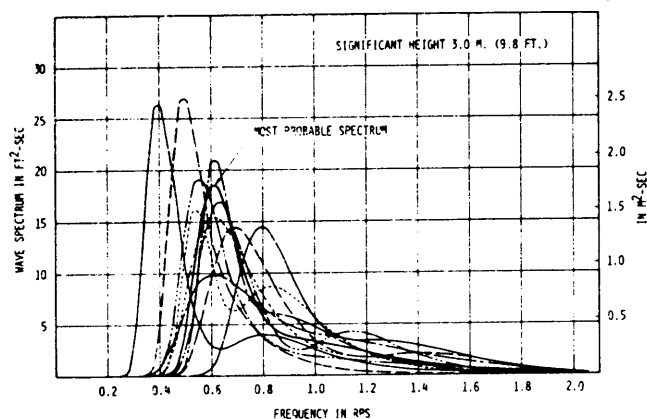


Fig. 35 Family of six parameter wave spectra for significant wave height 3.0 m (9.8 ft), from Ochi and Hubble (1976)

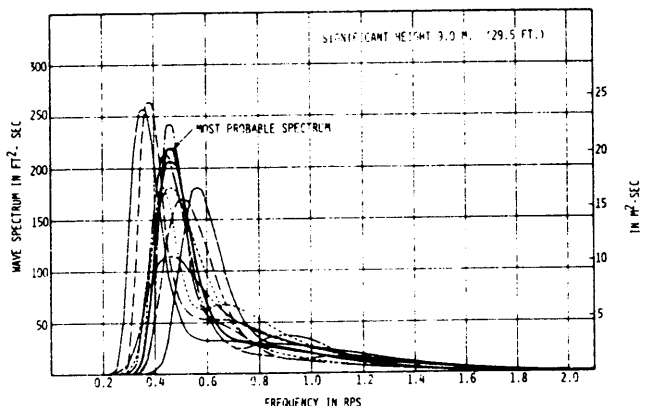


Fig. 36 Family of six-parameter wave spectra for significant wave height 9.0 m (29.5 ft), from Ochi and Hubble (1976)

Table 11—Ochi Six-Parameter Wave Spectrum Family—Values of Six Parameters as a Function of Significant Wave Height ( $H_s$ , m)

	$H_{s1}$	$H_{s2}$	$\omega_{m1}$	$\omega_{m2}$	$\lambda_1$	$\lambda_2$
Most Probable Spectrum	$0.84 H_s$	$0.54 H_s$	$0.70 e^{-0.046 H_s}$	$1.15 e^{-0.039 H_s}$	3.00	$1.54 e^{-0.062 H_s}$
0.95 Confidence Spectra	$0.95 H_s$	$0.31 H_s$	$0.70 e^{-0.046 H_s}$	$0.50 e^{-0.046 H_s}$	1.35	$2.48 e^{-0.102 H_s}$
	$0.65 H_s$	$0.76 H_s$	$0.61 e^{-0.039 H_s}$	$0.94 e^{-0.036 H_s}$	4.95	$2.48 e^{-0.102 H_s}$
	$0.84 H_s$	$0.54 H_s$	$0.93 e^{-0.056 H_s}$	$1.50 e^{-0.046 H_s}$	3.00	$2.77 e^{-0.112 H_s}$
	$0.84 H_s$	$0.54 H_s$	$0.41 e^{-0.016 H_s}$	$0.88 e^{-0.026 H_s}$	2.55	$1.82 e^{-0.089 H_s}$
	$0.90 H_s$	$0.44 H_s$	$0.81 e^{-0.052 H_s}$	$1.60 e^{-0.033 H_s}$	1.80	$2.95 e^{-0.105 H_s}$
	$0.77 H_s$	$0.64 H_s$	$0.54 e^{-0.039 H_s}$	0.61	4.50	$1.95 e^{-0.082 H_s}$
	$0.73 H_s$	$0.68 H_s$	$0.70 e^{-0.046 H_s}$	$0.99 e^{-0.039 H_s}$	6.40	$1.78 e^{-0.069 H_s}$
	$0.92 H_s$	$0.39 H_s$	$0.70 e^{-0.046 H_s}$	$1.37 e^{-0.039 H_s}$	0.70	$1.78 e^{-0.069 H_s}$
	$0.84 H_s$	$0.54 H_s$	$0.74 e^{-0.052 H_s}$	$1.30 e^{-0.039 H_s}$	2.65	$3.90 e^{-0.085 H_s}$
	$0.84 H_s$	$0.54 H_s$	$0.62 e^{-0.039 H_s}$	$1.03 e^{-0.030 H_s}$	2.60	$0.53 e^{-0.069 H_s}$

series of positions at various distances from the island of Sylt in the German Bight when the wind was offshore. The distances of the observation positions from the coast ranged up to 160 km (100 mi).

As a family, the spectra computed from these records had much narrower peaks than the Pierson-Moskowitz family. An extensive analysis found that the spectra could be fitted by the form;

$$S(\omega) = \alpha g \omega^{-5} \exp \left[ -\frac{5}{4} \frac{\omega}{\omega_m} \right]^{-4} \gamma^{\exp[-(\omega - \omega_m)^2 / 2\sigma^2 \omega_m^2]} \quad (87)$$

where

- $\gamma$  is 3.3
- $\sigma$  is 0.07 for  $\omega < \omega_m$   
is 0.09 for  $\omega > \omega_m$
- $\alpha$  is 0.076  $\tilde{x}^{-0.22}$
- $\omega_m$  is  $2\pi f_m g / V_{w10}$  (modal frequency)
- $\tilde{x}$  is  $g x / V_{w10}^2$
- $f_m$  is  $3.5 \tilde{x}^{-0.33}$
- $x$  is fetch
- $V_{w10}$  is wind speed at 10m (32 ft) above sea level

Note that the JONSWAP spectrum is simply a form of Bretschneider spectrum, Equation (87), multiplied by a frequency dependent factor;

$$\gamma^{\exp[-(\omega - \omega_m)^2 / 2\sigma^2 \omega_m^2]}$$

The JONSWAP spectra for a constant wind speed are shown in Fig. 32 for various fetches. However, recent research has shown that this parameter,  $\gamma$ , is affected by sampling variability and that reduced values may be more appropriate (Donelan and Pierson, 1983).

(d) *The Ochi 6-parameter spectrum.* As noted previously, the variability in form of point spectra is very great, and many of them do not resemble the Bretschneider form. Ochi and Hubble (1976) have developed a theoretical family which can provide a much better fit to most spectra derived from wave measurements (see also Ochi, 1978). They start with a basic form,

$$S(\omega) = \frac{1}{4} \frac{\left( \frac{4\lambda + 1}{4} \omega_m^4 \right)^\lambda}{\Gamma(\lambda)} \cdot \frac{H_s^2}{\omega^{4\lambda + 1}} \exp \left[ -\frac{(4\lambda + 1)}{4} (\omega_m / \omega)^4 \right] \quad (88)$$

using a new shape parameter,  $\lambda$ .  $\Gamma(\lambda)$  is a gamma function, and the parameter  $H_s$  is the significant wave height,  $H_{1/3}$ . This modification of the Bretschneider form reduces to the latter when  $\lambda = 1$ . It is unimodal, with the peak becoming sharper with increasing  $\lambda$ . By adding two of these forms, Ochi obtained a six-param-

eter spectral form with great latitude to match the shapes of observed spectra:

$$S(\omega) = \frac{1}{4} \sum_j \frac{\left( \frac{4\lambda_j + 1}{4} \omega_{mj}^4 \right)^{\lambda_j}}{\Gamma(\lambda_j)} \cdot \frac{H_{sj}^2}{\omega^{4\lambda_j + 1}} \exp \left[ -\frac{(4\lambda_j + 1)}{4} (\omega_{mj} / \omega)^4 \right] \quad (89)$$

where  $j = 1, 2$  stands for the lower and higher-frequency components, respectively. The six parameters,  $H_{s1}$ ,  $H_{s2}$ ,  $\omega_{m1}$ ,  $\omega_{m2}$ ,  $\lambda_1$  and  $\lambda_2$  may be determined numerically to minimize the difference from a specific observed spectrum. Figs. 33 and 34 suggest the range of shapes within the family in fitting to quite different spectral types. In the case of double peaks (Fig. 33), suggesting the superposition of waves from two different storms, no indication of their relative directions is given.

Ochi explored the statistics of the six parameters by fitting some 800 point-spectra from British weather ship wave records. From these, he developed statistically a specific set of 11 spectra for a given significant wave height for use in ship design. One spectrum, essentially that corresponding to the modal values of the various parameters, he calls the *most probable* spectrum. The other spectra are defined in terms of 0.95 confidence bands of the various parameters. These ten sets of parameters are specified as functions of the significant wave height,  $H_{1/3}$  or  $H_s$ ; see Table 11. Ochi recommends a weight of 0.5 for the most probable spectrum and 0.05 for each of the other spectra. The families for  $H_s$  equal to 3 m and 9 m, all unimodal, are shown in Fig. 35.

The sets of observational spectra that were used to explore the statistics of the six parameters include some inherent bias. The set used by Pierson and Moskowitz for the development of the full-developed sea spectrum was biased toward pure, uncontaminated local sea conditions; the stratified sample from Station *India* was biased toward severe sea conditions; and both of these sets were used by Ochi. All of these spectra were from British weather ships in the North Atlantic; so there is a geographical bias as well. The lack of directional information is a further limitation.

The Ochi six-parameter family should not be taken to be a valid statistical representation of all seas. But with this reservation, it can be very useful in exploring the range of response of any engineering structure as a function of spectral form. While the complexity of the form and the large number of members limit its attractiveness for desk calculator use, this is no handicap when a computer is available.

## Section 3

### Ship Responses to Regular Waves<sup>8</sup>

**3.1 Introduction.** The response of a ship advancing in a seaway is a complicated phenomenon involving the interactions between the vessel dynamics and several distinct hydrodynamic forces. It would be impossible to cover comprehensively the entire subject of ship motions in one short chapter. Therefore, we will concentrate on those aspects of ship motion theory and experiment that have proven useful to the designer. Specifically, a linear theory of ship motions will be presented. All ship responses are nonlinear to some extent, but in many cases when nonlinearities are small a linear theory will yield good predictions.

The assumption of linearity for the ship response allows us to use many powerful analysis techniques developed in other fields. As discussed in the previous section, the seaway can be considered a random process and spectral techniques can be used to define the characteristics of the seaway. The response of the ship to a seaway is also a random process, and therefore the same spectral techniques can be used to analyze the ship responses. In Section 4 of this chapter the applicable theory of random processes and linear system theory will be explained. For the present we need to note only that by knowing the responses of a ship to regular waves of different frequencies, we can predict the statistics of the responses to actual random seaways. Accordingly, in this section the responses of a vessel to regular waves will be discussed.

A ship advancing at a steady mean forward speed with arbitrary heading in a train of regular waves will move in six degrees of freedom. That is, the ship's motion can be considered to be made up of three translational components, surge, sway and heave, and three rotational components, roll, pitch and yaw (Fig. 37). Consequently, for an arbitrarily shaped vessel, six non-linear equations of motion, with six unknowns, must be set up and solved simultaneously. However, for slender vessels in low to moderate sea states it is possible to assume that the ship motions will be small and hence to develop a linearized theory. For the usual case of an unrestrained ship with port/starboard symmetry, the six non-linear equations reduce to two sets of three linear equations. The vertical-plane or longitudinal motions (surge, heave and pitch) are uncoupled from the horizontal-plane or transverse motions (sway, roll and yaw).

In this section, a strip theory will be developed for the motion of a ship in regular waves at forward speed and arbitrary heading. Strip theory is the method most widely used to predict ship motions; it gives reasonably accurate results over a wide range of parameters. Subsequent to the discussion of strip theory, a brief review of other ship motion theories under development will be presented. The final subsections will be devoted to

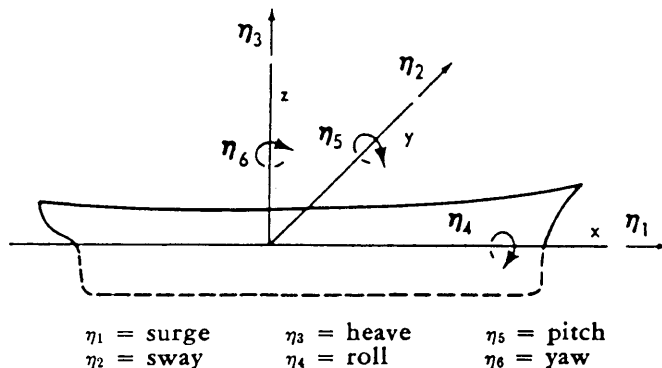


Fig. 37 Sign convention for translatory and angular displacements

discussing the various responses in detail. The coefficients and exciting forces in the equations of motion will be examined and comparisons between theory and experiment for the vessel responses will be made.

The derivation and solution of the equations that must be solved to determine the motions in all six degrees of freedom involve advanced calculus and hydrodynamics. As an aid to the reader not concerned with the theoretical details, the results for the simplified case of heave and pitch in head seas will be presented in the next sub-section. A discussion of the theory for all six degrees of freedom follows in Subsections 3.3-3.6. Some readers may wish to proceed from the simple case directly to the practical experimental and theoretical results presented in the remaining Sections 3.7 and 3.8. Newman (1978) gives a complete history of the development of theoretical methods to predict ship motions in regular waves.

**3.2 A Simplified Head-Sea Case.** As noted in the preceding sub-section, the longitudinal motions of pitch, heave and surge of a symmetrical ship in regular waves can be considered separately from the transverse modes. Furthermore, it has been found that for most comparatively long and slender ships surge has a minor effect and can be neglected. This implies that forward speed  $U_0$  is constant. The further simplification in this sub-section is to consider only the case of head seas, or waves from directly ahead ( $\mu = 180^\circ$ ). It is assumed that both the wave excitation forces and the resultant oscillatory motions are linear and harmonic, acting at the frequency of wave encounter,

$$\omega_e = \omega + \omega^2 g / U_0 \quad (90)$$

The equations of motion are based on Newton's second law of motion which in one form states that for

<sup>8</sup> Section 3 by Robert F. Beck, except for Subsection 3.8 by William C. Webster.

translational modes the forces acting on a body must equal the mass times the acceleration. For the rotational modes the moments acting on the body equal the mass moment of inertia times the angular acceleration. Thus, for heave,  $\eta_3$ , with the origin at the center of gravity (which must be located at the WL for this simple case),

$$\Delta \ddot{\eta}_3 = \mathbf{F}_3 \quad (91)$$

and for pitch,  $\eta_5$ ,

$$I_{55} \ddot{\eta}_5 = \mathbf{F}_5 \quad (92)$$

where  $\Delta$  is the mass (displacement),  $I_{55}$  is the mass moment of inertia about the  $y$ -axis and  $\mathbf{F}_3$  and  $\mathbf{F}_5$  represent the total force and moment, respectively, acting on the body, as functions of time. For the simplified case, the total force and moment consist mainly of fluid forces, both hydrostatic and hydrodynamic. (The heave gravitational force is balanced by the static buoyancy force in calm water and this defines the  $\eta_3 = 0$  position). In a linear theory, the fluid forces (and moments) can be conveniently divided between the forces due to the waves acting on a restrained ship, i.e., the forces that *excite* the motions, and the *radiation* forces due to the motions of the ship in an assumed calm sea. That is,

$$\begin{aligned} \mathbf{F}_3(t) &= F_{EX_3}(t) + F_{H_3}(t) \\ \mathbf{F}_5(t) &= F_{EX_5}(t) + F_{H_5}(t) \end{aligned} \quad (92)$$

The *excitations* for sinusoidal waves are expressed as,

$$\begin{aligned} F_{EX_3}(t) &= |F_{EX_3}| \cos(\omega_e t + \epsilon_3) \\ F_{EX_5}(t) &= |F_{EX_5}| \cos(\omega_e t + \epsilon_5) \end{aligned} \quad (93)$$

where  $|F_{EX_3}|$  refers to the amplitude of the heave force and  $|F_{EX_5}|$  to the amplitude of the pitch moment, and where  $\epsilon_3$  and  $\epsilon_5$  are the phase angles between the excitation and the waves.

In linear theory, the hydrodynamic *radiation* forces due to the coupled motions of the vessel in otherwise calm water can be expressed in terms that are directly proportional to the vertical displacements, velocities and accelerations. For *sinusoidal motions*, the hydrodynamic radiation force and moment can be written as,

$$\begin{aligned} F_{H_3} &= -[A_{33}(\omega) \ddot{\eta}_3 + B_{33}(\omega) \dot{\eta}_3 + C_{33} \eta_3 \\ &\quad + A_{35}(\omega) \ddot{\eta}_5 + B_{35}(\omega) \dot{\eta}_5 + C_{35} \eta_5] \\ F_{H_5} &= -[A_{53}(\omega) \ddot{\eta}_3 + B_{53}(\omega) \dot{\eta}_3 + C_{53} \eta_3 \\ &\quad + A_{55}(\omega) \ddot{\eta}_5 + B_{55}(\omega) \dot{\eta}_5 + C_{55} \eta_5] \end{aligned} \quad (94)$$

where  $A_{jk}(\omega)$  and  $B_{jk}(\omega)$  are coefficients that are functions of frequency. The minus sign is introduced for convenience in the final equations of motion.

The double-subscript notation for the coefficients

$A_{jk}$ ,  $B_{jk}$ ,  $C_{jk}$  is adopted in anticipation of its necessary use for the complete 6-degree of freedom case to be discussed subsequently. Where the subscripts are the same ( $A_{33}$ ,  $B_{33}$ ) a simple, uncoupled coefficient in the heave (3) or pitch (5) mode is intended. Where the subscripts are different ( $A_{35}$ ,  $B_{35}$ ) the meaning is that the  $k$ -mode is coupled into the  $j$ -mode (e.g.,  $A_{35} \ddot{\eta}_5$  represents the force in the heave mode due to a pitch acceleration).

The final coupled equations of motion for heave and pitch of a vessel in regular head seas are obtained by combining Equations (91), (92), (93) and (94). The radiation forces are moved to the left-hand side of the equations because they are proportional to the unknown motions. Thus,

$$\begin{aligned} (\Delta + A_{33}) \ddot{\eta}_3 + B_{33} \dot{\eta}_3 + C_{33} \eta_3 + A_{35} \ddot{\eta}_5 \\ + B_{35} \dot{\eta}_5 + C_{35} \eta_5 &= |F_{EX_3}| \cos(\omega_e t + \epsilon_3) \\ (I_{55} + A_{55}) \ddot{\eta}_5 + B_{55} \dot{\eta}_5 + C_{55} \eta_5 + A_{53} \ddot{\eta}_3 \\ + B_{53} \dot{\eta}_3 + C_{53} \eta_3 &= |F_{EX_5}| \cos(\omega_e t + \epsilon_5) \end{aligned} \quad (95)$$

The  $A_{jk}$ -terms correspond to *added mass*, in phase with vertical accelerations, the  $B_{jk}$ -terms to hydrodynamic *damping*, in phase with vertical velocity. Terms involving the coefficient  $C_{jk}$  are called *restoring* forces and moments, representing the net hydrostatic buoyancy effects of the ship motions. It should be noted that the  $C_{jk}$  are related to the hydrostatic coefficients used in ship stability calculations, i.e.,  $C_{33}$ ,  $C_{35}$ , and  $C_{55}$  are related to tons per cm immersion, change in displacement per cm of trim and moment to trim one cm, respectively.

Equations (95) are similar to the coupled equations that would be found for a two-degree-of-freedom spring-mass-damper system. There are mass, damping and spring terms on the left-hand side, and on the right-hand side the excitation. However, the equations are much different from the usual spring-mass-damper system in that the coefficients and the excitation are all functions of frequency. For a given frequency they are all constant and the system has a solution. For another frequency the values of the coefficients and the exciting forces will all be different. Hence, it has been shown (Ogilvie, 1964) that the correct solution of these equations of motion in the time domain requires the addition of complicated convolution integrals. To overcome this difficulty it is necessary only to consider the equations in the frequency domain, as shown subsequently. A complete discussion of these points can be found in Cummins (1962), Ogilvie (1964) and Wehausen (1971).

The cross-coupling between heave and pitch results from the coefficients with subscripts 35 or 53. For a fore-and-aft symmetric ship at zero forward speed the cross-coupling is zero. Even though typical ships are almost fore-and-aft symmetric, the cross-coupling between heave and pitch is very important and must be

retained in order to correctly predict the motions in head seas at forward speed.

The terms on the right-hand side of the equations represent the excitations, the forces or moments that would act on a restrained ship encountering waves at a forward speed  $U_0$ .  $|F_{EX_3}|$  and  $|F_{EX_5}|$  are the amplitudes of these harmonic forces and  $\epsilon_3$  and  $\epsilon_5$  the phase angles. In order to apply hydrodynamic theory to obtain expressions for the excitation amplitudes, the exciting forces and moments are usually subdivided into the Froude-Krylov and diffraction excitations. The Froude-Krylov excitations represent the integration of the pressure over the body surface that would exist in the incident wave system if the body were not present. The diffraction exciting forces and moments are caused by the diffraction or modification of the incident waves due to the presence of the vessel. The Froude-Krylov forces and moments are sometimes used to approximate the total exciting forces. This is a good approximation if the wavelength is much longer than the vessel length. For shorter wavelengths the approximation is increasingly inaccurate because the diffraction force becomes significant. For short waves the diffraction force may become approximately one-half of the total exciting force.

Thus, we have the two Equations (95) in two unknowns,  $\eta_3$  and  $\eta_5$ , which can be readily solved in this simple case of pitch and heave in head seas. To do this it is convenient to transform Equation (95) into complex number format, while at the same time taking the time derivatives to obtain velocity and acceleration.

In linear theory, the harmonic responses of the vessel,  $\eta_j(t)$ , will be proportional to the amplitude of the exciting forces and at the same frequency, but with phase shift. Consequently, the ship motions will have the form:

$$\begin{aligned}\eta_j(t) &= |\bar{\eta}_j| \cos(\omega_e t + \sigma_j) = \bar{\eta}_j e^{i\omega_e t} \\ \dot{\eta}_j(t) &= i\omega_e \bar{\eta}_j e^{i\omega_e t} \quad j = 3, 5 \\ \ddot{\eta}_j(t) &= -\omega_e^2 \bar{\eta}_j e^{i\omega_e t}\end{aligned}\quad (96)$$

where

$\bar{\eta}_j$  is the complex response amplitude, and  $j = 3$  represents heave;  $j = 5$  represents pitch,  
 $|\bar{\eta}_j|$  is the magnitude or absolute value of response amplitude, and  
 $\sigma_j$  is the phase shift of the response.

The complex amplitude is a complex number that contains both the magnitude and phase of the response. For example, the magnitude and phase of the heave response are given by

$$\bar{\eta}_3 = \bar{\eta}_{3_R} + i\bar{\eta}_{3_I} \quad (97)$$

where

$\bar{\eta}_{3_R}$  is the real part of  $\bar{\eta}_3$

$\bar{\eta}_{3_I}$  is the imaginary part of  $\bar{\eta}_3$

$|\bar{\eta}_3|$  is the magnitude of heave response amplitude and equals  $\sqrt{\bar{\eta}_{3_R}^2 + \bar{\eta}_{3_I}^2}$

$\sigma_3$  is the phase angle of heave response or  $\tan^{-1}(\bar{\eta}_{3_I}/\bar{\eta}_{3_R})$

In general it is understood that throughout this chapter, unless otherwise noted, the real part is to be taken in all expressions involving  $e^{i\omega_e t}$ .

Similarly the exciting force and moment can be expressed as

$$\begin{aligned}F_{EX_3}(t) &= |F_{EX_3}| \cos(\omega_e t + \epsilon_3) = F_{EX_3} e^{i\omega_e t} \\ F_{EX_5}(t) &= |F_{EX_5}| \cos(\omega_e t + \epsilon_5) = F_{EX_5} e^{i\omega_e t}\end{aligned}\quad (98)$$

where  $F_{EX_3}$  and  $F_{EX_5}$  are now taken to be the complex exciting force and moment amplitudes, containing both amplitude and phase. Making these substitutions in Equation (95), the  $e^{i\omega_e t}$  cancel out, and the resulting equations are:

$$\begin{aligned}(-\omega_e^2(\Delta + A_{33}) + i\omega_e B_{33} + C_{33})\bar{\eta}_3 \\ + (-\omega_e^2 A_{35} + i\omega_e B_{35} + C_{35})\bar{\eta}_5 = F_{EX_3}\end{aligned}\quad \text{(heave)} \quad (99)$$

$$\begin{aligned}(-\omega_e^2(I_{55} + A_{55}) + i\omega_e B_{55} + C_{55})\bar{\eta}_5 \\ + (-\omega_e^2 A_{53} + i\omega_e B_{53} + C_{53})\bar{\eta}_3 = F_{EX_5}\end{aligned}\quad \text{(pitch)} \quad (100)$$

$J = 3, 5 \quad k = 3, 5$

where

$A_{jk}$  is the added mass coefficient in  $j^{\text{th}}$  direction due to  $k^{\text{th}}$  motion.

$B_{jk}$  is the damping coefficient in  $j^{\text{th}}$  direction due to  $k^{\text{th}}$  motion.

$C_{jk}$  is hydrostatic restoring force coefficient in  $j^{\text{th}}$  direction due to  $k^{\text{th}}$  motion.

$F_{EX_j}$  are the complex exciting force and moment amplitudes in  $j^{\text{th}}$  direction.

Note that in Equations (99) and (100) the origin is at the center of gravity, which is assumed to lie in the WL. The more general case is given in the next sub-section.

The determination of the coefficients and exciting force and moment amplitudes represents the major problem in any ship motion calculation. The problem is simplified by applying a strip theory (as developed in the next sub-section), where the ship is divided into transverse strips, or segments. The added mass and damping for each strip are relatively easily calculated, using two-dimensional hydrodynamic theory or by equivalent two-dimensional experiments. The sectional values are then appropriately combined to yield values for  $A_{jk}$ ,  $B_{jk}$ ,  $C_{jk}$  and  $F_j$ . For the case of heave and pitch in head seas Table 12 lists the formulas for calculating the coefficients and the exciting forces. Actual theo-

Table 12—Head Sea Coefficients and Exciting Forces

$$\begin{aligned}
A_{33} &= \int a_{33} dx & B_{33} &= \int b_{33} dx \\
A_{35} &= - \int x a_{33} dx - \frac{U_0}{\omega_e^2} B_{33} & B_{35} &= - \int x b_{33} dx + U_0 A_{33} \\
A_{53} &= - \int x a_{33} dx + \frac{U_0}{\omega_e^2} B_{33} & B_{53} &= - \int x b_{33} dx - U_0 A_{33} \\
A_{55} &= \int x^2 a_{33} dx + \frac{U_0^2}{\omega_e^2} A_{33} & B_{55} &= \int x^2 b_{33} dx + \frac{U_0^2}{\omega_e^2} B_{33}
\end{aligned}$$

$$\begin{aligned}
C_{33} &= \int c_{33} dx = \rho g \int B(x) dx \\
C_{35} = C_{53} &= - \int x c_{33} dx = -\rho g \int x B(x) dx \\
C_{55} &= \rho g \nabla \overline{GM}_L + LCF^2 C_{33} \approx \int x^2 c_{33} dx = \rho g \int x^2 B(x) dx \\
F_{EX_3} &= \bar{\zeta} \int_L e^{ikx} e^{-kT^*(x)} [c_{33} - \omega_0(\omega_e a_{33} - ib_{33})] dx \\
F_{EX_5} &= -\bar{\zeta} \int_L e^{ikx} e^{-kT^*(x)} \left[ x(c_{33} - \omega_0(\omega_e a_{33} - ib_{33})) - \frac{U_0}{i\omega_e} \omega_0(\omega_e a_{33} - ib_{33}) \right] dx
\end{aligned}$$

where:

$a_{33}$  is the sectional heave added mass  
 $b_{33}$  is the sectional heave damping  
 $c_{33}$  is the sectional restoring force =  $\rho g B(x)$   
 $B(x)$  is the sectional waterline beam  
 $S(x)$  is the sectional area  
 $T^*(x)$  is the mean sectional draft or  $\frac{S(x)}{B(x)}$   
 $\bar{\zeta}$  is the incident wave amplitude

retical and experimental values for the sectional added mass and damping in heave for various section shapes are given in Section 3.5, and the overall coefficients and exciting forces are given in Section 3.7.

In Table 12 the approximate equation for  $C_{55}$  is based on the assumption that the vertical difference between the centers of gravity and buoyancy,  $\overline{BG}$ , and the longitudinal distance between  $CG$  and  $CF$  are both very small relative to the length of the ship.

It should also be noted that the amplitudes of the heave and pitch exciting force and moment listed in Table 12 depend directly on  $\bar{\zeta}$ , the incident wave amplitude. This is a consequence of the linear theory used in their development. The terms in brackets proportional to  $c_{33}$  are the Froude-Krylov exciting force and moment, and the terms involving  $a_{33}$  and  $b_{33}$  represent the hydrodynamic diffraction forces. That these forces are given in terms of the same added mass and damping coefficients used in calculating the radiation force coefficients,  $A_{jk}$  and  $B_{jk}$ , is the result of mathematical manipulation. Physically it can be viewed that the vertical motion of the wave relative to the fixed hull is

similar to the vertical motion of the hull relative to still water.

The factor  $e^{ikx}$  accounts for the wave profile along the length of the ship. Both the Froude-Krylov and diffraction parts of the exciting forces and moments are multiplied by the term  $e^{-kT^*(x)}$ , where  $k$  is the wave number and  $T^*(x)$  is the mean draft for the section, assumed to be  $S(x)/B(x)$ , where  $S(x)$  is the sectional area and  $B(x)$  is the local beam at the waterline. This is the result of the exponential decay of the dynamic pressure in the incident wave as one moves deeper below the free surface. This effect is often called the *Smith Effect* (Smith, 1883). For depths greater than approximately one wavelength no variation in pressure due to the incident waves can be felt. This decay in the incident wave dynamic pressure results in an equivalent reduction in the magnitude of the exciting forces.

To solve Equations (99) and (100) for the complex amplitudes, the equations are written in the form:

$$\begin{aligned}
P \bar{\eta}_3 + Q \bar{\eta}_5 &= F_{EX_3} \\
R \bar{\eta}_3 + S \bar{\eta}_5 &= F_{EX_5}
\end{aligned} \tag{101}$$



where

$$\begin{aligned} P &= -\omega_e^2 (\Delta + A_{33}) + i\omega_e B_{33} + C_{33} \\ Q &= -\omega_e^2 A_{35} + i\omega_e B_{35} + C_{35} \\ R &= -\omega_e^2 A_{53} + i\omega_e B_{53} + C_{53} \\ S &= -\omega_e^2 (I_{55} + A_{55}) + i\omega_e B_{55} + C_{55} \end{aligned}$$

The solutions to the coupled equations are then given by

$$\begin{aligned} \bar{\eta}_3 &= \frac{F_{EX_3} S - F_{EX_5} Q}{PS - QR} \\ \bar{\eta}_5 &= \frac{F_{EX_5} P - F_{EX_3} R}{PS - QR} \end{aligned} \quad (102)$$

The limiting forms of the solutions for  $\bar{\eta}_3$  and  $\bar{\eta}_5$  are easily determined from Equations (102). At the high-frequency limit, the exciting forces go to zero and therefore the motions must also approach zero. In the low-frequency limit,  $P$ ,  $Q$ ,  $R$ , and  $S$  approach the values of their respective hydrostatic restoring force coefficients. The low-frequency limit of  $F_3$  and  $F_5$  are found by using only the Froude-Krylov terms and expanding the  $e^{ikx}$  term for small  $k$ . The net result is that in the limit of low frequency:

$$\begin{aligned} \bar{\eta}_3 &\rightarrow \bar{\zeta} \\ \bar{\eta}_5 &\rightarrow -ik\bar{\zeta} \end{aligned} \quad (103)$$

Thus, for very long waves the heave amplitude approaches the wave amplitude and the pitch amplitude is the same as the maximum wave slope. The phasing is such that the vessel contours the waves. At intermediate frequencies the ship motions may peak. Depending on speed and hull form, typical peak values are in the range of 1 to 2 times the wave amplitude for heave and 1 to 1.5 times the wave slope for pitch. Examples of the pitch and heave motions in head seas are shown in Section 3.7.

The first strip theory for ship motions in regular waves was developed by Korvin-Kroukovsky (1955) to predict the heave and pitch motions of a vessel in head seas. Using concepts from slender-body theory in aerodynamics and shrewd physical insight, a linearized theory was developed to compute all the coefficients and the diffraction excitations. Some refinements and experimental comparisons were provided in the sequel by Korvin-Kroukovsky and Jacobs (1957). Further developments and extension to six degrees of freedom are discussed.

It is of interest to note that Equations (95), and hence the solutions given in (102), are basically the same as those developed by Korvin-Kroukovsky. The formulas for coefficients and for excitations listed in Table 12 are essentially the same except that they embody a more rigorous treatment of forward speed terms in the coefficients and have  $\omega_o \omega_e$  as the multiplier in the excitations instead of  $\omega_e^2$ .

**3.3 Motions in Regular Waves with Six Degrees of Freedom.** In order to be able to compute all responses of any vessel to regular waves, it is necessary to deal with the complete motions of a ship with six degrees of freedom, considering important couplings among them. The linear equations of motion will be presented for a ship advancing at constant mean forward speed with arbitrary heading in a train of regular sinusoidal waves. Detailed derivations of the equations of motion may be found in Salvesen, et al (1970), Newman (1977), Ogilvie (1964), or Wehausen (1971).

(a) *Equations of motion.* The linearization of the equations is made on the basis of small motions. The motions will in general be small if the ship is stable and the incident wave amplitude is relatively small. The principal exceptions to this rule are resonant situations where the damping is small, e.g., roll resonance in beam seas, near-pitch resonance of SWATH ships, heave resonance of semi-submersible oil-drilling ships, etc. Experimental and theoretical investigations have shown that a linear analysis of ship motions gives excellent predictions over a wide variety of sea conditions and vessel types (see Section 3.7), and that rolling at forward speed can be handled satisfactorily by equivalent linear equations (Section 3.8). Accordingly, the assumption of linearity will be retained here. However, in doubtful cases the admissibility of the assumptions inherent in linear theory can only be determined by comparing the results of calculations assuming linearity with experimental and full-scale measurements.

It is desirable first to define the three axis systems shown in Fig. 38. The  $(x_o, y_o, z_o)$  system is fixed in

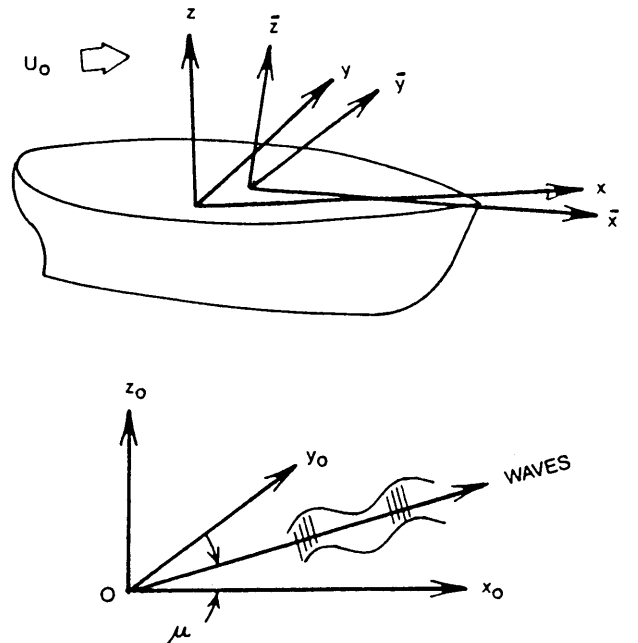


Fig. 38 Coordinate systems

relation to the earth, with the origin at any desired location. The  $z_0$ -axis is positive upwards and the  $x_0$ - $y_0$  plane (with origin 0) is usually coincident with the calm-water level. The  $x_0$  axis is normally set in the direction of travel of the ship. The  $(x_0, y_0, z_0)$  axis system is used to define the incident wave system.

The  $(x, y, z)$  system moves with constant velocity  $U_0$  in the positive  $x_0$ -direction, and is referred to as *inertial* coordinates. The  $x$ - $y$  plane is also aligned with the calm water level and  $z$  is positive upwards. The  $x$ -axis is coincident with the  $x_0$ -axis. The transformation from the  $(x_0, y_0, z_0)$  system to the moving system is then given by

$$\begin{aligned} x_0 &= x + U_0 t \\ y_0 &= y \\ z_0 &= z \end{aligned} \quad (104)$$

The  $\bar{x}, \bar{y}, \bar{z}$  axis system (body axes) is fixed in the ship and therefore moves with all the motions of the ship. The  $\bar{x}$ - $\bar{y}$  plane coincides with the ship's calm waterplane, with the  $\bar{z}$ -axis normal to it (positive upward) and the  $\bar{x}$ -axis pointing out the bow. In all the work described in this chapter it will be assumed that the ship has port/starboard symmetry and the  $\bar{x}$ - $\bar{z}$  plane is the plane of symmetry. Hence, the origin is in the center plane, in the calm waterplane and at any convenient fore-and-aft location, such as amidships.

The motions of the ship are determined by the orientation of the  $\bar{x}, \bar{y}, \bar{z}$  system relative to the  $x, y, z$  system. A total of six components are needed to uniquely define the motion, typically three translations and three rotations. The three translations are defined as surge, sway, and heave. The corresponding rotations of the  $\bar{x}, \bar{y}$ , and  $\bar{z}$  axes are called roll, pitch and yaw, respectively, Fig. 37.

It should be noted that with a ship moving at any angle,  $\mu$ , to regular waves the frequency of oscillation will be shifted to the frequency of wave encounter,

$$\omega_e = \omega_0 - \frac{\omega_0^2}{g} U_0 \cos \mu = \omega_0 - k U_0 \cos \mu \quad (105)$$

This shift is directly analogous to the Doppler shift in sound and electro-magnetic theory. For waves coming from ahead ( $\mu = 180$  deg) the frequency of encounter is higher than the absolute frequency. In stern seas ( $\mu = 0$  deg) the frequency of encounter is lower and may equal zero when the ship speed equals the phase velocity of the waves. For very high speeds in stern seas the frequency of encounter may obtain negative values. This corresponds to the case where the ship overtakes the waves so that the waves actually appear to be coming from ahead (Section 4). We shall see that the ship responds at the frequency of encounter and consequently the frequency shift caused by forward speed has a strong influence on the ship motions.

As in the simple case of a ship in head seas, the starting point in setting up the more complicated equations of motion for six degrees of freedom is Newton's second law, which must be written in an inertial co-ordinate system. But the forces and moments acting on the body are all defined in the body-axis system. Thus, transformations are used in order to write the equations of motion in the body-axis system. These transformations result in the so-called Euler equations of motion for a rigid body, which are highly nonlinear. For this reason most ship motion investigations first linearize the equations before attempting a solution.

The general form of the basic linearized equations in six degrees of freedom using body axes is,

$$\sum_{k=1}^6 \Delta_{jk} \ddot{\eta}_k(t) = F_j(t) \quad j = 1, 2, \dots, 6 \quad (106)$$

where  $\Delta_{jk}$  are the components of the generalized inertia matrix for the ship, in which the mass and moment of inertia terms,  $\Delta$  and  $I$ , and all possible couplings, are included.  $\ddot{\eta}_k$  are the accelerations in mode  $k$ ;  $F_j$  represent the total forces or moments acting on the body in direction  $j$ . The quantities  $F_j$ , as well as  $\eta_k$ , are harmonic functions of time.

In linearizing the equations many of the terms in  $\Delta_{jk}$  become zero, and Abkowitz (1969) has shown that for a ship with lateral symmetry (106) reduces to the following six explicit equations:

$$\begin{aligned} \Delta (\ddot{\eta}_1 + \bar{z}_c \ddot{\eta}_5) &= F_1 & (\text{surge}) \\ \Delta (\ddot{\eta}_2 - \bar{z}_c \ddot{\eta}_4 + \bar{x}_c \ddot{\eta}_6) &= F_2 & (\text{sway}) \\ \Delta (\ddot{\eta}_3 - \bar{x}_c \ddot{\eta}_5) &= F_3 & (\text{heave}) \\ I_{44} \ddot{\eta}_4 - I_{46} \ddot{\eta}_6 - \Delta \bar{z}_c \ddot{\eta}_2 &= F_4 & (\text{roll}) \\ I_{55} \ddot{\eta}_5 + \Delta \{ \bar{z}_c \ddot{\eta}_1 - \bar{x}_c \ddot{\eta}_3 \} &= F_5 & (\text{pitch}) \\ I_{66} \ddot{\eta}_6 - I_{64} \ddot{\eta}_4 + \Delta \bar{x}_c \ddot{\eta}_2 &= F_6 & (\text{yaw}) \end{aligned} \quad (107)$$

where

$F_j(t)$ ,  $j = 1, 2, 3$  are the total forces in the  $\bar{x}, \bar{y}, \bar{z}$  directions, respectively

$F_j(t)$ ,  $j = 4, 5, 6$  are the total moments acting about the  $\bar{x}, \bar{y}$ , and  $\bar{z}$  axes. Positive moments are in the right-hand sense

$\Delta$  is total mass of vessel

$I_{jj}$ ,  $j = 4, 5, 6$  are moments of inertia around the  $\bar{x}, \bar{y}, \bar{z}$  axes, respectively

$I_{46}$  is roll - yaw product of inertia  
=  $I_{64}$

$(\bar{x}_c, 0, \bar{z}_c)$  are coordinates of the center of gravity of the ship in the  $\bar{x}, \bar{y}, \bar{z}$  system.

$\ddot{\eta}_j(t)$  is acceleration in the  $j^{\text{th}}$  degree of freedom, where  $j = 1, 2, 3, \dots, 6$  refers to surge, sway, heave, roll, pitch and yaw, respectively.

It should always be kept in mind that the equations for  $j = 1, 2, 3$  are force equations and for  $j = 4, 5, 6$  are moment equations.

Comparing (106) to (107), the generalized inertia matrix is:

$$\Delta_{jk} = \begin{bmatrix} \Delta & 0 & 0 & 0 & +\Delta \bar{z}_c & 0 \\ 0 & \Delta & 0 & -\Delta \bar{z}_c & 0 & +\Delta \bar{x}_c \\ 0 & 0 & \Delta & 0 & -\Delta \bar{x}_c & 0 \\ 0 & -\Delta \bar{z}_c & 0 & I_{44} & 0 & -I_{46} \\ +\Delta \bar{z}_c & 0 & -\Delta \bar{x}_c & 0 & I_{55} & 0 \\ 0 & +\Delta \bar{x}_c & 0 & -I_{46} & 0 & I_{66} \end{bmatrix} \quad (108)$$

This matrix can be readily evaluated in any specific case. Of course, if the origin is vertically in line with the center of gravity, all  $\bar{x}_c$  terms will be zero (as in the simple head-sea case of Section 3.2).

As presented in Equation (107), the  $F_j$  represent the total forces (or moments) acting on the vessel resolved in the  $\bar{x}, \bar{y}, \bar{z}$  body-axis system. Likewise,  $\ddot{\eta}_j$  are the accelerations resolved in the body-axis system. In the formulation and solving of the hydrodynamic problems associated with ship motion it is often more convenient to work in the  $x, y, z$  or *inertial* system. As far as the linearized equations of motion are concerned, the resolution of the forces, moments, and motion amplitudes into one system or the other does not matter. The distinction between the two systems has been lost in the linearization. For the remainder of this section we shall in general work in the inertial ( $x, y, z$ ) reference frame. However, one must always be aware of the distinction between the two coordinate systems so that in the development of a linear hydrodynamic theory all the terms of the appropriate order of magnitude are retained.

The only product of inertia that appears is  $I_{46}$ , the roll-yaw product, which vanishes if the ship has fore-and-aft symmetry and is small otherwise. The other nondiagonal elements all vanish if the origin of the coordinate system coincides with the center of gravity of the ship; however, it is more convenient to take the origin in the waterplane at midship, in which case  $\bar{x}_c$  and  $\bar{z}_c$  are not equal to zero.

Writing Euler's equations of motion, Equations (106), with only gravitational and fluid forces acting on the ship results in

$$\sum_{k=1}^6 \Delta_{jk} \ddot{\eta}_k = F_j(t) = F_{Gj} + F_{Hj} \quad j = 1, 2, \dots, 6 \quad (109)$$

where

$F_{Gj}$  is the component of the gravitational force acting on the vessel in the  $j^{\text{th}}$  direction.

$F_{Hj}$  is the component of the fluid force acting in the vessel in the  $j^{\text{th}}$  direction.

$\Delta_{jk}$  is the inertia matrix given by Equation (108).

In a linear theory, the responses of the vessel will be linear with (i.e., directly proportional to) wave amplitude and occur at the frequency at which the ship perceives the incident waves. This is an important point. The use of linear analysis allows us to use the powerful analysis techniques of linear system theory and obtain many useful results. However, it also puts limitations on the results which must be recognized. Since only the vessel response to sinusoidal waves is being considered in this section, the time-dependent responses of the vessel,  $\eta_j(t)$ , will be sinusoidal at the frequency of encounter and can be written as:

$$\eta_j(t) = \bar{\eta}_j e^{i\omega_e t} \quad j = 1, 2, \dots, 6$$

where,

$\omega_e$  is the frequency of encounter (105), and equals

$$\omega_0 - \frac{\omega_0^2}{g} U_0 \cos \mu \quad (110)$$

$\bar{\eta}_j$  is the complex amplitude of vessel response in the  $j^{\text{th}}$  direction and  $j = 1, 2, \dots, 6$  refer to surge, sway, heave, roll, pitch, yaw, respectively.

The gravitational forces are simply due to the weight of the vessel applied at the center of gravity. Since the mean gravitational forces cancel the mean buoyant forces, they are usually combined with the hydrostatic part of the fluid forces to give the net hydrostatic forces.

The hydrostatic and hydrodynamic forces acting on the ship are obtained by integrating the fluid pressure over the underwater portion of the hull. The components of the fluid forces acting in each of the six degrees of freedom are thus given by

$$F_{Hj} = \iint_{S'} P n_j ds \quad j = 1, 2, \dots, 6 \quad (111)$$

where

$n_j$  is the generalized unit normal to the hull surface into the hull

$P$  is the fluid pressure

$s$  is the underwater hull surface area

The components of the generalized normal are equal to the usual hull surface normals for the translation modes ( $j = 1, 2, 3$ ) and equal to the moments of the unit normals for the rotational modes ( $j = 4, 5, 6$ ). Consequently, it may be written that

$$\begin{aligned} (n_1, n_2, n_3) &= \underline{n} \\ (n_4, n_5, n_6) &= \underline{r} \times \underline{n} \end{aligned} \quad (112)$$

where

$\underline{n}$  is the unit normal to the hull surface out of the fluid

$\underline{r}$  is the vector from origin to a point on the hull  
 $= x\underline{i} + y\underline{j} + z\underline{k}$

The pressure on the body can be found using Bernoulli's equation. Assuming an inviscid and irrotational flow, the equation for the pressure is

$$P = \frac{1}{2} \rho U_0^2 - \rho \frac{\partial \Phi}{\partial t} - \frac{1}{2} \rho (\nabla \Phi \times \nabla \Phi) - \rho g z \quad (113)$$

where  $\rho$  is density,  $\nabla \Phi$  is the total velocity vector representing the fluid flow, and  $U_0$  is the forward speed of the ship. The assumption of inviscid, irrotational flow is critical because it allows the development of a linear theory. However, the effects of viscosity and vortex shedding have been lost. For some cases (particularly roll and yaw) this may not be satisfactory and empirical corrections have to be added at a later stage.

In Equation (113), the first three terms represent the hydrodynamic contributions to the pressure and the last term represents the hydrostatic contribution. When the equation for the pressure is substituted into Equation (111), the fluid forces acting on the vessel may be divided into the following hydrostatic and hydrodynamic contributions:

$$F_{H_j} = F_{HS_j} + F_{HD_j}$$

where

$$F_{HS_j} \text{ (hydrostatic)} = -\rho g \iint_S z n_j ds \quad (114a)$$

$$F_{HD_j} \text{ (hydrodynamic)} =$$

$$-\rho \iint_S \left( \frac{1}{2} U_0^2 - \frac{\partial \Phi}{\partial t} - \frac{1}{2} \nabla \Phi \cdot \nabla \Phi \right) n_j ds \quad (114b)$$

In order to find expressions for the above to insert into the equations of motion, the hydrostatic and hydrodynamic forces will be considered separately.

(a) *Net hydrostatic forces.* To find the hydrostatic forces we must evaluate the integrals in Equation (114a), a straightforward but tedious process. The value of  $z$  must be replaced by its equivalent values in the  $(\bar{x}, \bar{y}, \bar{z})$  system and the integrals evaluated over the instantaneous underwater hull surface. Note that in linear theory the integrals need only be carried out on the instantaneous wetted surface up to the calm water level, since the contributions from the small area between the calm water level and the actual wavy water surface are of a higher order.

The details of the integral evaluation may be found in Newman (1977). Because the mean hydrostatic forces are cancelled by the mean gravitational forces, the two are usually combined to give the net hydrostatic force as follows:

$$F_{HS_j}^* = F_{G_j} + F_{HS_j} \quad j = 1, 2, \dots, 6 \quad (115)$$

where

$F_{HS_j}$  = hydrostatic force on the body in the  $j^{\text{th}}$  direction.

$F_{HS_j}^*$  = net hydrostatic force on the body in the  $j^{\text{th}}$  direction.

The final results for each of the six components for a vessel with port-starboard symmetry are:

where

$$F_{HS_1}^* = 0 \quad (116a)$$

$$F_{HS_2}^* = 0 \quad (b)$$

$$F_{HS_3}^* = -\rho g S \eta_3 + \rho g S_1 \eta_5 \quad (c)$$

$$F_{HS_4}^* = -\rho g \nabla (S_{22}/\nabla + \bar{z}_B - \bar{z}_C) \eta_4 \\ = -\rho g \nabla \overline{GM}_T \eta_4 \quad (d)$$

$$F_{HS_5}^* = \rho g S_1 \eta_3 - \rho g \nabla (S_{11}/\nabla + \bar{z}_B - \bar{z}_C) \eta_5 \\ = \rho g S_1 \eta_3 - \rho g \nabla (\overline{GM}_L + S \overline{LCF}^2/\nabla) \eta_5 \quad (e)$$

$$F_{HS_6}^* = 0 \quad (f)$$

where

$\overline{GM}_T$  is the transverse metacentric height  
 $\overline{GM}_L$  is the longitudinal metacentric height  
 $\bar{z}_B$  is the vertical center of buoyancy location  
 $\overline{LCF}$  is the longitudinal center of flotation

$S$  is the waterplane area  $= \int_L B(x) dx$

$S_1$  is the first moment of waterplane area around the  $y$ -axis

$$= \int_L x B(x) dx$$

$S_{11}$  is the second moment of waterplane area around the  $y$ -axis

$$= \int_L x^2 B(x) dx$$

$S_{22}$  is the second moment of waterplane area around the  $x$ -axis

$$= \iint_S y^2 dy dx = \int_L \frac{[B(x)]^3}{12} dx$$

$B(x)$  is the full breadth of waterplane at  $x$

In order to simplify the notation, the individual force components expressed in Equations (116) can be written in a more general matrix notation as

$$F_{HS_j}^* = - \sum_{j=1}^6 C_{jk} \bar{\eta}_k e^{i\omega_e t} \quad (117)$$

where

$C_{jk}$  are the hydrostatic restoring force coefficients and  $\bar{\eta}_k e^{i\omega_e t}$  replaces the arbitrary motions,  $\eta_k(t)$ .

(116) and (117). The final results are:

$$\begin{aligned}
C_{jk} &= 0 && \text{except for the values} \\
C_{33} &= \rho g \int B(x) dx \\
C_{35} &= C_{53} = -\rho g \int x B(x) dx \\
C_{44} &= \rho g \nabla \overline{GM}_r \\
C_{55} &= \rho g \nabla \left( \overline{GM}_L + \frac{\overline{LCF}^2}{\nabla} S \right) \approx \rho g S_{11} \\
&= \rho g S_{11} + \rho g \nabla (\overline{KB} - \overline{KG})
\end{aligned}
\tag{118}$$

where all integrals are taken over the length of the ship.

For many ships the vertical difference between the center of gravity and the center of buoyancy is very small relative to the length of the ship, so that in this case  $C_{55}$  can be approximated as

$$C_{55} \approx \rho g S_{11} = \rho g \int x^2 B(x) dx \quad (119)$$

It should be noted that, after appropriate changes in units, the hydrostatic restoring force coefficients,  $C_{jk}$ , are equivalent to the hydrostatic coefficients used in ship stability calculations. Tons per cm, change in displacement per cm of trim aft, righting moment per degree of heel, and moment to trim one cm are related to  $C_{33}$ ,  $C_{35}$ ,  $C_{44}$ , and  $C_{55}$ , respectively.

(b) *Hydrodynamic forces.* The hydrodynamic forces acting on the vessel can be found by evaluating Equation (114b). To accomplish this the total velocity potential for the fluid flow,  $\Phi(x, y, z, t)$ , must be known. At the present state of the art, this is impossible, so that several simplifications are necessary. The first is to assume that the total velocity potential can be subdivided into a simple summation of the various components as follows:

$$\begin{aligned}\Phi(x, y, z, t) &= [-U_0 x + \phi_s(x, y, z)] + \phi_T e^{i\omega_e t} \\ &= [-U_0 x + \phi_s(x, y, z)] \\ &\quad \text{steady part} \\ &\quad + \left[ \phi_I + \phi_D + \sum_{j=1}^6 \phi_j \bar{\eta}_j \right] e^{i\omega_e t} \\ &\quad \text{unsteady part}\end{aligned}\tag{120}$$

where,

$\phi_s$  is the perturbation potential due to steady translation

$\phi_T$  is the unsteady perturbation potential  

$$= \phi_I + \phi_D + \sum_{j=1}^6 \phi_j \bar{\eta}_j$$
 $\phi_I$  is the incident wave potential  
 $\phi_D$  is the diffracted wave potential  
 $\phi_j$  is the radiation potential due to unit motion  
in  $j$ th direction

Note that  $\phi_I, \phi_D, \phi_j$  are all independent of time and depend only on space variables. The steady part of  $\Phi$  results from the steady forward speed of the vessel. The  $-U_0x$  term is the free-stream velocity and the  $\phi_S$  is the steady perturbation velocity potential due to the presence of the ship hull. The term  $(-U_0x + \phi_S)$  is the solution to the problem of the ship advancing at constant forward speed in otherwise calm water. The velocity due to the steady advance of the vessel is given by

$$W = \nabla(-U_0 x + \phi_s) = -U_0 + \nabla\phi_s \quad (121)$$

where  $\nabla$  is the gradient differential operator.

The unsteady part contains all the time-dependent terms. As with the response amplitude, Equation (110), the time dependence is sinusoidal at the frequency of encounter. The unsteady part is subdivided into the incident wave potential  $\phi_i$ , the diffracted wave potential  $\phi_D$ , and the radiation potentials  $\phi_j$  due to motion in each degree of freedom. The potentials  $\phi_i$  and  $\phi_D$  result from solving the *diffraction problem* where incident waves act upon the vessel in its equilibrium position. The diffracted waves result from the scattering of the incident waves as they strike the body. The hydrodynamic forces that result from the incident plus diffracted waves are called the *exciting forces*. The radiation potentials ( $\phi_j$ ) are the solution to the *radiation problem* in which the vessel undergoes prescribed oscillatory motion in each of the six degrees of freedom in otherwise calm water. The hydrodynamic forces that result from the radiation problem involve added mass and damping.

The subdivision of the complete velocity potential into the components shown in (120) is not unique. Other subdivisions are possible, but the one shown has the advantage that the various contributions to the total potential are easily identifiable. In addition, the motion amplitudes,  $\bar{\eta}_j$ , are separated from the potentials so that the potentials can be found independently of the body motion. The interactions between the various unsteady components are all of higher order and are neglected in linear theory. As with the motion amplitudes, the assumption of linear theory has allowed simplification but at the cost of other harmonics in the response and interactions between the unsteady components.

The steady component ( $-U_0x + \phi_s$ ) is the solution to the wave resistance problem in calm water and can be determined independently of the unsteady components. In a consistent linear theory the boundary value

problem that must be solved to determine the unsteady components depends on  $\phi_s$ . Both the boundary conditions on the hull and the free surface contain terms involving  $\phi_s$ . Thus, there is an interaction between the steady and unsteady components. Unfortunately, developing a ship motion theory that properly accounts for this interaction is extremely difficult. For this reason, the interactions are usually ignored and the steady component is approximated by the free-stream value ( $-U_0 x$ ) in the unsteady problem. However, neglecting the interaction between the steady and unsteady perturbation potentials has significant effects on the ship motion predictions for high-speed ships and such problems as green water on deck and slamming. Hence, the interaction between the steady and unsteady problems has become an important area of current research. Further discussion can be found in Newman (1978) or Ogilvie (1977). Troesch (1981) uses the theory developed by Ogilvie and Tuck (1969) to compute the interaction in lateral motions. Inglis and Price (1981) use three-dimensional numerical techniques to compute the magnitude of the effects.

For the linear development of strip theory presented in this chapter, it is assumed that the steady velocity component can be approximated by the free-stream value. In this case, the value of  $\underline{W}$  is approximated by:

$$\underline{W} \approx (-U_0, 0, 0) \quad (122)$$

In addition, the nonlinearities associated with the  $\nabla\Phi \times \nabla\Phi$  term in the Bernoulli equation (113) are also dropped. Thus, the unsteady pressure equation becomes

$$P \approx -\rho \left[ i\omega_e - U_0 \frac{\partial}{\partial x} \right] \phi_T e^{i\omega_e t} \quad (123)$$

Using the approximation for the unsteady pressure given by (123), the expression, (114b), for the unsteady hydrodynamic force acting on the vessel reduces to

$$\tilde{F}_{HDj} \approx -\rho \iint_S n_j \left[ i\omega_e - U_0 \frac{\partial}{\partial x} \right] \phi_T e^{i\omega_e t} ds \quad (124)$$

where, consistent with the linearization, the integration is carried out over the mean underwater hull surface  $S$ . The tilde ( $\sim$ ) over the hydrodynamic force denotes that only the unsteady hydrodynamic forces are being considered.

Substituting the form of  $\phi_T$  from Equation (120) into (124) results in two distinct sets of unsteady forces acting on the vessel as follows:

$$\tilde{F}_{HDj} = F_{EXj} + F_{Rj} \quad (125)$$

where

$F_{EXj}$  are the exciting forces in the  $j$ th direction, and equal

$$\{F_j^I + F_j^D\} e^{i\omega_e t} \quad (a)$$

$F_j^I$  is the complex amplitude of the exciting force component due to incident waves, usually called the Froude-Krylov exciting force, and equals

$$-\rho \iint_S n_j \left( i\omega_e - U_0 \frac{\partial}{\partial x} \right) \phi_I ds \quad (b)$$

$F_j^D$  is the complex amplitude of the exciting force component due to diffracted waves, usually called the diffraction exciting force, equalling

$$-\rho \iint_S n_j \left( i\omega_e - U_0 \frac{\partial}{\partial x} \right) \phi_D ds \quad (c)$$

$F_{Rj}$  is the hydrodynamic force in the  $j$ th direction due to forced motion, represented by

$$\begin{aligned} & -\rho \iint_S n_j \left( i\omega_e - U_0 \frac{\partial}{\partial x} \right) \left( \sum_{k=1}^6 \phi_k \bar{\eta}_k e^{i\omega_e t} \right) ds \quad (d) \\ & = \sum_{k=1}^6 \left[ -\rho \iint_S n_j \left( i\omega_e - U_0 \frac{\partial}{\partial x} \right) \phi_k ds \right] \bar{\eta}_k e^{i\omega_e t} \end{aligned}$$

For convenience the above quantity in brackets is designated  $T_{jk}$ , so that

$$T_{jk} = -\rho \iint_S n_j \left( i\omega_e - U_0 \frac{\partial}{\partial x} \right) \phi_k ds$$

and

$$F_{Rj} = \sum_{k=1}^6 T_{jk} \bar{\eta}_k e^{i\omega_e t} \quad (126)$$

where  $T_{jk} \bar{\eta}_k$  is the complex amplitude of the hydrodynamic force in the  $j$ th direction due to forced motion in the  $k$ th direction.

**1. Exciting forces.** The exciting force amplitudes given in Equations (125b) and (125c) are the forces and moments that *excite* the motions of the vessel.  $F_j^I$  results from the integration over the body surface of the pressure which would exist in the wave system if the body were not present. This component is easily calculated since no hydrodynamic problem need be solved. The incident wave potential is known and only needs to be integrated over the body surface.  $F_j^I$  is usually called the Froude-Krylov exciting force after the classical work on ship rolling done by Froude (1861), and generalized to 6 degrees of freedom (Krylov, 1898). They were the first to make the approximation of using only the incident wave potential in computing the total exciting force. The Froude-Krylov approximation increases in accuracy as the wavelength

of the incident waves increases relative to the body dimensions. For short wave-lengths the diffraction potential cannot be neglected; in the limit of very short waves the total exciting force is approximately doubled over the Froude-Krylov approximation.

The second component of the exciting force,  $F_j^D$ , is caused by the diffraction of the incident waves due to the presence of the vessel. Mathematically the diffraction potential is necessary so that the combination of  $(\phi_I + \phi_D)$  meets the body boundary condition. In fact, it can be shown that  $F_j^D$  can be determined without ever solving for  $\phi_D$  (Newman, 1977). Because  $\phi_I$  and  $\phi_D$  solve very similar mathematical problems, the Green theorem and the body boundary condition can be used to derive the so-called *Haskind Relations*. These relations relate the diffraction exciting force to the incident wave and radiation potentials. They allow the computation of  $F_j^D$  without having to solve for the diffraction potential. This is important because it means substantial savings in computer time for ship motion programs. The development of strip theory in the next subsection will make use of the Haskind Relations.

**2. Radiation forces.** The final components of the unsteady hydrodynamic force are the radiation forces,  $F_{R_j}$ . These forces result from the *radiation* of waves away from a vessel that is forced to oscillate in the  $k$ th mode of motion in otherwise calm water. The term  $T_{jk}$  in Equation (125d) is seen to represent the hydrodynamic force on the vessel in the  $j$ th direction due to unit amplitude motion in the  $k$ th direction. It is effectively a transfer function from unit motion in the  $k$ th mode to hydrodynamic force in the  $j$ th mode. The real and imaginary parts of  $T_{jk}$  are usually separated as

$$T_{jk} = \omega_e^2 A_{jk} - i\omega_e B_{jk} \quad (127)$$

From Equation (125c),

$$F_{R_j} = \sum_{k=1}^6 (\omega_e^2 A_{jk} - i\omega_e B_{jk}) \bar{\eta}_k e^{i\omega_e t} \quad (128)$$

where

$A_{jk}$  is the added mass in the  $j^{\text{th}}$  mode due to unit motion in the  $k^{\text{th}}$  direction,  $Re(T_{jk}/\omega_e^2)$ .

$B_{jk}$  is the damping coefficient in the  $j^{\text{th}}$  mode due to unit motion in the  $k^{\text{th}}$  direction,  $Im(-T_{jk}/\omega_e)$ .

The products  $\omega_e^2$  and  $-i\omega_e$  are included in the definition of  $A_{jk}$  and  $B_{jk}$  for convenience when the terms are substituted back into the equations of motion. The names *added mass* and *damping* are chosen because of the physical significance the terms have in the equations of motion. As we shall see, the real part of the hydrodynamic force due to forced motion is in phase with the acceleration. Thus it acts as an apparent mass, adding to the mass of the body. Likewise, the damping term is the hydrodynamic force on the body that is in

phase with the velocity. It should also be noted that in general the added mass and damping are functions of frequency.

Various techniques have been developed to compute the exciting forces and the added mass and damping. In the next sub-section the strip theory technique will be discussed.

(c) *Linearized equations of motion.* The expressions for all the different forces can now be substituted back into the equations of motion (109).  $\ddot{\eta}_k$  can be expressed, from (110), as

$$\ddot{\eta}_k = -\omega_e^2 \bar{\eta}_k e^{i\omega_e t}$$

Taking account of the various force components developed in the preceding paragraphs, the right-hand side becomes

$$\begin{aligned} \mathbf{F}_j &= F_{G_j} + F_{H_j} = F_{G_j} + (F_{HS_j} + F_{HD_j}) \\ &= (F_{G_j} + F_{HS_j}) + (F_{EX_j} + F_{R_j}) \quad (129) \\ &= F_{HS_j}^* + F_{EX_j} + F_{R_j} \end{aligned}$$

Equation (109) then becomes

$$\mathbf{F}_j = \sum_{k=1}^6 -\omega_e^2 \Delta_{jk} \bar{\eta}_k e^{i\omega_e t} = F_{HS_j}^* + F_{EX_j} + F_{R_j} \quad j = 1, 2, \dots, 6 \quad (130)$$

Replacing  $F_{HS_j}^*$ ,  $F_{EX_j}$  and  $F_{R_j}$  by their components, given in (117), (125), and (128), gives

$$\begin{aligned} \sum_{k=1}^6 -\omega_e^2 \Delta_{jk} \bar{\eta}_k e^{i\omega_e t} &= -\sum_{k=1}^6 C_{jk} \bar{\eta}_k e^{i\omega_e t} + F_j^I e^{i\omega_e t} \\ &+ F_j^D e^{i\omega_e t} + \sum_{k=1}^6 (\omega_e^2 A_{jk} - i\omega_e B_{jk}) \bar{\eta}_k e^{i\omega_e t} \quad (131) \end{aligned}$$

Finally the hydrostatic restoring forces, the added mass, and damping terms are all brought to the left-hand side of the equations and the  $e^{i\omega_e t}$  are eliminated to yield the governing equations:

$$\begin{aligned} \sum_{k=1}^6 [-\omega_e^2 (\Delta_{jk} + A_{jk}) + i\omega_e B_{jk} + C_{jk}] \bar{\eta}_k \\ = F_j^I + F_j^D \quad j = 1, 2, \dots, 6 \quad (132) \end{aligned}$$

The right-hand side,  $F_j^I + F_j^D$ , represents the two components of the exciting force amplitude, as defined in Equation (125).

Equations (132) are the linearized equations of motion for an unrestrained vessel in sinusoidal waves. There are six coupled, linear equations for the six unknown complex amplitudes,  $\bar{\eta}_k$ . The mass matrix  $(\Delta_{jk})$  is given in Equation (108). The hydrostatic restoring force coefficient matrix  $(C_{jk})$  is presented in (117). The coefficients for added mass  $(A_{jk})$ , damping

$(B_{jk})$  and the exciting force complex amplitudes  $(\bar{F}_j^I, \bar{F}_j^D)$  are found by evaluating the integrals in Equations (125), (126) and (128). The evaluation requires the solution of the radiation and diffraction problems, and in the next subsection a strip theory to solve these problems will be discussed.

The equations of motion (132) look very similar to the equations of motion for a spring-mass-damper system with six degrees of freedom. There are mass terms  $(\Delta_{jk} + A_{jk})$ , damping terms  $(B_{jk})$  and spring constants  $(C_{jk})$  on the left-hand side. The exciting forces  $(\bar{F}_j^I + \bar{F}_j^D)$  are on the right-hand side. The cross-coupling between the modes results from the terms where  $j$  is not equal to  $k$ . The cross-coupling may be large or small depending on the modes of motion and the geometry of the vessel.

As previously noted, the principal difference between the equations of motion (132) and the simple spring-mass-damper system is that the coefficients  $A_{jk}$ ,  $B_{jk}$ ,  $F_j^I$ ,  $F_j^D$  are all *functions of frequency*. For the typical spring-mass-damper they are all constants. The frequency dependence of the coefficients in the equations of motion is the reason we cannot write the equations of motion in their usual differential equation form. Essentially we are solving the equations in the frequency domain where the coefficients are constant for a given frequency.

The mass term contains both the natural mass (or moments of inertia) of the vessel and the hydrodynamic added mass. The damping term is the result of wave damping of the free surface. The effects of viscous damping have been neglected; but if the incorporation of an equivalent viscous damping is necessary, it can be added to the  $B_{jk}$  term. Finally the spring constant terms are the result of the hydrostatic restoring forces and are proportional to the waterplane area. For modes of motion in which there are no hydrostatic restoring forces, the spring constant terms are zero. For example, the spring constant term in yaw ( $C_{66}$ ) is zero.

For an arbitrarily shaped vessel the six equations of motion must be solved simultaneously. However, for the case of an unrestrained ship with port/starboard symmetry the six equations in (132) may be uncoupled into two sets of three equations. The vertical-plane or longitudinal motions (surge, heave and pitch) are uncoupled from the horizontal-plane or transverse motions (sway, roll, and yaw). To see this we note that the cross coupling values of  $\Delta_{jk}$  and  $C_{jk}$  are zero if  $j = 1, 3, 5$  and  $k = 2, 4, 6$  or vice versa (for example,  $C_{12} = M_{36} = M_{63} = C_{43} \equiv 0$ ). As can be seen by examining Equations (125c) and (127), the same is true for  $A_{jk}$  and  $B_{jk}$ . For example,  $A_{23}$  and  $B_{23}$  are the added mass and damping in sway due to heave. From (125c) and (127) we have

$$\omega_e^2 A_{23} - i\omega_e B_{23}$$

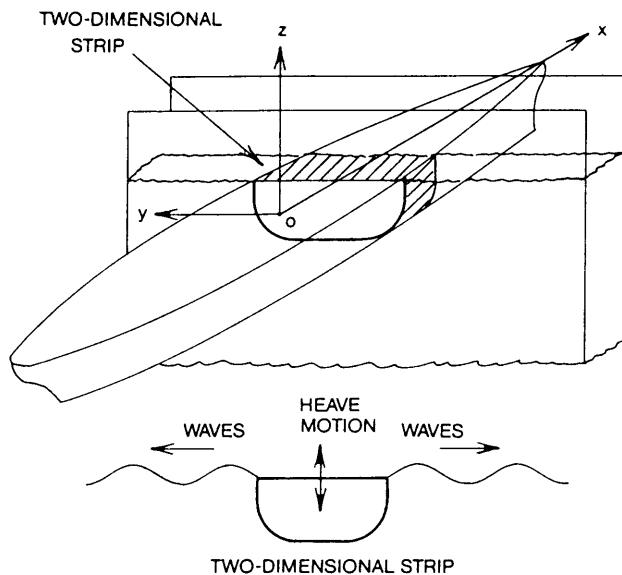


Fig. 39 Two-dimensional strip in heave

$$= -\rho \iint n_2 \left( i\omega_e - U_0 \frac{\partial}{\partial x} \right) \phi_3 ds \equiv 0 \quad (133)$$

The right-hand side equals zero because  $n_2$  is an odd function of the port and starboard sides while  $\phi_3$  is an even function. Consequently the integral over the entire hull surface must equal zero. Physically, it means that there is no hydrodynamic force in the sway direction due to a heave motion.

It should be noted that the lack of coupling between the vertical and horizontal modes is a consequence of linear theory. In nonlinear theories such cross-coupling may be present. For some ship motion problems this nonlinear coupling can be very important. For example, there is a nonlinear heave-roll cross-coupling that can lead to roll instabilities and eventual ship capsizing (Kerwin, 1955) or (Ogilvie and Beck, 1973). Another example is the nonlinear pitch-yaw coupling that results from varying submergence of the bow due to pitch motion (Korvin-Kroukovsky, 1980).

It should also be pointed out that the final equations of motion (132) are valid as long as the vessel is in sinusoidal waves and the responses are linear. Using different hydrodynamic theories will lead to different values of the added mass, damping and exciting forces, but the form of the equations remains the same. The effects of mooring lines, anti-roll fins, rudder, etc. can be added to the equations of motion by modifying the appropriate coefficients. Whether or not the vertical and horizontal plane motions are then uncoupled will depend on the form of the coefficients.

Assuming values for all the coefficients ( $A_{jk}$ ,  $\Delta_{jk}$ ,  $B_{jk}$ ,  $C_{jk}$ ) and the exciting forces ( $F_j^I$ ,  $F_j^D$ ) are known, the equations of motion can be solved using standard



techniques for the solution of complex simultaneous equations. For heave and pitch motion alone in head seas, the solution was given in Section 3.2.

In the next sub-section a method to determine the coefficients and exciting forces is given.

**3.4 Strip Theory.** Obtaining numerical values for the complex motion amplitudes,  $\bar{\eta}_k$ , requires that values for the coefficients  $\Delta_{jk}$ ,  $A_{jk}$ ,  $B_{jk}$ ,  $C_{jk}$  and the exciting force amplitudes  $\bar{F}_j^I$ ,  $\bar{F}_j^D$  can be determined and the equations of motion solved. The mass matrix,  $\Delta_{jk}$ , and the hydrostatic restoring forces,  $C_{jk}$ , can be evaluated directly by Equations (108) and (117). The Froude-Krylov exciting force can also be found by a direct integration of the incident wave potential over the ship hull. The major difficulty in determining the ship motions is to perform the calculations needed to find the coefficients of added mass, damping and the diffraction exciting forces, which requires the solution of difficult hydrodynamic problems. In this subsection we shall discuss a *strip theory* to compute the hydrodynamic forces. In a subsequent subsection a brief discussion of other techniques to compute the coefficients will be given.

(a) *Background.* While the details of the mathematical formulation for strip theory are still being debated, the physical assumptions are relatively easy to describe. First, it must be assumed that the vessel is a slender body, (i.e., its beam and draft are much less than the length and changes in cross-section vary gradually along the length). Restricting the discussion to zero forward speed and high frequencies, we would find that the fluid flow velocities in the transverse direction are much greater than in the longitudinal direction. Consequently, as shown in Fig. 39, the flow field at any cross section of the ship may be approximated by the assumed two-dimensional flow in that *strip*. To obtain the total effect on the ship, the effects of all individual strips are integrated along the length. For example, the strip theory approximation for the heave added mass is

$$A_{33} = \int_L a_{33}(x) dx \quad (134)$$

where

$a_{33}(x)$  is the two-dimensional added mass.

$L$  denotes that the integration is taken over the ship length.

The sectional added mass,  $a_{33}$ , is found by solving the two-dimensional hydrodynamic problem shown in Fig. 39. The essence of strip theory is thus to reduce a three-dimensional hydrodynamic problem to a series of two-dimensional problems which are easier to solve.

For low frequencies and vessels with high forward speed the strip theory approximation is no longer straightforward and different initial assumptions lead to different formulations. Newman (1978) gives a com-

plete history of the development of theoretical methods to predict ship motions in regular waves.

The previously mentioned Korvin-Kroukovsky and Jacobs (1957) strip theory has been modified and extended by many researchers. The most notable is probably the work of Gerritsma and Beukelman (1967). Their coefficients have been used extensively for the verification of strip theory against experimental results (Gerritsma and Beukelman, 1966), (Smith, 1967), (Salvesen and Smith, 1970), (Smith and Salvesen, 1969, 1970) and (Loukakis, 1971).

Even though the strip theories of Korvin-Kroukovsky and others have given reasonable comparisons with experiments, they were not entirely satisfactory. In general they were valid only for head seas. Furthermore, the forward-speed terms in the coefficients of the equations of motion did not satisfy the symmetry relations of Timman and Newman (1962). The Timman-Newman relations state that in a linear ship-motion theory the cross-coupling coefficients between the various modes of motion have certain symmetry properties. If a linear ship-motion theory does not have these symmetry properties, it must be in error. For these reasons, work has continued into the development of strip theories in order to give them a sounder mathematical foundation and more general applicability.

Ogilvie and Tuck (1969) (cf. Ogilvie, 1977) have performed a mathematically consistent analysis using slender-body theory. Their analysis reveals that the leading order terms involve only the zero-speed pure strip-theory coefficients. The effects of forward speed are of a slightly higher order and are present only in the cross-coupling coefficients. The cross-coupling coefficients include a term that is linearly proportional to  $U_0$  but involves the square of the potential over the free surface. These integral terms make the Ogilvie-Tuck coefficients impractical for routine calculations. Wang (1976) has re-derived the results from an energy analysis and Troesch (1981) has extended the analysis to horizontal-plane motions. Computations by Faltinsen (1975) and Troesch (1981) show improved agreement of the resulting cross-coupling coefficients with experiments. The net effect of the integral terms on the predictions of ship motions is not established. However, Ogilvie (1977) reports that the use of the complete Ogilvie-Tuck coefficients in a normal strip-theory computer program tends to worsen the predictions of the pitch and heave motions. This indicates that there must be other errors in the strip-theory approach; presumably in the exciting force terms.

There are several analyses that are not as rigorous as the Ogilvie-Tuck approach, but which are based on a stronger mathematical foundation than the original Korvin-Kroukovsky theory. The works of Salvesen, Tuck and Faltinsen (1970), Söding (1969), Tasai and Takaki (1969) and Borodai and Netsvetayev (1969) were all developed independently and at about the same time. Newman (1977) gives only results for heave

and pitch motions in head seas. His added mass and damping coefficients are the same as Salvesen, et al (1970), but the exciting forces are computed using two-dimensional results at the absolute wave frequency, rather than the frequency of encounter. All the methods are quite similar and the Salvesen, et al (1970), approach seems to have gained the widest acceptance. Therefore, it will be followed in this section.

The derivation of strip theory can be found in Appendix 1 of Salvesen, Tuck and Faltinsen (1970) and will not be reproduced here. In the summary of the theory that follows, two aspects of that original derivation will be modified. The first modification is the elimination of the transom stern corrections. These corrections result when Stokes' theorem is applied to underwater hull forms that are abruptly terminated. However, it has been found in practice that the ship motion predictions are usually better if the transom stern corrections are omitted. This is consistent with the Standard Ship Motion Program used by the U.S. Navy (Meyers, Applebee and Baitis, 1981).

The second modification concerns the surge degree of freedom. Salvesen, et al (1970) included surge motion only up to the point in their analysis where the hydrodynamic forces associated with surge become of a higher order. Various experiments have shown that the cross-coupling between surge motion and the other modes is normally small. As a result, it is usually neglected. However, surge is becoming more critical for certain specific problem areas, such as refueling at sea, towing in a seaway or broaching. More research into surge motion needs to be done; particularly into the coupling between the response of the propeller and the unsteady wake caused by the surge. Meanwhile, in the discussion that follows, the surge degree of freedom has been included by a straight-forward extension of the method of Salvesen, et al (1970).

(b) *Radiation problem.* To find the added mass and damping coefficients ( $A_{jk}$  and  $B_{jk}$ ), it should be recalled from Equations (125c) and (128) that they are defined by the complex force coefficient,

$$\begin{aligned} T_{jk} &= \omega_e^2 A_{jk} - i\omega_e B_{jk} \\ &= -\rho \iint n_j \left( i\omega_e - U_0 \frac{\partial}{\partial x} \right) \phi_k ds \end{aligned} \quad (135)$$

The determination of  $T_{jk}$  requires solving a boundary value problem for  $\phi_k$  and then integrating over the hull surface.

The radiation potentials,  $\phi_k$ , are the solution to the Laplace equation subject to boundary conditions on the hull surface, on the free surface and at infinity. The boundary condition on the hull is

$$\frac{\partial \phi_k}{\partial n} = i\omega_e n_k + U_0 m_k \quad k = 1, 2, 3, \dots, 6 \quad (136)$$

where

$n_k$  (or  $n_j$ ) is the generalized unit normal into the hull discussed later.

$m_k$  is the generalized vector involving the gradient of the forward speed potential.

The  $m_k$  vector is often approximated (as it is in Salvesen, et al, 1970) by

$$m_k \approx (0, 0, 0, 0, n_3, -n_2) \quad (137)$$

This approximation greatly simplifies the calculation but results in the loss of some forward speed effects.

On the free surface,  $\phi_k$  must satisfy the linearized free surface boundary condition

$$\left( i\omega_e - U_0 \frac{\partial}{\partial x} \right)^2 \phi_k + g \frac{\partial}{\partial z} \phi_k = 0 \text{ on } z = 0 \quad (138)$$

At infinity, the boundary conditions require that the gradient of  $\phi_k$  go to zero and that there be only outgoing waves. As discussed in Subsection 3.6, there are numerical methods to solve directly the complete three-dimensional problem for  $\phi_k$ , but they require a large computational effort. In strip theory, the mathematical problem for  $\phi_k$  is reduced to a series of simpler two-dimensional problems.

The body boundary condition, Equation (136) leads to two separate components for  $\phi_k$ , one meeting the  $n_k$  terms and the other the  $m_k$  terms. These components both satisfy the same boundary conditions on the free surface and at infinity. If the simplified form for the  $m_k$  terms (137) is used, then the two components are directly related since they solve the equivalent boundary value problems. In particular, Salvesen, et al show that

$$\begin{aligned} \phi_k &= \phi_k^0 \quad k = 1, 2, 3, 4 \\ \phi_5 &= \phi_5^0 + (U_0 / i\omega_e) \phi_3^0 \\ \phi_6 &= \phi_6^0 - (U_0 / i\omega_e) \phi_2^0 \end{aligned} \quad (139)$$

where  $\phi_k^0$  is a potential that satisfies the Laplace equation in the fluid domain, the conditions at infinity, the free surface boundary conditions Equation (138) and the condition on the hull surface,

$$\frac{\partial \phi_k^0}{\partial n} = i\omega_e n_k \quad (140)$$

Salvesen, et al then define a complex force coefficient based on  $\phi_k^0$  as

$$T_{jk}^0 = -\rho i\omega_e \iint n_j \phi_k^0 ds \quad (141)$$

The force coefficient of the added mass and damping,  $T_{jk}$  (135), may now be simplified using the expressions in (139) for  $\phi_k$  in terms of  $\phi_k^0$  and (141) for  $T_{jk}^0$ . The derivative with respect to  $x$  in (135) is eliminated using a variant of Stokes' theorem developed by Ogilvie and Tuck (1969). The final results in Salvesen are

$$T_{jk} = T_{jk}^0 \quad j, k = 1, 2, 3, 4 \quad (142)$$

For  $j = 5, 6$  and  $k = 1, 2, 3, 4$

$$T_{5k} = T_{5k}^0 - \frac{U_0}{i\omega_e} T_{3k}^0 \quad (143)$$

$$T_{6k} = T_{6k}^0 + \frac{U_0}{i\omega_e} T_{2k}^0$$

For  $j = 1, 2, 3, 4$  and  $k = 5, 6$

$$T_{j5} = T_{j5}^0 + \frac{U_0}{i\omega_e} T_{j3}^0 \quad (144)$$

$$T_{j6} = T_{j6}^0 - \frac{U_0}{i\omega_e} T_{j2}^0$$

And finally for  $j = k = 5, 6$

$$T_{55} = T_{55}^0 + \frac{U_0^2}{\omega_e^2} T_{33}^0 \quad (145)$$

$$T_{66} = T_{66}^0 + \frac{U_0^2}{\omega_e^2} T_{22}^0$$

At this point in the analysis, the slender body approximation and the linearization have allowed all the  $T_{jk}$  to be written in terms of  $T_{jk}^0$ . Further progress towards a strip theory requires that a means of evaluating  $T_{jk}^0$  in terms of two-dimensional sectional properties be found. The first step is to note that if the vessel is slender, then it is consistent with the previous assumptions to set  $ds = dl dx$  in the surface integrals so that

$$T_{jk}^0 = -\rho i \omega_e \int_L \int_{C_x} n_j \phi_k^0 dl dx \quad (146)$$

where the line integral in  $dl$  is around the section contour  $C_x$ , and the integral in  $dx$  is along the ship length  $L$ .

If the integrand in Equation (146) can be written in terms of two-dimensional section properties, then a strip theory will result. The potential  $\phi_k^0$  satisfies the three-dimensional Laplace equation subject to the body-boundary condition, the free surface boundary condition and the conditions at infinity. Several assumptions are used in order to allow  $n_j \phi_k^0$  to be replaced by its two-dimensional equivalent at each section. First, the slender-body approximation states that the derivatives in the longitudinal direction ( $x$ -direction) are small relative to the derivatives in the transverse ( $y$ - or  $z$ -) directions. This allows the Laplace equation to be reduced to the two-dimensional Laplace equation in the  $y$ - $z$ , or cross-flow plane. The radiation condition remains that there be outgoing waves at infinity.

The free surface boundary condition, Equation (138)

is reduced by assuming that  $U_0 \frac{\partial}{\partial x}$  is much smaller than  $\omega_e$ . This is equivalent to assuming that the frequency of encounter is large or that the wavelength is of the same order of magnitude as the beam. This assumption is critical for it makes strip theory a high frequency theory; at low frequencies, or long wave lengths, a different theory results. Newman's (1978) unified theory is an attempt to combine high and low-frequency theories.

The body-boundary condition is simplified by noting that for a slender body derivatives in the longitudinal direction are much smaller than in the transverse direction. The three-dimensional unit normals into the hull are defined as

$$\underline{n} = \nabla (b(x, z) \mp y) / |\nabla (b(x, z) \mp y)| \quad (147)$$

where  $y = \pm b(x, z)$  is the equation of the hull surface, and  $b(x, z)$  is the half beam, and  $\nabla$  is here the gradient differential operator.

For a slender body  $\frac{\partial b}{\partial x} \ll 1$ ;  $\frac{\partial b}{\partial z}$ , and the unit normals may be approximated by their two-dimensional equivalents,  $N_j$ :

$$n_1 \approx N_1 = \frac{\partial b}{\partial x} / \sqrt{1 + \left(\frac{\partial b}{\partial z}\right)^2} \quad (148a)$$

$$n_2 \approx N_2 = \mp 1 / \sqrt{1 + \left(\frac{\partial b}{\partial z}\right)^2} \quad (148b)$$

$$n_3 \approx N_3 = \frac{\partial b}{\partial z} / \sqrt{1 + \left(\frac{\partial b}{\partial z}\right)^2} \quad (148c)$$

Note that  $N_1$  is much smaller than  $N_2$  or  $N_3$ . Furthermore,  $N_1$  is usually much more difficult to compute than  $N_2$  or  $N_3$ . The hull offsets are normally entered into a computer on a station-by-station basis. Numerically, the computation of  $\frac{\partial b}{\partial z}$  is thus much easier than

$\frac{\partial b}{\partial x}$ , but in principle  $N_1$  can be computed at the same time that  $N_2$  and  $N_3$  are determined.

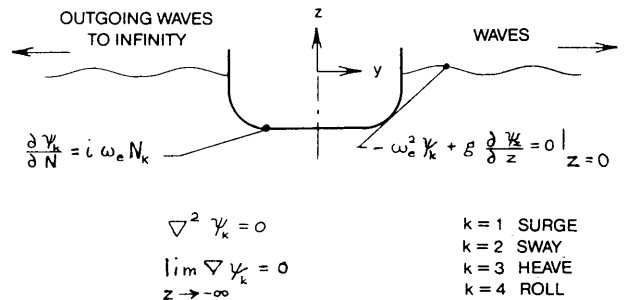


Fig. 40 Two-dimensional problem for  $\psi_k$

Table 13—Coefficients in Equations of Motion

## Vertical Mode

$$A_{11} = \int a_{11} dx$$

$$A_{13} = \int a_{13} dx$$

$$A_{31} = A_{13}$$

$$B_{11} = \int b_{11} dx$$

$$B_{13} = \int b_{13} dx$$

$$B_{31} = B_{13}$$

$$A_{15} = - \int x a_{13} dx - \frac{U_0}{\omega_e^2} B_{13}$$

$$B_{15} = - \int x b_{13} dx + U_0 A_{13}$$

$$A_{51} = - \int x a_{13} dx + \frac{U_0}{\omega_e^2} B_{31}$$

$$B_{51} = - \int x b_{31} dx - U_0 A_{13}$$

$$A_{33} = \int a_{33} dx$$

$$B_{33} = \int b_{33} dx$$

$$A_{35} = - \int x a_{33} dx - \frac{U_0}{\omega_e^2} B_{33}$$

$$B_{35} = - \int x b_{33} dx + U_0 A_{33}$$

$$A_{53} = - \int x a_{33} dx + \frac{U_0}{\omega_e^2} B_{33}$$

$$B_{53} = - \int x b_{33} dx - U_0 A_{33}$$

$$A_{55} = \int x^2 a_{33} dx + \frac{U_0^2}{\omega_e^2} A_{33}$$

$$B_{55} = \int x^2 b_{33} dx + \frac{U_0^2}{\omega_e^2} B_{33}$$

$$C_{33} = \int c_{33} dx = \rho g \int B(x) dx$$

$$C_{35} = C_{53} = - \int x c_{33} dx = -\rho g \int x B(x) dx$$

$$C_{55} = \rho g \nabla \overline{GM}_L + LCF^2 C_{33}$$

$$\approx \int x^2 c_{33} dx = \rho g \int x^2 B(x) dx$$

$$A_{44} = \int a_{44} dx$$

$$A_{46} = \int x a_{24} dx + \frac{U_0}{\omega_e^2} B_{24}$$

$$B_{22} = \int b_{22} dx$$

$$B_{24} = B_{42} = \int b_{24} dx$$

$$B_{26} = \int x b_{22} dx - U_0 A_{22}$$

$$B_{44} = \int b_{44} dx + B_e = B_{44}^*$$

$$B_{46} = \int x b_{24} dx - U_0 A_{24}$$

$$A_{62} = \int x a_{22} dx - \frac{U_0}{\omega_e^2} B_{22}$$

$$B_{62} = \int x b_{22} dx + U_0 A_{22}$$

$$A_{64} = \int x a_{24} dx - \frac{U_0}{\omega_e^2} B_{24}$$

$$B_{64} = \int x b_{24} dx + U_0 A_{24}$$

$$A_{66} = \int x^2 a_{22} dx + \frac{U_0^2}{\omega_e^2} A_{22}$$

$$B_{66} = \int x^2 b_{22} dx + \frac{U_0^2}{\omega_e^2} B_{22}$$

$$C_{44} \approx \rho g \nabla \overline{GM}_T$$

All integrals are taken over the ship length.

The generalized normals for  $k = 4, 5, 6$  can likewise be approximated by their two-dimensional equivalents,

$$\begin{aligned} n_4 &= yn_3 - zn_2 \\ &\approx N_4 \\ &= \left( y \frac{\partial b}{\partial z} + z \right) / \sqrt{1 + \left( \frac{\partial b}{\partial z} \right)^2} \end{aligned} \quad (149a)$$

$$\begin{aligned} n_5 &= zn_1 - xn_3 \\ &\approx -xN_3 \end{aligned} \quad (149b)$$

$$\begin{aligned} n_6 &= xn_2 - yn_1 \\ &\approx +xN_2 \end{aligned} \quad (149c)$$

It was at this point in the analysis by Salvesen, et al (1970) that the surge degree of freedom was eliminated by arguing that  $N_1 \ll N_k$ ,  $k = 2, 3 \dots 6$ .

## Horizontal Mode

$$A_{22} = \int a_{22} dx$$

$$A_{24} = A_{42} = \int a_{24} dx$$

$$A_{26} = \int x a_{22} dx + \frac{U_0}{\omega_e^2} B_{22}$$

The approximations just described allows the potentials  $\phi_k^0$  and the line integrals in Equation (146) to be found in terms of the solutions to a series of two-dimensional problems at various stations along the length of the ship. They consist of solving the two-dimensional Laplace equation subject to a normal boundary condition on the body, a free-surface condition, and conditions at infinity. As shown in Fig. 40, let  $\psi_k$ ,  $k = 1, 2, 3, 4$ , be the solution to this two-dimensional problem. For sway, heave and roll,  $\psi_k$  is the velocity potential for a cylinder with a cross-sectional shape equal to the ship section shape, oscillating on the free surface in the appropriate mode of motion.

At a given cross section the approximation is thus made that

$$\phi_k^0 \approx \psi_k \quad k = 1, 2, 3, 4 \quad (150)$$

It also follows from Equation (149b,c) and the body boundary condition that

$$\begin{aligned} \phi_5^0 &\approx -x \psi_3 \\ \phi_6^0 &\approx +x \psi_2 \end{aligned} \quad (151)$$

The solution of the  $\psi_k$  problem is difficult and requires the major portion of the running time in a strip-theory computer program. Some of the techniques for solving the  $\psi_k$  problem are mentioned in Subsection 3.5, along with the experimental determination of coefficients.

The section-wise approximations for  $\phi_k^0$  given in (150) and (151) may be substituted into Equation (146) to evaluate the line integral at each cross section.  $T_{jk}^0$  is then found by a simple integration along the ship length. However, since we first want the values of the coefficients  $a_{jk}$ ,  $b_{jk}$  and eventually  $A_{jk}$  and  $B_{jk}$ , it will be convenient to define the following sectional added mass and damping coefficients:

$$\begin{aligned} \omega_e^2 a_{jj} - i\omega_e b_{jj} &= -\rho i\omega_e \int_{Cx} N_j \psi_j dl \\ j &= 1, 2, 3, 4 \\ \omega_e^2 a_{13} - i\omega_e b_{13} &= \omega_e^2 a_{31} - i\omega_e b_{31} \\ &= -\rho i\omega_e \int_{Cx} N_1 \psi_3 dl \\ \omega_e^2 a_{24} - i\omega_e b_{24} &= \omega_e^2 a_{42} - i\omega_e b_{42} \\ &= -\rho i\omega_e \int_{Cx} N_2 \psi_4 dl \end{aligned} \quad (152)$$

where  $N_j$  are the 2-dimensional unit normals and  $\psi_j$  are the 2-dimensional velocity potentials previously discussed.

The added mass and damping coefficients are found

Table 14—Summary of Exciting Forces

$$F_{EX_j} = (F_j^I + F_j^D)e^{i\omega_e t}$$

$F_j^I$  is the Froude-Krylov Exciting Force amplitude

$F_j^D$  is the Diffraction Exciting Force amplitude

$$F_j^I = \int_L e^{-ikx \cos \mu} f_j(x) dx$$

$$j = 1, 2, 3, 4$$

$$F_5^I = - \int_L e^{-ikx \cos \mu} x f_3(x) dx$$

$$F_6^I = \int_L e^{-ikx \cos \mu} x f_2(x) dx$$

$f_j(x)$  are the sectional Froude-Krylov exciting force amplitudes

$$= \rho g \bar{\zeta} \int_{C_x} N_j e^{-iky \sin \mu} e^{kz} dl$$

$$j = 1, 2, 3, 4$$

$$F_j^D = \int_L e^{-ikx \cos \mu} h_j(x) dx \quad j = 1, 2, 3, 4$$

$$F_5^D = - \int_L e^{-ikx \cos \mu} \left( x + \frac{U_0}{i\omega_e} \right) h_3(x) dx$$

$$F_6^D = + \int_L e^{-ikx \cos \mu} \left( x + \frac{U_0}{i\omega_e} \right) h_2(x) dx$$

$h_j(x)$  are the sectional diffraction exciting force amplitudes

$$= \rho \bar{\zeta} \omega_0 \int_{C_x} (iN_3 + N_1 \cos \mu + N_2 \sin \mu) e^{-iky \sin \mu} \times e^{kz} \psi_j(y, z) dl \quad j = 1, 2, 3, 4$$

by recalling that  $\omega_e^2 A_{jk} - i\omega_e B_{jk} = T_{jk}$  and using the relations listed in Equations (142) through (152). The final results for the vertical and horizontal modes of a ship with port/starboard symmetry are given in Table 13. For convenience the values of  $C_{jk}$  are also listed. All coefficients not given are assumed to be zero.

It should be noted that the relations in Table 13 were derived on the basis of small motions. It is shown in Chapter II, for example, how the simple expression for  $C_{44}$  breaks down at large roll angles.

The cross-coupling coefficients between surge and heave and pitch shown in Table 13 are typically very small. The Standard Ship Motion program of the U.S. Navy (Meyers, Applebee, Baitis, (1981) sets the coefficients  $A_{13}$ ,  $A_{31}$ ,  $A_{15}$ ,  $A_{51}$ ,  $B_{13}$ ,  $B_{31}$ ,  $B_{15}$ ,  $B_{51}$  equal to zero, but there are indications that this simplification may not always be justified.

In Table 13 the term  $B_e$  added to the  $B_{44}$  coefficient signifies the additional damping that must be added to the strip theory result to give good predictions of

roll motion. Strip theory only predicts the inviscid wave damping acting on a vessel. Because roll wave generation is lightly damped, the other components of damping from viscous effects and lifting effects on the appendages are equally as important as the wave damping. In addition, the other horizontal mode coefficients may also have to be modified for the lifting effects of appendages. A discussion of the roll damping and appendage lifting effects will be given in Subsection 3.8, where  $B_{44}^*$  is defined as the complete equivalent linear damping coefficient.

(c) *Excitation.* The complex exciting force and moment amplitudes are found by evaluating Equations (125a) and (125b). To find the Froude-Krylov exciting force Equation (125a) the wave potential  $\phi_I$  is used, where  $\phi_I = (ig\bar{\zeta}/\omega_0) e^{-ik(x \cos \mu + y \sin \mu)} e^{kz}$ . Thus, the Froude-Krylov exciting force in the  $j^{\text{th}}$  direction,  $F_j^I$ , is found as

$$F_j^I = -\rho \iint n_j \left( i\omega_e - U_0 \frac{\partial}{\partial x} \right) \left( \frac{ig\bar{\zeta}}{\omega_0} e^{-ik(x \cos \mu + y \sin \mu)} e^{kz} \right) ds \quad (153)$$

$$\simeq +\rho g \bar{\zeta} \int_L dx e^{-ikx \cos \mu} \int_{C_x} n_j e^{-ky \sin \mu} e^{kz} dl$$

where use has been of the frequency of encounter relation,  $\omega_e = \omega_0 - k U_0 \cos \mu$ , and the slender-body approximation.

The line integral about the station in Equation (153) can be evaluated cross section by cross section. Using the slender-body approximations to the unit normals, Equations (148), (149) allow us to define the *sectional Froude-Krylov exciting force* amplitude,

$$f_j(x) = \rho g \bar{\zeta} \int_{C_x} N_j e^{-iky \sin \mu} e^{kz} dl \quad j = 1, 2, 3, 4 \quad (154)$$

In this case, the Froude-Krylov exciting force amplitudes become

$$F_j^I = \int_L e^{-ikx \cos \mu} f_j(x) dx \quad j = 1, 2, 3, 4$$

$$F_5^I = - \int_L e^{-ikx \cos \mu} x f_3(x) dx \quad (155)$$

$$F_6^I = \int_L e^{-ikx \cos \mu} x f_2(x) dx$$

The computation of the diffraction exciting forces,  $F_j^D$ , is more difficult because the diffraction potential,  $\phi_D$ , is unknown. However, since  $\phi_D$  and  $\phi_I$  satisfy very

similar boundary value problems, it is possible through the use of the Green theorem and the boundary conditions of the problem to find expressions for the diffraction exciting forces which involve only  $\phi_I$  and  $\phi_j$ . This interchange is known as the *Haskind relations*, and a complete discussion may be found in Newman (1965).

After eliminating  $\phi_D$  by using the Haskind relations, the resulting expressions are reduced to sectional calculations in a manner similar to that used for the Froude-Krylov exciting forces. Salvesen, et al, (1970), define the *sectional diffraction exciting force* amplitudes as,

$$h_j(x) = \rho \bar{\zeta} \omega_0 \int_{C_x} (iN_3 + N_1 \cos \mu + N_2 \sin \mu) \times e^{-iky \sin \mu} e^{kz} \psi_j(y, z) dl \quad j = 1, 2, 3, 4 \quad (156)$$

Integrating the sectional diffraction force along the ship length results in the following expression for the wave diffraction exciting force:

$$F_j^D = \int_L e^{-ikx \cos \mu} h_j(x) dx \quad j = 1, 2, 3, 4 \quad (157a)$$

$$F_5^D = - \int_L e^{-ikx \cos \mu} \left( x + \frac{U_0}{i\omega_e} \right) h_3(x) dx \quad (157b)$$

$$F_6^D = + \int_L e^{-ikx \cos \mu} \left( x + \frac{U_0}{i\omega_e} \right) h_2(x) dx \quad (157c)$$

A summary of the exciting forces for all six degrees of freedom is given in Table 14. Typical experimental and theoretical values are discussed in Section 3.5.

It should be noted that in the case of only pitch and heave motions in head seas ( $\mu = 180$  deg) the exciting forces can be further simplified. For head seas the sectional diffraction force can be written as:

$$h_3(x) = \rho \bar{\zeta} \omega_0 \int_{C_x} (iN_3 - N_1) e^{kz} \psi_3(y, z) dl \quad (158)$$

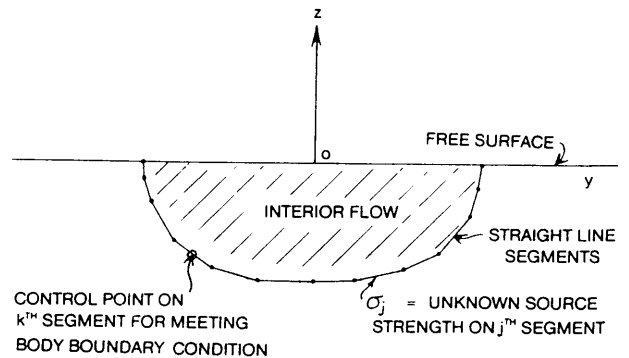


Fig. 41 Sectional approximation for Frank's method

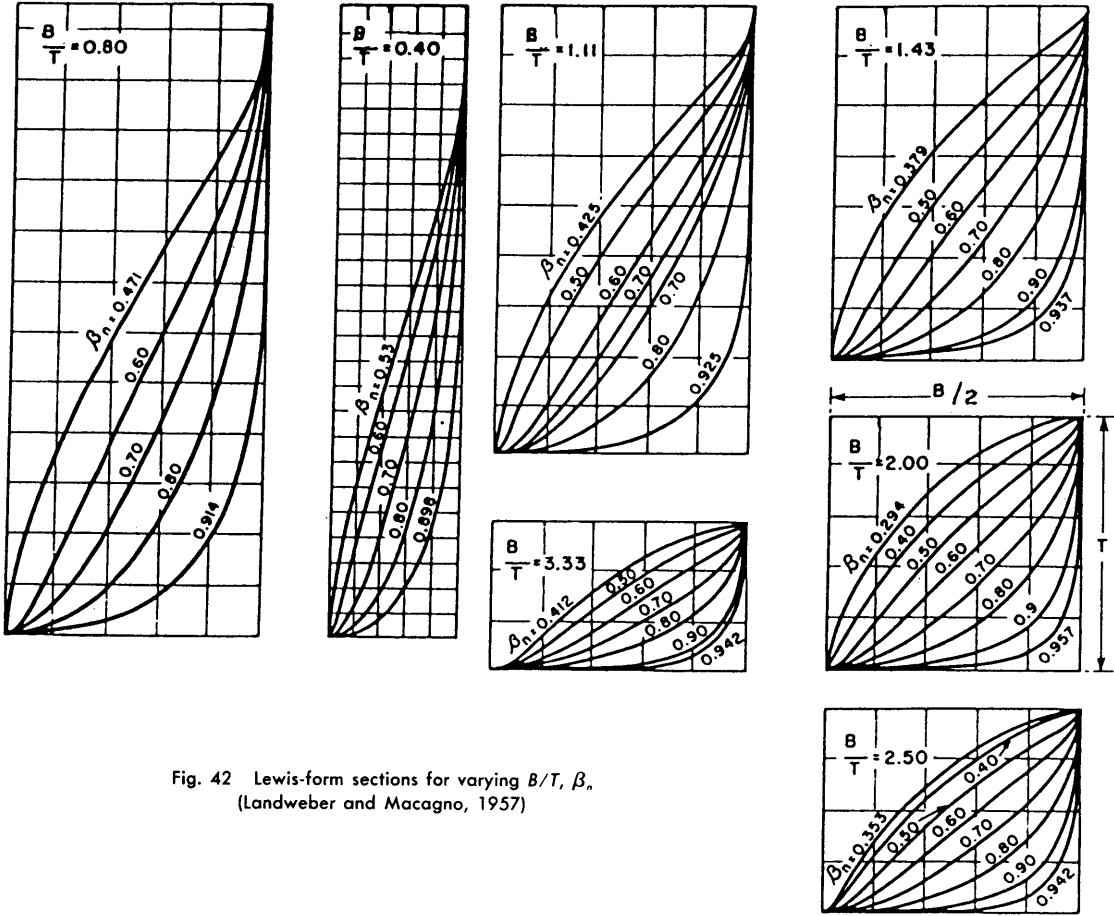


Fig. 42 Lewis-form sections for varying  $B/T$ ,  $\beta_n$   
(Landweber and Macagno, 1957)

The term  $(iN_3 - N_1)$  can be simplified to  $iN_3$  because the contribution to the value of the integral from the  $N_3$  term is much greater than the  $N_1$  term. Furthermore the exponential term is taken outside the integral by replacing  $e^{kz}$  with  $e^{-kT^*}$ , where  $T^*$  is a mean draft for the section, usually assumed to be

$$T^*(x) = S(x)/B(x) \quad \text{where}$$

$$S(x) = \text{sectional area}$$

$$B(x) = \text{waterline beam of section}$$

Using these simplifications, (158) becomes

$$h_3(x) = i\rho\bar{\zeta}\omega_0 e^{-kT^*(x)} \int_{C_x} N_3 \psi_3(y,z) dl \quad (159)$$

$$= -\bar{\zeta} \frac{\omega_0}{\omega_e} e^{-kT^*(x)} [\omega_e^2 a_{33}(x) - i\omega_e b_{33}(x)]$$

where the line integral around the section has been replaced by its equivalent value given by Equation (152).

Using the same assumptions, the sectional Froude-Krylov exciting force becomes

$$f_3(x) = \rho g \bar{\zeta} e^{-kT^*(x)} \int_{C_x} N_3 dl$$

$$= \rho g \bar{\zeta} e^{-kT^*(x)} B(x) = \bar{\zeta} e^{-kT^*(x)} c_{33}(x) \quad (160)$$

Finally the total heave and pitch exciting force amplitudes are given by:

$$F_{EX_3} = \bar{\zeta} \int_L e^{ikx} e^{-kT^*(x)} [c_{33}(x) - \omega_0[\omega_e a_{33}(x) - i b_{33}(x)]] dx$$

$$F_{EX_5} = -\bar{\zeta} \int_L e^{ikx} e^{-kT^*(x)} x [c_{33}(x) - \omega_0[\omega_e a_{33}(x) - i b_{33}(x)]] - \frac{U_0}{i\omega_e} \omega_0 [\omega_e a_{33}(x) - i b_{33}(x)] dx \quad (161)$$

Equations (161) allow the heave and pitch exciting forces to be computed in terms of the sectional geometry and the sectional added mass and damping.

**3.5 Computation of a Two-Dimensional Case.** The key to a successful strip-theory computer program for ship motions is to have a good method to solve the two-dimensional problem shown in Fig. 40. Mathe-

matically the problem so defined is called a mixed boundary value problem and there are many methods for its solution. In ship hydrodynamics the two most popular methods for solving the problem are boundary integral methods (Frank, 1967), (Yeung, 1982) and the multipole method (Ursell, 1949), (Porter, 1960), or (De Jong, 1973). The multipole method is often simplified using *Lewis-forms* (Lewis, 1929). In this subsection the two methods will be briefly discussed and then results for some standard shapes will be given. The mathematical details of each of the methods can be found in the appropriate references.

Many different boundary integral techniques have been proposed to solve the two-dimensional problem. Potash (1971) solves for the potential directly. Chang and Pien (1975, 1976) use a dipole distribution. Troesch (1979) and Frank (1967) use source distributions. It should be noted that the boundary integral methods used to solve the sectional problem are two-dimensional analogs of the three-dimensional methods of Faltinsen and Michelsen (1976), Chang (1977), Inglis and Price (1981), etc., to be discussed in the next subsection.

The method of Frank (1967) appears to be preferred in many, if not most, ship motion computer programs. As shown in Fig. 41, Frank's method consists of dividing the ship section into a series of straight-line

segments. Over each segment fluid sources with constant, but unknown, strengths are distributed. The form of the unit source potential is chosen so that the boundary conditions on the free surface and at infinity are met. The unknown source strengths are found by satisfying the body boundary conditions at the center point of each segment. Knowing the source strength, the velocity potential,  $\psi_k$ , can be found, and hence the sectional added mass and damping coefficients can be determined by integrating around the section, as given in Equation (152).

The advantages of Frank's method are that it is computationally fast and any ship cross-section can be approximated with as much accuracy as desirable. Typically, 8 to 10 segments on a half-section are enough to get accurate added mass and damping coefficients for motions in the vertical plane. Slightly more segments seem to be needed for the transverse motions, particularly for roll.

The primary disadvantage of Frank's method is the presence of irregular frequencies. In fact, most of the boundary integral methods are plagued by irregular frequencies when the cross-section is surface-piercing. This was first pointed out by John (1950) in the context of using source distributions to solve free-surface problems. The irregular frequencies fully discussed by Ohmatsu (1975) are a set of discrete frequencies at

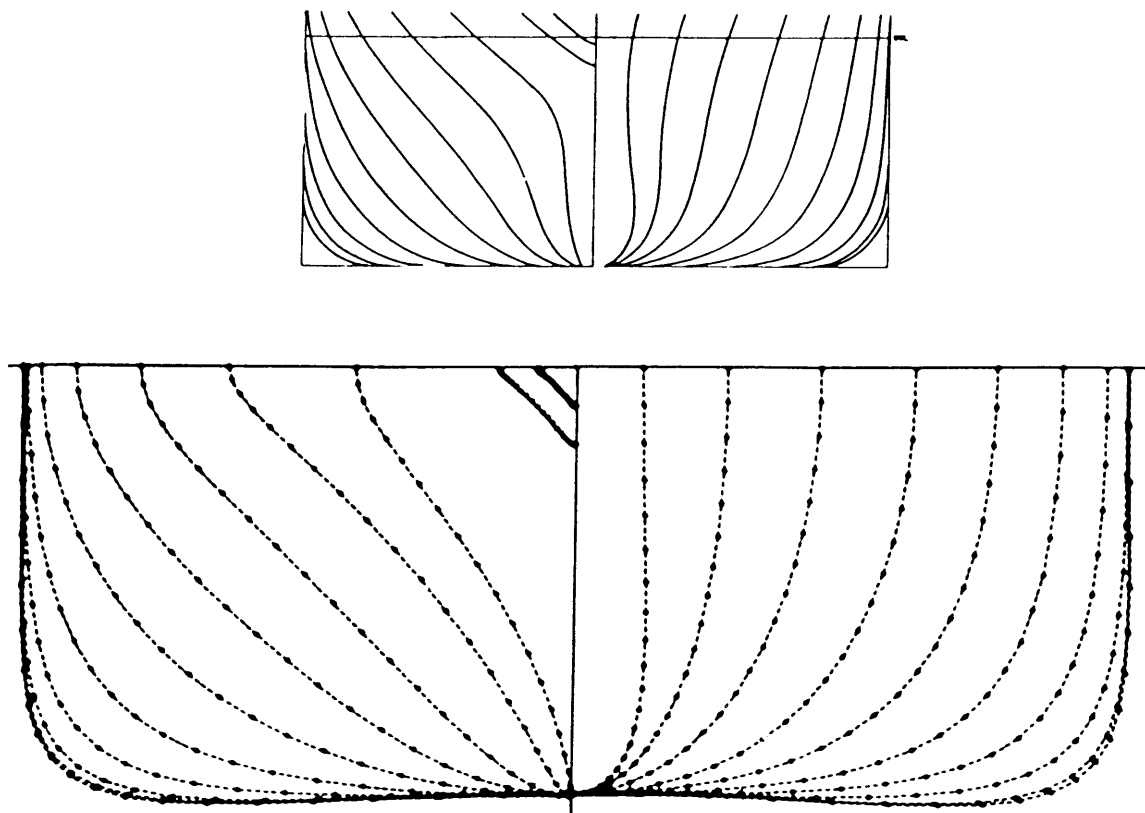


Fig. 43 Body plan and Lewis-form representation of *Mariner* hull



which the solution obtained from the boundary integral method is not unique or "blows up." The problem is associated with the resonant frequencies at which the interior flow in the "closed basin" inside the hull section breaks down.

Frank (1967) shows that for a rectangular cross section the irregular frequencies occur at

$$\omega_n^2 = n \frac{\pi g}{B} \coth(n\pi T/B) \quad n = 1, 2, 3, \dots \quad (162)$$

where

$$\begin{aligned} \omega_n &= n^{\text{th}} \text{ irregular frequency} \\ B &= \text{beam of rectangle} \\ T &= \text{draft of rectangle} \end{aligned}$$

The lowest value of the irregular frequency occurs for  $n = 1$ . Equation (162) shows that for fixed draft, the first irregular frequency decreases as the beam increases. For normal ship types the irregular frequencies are often above the range of practical interest. However, for certain section types, such as transom sterns or offshore transport barges, the irregular frequencies can cause calculation difficulties.

The irregular frequencies can be circumvented by various means. Ohmatsu (1975) suggested extending the source distribution along the free surface interior to the cross-section to put a "lid" on the body. Ogilvie and Shin (1978), Sayer and Ursell (1977), and Borresen (1980) all place concentrated sources or other singularities at the origin, with strength and phase selected so that the energy associated with a possible sloshing mode is absorbed by the concentrated singularity. Numerically, the proposed methods do not always seem to work, particularly in the transverse modes. Research is continuing, and a satisfactory method for removing the irregular frequencies should be available soon.

The multipole method was first developed by Ursell (1949). His method consists of the superposition of potential functions that all satisfy the Laplace equation, the free-surface boundary condition, and the condition at infinity. The potential functions represent a source and horizontal dipole at the origin, which give the radiated waves at infinity, and a series of multipole potentials that die off rapidly as one moves away from the origin. The strengths of the source, dipole and multipoles are all determined so that the body boundary condition is met. Ursell (1949) used the source and symmetric multipoles to solve the problem of a heaving circular cylinder. The dipole and asymmetric multipoles are used for sway and roll. The number of terms used in the multipole expansion are determined by the number of points on the body surface at which the body boundary condition is met.

For sections that are not circular in shape conformal mapping is used. Conformal mapping is a mathematical procedure in which one shape is *mapped* into an-

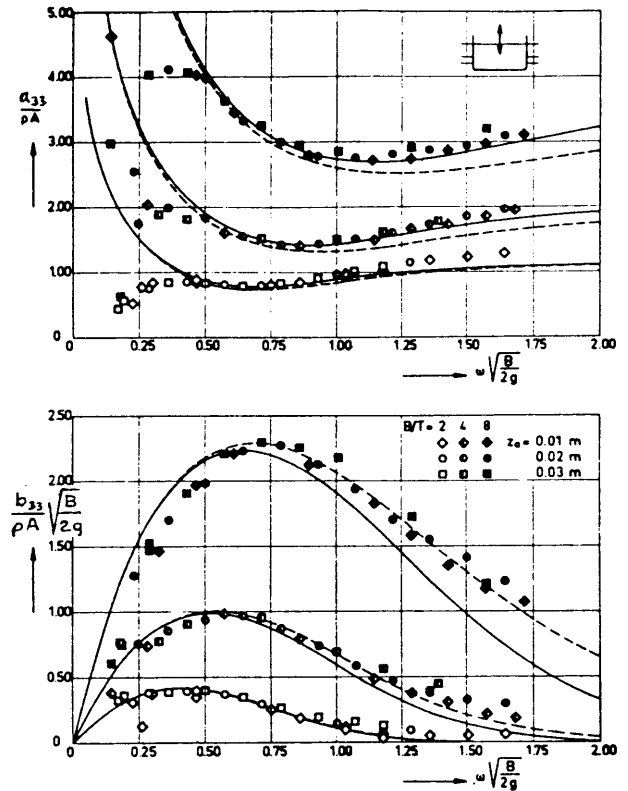


Fig. 44 Sectional added mass and damping coefficients in heaving (rectangle)

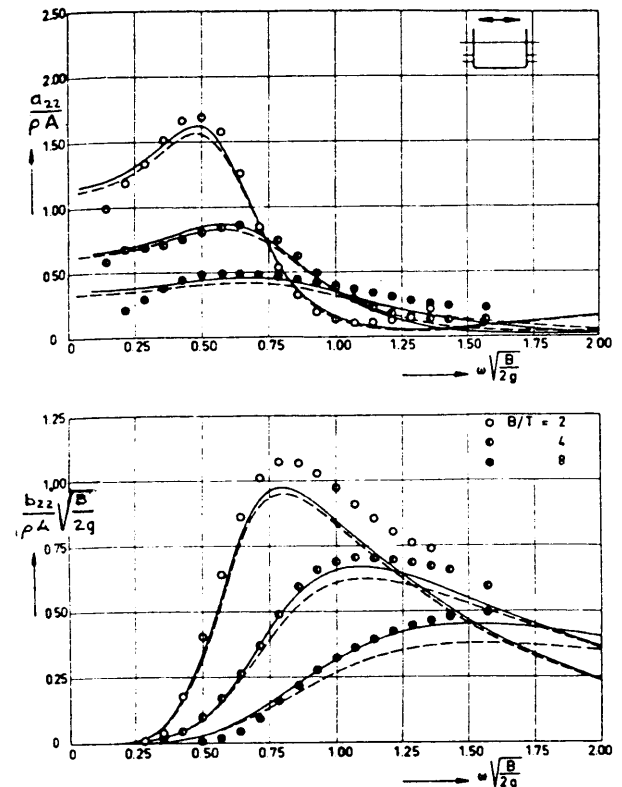


Fig. 45 Sectional added mass and damping coefficients in swaying (rectangle), (Vughts, 1968)

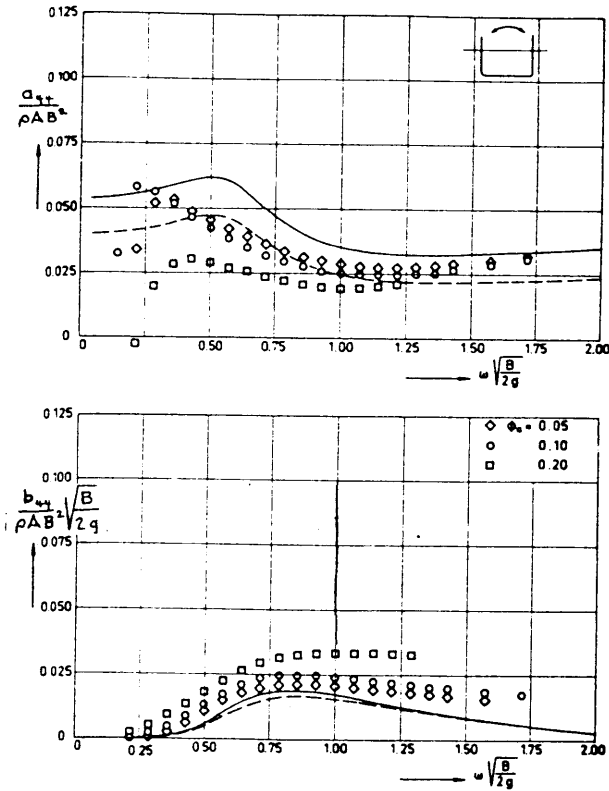


Fig. 46 Sectional added mass moment of inertia and damping coefficient in roll (rectangle)

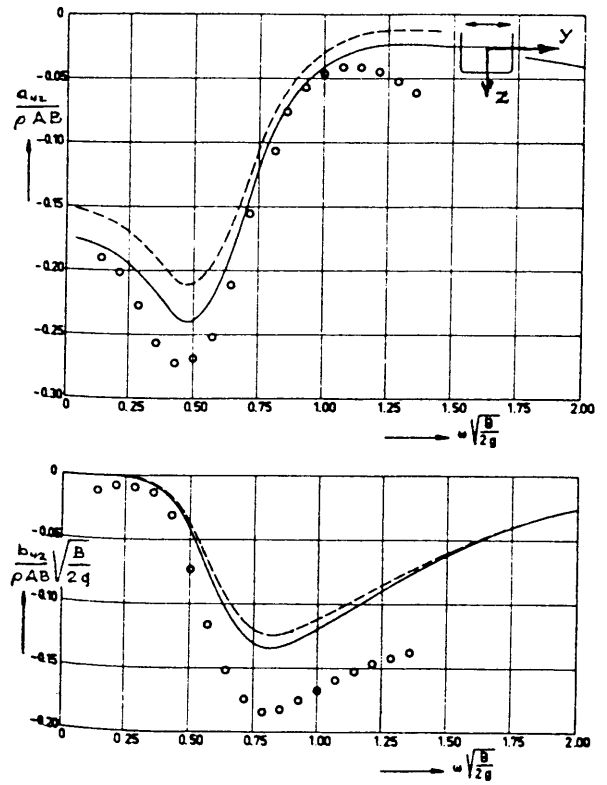


Fig. 47 Sectional coupling coefficients of sway into roll (rectangle)

other shape through a change in variables. The mathematical function that transforms the coordinates of the cross section into the coordinates of a different cross section is called the mapping function. In the multipole method, the mapping function that transforms the ship section into a semicircle is found. The mapping function can then be used in conjunction with Ursell's known solution for a circular cylinder to find the solution for the actual ship section. The difficulty in the technique is to determine the proper mapping function for each cross section. Various methods have been proposed to find the mapping function. De Jong (1973) gives a general description of the problem for both vertical and horizontal modes of motion. Von Kerczech and Tuck (1969) and Bishop, Price and Tam (1978) use different mathematical techniques to find the mapping functions. Bishop, et al (1980) give the added mass and damping for various sections in heave. Porter (1960) considered an arbitrarily-shaped cross section in heave and included experimental results. Bermijo (1965) developed a technique to find the mapping function coefficients for use in Porter's method. Specific mapping functions to give certain forms are discussed by Lewis (1929), Tasai (1959), Demanche (1968), and Landweber and Macagno (1957, 1959).

The most common mapping uses the so-called Lewis-forms (Lewis, 1929), (Landweber and Macagno, 1957). Lewis-forms use a two-parameter mapping function

based on the sectional beam-to-draft ratio,  $B(x)/T(x)$ , and the sectional area coefficient  $\left(\beta_n = \frac{S(x)}{T(x)B(x)}\right)$ .

Fig. 42 shows the sectional shapes for various combinations of beam-to-draft ratio and sectional area coefficient. Fig. 43 (Frank and Salvesen, 1970) shows how well Lewis-forms approximate the stations of a Mariner-type hull. Note that most of the stations are fairly well approximated. The bottom is not exactly flat, but this makes little difference in the added mass and damping. The bulb sections near the bow and the wine-glass sections near the stern are not well approximated, however.

Lewis-forms cannot fit all ship sections. For any given half-beam-to-draft ratio,  $B/2T$ , there is a permissible range for the sectional area coefficient. Landweber and Macagno (1957) derive the permissible range as

$$\frac{3\pi}{32} \left(2 - \frac{B}{2T}\right) \leq \beta_n \leq \frac{3\pi}{128} \left(\frac{B}{2T} + 12\right) \quad \frac{B}{2T} \leq 1 \quad (163)$$

$$\frac{3\pi}{32} \left(2 - \frac{2T}{B}\right) \leq \beta_n \leq \frac{3\pi}{128} \left(12 + \frac{2T}{B}\right) \quad \frac{B}{2T} \geq 1$$

where

$\beta_n$  is the sectional area coefficient.

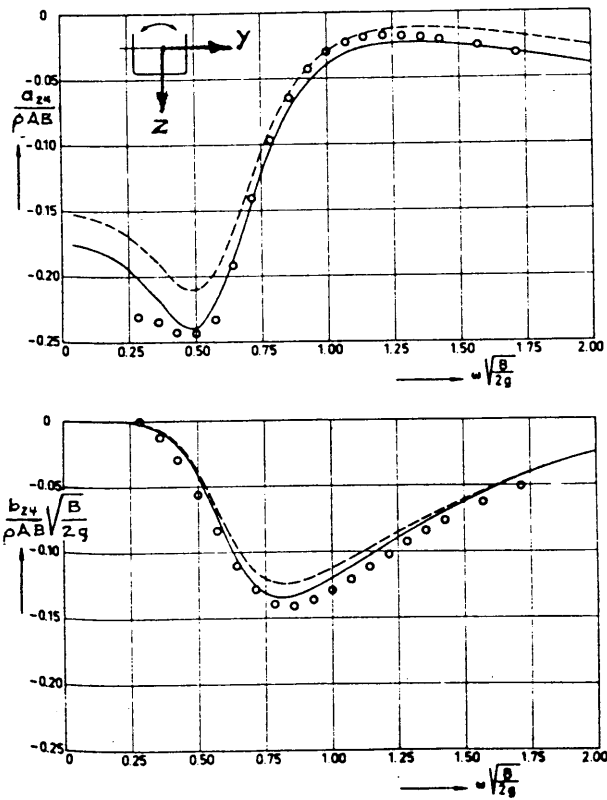


Fig. 48 Coupling coefficients of roll into sway (rectangle), from Vughts (1968)

For ship sections outside of the range shown in Equation (163) modifications must be made. Some ship motion programs artificially modify the sectional area and/or the half-beam to draft ratio until it fits into the range. For strip-theory calculations this approach is not too bad because the final computed motions are hardly affected. Another approach is to alter the mapping function slightly to give a different section shape for the same two parameters. Thus, Demanche (1968) uses the half-beam-to-draft ratio and sectional area coefficient as the two mapping parameters but obtains bulbous-bow type sections. The combination of Lewis-forms and Demanche bulb forms seems to cover most ship sections.

Summarizing, Frank's method and Lewis-forms are the two most common approaches to computing the two-dimensional coefficients for use in strip theory. Frank's method allows a more accurate description of the hull cross section, but it is troubled by irregular frequencies and requires more computer time. The Lewis-form approach does not have irregular frequencies, but it cannot accurately handle bulbous-bow sections, wine-glassed shaped sterns and barge sections with high  $B/T$  ratios. Lewis-forms are useful in preliminary design because only the load waterline beam, draft and sectional area need be known. These are the design parameters that are available early in the de-

sign stage. Late in the design stage, when a full set of hull offsets is known, the use of a boundary integral method (Frank's method) or a multiparameter conformal mapping is probably justified.

A new "hybrid" method to solve the two-dimensional problem has recently been developed by Yeung (1975) and Nestegard and Sclavounos (1983). The hybrid method uses a boundary integral technique in a region close to the body and a multipole expansion far from the body. The method eliminates the irregular frequencies but appears to use more computer time than Frank's method. Research on the hybrid method is continuing.

Several investigations have been carried out to compare the two-dimensional theoretical predictions of sectional coefficients with experimental results. Porter (1960) and Paulling and Richardson (1962) measured the vertical force and pressure at several locations for heaving sections. Vughts (1968) considered heave, sway, roll and sway-roll cross-coupling for five different section shapes (circle, rectangle, triangle and two ship-like sections). The results for the rectangle are shown in Figs. 44 through 48.

Fig. 44 shows the results for a heaving rectangle at various beam-to-draft ratios. The individual points are the experimental results; the solid curve is from conformal mapping; and the dashed curve is for the equivalent Lewis form. As can be seen, the experimental and theoretical results agree fairly well. The fall off in the heave-added-mass at low frequency is due to experimental inaccuracies and should be disregarded. The linearity of the results is verified by the fact that the experimental points for heave amplitudes of 0.01, 0.02 and 0.03 meters (0.38-1.1 in.) all fall along the same curve.

The curves in Fig. 44 clearly illustrate that added mass and damping in heave are greatly increased as the  $B/T$  ratio increases. This is to be expected in heave motion since, for a body of constant cross-sectional area, a wide, flat section will produce more of a fluid disturbance (hence larger hydrodynamic forces) than a narrow, deep section.

The solid and dashed curves demonstrate the differences in predicted added mass and damping using the Lewis-form approximation versus the more accurate multi-parameter conformal mapping. The results shown are for a rectangle, but the differences are typical for normal ship-like sections. Bishop, et al (1978) show that the differences between using Lewis-forms and multiparameter conformal mapping can be substantial for bow and stern sections. For normal ships, the predicted motions using Lewis-forms or more exact techniques usually do not differ very much. However, other quantities such as hydrodynamic pressure, shear or bending movements may be greatly affected.

The significant effects of oscillation frequency on the added mass and damping are apparent from Fig. 44. At high frequency the added mass approaches a constant and the damping tends to approach zero. This

is the result of the presence of the free surface. At high frequencies the free surface is dominated by inertial effects and consequently normal gravity waves are not generated. The damping, which results from energy carried away from the body by the gravity waves, tends to zero. The added mass approaches a value that is independent of frequency and equal to half the added mass of the equivalent double body in an infinite fluid. At low frequencies the free surface is dominated by gravity effects and acts like a rigid wall. The wave damping again approaches zero. The added mass coefficient,  $a_{33}$ , tends toward infinity. However, this does not mean the hydrodynamic force tends toward infinity since  $a_{33}$  must be multiplied by  $-\omega^2$  to obtain the force. The variation of the added mass and damping with frequency, which is an important aspect of ship-motion theory, is the result of the presence of the free surface and the generation of gravity waves by the body motion. The frequency dependence is responsible for the memory effects in the time domain and is the primary reason the solution of the ship motion problem is different from a multiple degree of freedom vibration problem.

The experimentally measured damping coefficients shown in Fig. 44 are higher than the solid lines because of viscous effects which tend to increase the damping over the ideal fluid wave damping. For heave and sway the viscous damping is only a small percentage of the total damping. Depending on the section shape, the viscous damping in roll can be the major component of the total damping.

The sectional coefficients of added mass and damping in sway are shown in Fig. 45. As expected, the effects of  $B/T$  are the opposite of heave in that  $B/T = 2$  has the larger hydrodynamic force. The effects of frequency are similar to heave except that the sway added mass approaches one-half of the double-body-in-an-infinite-fluid value at zero frequency instead of infinite frequency. Mathematically, this change in behavior between heave and sway is a result of the free-surface boundary condition and the required image system at high and low frequencies. A complete explanation may be found in Newman (1977); Section 6.17. Again the viscous damping tends to increase the experimentally measured damping coefficients.

Figs. 46, 47, and 48 show the added mass and damping in roll and the cross-coupling between sway and roll for  $B/T = 2$ . The results for other  $B/T$  ratios are similar. Fig. 46 clearly shows the nonlinearities associated with viscous effects in roll, because for three different roll amplitudes very different added mass and damping result. The theoretical results, which are linear, predict that the coefficients are independent of roll amplitude. The cross-coupling coefficients also show nonlinear effects, for theoretically the sway-into-roll and roll-into-sway coefficients should be identical. But the experiments indicate that they are similar but not identical. Presumably the differ-

ences are also the result of viscous effects. The nonlinearities associated with roll are very important in ship motion theory and are discussed in Subsection 3.8.

The added mass and damping of the various ship sections are usually computed by subroutines in a ship motion program. Several authors have published curves of added mass and damping versus frequency for various section shapes (Porter, 1960), (Jacobs, et al 1960), (Frank, 1967), and (Bishop, et al 1978b, 1980). Papanikolaou (1980) computed the added mass and damping in heave, sway and roll using a boundary integral method for triangles, ellipses and rectangles of widely varying  $B/T$  ratios. Such curves are useful for visualizing the effects of frequency; to obtain values of added mass and damping for specific sections; and to obtain numbers to check computer programs.

**3.6 Other Techniques to Compute the Hydrodynamic Forces.** Strip theory is probably the most widely used method to compute the hydrodynamic forces acting on a vessel in regular waves. However, under some circumstances (for example, high forward speed or non-conventional vessels) it does not necessarily give accurate answers. Many different techniques have been or are being developed to predict analytically the hydrodynamic forces on a vessel in waves. In this subsection several of the other techniques will be briefly described and appropriate references given, but a detailed description of all is beyond the scope of this chapter. Newman (1978) gives a history of the development of ship motion theory.

As previously mentioned, strip theory is a high-frequency theory in that the frequency of encounter is assumed large. It is also possible to develop the so-called *ordinary slender-body theory* of ship motions by assuming the frequency to be low. Newman and Tuck (1964) and Maruo (1967) assumed the wavelength of the incident waves to be the same order of magnitude as the ship's length. This leads to a theory in which the hydrostatic restoring forces and the Froude-Krylov exciting forces are the dominant terms, with the result that the leading-order equations of motion are nonresonant. For zero forward speed in head seas ordinary slender-body theory gives reasonable predictions, but the comparisons with experiment degrade as the speed and frequency increase.

Newman (1978), Newman and Sclavounos (1980) and Sclavounos (1985) have developed a unified theory to link ordinary slender-body theory and strip theory. At low frequencies, the unified theory approaches the ordinary slender-body theory and yields terms that involve longitudinal interference between sections. For high frequencies the longitudinal interferences disappear and the results are identical to the strip theory derived in the previous section. At zero forward speed the results of unified theory are similar to the *interpolation solution* of Maruo (1970). Sclavounos (1985) presents predictions using unified theory for the heave and pitch motions of a Series 60 ( $C_B = 0.70$ ) and a

destroyer model in head seas. For zero forward speed, the added mass and damping coefficients have been computed by Mays (1978) and Maruo and Tokura (1978). Good agreement is found with exact three-dimensional computations and experiments.

The typical strip theory (as presented in the preceding sub-section) uses the Haskind relations to compute the exciting forces. This eliminates the need to compute the diffraction potential, but it has also eliminated any information about the variation of the exciting forces and diffracted waves along the ship length, quantities that are needed to compute relative motion and wave-induced bending moments. Ad hoc methods have been developed that enable strip theory to compute these quantities, but they are not entirely satisfactory. For these reasons several researchers have investigated the direct solution of the wave diffraction problem. Ogilvie (1977) reviewed the various approaches using slender-body theory. Troesch (1979) considered the problem in non-head seas. Faltinsen (1971) developed a theory for ships in high-frequency head seas. Faltinsen's results are dominated by a singularity in the bow region. Maruo and Sasaki (1974) modified Faltinsen's approach in order to remove the singularity. Beck and Troesch (1980) used the Maruo and Sasaki theory to compute the pressure distribution, exciting forces and wave amplitude due to the incident plus diffracted wave system. Reasonable agreement was found with experiments. Liapis and Faltinsen (1980) extended the Maruo and Sasaki approach to non-head seas.

The unified theory for wave diffraction has been developed by Sclavounos (1984). For high-frequency oblique waves this unified theory yields the same results as Troesch (1979). For head waves the Maruo and Sasaki (1974) theory is recovered.

Recently, several researchers have proposed a new approach to the ship motion problem. The works of Chapman (1975), Faltinsen (1983), Loeser, Yue, and Salvesen (1982), and Yeung and Kim (1984) all have similar formulations. In principle the approach can be used to solve the nonlinear ship-motion problem, but to date numerical results are only available for the linear case. The approach consists of solving a series of two-dimensional initial-value problems in a control plane fixed in space through which the ship passes. The shape of the cross section of the hull in the control plane is continuously changing due to the ship motions and forward speed. The conditions on the free surface are stepped forward in time using the free-surface boundary condition. Consequently, as opposed to strip theory, the forward speed effects are brought into both the hull and free-surface boundary conditions. Numerical calculations for the added mass and damping show improved agreement with experiments and three-dimensional calculations.

The advent of large, high-speed computers has allowed the direct numerical solution of some three-di-

mensional seakeeping problems. For example, the use of numerical methods in free-surface flows is a growing field of research, much too large to discuss in this section (Yeung, 1982). However, it should be pointed out that offshore engineers routinely solve the linear, three-dimensional, zero-speed problem for a vessel in sinusoidal waves using source-panel methods. In offshore engineering the geometry of many of the vessels precludes the use of strip theory and the use of more involved theories has been necessary. Faltinsen and Michelsen (1975) and Garrison (1974, 1975, 1978) are examples of these calculations. Chang (1977) and Inglis and Price (1979, 1981) have extended the method to include forward speed. Liapis and Beck (1985) and King et al (1988) have solved the problem directly in the time domain. For problems with forward speed the time-domain solution appears to require less computational effort than the equivalent frequency-domain solution. Comparisons with available experimental data indicate that in general the three-dimensional numerical methods give better agreement than strip theory. The computation times for the three-dimensional methods are significantly larger than strip theory but this will become less significant with faster computers and improved computer codes. Further research is still necessary to define the trade-offs among the various numerical methods.

The next step in the evolution of pure numerical calculations appears to be the inclusion of nonlinearities in both the body-boundary condition and the free-surface boundary condition. The eventual goal would be to include viscous effects as well.

### 3.7 Longitudinal Motions.

(a) *General.* In this subsection the characteristics of the longitudinal or vertical-plane motions (surge, heave and pitch) will be discussed; the next subsection will analyze the transverse or horizontal-plane motions. As previously mentioned (in Section 3.2, Simplified Head Sea Case) the separation of the response of the ship into vertical and horizontal-plane motions is the result of linear theory and the fact that for a port/starboard symmetric ship there is no cross-coupling between them. If nonlinear motion or a ship with asymmetry (for example due to mooring lines) is investigated, all six degrees of freedom must be considered simultaneously.

The number of published investigations into the experimental and/or theoretical aspects of ship motions in regular waves is immense (see the Proceedings of the ITTC and ATTC seakeeping committees). There is space available here for only a few examples to illustrate various aspects of ship pitching, heaving and (to a limited extent) surging motions in regular waves. The coefficients in the equations of motion will be discussed first; followed by samples of computed ship motions.

(b) *Coefficients in the equation of motion.* To measure the distribution of the hydrodynamic forces

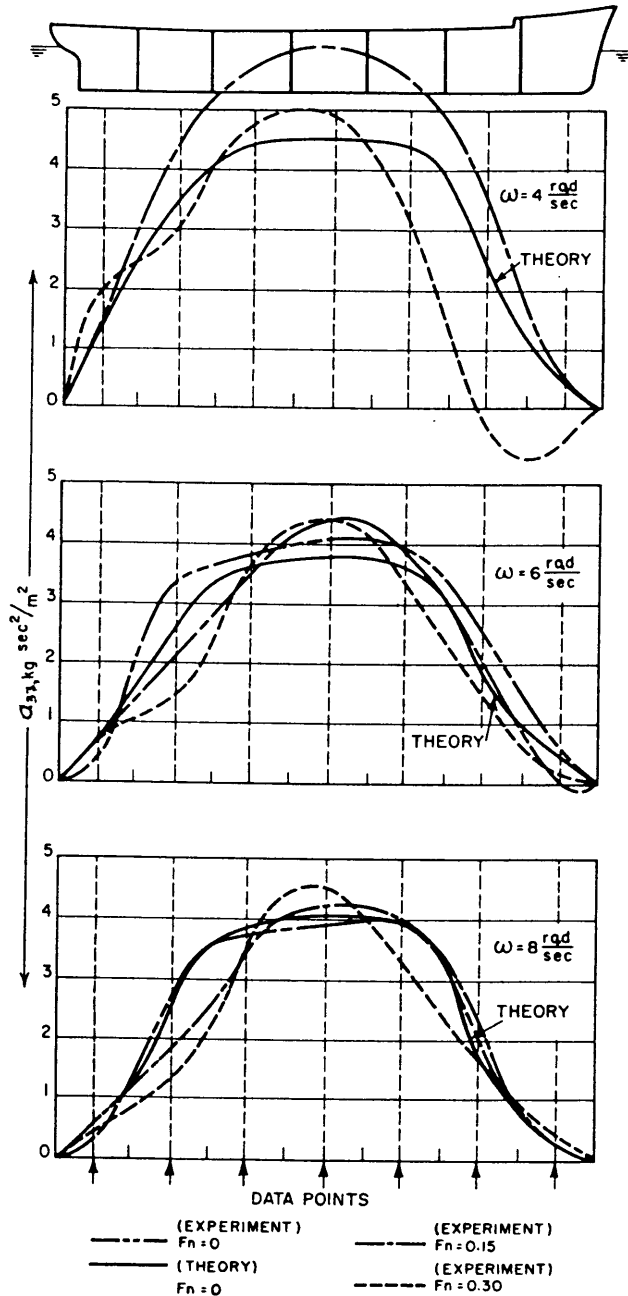


Fig. 49 Comparison of sectional values of added mass,  $a_{33}$ , from two-dimensional theory ( $F_n = 0$ ) and from experiment ( $F_n = 0, 0.15$  and  $0.30$ ) (Gerritsma and Beukelman, 1967)

along the length of a ship, Gerritsma and Beukelman (1964, 1965, 1967) and Gerritsma (1966) have tested a segmented model of a Series 60,  $C_B = 0.70$  ship. The added mass and damping terms were measured by forced oscillation testing at constant speeds in calm water. The exciting forces were determined by towing a fixed model in waves. Fig. 49 shows the distribution of the heave added mass along the length of the model at three different forward speeds and three oscillation

frequencies. As expected, the added mass is largest for the wide sections around midship and decreases to zero at the ends. For the lowest frequency, the disagreement between the theoretical and experimental curves shows the appreciable effects of three-dimensionality and forward speed. For the higher frequencies the agreement between the experiments and the two-dimensional strip theory approximation is reasonably good at zero speed, but it appears that the agreement between theory and experiment becomes divergent as the forward speed increases. Other coefficients show the same type of correlation.

The speed effects are more clearly seen by examining the total added mass coefficient in heave,  $A_{33}$ . Fig. 50 is taken from Faltinsen (1974) but is based on the work of Gerritsma and Beukelman. The added mass coefficient was computed by the formula given in Table 13, with the sectional added mass determined by using Lewis-form approximations. As can be seen, the experimental results are reasonably predicted by strip theory. The deep dip in the experimental results for  $F_n = 0.15$  around  $\omega_e \sqrt{L/g} = 2$  is probably due to tank wall effects and does not represent the actual values for a ship in the open ocean. The forward-speed dependence is clearly visible in the experimental results. The strip-theory results have no forward-speed dependence for a given frequency of encounter. The forward-speed effects tend to increase at low frequencies of encounter (i.e. long wavelengths). As we shall see, improper accounting for forward-speed effects in strip theory will carry right through to the motion and derived response predictions. One of the goals of present-day research into ship motion theory is to improve the prediction of forward-speed effects.

The complete set of coefficients have been experimentally determined by Gerritsma (1960) for three Series 60 parent forms of block coefficients  $C_B = 0.60, 0.70, 0.80$ . Models were oscillated at various frequencies while at constant speed in calm water. Fig. 51 shows the coefficients  $A_{33}, B_{33}, A_{55}$  and  $B_{55}$  as a function of frequency and block coefficient for four Froude numbers. The added mass coefficients are plotted as the nondimensional coefficients:

$$A'_{33} = \frac{A_{33}}{\Delta} \quad \text{and} \quad A'_{55} = \frac{A_{55}}{\Delta L^2} \quad (164)$$

where  $\Delta$  is ship mass,  $W/g$ , and  $L$  is length. The damping coefficients are nondimensionalized as

$$B'_{33} = \frac{B_{33} \sqrt{gL}}{\Delta} \quad \text{and} \quad B'_{55} = \frac{B_{55} \sqrt{gL}}{\Delta L^2} \quad (165)$$

Fig. 51 clearly illustrates the effect of body shape, the fuller form normally having larger added mass and less damping relative to its displacement. While not as obvious as in Fig. 50, the forward-speed effects are still present. The figure also indicates how the damping coefficient tends to zero at high and low frequencies.

The changes in the hydrostatic (restoring) coefficients with forward speed are shown in Fig. 52, which is also taken from Gerritsma (1960). The values are nondimensionalized with respect to the zero-speed values so that:

$$C'_{33} = \frac{C_{33}}{(C_{33})_{ST}} \text{ and } C'_{55} = \frac{C_{55}}{(C_{55})_{ST}} \quad (166)$$

where

$C_{33}$ ,  $C_{55}$  are the actual values of hydrostatic coefficients measured at forward speed, and  $(C_{33})_{ST}$ ,  $(C_{55})_{ST}$  are the values of hydrostatic coefficients computed at zero forward speed (see Table 13).

As can be seen, the pitch hydrostatic coefficient can vary appreciably with forward speed.  $C'_{55}$  is probably more affected by forward speed than  $C'_{33}$  because of the bow and stern wave systems. At the present time all ship motion programs assume  $C_{jk}$  to be speed independent. This could be one of the reasons that pitch predictions tend to become less accurate as forward speed increases.

The form of the cross-coupling coefficients,  $A_{35}$  and  $A_{53}$ , is illustrated in Fig. 53 (Faltinsen, 1974).<sup>9</sup> Equations listed in Table 13 show that for nearly fore-and-aft symmetric ships, the sign and magnitude of  $A_{35}$  and  $A_{53}$  are dominated by the forward-speed terms. At high frequency  $B_{33}$  tends toward zero so that  $A_{35}$  and  $A_{53}$  approach zero. The chain-dotted and dashed curves show the differences in computing  $A_{35}$  and  $A_{53}$  from Lewis-forms versus the Frank method. For normal ship sections the difference is expected to be small. Also shown on the graph are the results computed according to Ogilvie and Tuck (1969). The Ogilvie-Tuck coefficients contain integral terms which are extremely difficult to compute. However, Faltinsen's (1974) results show that for this particular ship the Ogilvie-Tuck coefficients give better agreement with experiments. Whether or not this conclusion holds in general is not known. At the present time research is continuing into improving the prediction of all the coefficients of the equations of motion.

(c) *Exciting forces.* Typical exciting force amplitudes in head seas for heave and pitch are shown in Fig. 54, which is taken from Gerritsma and Beukelman (1967). The non-dimensional force and moment coefficients are defined as

$$\begin{aligned} F'_3 &= \frac{F_3}{\rho g A_w \bar{\zeta}} \\ F'_5 &= \frac{F_5}{\rho g I_L k \bar{\zeta}} \end{aligned} \quad (167)$$

<sup>9</sup> The signs of the forward-speed term have been reversed from those in Table 13 because Faltinsen assumes positive  $x$  out of the stern.

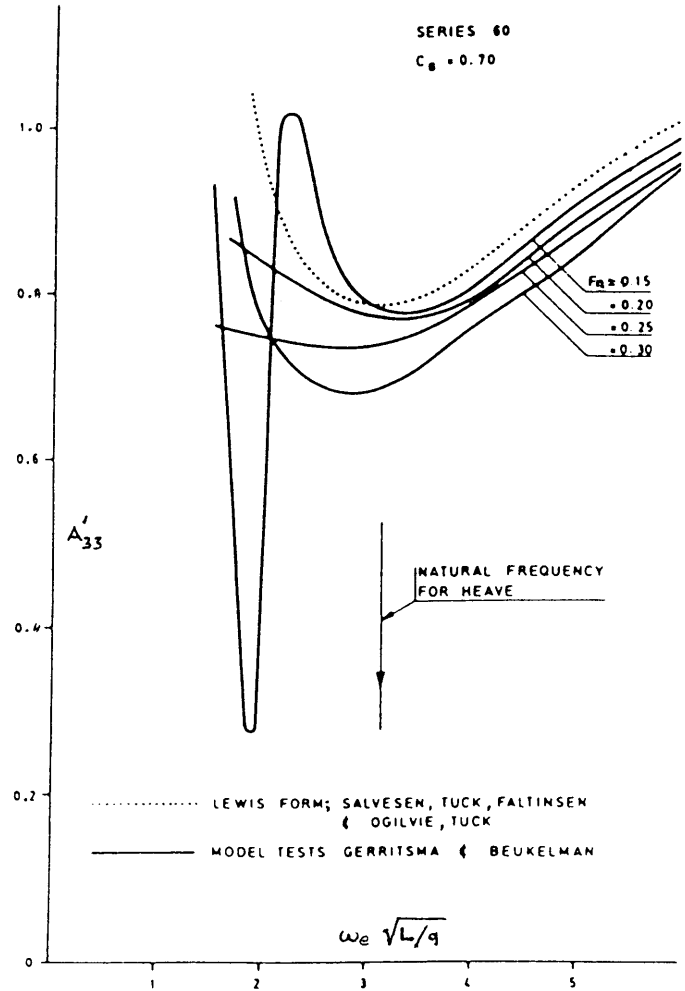


Fig. 50 Added-mass coefficient,  $A_{33}$  (nondimensionalized by  $\rho \nabla = \Delta$ ) for Series 60,  $C_B = 0.70$  (Faltinsen, 1974)

where

$A_w$  is the waterplane area

$I_L$  is the longitudinal moment of inertia of water-plane area about  $y$  axis

$\bar{\zeta}$  is the wave amplitude and  $k$  is the wave number

Gerritsma and Beukelman used the same segmented model for the experiments that was used to obtain the results reproduced in Fig. 49. As can be seen, the whole-model results and the sum of the sections show good agreement.

The pitch exciting force (moment) is non-dimensionalized relative to the maximum wave slope,  $k\bar{\zeta}$ . This means that while the nondimensional exciting force amplitude goes to 1.0 at low frequency, the dimensional pitch exciting force amplitude,  $|F'_5|$ , goes to zero. It is a maximum around  $L/L_w = 0.75$ . Note that the amplitudes of both  $F'_3$  and  $F'_5$  change significantly with incident wavelength. As previously noted, the change of exciting force with wavelength is very important and has a strong influence on the resulting ship mo-

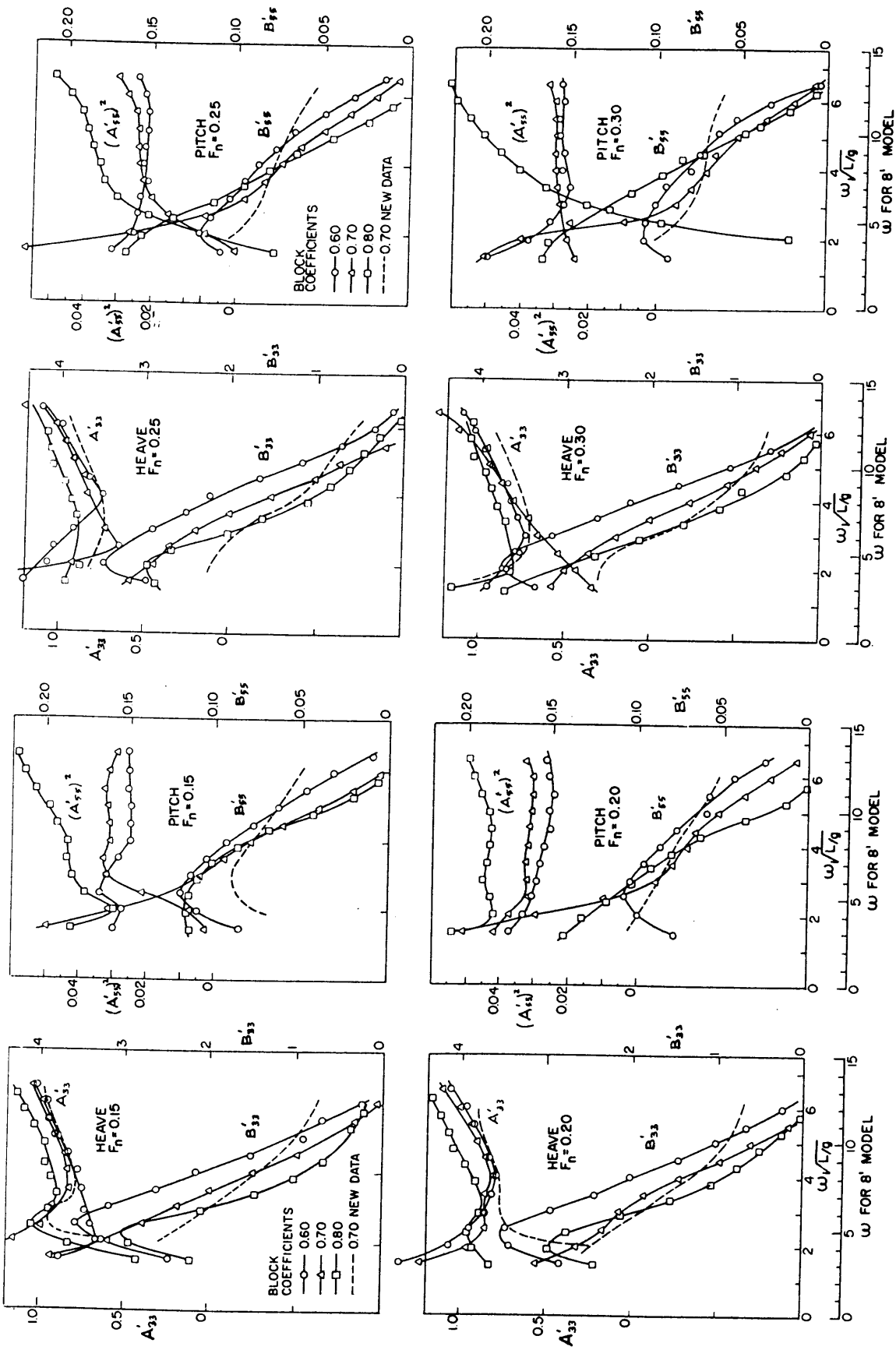


Fig. 51 Nondimensional heave and pitch coefficients for Series 60 forms at  $F_n = 0.15-0.30$  (Gerritsma, 1960)



tions. The zeros in the exciting force at short wavelengths are the result of cancellation along the hull. Depending on the wavelength, forward speed tends to increase the exciting force but the effects are generally small.

(d) *Natural frequencies.* As an aid in understanding the nature of the vertical-plane responses of a ship to sinusoidal waves, it is useful to derive the natural frequencies for heave and pitch. For an unrestrained ship, the surge natural frequency is, of course, zero since the spring constant term is zero. Unlike the spring-mass-damper system discussed in Chapter VI (Vol. II), the concepts of natural frequency and synchronism between the natural frequency and the frequency of the exciting forces do not necessarily give an accurate prediction of the magnitude of the ship motion responses. In a spring-mass-damper system that is not heavily damped the maximum motion always occurs at or very near the natural frequency. Thus, as shown in Chapter VI, the ratio of the excitation frequency to the natural frequency, or the so called *tuning factor*, is a good measure of the frequency range in which the response will be severe. In the ship motion problem, however, maximum motions do not necessarily occur around synchronism, because the magnitude of the exciting force and the coefficients in the equations of motion all depend on the encounter frequency—which in turn depends on wavelength, ship speed and heading. Hence, at low speeds synchronism, or resonance, occurs at such short wavelengths that the exciting force is very small, even at synchronism. However, at higher forward speeds the frequency of encounter shift can cause synchronism to fall within the range of wavelengths where the exciting forces are large; in this case significant peaks can occur in the heave and pitch response curves, Fig. 55. These peaks will not usually occur exactly at a tuning factor of 1.0 because of the strong coupling between heave and pitch, and the variation of added mass, damping and exciting force with frequency of encounter. In Section 4 the significance of the fact that the tuning factor alone does not give a good indication of the seakeeping performance of ships will be discussed in relation to design.

The natural frequencies of the uncoupled heave and pitch motions,  $\omega_{n_3}$  and  $\omega_{n_5}$ , respectively, are found by dividing the hydrostatic spring constant term by the mass plus added mass as follows:

$$\begin{aligned}\omega_{n_3} &= \sqrt{\frac{C_{33}}{\Delta + A_{33}}} \\ \omega_{n_5} &= \sqrt{\frac{C_{55}}{I_{55} + A_{55}}}\end{aligned}\quad (168)$$

Expressions to compute  $C_{33}$  and  $C_{55}$  may be found in Table 13. It should be noted that, as shown in Fig. 52,  $C_{33}$  and  $C_{55}$  can be changed by forward speed, but

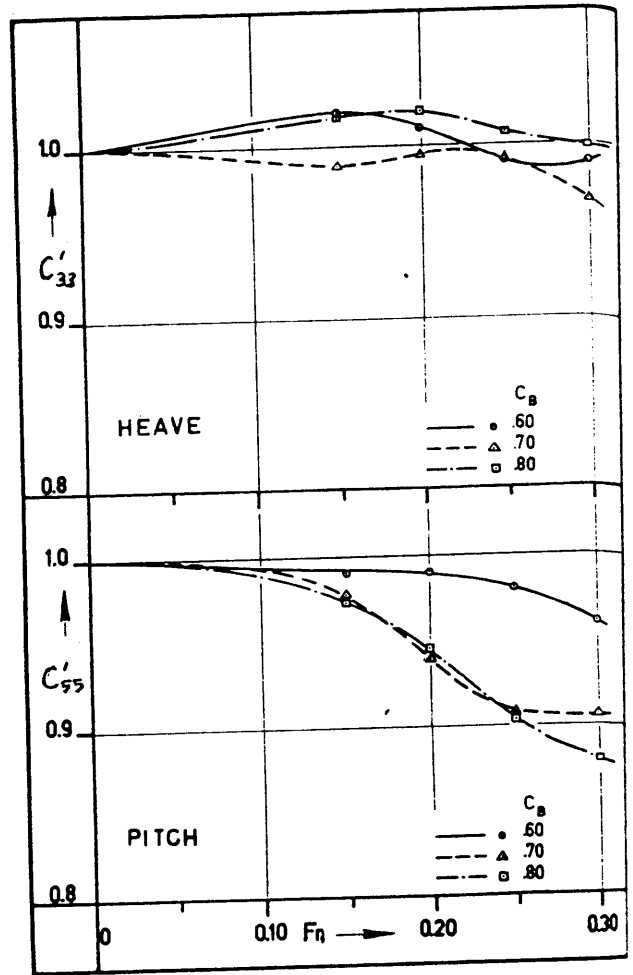


Fig. 52 Restoring force and moment coefficient as a function of speed (Gerritsma, 1960)

the effects on the natural frequencies are usually small.

The mass and pitch moment of inertia of the vessel are found knowing the displacement and pitch radius of gyration. The pitch radius of gyration is normally assumed to be  $0.25L$ . However, a Maritime Administration study in 1979 indicated that a value of  $0.267L$  might be more appropriate for average merchant ships. The added mass coefficients for such ships can be estimated from Fig. 51.

(e) *Experimental motions.* There are countless results available for both experimentally and theoretically determined vertical-plane motions. Most results are restricted to heave and pitch measurements because of the lack of coupling with surge and the difficulties associated with obtaining surge in both theory and experiment. Figs. 55 through 58 are intended to illustrate the nature of the vertical-plane motions in regular waves.

Gerritsma and Smith (1966), also Gerritsma (1980) have compared full-scale heave and pitch measure-

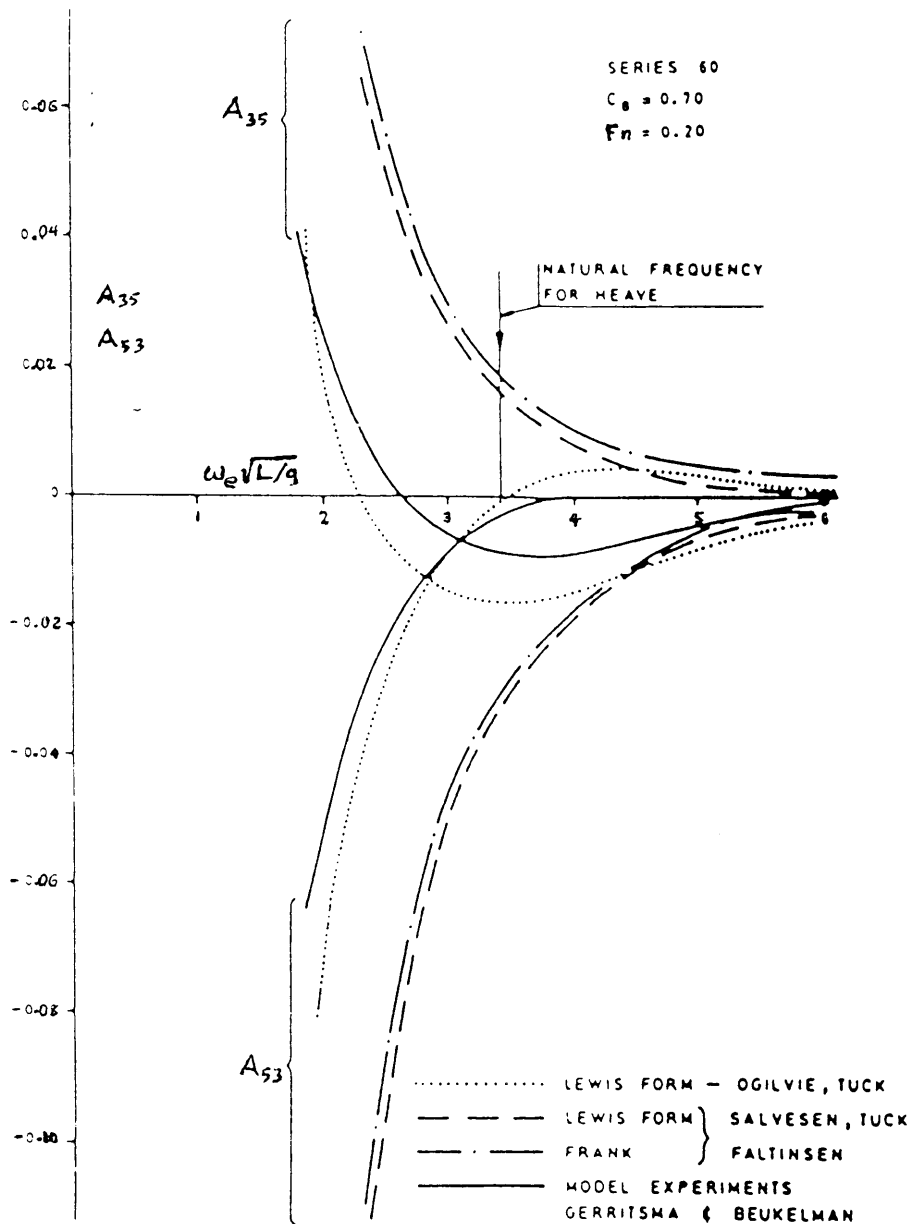


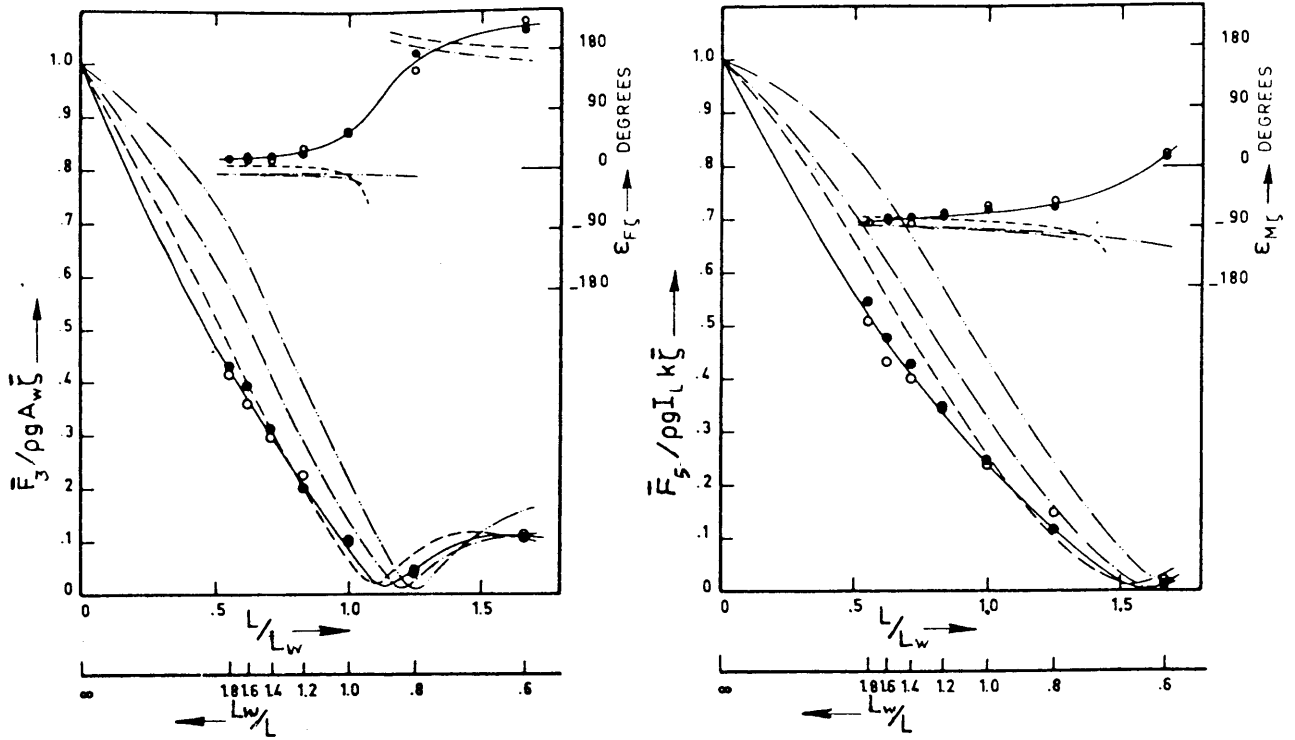
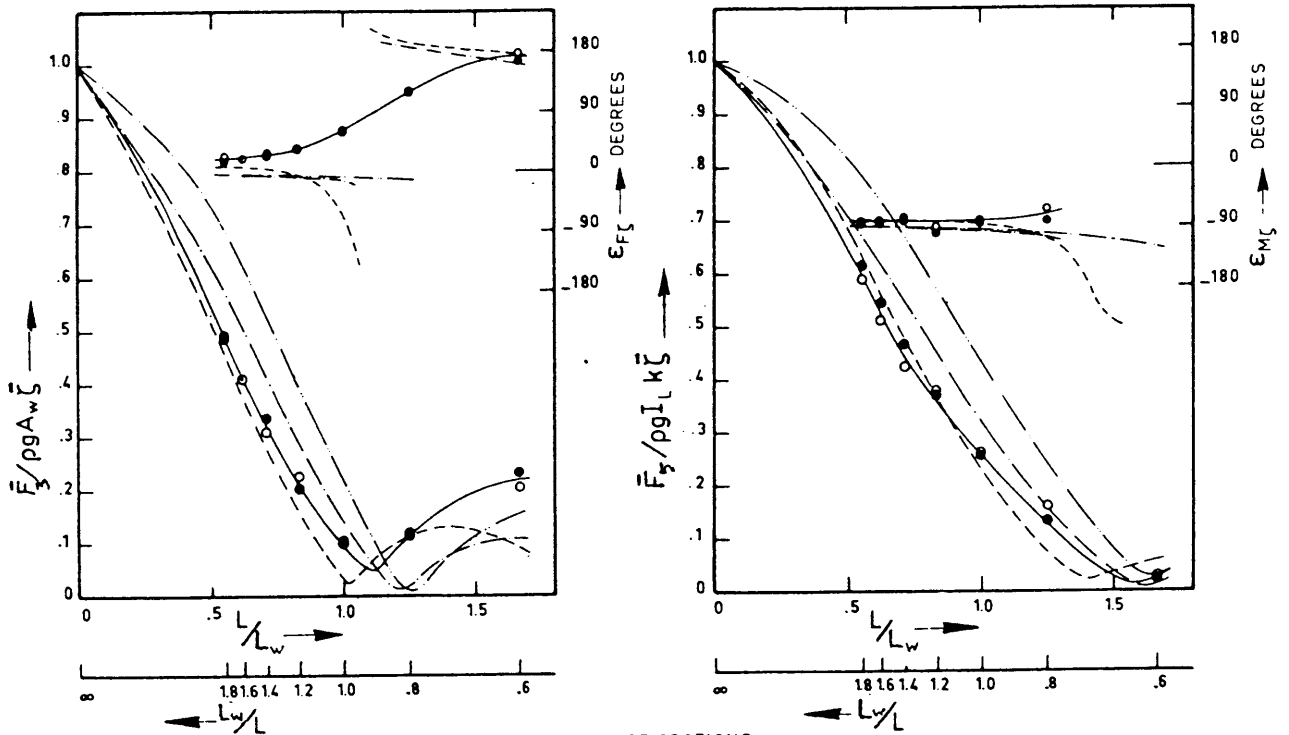
Fig. 53 Added-mass cross-coupling coefficients  $A_{35}$  and  $A_{53}$  (nondimensionalized) (Faltinsen, 1974)

ments with model tests and theoretical calculations. Fig. 55 shows the results of runs at three speeds in head seas of a *Frisland* class destroyer. The phase angles are relative to a wave crest at midship. No full-scale phase angles are available because random sea analysis was used. The theoretical calculations were based on the strip theory of Gerritsma and Beukelman (1967).

The agreement between theory, model tests and full scale is reasonably good. The scatter in the full-scale results is probably due to the inaccuracies of measuring the incident waves. At low frequencies (long

waves) the vessel contours the waves as shown by the fact that the heave amplitude approaches the wave amplitude, the pitch amplitude is the same as the wave slope, and the phase angles were 0 deg and -90 deg for heave and pitch, respectively. At high frequencies the motions go to zero. The heave natural frequency occurs where the heave phase angle shifts radically, but the maximum responses occur at much lower frequencies.

The two different theoretically calculated response curves shown in each graph of Fig. 55 are the result of using two different values of pitch radius of gyra-

(a)  $Fn = .15$ (b)  $Fn = .30$ 

— EXPERIMENT (● SUM OF SECTIONS, ○ WHOLE MODEL)  
 - - - CALCULATIONS  
 - · - CALCULATIONS WITHOUT DYNAMIC EFFECTS  
 - · - CALCULATIONS WITHOUT DYNAMIC EFFECTS AND SMITH EFFECT

Fig. 54 Total wave force and moment on a restrained ship model (Gerritsma and Beukelman, 1967)

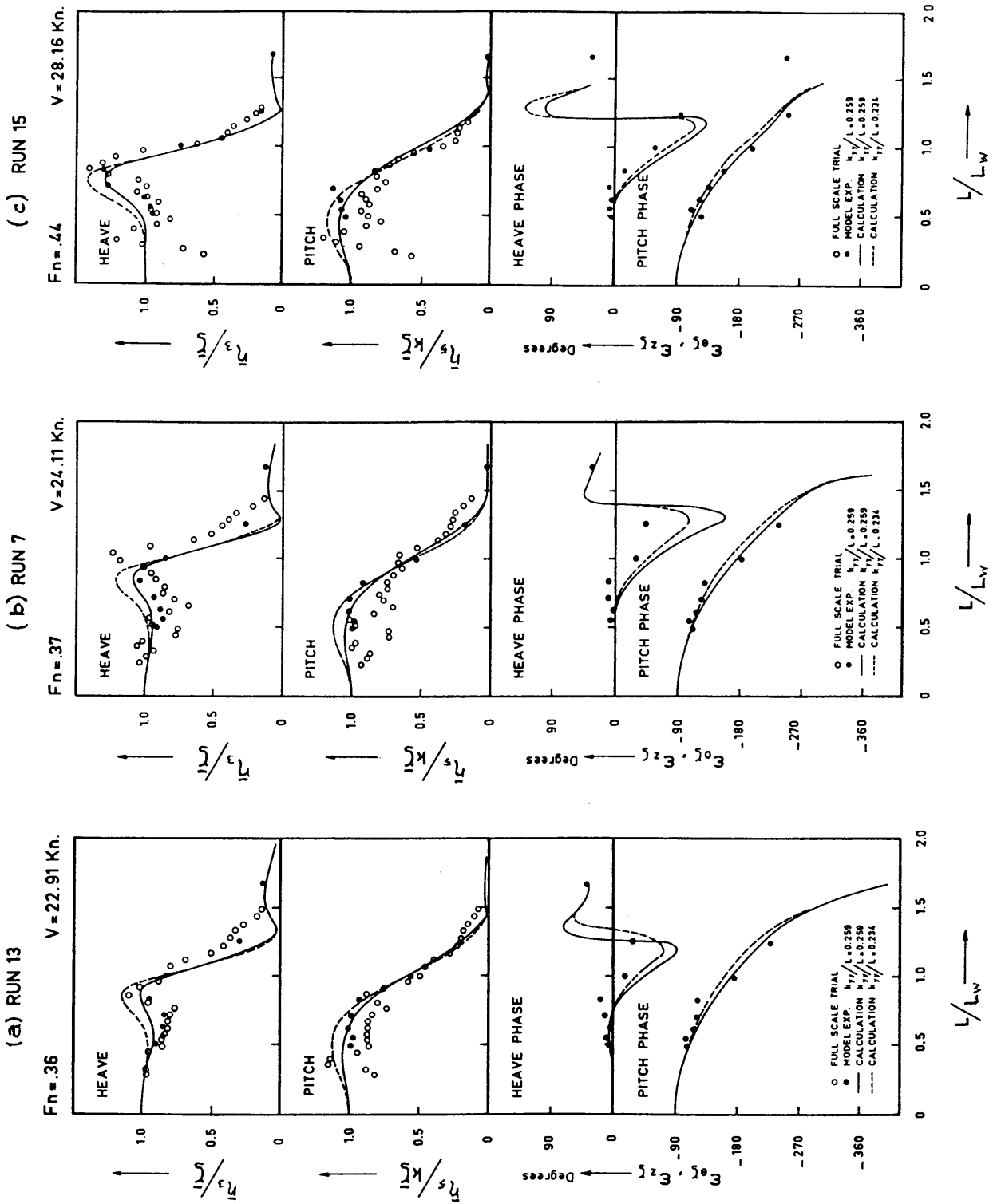


Fig. 55 Comparison of full-scale measurement, model experiment and calculation, H.M.S. Groningen, from Gerritsma and Smith (1966)

tion,  $k_5$ , where  $k_5^2 \Delta = I_{55}$ . The difference between the two curves shows the influence the pitch radius of gyration has on the heave and pitch motions in head seas. For this particular small, high-speed ship the peak motion amplitudes increase with decreasing radius of gyration and the responses at higher frequencies are in general decreased slightly. For other ships just the opposite behavior might result; it depends on the hull form, forward speed, and wavelength. Beukelman and Huijser (1977) and Loukakis and Chrysostomidis (1975) both discuss the effects of pitch radius of gyration on motions in head seas, showing in general a decrease in motions with a decreasing radius of gyration.

Fig. 56 shows a complete set of non-dimensional response amplitudes in all six degrees of freedom for an aircraft carrier at twenty-five knots. These results were computed by Baitis, et al (1981) using the U.S. Navy's SMP Program.

As can be seen, the theoretical results agree reasonably well with the experiments for most of the cases. The surge motion is small except in following seas, where the experimental results are larger than theory. In beam seas the theoretical surge motion is zero because the exciting force goes to zero and the program neglects almost all coupling between surge and the heave and pitch motions. The experiments show a small surge amplitude in beam seas which probably results from cross coupling between the modes and higher order terms in the exciting forces. The model tests were conducted with a self-propelled model. The effects of the unsteady motion on the propeller thrust, which is neglected in ship-motion theory, is probably a major source of disagreement. Surge motion is one of the areas in which more research is needed.

The pitch and heave motions are similar to the results we have seen previously. As in the case of surge, the pitch motion becomes very small in beam seas, but it is most severe in head seas. The sway, yaw and roll motions will be discussed in the next subsection.

Gerritsma (1960) has experimentally investigated the pitch and heave motions of Series 60 parent forms of  $C_b = 0.60, 0.70$  and  $0.80$ . Fig. 57 shows the non-dimensional results as a function of Froude number in head seas for different wavelength-to-ship length ratios. The low-speed trends were estimated because wall interference affected the results.

Fig. 57 clearly indicates the effects of wave frequency and forward speed in head seas. In general a reduction in forward speed will reduce the heave and pitch motion in long wavelengths and increase the motion in short wavelengths. The motions in short waves ( $L_w/L < 1.0$ ) are significantly less than in longer wavelengths.

Fig. 57 also shows that hull form has only minor effects on the motions in head seas. Although the three models covered a range of form parameters, relatively

small changes in the *nondimensional* amplitudes result. This indicates that the most important parameters for seakeeping responses in head seas are ship length, wavelength, wave amplitude and forward speed. In Section 8 of this Chapter a complete discussion of the influence of design parameters on seakeeping performance will be presented.

As a final example for this subsection, Fig. 58 (Takagi, et al 1985) shows the heave response versus wave period of a model ( $L=1.747\text{m}$  and scale ratio of  $1/64$ ) of a semi-submersible oil drilling rig in bow seas. This figure is intended to illustrate the fact that vessels that are not ship-shaped can have very different response curves from those previously shown. Semi-submersibles are designed to have a very low response at normal wavelengths. Note the zero heave response in wave periods below 1.0 sec model scale or 8.0 sec full scale. Consequently, the heave natural frequency is very low and the large response around a model wave period of 3 seconds in Fig. 58 results. It should be clear that semi-submersibles are typically much different from ships and that the strip theory presented in the previous section cannot be applied.

### 3.8 The Transverse Motions.

(a) *General.* The three motions, roll, sway and yaw, are known as the transverse motions of a vessel. If only linearized equations of motion are considered, these motions are uncoupled from the longitudinal motions discussed in the previous sub-section. That is, these motions can be computed without reference to heave, pitch and surge. The decoupling of these two sets of motions is a good assumption for typical ships in moderate seaways. However, extreme seaways, unusual ship forms or unsymmetric mooring systems may require the treatment of all six degrees of freedom simultaneously. In this section we will only consider the situation where the transverse motions are decoupled from the longitudinal motions. The transverse motions are strongly coupled to one another, but the character of each motion is different. Sway and yaw motions have no hydrostatic restoring forces and do not display any resonant behavior. Roll, on the other hand, has restoring forces and typically displays very marked resonant motions.

The transverse motions are important in the operation of a ship, but for much different reasons from those for the longitudinal motions. For instance, roll is certainly the most severe angular motion experienced by a ship, often exceeding the "small angle" range of ten or fifteen degrees. These large roll angles can make working on the ship difficult and can lead to motion sickness. Further, the transverse motions are responsible for significant athwartship accelerations. The forces resulting from these accelerations must be resisted by machinery foundations and cargo lashings. These same accelerations also make it difficult for the ship's personnel to operate the ship. In fact, roll motions are a major limiting factor in the operability of

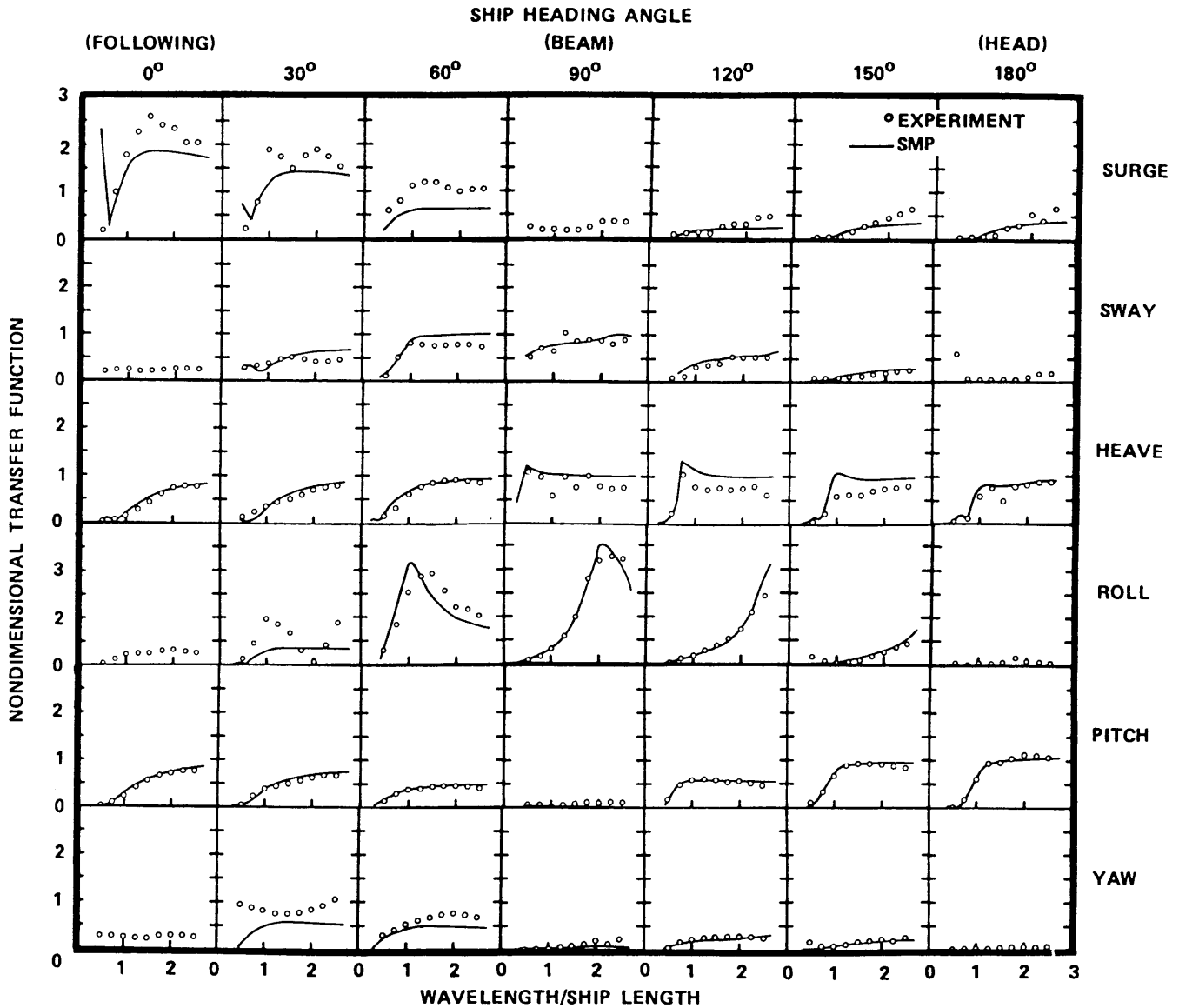


Fig. 56 Comparison of measured and predicted nondimensional transfer functions for the CVA-59 at 25 Knots ( $F_n=0.24$ ) (Baitis, et al, 1981)

offshore platforms.

The hydrodynamics involved in the computation of the transverse motions is more complicated than that of the longitudinal motions, since viscous effects play an important role. For instance, if a ship is underway, a sway velocity or a yaw angle relative to the path of the ship (or both) can place the ship hull at an apparent angle of attack to the flow. Significant transverse lift forces and moments are created on the ship hull and appendages as a result of the generation of vorticity. These forces are not modelled by the slender-body potential flow analysis covered in the previous subsections. For accurate predictions, terms representing these effects may have to be added to those shown in Table 13 in Section 3.4. There are indications that these

forces and moments are important at low frequencies (in the analysis of steering and maneuvering or of the motions in stern seas), at high forward speed, and in the computation of the roll damping. Their role in typical, wave-induced sway and yaw motions is not confirmed. In addition to lift effects, the hydrodynamics associated with roll motion includes many other important components, the overall effect of which is often treated simply as an effective roll damping, as suggested by the  $B_e$  term in  $B_{44}$ , Table 13.

Much less is known about the transverse motions in general, and yaw motions in specific, than is known about the longitudinal motions discussed in the previous sub-sections. A good part of this discrepancy is due to the fact that model testing of these motions is

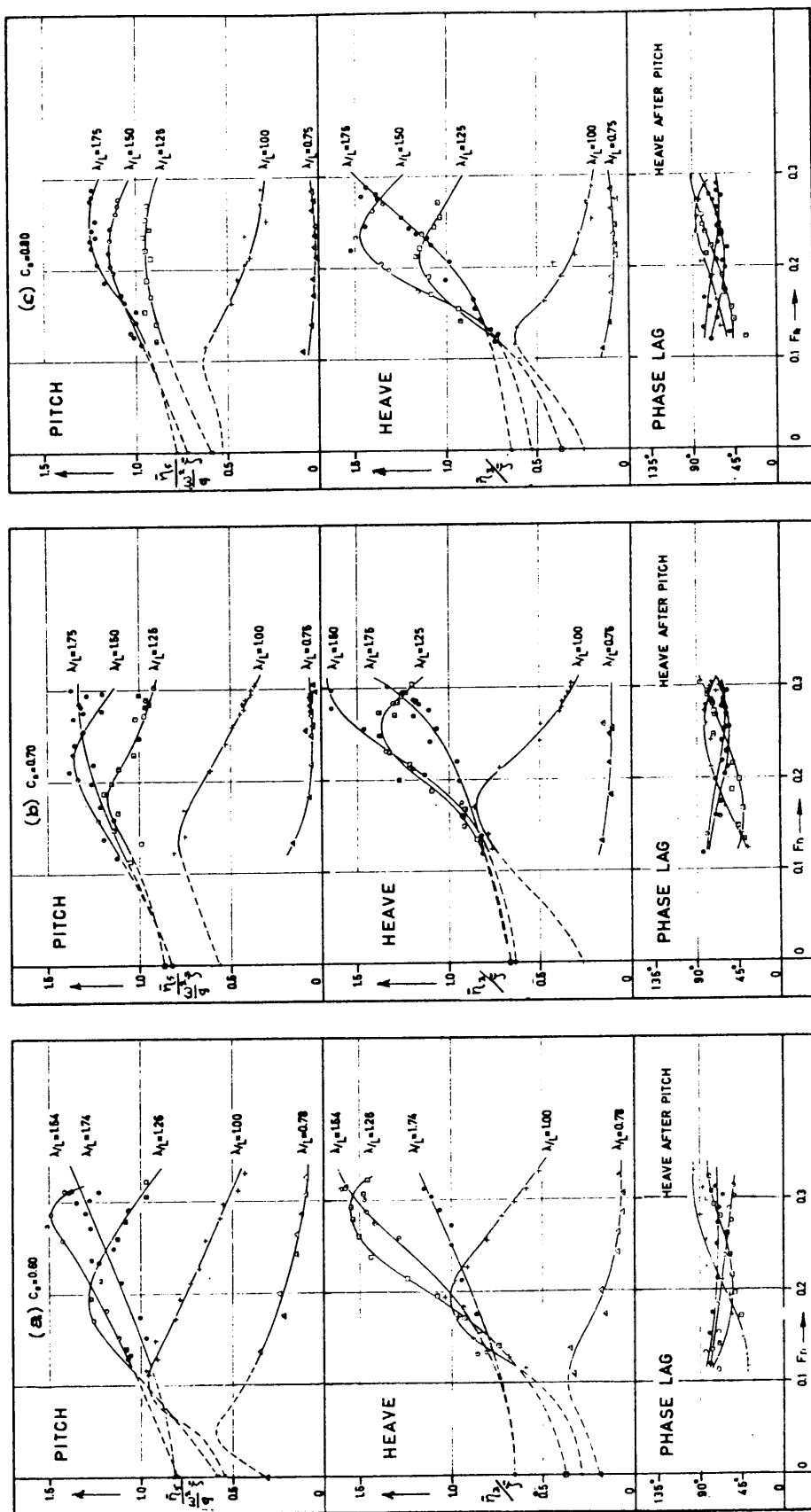


Fig. 57 Heave and pitch responses in regular head seas for three Series 60 models (Gerritsma, 1960) ( $\lambda$  is  $L_u$ )

more difficult. Longitudinal motions can be tested in an ordinary resistance towing tank fitted with a uni-directional wave marker at one end. Serious yaw motions only occur in quartering seas, and roll motions are also worst for most large ships when they are underway in quartering seas. These conditions can only be reproduced in a large basin in which the length and width dimensions are comparable. Further, tests in quartering seas require the model to have six degrees of freedom, and self-propelled models with automatic steering to maintain course are often required. It is possible to test for zero speed roll and sway motions in a narrow resistance towing tank by placing the model's centerline perpendicular to that of the tank. Indeed much of the insight into the nature of rolling that has been obtained comes from this kind of test. Comprehensive experimental validation of the theoretical prediction of transverse motion by slender body or other theories is, however, generally not available.

The results of application of the U.S. Navy's SMP slender-body program (Baitis, et al, 1981) for the aircraft carrier CVA 59 were shown in Fig. 56, Section 3.7, together with experimental results for waves at various headings. The comparison for sway, yaw and roll (rudder fixed) is shown to be good for beam and bow sea conditions. In quartering seas the yaw and roll predictions are less accurate. Special problems do arise in the experimental technique for tests in which the seas approach from the stern or nearly so. First, fewer waves are encountered during a run, since the ship and wave are travelling in the same direction. Second, the effects of the automatic steering become more significant. In the same report in which the CVA 59 results appear, Baitis gives the comparison of the predicted and measured results for the motions of a destroyer escort (DE-1006). The correlation between the motions predicted by SMP and the measurements is quite poor, and it is unclear whether the difficulty lies with the theoretical predictions or the experimental method.

Chapter IX, Controllability, discusses the motions of yaw and sway in relation to the problem of steering, or course-keeping, in both calm water and waves.

(b) *Roll motions.* Roll motions are by far the most difficult motions of a ship to predict. It is therefore appropriate to discuss this motion separately, even though it is strongly coupled with sway and yaw. It is an accepted fact of ship hydrodynamics that the damping arising from the creation of waves (the principal source of damping for heave, pitch, sway and yaw) is almost vanishingly small for the rolling of typical ship forms. Other mechanisms for damping, such as viscous effects, occur naturally. However, these mechanisms lead to roll dampings which are no larger than the wave damping, and thus the total damping from all sources is still small. It is typical for roll motions to have an effective nondimensional damp-

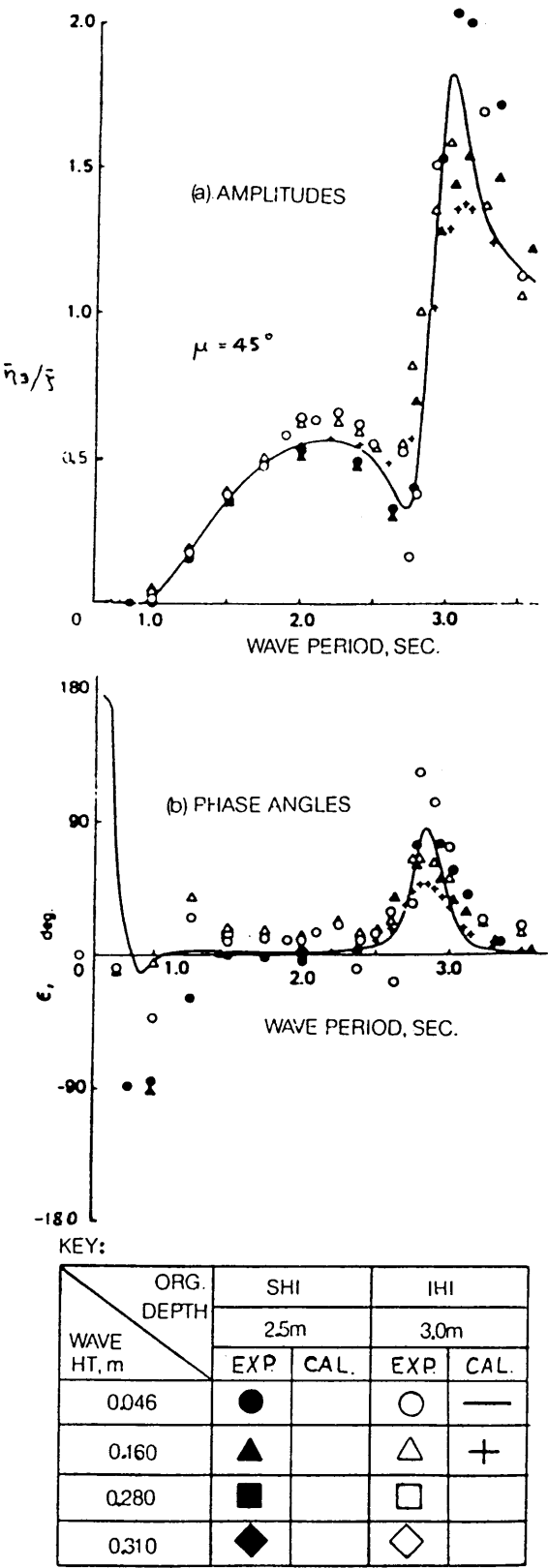


Fig. 58 Heave motion of semi-submerged drilling rig in regular bow waves (Takagi, et al, 1985)



ing ratio of considerably less than 5 percent for a bare-hulled ship. Waves that have an encounter frequency near roll resonance can, and do, cause typical ships to roll severely. These large roll angles can give rise to strong nonlinearities in the hydrodynamic damping and sometimes in the static roll restoring moment. These conditions further complicate any analysis of roll motions.

In order to discuss roll motions, we will assume that the ship is exposed to a single, unidirectional wave train and the transverse motions in response to this wave are sinusoidal. The linearized equations of motion for this situation based on slender-body theory were given in Section 3.4. Inclusion of the nonlinearities mentioned above is not generally possible in such a set of equations, since they lead to responses that include frequencies other than the exciting frequency. Exact treatment of these nonlinearities requires a solution in the time domain, with the hydrodynamic effects represented as convolution integrals.

However, it is common to include roll nonlinearities in an approximate way, using the concept of equivalent linear coefficients. These linear coefficients are selected so that they have the same integrated effect over one cycle of sinusoidal motion as the sum of the linear and nonlinear terms has over the same cycle. The assumption is that motion, including the nonlinearities, is still approximately sinusoidal, and that the principal effect of the nonlinearities is to change the amplitude of the response. The equivalent linear coefficients are not constants but depend primarily on the amplitude of the resulting motion and the ship's forward speed. Iteration is required to obtain correspondence between the values used in the equations of motion and the amplitude of the resulting motion. The U. S. Navy's SMP slender-body program previously mentioned incorporates such an iteration, although the formulation of equivalent linear roll damping is different from that presented later in this section.

For our purpose the three transverse equations of motion can be extracted from the general Equations (132), Section 3.3, by selecting  $j = 2, 4, 6$ . The equivalent linear damping coefficient for roll will be denoted by  $B_{44}^*(|\bar{\eta}_4|)$ , and the equivalent linear restoring coefficient for roll will be denoted by  $C_{44}^*(|\bar{\eta}_4|)$ . The nonlinearities become unimportant for small amplitudes of roll, and in this case  $B_{44}^*(|\bar{\eta}_4|) \rightarrow B_{44}$ , and  $C_{44}^*(|\bar{\eta}_4|) \rightarrow \Delta g \cdot GM_T$ , as given in Table 13. For convenience in notation,  $B_{44}^*$  and  $C_{44}^*$  will be presented without an argument in the development below and the dependence of these quantities on the sinusoidal amplitude  $|\bar{\eta}_4|$  is implied. The sway, yaw and roll equations of motion are, however, strongly coupled.

For the zero forward-speed case it is possible to isolate the effects of roll by a selection of a different ship-fixed coordinate system. The origin of the new system relative to the origin of the  $\bar{x}\bar{y}\bar{z}$  system is  $(\hat{x}, 0, \hat{z})$  and the axes of the new system are rotated an

angle  $\hat{\psi}$  about the  $\bar{y}$ -axis.  $\hat{x}$  and  $\hat{z}$  are chosen to be such that in the new system  $\hat{I}_{42} + \hat{A}_{42} = 0$  and  $\hat{I}_{62} + \hat{A}_{62} = 0$ . Thus,

$$\begin{aligned}\hat{x} &= (I_{62} + A_{62})/(\Delta + A_{22}), \text{ and} \\ \hat{z} &= (I_{42} + A_{42})/(\Delta + A_{22}).\end{aligned}\quad (169)$$

$\hat{\psi}$  is chosen so that  $\hat{I}_{46} + \hat{A}_{46} = 0$  in the new system. The roll equation of motion in this system becomes

$$[-\omega_e^2(\hat{I}_{44} + \hat{A}_{44}) + i\omega_e\hat{B}_{44}^* + C_{44}^*]\bar{\eta}_4 + \hat{B}_{42}\bar{\eta}_2 + \hat{B}_{46}\bar{\eta}_6 = \hat{F}_4 \quad (170)$$

The hydrodynamic coefficients and the roll moment are determined about this new origin, often called the *roll center*. A circumflex has been placed over these quantities as they do have magnitudes that differ from those previously given. Since the ship is assumed to be slender and  $\hat{\psi}$  is very little different from 0, the instantaneous roll angle measured about this new axis is not sensibly different from  $\eta_4$ . The hydrostatic term,  $\hat{C}_{44}^*$  is also not sensibly different from  $C_{44}^*$  since  $\hat{\psi}$  is small and there is no hydrostatic restoring in sway and yaw. In the subsequent discussion we assume that these two quantities can be interchanged with their circumflexed counterparts.

The sway, yaw and roll equations of motion are now inertially decoupled from each other. That is, if one measures the motions about the roll center, sway and yaw accelerations do not instantly lead to roll accelerations, and vice versa. The transformation is analogous to the selection of principal axes of inertia in rigid body mechanics, and the roll center plays the role of the effective center of gravity. However, one should realize that since the  $\hat{A}_{ij}$  are functions of encounter frequency, the roll center is also. A very rough estimate for the location of the roll center is halfway between the center of gravity and the center of buoyancy.

Roll is still coupled to the sway and yaw equations, but now only through the coefficients  $\hat{B}_{42}$  and  $\hat{B}_{46}$ , and this coupling is not strong. In particular, if these two coefficients are identically zero then the uncoupling is complete, even with forward speed. The motions resulting from an initial roll disturbance in calm water will result in pure roll about the roll center. One should note that a ship in a seaway does not actually roll about the roll center, since there will be other motions as well. This is important in design of devices to control rolling, for the apparent vertical for a shipboard observer is affected by these other motions (Section 6).

In order to characterize the roll behavior of a ship, the damped oscillatory motion in calm water that results from the application of a time-harmonic pure roll moment will be examined. If we ignore the coupling terms  $\hat{B}_{42}$  and  $\hat{B}_{46}$ . Equation (170) becomes that of a simple harmonic oscillator with nonlinear damping and restoring,

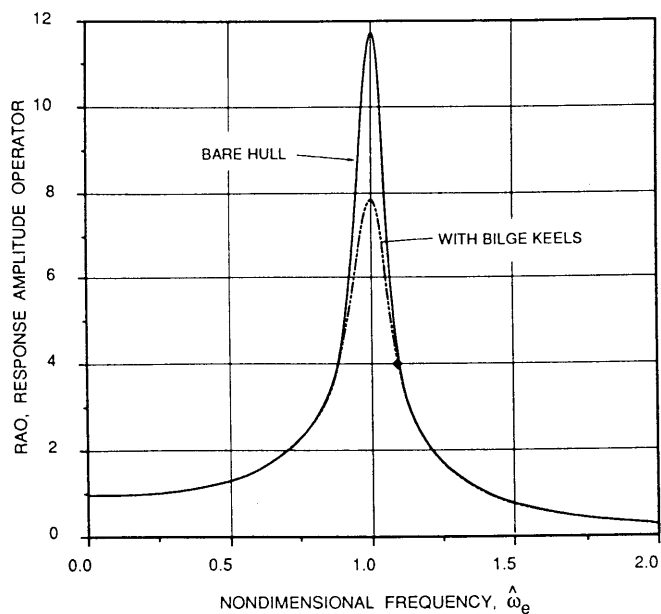


Fig. 59 Comparison of the computed roll response of a typical ship with and without bilge keels (RAO is magnification factor)

$$[-\omega_e^2(\hat{I}_{44} + \hat{A}_{44}) + i\omega_e\hat{B}_{44}^* + C_{44}^*]\bar{\eta}_4 = \hat{F}_4 \quad (171)$$

This is the equation usually adopted for the analysis of roll motions (Conolly, 1969). It should be emphasized that use of an uncoupled roll equation like (171) implies that the center of the coordinate system is at the roll center, that the above-mentioned two coupling terms are ignored, and that a different roll center may be required for each frequency. The roll moment about the roll center,  $\hat{F}_{EX_4}$ , is composed of both hydrostatic and hydrodynamic components. However, frequencies near the roll resonance are often so low that the principal component of  $\hat{F}_{EX_4}$  is the hydrostatic one. An estimate of  $\hat{F}_{EX_4}$  in such a region is  $g\Delta \cdot \overline{GM} \cdot \zeta'$  where  $\zeta'$  is the amplitude of wave slope in radians. For ships that have high metacentric heights relative to their beam (as is common in small craft) the hydrodynamic effects can be large and such an estimate may not be applicable.

Often a ship model in experimental studies is constrained to roll about an axis that passes through the ship's center of gravity. Tests of this type (or computations using slender-body theory in which the center of the coordinate system is different from the roll center) do yield the coefficients which appear in the full equations of transverse motion. However, these coefficients must be translated to the roll center if they are to be used directly in the single equation of roll (171). Finally, one is most often interested in the roll motion near resonance, since even in an irregular seaway most of the roll motion is due to the roll response in this neighborhood. In this case it is usually a satisfactory simplification to treat the roll center as fixed at its position at resonance. The errors involved at

other frequencies are usually not large.

To examine the roll behavior in the region of roll resonance, (171) is recast in nondimensional form by dividing by  $C_{44} = g\Delta \cdot \overline{GM}_T$ , yielding

$$[-\hat{\omega}_e^2 + 2i\hat{\omega}_e \cdot \beta^*(|\bar{\eta}_4|) + \gamma^*(|\bar{\eta}_4|)]\bar{\eta}_4 = f_4 \quad (172)$$

where

$\hat{\omega}_e = \omega_e/\omega_{n_4}$ , the nondimensional encounter frequency,

$\beta^*(|\bar{\eta}_4|) = \hat{B}_{44}^* \cdot \omega_{n_4}/(g\Delta \cdot \overline{GM}_T)$ , the nondimensional damping ratio,

$\gamma^*(|\bar{\eta}_4|) = \hat{C}_{44}^*/(g\Delta \cdot \overline{GM}_T)$ , the nondimensional roll restoring term,

$f_4 = \hat{F}_4/(g\Delta \cdot \overline{GM}_T)$ , the nondimensional roll moment amplitude, and

$\omega_{n_4} = \sqrt{g\Delta \cdot \overline{GM}_T/(\hat{I}_{44} + \hat{A}_{44})}$ , the roll resonance frequency.

Although  $\omega_{n_4}$  is called the roll resonance frequency, it should be noted that it can be considered to be so only for motions small enough for  $C_{44}^* = g\Delta \cdot \overline{GM}_T$  (i.e.,  $\gamma^* = 1$ ).  $\omega_{n_4}$  is simply a reference frequency used for nondimensionalization. Further,  $\omega_{n_4}$  is itself formally a function of encounter frequency, since the added mass moment of inertia,  $\hat{A}_{44}$ , is also. Fortunately,  $\hat{A}_{44}$  is much smaller than  $\hat{I}_{44}$  for typical ship forms, and the dependence of the sum,  $\hat{I}_{44} + \hat{A}_{44}$ , on frequency is quite weak. It will be assumed that the  $\hat{A}_{44}$  is constant and equal to its value at the roll resonance, since this discussion is aimed at the behavior near roll resonance. The quantity  $\beta^*(|\bar{\eta}_4|)$  is the ratio of the equivalent linear roll damping to the critical damping, and as indicated it is dependent on the roll amplitude,  $|\bar{\eta}_4|$ .

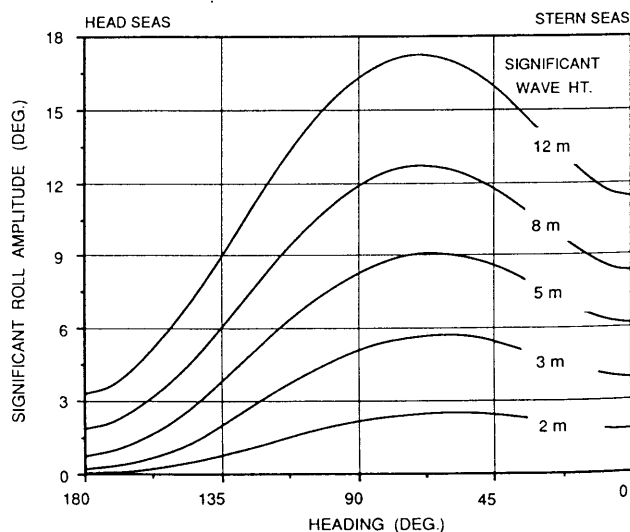


Fig. 60 Short-crested roll response at 18 knots as a function of seaway and heading

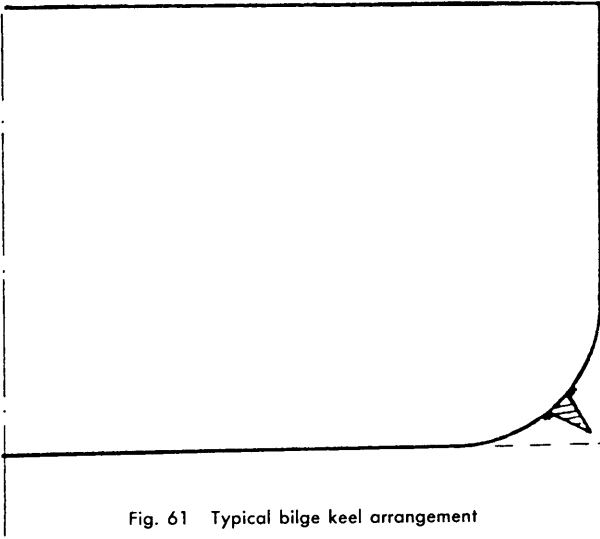


Fig. 61 Typical bilge keel arrangement

$f_4$  is often called the effective wave slope, since for long waves the amplitude of the nondimensional moment is exactly equal to the wave slope amplitude,  $\xi'$ , as discussed above.

The three quantities:  $\omega_{n_4}$ ,  $\beta^*(|\bar{\eta}_4|)$  and  $\gamma^*(|\bar{\eta}_4|)$  characterize the roll response and determination of these three quantities is normally the focus of an analysis of rolling.

For normal ship types  $\gamma^*(|\bar{\eta}_4|)$  is determined from ship hydrostatics, Chapter I. Unusual ship forms, and particularly high-speed craft, can have somewhat different roll stability at forward speed than at zero speed (see the previous sub-section). It is possible for there to be multiple solutions for the roll motion for a given roll moment input if the righting arm,  $\overline{GZ}$ , differs greatly from a linear relationship with the roll angle. Although this possibility is much discussed in the literature (see Battacharya, 1978), the righting arm curve for most ships is linear enough for this not to be a problem. A righting arm curve that increases with  $\bar{\eta}_4$  faster than  $\overline{GM}_T \cdot \bar{\eta}_4$  will lead to a roll resonant frequency that increases with roll amplitude and vice versa. The nonlinearity of the righting arm curve is usually not significant for roll angles less than about 20 deg. However, examination of the righting arm curve for the ship in question is necessary to determine if the predicted motions are sufficiently large for this effect to be important. It will be assumed below that the roll motion is small enough to approximate  $C_{44}^*$  by  $\gamma \Delta \cdot \overline{GM}_T$  (that is, it will be assumed that  $\gamma^* \equiv 1$ ).

The roll resonant period is given by

$$T_{n_4} = \frac{2\pi}{\omega_{n_4}} = \frac{2\pi k_4}{\sqrt{g \cdot \overline{GM}}} \quad (173)$$

where the radius of gyration

$$k_4 = \sqrt{\frac{\hat{I}_{44} + \hat{A}_{44}}{\Delta}}$$

For typical ship forms  $T_{n_4} \approx 2.27 \cdot B / \sqrt{(g \cdot \overline{GM})}$ , where  $B$  is the beam of the ship. The constant 2.27 can vary by as much as 20 percent for unusual ship forms. For instance, aircraft carriers have a flight deck much wider than  $B$  and, as a result,  $\hat{I}_{44}$  is much larger than for a normal ship of the same beam. For this case, a constant of 2.6 or more may be appropriate. On the other hand, submarines which are round and have no superstructure can have constants less than 2.0 when  $B$  is taken to be the maximum beam.

Of the three quantities that characterize roll motion,  $\beta^*(|\bar{\eta}_4|)$ , the damping parameter, is the most crucial one for the ship response. Equation (171) can be solved for  $|\bar{\eta}_4|/f_4$ , the ratio of the roll amplitude to the effective wave slope amplitude. This quantity is called the roll response amplitude operator (RAO). For ships with small roll damping in beam seas the peak of the RAO is equal to  $1/(2\beta^*)$ , and this occurs near the resonant frequency,  $\bar{\omega}_e \equiv 1$ . A typical ship without roll suppression devices such as bilge keels or the like will have a value of  $\beta^*$  less than 5 percent. This means that at resonance, the ship will roll at more than 10 times the effective wave slope (RAO > 10). Thus, it is not uncommon to observe significant rolling in what appears to be an almost calm sea. Figure 59 shows the computed roll response of a typical bare-hulled ship in beam seas. The very narrow and "spiked" response is typical of the motions measured in careful model tests.  $\beta^*$  is the most difficult parameter to estimate because the phenomena that govern roll damping are so complicated. Some details of the phenomena involved and current methods of estimating roll damping are discussed under the next heading.

The roll resonant periods of 10 to 16 seconds are normal for typical large ships. Waves with lengths corresponding to these periods are common only during heavy storm conditions. However, severe rolling can occur in much lighter seas with shorter wave periods if the ship is underway and the seas are coming

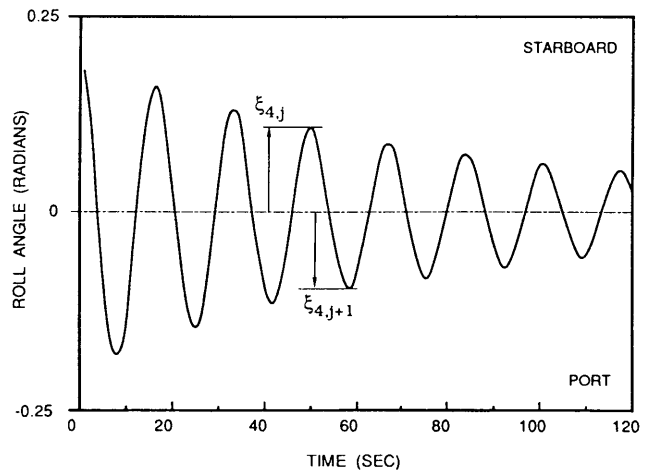


Fig. 62a Time history of the roll decay of a typical ship

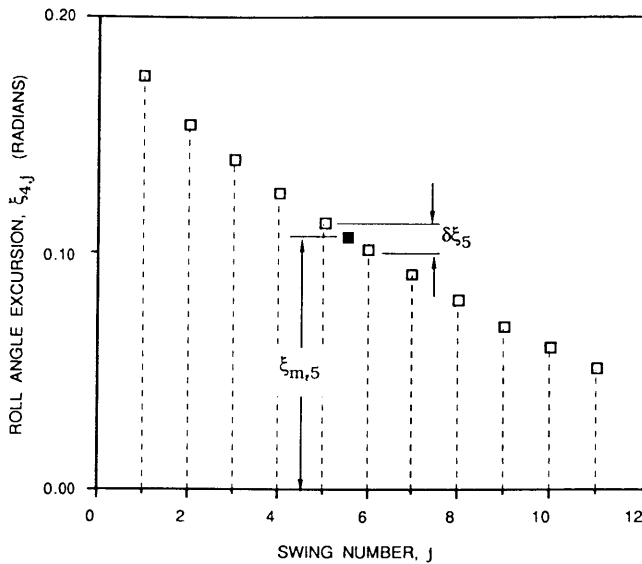
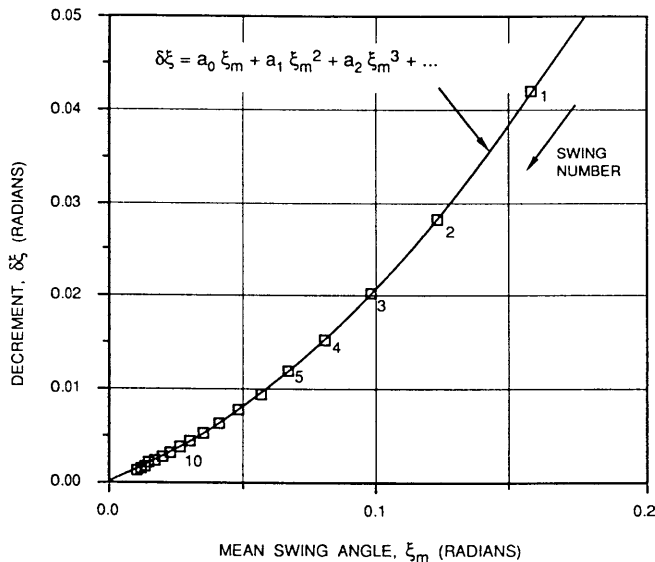
Fig. 62b Roll decay mean swing angle  $\xi_m$  and decrement,  $\delta\xi$ 

Fig. 62c Roll decay test data extinction curve

from the quarter. Although this orientation causes the effective wave slope to be reduced somewhat from its value in beam seas, the encounter period becomes greater than the wave period and resonance can occur. (See discussion Section 4.3). Fig. 60 shows the computed variation in significant roll response in short-crested seas for a typical ship proceeding at its design speed at various headings and sea states. For this ship the worst motions occur when the seas come from a heading from 15 to 30 deg aft of the beam. For ships with normal  $GM_T$ 's and speeds, this worst heading can vary from almost abeam to 45 deg abaft the beam. On the other hand, many barges and small ships have  $GM_T$ 's comparable to their beam and their resonant periods often correspond to the periods observed in

moderate seas. For these ships the rolling motions are worst in beam seas and severe rolling can occur even when not underway. Details of the phenomena involved and current methods of estimating roll damping are discussed under the next heading.

The fact that the roll response is so large has led to the development of a variety of different schemes for increasing the apparent roll damping. Most of these schemes are presented in Section 6. Bilge keels are so commonplace, however, that they deserve to be treated here. These appendages are usually constructed from flat plates that form a sharp obstruction to the roll motion, as shown in Fig. 61. The bilge keel is aligned with the calm water flow about the moving ship so that its effect on the resistance is minimal. Flow visualization studies are often performed during the resistance tests to aid in this placement. The height of the bilge keel is usually selected to be such that the tip of the bilge keel lies within the maximum beam of the ship and above the baseline. In this way the bilge keel is protected by the hull during docking, drydocking and in shallow water. Bilge keels offer a significant improvement in the roll damping over that of a bare ship hull, but fall far short of the damping that can be obtained from other roll stabilization devices. Nonetheless, it is considered prudent naval architecture to install bilge keels when practical, even when other stabilizers are fitted, since only bilge keels are effective in the severest of seas.

Using a theory similar to the one presented above, Schmitke (1978) presents comparisons of the theoretical rolling responses and model test results for a frigate over a range of wavelengths and for four different ship-wave headings. The measured effects of changing

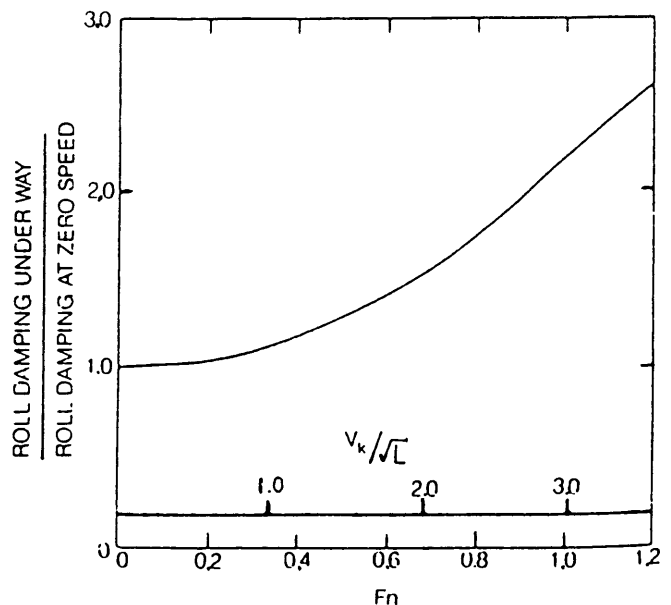


Fig. 63 Effect of speed on roll damping, for unstabilized ships with or without bilge keels (Miller, et al 1973)

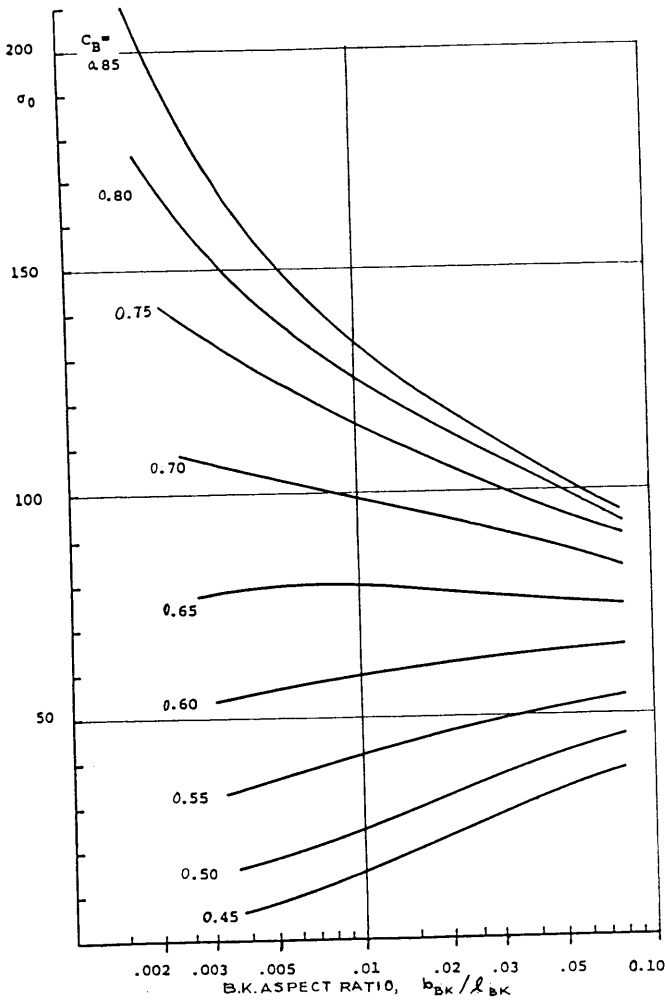


Fig. 64 Bilge-keel efficiency in Watanabe-Inoue method (Himeno, 1981)

speed,  $\overline{GM}_T$  and bilge keel configuration are shown to be in generally good agreement with the theoretical predictions.

(c) *Estimation of roll damping.* Two separate approaches have been used to estimate the roll damping of ship hulls, and both rely heavily on experimental results. The first approach involves direct experimentation and is appropriate in the final design stages. The second uses a combination of analysis of the mechanisms of roll damping coupled with a correlation of historical experimental data with ship characteristics. The resulting formulas are very useful during the preliminary design of the ship.

It has been found through careful experimentation that the part of the roll damping that is not predicted by potential theory is not only a nonlinear function of roll angle, but is also a nonlinear function of roll frequency and forward speed of the ship. It has also been found that there are many components to the roll damping, each of which arises through a separate physical process. It will be assumed that  $\beta^*$  can be

expressed in an expansion in  $|\overline{\eta}_4|$  given by

$$\beta^*(|\overline{\eta}_4|) = \sum_{n=0}^{\infty} \beta_n^* |\overline{\eta}_4|^n \quad (174)$$

$$= \beta_0^* + \beta_1^* |\overline{\eta}_4| + \beta_2^* |\overline{\eta}_4|^2 + \dots,$$

where each of the  $\beta_n^*$  are a function of forward speed. The first term represents linear damping and is associated principally with potential flow effects. This term includes contributions from the roll, sway and yaw damping coefficients listed in Table 13, resulting from the change in coordinate system involved in introducing the roll center. The second and third terms are associated with the damping that is due to real fluid effects, such as fluid drag and flow separation. In general,  $\beta_1^*$  and  $\beta_2^*$  are positive and the equivalent linear damping increases markedly with roll amplitude.

Careful sinusoidal tests to determine the nature of the roll damping for a prototype ship are exceedingly difficult; those for a model are time consuming. A simple alternative is to conduct a transient test, called the roll extinction test. The model (or ship) is inclined to a relatively large roll angle and then released impulsively. The time history of the motion is then recorded. Because roll is so lightly damped, the model (or ship) oscillates at its natural frequency and a large number of rolls can be observed before the motion decays to a roll amplitude too small to measure accurately. See Fig. 62a.

The information in the time history can be used to determine the nonlinear coefficients of roll damping at the roll resonance frequency. Let  $\xi_{4j}$  be the absolute value of the roll angle (in radians) at the  $j$ th maximum

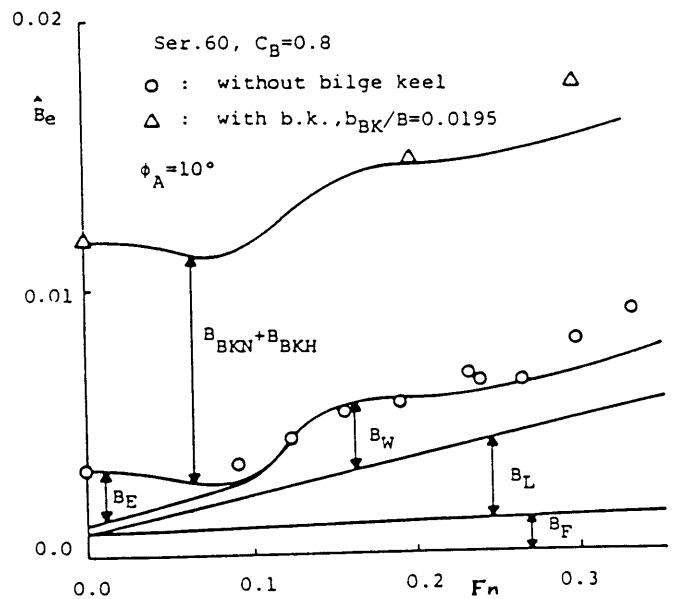


Fig. 65 Comparison of measured and estimated roll damping coefficient as functions of advance speed (Himeno, 1981)

(extreme value). The  $j^{\text{th}}$  decrement,  $\delta\xi_j$ , and the  $j^{\text{th}}$  mean maximum amplitude (port and starboard),  $\xi_m$ , are defined by:

$$\delta\xi_j = (\xi_{4,j-1} - \xi_{4,j}), \text{ and}$$

$$\xi_{m,j} = \frac{1}{2}(\xi_{4,j-1} + \xi_{4,j})$$

Fig. 62b shows the determination of these quantities graphically, and Fig. 62c is a plot of  $\delta\xi_j$  versus  $\xi_{m,j}$ , the so-called *extinction curve*. A cubic polynomial fitted to these discrete points yields

$$\delta\xi \approx a_0 \xi_m + a_1 \xi_m^2 + a_2 \xi_m^3 \quad (175)$$

For a linear system the equivalent linear damping ratio at any mean angle is equal to the decrement divided by  $\pi$ . Thus, the relation between these coefficients and the damping coefficients in Equation (174) is  $\beta_n^* = a_n/\pi$  for  $n = 0, 1, 2$ . An estimate of the nonlinear effects can therefore be made directly from an extinction test. Special caution should be observed when extinction tests are performed on small models since the viscous phenomena that produce these nonlinearities cannot be easily scaled and the model may not behave like the prototype.

For preliminary design purposes, it is necessary to estimate the roll damping of a design for which model or full-scale data are not available. Estimation procedures based on historical data have been developed and two examples are presented here.

The first was developed to predict the roll damping of typical naval ships. It was presented by Miller, et al. (1974) and represents the results of a regression analysis of a number of fairly round-bottomed and fine ships typically used by the U.S. Navy. The procedure involves two steps. First, the zero-speed damping ratio,  $\beta^{(0)}$ , is estimated as

$$\beta^{(0)}(|\bar{\eta}_4|) = 19.25 \left[ A_{BK} \sqrt{b_{BK}} + 0.0024 L B \sqrt{d} \right] \frac{d^2 \sqrt{d} |\bar{\eta}_4|}{(C_B L B^3 T)} \quad (176a)$$

where

$A_{BK}$  is the total area of the bilge keels (port and starboard),

$b_{BK}$  is the width of the bilge keel,

$C_B$  is the block coefficient,

$d$  is the distance from the centerline at the load waterline to the turn of the bilge,

$L$ ,  $B$  and  $T$  are the ship's length, beam and draft, respectively,

$|\bar{\eta}_4|$  is the roll amplitude in radians.

Second, the critical damping ratio,  $\beta^*(|\bar{\eta}_4|)$ , at forward speed is

$$\beta^*(|\bar{\eta}_4|) = \beta^{(0)}(|\bar{\eta}_4|) + 0.00085 (L/B) \sqrt{L/GM} F \{1 + F + 2F^2\} \quad (176b)$$

where

$$F = Fn/C_B, \text{ and } Fn = V/\sqrt{gL}, \text{ the Froude number.}$$

Fig. 63 shows a typical variation of roll damping with forward speed predicted by Equation (176b). Miller's presentation has the advantage of being very easy to apply, but should be used with caution for typical commercial ships with very high midships coefficients.

An alternate and more complicated approach was presented by Watanabe and Inoue (1964) and reported by Himeno (1981). This approximation was based on a detailed analysis of many typical commercial ships, including some very high-block coefficient tankers. This method addresses only the terms  $\beta_0^*$  and  $\beta_1^*$  in Equation (174). Using the same notation as above, Watanabe's method was simplified by Jan de Kat to yield

$$\begin{aligned} \beta^{(0)}_0 &= h [-2.03 (C_B T/L) + 1.6 (A_{BK} \sigma_0/L^2) + 0.064], \\ \beta^{(0)}_1 &= h [0.45 (C_B T/L) + 1.6 (A_{BK} \sigma_0/L^2) + 0.064], \end{aligned} \quad (177)$$

where

$$h = \left\{ \left( \frac{l}{B} \right)^3 \left[ 1.0 + \left( \frac{T}{2l} \right)^2 \right] + f \frac{B}{64 \cdot T} \right\} \times \frac{185}{C_B},$$

$$F = C_{WP}^2 + (C_{WP} - 1)/10,$$

$$l = \overline{KG} - T/2$$

$\overline{KG}$  is the height of the center of gravity above the keel, and

$C_{WP}$  is the waterplane coefficient.

The value  $\sigma_0$  is associated with the bilge keel efficiency and is a function of the block coefficient and the aspect ratio of the bilge keel, given by  $b_{BK}/l_{bk}$ , where  $b_{BK}$  is the width and  $l_{BK}$  is the length of the bilge keel. A plot of the bilge keel efficiency based on considerable experimental data is shown in Fig. 64. Himeno recommends the use of Takahashi's correction for forward speed, given by

$$\beta^{*n} = \beta^{(0)n} \left[ 1.0 + 0.8 [1.0 - e^{(-10Fn)/\hat{\omega}_e^2}] \right] \quad n = 0, 1 \dots \quad (178)$$

(d) *Mechanisms involved in roll damping.* A much more fundamental approach to the problem of roll damping involves the examination of the individual mechanisms that lead to roll damping. This method has been favored by Japanese researchers and most of the work on this approach has been done in Japan. A considerable insight into the most important parameters governing roll damping has been achieved by carefully examining each ingredient. Himeno (1981) plots qualitative graphs of these effects on the total roll damping of a ship. The various components shown are denoted by:

$B_F$ , the moment resulting from the drag (skin friction) of the hull in contact with seawater, a viscous fluid.

$B_E$ , the moment on the bare hull arising as a result of pressures caused by viscous separation of the flow and formation of eddies, principally near sharp bilges.

$B_L$ , the moment arising from hull side forces (lift forces), which are due to the apparent angle of attack of the hull when the ship is rolling under way.

$B_W$ , the moment resulting from the creation of waves when the ship rolls. This is the moment normally computed by linear potential theory.

$B_{BKN}$ , the moment resulting from normal (pressure) forces on just the bilge keels.

$B_{BKH}$ , the moment resulting from the modification of the flow around the hull caused by the existence of bilge keels.

$B_{BKW}$ , the moment arising from wave making of the bilge keels (normally a small quantity for normal-sized bilge keels).

Fig. 65 is reproduced from Himeno (1981) and shows a comparison of the measured and estimated roll damping coefficient for a Series 60, block 0.80 model. Although a promising procedure for performing the calculations is presented by Himeno, it is too complicated to duplicate here.

The figure shows the comparatively large effect of the bilge keel terms  $B_{BKN}$  and  $B_{BKH}$ . The second (interaction) term is due to a change in separation pattern around the hull resulting from a modification of the flow in the neighborhood of the bilge keel (Ikeda, et al., 1978). The figure also shows the strong effect of forward speed on the lift component,  $B_L$ .

(e) *Sway and yaw.* As previously noted, sway and yaw can be calculated by means of the complete equations for lateral motion (Sections 3.3, 3.4)—at least in bow and beam seas. Schmitke (1978) presents approximate solutions for sway assuming no coupling with roll and yaw, which compare moderately well with more exact results for a frigate at cruise speed.

However, sway and yaw motions are strongly influenced by ship steering, whether done manually or by means of an automatic control or auto-pilot. In turn, sway, yaw and roll characteristics all affect the design of the rudder, steering gear and control system. Swaying of a fast moving ship places it at an angle of attack, producing transverse forces and moments, just as yawing does. These problems are discussed in Chapter IX, Controllability. The ultimate merging of the fields of seakeeping (where the motions are at wave frequency) and coursekeeping (where the motions occur much more slowly) into a complete theory of steering in

waves has not yet been accomplished.

The relatively high-frequency yawing in bow seas generally poses no problems for either comfort of personnel or steering, since amplitudes are usually small. Hence, there is seldom any attempt made to control these motions in either hand or automatic steering. Early model tests in bow seas at the Davidson Laboratory (Lewis and Numata, 1960) and at the Netherlands Ship Model Basin (Vossers, 1962) revealed unexpectedly large values of leeway angle between the mean model heading and the path made good across the tank. This angle varied with wave length and speed. This important non-linear effect is not accounted for in the basic theory of ship motions in waves (See Section 5).

In quartering and following seas, the wave-encounter frequencies are much lower than in head seas or seas on the bow. This situation can lead to large amplitudes of the unrestored motions of sway and yaw, to serious interactions with the steering, and, as discussed in the previous sub-sections, to large resonant rolling angles. The combination of these three motions is uncomfortable to crew and passengers. It is sometimes called a "dutch roll," since it is comparable to this well known motion of airplanes.

In extreme high waves, where the water particle velocities become comparable to the ship speed, there is a possibility of loss of control and of broaching. This latter condition, when the ship yaws to an orientation parallel to the wave crests, is extremely dangerous and may lead to capsizing.

(f) *Roll instability and capsizing.* Capsize of large ships is fortunately very rare. Detailed theoretical and experimental studies of these phenomena have been conducted by Oakley, Paulling and Wood (1974). These show that there are several different mechanisms that can lead to capsize. Most of these mechanisms are essentially nonlinear in nature and cannot be investigated by the above simple frequency-domain approach. One mechanism, broaching, was discussed above.

Another mechanism involves the static stability characteristics of roll in a seaway Paulling (1961). The wave surface is not plane and thus the instantaneous load waterline is not either. The metacentric radius derived from this waterline may differ somewhat from that computed for the still waterline. The  $\overline{GM}_T$  is very sensitive to the metacentric radius, and the result is that significant variations in  $\overline{GM}_T$  can occur with a frequency equal to the encounter frequency. The parametric variation in  $\overline{GM}_T$  can lead to a roll instabilities, with roll motions increasing in time. These conditions are worst for ships with low initial stability and in stern seas or almost stern seas.

## Section 4

### The Ship in a Seaway<sup>10</sup>

**4.1 Theory of Linear Response to a Statistically Stationary Seaway.** Much if not most of the theory of the linear response of a marine system to random excitation was developed in the context of electronics and communication (Rice, 1944), (Lee, 1960). A great deal of the resulting theoretical detail has been directly transferred to marine applications where it has been called the theory of *linear superposition*. There are, however, some significant differences that are peculiar to this application. These have to do with the idea that the wave field (or excitation) is a function of space as well as time, and that the vessel of interest is more often than not moving at some speed within the wave system. St. Denis and Pierson (1953) introduced the basic concepts to the marine field, and resolved most of the problems peculiar to the application. Price and Bishop (1974) may serve those interested as a more modern and detailed treatment of both the basic theory and the problems of marine applications.

A reasonable and useful (if not exact) model for realistic seaways is described in Section 2 in terms of statistically stationary, zero-mean, Gaussian (or normal) random processes. While the wave elevations in a stationary wave process vary with time and position in the wave field, the probability structure of the process does not. That is, the statistical parameters that describe the process are constants. If the instantaneous wave elevations of a Gaussian process are sampled, the statistical properties of the sample are governed by a Gaussian probability density function; that is, the Gaussian assumption applies to wave elevation. In a zero-mean Gaussian process the only necessary statistical parameters are the wave variance and its frequency/direction decomposition (or spectrum).

Conceptually, once the spectrum of the stationary Gaussian process is fixed, the variance and other statistics of the process are determined for all time and space. This is not, of course, what happens in the ocean. The magnitude of ocean waves and their spectrum varies continuously in time and space. In the long term and over long distances ocean waves are non-stationary. Unfortunately, we do not have a rigorous statistical model for the response of a vessel to a non-stationary process. This conflict is resolved by the assumption that the evolution of the wave statistics in the vicinity of the vessel occurs gradually enough that we may approximate reality by a succession of space-time processes, each of which is considered statistically stationary in the short term and near field. This assumption allows the practical use of available theory for the response of a vessel to a stationary Gaussian random process.

In the study of the response of the ship to the sea-

way, the concepts of Section 2 that are of fundamental use are the wave *point spectrum*,  $S_{\zeta}(\omega)$ , and the *directional spectrum*,  $S_{\zeta}(\omega, \mu)$ . In this section a somewhat restrictive definition of the point spectrum will be employed. Here, we will use the point spectrum only to define *long-crested* random waves. It should also be noted at the outset that the direction variable,  $\mu$ , will be defined in the same way as in Section 3; that is, with respect to an  $x_0, y_0, z_0$  coordinate system fixed in the earth so that the  $x_0$ -axis is coincident with the heading or nominal course of the ship. The angle,  $\mu$ , in general will denote the direction of propagation of waves relative to the  $x_0$ -axis, and is taken to be positive counter-clockwise so as to conform to a right-hand rule. The reader may note that these conventions are opposite to those usually employed at sea where the angle denotes the direction from which the waves come, and the sense of the angle is in accordance with the compass. We lose no generality with the conventions of Section 3 since the directional spectrum may easily be transformed from one system to the other, and in any event, absolute directions come into play only in operational use of the final results of the theory.

Section 3 dealt with the physics of the response of a vessel to deterministic wave fields (regular waves), and it may perhaps not be immediately obvious how these results may be connected with the probabilistic model of Section 2. Broadly speaking, the analyses of Section 3 define the vessel response as a linear transformation of the wave elevation field. Results from the theory of probability say, in effect, that a linear transformation of a stationary Gaussian random process yields another stationary Gaussian random process. Thus, so long as the vessel's response is mathematically linear (or reasonably so) an immediate connection may be made between the stationary Gaussian wave field and a stationary Gaussian representation of the response. Moreover, once the response can be assumed to be Gaussian, the statistics of response maxima may be treated in the same manner as the wave maxima. Thus, the most important general observation about the deterministic development of vessel response in Section 3 is that all the analyses are linearized. Linearity of response is the fundamental assumption of the theory to be discussed here.

In studying the response of a vessel in a seaway the pertinent end result of Section 3 is the complex amplitude,  $\bar{\eta}_j$ , of the  $j$ th response to a regular wave of complex amplitude  $\zeta$ , whose phase is referenced to the origin of the coordinate system fixed in the vessel. Once the vessel geometry is fixed, there are four es-

<sup>10</sup> Section 4 written by John F. Dalzell.



essentially independent variables in the analysis of Section 3: regular wave amplitude,  $\bar{\zeta}$ , circular frequency,  $\omega = 2\pi/T$ , and direction,  $\mu$ , as well as vessel speed,  $U_0$ . These are the same four independent variables in a laboratory test of a model vessel in regular waves. Now the theory to be discussed cannot handle temporal variations in vessel speed within a particular realization of a random wave process. Thus for present purposes, the speed,  $U_0$ , must be considered to be a constant parameter, just as it is in practical implementations of the theory of Section 3, as well as many experimental investigations; i.e., surge is assumed to be zero.

The linearity assumption requires that the amplitude of the response be proportional to the exciting regular wave amplitude, and that the response phase be invariant with wave amplitude. Thus in the notation of Section 3, the ratio,  $\bar{\eta}_j/\bar{\zeta}$ , must be invariant with  $\bar{\zeta}$  for fixed  $\omega$ ,  $\mu$  and  $U_0$ . In numerical evaluations of the theory of Section 3 this invariance is assumed and computations are usually carried out for a unit regular-wave amplitude. Thus in practice, the results of the theory of Section 3,  $\bar{\eta}_j$ , are complex amplitudes per unit regular wave amplitude. Similarly, it is also conventional to normalize experimental determinations of the complex response amplitude in the same way. It is then natural to modify the notation of Section 3 and let  $\bar{\eta}_j$  represent  $\bar{\eta}_j/\bar{\zeta}_j$ . Thus, in this section

$\bar{\eta}_j(\omega, \mu; U_0) \equiv$  the complex  $j$ th response amplitude per unit regular wave amplitude, as a function of wave frequency  $\omega$ , and direction  $\mu$ , with constant vessel speed,  $U_0$  assumed.

As noted in Section 3, the vessel responses are physically related to *encounter frequency*,  $\omega_e$ . It will be noted from the definitions in Sections 2 and 3 that encounter frequency is determined by the variables in the argument of the function just defined. Thus, we may also consider the complex responses of a vessel to be functions of encounter frequency and define:

$\bar{\eta}_j(\omega_e, \mu; U_0) \equiv$  the complex  $j$ th response amplitude per unit regular wave amplitude, as a function of wave encounter frequency,  $\omega_e$ , and direction,  $\mu$ , with constant vessel speed,  $U_0$  assumed.

where it should be noted from Section 2.8 that the mapping from encounter to wave frequency may have to be handled carefully.

The functions that have just been defined are analogous to those that result from the application of generalized linear systems theory in other fields. In marine usage these functions bear various borrowed names; in particular, four common names used synonymously are: *transfer function*, *frequency response function*, *system function* and *receptance*. Whatever the terminology, the physical meaning is as defined above,

the relationships of the complex functions to normalized amplitude and phases of response are as defined in Section 3, and the underlying fundamental assumption is that the physical system is linear so that the relations between its response and its excitation may be completely defined in this way.

The modulus of the transfer function has special importance in the theory to be discussed, and bears a special name which is unique to marine usage. The terminology was originated by St. Denis and Pierson (1953) where  $|\bar{\eta}_j(\omega_e, \mu; U_0)|^2$  was defined as the *response amplitude operator*. Over the intervening years the custom much more often than not has been to define the unsquared  $|\bar{\eta}_j(\omega_e, \mu; U_0)|$  as the response amplitude operator, abbreviated RAO. The numerical consequences of confusing the squared and unsquared forms will be obvious to the reader, and it cannot be said that the squared form is no longer used in practice (Lackenby, 1978). However, for present purposes the unsquared form will be employed, and thus when response amplitude operator or RAO is used here it will mean the ratio of the (scalar) amplitude of response and the exciting regular wave amplitude, and will usually be expressed as  $|\bar{\eta}_j(\omega, \mu; U_0)|$  or  $|\bar{\eta}_j(\omega_e, \mu; U_0)|$ .

Now to illustrate the form of the connection between the theories of Sections 2 and 3, first note that from Section 3, Equation (96) the  $j$ 'th response to a regular wave may be written in real form as:

$$\eta_j(t) = |\bar{\eta}_j(\omega_e, \mu; U_0)| \bar{\zeta} \cos [\epsilon - \omega_e t + \sigma_j(\omega_e)]$$

where  $\sigma_j(\omega_e)$  is the phase of the response relative to the wave elevation and  $\epsilon$  represents an arbitrary phase that defines the elevation of a regular wave at time zero, as given in Equation (25) of Section 2.2. The definition of  $|\bar{\eta}_j(\omega_e, \mu; U_0)|$ , as noted above, corresponds to  $\bar{\eta}_j/\bar{\zeta}$  in the notation of Section 3. Thus the linear transformation of the motions analysis produces a shift in phase,  $\sigma_j(\omega_e)$ , and an amplitude proportional to the amplitude of the regular wave.

The linear superposition theory of Section 2, and indeed all general linear system theory, demands that the response to a sum of exciting waves be equal to the sum of the responses to each of the individual wave components. Thus the response to a sum of regular waves each defined by its wave frequency,  $\omega_m$ , direction,  $\mu_m$ , and amplitude,  $\bar{\zeta}_{mn}$ , becomes:

$$\eta_j(t) = \sum_m \sum_n |\bar{\eta}_j[(\omega_e)_{mn}, \mu_n; U_0]| \times \bar{\zeta}_{mn} \cos \left[ \epsilon_{mn} - (\omega_e)_{mn} t + \sigma_j[(\omega_e)_{mn}] \right] \quad (179)$$

The correspondence between Equation (179) and Equation (71) of Section 2.8 may be noted. The expressions are of identical form except that there is an additional factor of the  $mn$ 'th RAO and an additional deterministic phase in the argument of the cosine. If the arbitrary wave phases,  $\epsilon_{mn}$ , are assumed to be random

as in the representation of Section 2, the response may be interpreted as a random variable. Evaluating the variance of the response, (179), with the formalism of Section 2:

$$\text{Var}[\eta_j(t)] \equiv \langle [\eta_j(t)]^2 \rangle \\ = \frac{1}{2} \sum_m \sum_n |\bar{\eta}_j[(\omega_e)_{mn}, \mu_n; U_0]|^2 \bar{\zeta}_{mn}^2 \quad (180)$$

where the brackets  $\langle \rangle$  denote mean value. As in the random phase model of waves, Section 2, the variance of response becomes half the summation of squared response amplitudes.

In an analogy to the directional wave spectrum of Section 2, we may also define a continuous *pseudo-spectrum* of response,  $P_j(\omega_e, \mu)$ , whose integral equals the response variance:

$$\text{Var}[\eta_j(t)] = \int_0^{2\pi} \int_0^\infty P_j(\omega_e, \mu) d\omega_e d\mu \quad (181)$$

Comparing Eqs. (180) and (181), the pseudo-spectrum may be identified as a limit as  $\delta\omega_e \rightarrow 0$  and  $\delta\mu \rightarrow 0$ :

$$P_j[(\omega_e)_{mn}, \mu_n] \rightarrow \left[ \frac{1}{2} |\bar{\eta}_j[(\omega_e)_{mn}, \mu_n; U_0]|^2 \bar{\zeta}_{mn}^2 / \delta\omega_e \delta\mu \right] \quad (182)$$

This pseudo-spectrum expresses the contribution to response variance of the deterministic response to component waves of different frequencies and directions. Comparing Equation (182) and Equation (72) of Section 2.8, the relationship between the pseudo response spectrum and the directional wave spectrum becomes:

$$P_j(\omega_e, \mu) = |\bar{\eta}_j(\omega_e, \mu; U_0)|^2 S_\zeta(\omega_e, \mu) \quad (183)$$

Though the corresponding directional wave spectrum is "observable", the pseudo-spectrum of response is not. Any given response is an observable function of time. We can decompose an observable time function into frequency components, but cannot unambiguously determine the direction of the wave components that produced each frequency component. Thus it is necessary to define a response spectrum that is a function only of encounter frequency, and this may be done in the same manner as was done in Section 2 for the wave point spectrum:

$$S_j(\omega_e) = \int_0^{2\pi} P_j(\omega_e, \mu) d\mu \quad (184)$$

Comparing (184), (183), (182), and (180) the response spectrum may be identified as a limit as  $\delta\omega_e \rightarrow 0$ :

$$S_j[(\omega_e)_{mn}] \rightarrow \left\{ \frac{1}{2} \sum_n |\bar{\eta}_j[(\omega_e)_{mn}, \mu_n; U_0]|^2 \bar{\zeta}_{mn}^2 / \delta\omega_e \right\} \quad (185)$$

As one would expect by now, the response spectrum is the contribution to response variance of the deterministic responses to all those wave components that produce encounter frequencies within an infinitesimal encounter frequency band. The summation appears within the limiting form, (185) because, as pointed out in Section 2.8, the same encounter frequency may be produced by wave components having different directions.

The sections that follow contain a condensation of the principal results from response theory, and the resulting procedures, as applied to marine vehicles. They will begin with the simplest case and proceed to the more general.

**4.2 The Long-Crested, Zero-Speed Case.** The long-crested, zero-speed situation is at once the simplest case of interest, and one that is essentially the same as the basic communication or electronic theory. When the vessel is moored or hove-to an observer aboard the ship senses wave frequencies without distortion due to ship speed so that encounter and wave frequencies are the same. The long-crestedness assumption means that the direction of propagation of all wave components relative to ship heading is the same,  $\mu_0$ , say, and that the waves may otherwise be represented by a point spectrum,  $S_\zeta(\omega)$ . In this case the relationship between the variance spectrum of the  $j$ 'th response and the wave point spectrum becomes:

$$S_j(\omega) = |\bar{\eta}_j(\omega, \mu_0; 0)|^2 S_\zeta(\omega) \quad (186)$$

The response spectrum is thus equal to the product of the wave point spectrum and the squared modulus of the transfer function (or squared RAO according to the present definition). It might be noted again that the wave direction variable,  $\mu_0$ , is a constant parameter within the expression, and we have substituted  $U_0 = 0$  in the argument of the transfer function.

As has been implied by the treatment of the last section, the integral of the response spectrum over positive frequency is defined to be the response variance. (Variance spectra in this chapter are defined only for positive frequencies.) In simpler language, the area under the response spectrum is equal to the variance of the response. In this case, the spectral moments of response are defined in the same way as for point spectra of waves (see Section 2.6):

$$m_n = \int_0^\infty \omega^n S_j(\omega) d\omega \quad (187)$$

and as in the case of waves:

- $m_0$  is response variance
- $m_2$  is variance of response velocity
- $m_4$  is variance of response acceleration

Period averages for response are also defined as in Equations (49) through (52) of Section 2.6; that is, the same formulas hold, with response spectral moments

used instead of wave spectral moments. In practice, the estimates of response spectra and the moment integrals are done numerically; response amplitude operators almost never are obtained in continuous and sufficiently simple analytical forms that might allow purely analytical expressions for either the spectra or the moments (See 4.6, example computations).

**4.3 The Long-Crested, Forward-Speed Case.** As in the last section, the waves are assumed to be long-crested so that all wave components propagate in the same constant direction,  $\mu_0$ , relative to ship heading. As before, we also assume that a wave point spectrum is available to define the frequency content of the waves. In this case we consider non-zero vessel speed ( $U_0 \neq 0$ ). It has been pointed out in Section 2.8 that non-zero vessel speed can result in considerable complication, and it is at this point that we resume the discussion started there. In order to develop the response spectrum in a more practical form than has been indicated in Section 4.1 we must develop the encountered wave spectrum in some detail. We will consider encounter frequency to be positive always and write it in a slightly different form to express this:

$$\omega_e = |\omega - (\omega^2 U_0 / g) \cos \mu_0| \quad (188)$$

Now the transition from the wave point spectrum defining long-crested waves to the encountered spectrum is essentially a transformation of the frequency coordinate system such that the wave variance is preserved. In a similar way to the treatment of Section 2.8, the encountered spectrum for long-crested waves may be written:

$$S_\zeta(\omega_e; \mu_0, U_0) = S_\zeta(\omega) / |1 - (2\omega U_0 / g) \cos \mu_0| \quad (189)$$

where the value on the right-hand side must be associated with the proper value of  $\omega_e$  via the transformation, (188). The absolute value of the denominator (the *Jacobian* of the transformation) is taken because spectral density (the frequency decomposition of variance) must be positive. It may also be noted that the constant parameters,  $\mu_0$ ,  $U_0$ , have been added to the augment list of the encounter spectrum to emphasize the point that this function of encounter frequency depends upon the values assumed for speed and wave direction.

The detailed treatment of the encountered long-crested wave spectrum is dependent upon the sign of  $\cos \mu_0$  in the transformation (188). There are effectively three possibilities. The first is that the wave direction is 90 or 270 deg; that is, the vessel is proceeding in beam long-crested waves. In this event,  $\cos \mu_0 = 0$ , thus  $\omega_e = \omega$ , and the encountered spectrum is the same as the wave point spectrum regardless of speed. Thus in beam long-crested seas the relations between response spectra and wave spectra are the same as were noted in the last sub-section, the only difference being that the RAO would have to be that for a wave direction of 90 or 270 deg.

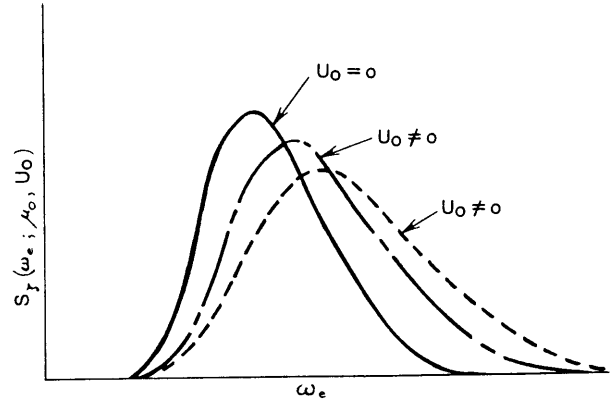


Fig. 66 Wave encounter spectra in long-crested head seas, at increasing ship speeds

The second possibility to be considered is that of head or bow waves. In this case  $\mu_0$  is between 90 and 270 deg, and  $\cos \mu_0$  is negative. In this circumstance the expression within the absolute value signs in (188) is always positive. This means that the transformation between  $\omega_e$  and  $\omega$  is one-to-one for all positive values of frequency, and that the denominator of (189) will not approach zero. Fig. 66 illustrates schematically the influence of speed upon the encountered long-crested sea spectrum for head or bow seas. Generally, the shape of the encountered spectrum is similar to that of the point spectrum regardless of speed. The effect of the transformation is to shift the spectrum to higher frequencies and flatten it a bit, while the area remains constant. Now turning to the relationships between the wave encounter and the response spectrum, the response spectrum for long-crested head or bow waves becomes:

$$S_j^H(\omega_e) = |\bar{\eta}_j(\omega_e, \mu_0; U_0)|^2 S_\zeta(\omega_e; \mu_0, U_0) \quad (190)$$

where  $90 \leq \mu_0 \leq 270$  deg, the transfer function is developed as a function of encounter frequency, and the transformation of the wave frequency spectrum is carried out as in (189). The superscript,  $H$ , is to call attention to the fact that the relationship holds only for long-crested head or bow waves.

With the last paragraph half of the possible directions of long-crested waves have been dealt with. The other half involves quartering and following seas. In this case  $0 \leq \mu_0 \leq 90$ , or  $270 \leq \mu_0 \leq 360$  deg, and  $\cos \mu_0$  is positive. The resulting variation of encounter frequency (188) with wave frequency is shown schematically in Fig. 67. In general, as wave frequency increases, encounter frequency goes through a maximum, returns to zero, and then increases once more. The figure illustrates the primary complication in the transformation between wave and encounter frequency for following or quartering waves; that is, for any value of  $\omega_e$  there correspond either one or three values of  $\omega$  (and one or three wave lengths). An observer aboard ship who senses an encounter frequency

less than  $g/(4U_0 \cos \mu_0)$  cannot work out the corresponding wave frequency without additional information. The wave frequency,  $g/(U_0 \cos \mu_0)$ , at which  $\omega_e = 0$  corresponds to the situation where the component of ship speed in the direction of wave propagation,  $(U_0 \cos \mu_0)$ , is exactly the same as the wave celerity,  $V_c$ . The maximum in the curve of  $\omega_e$  occurs at  $\omega = g/(2U_0 \cos \mu_0)$ , and at this point the component of ship speed in the direction of wave propagation is exactly equal to the group velocity of the waves,  $V_c/2$ . Near this maximum there is a broad range of wave frequencies,  $\omega$ , that will produce nearly the same frequency of encounter.

For the following or quartering wave case, the transformation between encounter and wave frequency is multi-valued, and this must be accounted for in the development of the encountered spectrum. For this purpose the wave frequency range may be divided into three regions as shown in Fig. 67. In the first, the component of ship speed in the direction of wave advance is less than the wave group velocity. In the second, the ship velocity component is between wave group velocity and celerity, and in the third, the ship velocity component is greater than the celerity. Physically, in Regions I and II the waves overtake the ship, and in Region III the ship overtakes the waves. Within each of the three regions the  $\omega, \omega_e$  transformation is one-to-one.

Fig. 68 illustrates schematically what happens when the transformation, Equation (189), is carried out for quartering or following waves. The (a) part of the figure indicates the wave frequency spectrum and the position of the three regions noted in Fig. 67. The (b) part of the figure indicates what happens when the operation defined by (189) is carried out. As  $\omega$  approaches  $g/(2U_0 \cos \mu_0)$  the denominator of (189) goes to zero and the result is a singularity in the encountered spectrum. The area under the spectrum at this

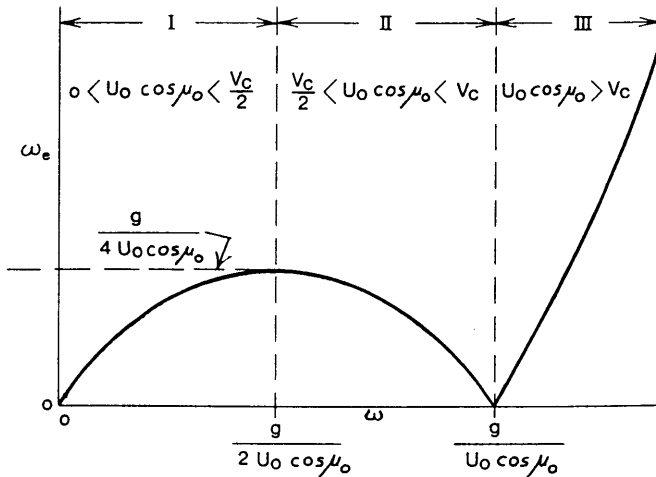


Fig. 67 Variation of encounter frequency with wave frequency for regular following or quartering waves

step is not equal to the wave variance because the transformation is not complete. The modified spectral densities have not been associated with the proper encounter frequency, a schematic scale of which is included beneath part (b) of the figure. Part (c) indicates the association step. The contribution of Region I extends from zero to  $\omega_e = g/(4U_0 \cos \mu_0)$ . The Region II contribution folds back and extends down to zero frequency, and the Region III contribution starts at zero and extends to indefinitely high encounter frequency. Part (d) of the figure indicates the wave spectrum as would be sensed aboard the moving ship. In the range  $0 \leq \omega_e \leq g/(4U_0 \cos \mu_0)$  the contributions from the three wave frequency regions are additive.

Thus, the encountered spectrum for quartering or following waves can be a practically unrecognizable modification of the wave frequency spectrum. It is worth noting that if the wave spectrum is appreciable at  $\omega = g/(2U_0 \cos \mu_0)$  the encounter spectrum will almost certainly have a strong peak at  $\omega_e = g/(4U_0 \cos \mu_0)$ . Within the range of typical ship sizes and speeds, the contribution of Region III tends to be unimportant, but there is a good possibility that both Regions I and II may be important for high-speed ships.

Now turning to the relation between the response and the encountered wave spectrum, the preceding discussion shows that, in order to estimate the response spectrum in quartering or following waves, we must handle the contributions from the three regions of wave frequency separately. In this case the response spectrum is formed by:

$$S_j^F(\omega_e) = |\bar{\eta}_j^I(\omega_e, \mu_0; U_0)|^2 S^I(\omega_e; \mu_0, U_0) + |\bar{\eta}_j^{II}(\omega_e, \mu_0; U_0)|^2 S^{II}(\omega_e; \mu_0, U_0) + |\bar{\eta}_j^{III}(\omega_e, \mu_0; U_0)|^2 S^{III}(\omega_e; \mu_0, U_0) \quad (191)$$

where for example,  $S^I(\omega_e; \mu_0, U_0)$  is the contribution to the wave encounter spectrum from Region I, and  $|\bar{\eta}_j^I(\omega_e, \mu_0; U_0)|$  is the response amplitude operator associated with the wave frequencies of Region I. It should be noted that the contributions from Regions I and II will contain singularities unless the response operator for  $\omega_e = g/(4U_0 \cos \mu_0)$  is zero, a relatively unlikely event. However, the area of the response spectrum will be finite and equal to the response variance.

In practice, the moments of the response spectrum are usually a more important result than the response spectrum itself. The response spectral moments are only meaningful in terms of encounter frequency, and are defined as follows:

$$m_n = \int_0^\infty (\omega_e)^n S_j(\omega_e) d\omega_e \quad (192)$$

so that once having the response spectrum, (190) or (191), the immediate next step is to integrate over

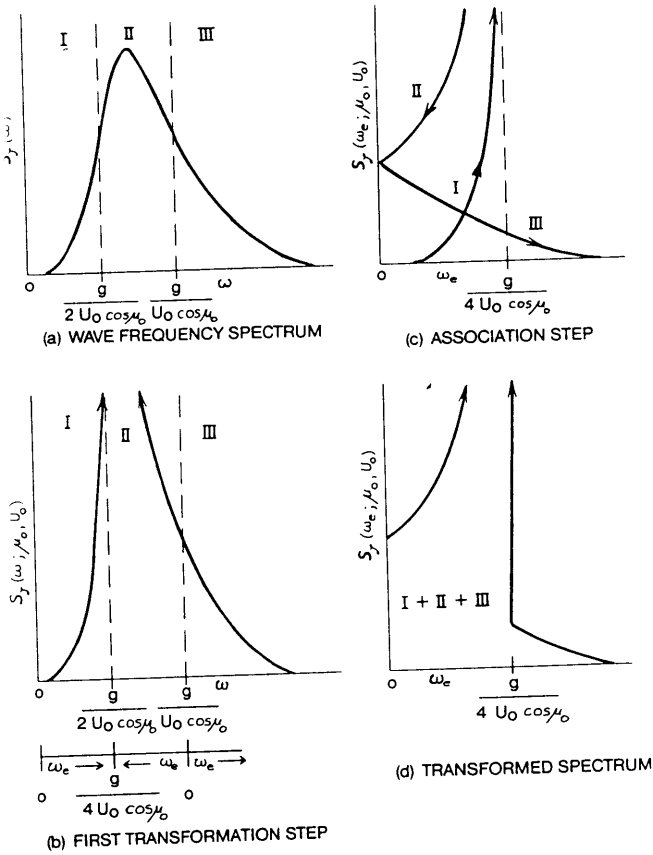


Fig. 68 Transformation of wave spectrum to encounter spectrum, following or quartering waves (long-crested)

encounter frequency. As mentioned previously, all practical work is done numerically. Because of the nature of the head or bow sea frequency transformation, numerical integration of (190) is hardly more difficult than in the zero speed case. However, because of the singularities in (191), which are brought on by the frequency transformation, numerical integrations for quartering or following waves become rather complicated exercises. For this reason it is customary to proceed in a different manner. The basic relationships between response variance or moments could have been developed in the wave frequency domain at the outset, and this was done in St. Denis and Pierson (1953). The frequency transformation was introduced in that reference only to develop the response spectrum properly. Thus, relative to the present treatment, if the expression for the response spectrum, (191), is substituted in (192), and a variance-preserving transformation from encounter to wave frequency is carried out, the expression for the moments becomes:

$$m_n = \int_0^\infty |\omega - (\omega^2 U_0 / g) \cos \mu_0| \times |\bar{\eta}_j(\omega, \mu_0; U_0)|^2 S_\zeta(\omega) d\omega \quad (193)$$

The same result is obtained when the head or bow sea response spectrum is substituted. Equation (192) for the response spectral moments as an integral over wave frequency thus holds for any speed and heading to long-crested waves. No singularities appear in the integrand and thus the numerical work is straightforward. In short, all moment calculations can be conveniently carried out in the wave frequency domain, with knowledge of the point spectrum of waves,  $S_\zeta(\omega)$ , and the response operator as a function of wave frequency.

It may be noted that the integrand of Equation (193) for  $n = 0$  is:

$$|\bar{\eta}_j(\omega, \mu_0; U_0)|^2 S_\zeta(\omega)$$

This is in the form of a spectrum, and the integral over frequency (the area) is the response variance, but it is *not* the spectrum of response as would be sensed by instrumentation aboard a moving ship. Depending upon ship speed and wave direction, the frequencies and the shape of the integrand of (193) may be completely incorrect as a representation of an observed response spectrum. Nevertheless, the integrand of (193) can be and is called a spectrum, and can be put to good use in practical analyses of the contributions of various wave frequencies to the response moments. If it is desired to work out the actual response spectral shape the wave spectrum must be transformed to the encounter frequency domain, and the operations of (190) or (191) must be carried out.

**4.4 The Short-Crested Sea Case.** The last of the complications in applying linear random theory to the response of a vessel is that introduced by the variation of direction of the wave components in a short-crested sea. In Sections 4.2 and 4.3 for the long-crested case the wave component direction was assumed to be a constant parameter,  $\mu_0$ . In the short-crested case the component wave direction,  $\mu$ , becomes a variable in the same sense as is wave or encounter frequency. In this case we must deal with waves that are defined by a directional spectrum,  $S_\zeta(\omega, \mu)$ , rather than the point spectrum,  $S_\zeta(\omega)$ . As before, we denote the spectrum of the  $j$ th response as  $S_j(\omega_e)$ , and note from the definition of the variance spectrum that the contribution to total response variance of response components of all directions with encounter frequencies within a small range,  $\delta\omega_e$ , of some frequency,  $\omega_e$ , may be represented as  $S_j(\omega_e) \delta\omega_e$ .

According to the simplified treatment of Section 4.1 we may think of  $S_j(\omega_e) \delta\omega_e$  as the sum of all the contributions to variance of the response to all the individual directional wave components that produce a response with frequency very near  $\omega_e$ . The indicated summation in Equation (184) is over wave direction, and we must thus anticipate that the response spectrum for short-crested seas will involve an integral over wave direction of the form:

$$\int |\bar{\eta}_j(\omega_e, \mu; U_0)|^2 S_\zeta(\omega_e, \mu) d\mu$$

where  $S_\zeta(\omega_e, \mu)$  is the result of transforming the wave directional spectrum into the encounter frequency domain. All the complications noted in the last section for long-crested waves enter into the transformation of the directional spectrum. Since the wave direction is a variable rather than a constant parameter, the boundaries of the various "regions" described in the last section become functions of encounter frequency as well as direction. Because of this, the response spectrum is not the straightforward direction integral of (190) or (191) that the form just noted might imply. However, the general form of the response spectrum is superficially similar to that for the long-crested case in that it may be written in the form:

$$S_j(\omega_e) = S_j^H(\omega_e) + S_j^I(\omega_e) + S_j^{II}(\omega_e) + S_j^{III}(\omega_e)$$

The first contribution is essentially that from wave directions corresponding to head and bow seas, and the second through fourth the contributions from the ambiguous quartering and following sea regions of the  $\omega, \omega_e$  transformation. Each of these contributions is an integral over wave direction, each with very precise, and different, domains of integration. As a practical matter, the complications are such that estimates of the response spectrum in short-crested seas are virtually never done, and the interested reader is referred to St. Denis and Pierson (1953), or Price and Bishop (1974) for further details.

As in the long-crested case, spectral moments are of more practical interest than the details of the form of the response spectrum. Thus it is fortunate that it is possible to substitute the detailed expression for the response spectrum in short-crested seas into the general expression for spectral moments. Equation (192) makes a variance-preserving transformation from the encounter to the wave frequency domain, and arrive at an expression that allows all moment calculations to be carried out in the wave frequency-direction domain. The resulting expression for the spectral moments is:

$$m_n = \int_0^\infty \int_0^{2\pi} |\omega - (\omega^2 U_0 / g) \cos \mu|^n |\bar{\eta}_j(\omega, \mu; U_0)|^2 S_\zeta(\omega, \mu) d\mu d\omega \quad (194)$$

As before, the expression holds regardless of speed and wave direction, and is free of singularities. The integrand is essentially that of Equation (193) and is thus *not* a proper response spectrum because it is not based on  $\omega_e$ . The main difference between this and (193) for the long-crested case is that the wave direction is a variable.

There is a manipulation of very practical significance that may be done to Equation (194) under the special

circumstance that the directional spectrum may be represented as the product of a point spectrum and a *spreading function*,  $M(\mu)$ ,

$$S_\zeta(\omega, \mu) \rightarrow S_\zeta(\omega) M(\mu)$$

As noted in Section 2.6, this is of practical influence in design application because of the dearth of information on directional wave spectra. It is easily seen that if this representation is substituted into (194), the computation of moments in short-crested seas may be split into two operations:

$$m_n = \int_0^{2\pi} m(n, \mu) M(\mu) d\mu \quad (195)$$

where:

$$m(n, \mu) = \int_0^\infty |\omega - (\omega^2 U_0 / g) \cos \mu|^n |\bar{\eta}_j(\omega, \mu; U_0)|^2 S_\zeta(\omega) d\omega \quad (196)$$

the function  $m(n, \mu)$ , (196), is simply the  $n$ 'th spectral moment in long-crested seas as a function of the wave direction,  $\mu$ . The  $n$ 'th moment in short-crested seas involves weighting the long-crested moments with the spreading function (See example in Subsection 4.6).

**4.5 Statistics of Maxima.** The shape of the spectrum of a vessel's response tells the analyst what frequencies are important contributors to the response variance. Thus the response spectrum may allow inferences to be made about why a response variance is what it turned out to be, or perhaps (indirectly) how a vessel might be modified for better performance. However, in practice the most important result of the theory described previously is the response variance (the zero'th spectral moment, or spectrum area) because this quantity is central to all the measures of response magnitude that are considered useful in design application.

In the marine field it is customary to estimate magnitudes of response in terms of quantities that have some connection with the qualitative aspects of waves or response to waves (visible crests, troughs, amplitudes, etc.). Mechanically, such estimates are made by multiplying the square root of response variance (the RMS response) by a constant that is derived from the theory for the probability density of the maxima of a stationary zero-mean Gaussian random process. The applicable probability theory was summarized in Section 2 for ocean waves and is applicable to the response if, as we have assumed here, the wave processes are Gaussian, and the response is linear. Hence, it may be assumed that all of the formulas and constants presented in Section 2 for wave heights apply to response *double amplitudes*. Since amplitudes, rather than heights or double amplitudes, are usually of more in-

terest for response, all the height constants presented in Section 2 should be multiplied by  $\frac{1}{2}$ . Hence,

$$\begin{aligned}\text{Average response amplitude} &= 1.25 \sqrt{m_0} \\ \text{Significant response amplitude} &= 2.0 \sqrt{m_0} \\ \text{Average of } \frac{1}{10} \text{ highest} \\ \text{response amplitudes} &= 2.55 \sqrt{m_0}\end{aligned}$$

The greatest response amplitude expected on the average in samples of size ( $N$ ) of independent observations of apparent response amplitudes are

$$\begin{aligned}N = 100, & \quad 3.25 \sqrt{m_0} \\ N = 1000, & \quad 3.85 \sqrt{m_0} \\ N = 10,000, & \quad 4.45 \sqrt{m_0}\end{aligned}$$

However, if a large number of samples of the stated size are taken, five percent of them would be expected to contain maximum amplitudes exceeding:

$$\begin{aligned}N = 100, & \quad 3.9 \sqrt{m_0} \\ N = 1000, & \quad 4.45 \sqrt{m_0}\end{aligned}$$

The above involves the concept of *confidence level*.

We may note that response spectra are generally narrower than wave spectra. Thus the narrow-band assumption normally applied to wave statistics (and to derive the numbers just given) is usually even more appropriate for responses. To restate the magnitude of the theoretical error introduced by the narrow-band assumption, for most response cases of interest the spectral broadness parameter,  $\epsilon$  is less than 0.6, and Fig. 32 (Section 2.6) shows, for example, that assuming  $\epsilon = 0$  leads to an error in the significant amplitude estimate of only about 5 percent. However, it should be noted that there are types of ship response in which the spectral broadness parameter can be greater than 0.6, and the conventions and numbers just given may be improper. The most common case is associated with the stress response of ships. Strong vibratory stress fluctuations can superimpose upon wave induced stresses in a way that produces double peaked response spectra which may be "broad" in the sense defined by the probability theory.

Since there are occasions when it is important to estimate extreme response magnitudes when response spectra are broad, a useful extension of the extreme value theory for the maxima was made by Ochi (1973). As was noted in Section 2.6, when the spectrum of a zero-mean process is broad, we have maxima that are negative and minima that are positive. However, these are of virtually no engineering interest if, as is common, we are interested in the possibility that some predetermined response amplitude might be exceeded. Thus Ochi (1973) derived the probability density of positive maxima (or negative minima) for processes with arbitrary broadness. In order to apply extreme value theory properly it is necessary first to define the level of confidence in the result. Suppose that  $\xi_n$  rep-

resents the largest positive maximum in a sample containing  $n$  positive maxima, and that  $\Xi_n = \xi_n / \sqrt{m_0}$  represents this sample extreme in non-dimensional form. Further, define an *estimated* non-dimensional extreme for samples of  $n$  maxima as  $\hat{\Xi}_n$ . The confidence level is defined by a probability statement that is valid before the data are collected:

$$\text{Prob}[\Xi_n \geq \hat{\Xi}_n] = \alpha$$

where  $\alpha$  is a "small" probability chosen to reflect the desired degree of confidence that the estimated extreme value will not be exceeded in one sample. If the value of  $\alpha$  is chosen to be 0.01 for instance, and a value of  $\hat{\Xi}_n$  estimated, the actual extreme in each of many samples of  $n$  maxima should exceed  $\hat{\Xi}_n$  only once on average in 100 such samples. Broadly, the development of Ochi (1973) involves estimates of extremes in which there is an  $100(1 - \alpha)$  percent confidence that the actual extreme in a sample of  $n$  maxima will not exceed the estimate.

The development of Ochi (1973) continued by developing a relatively simple formula for  $\hat{\Xi}_n$  from the density function for positive maxima previously mentioned. This led to the recognition that the number of observed maxima of interest,  $n$ , could be related to the duration of the observation of the process from which the positive maxima were derived if it be assumed that successive positive maxima are statistically independent. The final relatively simple result for the estimation of extreme positive maxima (or extreme negative minima) became:

$$\hat{\Xi}_D = \sqrt{2 \ln \left[ \frac{D}{2\pi\alpha} \sqrt{\frac{m_2}{m_0}} \right]} = \sqrt{2 \ln \left[ \frac{D}{\alpha T_z} \right]} \quad (197)$$

where  $\hat{\Xi}_D$  is the estimated non-dimensional extreme that should be exceeded only once on average in  $1/\alpha$  samples of  $D$  seconds duration. The second form of Equation (197) follows from the definition of the zero crossing period,  $T_z$ , in Section 2.6, and it may be illuminating to note that  $D/T_z$  is equal to the expected number of zero up-crossings in duration,  $D$ . More or less coincidentally, (197) is the same as the answer obtained when Ochi's assumptions are applied to the case of an ideally narrow band process. It must be noted that (197) holds for small values of  $\alpha$  and for values of spectral broadness parameter less than 0.9; that is for the vast majority of cases of practical interest. On the other hand, the necessary assumption that successive positive maxima be statistically independent is likely only to be true for processes with very broad spectra; that is, the assumption is normally violated for responses of interest. However, the effect of this violation is to inject some conservatism into the result in that (197) should usually yield answers larger than would be the case if statistical independence of successive maxima were considered rigorously. Due



to the sluggish numerical behavior of the square root of a logarithm, this conservatism is likely to amount to less than 10 percent, even for responses that are quite narrow band.

To take a simple example of practical application, suppose that the variance,  $m_0$ , of heave and the variance of heave velocity,  $m_2$ , are computed from a response spectrum to be

$$\begin{aligned} m_0 &= 4 \text{ (m)}^2 \\ m_2 &= 1 \text{ (m/sec)}^2 \end{aligned}$$

and assume that we wish to estimate an extreme heave amplitude that we are 99 percent confident will not be exceeded in 24 hours of statistically steady response. The duration,  $D$ , becomes 86,400 seconds,  $\alpha$  is 0.01, and substituting into (197) the result is:  $\hat{z}_D = 5.18$ . This is the non-dimensional extreme. The dimensional extreme is obtained by multiplying by  $\sqrt{m_0}$ , so that the estimated extreme heave amplitude in a 24-hour exposure becomes 10.36 m, with 99 percent confidence. For comparison, from the previous discussion the expected average of the  $\frac{1}{10}$  highest amplitudes for this case would be 5.1 m.

**4.6 Example Computations.** By comparison with the theoretical determinations of response functions, Section 3, the computation of response moments is quite straightforward, as is the computation of response spectra, so long as short-crested following seas are not involved. Such computations are ordinarily done on the computer to save time, but the more important ones can be done by hand, and will be illustrated here in forms that can be used for hand calculation.

As has been noted, the computation of spectral moments for the long-crested case is the basic operation, and a typical such hand calculation is illustrated in Table 15. The objective of the computation is to estimate the first three even spectral moments for one response to one long-crested wave system in accordance with Equation (193). If more than one response or more than one wave system is at issue, the computation is repeated with as many combinations of response and wave data as are required.

In the evaluation of (193) it is convenient to define both the response operator and the wave point spectrum at uniform increments of wave frequency, Column 1. In the table Column 3 reflects a heave response operator (RAO) typical of a ship proceeding in bow seas ( $\mu = 157.5^\circ$ ) at a Froude number of 0.2. For the example the ship was assumed to be 500 ft (152.4 m) in length so that speed,  $U_0$ , is 15.05 knots. This yields encounter frequencies, Column 2, according to  $\omega_e = \omega + 0.7294 \omega^2$ . The wave point spectrum, Column 4, was taken to be in the 15th ITTC form (Section 2.11b), with  $T_1$  at 10.8 seconds and a significant height of 5 m (16 ft). Ordinates of the integrand of Equation (193), Column 5, are the product of Column 4 and the square of Column 3. Columns 6 and 7 indicate the usual steps in a Simpson's integration of Column 5. Columns

8 and 9 are formed by successive multiplications with the square of encounter frequency, Column 2. These last operations result in Simpson's functions of ordinates for the second and fourth spectral moments,  $m_2$  and  $m_4$ . After summing Columns 7, 8 and 9, the three moments are worked out as indicated in the lower part of the table.

In setting up such computations it is clearly important to select wave frequency increments so as to define reasonably well both the peak of the spectrum and the peaks of the response operator. In some cases plots of the integrand may be required in order to confirm the adequacy of this choice. In this connection it might be noted that the extra work of Simpson's integrations is not absolutely required. In the example the simpler trapezoidal integration of Column 5 yields an answer only 0.8 percent different from that given in the table for  $m_0$ . The usual precision of the determination of response operators seldom justifies highly precise spectral moment integrations.

Computations such as outlined in Table 15 are inherently dimensional since the wave point spectrum and the wave frequency are dimensional. In the example the RAO happens to be non-dimensional since it is that for heave. It is important to note that if the example had involved pitch or roll response, the units of the RAO would have been degrees per meter, and thus the units of Column 5 would have been  $\text{deg}^2\text{-sec}$ , and those of the moments would have been  $\text{deg}^2$ ,  $(\text{deg/sec})^2$ , and  $(\text{deg/sec}^2)^2$ .

The usual next step after the moments have been obtained is to compute the statistical averages of interest. For example:

Average period between zero-up crossings of response:

$$T_z = 2\pi\sqrt{m_0/m_2} = 9.49 \text{ sec}$$

Average period between response maxima:

$$T_c = 2\pi\sqrt{m_2/m_4} = 8.86 \text{ sec}$$

Spectral broadness parameter:

$$\epsilon = \sqrt{1 - (T_c/T_z)^2} = 0.36$$

(so that the heave is relatively narrow-band.)

Significant amplitude estimates become:

Significant heave amplitude =  $2\sqrt{m_0} = 2.30 \text{ m}$ .

Significant amplitude of heave velocity

$$= 2\sqrt{m_2} = 1.52 \text{ m/sec}$$

Significant amplitude of heave acceleration

$$= 2\sqrt{m_4} = 1.08 \text{ m/sec}^2 = 0.11 g$$

Significant heave double amplitude

$$= 2(2.3) = 4.6 \text{ m}.$$

Considering other measures of response:

Average of the  $\frac{1}{10}$ th highest heave

$$\text{amplitudes} = 2.55\sqrt{m_0} = 2.94 \text{ m}.$$



Table 15—Example Computation of Heave Spectral Moments, Long-Crested Seas

①	②	③	④	⑤	⑥	⑦	⑧	⑨
$\omega$ rad/sec	$\omega_p$ rad/sec	RAO m/m	$Sg(\omega)$ m <sup>2</sup> -sec	$\textcircled{3}^2 \times \textcircled{4}$ m <sup>2</sup> -sec	SM	$\textcircled{5} \times \textcircled{6}$ m <sup>2</sup> -sec	$\textcircled{7} \times \textcircled{2}^2$ m <sup>2</sup> /sec	$\textcircled{8} \times \textcircled{2}^2$ m <sup>2</sup> /sec <sup>3</sup>
0.10	0.107	1.00	0	0				
0.15	0.166	1.00	0	0				
0.20	0.229	1.00	0	0				
0.25	0.295	1.00	0.00	0.000	1	0.000	0.000	0.000
0.30	0.365	1.00	0.20	0.200	4	0.800	0.106	0.014
0.35	0.439	1.01	2.04	2.081	2	4.162	0.802	0.154
0.40	0.517	1.03	4.27	4.530	4	18.120	4.843	1.294
0.45	0.598	1.07	4.98	5.702	2	11.404	4.078	1.458
0.50	0.682	1.20	4.50	6.480	4	25.920	12.056	5.607
0.55	0.770	1.22	3.62	5.388	2	10.776	6.389	3.788
0.60	0.862	0.80	2.75	1.760	4	7.040	5.231	3.887
0.65	0.958	0.50	2.06	0.515	2	1.030	0.945	0.868
0.70	1.057	0.24	1.53	0.088	4	0.352	0.393	0.439
0.75	1.160	0.09	1.14	0.009	2	0.018	0.024	0.032
0.80	1.267	0.03	0.86	0.0008	4	0.003	0.005	0.008
0.85	1.376	0.00	0.65	0.000	1	0.000	0.000	0.000
0.90	1.491	0	0.50	0				
0.95		0	0.38	0				
1.00		0	0.30	0				
1.05		0	0.24	0				
1.10		0	0.19	0				
1.15		0	0.16	0				
1.20		0	0.12	0				
1.25		0	0.10	0				
1.30		0	0.08	0				
1.35		0	0.07	0				
1.40		0	0.05	0				

$$\Sigma = 79.625 \quad \Sigma = 34.872 \quad \Sigma = 17.549$$

$$m_0 = \frac{0.05}{3} \times 79.625 = 1.3271 \text{ m}^2$$

$$m_2 = \frac{0.05}{3} \times 34.872 = 0.5812 \text{ (m./sec.)}^2$$

$$m_4 = \frac{0.05}{3} \times 17.549 = 0.2925 \text{ (m./sec}^2\text{)}^2$$

Greatest heave amplitude expected on  
the average in 1000 oscillations  
 $= 3.85 \sqrt{m_0} = 4.44 \text{ m.}$

The extreme heave amplitude that should not be exceeded in 24 hr exposure with confidence of 99 percent would be computed from Equation (197) as follows:

$$\hat{\Xi}_D = \sqrt{2 \ln \left[ \frac{86,400}{(0.01)(9.49)} \right]} = 5.24$$

thus the extreme sought equals  $5.24 \sqrt{m_0} = 6.04 \text{ m.}$

Typical computations of response moments in short-crested seas are of course more involved since heading is a variable rather than a constant parameter. However, the usual objective is the same as in the long-crested case; that is, to estimate spectral moments, which are used in the same way as in the preceding long-crested example. If the directional wave spectrum,  $S_{\zeta}(\omega, \mu)$ , is given as a general numerical function of wave frequency and direction, then the computation

would involve double integrations of the form of (194). At present, not enough detailed engineering data are available to define the directional spectrum this way, and virtually all computations of response to short crested seas have involved the approximation that the directional wave spectrum is the product of a point spectrum and a spreading function. Accordingly, the present illustration of short-crested computations will be confined to the approach indicated by (195) and (196).

To illustrate, the cosine-squared spreading function noted in Section 2.6 will be assumed, and the angular spread taken to be plus or minus 90 degrees. Thus:

$$M(\mu_w) = \frac{2}{\pi} \cos^2(\mu_w)$$

where  $-90 \text{ deg} \leq \mu_w \leq 90 \text{ deg}$

and  $\mu_w$  is the angle between a wave component and the dominant wave direction. The usual way to perform the numerical integrations over wave direction re-

Table 16—Derivation of Spreading Function Weights for 22.5 deg Heading Intervals

① $\mu_w$ deg.	② $M(\mu_w) = \frac{2}{\pi} \cos^2 \mu_w$	③ SM	④ $\frac{1}{3} \delta \mu \times \text{②} \times \text{③}$	⑤ $\mu_w$ , deg.
-90	.0000	1	0.0000	270.0
-67.5	.0932	4	0.0488	292.5
-45.0	.3183	2	0.0833	315.0
-22.5	.5434	4	0.2845	337.5
0.0	.6366	2	0.1667	0.0
22.5	.5434	4	0.2845	22.5
45.0	.3183	2	0.0833	45.0
67.5	.0932	4	0.0488	67.5
90	.0000	1	0.0000	90.0
$\Sigma = 0.9999$				

$$\delta \mu = 22.5 \text{ deg} = 0.3927 \text{ radians}$$

$$\frac{1}{3} \delta \mu = 0.1309$$

Note: Function,  $W(\mu_w)$  is zero outside the directional range shown.

quired by (195) is to choose an even divisor of 90 degrees as the wave direction increment and apply Simpson's rule. Essentially, the expression is turned into a weighted sum, in which the spreading function,  $M(\mu_w)$ , weighted by Simpson's rule is designated  $W(j\delta\mu)$ . Then:

$$m_n = \sum_j m(n, j\delta\mu) W(j\delta\mu) \quad (198)$$

Table 16 illustrates the computation of the function,  $W(j\delta\mu)$ , for a wave direction increment of 22½ deg. The computation is in the form of a Simpson's integration of the assumed function with the factor  $\delta\mu/3$  applied to the functions of ordinates rather than to the final summation. The required weighted function is given in Column 4. Since the integral of the spreading function must be unity, a check summation of Column 4 is performed. For later use Column 5 is added to express component wave direction,  $\mu_w$ , relative to the dominant direction, in a zero to 30 deg convention.

The next step in the short-crested moment computation is to evaluate the long-crested spectral moments of interest as functions of component wave direction,  $\mu$ , relative to the ship's heading, as indicated in (196). If "around the clock" results are desired and the spreading function integration is to be performed with 22½ deg intervals, as assumed for Table 16, Equation (196) would be evaluated for  $\mu = 0, 22.5, \dots 180$  deg. Each of these computations is the same as those shown in Table 15. The results of the long-crested computations for pitching may be arranged as in the first two columns of Table 17. Because phase relations are lost in a variance computation, and ships are ordinarily

Table 17—Example Computation of Zero<sup>th</sup> Spectral Moment for Pitching in Short-Crested Seas, Using the Wave Spreading Function Weights of Table 16

① $\mu$ deg	② $m(0, \mu)$	$\mu_a = 0^\circ$			$\mu_a = 157.5^\circ$		
		③ $\mu_w = \mu - \mu_a$ deg	④ $W(\mu_w)$	⑤ $\text{②} \times \text{④}$	⑥ $\mu_w = \mu - \mu_a$ deg	⑦ $W(\mu_w)$	⑧ $\text{②} \times \text{⑦}$
0	0.61	0	0.1667	0.1017			
22.5	0.65	22.5	0.2845	0.1849	202.5	0	0
45.0	0.65	45.0	0.0833	0.0541	225.0	0	0
67.5	0.36	67.5	0.0488	0.0176	247.5	0	0
90.0	0.03	90.0	0.0000	0	270.0	0	0
112.5	0.79	112.5	0.0000	0	292.5	0.0488	0.0015
135.0	1.99	135.0	0.0000	0	315.0	0.0833	0.0658
157.5	2.28	157.5	0.0000	0	337.5	0.2845	0.5661
180.0	2.21	180.0	0.0000	0	0	0.1667	0.3801
202.5	2.28	202.5	0.0000	0	22.5	0.2845	0.6287
225.0	1.99	225.0	0.0000	0	45.0	0.0833	0.1899
247.5	0.79	247.5	0.0000	0	67.5	0.0488	0.0971
270.0	0.03	270.0	0.0000	0	90.0	0	0
292.5	0.36	292.5	0.0488	0.0176	112.5	0	0
315.0	0.65	315.0	0.0833	0.0541	135.0	0	0
337.5	0.65	337.5	0.2845	0.1849	157.5	0	0
$\Sigma = 0.6149$					180.0	0	0
					$\Sigma = 1.9292$		

$$m_0 \text{ for ship heading to dom. wave dir. } 0 \text{ deg} = 0.6149 \text{ deg}^2$$

$$M_0 \text{ for ship heading to dom. wave dir. } 157.5 \text{ deg} = 1.9292 \text{ deg}^2$$

Note: The zero<sup>th</sup> moment (area) results were obtained for the pitch response of a ship 175 m in length at 22 knots by repeated application of the method illustrated in Table 15. The same 5 m (16 ft) sea spectrum is used as in Table 15.

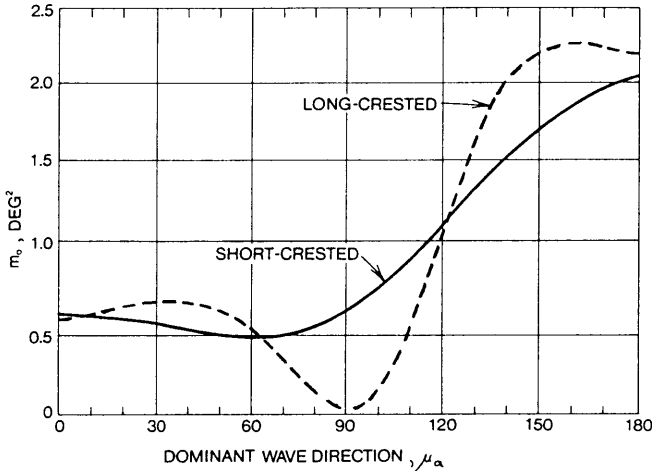


Fig. 69 Comparison of pitch variances computed for long and short-crested waves

symmetric about the center-plane, spectral moments for wave directions  $(360\mu)$  deg are the same as for wave direction  $\mu$ . Thus the numbers entered in Column 2 for directions greater than 180 deg are just a reflection of the computed results about  $\mu = 180$  deg. Note that the wave point spectrum is assumed constant for all the long-crested computations.

Next, the relationship between the wave direction,  $\mu_w$ , and the wave direction,  $\mu$ , must be clarified. The spreading function angles are defined with respect to a dominant wave direction, which in turn may be defined relative to the ship's heading as  $\mu_a$ . Thus the direction of a wave component relative to the ship's heading may be written:

$$\mu = \mu_a + \mu_w$$

$$\text{and: } \mu_w = \mu - \mu_a$$

This last relationship provides the connection between  $\mu_a$  and  $\mu$  required to complete the computation, Table 17. In the table, computations for dominant wave directions of 0 and 157.5 deg are indicated. Columns 3 and 6 indicate the values of  $\mu_w$  implied by  $\mu_a$  and  $\mu$  in a zero-to-360 deg convention. Now given  $\mu_w$  the function  $W(\mu_w)$  is entered in the appropriate places in accordance with the results in Table 16, noting that the weights are zero outside the range  $-90 \text{ deg} \leq \mu_w \leq 90 \text{ deg}$ . The computation for the zero'th moments are completed by forming the products of Columns 2 and 4, and Columns 2 and 7, and summing the results.

Fig. 69 compares graphically the pitch variance,  $m_0$ , obtained by performing the operations of Table 17 for dominant wave directions between zero and 180 deg with the original long-crested estimates. The effect upon variance of using the cosine-squared spreading function of Table 16 to estimate response in short-crested waves is usually as shown; that is, humps and hollows in the curve of long-crested variance vs. dominant wave direction tend to be smoothed out.

**4.7 Synthesis of Ship Response to Irregular Seas.** The theory outlined in the preceding subsections holds for any linear ship response to random waves, and for this reason it was convenient there not to go into details about particular responses. The intent in this sub-section is to illustrate the implications of the theory for specific vessel responses, mainly for the important case of pitch and heave in head seas.

(a) *Heave in irregular waves.* It was noted in Section 3.7 that one of the fundamental things to keep in mind when analyzing heave response to regular waves is that the non-dimensional response is always unity at zero wave frequency, and tends to zero at very high frequencies. As wave frequency approaches zero the wave length approaches infinity and the ship follows the wave surface, so that heave and wave amplitudes are equal. On the other hand, as wave frequency increases, wave lengths ultimately become very small; that is, become ripples to which ships and platforms do not respond.

Fig. 70 illustrates the typical shape of a ship heave response operator at fixed forward speed ( $F_n \approx 0.15$ ) in head seas. Usually the operator is very near unity for an appreciable range of wave frequency starting at zero. There is often an apparent resonance peak, and then a decline to zero. For ships at moderate speeds in head seas the range of frequencies where this transition is defined usually corresponds to a var-

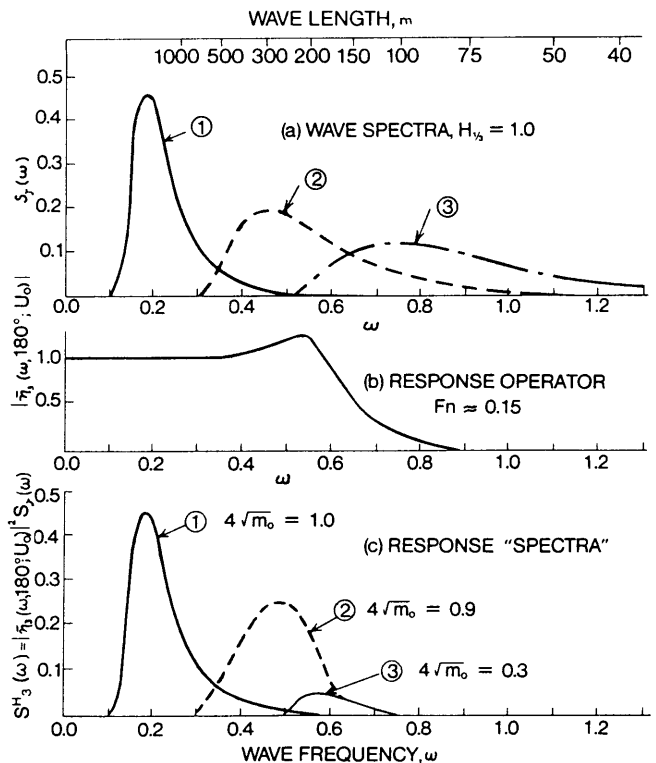


Fig. 70 Heave response in long-crested irregular head waves, with various wave spectra

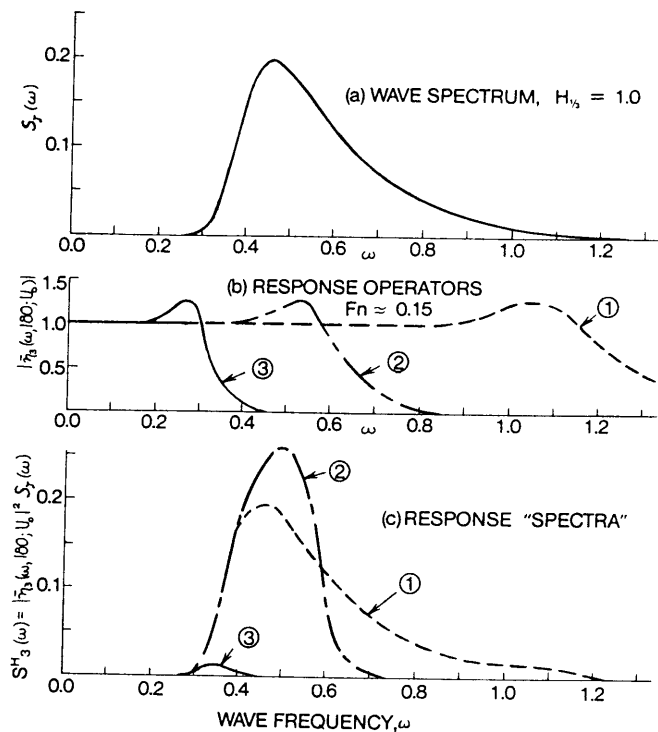


Fig. 71 Heave response in long-crested irregular head waves at various ship speeds

iation in wave length from 0.5 to 2.0 ship lengths. It should be noted that, though the heave response operators for all floating vessels involve a transition from unity to zero as wave frequency increases, the qualitative nature of the transition shown in Fig. 70 is not universal. For example, the heave response operator of a semi-submerged offshore platform may have a series of undulations in the high-frequency part, and a more pronounced peak. Unusually strong hydrostatic or dynamic coupling between heave and pitch of a vessel can produce either a "notch" or an accentuation of heave response in the vicinity of pitch resonance. A method of plotting data to identify the resonance peaks of both heave and pitch is in Section 8.

Fig. 70 has been prepared to illustrate heaving response of a ship heading into long-crested irregular waves. At the top of the figure are shown three wave point-spectra of the Bretschneider form (Section 2.11), having three different modal periods. The product of each of these spectra and the square of the response operator is shown at the bottom. Strictly, these products are the integrand of Equation (193) for the heave variance. It has been pointed out in Section 4.3 that such functions of wave frequency may be called heave response spectra though they do not reflect the contributions of various encounter frequencies to variance, and for present purposes this convention will be followed. For each of these heave "spectra", estimates of the significant heave double amplitude (4 times the square root of spectral area) are shown in the figure.

Considering the results corresponding to Spectrum 1, the important range of wave frequencies corresponds to the range where the response operator is essentially unity, the heave and wave spectra are almost identical, and the significant heave double amplitude is the same as the significant wave height. Generally, the significant heave double amplitude of a vessel in a wave system where most of the wave components are much longer than the vessel is about the same as the significant wave height. Spectrum 2 in the figure extends over the transition in the heave response operator. In this case the shape of the heave response spectrum is unlike that of the wave, though the significant heave double amplitude is almost as great as the significant wave height. Had the resonant peak of the RAO been higher, the heave response could have been much higher. Finally, only the high-frequency end of the response operator overlaps the low-frequency tail of Spectrum 3, with the result that the significant heave is much reduced. Ultimately, as the significant wave frequency range is moved higher relative to the response operator transition, the significant heave goes to zero because all wave components are relatively short. Ships and platforms do not respond to irregular ripples either.

Fig. 71 illustrates the same things from a slightly different point of view. Here one wave spectrum is shown in relation to three response operators. The response operators are typical of three geometrically similar ships whose heave resonant frequencies differ by factors of two, and whose lengths thus differ by

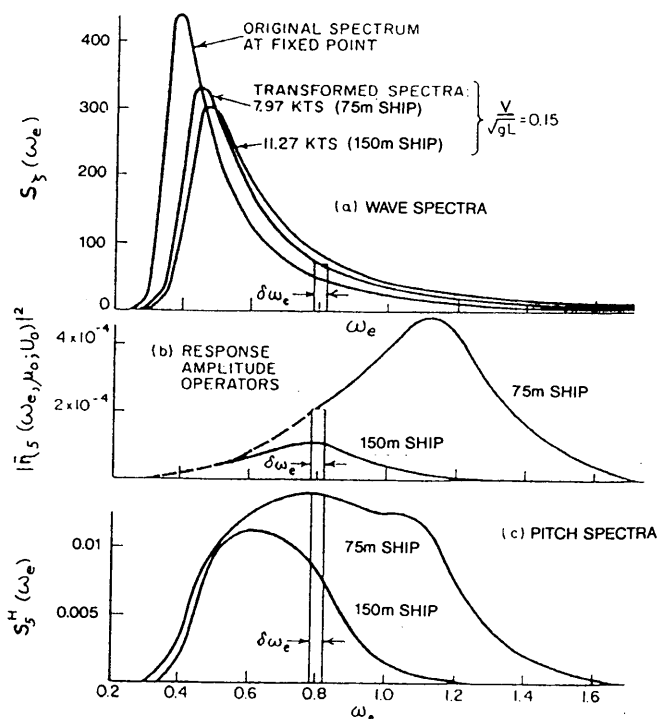


Fig. 72 Typical pitching response to irregular head sea (long-crested)

factors of four. The heave spectrum for the very small ship (No. 1) is nearly the same as the wave spectrum, and the significant heave double amplitude will thus be nearly the same as the significant wave height. The largest ship (No. 3), which would be sixteen times longer than ship No. 1, will have a relatively low heave response because most of the components of the irregular wave are of higher frequency than the range for significant heave response. This last condition corresponds to what is called *supercritical* heave response.

(b) *Pitch in irregular waves.* In principle, the analysis of pitching response to irregular long-crested head seas follows that for heave, except that the pitch response operator has different asymptotic properties. As with heave, pitch amplitude per unit wave amplitude approaches zero when wave frequency grows to the point that the corresponding wave length is small relative to vessel dimensions. However, as wave frequency approaches zero, wave length approaches infinity, the pitch of the vessel is controlled by hydrostatics, and the vessel follows the wave slope. Thus pitch amplitude per unit wave slope tends to unity for small wave frequency. For waves of amplitude  $\bar{\eta}$  the amplitude of wave slope (or "maximum" slope) is  $k\bar{\zeta} = \omega^2\bar{\zeta}/g$  for deep water. Thus, pitch amplitude per unit wave amplitude tends to  $k = \omega^2/g$ ; that is, to zero as wave frequency tends to zero.

Fig. 72 illustrates typical pitching response spectra for head long-crested waves, calculated according to the relation, Equation (190), for two geometrically similar ships at Froude Number 0.15. It should be emphasized that the calculations have been made in the encounter frequency domain. Accordingly, the single wave-frequency spectrum for which predictions are being made in the figure has been transformed into two encounter spectra by means of (189), one for each of the two absolute ship speeds. The response operators in Fig. 72 are plotted in squared form, a curve for each of the two ships, and the resulting pitch response spectrum for each ship size is shown in the lower part of the figure. Clearly in this case the average pitch response of the 250-ft ship is greater than that of the 500-ft ship because the RAO for the 250-ft ship is greater and covers a greater frequency range than does that of the 500-ft ship.

We note that the pitch amplitude per unit wave-slope amplitude for geometrically similar ships is the same for equal Froude numbers, and equal ratios of ship length to wave length. The large differences in response operator magnitude shown in Fig. 72 are a result of the scaling necessary to make predictions for the same absolute sea. When the size of the ship is changed the scale of frequency varies inversely with the square root of the linear scale ratio. Thus in Fig. 72 the frequency of peak pitch response and the range of frequency for significant response of the 250 ft ship is roughly  $\sqrt{2}$  greater than that of the 500 ft ship.

Similarly, the pitch response amplitude operator is dimensional (units of degrees per ft) and so must be scaled for different ship sizes inversely to the scale ratio. Thus the peak of the squared pitch response operator for the 250 ft ship is about four times the magnitude of that for the 500 ft ship. In this example it may be noted that the peak of the wave spectrum has little obvious effect upon the results because of its position on the frequency scale; that is, the wave spectrum peaks at a frequency where neither response operator is too significant. Under the circumstances indicated the larger pitch response of the smaller ship comes about because it responds not only to the long waves that affect the larger ship, but to the short (high frequency) components as well.

It is often helpful in the analysis of comparative response, such as that shown in Fig. 72, to consider the excitation and the response operators from the point of view of wave slope, as in Section 2.7. Whatever equivalent representation is considered, the pitch variance must be the same, and from (193) we may write (and manipulate) the pitch variance in long-crested waves as follows:

$$\begin{aligned} m_0 &= \int_0^\infty |\bar{\eta}_5(\omega, \mu_0 U_0)|^2 S_\zeta(\omega) d\omega \\ &= \int_0^\infty |\bar{\eta}_5(\omega, \mu_0 U_0)/k|^2 (\omega^4/g^2) S_\zeta(\omega) d\omega \quad (199) \\ &= \int_0^\infty |\bar{\eta}_5(\omega, \mu_0 U_0)/k|^2 S_\zeta(\omega) d\omega \end{aligned}$$

where the expressions have been specialized to pitch by choosing the subscript 5 in the response operator,  $|\bar{\eta}_5(\omega, \mu_0; U_0)|$ . The first of the three forms is the same as (193). The second is derived from the first by multiplying and dividing the integrand by the square of wave number,  $k$ , and to obtain the third form we set  $S_\zeta(\omega) = (\omega^4/g^2) S_\zeta(\omega)$  from Equation (67), Section 2.7, where  $S_\zeta(\omega)$  is the slope spectrum; that is, the spectrum of the slopes of the long-crested wave system. In the third form of the variance equation above,  $|\bar{\eta}_5(\omega, \mu_0; U_0)/k|$  is the pitch amplitude per unit wave slope; that is, the pitch response operator referred to wave slope. In this form the pitch RAO is nondimensional, and has the same low frequency asymptotic properties as heave. From the equations, the product of the slope spectrum and the squared nondimensional pitch RAO in the third of Equations (199) defines a pitch response spectrum equal to that implied by the first. As before, this spectrum is the same as that which would be sensed aboard a ship only if the speed were zero, but can be used to advantage for any speed in aid of analyses such as the present. (If desired, the

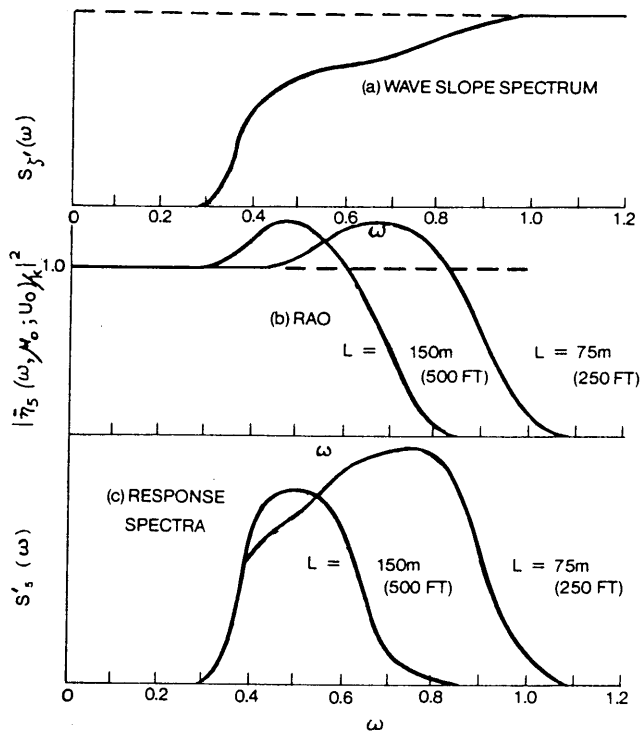


Fig. 73 Slope spectrum representation of pitching response to irregular head sea

slope spectrum for long-crested seas can be transformed into the encounter domain in the same way as was shown for wave elevation spectra in Section 4.1).

Fig. 73 shows the prediction of pitching response for the two geometrically similar ships of Fig. 72 using wave slope instead of elevation spectra. Note that the work in Fig. 72 was done in the encounter frequency domain, while Fig. 73 is in the wave frequency domain. However, the final plots of pitch response spectra look very similar, and would have been identical had both analyses been in the same frequency domain. An advantage of the slope spectrum way of looking at the problem is that it gives a better idea of the relative importance of the different wave spectral components for responses that depend upon wave slope. In particular in accordance with the discussion of Section 2.7, it may be noted that the spectral peak of Fig. 72 has been deemphasized, and that the largest contributions to the wave slope variance are in the high frequency range. In the figure the relative pitch response for the two ships is as before. We may amplify the reason for the much larger response of the smaller ship by noting that though the magnitude of the RAO referred to wave slope is the same for the two ship sizes, the smaller ship also responds to a wave frequency range where the wave slopes are greater.

As noted previously, the RAO curves in Fig. 72 for geometrically similar ships of differing size differ considerably in shape because both the wave frequency scale and the RAO itself are dimensional. The trans-

formation to the wave slope basis in Fig. 73 reduces the disparity, but does not eliminate it because the wave frequency scale is still dimensional. To make the response operator curves have the same shape for geometrically similar ships it is an advantage to plot them on the basis of  $\ln \omega$ , the natural logarithm of  $\omega$ , instead of  $\omega$ . Under this transformation RAO curves for geometrically similar ships are identical in shape, but are shifted along the  $\ln \omega$  scale in accordance with their size. This fact leads to a further transformation of the slope spectrum described in Section 2.7; that is, to the *log-slope form*,  $S_{\zeta'}(\ln \omega)$ . The transformation is variance-preserving, and it may be shown that:

$$m_0 = \int_{-\infty}^{\infty} |\bar{\eta}_5(\ln \omega, \mu_0, U_0)/k|^2 S_{\zeta'}(\ln \omega) d(\ln \omega) \quad (200)$$

which is to say that the area of the curve formed by a plot vs.  $\ln \omega$  of the product of the squared RAO and the log-slope spectrum is equal to the response variance, and thus that this product defines a response spectrum that may be interpreted in the same way as the others previously described.

Fig. 74 indicates the prediction in the log-slope form of the pitching response for the two geometrically similar ships of Figs. 72 and 73. The wave spectrum in log-slope form is shown at the top of the figure, and it should be noted that the log-frequency range of general interest is negative in sign, and that short waves are to the left. For later use a constant log-slope spectrum has been added. In this form the RAO curves for the different sized ships are identical in shape, but are shifted horizontally. The horizontal shift along the  $\ln \omega$  scale depends upon the scale ratio between the ship dimensions and in this case is  $\ln \sqrt{2} = 0.347$ . The plot at the bottom of the figure indicates the response spectra formed for the two ships of differing size, calculated both for the log-slope spectrum corresponding to the slope spectrum of Fig. 73 and the constant log-slope spectrum indicated in the figure. If all the components of the sea had the same relative slope; that is, if the log-slope spectrum were a horizontal straight line, the response spectra for geometrically similar ships would have identical shapes, as do the RAO's. For actual ocean-wave patterns this is not the case, and therefore the response spectra for similar ships of different size are also different, as shown in Fig. 74.

Comparing the magnitude of the pitching responses as measured by the spectral areas in Fig. 74 we see as before that the shape of the sea spectrum has less effect upon the result than does ship size, for even if the log-slope spectrum were a horizontal line (equal slope for all components) there would be but little difference in response at negative values of  $\ln \omega$  greater than  $-0.6$ . Hence, the larger pitching response of the small ship results almost entirely from its

smaller size—as indicated by the horizontal separation of the response spectrum curves—which adds the shaded area, Fig. 74 to the variance. However, in the case of a heavy swell, with most of the energy in long wave components, a situation might arise which was more favorable to the pitch response of the small ship.

Since we have just finished considering the effect of ship size on pitching response with three different representations of wave excitation spectra, it is probably worthwhile to consider the choice between the three approaches. As far as prediction of spectral moments is concerned, integrations similar to those indicated in Section 4.2 may be, and have been done, using the wave, the wave slope and the log-slope representations. The choice is largely a matter of what is wanted. If it is desired to clarify and separate the effects of ship size and wave spectral shape upon response (the intent in the immediately preceding paragraphs) the slope and log-slope approaches have much to recommend them. These approaches work particularly well with responses that are naturally dependent upon wave slope, such as pitch and roll, and make engineering sense with accelerations (to be discussed) and bending moments (Chapter IV, Vol. I). These ap-

proaches have little value in clarifying heave-related responses because such responses are not naturally dependent upon wave slope. On the other hand, if predictions of variances for a given set of sea conditions and responses is wanted, and as is usually the case, the details of the spectral shapes are not of primary concern, the approach outlined in Section 4.3 is ordinarily preferred because usually the wave data base exists in terms of elevation spectra.

(c) *Heave acceleration in irregular waves.* Displacements in heave are of less direct importance to personnel and equipment than heave accelerations. (For example, heave accelerations are linked to seasickness in Section 7.) The usual approach to measures of acceleration has been presented in Section 4.2. This approach involves the calculation of the fourth spectral moment of response, which is equal to the variance of response acceleration, and thus the variance of heave acceleration may easily be estimated once the basic heave displacement RAO is available.

However, for the sake of illuminating the effect of ship size upon heave acceleration response, it is of interest to consider an alternate approach similar to that employed for pitch response in the last subsection. Suppose first that consideration is restricted to long-crested waves and that heave acceleration is expressed in g's. On this basis, specializing Equation (193), the fourth spectral moment (the heave acceleration variance) may be written:

$$\begin{aligned}
 m_4/g^2 &= \int_0^\infty |\omega_e^2 \bar{\eta}_3(\omega, \mu_0; U_0)/g|^2 \times \\
 &\quad S_\zeta(\omega) d\omega \\
 &= \int_0^\infty \left| \frac{\omega_e^2 \bar{\eta}_3(\omega, \mu_0; U_0)/g}{\omega^2/g} \right|^2 \times \\
 &\quad (\omega^4/g^2) S_\zeta(\omega) d\omega \\
 &= \int_0^\infty |(\omega_e/\omega)^2 \bar{\eta}_3(\omega, \mu_0; U_0)|^2 \times \\
 &\quad S_{\dot{\zeta}}(\omega) d\omega
 \end{aligned} \tag{201}$$

where the encounter frequency is denoted by  $\omega_e$  instead of by the equivalent expression involving wave frequency and direction. Recalling the notation in Section 4.1, and the relations between displacement and acceleration shown in Section 3.2, the quantity inside the absolute value signs in the first form of the heave acceleration variance is the complex amplitude of heave acceleration, in g's per unit wave amplitude; that is, the absolute value of this complex number is the RAO of heave acceleration, with acceleration expressed in g's. The second form of the heave accel-

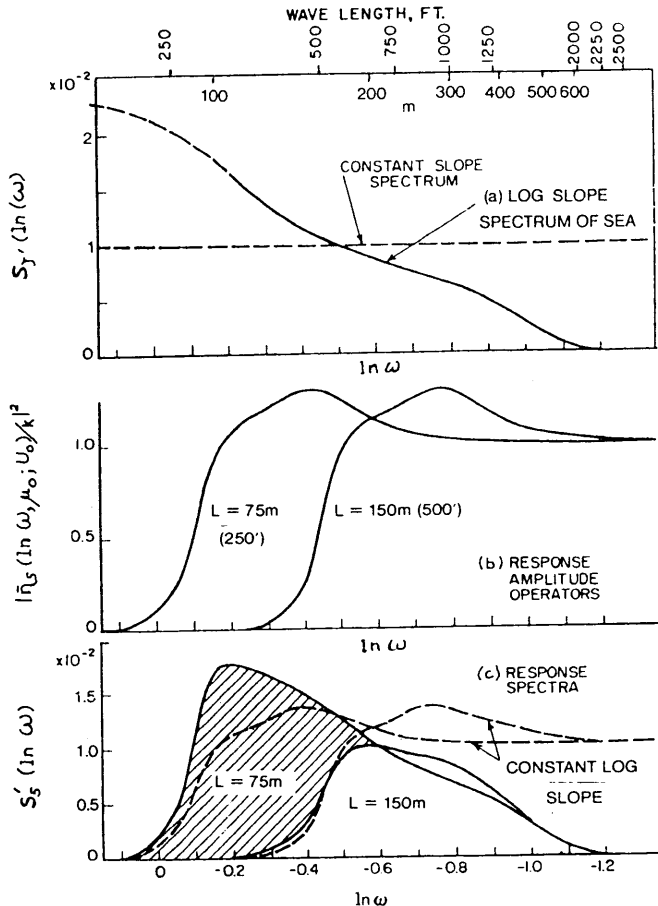


Fig. 74 Log-slope representation of pitching response to irregular head sea

eration variance above is obtained from the first by multiplying and dividing the integrand by  $\omega^4/g^2$ . The third form is obtained by cancelling out the  $g$ 's inside the absolute value signs, and setting  $S_{\zeta}'(\omega) = (\omega^4/g^2) S_{\zeta}(\omega)$ . Since we are dealing with long-crested waves we may again identify  $S_{\zeta}'(\omega)$  as the wave slope spectrum, Section 2.7. In a regular wave of amplitude,  $\zeta$ , the acceleration amplitude of a surface wave particle, expressed in  $g$ 's, is  $(\omega^2/g)\zeta$ , and it may be seen that this is numerically the same as the amplitude of the regular wave slope in deep water at any particular wave frequency. Noting that, in the notation of Section 4.1, the complex response is defined to be per unit wave amplitude, it may thus be seen that the expression within the absolute value signs in the second and third forms of the heave acceleration variance is the complex heave acceleration amplitude per unit vertical acceleration of a wave particle at the free surface. The absolute value of this expression is thus a nondimensional heave acceleration RAO. When vessel speed is zero the nondimensional heave acceleration RAO is equal to the dimensional heave displacement RAO. Regardless of speed it has the same asymptotic properties as heave. The integrands in all three representations

define a spectrum of heave acceleration that can be used for purposes of analysis as in the treatment of pitching; that is, the product of the wave slope spectrum and the square of the nondimensional heave acceleration RAO provides an alternate way to estimate a spectrum of heave acceleration. The wave slope form may also be transformed into the log-slope form.

A log-slope plot of the nondimensional acceleration prediction for the geometrically similar ships treated previously is shown in Fig. 75. In a similar fashion, the figure indicates the relation between the log-slope wave spectrum, the squared nondimensional heave acceleration RAO, and the resulting estimates of a heave acceleration spectrum (here denoted  $S_{\ddot{z}}(\ln\omega)$ ). The resulting picture is similar to that obtained for pitch, Fig. 74 and the same conclusion can be drawn; that is, the larger response of the small ship results almost entirely from its smaller size, because it responds to a wider range of frequencies. Again, a smaller ship will always be worse off in acceleration than a similar larger ship, except perhaps in long swells.

In most cases the vertical acceleration due to the combined effect of heave and pitch at a particular location in the ship is of more importance than heave acceleration alone. This can be analyzed in the same way, and can be expected to yield a picture similar to Fig. 75. This form of analysis is convenient for comparing either the performance of different ships of the same size or that of the same ship at different speeds. See Section 5.

(d) *Rolling in irregular waves.* Though there are some caveats that will be discussed later, the linear-random theory provides considerable insight into the rolling behavior of ships. The asymptotic behavior of the RAO for rolling in beam seas is the same as that for pitch in head seas; it tends toward zero at high wave frequency, and to wave slope at low. Rolling is far more dependent upon wave slope than amplitude, so that the remarks about the contrast between the dimensional and the nondimensional forms of the RAO for pitch apply in this case also. The main difference between the pitch and the roll RAO is that the rolling RAO almost always has a much more pronounced resonant peak, both higher and narrower than is the case for pitch. Because of the low damping, as noted in Section 3.8, resonant ship rolling amplitudes in response to regular waves vary typically between twice and ten times wave slope amplitude (pitch amplitudes tend to be less than twice wave slope) and this has an important effect upon the character of the rolling spectrum. Fig. 76 illustrates a typical situation of rolling in irregular long-crested waves where the wave direction is somewhere near the beam sea case, and there is significant energy in the wave spectrum at a wave frequency corresponding to the resonant encounter frequency. In the top frame a typical wave elevation spectrum is shown schematically; in the middle a squared roll RAO in the roll/wave amplitude form; and at the bottom the predicted roll spectrum. What

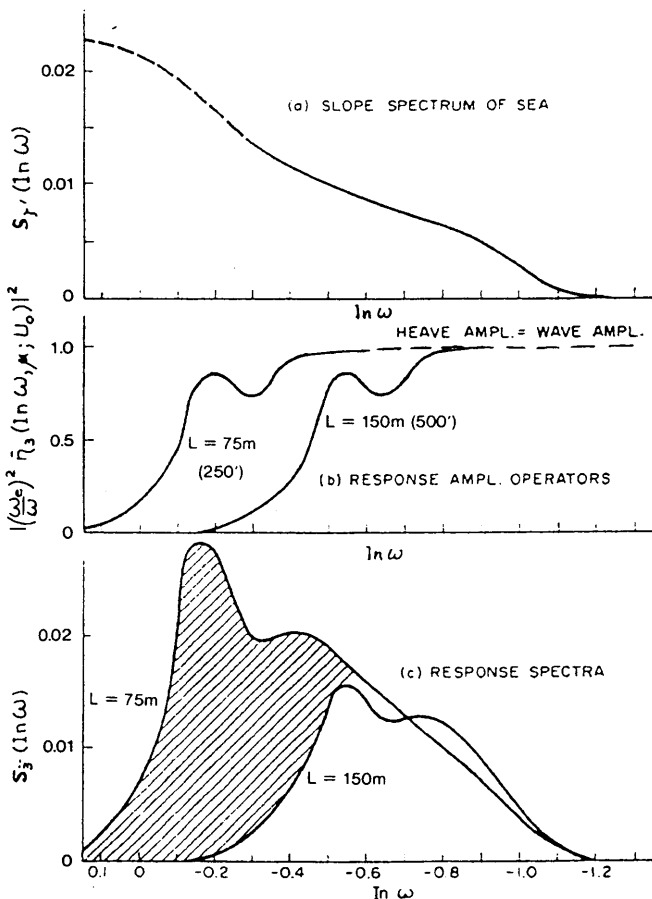


Fig. 75 Log-slope representation to heave acceleration response to irregular head sea



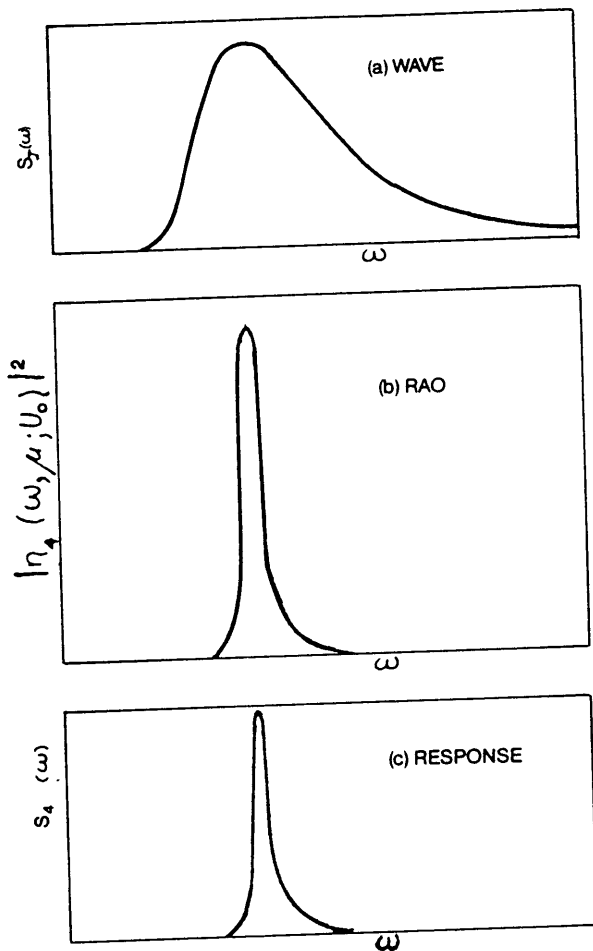


Fig. 76 Typical roll response to long-crested beam sea

happens is that once squared, the narrow peak of the RAO is the only part that is significant, the roll spectrum shape is controlled by the RAO, and the magnitude of roll depends almost entirely upon the magnitude of wave spectral density near resonance. Hence, there is little practical advantage in using slope or log-slope spectra.

Because ship rolling is ordinarily much more sharply "tuned" to a particular encounter frequency band than is pitch, ships often appear to roll mainly in their own natural rolling period rather than in the dominant period of encounter determined by vessel speed, wave direction, and the ambient wave spectrum. If there is some energy in the encountered wave spectrum in a frequency band that corresponds to roll resonance, the sharply peaked RAO of a lightly damped vessel can amplify the response to this portion of the wave spectrum to the point that the overall roll response is dominated by roll response components in the resonant period. This is why the relatively simple passive roll damping devices discussed in Section 6, which are effective mainly at resonance, are as successful as they

are when applied to an initially lightly damped ship.

In a very rough wind-driven beam or quartering sea almost any conventional ship will roll heavily because the range of practically attainable natural rolling periods is usually within the range of wave frequencies present. In more moderate wind-driven seas the rolling may be less severe, not only because the waves are less steep, but because lower frequency components which might cause resonant rolling may not be present. If the latter is the case, the ship is then in a supercritical condition with respect to rolling. It can also be concluded that a long rolling period can be advantageous, since in general it shifts the supercritical range to rougher seas.

The case of ship rolling when at speed at oblique headings to short-crested waves is much more complicated than in long-crested oblique waves. (See Subsection 4.9.) Relatively large changes in speed or heading may be required to reduce heavy resonant rolling because when the ship is moved out of synchronism with one band of wave components the many wave directions present makes it more likely to approach synchronism with another band.

The caveats previously alluded to about the application of the linear-random theory to rolling are centered upon whether or not the basic assumption, linearity of response, is satisfied. The mechanism producing the damping of pitch and heave is largely the radiation of ship generated waves (Section 3), a mechanism that is linear to reasonable accuracy. But, as explained in Section 3.8, in the case of rolling, theory usually predicts wave radiation damping that is relatively much smaller than model experiments suggest, unless the ship geometry is such that rolling will produce radiated waves of significant magnitude (extremely shallow draft barges, some work boats, and the like). For more normal large ship forms it is necessary to augment the wave radiation damping suggested by the basic theory by semi-empirical corrections for bilge keels, various viscous effects (Section 3.8) and the oscillatory dynamic lift forces upon appendages (Cox, et al 1977). Although the majority of these augmentations are nonlinear, Schmitke (1978) found that for high-speed ships (e.g., frigates and destroyers) including the important factor of dynamic lift on appendages, which is roughly linear, gave good agreement between linear calculations and model and full-scale tests in the vicinity of synchronism.

Thus, the degree to which linear-random theory will yield reasonable predictions for roll depends to an extent upon the vessel and operating conditions. Early experiments suggested that the rolling motion of a ship fitted with bilge keels and moving through the water is not too far from linear if the deck edges are not immersed (Lalangas, 1964), and that consequently the linear-random approach may be used in many cases. Since then, conclusions from experimental and theoretical research are less sanguine (Tasai, et al

1973), (Fujii, et al 1975), (ITTC, 1979, 1981). Depending upon speed, some fraction of roll damping appears to be nonlinear, which is to say dependent upon roll amplitude. As noted in Section 3.8, most theoretical treatments involve the form of damping nonlinearity postulated by Froude in the 19th Century (INA, 1955). In addition, model tests of beam-sea rolling often show evidence of a weak nonlinearity in restoring moment. Unfortunately, it is not now possible to give simple rules about the conditions and ship geometry where the nonlinear effects are important enough to invalidate the linear-random approach, except perhaps to suggest that the lower the speed and the lighter the apparent damping the more important the nonlinearities may become.

Because these nonlinearities are weak in the mathematical sense for moderate roll angles, and because roll is usually sharply tuned, there are practical ways of overcoming the difficulties in using linear spectral prediction methods. Several approaches have been suggested by Yamanouchi (1964), Kaplan (1966), Vassilopoulos (1971), Cox, et al (1977) and Schmitke (1978). Most involve an equivalent statistical linearization scheme where the nonlinear system is replaced by a conditionally linear one in which the RAO is a function of average or rms roll angle. This leads to an iterative solution where the roll magnitude predicted is compared with updated estimates until reasonable convergence is obtained.

**4.8 Validity of the Linear-Random Theory.** As noted earlier, there are two crucial assumptions that underlie the methods under discussion. These are that the response of the vessel is a mathematically linear function of wave elevation or slope, and that the wave field is Gaussian. In the strict sense it is obvious that neither can be true. The logical consequence of the Gaussian assumption is that regardless of wave height the troughs and crests must on average represent equal deviations from the mean water level, and further that wave elevation is unbounded. The strict interpretation of the linear assumption is that the vessel is wall-sided, travels on a straight course at constant speed, in waves of infinitesimal height, and never experiences motions that allow the forefoot or deck edge to approach the free surface. However, in engineering it is usually more important that an approach yield useful and reasonably correct results than that it be pure mathematically. In the present case, experience has shown that the linear and Gaussian assumptions usually take us a long way toward useful and reasonable answers, even under conditions where both assumptions are clearly violated. Thus when validity is mentioned in this context it means only the degree to which a valid engineering tool is available. How valid the tool is depends upon the type of vessel, to some extent its speed, the severity of the wave conditions, the mode of motion or the response of interest, and the nature of the statistics it is desired to predict.

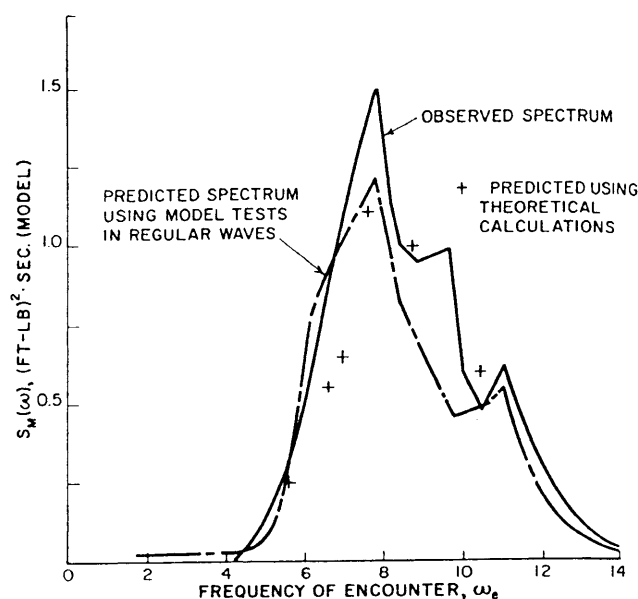


Fig. 77 Comparison of predicted and observed spectra of bending moment in irregular head seas

The early work in exploring the validity of the method for ship design concentrated upon longitudinal motions and bending moments. The theory of linear systems (Price and Bishop, 1974) (Ochi and Bolton, 1973), provides a number of approaches to the demonstration of validity in long-crested waves. One is that the observed response spectrum be the same as that predicted from RAO's obtained from theory or regular wave experiments. Fig. 77 (Jacobs, 1960) shows a three-way comparison of predicted bending moment spectra in long-crested irregular head seas: (a) As predicted from model tests in regular waves, (b) as predicted from calculated bending moments in regular waves, and (c) as determined directly from the record of bending moment obtained in an irregular tank sea. Though there are relatively large percentage differences in spectral density shown in Fig. 77, it should be remembered that the quantity used in a design application is the square root of the spectral area. Thus in application a margin of difference such as shown in the figure translates into statistical prediction uncertainties of the order of ten or fifteen percent, a magnitude which is usually less than the uncertainty in the definition of real wave conditions at sea. Ochi (1964) extended this approach to more severe towing tank waves and oblique seas, and to seakeeping parameters somewhat more sophisticated than just the spectra, with quite positive results.

Another more basic approach is to assess the degree to which RAO's derived from towing tank regular wave tests are invariant with regular wave height. Dalzell (1964) for example pursued this approach to extremely steep regular waves (length-to-height ratio up to 9). The conclusion was that amplitudes of head-

sea motion and bending moment response were reasonably proportional to wave amplitude for a range of wave steepnesses that covered a significant part of the physically possible range.

A third approach from the theory of linear systems is to identify the RAO's and transfer functions by *cross-spectral* analysis of observed wave and response time histories, and compare the answers with regular wave test results, as for example in Dalzell and Yamanouchi (1958) and Dalzell (1962). This type of analysis enables one to obtain phase information, an improved RAO estimate, and an estimate of statistical errors. A further variation on this theme (Dalzell, 1963) compared cross-spectral estimates of RAO's from experiments involving a range of wave severities, since the derived RAO must also be invariant with wave significant height. Finally, a fourth approach involved an inversion of the frequency domain descriptions of towing tank model response into the time domain according to linear theory, and using the result to calculate deterministic responses to known wave elevation records (Dalzell, 1963). The general conclusion from all the work was that the linear-random theory could be used for predictions, with practical validity, of the rms longitudinal motions (and derivations) of normal ships at reasonable speeds. More recent experience (Cummins, 1974) (Ochi, 1974), tends to bear this out. There are, however, two caveats associated with naval practice. It appears that nonlinearities in heave and pitch may become practically significant for Froude numbers in excess of 0.3, and for ships with extremely large bulbs (Smith and Salverson, 1970). Fortunately, these nonlinearities are relatively weak. One practical, but not rigorous, solution is to make predictions using RAO's from regular wave experiments in which the wave height is comparable to the significant irregular wave height of interest.

The situation with respect to ship rolling has been mentioned in the previous sub-section.

All the discussion just concluded involves model experiments, and it has been of concern to consider scale effects. There have been a number of full-scale ship trials in which the major objectives have included the examination of the validity of the linear-random theory; as noted for example, in Gerritsma and Smith (1967), Aertssen and van Sluijs (1972), Beukelman and Buitnhek (1973), and Taylor and Lundgren (1976). In cases where the apparent waves were unidirectional, some quite reassuring agreement among full-scale trials, model experiments and theory have been obtained. Fig. 55, Section 3, is an example of such results from Gerritsma and Smith (1967).

The validity of the linear-random approach for other than normal ship forms has been less well documented. In the case of the catamaran no adverse findings are known for the ordinary large-waterplane type. However, the low-waterplane type (SWATH) is known to have weak nonlinearities in longitudinal motions, even in the theory of Lee and Curphy (1977), so that some

caution is required. The theoretical nonlinearities are qualitatively similar to those discussed in the context of ship rolling. Experimentally, some SWATH concepts have displayed what may be considered strong nonlinearities, sub-harmonic response in roll for instance, and this is a problem not yet explained.

In most instances the linear-random approach is not considered applicable to planing craft at speeds above which significant dynamic lift is generated (Savitsky, 1968) (Savitsky and Brown, 1976) (Fridsma, 1969). It should also be noted that under some circumstances a planing vessel can experience strong nonlinear (sub-harmonic) response in heave and pitch. At present writing, argument exists about applicability to the surface effect ship concept. Some studies indicate that the linear-random approach is practically valid, others do not. In the case of the semi-submerged platform, complete applicability depends largely upon how heavily damped pitch, roll or heave is, and upon initial stability. Semi-submersibles with relatively low initial stability are prone to steady tilt (Numata, et al 1976), and sometimes to strong sub-harmonic response in pitch or roll. The more transparent the semi-submersible is to waves, the less likely that wave damping will control damping at motion resonances, and the more likely that the motion at resonance will be nonlinear. However, linear-random predictions that do not heavily involve wave excitation at a resonance are usually considered valid.

**4.9 Period Relationships.** The illustrative examples in the earlier part of this section show that in general the magnitude of vessel motions response will depend upon the interacting effects of vessel speed, wave spectrum, dominant wave direction and the characteristics of the response RAO, which depend in turn mainly upon the proportions and geometry of the ship's hull. Though the principles are not the same for all types of vessels, the intent here is to summarize some trends that have been found helpful to a general understanding of the relationship between the behavior in waves and the geometry of the conventional displacement ship.

Of the six modes of motion, the most important three (pitch, heave and roll) have natural frequencies, since in each case there is a hydrostatic restoring moment or force. As noted in Section 3, the regular wave response for these modes of motion may involve significant magnification due to resonance for wave encounter frequencies near the natural frequencies. It should be clear from the discussion of rolling in irregular seas that rolling motion should be much reduced if it is possible to avoid resonance (or synchronism) with wave components having significant energy. As also noted in Section 3, the magnitude of pitch and heave response to regular waves is not entirely determined by synchronism with wave encounter frequency since the magnitude of the wave excitation forces and moments varies with wave length as well as wave amplitude. However, for displacement ships of con-

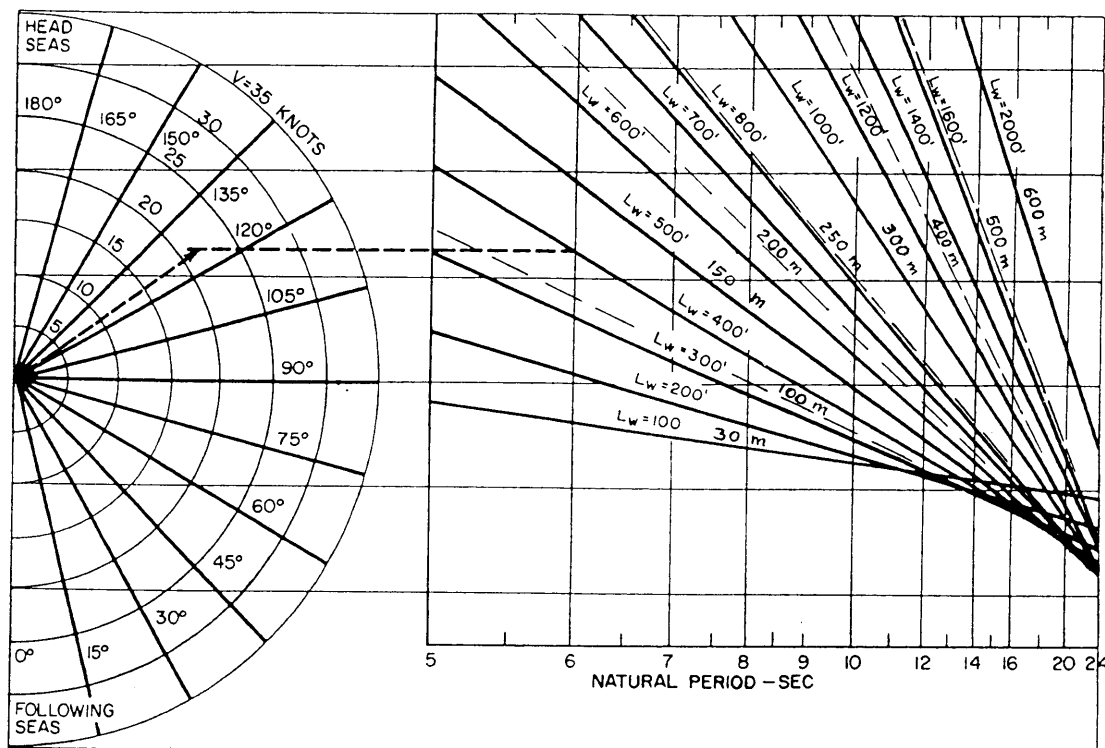


Fig. 78 Nomograph for determining conditions for synchronous oscillation in regular waves

ventional form the natural frequencies of pitch and heave usually locate roughly the dominant response, as discussed further in Section 8. This justifies further consideration of the conditions for synchronous motion. It has also been found that phase relationships leading to wet decks and slamming are associated with resonant conditions, which provide further justification (Szebehely, 1955) (Lewis, 1955).

For purposes of analysis of resonant behavior of ships it is useful to consider period and wavelength rather than frequency relationships. If we assume regular long-crested waves in deep water we have from Section 2, wave frequency,  $\omega = (2\pi g/L_w)^{1/2}$ , and from the basic definition the encounter period,  $T_e = 2\pi/\omega_e$ . Substituting these into Equation (188) for the encounter frequency, as well as expressing speed in terms of Froude number,  $F_n$ , the period of encounter becomes:

$$T_e = \frac{(L_w/g)^{1/2}}{|(2\pi)^{1/2} - (L/L_w)^{1/2} F_n \cos \mu|} \quad (202)$$

in which  $L$  is ship length. A convenient way of expressing how near the period of encounter is to synchronism is the *tuning factor*,  $\Lambda = T_j/T_e$ , where  $T_j$  is the natural period of the  $j$ 'th response. Then with the aid of the expression for the encounter period:

$$\Lambda = [T_{nj}(g/L)^{1/2}] (L/L_w)^{1/2} \times |(2\pi)^{-1/2} - (L/L_w)^{1/2} F_n \cos \mu|$$

Synchronism results when  $\Lambda = 1.0$ . Setting  $\Lambda$  to unity and solving the result for the Froude number for synchronism,  $F_{ns}$ ,

$$F_{ns} \cos \mu = (L_w/L)^{1/2} \left\{ \frac{1}{\sqrt{2\pi}} \pm \frac{(L_w/L)^{1/2}}{T_{nj}(g/L)^{1/2}} \right\} \quad (203)$$

Since the Froude number is considered positive in the conventions established thus far,  $\cos \mu$  fixes the sign of the left-hand side of the solution. Thus, for fixed  $\mu$ ,  $L$ ,  $L_w$  and  $T_{nj}$  there may be one, two or no solutions for the synchronous Froude number.

A dimensional form of the last relationship has been used in developing the nomograph shown in Fig. 78. This nomograph yields solutions within the ranges of speed, wave direction, wave length, and natural periods that are of importance for displacement ships. It may be noted in the lower right hand side of the nomograph that the lines for various wavelengths come together and cross one another so as to define an envelope. The envelope is defined by the relation,  $U_0 \cos \mu = gT_{nj}/8\pi$ , and corresponds to the condition where a singularity is expected in the encountered spectrum (See Section 4.3). Thus, for example, a ship having a 20-second roll period should experience near-resonant roll response to a broad range of wave lengths making up the peak of the encountered spectrum if it makes 20 knots in quartering waves (wave direction about 40 degrees from Fig. 78).

As may be noted from Fig. 78, wave direction affects the conditions for synchronism appreciably, but a good

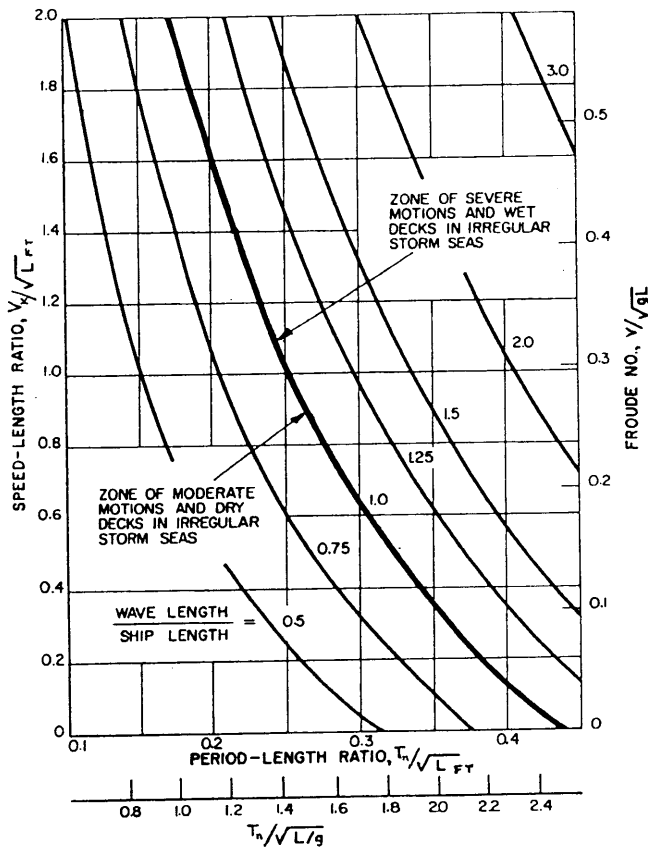


Fig. 79 Ship speeds for synchronism with regular head seas of various lengths ( $V \equiv U_0$ )

deal can be learned for the case of pitch or heave by considering the head-sea case alone. Fig. 79 was prepared by specializing the foregoing relation for the synchronous Froude number to the head-sea case. The figure shows the Froude number (and speed-length ratio) for synchronism with head seas of various wave lengths, for different values of the natural period parameter,  $T_n(g/L)^{1/2}$  (as well as a *period-length ratio* in English units). The range of the natural period parameter was chosen to reflect the attainable range for conventional ships, and will be elaborated upon later. It is clear from this figure that, in regular head waves, synchronism with a particular wave length can easily be avoided by a change in speed.

The discussions and examples in Section 3 and the earlier part of this section indicate certain general conclusions about ship behavior in head irregular waves:

- Only the wave components of about  $\frac{3}{4}$  ship length and above have appreciable effects on motions in head seas because the excitation in very short waves is much reduced, even at resonance.
- The most severe and objectionable results of ship motions (wet decks, slamming, high accelerations) result from the responses to wave components that are both relatively long and near synchronism with the ship's natural pitching and heaving periods.

These statements go some distance toward explaining the behavior of ships in head irregular storm seas. For instance, as a rule, ships are reasonably comfortable when they are hove to at very low speeds. The reason for this is that synchronism occurs only with wave components that are so short that they have only moderate effects. As the speed is increased, the period of encounter with longer wave components becomes short enough to approach synchronism with the ship's natural periods, and the motions become more violent. When violent motions occur, there will be the greatest likelihood of wet decks and slamming, since the ship is then responding predominantly to the wave components that lead to these effects. These trends are confirmed by model tests and by observations at sea.

Some ships must reduce speed more than others to ease motions in the same sea. For example, a 400-ft naval combatant generally can maintain higher speed than a 400-ft cargo ship. To obtain a general picture of the lowest speeds at which serious pitching and heaving are to be expected for ships of different proportions in irregular head seas, we may consider the conditions that result in synchronism with the wave components of approximately one ship length. Viewing the curves in Fig. 79 as representing the regular component waves of an irregular sea, one can see from the figure that, at any particular value of  $T_n(g/L)^{1/2}$ , Froude numbers on or above the curve for  $L_w/L = 0.75$  will result in synchronism with wave components as long as or longer than the ship, and may therefore lead to heavy pitching and/or heaving, wet decks, and slamming in a storm sea having a wide range of components. At speeds somewhat below the curve, synchronism will occur only with wave components shorter than the ship, which would not cause serious pitching. Thus the curve for  $L_w/L = 1.0$  may be considered as an approximate boundary between moderate and serious pitching and heaving in irregular head seas.

To an extent, this approximation to the boundary between moderate and severe longitudinal motions may be extended to oblique wave directions so long as the beam wave case is avoided. To accomplish this an *effective wavelength* is defined to be  $L_w/\cos \mu$ . When the effective length is substituted for the wavelength in the previous equation for the synchronous Froude number, it is possible to present the results as in Fig. 80, which defines zones of subcritical operation in oblique seas. Subcritical refers to the situation where synchronism occurs with waves that are too short to produce serious effects, i.e.,  $L_w \leq 0.75 L$ .

The generalizations for longitudinal motions of conventional displacement ships tend to be incomplete without some relatively simple connection between ship geometry and the magnitudes of pitch and heave periods. To start from the results in Section 3.7, we may take the expression for the uncoupled, undamped natural frequency of pitch and convert to natural period as follows:

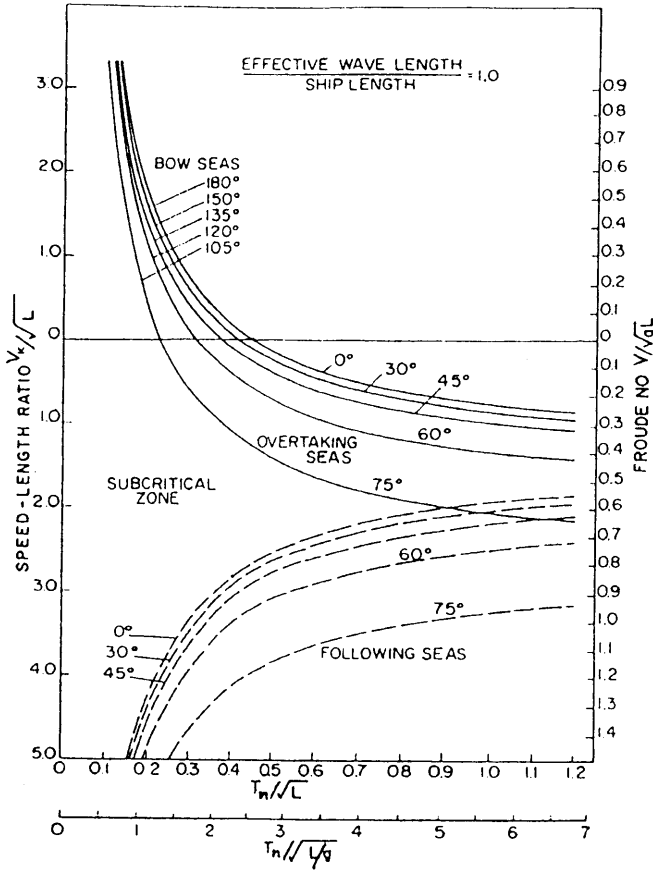


Fig. 80 Graph showing conditions for synchronism with waves of effective length equal to ship length ( $V \equiv U_0$ )

$$T_{n5} = 2\pi \left( \frac{I_{55} + A_{55}}{C_{55}} \right)^{1/2}$$

where  $I_{55}$  is the longitudinal mass moment of inertia,  $A_{55}$  is the hydrodynamic added moment of inertia and  $C_{55}$  is the pitch restoration coefficient. To clarify the effects of ship dimensions, form and other variables it is desirable to introduce non-dimensional coefficients in expressing each of these three terms. Thus  $I_{55} = \Delta k_{yy}^2 = \rho \nabla C_K^2 L^2$ , where  $C_K L$  is the longitudinal radius of gyration,  $k_{yy}$ , and  $C_K$  is the coefficient,  $k_{yy}/L$ .  $A_{55}$  represents the contribution to the longitudinal moment of inertia due to the *entrained water* and depends to a large extent on the longitudinal distribution of buoyancy. It can be expressed as  $A_{55} = \rho \nabla A'_{55} L^2$ , from Equation (164), where  $A'_{55}$  is a non-dimensional added mass moment of inertia coefficient analogous to  $C_K^2$ . Finally,  $C_{55}$  is given approximately in Table 13 of Section 3 (neglecting speed effect shown in Fig. 51) as  $C_{55} = \rho g \nabla \overline{GM}_L + LCF^2 C_{33}$ . Neglecting the second term and assuming  $\overline{GM}_L \approx \overline{BM}_L$ , we have roughly  $C_{55} \approx \rho g I_L$ , where  $I_L$  is the longitudinal moment of inertia of the waterplane. This can be rewritten as  $C_{55} \approx \rho g C_{IL} L^3 B$ , where  $C_{IL}$  is the conventional waterplane

inertia coefficient,  $C_{IL} = I_L / L^3 B$ . Making these substitutions and reducing, we obtain

$$\frac{I_{55} + A_{55}}{C_{55}} = \frac{\nabla C_K^2 + \nabla A'_{55}}{g C_{IL} B L}$$

Hence, the following three approximate expressions for the non-dimensional natural period of pitching result:

$$\begin{aligned} T_{n5} (g/L)^{1/2} &= 2\pi \left( \frac{\nabla}{B L^2} \right)^{1/2} \left( \frac{C_K^2 + A'_{55}}{C_{IL}} \right)^{1/2} \quad (a) \\ &= 2\pi \left( \frac{\nabla L}{L^3 B} \right)^{1/2} \left( \frac{C_K^2 + A'_{55}}{C_{IL}} \right)^{1/2} \quad (b) \\ &= \frac{2\pi}{1000(\rho g)^{1/2}} \left( \frac{W}{(L/100)^3 B} \right)^{1/2} \left( \frac{C_K^2 + A'_{55}}{C_{IL}} \right)^{1/2} \quad (c) \end{aligned} \quad (204)$$

These equations separate the influence of dimensions relative to displacement (first radical) from the influence of hull form and distribution of weights and buoyancy (second radical). In form (b) the ship's volume is expressed in terms of the nondimensional ratio  $\nabla/L^3$ , and  $L/B$  is a left-over ratio usually determined on the basis of other considerations than seakeeping. The third form (c) is obtained by substituting the conventional displacement-length ratio,  $W/(L/100)^3$ , where  $W$  is in long tons and  $\rho g = 1/35.0$  in salt water.

From the foregoing approximations it is clear that in order to shorten the period ratio,  $T_{n5} (g/L)^{1/2}$ , increased length relative to displacement is generally desirable. The appearance of the ratio,  $L/B$ , in the first radical of forms (b) and (c) means that  $\nabla/L^3$  is not as good a parameter as  $\nabla/B L^2$  and needs to be adjusted by multiplying by  $L/B$ —not that reducing  $L/B$  is desirable in itself (generally the reverse is the case). On the other hand, if  $L/B$  is determined by other considerations (such as stability), then  $\nabla/L^3$  and  $W/(L/100)^3$  are very useful indexes to use.

Fig. 81 shows typical values of pitching period-length ratio as functions of displacement-length ratio, as well as of  $\nabla/L^3$ ,  $\nabla/B L^2$ , and  $C_B T/L$ . Both model and full-scale data are presented, and the third form of the above approximation was used to curve-fit the data on the assumption (Lewis, 1955) that most of the variation occurs in the first radical of Equation (204c). It is clear from the figure that this last assumption is reasonable, since the spread of the data is well reflected by only a 20 percent variation in the curve-fitting constant,  $C$ , in which the second radical is embedded. For first approximations, values of  $A'_{55}$  of 0.03 or 0.04 are reasonable, and are consistent with Fig. 81 (See also Fig. 51, Section 3.7). The gyradius for conventional ships is typically between 24 and 26 percent of length, i.e.,  $C_K = 0.24$  to  $0.26$ . Noting that nearly the entire practical range of ship displacement-

length ratios is represented in Fig. 81, it appears that once length is established for a conventional ship the possibilities for variation of pitching period by changes in form or proportions are relatively limited. Hence, it is essential that a wide range of ship lengths be considered in design.

Finally, in order to clarify the design problem of improving subcritical performance by reducing the period ratio,  $T_{n5} (g/L)^{1/2}$ , another form of Equation (204) is useful. To obtain this the ship's volume is eliminated by substituting  $LBTC_B$  for  $\nabla$  and  $C_{IL}$  is eliminated by introducing a waterplane inertia coefficient,  $C_A = k_a^2/L$ , where  $k_a$ , the area radius of gyration, is defined by  $I_L = k_a^2 A_{WP}$ . Hence,

$$C_{IL} = I_L / L^3 B = \frac{k_a^2 A_{WP}}{L^3 B} = \frac{k_a^2}{L^2} \frac{A_{WP}}{LB} = C_A^2 C_{WP} \text{ and}$$

Equation (204a) becomes

$$T_{n5} (g/L)^{1/2} = 2\pi \left( \frac{T}{L} \right)^{1/2} \left( \frac{C_B}{C_{WP}} \right)^{1/2} \left( \frac{C_K^2 + A'_{55}}{C_A^2} \right)^{1/2} \quad (204d)$$

Note that  $C_B/C_{WP}$  is the vertical prismatic coefficient,  $C_{VP}$ . The period ratio has thus been expressed as three factors, covering: Dimensions, form coefficients and non-dimensional coefficients dependent on longitudinal distribution of hull mass, buoyancy and waterplane area. Since  $\nabla$  has been eliminated, this expression is independent of ship size.

Hence, the following specific steps appear to be favorable to reduced  $T_{n5} (g/L)^{1/2}$ :

- Decrease in draft-to-length ratio,  $T/L$ ;
- Increased waterplane area coefficient in conjunction with decreased  $C_B$  (i.e., reduced vertical prismatic and more V-shaped sections)
- Reduced mass moment of inertia coefficient,  $C_K = k_{yy}/L$  (i.e., reduced mass radius of gyration in relation to length), reduced added-inertia coefficient,  $A'_{55} = A_{55}/\rho \nabla L^2$  (which is not ordinarily calculated or assumed to be a variable, although it varies with speed and other factors, as shown in Section 3), and
- Increased waterplane inertia coefficient,  $C_A = k_a^2/L$  (i.e., increased waterplane radius of gyration in relation to length), which implies increased fullness of waterlines in the ends of the ship.

Another useful form for the equation of natural pitching period, assuming  $\overline{GM}_L \approx \overline{BM}_L = I_L/\nabla$ , is:

$$T_{n5} = \frac{2\pi}{g^{1/2}} \frac{k'_{yy}}{(\overline{BM}_L)^{1/2}} \quad (205)$$

where  $k'_{yy}$  is an effective radius of gyration,  $L(C_K^2 + A'_{55})^{1/2}$ , which with the typical values quoted above is about 30 percent of length.

As for heaving, we may adapt the results from Section 3 for the uncoupled natural heaving frequency to

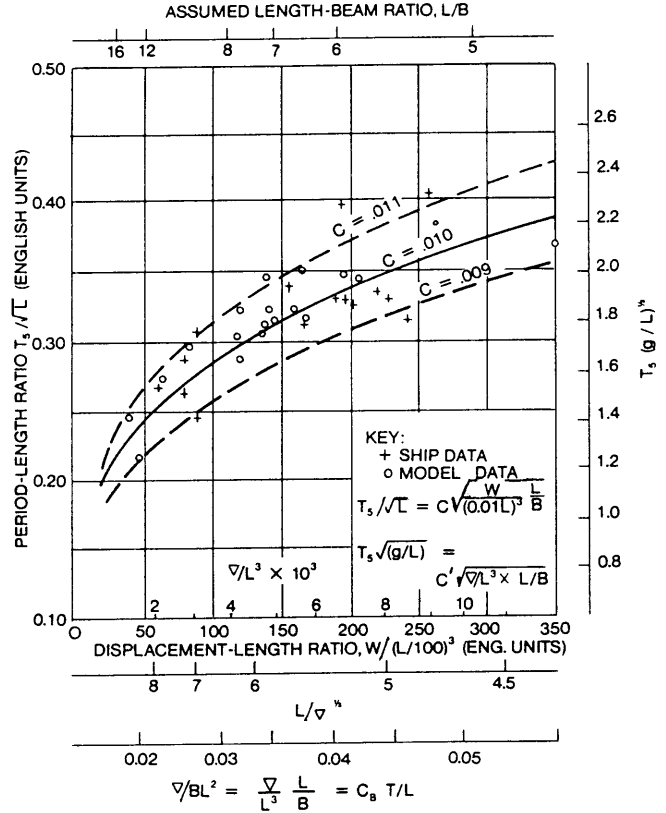


Fig. 81 Variation of natural pitching period with ship characteristics

produce the following estimate for the natural heaving period:

$$T_{n3} = 2\pi \left[ \frac{\rho \nabla + A_{33}}{C_{33}} \right]^{1/2}$$

We may express the heave restoration coefficient with the aid of the waterplane area coefficient,  $C_{WP}$ , as  $C_{33} = \rho g C_{WP} LB$ . Defining a nondimensional heave added mass coefficient as  $A'_{33} = A_{33}/\rho \nabla$ , the numerator of the expression for heave natural period becomes  $\rho \nabla (1 + A'_{33})$ . Making the substitutions and nondimensionalizing the expression, the approximation to the heave natural period ratio becomes:

$$T_{n3} (g/L)^{1/2} = 2\pi \left( \frac{T}{L} \right)^{1/2} \left( \frac{C_B}{C_{WP}} \right)^{1/2} (1 + A'_{33})^{1/2} \quad (206)$$

It appears that the draft-length ratio,  $T/L$  is again an important factor, followed by the vertical prismatic coefficient,  $C_{VP} = C_B/C_{WP}$ . The added mass coefficient,  $A'_{33}$ , varies very little for conventional ships, and is usually taken to be unity for first approximations, Fig. 51. Note the similarity to Equation (204d) for pitch.

The foregoing relationships allow the natural period



ratios to be estimated in very early stages of design (Section 3) and allow the conditions for synchronous pitching and heaving in regular waves to be determined. It has been noted that the most significant features of the heave and pitch RAO's are more or less dictated by natural periods. The fact that reasonably close estimates of natural periods can be made using only the most basic principal dimensions and form coefficients has an important consequence, which is that once the principal characteristics of the ship are selected a good part of its expected behavior in a seaway is determined. Over the years it has proven very difficult to produce large changes in the longitudinal motions of conventional displacement ships with small changes in form or size. But the importance of changes in proportions is considered further in Section 8.

The foregoing analyses raise the interesting technical possibility of attaining the supercritical condition of operation for ships; that is, going fast enough into head seas so that the periods of encounter with the longest important wave components are well under the natural pitching period. In other words, when the supercritical condition is reached the ship is going so fast that it does not have time to respond to a wave before it has passed and the next one has arrived. The possibility of attaining supercritical speeds depends upon the fact that there is an upper limit to the length of wave components normally found at sea. Oceanographers have established that the longer and harder the wind blows, the longer are the longest wave components present in the sea. The upper limit for different sea conditions has not been firmly established. However, Moskowitz, et al, (1963) indicated a limit between 625 and 1060m (2000 and 3400 ft), with about 800m (2600 ft) being average for a sample of severe North Atlantic seas (winds of 50-65 knots). In less severe storms the limit would be lower.

The other factors affecting supercritical operation are ship factors. The faster the ship and the longer the natural pitching and heaving periods, the easier it is to attain the supercritical condition. If the longest wave component in a given storm sea is 315 m (1000 ft), then the supercritical condition for a 155-m (500-ft) ship would lie above the curve for  $L_w/L = 2.0$  in Fig. 79. The speed required to attain it for any value of the period-ratio is also shown in the figure, which shows that the Froude numbers required would typically be in excess of those usually appropriate for merchant and most naval vessels. This illustrates the practical difficulties in assuring supercritical operation in all but very mild sea conditions. Attempts to develop supercritical ships usually involve radical departures from the usual ship form in order to lengthen natural periods. Furthermore, a considerable increase in bow freeboard may be required.

An early example of a ship designed for supercritical operation is the *Escort Research* ship design described by Oakley (1960). In this approach very large bow and

stern bulbs were incorporated so as to produce larger than normal added mass inertia, and thus longer than normal natural pitching periods.

Another method proposed for obtaining supercritical operation involves drastic reduction in longitudinal waterplane inertia coefficient, with a semi-submerged hull similar to a surfaced submarine (Lewis, et al 1960). Saunders (1965) points out that old style submersibles could often maintain high speeds in very rough seas, operating upon the surface in the supercritical condition. Such a hull pitches very little, though heaving accelerations may be rather high, and the decks are very wet.

The idea of design for supercritical operation has found most practical application in the design of semi-submerged platforms. In this case the natural periods achieved by the un-ship-like geometry are usually longer than the periods of typical waves encountered, but not usually longer than the longest components in a severe storm, so that the semi-submerged platform too is not always supercritical. The same may be said for the SWATH (Small Waterplane Twin-Hull) ship (Lee and Curphy, 1977) (See Section 8.5).

**4.10 Long-Term Performance Predictions.** The treatment thus far has been of measures of short-term response to one sea as defined by a spectrum that applies to a stationary process. The result is essentially conditional; that is, the response is predicated on the condition that the specified sea occurs. Practical performance predictions and design decisions have been made upon the results for one "design" sea, but current practice has tended away from this approach. The problem is that the probability of occurrence of any particular one of the sea spectra noted in Section 2 is virtually zero. Thus if the response in question is sensitive not only to the area but to the shape of the spectrum, or the range of significant frequencies, the answer obtained may correspond to an event of low probability and thus may be misleading. Accordingly, when practical performance predictions are at issue, current practice is tending toward the analysis and interpretation of collections of seaways, covering the expected range of spectral areas and shapes. Such analyses are particularly important in the synthesis of structural design loads, and in fact the concept of the synthesis of the response to collections of seaways originated in this context (See Chapter IV).

Several collections (families) of seaways have been discussed in Section 2. Mechanically, the response calculation involves repeating the linear-random predictions outlined in Section 4.1 for as many seaways as are defined in the collection, and then interpreting the collected results in the light of the expected frequency of occurrence of each member of the seaway collection. Essentially, the analysis of the response to collections of seaways is a strategy to overcome the statistical nonstationarity of real seas over the long term, and the fact just mentioned that there is negligible prob-



ability of any particular sea spectrum being exactly replicated.

The most important part of such procedures is the definition of the appropriate statistical measure or criterion of performance, to be discussed in Section 7. Once this is done the next step is to define the wave environment (Section 2) in terms of a collection of representative wave spectra, and a probability of occurrence for each. The linear-random prediction of response for each spectrum is then associated with the probability of occurrence of the spectrum. Finally, the predictions are weighted in accordance with the associated probabilities to form the desired statistical measure of performance for comparison with criteria. There are a number of variations of this type of analysis that follow from the various kinds of measures of performance to be discussed in Section 7, and doubtless others will arise. By far most of the numerical work and manual preparation for a collection analysis is in the generation of RAO's and the subsequent variance computations for a variety of wave spectra.

The increasing availability of computers with mass storage capability, has given rise to *seakeeping data base* development. To produce a data base of this type,

the geometry of a series of ship forms related in some way is assumed, motion RAO's are estimated for each, and the variances and spectral moments required for a large number of possible performance criteria are computed for each of a large number of hypothetical seaways. Computer storage of such results allows the major part of the numerical work to be recaptured when the undefined portions of the analysis (the exact criteria and the seaway probabilities) are defined. One of the primary justifications for the data base approach for ship design is the observation that large changes in a response statistic can ordinarily only be made by major changes in ship geometry; that is, by changes in principal dimensions and coefficients, the class of ship remaining constant. Examples incorporating a *standard series* approach to the geometry for merchant ships include Bales & Cummins (1970) and Loukakis & Chrysostomidis (1975). Examples including extensive variations of operational parameters for limited numbers of existing ships are: Bales, et al (1975), Baitis, et al (1976a & b). These latter are most useful in obtaining estimates of performance for existing ships, for comparison with estimates for a new design, or in the design of new ship systems on similar ships.

## Section 5

### Derived Responses<sup>11</sup>

**5.1 Introduction.** The aspects of ship response to rough seas that are generally of greatest importance to the evaluation of seakeeping performance will now be considered. These are the responses that can in principle be derived from the basic six modes of motion. They include:

- Vertical and/or lateral motions, velocities and accelerations at specific points, i.e. local motions.
  - Relative motions between a location in the ship (as the F.P.) and the encountered waves.
- Non-linear effects arise in connection with:

- Shipping water and slamming.
- Yawing and broaching.
- Added resistance and powering in waves.
- Wave bending moments and loads on hull and equipment.

All of these linear and non-linear responses will be considered in this section, first in regular and then in irregular seas.

#### 5.2 Local and Relative Motions.

(a) *General case of six degrees of freedom.* If amplitudes of motion in regular waves in all six degrees

of freedom, with phase angles, have been calculated by methods discussed in Section 3.3 to 3.5, it is possible to compute the resultant local motions, velocities and accelerations at any position in the ship (Hamlin, 1979). Such calculations are facilitated by the use of complex number notation, however.

The motions of any point  $(\bar{x}, \bar{y}, \bar{z})$  on the body may be defined by three translations and three rotations. Since the ship is assumed to be a rigid body, the rotational motions are the same at all points on the body. Thus, the complex amplitudes  $\bar{\eta}_4, \bar{\eta}_5, \bar{\eta}_6$  define the rotational motions at every point. In vector notation we may write

$$\begin{aligned}\underline{\Omega} &= \text{vector of rotational motion at any point} \\ &= (\bar{\eta}_4, \bar{\eta}_5, \bar{\eta}_6)\end{aligned}$$

The three translational motions at any point, resulting from the combined effect of rotation of the body and translation of its center of gravity, are defined in vector notation by

$$\bar{\xi} = (\bar{\xi}_1, \bar{\xi}_2, \bar{\xi}_3)$$

where  $\bar{\xi}_1, \bar{\xi}_2, \bar{\xi}_3$  are the complex local amplitudes at  $\bar{x}, \bar{y}, \bar{z}$  in surge, sway and heave, respectively.

To determine  $\bar{\xi}$  we must combine the motion at

<sup>11</sup> Section 5 written by Robert F. Beck, John F. Dalzell and the Editor.



the pitching terms usually have the effect of producing a much larger apparent resonance peak of vertical motion than for heave alone near midship. Because of the phasing between heave and pitch, the amplitude of vertical motion is usually much larger at the bow than at the stern. The longitudinal location of the center of flotation is also a factor.

In general, if the amplitude of heave—or of vertical motion at any point—is known in regular waves, the corresponding velocity and acceleration amplitudes can be determined from

$$\begin{aligned} |\dot{\xi}_3| &= \omega_e |\xi_3| \\ |\ddot{\xi}_3| &= \omega_e^2 |\xi_3| \end{aligned} \quad (212)$$

Hence, the response amplitude operators (squared) can be transformed from motion to velocity by multiplying successive points by  $\omega_e$  and to acceleration by multiplying by  $\omega_e^2$ . In evaluating ship performance the vertical acceleration at critical locations is of particular importance.

Also of interest is the relative vertical motion between a point in the ship and the surface of the encountered wave. This relative motion in regular wave is found by subtracting the free-surface motion from the vertical ship motion at the desired point, taking account of their phase relationship. The free-surface motion is composed of the incident wave, the diffracted

wave, the radiated wave (Section 3) and the wave due to the ship's steady forward speed. The traditional assumption is that the principal component is the incident wave and that the other components tend to cancel each other; i.e., the incident wave is not distorted by the presence of the ship. This may or may not be true and will be discussed further in the next subsection.

Assuming that the wave is not distorted by the presence of the ship and  $\bar{z} = 0$ , the amplitude of the relative vertical motion in general is given by

$$\begin{aligned} \bar{\xi}_R &= \bar{\xi}_3 - \bar{\zeta}_{\bar{x}\bar{y}} = \bar{\eta}_3 - \bar{x}\bar{\eta}_5 \\ &\quad + \bar{y}\bar{\eta}_4 - \bar{\zeta}_{\bar{x}\bar{y}} \\ &= \bar{\eta}_3 - \bar{x}\bar{\eta}_5 + \bar{y}\bar{\eta}_4 \\ &\quad - \bar{\zeta} e^{-ik(\bar{x} \cos \mu + \bar{y} \sin \mu)} \end{aligned} \quad (213)$$

where  $\bar{\zeta}_{\bar{x}\bar{y}}$  is the complex amplitude of the wave at  $x = \bar{x}$ ,  $y = \bar{y}$  relative to the body coordinate system. In the case of pitch and heave in head seas this reduces to

$$\bar{\xi}_R = \bar{\xi}_3 - \bar{\zeta}_{\bar{x}} = (\bar{\eta}_3 - \bar{x}\bar{\eta}_5 - \bar{\zeta} e^{ik\bar{x}}) \quad (214)$$

where  $\bar{\zeta}_{\bar{x}}$  is the complex wave amplitude at  $x = \bar{x}$  relative to the body coordinate system, or  $\bar{\zeta}_{\bar{x}} = \bar{\zeta} e^{ik\bar{x}}$ .

Then the RAO which requires only the scalar or absolute amplitude is

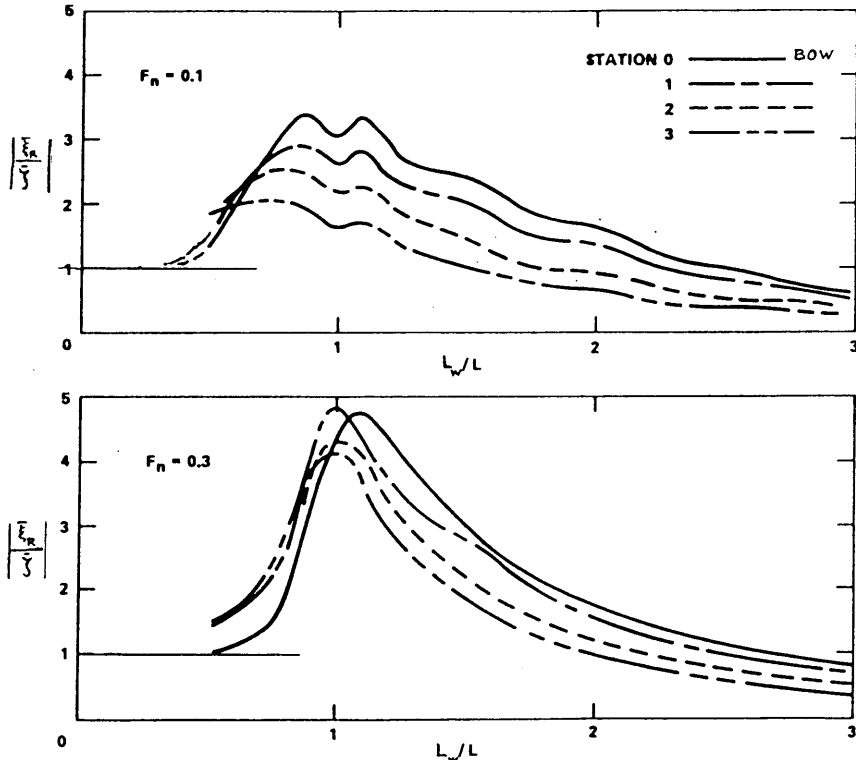


Fig. 83 Measured magnitude of relative motion RAOs in regular head waves (O'Dea, 1983)

$$|\bar{\xi}_R/\bar{\zeta}| = |(\bar{\eta}_3 - \bar{x}\bar{\eta}_5)/\bar{\zeta} - e^{ik\bar{x}}| \quad (215)$$

It is important to note that the relative motion RAO has entirely different asymptotic properties than heave. These properties are illustrated in Fig. 83 (O'Dea, 1983), which shows a plot of the total relative motion divided by the incident wave amplitude at stations 0–3 (on a 20-station ship) for a high-speed cargo ship (SL-7) model. At very long wavelengths the relative motion tends to zero because the ship contours the waves. For very short wavelengths both heave and pitch RAO's go to zero, and the relative motion is due only to the wave motion, yielding a value of around 1.0. In between the two extremes the relative motion peaks, typically around a wavelength to ship-length ratio of 1 to 1.5. In general the relative motion is greatest at the bow. However, as seen in the figure for Froude number 0.3, there are cases where the relative motion is greater abaft the bow. O'Dea also gives curves for non-head seas. For this case, the character of the relative motion curves is the same as Fig.

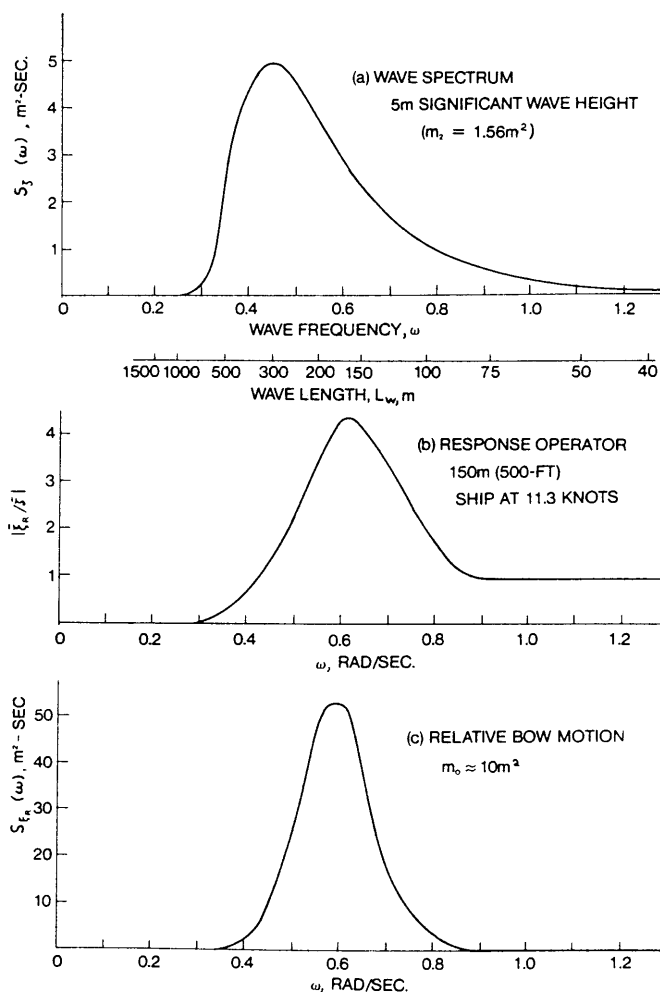


Fig. 84 Relative bow motion in an irregular head sea

83, except that the magnitude is increased on the weather side and decreased on the lee side.

It should be noted that the model test data given in Fig. 83 include certain dynamic effects to be discussed subsequently. So far our discussion of relative bow motion is based on the simplifying assumption that the ship and its motions do not affect the encountered wave, giving a so-called *kinematic solution*.

If the RAO's for absolute or relative motions have been calculated and the system is assumed to be linear, then the corresponding responses to irregular seas can be determined by the methods of Section 4. The calculation of relative bow motion in an irregular sea is of particular interest. Fig. 84 is an example of the prediction of relative bow motion for the 150-m (500-ft) ship of Fig. 72 (Section 4). In this example the influence of pitch is relatively strong and results in peak values of  $|\xi_R/\zeta|$  in excess of 4.0 at  $\omega = 0.6$  rad per sec. This is not an untypical magnitude for a ship at speed in head seas. Depending upon speed and fullness the peak relative motion RAO for ships can vary between 2 and 5. In the example of Fig. 84 the effect of unity high-frequency relative motion RAO is slight. It becomes of more concern as the RAO peak induced by pitch becomes smaller, or as the wave spectrum peak shifts to higher frequency.

The significance of the relative motion response is that the moments of the spectrum provide probability measures related to anticipated deck wetness and bow emergence—the latter affecting the likelihood of slamming—as discussed in the following sub-sections. However, in general we can expect that comparative calculations of relative bow motion will give useful qualitative information on the seakeeping performance of alternative ship designs. It should be emphasized that so far we have considered only the simplest possible, or kinematic, treatment of relative motion. Dynamic effects will be discussed under shipping water in the next sub-section.

**5.3 Shipping Water Forward.** An important aspect of relative bow motion is the probability of bow submergence and hence of shipping water on deck, particularly in head seas, since this greatly affects attainable speed in service. Predicting the shipping of water involves the comparison of the relative bow motion previously discussed with the available bow freeboard. One approach is to compute the probable fraction (or percentage) of time that the foredeck is awash or that the deck edge or bulwark is submerged, at a specific longitudinal location. This can be done on the basis of the underlying assumption that relative motion can be considered to be a Gaussian process, so that values taken at equal intervals of time follow a normal or Gaussian density function. The probability of relative bow motion exceeding a particular value of freeboard  $F_1$ , is 1 minus the cumulative normal distribution, which is readily obtainable from probability tables.



The water can be expected to reach the deck on the average  $N_T$  times per hour, so long as conditions remain unchanged and the total number of cycles  $N_L$  is large.

Probability techniques have been applied to determination of desirable trends in bow freeboard with ship type and size. For example, calculations were made (Band, 1964) beginning with relative bow motion for four lengths of full tankers in five different short-crested head seas. The probability of bow submergence at reasonable speeds in each sea was determined. Finally, considering the frequency of occurrence of each sea condition the combined probability of bow submergence in all head seas was calculated as a function of freeboard. Results are plotted in Fig. 85 in the form of required freeboard/length ratio versus ship length for different probabilities of bow submergence in both the North Atlantic and on typical tanker routes (Europe or U.S. to Mediterranean). In this case, absolute values are less important than trends, and it is interesting to note that all of the curves indicate approximately constant required freeboard for ship lengths above about 180m (600 ft). Hence, if a bow freeboard of  $0.05L = 9\text{m}$  (30 ft) has been found satisfactory for 600-ft cargo ships it would appear that 9m (30 ft) should be satisfactory for any longer ships of the same type in head seas.

However, if accurate quantitative predictions of shipping water for specific ships in specific seas are needed, a detailed analysis of the deck wetness problem reveals that the effective freeboard does not equal the nominal freeboard, and the relative motion is altered by hydrodynamic effects not accounted for in the simple kinematic approach. The actual effective freeboard can be considered as the sum of several components. The most important is the nominal freeboard, usually defined as the distance from the calm waterline to the deck or top of the bulwark at any longitudinal location. The second is the change in freeboard due to the sinkage and trim caused by the forward speed of the vessel. The forward speed also creates a calm water wave profile which further modifies the freeboard. Tasaki (1960) called these two effects *static swell-up*. Finally, as introduced by Newton (1960), the above-water body shape, freeboard, flare, knuckles, and other special features will alter the necessary relative motion required to produce deck wetness. Although this influence is often considered as a change in effective freeboard, it is convenient to consider it here along with the dynamic effects to follow.

Static swell-up can easily be evaluated by model tests in still water, and it can be assumed that there is linear superposition of the ship's wave and the encountered wave. The theoretical prediction of static swell-up has been extensively investigated in conjunction with ship wave-resistance theory. Various theoretical methods are available ranging from simple slender-body theories to "thin-ship" theory, to three-

dimensional source-panel distribution methods. A good summary may be found in Bai and McCarthy (1979) and Noblesse and McCarthy (1983). Lee, et al (1982) used a thin-ship theory to determine the steady wave profile and devised an empirical formula for the prediction of sinkage and trim of destroyer-type hulls (Bishop and Bales, 1978) and (Tasaki, 1963).

The actual relative motion may differ from that obtained by the simple kinematic approach because of the presence of the ship, as mentioned in Section 5.2. The first effect is the diffraction of the incident wave system and the second is the radiation of waves caused by the motions of the vessel. The change in relative motion due to the diffracted and radiated wave systems is often referred to as *dynamic swell-up* since it results from the dynamics of ship and wave motions.

Dynamic swell-up can again be determined by model tests. In model tests of a *Mariner* hull in head seas ( $C_B = 0.61$ ), Hoffman and Maclean (1970) found a dynamic swell-up factor of 1.12 to 1.15. Experimental trends of swell-up are given by Journee (1976a) for full-load and ballast conditions of a high-speed cargo ship (with bulb). It is noted that the dynamic swell-up is much greater at a station 10 percent of length abaft the FP than at the FP. O'Dea (1983) and O'Dea and Jones (1983) also measured the components on a model of an SL-7 high-speed containership.

Since simple general formulas for all types of ship are not yet available, the best solution in a specific case appears to be model experiments for the designs under consideration. However, theoretical and experimental research continues and some highlights will be mentioned.

Lee, O'Dea and Meyers (1982) extended the basic ship motion theory, as presented in Section 3, to predict the vertical motions of a point in a ship relative to the free surface, retaining the assumptions of strip theory and linearity. Calculations for a high-speed containership and a typical naval combatant were then compared with model tests in head and bow seas. Results showed some discrepancies at the higher speed, which were attributed to inaccuracies in prediction of the phase relations among the incident, diffracted and radiated wave components, and may be due in part to neglect of non-linear effects, including the influence of above-water hull form. On the other hand, the comparisons reveal no conclusive evidence that the theoretical refinements in calculation of relative motions provide much improvement compared to using only the kinematic solution.

Beck (1982) measured experimentally the radiation and diffraction components in head seas about a mathematical hull form with parabolic waterlines. The components were also predicted theoretically using a strip theory for the radiated waves and a slender-body theory for the diffracted waves. Researchers have used three-dimensional computations to improve the agreement between theory and experiment for the mathe-

mathematical model. The general conclusion from the investigations is that the individual components taken separately may substantially alter the relative motion. However, in many cases the various components tend to cancel one another so that the simple kinematic approach gives reasonable answers.

For example, Lloyd, et al (1979), reporting on model tests on a "typical modern warship" without bulb, found that, "The computed relative bow motion . . . with no allowance made for any distortion of the waves by the ship," gave reasonably good agreement with experimental measurements at the stem of the model.

The effect of above-water bow shape (flare, knuckles, etc.) on relative motion, and hence on effective freeboard, has been investigated by several researchers. In general above-water bow section shape has very little, if any, effect on the primary ship motions (pitch and heave), but the influence of flare on deck wetness is more significant, although it is not clearly defined. O'Dea and Walden (1984) and Newton (1960) found that increased flare reduced deck wetness. On the other hand, the relative motions measured by Swaan and Vossers (1961) and Lloyd, et al (1985) were increased as the flare increased. This was apparently caused by increased dynamic swell-up. The increased flare was effective at shielding water on either side of the bow. However, the increased swell-up caused by the flare propagates forward as the bow pitches down into an approaching wave and may be responsible for increased shipping of water over the stem. The O'Dea and Walden experiments were conducted in regular waves while Lloyd, et al, used more realistic irregular seas; this might account for the different conclusions. Furthermore, O'Dea and Walden kept the same stem profile, while Lloyd, et al, increased stem rake as the flare increased. It is possible that the differences in deck wetness were caused by differences in the detailed design of the bows. It is obvious that non-linear effects are present here. Salvesen (1978b) has shown that significant second-order terms can be introduced without excessive complications.

Although all factors affecting relative motions are not yet fully understood, a tentative procedure based on Bales (1979) has been adopted by the U.S. Navy for checking bow freeboard in the contract design stage of combatant ships (NAVSEA, 1982). It makes use of computer calculations of motions and empirical data for the static and dynamic build-up, neglecting the influence of above-water hull form.

Relative motions at other longitudinal locations may be of importance also, particularly at the stern where shipping water in following seas, or *pooping*, may be a problem for some ships. Comparison between experiment and theory for a cargo ship hull by Journee (1976b) showed that, although calculated relative motions at the stern agreed with those determined from measured pitch, heave and wave, the measured relative motions were generally  $\frac{1}{3}$  to  $\frac{1}{2}$  as great, as a result of

dynamic effects. It is clear that further work is needed on such effects in following as well as head seas.

**5.4 Slamming.** Another phenomenon related to relative bow motion is bow emergence and bottom slamming. Impact of the ship's bottom on the surface of a wave can cause not only decelerations and local structural damage but transient vibratory stresses (whipping) elsewhere in the hull, as discussed in Chapter IV. It might be expected that the prediction of bow emergence in regular waves from kinematic calculations of pitch and heave and the incident wave amplitude would be reasonably reliable, since the previously mentioned effects of ship's above-water bow form and interaction of ship motion with the encountered wave should here be less. A simplified probability of bow emergence in irregular head seas can be determined in the same way as for deck wetness (sub-section 5.3) by substituting still water draft forward,  $T_f$ , for freeboard,  $F_1$ .

However, whether or not bottom slamming impact will occur when the bow emerges depends also on factors such as relative vertical velocity at the fore-and-aft location where slams occur, section shape, particularly extent of flat of bottom, and angle between keel and wave slope at entry. On the basis of experiments with a model of a 160-m (525-ft) *Mariner* class cargo ship, Ochi (1964) found that slamming occurred when the bow emerged and the relative velocity exceeded a threshold value of 3.65m/sec (12 ft/sec) (full-scale), regardless of angle of entry. He suggested that for other similar ships the threshold velocity would depend on ship length in accordance with Froude scaling (i.e., proportional to  $\sqrt{L}$ ).

Calculation by the techniques of Section 4 of the probability of slamming in irregular head seas having a specified spectrum requires first the evaluation of a suitable RAO for relative vertical velocity. As previously explained in Equation (212), this involves multiplying the relative motion RAO (Equation 215) by  $\omega_e$ . That is,

$$|\dot{\xi}_R| = \omega_e |\bar{\xi}_R| \quad (219)$$

The probability of exceeding a given relative vertical velocity can then be determined using the area under the response spectrum, in the same manner as for bow emergence or shipping water. Alternatively, the identical result can be obtained by taking the second moment,  $m_2$ , of the response spectrum for local relative motion.

On the basis of work of Ochi (1964), one can go on to predict the joint probability of forefoot emergence and vertical velocity exceeding a critical value  $\dot{\xi}_{RC}$ , which is given by

$$\exp -\frac{1}{2}[T_1^2/m_0 + \dot{\xi}_{RC}^2/m_2] \quad (220)$$

where  $T_1$  is forward draft and the moments,  $m_0$  and

$m_2$  apply to relative ship-to-wave motion near the bow and relative velocity, respectively. Details of calculations to predict the occurrence of slamming in irregular seas are thoroughly covered by Ochi (1964) and Ochi and Motter (1973).

For structural design purposes magnitudes of bottom impact pressures are needed. The prediction of such impact pressures is a complex problem that is far from a satisfactory solution. Some of the important factors:

- Relative vertical velocity at bow entry.
- Section shape, particularly whether bottom is flat.
- Angle between keel and wave slope at entry.
- Area of impact on flat of bottom.
- Duration of impact.

In general there seems to be reasonable agreement between pressures obtained by two-dimensional drop tests and by theory, when theory includes the effect of entrapped air and water surface deformation. However, hydrodynamic pressures obtained in two-dimensional experiments are consistently higher than those obtained in ship model tests. The difference is believed to be due to the effect of surface waves, air entrapment and three-dimensional effects. Work by Beukelman (1979) has shown that at forward speed impact pressures are significantly increased if there is an angle between the centerline of the keel and the wave surface.

In spite of the above difficulties, two approximate methods of calculating impact pressures are now available, one by Ochi and Motter (1973) for merchant hull forms and the other by Stavovy and Chuang (1976) for high-speed vehicles. The former assumes that the local pressure at a critical section is the product of the square of the relative vertical velocity and a form factor dependent on section shape. Form factors are derived empirically from model tests and full-scale data, using Froude scaling. No account is taken of angle between keel and wave slope nor of differences in ship speed. The second method is applicable to V-shaped forms without significant flat of bottom and takes account of the angle between keel and wave slope. Because of the latter refinement, this method is more difficult to incorporate into conventional ship motion calculations, but it has considerable promise for the future (Troesch and King, 1986).

From the point of view of hull structural design (Chapter IV), impact on bow flare may be even more serious than bottom slamming, since the duration of the impulse is longer and the dynamic magnification factor therefore is usually greater. Kaplan and Sargent (1972) have presented a method for calculating forces due to flare entry. The applied load is computed on the basis of the "non-linear variations in buoyancy and inertial forces, over and above those used in the linear ship motion analysis." Results are obtained as time domain solutions of structural response to various

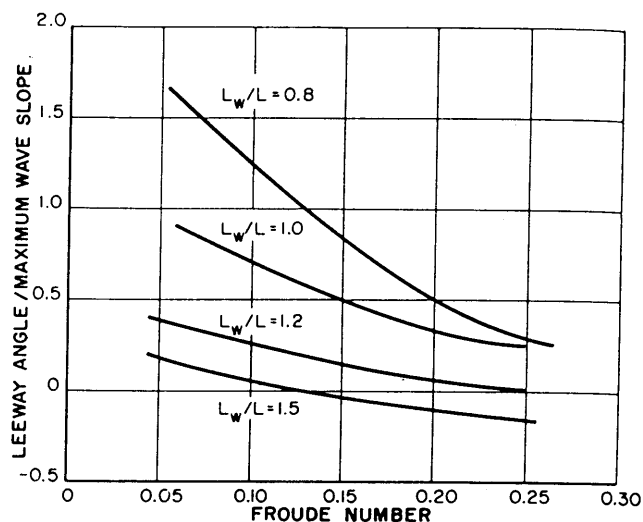


Fig. 86 Leeway angle of a Victory model in bow seas ( $\mu_w = 120^\circ$ ), (Vossers, 1962)

wave inputs, as well as rms values and other statistical properties. Work has also been done by Kumai and Tasai (1970) and O'Dea and Walden (1984).

Pending the development of completely reliable theoretical methods for predicting bottom and flare entry slamming, the value of direct experimental determination of deck wetness and slamming features of a new design should be recognized (Murdey, 1979). Such model tests in irregular waves can be considered to be a form of analog computer solution in which all non-linearities are automatically taken into account, and a single model can be fitted with a number of alternative bows or bow segments. Of course, wind and spray effects are not usually reproduced in model tests.

**5.5 Yawing and Broaching.** The problems of steering and maneuvering in waves depend upon systems for ship control, and therefore they are discussed in Chapter IX, as well as in Section 3 of this chapter. However, since they also involve ship motions—including important non-linear behavior—they need to be mentioned here.

The interacting effects of sway, yaw and roll are shown mathematically in the equations of motion developed in Section 3, which apply very well for head and bow seas (with rudder fixed). Only the hull lift effects resulting from the changing angle of attack due to yaw and sway are not included.

As noted in Section 3.8, early model tests in regular oblique bow waves revealed unexpectedly large values of leeway angle between the mean model heading and the path made good across the tank. This angle varied with wavelength and speed, as shown in Fig. 86. Consequently, when many wave components are present simultaneously, as in the case of irregular seas, a ship will continually change its heading to the sea unless



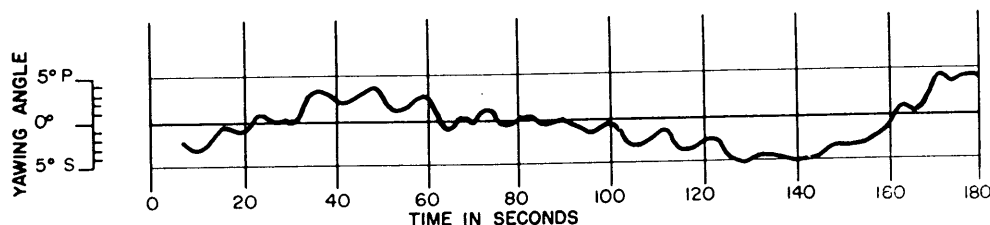


Fig. 87 Record of yawing motion in bow seas, S.S. *Nissei Maru* (Exp. Tank Com. of Japan, 1954)

controlled by rudder action. At the same time, tests showed that the model also oscillated in yaw about its mean heading. Thus a ship or model's heading in bow seas changes as a result of both high-frequency yawing and slower changes in leeway angle. The former is affected very little by the action of the rudder and hence may result in unnecessary steering-gear wear. But the latter depends greatly on the efficacy of steering gear and helmsman or automatic steering system. Fig. 87 shows both types of change of heading in records taken on the *Nissei Maru* at sea (Exp. Tank Committee, Japan, 1954).

Salvesen (1974) has investigated the causes of the observed leeway angles in oblique waves. He states, "In the horizontal modes of motion the ship will experience steady drift motions in addition to periodic motions, because of the lack of hydrostatic restoring forces and moments in these modes. Similarly, in irregular seas a ship will experience slowly varying surge, sway, and yaw motions with non-zero means in addition to motion with frequency components equal to the frequency of encounter of the individual wave components . . . the drift and slowly varying motions are caused by wave excitation which is of higher order according to the conventional formulation of ship motion."

Thus leeway angle in oblique seas, as well as added resistance at all headings, requires a more advanced second-order theory. He stated, "It should be recognized that the motions resulting from second order slowly-varying excitation can be determined from equations of motion which are otherwise linear because the motions may be assumed to be linear even though the excitation is non-linear." Newman (1974) has shown, that the slowly varying exciting forces and moments in irregular seas, which are caused by the interaction between the different frequency components, can in some cases be approximated by the steady-state forces in regular waves. In other cases a completely non-linear solution may be required, and research continues on the subject.

In quartering seas, the wave-encounter frequencies are much lower and good steering is particularly important. Theoretical treatment of this case requires the inclusion of at least coupled yaw and sway equa-

tions, for sway with forward speed induces a lateral force and yawing moment. Rydill (1959) has made such a study and evaluated the effectiveness in irregular quartering seas of various rudder-control parameters in the automatic steering system—heading, rate of change of heading, and integral of heading change. Korvin-Kroukovsky has pointed out, however, that an important factor not included in Rydill's treatment is the effect of other modes of motion on the coefficients in the equations of yaw-sway. Pitching in particular has a large cyclical effect on lateral coefficients, as the underwater profile is continually changing as bow and stern pitch in and out of the waves. This effect is not allowed for in a linear theory.

At very low encounter frequencies, i.e., when the wave and ship speeds are nearly equal, the danger of loss of control and broaching arises. Here the pressures may actually turn the ship broadside to the waves, and excessive rolling or structural damage, or even the capsizing of small vessels, may result. This phenomenon was investigated as a quasi-static phenomenon by Davidson (1948) and later by Grim (1963), who concluded that nonlinear surging, as well as swaying and yawing, plays an important part. He found that broaching is more probable for a ship that is unstable on course in calm water than for one that is stable.

The theoretical approach of Paulling, et al (1974), also Chou, Oakley, Paulling, et al (1974) is particularly promising. Quoting from Salvesen (1978b), "J. R. Paulling has worked for several years on the nonlinear problem of large-amplitude ship motions in following and quartering waves. With the assistance of some of his students, he has developed a time-domain numerical simulation technique . . . which has been used to predict even the very nonlinear phenomena of capsizing. In this method the forces due to body-generated waves (i.e., added mass, damping, and diffraction) are assumed to be small due to the low encounter frequency and therefore are estimated very crudely; the hydrostatic forces are assumed to dominate the problem and are computed to a high order of accuracy for the actual instantaneous submerged hull shape. The good agreement between computational and experimental results shown seems to indicate that this time-

domain numerical method may not only be a useful tool for predicting capsizing but it may also be useful for the general dynamical problem of ship motions and course-keeping at low encounter frequencies." Work in Japan was also reported in the *Proceedings of Stability '81* and subsequent conferences.

**5.6 Added resistance.** The increase in required power resulting from ship motions in heavy seas arises from the combined effect of several factors:

- (a) *Added resistance caused by*
  - Direct wind and wave action.
  - Indirect effect of waves associated with ship motions (all six components).
  - Rudder action.
- (b) *Reduced propulsive efficiency caused by*
  - Increased propeller loading.
  - Propeller racing or air drawing.
  - Unsteady propeller effects.
  - Reduced hull efficiency.

Added resistance will be discussed here; factors involving propulsive efficiency are discussed in Section 5.7. The resistance caused by wind is discussed in Chapter V, Vol. II.

When a ship is subjected to pitching and heaving, the effect of the motions on resistance may be considerable. Havelock (1945) first investigated this problem, and more recently Maruo (1957) developed an advanced theory.

Vossers (1962) summarized this and other work by explaining that the added resistance in head seas may be considered to be made up of three components:

- (a) One corresponding to that experienced by a ship forced to oscillate in calm water, generating damping waves that dissipate energy.
- (b) Another caused by the phase shift between wave excitation and ship motions, analogous to the power loss in an alternating-current circuit associated with phase shift between voltage and current.
- (c) One resulting from the reflection and refraction of oncoming waves by the ship.

Maruo (1957) reached the following conclusions, which seem valid for head seas even though his equations have not been fully substantiated for general use:

- (a) The excess resistance is independent of the still water resistance.
- (b) The additional resistance is proportional to the square of the wave height.
- (c) The pitching motion has a dominating effect upon the resistance increase.
- (d) The direct effect of the reflection of sea waves is comparatively small.
- (e) The maximum increase of resistance occurs at a slightly higher speed than that for pitch synchronism, if the natural pitching period is longer than the natural heaving period.

A comparatively simple theoretical approach by Gerritsma and Beukelman (1972) considered the added re-

sistance to be primarily the result of the damping waves radiated from the oscillating ship's hull. The method is simpler to use than other methods, but is not applicable to the case of the relatively small added resistance due to waves that are too short to cause appreciable ship motions. Model tests by Strom-Tejsen, et al (1973) on Series 60 models (0.60 and 0.70 block coefficients) and a destroyer hull showed better agreement with Gerritsma and Beukelman (1972) than with other theories investigated (Maruo, 1957) and (Joosen, 1966).

Equating added resistance to energy radiated by the pitching and heaving ship, Gerritsma and Beukelman (1972) arrived at the simple relation for a ship in regular head seas,

$$\langle \delta R \rangle = (\pi / L_w \omega_e) \int b(x) |\dot{\xi}_R|^2(x) dx \quad (221)$$

where  $\dot{\xi}$  is the scalar amplitude of relative vertical velocity at any section between ship and wave surface as a function of  $x$  and  $b(x)$  is the sectional value of total damping coefficient. Using the notation of Section 3,

$$b(x) = b_{33}(x) - U_0 (d a_{33}(x) / dx) \quad (222)$$

where  $a_{33}(x)$  and  $b_{33}(x)$  are sectional heave virtual mass and damping coefficients, respectively. The second term involving  $U_0$ , the ship forward speed, is what Korvin-Kroukovsky, et al (1957) referred to as *dynamic damping*.

Assuming  $a_{33}$  goes to zero at the ends of the ship, after partial differentiation and substitution, the mean added resistance at  $U_0$  and  $\omega_e$  becomes

$$\langle \delta R \rangle = (\pi / L_w \omega_e) \times \int [b_{33}(x) |\dot{\xi}_R| + 2U_0 a_{33}(x) d|\dot{\xi}_R| / dx] |\dot{\xi}_R| dx \quad (223)$$

Since  $|\dot{\xi}|$  represents the amplitude of *relative velocity*, it must be calculated by combining the effects of pitch, heave and wave elevation, considering their phase relations, as discussed in Section 5.2. A dynamic factor is also introduced and applied to the encountered wave height to correct for refraction effects resulting from the distortion of the incident waves by the presence of the ship.

Salvesen (1978a) has presented another theory in which second-order effects are expressed as a product of first-order terms that are all computed by programs presently in use for predicting linear heave and pitch motions. Furthermore, the theory applies to oblique waves as well as head seas. Comparisons were made between theory and experiment in head seas for Series 60 hulls ( $C_B = 0.60, 0.70, 0.80$ ) for a destroyer at  $Fn = 0.25$  and  $0.35$  and for a high-speed, bulbous-bow form at  $Fn = 0.20 - 0.50$ . In a few cases the new

theory was not quite as good as that of Gerritsma/Beukelman (1972) (destroyer hull at low speed), but in other cases it was much better (fine Series 60 models).

Others contributing to the subject of added resistance in waves have been Vossers (1961), Joosen (1966), Newman (1967), Lee and Newman (1971), Lin and Reed (1976), Dalzell and Kim (1976), and Ankudinov (1972).

The most significant aspect of all theories is that, in regular waves of any particular length, the added resistance is proportional to the square of wave height. This is highly significant, for it means that the principle of superposition can be applied to added resistance in irregular waves, as well as to ship motions. The superposition principle for the mean added resistance (or drift force or moment) was first noted without elaboration by Maruo (1957). Early experimental validation was carried out by Kawashima, et al (1959) and Gerritsma, et al (1961). Later Hasselmann (1966) and Vasilopoulos (1966) pointed out that the basic result could be explained in terms of the theory of quadratic, non-linear systems. Though this latter theory has been used to develop approaches for other statistics (Dalzell, 1976) (Pinkster, 1980), we will concentrate upon the

estimator for the mean value since it is of primary practical interest.

The usual estimator for the mean value of added resistance,  $\langle \delta R_w \rangle$ , or drift force, in irregular seas takes the form

$$\langle \delta R_w \rangle = 2 \int [\delta R(\omega_e) / \bar{\zeta}^2] S_{\zeta}(\omega_e) d\omega_e \quad (224)$$

This estimator has a strong, but entirely coincidental, resemblance to that for the variance of a linear response (Section 4). The mean value on the left-hand side is a statistical mean, conceptually the result of averaging the fluctuations in added resistance or drift force over a very long time under statistically stationary conditions. The factor  $[\delta R(\omega_e) / \bar{\zeta}^2]$  in the integrand is the normalized mean value of added resistance in regular waves of encounter frequency  $\omega_e$  and scalar amplitude  $\bar{\zeta}$ . (Head, bow or beam seas are assumed if the ship is at speed). This added resistance or *drift force* operator is sometimes called an RAO, but it is to be noted that the normalization is by the square rather than the first power of wave amplitude, as in the linear case, and the entire quantity is not squared in the integral. The factor  $S_{\zeta}(\omega_e)$  in the integrand is the encountered variance spectrum of wave elevation defined, as in Section 4, so that the area over positive

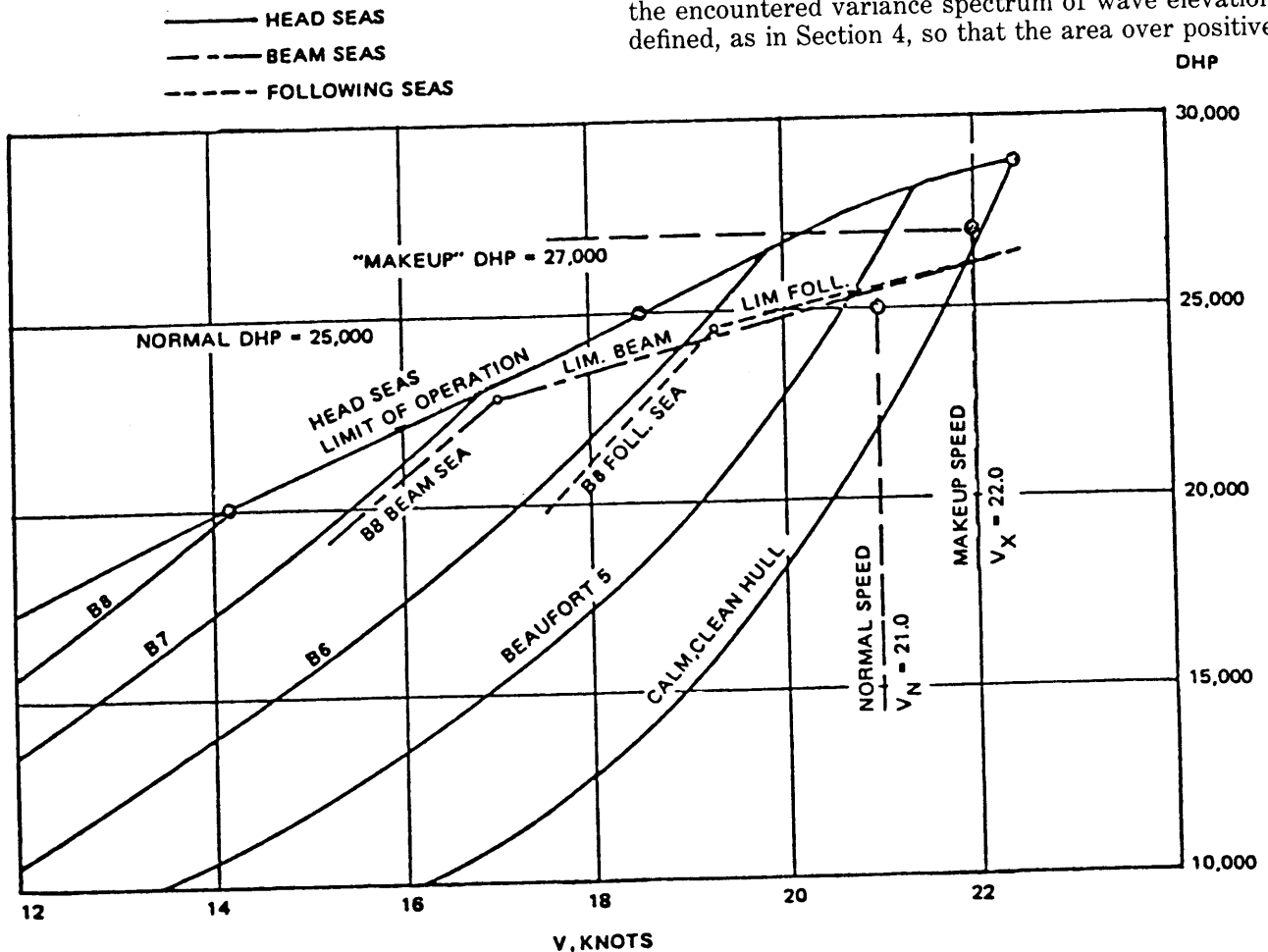


Fig. 88 Service performance of *Dart Europe* in full load condition (Aertssen and van Sluijs, 1972)

frequency is equal to the variance. The leading factor of 2 falls out of the derivation for the statistical mean, and is not to be confused with the various multipliers for significant amplitudes noted previously. If the mean value has units of force  $F$ , and the wave spectrum has units of  $(L^2 \times T)$  (where  $T$  is time), the added resistance operator  $[\delta R(\omega_e)/\xi^2]$  must have units of  $F/L^2$ , and accordingly the integrand must have units of  $(F \times T)$ , which are not those of a variance spectrum. While the integrand can be, and often is, called a *spectrum* of added resistance or drift force, it is not a variance spectrum and cannot be interpreted as such.

Hence, it is possible to compute the added resistance in different representative sea conditions at various speeds and prepare rough-sea resistance curves for each condition. Furthermore, Gerritsma, et al (1961) have found that, as shown in the next subsection, added thrust and torque can be estimated in the same way.

Rolling presumably increases resistance, particularly when bilge keels are fitted, although little quantitative data are available. Anti-rolling devices may be expected to have a net favorable effect on powering, particularly if they are internal types that do not have their own drag.

Yawing and swaying in oblique seas, with the related rudder action, also increase resistance, but this effect is relatively minor. A more important aspect is the leeway angle that is experienced in bow seas, which, as noted in the preceding sub-section, give rise to an induced drag of appreciable magnitude.

An important consideration, especially for ship operation, is resistance at oblique headings to waves, since it is often desirable to compare a change of course with a speed reduction. Furthermore, to obtain accurate calculations of added resistance in short-crested seas, the effect of different directional wave components is needed. Some experimental work along this line has been done, as for example a study by Fujii and Takahashi (1975) on resistance increase in oblique seas. Such oblique wave tests require rather complex instrumentation, as discussed in the Proceedings of ITTC '78. The added resistance, as well as the sideways drift force, was derived theoretically by N. Salvesen (1974) (1978), as well as by Maruo (1963).

**5.7 Powering in Waves.** Fig. 88, derived from Aertssen and van Sluijs (1972), gives a broad overall picture obtained from service records of speed-power relationships in rough seas for a large containership. It shows a series of average power curves corresponding to different degrees of sea severity. The limit lines indicate the upper limits of attainable speed (based on wet decks, slamming, etc.) that provide cut-off points on each power curve. The plot also shows the effect of ship's heading to the waves.

Two basic approaches have been used for estimation of power requirements in rough seas:

(a) Direct self-propelled testing in waves, some-

times in irregular waves but usually in regular waves, with calculation of power in irregular waves by superposition.

(b) Measurement or calculation of added resistance, estimation of propulsion factors and calculation of power and rate of rotation in waves, using these values.

For many years some model basins have made use of self-propelled model tests in regular waves for limited comparative purposes (for example, Kempf, 1934). Such tests repeated for many different conditions can provide an indication of the effect of speed, heading, and wavelength on added power requirements in regular waves, as shown in Fig. 89 (Vossers and Swaan, 1960). (Added power in quartering and following seas was found to be insignificant).

Of course, power is not usually measured directly in self-propelled model tests, but is calculated from measured mean torque and rate of rotation, since  $P_D = 2\pi Qn$ , where  $P_D$  is in kW if  $Q$  is in kNm and  $n$  is in RPS. It is customary to carry out tests in regular waves at model self-propulsion point and to maintain constant shaft rotation throughout each test run in waves, but for accurate evaluation of performance it is necessary to take account of the response of the power plant itself. Reciprocating steam engines and diesel engines produce essentially constant torque, so that as RPM is reduced by added resistance, the power falls off. Geared-turbine and electric drive, on the other hand, produce essentially constant power as RPM is reduced. Hence, the nature of the power plant has a great deal to do with the power and speed that can be maintained. A more satisfactory approach than constant-rotation testing was described by Nakamura and Fujii (1977). A speed control was built that enables the engine characteristics to be simulated during model tests, i.e., constant RPM, constant torque or constant power. Results are presented of tests on a containership model in regular and irregular head seas in which speed reduction was determined under either constant torque (decreasing power) or constant RPM (increasing power). The experimental approach is recommended as the most direct way to obtain the data needed to evaluate attainable sea speed under different irregular sea conditions.

The report of the ITTC Seakeeping Committee (1978) discusses the relative merits of the above direct power measurements in waves and the so-called thrust method, which uses thrust increase measured on a self-propelled model in waves together with propulsion factors from overload tests in calm water. No conclusion could be reached other than a recommendation that work be continued and no significant changes have been made in subsequent conferences. A survey of alternative test methods was given by Day, Reed, and Lin (1977) along with a description of the technique then in use at DTRC.

The second method for determining power required

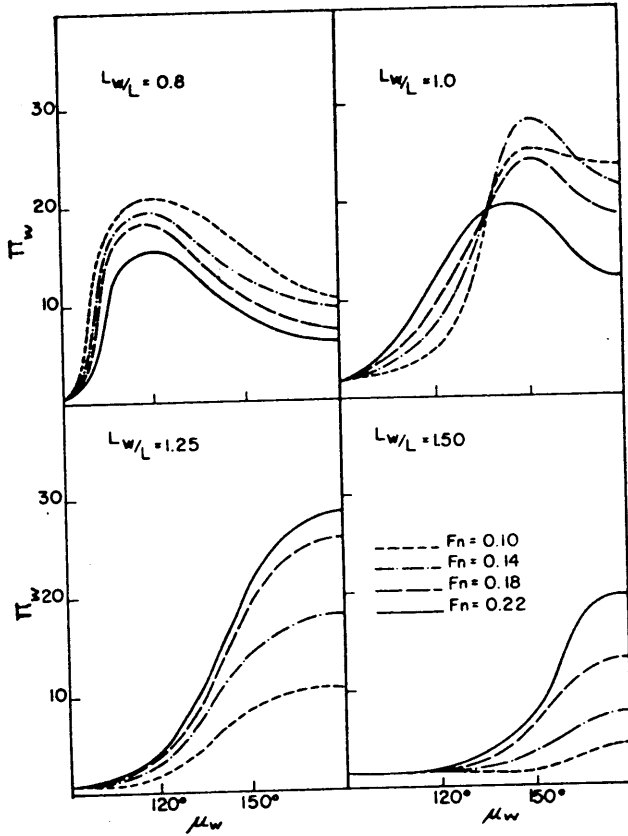


Fig. 89 Power increase in waves for a Victory type ship model as a function of wave length, ship heading, and Froude No. (Vossers and Swaan, 1960)

in a seaway—a direct calculation procedure without model tests in waves—is the ultimate goal. This involves first the calculation of added resistance due to waves (Section 5.6) and wind resistance (Chapter V, Vol II). But added resistance model tests can be used. Then it is necessary to estimate the propulsion factors in waves, i.e., wake, thrust deduction and relative rotative efficiency. Gerritsma (1976) states that, “Experiments by Goeman, who used a forced oscillating ship model with a propeller running at constant speed, have shown that the influence of frequency of motion on the mean thrust and power is very small and can be neglected for practical purposes, when the propeller does not suffer from air suction. Thus for the sustained sea speed calculation only the decrease of efficiency due to the higher loading is of interest, provided that extreme conditions are excluded.” However, recent open-water propeller tests at the University of Michigan yielded a 5 to 10 percent change in  $K_T$  and  $K_a$ . Finally propeller characteristic curves are used to determine propeller efficiency under the overload condition.

However, Murdey (1979) says that it is usually assumed that all of the above propulsion factors are “the same as in calm water with the propeller loading the same as the average loading in waves.” Although this

assumption has been used satisfactorily to provide engineering solutions (Journée, 1976), there is evidence (Nakamura and Naito, 1977) that the propulsion factors in waves are not the same as in calm water. These differences are most marked for models of ships tested at ballast drafts and therefore may be due to air drawing. More study of propulsion factors is clearly needed. Nevertheless, assuming that propulsion factors can be determined by overload self-propelled tests in calm water, the added power in regular wave trains can be approximated.

Coming to the problem of added power in irregular waves, we find that knowing the added torque, rate of rotation and power in regular waves, obtained either by model tests or calculations, it is possible to determine mean values of these quantities in irregular waves. They are determined for any specific wave spectrum in the same manner as that used for added resistance (Section 5.6).

Fig. 90 shows graphically a typical calculation of added power for two ships of different sizes in non-dimensional form. The influence of spectrum shape is clearly presented. The log-slope form of plotting was used in this figure, with an added power operator, normalized by the square of the scalar wave amplitude, as given by

$$\Pi'_w / \left( \frac{\omega^2}{g} \bar{\xi} \right)^2$$

where  $\Pi'_w$  is a non-dimensional coefficient of added power,  $\delta P$ , derived from one given by Gerritsma, et al (1961),

$$\Pi'_w = \delta P / \rho g B^2 L V \quad (225)$$

Hence, with  $\omega^2/g = 2\pi/L_w$ , the scalar operator's

$$\delta P L_w^2 / 4\pi^2 \rho g B^2 L V \bar{\xi}^2 \quad (226)$$

But the common (dimensional) plot, on the basis of  $\omega$ , is equally suitable. The added power operator is then of the form,

$$\delta P / \bar{\xi}^2$$

Mean added power in irregular long-crested head seas is, in form similar to Equation (224) for mean added resistance,

$$\langle \delta P_D \rangle = 2 \int [\delta P(\omega_e) / \bar{\xi}^2] S_\zeta(\omega_e) d\omega_e \quad (227)$$

Thus it is clear that systematic self-propelled model tests or calculations for different speeds and headings (head and bow seas) make it possible to predict rough curves of sea speed vs. power for various representative ocean wave spectra similar to Aertssen's curves, Fig. 88. These curves can be of great value in estimating the maximum required power in service, or service power factor, for a new ship design as discussed in Section 8.

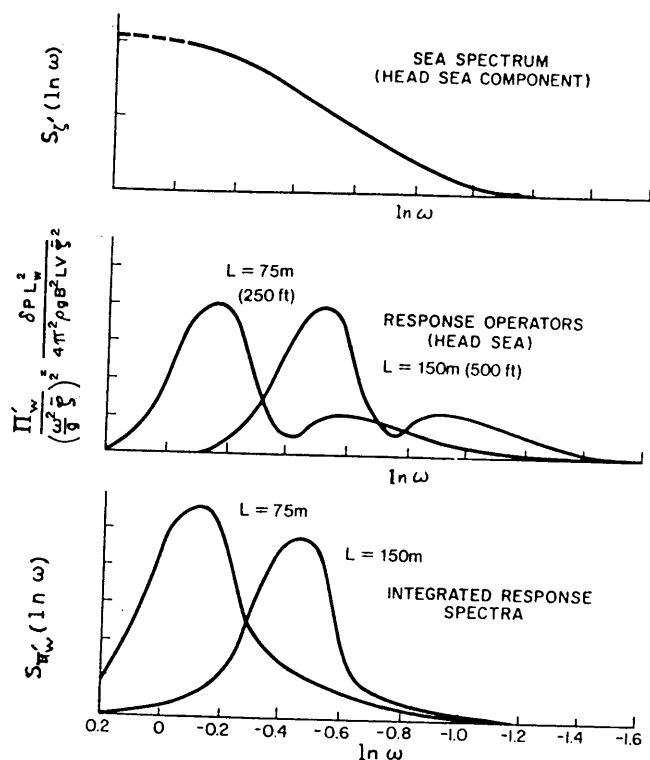


Fig. 90 Prediction of added power in irregular waves for Series 60, 0.60 block ships at  $FN = 0.15$

### 5.8 Wave loads.

(a) *General.* Although wave loads enter implicitly into the calculation of ship motions, they are considered here under the heading of derived responses because, in order to determine the loads at a particular instant of time, a solution to the ship motions must first be obtained.

There are three different levels at which wave loads may be needed for structural design purposes:

1. Instantaneous local hydrodynamic pressures on the surface of the hull as a result of ship motions and ship-wave interactions. These pressures may be needed over the entire hull surface or only some portion of it.
2. Integrated instantaneous pressures yielding the longitudinal and torsional bending moments and shear force at midships or other stations.
3. Impulsive pressures on local areas of the hull (flat bottom, flare, sponson, or stern) which can cause vibratory hull response (slamming, whipping, springing). See Section 5.4 and Chapter IV, Vol I.

(b) *Local Pressures.* The introduction of finite element structural analysis techniques has given impetus to the development of methods of calculating the distribution of instantaneous hydrodynamic pressures over individual sections and hence over the entire surface of a hull oscillating in waves. It was shown in Section 3 that the calculation of ship motions requires

the determination of hydrostatic and hydrodynamic pressures over the surface of the hull. Hence, there is no basically difficult problem in determining these pressures at a particular instant in time, with the ship in any desired position relative to an encountered regular wave.

Hoffman (1966) and Tasai (1966) simultaneously, but separately, published papers showing the methods to compute the wave-induced pressures on the hull surface of a ship heaving and pitching in regular longitudinal waves. Hoffman also measured the pressure distribution on a T-2 tanker model, and found that the experimental results had good agreement with theoretical calculations.

(c) *Wave Bending Moments.* The ship motion theory of Section 3 can be extended to permit the calculation of wave-induced shearing forces and longitudinal bending moments on the hull girder. First it is necessary to solve the equations of motion for the motion amplitudes. Then one can evaluate the incremental vertical forces (in excess of or less than the still-water buoyant force) acting at any instant of time along the length of the ship. The shear and bending moment in regular waves were shown to be the result of integrating vertical hydrodynamic pressures and inertia (D'Alembert) forces over the ship length at a fixed time (Jacobs, 1958). The work explained experimental observations of the reduction in dynamic wave bending moments on the basis of two factors: The so-called *Smith effect*, which accounts for the pressure reduction in a wave crest and increase in a trough resulting from the orbital motion of wave particles, and a second effect of comparable magnitude resulting from ship-wave interaction (Salvesen, et al 1970).

The study of longitudinal wave-induced shear and bending moments in irregular seas according to the linear-random theory (assuming bending moment amplitude proportional to wave amplitude) has had important consequences in the strength standards for large ships, as discussed in Chapter IV, Vol I. Bending moment RAO's in terms of scalar moment/unit wave amplitude tend toward zero for both very low and very high frequencies. They often are "double humped," i.e., one peak corresponding to a motions resonance, and another to the wavelength that produces the greatest re-distribution of buoyancy (Moor, 1966). Prediction of statistical parameters according to methods illustrated in Section 4.1 is one of the important steps in calculating short-term magnitudes and in the synthesis of long-term trends for design purposes.

A revealing early study of bending moments used the log-slope form of presentation to show clearly the effect of size alone on ships in the same seaway. To carry out the prediction of bending moments in irregular waves in this way, wave bending moment may in regular waves be expressed in nondimensional form by dividing by maximum wave slope, giving a bending moment operator,

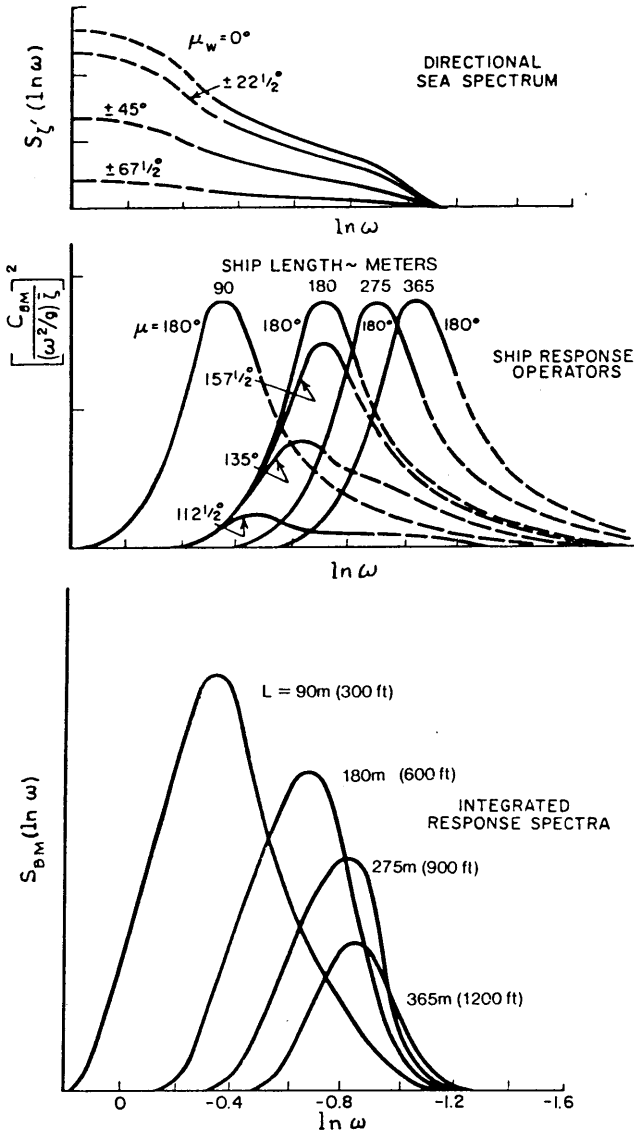


Fig. 91 Prediction of bending moments for Series 60 Ships of various lengths in a severe short-crested head sea

$$\left| \frac{C_{BM}}{(\omega^2/g) \zeta} \right|$$

where  $C_{BM}$  is a nondimensional bending moment coefficient,

Fig. 91 summarizes graphically the calculation of wave bending moments in a severe irregular short-crested head sea for a family of geometrically similar ships of 0.80 block coefficient. From the bending moment spectra at the bottom of the figure one can compute the average short-term bending moments for ships of all lengths or the highest expected bending moments in 10,000 cycles, for example. However, it should be emphasized that trends here apply only to geometrically similar ships with similar weight distribution. Methods of taking into account many different

sea conditions to obtain long-term probability trends are discussed in Chapter IV, Vol. I.

(d) *Springing*. An important effect of sea waves on some ships is the excitation of random hull vibration that may continue for extended periods of time. This phenomenon, known as *springing*, has been noticed particularly in Great Lakes bulk carriers (Matthews, 1967), but it has also been reported on large ocean-going ships of full form (Goodman, 1971). The springing excitation and response can be treated as stochastic processes that can be handled by the techniques discussed in Section 4. However, it has been shown by Kumai (1972) and Troesch (1984b) that longer waves in the spectrum can also excite the hull vibration. This introduces non-linear aspects that are important to consider here.

Experiments in waves were carried out by Troesch (1984a) on a model jointed amidships, to measure both wave excitation and springing response. He found that if the incident wave amplitude is given as  $\zeta(t) = \zeta \cos(\omega_e t)$ , then "there is a measurable springing excitation at  $2\omega_e$  and, sometimes  $3\omega_e$ . Here  $\omega_e$  is the encounter frequency and  $\zeta$  is the incident wave amplitude. Should  $2\omega_e$  or  $3\omega_e$  equal  $\omega_n$ , the natural frequency of the hull, there will be a large increase in the springing response. This non-linear response is quadratic in wave amplitude. In other words, if  $\zeta$  doubles, then the response increases by a factor of four." Furthermore, wave components at one frequency will interact with components at other frequencies. A good description of the theory is given by Longuet-Higgins (1963), who said, "The implication for ship springing is that, in addition to the long-wave excitation resulting from  $2\omega_e$  and  $3\omega_e$ , there will also be long-wave excitation at  $\omega_n$  from  $\omega_i + \omega_j = \omega_n$ , where  $\omega_i$  and  $\omega_j$  are frequencies of first-order wave components."

Summarizing, the response at  $\omega_n$  is the result of the following sources of excitation:

1. Waves with a frequency of  $\omega_n$ . (This is the linear case).
2. Waves with a frequency of  $\omega_1$ , where  $2\omega_1 = \omega_n$ . (This is the non-linear excitation due to harmonics of long waves).
3. Waves with encounter frequencies of  $\omega_i$  and  $\omega_j$  where  $\omega_i + \omega_j = \omega_n$ . (This is also a non-linear excitation caused by the interaction of two different wave components).

Jensen and Pedersen (1981) give the total bending moment response as follows:

$$m(x, t) = m^{(1)}(x, t) + m^{(2)}(x, t) + \dots \quad (228)$$

where  $m^{(1)}(x, t)$  is the linear moment due to wave excitation as previously described in 1, and  $m^{(2)}(x, t)$  is the non-linear moment due to wave excitation described by 2. and 3. They next show how a spectrum of bending moment can be calculated if the spectrum of the incident wave is known and if the bending moment response amplitude operator (RAO) is given or

can be determined. The RAO is the bending moment due to waves of unit amplitude and may include the effects of non-linearities, which requires iterative procedures to be followed. The bending moment spectrum would then include both linear and non-linear parts.

Troesch (1984a) determined springing excitation experimentally for a Great Lakes bulk carrier, which showed an oscillatory character when plotted against encounter frequency. (Peaks correspond to wave lengths such that forces at bow and stern reinforce one another). The complete solution to the springing problem requires consideration of the hull structural properties as well as the hydrodynamic excitation (Chapter IV, Vol. I).

(e) *Forces due to ship motions.* The local forces acting upon parts of a vessel subject to motions in waves consist primarily of inertial reactions (*d'Alembert forces*) which depend on the accelerations discussed in Section 5.1. In addition, angular motions produce changes in the direction of the gravity forces, which affect the components along the three ship axes. In general, determining these forces for a ship in regular waves permits statistical estimates to be made of the local forces in irregular seas according to the spectral method. Before considering these, however, it is important to note that the time-honored deterministic approach for a ship subject only to rolling in regular beam seas can provide useful approximation for some purposes and is thus worth repeating at this point. All parts of a rolling ship are acted upon by two inertial reactions (*d'Alembert forces*) in addition to gravity; viz., a centrifugal force and a tangential force. The force of gravity may be resolved into components parallel and perpendicular to the centerline plane of the ship. These components are equal, respectively, to  $w \cos \phi$  and  $w \sin \phi$ , where  $w$  is the weight of the part. See Fig. 92.

The centrifugal force, which acts radially away from the axis of roll, is equal to  $(w/g) \dot{\phi}^2 r$ , where  $\dot{\phi}$  is the angular velocity of the ship and  $r$  is the distance from the axis of roll to the center of gravity of the part under consideration. Since  $\dot{\phi}$  is seldom greater than 0.15 radian per sec, the centrifugal force is usually negligible in magnitude. For example, if  $\dot{\phi}$  is 0.1 radian per sec and  $r$  is 150 ft, the centrifugal force is about 5 percent of  $w$ . If the center of gravity of the part is above the CG of the ship, the centrifugal force opposes the gravity component  $w \cos \phi$  and therefore reduces the force on the supports. Since the static downward force on the supports when the ship is not rolling is  $w$ , the effect of centrifugal force is to reduce this force by a small amount. It should be noted that  $\dot{\phi}$  and consequently the centrifugal force has its maximum value when the rolling ship is upright ( $\phi = 0$ ). The value of  $\dot{\phi}$  when  $\phi$  is zero, is  $\omega \phi_A$  where  $\phi_A$  is the maximum angle of roll in radians. The angular velocity of roll and centrifugal force are zero where  $\phi = \phi_A$ .

The tangential force is an inertial reaction to the

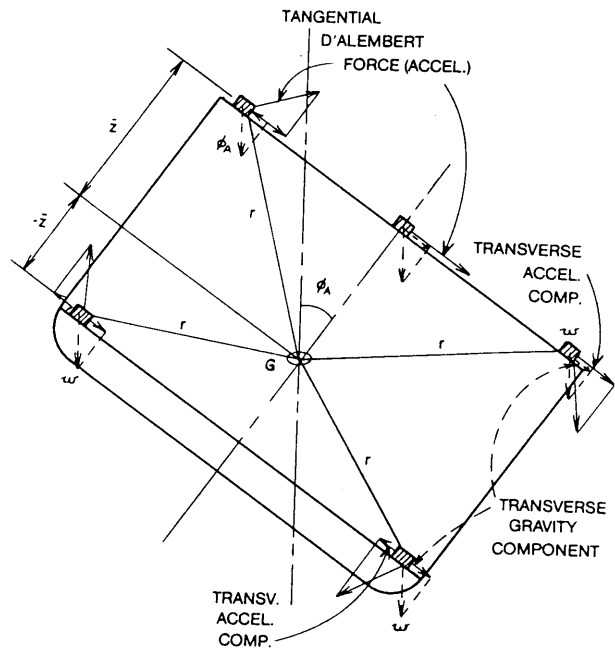


Fig. 92 Forces due to rolling (at maximum angle)

angular acceleration of the ship, which is a maximum when  $\phi = \phi_A$ . Its maximum value then is  $\omega^2 \phi_A$  where  $\phi_A$  is in radians. The linear acceleration acts in a direction normal to the radius that connects the center of gravity of the part to the axis of roll, usually assumed to be through the center of gravity of the ship. The maximum value of the tangential acceleration is  $r \omega^2 \phi_A$  and therefore when  $\phi = \phi_A$  the tangential force is  $(w/g) r \times \omega^2 \phi_A$  (Fig. 92).

In designing foundations or restraining devices the main interest is in the transverse components (parallel to the deck) of the tangential and gravity forces. In general, the transverse component of the tangential force is obtained by substituting  $\bar{z}$  for  $r$ , where  $\bar{z}$  is the height of the part above the CG (assumed rolling center), using ship axes. (Determining the true rolling center is discussed in Section 3.8.) Combining this transverse component with the transverse gravity component,  $w \sin \phi_A$ , gives the total transverse force acting at any point on a rolling ship as

$$(w/g) \bar{z} \omega^2 \phi_A \pm w \sin \phi_A \quad (229)$$

If the center of gravity of the part is above the CG of the ship, this force acts in the same direction as the  $w \sin \phi_A$  component of the force of gravity; if the part is below the CG the reverse is true. This explains the greater likelihood of cargo shifting in the 'tween decks than in the hold.

*A numerical example.* A gun turret mounted on the centerline of a naval vessel has its center of gravity at a height of 9 m above the waterline. The turret's mass is 1000 kg. The period of roll is 15 sec. Calculate the transverse reaction on the turret foundation when



the ship is rolling to a maximum inclination of 30 deg assuming that the axis of roll is at the waterline.

$$\phi_A = \frac{\pi}{180} \times 30 \text{ deg} = \frac{\pi}{6} \text{ radians}$$

Maximum tangential force

$$= 1000 \times \frac{4\pi^2}{(15)^2} \times \frac{\pi}{6} \times 9 = 827 \text{ kN}$$

Transverse component of weight ( $g = 9.81 \text{ m/sec}^2$ )

$$= 1000 \times 9.81 \times 0.5 = 4905 \text{ kN}$$

Maximum transverse reaction

$$= 5732 \text{ kN}$$

In addition to this reaction the foundation bears a transverse moment that is equal to the maximum transverse force times the height of the center of gravity of the turret above the top of the foundation.

The more general approach to the same problem, involving irregular waves and all modes of motion, follows the linear random theory discussed in Section 4, including the estimation of extreme values. The only different aspect is the construction of RAO's or force operators relating force amplitudes to wave amplitudes. The "forces" are the sum of gravity components and inertial reactions dependent upon the mass,  $m$ , of the component under consideration and its acceleration,

$a$ ; i.e.,  $F = ma = \frac{w}{g} a = w \frac{a}{g}$ , where  $w$  is the weight of the element and  $a/g$  is the acceleration in  $g$ 's. Hence, the inertial reaction may be expressed as the product of the weight of the element,  $w$ , and an effective acceleration in  $g$ 's. The usual final scalar force operator is computed in  $g$ 's and may be interpreted as the amplitude of acceleration in  $g$ 's per unit wave amplitude per unit element weight. With an operator so defined the measures of response computed for irregular waves by means of the methods of Section 4 will be in the nature of effective accelerations in  $g$ 's which may then be applied to the weight of the element of interest. However, it is important to bear in mind that what is desired is the effect of the vector sum of a gravitational component and an acceleration in some direction.

The derivation of the RAOs for force per unit weight proceeds as follows. It is first assumed that the basic complex ship motion amplitudes of Sections 3, 4 and 5.2 ( $\bar{\eta}_1 \dots \bar{\eta}_6$ ) are obtained per unit regular wave amplitude,  $\bar{\zeta}$ , as a function of frequency. Thus following Equations (208) and (209), retaining the complex notation, and dividing by  $g$  to express accelerations in  $g$ 's, the complex amplitudes of the three components of acceleration at a point ( $\bar{x}, \bar{y}, \bar{z}$ ) relative to the origin of the ship coordinate system may be written:

$$\text{Longitudinal: } \ddot{\xi}_1/g = -\frac{\omega_e^2}{g} \bar{\xi}_1 =$$

$$-\frac{\omega_e^2}{g} (\bar{\eta}_1 + \bar{z} \bar{\eta}_5 - \bar{y} \bar{\eta}_6)$$

$$\text{Lateral: } \ddot{\xi}_2/g = -\frac{\omega_e^2}{g} \bar{\xi}_2 = \quad (230)$$

$$-\frac{\omega_e^2}{g} (\bar{\eta}_2 + \bar{x} \bar{\eta}_6 - \bar{z} \bar{\eta}_4)$$

$$\text{Vertical: } \ddot{\xi}_3/g = -\frac{\omega_e^2}{g} \bar{\xi}_3 =$$

$$-\frac{\omega_e^2}{g} (\bar{\eta}_3 + \bar{y} \bar{\eta}_4 - \bar{x} \bar{\eta}_5)$$

The first two components above include the tangential acceleration components that determine the inertial reactions due to pitch and roll in the conventional analysis, and the third includes modifications to the heave acceleration due to pitch and roll which, in the end, determines a "virtual weight." The expressions are more complicated than those given in the simpler analysis because they take into account the influence of heave, sway, surge, pitch and yaw accelerations which are neglected in simplified analyses. In a sense, the expression for the lateral acceleration is less complicated than that of the simplified analysis because it is linearized and uses complex notation with a consistent coordinate system. The lateral acceleration associated with the centrifugal force can be neglected in the construction of the RAO's because it is nonlinear, and in any event small.

The gravitational component is accounted for next. In the simpler analysis the lateral component of force on a part of the ship due to gravity and a roll angle  $\phi$  is  $w \sin \phi$ . Linearizing, this becomes  $w\phi$ , or just  $\phi$  in terms of an increase in lateral force per unit weight. The complex amplitude of roll,  $\bar{\eta}_4$ , corresponds to the negative of the complex amplitude of the lateral component of (gravitational force per unit weight) if the axis sense conventions of Section 3 are observed. Observing the axis conventions of Section 3 in a similar fashion, the complex amplitude of pitch ( $\bar{\eta}_5$ ) corresponds to the complex amplitude of the longitudinal component of (gravitational force per unit weight). Finally, the change in the vertical (gravitational force per unit weight) due to roll and pitch, relative to the static  $1g$  case, is of the order of  $(1 - \cos |\bar{\eta}_4| \cos |\bar{\eta}_5|)$ , which is zero to the present linear approximation.

To construct the force-per-unit-weight RAO's the signs of the acceleration components of Equation (230) are changed in accordance with d'Alembert's principle, and added to the complex amplitudes of the gravitational components noted above the absolute values of the results are taken to yield the scalar amplitudes of force per unit weight for the regular wave amplitude,  $\bar{\zeta}$ , assumed in the original motions computations. Dividing these results by the wave amplitude,  $\bar{\zeta}$ , the RAO's for force per unit weight then become:

$$\text{Longitudinal: } \left| \frac{\omega_e^2}{g} (\bar{\eta}_1 + \bar{z} \bar{\eta}_5 - \bar{y} \bar{\eta}_6) + \bar{\eta}_5 \right| / \bar{\zeta}$$

$$\text{Lateral: } \left| \frac{\omega_e^2}{g} (\bar{\eta}_2 + \bar{x} \bar{\eta}_6 - \bar{z} \bar{\eta}_4) - \bar{\eta}_4 \right| / \bar{\zeta}$$

$$\text{Vertical: } \left| \frac{\omega_e^2}{g} (\bar{\eta}_3 + \bar{y} \bar{\eta}_4 - \bar{x} \bar{\eta}_5) \right| / \bar{\zeta}$$

The net result from analyses utilizing these RAO's will be the deviations from the static case (1g vertically and zero laterally and longitudinally). In the spectral approach it is not necessary to assume pitch or roll periods, since these are factored into the definition of the force-per-unit-weight RAO's and the sea spectrum.

For the simple case of rolling alone (at zero speed where  $\omega_e = \omega$ ), assuming sway and yaw to be zero,

the preceding expression for the amplitude of lateral force on a part of the ship per unit weight and unit wave amplitude reduces to

$$\left| -\frac{\omega^2}{g} \bar{z} \bar{\eta}_4 - \bar{\eta}_4 \right| / \bar{\zeta}$$

Then the total lateral force amplitude becomes, in agreement with the simpler case previously given, Equation 229,

$$\bar{\zeta} w \left| -\frac{\omega^2}{g} \bar{z} \bar{\eta}_4 - \bar{\eta}_4 \right| / \bar{\zeta} = w \left[ \frac{\omega^2}{g} \bar{z} \phi_A + \phi_A \right] \quad (231)$$

where  $|\bar{\eta}_4| = \phi_A$ , the amplitude or maximum angle of roll in rad. ( $\phi_A \approx \sin \phi_A$ ) and  $w$  is the weight of the item under consideration ( $w/g$  is its mass).

## Section 6

### Control of Ship Motions<sup>12</sup>

**6.1 General.** The reasons for attempting to control and reduce the motions of a ship are as varied as the types of ships. Excessive motions would interfere with the recreational activities of passengers on a cruise ship. Often more than half of the load of a container ship is stowed above deck where it is subjected to large accelerations due to rolling. In some situations this may cause some internal damage to the contents of the containers; in more severe situations failure of the lashing can occur and containers may be lost overboard. Underdeck cargo in ordinary cargo ships and bulk commodities in colliers, ore ships and grain ships can shift if the motions become too severe. Excessive motions of warships can both seriously degrade the combat readiness of its crew and adversely affect the performance of its weapons systems. Finally, offshore platforms, pipe-laying ships and drill ships require only very small motions to perform many of the individual operations. The amplitude of the motions may be the most important feature in these latter ocean engineering tasks, whereas in some of the other situations mentioned, the velocity or acceleration of the motions may be of principal concern.

The purpose of this section is to concentrate on the *additions*, either internal or external to the hull, that reduce or otherwise improve the motion responses of the hull. It is assumed that the additions are such that their benefit to the motions of the ship outweighs any impact on the ability of the ship to perform its assigned task. It is particularly challenging to obtain large improvements in the motion characteristics of existing

ships that are being rebuilt or modified for some task not anticipated in their original design.

In light of the foregoing discussion, it is appropriate to ask what motions can be sensibly influenced by a small addition to the ship. Let us first consider the unrestored (horizontal) motions of the ship: sway, yaw and surge. These motions exhibit no resonance, and their amplitudes in deep water are never greater than the wave amplitude, or in the case of yaw, never greater than the wave slope. Thus, these motions are rarely a significant problem of themselves. Further, these motions are caused by exciting forces that are comparable to the ship's weight or, in the case of yaw, the product of the weight times the ship length. It is unreasonable to expect that any small addition will be able to produce an effect comparable in magnitude. Only the usual directional control, or steering, is needed, as discussed in Chapter IX.

Motions that have vertical components (heave, pitch and roll) have restoration forces. For these motions, the ship behaves somewhat like a damped spring-mass system. These motions exhibit resonance and respond with amplitudes sometimes greater than the wave slope or, in the case of heave, greater than the wave amplitude. The magnification factor or nondimensional RAO, the ratio of the amplitude of motion in regular waves to the wave amplitude (or amplitude of the wave slope) at the resonant frequency, varies greatly amongst the three motions. The magnification factor for heave for a typical ship is less than 1.3 and is frequently less than 1.0. That for pitch is rarely more than 1.5, but that for roll can be 10 or more for the bare hull, and 7 or more for a ship equipped with bilge keels.

<sup>12</sup> by William C. Webster.

The foregoing serves to illustrate that resonant roll motions in waves are perhaps the most attractive candidate for control. These motions are large enough to be important in most applications. The almost total lack of inherent roll damping means that small additions to this damping can produce large reductions in the response. The possibility of controlling pitch motions is entertained from time to time, but the prospects are certainly not as good as they are for roll. It appears neither feasible nor necessary to attempt to control heave for normal ship forms. The subsequent parts of this section explore methods that have been investigated and used to control motions, with the predominant emphasis on roll motions.

**6.2 Control of Roll.** Since, as described in Section 3.8, the most severe roll motion occurs at resonance (sometimes referred to as synchronous rolling) the best way of reducing it is to increase damping. The most common means of doing so is the installation of bilge keels. If more control of the roll motions is required, the use of special anti-rolling devices may be called for. A multitude of different devices for this purpose have been invented but only a few types are in common usage. In the following discussion these devices are described in general, but special emphasis is placed on the popular devices. The stabilizers can be grouped by general categories, depending on how they achieve the stabilization; i.e., *passive*, *controlled-passive* or *active*.

(a) *Passive Stabilizers.* These devices do not require power or a control system to operate. They belong to two separate sub-categories: those that do not have moving parts and those that do.

The primary devices with no moving parts are bilge keels (which have been discussed in Section 3.8) and sails. Sails are a very effective roll stabilizer for small ships and have been used extensively in fishing boats. The lift on the stabilizing sail changes as the ship rolls and the phasing of these lift forces is such that roll energy is removed from the ship. The size of sail required and complexity associated with rigging the sail are modest for a small boat, but generally prohibitive for large ships.

There are a variety of devices that rely on motion of the stabilizer to interact with and to reduce the roll motions. These stabilizers are passive in the sense that they are unattended and do not rely on special sensors or actuators. Typical stabilizers of this type include passive antiroll tanks and moving-weight stabilizers. Three types of antiroll tanks have been used and sketches of them are shown in Fig. 93, adapted from Bhattacharyya (1978).

The free surface tank shown at the top (a) of this figure is a single, partially-filled tank which typically extends across the full beam of the ship. Its shape and internal baffles allow the liquid in the tank to slosh from side-to-side in response to the roll motions. The phasing of the roll moments acting on the ship as the result of the fluid motion in a well-designed tank are

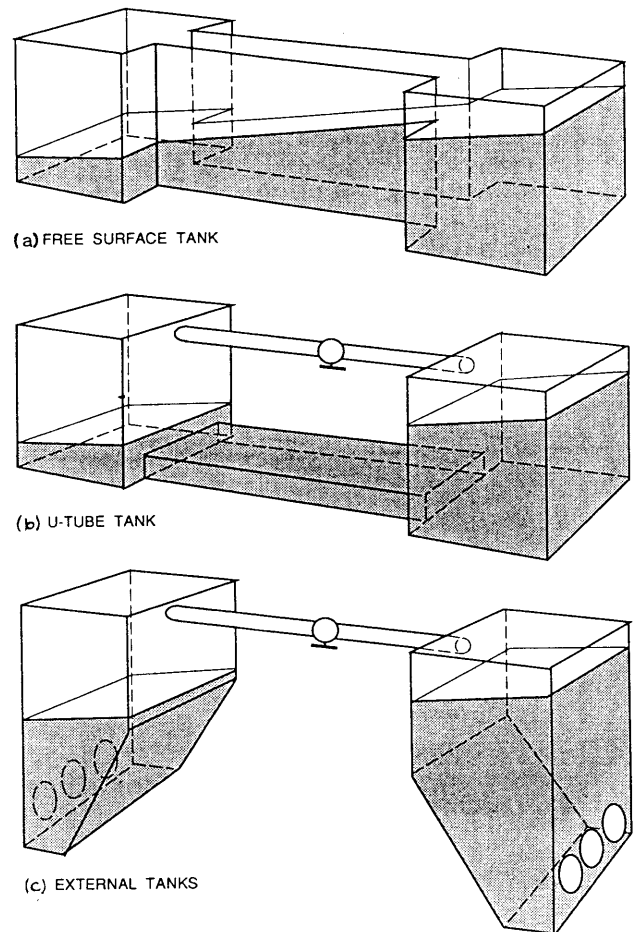


Fig. 93 Different types of passive antiroll stabilizing tanks

such that they reduce the roll motion. This type of tank was first investigated by Froude, but did not receive much attention until the 1950's when it was rediscovered and used in several naval vessels.

A related concept is that of the U-tube antiroll tank, a perspective view of which is shown in the middle (b) of Fig. 93. The use of these tanks was pioneered in Germany by Frahm around the turn of the century and they are often referred to as Frahm tanks. This stabilizer consists of two wing tanks connected on the bottom by a substantial crossover duct. These tanks are also partly filled, and the air spaces above the fluid in each wing are connected by a duct. As in the free surface tanks, when the ship begins to roll, fluid flows from wing tank to wing tank causing a time-varying roll moment on the ship. With careful design this roll moment is of the correct phasing to reduce the roll motions (see Fig. 94). As shown in this figure, both the roll motion and the motion of the fluid in the tank are at a larger amplitude than the wave slope.

Another stabilizer concept introduced by Frahm was the external stabilizer tanks, also shown in Fig. 93. These tanks were used in several ships (including some naval ships) in the early 1900s. In this configuration,

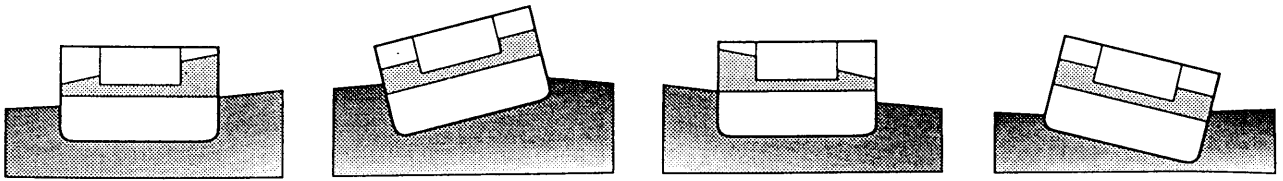


Fig. 94 Motion of the fluid in an antiroll tank

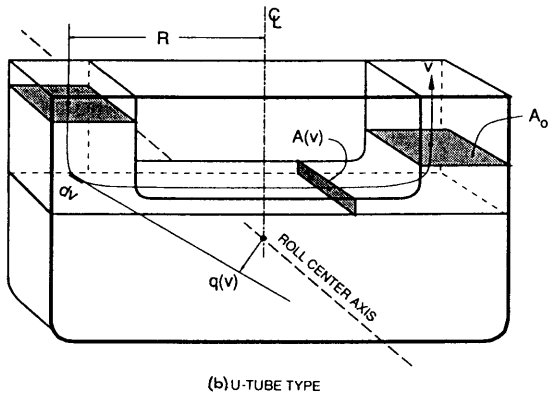
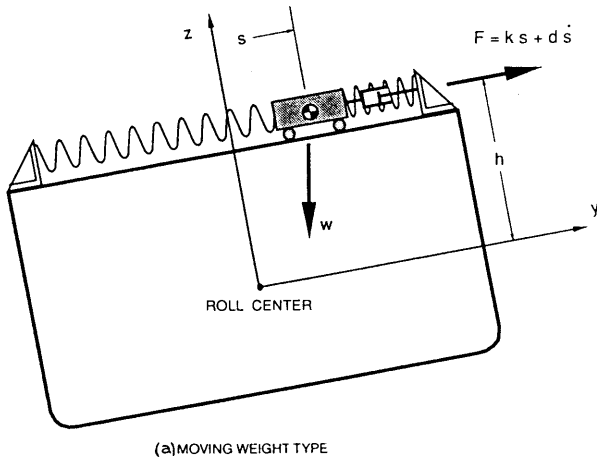


Fig. 95 Definitions of variables used in the analysis of stabilizers

the two wing tanks are not connected to one another except perhaps by an air duct at the top. Water flows in and out of each tank through openings in the hull to the sea. This configuration eliminates the duct filled with water, which exists in either the free-surface tank or the U-tube tank, but has its own set of disadvantages. These include corrosion due to the seawater in the tank, and resistance to forward motion due both to the holes in the hull and the force required to accelerate the seawater outside the ship (which is initially almost at rest) to the speed of the ship as it enters the tank. The horsepower required by this latter drag component (sometimes called momentum drag) increases with the square of the ship speed and can be substantial. More recently, a variation of external tanks have

been used in oil drilling rig applications where forward speed is not a concern. A comparison of different tanks is given by Vugts (1969).

A fourth concept is that of a moving weight stabilizer (see Fig. 95a). In this scheme a large weight is allowed to move athwartships on a track. It is kept near the center of the travel by either a spring (as shown) or a curved track, and it is also restrained by a damping mechanism. These mechanisms produce a force,  $F$ , acting on the moving weight that is given by

$$F = ks + d \dot{s} \quad (232)$$

where  $k$  is the spring constant,  $s$  is the distance of the moving weight from the ship centerline,  $d$  is the damping constant and  $\dot{s}$  is the moving weight's velocity. The motion of the ship leads to other forces on the moving weight which cause it to respond in such a way as to create roll moments that counteract the wave exciting moments. Its action is therefore similar to that of the fluid in the antiroll tanks.

All four of these concepts rely on a common, underlying physics as a basis for operation. Each has a mass that can transfer from one side of the ship to the other, and each has a design feature that restores this mass to amidships when the ship is near upright. The result is that each of these passive stabilizers is a damped mass-spring system that moves in response to all three transverse motions. In a properly designed stabilizer, the roll moments generated by the stabilizer movement will counteract part of the roll moment applied to the ship by the seaway, and will reduce the overall roll motion. None of these stabilizers can eliminate roll motions entirely, since the stabilizer does not move until the ship moves. In concept all of these devices are similar to the classic vibration absorber.

The equations of motion for the ship and stabilizer system for all four devices are of exactly the same form and the design parameters used for each are similar. The equations of motion are too complex to derive here, but details can be found in Vasta, et al (1961) or in Webster (1967). A careful analysis of the resulting coupled roll, sway, yaw and stabilizer system shows that the stabilization performance depends principally on five parameters:

1. *Stabilizer size*,  $\mu = \delta \overline{GM}_T / \overline{GM}_{T0}$ , the loss of metacentric height caused by the stabilizer divided by the metacentric height with the stabilizer weight or liquid frozen in mid-position. Each of these passive

stabilizers has the characteristic that, when the ship has a heel, the weight in the stabilizer moves to cause a moment that increases the heel. In the tank configurations this loss of stability is simply the free surface loss. In moving weight stabilizer,  $\delta \overline{GM}_T$  is given by  $w^2/gk\Delta$ , where  $w$  is the moving weight (mass =  $w/g$ ),  $k$  is the spring constant restoring the weight to the center of its track and  $g\Delta$  is the displacement weight,  $W$ . The parameter  $\mu$  measures the static effect of a motion of the stabilizer on the roll motion. All three tanks shown in Fig. 93 have the same  $\mu$ , even though their other characteristics may be different.

2. *Stabilizer coupling*,  $\sigma_i = \omega_i/\omega_{n4}$ , the ratio of the natural frequency of the stabilizer to the roll natural frequency (also known as *stabilizer tuning factor*, in order to avoid confusion with the *ship tuning factor*, used elsewhere, which is the ratio of encounter frequency to ship roll natural frequency). When the ratio,  $\sigma_i$ , is near unity, the worst motions of the ship (those near the resonant frequency) couple easily into motions of the stabilizer. In practice, it is typical for this ratio to be slightly larger than unity to account for the difference in damping between the ship and the stabilizer. The natural frequency of a U-tube tank system can be estimated by  $\omega_i = \sqrt{2g/S'}$ , where

$$S' = \int_0^L \frac{A_0}{A(v)} dv$$

and where the girth parameter  $v$ , the U-tube free surface area  $A_0$  and cross-section area  $A(v)$  are defined in Fig. 95a. The natural frequency of the other types of stabilizer tanks can be estimated on the basis of an equivalent U-tube (Vasta, et al 1961). The natural frequency of the moving weight is simply  $\sqrt{gk/w}$ .

3. *Nondimensional stabilizer damping*,  $\zeta_i$ , the ratio of the stabilizer's equivalent linear damping to its critical damping. This parameter is comparable to  $\beta^*$  in the ship roll equation; see Section 3.8, Equation (172). Stabilizers are typically moderately damped and the damping is usually quite nonlinear. Values of  $\zeta_i$  of 0.2–0.4 are typical for moderate motions. Therefore, these stabilizers do not exhibit a resonance as marked as the ship in roll. The damping in a tank depends on the details of the shape of the wing tanks and especially of the crossover duct or, in the case of external tanks, on the details of the hull openings. Since the fluid drag associated with flow in this type of complicated geometry is difficult to predict, it is common to construct a reasonably large scale model of the tank to confirm the damping. Analysis of free surface tanks is somewhat more difficult since both the natural frequency and the damping of the tank are sensitive to the water depth.

4. *Stabilizer capacity*,  $\eta_s$ , the maximum angle to which the stabilizer can heel the ship with all of the weight in the stabilizer on one side. For instance, for a U-tube tank,  $\eta_s$  is computed as the static heel angle induced when the fluid inside has moved to one side and completely fills one wing tank. Typical values of capacity are 0.03 to 0.10 rad., corresponding to a capability of the stabilizer to cause a static roll of 2 to 6 deg. A stabilizer loses effectiveness if the effective wave slope is greater than  $\eta_s$ , and in very heavy seas the stabilizer might be only marginally effective.

5. *Stabilizer height parameter*,  $\xi_i$ . This parameter is given either as

$$\xi_i = \frac{h\omega_i^2}{g}$$

for the moving weight stabilizer, where  $h$  is the height of the center of gravity of the moving weight above the roll center, or as  $\xi_i = S''/S'$  for the U-tube tank, where

$$S'' = \int_0^L \frac{q(v)}{R} dv,$$

$S'$  is as before, and where  $R$  and  $q(v)$  are defined in Fig. 95b. Here  $q(v)$  is defined to be negative if the tangent line to the flow path at the point  $v$  is below the roll center axis and to be positive if it is above. The height parameter for the other tank configurations can be determined by analogy to the U-tube configuration.

The roll moments that arise due to the acceleration

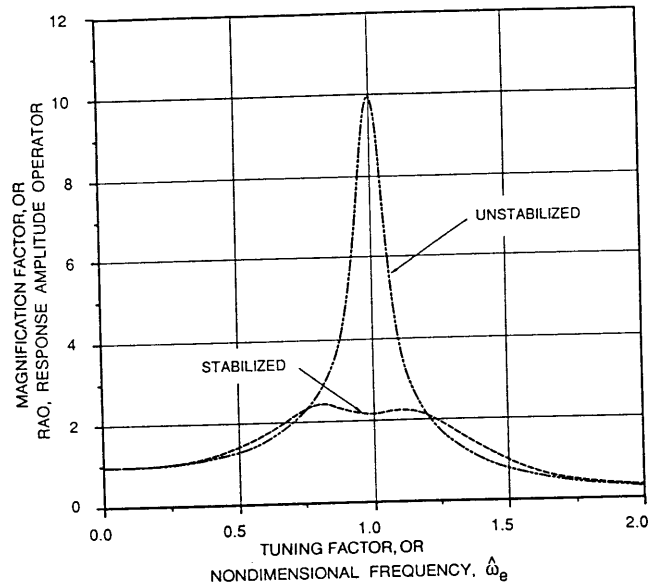


Fig. 96 Comparison of the computed roll response of a typical ship with and without a good passive roll tank

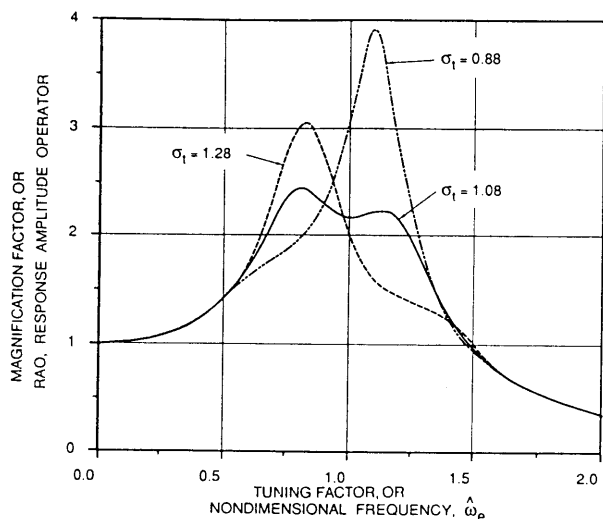


Fig. 97 Effect of variations of stabilizer tuning on roll stabilization

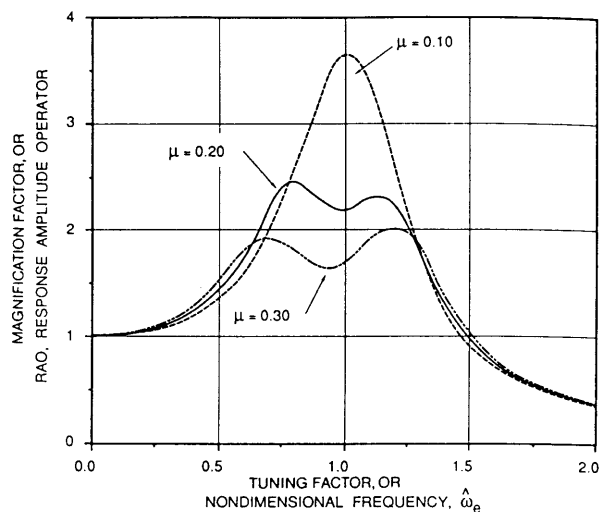


Fig. 98 Effect of variations of stabilizer size on roll stabilization

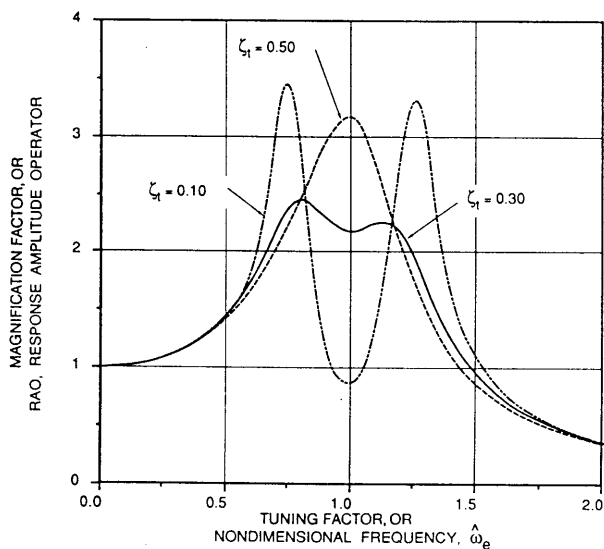


Fig. 99 Effect of variations of stabilizer damping on roll stabilization

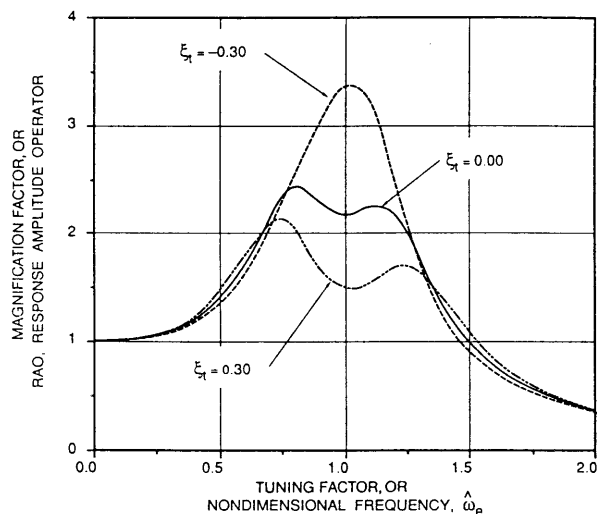


Fig. 100 Effect of variations of stabilizer height on roll stabilization

of the mass of the stabilizer weight or fluid from one side of the ship to the other counteract the static moment of the weight or fluid if the stabilizer is mounted far below the roll center ( $\xi_t < 0$ ), and add if the stabilizer is mounted far above the roll center ( $\xi_t > 0$ ). That is, the higher the stabilizer is located in the ship, the more effective it is. Because of the factor  $\omega_e^2$  in the parameter, stabilizers for ships with high meta-centric stability (high roll resonant frequencies) require stabilizers to be mounted high in the ship if they are to be effective.

The roll magnification factor or RAO (amplitude of roll divided by effective maximum wave slope) is a simple and effective measure to explore the effect of the various stabilizer parameters, when plotted

against non-dimensional frequency,  $\hat{\omega}_e = \omega_e / \omega_{n_4}$  (or tuning factor). The following parameters represent a typical good design of a stabilizer:

$$\begin{aligned} \mu &= 0.20 \\ \sigma_t &= 1.08 \\ \zeta_t &= 0.30 \\ \eta_s &= 0.05 \\ \xi_t &= 0.00 \end{aligned} \quad (233)$$

We first consider motions that are small enough so that the capacity of the tank,  $\eta_s$ , is not a question. Fig. 96 shows a sample calculated magnification factor or RAO for a ship in beam seas with a roll damping ratio of 0.05 (typical for a large ship fitted with bilge keels) with and without a stabilizer defined by the

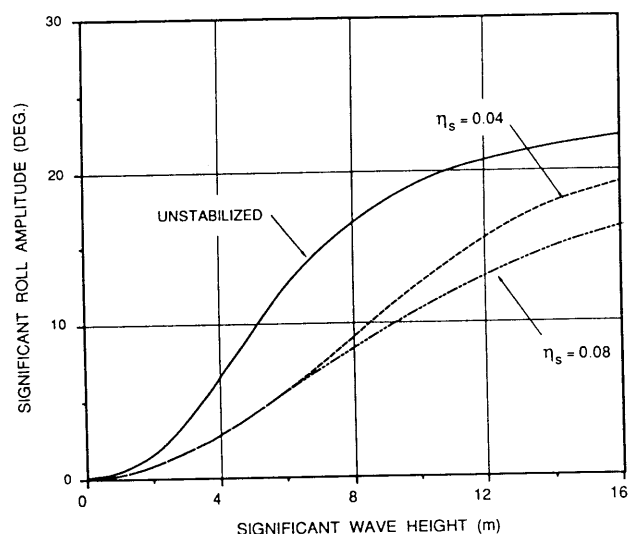


Fig. 101 Effect of stabilizer capacity on roll stabilization in short-crested random seas

parameters given in Equations (233). At very low frequencies both the stabilized and unstabilized ships have an RAO of unity. In other words, in very long waves the ship rolls with an amplitude equal to the effective wave slope and at these frequencies the stabilizer has no motion relative to the ship. The ship alone has a sharp peak at its resonant frequency, and this peak is greatly reduced by the stabilizer. However, for non-dimensional frequencies (tuning factors) below about 0.7 and above 1.25, the RAO's are larger for the ship with the stabilizer. That is, the stabilizer does not improve motions at all frequencies.

It is rare that a ship experiences a seaway that is composed of regular waves of a single frequency. Typical situations involve random seas with component waves of many different frequencies and the effect of the stabilizer over all these frequencies is important. The extremely large roll reductions observed near roll resonance are not realized in a real seaway. In particular, the average roll reduction in a real seaway is typically of the order of 50 percent for a well-designed stabilizer, even though the reduction at resonance is 90 percent or more.

It is interesting to examine typical variations in the calculated beam-seas motions with changes in stabilizer size, tuning, damping, and stabilizer height parameters. Fig. 97 shows the effect on stabilization of changes in the stabilizer tuning,  $\sigma_t$ . One sees that changes in tank tuning factor,  $\sigma_t$ , either above or below the baseline frequency given in Equation (232) lead to significant changes in the shape of the response curve. A stabilizer with a natural frequency much higher than the ship's roll resonance frequency,  $\sigma_t \gg 1$ , is effective only at high frequencies. A similar statement also applied to a tank with a much lower natural frequency.

Fig. 98 shows the effect of changes in stabilizer size,  $\mu$ . Increases in  $\mu$  further reduce the peak of the RAO at resonance, but also increase the response in the low and high-frequency regions where the stabilized ship rolls more than the unstabilized ship. The selection of a  $\mu = 0.2$  represents a typical compromise between these competing effects.

Fig. 99 shows the effect of changes in the stabilizer damping,  $\zeta_t$ . When the damping is much smaller than the baseline damping given in Equation (232) the motions at the original roll resonance becomes small, but two large resonances at frequencies above and below the original resonance appear. If the damping is too high the roll motions are little different from their unstabilized counterparts.

Fig. 100 shows the effect of stabilizer height,  $\xi_t$ . It is clear that stabilizer performance improves with increase in height above the roll center. However, the topside space on board a ship is usually more valuable for other purposes and stabilizers are often placed deep in the ship. This figure shows that if the stabilizer is placed too deep in the ship its performance may be marginal.

When roll motions become larger, the nonlinear roll characteristics and nonlinear tank damping play a more important role. As a result, the stabilization performance in these situations can vary considerably from one ship to another. The most important single parameter governing these differences is the tank capacity,  $\eta_s$ . Fig. 101 shows the variation of the significant roll motions as a function of significant wave height for a typical unstabilized ship, and for the same ship with stabilizers that differ only in their capacity,  $\eta_s$ . The motions are in a short-crested irregular seaway at the worst heading. It is seen that in low and moderate seas the stabilizers are quite effective and do not differ in performance. As the sea state increases the stabilizer with the lowest capacity saturates first and its stabilization is not as good as for the higher-capacity tank. The effects of tank saturation appear at small roll angles when  $\eta_s$  is small and not until larger roll angles when  $\eta_s$  is large. Thus, the capacity parameter must be considered in relation to the mission profile of the ship in which it will be installed.

Selection of the appropriate passive stabilizer for a given application requires consideration of several different factors. Within a rough approximation all four types of passive stabilizers discussed, i.e., moving weight, U-tube, free surface and external tanks, are not grossly different in weight for a given set of design parameters. The moving weight can be much smaller in volume, since the weight can be constructed using steel and even denser materials. However, the size of the weight increases in direct proportion to the ship displacement and safety considerations restrict moving weight stabilizers to small ships. U-tube tanks require somewhat more internal structure for the bulkheads and ducts than do free surface tanks but

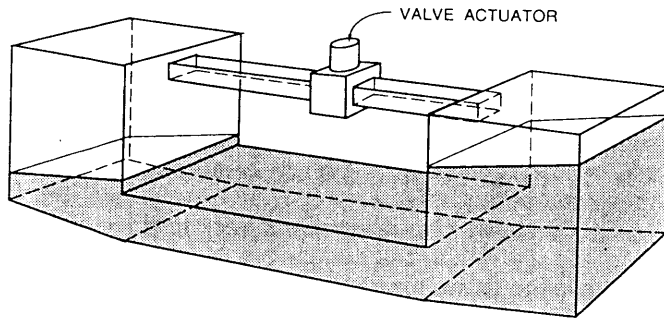


Fig. 102 Schematic of controlled-passive antiroll stabilizing tanks

have the advantage that they do not restrict fore-and-aft passage. That is, the space above and below the water cross-over duct is available for other purposes. Free surface tanks have the advantage that it is possible to vary the tank natural frequency by changes in water level and thus accommodate changes in the ship's metacentric height. It is, however, difficult to measure the water level at sea and it is not easy for the crew to decide the best water level setting for a given situation. External tanks do not restrict fore-and-aft passage inside the ship but have unique corrosion problems and high added resistance.

Several features of all four passive stabilizers require special emphasis:

- These stabilizers cannot eliminate all of the roll motions. Each relies on the ship motions to generate the sloshing in the tanks or the motion of the weight. The principal effect is a significant decrease in the level of roll motions in the neighborhood of roll resonance.
- All passive stabilizers of this type increase the roll motions at frequencies significantly away from the roll resonance. For instance, in seas that are predominantly from the stern, the encounter frequency may be quite low and the ship may actually roll more with the stabilizer in operation.
- Passive stabilizers do not require the ship to have forward way. In fact, passive stabilizers are perhaps the most effective system of roll reduction at zero speed. This is often a critical consideration for drill ships and other ocean engineering vehicles.
- The action of the stabilizer is to eliminate the sharp peak in the roll RAO at resonance. The stabilized RAO curve is more or less flat over a large frequency band. The roll motions of the stabilized ship therefore have a random or unpredictable characteristic similar to that of the seaway. This is in sharp contrast to the unstabilized ship motions which tend to have regular and predictable, although larger, roll motions. The result is that the stabilized ship may be perceived subjectively by the on-board personnel as less comfortable.
- The motion of the passive stabilizer's fluid or weight in high sea states may become so severe that

saturation occurs. The fluid can hit the tank top or the weight can come to the end of its track. In either case the stabilizer loses effectiveness and the ship roll behavior becomes more like the unstabilized ship. Prudence dictates, therefore, that other means of stabilization, particularly bilge keels, also be installed.

• In anti-roll tanks it is common to use fresh water with additives to prevent corrosion. It is possible to use other liquids including fuel oils and ordinary sea water. These latter liquids may require special attention to combat corrosion and flammability dangers.

(b) *Controlled-passive stabilizers.* In the event that the roll stabilization offered by ordinary passive stabilizers (such as described in the previous sub-section) is not sufficient, it may be possible to use a slightly more complex stabilization system known as a controlled-passive roll stabilizer. The concept is to improve the performance of a passive system by adding a sophisticated control system which, although it does not change the basic action of the stabilizer, modifies this action to make it more effective.

A typical stabilizer of this variety is the so-called *controlled-passive* roll tank discussed in Bell & Walker (1966) and sketched in Fig. 102. This tank is similar in shape to the U-tube but the water cross-over is much larger in cross section and the air cross-over duct contains a servo-controlled valve system. Since these valves control only the flow of air, very little power is required for their activation. When the valve is closed, the passage of air from one wing tank to the other is prevented and the motion of the water between the wing tanks is restricted by the resulting compression of the air in the top of each tank. When the valve is open, the air can pass freely and the water can slosh without restriction from wing tank to wing tank.

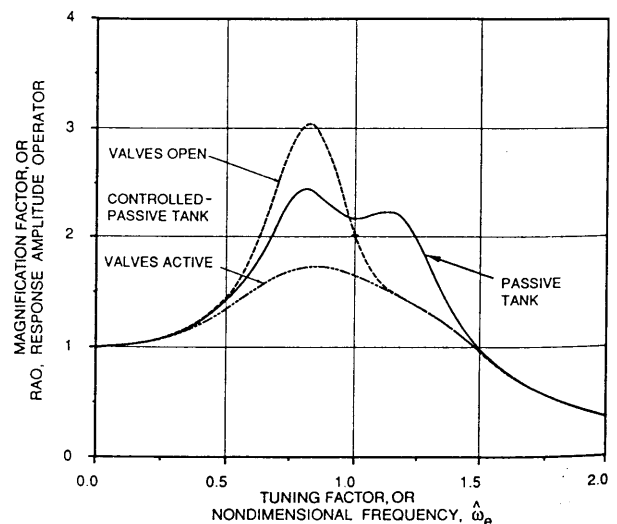


Fig. 103 Comparison of passive and controlled-passive roll stabilizing tanks



The typical controlled-passive roll tank is designed to have a tank tuning factor,  $\sigma_t$ , well above unity. Fig. 103 shows three RAOs: one for a ship stabilized by a good passive tank, one for a ship stabilized with a controlled-passive tank, and one for a ship with the controlled-passive tank but with the valves locked in the open position. The first and third of these curves are duplicates of curves in Fig. 98. As seen in these figures, there is little difference between the controlled-passive tank and the equivalent high-tuning-factor, (i.e., high-natural-frequency) passive tank at frequencies above the roll resonance. Both tanks produce smaller roll motions at these frequencies than either the ship alone or the ship with a well designed passive tank.

At frequencies in the neighborhood of the roll resonance and below the roll resonance, however, the fluid in the high-natural-frequency tank with the valves locked open can slosh from one side of the ship to the other much too fast. The result is the greatly exaggerated low-frequency roll motions which are more severe than either the ship alone, or the ship with a well designed passive tank. The control system prevents this unsatisfactory behavior at low frequencies by closing the valves and slowing the flow whenever it would otherwise lead to large roll motions. The control system thus regulates the phasing of the fluid motion primarily in the low-frequency regime. A well designed controlled-passive tank has superior roll stabilization (as much as a 20-40 percent better) over all frequencies compared to those of a well designed passive tank of the same size,  $\mu$ .

Controlled-passive tanks have several disadvantages, and these have generally prevented their widespread use. First, in order to achieve the high-natural-frequency tank that a simple control system can slow down, a large crossover duct is required. Therefore, a controlled passive tank has a larger weight of fluid for a tank of the same size,  $\mu$ . Second, a controlled-passive tank depends on the operation of both the control system (which normally includes gyros and sophisticated electronics) and the mechanical activation system for the valves. If any of this mechanical equipment fails, the tank is either ineffective (the valves locked closed) or inferior (the valves locked open). Nonetheless, several of these stabilizers have been installed and they appear to have a good operating record.

(d) *Active stabilization.* The border between controlled-passive and active stabilization is not distinct. Active stabilization generally implies that the system requires the use of machinery of significant power and, in order to justify the expense of this equipment, the system is designed to be much more effective in eliminating roll motions than passive systems. Each system consists of two essential parts: a control system to detect motions of the ship and to predict the roll moment that will be applied to the ship by the seaway in the immediate future and a moment generating system

that will apply a roll moment to cancel the predicted moment.

The possible moment-generating systems include: fin stabilization, gyro stabilization and active-tank stabilization. Whereas the control system for each type of stabilization system is similar, the means by which the counteracting roll moment is produced is entirely different. The control system will be discussed first, followed by a more detailed discussion of each of these different physical systems.

1. *Control system.* It is the job of the control system to command the moment-generating system to act in such a way that the roll motions are reduced. It is possible to develop such a control system that ignores the cause of the roll and produces the desired command signal on the basis of measured roll motions and empirically determined constants (known as gains). However, an insight into the capabilities and limitations of an active system can be gained by use of the equations of motion.

For perfect stabilization, the roll moment that the seaway will apply to the ship must be known *in advance* of its actual application, since all of the means of producing counteracting roll moments on the ship have a lag between the time when the commanded moment is received and the time when the roll moment is actually produced. Without constantly measuring the seaway in the neighborhood of the ship, it is clear that the current motions of the ship alone, even if measured perfectly, would at best yield the instantaneous roll moment acting on the ship. However, if the stabilizer has a relatively small lag in its response, then an estimate of the current seaway-induced roll moment is sufficient to produce very good stabilization.

In principle, Equation (171) in Section 3 can be used for this purpose. Its use, however, is complicated by the fact that it is a statement in the frequency domain (as a consequence of the coefficients  $\hat{A}_{44}$  and  $\hat{B}_{44}$  being frequency dependent). Using a mathematical procedure known as convolution, this equation can be transformed so that the required roll moment can be expressed as the sum of a constant times the instantaneous roll acceleration plus an integral over all previous time of the roll acceleration history. In practice, one is principally interested in the roll moments applied to the ship at frequencies in the neighborhood of the roll resonance. In this case, one can approximate Equation (171) by a differential equation,

$$(\hat{I}_{44} + \bar{A}_{44}) \ddot{\eta}_4 + \bar{B}_{44} \dot{\eta}_4 + \hat{C}_{44} \eta_4 = \hat{F}_4(t) \quad (234)$$

where the constants  $\bar{A}_{44}$  and  $\bar{B}_{44}$  are chosen to be  $\hat{A}_{44}(\omega_{n4})$  and  $\hat{B}_{44}(\omega_{n4})$ , the values of these parameters at roll resonance. If, in a specific sea condition, the roll angle, the roll rate and the roll acceleration can be accurately measured, then Equation (234) gives an estimate of the instantaneous roll moment,  $\hat{F}_4(t)$ , in that sea state. Accurate full-scale measurements of roll velocity are not easy and measurements of roll accel-

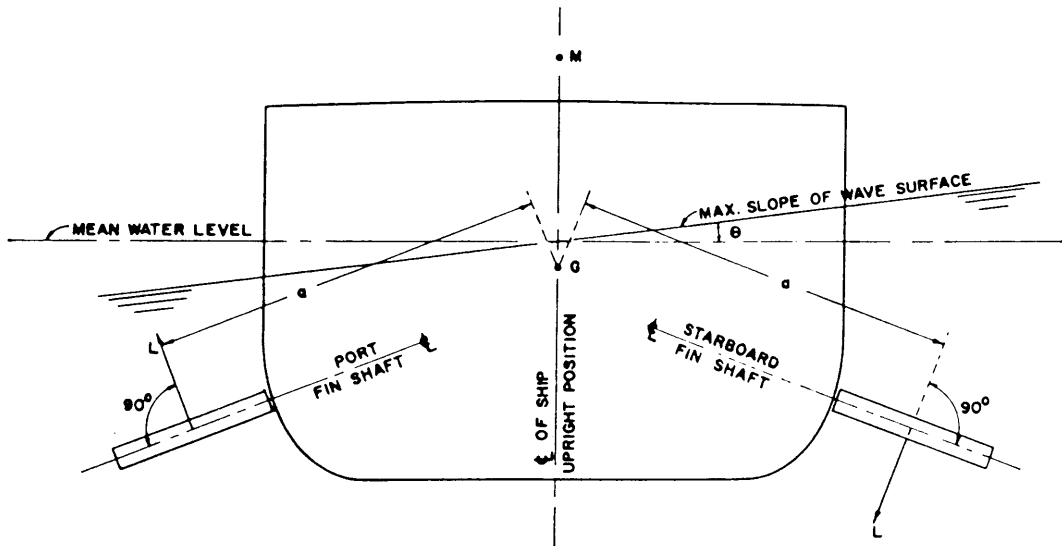


Fig. 104 Active fin stabilization diagram

eration are difficult. Instruments that perform these tasks are susceptible to errors from many sources, including noise originating from ship vibrations and electrical noise. These errors are reflected in  $\hat{F}_4(t)$ .

The control system most frequently adopted makes use of yet another simplifying assumption. It is usually assumed that the commanded roll moment is given as

$$\hat{F}_4(t) \approx C_1 \dot{\eta}_4 + C_2 \eta_4 \quad (235)$$

Where  $C_1$  and  $C_2$  are comparable in size to  $\hat{B}_{44}^*$  and  $\hat{C}_{44}^*$ , and are chosen to best stabilize the roll angle with the given stabilizer hardware.

It should be clear that the use of Equation (235) represents a compromise between what is required and what is measurable. However, with responsive roll stabilization systems such as fin stabilizers, the approximation is less severe than one would first surmise. For waves with encounter frequencies near resonance, the first and third terms in Equation (234), nearly cancel out (the cancellation is exact at resonance). Thus, at this critical frequency, the seaway-applied roll moment is in phase with the roll rate, and roll acceleration is not required. In classical control theory this type of input to the moment generation system (Equation 235) is called position and rate feedback.

**2. Stabilizing fins.** By far the most popular (and most effective) means of active stabilization of ship roll is through the use of fins. Fins are mounted on the side of a hull, usually near the turn of the bilge. During operation the fins usually extend beyond the beam of the ship and sometimes below the baseline of the ship. See Fig. 104. As a result, some additional mechanism must be provided for their retraction while maneuvering in port and for docking. During transit of the ship, the fins also are usually retracted unless they are

needed to reduce motions, since their drag is significant. Many manufacturers have designed and installed stabilizers. Each is different in the controls, shape of the fin, the exact mechanical details of operation, etc. Fin stabilizers have been used extensively for high-speed vessels, particularly on warships, cruise ships and luxury liners.

When the fins are placed at an angle of attack, the flow over them resulting from the forward speed of

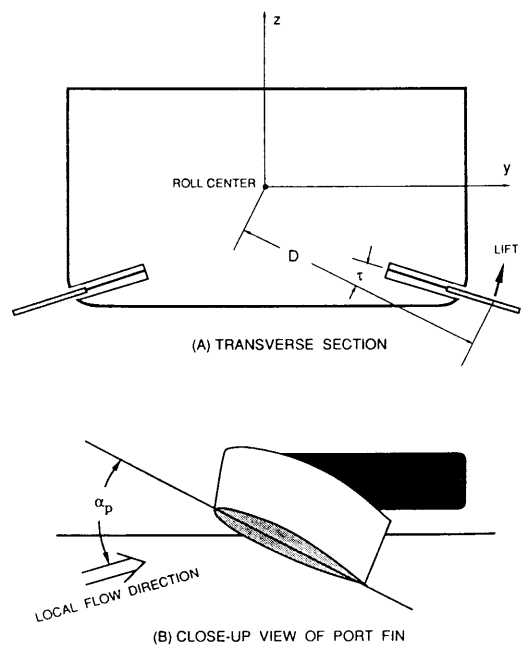


Fig. 105 Location and orientation of active antiroll fins

the ship causes a lift; if the lifts are opposite from one side of the ship to the other, the difference results in a roll moment acting on the ship. The geometric fin angle of attack (relative to the ship axes) can be varied by an actuator, which is usually hydraulic. The roll moment,  $F_{4f}$ , available from a pair of fins, each of planform area,  $A_0$ , on a ship proceeding at a speed,  $V$ , can be estimated as

$$F_{4f} = \rho V^2 A_0 \frac{\partial C_L}{\partial \alpha} (\alpha_p - \alpha_s) D \cos \tau \quad (236)$$

where  $D$  is the distance along a line from the roll center to the center of effort of one fin, and  $\tau$  is the angle between the fin axis and this line (see Fig. 105),  $\partial C_L / \partial \alpha$  is the fin lift coefficient slope,  $\alpha_p$  and  $\alpha_s$  are the effective angles of attack of the port and starboard fins, respectively (measured relative to the local instantaneous flow and opposite in sign). The orientation of typical fins is such that  $\cos \tau$  is very close to unity. Lift on the fins also gives rise to an induced drag on the fins, and this in turn is exhibited as an increase in the resistance of the ship. Since induced drag is approximately proportional to the square of the fin lift, the increase in ship resistance can be noticeable in severe seaways.

Equation (236) shows that the moment available depends on the square of the forward velocity and the surface area. The maximum value of  $\partial C_L / \partial \alpha (\alpha_p - \alpha_s)$  is in the neighborhood of  $\pm 1.0$  for the symmetric foil sections used for fins. Since the magnitude of the roll moment applied by the seaway is not greatly affected by the ship's speed, it is clear that the ship must either have large enough fins or be travelling fast enough for the fins to develop moments comparable to those induced by the seaway. In particular, fin stabilization is not appropriate for ships that need stabilization at zero speed (such as oil drilling vessels) or those with low-speed tasks (such as oceanographic vessels).

The relationship between the geometric angle of attack (relative to the ship) and the effective angle of attack (relative to the local flow) of each fin is difficult to determine since waves in the neighborhood of the fins strongly affects the local flow. In many modern fin stabilizers, the achieved roll moment from the fins is determined by measuring directly the force on the

fin using strain gauges on the fin-hull attachment. When the achieved force from either fin is less than the commanded force the angle of the fins is increased and vice versa.

The limitations in predicting the roll moment that will act on the ship and the time lag in controlling the fins prevent perfect stabilization. Further, in extremely high seas, the commanded force on a fin may be larger than the fin is able to produce and a degradation in the stabilizer effectiveness occurs. However, a well designed fin stabilizer system will provide better stabilization than other known stabilizers. Fig. 106 (Chadwick, 1955) shows the stabilization achieved with a Denny-Brown fin stabilizer.

3. *Rudder stabilization.* Baitis, et al (1983) and Källström, et al (1988) discuss an interesting variation of fin stabilization which is possible to use in special cases. In some ships, the service speed is high enough and the center of effort of the rudder is far enough below the roll center that placing the rudder at an angle of attack will produce a substantial roll moment. The effect of this moment is frequently observed as an initial heel into a turn in the first instants after initiating a hard turn at full speed.

If the responsiveness of the steering machinery is such that the rudder can be quickly moved from side to side, it may be possible to use the rudder forces (and the corresponding roll moments) for roll stabilization. In such a system the commanded rudder angle for roll stabilization would be simply added to that required for course keeping. The frequencies at which the stabilizing roll moments are required are sufficiently high compared to those to which the ship responds in turning, that such a system would not adversely affect the course keeping.

Naval ships are good candidates for this type of stabilization since they are of high speed and have large rudders mounted low on the ship (sometimes even below the baseline). The rudders of typical commercial ships may not be sufficient to generate adequate roll moments for this type of stabilization. In almost all cases the moment arm for a rudder is much less than that for a fin mounted at the bilge and thus, for an equivalent stabilization, the instantaneous forces developed on the rudder must be much larger. Although rudders are much bigger than typical fins, the induced drag associated with the larger forces may or may not be larger than that for the fins.

4. *Gyro stabilization.* Gyros have been used for roll stabilization for over 80 years, principally in passenger ships and later in submarines. The idea is simply that a gyro spinning about a vertical axis exerts a substantial roll moment on its foundation proportional to its precession rate about a transverse axis. In the active systems the precession rate is forced in order to develop the commanded roll moment. It is possible to have a passive gyro design (sometimes called a Schlick type after its original designer), but

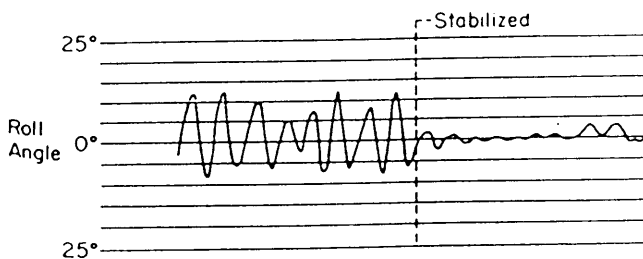


Fig. 106 Measured roll motions before and after activating fin stabilization

these have not been used in many years. Several designs of active gyro stabilizers have been put into practice, notably the designs by Sperry. Unlike fin stabilization, gyro stabilization does not increase the drag of the ship. However, in order to generate roll moments of a size comparable to the roll moments applied by the seaway, the gyros must be physically quite large and will consume considerable power. Generally the cost, weight and space requirements have mitigated against their recent application.

5. *Active tank stabilizers.* It is possible to conceive of an active stabilizer using a tank of fluid, and one such system was actually constructed by Minorsky (Chadwick & Klotter, 1954). This concept uses an axial flow pump to force the water in the tank from one side of the ship to the other, rather than to have it slosh under the natural roll, sway and yaw forces, as happens in a passive tank. Webster (1967) studied the problem of the design of such a system in some detail.

For a number of reasons this concept is not as attractive as the other active systems. First, the pump when activated in such a system accelerates the fluid in the tank either to the port or starboard side of the ship. A sizable amount of fluid arrives at that side only some time after pumping begins. That is, a considerable lag exists between the time that the water is set into motion and when the desired roll moment is achieved. As discussed above, it is not really possible to anticipate the required roll moment, and the addition of this large lag in the tank response limits the effectiveness of the roll stabilization. Therefore, fundamental reasons exist that prevent active roll tanks from achieving the stabilization level of a good, rapidly responding active fin system.

The amount of instantaneous pumping power required to achieve considerably better stabilization than a passive roll tank is substantial and might be as high as 10 percent of the installed shaft power of the ship. The average power, on the other hand, is theoretically negative (out of the tank) since the stabilizer acts as a wave power absorber. It is unlikely that such a system would actually yield any net useful power, since

the types of pumps required do not have extremely high efficiency.

**6.3 Control of Pitch.** The possibilities of anti-pitching devices must be considered, although the wave forces and moments on a ship are much greater than those that cause rolling. One device of demonstrated effectiveness is a pair of fixed fins near the bow (Abkowitz, 1959). During synchronous pitching, the bow motion is nearly out-of-phase with that of the oncoming waves, and the relative vertical velocity between ship and wave is greatest at this location. Fixed fins develop, therefore, large forces and pitch moments as a result. Use of these devices has been very limited as a result of the vibration associated with the separated flow around the foils and the increased resistance which accompanies the development of the large fin forces. Some solutions to the former problem have been proposed (Cummins, 1959) (Ochi, 1961).

Bow bulbs of the type used by Taylor appear to have comparatively little damping effect, since they are streamlined and normally well below the surface. The very large bulbs that have become common in the last twenty years have been reported to provide some pitch damping. However, they also increase both the pitch moment of inertia and added mass moment of inertia. These tend to lengthen the natural pitching period, which is generally undesirable.

Fixed fins at the stern have been long used to improve the flow and hence reduce propeller vibration. Their effectiveness in producing pitch damping is, however, small since the relative velocity between ship and wave is small at this location. The possibility of activated stern fins has been suggested as a supplement to fixed bow fins. The use of bow and/or stern tanks with openings to the sea that allow water to flow in and out like an external roll tank has also been discussed. To be effective for a conventional ship hull, these tanks would have to occupy approximately 20 percent of the ship length. Their use at forward speed would incur an enormous momentum drag penalty. As a result, it seems unlikely that external pitch tanks would be attractive for most applications.

## Section 7

### Assessing Ship Seaway Performance<sup>13</sup>

**7.1 Measures of Performance.** The necessity to forecast the operational worth of a ship long before it is completed and goes to sea poses a multifaceted challenge to the ship designer. One of those facets is the ship's response to its environment, particularly its motions in various seaways to be encountered. Not only must the naval architect be able to predict the performance of a ship in any seaway during its design stage, but he or she also needs a methodology to assess the overall adequacy of its predicted seaway performance. Such a methodology is described in this section. It is intended to be useful in assessing the seaway performance of ships engaged in their normal, operational missions, not to be used to assess the survivability of ships in extreme seas, a topic discussed in Chapters II, III and IV, Vol. I.

St. Denis (1976) has suggested an appropriate general measure for assessing a ship's operational performance in a seaway, which he calls *environmental operability*: "Given a mission and a sea-based system by which to fulfill it," he said, "the environment of weather and sea will tend to degrade the effectiveness in which the system will perform the mission. It is this environmental degradation that is the central subject of inquiry. Since in airs and seas that are calm the environmental degradation is nil, the system's calm air and calm sea performance of its mission can be taken as the standard of reference. By so doing, environmental operability is defined as and measured by the degree of attainment of calm air and still water mission performance. It is this ratio that is the index of environmental operability."

The above will be referred to here as the measure or index of seakeeping performance. In general, the methodology for assessing seakeeping performance depends upon four factors, which need definition and quantification:

(a) *Mission.* Missions are assigned to the ship, including appropriate conditions of loading. The overall missions of virtually all the ships of the world may be subdivided into three categories:

1. Port-to-port transportation of goods or people either by ships operating on a fixed schedule (liners) or by ships engaged in continuous operation (tramps and bulk carriers).

2. Military missions carried out entirely at sea, such as ocean surveillance, defensive or offensive operations of and against forces at sea or against shore targets.

3. Commercial missions at sea, such as fishing, oil drilling, or ocean mining.

Each mission in any of these three overall categories may include several different ship functions. Typical military ship functions under a surveillance mission, for example, are transit, helicopter launch and recovery, and at-sea replenishment.

(b) *Environment.* Ocean surface roughness and wind speeds are defined and quantified as a function of both location and time in Section 2. For the purposes of this section, the common maritime practice of quantifying ocean surface roughness by strata called sea state numbers is employed. The strata used in this section are characterized by the significant wave heights (and modal wave periods) shown in Tables 6 and 7 (Section 2). While significant wave height,  $H_{1/3}$ , and modal wave period,  $T_m$ , are the two parameters currently used to characterize the sea state,  $H_{1/3}$  is the prime parameter.  $T_m$ , while important, is secondary because for every possible value of  $T_m$  there is always a positive limiting value of  $H_{1/3}$ , governing ship speed within the ship's operating envelope. The opposite is not always true. For large values of  $H_{1/3}$ , there is very likely to be no value of  $T_m$  within the bound of possible  $T_m$  values observed to exist in the ocean ( $0 < T_m < 24$  sec) that will permit operation within the desired ship's speed operating envelope.

(c) *Ship responses.* Specific responses are examined as a function of ocean surface roughness, ship speed and ship-wave heading angle, maximum attainable speed in both calm and rough water. Ship responses, include all of the ship responses, both absolute and relative, discussed in Section 7.3. Methods of calculating the responses are treated in Sections 3,4 and 5.

(d) *Seakeeping performance criteria.* These are a key element in developing a methodology for assessing a ship's seaway operational performance, and with their prescribed limiting values, determine whether or not a mission(s) can be carried out. This factor is covered fully in sub-sections 7.3-7.6.

Before proceeding to discuss quantitative measures of the seakeeping performance of ships it is well to note that the single word ship is used throughout this section to include all marine vehicles such as the monohull, SWATH, hydrofoil, planing, and surface effect ships, as well as air cushion vehicles. The single word ship is also used to denote the total ship system, which in all cases comprises at the minimum the following four elements:

1. The hull or platform; its type, geometry, and structure.

2. The systems needed to operate the hull of platform, (here called platform systems) i.e., its power plant, steering system, motion control systems, etc.

3. The systems needed to perform the mission or missions assigned to the ship (called mission systems).

<sup>13</sup> Section 7 written by Philip Mandel.

4. The people (in number, kind and training) necessary to operate the total ship system.

Two quantitative measures of ship seakeeping performance, called *Seakeeping Performance Indexes* (SPI), have been recognized conceptually for years. Both of them are in accord with the St. Denis general index. One measure, here called SPI-1, is defined as *mission effectiveness*. This is the fraction of time that a given ship in a given condition of loading can perform a specified military or commercial mission (or mix of missions), for a predetermined profile of ship speeds and headings in a specified ocean area and season.

The second measure, here called SPI-2, is a transit time index. It is uniquely appropriate for the many ships of the world devoted solely to port-to-port transportation. It also applies to fishing boats traveling to and from fishing grounds, and it may apply to naval vessels en route to a specific destination when minimum elapsed time of transit is of overriding importance. SPI-2 is defined as *transit time index*, which is the ideal time that a ship needs for a transit in calm water between two or more specified ports divided by the actual time that the ship would require to travel between the same two ports in seas appropriate to a specified season or seasons. For a designated minimum-distance route SPI-2 is also the ratio of the average speed of that ship on that route in the designated seas to the calm water speed of that ship in the same condition of loading and with the same bottom fouling. This index is called the *expected speed fraction* (St. Denis, 1976).

The details of how to calculate the Mission Effectiveness Index, SPI-1 and the Transit Time Index, SPI-2 are outlined in Sub-Sections 7.7 and 7.8. Their general significance is discussed here.

SPI-1 is directly useful in assessing the operational worth of the many military ships, and some commercial ships—such as cruise ships—whose primary missions are conducted and completed at sea. Assuming that a correct set of seakeeping performance criteria and their prescribed limiting values are available for each particular ship mission and that the probabilities of occurrence of wave conditions in the desired ocean areas and over the desired time periods are known, SPI-1 can be determined. We must calculate the percent of time (i.e., probability) that the actual values of various ship response never exceed the prescribed values of the applicable performance criteria. This percent of time, SPI-1, is used directly in judging the operational worth of a ship. Performance limitations, other than seakeeping, may even more severely constrain this percent of time, but the percent of time measured by SPI-1 can never be exceeded unless the ship or its operational doctrine is altered.

Because of its restriction to a predetermined mix of fixed speeds, SPI-1 is not useful in calculating the operational worth of ships engaged in the common, commercial function of port-to-port transportation of

cargo or people. For this function, SPI-2, the ratio of ideal transit time in smooth water to the actual transit time, is appropriate. SPI-2 is one of the key factors needed to calculate voyage time on a particular route and in a particular season to a specified degree of certainty. This is the most essential ingredient in assessing the operational worth of transportation ships engaged in regular or a scheduled service. Other key factors involved in calculating voyage time to a specified degree of certainty are not included in SPI-2 because they are not directly associated with ship performance in rough seas. These key factors are associated with ocean currents, wind drag, fouling, visibility conditions, deterioration of power output, cost of fuel, harbor conditions, etc. It should be noted that just as SPI-1 is not applicable to the transportation mission, SPI-2 is not suitable for the ship missions for which SPI-1 is useful. Both SPI-1 and SPI-2 may be useful for frigates and destroyers on convoy duty.

**7.2 Involuntary and Voluntary Speed Reductions.** The values of both SPI-1 and 2 are intimately linked to seaway-induced restrictions on ship speed and on ship-wave heading direction. In this sub-section primary emphasis is on the restrictions on ship speed in head seas, which is the critical ship-wave heading for most ships. The restrictions on ship speed at other ship-wave headings are discussed in sub-sections 7.5 and 7.7.

It was shown in Section 5 that maximum power-limited speed at any heading, in any seaway, occurs at the point on the appropriate curve of required power of the ship, plotted as a function of speed, corresponding to the available propulsion power, Fig. 88. Available power in different sea conditions is dependent mainly on the characteristics of the propulsion plant and the propulsor's interaction with the waves and the hull of the ship. Required power as a function of speed is dependent on sea state, ship heading, ship size and configuration. The increase in required power due to rough water is attributable mainly to added drag in a seaway. But the reduction in available power in rough water results from both the drop in power plant output under overload and the effect of ship motions in reducing propulsive efficiency. The reductions in ship speed attributable to both reduced available power and increased required power are called involuntary speed reductions because they occur whether the ship captain wants them to occur or not.

The attainable speed of large, full low-powered ships in rough seas is determined primarily by this involuntary speed reduction. In fact, large low-powered supertankers are usually slowed down sufficiently by rough seas to avoid problems of severe motions.

But for moderate to high-speed ships there is also a voluntary speed reduction related to ship motions. Fig. 107 (Mandel, 1979) shows for a hypothetical high-speed monohull ship, in two different conditions of loading, how attainable speed varies with head seas

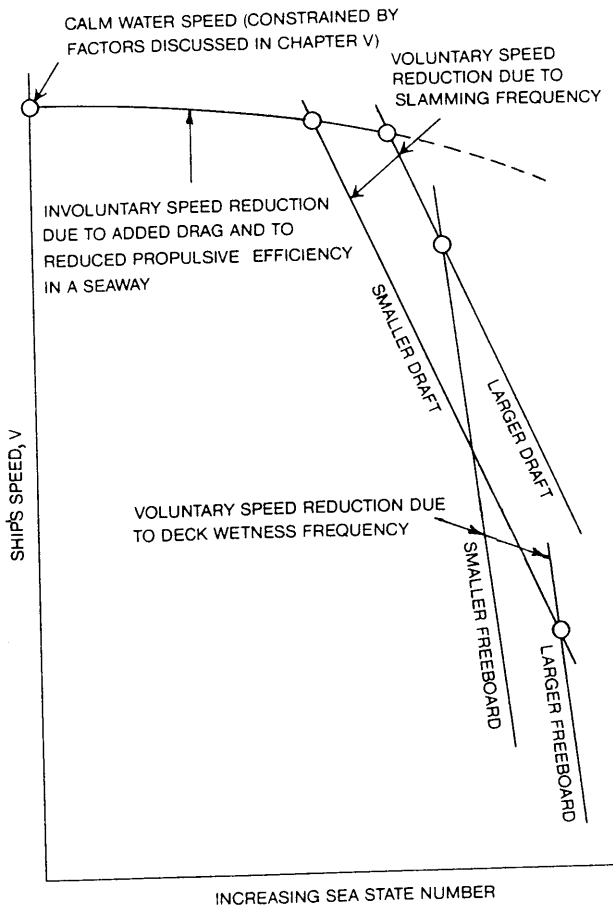


Fig. 107 Involuntary and voluntary speed reduction from calm water speed for a high-speed mono hull in head seas (Mandel, 1979)

of different significant heights. It illustrates both the involuntary speed reduction, caused by added required power and reduced available power, and the voluntary speed reduction caused by slamming (at the lighter draft) and by deck wetness (at the deep draft). The figure suggests that the involuntary speed reductions are relatively small, although this may not always be the case. As the sea state severity increases, and amplitudes of motion of this high-speed ship increase, and eventually, even with active motion stabilizers, the motions of the ship will become so severe that the captain fears for the ability of his crew to carry out their function, for the comfort of his passengers or for possible damage to the ship or its systems and its payload. In the case of military ships, the motions may become so severe that one or more ship functions cannot be performed. Vital operational capabilities, like launch and recovery of aircraft, become very hazardous, or detection of other ships by means of sonar may become impossible. (In all of these cases, the seas are severe enough to reduce operational capability, but they are not so severe that ship survivability is threatened). The only recourse that the ship captain has is either to reduce the speed of his ship, or to change its heading

with respect to the waves, or both. These speed reductions and heading changes are called voluntary because they are brought about by a decision of the master and are not imposed by factors like added drag or decreased propulsive efficiency over which he has no control.

Fig. 108, taken from Lewis (1959) and Marks and Ferdinande (1960), shows quantitative speed reduction data similar to the hypothetical data of Fig. 107 for two classes of general cargo ships at five different ship-wave heading angles taken from actual voyage records. The two curves labeled "power reduced" indicate very roughly the points of transition between involuntary and voluntary speed reduction for these two types of cargo ship.

Fig. 109 shows full-scale log data for the 218-m (715-ft) 21-knot containership *Dart Europe* (the same ship as in Fig. 88) in head seas, as plotted by Sellars and Setterstrom (1987) from data in Aertssen and van Sluijs (1972). The figure shows greater involuntary speed reductions for this ship before power was voluntarily reduced than in Figs. 108 and 109 and correspondingly less voluntary speed reduction as sea conditions become more severe.

Because SPI-2 is concerned with maximum attainable ship speed in all seas from calm to rough, it is likely that both involuntary and voluntary speed reductions may be important in calculating SPI-2. On the other hand, because SPI-1 is only concerned with predetermined or specified speed values (which are almost always below the maximum calm water speed), it is

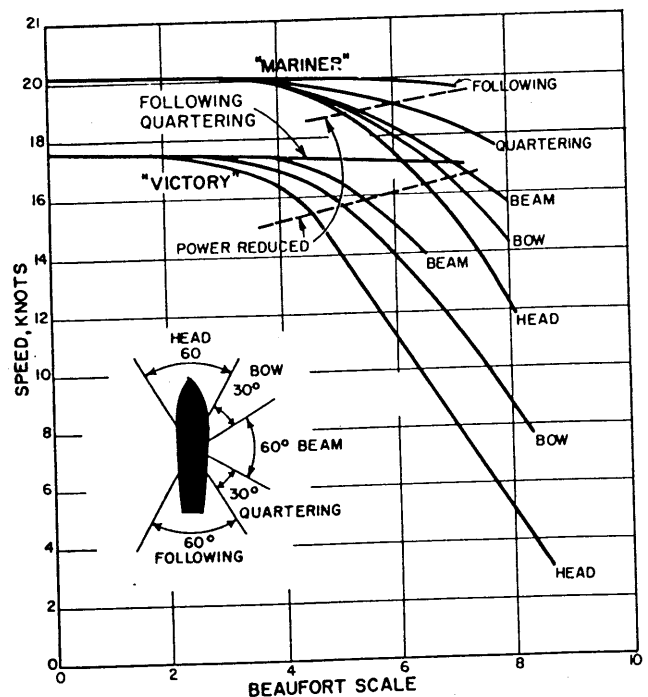


Fig. 108 Attainable sea speed in different sea conditions for two classes of cargo ships (Lewis, 1959, and Marks and Ferdinande, 1960)



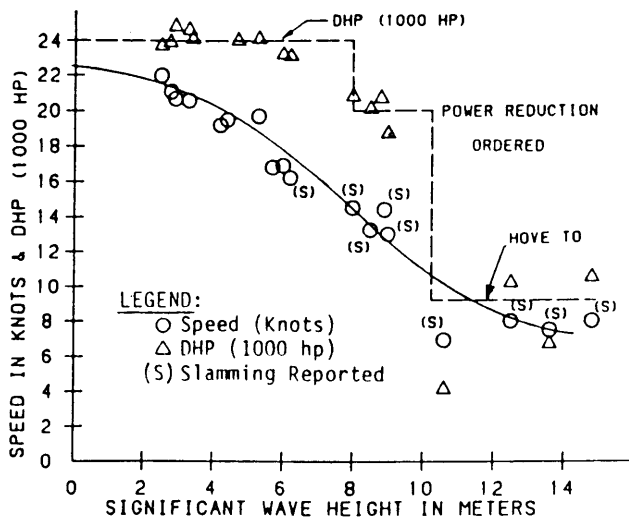


Fig. 109 Service performance of 218-m (715-ft) containership in head seas (Sellars and Setterstrom, 1987)

most probable that only voluntary speed reductions and heading restrictions will be important for SPI-1. Of course, if the specified speed values are very close to the ship's maximum calm water speed, then Fig. 108 shows that the involuntary speed reduction might slightly degrade the range of sea state severities in which the ship may carry out its mission. However, in most practical cases, the values of speed at which it is desired to calculate the values of SPI-1 are below the speed at which the involuntary speed reductions play a large role, and the voluntary speed reductions are more important.

The process by which a ship captain makes his decision to voluntarily reduce ship speed or change the ship-wave heading direction is necessarily subjective. The concepts of seakeeping performance criteria and of limiting prescribed values for those criteria discussed in the following sections were developed to quantify this subjective process. The increasing trend toward installing motion monitoring instrumentation on modern ships can be of great assistance in developing useful and reliable limiting values of the various performance criteria, as well as providing useful operating guidance to the ship master.

In this section emphasis is on the medium and high-speed ship for which voluntary speed reductions are of particular importance. It is assumed that available power is always adequate, and both mission performance (SPI-1) and attainable speed (SPI-2) depend mainly on direct and indirect effects of motions. For slow-speed vessels where available power affects SPI-2, and for all ships where lost time in rough seas must be made up in good weather, the problem of required maximum installed power (or service power allowance) is important. See Sections 5 and 8.

**7.3 Seakeeping Performance Criteria and Ship Seaway Responses.** In general usage, the words *index*

**way Responses.** In general usage, the words *index* and *criterion* have similar meanings. But in the literature on seakeeping, a clear distinction has gradually taken form. The term *seakeeping performance index*, or index of environmental operability (Section 7.1), is used here as an overall statistical measure of the degradation of seaway performance of a total ship system over a period of time. In contrast, the term *seakeeping performance criterion* refers to a specific aspect of ship response to a seaway (amplitude of motion, individual event or frequency of occurrence of events), each of which—if severe enough—can degrade the performance of one or more of the elements of a total ship system to an unacceptable level. (See sub-section 7.4).

Twelve examples of currently used seaway performance criteria are given in Table 19, together with the elements of the total ship system that they may affect and the performance degradations they may cause. The twelve seakeeping performance criteria are subdivided in the table into four categories of response, as follows:

(a) Amplitudes of motion, such as absolute displacements and roll, pitch, and yaw angles of the ship.

(b) Absolute vertical, transverse, and longitudinal velocities and accelerations of points at selected locations on the ship with respect to the earth.

(c) Relative vertical displacements and velocities of points at selected locations on the platform with respect to the ocean surface at these locations.

(d) Relative motions between platform and aircraft.

All twelve criteria of Table 19 may apply to both commercial and military ships. However, Criteria Nos. 3, 9 and 12 apply primarily to military ships. Criterion 6 is defined and discussed in Section 7.6.

There is a fifth category of seaway responses that is important to some ships but is not reflected in any of the criteria of Table 19. This category is:

(e) Vertical, transverse, and longitudinal displacements, velocities and accelerations of platform or payload components with respect to the ship, caused by ship motions.

This category includes the motions of ship or payload components sliding on a ship's deck because of the motions of the ship. Aspects of these motions are further discussed at the end of this subsection, but data are scarce.

The evaluation of the long-term seakeeping performance of a proposed new design, to operate on an assigned mission in a specified environment (Sections 7.7 and 7.8), involves the comparison of calculated responses against the prescribed values of the appropriate criteria, such as those given subsequently in Table 20 and discussed fully in Sections 7.4 and 7.6, for many short-term situations. The actual values of the responses measure the severity of the motions and the frequency of the seakeeping-related events that a ship experiences while at sea. How to predict these values is the major subject of Sections 3, 4, and 5 of



Table 19—Twelve Examples of Seakeeping Performance Criteria

No.	Seaway Performance Criteria	Affected Elements	Performance Degradations
(a) Absolute Motion Amplitudes			
1. Roll angle } 2. Pitch angle }	People, Mission and Platform Systems	{ People Mission Systems	{ Personnel injury, reduced task proficiency, and mission and hull system degradation.  Injury to personnel handling aircraft. Inability to safely launch or recover aircraft.
3. Vertical displacement of points on flight deck			
(b) Absolute Velocities and Accelerations			
4. Vertical acceleration } 5. Lateral acceleration }	People and Mission Systems	{ Personnel fatigue, reduced task proficiency and mission system degradation  Reduced task proficiency.	
6. Motion sickness incidence (MSI)			
7. Slam acceleration (vibratory, vertical)	People, Mission and Platform Systems	{ Personnel fatigue, injury, reduced task proficiency and mission and hull system degradation. Preclusion of towed sonar operation.	
(c) Motions Relative to Sea			
8. Frequency of slamming. (Simultaneous bow reimmersion & exceedance of a threshold vertical velocity.)	{ Mission Systems Platform System	{ Hull Whipping stresses and damage to sensors on the masts  Slamming damage to bottom forward hull structure.	
9. Frequency of emergence of a sonar dome			
10. Frequency of deck wetness (submergence of the main deck forward.)	{ People Mission Systems	{ Injury or drowning of personnel. Damage to deck-mounted equipment.	
11. Probability of propeller emergence	Platform System	Damage to the main propulsion plant.	
(d) Motions relative to aircraft			
12. Vertical velocity of aircraft relative to the flight deck	Mission Systems	Damage to aircraft landing gear and/or loss of aircraft.	

this chapter.

The actual values of all responses, except those involving the motions of a body independent of the ship platform (like Criterion No. 12 of Table 19, are totally dependent on the motions of the ship in the seaway. Hence the values of the responses corresponding to Criteria 1 through 7 are directly calculable from the response spectra associated with Categories (a) and (b). The motion sickness corresponding to Criterion No. 6 is assumed to be dependent on the values of vertical acceleration and on the frequency of occurrence of those values of acceleration, as discussed in Section 7.6. Under Criterion No. 7 the actual values of peak vertical acceleration due to slamming are difficult to calculate because they are the result of a transient event. The actual values of the responses corresponding to Criteria Nos. 8–11, category (c), can be calculated using the methods of Sections 4 and 5 to obtain the spectra of responses at different speeds and headings in representative sea spectra. Finally, the actual

values of response for Criterion No. 12 are calculable from the spectra of the vertical velocities of Category (b) for both the flight deck and the aircraft. (A more accurate but much more expensive determination of the values of these responses can be obtained by repeated time domain solutions).

A short-term evaluation of ship performance can be obtained by making systematic calculations of the various responses at different speeds and headings in specific sea conditions, as defined by their directional sea spectra. Results can then be plotted on the basis of speed. For any specific set of performance criteria, the speeds at which the criteria will be met can then be determined for any combination of sea state and ship heading. Such plots form the basis for the long-term evaluations discussed in Sections 7.7 and 7.8.

The ship response spectra mentioned in the previous paragraphs can be calculated by a Standard Ship Motion Program, utilizing the most suitable of the procedures described in Sections 3 and 4, as published by

Meyers, et al (1981). Some users of this (and other) programs have developed their own extensions to time-domain solutions.

Baitis, et al (1976b) utilized earlier versions of the above standard program to create a comprehensive ship motion data base, including both frequency domain and time domain responses, for five current classes of Navy ships. A somewhat less comprehensive data base exists for four classes of U.S. commercial ships and for several liquefied natural gas (LNG) carriers (S. Bales, et al 1975) (Baitis, et al 1976a). Such data bases are useful for readily obtaining seaway performance information on existing ships, either for comparison with similar information on new designs or for use in the design of new ship systems and/or components, Section 4.

While a frequency-domain data base is sufficient to calculate the actual values of most responses of specific ships, it is not sufficient for the responses corresponding to all applicable criteria. Vehicle motions in the time domain are often desirable for the four classes of criteria that:

(a) Involve the relative motion of two bodies whose motions are independent of one another (e.g., Criterion No. 12 of Table 19).

(b) Involve highly nonlinear combinations of various ship motion components (e.g., shoring forces on objects carried on a deck of a ship that involve motion dependent friction forces).

(c) Depend on the joint (simultaneous) occurrence of any two or more independent ship motion components exceeding a certain specified value (e.g., a criterion that stated that the joint probability of occurrence of roll = 5 deg and pitch = 2 deg could not be tolerated).

(d) Involve time in an absolute, not relative, sense (e.g., a criterion that states that a specified event cannot occur at intervals less than  $x$  seconds duration).

These considerations account for the fact that many computer programs, as well as the Baitis data base, have been extended to obtain time domain responses.

**7.4 Prescribed Limiting Values of the Seaway Performance Criteria.** Given that ship motions do degrade the performance of elements of the total ship system, the prescribed limiting values of the seaway performance criteria are intended to correspond to the boundary between acceptable and unacceptable performance, i.e., the limit of operability. Ideally, it would be very helpful if acceptability corresponded to an abrupt discontinuity in the relation between motions and performance degradation. In reality such abrupt discontinuities do not, of course, exist. It should be possible, however, to establish relationships in probability terms between motions and degradation of performance for the various criteria (referred to as *degradation functions* by Comstock and Keane (1980)). Such a scheme can be fully realized only through the collection and statistical analysis of large amounts of service data. It would permit a more precise definition

to be made of limits associated with different levels of performance.

Actually, the prescribed values are largely judgment values coming from the experience and knowledge of those who formulate the operational requirements for ships, the medical profession concerned with human performance, the naval architects and other engineers concerned with the design and performance of the ship and its subsystems, the various kinds of engineers concerned with the mission systems, and—most important—the officers and men who operate the systems. Each of the prescribed values is viewed by these people as a reasonable, average operational limit associated with no significant impairment of functions or degradation of performance (unless otherwise stated) in one of the following three categories:

(a) Personnel

- Comfort
- Motion sickness
- Personnel fatigue
- Task proficiency
- Safety

(b) Ship payload

- Helicopter and aircraft landing
- Cargo shifting.

(c) The ship

- Hull damage
- Deck equipment damage
- System damage
- System efficiency
- Propulsion plant.

The prescribed values of the seakeeping criteria developed for Categories (a) and (b) should be completely independent of sea, wind, and weather conditions; location on the ship; or the presence or absence of active motion controls. They are dependent on ship function (mission) and crew experience, and may be dependent on ship type, size, and/or mission duration. Similarly, the prescribed values of seakeeping criteria developed for Category (c) are also completely independent of sea, wind, and weather conditions, and are dependent on ship function. But they, unlike the preceding prescribed values, are dependent on location in the ship.

Prescribed values for five different naval and four commercial ship configurations, taken from several sources, for the twelve seaway performance criteria of Table 19 are given in Table 20 for several ship functions. These values, and those given subsequently in Section 7.7, are the best currently available in the literature, but uncertainties remain in regard to many of them. Hence, they should be considered tentative and subject to revision as more instrumented ship data become available. The five naval ship configurations include monohull, SWATH, planing, hydrofoil and surface effect ships. Although not necessarily so specified in each source, it may be assumed that the prescribed values of Table 20, except those for Criterion No. 6, correspond to observed average operational limits for no significant degradation of performance.

Table 20—Prescribed Values for the Twelve Performance Criteria of Table 19

Criterion No.	Column No.	1	2	3	4	5	6	7	8	9	10	11	12	13	14
	Ship type	Naval mono-hull	3350 t. SWATH	Planing craft	Hydro-foil	2000–3000 t SES		Naval mono-hull		Naval mono-hull		Commerical Monohulls			
	Function	Point-to-point transit						Helicopter operation		At sea replen.	Sonar search	Transit			
	Source	Olson (1977)	Comstock et al. (1980)	Olson (1977)	Allen et al (1978)	Stark (1977)	Mandel (1979)	Olson (1977)	Comstock et al. (1980)	Olson (1977)	Olson (1977)	Aertssen (1968, 1972)			
1	Rms Roll Angle, deg.	9.6	4.	9.6	—	1.25	1.5	3.2	2.5	—	9.6	—	—	—	—
2	Rms Pitch Angle, deg.	—	1.5	—	—	1.5	1.5	—	1.5	2.4	—	—	—	—	—
3	Rms Vert. Disp., m.	—	—	—	—	—	—	1.26	—	—	—	—	—	—	—
4	Rms Vert. Accel., g	—	0.2	—	—	0.11	0.1	—	0.2	—	—	0.5	0.9	1.4	1.0
5	Rms Lat. Accel., g	—	0.1	—	—	0.06	0.1	—	0.1	—	—	—	—	—	—
6	Mot. Sickness Incidence	20% in 2 hrs	—	20% in 2 hrs.	—	10% in 4 hrs.	10% in 2 hrs.	—	—	—	20% in 2 hrs.	—	—	—	—
7	Slam Accel., g.	0.2	—	—	4*	0.5*	0.6*	0.2	—	0.2	0.2	0.2	0.2	0.9	0.4
8	Slam Freq.	$\frac{3}{100}$	$\frac{20}{\text{hr.}}$	#	—	—	—	$\frac{3}{100}$	$\frac{20}{\text{hr.}}$	$\frac{3}{100}$	$\frac{3}{100}$	$\frac{3}{100}$	$\frac{4}{100}$	$\frac{6}{100}$	$\frac{5}{100}$
9	Sonar Dome Emerg. Freq.	—	—	—	—	—	—	—	—	—	$\frac{120}{\text{hr.}}$	—	—	—	—
10	Dk. Wetness Freq.	$\frac{30}{\text{hr.}}$	$\frac{30}{\text{hr.}}$	—	—	—	—	$\frac{30}{\text{hr.}}$	$\frac{30}{\text{hr.}}$	$\frac{30}{\text{hr.}}$	$\frac{30}{\text{hr.}}$	$\frac{5}{100}$	$\frac{5}{100}$	—	—
11	Prop. Emerg. Freq.	—	—	#	—	—	—	—	—	—	—	$\frac{25}{100}$	$\frac{25}{100}$	—	—
12	Rms Rel. V. Velocity, m/s	—	—	—	—	—	—	1.83	1.0	—	—	—	—	—	—

Notes: All values of response (angles, displacements, accelerations) are rms (root mean square) peak-to-mean (single amplitude) values unless otherwise noted.

\* Extreme peak-to-mean value.

# See text, Section 7.6

Seakeeping Performance Criteria—Table 2

The prescribed values of the criteria of Table 20, in accordance with a principle stated early in this section, can be applied to any location aboard ship. However, because most of the actual values of the responses corresponding to the criteria are very location dependent (the only two exceptions are Criteria 1 and 2) use of the seaway performance methodology requires knowledge of the locations to be considered. The locations at which responses should be compared with prescribed values of Criteria 3 through 12 of Table 20 are as follows, considering longitudinal, vertical and lateral coordinates:

Criteria 3: Helicopter landing pad.

Criteria 4, 5 & 6: All locations in the ship where personnel eat, sleep, and work (and on passenger ships, recreate).

Criteria 7 & 8: For planing craft, hydrofoils, SES, and ACVs: The same locations as for Criteria 4, 5 and 6. For monohulls and SWATHs:

Locations that are dependent on hull fullness and particularly on the extent of the flat of bottom. The location assumed for the values given in Table 20 is 15 percent of the ship length abaft the bow, which is the value for the 528-ft *Mariner* cargo ship used by Ochi and Motter (1973).

Criterion 9: The location of the sonar dome.

Criterion 10: Any location on or above the deck of the ship where personnel, payload, ship structure or ship systems may be injured or damaged by impacting sea water.

Criterion 11: The location of the propeller.

Criteria 3 and 12: The location (called the bull's eye) where the helicopters are launched and recovered.

Each of the prescribed values of Table 20 is discussed in detail in Section 7.6.

**7.5 Governing Criteria.** For a given ship, in a given condition of loading, operating in a given sea state, the prescribed values of one or more criteria from Table 20 will constrain ship speed and ship-wave heading direction. These criteria are called the governing criteria. The governing criteria will change as speed and ship-wave heading direction are altered, and they will also change as the sea state changes. Insuring that the governing criteria are identified for each sea state and each ship condition requires that all of the seakeeping criteria applicable to the ship and to its function(s) be individually considered.

The governing criteria for a given mission, speed, and heading may also be different for different ships of the same general type and may even be different for the same ship in different conditions of loading. The latter point is illustrated in Fig. 109 for ahead seas. In a light condition of loading (shallow draft and large freeboard) the governing criterion for a monohull performing the transit function is the slamming frequency criterion No. 8 for the greater part of the speed regime. Only at speeds in the lower 28 percent of the speed regime is the deck wetness Criterion No.

10 governing. However, in a heavy condition of loading (large draft and smaller freeboard), the slamming criterion is governing only in the upper 20 percent of the speed regime, whereas the wetness criterion is governing over most of the speed range.

**7.6 Discussion of Prescribed Values.** The bases for the prescribed values, identified by the criteria numbers and column numbers of Table 20, are discussed in this section. For SES, monohull, planing and SWATH ships, some information concerning the governing seakeeping criteria is also given. It will be clear from the discussion below that all prescribed values are tentative, subject to revision as information accumulates.

(a) *Criterion No. 1: Rms (root mean square) roll angle.* Motion sickness or nausea has a long historical connection with the rolling of ships at sea (the word nausea comes from the Greek word "naus" meaning ship). However, the research of O'Hanlon and McCauley (1973) revealed that it is the vertical accelerations associated with roll angle, pitch angle and heave (not the roll angle itself) occurring within a very narrow band of frequencies, all well below one hertz, that induce motion sickness. As a result of this research, discussed further under Criterion No. 6, none of the prescribed values for roll angle in Table 21 were determined on the basis of motion sickness. Rather the basis for each value of the roll angle criteria in Table 20 is as follows:

Cols. (1), (3) and (10); 9.6 deg: Olson (1977) could not really substantiate this relatively large value; although he related it to personnel effectiveness. It is interesting to observe in the summary of Olson's work by Mandel (1979) that, in spite of its large magnitude, this prescribed value caused roll angle to be the governing criterion for monohulls for the transit-alone function in 75 out of 80 possible cases at a ship-wave heading angle of 75 deg (285 deg), where 180 deg represents head seas. Roll angle was also the most prevalent governing criterion at all ship-wave heading angles between 50 deg (310 deg) and 82 deg (278 deg). (Olson's work covered four different military monohulls operating at five different speeds in seas of four different modal periods). In contrast, for SWATH ships, roll angle with this same prescribed value is never a governing criterion.

Col. (2); 4 deg: The given basis for the value is personnel considerations; it is not related to limits on ship or mission equipment or to the ship itself. There is some evidence that this prescribed value is unduly restrictive for the transit function.

Col. (5); 1.25 deg: Stark (1977) suggests this value as an approximate guideline for subsequent combat system requirements, to ensure crew proficiency in rough water and to constrain structural loads on equipment located at ship extremities.

Col. (6); 1.5 deg: The significance of this value for rms roll (and pitch) angle is that in unpublished sim-

ulation studies this value was never exceeded in sea states where Criterion No. 4 (rms vertical acceleration) with the prescribed value of  $0.1g$  (given in Column 6 of Table 20) was governing. Presumably the actual rms value of roll and pitch angle could be larger than  $1.5$  deg without reducing task proficiency or increasing motion sickness so long as the prescribed value of Criterion No. 4 was not exceeded. This is in accord with the findings of O'Hanlon and McCauley (1973) mentioned in the introduction to this subsection.

Because of uncertainties, data on ACVs are not included in Table 21. However, a prescribed value of  $3.4$  deg for rms roll was obtained from actual measurements by Wachnik and Pierce (1967) on one of England's cross-channel, passenger-carrying SRN4 class of ACV's in seas of  $8.9$  ft ( $2.7$  m) significant wave height as measured by wave buoys at selected points on the route. The significance of this sea condition is that it represents the level of sea severity at which the operators of these vehicles suspend them from service because of passenger intolerance, although the vehicles themselves could tolerate more severe seas.

Since these vehicles are engaged in a strictly commercial, profit-motivated service, the decision to suspend service is not taken lightly. Furthermore, the fact that these vehicles have been in service for well over a decade means that such decisions are based on firm knowledge of passenger tolerance of severe motions. However, based on experience with the SES as noted in the discussion of the prescribed values of Col. (6), it is likely that the true governing criterion for ACV's is the rms vertical acceleration with a value of  $0.1g$  from Column (6), not the rms roll angle of the preceding paragraph.

Cols. (7) and (8);  $3.2$  deg and  $2.5$  deg: These values prescribed by Olson (1977) and Comstock and Keane (1980) for monohull (and also SWATH) ships launching or recovering helicopters are both based on work by Baitis (1975). They are intended to define the safe limits for the personnel who are out on deck handling helicopter launch or recovery. The summary of Olson's (1977) report by Mandel (1979) shows that these prescribed values caused roll angle to be the most prevalent governing criterion for the four monohull destroyers treated by Olson performing the helicopter launch or recovery function at all ship-wave heading angles between  $40$  deg ( $320$  deg) and  $100$  deg ( $260$  deg). For SWATH, the prescribed value of  $3.2$  deg causes roll angle to be governing in one case out of 32 at ship-wave heading angles between  $40$  deg ( $320$  deg) and  $70$  deg ( $290$  deg), one SWATH operating at eight different speeds in seas of four different modal periods.

(b) *Criterion No. 2; Rms pitch angle.* The bases for each of the prescribed values of pitch angle in Table 20 are the same as those for roll angle. With respect to the value in Column 9, Olson (1977) states, "While we found no specific pitch criterion based on consid-

eration of human effectiveness, a  $2.4$  deg rms pitch is frequently cited as an operational limit on ship sub-systems such as replenishment-at-sea equipment."

(c) *Criterion No. 3; Rms vertical displacement.* The consideration behind Criterion No. 3 is the ability of the flight deck crew to safely handle helicopters before launch and at recovery. The prescribed rms single amplitude value of  $4.17$  ft ( $1.26$  m) entered in Table 20, was obtained from Baitis (1975) and Olson (1977). Olson's results show that this prescribed value caused Criterion No. 3 to be the major governing criterion for the helicopter launch and recovery functions at all ship-wave heading angles between  $120$  deg and  $240$  deg and between  $0$  ( $360$  deg) and  $40$  deg ( $320$  deg) for monohulls and between  $0$  ( $360$  deg) and  $75$  deg ( $285$  deg) for SWATH ships. However, Fig. 115 discussed in the next section shows Criterion No. 12, not Criterion No. 3, to be the governing criterion for the helicopter launch and recovery function. Hence, these Olson results should be considered tentative.

(d) *Criteria Nos. 4 and 5; Rms vertical and lateral accelerations.* The close relation between Criteria 4 & 5 and personnel fatigue and reduced task proficiency have been recognized for decades. Prescribed values of these two criteria at frequencies above  $1$  Hertz and in association with stated time durations have been promulgated by the International Standards Organization (ISO, 1978) and used as military standards (MIL-STD-1472) for many years.

At frequencies lower than  $1$  hertz, which were not included in ISO standards, Stark (1977) adopted frequency weighted values of the vertical acceleration using the Motion Sickness Incidence discussed in the next section. These are the values in Table 20, Column 5. Virtually identical values of vertical acceleration obtained from the simulation tests of SES's and from the trials of the SRN4 class of ACVs are reported in Column (6) of Table 20. Aertssen (1968) gives much larger limiting values for commercial vessels (Columns 11-14).

Stark's (1977) prescribed value for rms lateral acceleration (Criterion 5) in Column (5) is  $0.06g$ . He states that he obtained this value by extrapolating the MIL-STD value (for a four-hour duration limit) which is constant at frequencies between  $1$  and  $2$  hertz down to the synchronous rolling frequency of hydrofoil craft ( $\sim 0.25$  hertz). The prescribed value of this criterion for SES's in Column (6) is related to turning characteristics, not to motions in waves (see Chapter VI), as is the value for monohull ships in Columns (2) and (8).

A recent approach developed from that of Stark (1977) for evaluating human performance limits is described in Dept. of Defense publication (DOD, 1981).

(e) *Criterion No. 6; Motion sickness incidence.* In the early 1970's, O'Hanlon, et al, (1973) conducted experiments with a group of young men, unacclimated to motions, subjecting them to a series of single frequencies of vertical sinusoidal motion (no roll motion).

The results of these experiments were expressed in terms of a Motion Sickness Incidence, MSI, which is defined as the percent of individuals who would become physically ill if subjected to motions of prescribed characteristics for a given time interval  $t_1$ . Results of the O'Hanlon, et al, experiments in the form of values of rms vertical acceleration and frequency corresponding to four different combinations of values of MSI and  $t_1$  are plotted in Fig. 111. This figure shows that at a rms vertical acceleration value of  $1 \text{ m/s}^2$  ( $0.1g$ ), 20 percent of unacclimated men threw up in two hours, at frequencies of 0.1 and 0.29 hertz (periods of 3.4 and 10 sec). At frequencies (and periods) intermediate between these two sets of values, the MSI value is greater than 20 percent. At a rms vertical acceleration of  $2 \text{ m/s}^2$ , 35 percent of such people became sick in two hours at frequencies of 0.09 and 0.34 hertz (periods of 2.9 and 11.4 sec). These ranges of periods happen to coincide fairly strongly with the actual roll periods of most monohull ships, with synchronous rolling of such ships most commonly occurring in the range of 6 to 25 sec. The O'Hanlon, et al, work revealed this coincidence of periods and thereby shed light on the historical association between ship roll angle and motion sickness; it also simultaneously disclosed that it was not necessarily the roll motion itself, but rather the vertical acceleration associated with roll, pitch and heave motion that may be the base cause of motion sickness.

Fig. 110 also shows the very rapid decrease in motion sickness incidence with increase in period above the usual synchronous roll period of ships. With increase in period above about 7 seconds (frequency below 0.14 hertz), MSI decreases rapidly at all values of rms vertical acceleration above about  $1 \text{ m/s}^2$ . This accounts for the great interest on the part of naval architects in the early years of this century, during the heyday of trans-Atlantic passenger liners, in increasing the roll period of these ships by reducing the metacentric height. U.S. designers were more restricted in this regard than designers abroad because of the correct perception in the U.S. that the low metacentric heights needed to achieve long roll periods (see Chapter II) severely jeopardized damage stability and ship survivability.

The weakness of the O'Hanlon, et al (1973) results of Fig. 110 is that their experiments were conducted with people totally unacclimated to motion. In reality, acclimation is a vitally important parameter in determining motion sickness incidence. In a study in the Royal Navy it was shown that even at rms vertical accelerations greater than  $1.2 \text{ m/sec}^2$ , associated with  $\text{MSI} = 35$  percent in Fig. 110, motion sickness was not the governing criterion because the sailors were so acclimated to motion. It follows that the prescribed MSI values of 10 and 20 percent shown in Table 20 for monohulls, hydrofoil ships and SES are realistic only for passenger ships or for ships manned with

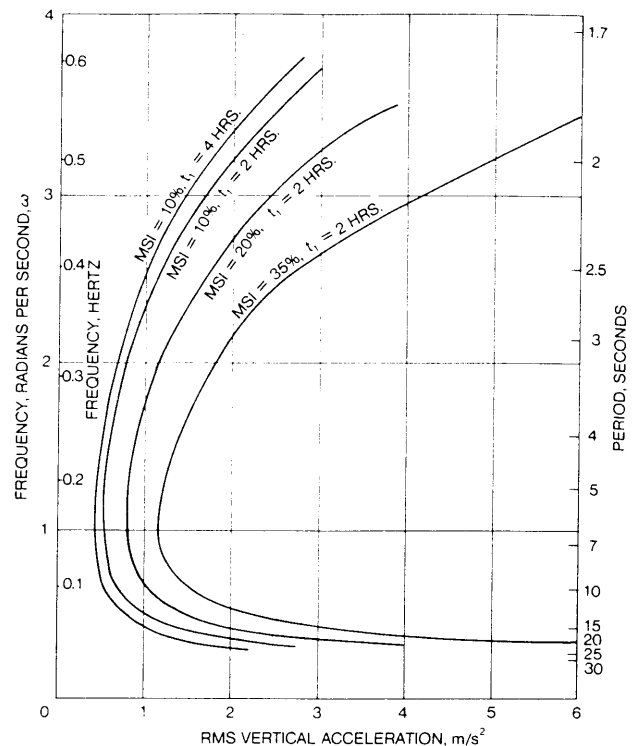


Fig. 110 Values of vertical acceleration and frequency corresponding to four specified values of Motion Sickness Index (MSI) and motion exposure time ( $t_1$ ) (Mandel, 1979)

crews unacclimated to motion. For non-passenger ships with crews acclimated to motions, it seems likely that, based on the O'Hanlon, et al data, a prescribed MSI value of 35 percent in conjunction with a  $t_1$ -value of two hours would be adequate.

Once MSI and  $t_1$ -values are prescribed, the corresponding prescribed value of the rms vertical acceleration (Criterion No. 4) can be read from Fig. 110, using the estimated synchronous roll period of the ship or new design being considered. For example, if a ship has prescribed values of  $\text{MSI} = 35$  percent and  $t_1 = 2$  hrs and a natural roll period of 10 sec (natural frequency = 0.1 hertz), the prescribed upper limit of rms vertical acceleration read from Fig. 110 is  $1.50 \text{ m/s}^2$ . For prescribed values of 20 percent and 10 percent, it drops to  $1.05$  and  $0.7 \text{ m/s}^2$ , respectively.

(f) *Criterion No. 7: Slamming acceleration.* The occurrence of severe and frequent slamming is well recognized as a limitation on sea speed in rough seas. Its severity may be judged either by the high local vertical acceleration at impact or by the subsequent vibratory response (or whipping) experienced throughout the ship, involving both accelerations and hull bending stresses. The magnitude of local slamming acceleration at impact is often used as a criterion of seakeeping performance, especially for small craft. An accelerometer record near the bow may indicate either

a distinct peak in acceleration or a relatively small response superimposed on the acceleration due to ordinary ship motions, as for a large mono-hull. The vertical motion of a light planing craft can be stopped dead by impact on the water surface, while the motion of a heavy ship will only be slightly modified.

This difference has very significant ramifications. The very large peak slamming accelerations experienced with planing craft can be injurious, even lethal, as far as personnel are concerned (Payne, 1978). On the other hand, the smaller slamming accelerations experienced by large ships are not injurious to personnel but may involve local structural damage and strong whipping stresses in the hull (Chapter IV, Vol. I).

With planing craft, slamming introduces very large upward accelerations at very frequent intervals even in moderately rough seas. A small sample of a planing craft vertical acceleration time history in Sea State No. 6, head seas, is shown in Fig. 111a. The frequent, large, upward accelerations are attributable to three planing craft features:

1. Relatively low deadrise hull shape, which results in a relatively large slamming impact area compared to a monohull.
2. Small displacement, which makes them much more responsive to impact loads.
3. High speed, which increases the frequency of wave encounter and of slamming severity in head seas.

Because the upward slamming acceleration peaks on a planing craft are so frequent and so large (greater than  $1.0g$  in Fig. 111), their Criterion No. 7 value is dictated by human fatigue and proficiency considerations, not by fear of hull damage as it is on some large monohulls. On the other hand, because slamming ac-

celerations occur so frequently with planing craft and are so severe, other seakeeping events evidently do not constrain its operations. For example, motion sickness does not appear to be an issue in high-speed planing craft ride qualities at all, probably because the low-frequency motions that induce seasickness are scarcely perceived by planing craft personnel subjected to the higher frequency, high-level slamming accelerations characteristic of these craft. Evidently, the personnel who ride planing craft are expected to tolerate a much more severe ride than personnel on other vehicle types. See Payne (1978) for a good further discussion of ride quality criteria for craft subject to frequent slamming.

Allen and Jones (1978) suggested prescribed peak of maximum values of slamming acceleration of  $4.0g$  for 100-ton planing craft (for very short exposure times of 20 minutes or less), as shown in Table 20.

The peak slamming vertical acceleration value of  $0.5g$  prescribed by Stark (1977) in Table 20 for hydrofoil craft (of unspecified size) in the foilborne condition for longer periods of time is far below the peak value of  $4.0g$  suggested by Allen and Jones (1978) for 100-ton planing craft. Stark's low prescribed value is a reflection of his firm view that slamming vertical acceleration represents the most severe constraint on hydrofoil seaway performance. His low prescribed value is intended to insure that human fatigue will not play a role in evaluating the quality of the hydrofoil ride in rough seas. Note the total absence of any peak slamming acceleration in the hydrofoil motion time history shown in Fig. 111b in extremely severe, Sea State 8, head seas.

Stark's concern with slamming acceleration is associated with the fact that as the foils of a hydrofoil

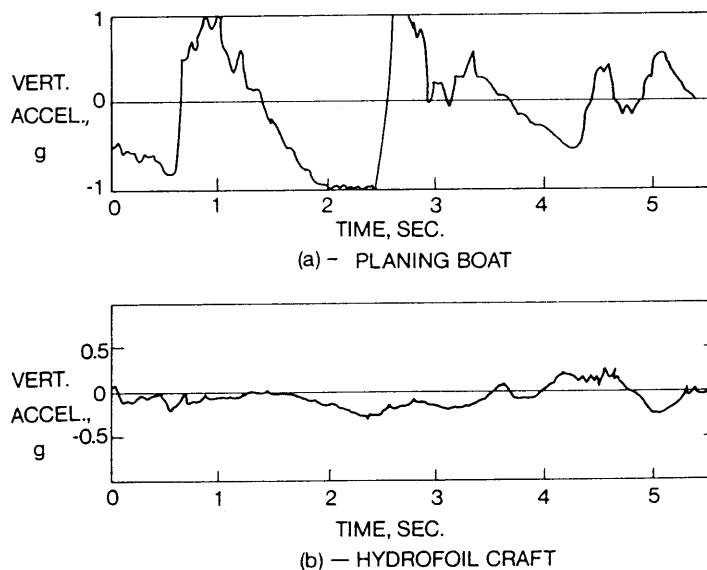


Fig. 111 Typical time histories of the vertical acceleration of a planing boat and a hydrofoil craft in head seas of stated severities (Mandel, 1979)

ship come close to the surface in rough water, they may emerge and the lift they provide may momentarily go to zero. This condition is referred to as *foil broaching*. For severe broaches, large downward vehicle accelerations will occur and subsequent to a broach, the hull itself will slam into the oncoming wave crest. The upward acceleration associated with this slam will be larger than the downward accelerations associated with broaching. The values of the slamming acceleration peaks thus become the constraining limit on hydrofoil operations in extremely severe seas.

SES's and ACV's also experience slamming. In heavy seas, the pitch angle of these vehicles may become so large that there is leakage of cushion air from under the bow seal. If this occurs, the resulting downward acceleration of the bow will cause large slamming accelerations.

The prescribed slamming acceleration peak value of  $0.6g$  for the 2,000–3,000-ton SES in Table 20 conforms to the values ( $0.55g$  to  $0.70g$ ) for 2,000–3,000-ton vehicles given by Allen and Jones (1978). Mandel (1979) gives a similar value for an ACV. As with hydrofoils, the effect of slamming accelerations on personnel fatigue and crew proficiency is a cause of very serious concern with SES vehicles, and active motion alleviation systems may be essential for them.

Allen and Jones (1978) suggest that the prescribed peak value of the slamming acceleration should be a function of ship size to reflect the very different impact of slamming on large ships, like monohulls, compared to small ships like planing craft. Hence they suggest an extreme peak-to-mean value of  $0.5g$  for 4,000-ton monohulls. In this case slamming introduces large impact pressures acting on a limited area of the ship's bottom which may cause local ship structural damage, or it may introduce large whipping stresses in the ship's hull. However, slamming generates smaller relative upward acceleration peaks on monohulls than on planing craft because of the usually larger size (displacement) of monohulls and their hull shape which greatly reduces the area of the hull impacted by a slam. As previously noted therefore, the motion of a ship is only slowed by a slam, not stopped as is often the case with planing craft.

In spite of the emphasis on peak values of acceleration in the previous paragraph, the prescribed values of slamming acceleration given in Table 20 for monohulls are single amplitude rms accelerations, not peak values. Unfortunately these are the only values recorded in the literature for these ship types.

The prescribed value of  $0.2g$  rms for monohulls in Columns (1), (7) and (9)–(12) of Table 20 were calculated from spectral analysis of vertical acceleration records taken during special trials of a large container ship and reported by Aertssen and van Sluijs (1972). During these trials, the ship motions became so severe that the captain slowed the ship, fearing slamming damage to the hull. The actual rms vertical accelera-

tion value of  $0.2g$  obtained from records in this sea state was, therefore, taken as the prescribed value of Criterion No. 7 for monohulls. However, this should be taken as only a rough guide for large ships; the frequency of slamming (Criterion No. 8), or the magnitude of midship slam stress, may be considered more reliable for such ships (Aertssen, 1968). The prescribed values for trawlers and cross-channel vessels (columns 13 and 14) are also from Aertssen (1968).

(g) *Criterion No. 8: Slamming frequency.* While peak slamming acceleration is an adequate criterion for part of the ride quality evaluation of SES, hydrofoil, and planing craft, it is not an adequate criterion for assessing the importance of slamming on large monohull and SWATH ships. In the opinion of Aertssen and van Sluijs (1972), and other investigators, it is the frequency of occurrence of severe slams, in addition to excessive slamming accelerations and vibratory whipping that induces a ship captain to slow his ship's speed or change its course. Tick (1958) and others postulated that a severe slam occurs on monohulls when two events occur simultaneously. These two events are:

- Reentry of the ship's bow into the water after it has risen above the surface.
- The relative vertical velocity between the ship's flat of bottom and the water surface exceeds a certain critical specified value.

This critical vertical velocity value, according to Ochi and Motter (1973), is 12 ft per sec (3.66 m/s) for a 520-ft (158m) ship, at a point 15 percent of length from the bow. Calculations indicate that the Ochi, Motter critical velocity corresponds to a slam of considerable magnitude. For ship lengths other than 158m., the value of the critical vertical velocity may be obtained by means of Froude scaling. The location at which this velocity is to be measured actually depends on hull fullness and particularly on the extent of the flat of bottom (Section 5).

A method of predicting the joint probability of forefoot emergence and relative vertical velocity exceeding a critical value is given by Ochi (1964) and Ochi and Motter (1973). Aertssen (1968) states that a commercial ship captain will slow down or alter course if a severe slam occurs more frequently than 3 to 6 times in 100 ship-wave encounters, depending on the type of vessel, as shown in Table 20. A frequency of 3 times in 100 cycles is equivalent to one slam every 2 to 5 minutes, or a slamming frequency of 12–30 per hour, depending on ship size. Since pitch natural period tends to increase with length of ship (Mandel, 1960), the number of pitch cycles per unit time tends to decrease with increasing length. The range 12–30 per hour spans the average value given in Columns (2) and (8), from Comstock, et al (1980). Bales (1978) suggests similar values.

Fig. 111 shows an interval of only 1.7 seconds between two slams of a planing craft, corresponding to



a frequency of 35 slams per minute. This should be compared to the prescribed slam frequency (Criterion No. 8) value of 12 to 30 slams per hour for monohulls, given in the previous paragraph.

In the case of SWATH ships, Criterion No. 8 is not related to slamming frequency but rather to the frequency of contact between a wave and the underdeck of the cross structure of the SWATH. Evidently, the flat underdeck of this structure and the confinement of the water by the side struts cause wave contact to be a significant seakeeping event for SWATH ships. According to Lamb (1975), the prescribed frequency of wave contacts for SWATH's occurs when the average of the 1/10-highest values of the relative vertical displacement, between the underdeck of the SWATH and the rough sea surface beneath it, exceeds the smooth water clearance to the underdeck.

Olson (1977) results show for the SWATH ship of Table 20 that this prescribed value resulted in Criterion No. 8 being the governing criterion for the SWATH ship functions of Table 20, at all ship-wave heading angles between 130 and 230 deg (180 deg represents ahead seas) in more than 20 out of a possible 32 cases. Thus wave contact is a very significant seaway performance criterion for SWATH ships.

(h) *Criterion No. 9 Frequency of sonar dome emergence.* While the ping of a sonar is a short pulse, a long listening period, called the ping interval, is required after the ping in order to be able to detect the returning target echo. The duration of the ping interval is a direct function of the range of the sonar and the speed of sound in water. If an active search is being conducted out to a range of 10 miles, Olson (1977) suggests a ping interval of about 30 seconds. In order to receive an echo back from a target located anywhere from 0 to 10 miles away, the sonar dome must remain completely submerged during the entire ping interval. For longer sonar ranges, the sonar dome must remain completely submerged for much longer intervals (Fig. 12 of Section 7.7).

The prescribed value of Criterion 9 in Table 20 is 120 sonar dome emergences per hour, which corresponds approximately to Olson's (1977) ping interval of 30 seconds. Of course, the prescribed value of 120 emergences per hour does not insure that all ping intervals will be longer than 30 seconds. If this sacrifice in precision is not acceptable a more refined probability-based solution could be obtained. Although time-domain calculations may seem to provide a more definite answer, they actually must be repeated many times to provide a reliable statistical conclusion.

(i) *Criterion No. 10: Deck wetness frequency.* Olson (1977) states, "... it is suggested that ships rarely choose to take green water over the bow more than once every 2 to 5 minutes especially if gun mounts, missile launchers, or major deck equipment are located forward." Thirty wetnesses per hour was selected by Olson as the prescribed value for mono-

hulls. Bales (1978) suggests a similar value, but Andrew and Lloyd (1981) suggest 90 wetnesses per hour for the prescribed value for frigates, and Aertssen, in a discussion of the Andrew and Lloyd paper, suggests 36 wetnesses per hour as the prescribed value for container ships, or 5 per 100 cycles (Aertssen, 1968).

Olson's results show that for the four destroyer-like ships he analyzed, his prescribed value resulted in deck wetness being the governing criterion in only six out of a possible 80 cases at ship-wave heading angles between 160 and 200 deg. According to Table 20, deck wetness is evidently an important seaway performance criterion only for monohulls.

(j) *Criterion No. 11: Propeller emergence.* Propeller emergence in severe seas, resulting in propeller racing, is a common event with single-screw merchant ships, particularly those that are diesel propelled, and with SWATH ships. By observing when the chief engineer ordered a reduction in propeller RPM because of racing, Aertssen (1966) established for a single-screw diesel cargo ship a prescribed value of 25 propeller emergences per 100 ship oscillations.

According to Olson (1977), the criterion for SWATH ships is the probability that the vertical displacement of the propeller relative to the free surface of the water will not cause more than 25 percent of the disk area of the propeller to emerge. This prescribed value for the 3,350-ton SWATH ship of Table 20, according to Lamb (1975), corresponds to the significant value of vertical displacement of the propeller relative to the surface of the water not exceeding 12.8 ft (3.90 m).

Olson's results show that with this prescribed value propeller emergence is a significant governing criterion for the SWATH ship transit function of Table 20 at all ship-wave heading angles. At ship-wave heading angles between 0 (360 deg) and 110 deg (250 deg), it is the governing criterion in well over a fourth of the 32 SWATH cases.

(k) *Criterion No. 12: Rms relative vertical velocity.* The prescribed value of Criterion No. 12 is intended to limit the maximum impact forces sustained by the helicopter landing gear during recovery operations. According to Olson (1977) the maximum allowable significant relative velocity between the SH2F (Lamps) helicopter and the flight deck is approximately 12 ft/sec (3.65 m/s). This corresponds to the prescribed 1.83 m/s rms value given in Column 7 for monohulls in Table 20. Since the SH2F helicopter has a sink rate of 5 ft/sec (1.52 m/s), this implies a limiting significant vertical velocity of the ship relative to the earth of 2.13 m/s (7 ft/sec). Although Olson's results show that with the 1.83 m/s rms prescribed value, Criterion No. 12 was never a governing criterion for the monohulls he treated, it was the major governing criterion for SWATH ships at ship-wave heading angles between 85 deg (275 deg) and 120 deg (240 deg). However, more recent NAVSEA analysis has shown

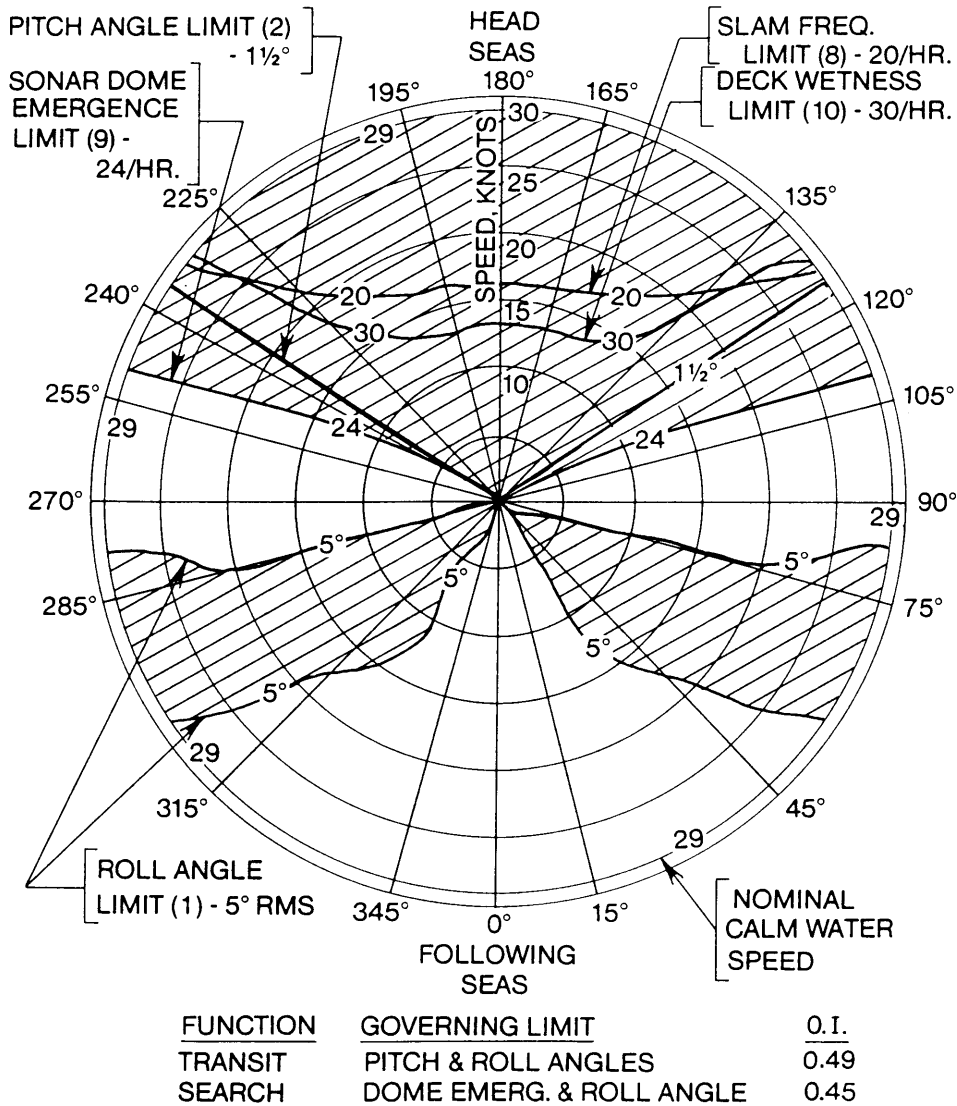


Fig. 112 Speed-polar plot, showing Seakeeping Operating Envelopes (SOE) and Operability Index (O.I.) values for a destroyer in sea state 6. (Transit and/or sonar search functions)

that with a lower prescribed significant value of 0.67 m/s (flight deck with respect to the earth), Criterion No. 12 is the governing criterion for a destroyer performing the helicopter recovery function at all ship wave heading angles between 70 deg and 290 deg (head seas correspond to 180 deg). This is shown subsequently in Fig. 115b. Comstock, et al (1980) give a limiting value for monohulls of only 1.0 m/s, Column (8).

**7.7 Steps in Obtaining the Seakeeping Performance Index SPI-1.** So far in Section 7 we have dealt primarily with the concept of seakeeping performance criteria, the nature of these criteria for different ship missions, available data on limiting or prescribed values of the criteria, and methods of using available theoretical techniques to calculate actual short-term responses.

These steps permit us to predict performance in assumed conditions under which ship loading, sea state, ship speed and heading remain essentially constant and hence to evaluate short-term performance. We are now ready to proceed to the problem of evaluating long-term seakeeping performance, considering profiles of missions, loadings, sea conditions, headings and speeds, in short, determining values of a Ship Performance Index, as defined and discussed in Sections 7.1 and 7.3, for any new or existing ship design. This can be accomplished in various ways, but the method of Comstock, et al (1980), as effectively used in U.S. Navy preliminary design, will be described here.

(a) *Speed polar plot.* The first step is to adopt a method of presenting results of many short-term performance evaluations (Section 7.3) in a convenient manner. This can be done by means of the *Speed Polar*

Plot utilized extensively by Comstock, et al (1980), which is an ideal vehicle for displaying the boundaries between ship speeds and ship-wave heading angles associated with acceptable motions and those associated with unacceptable motions in a particular sea state. Here "acceptable" is used in the sense that the prescribed values correspond to impairment of function if the prescribed value is exceeded, i.e., that the ship is operable (Section 7.4).

Fig. 112 shows such a speed polar plot for a large destroyer performing the transit and sonar search functions in rough seas corresponding to Sea State Number 6. The limits on ship's speed and heading angle imposed by the Comstock, et al (1980) prescribed values of Criteria Numbers 2, 8 and 10 of Table 20, Column 2, are shown on Fig. 112, as well as the limits on ship's speed and heading angle imposed by a prescribed rms roll value of 5 deg on Criterion Number 1 (in lieu of 4 deg by Comstock, 1980) and by a prescribed value of 24 sonar dome emergences per hour imposed by Criterion Number 9 (in lieu of 120 per hour by Olson, 1977). It is clear from Fig. 112 that for the sonar search function the latter two criteria (i.e., 1 and 9) with their prescribed values are the governing criteria for this particular destroyer. For the transit function alone, Fig. 112 shows that the roll angle limit of 5 deg and the pitch angle limit of  $1\frac{1}{2}$  deg make Criteria Nos. 1 and 2 the governing criteria.

(b) *Seakeeping operating envelope.* The boundary of the operable regime of speeds and headings, shown unshaded in Fig. 112 (for the sonar search function), is called the *Seakeeping Operating Envelope* (SOE) (Comstock, et al 1980). Roughly speaking, the bigger the unshaded area within the SOE the better the seakeeping performance of the ship. But more quantitative conclusions can also be drawn; for example, it is clear that at certain ship-wave heading angles, operability is independent of speed (e.g., 0, 90, 270 deg in Fig. 112). On the other hand, with speed fixed there are some headings that are operable and some that are not. Furthermore, the fraction of time the ship is able to perform its stated function at a particular speed and sea state can be obtained, assuming equal probability of all headings, by taking the ratio of the total angle subtended by the unshaded arcs around any constant-speed circle to 360 deg. Thus at a speed of 10 knots the designated sonar search function will not be constrained in Sea State 6 by seakeeping considerations in about 39 percent of all possible ship-wave heading angles; at 15 knots this increases to 42 percent and at all speeds between 20 to 29 knots to about 45 percent. These values correspond to what Comstock, et al (1980), call the *Operability Index* (OI), based on the assumption that all possible heading angles are equally probable for the sonar search function. If, in addition, use of all possible speeds were equally probable for the sonar search function, the OI value in Sea State 6 would be ap-

proximately equal to the ratio of the unshaded area of Fig. 112 to the area of the whole polar diagram. The ratio of those areas for the sonar search function in the figure is 0.45.

(c) *Operability Index.* Data like those shown in Fig. 112 are needed to calculate OI even if all speeds and all headings are not equally probable. To determine the value of OI for other distributions of speed and heading angle it is necessary to segregate the speeds and headings of Fig. 112 into discrete elemental areas and to estimate (visually if necessary) the local probability,  $p_i$ , within each elemental area that the ship's function can be accomplished. For example the value of  $p_i$  within the elemental area

$$\int_{10 \text{ kts}}^{15 \text{ kts}} \int_{165^\circ}^{180^\circ} dV d\mu$$

is zero, whereas the  $p_i$  value within the elemental area

$$\int_{25 \text{ kts}}^{29 \text{ kts}} \int_{75^\circ}^{90^\circ} dV d\mu$$

is approximately 0.5.

It is also necessary to specify the probable fractions of time,  $p_v$  and  $p_\mu$  that the ship will travel at each combination of speed and heading angle, respectively.

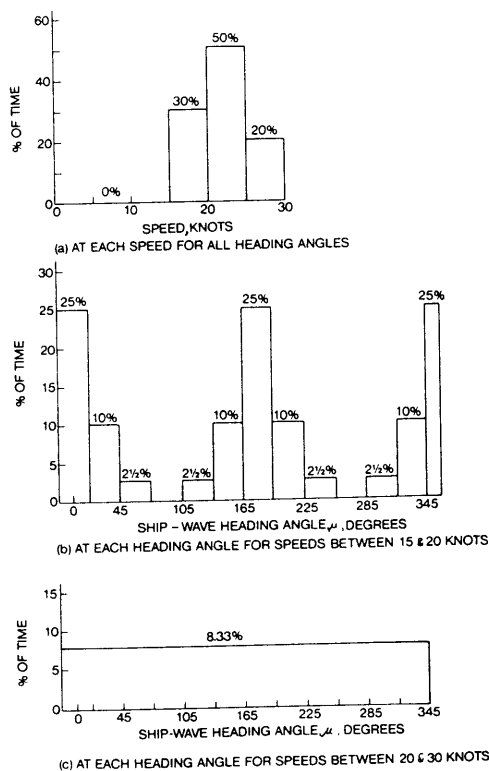


Fig. 113 Sample specifications of probable fractions of time at various ship speeds and ship-wave heading angles (sea state 6)

An example of such specification with elemental areas contained within broadband widths of 5 knots and 30 deg heading angle is shown on Fig. 113. Assuming the variables to be independent, the data of Figs. 112 and 113 may be combined to calculate the overall OI for any specified distribution of speeds and heading angles thus,

$$OI = \sum_v \sum_\mu p_i \times p_v \times p_\mu \quad (237)$$

Table 21 shows for the destroyer of Fig. 111 performing the sonar search function that the overall OI value in Sea State Number 6 for the speed and heading distributions of Fig. 112 is 0.453 (Row 15, Col. 11). The value in Col. 10, Row 16 of Table 21 indicates that the overall OI value, if all speeds between 15 and 30 knots and all headings were equally probable, is virtually the same in this case. If all speeds between zero and 30 knots and all heading angles were equally probable, the OI value is 0.45 for the sonar search function, as indicated in Fig. 112. On the other hand, if the ship-wave heading angles are restricted to head and bow seas ( $120 \text{ deg} \leq \mu \leq 240 \text{ deg}$ ), the OI value is reduced to zero for any speed or combination of speeds.

For the transit alone function, the OI value calculable from Fig. 112 increases (in Sea State 6) to over 0.50, assuming equal probability of all possible speeds and headings, but only to 0.02 if the heading angles are restricted to  $120 \text{ deg} \leq \mu \leq 240 \text{ deg}$ .

The operational significance of these OI values is that they correspond to the expected fraction of time (or probability) that a ship can perform its designated ship functions in the designated sea state. That is, assuming that all ship speeds and all ship-wave headings are equally probable, the destroyer of Fig. 112 can be expected to perform the sonar search function, at most, for 45 percent of the total time it operates in Sea State Number 6. This restriction is imposed solely by seakeeping considerations. Other important factors, such as visibility conditions, equipment failures, etc., which must be taken account of in the overall operational evaluation of the ship, will restrict this fraction of time even more.

Plots similar to Fig. 112 can be prepared for sea states other than Sea State 6, thus providing a concise picture of conditions for acceptable and for unacceptable short-term performance—or operability—for one or more ship functions. A number of OI curves can then be plotted against Sea State Number, each for a different ship speed, provided equal probability of use of all possible ship-wave heading angles is assumed. This is done in Fig. 114 at 10, 20 and 30 knots for five ships of increasing displacements, all performing the full combat-support mission of Bales-Cieslowski (1981). The hull forms of all five ships correspond to the “optimum” Bales-Cieslowski seakeeping hull. Using Fig. 114 one can assess performance by interpolation, assuming equal probability of all possible ship-wave

heading angles, under a variety of conditions, such as:

- What is the highest speed at which a ship of 16,000 t can be expected to carry out full combat support in Sea State 6 at least 75 percent of the time? (16 knots).
- What is the highest sea state in which a ship of 1,000 t can be expected to carry out full combat support at a sea speed of 20 knots at least 75 percent of the time? See also McCreight and Stahl (1985) (4 t).

Fig. 115 shows the Seakeeping Operating Envelopes for two ship functions in addition to the two shown in Fig. 112. Fig. 115(a) is for the at-sea-replenishment function in Sea State Number 5 and Fig. 115(b) is for the helicopter launch and recovery function in Sea State Number 6. In preparing both figures the prescribed values of Criteria 8 and 10 of Table 20, Column 2 were considered. In addition, Fig. 115 utilizes the values in Table 22 for Criteria 1, 2 and 12:

Trends of Operability Index with sea state number for the destroyer of Figs. 112 and 115 are shown for four ship functions in Fig. 116. In this figure the shape of the curves was approximated by following the trend of the 8,000-t optimum hull of Bales and Cieslowski (1981) shown in Fig. 114, replotted as a solid curve in Fig. 116.

(d) *Seakeeping Performance Index SPI-1*. The Mission Effectiveness Index, SPI-1, introduced in Section 7.1, is computed by summing the OI values for the ship function weighted by the probabilities,  $p_s$  (expected frequency of occurrence), of the sea state conditions in which that function is to be carried out. This will provide a value of SPI-1 for the particular ship function considered. If the evaluation is to cover a number of ship functions, another factor,  $I_R$ , must be included that represents the relative importance of that function. Equation (238) expresses this mathematically, and Table 23 is a sample calculation,

$$SPI-1 = \sum_{\text{All Functions}} \sum_{\text{All Functions Sea States}} OI \times p_s \times I_R \quad (238)$$

The values of OI as functions of sea state utilized in Table 23 for the four ship functions of Figs. 112 and 115 were obtained from Fig. 116. Table 23 also incorporates the following two simplifying assumptions:

- The same distribution of sea state severity (given in the 1st column) applies for all four ship functions.
- Use of all possible ship speeds and ship-wave heading angles is equally probable for each of the ship functions.

If the first assumption is not valid, then new data for Column (1) of Table 23 must be estimated for each ship function and incorporated into the calculation. These data may be obtained from the information on sea state frequency of occurrence in the Northern Hemisphere (S. Bales, et al 1981). (See also Section 2.)

Table 21—Sample Computation of the Value of the Operability Index (OI) for the Destroyer of Fig. 112 Performing the Sonar Search Function in Sea State 6.

		Ship Speeds									Calculation of Values of O.I.	
		15-20 Knots			20-25 Knots			25-30 Knots				
Column No.		1	2	3	4	5	6	7	8	9	10	11
Row No.	Ship-Wave Heading Angle, $\mu$ , deg (See Fig. 113)	$p_i$ (Estimated From Fig. 113)	$p\mu$ (See Fig. 114b)	Cols. 1 $\times$ 2 (Rows 1-12 Only)	$p_i$ (Estimated From Fig. 113)	$p\mu$ (See Fig. 114c)	Cols. 4 $\times$ 5 (Rows 1-12 Only)	$p_i$ (Estimated From Fig. 113)	$p\mu$ (See Fig. 114c)	Cols. 5 $\times$ 6 (Rows 1-12 Only)	Cols 1 + 4 + 7	Cols 3 + 6 + 9 OI Value For Various Headings
1	345-15	1.00	.250	0.250	1.00	.0833	0.0833	1.00	.0833	0.0833	3.00	0.4167
2	15-45	0.94	.100	0.094	1.00	.0833	0.0833	1.00	.0833	0.0833	2.94	0.2607
3	345-315	0.94	.100	0.094	1.00	.0833	0.0833	1.00	.0833	0.0833	2.94	0.2607
4	45-75	0.02	.025	0.000	0.15	.0833	0.0125	0.31	.0833	0.0258	0.48	0.0383
5	315-285	0.02	.025	0.001	0.15	.0833	0.0125	0.31	.0833	0.0258	0.48	0.0389
6	75-105	0.99	0	0	0.91	.0833	0.0758	0.72	.0833	0.0600	2.62	0.1358
7	285-255	0.99	0	0	0.91	.0833	0.0758	0.72	.0833	0.0600	2.62	0.1358
8	105-135	0.23	.025	0.006	0.18	.0833	0.0150	0.15	.0833	0.0125	0.56	0.0335
9	255-225	0.23	.025	0.005	0.18	.0833	0.0150	0.15	.0833	0.0125	0.56	0.0334
10	135-165	0	.100	0	0	.0833	0	0	.0833	0	0	0
11	225-195	0	.100	0	0	.0833	0	0	.0833	0	0	0
12	165-195	0	.250	0	0	.0833	0	0	.0833	0	0	0
13	Sums of Rows 1 thru 12	5.36	1.000	0.450	5.48	1.000	0.4566	5.36	1.000	0.4466	16.20	1.3534
14	$p_v$ (see Fig 114a)			0.30	—	—	0.50	—	—	0.20	—	—
15	Row 13 $\times$ 14			0.1350	—	—	0.2283	—	—	.0893	—	0.4527

NOTES: Table is based on Equation (237) and the speed and heading distribution given in Fig. 114. Summation in row 15 gives O.I.

OI Value Assuming Equal Probability of all Speeds and Headings: Row 13, Col 10  $\div$  36\* = 0.450

\* 12 Bands of heading angles times 3 bands of speeds = 36.

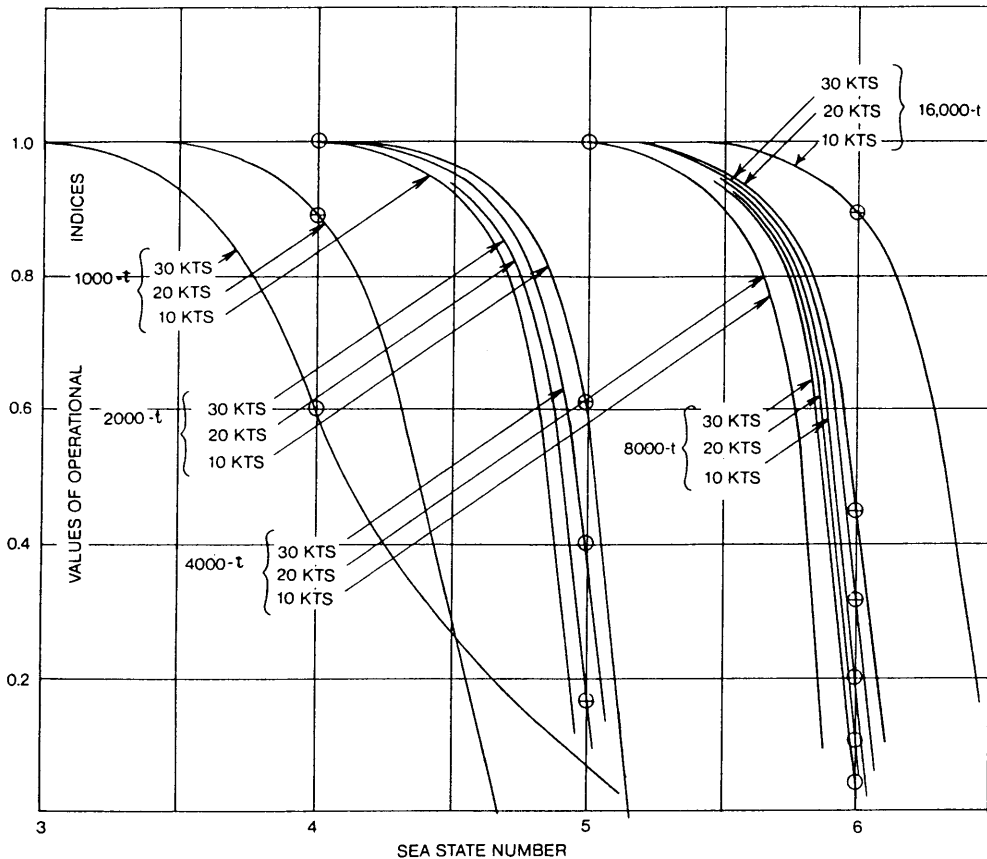


Fig. 114 Approximate trends of the Operating Index (O.I.) for an "optimum" seakeeping hull as a function of sea state, ship speed and ship size

NOTE: Plots are for the full combat support mission, Criteria Set A of Bales/Cieslowski (1981), assuming equal probability of all possible heading angles

This reference gives data on sea state occurrence in terms of the joint probability of occurrence of significant wave height and wave modal period as a function of time, location and season for all NATO operating areas. If the second assumption is not valid, then OI values as a function of sea state, similar to those of Fig. 116, must be calculated for the desired distribution of ship speeds and ship-wave heading angles, in accordance with the procedure of Equation (237) outlined

in Table 20. These data must then be utilized in place of the data given in Columns (2), (5), (8) and (11) of Table 23.

As indicated in Section 7.1, SPI-1 has very important quantitative operational significance. Its value is the probability or expected fraction of total time that the operational mission for which the ship was designed can be performed while in its operating area, subject to the constraints imposed by the seaway on the performance of the ship and its systems. As previously noted, other performance limitations may be even more severe constraints, but the percent of time measured by SPI-1 can never be exceeded unless the ship is altered or unless that part of its operating doctrine determined by the prescribed values of the seaway performance criteria is changed. Hence, it is a unique quantitative measure of the operational utility of a ship and is ideally suited to assess the seakeeping performance of most ships not engaged in the routine transportation of goods or people.

Calculated SPI-1 values for notational ships, capable of launching, recovering and supporting various types of naval aircraft are compared by Comstock, et al

Table 22—Criteria 1, 2 and 12

Criterion	Prescribed rms Limiting Values, Fig. 115	
	(a)	(b)
1. Roll Angle, deg.	2.5	6.8
2. Pitch Angle, deg.	1.0	1.35
12. Vertical Velocity	—	0.67 m/sec. (2.2 ft/sec)

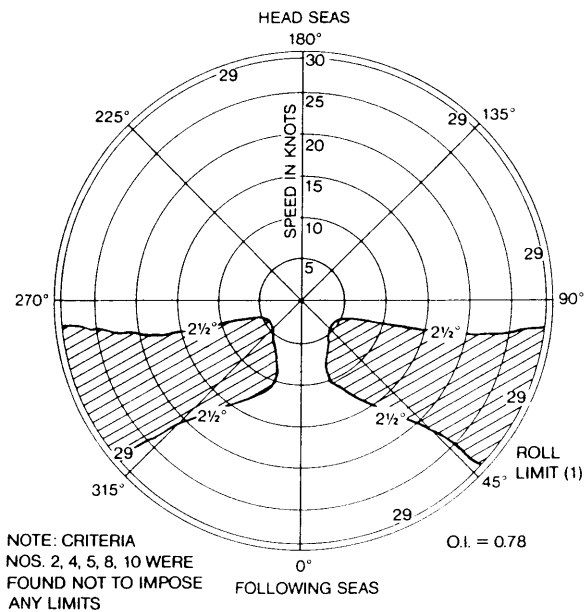
Note: Only Criterion No. 1 appears in Fig. 115a because in Sea State 5 the other criteria do not actually impose any limitations.

Table 23—Sample Computation of SPI-1 for a Destroyer Performing Four Ship Functions

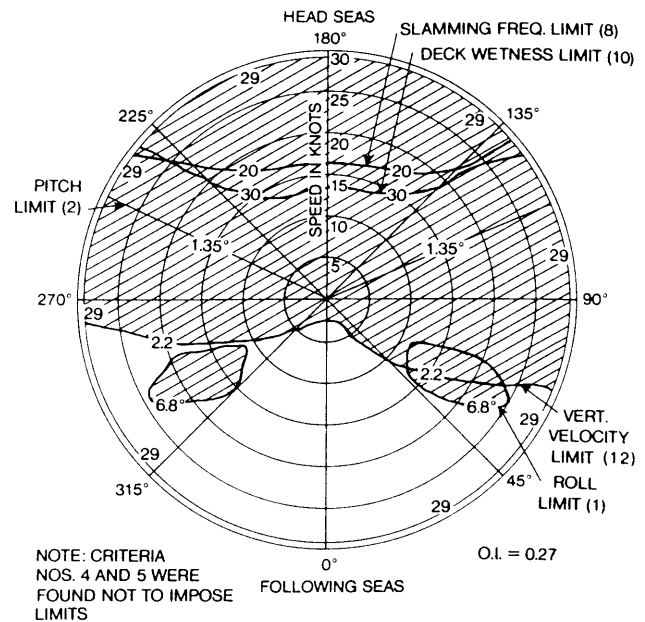
Row No.	Ship Functions		1. Transit			2. Sonar Search			3. At Sea Replenishment			4. Helicopter Operations			SPI-1
0	$I_R$ Value (Assumed)		0.40			0.25			0.10			0.25			
	Col. No.	1	2	3	4	5	6	7	8	9	10	11	12	13	14
					Col 3 $\times$ $I_R$ Value From Row 0			Col 6 $\times$ $I_R$ Value From Row 0			Col 9 $\times$ $I_R$ Value From Row 0			Col 17 $\times$ $I_R$ Value From Row 0	Col 4 + 7 + 10 + 13
	Sea State Number	Probabil- ity of Sea State	Value of O.I. Fig. 116	Col 1 $\times$ Col 2		Value of O.I. Fig. 116	Col 1 $\times$ Col 5		Value of O.I. Fig. 116	Col 1 $\times$ Col. 8		Value of O.I. Fig. 116	Col 1 $\times$ Col 11		
1	0-1	0	1.00	0	0	1.00	0	0	1.00	0	0	1.00	0	0	
2	1-2	0.057	1.00	0.057	0.023	1.00	0.057	0.014	1.00	0.057	0.006	1.00	0.057	0.014	
3	2-3	0.197	1.00	0.197	0.079	1.00	0.197	0.049	1.00	0.197	0.020	1.00	0.197	0.049	
4	3-4	0.283	1.00	0.283	0.113	1.00	0.283	0.071	1.00	0.283	0.028	1.00	0.283	0.071	
5	4-5	0.195	1.00	0.195	0.078	1.00	0.195	0.049	0.78	0.152	0.015	1.00	0.195	0.049	
6	5-6	0.175	0.49	0.086	0.034	0.043	0.075	0.019	0	0	0	0.27	0.047	0.012	
7	6-7	0.076	0	0	0	0	0	0	0	0	0	0	0	0	
8	7-8	0.017	0	0	0	0	0	0	0	0	0	0	0	0	
9	> 8	0.001	0	0	0	0	0	0	0	0	0	0	0	0	
10	Sum of Rows 1-9	1.00	—	0.818	0.327	—	0.807	0.202	—	0.689	0.069	—	0.779	0.195	$\Sigma 0.793 = \text{SPI}-1$

NOTES: Table is based on using Equation (238, Figs. 112, 115 and 116, and the two simplifying assumptions given in the text.

Summation in Row 11 gives SPI-1 for Relative Importance  $I_R$  given in Row 0.  
 SPI-1 Value for the Same Relative Importance of all Ship Functions in Given by Sum of Values of Cols. 3, 6, 9 & 12 of Row 10  $\div 4 = 0.773$



(a) PERFORMING AT - SEA REPLENISHMENT IN SEA STATE 5



(b) ENGAGED IN HELICOPTER OPERATIONS IN SEA STATE 6

Fig. 115 Seaking Operating Envelopes (SOE) for other functions of the destroyer of Fig. 113

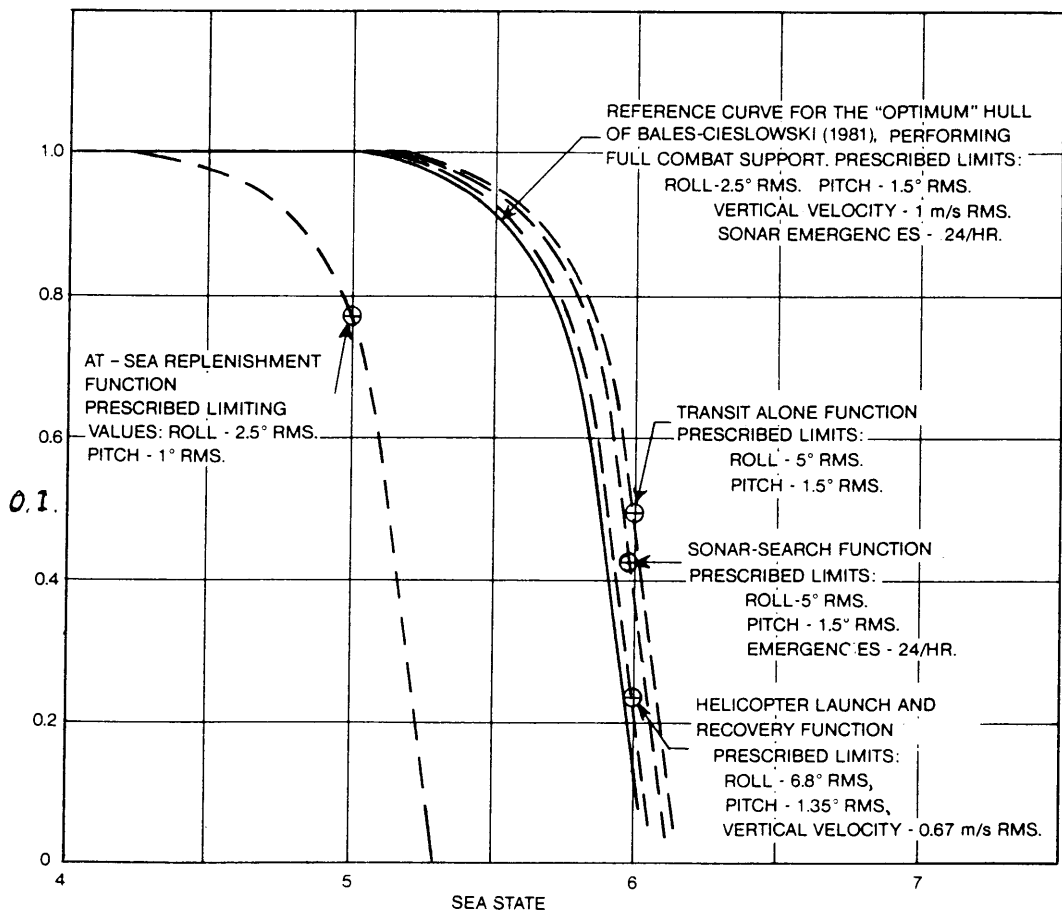


Fig. 116 Approximate trends of O.I. as a function of sea state for four destroyer functions, based on Figs. 113 and 116 (assuming equal probability of all possible ship speeds and wave heading angles)



(1980). The calculations are based on the same two simplifying assumptions stated in connection with Table 23. The Comstock work presents results for a 20,000-ton aircraft carrier of SWATH configuration and for monohull destroyers and aircraft carriers varying in displacement from 7000 to 95,000 tons. The SPI-1 values show a significant degradation with decreasing size for monohull ships handling vertical takeoff and landing aircraft from SPI-1 = 0.91 for a 95,000-ton aircraft carrier to 0.87 for a 20,000-ton aircraft carrier down to SPI-1 < 0.5 for a 7,000-ton destroyer. In contrast, the study shows an SPI-1 value of 0.99 for a 20,000-ton SWATH aircraft carrier.

**7.8 The Seakeeping Performance Index, SPI-2.** The Transit Speed Measure, SPI-2 of Section 7.1, is appropriate for assessing the overall seaway performance of the vast majority of ships of the world, i.e., those engaged in point-to-point transportation of goods and people. As noted in Section 7.2, SPI-2, unlike SPI-1, involves both involuntary and voluntary speed reductions. Thus, in addition to the performance criteria and their prescribed values, the calculation of SPI-2 may also involve consideration of added resistance and reduced available power in a seaway. These involuntary

speed reduction factors are discussed in Section 5, and, if necessary, the procedures outlined there may be used to estimate their value.

As seen in Figs. 108 and 109 the involuntary speed reductions usually apply mainly in moderate, not severe, seas. They, therefore, often have a smaller effect on ship speed than do the voluntary speed reductions. Hence the value of SPI-2 is not very sensitive to the values of the involuntary speed reductions. For this reason, only the calculation of the voluntary speed reductions is generally carried out during the design stage of moderate and high-speed ships. The situation may be different for large, full, slow-speed bulk carriers, where involuntary speed reductions govern.

Voluntary speed reductions can be calculated in the design stage by the procedures of Sub-Section 7.7. As in that section the first step is to construct SOE diagrams similar to Fig. 113 for the transit-alone function in seas of progressively increasing severity. Figs. 117(a)–(c) show such calculated SOE diagrams in sea states 5, 6 and 7 for a 4,000-t monohull whose hull form corresponds to the “optimum” seakeeping hull (Bales-Cieslowski, 1981).

Fig. 117d shows the SOE diagram for a 4,000-t mo-

Table 24—Sample Computation of SPI-2 (Expected Speed Fraction) for the Two Ship Hulls of Fig. 118.

Sea State Number	0-4	5	6	
Sea State Probability, <i>ps</i>	0.537	0.195	0.175	0.076

(a) 4,000-t Optimum Hull of Bales—Cieslowski (1981)

Ship-Wave Heading Angles, deg	Attainable Ship Speeds From Fig. 117—(Optimum Roll Only)				Sum of Speeds, Weighted
10	25	25	25	0	22.68
30	25	25	25	0	22.68
50	25	25	25	0	22.68
70	25	25	25	0	22.68
90	25	25	25	0	22.68
110	25	25	25	0	22.68
130	25	25	25	0	22.68
150	25	25	16	0	21.10
170	25	25	6	0	19.35

Sum over 9 Headings = 799.21  
Average Speed Over all Hdgs =  $799.21 \div 9 = 22.13$  kts.  
SPI-2 =  $22.13/25 = 0.885$

(b) 4,000-t Anti-Optimum Hull of Bales—(Ieslowski (1981)

10	25	25	25	0	22.68
30	25	25	25	0	22.68
50	25	25	25	0	22.68
70	25	25	25	0	22.68
90	25	25	15	0	20.93
110	25	25	0	0	18.30
130	25	25	0	0	18.30
150	25	25	0	0	18.30
170	25	25	0	0	18.30

Sum over 9 Heading = 184.85  
Average Speed Over all Headings =  $184.85 \div 9 = 20.54$  kts.  
SPI-2 =  $20.54/25 = 0.822$

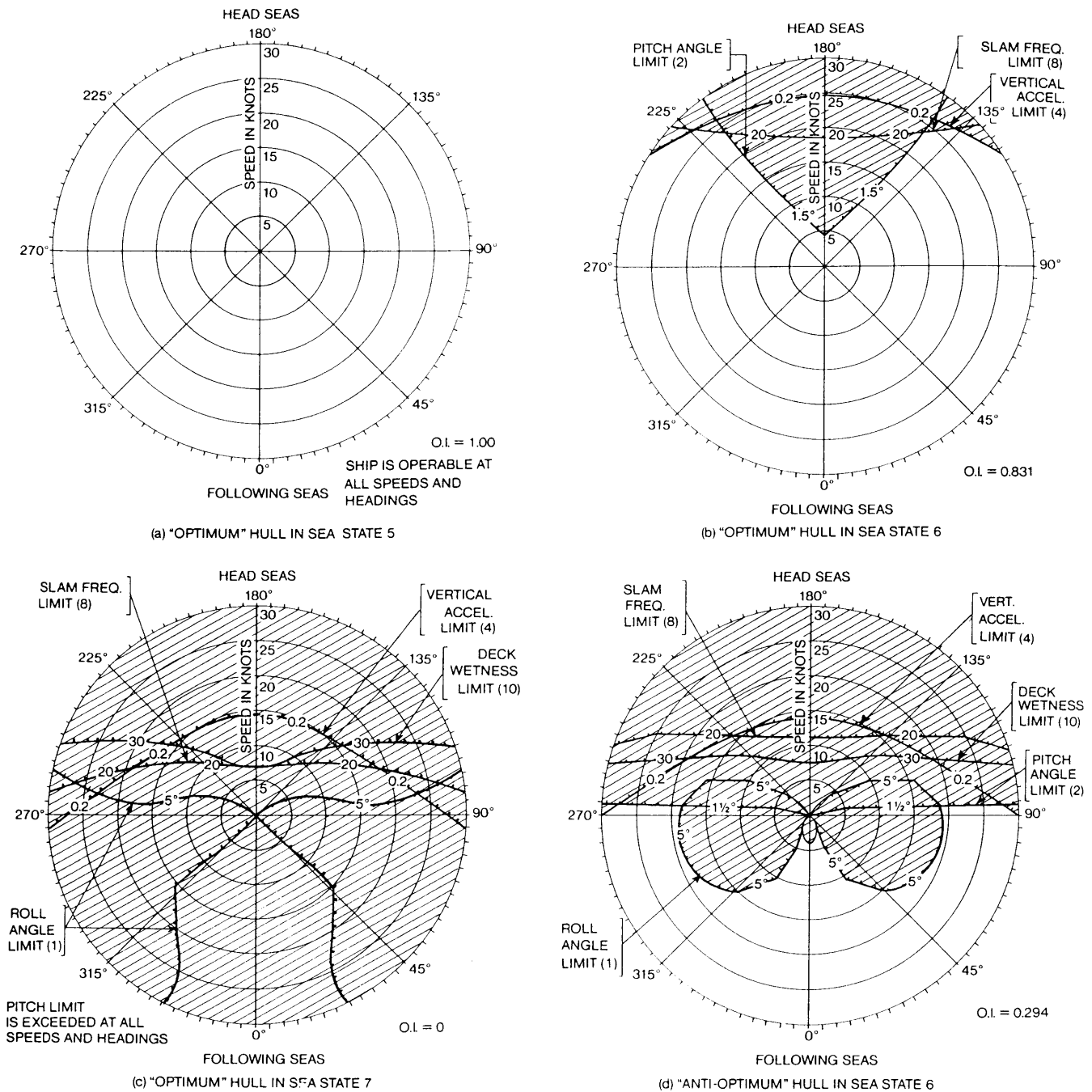


Fig. 117 Seakeeping Operating Envelopes for a 4000-t monohull performing a pure transit function

nohull in Sea State 6 with the "anti-optimum" form of the same reference. The allowable ship speeds up to a maximum speed of 25 knots taken from these figures are shown shaded in Fig. 118(a) for the "optimum" hull and in Fig. 118(b) for the "anti-optimum" hull.

The basic features of the speed plots of Fig. 118 are not dissimilar from those of the larger commercial

ships of Fig. 109 with two exceptions:

- The degradation in allowable speed with increasing sea state is much more abrupt in Fig. 118 than in Fig. 109.
- In beam, quartering, and stern seas, Fig. 118(b) shows that speeds between zero and 4 to 18 knots are prohibited in Sea State 6 whereas higher speeds are

permissible. Fig. 118 shows no such anomaly.

The reason for the anomaly is evident in Fig. 117(d). It shows that the prescribed values of 5 deg rms roll, which has no effect on the optimum hull (Fig. 117b), has a big effect on the "anti-optimum" hull, but only at low speeds and at certain headings.

The information provided by Figs. 109 and 118 is only one of three essential parts of the data needed to calculate SPI-2. The second part of needed data is a description of the kind of seas that a ship will experience as a function of time, location, and season in the oceans between its designated ports. As noted in Section 7.7, these data are available in Bales, et al (1981). See also Section 2.

The third part of the data needed to calculate SPI-2 is the route the ship will follow between its ports. One such obvious route is the minimum distance route, which in calm water would also be the minimum elapsed time route. However, because of the powerful impact of seaway-induced speed reductions on voyage elapsed time, the minimum distance route is seldom the minimum elapsed time route. It is for this reason that weather routing, where the objective of achieving minimum voyage elapsed time determines the route, has become so commonplace for ships. With weather routing, the actual route that the ship will follow is time-dependent on the information available from weather forecasts made during the voyage. Hence, calculation of SPI-2 can only be made *ex-post-facto*, unless an on-board computer is installed. However, for the purposes of making reliable estimates of the economic viability of a proposed ship during its design

stage and for the purpose of selecting optimum hull characteristics on the basis of expected superior performance in the real seaway, the assumption of a minimum-distance route is appropriate. With the use of a minimum-distance route, the value of SPI-2 expressed either as a ratio of elapsed voyage times or expected speed fraction is identical (Sub-Section 7.1).

Table 25 shows a sample computation of SPI-2 expressed as expected speed fraction on hypothetical voyages of the two hulls of Fig. 118. The following two arbitrary assumptions concerning the voyages were made in Table 25:

- Equal time is spent at each of the nine headings.
- The probability distribution of sea state severity used in Table 24 (for all-season operation in the Northern Hemisphere) is applicable to these voyages. (For ships on scheduled liner services, the weather statistics for the winter season—or worst winter month—may be more appropriate).
- For the "anti-optimum" hull, the low-speed restrictions in quartering and following seas can be ignored.

The 11.8 to 17.1 percent reduction in average sea speed from the smooth water speed of 25 knots shown in Table 24 illustrates the crucial impact that seaway performance can have on the economic viability of a commercial ship. Similar computations for the Victory ship of Fig. 109 indicate a 16.5 percent reduction to an average sea speed of 14.6 knots from a smooth water speed of 17.5 knots.

The importance of the methodology presented in this section is that it can forecast the magnitude of the

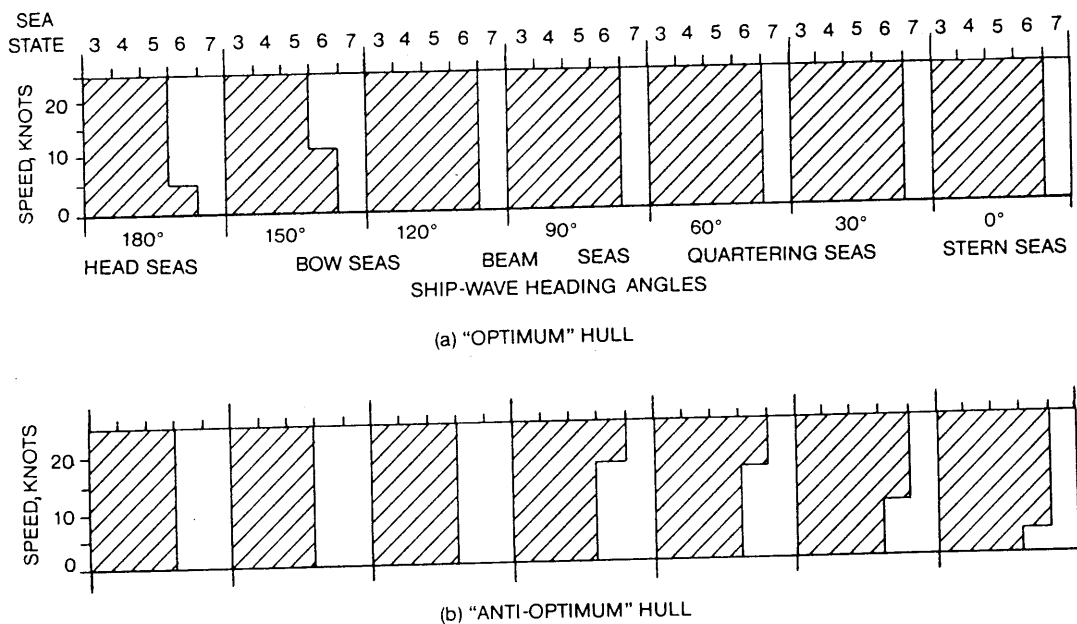


Fig. 118 Allowable ship speeds as a function of sea state and ship-wave heading angle, for the two 4000-t hulls of Bales and Cieslowski (1981) performing the transit function (Criteria Set B)

speed reduction before a ship is built. As shown in Table 25, this speed reduction may be a strong function of hull shape, for the "anti-optimum" hull form of Bales, Cieslowski (1981) has an average speed loss that is 1.6 knots or 6.4 percent greater than that of the "optimum" hull. It is also shown in Section 8 that speed reduction is a strong function of ship proportions.

Hence, its magnitude can change significantly from ship to ship of identical displacements. Furthermore, the magnitude of the speed reduction must be known before realistic estimates of the economic viability of a proposed ship can be made. For these reasons it is important that the calculation of SPI-2 should become routine in the design stage of all transportation ships.

## Section 8

### Design Aspects<sup>14</sup>

**8.1 Introduction.** Sections 2 to 5 have presented procedures whereby predictions can be made of all aspects of the seakeeping performance of ships, both in idealized regular waves and in the irregular patterns actually experienced at sea. Such predictions cover not only motion responses in six degrees of freedom, but derived responses, such as vertical accelerations, shipping of water, slamming, added power requirements and wave-induced loads. Section 6 discussed the effects of various motion-control devices. Finally, the preceding Section 7 dealt in detail with criteria of seakeeping performance that define acceptable limits of ship response for specific ship missions or functions. Furthermore, it showed that comparing predicted performance over a range of expected sea conditions, ship speeds and headings with the appropriate criteria permits the evaluation of seakeeping performance of a new design in terms of a *Seakeeping Performance Index* (SPI).

It is the object of this section first to draw upon the earlier sections to offer guidelines that will assist the designer in selecting ship characteristics favorable to good seakeeping behavior. Theory shows (Section 3) that the effects of longitudinal motions (pitch, heave and surge) and of transverse motions (roll, yaw and sway) can, for practical purposes, be considered separately. This will be done here, since design features to reduce motions are generally different for the two cases. The longitudinal motions (particularly heave and pitch) will be considered first, since they are affected more by choice of ship dimensions, have a greater effect on attainable speeds in rough seas, and are less amenable to artificial control. Attention will then be given to other design considerations, such as above-water hull form and added power in waves, followed by the effects of transverse motions (rolling in particular) and discussion of special considerations affecting high-performance ships.

Finally, suitable design procedures will be consid-

ered, including comparative evaluation of the seakeeping performance of alternative designs and selection of an optimum on the basis of economic considerations.

**8.2 Factors affecting pitching and heaving.** (a) *Theoretical considerations.* Theory, supported by model tests and full-scale observations, provides some good general guidance to the designer. First may be mentioned the dimensional effect of ship size (particularly length) in relation to sea conditions encountered. Sellars (1983) has pointed out that in general, for conventional mono-hulls in head seas, the longer the ship the less the average wave excitation. This is mainly because the probability of encountering waves of near ship length decreases with increasing length, but also because the average height of long waves, and hence wave slope, is less than short waves. Sellars (1983) has calculated the probabilities of encountering conditions leading to large heave and pitch excitation in average North Atlantic weather as a function of ship length, as shown in Fig. 119. See also Fig. 74 and discussion in Section 4.7.

The advantage of greater length applies whether overall size, as indicated by displacement, remains the same or increases with length. The favorable effect of increasing all dimensions together is discussed in Section 4.7, where the non-dimensional plots in Figs. 74 and 75 show clearly the comparative pitching and heaving motions of two geometrically similar ships in irregular head seas. However, this is an extreme case of a large size difference (ratio of 8 in displacements), while even a modest increase in size would be an expensive way to improve seakeeping qualities. The effects of increasing length with displacement fixed are of greater interest and will be discussed further in this section.

It has been suggested in Section 4.9 that the next consideration is whether the ship is expected to reduce speed in order to operate in sub-critical conditions in rough seas or can remain in a high-speed supercritical state. The first case applies to the majority of normal commercial and naval vessels, while the latter case is characteristic of some of the high-performance craft to be considered separately.

<sup>14</sup> Section 8 written by Edward V. Lewis, assisted by Philip Mandel, particularly with sub-section 8.5, High-performance Ships.

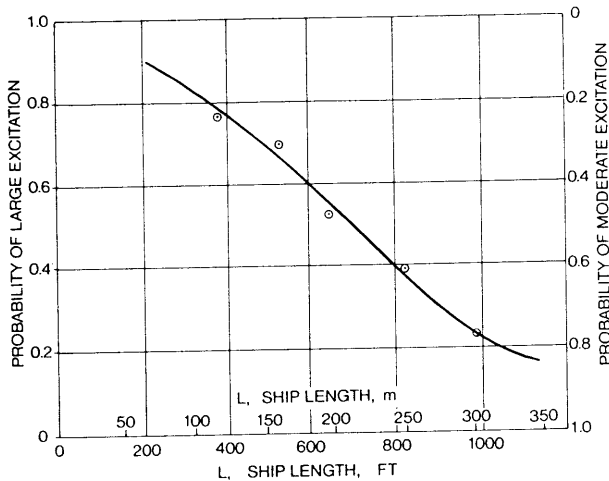


Fig. 119 Probability of conditions for large pitch and heave excitation, i.e., probability ( $L_w \geq 0.75L$ ) (Sellars, 1983)

The problem of attaining sub-critical pitching and heaving behavior of normal ships over as wide a range of speed as possible requires consideration at early stages of design of the relationship of length—the most important dimension—and other hull characteristics to the natural periods of oscillation, as discussed in Section 4.9. This important influence of natural periods of oscillation on motions in waves is often overlooked because of the difficulty in determining natural periods experimentally. A solution to the problem is to plot model test (or calculated) responses on a basis of ship speed or encounter frequency, with wave length constant. The resulting peaks will define an effective natural frequency that is of prime interest.

Fig. 120 is a plot of experimental model data (Stefun, 1958) that illustrates the complex relationships existing between non-dimensional ship motion amplitudes and both wavelength-to-ship length ratio,  $L_w/L$ , and tuning factor.  $\Lambda = \omega_e/\omega_n$ , where  $\omega_e$  is the frequency of encounter, varies with both wavelength and ship speed ( $\omega_n$  is the natural frequency of pitch or heave.) It can be seen that only the curves plotted for constant values of  $L_w/L$  (solid lines) have clearly defined maxima, because  $\omega_e$  and hence  $\Lambda$  here depend only on model speed. Higher speeds would be required to define the maxima for longer waves ( $L_w/L \geq 1.25$ ) (Fig. 57). The maxima are shown to occur in this case at a  $\Lambda$ -value of about 1.1 rather than 1.0 because of approximations made (Section 3.7).

The dashed curves in Fig. 120 drawn for constant Froude Number and varying  $L_w/L$  do not show distinct peaks because wavelength has a greater direct effect on excitation than indirect effect through changing  $\omega_e$ . All non-dimensional responses go to 1.0 in very long (infinite) waves in which the ship simply follows the wave contour, as shown by a replot of the data in Fig. 121.

Fig. 121 also shows how, with speed constant, the ship response can be separated into a static value—dependent on ship-wave geometry—and a magnification effect depending mainly on tuning factor.

Another effect of tuning factor is on phase relations. Szebehely (1955) showed that in waves around ship length the incidence of shipping water over the bow and bow emergence leading to slamming are both associated with synchronous response; bow down into crest, bow up into hollow, with high relative vertical velocity (Lewis, 1955).

Fig. 79 defines in a general way the conditions for critical operation in head seas, which generally give the worst pitching and heaving behavior. It is clear from the figure that the lower the period ratio,  $T_n(g/L)^{1/2}$ , the higher the speed before critical conditions are reached. Hence, the period ratios for pitching and heaving have a vital effect on ship behavior and on attainable sea speed. The natural periods of pitching and heaving are usually quite close together, but attention is focused here on the pitching period,  $T_{n5}$ , since it has the greater effect on wetness, slamming, and vertical accelerations. The influence of ship proportions and form on  $T_n(g/L)^{1/2}$  was discussed in Section 4.9 and general trends shown in Fig. 81.

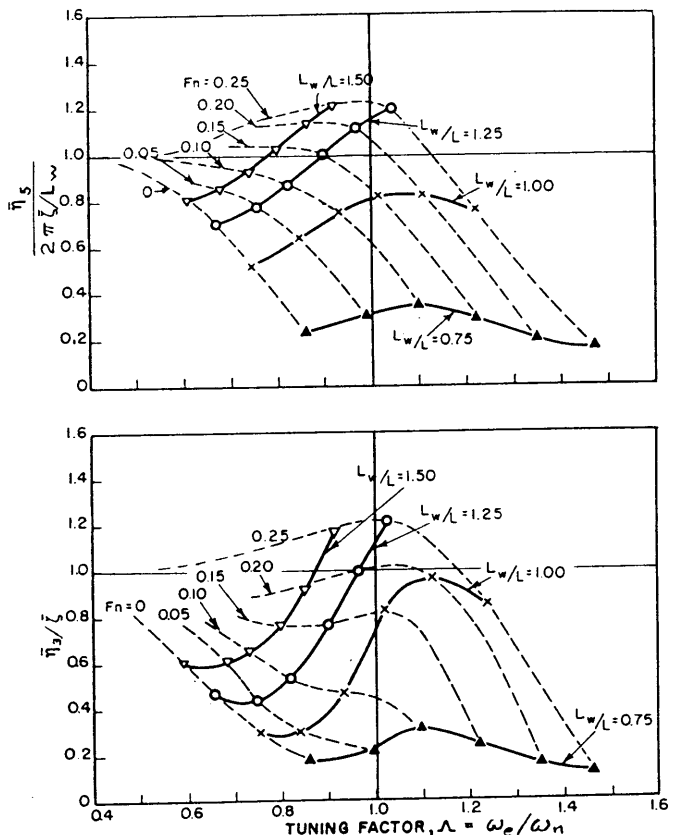


Fig. 120 Pitching and heaving amplitudes for a Series 60, 0.60 block model in head seas (Stefun, 1958)

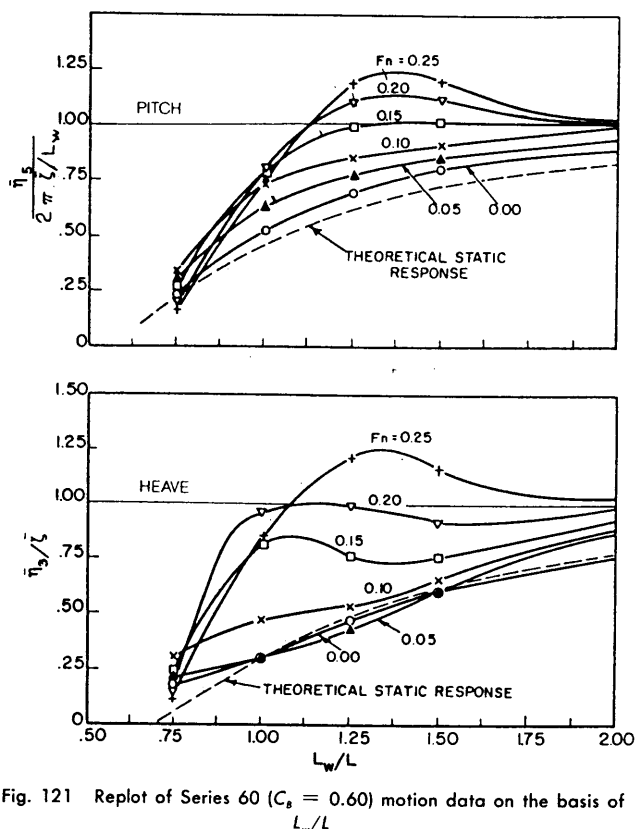


Fig. 121 Replot of Series 60 ( $C_s = 0.60$ ) motion data on the basis of  $L_w/L$

In order to obtain a picture of the possibilities of subcritical operation, Figs. 79 and 81 (Section 4) have been combined in Fig. 122, which shows the relationship between ship proportions—as indicated by  $L/\nabla^{1/3}$ ,  $W/(L/100)^3$  or  $C_B T/L$ —and the Froude number for synchronism with waves of length equal to ship length. Since peak amplitudes for some ships may occur at a tuning factor somewhat below 1.0, a curve for  $\Lambda = 0.9$  is also shown. For ships heading directly into irregular seas, with a wide range of wave components present, the zone above these boundary curves represents conditions for intermittently violent pitching motion, wet decks, bow emergence with possible slamming, and high accelerations. The zone below the curves represents conditions for less severe motions, fairly dry decks, less bow emergence, and moderate accelerations in the same type of sea. Whether slamming occurs or not depends on draft and on section shapes. Fig. 122 may be considered as a basic general picture of the conditions for moderate (subcritical) and serious (critical) pitching motions of typical ships heading into severe storm seas. It is apparent that the choice of high  $L/\nabla^{1/3}$  and high  $L/T$ , usually adopted for ships intended for high speed in calm water also confers a distinct advantage for speed in rough water—provided that it is not accompanied by excessive draft reduction, which might lead to slamming.

It may be of interest to consider a few specific examples of ship performance in heavy seas to illustrate the significance of Fig. 122. James L. Bates (1945) mentions the difficulty experienced by 30-knot destroyers in keeping station with the 23-knot *Leviathan* in rough weather during World War I. In his reply to the discussion of his paper, he points out that the motions of these destroyers were very comfortable when speeds were reduced to about  $V_K/L^{1/2} = 1.0$ . The old destroyer *Pruitt*, mentioned by Bates, has been plotted in Fig. 122, first at 30 knots—well up in the heavy pitching zone—and then at 17½ knots, which Bates states to have been a comfortable speed. At the reduced speed, the ship may be seen to lie close to the moderate pitching zone.

The *Victory*-type cargo ship may be considered as an example of a much higher displacement-length ratio. At the normal design speed of 16½ knots, this ship is shown in Fig. 122 to be well up in the heavy pitching zone. Log data show that, in meeting severe North Atlantic weather, its speeds are reduced to 5 to 9 knots in order to ease the motions. It can be seen in the figure that an average reduced speed of 7 knots brings this ship into the moderate pitching zone.

Another example is furnished by Möckel's data on typical European trawlers (1953). Like the *Victory* ship, his trawler "A" lies in the heavy pitching zone at the normal free-running speed of 11 knots. Möckel states that, at a trawling speed of 3 knots, the ship was comfortable in winds up to force 7 (30 knots) and able to continue normal trawling operations. Both speeds are shown in Fig. 122. (Möckel believes that a somewhat higher speed could have been maintained if sufficient power had been available.) It is clear from the figure that "fat" vessels such as trawlers must be designed for severe motions (high freeboard, V-form sections, and so on) if they are to maintain headway in rough weather.

Finally, Fig. 122 shows points for the transatlantic liner *United States* which had a reputation for maintaining high speed in rough weather. The points correspond to the good-weather speed of 35 knots and the average (not the minimum) speed of 27 knots reported on a typical rough crossing. Again, a shifting from the heavy to the moderate pitching zone is indicated. The lengthening of T-2 tankers, C-4 type cargo ships, and Libertys would likewise be expected to improve their seakeeping qualities, and this has been found to be the case.

Aertssen (1958–59) plotted all his voyage data on cargo ships obtained up to that time on a graph based on Fig. 122 with the result shown in Fig. 123. This confirms the value of Fig. 123 as a guide to the choice of ship proportions for service in severe sea conditions.

As previously noted, there has been a gradual trend to higher  $L/\nabla^{1/3}$  (lower displacement-length ratios) and hence higher  $L/T$  values as ship speeds have increased through the years. This trend undoubtedly has been

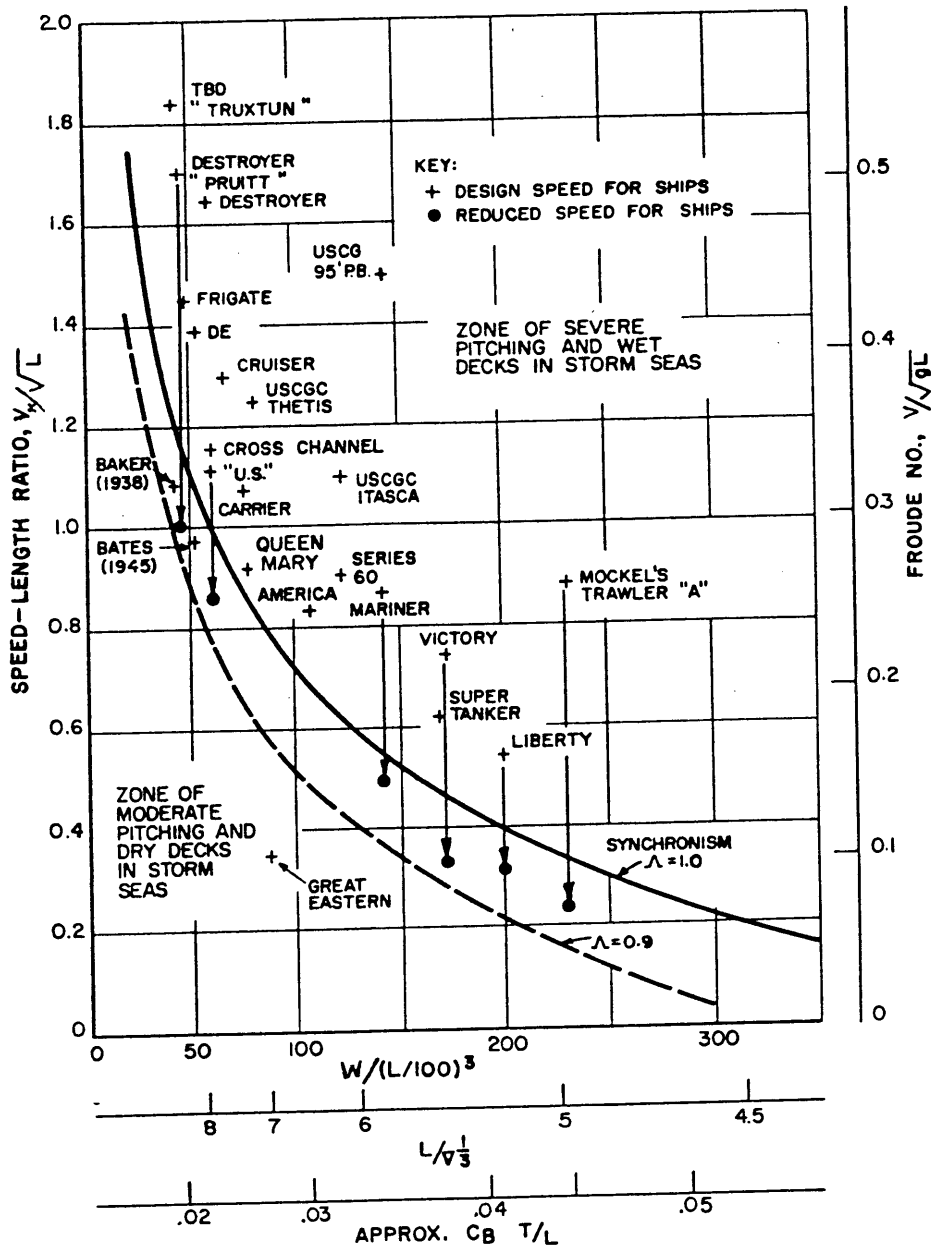


Fig. 122 Trends of speeds for synchronous pitching, defining zones of serious and moderate motions in irregular head seas

dictated by calm-water considerations rather than by rough-water performance. It may be that in many cases seakeeping considerations will encourage this trend.

(b) *Damping*. It is normally impossible or uneconomical to design ships for operation in the favorable speed zone only, and therefore an important problem is how to improve ship performance in the critical region of Fig. 123. In this zone, the problem of reducing motions and thereby permitting higher speeds is predominantly one of minimizing near-synchronous re-

sponses, which means increased damping and hence reduced magnification factor. An increase of damping is effective in an irregular sea in which synchronism with component waves occurs, just as it is under conditions of synchronism with regular waves.

Some of the trends of proportions and form that are beneficial to reducing natural periods of pitch and heave are also favorable to increased damping; such as reduced  $C_M$  and coefficients of other sections, increased  $C_{WP}$  (hence more V-form and reduced  $C_{VP}$ ) and filling the waterlines toward the ends. Work of Grim

(1959) and Porter (1960) show a distinct increase in damping with increasing  $B/T$ , although it may not always be favorable for reduced natural periods. But since the effect of beam increase is felt mostly near midship, this factor may be less important for pitching than filling out the waterplane of the ends (increase in  $C_{WP}$ ).

Various writers agree on the importance of increasing  $C_{WP}$ , which can also be expressed as a decreasing  $C_{VP}$ , especially for high-speed ships (Lewis, 1955) (Blok and Buekelmann, 1984). Bales (1980) found that the increase of  $C_{WP}$  or decrease in  $C_{VP}$  using V-sections was more effective in the forebody than in the aftbody. However, V-form forward may exact a penalty in added resistance in calm water and/or waves.

There is also evidence of the advantage of a wide longitudinal separation of LCF and LCB. (However, supercritical ships such as SWATHs show a strong disadvantage to such separation). With LCF 5.5 percent  $L$  abaft the LCB, Moor (1970) showed a significant reduction in pitch and heave motions, vertical acceleration forward, relative bow motion, and speed loss in waves for a series of models of a 770-ft. (250-m), 26-knot passenger ship. However, trial speed was reduced by 3 percent. Naval vessels with wide transom sterns have been able to take advantage of this favorable effect of LCF and LCB separation. Finally there is the possibility of using fixed fins for damping of pitch (Section 6).

Of course, some of the factors that increase damping will also increase the excitation. However, under conditions of severe synchronous responses the damping effect is always at its greatest and hence would be expected to predominate.

(c) *Model test results.* Before adopting guidelines derived from simplified theoretical period relationships, some confirmation is needed and the best method for that purpose is model tests in waves. Unfortunately, comparative model experiments that isolate the effects of specific changes in hull proportions and form are rare. For example, the extensive tests of Series 60 hulls in regular waves (Vossers, et al 1960), which reveal trends of motions and power with  $L/T$ ,  $L/B$  and  $C_B$ , include inadvertent effects of changes in displacement,  $L/\nabla^{1/3}$  and  $B/T$  as well, and do not compare performance under realistic irregular sea conditions.

However, Hamlin and Compton (1966) made use of Vossers' model data to show the results of calculations on Series 60 models of different  $L/T$  (and  $L/\nabla^{1/3}$ ) ratios in a severe irregular sea. Fig. 124 confirms the advantage of a large  $L/T$  value for minimum relative bow motion,  $\bar{s}/L$ . Calculations of heave acceleration show a similar advantage. Furthermore, if bow freeboard is proportional to length, the shipping of water should decrease with increasing  $L/T$ . The situation regarding slamming is somewhat different. Here the more slender ship shows up poorly, because even though the relative bow motion in relation to length is less, the reduced draft would result in more frequent bow emergence and higher relative velocities (Vossers, et al 1960). It should be noted that the model data on which these conclusions were based assumed constant  $L/B$  values, which could lead to excessive beam, from a stability viewpoint, in the longest ship.

Subsequent studies have used the same or similar data to calculate and compare the predicted behavior of ships of equal displacement in irregular head seas,

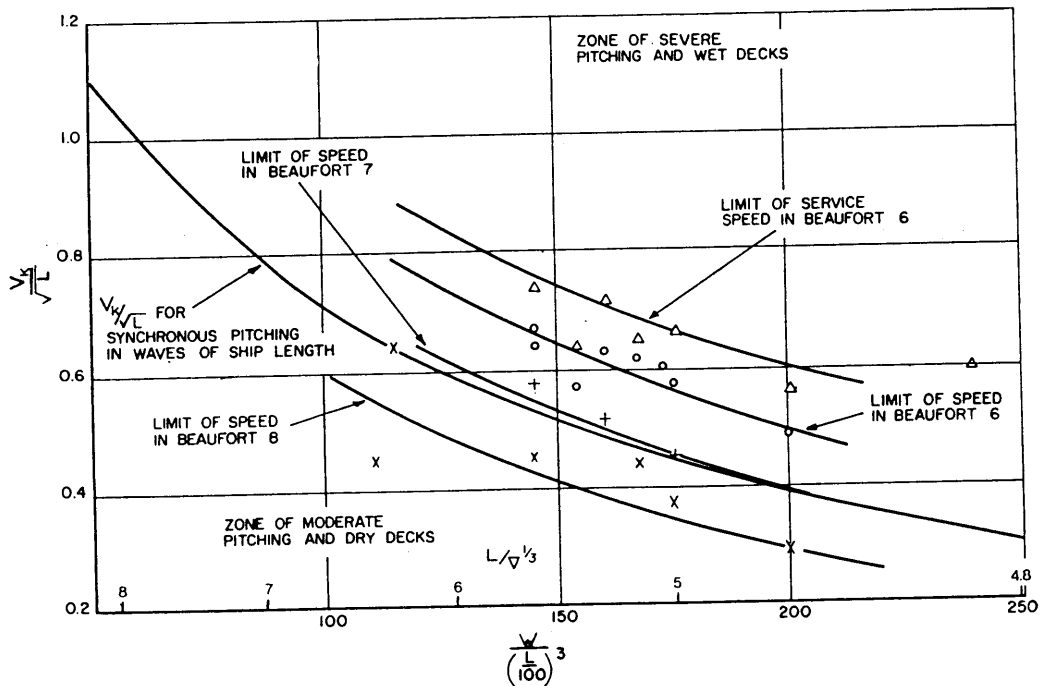


Fig. 123 Trends of attainable speed in different sea conditions, from logbook analysis compared with theoretical trends (Aertssen, 1958-59)



including the effects of variation in forebody shape, longitudinal radius of gyration, etc. (Swaan, 1961) (Swaan and Vossers, 1961) (Swaan and Rijken, 1964) (Ewing, 1967). St. Denis (1983) has reviewed much of this work and has drawn some general conclusions. The research confirms that, for moderate to high-speed ships, there are advantages to be gained in pitch and heave—and related responses—by increasing  $L/T$  and  $B/T$ , reducing  $C_B$  while increasing  $C_{WP}$  (more V-shaped sections) and reducing longitudinal radius of gyration. It also shows that for low-speed ships ( $Fn < 0.3$ ) some of the above, such as the advantage of high  $L/T$  or a low  $C_B$ , may not apply, especially for large tankers where powering is more of a problem than motions in waves.

A recent model investigation by Schmitke and Murdey (1980) and later extended by Murdey and Simoes Ré (1985) is based on a well-chosen range of hull characteristics and again evaluates the models by comparing their predicted behavior at constant displacement in a typical long-crested head sea. Although these results apply specifically to fine frigate/destroyer hull forms (Fig. 125) they are believed to provide useful guidance for other relatively high-speed displacement craft. These studies employed the slenderness parameter  $L^2/BT$ , which indicates length (squared) relative to the area,  $BT$ , of the midship circumscribing rectangle. Further definition of proportions is given by the ratio  $B/T$ , and hull form by  $C_B$  and  $C_{WP}$ .

Results showing trends with all these parameters are given in Figs. 126–129 for pairs of models at a constant displacement of 3500 t. In evaluating these results it is important to note that  $L^2/BT$  and  $B/T$  are not independent parameters, since they both involve  $B$ . However, the product of  $L^2/BT$  and  $B/T$  is  $(L/T)^2$ , and  $T/L$  is an independent parameter that has been shown to be important in studying natural periods of pitch and heave (Equation 204d, Section 4.9.) Similarly the ratio  $C_B/C_{WP} = C_{VP}$  may be more significant than the two coefficients considered separately.

The comparative findings in Figs. 126–129 are based on self-propelled experiments on 10 models in regular head waves (with wavelengths varied in about 20 steps from  $L/2$  to  $3L$ ; heights  $1/50 L_w$ ) at each of four speeds corresponding to  $Fn = 0.2, 0.3, 0.4$ , and  $0.5$ . Faired results were used as RAOs to calculate significant responses in irregular head seas, using the “quadratic regression spectrum” (Gospodnetic and Miles, 1974) for a significant height of 3.66m (12 ft). Response data were averaged over a wave modal period range of 7.28 to 10.92 sec and over a speed range of 15 to 30 knots. They have been made non-dimensional by dividing by the appropriate response value for the basic hull of the series (No. 6).

First, it may be seen in Fig. 127 that with displacement constant there is in all cases a distinct reduction in pitch and heave amplitudes, and in vertical acceleration at  $0.25L$  from the bow, as  $L^2/BT$  increases. This shows the clear value of increasing length and

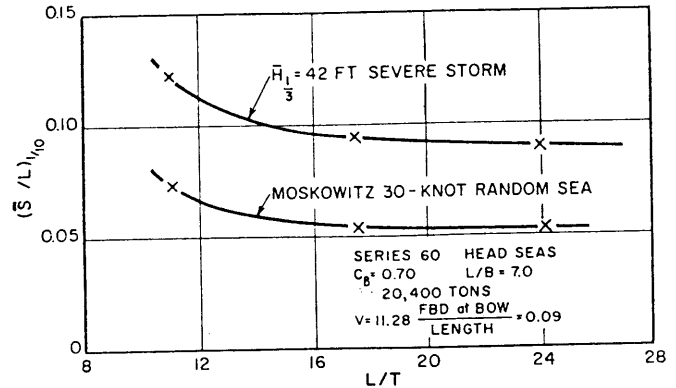


Fig. 124 Relative bow motion trends with  $L/T$  ratio in irregular head seas, 500-ft. ships (Hamlin and Compton, 1965)

reducing  $BT$ . Furthermore, since  $L^2/BT$  is equal to  $C_B L^3/\nabla$  and  $C_B$  is held constant, Fig. 127 also implies the same favorable trend with increasing  $L^3/\nabla$ , or  $L/\nabla^{1/3}$ , the length-displacement ratio (Froude's  $M$ ), as previously suggested (Section 4.9) on the basis of period considerations.

However, predicted relative bow motion (RBM) shows little change—or even a reverse trend—with increasing  $L^2/BT$ . This picture changes if the non-dimensional ratio  $\bar{s}/L$  is used as an index of RBM instead of  $\bar{s}$ . (See Fig. 126, where  $\bar{s}/L$  reduces significantly with increasing  $L/T$ ). If the RBM data in Fig. 127 are replotted in terms of  $\bar{s}/L$  it will be found that there is a distinct reduction in response with increasing  $L^2/BT$  in all cases. The question in any specific situation, such as evaluation of probabilities of shipping water or slamming is, which is a more suitable index of performance,  $\bar{s}$  or  $\bar{s}/L$ ? In the case of wet decks, it is often feasible to increase bow freeboard in proportion to increasing length by simply extending the sheer curve forward. This would mean that  $\bar{s}/L$  is appropriate. On the other hand, an increase in ship length may entail a reduction in draft forward, which would suggest that the absolute value,  $\bar{s}$ , is significant for consideration of bow emergence and slamming. Such reduction in draft with increasing  $L^2/BT$  would be expected to increase the probability of bow emergence and slamming, as previously noted. This is not always true, however. Bales (1980) found that “bottom slamming per se may be reduced or stabilized by reductions in relative motion attendant to reductions in  $T/L$ .”

Fig. 127 (as well as Fig. 126) shows a clear advantage of increasing  $B/T$ . This is consistent with the conclusion in sub-section 8.2(b) that increases in  $B/T$  are favorable for reduced pitching and heaving, because of increased damping. Furthermore, since increasing both  $L^2/BT$  and  $B/T$  is shown to be beneficial, increasing their product  $(L/T)^2$  should also be beneficial. This is as predicted on the basis of favorable natural periods alone in Equations (204d) and (206), Section 4.9.

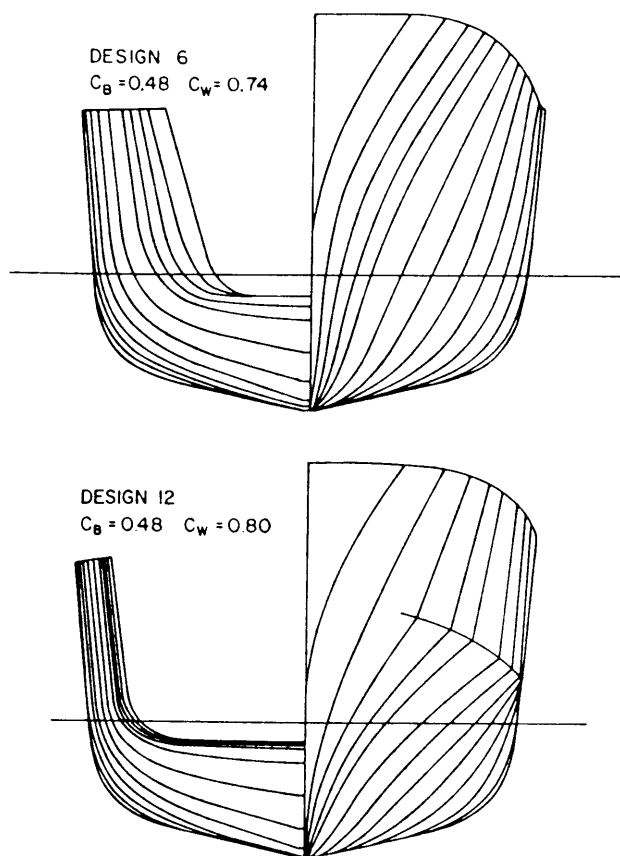


Fig. 125 Body plans of two frigate models tested by Schmitke and Murdey (1980); Design 6 is the basic model

Figs. 128 and 129 show gains in increasing  $C_{WP}$  and decreasing  $C_B$ , hence reducing  $C_{VP} = C_B / C_{WP}$ . However, the situation regarding relative bow motion in Fig. 129 is again ambiguous. Hence, an obvious conclusion is that special attention in design for good seakeeping should be given to obtaining adequate freeboard forward and adopting section shapes that reduce slamming probabilities.

Results of the extension of this model series to a total of 31 models were reported by Murdey and Simoes Ré (1985), and some are shown in Figs. 130 and 131. Although data are presented in a similar manner as before, an ITTC spectrum with 4.0-m (13-ft.) significant height was used as a basis for predictions. The range of zero-crossing period for averaging responses was 6.1–9.1 sec, and ship speeds of 13–33 knots.

Fig. 130 shows similar trends with  $L^2/BT$  as Fig. 126, but over a much wider range, with displacement again constant (Curves added for constant length are of less interest).

The extended series also confirms with more data the trends of Figs. 127 and 128 and 129 that increasing  $B/T$  and  $C_{WP}$ , and decreasing  $C_B$ , are favorable to reduced pitching and heaving. However, there is some ambiguity in the case of  $C_{WP}$  with respect to relative

bow motion. The more complete data on  $C_B$  (Fig. 131) also show some ambiguity. Supplementary analyses by Simoes Ré (1986) have shown that, using data from the extended series, the relationship between  $L^2/BT$  and  $C_B$  is clarified. He found that for pitch and bow acceleration, with displacement fixed, there are:

- Decreased responses when  $C_B$  decreases and  $L^2/BT$  increases
- Increased responses when both  $C_B$  and  $L^2/BT$  decrease
- Uncertain effect when  $L^2/BT$  stays constant.

Hence, a clear conclusion emerges that using reduced  $C_B$  to increase length is advantageous but using it otherwise of doubtful value. Trends of relative bow motion with  $C_B$  in the expanded study remained ambiguous.

Some supplementary tests with different combinations of bows and sterns of two models ( $C_B = 0.48$ ) showed a clear advantage for all responses in increased V-ness of the bow, with or without a wide transom. At the same time, a wide transom showed an advantage in pitch and bow acceleration over a narrow-transom stern, while showing only slight improvement in heave and relative bow motion.

(d) *Specific guidelines for design.* We are now in a position to state a number of specific conclusions on the basis of both experimental studies and the theoretical relationships considered in Section 4, Equations (204) and (206), to reduce the period ratios and increase damping. These apply to moderate to high-speed ships intended to operate in the critical and sub-critical speed zones, and should lead to reduced pitching and heaving motions:

- Ship proportions—Increase length relative to draft  $T$ , or  $BT$ , which generally implies increased  $L/\nabla^{1/3}$ . Increase  $B/T$  for greater damping (if feasible).
- Coefficients of form—Reduce  $C_{VP}$  (more V-form, especially in forebody) with reduced  $C_B$  and increased  $C_{WP}$ . Decrease  $C_B$  by increasing length. (If length is decreased, effect is generally doubtful).

To reduce pitching, and hence relative bow motion, but not heaving:

- Longitudinal distribution of W.P.—Increase the coefficient of waterplane inertia,  $C_A$  (filling WL's at ends). (Increase transom width in naval vessels).
- Longitudinal mass distribution—Reduce the coefficient of mass moment of inertia,  $C_K^2$ .

The above are also generally favorable to reduced vertical accelerations, and usually, but not always, to relative bow motion. This means that separate consideration must be given to ensuring adequate freeboard forward to avoid excessive wetness and bow section shapes to minimize slamming.

Note that the effects of changes in coefficients of added mass (heave,  $A'_{33}$ ) and added inertia (pitch,  $A'_{55}$ ) are assumed to be negligible.

It can be seen that one of the important parameters affecting pitching motion is longitudinal mass radius

of gyration. Although this is not often under the control of the designer, there are exceptions, and therefore this factor should not be overlooked. For example, locating machinery space amidships results in cargo being located closer to the ends than with (comparatively light) machinery way aft, with a correspondingly long gyradius. In ships carrying high-density cargo all available cargo volume may not be needed, and therefore arrangements to concentrate cargo closer to midship may be feasible. This will reduce radius of gyration, shorten the natural pitching period and permit somewhat higher subcritical speed in irregular head seas. However, an increased midship sagging moment, both static and wave-induced, will result (Dallzell, 1964).

**8.3 Other Design Considerations.** (a) *Above-water form.* An important criterion of seakeeping performance discussed in Section 7 is frequency of deck wetness forward. It has been shown in sub-section 8.2 that, if the ratio between relative bow motion and length,  $\bar{s}/L$ , is considered, the same trends of hull characteristics that favor reduced pitch and heave apply. But shipping water depends not only on the rel-

ative bow motion but on the above-water form and section shapes. Therefore, every effort must be made to ensure not only that the freeboard ratio,  $F/L$ , selected is adequate, but that bow section shapes are suitable.

It was shown in section 5.3 that calculations of relative bow motion can be used to predict trends of required freeboard in relation to ship length on the basis of probabilities of shipping water (see Fig. 85). Bales (1979) has carried this approach even further.

In Section 5.3 the non-linear factors that influence the true relative bow motion are also discussed and the difficulties of calculation explained. It is there recommended that, if possible, model tests in irregular waves be used for a final determination of freeboard—as well as of the amount and shape of flared sections, use of knuckles, etc. General guidance derived from model tests is given by Newton (1960) for cargo ships, Moor and Luyster (1960) for tankers, and Van Sluijs and Tan (1972) for frigates.

Some empirical guidance regarding suitable bow freeboard is given in Fig. 132, showing freeboard/length ratios for a number of ships, as well as trends

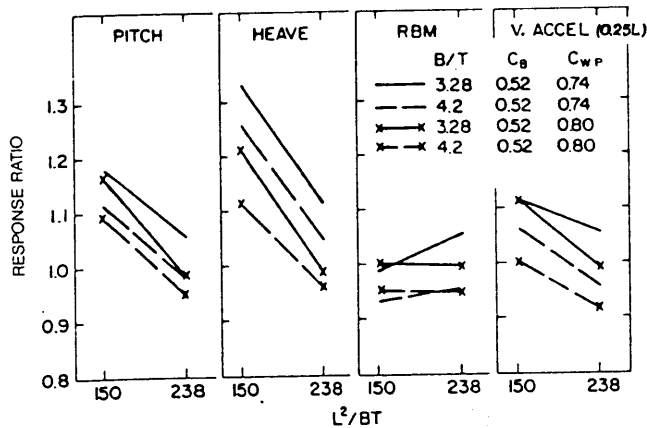


Fig. 126 Effect of  $L^2/BT$  on seakeeping

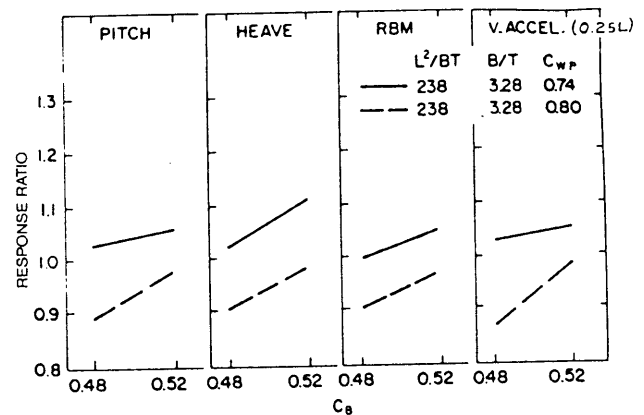


Fig. 128 Effect of  $C_B$  on seakeeping

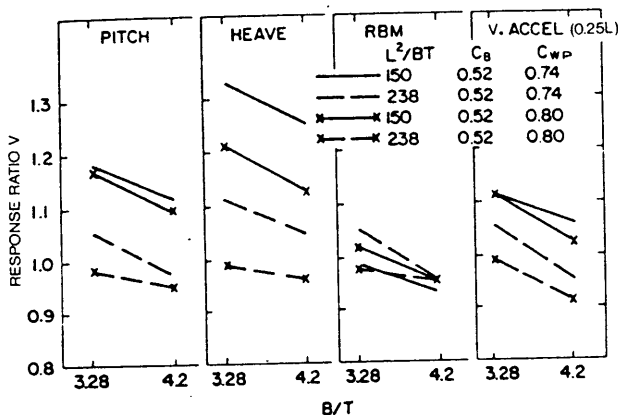


Fig. 127 Effect of  $B/T$  on seakeeping

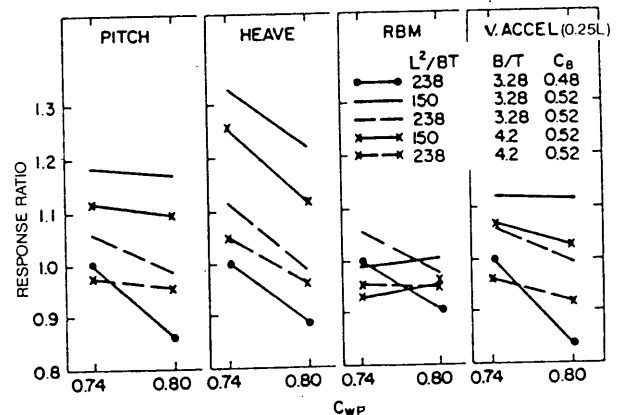


Fig. 129 Effect of  $C_{wp}$  on seakeeping,  $\Delta = 3500t$  all from Schmitke and Murdey (1980)

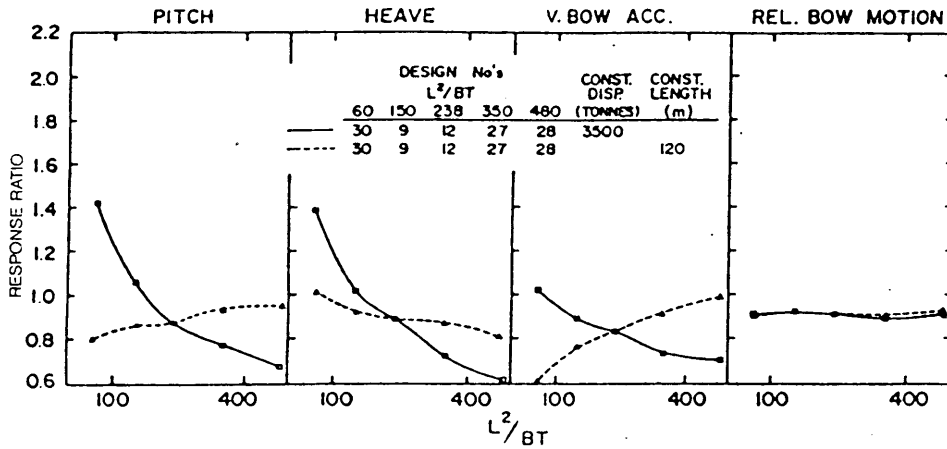


Fig. 130 Effect on seakeeping of increasing  $L^2/BT$  at constant displacement (3500t) and at constant length, 120 m (Murdey and Simoe's Re; 1985)

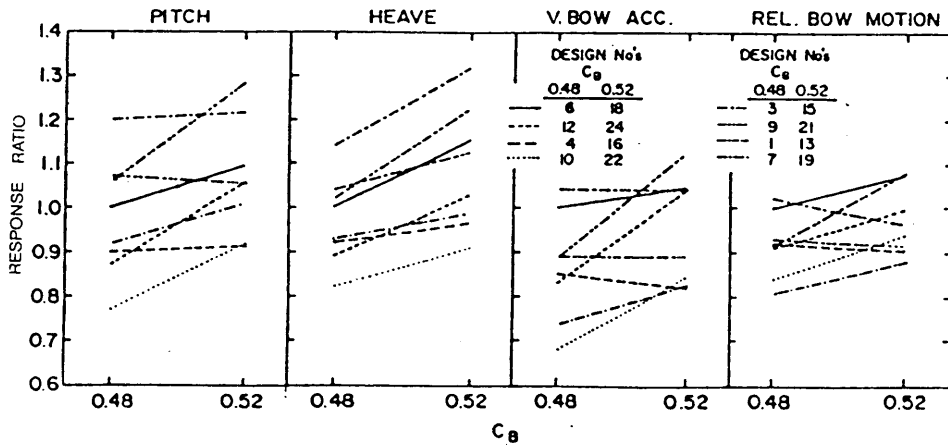


Fig. 131 Effect on seakeeping of increasing  $C_B$

obtained from the various sources indicated. In the case of large passenger liners it is generally considered that the bow freeboard of the *Europa* was inadequate, the *America* somewhat borderline, and the *United States* satisfactory. The left-hand part of the figure must be considered only as a general guide, however, since it has been shown in Section 5 that required bow freeboard depends greatly on the speed of the ship, as shown in the right-hand part of the figure, as well as above-water form.

U.S. Navy procedures for determining minimum freeboard for various types of naval vessels is given in a Design Data Sheet (NAVSEA, 1982). Recommendations regarding other above-water hull design parameters:

*"A sufficient amount of flare is helpful in deflecting water outward as the bow moves downward into a wave to decrease the occurrences of deck wetness and to increase effective freeboard. However, extreme flare may intensify slamming impact and may also cause greater speed loss than would be necessary to limit wetness. Ships with superior wetness have flare angles between 20 and 25 deg.*

*"A knuckle is often used in combination with flare on ships in which there is a requirement to maintain arrangeable deck area forward and which would result in excessive flare if the flare were carried to the weather deck. ....*

*"Spray rails provide a simple way of reducing deck wetness on designs in which wind driven spray is brought on deck or whipped into the bridge. Spray rails are fitted forward below the edge of the weather deck. It should be pointed out that once the ship's motions become so severe that the rails are submerged, the increase in effective freeboard is lost.*

*"Sheer is increased forward in order to provide the required freeboard. If excessive sheer is required, then a bulwark may be indicated or a raised fo'c'sle added. ....*

*"Breakwaters are important to above-water hull design because they protect deck equipment once green water has been shipped on deck. The breakwater is vee-shaped and is located forward of the forward-most gun or missile launcher on the weather deck. ...."*

(b) *Slam avoidance.* Another important criterion of seakeeping performance discussed in Section 7 is the probability of slamming. Calculated relative bow motion is a good basis for determining the probability of bow emergence. However, the occurrence of bottom slamming depends also on other factors: hull form (particularly shape of bottom sections forward) and relative vertical velocity at impact locations. V-shaped sections and minimum flat of bottom are desirable. These effects are discussed in Section 5, where it is shown that available methods of predicting slamming probabilities by calculation must be considered approximate for design use. Flare-entry slamming is even more difficult to calculate.

For merchant ships and tankers that may operate over a wide range of drafts, the light-load or ballast condition is critical. Adequate ballast water capacity to keep the forward draft reasonably large is essential.

To determine the acceptability of a new design the designer also has recourse to the slamming experience of other similar ships. For unusual designs model tests in irregular waves are undoubtedly the most reliable method to use for evaluation.

(c) *Added power requirements.* Because of today's high cost of fuel the search for good seakeeping qualities must include consideration of the effects of optimum choice of ship proportions on power requirements, under both calm sea and rough water conditions. As pointed out in Section 5, both added resistance and reduced propulsive efficiency enter in. The biggest factor in added resistance for high-speed ships is the effect of severe pitching and heaving, and

therefore steps taken to reduce these motions will be advantageous for resistance. Fortunately, for high-speed ships the trend toward increased  $L/\nabla^{1/3}$  dictated by seakeeping considerations should have a favorable effect on calm water resistance and power. This has been confirmed by calculations and model tests, such as those reported by Schmitke and Murdey (1980), also (Bales and Day, 1982). Propulsive efficiency for all types of ships is also adversely affected by pitching and heaving motion. Hence, reduction in motions should be generally favorable to low loss of propulsive efficiency. Trends toward reduced draft at the stern can lead to more frequent propeller emergence, or to restrictions on propeller diameter, either of which may have an unfavorable effect.

The situation may be quite different for full bodied, low-speed ships where energy losses in the reflection of on-coming waves may be a more important factor in resistance than motions and may call for U rather than V-form sections forward (finer waterline endings). In such cases there may be a trade-off between damping of motions and added resistance in waves. Furthermore, if motions are less of a problem at low speeds, a shorter hull length may be advantageous, and economic trade-off studies are called for as discussed as Sub-section 8.6.

Bulbous bows are often used to reduce wave-making resistance of high-speed ships and to improve flow conditions of low-speed, full-form ships (Chapter V). The question arises as to their effects on seakeeping performance. In general, model tests in waves show little effect of bulbs on motions, but an increased prob-

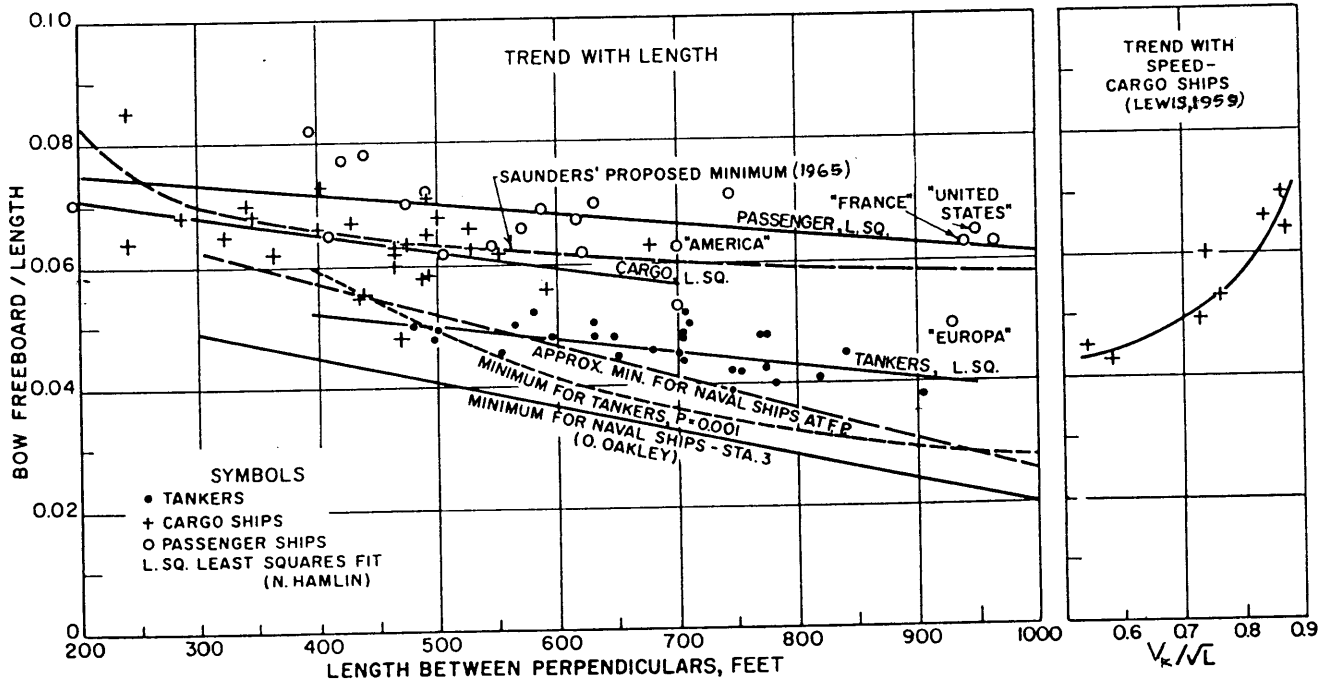


Fig. 132 Suitable bow freeboard trends

ability of slamming in severe seas, especially with larger bulbs. High-speed ships in waves shorter than their lengths may show somewhat less added resistance when fitted with moderate-sized bulbs (Dillon and Lewis, 1955). But this is not always the case, and if slamming occurs it will, of course, limit the attainable rough water speed (Wahab, 1966). It seems best to adopt a bulbous bow only for reasons of calm water resistance, after making sure that any adverse effects in rough water are acceptable.

Bow sonar domes may be a problem with naval vessels. Since they are relatively "soft" structures, in order to transmit sound, they can be easily damaged by slamming. Usually they are located deeper in the water than conventional bulbous bows and therefore may have less effect on motions.

**8.4 Factors Affecting Rolling.** Considering the transverse motions (roll, yaw and sway), roll is of particular interest for conventional ships because it makes the largest contribution to the objectionable accelerations. For most ships the magnitude and frequency range of these accelerations happen to correspond to those of maximum human sensitivity and thus are very likely to produce motion sickness in rough seas. However, in the design of high-performance craft the resulting unique hull forms often have motion characteristics such that some other motion (say, pitch) is more likely to produce sickness. For conventional ships, although roll is the most noticeable component of transverse motions, yaw and sway (also heave), contribute to the accelerations experienced by personnel and equipment. Hence, as noted previously, the apparent vertical reference is actually normal to the wave surface in relatively long beam seas. The ideal for comfort is for the ship to follow the wave slope, i.e., to roll very little with respect to the apparent vertical, rather than to the gravity vertical (Chadwick, 1955).

The magnitude of rolling depends both on the relationship between ship and wave dimensions and on resonance effects; just as in the case of longitudinal motions. But since a ship's breadth is always less than its length, the wavelengths having significant effects on rolling are usually much shorter and therefore occur more frequently. Furthermore, the usual  $L/B$  ratios result in less transverse stability and less damping of transverse motions, with consequent greater sensitivity to resonance effects. It was noted in Section 3.8 that magnification factors of 10 are common when no artificial damping is introduced. At the same time, passive or active damping devices can be more effective than for other motions, such as pitch.

Hence, the first step in design for reduced rolling is to introduce artificial damping, bilge keels being the simplest and most effective device. Sharp or short-radius bilges may be helpful and also an increase in ship breadth. The latter will tend to increase slightly the length of waves required to excite rolling, but it

may also have the more unfavorable effect of increasing the roll natural frequency.

Since resonance effects are very important in rolling, it would be desirable to design for a natural period that avoids resonance entirely. This is seldom possible because of the wide range of wavelengths to which a ship will respond in beam or quartering seas. However, it is fortunate that roll amplitudes are asymptotic to maximum wave slope in long waves (low frequencies), and therefore, except in the vicinity of resonance, the response will tend to the ideal situation—i.e., following the wave slope. Fig. 133 shows typical rolling response of a cargo ship to the angular components of both a mild and a rough short-crested beam seaway. Since this figure is in the log-slope format, the longer waves and lower frequencies are to the right. It is clear that moving the roll RAO to the right (lower natural frequency) would lead to a reduction in roll response, even to attainment of a supercritical condition as defined in Section 4. Furthermore, as the natural frequency is reduced (natural period increased) the resulting accelerations, with constant roll amplitude, would reduce as  $\omega_n^{-2}$ . A long natural period also reduces the likelihood of synchronous rolling, as a study of Fig. 134 (based on Fig. 78) will show. For any given range of wavelengths, the longer the natural period the narrower the range of directions and speeds at which synchronism will occur.

With this approach, as noted in Section 7.6 (Fig. 110), the longest practicable natural roll period of ships is favorable as far as reducing seasickness (MSI) is concerned. Ships with low natural frequency are usually known as *easy* rollers, while ships with high natural frequency are *stiff* and usually experience abrupt and unpleasant rolling. An example was the liner *Malolo* which was known as an uncomfortable ship until extensive alterations were made to reduce its  $\overline{GM}$ . (It was then renamed *Matsonia*).

A study of Equation (173), Section 3.8, shows that the simplest way to achieve a long natural period of roll is to adopt a low value of metacentric height,  $\overline{GM}$ . Unfortunately, this affects the ship's transverse stability adversely, and the minimum stability standards discussed in Chapters II and III may not be met. Reduction in  $\overline{GM}$  may involve reduction in beam, which is generally unfavorable to damping. Reducing the transverse gyradius is helpful in increasing the natural period, but it is usually governed by other design considerations.

A special case is the semi-submersible floating platform often used for oil drilling. It makes use of buoyancy cylinders located well below the sea surface, with an open structure of struts connecting them and supporting the platform above the water. These design features take advantage of the fact that wave excitation reduces rapidly with draft (i.e., depth below the surface) and the open construction leads to small waterplane moments of inertia, hence low stability but

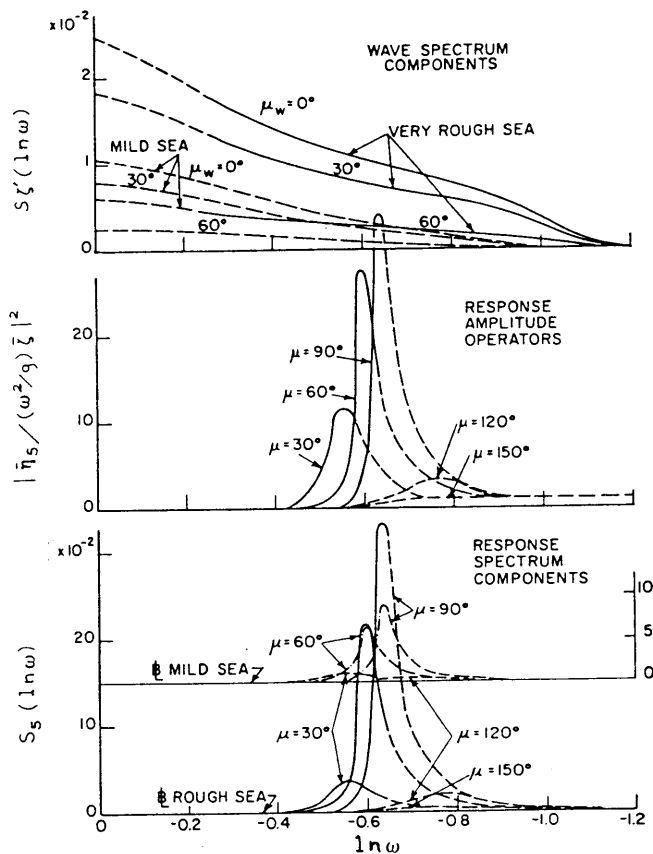


Fig. 133 Rolling response in short-crested irregular beam seas

long rolling period. The result is small rolling motion over a wide range of sea conditions.

Another approach to the reduction of rolling is to go in the direction of subcritical operation (Hutchison and Laible, 1987). This implies reduced natural period (increased natural frequency), which involves increased  $\overline{GM}$  and often increased beam. If carried far enough—as with a rectangular barge or floating platform—this could mean that resonant response, if limited by a high  $\overline{GM}$  to a range of wavelengths of say  $B/2$  and less, would be negligibly small because the hull would span at least two wavelengths and damping would be very high. Rolling in response to longer waves would tend to follow the wave slope and therefore would not be objectionable.

Hutchison and Laible (1987) have shown that a research vessel could be designed to provide an exceptionally steady platform with  $L/D = 3.4$  (instead of the usual 4.5 – 5.5). Of course, this vessel would not be expected to fully attain subcritical operation in all circumstances, but the design did move in that direction.

Although design for reduced rolling is difficult, roll is much easier to control than any other ship motion because transverse wave moments are relatively small. Since rolling response operators show sharp

peaks at resonance, over a narrow spread of wave frequencies, various devices other than bilge keels can be installed to further damp or otherwise reduce rolling, as discussed in Section 6. Many cruise ships and naval vessels are fitted with anti-rolling fins or passive anti-roll stabilizers, which are very effective in reducing roll. Cargo ships can also benefit from having one or the other of these devices installed. But as with all ships, the reduction in rolling attainable must be weighed against the disadvantages of the added direct cost of the anti-roll device, and its added weight, drag and required space, all of which may detract from the earning power of the ship. Fortunately, with the procedure for calculating voyage time as a function of season and route outlined in Section 7.8, the economic advantage of anti-roll stabilization can be quantified. Thus, the economic arguments for and against roll stabilization can be satisfactorily resolved, as considered in Section 8.6.

Another interesting possibility discussed in Section 6 is the use of rudders for control of roll as well as of heading of the ship. This scheme has the advantage of making use of an existing system, with some modifications, thus substantially reducing the cost, weight and resistance penalties. However, special care is required to the design of rudders that will produce large transverse as well as longitudinal moments.

Rolling is known to increase the resistance of a ship, although little quantitative data are available. External devices such as bilge keels or anti-rolling fins add their own resistance, but this effect is usually more than balanced by the reduction in roll-induced resistance produced. Hence, well-designed devices may be expected to have a favorable effect on powering and hence on fuel consumption.

Yawing and swaying in oblique seas, with the related rudder action, also increase resistance, but these effects are relatively minor. A more important aspect may be the leeway angle experienced in bow seas. This leeway angle may give rise to an induced drag of appreciable magnitude.

**8.5 High-performance ships.** The main emphasis of this book has been on conventional, monohull ships, but attention has also been given to other vehicle types that operate at the water-air interface. Since a good deal of the incentive for investigating some of the newer interface vehicle types resides in their promise to reduce motions in a seaway, some of the important seakeeping features of these newer vehicle types will be discussed in this section. For a more complete and also realistic discussion and appraisal of each type, particularly for naval applications, the reader is referred to Eames (1981) and to the special February, 1986, issue of the *Naval Engineers Journal*.

(a) *Catamarans.* An old type of craft that has been receiving attention in recent years is the catamaran, which can provide large deck areas and any degree of transverse stability, for use as a ferry, oceanographic

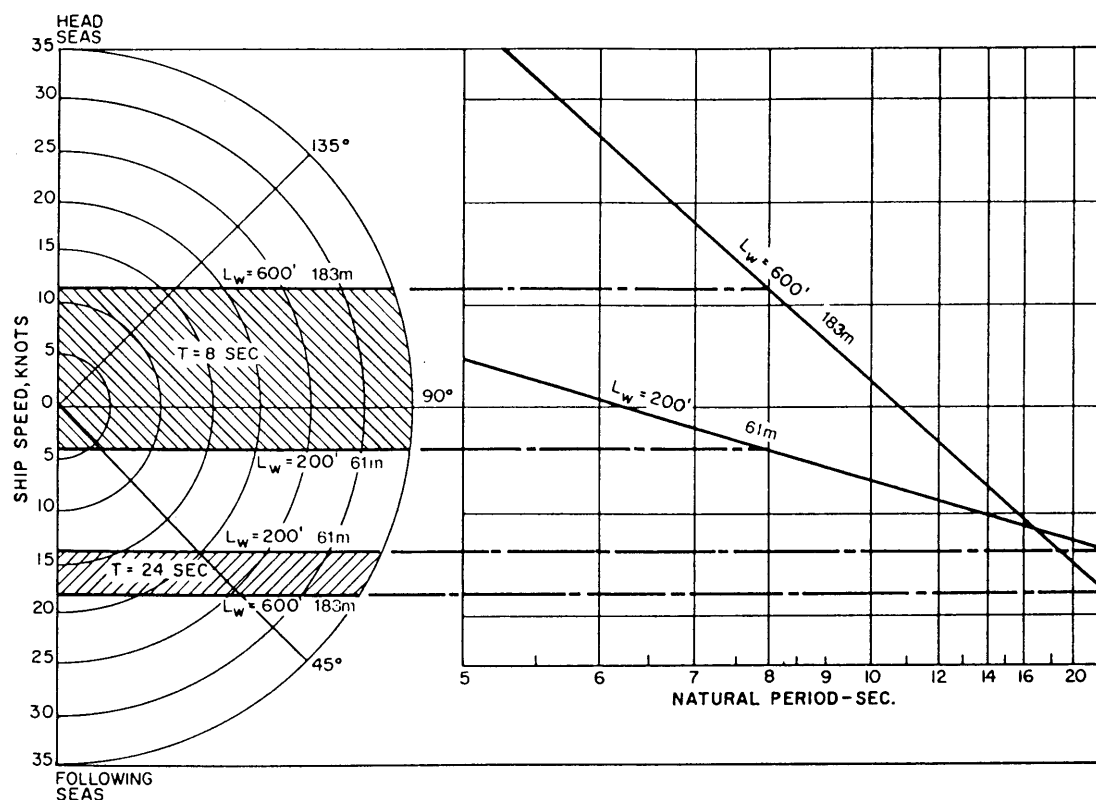


Fig. 134 Zones of probably heavy rolling of ships with 8 and 24-second roll periods among waves of 61 to 183-m (200-600-ft) length (see Fig. 78)

research ship or oil-drilling platform. Navy experience with the design of the oceanographic research catamaran *Hayes* (Hadler, Lee, et al 1974) has shown that relative bow motions were excessive in the open North Atlantic, resulting in slamming on the cross-structure. On the basis of research and development work at DTRC, a fixed hydrofoil was designed and installed forward between the two hulls to provide damping of pitch and heave. This was found to reduce relative bow motion and slamming to acceptable levels, and also reduced coupled roll-pitch or *corkscrew* motion.

The above paper also discusses other aspects of the seakeeping design problems of the catamaran, including choice of overall dimensions and the ratios  $L/B$  and  $L/T$ . It is recommended that roll and pitch natural periods be kept as far apart as possible to minimize corkscrew motion. An extension of basic ship motion theory is presented to permit the calculation of coupled pitch-heave motions, and in addition the loads on cross-structure connecting the two hulls. It is recommended that the design of the damping foil be undertaken at the beginning of the catamaran design, and a method for designing the foil is given.

(b) *SWATH*. A relatively new version of the older, twin-hull catamaran is the Small-Waterplane-Area Twin-Hull (SWATH), which is a noteworthy applica-

tion of the principle of supercritical operation discussed in Section 4. The SWATH configuration includes two streamlined, totally submerged, longitudinally oriented, buoyant hulls of circular or elliptical cross section. These two hulls support, by means of one or more vertical surface-piercing streamlined struts, the weight of a wide ship platform spanning both hulls located substantially above the air-water interface. Since the rough water surface is penetrated only by the thin, small-waterplane-area struts, not only is the excitation by ocean waves of the vertical motions of the SWATH reduced, compared to a conventional surface ship or to a traditional catamaran, but long natural pitching and heaving periods result. Hence, the SWATH is capable of attaining high-speed supercritical operation in moderately rough head seas, up to the point at which severe slamming on the cross-structure begins.

Numata (1980) described a number of SWATH vessels and gave results of model tests of four of them in calm water and in waves. These showed clearly the relatively light damping in pitch and heave, as well as roll, which makes them very sensitive under conditions of resonance, also (Lee and Curphey, 1977). Numata shows how the conditions for severe motion can be estimated by calculating the undamped natural period



of pitch and determining the forward speed that produces resonance with the component wave corresponding to the peak of the wave spectrum (modal period). (Use is made of Fig. 78, Section 4, for this purpose). To attain supercritical operation in head seas the forward speed must be well above this critical speed. However, as resonant conditions are approached, it has been found that fixed or controllable foils can provide effective damping of pitch and heave.

In stern seas the long natural pitching and heaving periods may delay achievement of supercritical operation until very high, perhaps unrealistic, speeds, and will contribute to critical yaw motions at low speeds. To minimize these effects, the anti-pitching fins fitted forward and aft are effective. By canting these fins downward they may also be used as rudders, thus obviating the need for a separate rudder system for steering.

Lee and Curphey (1977) have presented a modified linear theory for calculating SWATH motions. A strip method is used for obtaining hydrodynamic coefficients, and allowance is made for viscous damping effects and for the lift and moment of the stabilizing fins. Good results were obtained in comparing theoretical calculations of motion with experimental data on two models. However, improvement in theory is needed for the case of following waves, especially when controllable fins are to be used. McCreight (1987) gives a methodology for investigating the relationship between hull characteristics and seakeeping performance. See also Lamb (1987).

It is important to notice that SWATH ships (and most supercritical ships) must be designed to make a smooth transition between sub-critical and super-critical modes of operation. In the case of SWATH, as the wave height gets so large that cross-structure slamming would occur, so does the wave period get large. This long wave period is in better tuning to the ship's heave period, and results in increased heave response, which may assist the ship in lifting itself above the oncoming wave and avoiding slams. In SWATH design the selection of heave natural period as a function of cross structure height is important.

(c) *Planing craft* develop dynamic lift not by means of foils but rather by virtue of the angle of attack of the relatively flat bottom of their hulls. At low speed they are completely buoyantly supported, while at top speed they are partially supported by dynamic lift and partially by buoyancy.

In smooth water and slightly rough seas planing craft can attain high (super-critical) speeds. But as seas become rougher severe pounding, with high vertical accelerations, are experienced in head seas. Hence, the selection of suitable dead-rise angles is vitally important (Savitsky and Brown, 1976), (Martin, 1978).

An interesting development of a planing craft with high rough-water speeds is the so-called *Sea Knife*

(Payne, 1974). The hull is narrow, so that the planing surface is relatively small and the waterline endings very sharp. This permits the hull to cut through the waves and attain a supercritical condition of operation.

(d) *Hydrofoil craft*. Among the dynamically supported vehicles, the hydrofoil ship is like the SWATH ship in that the hull is also carried above the water surface by struts. But in the hydrofoil case the support is provided by transversely oriented, hydrodynamic lifting surfaces (hydrofoils) rather than by longitudinally-oriented buoyant hulls. Many commercial hydrofoil ships are built with fixed transverse foils incorporating a dihedral so oriented that the hydrofoils pierce the free surface in the normal flying mode. This arrangement provides the vehicle with inherent vertical, transverse and longitudinal stability. On the other hand, most military and some commercial hydrofoil craft are built with completely submerged hydrofoils, having little or no dihedral, which require an automatic control system to provide vehicle stability. Ships with submerged foils have the advantage of reduced drag and reduced motions in rough seas, but are considerably more expensive to build than hydrofoil craft with surface-piercing foils.

Hydrofoil craft can easily attain supercritical operation in seas of moderate severity, when the hull is carried clear of the wave crests. Some problems in seakeeping design of both types of hydrofoil craft and methods of solution are discussed by Hirsch (1967) and Johnson (1985).

(e) *ACV and SES craft*. Both Air Cushion Vehicles (ACV) and Surface Effect Ships (SES) are supported by a pressurized cushion of air between the water surface and the bottom of the vehicle. With the ACV the air cushion is contained within a flexible peripheral skirt around the entire hull. Using air propulsion, ACV may be a truly amphibious craft. In contrast to the ACV, the SES has two sidewalls that penetrate the water surface and help contain the air cushion. They not only decrease cushion air losses but also increase water drag and deny amphibious operation to the SES. Resistance "hump" characteristics dictate that an SES designed for speeds between 40 and 60 knots incorporate a high length-to-beam ratio. These speeds may be sub-or supercritical depending on sea conditions.

ACVs have been extensively developed in Great Britain under the designation *hovercraft*. They have been successful in commercial operation, notably in providing regular ferry service across the English Channel. These craft have low  $L/B$  ratios, and their seakeeping performance depends greatly on their ability to maintain height above the water surface to clear the tops of the waves. Seakeeping problems are discussed by Lavis (1972), Moran, Fein and Magnuson (1974) and Bebar, Kennell, et al (1985).

For SES craft equations of motion with six degrees of freedom are presented in a paper by Kaplan, Benton and Davis (1981), where the important differences

in dynamic behavior between SES and conventional mono-hulls are discussed. It is interesting to note that pitch/heave wave excitation forces on the SES arise mainly from variations in the buoyancy of the immersed sidewalls, since "the greater part of the wave-induced forces are imparted through the air cushion at a uniform pressure." Rolling motion is affected by sidewall draft, which determines when sidewall emergence will occur, and by distance between sidewalls relative to  $KG$ , which affects the natural period of roll.

Verification of theoretical motion calculations by model tests is complicated by the fact that cushion air pressure does not follow Froude scaling. The procedure adopted is to carry out computer calculations "for the same test conditions at the same scale as the model itself is experiencing. The results of the model test and the computer program outputs are then to be compared." If the theory is thus verified for model scale, then it can be used with confidence to compute full-scale motions. In the work of Kaplan, et al (1981), the theory was found to agree reasonably well with model tests for pitch and heave in head seas for six SES designs for which model results were available. A few comparisons with full-scale test craft have indicated generally good results from combined model tests and theoretical calculations. But direct comparisons are difficult because of wave measurement problems at sea.

In general, SES craft experience high vertical accelerations in head seas because of the high frequencies of wave encounter and the pressure pulses experienced with air leakage in the bow-up condition. Hence, some type of *ride control system* is required on an SES operating in the open sea. This involves the controlled alteration of cushion air pressure and has been quite successful (Kaplan, et al 1981).

### 8.6 Seakeeping Design Procedures. (a) General.

Because of the importance to seakeeping performance of ship or "platform" configuration and dimensions, it is clear that for best results seakeeping considerations should be taken into account at the earliest stages of design, before basic dimensions and other parameters have been selected. Hence, it is important to consider rational design procedures that make this possible.

For high-speed ships an early consideration is whether the mission or service of the ship involves primarily sub- or super-critical operation in rough seas. All ships, no matter how designed, achieve super-critical operation if the sea state is mild enough, but in the severe seas often experienced in the open ocean most ships cannot be expected to push above the critical zone, and therefore the sub-critical (or critical) regime has more influence on design. However, for high-performance craft, such as are discussed in the preceding sub-section, there may be a choice, which can have a drastic effect on the design.

For example, there are certain missions for which either a fine, monohull with short pitching period or a

SWATH design with a long period might be suitable. In fact, McCreight and Stahl (1985) have attempted a seakeeping performance assessment of several designs of each type, indicating the circumstances under which either might be preferred. Kennell, et al (1985) compared two monohull designs and a SWATH.

For most ships, regardless of speed, the critical and sub-critical ranges of operation govern design for seakeeping. This usually calls for short natural periods of pitch and heave, together with as high damping as possible.

It is also important to decide as soon as possible in the design as to whether or not special anti-rolling devices (other than bilge keels) or anti-pitching fins are to be considered (See Section 6).

In a chapter, "Mission Analysis and Basic Design," by R. K. Kiss (Taggart, 1980) the importance of considering rough weather performance early in the design of any ship is emphasized (Section 3, Concept Design). It is explained that, "for any particular set of requirements, there is an infinite number of combinations which give the transport or mission capability desired; i.e., for cargo ships: capacity, deadweight, speed and endurance." Computer-aided parametric studies provide a means for exploring a wide range of ship proportions and form, and determining those combinations that provide acceptable technical solutions. The guidelines in Sections 8.1–8.5 can be used in deciding what alternate design configurations and range of hull characteristics are to be explored. It is particularly important that a wide range of lengths be included. The next step is then to produce alternate preliminary or concept designs for consideration. Seakeeping evaluations can then be carried out and finally, a selection made of the final design on the basis of economics, as discussed subsequently.

For the seakeeping evaluation, the theory of ship motions presented in Sections 3 and 4 provides valuable tools for predicting the motions of a specific hull, or comparing alternative designs, in specific sea conditions at stated speeds and headings. For our purpose these studies must include the derived responses discussed in Section 5 that correspond to the criteria presented in Section 7. These include accelerations at critical points, frequency of slamming and of shipping water, and added resistance and power. Calculations may be supplemented by self-propelled model tests in irregular waves, especially when estimates based on empirical data must be used.

Repeated computer calculations provide the best means of identifying directly the precise effect of changing the various parameters defining hull proportions and form. Each parameter affects the various coefficients in the equations of motion differently, and the coefficients depend in turn on frequency of wave encounter, forward speed, etc. Furthermore, coupling between modes of motions, phase angles and forward speed influence the manner in which the various terms

in the equations interact. Therefore, several sets of calculations—perhaps supplemented by comparative model tests—are needed.

It should be noted that the calculation of power requirements in different sea conditions, ship headings and speeds is needed not only for the seakeeping evaluation (SPI-2) but also for the reliable determination of required installed power for the machinery design of a fast ship in a rough-weather service, where an arbitrary percentage addition to trial power would be unsatisfactory (Lewis, 1958). If the calculated average voyage speed is not adequate for the proposed operating schedule there are two steps possible in the design stage. One is to increase the maximum power in order that speed can be increased when the more moderate sea conditions prevail; the service power requirement would then be determined by the duration of the periods of more moderate seas during which the time lost must be made up. The other method of decreasing voyage time is to modify ship size, proportions, freeboard, ballast capacity, or other characteristics in order to raise the limiting speeds in the more severe sea conditions.

The seakeeping evaluation of alternative designs involves the choice of a suitable index, as discussed in Section 7. For merchant ships, and naval transit missions, the principal measure of seakeeping performance is the Transit Speed Index, SPI-2. Since this involves both voluntary and involuntary speed reduction it depends on both ship motions and added power required in waves. For most naval ships the principal index is that of Mission Effectiveness, SPI-1, which involves the many factors discussed in Section 7. This index also applies to survey vessels and fishing craft on station.

Although the procedures discussed in Section 7 for calculating the seakeeping performance indexes were intended mainly for naval vessels, they can be applied—perhaps with some shortcuts—to commercial ships as well. These techniques involve the use of Speed Polar Plots, with Seakeeping Operating Envelopes (SOE), the Operability Index (OI) as a function of sea state and finally the appropriate overall, long-term Seakeeping Performance Index (SPI-1 or 2). Separate discussions follow for merchant and naval ships.

(b) *Merchant ship evaluation.* Having established a number of alternative acceptable concept hull designs, the principal subjects for study are motions and added power requirements in waves. Using the techniques discussed in previous sections, ship responses can be predicted in different representative sea conditions, at various speeds and headings, and estimates made of attainable speed and required power. Considering the frequency of occurrence of the different sea conditions expected in the ship's service, the average voyage speeds or times (SPI-2) can be estimated for different seasons, along with the corresponding power requirements.

Procedures for technical evaluation have been presented by Chrysosostomidis (1972), Bringloe (1978) and Hutchison (1981) in more or less detail. However, the final evaluation should be in economic terms (Mandel and Leopold, 1966). This may be done on the basis of Required Freight Rate (RFR), computed first for each design under ideal fine weather conditions. To obtain RFR under operational sea conditions the ship performance calculations must be extended to cover fuel consumption at reduced speeds, and effects of rough weather delays on port times, hence on cargo handling and other terminal costs. The final evaluation may then be in the form of a plot of overall annual RFR against ship length, first under ideal calm weather and then under actual anticipated service conditions. Such a plot would not only establish the optimum design but would indicate the penalties involved in departure from the optimum because of considerations of first cost, terminal or port restrictions, etc.

Although the approach to merchant ship design just described is not in general use, current research sponsored by the H-7 Panel of SNAME has developed the procedure in more detail and applied it to the design of a 21-knot container ship for North Atlantic service (Sellars and Setterstrom, 1987). Fig. 135 is a plot of results tabulated in the paper for alternative designs intended to provide regular weekly liner service between New York and a European port with three ships of 1290 TEU capacity (7,600 miles round trip). Preliminary economic studies of ships 175 to 251 m (575 to 825 ft) in length had established that under ideal calm water conditions the minimum RFR was obtained with a 183-m (600-ft) ship (0.55 block coefficient). Designs for seakeeping evaluation in the figure ranged from 183 to 251m (600 to 825 ft) in length and 169 to 78 in  $W/(L/100)^3$ , using the better of two operating schedules studied. Comparative costs are expressed in terms

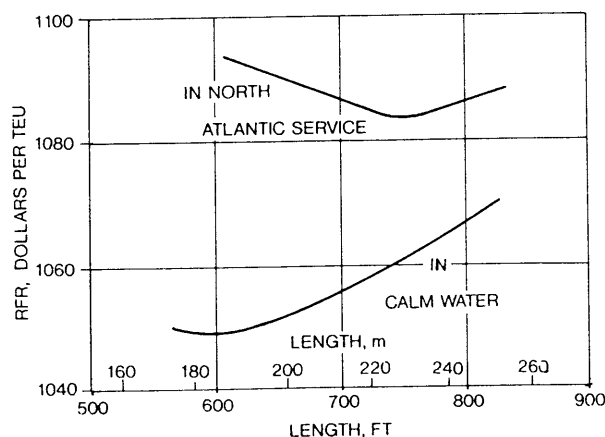


Fig. 135 Variation of Required Freight Rate with ship length

of RFR/TEU, where RFR is based on total operating costs, including annualized initial costs and costs of cargo handling and of fuel at \$156 per long ton.

It may be seen in the figure that the optimum design under realistic operating conditions is the one with 229-m (750-ft) length, which is substantially different from the 183-m (600-ft) length determined for calm water. However, the difference in RFR is only \$10/TEU or about 1 percent. The question remains as to whether or not the saving (in fuel and cargo handling costs) is worth the extra initial and operating costs. The paper notes that a *benefit-to-cost ratio*, defined as the ratio of fuel and cargo handling cost reductions to the sum of increases in capital and operating costs, is about 1.8 for the 229-m (750-ft) ship; 2.0 for the 312-m (700-ft) design. For longer trade routes, such as Seattle to Tokyo, the savings are expected to be greater.

(c) *U.S. Navy design procedure.* Following a Navy Seakeeping Workshop (NAVSEC, 1975) the U.S. Navy not only accelerated its seakeeping research but began the development of procedures that allowed seakeeping to be incorporated into the routine process of surface ship hull design. The procedure, as described in Section 7 and in Keane and Sandberg (1984), involves the evaluation of seakeeping performance of alternative designs, along with the evaluation of speed and power and of maneuverability. Use is made of the Seakeeping Performance Indexes also discussed in Section 7, and described by Comstock and Keane (1980). Examples of the evaluation of alternative naval designs were given in Comstock, et al (1980), McCreight and Stahl (1985) and Kennell, et al (1985), as well as in Sections 7.7-7.8.

An important refinement introduced by Lin, Day, et al (1984) was to "evaluate the seakeeping performance at the same time, or preferably before, optimizing the hull form for powering, within given constraints." As they explain, in the traditional hydrodynamic design of hull forms, the primary consideration has been to achieve good performance in calm-water resistance and powering. Seakeeping usually has not been considered in selecting the primary hull form design parameters. However, Bales (1980) developed an approximate Seakeeping Rank Estimator and demonstrated that the use of such a method based on ship-motion theory can provide major improvements in the seakeeping characteristics of a hull design. It was feared that such hull designs optimized for seakeeping alone might sustain higher-than-normal resistance.

Experience and theoretical analyses have shown that calm-sea resistance characteristics of a hull design are more sensitive than seakeeping characteristics to local hull geometry changes. Therefore, Lin, Day, et al felt that if a hull is optimized first for seakeeping, it is likely to have enough flexibility for additional modifications in local geometry to reduce resistance while maintaining good seakeeping characteristics, but not vice versa.

An example is given by Lin, Day, et al (1984) in which the foregoing procedure was followed in a naval ship design and an excellent compromise obtained by:

- Keeping a large value of  $C_w$  and small value of  $C_{vp}$  in the forebody to favor good seakeeping without significant effect on resistance.
- Adopting a wide transom stern instead of a cruiser stern, to improve the resistance without reducing waterplane coefficient.

Economics should not be neglected in the case of naval vessels, but design studies are often limited to considering initial cost in relation to overall mission performance, without attention to operating costs. In time of war it can be argued that economic considerations in the design of naval ships are definitely secondary to mission performance. Yet even then, since cost represents an index of resources expended, both physical and manpower, economics cannot be overlooked. In any case, it can also be argued that in peacetime federal budget limitations dictate that both initial and operating costs be given full consideration in design (Leopold, 1974).

It has been shown that the economic evaluation of commercial ship designs usually involves the total annual cost, including both the annualized (or amortized) initial cost and the annual operating cost; which can then be related to the annual quantity of cargo carried. In the case of many government projects, it has been customary to take the alternative approach of determining the life-cycle cost, i.e., the initial cost plus the total lifetime operating cost. For ships (or fleets of ships) the design that would accomplish a desired mission (or group of missions) at the lowest life-cycle cost would then be the optimum design. As a practical matter, only initial costs are usually considered in naval design procedures.

An example of a military economic study was given by Gatzoulis and Keane (1977) for the case of proposed installation of active fin stabilizers on a class of frigates, with respect to helicopter operations. Operational effectiveness was evaluated in terms of percentage-time that helicopter operations could be performed with certain assumed profiles of ship speed vs. time, heading to the sea and sea state. Hence, it was possible to determine the improved effectiveness of the frigate with stabilizers and to compare this with the initial cost of their installation. In this case it was found that the effectiveness increased many times faster than the cost.

Brown (1985) presents a method of placing a dollar value on the seakeeping performance of surface warships. The method is based on the assumption that the value of the ship is equal to the total cost per day (capital charges plus operating expenses) of keeping the ship at sea. This value can be determined both for ideal, calm sea conditions and for several sea states, and then a weighted average calculated for an expected profile of sea states.

## REFERENCES

- Abkowitz, M.A. (1959), "The Effect of Antipitching Fins on Ship Motions," *SNAME Transactions*, Vol. 67.
- Abkowitz, M.A., Vassilopoulos, L.A. and Sellars, F. (1966), "Recent Developments in Seakeeping Research and its Application to Design," *SNAME Transactions*, Vol. 74.
- Abkowitz, M.A. (1969), "Stability and Control of Ocean Vehicles," MIT Press, Cambridge, Mass.
- Aertssen, G. (1966), "Service Performance and Seakeeping Trials of M.V. *Jordaens*," *Trans. RINA*, London, Vol. 114.
- Aertssen, G. (1968), "Laboring of Ships in Rough Seas with Special Emphasis on the Fast Ship," *SNAME Diamond Jubilee International Meeting*.
- Aertssen, G., and van Sluijs, M.F. (1972), "Service Performance and Seakeeping Trials on a Large Container Ship," *Trans. RINA*, London, Vol. 114.
- Allen, R.G. and R.R. Jones (1978), "Structural Design-Limit Pressures on High Performance Marine Vehicles," AIAA and SNAME Advanced Marine Vehicles Conference.
- Andrew, R.N. and A.R.J.M. Lloyd (1981), "Full-Scale Comparative Measurements of the Behavior of Two Frigates in Severe Rough Seas," *Trans. RINA*, London, Vol. 116.
- Ankudinov, V.K. (1972), "The Added Resistance of a Moving Ship in Waves," *International Shipbuilding Progress*, Vol. 19.
- Bai, K.J. and McCarthy, J.H. (Eds.) (1979), *DTRC Proceedings*, Workshop on Ship Wave-Resistance Computations.
- Baitis, A.E. et al (1976a), "Prediction of Extreme Ammunition Cargo Forces at Sea," *DTRC Report SPD-704-01*.
- Baitis, A.E. (1975), "Influence of Ship Motion on Operations of SH-2F Helicopters from DE 1052 Class Ships," *DTRC Report SPD-556-01*.
- Baitis, A.E., Appleby, T.R. and Meyers, W.G. (1981), "Validation of the Standard Ship Motion Program, SMP: Ship Motion Transfer Function Prediction," *DTRC Report SPD-0936-03*.
- Baitis, A.E., Woolaver, D.A., and Beck, T.A. (1983), "Rudder Roll Stabilization for Coast Guard Cutters and Frigates," *Naval Engineers Journal*.
- Baitis, A.E. et al (1976b), "A Non-Aviation Ship Motion Data Base for the DD963, CC 26, FF 1052, FFG 7 and the FF 1040 Ship Classes," *DTRC Report SPD-788-01*.
- Bales, N.K. and Cummins, W.E. (1970), "The Influence of Hull Form on Seakeeping," *SNAME Transactions*, Vol. 78.
- Bales, N.K. (1978), "Notes Regarding Wave-Induced Performance Limitations of Destroyer and Frigates (U)," *DTRC Report SPD-C-811-02*.
- Bales, N.K. (1979), "Minimum Freeboard Requirements for Dry Foredecks: A Design Procedure," *Proceedings*, SNAME Star Symposium, Houston.
- Bales, N.K. (1980), "Optimizing the Seakeeping Performance of Destroyer-Type Hulls," 13th ONR Symposium on Naval Hydrodynamics, Tokyo.
- Bales, N.K., and Day, (1982), "Experimental Evaluation of a Destroyer-Type Hull Optimized for Seakeeping," *SNAME, STAR Symposium*.
- Bales, N.K., and Cieslowski, D.S. (1981), "A Guide to Generic Seakeeping Performance Assessment," *Naval Engineers Journal*, April.
- Bales, S.L. et al (1975), "Rigid Body Ship Responses for a Series of LNG Ships," *DTRC Report SPD-517-04*.
- Bales, S.L., Lee, W.T. and Voelker, J.M. (1981), "Standardized Wave and Wind Environments for NATO Operational Areas," *DTRC Report SPD-0919-01*.
- Bales, S.L., Cummins, W.E., and Comstock, E.N. (1982), "Potential Impact of Twenty Year Hindcast Wind and Wave Climatology in Ship Design," *Marine Technology*, Vol. 19 No. 2, April.
- Bales, S.L. (1982), "Development and Application of a Deep Water Hindcast Wave and Wind Climatology," *International Symposium on Wave and Wind Climate Worldwide*, RINA, London.
- Band, E.G.U. (1964), "A Rational Basis for Determining Bow Freeboard of Large Tankers," *Webb Institute Report*.
- Barber, N.F. (1963), "The Directional Resolving Power of an Array of Wave Detectors," in *Proceedings of Conf.*, published as *Ocean Wave Spectra*, Prentice-Hall, New York.
- Barr, R.A. and Ankudinov, V. (1977), "Ship Rolling, Its Prediction and Reduction Using Roll Stabilization," *Marine Technology*, Vol. 14, No. 1.
- Bassett, P.R. and Hodgkinson, F.P. (1935), "New Studies of Ship Motions," *SNAME Transactions*, Vol. 43.
- Bates, J.L. (1945), "Large Passenger-Carrying Ships for Certain Essential Trade Routes," and Discussion, *SNAME Transactions*, Vol. 53.
- Bebar, M.R., Kennell, C., White, W. and Lavis, D. (1985), "Advanced Marine Vehicles—a Review," *Workshop on Hull Form Design*, MARIN, Wageningen, the Netherlands.
- Beck, R.F. (1982), "Relative Motion Components for a Mathematical Form in Regular Waves," *Proceedings*, 14th Symposium on Naval Hydrodynamics, University of Michigan, Ann Arbor, Mich.
- Beck, R.F. and Troesch, A.W. (1980), "Wave Diffraction Effects in Head Seas," *International Shipbuilding Progress*, Vol. 27.
- Bell, J. and Walker, W.P. (1966), "Activated and Passive Controlled Fluid Tank System for Ship Stabilization," *SNAME Transactions*, Vol. 74.
- Bendat, J.S., and Piersol, A.G. (1971), *Random*

*Data: Analysis and Measurement Procedures*, Wiley-Interscience, New York.

Bermejo, R.T. (1965), "Added Mass and Damping Coefficients for Ships Heaving in Smooth Water," MIT Report No. 65-5.

Beukelman, W. and Buitnhek, M. (1973), "Full Scale Measurements and Predicted Seakeeping Performance of the Container Ship *Atlantic Crown*," *International Shipbuilding Progress*, Vol. 21, No. 243.

Beukelman, W. and Huijser, A. (1977), "Variations of Parameters Determining Seakeeping," *International Shipbuilding Progress*, Vol. 24, No. 275.

Beukelman, W. (1979), "Bottom Impact Pressures Due to Forced Oscillations," Delft Technical University Report No. 479.

Bhattacharyya, R. (1978), *Dynamics of Marine Vehicles*, Chapter 14 - "Motion Stabilization," Wiley-Interscience, New York.

Bishop, R.C., and Bales, N.K. (1978), "A Synthesis of Bow Wave Profile and Change of Level for Destroyer-type Hulls, with Application to Computing Freeboard Requirements," DTRC Report No. 78-SPD-811-01.

Bishop, R.E.D., Price, W.G. and Tam, P.K.Y. (1978a), "The Representation of Hull Sections and its Effects on Estimated Hydrodynamic Actions and Wave Responses," *Trans.*, RINA, Vol. 121.

Bishop, R.E.D., Price, W.G. and Tam, P.K.Y. (1978b), "Hydrodynamic Coefficients of Some Heaving Cylinders of Arbitrary Shape," *International Journal for Numerical Methods in Engineering*.

Bishop, R.E.D., Price, W.G. and Temarel, P. (1980), "Hydrodynamic Coefficients of Some Swaying and Rolling Cylinders of Arbitrary Shape," *International Shipbuilding Progress*, Vol. 27, Number 307.

Blok, J.J. and Beukelman, W. (1984), "The High-Speed Displacement Ship Systematic Series Hull Forms — Seakeeping Characteristics," *SNAME Transactions*, Vol. 92.

Borodai, I.K. and Netsvetayev, Y.A. (1969), *Ship Motions in Ocean Waves*, (in Russian), *Sudostoren*, Leningrad.

Borresen, R. (1980), "On the Irregular Frequency Problem in the Theory of Ship Motions," Det norske Veritas, Report No. 80-0674.

Bretschneider, C.L. (1952), "The Generation and Decay of Wind Waves in Deep Water," *Trans. American Geophysical Union*, Vol. 37.

Bretschneider, C.L. (1957), "Review of Practical Methods for Observing and Forecasting Ocean Waves by Means of Wave Spectra and Statistics," *Trans. American Geophysical Union*, April.

Bringle, J.T. (1978), "Application of Seakeeping Analysis," *Marine Technology*, Oct.

Brown, D.K. (1985), "The Value of Reducing Ship Motions," *Naval Engineers Journal*, March.

Canham, H.J.S., Cartwright, D.E., Goodrich, G.J., and Hogben, N. (1962), "Seakeeping Trials on O.W.S. *Weather Reporter*," *Trans.*, RINA, London.

Cartwright, D.E., and Longuet-Higgins, M.S. (1956), *Proceedings*, Royal Society of London, Series A., Vol. 237.

Chadwick, J.H. and Klotter, K. (1954), "On the Dynamics of Anti-Rolling Tanks," *Schiffstechnik*, Band 2, Heft 3.

Chadwick, J.H., (1955), "On the Stabilization of Roll," *SNAME Transactions*, Vol. 63.

Chang, M-S and Pien, P.C. (1975), "Hydrodynamic Forces on a Body Moving Beneath a Free Surface," *Proceedings*, First International Conference on Numerical Ship Hydrodynamics, DTRC, Bethesda, Md.

Chang, M-S. and Pien, P.C. (1976), "Velocity Potentials of Submerged Bodies Near a Free Surface-Appliation to Wave-Excited Forces and Motions," *Proceedings*, 11th Symposium on Naval Hydrodynamics, London.

Chang, M-S. (1977), "Computations of Three-Dimensional Ship Motions with Forward Speed," *Proceedings*, 2nd International Conference on Numerical Ship Hydrodynamics, University of California, Berkeley, Cal.

Chapman, R.B. (1975), "Numerical Solution for Hydrodynamic Forces on a Surface-Piercing Plate Oscillating in Yaw and Sway," *Proceedings*, 1st International Conference on Numerical Ship Hydrodynamics, DTRC, Bethesda, Md.

Chase, J., Cote, L.J., et al. (1960), "The Directional Spectrum of a Wind-Generated Sea as Determined from Data Obtained by the Stereo Wave Observation Project," New York University, College of Engineering Report.

Chen, H.T., Chen, H.H., and Hoffman, D. (1979), "The Implementation of the 20-year Hindcast Wave Data in the Design and Operation of Marine Structures," Offshore Technology Conference.

Chou, S.J., Oakley, O.H., Paulling, J.R., van Slyke, R., Wood, P.D. and Zink, P.F. (1974), "Ship Motions and Capsizing in Astern Seas," U.S. Coast Guard Report, No. CD-D-103-75.

Chrysostomidis, C. (1972), "Seakeeping Considerations in a Total Design Methodology," 9th ONR Symposium on Naval Hydrodynamics.

Comstock, E. and Keane, R.G., (1980), "Seakeeping by Design," *Naval Engineers Journal*, Vol. 92, No. 2.

Comstock, E.N., Bales, S.L. and Keane, R.G. (Comstock, et al) (1980), "Seakeeping in Ship Operations," SNAME STAR Symposium, San Diego.

Conolly, J.E. and Goodrich, G.J. (1970), "Sea Trials of Antipitching Fins," *Trans. RINA*, Vol. 112.

Cox, G.G. and Lloyd, A.R. (1977), "Hydrodynamic Design Basis for Navy Ship Roll Motion Stabilization," *SNAME Transactions*, Vol. 85.

Cummins, W.E. (1959), Discussion of Abkowitz (1959).

Cummins, W.E. (1962), "The Impulse Response Function and Ship Motions," *Schiffstechnik*, Vol. 9.

Cummins, W.E. (1974), "Pathologies of the Transfer



Functions," SNAME T&R Symposium S-3 on Sea-keeping.

Cummins, W.E. and Bales, S. (1980), "Extreme Value and Rare Occurrence Wave Statistics for Northern Hemispheric Shipping Lanes," SNAME STAR Symposium.

Cummins, W.E., Bales, S.L., and Gentile, D.M. (1981), "Hindcasting Waves for Engineering Applications," *Proceedings of the Symposium on Hydrodynamics in Ocean Engineering*, Norwegian Hydrodynamic Laboratories, Trondheim, Norway.

Dalzell, J.F. and Yamanouchi, Y. (1958), "Analysis of Model Tests in Irregular Seas to Determine Motions Amplitudes and Phase Relationships to Waves," Davidson Laboratory Report, Stevens Institute of Technology.

Dalzell, J.F. (1962), "Cross-spectral Analysis of Ship Model Motions: a Destroyer Model in Irregular Long-crested Head Seas," Davidson Laboratory Report 810, Stevens Institute of Technology.

Dalzell, J.F. (1963), "Some Further Experiments on the Application of Linear Superposition Techniques to the Responses of a Destroyer Model in Extreme Long-crested Head Seas," Davidson Laboratory Report 918, Stevens Institute of Technology.

Dalzell, J.F. (1964), "An Investigation of Midship Bending Moments Experienced in Extreme Regular Waves by Models of the Mariner Type Ship and Three Variants," Ship Structure Committee, SSC-155.

Dalzell, J.F. (1964), "An Investigation of Midship Bending Moments Experienced in Extreme Regular Waves by Models of a Tanker and a Destroyer," Ship Structure Committee, SSC-156.

Dalzell, J.F. (1976), "Application of the Functional Polynomial Model to the Ship Added Resistance Problem," 11th Symposium on Naval Hydrodynamics, University College, London.

Dalzell, J.F., and Kim, C.H. (1976), "Analytical Investigation of the Quadratic Frequency Response for Added Resistance," Davidson Laboratory Report SIT-DL-76-1878, Stevens Institute of Technology.

Davidson, K.S.M. (1948), "A Note on Steering of Ships in Following Seas," *Proceedings*, 7th International Congress for Applied Mechanics, London, Vol. 2.

Day, W.G., Reed, A.M. and Lin, W.C. (1977), "Experimental and Prediction Techniques for Estimating Added Power Requirements in a Seaway," *Proceedings*, 18th ATTC, Annapolis, Md.

DeJong, B. (1973), "Computation of the Hydrodynamic Coefficients of Oscillating Cylinders," Netherlands Ship Research Center Report.

Demanche, J.F. (1968), "Added Mass and Damping Coefficients for Cylinders with a Bulb-Like Cross-Section Oscillating in a Free Surface," M.S. Thesis, MIT, Cambridge, Mass.

Dillon, E.S., and Lewis, E.V. (1955), "Ships with Bulbous Bows in Smooth Water and in Waves," SNAME Transactions, Vol. 63.

DOD (1981), "Human Engineering Design Criteria for Military Systems, Equipment and Facilities," MIL-STD 1472c.

Donelan, M., and Pierson, W.J. (1983), "The Sampling Variability of Estimates of Spectra of Wind-Generated Gravity Waves," *Journal of Geophysical Research*, Vol. 88, No. C7.

Eames, M.C. (1980), "Advances in Naval Architecture for Future Surface Warships," *The Naval Architect*.

Ewing, J.A. (1967), "The Effect of Speed, Forebody Shape and Weight Distribution on Ship Motions," *Trans. RINA*, London.

Ewing, J.A. (1975), "Some results from the Joint North Sea Wave Project of Interest to Engineers," *Proceedings*, Symposium on the Dynamics of Marine Vehicles and Structures in Waves, April 1974, Institution of Mechanical Engineers, London.

Exp. Tank Com. of Japan (1954), "An Investigation into the Seagoing Qualities of the S.S. *Nissei Maru* by Actual and Model Ship Experiments," Seventh ITTC.

Faltinsen, O. (1971), "Wave Forces on a Restrained Ship in Head Sea Waves," Ph.D. Thesis, University of Michigan, Ann Arbor, Mich.

Faltinsen, O.M. (1974), "A Numerical Investigation of the Ogilvie Tuck Formulas for Added Mass and Damping Coefficients," *Journal of Ship Research*, Vol. 18, No. 2.

Faltinsen, O.M., and Michelsen, F.C. (1974), "Motions of Large Structures in Waves at Zero Froude Number," *Proceedings*, International Symposium on Dynamics of Marine Vehicles in Waves, University College, London.

Faltinsen, O.M. (1983), "Bow Flow and Added Resistance of Slender Ships at High Froude Number and Low Wave Lengths," *Journal of Ship Research*, Vol. 27, Number 3.

Frank, W. (1967), "Oscillation of Cylinders in or Below the Free Surface of Deep Fluids," Report Number 2375, DTRC, Bethesda, Md.

Frank, W. and Salvesen, N. (1970), "Frank Close-Fit Ship-Motion Computer Program," Report No. 3289, DTRC, Bethesda, Md.

Fridsma, G. (1969), "A Systematic Study of the Rough Water Performance of Planing Boats," Davidson Laboratory Report 1275, Stevens Institute of Technology.

Froude, W. (1861), "On the Rolling of Ships," *Trans., INA*, London.

Fujii, H. and Takahashi, T. (1975), "Experimental Study on Lateral Motions of a Ship in Waves," International Conference on Stability of Ships and Ocean Vehicles, University of Strathclyde, Glasgow.

Garrison, C.J. (1974), "Hydrodynamics of Large Objects in the Sea Part I: Hydrodynamics Analysis," *Journal of Hydronautics*, Vol. 8.

Garrison, C.J. (1975), "Hydrodynamics of Large Ob-

jects in the Sea Part II: Motion of Free-Floating Bodies," *Journal of Hydronautics*, Vol. 9.

Garrison, C.J. (1978), "Hydrodynamic Loading of Large Offshore Structures: Three-Dimensional Source Distribution Methods," *Numerical Methods in Off-shore Engineering*.

Gatzoulis, J. and Keane, R.G. (1977), "Upgrading Mission Capability and Performance Effectiveness of Naval Ships by the Use of Active Fin Stabilizers," Association of Scientists and Engineers, NAVSEA.

Gerritsma, J. (1960), "Ship Motions in Longitudinal Waves," *International Shipbuilding Progress*, Vol. 7, No. 66.

Gerritsma, J., Bosch, J. van den, and Beukelman, W. (1961), "Propulsion in Regular and Irregular Waves," *International Shipbuilding Progress*, Vol. 8, No. 82.

Gerritsma, J. (1966), "Distribution of Hydrodynamic Forces along the Length of a Ship Model in Waves," Report No. 144, Technical University of Delft, Netherlands.

Gerritsma, J. (1980), "Results of Recent Full Scale Seakeeping Trials," *International Shipbuilding Progress*, Vol. 27.

Gerritsma, J. and Beukelman, W. (1966), "Comparison of Calculated and Measured Heaving and Pitching Motions of a Series 60,  $C_B = .70$  Ship Model in Regular Longitudinal Waves," Report No. 139, Netherlands Ship Research Center, Delft.

Gerritsma, J. and Smith, W.E., (1966). "Full Scale Destroyer Motion Measurements," Report No. 142, Netherlands Ship Research Center, Delft, (1967) *Journal of Ship Research*, Vol. 11, No. 1.

Gerritsma, J. and Beukelman, W. (1964), "The Distribution of the Hydrodynamic Forces on a Heaving and Pitching Ship Model in Still Water," *Proceedings*, 5th Symposium on Naval Hydrodynamics, Washington, D.C.

Gerritsma, J. and Beukelman, W. (1965), "The Distribution of the Hydrodynamic Forces on a Heaving and Pitching Ship Model, with Zero Forward Speed in Still Water," Report No. 124, Netherlands Ship Research Center, Delft.

Gerritsma, J. and Beukelman, W. (1967), "Analysis of the Modified Strip Theory for the Calculation of Ship Motions and Wave Bending Moments," *International Shipbuilding Progress*, Vol. 14, No. 156.

Gerritsma, J. and Beukelman, W. (1972), "Analysis of the Resistance Increase in Waves of a Fast Cargo Ship," *International Shipbuilding Progress*, Vol. 19.

Gerritsma, J. (1976), "A Note on the Application of Ship Motion Theory," *Schiffstechnik*, Vol. 23.

Goodman, R.A. (1971), "Wave Excited Main Hull Vibration in Large Bulk Carriers and Tankers," *Trans. RINA*, Vol. 113, London.

Gospodnetic, D., and Miles, M. (1974), "Some Aspects of the Average Shape of Wave Spectra at Station India," Symposium on the Dynamics of Marine Vehicles and Structures in Waves, London.

Grim, O. (1959), "Die Schwingungen von Schwimmenden, Zweidimensionalen Körpern," Hamburg Model Basin Report 1171.

Grim, O. (1963), "Surging Motion and Broaching Tendencies in a Severe Irregular Sea," *Deutsche Hydrographischen Zeitschrift*, Vol. 16, No. 5.

Hadler, J.B., Lee, C.M., Birmingham, J.T. and Jones, H.D. (1974), "Ocean Catamaran Seakeeping Design Based on Experiences of USNS *Hayes*," *SNAME Transactions*, Vol. 82.

Hamlin, N.A., and Compton, R. (1966), "Assessment of Seakeepability," *Marine Technology*, Oct.

Hamlin, N.A. (1979), "Analysis of Ship Acceleration and Resultant Forces Resulting in Damage," Appendix C of *Guidelines for Deck Stowage of Containers*, J.J. Henry Co., Inc.

Hasselmann, K. (1966), "On Non-linear Ship Motions in Irregular Waves," *Journal of Ship Research*, Vol. 10, No. 1.

Hasselmann, K., et al (1973), "Measurements of wind-wave growth and swell decay during the Joint North Sea Wave Project (JONSWAP)," *Deutsche Hydrographischen Zeitschrift*, A8, 12.

Hasselmann, K., et al (1976), "A Parametric Wave Prediction Model," *Journal of Physical Oceanography*, Vol. 6.

Havelock, T.H. (1945), "Notes on the Theory of Heaving and Pitching," *Trans. RINA*, London.

Himeno, Y. (1981), "Prediction of Ship Roll Damping - State of the Art," University of Michigan Report No. 239.

Hirsch, I. (1967), "On the Prediction of the Seakeeping Characteristics of Hydrofoil Ships," *SNAME/AIAA Symposium on Advanced Marine Vehicles*.

Hoffman, D. (1966), "Distribution of Wave Caused Hydrodynamic Pressures and Forces on a Ship Hull in Waves," Norwegian Ship Model Tank publication 94, Trondheim.

Hoffman, D. and Maclean, W.M. (1970), "Ship Model Study of Incidence of Shipping Water Forward," *Marine Technology*, April.

Hoffman, D. and Miles, M. (1976), "Analysis of a Stratified Sample of Ocean Wave Records at Station India," *SNAME T and R Bulletin* No. 1-35.

Hogben, N. and Lumb, F.E. (1967), *Ocean Wave Statistics*, Her Majesty's Stationery Office, London.

Hutchison, B.L. (1981), "Risk and Operability Analysis in the Marine Environment," *SNAME Transactions*, Vol. 89.

Hutchison, B.L., and Laible, D.H. (1987), "Conceptual Design of a Medium-Endurance Research Vessel Optimized for Mission Flexibility and Seakeeping," *Marine Technology*, April.

Ijima, T. (1957), "The Properties of Ocean Waves on the Pacific Coast and the Japan Sea Coast of Japan," Report No. 25, Transportation Technical Research Institute, Tokyo.

Ikeda, Y., Himeno, Y., and Tanaka, N., (1978) "Com-



ponents of Roll Damping at Forward Speed," *Trans. Japan Society of Naval Architects*, Vol. 143.

Inglis, R.B. and Price, W.G. (1981), "A Three Dimensional Ship Motion Theory Comparison between Theoretical Prediction and Experimental Data of the Hydrodynamic Coefficients with Forward Speed," *Trans. RINA*, Vol. 124.

INA (1955), "The Papers of William Froude," The Institution of Naval Architects, London.

ISO (1978), "Guide for the Evaluation of Human Exposure to Whole-body Vibration," 2nd Edition. ISO-2631.

ITTC, Report on Seakeeping Committee (1978), *Proceedings*, 15th International Towing Tank Conference.

ITTC (1979), (1981), Reports of the Seakeeping Committees, 15th and 16th International Towing Tank Conferences.

Jackson, F.C., Walton, W.T., and Baker, P.L. (1985), "Aircraft and Satellite Measurement of Ocean Wave Directional Spectra using Scanning-Beam Microwave Radars," *Journal of Geophysical Research*, Vol. 90.

Jacobs, W.R. (1958), "The Analytical Calculation of Ship Bending Moments in Regular Waves," *Journal of Ship Research*, June.

Jacobs, W.R., Dalzell, J. and Lalangas, P. (1960), "Guide to Computational Procedure for Analytical Evaluation of Ship Bending-Moments in Regular Waves," Davidson Laboratory Report No. 791, Stevens Institute of Technology.

Jacobs, W.R. and Dalzell, J.F. (1960), "Theory and Experiment in the Evaluation of Bending Moments Acting upon a Ship in Waves," *International Shipbuilding Progress*, September.

Jensen, J.J., and Pedersen, P.T. (1981), "Bending Moments and Shear Forces in Ships Sailing in Irregular Waves," *Journal of Ship Research*, December.

John, F., (1950), "On the Motion of Floating Bodies II," *Communications on Pure and Applied Mathematics*, Vol. 3, Interscience Publishers, New York.

Johnson, R.J. (1985), "Hydrofoils," *Naval Engineers Journal*, Feb.

Joosen, W.P.A. (1966), "Added Resistance of Ships in Waves," 6th Symposium on Naval Ship Hydrodynamics, ONR, Washington, D.C.

Journeé, J.M.J. (1976a), "Motions, Resistance and Propulsion of a Ship in Longitudinal Regular Waves," Delft University of Technology, Hydrodynamics Report No. 428.

Journeé, J.M.J. (1967b), "Motions and Resistance of a Ship in Regular Following Waves," Delft Technical University, Hydromechanics Report No. 440.

Kaplan, P. (1966), "Lecture Notes on Nonlinear Theory of Ship Roll Motion in a Random Seaway," *Proceedings*, International Towing Tank Conference.

Kaplan, P., and Sargent, T.P. (1972), "Further Studies of Computer Simulation of Slamming and Other Wave-Induced Vibratory Structural Loadings on Ships

in Waves," Ship Structure Committee Report No. SSC-231.

Kaplan, P., Bentson, J., and Davis, S. (1981), "Dynamics and Hydrodynamics of Surface-Effect Ships," *SNAME Transactions*, Vol. 89.

Källström, C.G., Wessel, P. and Sjölander, S. (1988), "Roll Reduction by Rudder Control," SNAME Star Symposium.

Kawashima, E., Sakao, M., and Tasaki, R. (1959), "On the External Force Acting on the Marine Reactor Due to Ship Motion in Rough Sea," *Journal of Zosen Kiokai*, No. 105.

Keane, R.G., and Sandberg, W.C. (1984), "Naval Architecture for Combatants: a Technology Survey," *Naval Engineers Journal*, Sept.

Kempf, G. (1934), "Effect of Pitching on Resistance and Propeller Efficiency," *Jahrbuch der Schiffbau Technische Gesellschaft*.

Kennell, C.G., White, B.L. and Comstock, E.N. (1985), "Innovative Naval Designs for North Atlantic Operations," *SNAME Transactions*, Vol. 93.

Kerwin, J.E. (1955), "Notes on Rolling in Longitudinal Waves," *International Shipbuilding Progress*, Vol. 2.

Kimura, A. (1980), "Statistical Properties of Random Wave Groups," *Proceedings*, 17th Conference Coastal Engineers, Vol. 3.

King, B.K. (1987), "Time-Domain Analysis of Wave Exciting Forces on Ships and Bodies," Ph.D. Thesis, University of Michigan, Ann Arbor.

King, B., Beck, R., and Magee (1988), "Seakeeping Calculations with Forward Speed Using Time-Domain Analysis," *Proceedings*, 18th Symposium on Naval Hydrodynamics, Delft, Netherlands.

Korvin-Kroukovsky, B.V. (1955), "Investigation of Ship Motions in Regular Waves," *SNAME Transactions*, Vol. 63.

Korvin-Kroukovsky, B.V., and Jacobs, W.R. (1957), "Pitching and Heaving Motions of a Ship in Regular Waves," *SNAME Transactions*, Vol. 65.

Korvin-Kroukovsky, B.V. (1961), *Theory of Seakeeping*, SNAME, New York.

Korvin-Kroukovsky, B.V. (1970), "Discussion of Salvesen, et al."

Korvin-Kroukovsky, B.V. and Jacobs, W.R. (1957), "Pitching and Heaving Motions of a Ship in Regular Waves," *SNAME Transactions*, Vol. 65.

Krylov, A. (1898), "A New Theory of the Pitching Motion of Ships on Waves, and of the Stresses Produced by this Motion," *Trans.*, INA, London.

Kumai, T., and Tasai, F. (1970), "On the Wave Exciting Force and Response of Whipping of Ships," *European Shipbuilding*, Vol. 4.

Kumai, T. (1972), "Wave-Induced Force Exciting Hull Vibration and Its Response," *Trans. Society of Naval Architects of West Japan*.

Lackenby, H. (1978), "ITTC Dictionary of Ship Hy-

- drodynamics," Maritime Technology Monograph No. 6, RINA, London.
- Lalangas, P.A. (1964), "Application of Linear Superposition Technique to the Roll Response of a Ship Model in Irregular Beam Seas," Stevens Institute of Technology, Davidson Laboratory Report 983.
- Lamb, Horace (1924), *Hydrodynamics*, Cambridge University Press, England.
- Lamb, G.R. (1975), "The SWATH Concept; Designing Superior Operability into a Surface Displacement Ship," DTRC Report No. 4570.
- Lamb, G.R. (1988), "Some Guidance for Hull Form Selection for SWATH Ships," *Marine Technology*, October.
- Landweber, L. and Macagno, M.C. (1957), "Added Mass of Two Dimensional Forms Oscillating in a Free Surface," *Journal of Ship Research*, Vol. 1, No. 3.
- Landweber, L. and Macagno, M.C. (1959), "Added Mass of a Three Parameter Family of Two-Dimensional Forces Oscillating in a Free Surface," *Journal of Ship Research*, Vol. 2, No. 4.
- Landweber, L. and Macagno, M. (1967), "Added Masses of Two-Dimensional Forms by Conformal Mapping," *Journal of Ship Research*, Vol. 11, No. 2.
- Landweber, L. and Macagno, M. (1975), "Accurate Parametric Representation of Ship Sections by Conformal Mapping," *Proceedings*, First International Conference on Numerical Ship Hydrodynamics, DTRC, Bethesda, Md.
- Lavis, D.R. (1972), "On the Prediction of Acceleration Response of Air Cushion Vehicles to Random Seaways," SNAME/AIAA Symposium on Advanced Marine Vehicles.
- Lee, C.M., and Newman, J.N. (1971), "The Vertical Mean Force and Moment of Submerged Bodies Under Waves," *Journal of Ship Research*, Vol. 15.
- Lee, C.M., O'Dea, J.F., and Meyers, W.G. (1982), "Prediction of Relative Motion of Ships in Waves," 14th ONR Symposium on Naval Hydrodynamics, Ann Arbor, Mich.
- Lee, C.M., Curphey, R.M. (1977), "Prediction of Motion, Stability, and Load of Small-Waterplane-Area, Twin-Hull Ships," SNAME *Transactions*, Vol. 85.
- Lee, W.T., and Bales, S.L. (1984), "Environmental Data for Design of Marine Vehicles," SSC/SNAME Symposium, Arlington, Va.
- Lee, W.T., Bales, S., and Sowby, S.E. (1985), "Standardized Wind and Wave Environments for North Pacific Ocean Areas," DTRC Report SPD-0919-02.
- Lee, Y.W. (1960), *Statistical Theory of Communication*, John Wiley and Sons, New York.
- Leopold, R. (1974), "Design-to-Cost of Naval Ships," SNAME *Transactions*, Vol. 82.
- Lewis, E.V. (1955), "Ship Speeds in Irregular Waves," SNAME *Transactions*, Vol. 63.
- Lewis, E.V. (1958), "The Problem of Service Power Margins," International Design and Equipment Number, *Shipbuilding and Shipping Record*.
- Lewis, E.V. (1959), "Increasing the Sea Speed of Merchant Ships," SNAME *Transactions*, Vol. 67.
- Lewis, E.V., and Breslin, J.P. (1960), "Semi-submerged Ships for High-Speed Operation in Rough Seas," 3rd ONR Symposium on Naval Hydrodynamics, Washington, D.C.
- Lewis, E.V., and Numata, E. (1960), "Ship Motions in Oblique Seas," SNAME *Transactions*, Vol. 68.
- Lewis, F.M. (1929), "The Inertia of the Water Surrounding a Vibrating Ship," SNAME *Transactions*, Vol. 37.
- Liapis, N. and Faltinsen, O. (1980), "Diffraction of Waves Around a Ship," *Journal of Ship Research*, Vol. 24, No. 3.
- Liapis, S. and Beck, R.F. (1985), "Seakeeping Computations Using Time-Domain Analysis," *Proceedings*, Fourth International Conference on Numerical Ship Hydrodynamics, Washington, D.C.
- Lin, W.C., and Reed, A.H. (1976), "The Second-Order Steady Force and Moments on a Ship Moving in an Oblique Seaway," 11th Symposium on Naval Hydrodynamics, London.
- Lin, W.C., Day, W.G., Hough, J.J., Keane, R.G., Walden, D.A., and Koh, I-Y, (1984), "An Advanced Methodology for Preliminary Hull Form Development," *Naval Engineers Journal*, July.
- Lloyd, A.R.J.M., Brown, J.C. and Anslow, J.F.W. (1979), "Motions and Loads on Ship Models in Regular Oblique Waves," *Trans. RINA*, Vol. 121, London.
- Lloyd, R.J.M., Salsich, J.O., and Zselezky, J.J. (1985), "The Effect of Bow Shape on Deck Wetness in Head Seas," *Trans. RINA*, London.
- Loeser, D.J., Yue, Dick K. and Salvesen, N. (1982), "Slender-Body Calculations of Large-Amplitude Ship Motions," *Proceedings*, 14th Symposium on Naval Hydrodynamics, University of Michigan, Ann Arbor, Mich.
- Lofft, R.F., and Price, W.G. (1973) "Ocean Wave Statistics-Frequency of Occurrence of Sea States," Admiralty Experiment Works, Haslar, England, No. 19.
- Longuet-Higgins, M.S. (1963), "The Effects of Non-linearities on Statistical Distributions in the Theory of Sea Waves," *Journal of Fluid Mechanics*, Vol. 17, Part 3.
- Longuet-Higgins, M.S. (1984), "Statistical Properties of Wave Groups in a Random Sea State," *Philosophical Trans.*, Royal Society of London, Vol. 312.
- Longuet-Higgins, M.S., Cartwright, D.C., and Smith, N.P. (1963), "Observations of the Directional Spectrum of Sea Waves Using the Motions of a Floating Buoy," *Ocean Wave Spectra, Proceedings of a Conference*, Prentice-Hall, Englewood Cliffs, N.J.
- Loukakis, T.A. (1970), "Computer Aided Prediction of Seakeeping Performance in Ship Design," Report No. 70-3, MIT, Cambridge, Mass.
- Loukakis, T.A. and Chrysostomidis, C. (1975), "Seakeeping Standard Series for Cruiser-Stern Ships," SNAME *Transactions*, Vol. 83.

Mandel, P. (1960), "Subcritical and Supercritical Operation of Ships in Waves and the Coincidence of Maximum Damping," *Journal of Ship Research*, June.

Mandel, P. (1979), "Seagoing Box Scores and Seakeeping Criteria for Monohull, SWATH, Planing, Hydrofoil, Surface Effect Ships and Air Cushion Vehicles," DTRC Report SPD-79/1.

Mandel, P. and Leopold, R. (1966), "Optimization Methods Applied to Ship Design," *SNAME Transactions*, Vol. 74.

Mantle, P.J. (1976), "Cushions and Foils," SNAME Spring Meeting, Philadelphia.

Marks, W. and Ferdinande, V. (1960), "Effect of Sea State on Attainable Ship Speed for Some *Mariner* Class Ships," Davidson Laboratory Note No. 606.

Martin, M. (1978), "Theoretical Prediction of Motions of High-Speed Planing Boats," *Journal of Ship Research*, Sept.

Maruo, H. (1957), "The Excess Resistance of a Ship in Rough Seas," *International Shipbuilding Progress*, Vol. 4.

Maruo, H. (1967), "Application of the Slender Body Theory to the Longitudinal Motion of Ships among Waves," *Bulletin of Faculty of Engineering*, Yokohama National University, Vol. 16.

Maruo, H. (1963), "Resistance in Waves, Researches into Seakeeping Qualities of Ships," Society of Naval Architects of Japan, 60th Anniversary Series, Vol. 8.

Maruo, H. (1970), "An Improvement of the Slender Body Theory for Oscillating Ships with Zero Forward Speed," *Bulletin of Faculty of Engineering*, Yokohama National University, Vol. 19.

Maruo, H. and Sasaki, N. (1974), "On the Wave Pressure Acting on the Surface of an Elongated Body Fixed in Head Seas," *Journal of Society of Naval Architects of Japan*, Vol. 136.

Maruo, H. and Tokura, J. (1978), "Prediction of Hydrodynamic Forces and Moments Acting on Ships in Heaving and Pitching Oscillations by Means of an Improvement of the Slender Ship Theory," *Journal of Society of Naval Architects of Japan*, Vol. 143.

Matthews, S.T. (1967), "Main Hull Girder Loads on a Great Lakes Bulk Carrier," *SNAME Spring Meeting Proceedings*.

Mays, J.H. (1978), "Wave Radiation and Diffraction by a Floating Slender Body," Ph.D. Thesis, Massachusetts Institute of Technology, Cambridge, Mass.

McCreight, K.K., and Stahl, R.G. (1985), "Recent Advances in the Seakeeping Assessment of Ships," *Naval Engineers Journal*, Vol. 97.

McCreight, K.K. (1987), "Assessing the Seaworthiness of SWATH Ships," *SNAME Transactions*, Vol. 95.

Meyers, W.G., Applebee, T.R. and Baitis, A.E. (1981), "User's Manual for the Standard Ship Motion Program, SMP," DTRC Report SPD-0936-01.

Miles, J.W. (1957, 1959), "On the Generation of Sur-

face Waves by Shear Flows," Parts I and II, *Journal of Fluid Mechanics*, 3 and 6.

Miller, E.R., Slager, J.J. and Webster, W.C. (1974), "Phase I Report on the Development of a Technical Practice for Roll Stabilization System Selection," NAVSEA Report 6136-74-280.

Milne-Thompson, L.M. (1960), *Theoretical Hydrodynamics*, MacMillan Company, New York.

Mitsuyasu, H., et al (1975), "Observations of the Directional Spectrum of Ocean Waves Using a Cloverleaf Buoy," *Journal of Physical Oceanography*, Vol. 5, No. 4.

Möckel, W. (1953), "Seaworthiness and Safety of Trawlers in a Seaway," International Fishing Boat Congress, FAO of the United Nations, Rome.

Moran, D.D., Fein, J.A., and Magnuson, A.H. (1974), "Dynamic Performance of an Air Cushion Vehicle in a Marine Environment," AIAA/SNAME Symposium.

Moor and Luyster (1960), "Bow Freeboard" *Trans. RINA*, London.

Moor, D.I. (1966), "Longitudinal Bending Moments on Models in Head Seas," *Trans. RINA*, London.

Moor, D.I. (1970), "Effects on Performances in Still Water and Waves of Some Geometric Changes to the Form of a Large Twin-Screw Ship," *SNAME Transactions*, Vol. 78.

Moskowitz, L., Pierson, W.J. and Mehr, E. (1962, 1963), "Wave Spectra Estimated from Wave Records Obtained by the OWS *Weather Explorer* and OWS *Weather Reporter*," New York University, College of Engineering.

Moskowitz, L., Pierson, W.J., and Mehr, E. (1963), "A Proposed Spectral Form for Fully Developed Wind Seas Based on the Similarity Theory of S.A. Kitaigorodskii," Technical Report for U.S. Naval Oceanographic Office, New York University.

Murdey, D.C. (1979), "Experiment Techniques for the Prediction of Ship Seakeeping Performance," *Proceedings*, International Symposium on Marine Technology, Trondheim, Norway.

Murdey, D.C., and Simoes Ré, A.J. (1985), "The NRC Hull Form Series—an Update," MARIN Workshop on Hull Form Design, Wageningen, the Netherlands.

Nakamura, S., and Fujii, H. (1977), "Nominal Speed Loss of Ships in Waves," Symposium on Practical Design in Shipbuilding (PRADS), Tokyo.

Nakamura, S., and Naito, S. (1977), "Propulsive Performance of a Container Ship in Waves," *Journal of Society of Naval Architects of Japan*.

NAVSEA (1982), "Minimum Required Freeboard for U.S. Naval Surface Ships," Design Data Sheet, DDS-079-2.

NAVSEC (1975), "Seakeeping in the Ship Design Process," Report of a Seakeeping Workshop, Annapolis.

Nestegard, A. and Sclavounos, P. (1984), "A Nu-

merical Solution of Two-Dimensional Deep Water Wave-Body Problems," *Journal of Ship Research*, Vol. 28.

Newman, J.N. and Tuck, E.O. (1964), "Current Progress in the Slender Body Theory of Ship Motions," *Proceedings*, 5th Symposium on Naval Hydrodynamics, ONR, Washington, D.C.

Newman, J.N. (1965), "The Exciting Forces on a Moving Body in Waves," *Journal of Ship Research*, Vol. 9.

Newman, J.N. (1967), "The Drift Force and Moment on Ships in Waves," *Journal of Ship Research*, Vol. 11.

Newman, J.N. (1970), "Applications of Slender Body Theory in Ship Hydrodynamics," *Annual Review of Fluid Mechanics*, Vol. 2.

Newman, J.N. (1974), "Second-order, Slowly Varying Forces on Vessels in Irregular Waves," Symposium on Dynamics of Marine Vehicles and Structures in Waves, London.

Newman, J.N. (1977), *Marine Hydrodynamics*, Massachusetts Institute of Technology Press, Cambridge, Mass.

Newman, J.N. (1978), "Theory of Ship Motions," *Advances in Applied Mechanics*, Vol. 18.

Newman, J.N. and Sclavounos, P. (1980), "The Unified Theory of Ship Motions," *Proceedings*, 13th Symposium on Naval Hydrodynamics, Tokyo.

Newton, R.N. (1960), "Wetness Related to Freeboard and Flare," *Trans. RINA*, Vol. 102.

Nobless, F. and McCarthy, J.H. (1983), "Ship Wave Resistance Computations," *Proceedings*, David Taylor Research Center Workshop on Ship Wave Resistance Computations, Washington, D.C.

Nordenstrom, N. (1969), "Methods for Predicting Long-Term Distributions of Wave Loads and Probability of Failure for Ships, Appendix II, Relationships Between Visually Estimated and Theoretical Wave Heights and Periods," Det norske Veritas Report No. 69-22-S, Oslo.

Numata, E., Michel, W.H., and McClure, A.C. (1976), "Assessment of Stability Requirements for Semisubmersible Units," *SNAME Transactions*, Vol. 84.

Numata, E. (1980), "Predicting Hydrodynamic Behavior of Small Waterplane Area, Twin-Hull Ships," SNAME Section paper, April.

Oakley, O.H. (1960), "High Performance Ships, Promises and Problems," Third Symposium on Naval Hydrodynamics, Office of Naval Research, Washington, D.C.

Oakley, O.H., Paulling, J.R., and Wood, P. (1974), "Ship Motions and Capsizing in Astern Seas," 10th Symposium on Naval Hydrodynamics, ONR.

Oakley, O.H., Jr. (1974), "Directional Wave Spectra Measurement and Analysis Systems," *Proceedings*, SNAME T&R Symposium S-3.

Ochi, M.K. (1961), "Hydroelastic Study of a Ship Equipped with an Antipitching Fin," *SNAME Trans-*

*actions*, Vol. 69.

Ochi, M.K. (1964), "Extreme Behavior of a Ship in Rough Seas—Slamming and Shipping of Green Water," *SNAME Transactions*, Vol. 72.

Ochi, M.K. and L.E. Motter (1973), "Prediction of Slamming Characteristics and Hull Responses for Ship Design," *SNAME Transactions*, Vol. 81.

Ochi, M.K. (1973), "On Prediction of Extreme Values," *Journal of Ship Research*, Vol. 17, No. 1.

Ochi, M.K. and Bolton, W.E. (1973), "Statistics for the Prediction of Ship Performance in a Seaway," *International Shipbuilding Progress*, Vol. 22.

Ochi, M.K. (1974), "Review of Recent Progress in Theoretical Prediction of Responses to Random Seas," SNAME T&R Symposium S-3.

Ochi, M.K., and Hubble, E.N. (1976), "On Six-Parameter Wave Spectra," *Proceedings*, 15th Coastal Engineers Conference, ASCE, New York.

Ochi, M.K. and Bales, S.L. (1977), "Effect of Various Spectral Formulations in Predicting Responses of Marine Vehicles and Ocean Structures," *Proceedings*, Offshore Technology Conference, Houston, Tex.

Ochi, M.K. (1978), "Wave Statistics for the Design of Ships and Ocean Structures," *SNAME Transactions*, Vol. 86.

Ochi, M.K. (1986), "Non-Gaussian Random Processes in Ocean Engineering," *Probabilistic Engineering Mechanics*, Vol. 1.

O'Dea, J.F. (1983), "Wave Induced Mean Shift in Vertical and Absolute Relative Motion," *Proceedings*, International Workshop on Ship and Platform Motions, Berkeley, Cal.

O'Dea, J.F., and Walden, D.A. (1984), "Effect of Bow Shape and Non-Linearities on the Prediction of Large Amplitude Motions and Deck Wetness," 15th ONR Symposium on Naval Hydrodynamics, Hamburg.

Ogilvie, T.F. and Beck, R.F. (1973), "Transfer Functions for Predicting Ship Motions: A Review of the Theory," SNAME T&R Symposium S-3.

Ogilvie, T.F. (1964), "Recent Progress Toward the Understanding and Prediction of Ship Motions," *Proceedings*, 5th Symposium Naval Hydrodynamics, ONR, Washington, D.C.

Ogilvie, T.F. (1977), "Singular Perturbation Problems in Ship Hydrodynamics," *Advances in Applied Mechanics*, Vol. 17.

Ogilvie, T.F. and Shin, Y.S. (1978), "Integral-Equation Solutions for Time-Dependent Free Surface Problems," *Trans.*, Society of Naval Architects of Japan.

Ogilvie, T.F. and Tuck, E.O. (1969), "A Rational Strip Theory for Ship Motions Part 1," Report No. 013, University of Michigan, Ann Arbor.

O'Hanlon, J.F., and M.E. McCauley (1973), "Motion Sickness Incidence as a Function of the Frequency and Acceleration of Vertical Sinusoidal Motion," Human Factors Research, Inc. Technical Memorandum 1973-1.

Ohmatsu, S. (1975), "On the Irregular Frequencies

in the Theory of Oscillating Bodies in a Free Surface," *Papers of Ship Research Institute of Japan*, No. 48.

Olson, S.R. (1977), "A Seakeeping Evaluation of Four Naval Monohulls and a 3,250 ton SWATH," Center for Naval Analysis Memorandum 77-0640.

Papanikolaou, A. (1980), "Schwingungen von Schwimmenden Zylindern," *Schiffstechnik*, Bd. 27.

Paulling, J.R. (1961), "The Transverse Stability of a Ship in Longitudinal Seaway," *Journal of Ship Research*, March.

Paulling, J.R. and Richardson, R.K. (1962), "Measurement of Pressures, Forces and Radiating Waves for Cylinders Oscillating in a Free Surface," University of California, Berkeley, Series 82, Issue 23.

Paulling, J.R., and Wood, P.D. (1974), "Numerical Simulation of Large-Amplitude Ship Motions in Astern Seas," SNAME T&R Symposium S-3.

Payne, P.R. (1974), "Supercritical Planing Hulls," AIAA/SNAME Symposium on Advanced Marine Vehicles, Feb.

Payne, P.R. (1978), "On Quantizing Ride Comfort and Allowable Accelerations," AIAA-SNAME Symposium on Advanced Marine Vehicles.

Phillips, O.M. (1957), "On the Generation of Waves by Turbulent Wind," *Journal of Fluid Mechanics*, Vol. 2, part 5.

Phillips, O.M. (1966), *The Dynamics of the Upper Ocean*, Cambridge University Press, England.

Pierson, W.J., Neumann, G. and James, R.W. (1955), "Practical Methods for Observing and Forecasting Ocean Waves by Means of Wave Spectra and Statistics," H.O. Publication 603, U.S. Navy Hydrographic Office, Washington, D.C.

Pierson, W.J. and Moskowitz, L. (1964), "A Proposed Spectral Form for Fully Developed Wind Seas Based on the Similarity Theory of S.A. Kitaigorodskii," *Journal of Geophysical Research*, Vol. 69.

Pierson, W.J. (1974), "Forecasting and Observing Waves, Winds and Weather at Sea," SNAME Technical and Research Symposium S-3.

Pierson, W.J. (1982), "The Spectral Ocean Wave Model (SOWM) . . .," DTRC Report 82/011.

Pinkster, J.A. (1980), "Low Frequency Second Order Wave Exciting Forces on Floating Structures," MARIN Pub. 650, Wageningen.

Porter, W.R. (1960), "Pressure Distributions, Added Mass and Damping Coefficients for Cylinders Oscillating in a Free Surface," University of California, Berkeley, Report, 82-16.

Potash, R.L. (1971), "Second-Order Theory of Oscillating Cylinders," *Journal of Ship Research*, Vol. 15, Number 4.

Price, W.G. and Bishop, R.E.D. (1974), *Probabilistic Theory of Ship Dynamics*, Chapman and Hall, London.

Research Panel (1980), "Winds and Waves of the North Pacific Ocean," Shipbuilding Research Association of Japan.

Rice, O. (1944-45), "Mathematical Analyses of Random Noise," *Bell System Technical Journal*, Vols. 23, 24.

Roll, H.U. (1958), "Height, Length and Steepness of Seawaves in the North Atlantic," and "Dimensions of Seawaves as Functions of Wind Force," Translation by M. St. Denis, SNAME T&R Bulletin, No. 1-19.

Rydill, L.J. (1959), "A Linear Theory for the Steered Motion of Ships in Waves," *Trans. RINA*, London.

Salvesen, N. and Smith, W.E. (1969), "Comparison of Ship Motion Theory and Experiment for Mariner Hull," Technical Note 104, DTRC, Bethesda, Md.

Salvesen, N. and Smith, W.E. (1971), "Comparison of Ship-Motion and Experiment for Mariner Hull and a Destroyer Hull with Bow Modification," Report No. 3337, DTRC, Bethesda, Md.

Salvesen, N., Tuck, E.O. and Faltinsen, O. (1970), "Ship Motions and Sea Loads," *SNAME Transactions*, Vol. 78.

Salvesen, N. (1974), "Second-order Steady-State Forces and Moments on Surface Ships in Oblique Regular Waves," Symposium on Dynamics of Marine Vehicles and Structures in Waves, London.

Salvesen, N. (1978a), "Added Resistance in Waves," *Journal of Hydronautics*, Vol. 12, January.

Salvesen, N. (1978b), "Ship motions in Large Waves," *Proceedings*, Symposium on Applied Mathematics, Delft.

Saunders, H.E. (1965), *Hydrodynamics in Ship Design*, Author's Notes, Vol. III, SNAME.

Savitsky, D. (1968), "On the Seakeeping Performance of Planing Hulls," *Marine Technology*, Vol. 5, No. 2.

Savitsky, D. and Brown, P.W. (1976), "Procedures for Hydrodynamic Evaluation of Planing Hulls in Smooth and Rough Water," *Marine Technology*, Vol. 13, No. 4.

Sayer, P. and Ursell, F. (1977), "Integral-Equation Methods for Calculating the Virtual Mass in Water of Finite Depth," *Proceedings*, Conference on Numerical Ship Hydrodynamics, University of California, Berkeley.

Schmitke, R.S. (1978), "Ship Sway, Roll and Yaw Motions in Oblique Seas," *SNAME Transactions*, Vol. 86.

Schmitke, R.T., and Murdey, D.C. (1980), "Seakeeping Resistance Trade-Offs in Frigate Hull Form Design," 13th ONR Symposium on Naval Hydrodynamics, Tokyo.

Slavounos, P. (1984), "The Diffraction of Free-Surface Waves by a Slender Ship," *Journal of Ship Research*, Vol. 28, No. 1.

Slavounos, P. (1985), "The Unified Slender-Body Theory: Ship Motions in Waves," *Proceedings*, Symposium Naval Hydrodynamics, University of Michigan, Ann Arbor.

Sellers, F. (1983), Memo to Panel H-7, "Seakeeping Design Procedure," Oct. (unpublished).

- Sellars, F.H. and Setterstrom, C.R. (1987), "Analysis of Effects of Seakeeping on Ship Operating Economics," SNAME Ship Operations, Management and Economics Symposium, Kings Point, N.Y.
- Simoes Ré, A.J. (1986), unpublished communication to the Editor.
- Smith, W.E. (1883), "Hogging and Sagging Strains in a Seaway as Influenced by Wave Structure," *Trans. INA*, Vol. 24.
- Smith, W.E. and Salvesen, N. (1969), "Comparison of Ship Motion and Experiment for Davidson A Destroyer Form," Technical Note 102, DTRC, Bethesda, Md.
- Smith, W.E. and Salveson, N. (1970), "Comparison of Ship Motion Theory and Experiment for Destroyer with Large Bulb," *Journal of Ship Research*, Vol. 14, No. 1.
- Soeding, H. (1969), "Eine Modifikation der Streifenmethode," *Schiffstechnik*, Bd. 16, Heft 80.
- St. Denis, M. and Pierson, W.J. (1953), "On the Motions of Ships in Confused Seas," *SNAME Transactions*, Vol. 61.
- St. Denis, M. (1976), "On the Environmental Operability of Seagoing Systems," *SNAME T&R Bulletin* No. 1-32.
- St. Denis, M. (1980), "On the Statistical Description of Seaways of Moderate Severity," *SNAME STAR Symposium*.
- St. Denis, M. (1980), "Some Comments on Certain Idealized Variance Spectra of the Seaway Currently in Fashion," *Journal of Ship Research*, December.
- St. Denis, M. (1983), "On the Empiric Design of Seakindly Ships," 2nd International Symposium on Practical Design in Shipbuilding (PRADS), Tokyo.
- Stability '81 (1981) Proceedings of a Symposium.
- Stark, D.A. (1977), "Hydrofoil Control and Dynamics Criteria (Technical Substantiation)," Vol. IIIA Boeing Marine Systems Report BMS D321-51313-2.
- Stavovy, A.B. and Chuang, S.L. (1976), "Analytical Determination of Slamming Pressures for High-Speed Vehicles in Waves," *Journal of Ship Research*, December.
- Stefun, G.P. (1958), "The Influence of Ship Form on Pitch and Heave Amplitudes," DTRC Report 1235.
- Stokes, G.G. (1847), "On the Theory of Oscillatory Waves," *Trans. Cambridge Philosophic Society*.
- Strom-Tejsen, J. Yeh, H.Y.H. and Moran, D.D. (1973), "Added Resistance in Waves," *SNAME Transactions*, Vol. 81.
- Swaan, W.A., and Vossers, G. (1961), "The Effect of Forebody Section Shape on Ship Behavior in Waves," *Trans. RINA*, Vol. 103.
- Swaan, W.A. (1961), "The Influence of the Principal Dimensions on Ship Behavior in Irregular Waves," *International Shipbuilding Progress*, Vol. 8.
- Swaan, W.A., and Rijken, H. (1964), "Speed Loss at Sea as a Function of Longitudinal Weight Distribution," *Trans. NECIES*.
- Szebehely, V.G. (1955), "Ship Slamming in Head Seas," DTRC Report 913.
- Takagi, M., Arai, S.-I., Takezawa, S., Tanaka, K. and Takarada, N. (1985), "A Comparison of Methods for Calculating the Motion of a Semi-Submersible," *Ocean Engineering*, Vol. 12, No. 1.
- Tasai, F. (1959), "On the Damping Force and Added Mass of Ships Heaving and Pitching," *Journal of Society of Naval Architects of Japan*, Vol. 105, Translation published by University of California, Berkeley.
- Tasai, F. (1966), "An Approximate Calculation of Hydrodynamic Pressure on the Midship Section Contour of a Ship Heaving and Pitching in Regular Head Waves," Reports of Research Institute for Applied Mechanics, Kyushu University, Japan.
- Tasai, F. et al (1973), "Model Experiments and Theoretical Calculations in Waves on a High-Speed Containership with Triple Screws," *Journal, Society of Naval Architects of Japan*.
- Tasaki, R. (1963), "On the Shipping of Water in Head Waves," *Trans. Society of Naval Architects of Japan*, Vol. 107 (in Japanese). Also *Proceedings of 10th ITTC, London (1963)* and *60th Anniversary Series of SNA of Japan (in English)*.
- Taylor, K.V. and Lundgren, J. (1976), "Full Scale Static and Dynamic Measurements on MV *Nihon*," *The Naval Architect*, March.
- Tick, L.J. (1958), "Certain Probabilities Associated with Bow Submergence and Ship Slamming in Irregular Seas," *Journal of Ship Research*, Vol. 2, No. 1.
- Timman, R. and Newman, J.N. (1962), "The Coupled Damping Coefficients of Symmetric Ships," *Journal of Ship Research*, Vol. 5, No. 4.
- Troesch, A.W. (1976), "The Diffraction Potential for a Slender Ship Moving through Oblique Waves," Ph.D. Thesis, University of Michigan, Ann Arbor.
- Troesch, A.W. (1979), "The Diffraction Forces for a Ship Moving in Oblique Seas," *Journal of Ship Research*, Vol. 23, No. 2.
- Troesch, A.W. (1981a), "Sway, Roll, and Yaw Motion Coefficients Based on a Forward Speed Slender Body Theory - Part 1," *Journal of Ship Research*, Vol. 25, No. 1.
- Troesch, A.W. (1981b), "Sway, Roll, and Yaw Motion Coefficients Based on a Forward Speed Slender Body Theory - Part 2," *Journal of Ship Research*, Vol. 25, No. 1.
- Troesch, A.W. (1984a), "Wave-Induced Hull Vibrations: an Experimental and Theoretical Study," *Journal of Ship Research*, June.
- Troesch, A.W. (1984b), "Effects of Nonlinearities on Hull Springing," *Marine Technology*, Oct.
- Troesch, A.W. and Kang, C.G. (1986), "16th Symposium on Naval Hydrodynamics, Berkeley, CA.
- Tsai, F. and Takaki, M. (1969), "Theory and Calculation of Ship Responses in Regular Waves," (in Japanese), Symposium, Seaworthiness of Ships, Society of Naval Architects of Japan.

- Tucker, M.J. (1956), "A Shipborne Wave Recorder," *Trans. RINA*, Vol. 98.
- Tukey, J.W. (1949), "The Sampling Theory of Power Spectrum Estimates," Symposium on Applications of Autocorrelation Analysis to Physical Problems, ONR, Woods Hole, Mass.
- Ursell, F. (1949), "On the Heaving Motion of a Circular Cylinder on the Surface of a Fluid," *Quarterly Journal of Applied Mathematics*, Vol. 2.
- Ursell, F., "Wave Generation by Wind," *Surveys in Mechanics*, pp. 216-249, G.K. Batchelor and R.M. Davies, Cambridge University Press, England.
- U.S. Navy (1983), "Hindcast Spectral Ocean Wave Model Climatology Atlas: North Atlantic," Naval Oceanography Command, Asheville, N.C., NAVAIR 50-1C-538.
- U.S. Navy (1985), "Hindcast Spectral Ocean Wave Model Climatology Atlas: North Pacific," Naval Oceanography Command, Asheville, N.C., NAVAIR 50-1C-539.
- Van Sluijs, M.F., and Tan, S.G. (1972), "Behavior and Performance of Compact Frigates in Head Seas," *International Shipbuilding Progress*, Vol. 19.
- Vassilopoulos, L.A. (1966), "The Application of Statistical Theory of Non-linear Systems to Ship Performance in Random Seas," Ship Control Systems Symposium, Annapolis, November.
- Vassilopoulos, L. (1971), "Ship Rolling at Zero Speed in Random Beam Seas with Nonlinear Damping and Restoration," *Journal of Ship Research*, Vol. 15.
- Vasta, J., Giddings, A.J., Taplin, A. and Stilwell, J.J. (1961), "Roll Stabilization by Means of Passive Tanks," *SNAME Transactions*, Vol. 69.
- Von Kerczek, C. and Tuck, E.O. (1969), "The Representation of Ship Hulls by Conformal Mapping Functions," *Journal of Ship Research*, Vol. 13, No. 4.
- Vossers, G., and Swaan, W.A. (1960), "Some Sea-keeping Tests with a Victory Model," *International Shipbuilding Progress*.
- Vossers, G., Swaan, W.A., and Rijken, H. (1960), "Experiments with Series 60 Models in Waves," *SNAME Transactions*, Vol. 68.
- Vossers, G. (1962), "Behavior of Ships in Waves," *Resistance, Propulsion and Steering of Ships*, Vol. C; H. Stam N.V., Haarlem, the Netherlands.
- Vughts, J.H. (1968), "The Hydrodynamic Coefficients for Swaying, Heaving and Rolling Cylinders in a Free Surface," *International Shipbuilding Progress*, Vol. 15.
- Vughts, J.H. (1969), "A Comparative Study on Four Different Passive Roll Damping Tanks (Part II)," *International Shipbuilding Progress*, Vol. 16.
- Wachnik, Z.G., and Pierce, R.D. (1967), "SR.N4 Motions," DTRC Report.
- Wahab, R. (1966), "Research on Bulbous Bow Ships," Part 1.B, *International Shipbuilding Progress*, Vol. 13.
- Walden, H. (1964), "Die Eigenschaften der Meeresswellen im Nordatlantischen Ozean," *Deutscher Wetterdienst*, No. 41, Hamburg.
- Wang, S. (1976), "Dynamical Theory of Potential Flows with a Free Surface," *Journal of Ship Research*, Vol. 20, No. 3.
- Watanabe, Y., Inoue, S., and Murahashi, T. (1964), "The Modification of Rolling Resistance for Full Ships," *Trans. West-Japan SNA* (in Japanese).
- Webster, W.C. (1967), "Analysis of the Control of Activated Antiroll Tanks," *SNAME Transactions*, Vol. 75.
- Wehausen, J.V. (1971), "The Motion of Floating Bodies," *Annual Review of Fluid Mechanics*, Vol. 3.
- Wiener, N. (1930), "Generalized Harmonic Analysis," *Acta Mathematica*, Vol. 55.
- Wiener, N. (1949), *The Extrapolation, Interpolation and Smoothing of Stationary Time Series*, John Wiley & Sons, New York.
- Yamanouchi, Y. (1964), "On Some Remarks on the Statistical Estimation of Response Functions of Ships," Fifth Symposium on Naval Hydrodynamics, Bergen, Norway.
- Yamanouchi, Y. and Ogawa, A. (1970), "Statistical Diagrams on the Winds and Waves on the North Pacific Ocean," Ship Research Institute, Tokyo.
- Yeung, R.W. (1975) "A Hybrid Integral Equation Method for Time-harmonic Free-surface Flow," First International Conference on Numerical Ship Hydrodynamics, DTRC, Washington, D.C.
- Yeung, R.W. (1982), "Numerical Methods in Free-Surface Flows," *Annual Review of Fluid Mechanics*, Vol. 14.
- Yeung, R.W. and Kim, S-H. (1981), "Radiation Forces on Ships with Forward Speed," *Proceedings*, Third International Conference on Numerical Ship Hydrodynamics, Paris.
- Yeung, R.W. and Kim, S.H. (1985). "A New Development in the Theory of Oscillating and Translating Slender Ships," *Proceedings*, Fifteenth Symposium on Naval Hydrodynamics, Hamburg.
- Yeung, R.W. (1975), "A Hybrid Integral Equation Method from Time-Harmonic Free-Surface Flow", *Proceedings*, First International Conference on Numerical Ship Hydrodynamics, Washington D.C. pp 581-608.



# Nomenclature

## Motions in Waves

The following symbols apply to Chapter VIII only. The phrase "stands for" is understood between the symbol and its definition.

$A_{BK}$	stands for area of bilge keel
$A_w$	waterplane area
$A'_{33}$	non-dimensional coefficient of added mass (heave)
$A'_{55}$	non-dimensional coefficient of added inertia (pitch)
$B$	breadth
$b_{BK}$	width, bilge keel
$C$	coefficient, generally
$C_B$	block coefficient
$C_A$	coefficient, waterplane longitudinal radius of gyration
$C_k$	ratio, longitudinal gyradius to ship length
$C_{IL}$	waterplane inertia coefficient
$C_{BM}$	non-dimensional hull bending movement coefficient
$C_m$	midship section coefficient
$C_{wp}$	waterplane area coefficient

### Coefficients in Equations of Motion

$\left\{ \begin{array}{ll} a_{jk}, A_{jk} & \text{sectional and overall added mass} \\ b_{jk}, B_{jk} & \text{sectional and overall damping} \\ c_{jk}, C_{jk} & \text{sectional and overall restoring} \end{array} \right\}$	
---	--

(subscripts  $j, k$  indicate mode)

$CB$	center of buoyancy
$CG$	center of gravity
$D$	duration; diameter
$e$	base of logarithm, ln
$E$	total variance of a wave system
$F$	force; freeboard at FP; $F_1$ freeboard at specified point
FP	forward perpendicular
$F_j$	total force on moment acting on ship in waves in $j$ th mode

$F_{EXj}$	exciting force on moment in $j$ th mode
$F_{Rj}$	hydrodynamic force on moment due to forced motion in $j$ th mode
$F_{HSj}^*$	net hydrostatic force on moment in $j$ th mode
$Fn$	Froude number
$f_4$	non-dimensional roll moment amplitude
$\overline{GM}$	metacentric height
$\overline{Gz}$	righting arm
$g$	acceleration due to gravity
$H_{1/3}$	(or $\langle(h_w)1/3\rangle$ ) average height of the 1/3 highest waves, or <i>significant</i> height
$H_{1/10}$	(or $\langle(h_w)1/10\rangle$ ) average height of the 1/10th highest waves
$H_v$	visually estimated wave height
$h$	depth of water
$h_w = 2\bar{\zeta}$	height of regular wave, crest to trough
$I$	mass moment of inertia
$I_R$	coefficient indicating relative importance of particular ship functions
$I_{jk}$	component, generalized inertia matrix of ship including all inertia terms; mass terms, $\Delta jk$
$\overline{KG}$	height of CG above keel
$k$	wave number = $2\pi/L_w = \omega^2/g$
$k_a$	longitudinal waterplane radius of gyration
$k_{yy}$	longitudinal gyradius or mass radius of gyration
$L$	length of ship
$L_w$	wavelength
LCB	longitudinal center of buoyancy
LCF	longitudinal center of flotation
ln	logarithm to base e
$M(\mu)$	spreading function for short-crested sea
$M_w$	wave bending moment
MSI	motion sickness incidence



$m$	moment, generally; also mass of object in or on ship
$m_n$	spectral moments of area under $S(\omega)$ subscript indicating 0-4th moments
$N, n$	number of cycles of response
$N_j, n$	two-dimensional and generalized unit normals
OI	operability index
$P, p$	probability; fluid pressure; power
$P_j$	pseudo-spectrum (directional) of response
$p_s$	probability of a given sea state
$p_u$	probability of a given ship-wave heading
$p_v$	probability of a given ship speed
$p_i$	probability of a ship being operable at a given speed and heading in a given sea state
$R$	resistance; radius
$r$	segment radius
$r$	$= (\bar{x}, \bar{y}, \bar{z})$ the position vector of point $(\bar{x}, \bar{y}, \bar{z})$
RAO	Response Amplitude Operator
RBM	Relative Bow Motion, vertically, between a point at the bow and the wave surface
RFR	Required Freight Rate for even trade-off between estimated expenses and revenues
$S$	area, in general
$S'$	underwater hull surface area
$S(\omega)$	wave spectrum (as a function of frequency)
$S_i(\omega)$	wave spectrum at a point
$S'_i(\omega)$	wave slope spectrum at a point
$S_j(\omega)$	response spectrum in $j$ -mode as a function of $\omega$
$S_j(\omega_c)$	response spectrum in $j$ -mode as a function of $\omega_c$
SOE	Seakeeping Operability Envelope
SPI-1	Seakeeping Performance Index; transit speed
SPI-2	Seakeeping Performance Index; mission effectiveness
$s$	relative bow motion (RBM) between a point on the bow and the water surface (scalar value of $\xi_R$ at FP)
$\bar{s}$	amplitude of relative bow motion
$T$	wave period; draft
$T_c$	average period between peaks (or hollows) of wave record
$T_e$	period of wave encounter
$T_f$	still-water draft forward
$T_m$	modal wave period; period corresponding to peak of $S(\omega)$

$T_v$	visually estimated wave period
$T_w$	period of a regular wave
$T_z$	average period between zero up-crossings (wave record)
$T_{-1}$	average period of component waves in a seaway
$T_1$	period corresponding to average frequency of component waves
$T_{nj}$	ship's natural period of oscillation in $j$ th mode
TEU	Twenty-ft Equivalent Unit (cargo containers)
$U_0$	forward velocity of ship (or $V$ )
$V_c$	wave velocity or <i>celerity</i>
$v$	dummy variable
WP	waterplane

## Coordinates of Axis Systems

$x, y, z$	moving with same velocity as the ship ( <i>inertial</i> coordinates)
$x_0, y_0, z_0$	<i>fixed</i> in relation to the earth, with $x_0$ axis set in direction of travel of ship
$\bar{x}, \bar{y}, \bar{z}$	fixed in the ship (body axes)
$x$	distance from origin along X-axis, normal to $y, z$
$y$	distance from origin along Y-axis, normal to $x, z$
$z$	distance from origin along Z-axis, normal to $x, y$

## Greek Symbols

$\alpha$ (alpha)	angle, generally; confidence level parameter (Ochi)
$\beta^*$ (Beta)	non-dimensional roll damping ratio
$\gamma^*$ (gamma)	non-dimensional roll restoring force
$\Delta$	mass displacement
$\Delta k$ (Delta)	mass components of generalized inertia matrix of ship
$\delta$ (delta)	a finite increment; $\delta_R$ rudder angle
$\delta R$	added resistance in waves
$\delta P$	added power in waves
$\epsilon$ (epsilon)	phase angle; spectral broadness parameter
$\zeta$ (zeta)	wave surface elevation
$\bar{\zeta}$	wave amplitude
$\zeta'$	wave slope
$\bar{\zeta}' = 2\pi\xi/L_w$	wave slope amplitude (maximum value)
$\zeta_{\bar{x}, \bar{y}, \bar{z}}$	local wave surface elevation at a point in ship
$\zeta_0$	surface wave profile
$\eta_j$ (eta)	complex response of ship to waves in $j$ th mode, where $j = 1, 2, 3, \dots, 6$ refers to surge, sway, heave, roll, pitch, yaw, respectively

$\bar{\eta}_j$	complex amplitude of ship response to waves in $j$ th mode; response per unit wave amplitude	$\Xi_D$	non-dimensional largest maximum expected to be exceeded in $1/\alpha$ samples of $D$ sec. duration
$ \bar{\eta}_j $	scalar amplitude of ship response	$\Xi$	non-dimensional largest maximum expected to be exceeded once in $1/\alpha$ samples of $n$ maxima
$\eta$	$= (\bar{\eta}_1, \bar{\eta}_2, \bar{\eta}_3)$ vector of translational motions at the origin in terms of complex amplitudes	$\Pi'_w$ (Pi)	non-dimensional coefficient of added power
$\theta$ (Theta)	angle generally	$\rho$ (rho)	density
$\Lambda$ (Lambda)	tuning factor, $T_{nj}/T_e = \omega_e/\omega_{nj}$	$\Phi$ (Phi)	velocity potential, also $\phi$ (phi)
$\mu$ (mu)	angle of wave propagation relative to ship's heading	$\phi_\kappa$	radiation potential
$\mu_a$	dominant direction of propagation of short-crested sea relative to ship's heading	$\phi$	angle of heel (or roll)
$\mu_\omega$	angle of propagation of wave component relative to dominant wave direction	$\dot{\phi}$	velocity of roll
$\mu_0$	angle of long-crested sea relative to ship's heading	$\psi_j$ (psi)	two-dimensional velocity potential
$\xi_1, \xi_2, \xi_3$ (xi)	local translational motion at a point in surge, sway, heave (as in Section 5)	$\Omega$ (Omega)	$= (\eta_4, \eta_5, \eta_6)$ vector of rotational motion at a point in terms of complex amplitudes
$\bar{\xi}_1, \bar{\xi}_2, \bar{\xi}_3$	complex amplitudes of local motion at a point	$\omega$ (omega)	circular frequency of a regular wave; angular velocity
$\bar{\xi}$	$= (\bar{\xi}_1, \bar{\xi}_2, \bar{\xi}_3)$ vector of translational motion at a point in a ship	$\omega_e$	frequency of encounter ( $2\pi/T_e$ )
$\bar{\xi}_R$	complex amplitude of vertical motion relative to the wave surface	$\hat{\omega}_e$	tuning factor ( $\omega_e/\omega_n$ ), also $\Lambda$
$\xi$ (xi)	magnitude of a maximum o-mean process; peak-to-mean value of wave or response record	$\omega_n, \omega_{nj}$	natural frequency of response (in $j$ th mode)
$\xi_n$	largest positive maximum in a sample of $n$ maxima	<b>Mathematical symbols</b>	
$\Xi$ (Xi)	$= \xi/\sqrt{M_0}$ normalized maxima of an o-mean process	$\partial$	the partial derivative sign
$\Xi_n$	$= \xi/\sqrt{2M_n}$ non-dimensional largest maximum in a sample of $n$ maxima	$f$	a function of
		$\sum$	summation
		$\Delta$	mass displacement volume
		$\delta$	increment
		$\int$	integrate
		$\langle \rangle$	average value of
		$\nabla$	vector differential operator on a function of three variables
		$\boxtimes$	mid-length (amidships)

See also list on page 420.

C. L. Crane, H. Eda,  
A. Landsburg

# Controllability

## Section 1 Introduction

**1.1 Definition and Scope.** Controllability encompasses all aspects of regulating a ship's trajectory, speed, and orientation at sea as well as in restricted waters where positioning and station keeping are of particular concern. Controllability includes starting, steering a steady course, turning, slowing, stopping, backing, and in the case of submarines, diving. The study of the complex subject of controllability is usually divided into three distinct areas or functions:

(a) **Coursekeeping (or steering)**—The maintenance of a steady mean course or heading. Interest centers on the ease with which the ship can be held to the course.

(b) **Maneuvering**—The controlled change in the direction of motion (turning or course changing). Interest centers on the ease with which change can be accomplished and the radius and distance required to accomplish the change.

(c) **Speed Changing**—The controlled change in speed including stopping and backing. Interest centers on the ease, rapidity and distance covered in accomplishing changes.

Performance varies with water, depth, channel restrictions, and hydrodynamic interference from nearby vessels or obstacles. Coursekeeping and maneuvering characteristics are particularly sensitive to ship trim. For conventional ships, the two qualities of coursekeeping and maneuvering may tend to work against each other; an easy turning ship may be difficult to keep on course whereas a ship which maintains course well may be hard to turn. Fortunately a practical compromise is nearly always possible.

Since controllability is so important, it is an essential consideration in the design of any floating structure. Controllability is, however, but one of many considerations facing the naval architect and involves compromises with other important characteristics. Some solutions are obtained through comparison with the

characteristics of earlier successful designs. In other cases, experimental techniques, theoretical analyses, and rational design practices must all come into play to assure adequacy.

Three tasks are generally involved in producing a ship with good controllability:

(a) Establishing realistic specifications and criteria for coursekeeping, maneuvering, and speed changing.

(b) Designing the hull, control surfaces, appendages, steering gear, and control systems to meet these requirements and predicting the resultant performance.

(c) Conducting full-scale trials to measure performance for comparison with required criteria and predictions.

This chapter will deal with each of these three tasks in detail.

**1.2 Goal and Organization of the Chapter.** The goal of this chapter is to introduce the basics of controllability analysis and its many facets in a manner that will lead to the use of rational design procedures to assure adequate ship controllability.

The chapter is organized to provide an understanding of controllability and for influencing it while interacting with the design of the vessel's hull, machinery, and other features. The material is arranged to provide a progression of information starting with general principles (Sections 2 through 11 on theory and analysis), the influences of factors such as environment and channel restrictions (Sections 12 and 13), the hydrodynamics of control surfaces (Section 14), and trials and performance requirements (Section 15). The final Sections (16 and 17) provide an introduction to the application of maneuverability analysis tools and methods to the design of the ship and its appendages for satisfactory control by the helmsman and autopilot. The design-oriented naval architect should find Sections 15–17 most helpful.

## Section 2

### The Control Loop and Basic Equations of Motion

**2.1 The Control Loop.** For surface ships, course-keeping, speed changing, and maneuvering involve primarily forces, moments, and motions acting in all directions in the horizontal plane. For submarines, the third dimension also comes into play. Hydrodynamic motion forces and interactions acting on the vessel's hull, rudder, and other appendages are of first consideration and difficulty. However, it is important to recognize that the responses of a large number of other mechanical, electronic, environmental and, most importantly, human factors all influence controllability. The following discussion of controllability based on the concept of control loops illustrates the role of these many factors.

Consider first the closed-loop directional control system from Segel (1960)<sup>1</sup> shown in Fig. 1. Starting at the left of the figure, there is a desired path or trajectory that the ship's conning officer wants to follow either under conditions of steady steaming at sea or in maneuvering. In an idealistic case, the desired path would be displayed for use by the helmsman (or alternatively by an autopilot). Simultaneously, again for the idealistic case, the path actually being traversed would also be shown on the display. If these two paths do not coincide, corrective action is taken by the helmsman or autopilot by changing the helm in a direction that will tend to correct the path error. This action activates the steering gear which changes the rudder position which in turn exerts a control force on the ship. This control force acts to induce on the hull an angle of attack, an angular velocity, and other motions. These motions of the hull introduce the major hydrodynamic forces and moments that effect the change in heading and path.

In addition to control and hydrodynamic forces and moments, external disturbances such as the wind, current, or waves may also be simultaneously acting on the ship. Ideally, the resultant heading and actual path coordinates can then be fed continuously back to the helmsman's display. This last step closes the control loop.

In the real case, all of the information concerning the actual instantaneous path is rarely known. On most ships only the heading and sometimes the rate of turn are continuously determinable, while the coordinates of position are available only occasionally. In spite of the shortcomings of the real case, the control loop still functions as shown in Fig. 1 but with less than complete information available to the conning officer and helmsman (or autopilot). Relatively large-scale changes in position are determined or deduced in restricted water conditions from visual observations, a radar display, or from visual cross bearings. Modern electronic navigation systems such as Loran C and Global Positioning System (GPS) also offer a means for determining large scale changes in position.

Consideration of the control loop of Fig. 1 shows that each of its elements plays a vital role in the overall controllability of the ship. The last two elements of the loop, the "ship" and the "steering gear and rudder," are of the greatest concern to the naval architect although the human factors present must be continually reviewed to develop a successful design.

Whereas the directional control loop of Fig. 1 functions to determine the path, a second loop of interest, the speed control loop, functions to determine the speed along the path. The only common link between the two loops is the conning officer, who issues the orders in both cases. In the case of the speed control loop, an operator or engineer receives the orders of the conning officer and manipulates the power output and direction of rotation of the main propulsion machinery to maintain, accelerate, slow down, stop, or reverse the speed of the ship. In the open sea where decisions can be made in a more leisurely manner, the conning officer has ample time to issue the necessary orders to both control loops. In restricted and congested waters, however, orders to both control loops may have to be issued simultaneously. With development of automation, the integration of these loops and the elimination of the intermediate roles of the helmsman on the bridge and the operator in the engine room is becoming commonplace.

With today's sophisticated drill rigs and track-keeping vessels, the automatic controller has indeed be-

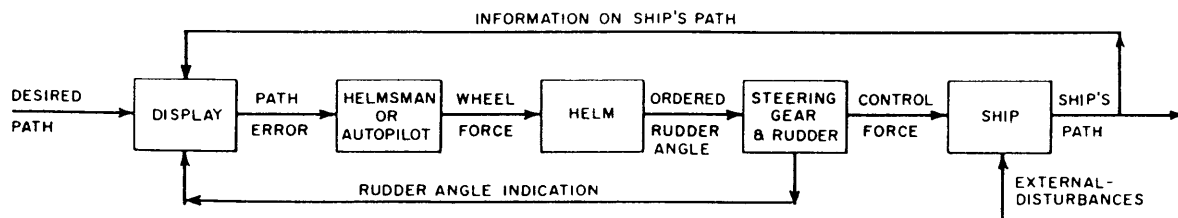


Fig. 1 Closed-loop control system ship controllability (Segel, 1960)

<sup>1</sup> Complete references are listed at the end of the chapter.

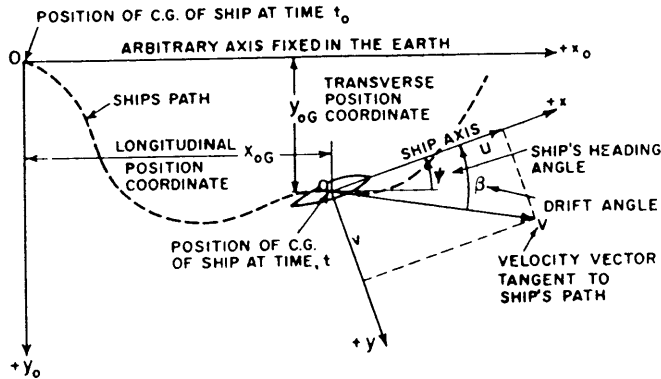


Fig. 2 Orientation of fixed axes and moving axes (Hoyt, 1948)

come quite advanced. Heading and speed, plus transverse position error and fore and aft position error are used to compute vector thrusts required of the various force effectors (propellers, rudders, thrusters, etc.), and proper distribution of correction forces/moments is automatically ordered.

**2.2 Axes Fixed Relative to the Earth.** The basic dynamics of maneuvering and coursekeeping can be described and analyzed using Newton's equations of motion. Basic equations in the horizontal plane can be considered first with reference to one set of axes fixed relative to the earth and a second set fixed relative to the ship.

Fig. 2 shows typical fixed and moving axes for a surface ship. The path is usually defined as the trajectory of the ship's center of gravity. Heading refers to the direction ( $\psi$ , angle of yaw) of the ship's longitudinal axis with respect to one of the fixed axes. The difference between the heading and the actual course (or direction of the velocity vector at the center of gravity) is the drift or leeway angle,  $\beta$ . When the ship is moving along a curved path, the drift angle is thus the difference in direction between the heading and the tangent to the path of the center of gravity.

There are significant factors that couple the speed of a ship and its path. For example, it is shown later that path changing (turning) and even path keeping (coursekeeping) cause involuntary speed reductions. These effects arise from the fact that any misalignment between the  $x$ -axis of the ship as shown in Fig. 2 and its velocity vector,  $V$ , increases the drag force acting on the ship. In addition, on multiple-screw vessels the thrust produced by each propeller can be controlled individually so as to influence the path as well as the speed. On ships with an odd number of propellers, or with any number of unirotating propellers, the direction of rotation of the uncompensated-for propeller(s) influences the path. Even on ships where the trajectory control and speed control loops operate independently, changes in the direction of propeller rotation are commonly used in conjunction with rudder action to control the motion in restricted waters.

Fig. 2 shows a right-hand orthogonal system of ref-

erence axes  $x_0$  and  $y_0$  whose directions are fixed with respect to the surface of the earth. For surface ships in calm water, it is obvious that the path of the center of gravity is restrained at all times to the horizontal plane  $x_0y_0$ . The positive direction of the  $x_0$ -axis is taken to be in the general direction of the motion; its precise direction is arbitrary, but is fixed with respect to the earth. Positive  $z_0$  is taken downward or into the plane of the paper, positive  $y_0$  is to starboard. The motion of the ship subsequent to time,  $t = t_0$ , is completely defined by the coordinates  $x_{0G}$ ,  $y_{0G}$  and the angle of yaw,  $\psi$ . Since in Fig. 2,  $Z_0$  is positive downward into the paper, the sign of  $\psi$  shown in Fig. 2 is negative. Referring to these axes fixed in the earth, the Newtonian equations of motion of the ship are:

$$\begin{aligned} X_0 &= \Delta \ddot{x}_{0G} \quad (\text{Surge}) \\ Y_0 &= \Delta \ddot{y}_{0G} \quad (\text{Sway}) \\ N &= I_z \ddot{\psi} \quad (\text{Yaw}) \end{aligned} \quad (1)$$

where the two dots above the symbols  $x_{0G}$ ,  $y_{0G}$  and  $\psi$  indicate the second derivatives of those values with respect to time,  $t$ , and,

$X_0$  and  $Y_0$  = total forces in  $x_0$  and  $y_0$  directions respectively

$\Delta$  = mass of ship

$N$  = total moment about an axis through the center of gravity of ship and parallel to the  $z_0$ -axis

$I_z$  = mass moment of inertia of ship about the  $z_0$ -axis

$\psi$  = yaw angle in the horizontal plane measured from the vertical  $x_0 z_0$  plane to the  $x$ -axis of the ship.

**2.3 Axes Fixed in the Ship.** In spite of the apparent simplicity of Equations (1), the motion of a ship is more conveniently expressed when referred to the axes  $x$  and  $y$  fixed with respect to the moving ship as also shown in Fig. 2. The moving axes, like the fixed axes  $x_0$  and  $y_0$ , form a right-hand orthogonal system, but with the difference that the origin stays at the center of gravity for all time,  $t$ . The  $x$ -axis is along the centerplane, coincident with the longitudinal axis of inertia which may be assumed, with very small error, to be parallel to the baseline of the ship. Its positive direction is forward. The direction of the  $x$ -axis is referred to as the heading; hence  $\psi$  is the heading angle as well as the yaw angle. The  $z$ -axis is also in the centerplane of the ship, but is normal to  $x$  and is positive downward; the  $y$ -axis is normal to  $x$  and  $z$  and is positive to starboard. The instantaneous linear velocity of the origin of the moving axes is represented by the vector  $V$  and the orientation of the moving axes with respect to the direction of motion is given by the angle,  $\beta$ , the so-called drift angle, or angle of attack measured from  $V$  to  $x$  as shown in Fig. 2. The velocity  $V$  is, of course, always tangent to the path of the ship. The

orientation of the moving axes with respect to the  $x_0$ ,  $y_0$  axes is, as noted earlier, the angle of yaw  $\psi$ . In the particular case shown in Fig. 2, both  $\beta$  and  $\psi$  are negative.

In order to convert Equations (1) from axes fixed in the earth to axes fixed in the moving ship, the total forces  $X$  and  $Y$  in the  $x$  and  $y$ -directions, respectively, are expressed in terms of  $X_0$  and  $Y_0$ :

$$\begin{aligned} X &= X_0 \cos \psi + Y_0 \sin \psi \\ Y &= Y_0 \cos \psi - X_0 \sin \psi \end{aligned} \quad (2)$$

likewise

$$\begin{aligned} \dot{x}_{0G} &= u \cos \psi - v \sin \psi \\ \dot{y}_{0G} &= u \sin \psi + v \cos \psi \end{aligned} \quad (3)$$

where the dot above the symbol signifies the first derivative of the quantity with respect to time, and  $u$  and  $v$  are the components of  $\mathbf{V}$  along  $x$  and  $y$ , respectively. Then

$$\begin{aligned} \ddot{x}_{0G} &= \dot{u} \cos \psi - \dot{v} \sin \psi - (u \sin \psi + v \cos \psi) \dot{\psi} \\ \ddot{y}_{0G} &= \dot{u} \sin \psi + \dot{v} \cos \psi + (u \cos \psi - v \sin \psi) \dot{\psi} \end{aligned} \quad (4)$$

Substituting Equation (4) in Equation (1) and inserting the resulting values of  $X_0$  and  $Y_0$  in Equation (2) yields the simple expressions:

$$\begin{aligned} X &= \Delta(\dot{u} - v\dot{\psi}) \\ Y &= \Delta(\dot{v} + u\dot{\psi}) \end{aligned}$$

These and the third member of Equations (1) comprise the pertinent equations of motion in the horizontal plane assuming zero roll, pitch, and heave. Roll, pitch, and yaw are the rotary ship motions about the  $x$ ,  $y$ , and  $z$ -axes, respectively. Surge, sway and heave are the translatory motions along the same axes. For completeness:

$$\begin{aligned} X &= \Delta(\dot{u} - v\dot{\psi}) && \text{is surge} \\ Y &= \Delta(\dot{v} + u\dot{\psi}) && \text{is sway} \\ N &= I_z \ddot{\psi} && \text{is yaw} \end{aligned} \quad (5)$$

Note the existence of the term  $\Delta u\dot{\psi}$  in the equation for  $Y$  and  $\Delta v\dot{\psi}$  in the equation for  $X$ , whereas terms like these were not present in Equations (1). These are the so-called centrifugal-force terms which exist when systems with moving axes are considered, but do not exist when the axes are fixed in the earth.

Equations (5) have been developed for the case where the origin of the axes,  $O$ , is at the center of gravity of the ship. For many reasons, it is frequently desirable to locate the origin not at the center of gravity but rather at the intersection of planes of symmetry. For example, for body-of-revolution submarines, if  $O$  is located at the axis of symmetry rather than at the vertical position of the center of gravity, important simplifications are achieved. For surface ships, locating the origin at the midlength rather than

at the longitudinal position of the center of gravity is desirable for two reasons; one is to simplify certain computations, the other is that the location of the center of gravity is not constant but changes with the condition of loading. (Throughout this chapter it is assumed that LCG coincides with LCB and with the midship location.)

**2.4 Forces Acting on a Vessel During a Maneuver.** The forces and moments (left hand side) of the equations of motion (5) are built up of four types of forces that act on a ship during a maneuver:

- (a) Hydrodynamic forces acting on the hull and appendages due to ship velocity and acceleration, rudder deflection, and propeller rotation.
- (b) Inertial reaction forces caused by ship acceleration.
- (c) Environmental forces due to wind, waves and currents.
- (d) External forces such as tugs or thrusters.

The first two types of forces generally act in the horizontal plane and involve only surge, sway and yaw responses, although rolling effects (heel) occur in the maneuvering of high-speed ships and the Small Waterplane Area Twin Hull (SWATH) vessels. Hydrodynamic forces fall into two basic categories, those arising from hull velocity through the water (damping forces) and those arising from hull accelerations through the water (added mass forces). The ship accelerations produced by these and any external forces result in balancing inertial reaction (*d'Alembert forces and moments*), especially when turning.

The effect of a rudder on turning is indirect. Moving the rudder produces a moment that causes the ship to change heading so as to assume an angle of attack (leeway angle) to the direction of motion of the center of gravity. Consequently, hydrodynamic forces on the hull are generated which, after a time, cause a change of lateral movement of the center of gravity. The lateral movement is opposed by the inertial reactions. If the rudder remains at a fixed position, a steady turning condition will evolve when hydrodynamic and inertial forces and moments come into balance.

When in shallow or restricted waters, various complex effects come into play. Interactions between vessels further complicate hydrodynamic and inertial force analysis. Section 13 describes how some of these complications have been treated.

The ship may also be operating and maneuvering in an environment where wind, waves, and current are present. The effect of current is usually incorporated with the hydrodynamic forces by considering the relative velocity between the vessel and the water although studies in restricted waters require more careful analysis. Wind and wave forces are generally treated as external forces as described in Section 12.

Wind velocity is generally unsteady and hence forces

and moments due to wind will be time dependent. These forces are generally proportional to the above water area of the ship and the square of the relative velocity between the ship and the wind. Forces and moments also vary with the direction of the wind velocity relative to the ship's axes.

Two distinct types of wave forces act. The steady and slowly varying forces due to second-order wave drift effects are generally more important for ship controllability than the first-order forces, which are of primary importance for seakeeping, as described in Chapter VIII. However, the latter can be important for the case of following seas where frequency of encounter is small. Wave drift forces depend primarily

on ship length and on the relative magnitudes of wave length and amplitude.

Pitching motion changes the shape of the immersed hull and can therefore have significant effects on the coefficients in the equations of motion, particularly in quartering and following seas.

Finally, tugs and thrusters create effective forces when utilized at relatively slow speeds. The forces they develop are for the most part external to the hydrodynamics of the maneuver and are normally treated as independent additions.

The simple case of controllability, assuming a calm open sea without wind, waves, current, and external forces, will be considered first.

## Section 3

### Motion Stability and Linear Equations

**3.1 Definitions of Motion Stability.** The concept of path keeping is strongly related to the concept of course stability or stability of direction. A body is said to be stable in any particular state of equilibrium in rest or motion if, when momentarily disturbed by an external force or moment, it tends to return, after release from the disturbing force, to the state of equilibrium existing before the body was disturbed. In the case of path keeping, the most obvious external disturbing force would be a wave or a gust of wind. For optimum path keeping, it would be desirable for the ship to resume its original path after passage of the disturbance, with no intervention by the helmsman. Whether this will happen depends on the kind of motion stability possessed.

The various kinds of motion stability associated with ships are classified by the attributes of their initial state of equilibrium that are retained in the final path of their centers of gravity. For example, in each of the cases in Fig. 3, a ship is initially assumed to be traveling at constant speed along a straight path. In Case I, termed straight-line or dynamic stability, the final path after release from a disturbance retains the straight-line attribute of the initial state of equilibrium, but not its direction. In Case II, directional stability, the final path after release from a disturbance retains not only the straight-line attribute of the initial path, but also its direction. Case III is similar to Case II except that the ship does not oscillate after the disturbance, but passes smoothly to the same final path as Case II. The distinction between these two cases is discussed in Section 4. Finally, in Case IV, positional motion stability, the ship returns to the original path, ie: the final path not only has the same direction as the original path, but also its same transverse position relative to the surface of the earth.

The foregoing kinds of stability form an ascending

hierarchy. Achieving straight-line stability (Case I) is the designer's usual goal for most ships when steered by hand. The other cases require various degrees of automatic control.

**3.2 Course Stability With Controls Fixed and Controls Working.** All of these kinds of stability have meaning with control surfaces (rudders) fixed at zero, with control surfaces free to swing, or with controls either manually or automatically operated. The first two

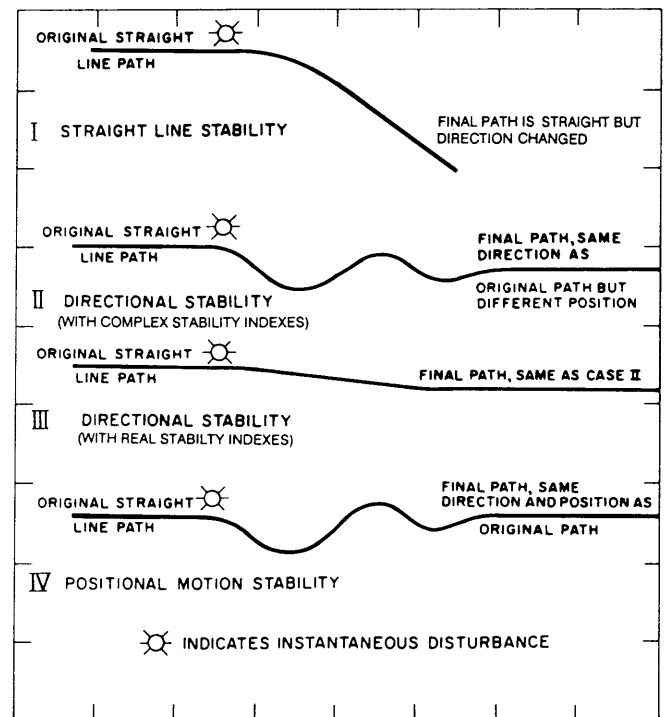


Fig. 3 Various kinds of motion stability (Arentzen, 1960)

cases involve only the last two elements of the control loop of Fig. 1, whereas the last case involves all of the elements of the control loop. In normal marine usage the term stability usually implies controls-fixed stability; however, the term can also have meaning with the controls working. The following examples indicate distinctions:

(a) A surface ship sailing a calm sea possesses positional motion stability in the vertical plane (and therefore directional and straight-line stability in this plane) with controls fixed. This is an example of the kind of stability shown by Case IV of Fig. 3. In this case, hydrostatic forces and moments introduce a unique kind of stability which in the absence of these forces could only be introduced either by very sophisticated automatic controls or by manual control. The fact that the ship operator and designer can take for granted this remarkable kind of stability does not detract from its intrinsic importance.

(b) In the horizontal plane in the open sea with stern propulsion, a self-propelled ship cannot possess either positional or directional stability with controls fixed because the changes in buoyancy that stabilize in the vertical plane are nonexistent in the horizontal plane. However, a ship must possess both of these kinds of stability with controls working either under manual or automatic guidance. Possible exceptions include sailing vessels, some multi-hull ships, and foil or planing craft but not other surface effect ships.

(c) The only kind of motion stability possible with self-propelled ships in the horizontal plane with controls fixed is straight-line stability. In fact, many ships do not possess it. In subsequent sections of this chapter, with some exceptions, whenever controls-fixed stability is mentioned, the intended meaning is controls-fixed straight-line stability. This kind of stability is desirable, but not mandatory.

With each of the kinds of controls-fixed stability, there is associated a numerical index which by its sign designates whether the body is stable or unstable in that particular sense and by its magnitude designates the degree of stability or instability. To show how these indexes are determined, one must resort to the differential equations of motion.

**3.3 Assumptions of Linearity and Simple Addable Parts.** In order to understand the impact of various ship design characteristics and features on ship controllability, it is necessary to first become familiar with certain fundamental aspects relating to the concept of stability and to the development and use of the linear equations of motion. The use of non-linear equations for analysis and prediction and the determination of coefficients through captive model tests, use of theoretical and empirical coefficient determination methods, and systems analysis is introduced in Sections 8 and 9.

The force components  $X$ ,  $Y$  and the moment component  $N$  in Equation (5) are assumed to be composed

of several parts, some of which are functions of the velocities and accelerations of the ship. In the most general case they also include terms dependent on the orientation of the ship relative to the axis of the earth as well as excitation terms such as those arising from the seaway or from use of the rudder, but these will be introduced later. For the present they are assumed to be composed only of forces and moments arising from motions of the ship which in turn have been excited by disturbances whose details we need not be concerned with here. Expressed functionally  $X$ ,  $Y$ , and  $N$  are:

$$\begin{aligned} X &= F_x(u, v, \dot{u}, \dot{v}, \dot{\psi}, \ddot{\psi}) \\ Y &= F_y(u, v, \dot{u}, \dot{v}, \dot{\psi}, \ddot{\psi}) \\ N &= F_\psi(u, v, \dot{u}, \dot{v}, \dot{\psi}, \ddot{\psi}) \end{aligned} \quad (6)$$

In order to obtain a numerical index of motion stability, the functional expressions shown in Equation (6) must be reduced to useful mathematical form. This can be done by means of the Taylor expansion of a function of several variables. The Taylor expansion of a function of a single variable states that if the function of a variable,  $x$ , Fig. 4, and all its derivatives are continuous at a particular value of  $x$ , say  $x_1$ , then the value of the function at a value of  $x$  not far removed from  $x_1$  can be expressed as follows:

$$\begin{aligned} f(x) &= f(x_1) + \delta x \frac{df(x)}{dx} + \frac{\delta x^2}{2!} \frac{d^2f(x)}{dx^2} \\ &+ \frac{\delta x^3}{3!} \frac{d^3f(x)}{dx^3} + \dots + \frac{\delta x^n}{n!} \frac{d^nf(x)}{dx^n} \end{aligned} \quad (7a)$$

where

$f(x)$  = value of function at a value of  $x$  close to  $x_1$

$f(x_1)$  = value of function at  $x = x_1$

$\delta x = x - x_1$

and

$\frac{d^nf(x)}{dx^n}$  =  $n$ th derivative of function  
evaluated at  $x = x_1$

If the change in the variable,  $\delta x$ , is made sufficiently small, the higher order terms of  $\delta x$  in Equation (7a) can be neglected. Equation (7a) then reduces to

$$f(x) = f(x_1) + \delta x \frac{df(x)}{dx} \quad (7b)$$

It may be seen from Fig. 4 that Equation (7b) is a linear approximation to the real function  $f(x)$  at  $x = x_1 + \delta x$  and that (7b) becomes increasingly accurate as  $\delta x$  is reduced in magnitude. Equation (7b) is called the linearized form of (7a).

The linearized form of the Taylor expansion of a



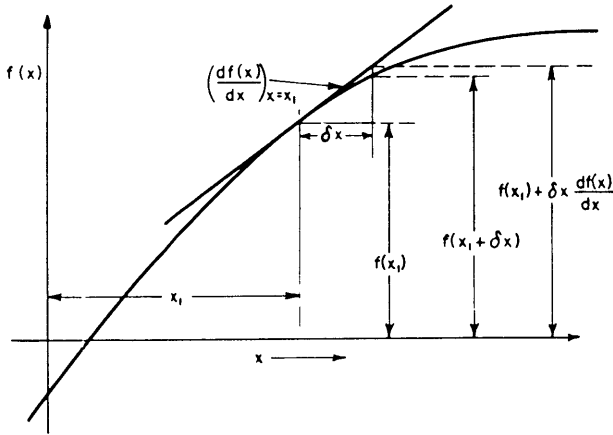


Fig. 4 Linearization of Taylor expansion of a function of a single variable,  $f(x)$

function of two variables  $x$  and  $y$  is a simple sum of three linear terms as follows:

$$f(x, y) = f(x_1, y_1) + \delta x \frac{\partial f(x, y)}{\partial x} + \delta y \frac{\partial f(x, y)}{\partial y} \quad (7c)$$

where both  $\delta x$  and  $\delta y$  must be small enough so that higher order terms of each can be neglected as well as the product  $\delta x \delta y$ .

The assumption that renders linearization reasonably accurate, namely, that the admissible change in variables must be very small, is entirely compatible with an investigation of motion stability. Motion stability determines whether a very small perturbation from an initial equilibrium position is going to increase with time or decay with time. Thus, it is consistent with the physical reality of motion stability to use the linearized Taylor expansions in connection with equation (6). For example, by analogy with Equation (7c), the linearized  $Y$ -force of (6) can now be written as:

$$Y = F_y(u_1, v_1, \dot{u}_1, \dot{v}_1, \dot{\psi}_1, \ddot{\psi}_1) + (u - u_1) \frac{\partial Y}{\partial u} + (v - v_1) \frac{\partial Y}{\partial v} + \dots + (\ddot{\psi} - \ddot{\psi}_1) \frac{\partial Y}{\partial \ddot{\psi}} \quad (8)$$

where the subscript 1 refers in all cases to the values of the variables at the initial equilibrium condition and where all of the partial derivatives are evaluated at the equilibrium condition. Since the initial equilibrium condition for an investigation of motion stability is straight-line motion at constant speed, it follows that  $\dot{u}_1 = \dot{v}_1 = \dot{\psi}_1 = \ddot{\psi}_1 = 0$ . Furthermore, since most ships are symmetrical about their  $xz$ -plane, they travel in a straight line at zero angle of attack; therefore  $v_1$  is also zero but this is not necessarily true on ships with an odd number of propellers or with any number of unirotating propellers, Sections 5.3 and 11.0). Also because of symmetry  $\partial Y / \partial u = \partial Y / \partial \dot{u} = 0$  since a

change in forward velocity or forward acceleration will produce no transverse force with ship forms that are symmetrical about the  $xz$ -plane. Finally, if the ship is in fact in equilibrium in straight-line motion, there can be no  $Y$ -force acting on it in that condition, therefore  $F_y(u_1, v_1, \dot{u}_1, \dot{v}_1, \dot{\psi}_1, \ddot{\psi}_1)$  is also zero. Only  $u_1$  is not zero but is equal to the resultant velocity,  $V$ , in the initial equilibrium condition. With these simplifications, Equation (8) reduces to

$$Y = \frac{\partial Y}{\partial v} v + \frac{\partial Y}{\partial \dot{v}} \dot{v} + \frac{\partial Y}{\partial \dot{\psi}} \dot{\psi} + \frac{\partial Y}{\partial \ddot{\psi}} \ddot{\psi} \quad (9a)$$

and similarly the surging force and the yawing moment can be written as:

$$X = \frac{\partial X}{\partial \dot{u}} \dot{u} + \frac{\partial X}{\partial u} \delta u + \frac{\partial X}{\partial v} v + \frac{\partial X}{\partial \dot{v}} \dot{v} + \frac{\partial X}{\partial \dot{\psi}} \dot{\psi} + \frac{\partial X}{\partial \ddot{\psi}} \ddot{\psi} \quad (9b)$$

$$N = \frac{\partial N}{\partial v} v + \frac{\partial N}{\partial \dot{v}} \dot{v} + \frac{\partial N}{\partial \dot{\psi}} \dot{\psi} + \frac{\partial N}{\partial \ddot{\psi}} \ddot{\psi} \quad (9c)$$

where the cross-coupled derivatives  $\partial Y / \partial \dot{\psi}$ ,  $\partial N / \partial v$ , and  $\partial N / \partial \dot{v}$  usually have small nonzero values because most ships are not symmetrical about the  $yz$ -plane even if that plane is at the midlength of the ship (bow and stern shapes are normally quite different). However, the cross-coupled derivatives  $\partial X / \partial v$ ,  $\partial X / \partial \dot{v}$ ,  $\partial X / \partial \dot{\psi}$ , and  $\partial X / \partial \ddot{\psi}$ , like  $\partial Y / \partial \dot{u}$  and  $\partial Y / \partial \ddot{u}$  are zero because of symmetry about the  $xz$ -plane. Hence, equation (9b) reduces to:

$$X = \frac{\partial X}{\partial \dot{u}} \dot{u} + \frac{\partial X}{\partial u} \delta u \quad (9d)$$

where  $\delta u = u - u_1$ .

**3.4 Notation of Force and Moment Derivatives.** In the simplified derivative notation of SNAME (Nomenclature, 1952),  $\partial Y / \partial v = Y_v$ ,  $\partial N / \partial \dot{\psi} = N_{\dot{\psi}}$ , and so on. Also for motions restricted to the horizontal plane  $\dot{\psi} \equiv r$  and  $\ddot{\psi} \equiv \dot{r}$ . Using this notation and substituting (9) into (5), the linear equations of motion with moving axes in the horizontal plane are:

$$\left. \begin{aligned} -X_u(u - u_1) + (\Delta - X_{\dot{u}}) \dot{u} &= 0 \\ -Y_r v + (\Delta - Y_{\dot{v}}) \dot{v} - (Y_r - \Delta u_1) r - Y_{\dot{r}} \dot{r} &= 0 \\ -N_r v - N_{\dot{u}} \dot{v} - N_{\dot{r}} r + (I_z - N_{\dot{r}}) \dot{r} &= 0 \end{aligned} \right\} \quad (10)$$

Every term of the first two equations of (10) has the dimensions of a force whereas every term in the third equation of (10) has the dimensions of a moment. Therefore, to nondimensionalize (10), which is convenient for several reasons, the force equations are divided through by  $(\rho/2)L^2V^2$  and the moment equations by  $(\rho/2)L^3V^2$ . (Note the similarity between  $(\rho/2)L^2V^2$  used as a nondimensionalizer in this case and  $(\rho/2)SV^2$

used to obtain the resistance coefficients in Chapter V). Further, as in (Nomenclature, 1952) a primed symbol will be used to designate the nondimensional form of each of the factors appearing in (10). For example:

$$\Delta' = \frac{\Delta}{\frac{\rho}{2}L^3}; v' = \frac{v}{V}; \dot{v}' = \frac{\dot{v}}{V^2}$$

$$I'_z = \frac{I_z}{\frac{\rho}{2}L^5}; r' = \frac{rL}{V}; \dot{r}' = \frac{\dot{r}L^2}{V^2}$$

$$Y'_v = \frac{Y_v}{\frac{\rho}{2}L^2V}; Y'_r = \frac{Y_r}{\frac{\rho}{2}L^3V}; N'_v = \frac{N_v}{\frac{\rho}{2}L^3V}; N'_r = \frac{N_r}{\frac{\rho}{2}L^4V}$$

$$Y'_\dot{v} = \frac{Y_{\dot{v}}}{\frac{\rho}{2}L^3}; Y'_{\dot{r}} = \frac{Y_{\dot{r}}}{\frac{\rho}{2}L^4}; N'_{\dot{v}} = \frac{N_{\dot{v}}}{\frac{\rho}{2}L^4}; N'_{\dot{r}} = \frac{N_{\dot{r}}}{\frac{\rho}{2}L^5}$$

Thus, for example, the nondimensional forms of the first couple of terms of the last of Equations (10) are:

$$N'_v v' = \left( \frac{N_v}{\frac{\rho}{2}L^3V} \right) \left( \frac{v}{V} \right) = \frac{N_v v}{\frac{\rho}{2}L^3V^2};$$

$$N'_{\dot{v}} \dot{v}' = \left( \frac{N_{\dot{v}}}{\frac{\rho}{2}L^4} \right) \left( \frac{\dot{v}L}{V^2} \right) = \frac{N_{\dot{v}} \dot{v}}{\frac{\rho}{2}L^3V^2};$$

etc.

If the surge equation is neglected and if the previous notation is adopted, (10) becomes in nondimensional form:

$$\begin{aligned} -Y'_v v' + (\Delta' - Y'_{\dot{v}}) \dot{v}' - (Y'_r - \Delta') r' \\ -Y'_{\dot{r}} \dot{r}' &= 0 \\ -N'_v v' - N'_{\dot{v}} \dot{v}' - N'_r r' \\ + (I'_z - N'_{\dot{r}}) \dot{r}' &= 0 \end{aligned} \quad (11)$$

where the main difference between (10) and (11), aside from the prime notation, is that  $u_1$  has disappeared since  $u_1/V \approx 1$  for small perturbations.

Because of the fact that the derivative  $Y'_{\dot{v}}$  enters into Equation (11) as an addition to the mass term, it is termed the virtual mass coefficient. (The term  $Y'_{\dot{v}}$  is always negative; i.e.,  $Y$  acts to oppose positive  $\dot{v}$ , see Section 4.2.) It is thus identical to the concept of added mass. (The force required to accelerate a body in a fluid is always larger than the product of the actual mass of the body times its acceleration. This fact has given rise to the concept of "entrained" or "added" mass. However, this added force should be really in-

terpreted as the hydrodynamic force arising because of the acceleration of the body in the fluid. This is precisely the definition of the  $Y_{\dot{v}}$  force in (10)). Similarly,  $N'_{\dot{r}}$  is termed the virtual moment of inertia coefficient. The derivatives  $Y'_{\dot{r}}$  and  $N'_{\dot{v}}$  are termed coupled virtual inertia coefficients. As noted earlier, these derivatives would be zero if ship hulls, including their appendages, were symmetrical about their  $yz$ -planes.

It is convenient to use a notation that distinguishes the forces and moments according to their origins. For example the notation  $Y_{v,v}$  will be used to denote the  $y$ -component of the hydrodynamic force acting at the center of gravity of the ship that is developed as a result of an angle of attack,  $\beta$ . As has been shown,  $Y_{v,v}$  is only a linear approximation to, or linearization of, this  $Y$ -force as will be further evident from later examination of Fig. 10. Similar symbols and definitions are included in the nomenclature for other forces and moments.

**3.5 Control Forces and Moments.** It is important to note that all of the terms of (10) or (11) must include the effect of the ship's rudder held at zero degrees (on the centerline). On the other hand, if we want to consider the path of a ship with controls working, the equations of motion (10) or (11) must include terms on the right-hand side expressing the control forces and moments created by rudder deflection (and any other control devices) as functions of time. The linearized  $y$ -component of the force created by rudder deflection acting at the center of gravity of the ship is  $Y_{\delta} \delta_R$  (see Fig. 5) and the linearized component of the moment created by rudder deflection about the  $z$ -axis of the ship is  $N_{\delta} \delta_R$  where

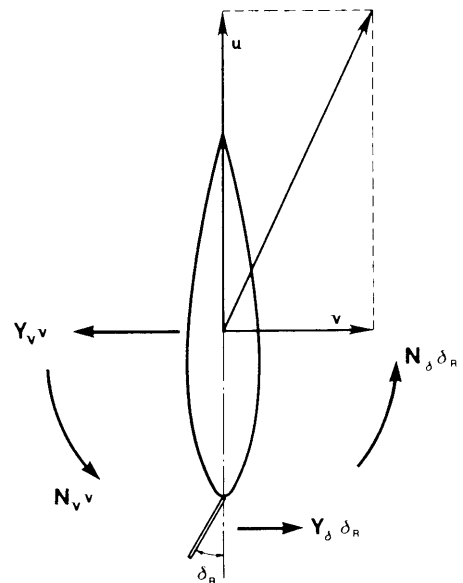


Fig. 5 Rudder-induced turning moments

$\delta_R$  = rudder-deflection angle, measured from  $xz$ -plane of ship to plane of rudder; positive deflection corresponds to a turn to port for rudder(s) located at stern

$Y_\delta, N_\delta$  = linearized derivatives of  $Y$  and  $N$  with respect to rudder-deflection angle  $\delta_R$

The lateral force from the deflected rudder thus creates a moment to turn the ship. This turning action causes the ship to develop an angle of attack with respect to its motion through the water. The lateral forces then generated by the well designed ship (acting as a foil moving in a liquid at an angle of attack) create a moment,  $N_v v$ , that *greatly augments* the rudder moment. The combined moments cause the turning motion as indicated in Fig. 5.

For the case of small perturbations, which is the only case where (10) and (11) apply, only small deflections of the rudder are admissible. With this restriction, the derivatives such as  $Y'_v, N'_v, Y'_r$ , and  $N'_r$  are evaluated at  $\delta_R = 0$  and are assumed not to change at other admissible values of  $\delta_R$ . Furthermore, for usual ship configurations,  $Y'_r \approx 0$  and  $N'_v \approx 0$ .

With these assumptions the equations of motion including the rudder force and moment, are as follows:

$$\begin{aligned} \text{Moment:} \quad n'_z \dot{r}' - N'_v v' - N'_r r &= N'_\delta \delta_R \\ (\text{Yaw}) & \\ \text{Force:} \quad \Delta'_y \dot{v}' - Y'_v v' - (Y'_r - \Delta) r' & \\ (\text{Sway}) &= Y'_\delta \delta_R \end{aligned} \quad (12)$$

where:

$$\begin{aligned} n'_z &= I'_z - N'_r \approx 2 I_z \\ \Delta'_y &= \Delta' - Y'_v \approx 2 \Delta' \end{aligned}$$

It will be shown in the next three sections how the linearized equations developed so far can be used to analyze the problem of course stability and steady turning. But to make numerical predictions it is necessary to obtain values for some or all of the coefficients or derivatives involved. This is primarily done by means of captive model tests, as discussed in Sections 8, 9 and 16. Theoretical approaches to estimating some coefficients and approaches are also described in Section 16.

## Section 4

### Analysis of Coursekeeping and Controls-Fixed Stability

**4.1 Stability Indexes.** Using only linear terms, solutions to the sway and yaw equations provide linear transfer functions permitting the review of the stability of motion. This Section develops the basic stability indexes and describes the definitive spiral maneuver whose numerical measures are indicative of the stability characteristics of a ship.

Equations (12) are two simultaneous differential equations of the first order in two unknowns, the horizontal-velocity component,  $v'$ , and the yaw angular-velocity component  $r'$ . The simultaneous solution of these two equations for  $v'$  and  $r'$  yields a second-order differential equation which leads to the concept of straight-line stability. The solutions for  $v'$  and  $r'$  correspond to the standard solutions of second-order differential equations which are as follows:

$$\begin{aligned} v' &= V_1 e^{\sigma_1 t} + V_2 e^{\sigma_2 t} \\ r' &= R_1 e^{\sigma_1 t} + R_2 e^{\sigma_2 t} \end{aligned} \quad (13)$$

where  $e = 2.718$ ;  $V_1, V_2, R_1$ , and  $R_2$  are constants of integration;  $\sigma_1$  and  $\sigma_2$  are the stability indexes with dimensions of  $1/t$  and  $t$  is time. It is seen from solution (13) that if both values of  $\sigma$  are negative,  $v'$  and  $r'$  will approach zero with increasing time which means that the path of the ship will eventually resume a new straight-line direction. This corresponds to Case I of Fig. 3. If either  $\sigma_1$  or  $\sigma_2$  is positive,  $v'$  and  $r'$  will

increase with increasing time, a straight-line path will never be resumed, and the ship may end up in a steady turn with its rudder held fixed at zero.

The relationship between the stability indexes,  $\sigma$ , of solution (13) and the stability derivatives of (11) can be obtained by substituting the solutions (13) back into (11). If this is done, a quadratic equation in  $\sigma$  is obtained:

$$A\sigma^2 + B\sigma + C = 0 \quad (14)$$

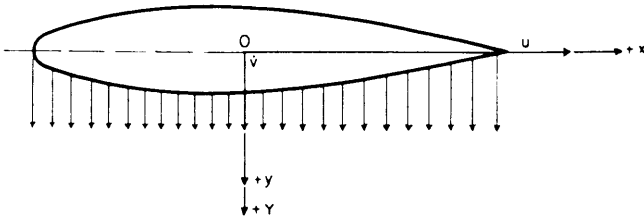
where

$$\begin{aligned} A &= n'_z \Delta'_y \\ B &= -n'_z Y'_v - \Delta'_y N'_r \\ C &= Y'_v N'_r - (Y'_r - \Delta') N'_v \end{aligned}$$

The two roots of Equation (14), both of which must be negative for controls-fixed stability are:

$$\sigma_{1,2} = \frac{-B/A \pm [(B/A)^2 - 4C/A]^{1/2}}{2} \quad (14a)$$

From a practical standpoint,  $\sigma_1$  alone is usually given for surface ships. This is because the size for  $\sigma_2$  is algebraically less than  $\sigma_1$  and thus it is clear from Equations (13) that the motion description by the  $\sigma_1$  term is larger than the  $\sigma_2$  term after the distur-

Fig. 6 Ship with a transverse acceleration,  $\dot{v}$ 

bance has ended. Hence  $\sigma_1$  alone is rather a good negative quantitative measure of the degree of stability.

**4.2 The Stability Criterion.** Expression (14a) reveals that the two essential conditions for both  $\sigma_1$  and  $\sigma_2$  to be negative are:

(a) That  $C/A$  be positive, i.e.,  $C/A > 0$ . If  $C/A$  is negative

$$\left[ \left( \frac{B}{A} \right)^2 - \frac{4C}{A} \right]^{1/2}$$

will be greater than  $B/A$  and whether  $B/A$  is positive or negative, one value of  $\sigma$  will always be positive.

(b) That  $B/A$  be positive. If  $B/A$  is negative and  $C/A$  is positive, then both  $\sigma_1$  and  $\sigma_2$  will always be positive. As noted before, if both  $B/A$  and  $C/A$  are negative, one value of  $\sigma$  will be positive.

Thus, the conditions for stability are reduced to the requirements that  $B/A$  and  $C/A$  must both be positive quantities. Since each of the terms of  $A$ ,  $B$ , and  $C$  are nondimensionalized by the same quantities, the magnitudes and the signs of  $A$ ,  $B$ ,  $C$  may be determined by examination of either the dimensional or nondimensional derivatives appearing in the definitions of  $A$ ,  $B$ , and  $C$  in Equation (14). Because the nondimensionalizing items,  $\rho$ ,  $V$ , and  $L$  are always taken as positive, they do not change the signs of the derivatives.

The derivative  $Y_{\dot{v}}$  will be treated first. It is the slope of the  $Y$ -force with respect to an acceleration  $\dot{v}$ , and appears in the definition of both  $A$  and  $B$  of (14). The sketch shown in Fig. 6 represents a ship with an ac-

celeration  $+\dot{v}$  with the origin taken at the midlength of the ship. Under these circumstances, both the bow and stern experience a  $\dot{v}$ -acceleration in the positive  $y$ -direction. Therefore, the inertial reaction pressure of the water being accelerated by the hull produces forces in the negative  $y$ -direction on both the bow and stern. Hence, the bow and the stern effects add to give a relatively large negative  $Y$ -force resulting from a positive  $\dot{v}$ . If a disturbance of a negative  $\dot{v}$  is placed on the ship, the inertial pressures on the bow and the stern will add together to give a relatively large  $Y$ -force in the positive  $y$ -direction. Hence, the plot of  $Y$  versus  $\dot{v}$  would appear as shown in Fig. 7, and the slope  $Y_{\dot{v}}$  taken at  $\dot{v} = 0$  would be a negative value of relatively large magnitude. For ship-shaped bodies with large length to beam ( $L/B$ ) ratios, the magnitude of  $Y_{\dot{v}}$  is approximately that of the ship's displacement,  $\Delta$ . For example, theoretically calculated values of  $Y_{\dot{v}}$  for ellipsoids give values of  $-0.9 \Delta$  for  $L/B = 5$ ;  $-0.95 \Delta$  for  $L/B = 8.5$ ; and  $-1.0 \Delta$  for  $L/B = \infty$ . Thus, the term  $(\Delta - Y_{\dot{v}})$  which occurs in both  $A$  and  $B$  is a large positive number with a magnitude of almost  $2 \Delta$  Equation (12).

Like  $Y_{\dot{v}}$ , the derivative  $N_{\dot{r}}$  appears in both  $A$  and  $B$ , and is also always negative and relatively large as will be shown in Fig. 8. A sample plot of  $N$  versus  $\dot{r}$  follows the same relationship as  $Y$  versus  $\dot{v}$  in Fig. 7.

Just as the magnitude of  $Y_{\dot{v}}$  is almost as large as  $\Delta$  for ship-like forms, the magnitude of  $N_{\dot{r}}$  is almost as large as  $I_z$ . Theoretical calculations for ellipsoids show that  $N_{\dot{r}} = -0.7 I_z$  for  $L/B = 5$ ;  $N_{\dot{r}} = -0.8 I_z$  for  $L/B = 8.5$ ; and  $N_{\dot{r}} = -1.0 I_z$  for  $L/B = \infty$ .

As was indicated in the analysis of the derivative  $Y_{\dot{v}}$ , both the bow and the stern add to contribute to a large negative  $Y_{\dot{v}}$ . However, in the case of  $N_{\dot{r}}$ , again the bow and stern oppose each other and  $N_{\dot{r}}$ , like  $Y_{\dot{r}}$ , is usually a relatively small quantity of uncertain sign provided the origin is taken close to the ship midlength.

The sign and magnitude of  $A$  may now be determined:

$$A = n'_z \Delta'_{y'} = (I'_z - N'_{\dot{r}}) (\Delta' - Y'_{\dot{v}}) > 0$$

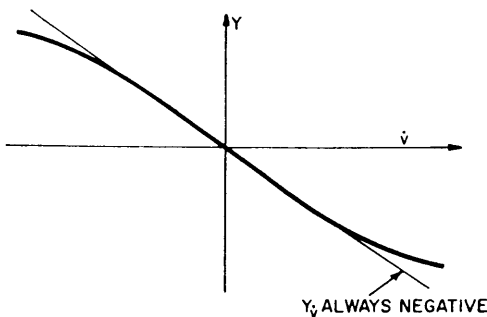
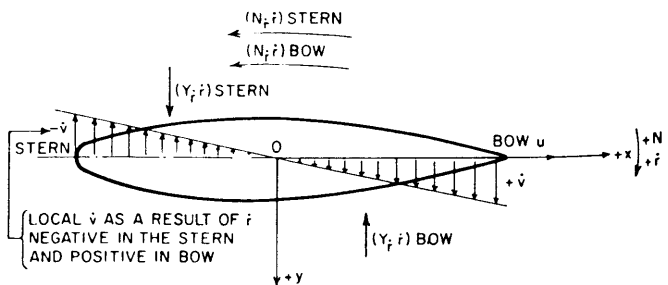
Fig. 7 Typical  $Y$  versus  $\dot{v}$  relationship

Fig. 8 Ship with an angular acceleration

To evaluate the relative magnitudes of  $B$  and  $C$ , it is necessary to examine the nature of the derivatives  $Y_v$ ,  $N_v$ ,  $Y_r$ , and  $N_r$ . In Fig. 9, the nature of the forces acting on a body with a velocity  $v$  added to a forward velocity  $u$  is shown. It is seen that as a result of the angle of attack,  $\beta \approx -v/V$  on the body, both the bow and the stern experience a lift force oppositely directed to  $v$ . Hence,  $Y_v$  is always negative. However, the bow contribution to the total  $Y_v$ -force is usually larger than that of the stern so that the center of action of the total force in the  $y$ -direction owing to  $v$  is considerably forward of the midlength of the ship. Hence, with the origin at the midlength,  $N_v$  is also usually a negative quantity for ships without fins or rudders. It is obvious that the addition of a rudder at the stern of a ship, for example, will increase the magnitude of  $(Y_v)_{\text{stern}}$  and hence decrease the negative magnitude of  $N_v$ . If the rudder were sufficiently large, it might even cause  $N_v$  to become positive; however, this is not usually the case. A typical plot of  $Y$  versus  $v$  and possible plots of  $N$  versus  $v$  with the origin at  $\mathcal{O}$  are shown in Fig. 10.

In analyzing the effect of an angular velocity  $r$  on  $Y$  and  $N$ , a location  $B$  forward and  $S$  aft are assumed as shown in Fig. 11. The origin is again taken at the midlength. When the ship is moving ahead with a velocity  $V$  and an angular velocity  $+r$  is added, point  $B$  at the bow has an angle of attack from starboard ( $\approx rd_1/V$  for small  $r$ ) producing a negative  $Y$ -force and a negative  $N$ -moment on the bow. Similarly, point  $S$  at the stern experiences an angle of attack from the port side producing a positive  $Y$ -force at the stern and a negative  $N$ -moment. Hence, the bow and the stern add to give a large negative  $N$  for a positive  $r$ , whereas bow and stern oppose each other to give either a small positive or negative  $Y$ -force for a positive  $r$ , negative if the bow dominates. For a negative  $r$ , the angles of attack change to opposite sides and hence the force and moment contributions change sign. Sample curves of  $Y$  versus  $r$  and  $N$  versus  $r$  for  $\mathcal{O}$  at  $\mathcal{O}$  are shown in Fig. 12.

Since  $B$  like  $A$  is always a large positive quantity for ships, independent of the choice of origin, the condition for stability reduces from  $B > 0$  and  $C > 0$  to only  $C > 0$ .

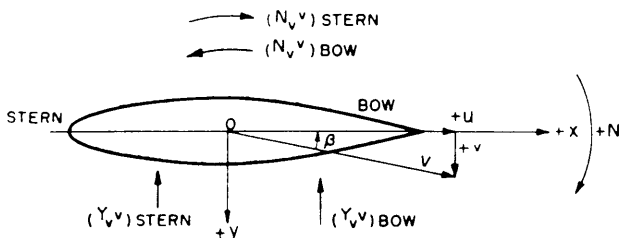


Fig. 9 Ship with a forward velocity,  $u$ , and a transverse velocity,  $v$

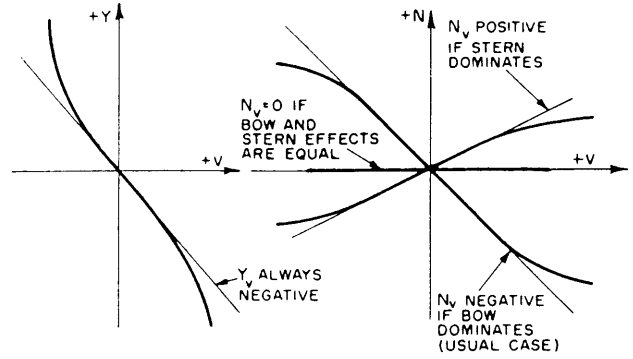


Fig. 10 Typical  $Y$  versus  $v$  and  $N$  versus  $v$  relationships

Hence,  $C$  is considered the discriminant of dynamic stability. From Equation (14),

$$C = Y'_v N'_r - N'_v (Y'_r - \Delta') \quad (14b)$$

and the condition for stability is simply:

$$Y'_v N'_r - N'_v (Y'_r - \Delta') > 0 \quad (14c)$$

or

$$Y'_v N'_r > N'_v (Y'_r - \Delta') \quad (14d)$$

with the inequality of Equation (14c) expressed as

$$\frac{N'_r}{Y'_r - \Delta'} - \frac{N'_v}{Y'_v} > 0 \quad (14e)$$

the solution can be viewed as a relationship between the lever arm of forces due to yawing and sway. The inequalities of Equation (14c) and (14d) provide the basic criterion for dynamic course stability, indicating whether or not the ship is stable but not giving a quantitative measure—as do the  $\sigma$ s of (13) and (14).

Methods for estimating stability ( $\sigma_1$ ) early in a design effort based only on major dimensions have been developed by Clark (1982) based on regression analyses and are mentioned in Section 16.3. Another closely related index  $T$  (approximately equal to  $1/\sigma_1$ ) of the  $K$  and  $T$  pair of indexes is introduced later in Section 5.4.  $T$  and  $K$  can be developed from common trials and are useful in comparing vessels.

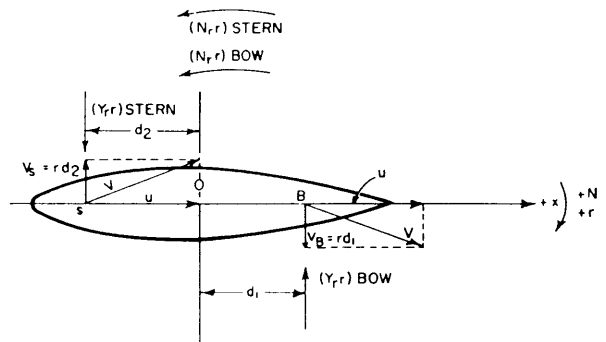


Fig. 11 Ship with a forward velocity,  $v$ , and an angular velocity,  $r$

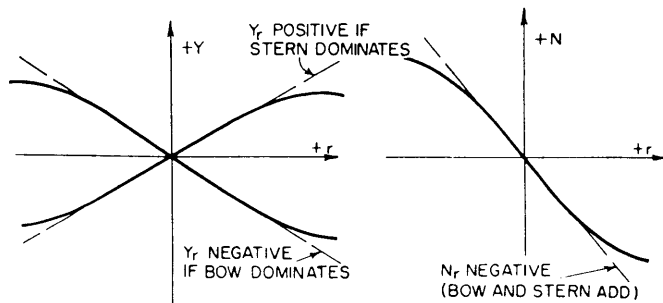


Fig. 12 Typical  $Y$  versus  $r$  and  $N$  versus  $r$  relationships

The  $\sigma$  stability indexes in the horizontal plane are not speed dependent in the range of low and moderate Froude numbers where the resistance coefficient,  $C_T$ , is essentially constant, since the nondimensionalized stability derivatives are sensibly constant in this speed range. Thus, if a ship possesses controls-fixed, straight-line stability in the horizontal plane at low speeds, it will also be stable in this sense at higher speeds, at least up to the limiting Froude number to which the nondimensional motion stability derivatives remain constant; or vice versa, if a ship is unstable at low speeds, it will also be unstable at higher speeds.<sup>2</sup>

**4.3 The Dieudonne' Spiral Maneuver.** The direct or Dieudonne' spiral maneuver is a definitive ship trial (Dieudonne', 1953) which identifies the directional stability characteristics of the vessel. The maneuver consists of the following:

(a) The ship is "steadied" on a straight course at a preselected speed and held on this course and speed for about 1 min. Once a steady speed is established, the power plant controls are not manipulated for the duration of the maneuver.

(b) After about 1 min, the rudder is turned to an angle,  $\delta_R$ , of about 15 deg and held until the rate of change of yaw angle maintains a constant value for about 1 min.

(c) The rudder angle is then decreased by a small amount (about 5 deg) and held fixed again until a new value of  $\psi$  is achieved and is constant for several minutes.

(d) The foregoing procedure is repeated for different rudder angles changed by small increments from, say, large starboard values to large port values and back again to large starboard values.

The numerical measures obtained from the preced-

ing spiral maneuver are the steady yawing rates as a function of rudder angle. A plot of these values is indicative of the stability characteristics of a ship. For example, if the plot is a single line going from starboard rudder to port and back again, as shown for ship A in Fig. 13, the ship possesses controls-fixed, straight-line stability; that is, it has a negative directional stability index. If, however, the plot consists of two branches joined together to form a "hysteresis" loop, as shown in ship B of Fig. 13, the ship is unstable; that is, it has a positive stability index. In addition, the height and width of the loop are numerical measures of the degree of instability; the larger the loop the more unstable the ship. The slope of the yaw-rate curve at zero rudder angle is a measure of the degree of stability or instability. It may be predicted using Equation (26) or measured from plotted ship trial data.

However, the linear theory used to develop (26) is unable to predict the characteristics of the hysteresis loop for unstable ships. For this purpose the nonlinear theory of Section 8 is essential. Nevertheless, it is clear that a ship with a hysteresis loop must have a positive control-fixed stability index. The existence of a loop means that with the rudder fixed at zero,  $\psi$  is not necessarily zero; that is, the ship may continue to turn with the rudder amidships. The mere possibility of this, with no external disturbances acting or having acted in the recent past, testifies to controls-fixed instability.

Abkowitz (1964) has pointed out the analogy between stability in straight-line motion and stability in heel. Fig. 14 is a plot of the conventional righting-moment curve versus the angle of heel,  $\phi$ , for both stable and unstable ships. The resemblance between Figs. 13 and 14 is apparent immediately. For ship A of Fig. 14, which is stable in heel, the slope of the righting-moment versus heel angle curve at  $\phi = 0$  is positive, indicating stability. Similarly, in Fig. 13, the positive slope (as drawn) of  $\psi$  versus  $\delta_R$  for ship A indicates that that ship is stable in straight-line motion. Likewise for the unstable ships B in Figs. 13 and 14. The slope at the origin of both curves is negative, indicating instability.

In the case of the stable ship A in Fig. 13 only one angular velocity (or turning rate) can result from any given rudder deflection. For the unstable ship B in Fig. 13, there are regions between the lines  $aa_1$  and  $bb_1$  where there is more than one turning angular velocity for a given rudder deflection. For the ship unstable in straight-line motion, there is a region where the ship can turn against its rudder.

During a spiral test, no data can be obtained for the unstable ship B on the dotted curve between (a) and (b) in Fig. 13, because these are points of unstable equilibrium for the particular rudder angles. For example, at zero rudder angle, the ship will tend to move to either positions (c) or (c<sub>1</sub>) depending on the previous time history of the motion because these are positions

<sup>2</sup> At first glance, this may seem contrary to operating experience where, in the presence of variable winds or currents the pathkeeping ability of a ship may improve with increasing ship speed. However, the presence of continuing disturbances is precluded in the present context by the definition of stability stated in the beginning of Section 3. Path keeping in the presence of such continuing disturbances is discussed in Section 11.3.

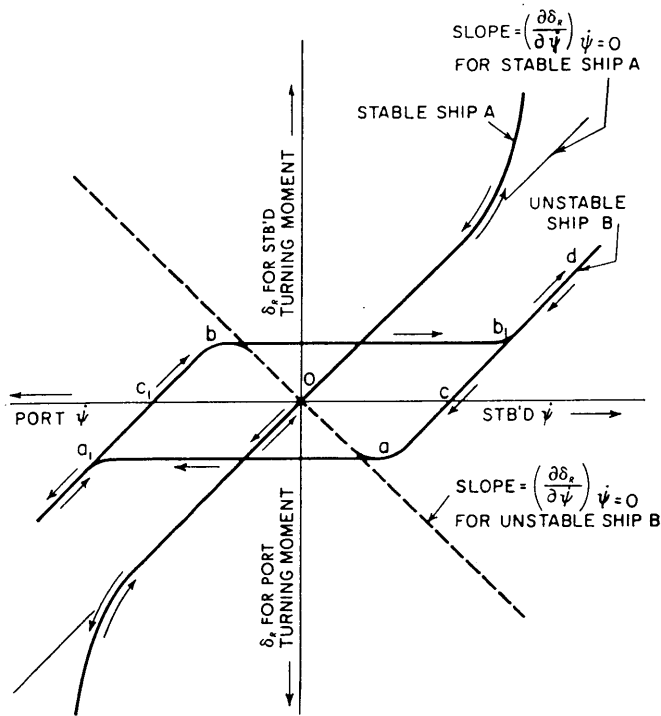


Fig. 13 Relation between angular velocity ( $\psi$ ) and rudder deflection angle ( $\delta_r$ ) for stable and unstable ships

of stable equilibrium for zero rudder deflection since the slopes, as drawn, of the  $\delta_r$  versus  $\psi$  curve at these points are positive.

For a spiral test conducted from starboard to port, the unstable ship B may start with an angular velocity denoted by point ( $d$ ) in Fig. 13. As the rudder angle is reduced, the angular velocity is reduced following curve B, until at zero rudder deflection an angular velocity indicated by point ( $c$ ) is obtained. Upon continuing the rudder deflection to port, the ship still continues to turn to starboard against the direction of the rudder deflection until point ( $a$ ) on curve B is reached. Any increase of the rudder angle to port beyond point ( $a$ ) will cause the ship to suddenly assume the large angular velocity to port indicated by point ( $a_1$ ), and perhaps temporarily even overshoot ( $a_1$ ). Similarly, when the spiral is repeated from port to starboard, an increase in the rudder angle beyond point ( $b$ ) in Fig. 13 will cause the ship to swing as fast as its inertia will let it to the angular velocity indicated by point ( $b_1$ ). Hence, an unstable ship can turn against its rudder up to a certain rudder angle and then suddenly swing in the opposite direction to a new stable position for that rudder-deflection angle.

This behavior of a ship unstable in straight-line motion is exactly analogous to the behavior of a ship which is transversely unstable. The transversely unstable ship cannot remain upright even in the absence

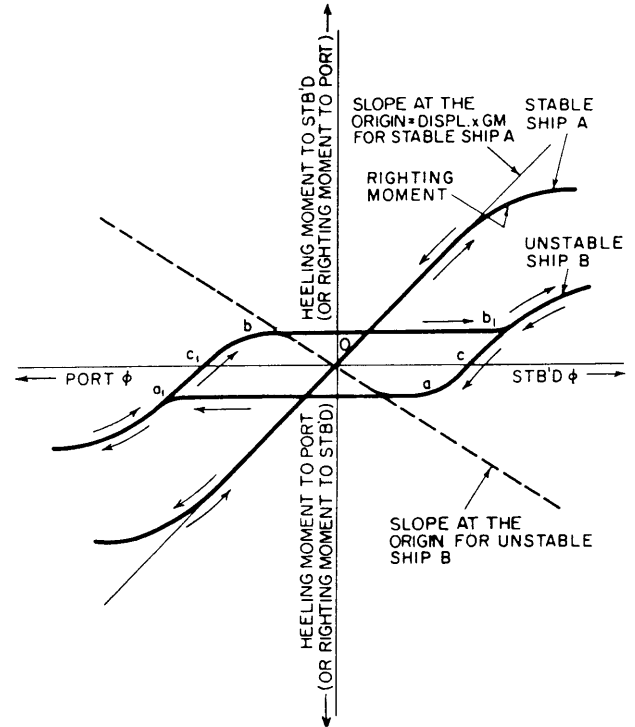


Fig. 14 Relation between heeling angle ( $\alpha$ ) and heeling (or righting) moment for stable and unstable ships

of a heeling moment. It will heel either to port or starboard to an angle of heel indicated by either ( $c$ ) or ( $c_1$ ) for ship B of Fig. 14. These are positions of equilibrium since the slope of curve B is positive at these points. If a port heeling moment is applied to the unstable ship B which is initially heeled to the starboard angle ( $c$ ) in Fig. 14, the angle of heel will be reduced, but will still remain to starboard until point ( $a$ ) is reached. Any further increase in the heeling moment to port will cause ship B of Fig. 14 to lurch from point ( $a$ ) to point ( $a_1$ ), which is a stable position of large heel to port. [The heel angle will overshoot ( $a_1$ ), but will finally settle down at ( $a_1$ ).] Hence, no points in the unstable region between ( $a$ ) and ( $b$ ) can be obtained for ship B during an inclining experiment. Thus, the behavior of an unstable ship in an inclining experiment would be completely analogous to that of a unstable ship in its spiral test.

It was noted in Section 4.2 that the controls-fixed stability indexes are not speed dependent at low and moderate speeds for motions in the horizontal plane. Based on this conclusion, the results of spiral maneuvers conducted at different speeds should not differ from one another significantly. It should also be noted that the results of the spiral maneuver shown in Fig. 13 are essentially symmetrical about zero rudder angle and zero yaw rate. These are typical of results obtained with ships that are both dynamically and geometrically

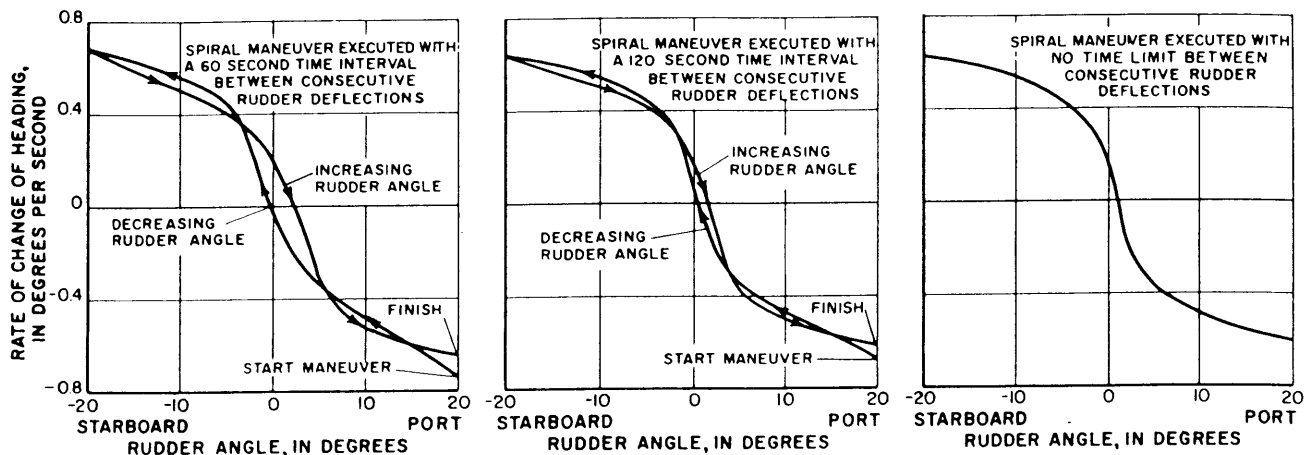


Fig. 15 Results of spiral maneuver (Strom-Tejsen, 1965)

symmetrical about the  $xz$ -plane. However, because of propeller rotation, ships with an odd number of propellers or with any number of unirotating propellers are not dynamically symmetrical about the  $xz$ -plane. Therefore, the results of spiral maneuvers conducted with such ships are likely to be displaced to one side or the other depending on the direction of rotation of the uncompensated propeller. For a stable ship, the rudder angle at  $\psi = 0$  is the rudder angle needed to maintain a straight course. This is the initial equilibrium rudder angle or  $\delta_1$  in the symbology of Section 3.3. It will also usually be associated with a nonzero value of  $v_1$ . The values of  $\delta_1$  and  $v_1$  are also called neutral angles. For an unstable ship, the rudder angle corresponding to the position of half the loop height shown in Fig. 13 is the approximate neutral angle.

It is essential in conducting a spiral maneuver to allow sufficient time for conditions to "steady" at each rudder angle otherwise spurious results are obtained. Fig. 15 (Strom-Tejsen, 1965) shows results of nonlinear predictions (based on systems of equations similar to those introduced in Section 8) which are three spiral tests conducted with three different time intervals between consecutive rudder deflections:

- 60 sec.
- 120 sec.
- no time limit.

In the first two cases the results show a sloped "hysteresis" loop giving the impression that the ship is unstable whereas in reality, the last case shows that the ship is quite stable.

As will be discussed in Sections 15 and 16, directional instability is not necessarily bad. Large, slow moving ships with directional instability can be handled in a quite satisfactory manner. The degree of instability relative to the type, size, and speed of the ship is important.

It is obvious that the spiral maneuver cannot be conducted with submarines in the vertical plane. Here

a very simple test, called the meander test, suffices. In this test the stern planes are deflected to a preselected value for a very short time and then returned to their neutral angle. If the subsequent path followed by the submarine in the vertical plane is a decaying oscillation as shown in Fig. 3, Case II, the submarine is directionally stable. If the path is an increasing oscillation, the submarine is directionally unstable. Because ships do not possess directional stability in the horizontal plane, the meander test is not used in that plane and recourse is made to the spiral maneuver.

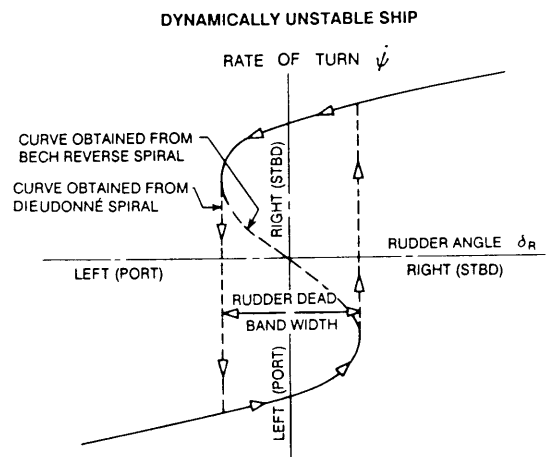


Fig. 16 Reverse spiral test

**4.4 The Bech Reverse Spiral and Pullout Maneuvers.** The Bech or reverse spiral maneuver (Bech, 1968) is an alternative test to the direct spiral maneuver. In the reverse spiral test the ship is steered at a constant rate of turn and the mean rudder angle required to produce this yaw rate is measured. This procedure is repeated for a range of yaw rates (from 0.5 deg per sec port to 0.5 deg per sec starboard, for



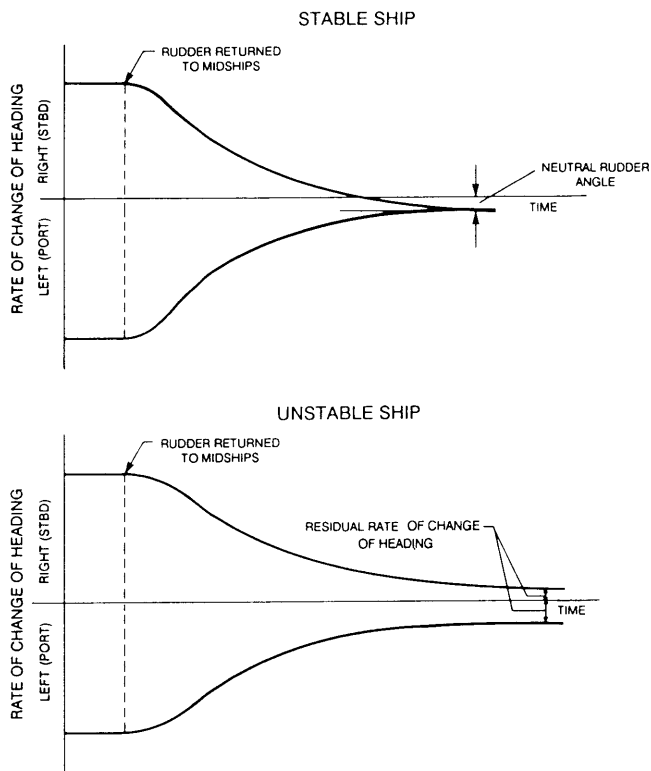


Fig. 17 Presentation of pullout tests results

instance) until a complete yaw rate versus rudder angle relationship is established. Results for a directionally stable vessel are similar to results from the direct spiral. For unstable vessels however, a hysteresis loop is identifiable although a definite relationship is indicated within the loop, Fig. 16. This is because the test condition is no longer controls-fixed. The results still provide the shape of the loop for evaluation of the degree of instability.

A properly calibrated rate-gyro and an accurate rudder angle indicator are required although in certain cases the test may be performed with the automatic steering devices available on board. If manual steering is used, the instantaneous rate of turn must be visually displayed for the helmsman, either on a recorder or on a rate-of-turn indicator. Using the reverse spiral test technique, points on the curve of yaw rate versus rudder angle may be taken in any order.

Although not commonly in use, the pullout tests, Fig. 17, provide a indication of a ship's stability on a straight course (Burcher, 1972). The ship is first made to turn with some rate of turn in either direction. The rudder is then returned to midships (neutral position). If the ship is stable, the rate of turn will decay to zero for turns to both port and starboard. If the ship is only moderately unstable, the rate of turn will reduce to some residual rate. The pullout tests should be performed to both port and starboard to show possible asymmetry. Normally, pullout tests can easily be performed in connection with other tests being run.

## Section 5

### Stability and Control

**5.1 General.** The controls-fixed stability indexes discussed in the preceding section constitute one of the important elements of path keeping at sea. Because the practical problem of path keeping involves repeated instances of path correction, its basic elements tend to merge with those of path changing. These basic elements are shown on the control loop of Fig. 1. Path keeping and path changing ability of a ship depends on:

(a) The magnitude and frequency of any yawing moments and sway forces acting to disturb the ship from the desired path.

(b) The character of the response of the ship with controls fixed to these disturbances. This response will be reflected in changes in the ship's path shown at the extreme right of Fig. 1.

(c) The rapidity with which the error between the ship's path and the desired path can be detected, and with which corrective action can be initiated.

(d) The rate at which the corrective action is translated into movement of the rudder. This is a function

of the play between the third and fourth elements of the control loop and the rate at which the steering gear can deflect the rudder in the fourth box of Fig. 1.

(e) The magnitude of the control force and moment applied to the ship by the rudder.

Of these five elements, only the second is dependent on the controls-fixed stability of the ship. This is an important element, but so are all the others. Usually, deficiencies in any single element of the control loop can be compensated for by improvements in other elements. For example, it is shown in Section 11.2 that the use of properly designed automatic controls in element (c) can correct for controls-fixed instability in element (b). Often it is assumed that increases in rudder size, element (e), or in the rate of rudder deflection, element (d), can correct for deficiencies in the path keeping or path-changing ability of a ship. The latter view is shown in Section 17 to be incorrect. Although minor degrees of controls-fixed instability are commonplace in ships, the best design is likely to be that

which possesses minimum deficiencies in each element of the control loop.

**5.2 Definitive Maneuvers.** The naval architect is mainly concerned with elements (b), (d), and (e) of the path-keeping and path-changing problems. Therefore, certain definitive maneuvers have been devised to demonstrate the efficacy of these elements of the control loop and to exclude as much as possible the influence of element (c). Essentially, these maneuvers establish the basic stability and control characteristics of a ship independent of its helmsman or autopilot:

- (a) Direct or reversed spiral (see Section 4.3)
- (b) Zigzag, Z, or *Kempf overshoot* (see Section 5.3)
- (c) Turning (see Section 6.1)

The spiral maneuver as described earlier serves mainly to determine stability characteristics, whereas the zigzag maneuver is to determine control characteristics. The turning maneuver denotes turning qualities. All three maneuvers are important for both merchant and naval ships. Specific performance criteria and other related trials are discussed in Section 14.

**5.3 ZigZag Maneuver.** Second to the spiral maneuver in importance is the zigzag maneuver, also known as the *Kempf overshoot* or "Z" maneuver (Kempf, 1944).

The results of this maneuver are indicative of the ability of a ship's rudder to control the ship. However, just as the results of the spiral maneuver give some indication of control effectiveness (yaw-angle rate versus rudder angle), so do the results of the zigzag test depend somewhat on the stability characteristics of the ship as well as on the effectiveness of the rudder. The typical procedure for conducting the test is as follows (Gertler, 1959):

(a) Steady the ship as in step (a) of the spiral maneuver. (See Section 4.3).

(b) Deflect the rudder at maximum rate to a preselected angle, say 20 deg, and hold until a preselected change of heading angle, say 20 deg, is reached.

(c) At this point, deflect the rudder at maximum rate to an opposite (checking) angle of 20 deg and hold until the execute change of heading angle on the opposite side is reached. This completes the overshoot test.

(d) If a zigzag test is to be completed, again deflect the rudder at maximum rate to the same angle in the first direction. This cycle can be repeated through the third, fourth, or more executes although characteristics through the first overshoot are most important as discussed in Section 15.

Fig. 18 shows the results of a zigzag maneuver carried through five executes. The results shown are those that can be readily obtained with a controlled model in a towing tank or with a well-instrumented ship at sea. With ordinary ship navigational aids, only the rudder angle and yaw-angle curves are readily obtainable.

The principal numerical measures of control obtained from the overshoot maneuver as illustrated in

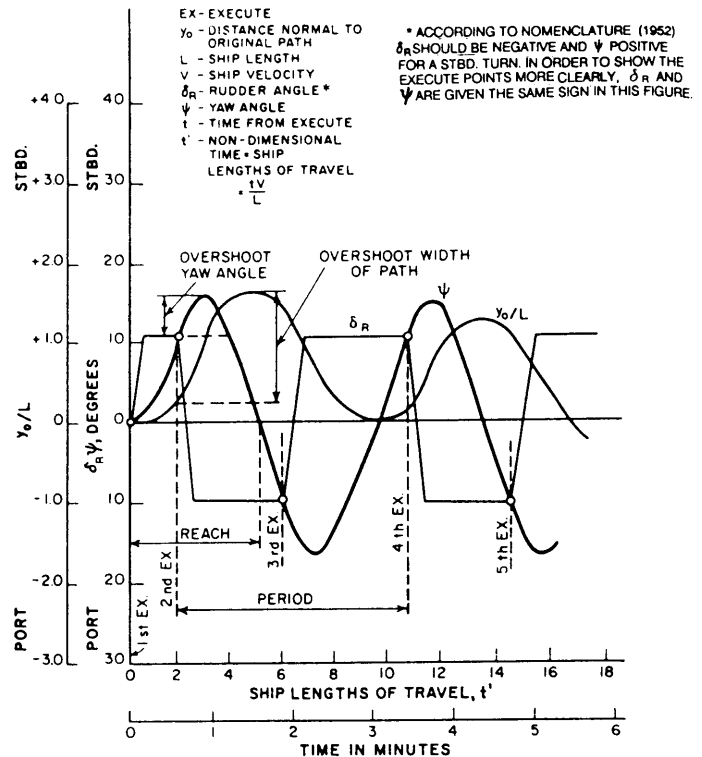


Fig. 18 Results of an overshoot and zigzag maneuver (Morse and Price, 1961)

Fig. 18 are: (a) The time to reach the second execute yaw angle; (b) the overshoot yaw angle; and (c) the overshoot width of path. All of these are important operational parameters. The first is a direct measure of the ability of a ship to rapidly change course. It improves with increased rudder effectiveness and with decreased controls-fixed stability (Arentzen and Mandel, 1960). The second and third are numerical measures of countermanning ability and are indicative of the amount of anticipation required of a helmsman while operating in restricted waters. It was shown that the magnitude of the yaw-angle overshoot decreases with increased stability but increases with increased rudder effectiveness. On the other hand, the overshoot width of path decreases with both increased stability and increased rudder effectiveness.

The results of the zigzag maneuver are speed dependent. In general, for any given ship the time to reach execute decreases with increasing speed, and the overshoot yaw angle and the overshoot width of path increase with increasing speed. However, the non-dimensional time to reach execute, interpreted in Fig. 18, as ship lengths of travel to execute, increases with increasing speed because of the influence of the rate of rudder deflection,  $\delta'_R$ . When  $\delta'_R$  is nondimensionalized,  $\delta'_R = \delta_R L/V$ , it may be interpreted as degrees of rudder deflection per ship length of travel. At low speeds, this nondimensional rate is much higher than at higher speeds since  $\delta_R$  is essentially indepen-

dent of speed. Hence, with respect to the ship length of travel scale in Fig. 18, the rudder would be deflected more rapidly at low speeds than at high. Hence, the rudder exerts its full influence longer at low speeds, which tends to reduce the nondimensional time to reach execute as speed is reduced. However, in spite of this beneficial effect as speed is decreased, the time to reach execute usually increases with decreasing speed. (The effects of the rudder are reviewed further in Section 17).

In the case of submarines, the overshoot maneuver is employed in both the horizontal and vertical plane and its results are perhaps even more operationally significant in the vertical plane than in the horizontal. This is true because in the vertical plane submarines must operate within a relatively shallow layer of water, while they usually have ample freedom of motion in the horizontal plane except when they are in restricted or congested waterways. Hence, to the submarine operator, overshoot pitch angle and overshoot change of depth are very important parameters.

**5.4 The K and T Coursekeeping and Turning Indexes.** This section presents the Nomoto simplified analysis of  $K$  and  $T$  indexes which can be developed from zigzag trial data. These indexes are widely used, simplified analysis tools developed from the linear equations of motion. They are useful in comparing coursekeeping as well as turning abilities, which will be presented further in Section 6.

While Equations (11) and (12) expressed the linear equation as a pair of simultaneous first order differential equations, where the constant coefficients are the dimensionless acceleration and velocity derivatives, it is possible to express these equations in an alternative form. It was first shown by Nomoto (1957) that these equations can be written as a pair of decoupled second order equations as follows:

$$\begin{aligned} T_1' T_2' \ddot{r}' + (T_1' + T_2') \dot{r}' + r' &= K' \delta_R \\ &+ K' T_3' \dot{\delta}_R' \\ T_1' T_2' \ddot{v}' + (T_1' + T_2') \dot{v}' + v' &= K_v' \delta_R \\ &+ K_v' T_4' \dot{\delta}_R' \end{aligned} \quad (15)$$

This expression for the coefficients in terms of the time constants  $T_1'$ ,  $T_2'$ ,  $T_3'$  and  $T_4'$  as well as a system gain  $K'$  is consistent with control engineering practice.

Since Equations (15) are a linear system as are (11), a solution similar to (13) may be derived and it may be seen that the roots of the solutions are related to the time constants as follows:

$$\sigma_1 = -\frac{1}{T_1'}, \quad \text{and} \quad \sigma_2 = -\frac{1}{T_2'}$$

Returning to the linear yaw and sway (11) and (12), it can be seen that they are coupled only through the terms  $N_v' v'$  and  $Y_r' r'$ , which are typically small, particularly for ships with near fore-and-aft symmetry. If these cross-coupling terms are neglected and sway

velocity or side slip angle thus eliminated, turning depends only upon yaw rate,  $r$ , and is defined by the simplified non-dimensional yaw equation of motion:

$$n_z' \dot{r}' - N_r' r' = N_{\delta_R}' \delta_R \quad (16)$$

Nomoto (1957, 1960, and 1966) noted that this equation could be divided by the yaw damping coefficient,  $N_r'$ , and rewritten in the parametric form:

$$T' \dot{r}' + r' = K' \delta_R \quad (17)$$

where the non-dimensional parameters or indexes  $T'$  and  $K'$  are given by:

$$\begin{aligned} T' &= n_z' / N_r' = (I_z' - N_r') / N_r' \\ &= T_1' + T_2' - T_3' \\ K' &= N_{\delta_R}' / N_r' \end{aligned} \quad (18)$$

In dimensional form the equation is  $T\dot{r} + r = K\delta_R$ , where the non-dimensional parameters are related to the dimensional Nomoto parameters  $T$  and  $K$  by:

$$\begin{aligned} T' &= T(V/L) \\ K' &= K(L/V) \end{aligned}$$

The indices  $T'$  and  $K'$  represent ratios of non-dimensional coefficients from (18):

$$\begin{aligned} T' &= \frac{\text{yaw inertia coefficient}}{\text{yaw damping coefficient}} \\ K' &= \frac{\text{turning moment coefficient}}{\text{yaw damping coefficient}} \end{aligned}$$

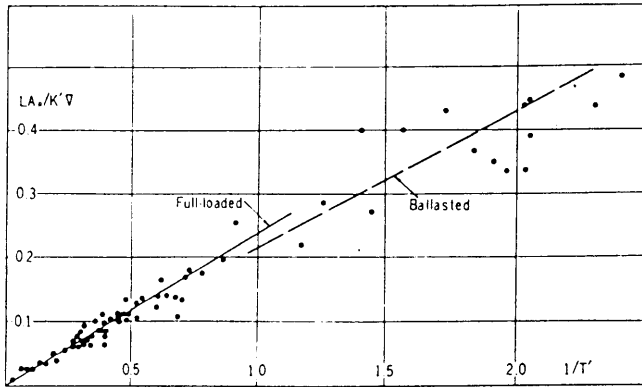
Dividing  $K'$  by  $T'$  shows that the two indexes are related by:

$$\frac{K'}{T'} = \frac{\text{turning moment coefficient}}{\text{yaw damping coefficient}}$$

In practice, Equation (15) can be solved by numerical integration. For the simple case where the rudder is put over suddenly to an angle  $\delta_0$  and held there, the solution for  $r$  is given, in terms of  $T$  and  $K$ , by:

$$r = K \delta_0 (1 - e^{-t/T}) \quad (19)$$

This shows that the yaw rate  $r$  increases exponentially with time but at a declining rate dependent on  $T$  and approaches a steady value  $K\delta_0$  (or  $K'V\delta_0/L$ ). A larger  $K$  thus provides greater steady-state turning ability, and a smaller value of  $T$  provides a quicker initial response to the helm. Quick response implies good course-changing ability and good course-checking ability when a turn (or other maneuver) is completed. Since quick response is obviously valuable in course-keeping (steering), it is thus consistent with a smaller  $T$ . The above discussion of Equation (19) shows that  $T$  has no effect at all on steady turning rate, but a small  $T$  would reduce the time required to reach a steady turn. At the same time, the index  $T$  is a reciprocal measure of

Fig. 19  $K' - T'$  Diagram (Nomoto 1966)

course stability, with stability increasing with decreasing  $T$ . However, a negative value indicates an unstable dynamic character. The steering quality indexes  $K$  and  $T$  have an immediate relationship to the conventional measures of ship turning. It may be shown that, under the previously stated simplifying assumption that sway can be neglected:

$$\sigma_1 = -\frac{1}{T'}$$

where  $\sigma_1$  is the stability index of Section 4. Thus,  $T'$  offers a direct quantitative measure of straight-line stability.

For steady turning at constant rudder angle  $\delta_{R_0}$ ,

$$r = K\delta_{R_0} = K' V \delta_{R_0} / L \quad (20)$$

Steady turning diameter,  $D_0$ , by definition is:

$$D_0 = \frac{2V}{r} \quad (21)$$

and hence non-dimensional turning diameter,  $D_0/L$ , and  $K'$  are related by:

$$D_0/L = 2V/rL = 2/K'\delta_{R_0} \quad (22)$$

This relation can be derived from (16) in Section 5 by neglecting sway (placing  $N'_v = 0$ ). This is in accord with the statement in Section 5.3 that  $R/L$  depends on the relative magnitudes of  $N'_r$  and  $N'_{\delta_R}$ . It shows that with a larger value of  $K'$  a smaller rudder angle may be used in achieving a given turning diameter.

The main maneuvering qualities of a ship using linear analysis can thus be characterized using only the indexes  $T'$  and  $K'$ , where increasing values indicate improving performance:

$T'$	Course stability
$1/T'$	Responsiveness to rudder
$K'$	Turning ability

A highly maneuverable ship (with high responsiveness to rudder and both good turning and low course

stability) will have a small value of  $T'$  and a large value of  $K'$ . In other words, a large ratio  $K'/T'$ , or *Norrbin parameter*,  $P = K'/2T'$ , (Nomoto and Norrbín, 1969) is indicative of good maneuverability. It is not a good indicator of course-keeping ability (or good steering) however, because this can be achieved either by high course stability and low responsiveness (high  $T'$ ) or by low or even negative stability and high responsiveness (high  $1/T'$ ) plus superior automatic control. In short, a large ratio  $K'/T'$  suggests good overall controllability only if stability is no greater than necessary.

Overshoot angle, which is obtained from the zigzag maneuver (Section 4) has often been used as a measure of controllability. Nomoto (1966) has shown that overshoot angle is, for a given rudder angle, nearly proportional to the product  $K'T'$ . Overshoot angle thus has the inherent weakness that it cannot be used to discriminate between a ship with: (a) good turning and fast response or good course stability (large  $K'$  and small  $T'$ ) and (b) poor turning and slow response or course stability (small  $K'$  and large  $T'$ ). The former with large  $K'/T'$ , is clearly a far superior ship in overall controllability. But overshoot angle does indicate turn-checking ability.

For further guidance Nomoto has suggested that:

Turning moment coefficient  $\propto A_R/LT$  and

Yaw inertia coefficient  $\propto \nabla/L^2T$

where  $A_R$  is rudder area, and  $\nabla$  is displaced volume. Using these approximations:

$$\frac{K'}{T'} \propto \frac{A_R L}{\nabla} = c_1 \frac{A_R L}{\nabla} \quad (23)$$

where  $c_1$  is a constant of proportionality. Fig. 19 summarizes results for various ships and rudder angles, and indicates by the straight lines that  $c_1$  tends to be independent of ship type and rudder angle. It is clear from (23) that, since large  $K'/T'$  is favorable, a large value of  $A_R L/\nabla$  is desirable. This simplified linear analysis indicates that ship dimensions (particularly  $L$  and  $\nabla$ ), as well as rudder area, will have a significant effect. Once overall ship dimensions are established, both aspects of controllability can be significantly improved by increasing rudder size or effectiveness.

The indexes  $T'$  and  $K'$  can be calculated numerically using Equation (15) if hydrodynamic and mass coefficients for the ship are known. One advantage of these indexes is that they can be derived from the results of the standard trials or free-running model maneuvers for comparison with calculation. They give physical meaning to the standard trials.

The application of  $T'$  and  $K'$  to determining criteria of controllability is discussed in Section 14.7. The elements of turning performance as separated from coursekeeping and control are introduced and addressed more fully in Section 6.

## Section 6

### Analysis of Turning Ability

**6.1 Characteristics of the Turning Path.** All ship maneuvering, except some stopping maneuvers, involves turning. The response of the ship to deflection of the rudder, and the resulting forces and moments produced by the rudder, can be divided into two portions:

- (a) An initial transient one in which significant surge, sway, and yaw accelerations occur.
- (b) A steady turning portion in which rate of turn and forward speed are constant and the path of the ship is circular (in the absence of significant external forces).

Fig. 20 is a definition diagram for turns of any diameter. Generally, the turning path of a ship is characterized by four numerical measures; advance, transfer, tactical diameter, and steady turning diameter. As shown in Fig. 20, all but the last are related to heading positions of the ship rather than to tangents to the turning path. The advance is the distance from the origin at "execute" to the  $x$ -axis of the ship when that axis has turned 90 deg. The transfer is the distance from the original approach course to the origin of the ship when the  $x$ -axis has turned 90 deg. The tactical diameter is the distance from the approach course to the  $x$ -axis of the ship when that axis has turned 180 deg. These parameters of a ship's turning path are useful for characterizing maneuvers in the open sea. Section 15 discusses the use of the turning circle further as a definitive and practical test for assessing maneuverability.

Fig. 20 also shows the position of the so-called *pivot point* in a steady turn. This point is of interest, because to an observer aboard a turning ship it appears as if the ship were pivoting about a point usually somewhat abaft the bow. At this point, because of the combination of the drift angle on the ship and the rotation of the ship, the flow of water past the ship is parallel to the  $x$ -axis of the ship. Forward of this point, for a starboard turn the flow approaches from off the starboard side of the ship as shown in Fig. 20, and aft of this point the flow approaches from the port side. Thus, a fixed vertical fin in the plane of symmetry of the ship would experience no angle of attack at this location (see also Section 16.3). According to Fig. 20, the distance between the pivot point and the center of gravity of the ship  $x_c = R \sin \beta$ . Because small radius turns are usually associated with large drift angles, and large radius turns with small drift angles, the product  $R \sin \beta$  does not vary significantly for different ships or for the same ship at different turning radii. For most ships the pivot point is somewhere between the bow and about  $1/5 L$  aft of the bow (Mandel, 1953). Based on empirical data, the drift angle,  $\beta$ , in degrees, generally falls within the following range of values:  $\beta = 22.5 L/R + 1.45$  and  $\beta = 18 L/R$ . The former

relationship yields values of  $x_c$  from 0.4 to 0.5  $L$  depending on the  $L/R$  ratio. The latter relationship yields values of  $x_c = 0.3L$ .

During the first phase of the turn, before it becomes steady, there is also an apparent "pivoting" point. This point near the bow of the ship initially follows a path which is a straight-line extension of the approach path, while the stern deviates outward of the approach path and the bow deviates inward of it.

The turning circle maneuver has traditionally received the most attention in treatises on ship maneuverability. One reason for this is that it has been and still is an important practical maneuver that ships frequently perform. Also, because the final phase of the turning path is a steady-state maneuver, it has lent itself more readily to analytical treatment than have transient maneuvers.

**6.2 The Three Phases of a Turn.** Suppose that a ship is advancing on a straight path when its rudder is deflected and held at a fixed angle as in Fig. 20. The resulting path of the ship may be divided into three distinct phases.

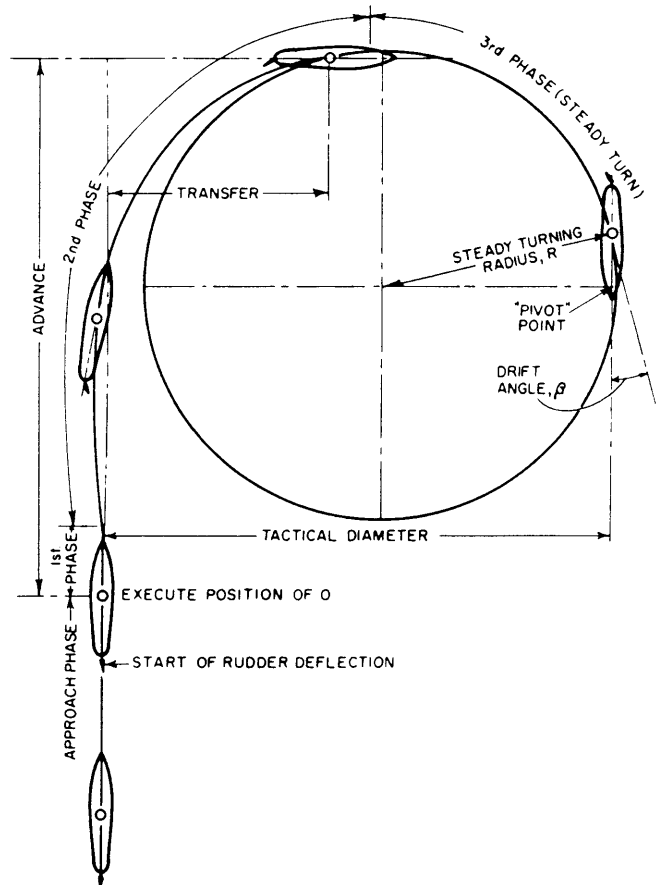


Fig. 20 Turning path of a ship

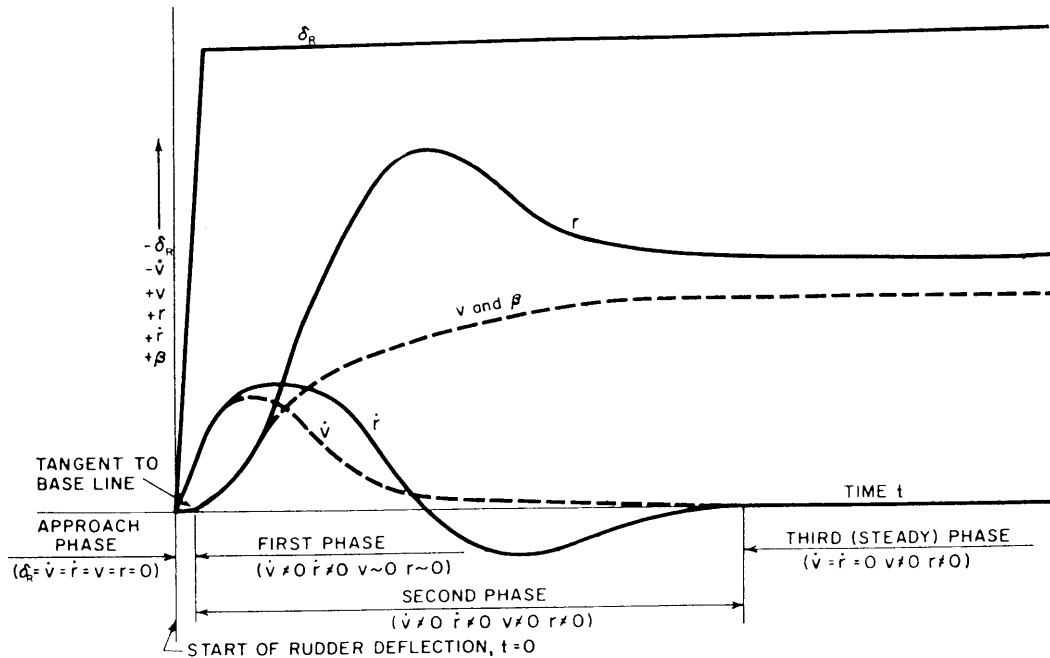


Fig. 21 Characteristics of transient phases of a turn

The first phase starts at the instant that the rudder begins to deflect and may be complete by the time the rudder reaches its full deflection angle. During this period, the rudder force,  $Y_\delta \delta_R$ , and rudder moment,  $N_\delta \delta_R$ , produce accelerations and are opposed solely by the inertial reaction of the ship because there has not yet been an opportunity for development of hydrodynamic forces arising from a substantial drift angle,  $\beta$ , or a rotation,  $r$ , to develop. Hence, in this stage,  $\beta = v/V = r = 0$ . Using the dimensional Equation (10) and introducing the rudder force and moment, the linearized equations of motion in the first phase of turning are:

$$(\Delta - Y_{\dot{v}})\dot{v} - Y_{\dot{r}}\dot{r} = Y_\delta \delta_R \quad (24)$$

$$(I_z - N_{\dot{r}})\dot{r} - N_{\dot{v}}\dot{v} = N_\delta \delta_R$$

The values of the accelerations,  $\dot{v}$  and  $\dot{r}$  that occur in this phase can be obtained from these equations. It may be noted in Figs. 20 and 21 that the transverse acceleration,  $\dot{v}$ , is negative or directed to port in this phase, whereas the turn will eventually be to starboard. This is because (for a rudder at the stern) the rudder force  $Y_\delta \delta_R$  is directed to port for a starboard turn.

The accelerations  $\dot{v}$  and  $\dot{r}$  can exist in isolation only momentarily, for they quickly give rise to a drift angle,  $\beta$ , and a rotation,  $r$ , of the ship. With the introduction of these parameters, the ship enters the second phase of turning. Here the accelerations of the ship coexist with the velocities and all of the terms of Equation

(10) along with the excitation terms  $Y_\delta \delta_R$  and  $N_\delta \delta_R$  are fully operative (12). The crucial event that takes place at the beginning of the second phase of the turn is the creation of a  $Y_v v$ -force positively directed to starboard in Fig. 20 towards the center of the turn, resulting from the introduction of the drift angle,  $\beta$ . The magnitude of this force soon becomes larger than the  $Y_\delta \delta_R$ -force which is directed to port (Fig. 5). As shown in Fig. 21 this causes the acceleration  $\dot{v}$  to cease to grow to port and eventually to be reduced to zero as the inwardly directed  $Y_v v$ -force comes into balance with the outwardly directed centrifugal force of the ship. However, in the second phase of the turn, the path of the center of gravity of the ship at first responds to the  $Y_\delta \delta_R$ -force and tends to port before the  $Y_v v$ -force grows large enough to enforce the starboard turn. This port offset although visibly portrayed in Fig. 20 is negligible or nonexistent in practice because of the shortness of phase 1, and the quick development of the large  $N_v v$ -moment in ship forms.

**6.3 Steady Turning Radius.** Finally, after some oscillation (some of which is due to the settling down of the main propulsion machinery and is characteristic of the particular type of machinery and its control system) the second phase of turning ends with the establishment of the final equilibrium of forces. When this equilibrium is reached, the ship settles down to a turn of constant radius as shown in Fig. 20. This is the third, or steady, phase of the turn. Here  $v$  and  $r$  have nonzero values, but  $\dot{v}$  and  $\dot{r}$  are zero. Thus, using Equations (10) the linearized equations of motion in a steady turn are:

$$\begin{aligned} -Y_v v - (Y_r - \Delta' u_1) r &= Y_\delta \delta_R \\ -N_v v - N_r r &= N_\delta \delta_R \end{aligned} \quad (25)$$

These two simultaneous equations can be solved for  $r$  and  $v$  provided that the stability derivatives  $Y_v$ ,  $Y_r$ ,  $N_v$ ,  $N_r$  and the control derivatives  $Y_\delta$  and  $N_\delta$  are known. Noting that  $r' \equiv \dot{\psi} = rL/V$  and that the steady turning radius  $R = V/r$ , then  $r' = L/R$  or the reciprocal of the ratio of the steady turning radius to the ship length. Solving the nondimensional version of (25) we obtain:

$$R = \frac{-L}{\delta_R} \left[ \frac{Y'_v(N'_r) - N'_v(Y'_r - \Delta')}{Y'_v N'_\delta - N'_v Y'_\delta} \right] \quad (26)$$

and

$$v' = -\beta = \delta_R \left[ \frac{N'_\delta(Y'_r - \Delta') - Y'_\delta N'_r}{Y'_v N'_r - N'_v(Y'_r - \Delta')} \right] \quad (27)$$

where  $\beta$  and  $\delta$  are in radians and positive  $R$  denotes a starboard turn.

Thus, according to the preceding linear theory, the steady turning radius would be proportional to the ship length,  $L$ , and inversely proportional to the rudder-deflection angle,  $\delta_R$ , and the drift angle  $\beta$  would be directly proportional to  $\delta_R$ .

Solutions (26) and (27) are useful for estimating the steady turning radii and drift angles of stable ships with fairly large diameter turns of about four ship lengths or more. They are used to estimate the turning radii of torpedoes, and are useful for estimating the turning radii of ships at less than maximum rudder angles.

The great majority of merchant ships have turning diameters of from two to four ship lengths at full rudder angle, and many ships have turning diameters of two ship lengths or less. Such tight turns introduce strong nonlinearities that tend to reduce the validity of the linear equations of motion. Procedures for predicting the maneuvers of tight-turning ships are discussed in Section 8.

**6.4 Relationship Between Steady Turning Radius and the Hydrodynamic Derivatives.** Equation (26) developed from linear theory may be used for stable ships to predict the effect of changes in the hydrodynamic derivatives on the turning radius. In slightly modified form, Equation (26) is:

$$\frac{R}{L} = -\frac{1}{\delta_R} \left[ \frac{Y'_v N'_r - N'_v(Y'_r - \Delta')}{Y'_v N'_\delta - N'_v Y'_\delta} \right] \quad (26a)$$

It is seen that the numerator is identically the stability criterion,  $C$ , Equation (14b) of Section 4.2; it was shown in Section 4.2 that the value of the numerator is independent of the choice of origin. If the relationships

$$N'_\delta = (N'_\delta)_{\infty} + (Y'_\delta)x'_{\infty}$$

and

$$N'_v = (N'_v)_{\infty} + Y'_v x'_{\infty}$$

are substituted in the denominator, it reduces to  $Y'_v(N'_\delta)_{\infty} - Y'_\delta(N'_v)_{\infty}$  which is also independent of the choice of origin, thus if the ship is stable the numerator is positive and if the ship is unstable the numerator is negative. The sign of the denominator is always positive for the following reasons:

(a)  $Y'_v$  is always negative and  $N'_\delta$  is always negative for rudders located at the stern (Fig. 22). In the figure  $\delta_R$  is negative following the definition of these  $\delta$ 's given in Section 3.5 and following the sign convention given in the nomenclature at the end of this chapter. The moment  $N$  resulting from negative  $\delta$ , however, is positive according to the same sign convention. Similarly, if  $\delta$  were positive,  $N$  would be negative. Hence, the derivative  $N'_\delta$  is always negative for rudders at the stern. In Fig. 22, the force,  $Y$ , arising from the negative  $\delta$  is also negative, if  $\delta$  were positive,  $Y$  would be positive; hence, the derivative,  $Y'_\delta$ , is always positive hence, their product is positive.

(b)  $Y'_\delta$  is always positive,  $N'_v$  is almost always negative; hence, subtracting their product will add positively to  $Y'_v N'_\delta$ .

(c) If  $N'_v$  is positive (it is rarely so), its magnitude

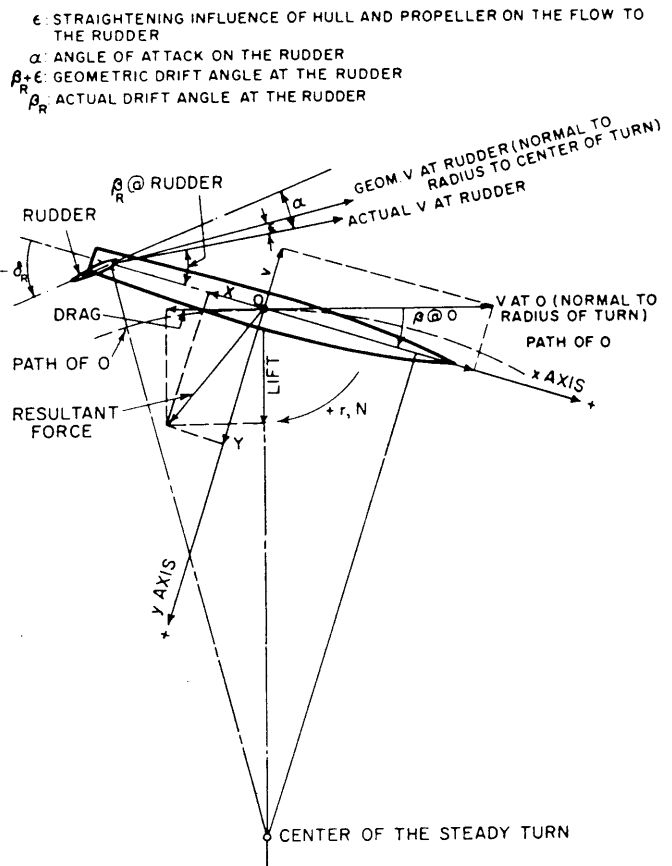
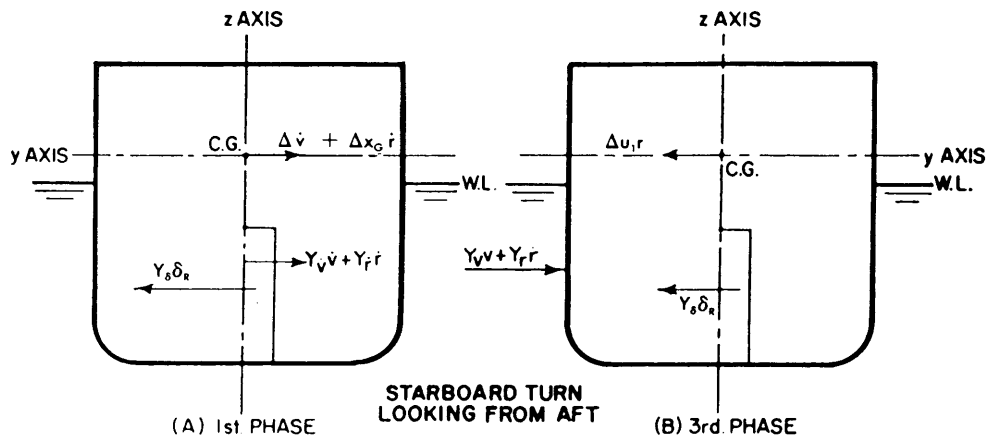


Fig. 22 Orientation of ship and rudder in a steady turn to starboard

Fig. 23 Disposition of forces in  $yz$  plane in a turn

is bound to be small so that the larger positive  $Y'_v N'_s$  product will determine the sign of the denominator.<sup>3</sup>

It may therefore be concluded that if a ship is stable and its rudder is located at the stern, a positive (starboard)  $R$  will always result from a negative  $\delta$  and vice versa. However, if the ship is unstable, then the numerator of the right-hand side of Equation (26) is negative and  $R$  will have the same sign as  $\delta$ . Physically this means that a ship will turn against its rudder, which is in accord with the behavior of an unstable ship. Since Equation (26) deals only with the slope of the  $R$  versus  $\delta$  curve at  $\delta = 0$ , which is a region of unstable equilibrium for unstable ships, it cannot be used to predict the turning radii of unstable ships.

For stable ships, Equation (26) may be used to examine the effect of changes in the individual derivatives on the turning radius. Equation (26) shows that the effect of changes in  $Y'_v$  on  $R$  depends on the relative magnitude of  $(N'_v)$  compared to  $N'_s$ . If  $N'_s$  has a greater magnitude than  $(N'_v)$  then increasing the magnitude of  $Y'_v$  would decrease the radius of turn. On the other hand, if the magnitude of  $(N'_v)$  is larger than  $N'_s$ , then an increase in the magnitude of  $Y'_v$  will usually increase the radius of the turn. Since for stable ships,  $(N'_v)$  is usually much more negative than  $N'_s$ , the usual effect of increasing the magnitude of  $Y'_v$  is to increase the radius of the turn. Thus, while the  $Y_v v$ -force is responsible for the initiation of a turn in the desired direction, an increase in the magnitude of  $Y_v$  does not necessarily reduce the steady turning radius.

The effect of  $N'_v$  on  $R$  is readily predictable. If  $N'_v$  is negative, increasing its magnitude will decrease the positive value of the numerator of the right-hand side of (26) and increase the positive value of the denomi-

nator, hence  $R$  will decrease on two counts. On the other hand, if  $N'_v$  were positive, increasing its magnitude would increase the numerator and decrease the denominator, and hence  $R$  would be increased.

The effect of  $N'_r$  and  $N'_s$  on  $R'$  is equally clear. According to Equation (18), an increase in the magnitude of  $N'_r$  will increase  $R$  while an increase in the magnitude of  $N'_s$  will decrease  $R$ . This result is in accord with an intuitive examination of the question.

The effects of the remaining derivatives on  $R$  depend on the sign of  $N'_v$ , and can be deduced from Equation (26) when the sign of the derivative is known (see Table 1).

**6.5 Heel Angle in a Turn.** While use of the rudder is intended to produce motions only in the yaw ( $xy$ ) plane, motions are also induced by cross coupling into the pitch ( $xz$ ) and roll ( $yz$ ) planes. The unwanted mo-

Table 1—Effect of Changes in the Derivatives on Steady Turning Radius (for Stable Ships with Rudder(s) at the Stern)

Derivative	Sign of the derivatives for ships
$Y'_v$	always negative
$N'_r$	always negative
$N'_s$	always negative
$N'_v$	either positive or negative
$Y'_r$	either positive or negative
$Y'_\delta$	always positive
$\Delta'$	always positive

NOTES:

1.  $\Delta'$  is not a derivative but is included here for convenience.

2. Signs in italics refer to the signs of the derivatives for usual ship forms.

3. For typical values of the foregoing derivatives for a wide range of merchant ship forms (nondimensionalized on the basis of  $\rho$ ,  $L$ ,  $T$  and  $V$ ), see Table 6.

<sup>3</sup> For rudders located at the bow,  $N'_s$  will always be positive and  $R$  will always have the same sign as  $\delta_r$  for stable ships. The sign of  $Y'_s$  is always positive whether the rudder(s) are located at the bow or at the stern.



tions in the roll plane, particularly, are likely to be large enough to be of significance.<sup>4</sup> The magnitude of the heel angles induced by the rudder can be estimated by considering the heeling moments arising from the vertical disposition of the forces described in the preceding section. That disposition for the first phase of a starboard turn, is shown in Fig. 23(a). The direction of most of the forces may be obtained from the first of Equations (24) if all terms are gathered on one side and equated to zero as follows:

$$Y_{\delta}\delta_R + Y_v\dot{v} + Y_r\dot{r} - \Delta v = 0 \quad (28)$$

Since  $Y_{\delta}$  is always positive and  $\delta_R$  is negative for a starboard turn,  $Y_{\delta}\delta_R$  is negative or directed to port. Since  $Y_u$  is always negative and  $\dot{v}$  is negative in the first phase of a starboard turn,  $Y_v\dot{v}$  is positive or directed to starboard. Since  $Y_r$  may be either positive or negative, the sign of  $Y_r\dot{r}$  is not predictable from (28). In any event,  $Y_r\dot{r}$  is very small compared to  $Y_v\dot{v}$ . Finally, since  $\dot{v}$  is negative and  $\Delta$  is positive,  $(-\Delta v)$  is positive or directed to starboard.

The approximate angle of heel,  $\phi$ , may be obtained by equating the resultant heeling moment, which is the sum of the moments of each of the forces in the  $yz$ -plane, Fig. 23(a), to the hydrostatic righting moment. A graphical solution of this equation is described in Section 7 of Chapter II. For this purpose  $Y_v\dot{v}$ ,  $Y_r\dot{r}$  may be taken to be acting at half draft,  $Y_{\delta}\delta_R$  at the vertical center of the rudder and  $\Delta v$  and  $\Delta x_G\dot{r}$  at the center of gravity of the ship. If moments are taken about the half draft, it is obvious from Fig. 23(a) that the heel angle,  $\phi$ , will be to the starboard (positive) in the first phase of a starboard turn.

The forces acting in the  $yz$ -plane taken from Equation (25) for the third phase of a starboard turn are shown in Fig. 23(b). If moments are taken about the center of gravity of the ship, it is seen that the heel angle,  $\phi$ , is likely to be to port (negative) since  $Y_v\dot{v} + Y_r\dot{r}$  must be much larger than  $Y_{\delta}\delta$  in order to enforce the starboard turn. Thus, between the first and third phase of a turn, the heel angle of a surface ship changes sign. The heel-angle time record of ship with a large turning heel angle is shown for a starboard turn in Fig. 24. It is seen that the amplitude of the initial heel to starboard in the first phase of the turn is small compared to the amplitude of the second heel to port. This second heel involves a large overshoot angle beyond the equilibrium value computed in accordance with Fig. 23(b). However, eventually the port heel settles down to a fairly steady value corresponding to the computed value for the final phase of the turn.

From an operational point of view, a potentially dan-

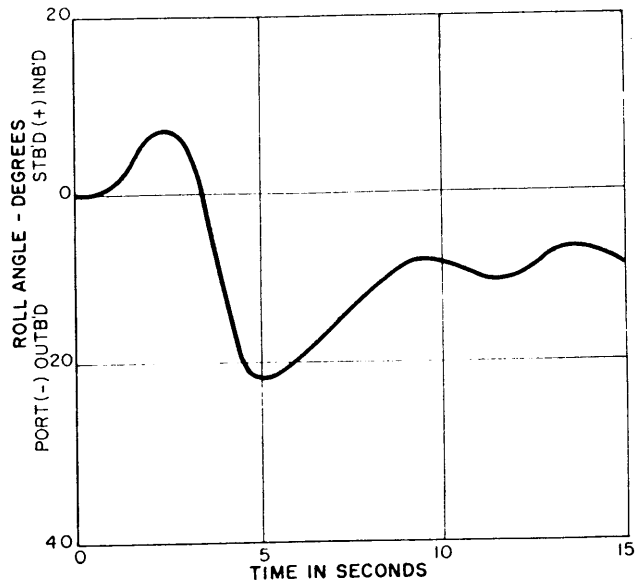


Fig. 24 Roll-angle time records for a starboard turn

gerous situation exists just prior to the completion of the first large heel to port. A helmsman, fearing too large a heel to port, might at this instant decide to return the rudder quickly to amidships. This would eliminate the  $Y_{\delta}\delta_R$  force and the heel to port would be aggravated rather than alleviated. The only safe action to take in such a situation is to immediately, but slowly and cautiously, reduce the rudder angle and at the same time reduce speed as quickly as possible.

In the case of a submarine turning, submerged, the heel angle is inboard (starboard heel for a starboard turn) throughout all phases of a turn. The reason for this is that the positions of both the  $Y_v\dot{v} + Y_r\dot{r}$  force of Fig. 23(a) and the  $Y_{\delta}\delta + Y_r\dot{r}$  force of Fig. 23(b) are considerably higher relative to the center of gravity on a submerged submarine than on a surface ship. In particular, the bridge fairwater existing on practically all submarines is an effective lifting device and contributes heavily to both the magnitude and the height of the  $Y_v\dot{v}$ -force of Fig. 23(b), increasing rolling moment,  $K_v\dot{v}$ . It is clear that if the  $Y_v\dot{v} + Y_r\dot{r}$  force is raised sufficiently high (on some submarines it is raised to a position above the center of gravity), the heel in the third phase of a turn will be in the same direction as in the first phase of a turn. Thus, the first heel of a submerged turning submarine is an inboard heel of very large amplitude called the *snap roll* with subsequent inboard rolls of diminished mean values. According to Arentzen and Mandel (1960), the ratio of the snap roll in the first phase of a turn to the steady heel in the final phase of a turn may be as large as  $3\frac{1}{2}$  for a submarine with a large bridge fairwater and as large as 5 for a submarine without a fairwater. The latter submarine, however, has a much smaller steady

<sup>4</sup> For submerged submarines, the pitch angles induced in turning by the rudder as well as by hull asymmetries are also frequently large enough to be of concern.

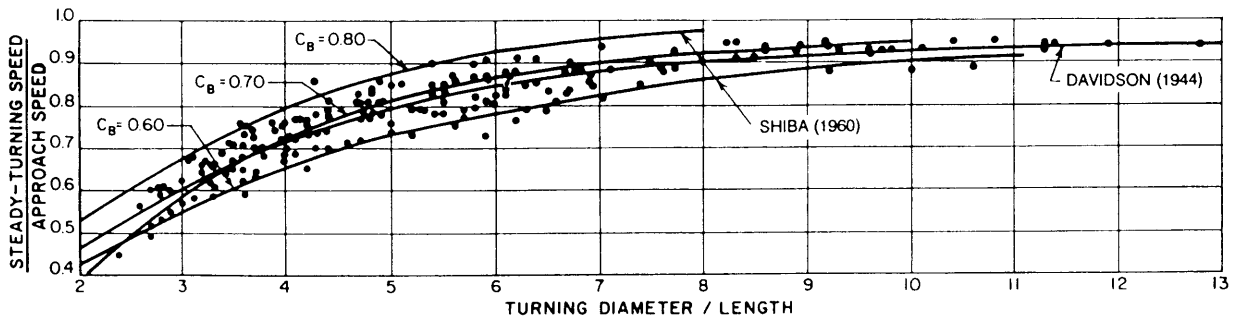


Fig. 25 Speed reduction as a function of turning diameter and block coefficient

heel angle than a submarine with a fairwater. Thus, the fairwater plays a dual role in turning:

(a) It increases the roll excitation in a turn because of its large influence on the roll moment due to the transverse velocity  $K_v v$ .

(b) It increases the magnitude of the roll damping moment,  $K_p p$ , and hence, dampens the amplitude of the overshoot of the snap roll.

See Section 12 and 15.7 for description of yaw-roll coupling effects in waves and further discussion.

**6.6 Reduction of Speed in a Turn.** Part of the reason that the initial snap roll of a submarine is so much larger than subsequent rolls is that the speed of the submarine is rapidly reduced as soon as it develops a substantial drift angle. This is also part of the reason why the first roll to port of the surface ship in Fig. 24 is much larger than subsequent rolls. However, in the case of the surface ship, its speed is more greatly reduced by the time it experiences its largest heel angle than in the case of the submarine. This partially accounts for the fact that the ratio of the value of the first large roll to the steady heel shown in Fig. 24 is not nearly as large as the comparable ratios for submarines cited from Arentzen and Mandel (1960).

The magnitude of the speed reduction in a turn is largely a function of the tightness of the turning circle (Davidson, 1944). Fig. 25 shows the empirical relationship between the ratio of the speed in a steady turn to the approach speed and of the turning diameter to the ship length, developed by Davidson on the basis of a large number of ship trial and model results. The discounting by Davidson of the differences between full-scale and model results has been shown to be erroneous by Strom-Tejsen (1965), among others. Superimposed on the Davidson results in Fig. 25 are Shiba's (1960) results. Davidson and Shiba concluded that the relatively small scatter of data shown could not be related to rudder angle, approach speed, or rudder-area ratio, which were, of course, among the variables of the tests. The effect of changes in type of ship power plant and in ship configuration on the speed

reduction during maneuvers is discussed in Sections 8.7 and 16.4.

In spite of the increasingly severe speed loss associated with tighter turns, Davidson showed that by decreasing the tactical diameter to two ship lengths or less, significant operational aspects of turning are improved. For example, Fig. 26 shows that a 122 m (400 ft) long, 20-knot ship with a  $TD/L = 2.0$  achieves a full course reversal and has almost completely regained its approach speed in the  $1\frac{1}{4}$  min that are required for the ship to pass its original execute point headed in the opposite direction. On the other hand, the same ship with a  $TD/L = 4.5$  required  $2\frac{1}{2}$  min and

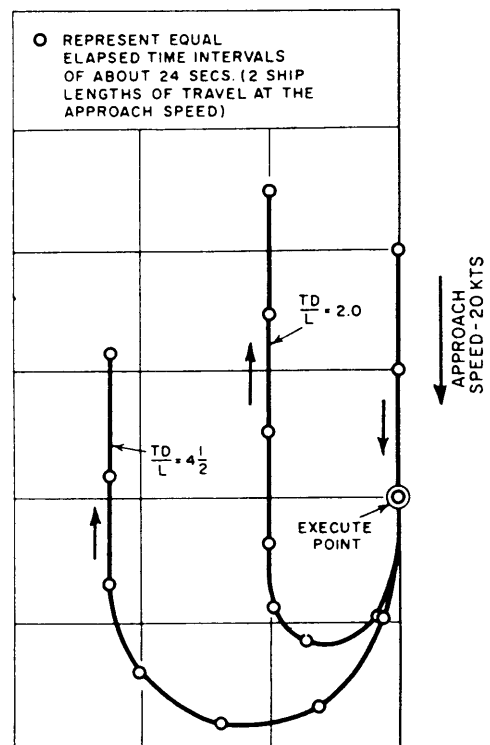


Fig. 26 Comparison of 180 deg turn and speed recovery characteristics of 152-m (400-ft) ship (Davidson, 1944)

much more sea room for the same maneuver.

The speed used in the computation of heel angle in the final phase of a turn in accordance with Fig. 23(b) should of course be the reduced speed as determined from Fig. 25 and not the approach speed.

Transient turning and complex maneuvers cannot be predicted by linear theory. Instead one must resort either to non-linear theory in conjunction with captive model tests (Section 7) or to free-running radio-controlled model tests (Section 8).

## Section 7

### Free-Running Model Tests and Hydraulic Models

**7.1 Free-Running Model Tests.** There are two distinct types of model tests used in the calculation of ship controllability: forced captive model tests and free-running model tests. Captive model tests will be described in Section 8 and are useful in developing coefficients for use in ship trajectory prediction equations. Free-running model tests are more direct and make use of a self-propelled scale model of the ship fitted with all appendages and remote control, so that actual maneuvers can be performed and controllability evaluated.

Simple free-running models are typically used to evaluate turning performance and course keeping stability. Such testing can be used to obtain numerical measures of stability when the model is fitted with a sophisticated sensor-control and a position recording system. Measured trajectories from the circle, zigzag, and reverse spiral definitive maneuvers can directly yield index values for comparison with established criteria or similar values from an acceptable design. Section 15 discusses further the development and assessment of performance requirements.

Controllability in shallow water can also be evaluated if a test facility with variable water depth is available. Free-running model tests, however, are not generally suitable for evaluating stopping performance since scale effects are difficult to overcome.

Free-running ship models can also be used in hydraulic models of harbor and waterway situations. Piloted remotely, such models provide a method of evaluating various arrangements on the hull, and the effectiveness of various types of vessels under particular shallow and restricted waterway conditions. Some large piloted models are also used for training, and research in facilities such as the one in Sogreah, France (Demenet, Lewis, et al; 1987).

**7.2 Free-Running Model Test Techniques.** Free-running model tests require a model whose propeller rotation and control-surface position may be remotely controlled and recorded as a function of time. They also require a large maneuvering basin, as well as means for determining and recording the  $x_0$  and  $y_0$  coordinates of the origin of the model, the model heading angle  $\psi$ , and, if desired, the model heel angle  $\phi$ , all as a function of time. Using instructions like those for the full-scale ship, the turning, zigzag, and re-

versed spiral definitive maneuvers may be carried out with a free-running model and the resulting characteristics of these maneuvers may be directly determined. For this reason, free-running model tests have been, and still are, extensively used for predicting the maneuvering characteristics of surface ships, and have even been used to determine the maneuvering characteristics of submerged submarines in the horizontal plane.

Martinussen and Linnerud (1987) provide a current status of the use of free-running models for predicting maneuvering characteristics at the design stage. Some of the difficulties in developing test techniques are connected with the question of viscous scale effects as addressed by many including ITTC (1984), Burcher (1975), Okamoto, Tamai, and Oniki (1972), and Nikolaev and Lebedeva (1980). Some detailed discussion of scale effects, particularly with regard to control surfaces, will also be presented in Section 14.2. Other difficulties are related to the physical execution of the tests.

On the physical side, cost considerations normally result in utilizing the same model used for towing and propulsion tests to perform free-running maneuvering tests. Large models are thus often used which help in the reduction of scale effects but require careful test execution to complete maneuvers because of space limitations even when performed in large basins.

As Martinussen and Linnerud (1987) recount, five conditions should be met at the start of a maneuver; forward speed equal to approach speed with the corresponding propeller revolutions, rudder angle at neutral, and sway and yaw velocities at zero. It is difficult to satisfy all five when testing large models of unstable ships. Priority is thus given to forward speed, propeller RPM, and yaw velocity over rudder angle. During each maneuver, the controller must carefully optimize use of the basin to allow full maneuvers to be accomplished.

In order that free-running model test results may be directly applicable to a full-scale ship, the following additional conditions, added to that of geometric similitude, should be satisfied:

(a) The nondimensional mass moment of inertia of the model about the  $z$ -axis,  $I'_z$ , should be identical to that of the ship.

(b) The model rudder should be deflected to the

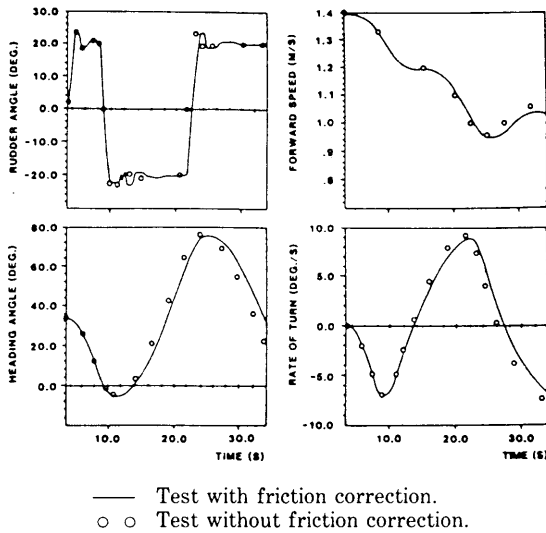


Fig. 27 20/20 zigzag test. Model scale result

same maximum angle as the ship rudder at the same nondimensional deflection rate as that of the ship, i.e.,

$$\dot{\delta}'_{Rm} = \dot{\delta}'_s = \frac{\dot{\delta}_m L_m}{V_m} = \frac{\dot{\delta}_s L_s}{V_s} \quad (29)$$

where the subscript  $m$  refers to model values and the subscript  $s$  to ship values. Thus the model dimensional rudder rate  $\dot{\delta}_m$  is different from that of the ship,  $\dot{\delta}_s$ .

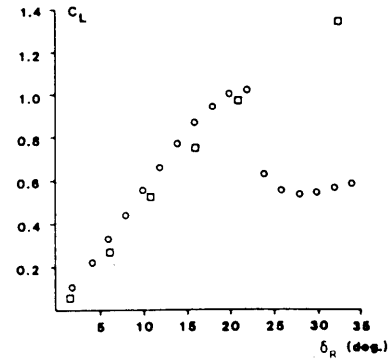
(c) If the ship heel in maneuvers is to be properly simulated, the  $I'_x$  of the model as well as its nondimensional transverse metacentric height must be identical to that of the ship. (In practice, these are difficult conditions to fulfill.)

(d) The model propeller operating slip ratio should be identical to the ship propeller slip ratio. This is particularly important if the rudder is located in the propeller race.

(e) If the speed loss in maneuvers is to be properly simulated, the response of the motor that drives the model propeller to an augment in model resistance should duplicate the response of the power plant of the full-scale ship to a corresponding augment in ship resistance.

Condition (d) is fulfilled in the ordinary self-propulsion test by having the towing carriage provide part of the thrust necessary to drive the model. If not accounted for, some models will maneuver more sharply than the full-scale ship because the rudder force (and hence rudder moment) is larger for the model as a result of more flow past the rudder.

For free-running models this condition is commonly fulfilled with by using an air propeller to provide part of the thrust. This air force can be measured and dynamically changed as a function of measured model speed to improve results. Fig. 27 shows a comparison of results from similar zig-zag tests run with and with-



○ ○ Open water test, turbulence provided by wire mesh upstream of rudder.

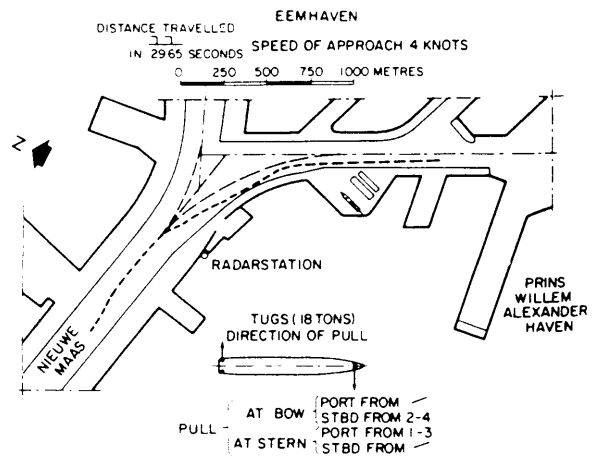
□ □ Behind hull and propeller.  $C_L$  based on model speed.

Fig. 28 Rudder lift coefficient  $C_L$  as function of rudder angle (Martinussen and Linnerud, 1987)

out friction correction, showing the effect of a more effective rudder in the latter case.

Condition (e) is usually ignored with a constant RPM held. Free-running model tests thus show less speed loss in a maneuver than do full-scale results. Results are often considered acceptable for diesel powered ships which normally show only a 10–15 percent reduction in revolutions in a turning circle with a 35 deg rudder angle. Use of a thrust and torque transducer would allow simulation of the propulsion engine characteristics during tests.

As will be presented later in Section 14.2, a rudder in a free stream will encounter flow separation at smaller rudder angles in model scale. There is a general belief that a model rudder when placed in the propeller race, encounters a high turbulence level



WATER DEPTH 13.80 m (14.2 x DRAFT), TIDE CONDITION LOW, CURRENT SPEED 1.0 m/sec, WIND DIRECTION — SPEED 0 m/sec

Fig. 29 Typical record of hydraulic model test (Panel H-10, 1975)

which makes this scale effect negligible. Fig. 28 supports this conclusion through its comparison of results for a model rudder tested in open water with test results with a rudder behind a propeller on a captive model running at the ship self-propulsion point.

The general problem remains of having different model vs full-scale boundary layer thickness, after-body separation, and cross-flow separation. In addition to the traditional bow trip wire Nikolaev and Lebedeva (1980) have applied turbulence stimulation on other parts of the underwater hull.

Results reported by Dand (1983) indicate that the model is normally more directionally stable than the ship. Martinussen and Linnerud (1987), however, indicate that by using large models, predictions of stability characteristics can be reasonably accurate for quite different hull forms. The free-running model in open water has long been a tool in the analysis of maneuverability. The series type test results of Shiba (1960) have been very instructive as to the effect of basic dimensions and rudder area on maneuvering characteristics.

Because of the numerous scaling and other difficulties noted above, and because free-running model tests yield terminal results only providing little insight into the many individual factors, and because large maneuvering basins are required, alternate procedures employing computer simulation in conjunction with captive model test results have been developed and will be presented in Section 8.

Before leaving the free-running model, its utility when operated in a hydraulic model of a waterway will next be introduced.

**7.3 Hydraulic Models.** Models of harbor and vessel waterway systems accurately modeling hydraulic flows can be constructed and then free running models

piloted remotely through them to determine safety and efficiency of the operation. Fig. 29 shows one such hydraulic model test scenario, the Port of Eemhaven, Netherlands (Panel H-10, 1975).

In this particular case the channel bend was determined, after survey, to present the most critical problem in the maneuvering of container ships. While the existing channel was wide enough to accommodate a large container ship, the combined effects of the turning maneuver and wind and current restricted entry time to a window of only two hours a day. And even with this restraint, entry was still judged to be risky by the Rotterdam pilots.

A hydraulic model was set up at MARIN of the Eemhaven waterway configuration and many different large proposed container ship models were run through the turning maneuver. The rate of groundings was 30 percent of the transits, reinforcing the pilots' fears. When proposed dredging to ease the bend was tried in the hydraulic model, groundings were reduced to zero with proper tug assistance (tug usage was simulated using small fans mounted on the model).

Fig. 29 shows a sample trajectory resulting from the Eemhaven study. As a result of the project, the Rotterdam Port Authority authorized an expensive easing of the channel bend entering Eemhaven.

While the hydraulic modeling of the waterway can be made quite accurate reflecting correctly the flows of water, scaling problems still exist and the difficulties mentioned in the previous sections apply. Scales are usually small (1 to 100 is common) because of the expense of building waterway models.

Pilot or helmsman control is from a bird's eye position which provides a better understanding of what is happening, but in a compensating manner, movements take place many times faster than in real life.

## Section 8

### Nonlinear Equations of Motion and Captive Model Tests

**8.1 Nonlinear Equations of Motion.** Captive model tests and associated simulation studies using nonlinear equations are the most powerful and flexible means available today for predicting controllability. This approach may be initially more costly than a free-running model test program, but once the required hydrodynamic coefficients are determined from the model test data, a wide variety of more accurately predicted maneuvers and ship operations can be rapidly and economically simulated, with the effects of environment, control systems, and external forces readily studied.

Linear theory as discussed in prior sections is useful for analyzing the influence of ship features on controls-fixed stability and on the turning ability of directionally stable ships in the linear range. Captive model tests

can be used to develop coefficients for these equations. However, as previously noted, linear theory fails to predict accurately the characteristics of the tight maneuvers that most ships are capable of performing, and it cannot predict the maneuvers of directionally unstable ships.

There is no completely analytical procedure available to this date (1989) for predicting the characteristics of these nonlinear maneuvers. As a result, current computer-aided techniques utilize the experimental results from captive model tests, with the equations of motion expanded to include significant nonlinear and coupled terms.

A variety of different approaches to developing a set of nonlinear equations of motion exist, ranging

from using wing theory to applying a Taylor's series expansion to force and moment parameters. A "Catalog of Existing Mathematical Models" (Hagen, 1983) provides a primer on nonlinear models and reporting of coefficients and data. The works of Abkowitz (1964, 1965), Strom-Tejsen (1965), Eda and Crane (1965), Norrbin (1971), Goodman and Gertler (1976), and others should also be reviewed. Fedyayevsky (1964) developed a modular system based on physical relationships and the use of wing theory, and more recently, the Japanese Mathematical Modeling Group (MMG) through Kose (1982) and others has developed a similar modular model (Section 16 addresses these developments and the modular approach).

The Abkowitz and Strom-Tejsen Taylor's expansion approach is herewith presented to give an understanding of the development of this popular non-modular model. The approach is based on a restatement of Equation (6) to include rudder angle as follows:

$$\left. \begin{matrix} X \\ Y \\ N \end{matrix} \right\} = f(u, v, r, \dot{u}, \dot{v}, \dot{r}, \delta_R) \quad (30)$$

It is assumed in Equation (30) that the only important forces and moments acting on the ship induced by the rudder are those due to rudder deflection,  $\delta_R$  and that the forces and moments produced on the ship as a result of  $\dot{\delta}_R$  and  $\ddot{\delta}_R$  are negligible.

The complete Taylor expansion of Equation (30) with terms up to the third order is as follows for  $X$  with similar expressions for  $Y$  and  $N$ .

(As noted in Section 6.7, tight maneuvers involve large speed losses; hence, consideration of the  $X$ -equation constitutes a vital part of this section whereas it could legitimately be neglected in the earlier considerations of linear maneuvers):

$$\begin{aligned} X = & X^0 + [X_u \delta U + X_v v + X_r r + X_{\dot{u}} \dot{u} \\ & + X_{\dot{v}} \dot{v} + X_{\dot{r}} \dot{r} + X_{\delta} \delta_R] + \frac{1}{2!} [X_{uu} \delta u^2 \\ & + X_{vv} v^2 + \dots + X_{\delta\delta} \delta_R^2 + 2X_{uv} \delta u v \\ & + 2X_{ur} \delta u r + \dots + 2X_{\dot{v}\delta} \dot{v} \delta_R] \\ & + \frac{1}{3!} [X_{uuu} \delta u^3 + X_{vvv} v^3 + \dots + X_{\delta\delta\delta} \delta_R^3 \\ & + 3X_{uuv} \delta u^2 v + 3X_{uur} \delta u^2 r + \dots + 3X_{\dot{v}\delta\delta} \dot{v} \delta_R^2 \\ & + 6X_{uvr} \delta u v r + 6X_{u\dot{v}\delta} \delta u v \dot{v} \\ & + \dots + 6X_{\dot{v}\dot{r}\delta} \dot{v} \dot{r} \delta_R] \end{aligned} \quad (31)$$

where  $X^0$  is the force in the  $x$ -direction at the equilibrium condition, that is,  $u_1 = V$

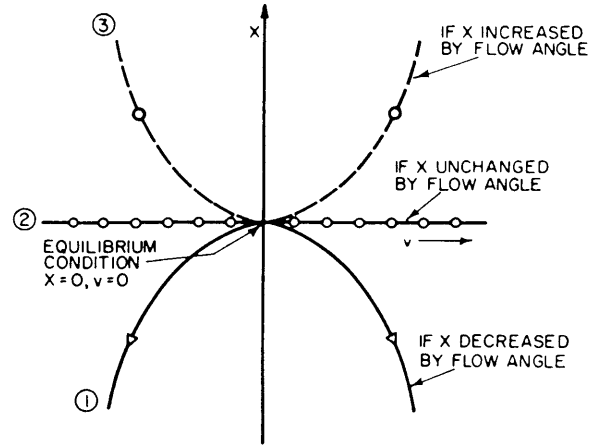


Fig. 30 Three possible relationships between  $X$  and  $v$

$$X_{uu} = \frac{\partial^2 X}{\partial u^2}, X_{\delta\delta} = \frac{\partial^2 X}{\partial \delta_R^2}, X_{uv} = \frac{\partial^2 X}{\partial u \partial v}$$

$$X_{uuu} = \frac{\partial^3 X}{\partial u^3}, X_{uur} = \frac{\partial^3 X}{\partial u^2 \partial r}, \text{ etc.}$$

Terms higher than third order are not included in Equation (31) because experience has shown that accuracy is not significantly improved by their inclusion. Furthermore, practical limitations of measurement techniques and the state of refinement of present theory do not justify the inclusion of higher order terms.

As a consequence of the geometrical symmetry of ships about the  $xz$ -plane, the relationship between  $X$  and  $v$ , for example, must correspond in general form to one of the three relationships shown in Fig. 30. The feature common to all three relationships is that they are symmetrical about the ordinate  $X$ . If the relationship between  $X$  and  $v$  as depicted by curves 1 or 3 of Fig. 30 is to be expressed as an expansion in powers of  $v$  beyond the first power, then only the even powers of  $v$  can appear in the expression and the coefficients of the odd powers must be zero. That is,  $X$  is an even function of  $v$  which takes the form:

$$X(v) = a_2 v^2 + a_4 v^4 + a_6 v^6 + \dots \quad (32)$$

where

$$a_2 = \frac{1}{2} X_{vv}; a_4 = \frac{1}{24} X_{vvv}, \text{ etc., from Equation (31)}$$

Again, as a result of symmetry about the  $xz$ -plane, Abkowitz (1964) shows that  $X$  is also an even function of  $r$ ,  $\delta_R$ ,  $\dot{v}$  and  $\dot{r}$ , that is,

$$X(r) = b_2 r^2 + b_4 r^4 + b_6 r^6 + \dots \quad (33)$$

$$X(\delta_R) = c_2 \delta_R^2 + c_4 \delta_R^4 + c_6 \delta_R^6 + \dots \quad (34)$$

It follows from the previous analysis that cross-coupled terms in Equation (31) such as  $X_{uv} v \delta u$ ,

$X_{ru} r \delta u$ ,  $X_{\delta u} \delta_R \delta u$ ,  $X_{vvu} v^3 \delta u$ ,  $X_{rru} r^3 \delta u$ , and so on, involving odd powers of  $v$ ,  $r$ , and  $\delta_R$  are also zero. However, cross-coupled terms such as  $X_{vvu} v^2 \delta u$ ,  $X_{rru} r^2 \delta u$ ,  $X_{\delta \delta u} \delta_R^2 \delta u$ , and so on, are nonzero because they involve even powers of  $v$ ,  $r$ , and  $\delta_R$ . Also, terms such as  $X_{vr} vr$ ,  $X_{v\delta_R} v \delta_R$ ,  $X_{r\delta_R} r \delta_R$ ,  $X_{vru} vr \delta u$ , and  $X_{r\delta u} r \delta_R \delta u$  are nonzero because they involve even-powered products of  $v$ ,  $r$ , and  $\delta_R$  (see also Section 8.6).

In contrast to  $X$ , the expressions for  $Y$  and  $N$  are odd functions of  $v$ ,  $r$ ,  $\delta_R$ ,  $\dot{v}$ , and  $\dot{r}$ ; that is, only the coefficients of the terms in the expansion with odd powers are non-zero; those with even powers are zero. Odd functions are like those shown in Figs. 6, 8, 11, and 13 where in all cases the graph of the function is reflected about the origin. The expansion of  $Y$  or  $N$  as a function of  $v$ ,  $r$ ,  $\delta_R$ ,  $\dot{v}$ , or  $\dot{r}$  is typically as follows:

$$Y(v) = d_1 v + d_3 v^3 + d_5 v^5 + \dots \quad (35)$$

$$Y(\delta_R) = e_1 \delta_R + e_3 \delta_R^3 + e_5 \delta_R^5 + \dots \quad (35a)$$

Although superficially it appears that there should be a correspondence between the relationship of  $Y$  to  $v$  shown in Equation (35) and the relationship of  $X$  to  $u$ , in reality they are vastly different, for several reasons. One is that the equilibrium value of  $v$ , designated  $v_1$  in Section 3, is taken as zero. (Any asymmetry due to propeller rotation is neglected for this restricted purpose but is taken account of later in Equations (37) and (38).)

The equilibrium value of  $u$ ,  $u_1$  is not zero but is equal to the ship velocity,  $V$ . Another reason is that the  $X$ -force is the component along the  $x$ -axis of the difference between two oppositely directed forces, namely, the ship resistance and the propeller thrust, whereas the  $Y$ -force is the component of a direct hydrodynamic force. For these reasons and others,  $X$  is neither an odd nor an even function of  $u$  but rather its expansion includes all powers of  $\delta u$ .

Additional terms of the nonlinear equations can be eliminated by considering the nature of acceleration forces. Abkowitz (1964) states that no second or higher order acceleration terms can be expected, on the assumption that there is no significant interaction between viscous and inertia properties of the fluid and that acceleration forces calculated from potential theory when applied to submerged bodies give linear terms. Hence all terms such as  $X_{\ddot{u}} \ddot{u}^2$ ,  $X_{\ddot{v}} \ddot{v}^2$ ,  $X_{\ddot{r}} \ddot{r}^2$ ,  $X_{\ddot{u}\ddot{u}} \ddot{u}^3$ , and so on, of Equation (31) are taken as zero. Since  $X_{\dot{v}}$  and  $X_{\dot{r}}$  are also zero because of symmetry, the only acceleration derivative that is not taken as zero in the nonlinear equation of motion for  $X$  is  $X_{\ddot{u}}$ , which is also the only acceleration derivative that appears in the linear equation for  $X$  (10).

Combining the nonlinear Taylor expansion for  $X$ , Equation (31) with the dynamic response terms of the  $X$ -equation, Equation (5), and taking all of the preced-

ing considerations into account, the equation for  $X$  becomes:

$$(\Delta - X_{\ddot{u}}) \ddot{u} = f_1(u, v, r, \delta_R) \quad (36)$$

where

$$\begin{aligned} f_1(u, v, r, \delta_R) = & X^0 + X_u \delta u + \frac{1}{2} X_{uu} \delta u^2 + \frac{1}{6} X_{uuu} \delta u^3 \\ & + \frac{1}{2} X_{vv} v^2 + \frac{1}{2} X_{rr} r^2 + \frac{1}{2} X_{\delta\delta} \delta_R^2 \\ & + \frac{1}{2} X_{vvu} v^2 \delta u + \frac{1}{2} X_{rru} r^2 \delta u + \frac{1}{2} X_{\delta\delta u} \delta_R^2 \delta u \\ & + (X_{vr} + \Delta) vr + X_{v\delta_R} v \delta_R + X_{r\delta_R} r \delta_R + X_{vru} vr \delta u \\ & + X_{v\delta u} v \delta_R \delta u + X_{r\delta u} r \delta_R \delta u \end{aligned}$$

The relationship between  $Y$  or  $N$  and  $\delta u$  corresponds to that shown in curve 2 of Fig. 30 for  $X$  versus  $v$ . That is, because of symmetry about the  $xz$ -plane,  $Y(u) = N(u) = 0$  and the derivatives  $Y_u$ ,  $Y_{uu}$ ,  $Y_{uuu}$ ,  $Y_{\dot{u}}$ ,  $N_{\dot{u}}$ ,  $N_{uu}$ ,  $N_{uuu}$ , and  $N_{\dot{u}}$  are all zero.

As stated earlier,  $Y$  and  $N$  are odd functions of  $v$ ,  $r$ ,  $\delta_R$ ,  $\dot{v}$ , and  $\dot{r}$ . It follows that all the cross-coupled terms in the complete Taylor expansion of  $Y$  and  $N$  involving even powers or even-powered products of  $v$ ,  $r$ ,  $\delta_R$ ,  $\dot{v}$ , and  $\dot{r}$  are zero. Thus  $Y_{vvu} v^2 \delta u$ ,  $Y_{rru} r^2 \delta u$ ,  $Y_{vr} vr$ ,  $Y_{v\delta_R} v \delta_R$ ,  $Y_{r\delta_R} r \delta_R$ ,  $Y_{vru} vr \delta u$ ,  $Y_{v\delta u} v \delta_R \delta u$ , etc., and similar terms for  $N$ , are all zero.

The  $Y$ -force and  $N$ -moment induced by the rotation of a single propeller or by unirotating multiple propellers, at  $v = \delta_R = 0$ , identified as  $Y^0$  and  $N^0$  in Equation (26) must, of course, be included in the nonlinear equations for  $Y$  and  $N$ . In addition, since  $Y^0$  and  $N^0$  are likely to be speed dependent, the following terms are also taken as nonzero in the Taylor expansion:

$$\begin{array}{ll} Y_u^0 \delta u & N_u^0 \delta u \\ Y_{uu}^0 (\delta u)^2 & N_{uu}^0 (\delta u)^2 \end{array}$$

The  $Y$ -force and  $N$ -moment induced by propeller rotation at  $v \neq 0$ , also discussed in Section 17.9 (see Fig. 253), as well as their speed dependency, are included in the following nonzero terms in the Taylor expansion:

$$\begin{array}{ll} Y_{vu} v \delta u & N_{vu} v \delta u \\ Y_{vuu} v (\delta u)^2 & N_{vuu} v (\delta u)^2 \end{array}$$

Following Abkowitz's reasoning as noted in the discussion of Equation (31) the only acceleration derivatives not taken as zero in the nonlinear expansion of  $Y$  and  $N$  are those appearing in the linear equations of motion. These are  $Y_{\ddot{v}}$ ,  $Y_{\ddot{r}}$ ,  $N_{\ddot{v}}$ , and  $N_{\ddot{r}}$ .

Combining the third-order Taylor expansions for  $Y$  and  $N$  [similar to that shown for  $X$  in (31)], with the dynamic response terms of the  $Y$  and  $N$ -equations of Equation (5) and taking all of the preceding consid-

erations into account, the nonlinear equations of motion for  $Y$  and  $N$  are as follows:  $Y$ -Equation:

$$(\Delta - Y_i)\dot{v} - Y_i\dot{r} = f_2(u, v, r, \delta_R) \quad (37)$$

$N$ -Equation:

$$-N_i\dot{v} + (I_z - N_i)\dot{r} = f_3(u, v, r, \delta_R) \quad (38)$$

where

$$\begin{aligned} f_2(u, v, r, \delta_R) = & Y^0 + Y_u^0 \delta u + Y_{uu}^0 \delta u^2 + Y_v v \\ & + \frac{1}{6} Y_{vvv} v^3 + \frac{1}{2} Y_{vrr} v r^2 + \frac{1}{2} Y_{v\delta\delta} v \delta_R^2 + Y_{vu} v \delta u \\ & + \frac{1}{2} Y_{vu u} v \delta u^2 + (Y_r - \Delta u_1) r + \frac{1}{6} Y_{rrr} r^3 + \frac{1}{2} Y_{rvv} r v^2 \\ & + \frac{1}{2} Y_{r\delta\delta} r \delta_R^2 + Y_{ru} r \delta u + \frac{1}{2} Y_{ruu} r \delta u^2 + Y_{\delta} \delta_R \\ & + \frac{1}{6} Y_{\delta\delta\delta} \delta_R^3 + \frac{1}{2} Y_{\delta vv} \delta_R v^2 + \frac{1}{2} Y_{\delta rr} \delta_R r^2 \\ & + Y_{\delta u} \delta_R \delta u + \frac{1}{2} Y_{\delta uu} \delta_R \delta u^2 + Y_{vr\delta} v r \delta_R \end{aligned}$$

$$\begin{aligned} f_3(u, v, r, \delta_R) = & N^0 + N_u^0 \delta u + N_{uu}^0 \delta u^2 + N_v v \\ & + \frac{1}{6} N_{vvv} v^3 + \frac{1}{2} N_{vrr} v r^2 + \frac{1}{2} N_{v\delta\delta} v \delta_R^2 + N_{vu} v \delta u \\ & + \frac{1}{2} N_{vu u} v \delta u^2 + N_r r + \frac{1}{6} N_{rrr} r^3 \\ & + \frac{1}{2} N_{rvv} r v^2 + \frac{1}{2} N_{r\delta\delta} r \delta_R^2 + N_{ru} r \delta u + \frac{1}{2} N_{ruu} r \delta u^2 \\ & + N_{\delta} \delta_R + \frac{1}{6} N_{\delta\delta\delta} \delta_R^3 + \frac{1}{2} N_{\delta vv} \delta_R v^2 + \frac{1}{2} N_{\delta rr} \delta_R r^2 \\ & + N_{\delta u} \delta_R \delta u + \frac{1}{2} N_{\delta uu} \delta_R \delta u^2 + N_{vr\delta} v r \delta_R \end{aligned}$$

An equation similar to Equation (38) could also be developed for the roll moment,  $K$ , which could be used to solve for the heel angle,  $\phi$ , as a function of time.

Equations (36), (37) and (38) can be solved simultaneously for the accelerations  $\dot{u}$ ,  $\dot{v}$ , and  $\dot{r}$ , as follows:

$$\begin{aligned} \dot{u} &= \frac{f_1(u, v, r, \delta_R)}{(\Delta - X_u)} \\ \dot{v} &= \frac{(I_z - N_i)f_2(u, v, r, \delta_R) + Y_i f_3(u, v, r, \delta_R)}{(\Delta - Y_i)(I_z - N_i) - N_i Y_i} \\ \dot{r} &= \frac{(\Delta - Y_i)f_3(u, v, r, \delta_R) + N_i f_2(u, v, r, \delta_R)}{(\Delta - Y_i)(I_z - N_i) - N_i Y_i} \end{aligned} \quad (39)$$

These solutions can be rewritten in the form:

$$\frac{du}{dt} = g_1[t, u(t), v(t), r(t), \delta_R(t)]$$

$$\frac{dv}{dt} = g_2[t, u(t), v(t), r(t), \delta_R(t)] \quad (40)$$

$$\frac{dr}{dt} = g_3[t, u(t), v(t), r(t), \delta_R(t)]$$

where  $u(t)$ ,  $v(t)$ ,  $r(t)$ , and  $\delta_R(t)$  are the instantaneous values of  $u$ ,  $v$ ,  $r$ , and  $\delta_R$  at any time,  $t$ .

Equation (40) is a set of three first-order differential equations for which approximate numerical solutions are readily obtained on a digital computer. The key to the numerical solution is that values of  $u$ ,  $v$ , and  $r$  at time  $t + \delta t$  are obtained from knowledge of the values of  $u$ ,  $v$ ,  $r$ , and  $\delta_R$  at time  $t$  using a simple first-order expansion; that is,

$$u(t + \delta t) = u(t) + \delta t \dot{u}(t)$$

$$v(t + \delta t) = v(t) + \delta t \dot{v}(t) \quad (41)$$

$$r(t + \delta t) = r(t) + \delta t \dot{r}(t)$$

This method is found to give adequate accuracy for the present type of differential equations because the accelerations  $\dot{u}$ ,  $\dot{v}$ , and  $\dot{r}$  vary but slowly with time, owing to the large mass or inertia of a ship compared to the relatively small forces and moments produced by its control surface. Any desired accuracy of the solutions can be obtained with a computer by using smaller time intervals  $\delta t$ .

The mathematical model has been developed in dimensional form. The equations are equally valid in nondimensional form with the stipulation that the velocity used for nondimensionalization should be the velocity at any time,  $t$ , but not the initial velocity. For further simplification, the nondimensionalizing velocity in the nonlinear equations is taken as  $u(t)$  rather than  $V(t)$ .

One reason cited in this chapter for non-dimensionalization is that the nondimensional derivatives are independent of speed. The extent to which this assumption is not true for nonlinear maneuvers is taken account of in Equations (36), (37), and (38) by the inclusion of such terms as  $Y'_{vu}$ ,  $Y'_{vu u}$ ,  $Y'_{ru}$ ,  $Y'_{ru u}$ ,  $Y'_{\delta u}$ ,  $Y'_{\delta u u}$ , and so on, which represent the changes in the nondimensional derivatives  $Y'_v$ ,  $Y'_r$ ,  $Y'_\delta$  with speed.

Assuming that a full set of hydrodynamic coefficients ( $X'_u$ ,  $X'_{uu}$ ,  $X'_{uuu}$ ,  $Y'_v$ , etc.) is available, and that the rudder deflection  $\delta_R$  is defined as a function of time, the first step in the calculation of the trajectory of a ship would be to set the values of  $u$ ,  $v$ ,  $r$ , and  $\delta_R$  at time  $t = 0$ . In the most usual case  $u$ ,  $v$ , and  $\delta_R$  at



$t = 0$  would be zero and  $u$  would be equal to  $u_1$ . Having done this,  $\dot{u}$ ,  $\dot{v}$ , and  $\dot{r}$  can be calculated from Equations (39) and the new velocities at time  $t = \delta t$  can be obtained from Equations (41). The process is then repeated using the new values for  $u$ ,  $v$ ,  $r$ , and  $\delta_R$  in Equations (39) and so on. The values of the velocities at a time  $t$  are thus obtained from

$$\begin{aligned} u(t) &= u(0) + \sum_{\tau=0}^{t-\delta t} \dot{u}(\tau) \delta t \\ v(t) &= v(0) + \sum_{\tau=0}^{t-\delta t} \dot{v}(\tau) \delta t \\ r(t) &= r(0) + \sum_{\tau=0}^{t-\delta t} \dot{r}(\tau) \delta t \end{aligned} \quad (42)$$

where  $u(0)$ ,  $v(0)$ , and  $r(0)$  are the values of  $u$ ,  $r$ , and  $v$  at  $t = 0$  and  $\tau$  represents intermediate values of time (between time 0 and time  $t - \delta t$ ) at which the accelerations  $\dot{u}(t)$ ,  $\dot{v}(t)$ , and  $\dot{r}(t)$  are determined.

The instantaneous values of the linear velocities of the ship relative to earth axes (which are needed to plot trajectories) instead of relative to ship axes are obtained from Equation (3) re-expressed as:

$$\begin{aligned} \dot{x}_{0o}(t) &= u(t) \cos \psi(t) - v(t) \sin \psi(t) \\ \dot{y}_{0o}(t) &= u(t) \sin \psi(t) + v(t) \cos \psi(t) \end{aligned} \quad (43)$$

where  $\dot{x}_{0o}(t)$  and  $\dot{y}_{0o}(t)$  are the components of the instantaneous resultant velocity of the origin,  $O$ , of the ship along a fixed set of earth axes  $x_0$  and  $y_0$ , respectively.

The instantaneous coordinates of the path of the origin of the ship  $x_{0o}(t)$  and  $y_{0o}(t)$  relative to the fixed set of earth axes and the orientation of the ship,  $\psi(t)$ , can then be obtained by integration of the last of Equations (42) and (43). These are as follows:

$$\begin{aligned} \psi(t) &= \psi(0) + \sum_{\tau=0}^{t-\delta t} r(\tau) \delta t \\ x_{0o}(t) &= x_{0o}(0) + \sum_{\tau=0}^{t-\delta t} \{v(\tau) \cos \psi(\tau) \\ &\quad + [u(\tau) + u(0)] \sin \psi(\tau)\} \delta t \\ y_{0o}(t) &= y_{0o}(0) + \sum_{\tau=0}^{t-\delta t} \{[u(\tau) + u(0)] \cos \psi(\tau) \\ &\quad - v(\tau) \sin \psi(\tau)\} \delta t \end{aligned} \quad (44)$$

There remains the question of defining the rudder deflection as a function of time. It is assumed that the

rudder moves with a constant rate of deflection,  $\dot{\delta}_R$ , determined in accordance with condition 2 of Section 9.2, and that there is a fixed time lag between the instant that rudder deflection is ordered and the instant that the rudder begins to move (see item (d) of Section 5.1). A rudder deflection up to a certain maximum angle  $\delta_R$  would be simulated in a computer program as follows:

$$\delta_R(t) = \delta_R(t_o) \quad \text{until } t > t l_{lag} + t_o$$

$$\text{then } \delta_R(t) = \delta_R(t_o) + \text{rate} (t - t_o - t_{lag})$$

$$\text{until } \delta_R(t) = \delta_{const}$$

$$\text{then } \delta_R(t) = \delta_{const}$$

A rudder function of this type gives a very close approximation to the actual time history of a ship's rudder when a maneuver is ordered from the bridge.

**8.2 Captive Model Tests.** Captive model tests in tanks are now carried out using a planar motion mechanism (PMM) or a rotating arm. In either case the model is tested over a suitable range of important variables such as drift angle, yaw rate, sway acceleration, yaw acceleration, propeller RPM and rudder angle, and the results are analyzed to obtain the hydrodynamic coefficients required in the equations of motion. Development of the linear coefficients will be addressed first.

For design of a control surface, knowledge of the lift, drag and center-of-pressure location as a function of angle of attack, velocity, and control-surface configuration as given in Section 14 is adequate for most practical problems. Knowledge of the forces and moments generated by control-surface rate of deflection,  $\dot{\delta}_c$  and angular acceleration,  $\ddot{\delta}_c$  are only occasionally important to the design of the steering engine that deflects the control surface and rarely, if ever, to the motion of the ship v.s. the control-surface system as a whole. However, it was found in Equation (14a) that to determine whether a ship is stable or unstable in straight-line motion, one must know not only the forces and moments generated by angle of attack on the ship, but also those generated by angular velocity. In addition to these, the forces and moments generated by linear and angular acceleration must be known in order to determine the magnitude of the stability indexes, Equation (14) or to compute the trajectory of a ship from the equations of motion.

The experimental techniques necessary to measure the significant forces and moments generated by a ship's hull are much more elaborate and sophisticated than those necessary to measure the significant control-surface forces. Only in the case of the determination of the velocity-dependent derivatives of the hull is the experimental technique similar in principle to that used to determine control-surface forces and mo-

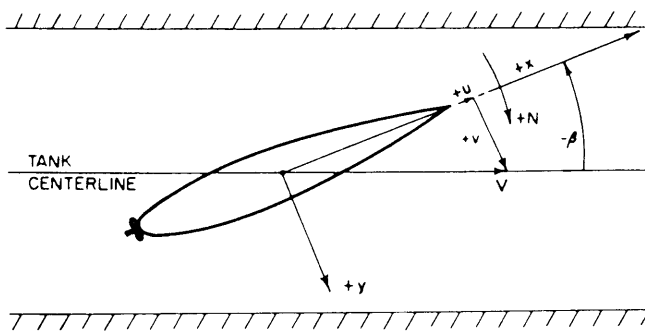


Fig. 31 Orientation of model in towing tank to determine  $Y$  and  $N$  (Abkowitz, 1964)

ments as used for this purpose in a modern wind tunnel (Whicker, 1958), or by Joessel in the river Loire in 1873 (Van Lammeren, et al 1948).

**8.3 Straight-Line Tests in a Towing Tank.** The velocity-dependent derivatives  $Y_v$  and  $N_v$  of a ship at any draft and trim can be determined from measurements on a model of the ship, ballasted to a geometrically similar draft and trim, towed in a conventional towing tank at a constant velocity,  $V$ , corresponding to a given ship Froude number, at various angles of attack,  $\beta$ , to the model path. Fig. 31 indicates the orientation of the model in the towing tank. From this orientation it is seen that a transverse velocity component,  $v$ , is produced along the  $y$ -axis such that:

$$v = -V \sin \beta$$

where the negative sign arises because of the sign convention adopted in this chapter, Fig. 2.

A dynamometer at the origin,  $O$ , measures the force  $Y$  and the moment  $N$  experienced by the model at each value of  $\beta$  tested. These measurements are then plotted as a function of  $v$  (Fig. 10) and the slopes of the curves taken at  $v = 0$ , give numerical values for the derivatives  $Y_v$  and  $N_v$  for the model. These values can be reduced to nondimensional form by dividing by the proper combination, given in Section 3.4, of model length  $L$ , model speed  $V$ , and towing-tank water density,  $\rho$ . The dimensional ship values of the derivatives can then be obtained by multiplying the nondimensional derivatives by the same respective combinations of ship length, ship speed, and seawater density.

With reference to Equation (10), it is not really necessary that the origin, and hence the dynamometer, be located at the center of gravity of model. The results are independent of the location of  $G$ . Rather it is most convenient that the origin and the dynamometer be located at  $\infty$  so that  $x_\infty = 0$ . If the dynamometer is not located at  $\infty$ , the derivative  $N_v$  should be corrected so that it applies to  $O$  at  $\infty$ .

As described in Section (17), the propeller will usually exert an important influence on the hydrodynamic derivatives. Therefore, model tests to determine these derivatives should be conducted with propellers operating, preferably at the ship propulsion point. Also,

since the undeflected rudder contributes significantly to the derivatives the model tests should also include the rudder in the amidship position.

The technique just described can also be used to determine the control derivatives  $Y_\delta$  and  $N_\delta$ . If in Fig. 31 the model were oriented with zero angle of attack,  $\beta$ , to the flow but the model were towed down the tank at various values of rudder angle  $\delta_R$ , the dynamometer measurements would determine the force  $Y$  and the moment  $N$  as a function of rudder angle. Plots of these against rudder angle would thus indicate the values of the derivatives  $Y_\delta$  and  $N_\delta$ . In addition to these important data, comparison of the values of  $Y_\delta$  and  $N_\delta \delta_R$  obtained by this means at any given rudder angle with the values obtained from Equation (120) at  $\beta_R = 0$  using isolated control-surface lift and drag data would indicate the magnitude of the interaction effects arising because of the close proximity of the rudder to the hull.

Straight-line tests in a towing tank can also be used to determine the cross-coupling effect of  $v$  on  $Y_\delta$  and  $N_\delta$  and of  $\delta_R$  on  $Y_v$  and  $N_v$ . While such information is inadmissible within the context of the linear theory, it is important for the nonlinear theory. Also for the purpose of this theory, knowledge of the shape of the  $Y$  versus  $\delta_R$ ,  $Y$  versus  $v$ ,  $N$  versus  $\delta_R$  and  $N$  versus  $v$  curves at large values of  $v$  and  $\delta_R$  will be of importance.

**8.4 Rotating-Arm Technique.** To measure the rotary derivatives  $Y_r$  and  $N_r$  on a model, a special type of towing tank and apparatus called a rotating-arm facility is occasionally employed. In this facility, an angular velocity is imposed on the model by fixing it to the end of a radial arm and rotating the arm about a vertical axis fixed in the tank as seen in Fig. 32. The model is oriented with its  $x$ -axis and  $z$ -axis normal to

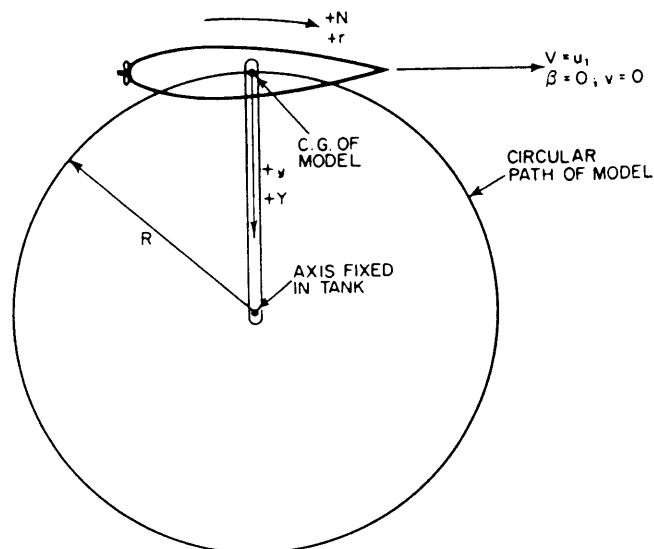


Fig. 32 Orientation of model in rotating-arm facility to determine  $Y_r$  and  $N_r$  (Abkowitz, 1964)

the radial arm and it is attached to the arm preferably at the model's midlength. As a result of this particular orientation, as the model revolves about the tank axis, rotates at rate  $r$  while its transverse velocity component  $v$  is at all times zero (yaw angle of attack  $\beta = 0$ ), and its axial velocity component  $u_1$  is identical to its linear speed. The model is rotated at a constant linear speed at various radii,  $R$ , and a dynamometer measures the force  $Y$  and the moment  $N$  acting on the model. Since the angular velocity  $r$  is given by

$$r = \frac{u_1}{R}$$

the only way to vary  $r$  at constant linear speed is to vary  $R$ . Typical plots of the resulting measurements (after model inertial effects are deducted) are shown in Fig. 12 and the derivatives  $Y_r$  and  $N_r$  are obtained by evaluating the slopes at  $r = 0$ . Because of ship symmetry, the values of  $Y_r$  and  $N_r$  at the negative values of  $r$  shown in Fig. 12 are a reflection of their values at positive  $r$  but with opposite sign.

The model must be ballasted so that it floats at the proper draft and trim. Since the rotating-arm tests are conducted with  $\dot{r} = 0$ , the results of rotating-arm tests are independent of the model radius of gyration. If the radial arm shown in Fig. 32 is attached to the model at its midlength, a distance  $x_G$  from the longitudinal center of gravity of the model, then the dynamometer measurements will yield values for  $(N_r - \Delta x_G u_1)$  and

$(Y_r - \Delta u_1)$ . Since values of  $\Delta$ ,  $x_G$  and  $u_1$  are known for the model, the dynamometer measurements can be used to determine the hydrodynamic derivatives  $N_r$  and  $Y_r$ . Values of these hydrodynamic derivatives for the full-scale ship can be determined from their nondimensional values. For the same reasons as indicated in the model tests for  $N_v$  and  $Y_v$ , the model used in the rotating-arm tests should have the rudder in the amidship position and the propellers operating at the ship propulsion point.

In contrast to the results of the towing tank test for  $Y_v$  and  $N_v$ , the results of the rotating-arm tests are dependent on the location of the center of gravity of the model. If, however, the procedure described in the preceding paragraph is followed, the model center of gravity need not be located at the same geometrical position as the  $G$  of the ship. The latter position is, of course, dependent on the condition of loading of the ship and needs to be known for insertion in the equations of motion of the full-scale ship. If the radial arm shown in Fig. 32 is not attached to the model at the midlength, the results should be corrected to the midlength position.

The rotating-arm facility can also be used to determine  $Y_v$  and  $N_v$  as well as  $Y_r$  and  $N_r$ . This is accomplished by towing the model at a variety of values of  $\beta$  for each  $r$ -value, not just at  $\beta = 0$  as in Fig. 32. These tests should include both plus and minus values of  $r$ . By cross plotting the values of  $Y_v$  and  $N_v$  obtained at each  $r$ -value against  $r$ , the values of  $Y_v$  and  $N_v$  at  $r = 0$  can be obtained. Within the range of values of

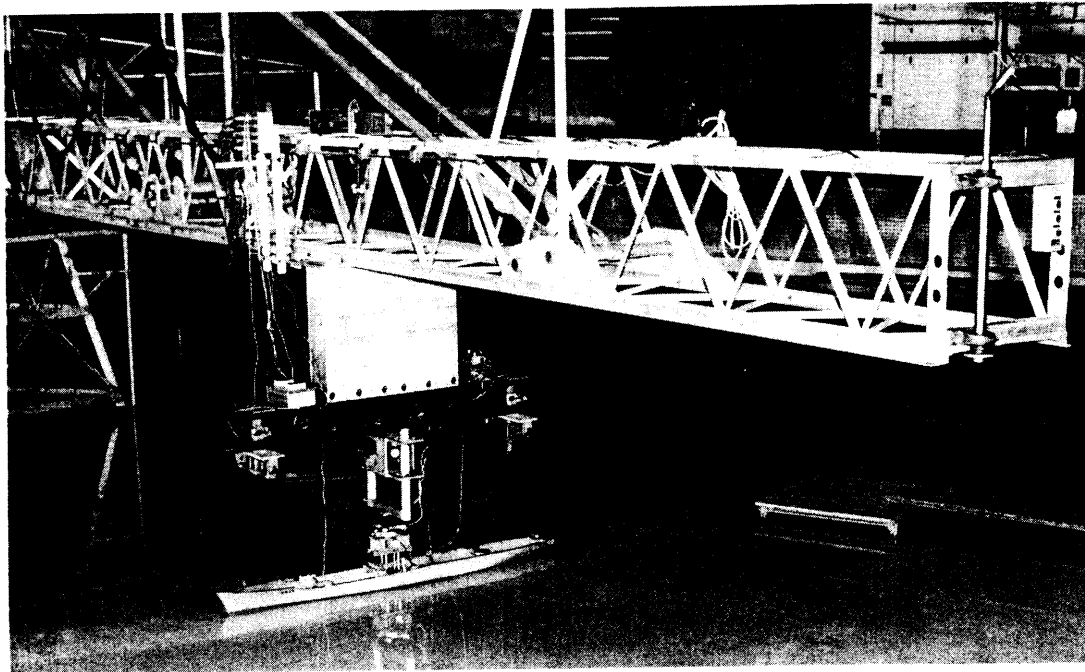


Fig. 33 Rotating Arm Facility at Davidson Laboratory, Stevens Institute, is the first of its kind, is about 22m (70 ft) in diameter

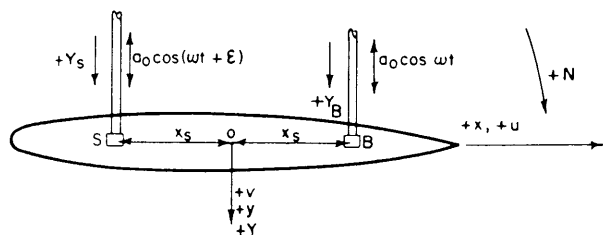


Fig. 34 Model setup for planar motion tests (Abkowitz, 1964)

$r$  in which linear theory is applicable, this cross plot should show that  $Y_v$  and  $N_v$  are substantially independent of  $r$ . Values of the control derivatives  $Y_\delta$  and  $N_\delta$  can also be obtained from rotating-arm tests in a manner exactly analogous to that just described for  $Y_v$  and  $N_v$ . Unfortunately values of  $Y_\delta$ ,  $N_\delta$ ,  $Y_v$  and  $N_v$  obtained in this manner do not always agree with values obtained from straight-line tests.

For the purposes of the nonlinear theory discussed in Sections 8.1 and 8.6, the rotating-arm facility can provide not only values of the hydrodynamic forces and moments at large values of  $r$ ,  $v$ , and  $\delta_R$  but also information on the cross coupling between these three parameters. Furthermore, with sufficient components the dynamometer used in the rotating-arm experiments can also be used to measure the  $X$ -force and the roll moment,  $K$ , as a function of  $r$ ,  $v$  and  $\delta_R$ . These are needed with nonlinear theory to predict speed loss and heel during maneuvers. If the model at the end of the rotating arm is tested at various heel angles,  $\phi$ , as well as at various values of  $r$ ,  $v$ , and  $\delta_R$ , the nonlinear effects of heel and the cross-coupling effects between  $\phi$ ,  $r$ ,  $v$  and  $\delta_R$  can be obtained.

A major drawback associated with rotating-arm tests is that they require a specialized facility of substantial size; they cannot be conducted in the long narrow tank conventionally used for resistance and propulsion testing. There are only a few rotating-arm facilities in the world. The largest in this country is at the David Taylor Research Center, Carderock, Md., with a diameter of 80 m (260 ft). See Fig. 33 for a view of the apparatus at Davidson Laboratory.

Other problems associated with the rotating-arm technique are:

(a) The model must be accelerated and data obtained within a single revolution. Otherwise, the model will be running in its own wake and its velocity with respect to the fluid will not be accurately known.

(b) In order to obtain values of the derivatives  $Y_r$ ,  $N_r$ ,  $Y_v$  and  $N_v$  at  $r = 0$ , data at small values of  $r$  are necessary. This means that the ratio of the radius of turn,  $R$ , to the model length,  $L$ , should be large. For large models, a large facility is required. Smaller models may use a smaller tank, but models too small will lead to scale effects in the ship prediction.

**8.5 Planar Motion Mechanism ("PMM") Technique.** In order to avoid the large expense of a ro-

tating arm facility, a device known as a Planar Motion Mechanism (PMM) was developed for use in the conventional long and narrow towing tank to measure the velocity-dependent derivatives,  $Y_v$  and  $N_v$ , the rotary derivatives  $Y_r$  and  $N_r$ , as well as the acceleration derivatives  $N_{\dot{r}}$ ,  $Y_{\dot{r}}$ ,  $Y_{\dot{v}}$  and  $N_{\dot{v}}$ . This apparatus, described by Gertler (1959) and Goodman (1960), was developed at the David Taylor Research Center to determine submarine derivatives in the horizontal and vertical planes. Subsequently by similar devices, described by Strom-Tejsen (1964), Paulling and Sibyl, (1962), and Van Leeuwen (1964), were developed elsewhere for surface ship models.

Basically the PMM consists of two oscillators, one of which produces a transverse oscillation at the bow and the other a transverse oscillation at the stern while the model moves down the towing tank at a constant velocity  $u_0$  as measured along the centerline of the towing tank. The subscript zero is used here to designate the velocity component measured along the  $x_0$ -axis fixed in the earth, i.e., in the towing tank. Therefore, the magnitude of the resultant velocity vector  $V$  of the model is not strictly speaking a constant in the planar motion tests. However, for the small motions admissible within linear theory,  $V \approx u_0$ .

The PMM, however, is more than a mechanical means of oscillating a model in a prescribed manner. The transducers used to measure the forces on the model, and the special instrumentation required for the proper resolution of the forces, are vital parts of the PMM.

The setup for planar motion tests is shown in Fig. 34. Near the bow a point  $B$ , located a distance  $x_s$  forward of the origin  $O$ , (preferably taken at  $\infty$ ) is oscillated transversely with a small amplitude  $a_0$  and at angular frequency  $\omega$ . Point  $S$  near the stern at an identical distance,  $x_s$ , aft of the origin is oscillated transversely with the same amplitude,  $a_0$ , and the same frequency,  $\omega$ . The phasing of the oscillation of the stern relative to that of the bow can be adjusted and is indicated by the phase angle  $\epsilon$ . If  $\epsilon = 0$ , the model

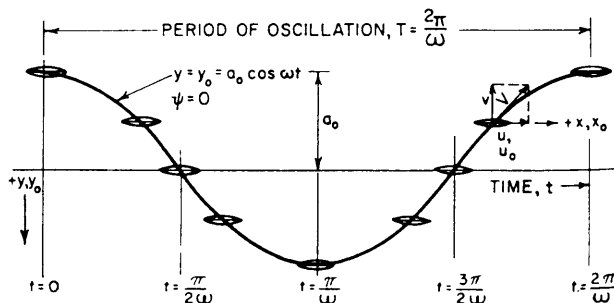


Fig. 35 Path and orientation of model from determining velocity and linear acceleration dependent derivatives—pure sway motion (Abkowitz, 1964 and Gertler, 1959)

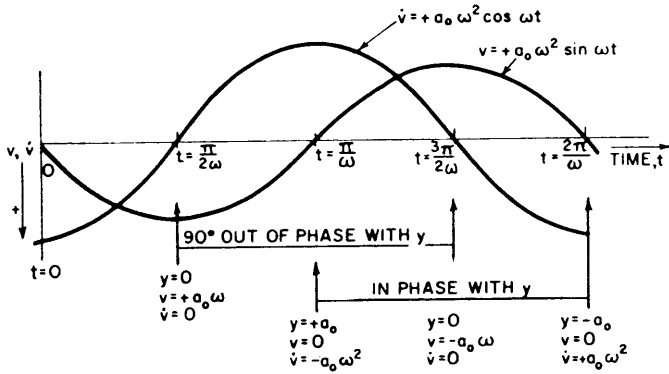


Fig. 36 Transverse linear velocity and acceleration of model corresponding to Fig. 35 (Abkowitz, 1954 and Gertler, 1959)

experiences an oscillation in pure sway with zero yaw, as shown in Fig. 35. The sway oscillation is of the form:

$$y_0 = y = a_0 \cos \omega t$$

$$\frac{dy}{dt} = v = -a_0 \omega \sin \omega t \quad (45)$$

$$\frac{d^2y}{dt^2} = \dot{v} = -a_0 \omega^2 \cos \omega t$$

Two dynamometers located at  $B$  and  $S$  in Fig. 34 measure the oscillatory  $Y$ -forces experienced by the model as a result of its swaying motion. These are the forces,  $Y_B$  and  $Y_S$ . As shown in Equation (45), the velocity  $v$  is a sine function, 90 deg out of phase with the displacement  $y_0$ , (or  $y$ ) and the acceleration,  $\dot{v}$ , both of which are cosine functions. Hence the measurements of  $Y_B$  and  $Y_S$  taken when the time variable has values 90 deg out of phase with the displacement,  $y_0$ , are forces arising from the effects of  $v$  and not from the effects of  $\dot{v}$  since the latter is zero at these times. This is shown in Fig. 36. The velocity-dependent derivatives  $Y_v$  and  $N_v$  are then obtained from the following relationships:

$$Y_v = \frac{\partial Y}{\partial v} = \pm \frac{(Y_B)_{out} + (Y_S)_{out}}{-a_0 \omega} \quad (46)$$

$$N_v = \frac{\partial N}{\partial v} = \pm \frac{[(Y_B)_{out} - (Y_S)_{out}]x_s}{-a_0 \omega}$$

where the subscript "out" refers to the amplitudes of  $Y_B$  and  $Y_S$  taken 90 deg out of phase with the displacement  $y_0$ .

For both  $Y_v$  and  $N_v$ , the positive sign in front of the expression should always be associated with the case when  $Y_B$  is positive and the negative sign when  $Y_B$  is negative. This is necessary because the amplitude  $a_0$  and the frequency  $\omega$  are always taken as positive val-

ues and, as was shown in Section 4.2,  $Y_v$ , for example, is always negative. Because of the oscillatory nature of both  $Y_B$  and  $Y_S$ , they can be either positive or negative, hence the alternate sign designation is essential. The sign of  $N_v$ , which can be either positive or negative, will be determined from Equation (46) according to whether the absolute magnitude of  $Y_B$  is greater or less than  $Y_S$ . If  $Y_B$  is greater,  $N_v$  will be negative and vice versa. With the PMM, the proper signs are obtained directly by establishing a given sign convention initially in the electronic measuring equipment.

In order to obtain the coefficients of the linear acceleration terms of Equation (10), the in-phase amplitudes of  $Y_B$  and  $Y_S$  must be measured, since, as shown in Fig. 36, these correspond to the times when  $\dot{v}$  is a maximum and  $v = 0$ . The relationships for these coefficients are:

$$Y_v - \Delta = \pm \frac{(Y_B)_{in} + (Y_S)_{in}}{-\omega^2 a_0} \quad (47)$$

$$N_v - \Delta x_G = \pm \frac{[(Y_B)_{in} - (Y_S)_{in}]x_s}{-\omega^2 a_0}$$

where the subscript "in" refers to the amplitudes of  $Y_B$  and  $Y_S$  taken in phase with the displacement,  $y_0$ .

The remarks concerning the use of the  $\pm$  signs made with regard to Equation (46) apply also to Equation (47) as well as to Equation (49) to be developed subsequently.

In order to obtain the rotary derivatives  $Y_r$  and  $N_r$  from planar motion tests, the measurements must be made when  $\dot{r} = 0$ ,  $v = 0$ , and  $\dot{v} = 0$ . Similarly for  $Y_r$  and  $N_r$ , the measurements must be taken when  $r = 0$ ,  $v = 0$ , and  $\dot{v} = 0$ . In order to impose an angular velocity and an angular acceleration on the body with  $v$  and  $\dot{v}$  both equal to zero, the model must be towed down the tank with the centerline of the model always tangent to its path, Fig. 37. This means that the  $v$ -component of the resultant velocity,  $V$ , is always zero, which is not the case in the situation shown in Fig. 35. However, the velocity, which strictly speaking is held constant in the experiment depicted by Fig. 37, is  $u_0$  just as it was in Fig. 35.

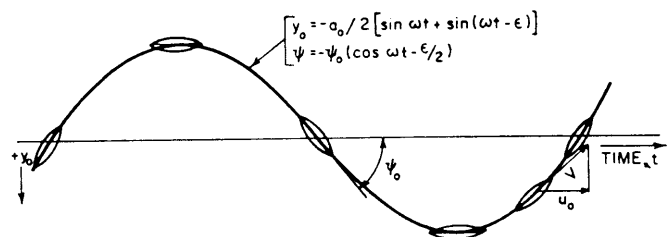


Fig. 37 Path and orientation of model for determining rotary and angular acceleration dependent derivatives—pure yawing motion (Abkowitz, 1964 and Gertler, 1959)

Whereas the motion shown in Fig. 35 is pure sway with zero yaw, that shown in Fig. 37 is pure yaw with zero sway, since sway is defined as a translation along the  $y$ -axis fixed in the model. Since  $r$  is set equal to zero for all time in Fig. 37, there is no motion along the  $y$ -axis fixed in the model; only along the  $y_0$ -axis fixed in the towing tank and shown as the ordinate of Fig. 37. Since the  $y$ -axis is constantly oscillating in direction in Fig. 37, the ordinate of that figure can be identified only as the  $y_0$ -axis whereas in Fig. 35, the ordinate could be identified as both the  $y_0$  and  $y$ -axes.

In order to achieve the kind of motion shown in Fig. 37, it has been shown by Goodman (1960) that the phase angle  $\epsilon$  between the bow and stern oscillators (see Fig. 34) must satisfy the condition:

$$\cos \epsilon = \frac{1 - \left(\frac{\omega x_s}{u_0}\right)^2}{1 + \left(\frac{\omega x_s}{u_0}\right)^2}$$

which is equivalent to the simpler expression:

$$\tan \epsilon/2 = \frac{\omega x_s}{u_0}$$

where  $x_s$  in both cases is the distance from the origin of the model to each oscillator.

The yaw oscillation shown in Fig. 37 is of the form:

$$\begin{aligned}\psi &= -\psi_0 \cos(\omega t - \epsilon/2) \\ \dot{\psi} &= r = +\psi_0 \omega \sin(\omega t - \epsilon/2)\end{aligned}\quad (48)$$

$$\ddot{\psi} = \dot{r} = +\psi_0 \omega^2 \cos(\omega t - \epsilon/2)$$

where  $\psi_0$  is the amplitude of the yaw oscillation. In Equation (48),  $r$  is out of phase with  $\psi$  and  $\dot{r}$  is in phase with  $\psi$ . Therefore, the amplitudes of  $Y_B$  and  $Y_S$  measured 90 deg out of phase with  $\psi$  will determine the force and moment due to rotation,  $r$ , and the amplitudes of  $Y_B$  and  $Y_S$  measured in phase with  $\psi$  will determine the force and moment due to angular acceleration,  $\dot{r}$ . The force and moment derivatives with respect to  $r$  and  $\dot{r}$  are then expressed as follows:

$$\begin{aligned}Y_r - \Delta u_1 &= \pm \frac{(Y_B)_{\text{out}} + (Y_S)_{\text{out}}}{-\psi_0 \omega} \\ N_r - \Delta x_G u_1 &= \pm \frac{[(Y_B)_{\text{out}} + (Y_S)_{\text{out}}] x_s}{-\psi_0 \omega} \\ Y_{\dot{r}} - \Delta x_G &= \frac{\pm [(Y_B)_{\text{in}} + (Y_S)_{\text{in}}]}{-\psi_0 \omega^2} \\ N_{\dot{r}} - I_z &= \frac{\pm [(Y_B)_{\text{in}} - (Y_S)_{\text{in}}] x_s}{-\psi_0 \omega^2}\end{aligned}\quad (49)$$

where the amplitude of the yaw oscillation  $\psi_0$  as well as the frequency  $\omega$  are always taken as positive.

The last equation shows that the results of the PMM tests are dependent on the model mass moment of inertia, and, hence its radius of gyration, as well as on the distance  $x_G$ . The procedure described in Section 8.4 for expanding the results of rotating-arm tests to the full scale in the event that  $x_G/L$  is not the same between model and ship applies to the results of the PMM tests in the event that neither  $x_G$  nor the radius of gyration is scaled properly. Thus, the longitudinal radius of gyration of the model need not be proportional to that of the ship. The model must, of course, be ballasted to the proper draft and trim and it should be self-propelled at the ship propulsion point with the rudder, in the amidship position, included.

Caution is necessary in using the results of planar motions tests. Since the ship model is at the water surface, its oscillatory motions create waves whose properties depend on the frequency of wave generation. By testing at various frequencies with the PMM the frequency dependence of the derivatives can be determined. However, for many problems in maneuvering, we are most interested in zero or very low frequencies. For example, the maneuver of a ship going into a turn is at zero frequency. To determine the values of the derivatives at zero frequency from planar motion tests, it is necessary to plot the derivatives against frequency and to extrapolate to zero frequency; hence, the desirability of testing at low frequencies. However, for many problems, including transient maneuvers and motions in rough seas, we are extremely interested in the extent to which the hydrodynamic derivatives are in fact frequency dependent. For this information the planar motion tests are indispensable. Van Leeuwen (1964) presents extensive plots of the hydrodynamic derivatives of a Series 60,  $C_B = 0.70$ , model as a function of both frequency of oscillation and ship speed.

It should be noted that the values of the derivatives determined either in straight-line tests in the towing tank or on a rotating-arm facility are the values at zero frequency of oscillation. These should correspond to the values obtained from planar motion tests extrapolated to zero frequency.

The PMM, like the rotating arm, can also be used to determine nonlinear and cross-coupling effects which are essential for the prediction of nonlinear maneuvers. Sample results from PMM experiments relating  $Y$  and  $N$  to simultaneously large values of  $\beta$  and  $\delta_R$  are shown in Fig. 38 and related to the nonlinear equations of motion in Section 8.6. Similar results can also be obtained from the PMM not only relating  $Y$  and  $N$  to  $r$  as well as  $\beta$  and  $\delta_R$ , but also relating the longitudinal force  $X$  to  $\beta$ ,  $\delta_R$ , and  $r$ . The PMM like the rotating arm can also be used to determine the rolling moment,  $K$ , as a function of  $\beta$ ,  $\delta_R$ ,  $r$ , and  $\phi$ .

The use of model test data immediately suggests

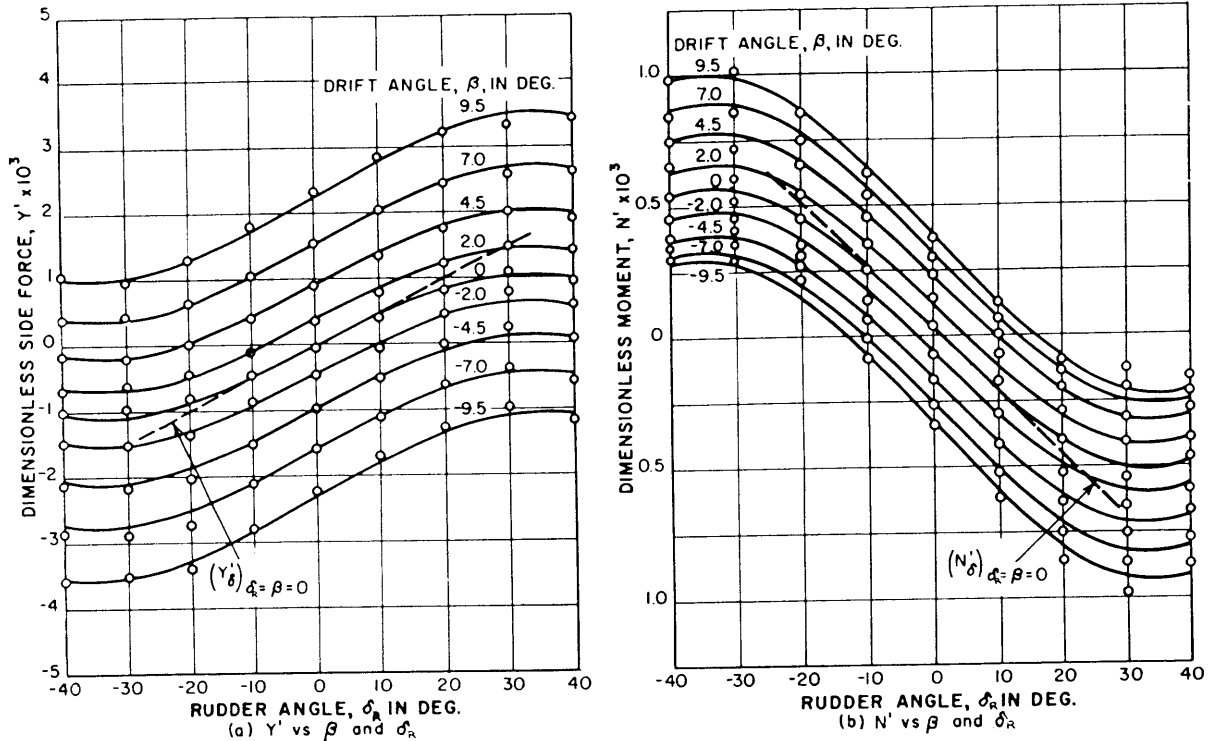


Fig. 38  $Y$  and  $N$  versus  $\beta$  and  $\delta$  for Mariner-class model (Chislett and Strom-Tejse, 1965). Curves fitted to experimental values by least-squares technique

the possibility of scale effects as introduced in the discussion of free-running models (Section 7.2). If the Froude number is satisfied, the Reynolds number will not be satisfied. However, in determining the  $Y$ -forces and  $N$ -moments, lift and circulation effects are involved and it is shown in Section 14.2 that there is very little scale effect on the slope of lift coefficient versus angle of attack. However, separation or breakdown of lift does occur at lower angles of attack at lower Reynolds number. For example Fig. 38 does show a decrease in the values of  $Y$  and  $N$  at large values of  $\delta_R$ . This may be, but is not necessarily, evidence of stall. If the cause is stall, and it is suspected that stall in the full scale would occur at larger values of  $\delta_R$ , the data of Fig. 38 could be empirically corrected at large values of  $\delta_R$  before using the data for predicting nonlinear maneuvers. In this way, errors in predictions of maneuvering characteristics due to premature stall of the model may be minimized.

**8.6 Evaluation of the Coefficients of the Nonlinear Equation of Motion.** All of the derivative coefficients of Equations (36), (37), and (38) with the exception of some of those involving  $u$  are best evaluated on the basis of experimental data obtained from captive model tests. For example, from experimental data like those given in Fig. 38 relating  $Y'$  and  $N'$  to  $\delta_R$  and  $\beta$ , all of the derivatives involving  $\delta_R$  and  $v'$  in Equations (37) and (38) may be determined. Similar experimental

data for  $X$  as a function of  $\delta_R$  and  $\beta$  can also be used to determine all of the derivatives involving  $\delta_R$  and  $v'$  in Equation (36).

Starting with  $Y'_\delta$  and  $Y'_{\delta\delta}$ , the first step is to evaluate the coefficients  $e_1$  and  $e_3$  of the polynomial Equation (35a) so that it forms the best least-squares fit to the curve through the experimental data given in Fig. 38(a) for  $\beta = 0$ . The coefficients,  $e_1$  and  $e_3$ , are related to  $Y'_\delta$  and  $Y'_{\delta\delta}$  as follows through Equation (37):

$$e'_1 = Y'_\delta \text{ and } e'_3 = \frac{1}{6} Y'_{\delta\delta}$$

In an exactly analogous manner, the derivatives  $Y'_v$ ,  $Y'_{vvv}$ ,  $N'_\delta$ ,  $N'_{\delta\delta\delta}$ ,  $N'_v$ , and  $N'_{vvv}$  may be determined recollecting that  $v' = -\sin \beta$ . Similarly, the derivatives  $X'_{vv}$ ,  $X'_{vvv}$ , and  $X'_{\delta\delta}$  of Equation (36) can be determined by fitting Equations (32), (33), and (34) to experimental data relating  $X$  to  $\delta_R$  and  $\beta$ .

The cross-coupled derivatives involving  $\delta_R$  and  $v'$  may also be determined from data like those given in Fig. 38. For example, to determine  $Y'_{\delta vv}$ , the first step is to measure  $(Y'_\delta)_{\delta=0}$  from Fig. 38(a) for all given values of  $v' = -\sin \beta$ . The next step is to fit a polynomial to these values of  $Y'_\delta$  as a function of  $v'$ . Because all values of  $Y'_\delta$  are positive and also because of symmetry port and starboard,  $Y'_\delta$  is an even function  $v'$ ; i.e.,

$$Y'_\delta(v) = h'_2 v'^2 + h'_4 v'^4 + \dots$$

Table 2—Assessment of the Coefficients in the X-Equation

Variable	Coefficient	Value of Coefficients		Relative Importance of Coefficients (see note 1)	
		Mariner Class	Series 60, Model 5, 1, 1	Strom-Tejsen (1965)	Eda and Crane (1965)
$\dot{u}$	$\Delta' - X'_u$	+0.177	+0.175	A	B
$\delta u$	$X'_u$	-0.0253	—	A	
$\delta u^2$	$\frac{1}{2}X'_{uu}$	+0.00948	—	A	B
$\delta u^3$	$\frac{1}{6}X'_{uuu}$	-0.00217	—	A	
$v^2$	$\frac{1}{2}X'_{vv}$	-0.189	—	C	
$r^2$	$\frac{1}{2}X'_{rr} + m'x'_G$	+0.00379	—	C	
$\delta_R^2$	$\frac{1}{2}X'_{\delta\delta}$	-0.02	—	C	B
$v^2\delta u$	$\frac{1}{2}X'_{vvu}$	—	—	E	
$r^2\delta u$	$\frac{1}{2}X'_{rru}$	—	—	E	
$\delta_R^2\delta u$	$\frac{1}{2}X'_{\delta\delta u}$	—	—	E	
$vr_R$	$X'_{vr} + \Delta'$	+0.168	—	D	B
$v\delta_R$	$X'_{v\delta}$	+0.0196	—	D	
$r\delta$	$X'_{r\delta}$	0	—	D	
$vr\delta u$	$X'_{vru}$	—	—	E	
$v\delta_R\delta u$	$X'_{v\delta u}$	—	—	E	
$r\delta_R\delta u$	$X'_{r\delta u}$	—	—	E	
—	$(X^0)'$	0	—	D	B

NOTE 1 The symbols used in these two columns have the following meanings:

A — Evaluated and deemed important.

B — Evaluated but no opinion as to importance.

C — Evaluated and deemed of minor importance.

D — Evaluated and deemed negligible.

E — Considered but not evaluated since deemed negligible.

No entry in these columns means the coefficient was ignored.

NOTE 2 All derivatives are nondimensionalized on basis of  $\rho$ ,  $L$ ,  $T$ , and  $V$ .

where  $h'_2 = \frac{1}{2}Y'_{\delta vv}$ ,  $h'_4 = 0$  for a third-order expansion. For  $Y'_{v\delta\delta}$ , the first step is to measure  $(Y'_v)_{v=0}$  at all given values of  $\delta_R$  on Fig. 38 and then proceed in the same way as described for  $Y'_{\delta vv}$ ; similarly for  $N'_{v\delta\delta}$  and  $N'_{\delta vv}$ . The cross-coupled derivatives  $X'_{vr}$ ,  $X'_{v\delta}$  and  $X'_{\delta r}$  can also be similarly determined from experimental data relating  $X$  to  $\delta_R$  and  $\beta$ .

Fig. 38 applies only to  $r' = 0$ . Data like these can be obtained for all values of  $r'$  from either rotating-arm or PMM tests. Given all these additional experimental data, all the coefficients of Equations (37) and (38) involving  $v$ ,  $\delta_R$ , and  $r$  may be derived. In addition,  $(Y^0)'$  of Equation (37) is the value of  $Y'$  at  $\beta = \delta_R = 0$  in Fig. 38(a) and  $(N^0)$  is the value of  $N'$  at  $\beta = \delta_R = 0$  in Fig. 38(b).

If, in addition, the prediction of heel angle during maneuvers is desired, experimental data like that shown in Fig. 38 are required, relating the rolling moment  $K$  to  $v$ ,  $\delta_R$ ,  $r$  and the heel angle  $\phi$ . The feasibility of obtaining these data was discussed in Section 8.4 and 8.5.

The coefficients of the equation expressing the re-

lationship between  $X$  and  $u$  are best determined from the results of open-water propeller tests and ship resistance data rather than from either rotating-arm or PMM tests. The reasons for this are outlined in the following.

As long as a ship is moving in a straight line at constant speed,  $V = u_1$ , the following relationship is true:

$$X = T(1 - t) - R = 0$$

where

$T$  = propeller thrust

$t$  = thrust deduction coefficient

$R$  = total ship resistance

This equilibrium condition defines the initial propeller thrust and the corresponding propeller torque and revolutions. However, as soon as a maneuver is initiated, this equilibrium condition is disturbed and the  $X$ -force varies as a function of speed. While  $R$  and  $t$  as functions of speed may be obtained from ship resistance



Table 3—Assessment of the Coefficients in the Y-Equation

Variable	Coefficient	Value of Coefficients		Relative Importance of Coefficients (see note 1)	
		Mariner Class	Series 60, Model 5, 1, 1	Strom-Tejsen (1965)	Edu and Crane (1965)
$\dot{v}$	$(\Delta' - Y'_v)$	+0.327	+0.309	A	B
$\dot{r}$	$(\Delta' x'_G - Y'_r)$	-0.0018	—	A	
$v$	$Y'_v$	-0.244	-0.260	A	B
$v^3$	$\frac{1}{6} Y'_{vvv}$	-1.702	-2.15	C	B
$vr^2$	$\frac{1}{2} Y'_{vrr}$	0	-1.18	D	B
$v_\delta^2$	$\frac{1}{2} Y'_{v\delta\delta}$	-0.0008	—	D	
$v\delta u$	$Y'_{vu}$	—	—	E	
$v\delta u^2$	$\frac{1}{2} Y'_{vu u}$	—	—	E	
$r$	$(Y'_r - \Delta')$	-0.105	-0.0781	A	B
$r^3$	$\frac{1}{6} Y'_{rrr}$	0	-0.0461	D	B
$rv^2$	$\frac{1}{2} Y'_{rvv}$	+3.23	-0.0994	A	B
$r\delta_R^2$	$\frac{1}{2} Y'_{r\delta\delta}$	0	—	D	
$r\delta u$	$Y'_{ru}$	—	—	E	
$r(\delta u)^2$	$\frac{1}{2} Y'_{ru u}$	—	—	E	
$\delta_R$	$Y'_\delta$	+0.0586	+0.050	A	B
$\delta_R^3$	$\frac{1}{6} Y'_{\delta\delta\delta}$	-0.00975	—	C	
$\delta_R v^2$	$\frac{1}{2} Y'_{\delta vv}$	+0.25	—	C	
$\delta_R r^2$	$\frac{1}{2} Y'_{\delta rr}$	0	—	D	
$\delta_R \delta u$	$Y'_{\delta u}$	0	—	C	
$\delta_R (\delta u)^2$	$\frac{1}{2} Y'_{\delta u u}$	—	—	E	
$vr\delta_R$	$Y'_{vr\delta}$	0	—	D	
—	$(Y^0)'$	-0.0008	+0.00016	C	B
$\delta u$	$(Y_u^0)'$	0	—	D	
$(\delta u)^2$	$(Y_{uu}^0)'$	—	—	E	

and self-propulsion tests, the propeller thrust  $T$  as a function of  $u$  is dependent on the type of power plant and the power-plant settings that are maintained during a maneuver.

For example, a diesel engine is essentially a constant-torque machine whereas a turbine is a constant-power machine. When a diesel ship enters a maneuver there is therefore a decrease in RPM and hence in thrust. On a turbine-driven ship, any reduction in RPM is accompanied by an increase in torque; hence, the reduction in thrust in a maneuver is less than on a diesel ship (Fig. 44). These considerations governing the relationship between  $T$  and  $u$  are best taken account of by means of open-water propeller test data as shown in Strom-Tejsen (1965).

Data from Strom-Tejsen and Chislett (1964) for the Mariner Class model and from Eda and Crane (1965) for the Series 60, Model 5,1,1, corresponding most closely to the Mariner Class model are summarized in

Tables 2, 3 and 4. Both models are described in Table 5. An assessment of the importance of the various coefficients made in Strom-Tejsen (1965) is also contained in Table 4. The two references do not agree as to the importance of the various derivatives.

**8.7 Sample Results of Nonlinear Model-Predictions.** The overall precision of the nonlinear model-prediction technique as developed by Strom-Tejsen (1965) and utilizing PMM experimental data from Chislett and Strom-Tejsen (1965) is shown in Figs. 39, 40, and 41. A comparison is made in these figures between the results of full-scale turning tests, zigzag and spiral maneuvers conducted with a Mariner Class ship (Morse and Price, 1961) and the prediction of the identical maneuvers made in Chislett and Strom-Tejsen (1965). The overall agreement for all of these maneuvers is reasonably good except for the fact that the model prediction in Fig. 39 shows a small tendency to turn better to starboard whereas the full-scale ship shows

Table 4—Assessment of the Coefficients in the  $N$ -Equation

Variable	Coefficient	Value of Coefficients -		Relative Importance of Coefficients (see note 1)	
		Mariner Class	Series 60, Model 5-1-1	Strom-Tejsen (1965)	Eda and Crane (1965)
$\dot{v}$	$(\Delta'x'_G - N'_v)$	-0.00478	—	A	
$\dot{r}$	$(I'_g - N'_r)$	+0.0175	+0.0202	A	B
$v$	$N'_r$	-0.0555	-0.075	A	B
$v^3$	$\frac{1}{6}N'_{vvv}$	+0.345	-0.385	C	B
$vr^2$	$\frac{1}{2}N'_{vrr}$	0	-0.306	D	B
$v\delta_R^2$	$\frac{1}{2}N'_{v\delta\delta}$	+0.00264	—	D	
$v\delta u$	$N'_{vu}$	—	—	E	
$v\delta u^2$	$\frac{1}{2}N'_{vu u}$	—	—	E	
$r$	$(N'_r - \Delta'x'_G u)$	-0.0349	-0.0569	A	B
$r^3$	$\frac{1}{6}N'_{rrr}$	0	-0.101	D	B
$rv^2$	$\frac{1}{2}N'_{rvv}$	-1.158	-1.42	A	B
$r\delta^2$	$\frac{1}{2}N'_{r\delta\delta}$	0	—	D	
$r\delta u$	$N'_{ru}$	—	—	E	
$r\delta u^2$	$\frac{1}{2}N'_{ru u}$	—	—	E	
$\delta_R$	$N'_\delta$	-0.0293	-0.024	A	B
$\delta_R^3$	$\frac{1}{6}N'_{\delta\delta\delta}$	+0.00482	—	C	
$\delta_R v^2$	$\frac{1}{2}N'_{\delta vv}$	+0.1032	—	C	
$\delta_R r^2$	$\frac{1}{2}N'_{\delta rr}$	0	—	D	
$\delta_R \delta u$	$N'_{\delta u}$	0	—	C	
$\delta_R \delta u^2$	$\frac{1}{2}N'_{\delta u u}$	—	—	E	
$vr\delta_R$	$N'_{vr\beta}$	0	—	D	
—	$(N^0)'$	+0.00059	-0.0003	C	B
$\delta u$	$(N^0)'_u$	0	—	D	
$\delta u^2$	$(N^0)'_{uu}$	—	—	E	

a tendency to turn better to port. The results of the spiral maneuvers of Fig. 40 confirm these small opposite tendencies since, at zero rudder, the model prediction indicates a tendency to turn to starboard, whereas the ship tends to turn to port. This latter tendency is in accord with Section 17.9

Predicted data on the speed loss during the turning and zigzag maneuvers shown in Figs. 39 and 41 are shown in Figs. 42 and 43. Three conditions are shown on each figure: that corresponding to constant RPM, as prevails, for example, in the usual free-running model turning test; that corresponding to constant power, as for a turbine-driven ship; and that corresponding to constant torque, as for a diesel-driven ship. The RPM-speed relationships for these three cases are shown in Fig. 44. It is clear from these data that free-running model tests seriously underpredict the speed loss in a turn for either a turbine or diesel-driven ship, whereas the prediction method outlined in this section can accommodate realistically the effects of different power plants on the speed loss.

The ability of the nonlinear model technique to predict the spiral maneuvers of unstable ships is shown in Fig. 45. As noted in Section 4.3, these maneuvers cannot be predicted by linear theory. The derivatives

of the marginally stable ship were obtained by decreasing the magnitude of  $Y'_v$ ,  $Y'_r$ , and  $N'_r$  of the stable ship by 10 percent and increasing the magnitude of  $N'_v$  of the stable ship by 10 percent. Similarly, the derivatives of the unstable and very unstable ships correspond to 20 and 30 percent changes, respectively, from the stable ship. Also shown in Fig. 45 are the slopes of the  $r - \delta_R$  curves taken from Fig. 174 for these same ships. The dimensional slopes,  $\partial r / \partial \delta_R$ , shown are obtained from the nondimensional slopes,  $\partial r' / \partial \delta$ , given in Fig. 174 by multiplying the latter by  $V/L = 15 \times 1.689/528 = 0.479$ , where 161m (528 ft) is the length of the Mariner Class and 15 knots is the speed at  $\delta_R = 0$  deg. The slopes correlate nicely with the characteristics of the spiral maneuvers of the unstable ships as predicted by the nonlinear model techniques.

**8.8 Comparison of Experimental Techniques and Quasi-Steady Theory.** Much testing and correlation work has been accomplished with free running, and captive model tests over the years. Free running and captive model tests using a model of the Mariner-class cargo ship *SS Compass Island* for which extensive full-scale data are available (Morse and Price, 1961) have been collected and compared under the auspices

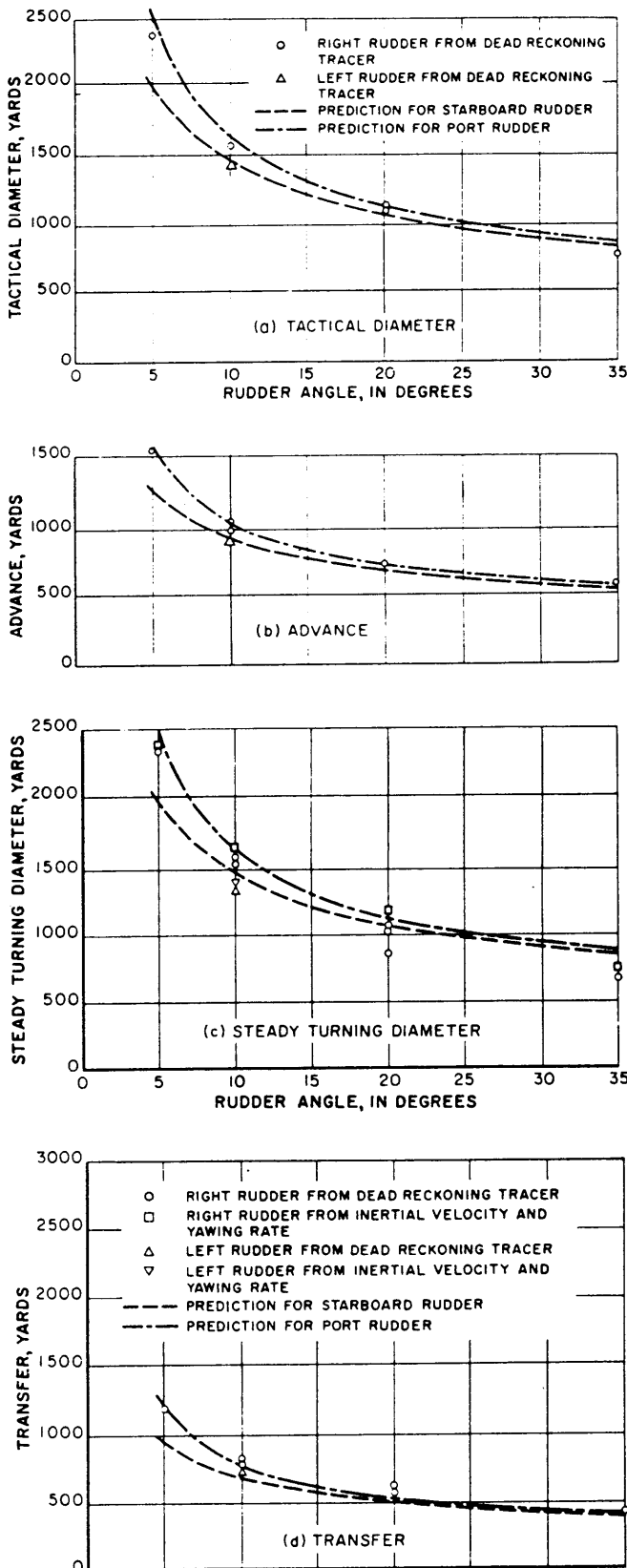


Fig. 39 Comparison of turning circles from full-scale trials and predictions from model tests; 15-knot approach speed (Chislett and Strom-Tejsen, 1965)

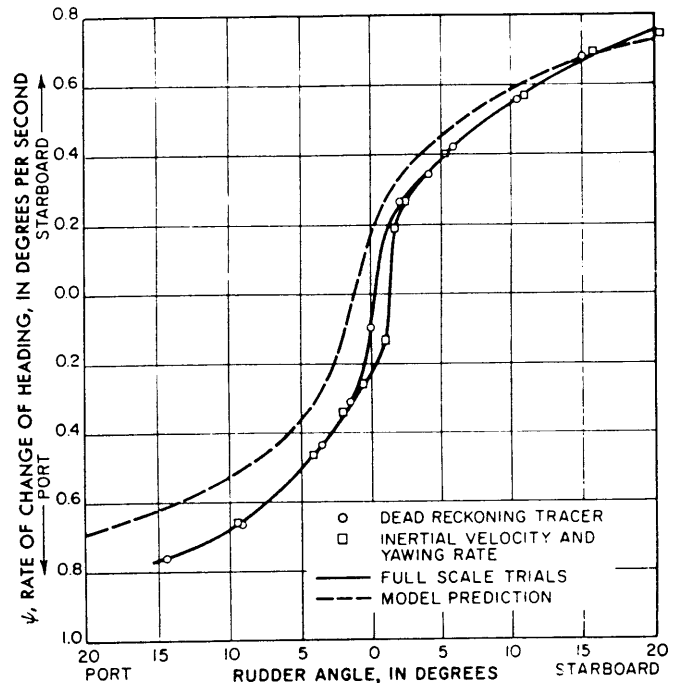


Fig. 40 Comparison of spiral results from full-scale trials and prediction from model tests; 15-knot approach speed (Chislett and Strom-Tejsen, 1965)

of the International Towing Tank Conference. Results of an investigative program concentrating on turning circles were reported at the Thirteenth Conference in 1972 with favorable comparisons. The measurements of the linear force derivatives by various model test towing tanks using the rotating arm and PMM testing facilities have also been studied.

Concern for frequency dependence in PMM testing and a desire to provide accurate predictions of extreme maneuvers, resulted in the development of larger amplitude PMMs (LAPMM) such as that used at the Danish tank. Smitt and Chislett (1974) Marine LAPMM results are compared with data from oblique towing tests and rotating arm tests (Smitt, 1975). This paper and a related one by Eda at the 1975 conference conclude that comparable linear force data from carefully conducted rotating arm and PMM tests are essentially identical for the Mariner hull form.

Development in the early 1970's of the high block ( $C_B$ ) tanker forms showing instability of flow around the ship stern caused concern for the effects of scale on maneuverability predictions. Numerous tests were consequently performed to verify the maneuvering capability of such forms. Nomoto and Fujii report on tests performed by several researchers addressing the scale problem (Burcher, 1975). Among the tests were those of Sato, et al (1973) who utilized a 30 meter free-running model in addition to 4 and 10 meter free running models to investigate scale effects.

Trials of the *Esso Osaka* discussed in Section 13 have paralleled the Mariner trials as a standard for

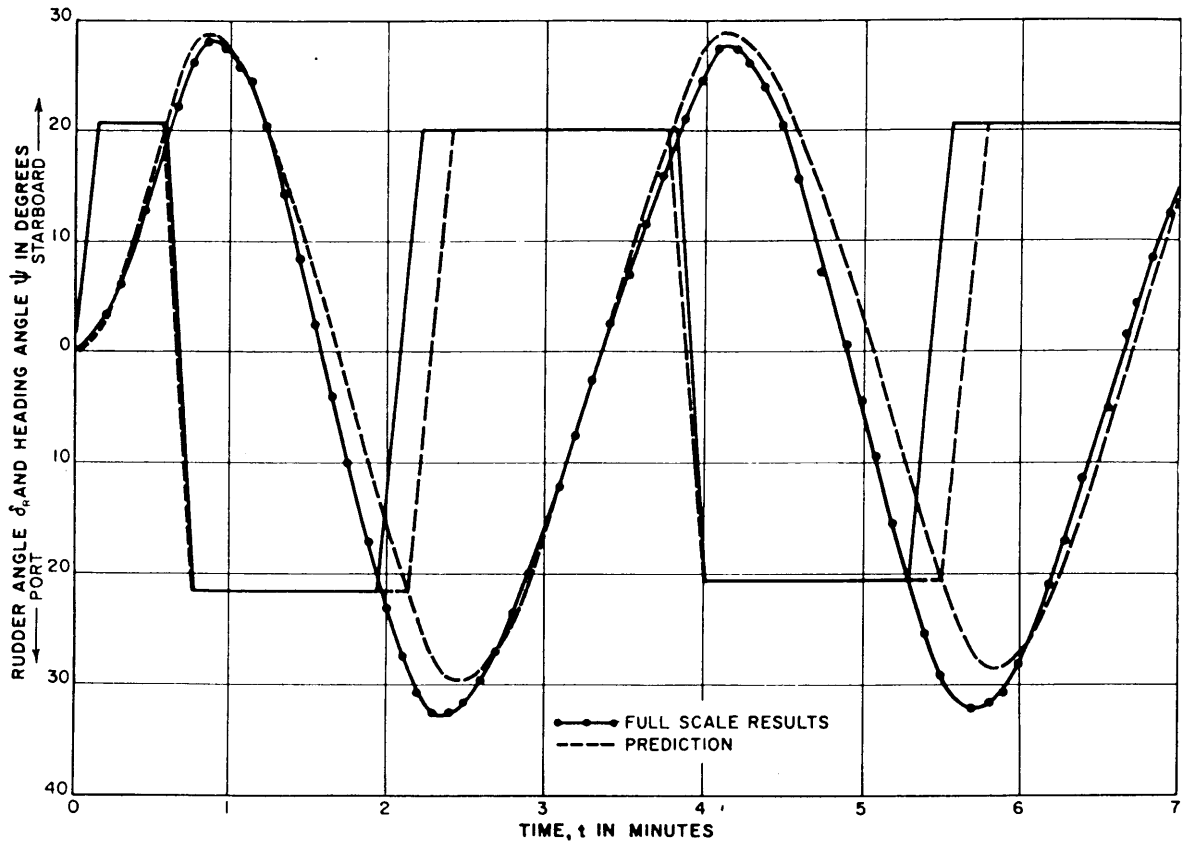


Fig. 41 Comparison of zigzag maneuver from full-scale trials and prediction from model tests; 15-knot approach speed (Chislett and Strom-Tejsten, 1965)

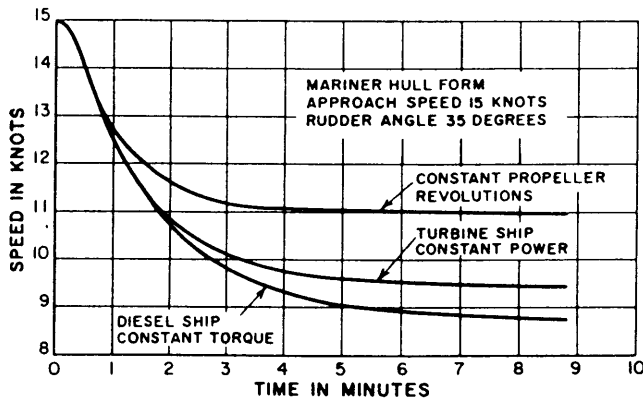


Fig. 42 Time history of velocity during transient and steady turning computed for different types of power plants (Strom-Tejsten, 1965)

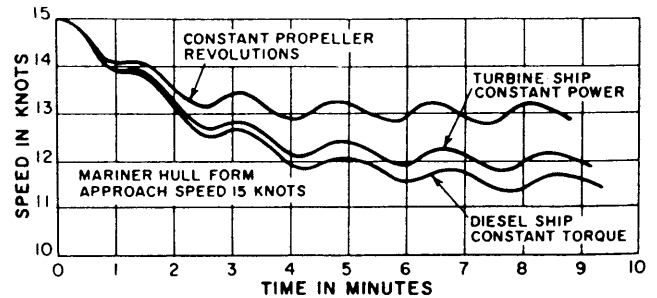


Fig. 43 Time history of velocity in zigzag maneuver computed for different types of power plants (Strom-Tejsten, 1965)

maneuvering prediction correlation of a full form in both deep and shallow water (Crane, 1979). Numerous model towing tanks have tested models of the *Osaka* with good correlation. See "Model Test," (1980), Dand and Hood, (1983) and others.

With regard to the validity of captive model tests, quasi-steady state theory is the basis upon which hydrodynamic conditions of steady motions are assumed to apply in transient conditions. Burcher (1975) and

Nomoto (1975) provide discussion of the applicability of the theory particularly with reference to the oscillatory derivatives obtained by PMM experiments where the motion is induced by rudder deflection. It is difficult to justify the quasi-steady assumption on purely theoretical grounds but the method has been widely used in hydrodynamics and aerodynamics and in practical terms appears to work.

The use of captive model test data to develop coefficients in motion equations is assumed to be valid according to the quasi steady state theory as long as the motion is "slow." An expression such as Equation

(12) for the forces due to sway motion, should be written with each variable as a function of time. Thus, these equations can be misleading if applied to ship and model motions indiscriminately. Bishop, Burcher and Price (1975) reported on investigations into the time history effect in captive ship model testing. Nomoto (1975) concludes that

$$\omega' = \frac{\omega L}{v} = 2 \text{ to } 2.5$$

may be the highest limit at which PMM tests can safely obtain the slow motion derivatives. The general indications concluded by Burcher are that frequency effects do not play a significant part in the steered motions of ships in calm water.

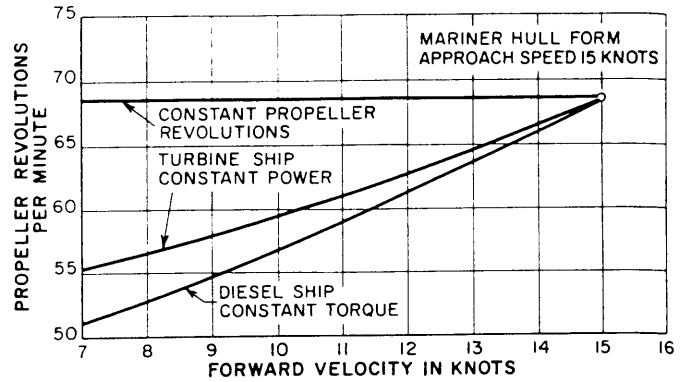


Fig. 44 Change of propeller revolutions as function of speed-loss in maneuvers for different types of power plants (Strom-Tejsen, 1965)

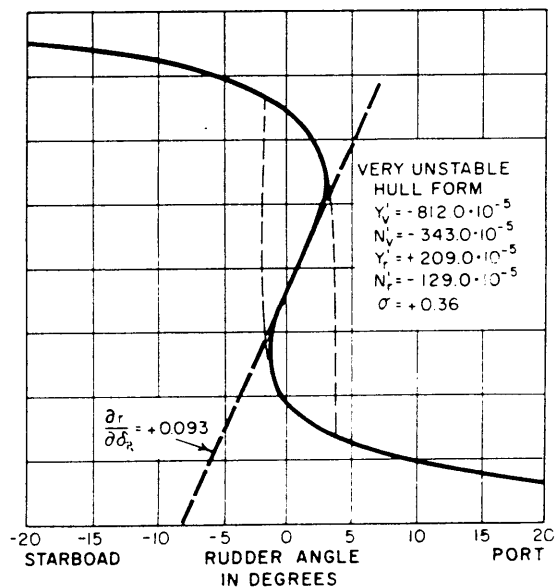
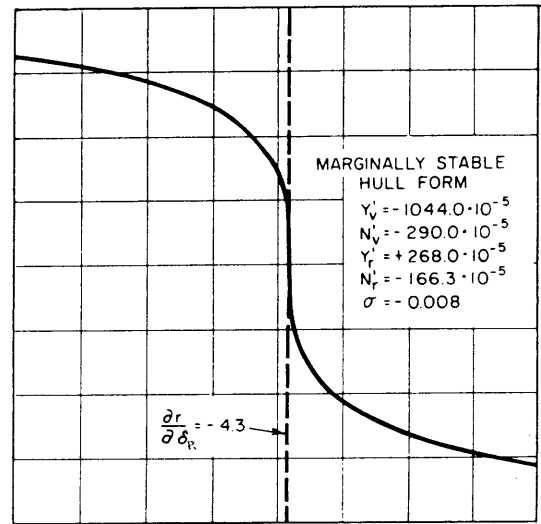
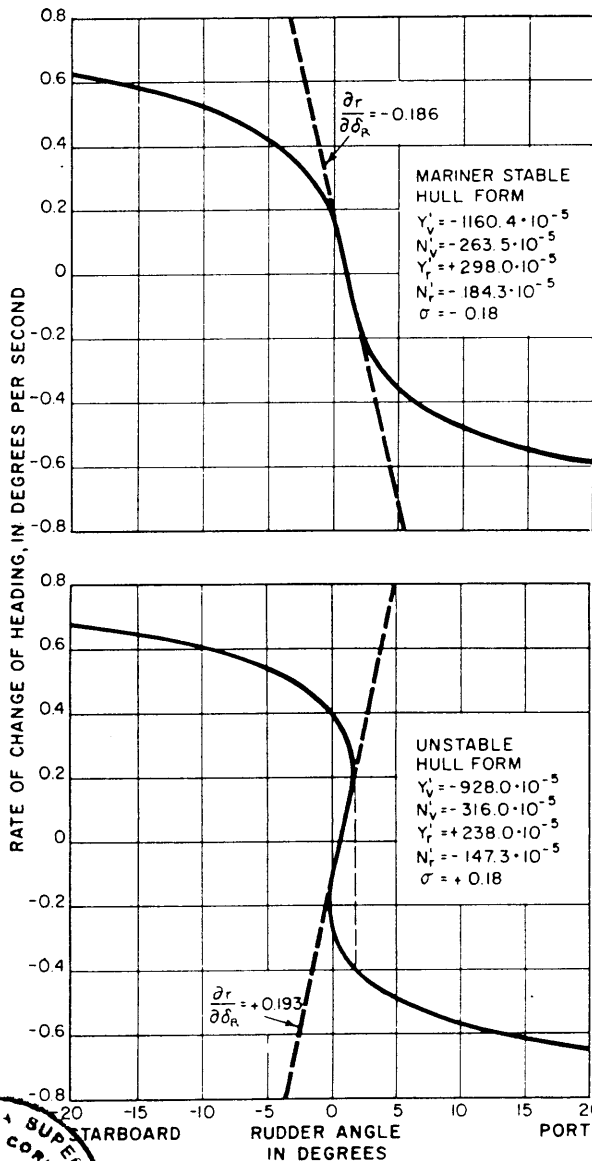


Fig. 45 Prediction of spiral maneuvers for stable, marginally stable, and unstable hull forms; 15-knot speed at  $\delta_e = 0$  deg (all derivatives nondimensionalized on basis of  $p, L, T$  and  $V$ ) (Strom-Tejsen, 1965)



## Section 9

### Theoretical Prediction of Hydrodynamic Coefficients and Systems Identification

**9.1 General.** While experimental techniques as described in Section 8 allow measuring forces and moments in the nonlinear as well as the linear range of motions, the theoretical prediction of these forces and moments has not yet been refined, particularly for the nonlinear range. This section introduces the theoretical development of hydrodynamic coefficients for the linear range. Current developments in the calculation of coefficients including the "systems identification" approach are summarized in this section.

One of the many assumptions made in linear theory is that the interference effects of the ship's hull on its appendages such as fixed fins and rudders and hull are negligible. While it is hard to justify this assumption on physical grounds and it is obviously not justified for tight maneuvers (see Section 6.4 and Fig. 22), it is shown in Section 6.4 that it and the other assumptions made in the linear prediction do lead to reasonable correlation with experimental data for small motions within the linear range.

**9.2 Contribution of Fixed Fins.** The contribution of a lifting surface or fixed fin located at the extremity of a ship's hull, several chord lengths from the origin of the ship, to the hydrodynamic derivatives of that hull will be considered first. Such a fin could be a rudder held in the amidship position, the ship's deadwood aft or a foil located anywhere along the ship length. Although the example treated deals with a fin a distance  $+x_f$  forward from the origin, the formulation resulting from the forthcoming analysis gives the effect of such a fin aft of the origin provided a negative value of  $x_f$  is used.

If the body and fin shown in Fig. 46 are initially travelling at a forward velocity  $u$ , and the body is given a transverse-velocity disturbance,  $+v$ , then the fin also experiences a transverse velocity of  $v_f = v$ . For small values of  $v_f$  relative to  $u$ , the angle of attack at the fin,  $\beta_f$ , in radians is

$$\beta_f = \frac{v_f}{u_f} \quad (50)$$

where  $u_f$  is the forward velocity of the fin, and the resultant velocity

$$V = u_f(1 + \beta_f^2)^{1/2} \approx u_f$$

The  $Y$ -force and the  $N$ -moment produced by the fin as a result of this angle of attack are given by

$$Y_f = \pm (L_f \cos \beta_f + D_f \sin \beta_f) \quad (51a)$$

$$N_f = Y_f x_f \quad (51b)$$

where  $L_f$  and  $D_f$  are the lift and drag forces on the fin. The signs of  $L_f$ ,  $D_f$ , and  $\beta_f$  are assumed to always be positive, hence, the necessity for the  $\pm$  signs.

The derivative of  $Y_f$  with respect to  $v_f$  taken at  $v_f = 0$  is the fin velocity-dependent force derivative,  $(Y_v)_f$ :

$$(Y_v)_f = - \left| (Y_\beta)_f \left( \frac{\partial \beta}{\partial v} \right)_f \right| \quad (52)$$

where the negative sign in association with the absolute magnitude symbol  $| |$  is necessary because as shown in Section 4.2,  $Y_v$  is always negative.

From Equation (50):

$$\left( \frac{\partial \beta}{\partial v} \right)_f = \frac{1}{u_f} \approx \frac{1}{V} \quad (53)$$

From Equation (51a)

$$(Y_\beta)_f = L_f \sin \beta_f - \left( \frac{\partial L}{\partial \beta} \right)_f \cos \beta_f - D_f \cos \beta_f - \left( \frac{\partial D}{\partial \beta} \right)_f \sin \beta_f$$

and for  $\beta_f = 0$

$$(Y_\beta)_f = - \left[ \left( \frac{\partial L}{\partial \beta} \right)_f + D_f \right] \quad (54)$$

The fin lift and drag can be expressed in terms of the lift and drag coefficients and the fin area,  $A_f$ , as follows (see also Section 14.1):

$$L_f = (C_L)_f (\rho/2) A_f V^2 \quad (55a)$$

$$D_f = (C_D)_f (\rho/2) A_f V^2 \quad (55b)$$

and from Equation (55a):

$$\left( \frac{\partial L}{\partial \beta} \right)_f = (\rho/2) A_f V^2 \left( \frac{\partial C_L}{\partial \beta} \right)_f \quad (56)$$

Substituting Equations (56) and (55b) into Equation (54) and Equations (54) and (53) into (52), one obtains finally for  $\beta_f = 0$ :

$$(Y_v)_f = - \left| (\rho/2) A_f V \left[ \left( \frac{\partial C_L}{\partial \beta} \right)_f + (C_D)_f \right] \right| \quad (57)$$

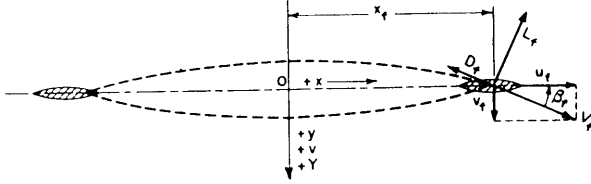


Fig. 46 Fin arrangement showing forces and velocities (Abkowitz, 1964)

Values of the lift-curve slope,  $\partial C_L / \partial \beta$ , needed for insertion in Equation (57), may be estimated from Equation (122b) of Section (14.5) or from Abbott and Doenhoff (1958). A much simpler expression of reasonable accuracy for very low aspect-ratio fins is the Jones' formula (Abbott and Doenhoff, 1958)

$$\frac{\partial C_L}{\partial \beta} = \left( \frac{\pi}{2} \right) a \text{ (per radian)}$$

where  $a$  is the effective aspect ratio. This relationship is compared to (122b) Fig. 137 where it is seen that for  $a < 0.5$  and for sweep angle  $\Lambda = 0$  the two relationships are in excellent agreement. (Note that the values of  $\partial C_L / \partial \alpha$  are per degree whereas values needed for insertion in Equation (57) are per radian.) The drag coefficient  $(C_D)_f$  at zero angle of attack may be estimated as essentially the skin-friction drag of the fixed fin; however, it is usually so small in relation to  $\partial C_L / \partial \beta$  that it is frequently ignored. Thus:

$$(Y_v)_f = - \left| (\rho/2) A_f V \left( \frac{\partial C_L}{\partial \beta} \right)_f \right| \left( \frac{\partial C_L}{\partial \beta} \text{ per radian} \right) \quad (58)$$

and, with draft  $T$  introduced

$$(Y_v)_f = - \left| \frac{(\rho/2) A_f V \left( \frac{\partial C_L}{\partial \beta} \right)_f}{(\rho/2) L T V} \right| = - \left| A'_f \left( \frac{\partial C_L}{\partial \beta} \right)_f \right|$$

Because of the prominence of the ship's draft,  $T$ , in the formulations of this and subsequent sections, it is often used in association with the ship's length,  $L$ , as a nondimensionalizing parameter.

Also, from Equation (51b)

$$(N'_v)_f = (Y'_v)_f x'_f \quad (59a)$$

from which it may be seen that  $(N'_v)_f$  is positive (and hence stabilizing according to Table 1) if the fin is aft of the origin ( $x'_f$  negative) and negative and destabilizing if the fin is forward of the origin.

The contribution of a fin to the derivatives  $Y'$ , and  $N'$ , is readily calculable from the expressions developed in Section 4.2. Noting that  $x_f$  in Fig. 46 is anal-

ogous to  $x_{\infty}$  in Fig. 9, and neglecting the fin derivatives taken about the fin's own midlength (which are negligibly small), it follows from Equation (13) that:

$$(Y'_r)_f = x'_f (Y'_v)_f \quad (59b)$$

and

$$(N'_r)_f = x'^2_f (Y'_v)_f \quad (59c)$$

Equations (59a, b, and c) show that the contributions of a fixed fin to the velocity-dependent moment derivative and to the rotary derivatives are all functions of the fin velocity-dependent force derivative  $(Y'_v)_f$ . Similarly, the contributions of a fixed fin to the acceleration derivatives of a ship's hull are functions of the acceleration-dependent force derivative of the fin,  $(Y''_v)_f$ . This derivative corresponds to the "added mass" of a flat plate for accelerations perpendicular to the plate and may be approximated as follows:

$$(Y''_v)_f = - \frac{\pi \rho b A_f}{(a_G^2 + 1)^{1/2}} \times \frac{1}{(\rho/2) L^2 T} = - \frac{2 \pi b' A'_f}{(a_G^2 + 1)^{1/2}} \quad (60)$$

where  $A_f$  is the area of the fin,  $b$  is the geometric span, and  $a_G$  is its geometric aspect ratio  $b^2/A_f$ . For a fin attached to a ship's hull so that its effective aspect ratio is  $2a_G$ , (60) becomes:

$$(Y''_v)_f = - \frac{2 \pi \rho b A_f}{(4 a_G^2 + 1)^{1/2}} \times \frac{1}{(\rho/2) L^2 T} = - \frac{4 \pi b' A'_f}{(a^2 + 1)^{1/2}} \quad (61)$$

from which it may be seen that for the limiting case of zero aspect ratio the "added mass" of a fin with its root chord adjacent to a bounding surface is twice that of the same fin without the bounding surface.

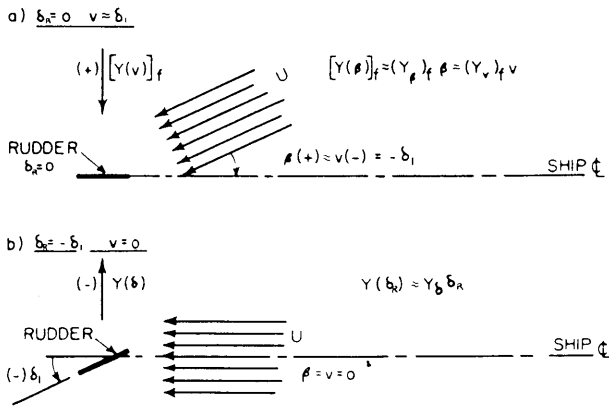
The expressions for the contributions to the other acceleration derivatives of a fixed fin remote from the origin of the ship to which it is attached are exactly analogous to Equations (59a, b, and c)

$$(N''_v)_f = x'_f (Y''_v)_f \quad (62a)$$

$$(Y''_r)_f = x'_f (Y''_v)_f \quad (62b)$$

$$(N''_r)_f = (x'_f)^2 (Y''_v)_f \quad (62c)$$

The magnitudes of the fin acceleration derivatives determined from Equations (61) and (62) are generally small and of minor significance compared to the fin velocity and rotary-dependent derivatives. The contribution that a fixed fin such as a rudder or deadwood makes to the latter derivatives is often decisive in determining whether a ship possesses control-fixed stability or not. This is further discussed in Section 16.2.

Fig. 47 Relationship between  $Y_\delta$  and  $(Y_v)_f$ .

**9.3 Prediction of the Control Derivatives.** By treating the fixed fin of the previous section as a control surface, values of the control derivatives  $Y_\delta$  and  $N_\delta$  can be computed in the same manner as the fixed fin contributions  $(Y_v)_f$  and  $(N_v)_f$ . It is clear from Fig. 47 that neglecting interference effects from the hull and the propellers, the net effect of both a drift angle  $\beta$  at the stern and a control-surface deflection angle  $\delta_c$  is to introduce an angle of attack on the control surface so that in both cases the slope of the nondimensional  $Y$ -force versus angle of attack can be computed as a product of  $A'_T$  and  $\partial C_L / \partial \alpha$ , that is,

$$(Y'_\beta)_f = A'_T \left( \frac{\partial C_L}{\partial \alpha} \right) \quad (63a)$$

and

$$Y'_\delta = A'_G \left( \frac{\partial C_L}{\partial \alpha} \right)_f \left( \frac{\partial C_L}{\partial \alpha} \text{ per radian} \right)$$

where  $\partial C_L / \partial \alpha$  may be estimated from Equation (122b). From the preceding

$$Y'_\delta = (Y'_\beta)_f$$

and since

$$\begin{aligned} Y'_\beta &= -Y'_v \\ Y'_\delta &= -(Y'_v)_f \end{aligned} \quad (63b)$$

And from Equation (59a) for  $x'_f = -\frac{1}{2}$

$$N'_\delta = -\frac{1}{2} Y'_\delta$$

**9.4 Prediction of the Bare Hull Hydrodynamic Derivatives.** It is shown in Chapter V that no adequate theory exists to predict the resistance of a ship in simple straight-line motion with zero angle of attack at constant speed; that to predict such resistance, one must resort to model data or to other empirical approaches. The theory for predicting the hydrodynamic

derivatives of a ship's hull is even less well developed than that for predicting ship's resistance. What is presented in this section is a procedure for predicting the hydrodynamic derivatives using a combination of theoretical and empirical inputs.

For the purposes of this section, the ship's hull may be viewed as a very low aspect-ratio fin of very large area. The geometric aspect ratio of the hull is its draft-to-length ratio, its thickness-to-chord ratio is its beam-to-length ratio, its taper ratio is usually close to 1.0, its sweepback angle is usually slightly negative and its mean section shape corresponds to the shape of its water plane at half draft. At the low speeds ( $Fn < 0.25$ ) where the influence of wavemaking may be neglected and to which the current approaches are strictly limited, it was shown by Tsakonas (1959) that the free water surface serves as a groundboard for the ship's hull, hence, the effective aspect ratio of the hull may be taken as  $2T/L$ . Because of its poor section shape as a lifting surface and because of its extremely low aspect ratio, it might be expected that a ship's hull would generate very small hydrodynamic forces and moments compared to its rudder; however, because of its very large profile area, a ship's hull does in fact generate forces and moments far larger than the control forces generated by its rudder.

Viewed in this light, the velocity-dependent force derivative,  $(Y_v)_h$ , for the bare hull is identical in form to that of the fin  $(Y_v)_f$  given by (57):

$$(Y_v)_h = -(\rho/2)A_h V \left[ \left( \frac{\partial C_L}{\partial \beta} \right)_h + (C_D)_h \right] \quad (64a)$$

where the subscript  $h$  refers to the bare hull and  $A_h$  is the profile area of the ship's hull. Since the effective aspect ratio of a ship's hull,  $2T/L$ , is rarely greater than about  $\frac{1}{2}$ , the Jones formula shown in Fig. 137 is of ample accuracy. Thus,

$$\left( \frac{\partial C_L}{\partial \beta} \right)_h = \left( \frac{\pi}{2} \right) a = \pi T/L \text{ per radian} \quad (65)$$

Substituting this expression in Equation (64a) and nondimensionalizing on the basis of  $\rho$ ,  $L$ ,  $T$ , and  $V$ , we obtain:

$$(Y'_v)_h = \frac{(Y_v)_h}{(\rho/2)LT^2V} = -\left( \frac{\pi T}{L} \right) + (C_D)_h \quad (64b)$$

where  $(C_D)_h$  may be obtained from the drag characteristics of the ship at zero angle of attack.

The velocity-dependent moment derivative of a ship's hull  $(N_v)_h$  includes a term that is negligible for a fixed fin remote from the origin of the hull and is therefore not included in the expression for  $(N_v)_f$  given in (59a). This term, commonly called the Munk moment, Munk (1934), is derived in Lamb (1945) for an ellipsoid, deeply submerged in an ideal fluid. The nondimensional derivative of the Munk moment with respect to an



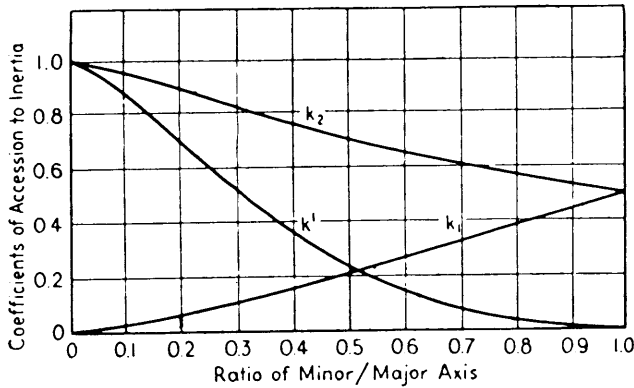


Fig. 48 Coefficients of accession to inertia for prolate spheroids (Davidson and Schiff, 1946)

angle of attack,  $\beta$ , for an ellipsoid may be expressed as follows:

$$(N'_{\beta})_i = +(k_2 - k_1)\Delta$$

or equivalently

$$(N'_v)_i = -(k_2 - k_1)\Delta' \quad (66)$$

where

the subscript  $i$  refers to the value of the derivative in an ideal fluid

$k_2$  = coefficient of accession to inertia in lateral,  $y$ -direction as given in Lamb (1945)

$k_1$  = Lamb coefficient of accession to inertia in longitudinal,  $x$ -direction

$\Delta'$  = nondimensional mass of ellipsoid

Fig. 48 shows values taken from Lamb, (1945) for  $k_1$ ,  $k_2$  and  $k'$  (being the coefficient for accession to inertia in rotation). Since Fig. 48 indicates that  $k_2$  is always larger than  $k_1$ ,  $(N'_v)_i$  is always negative according to Equation (66) and hence always destabilizing.

The Munk moment arises from the fact that in an ideal (nonviscous) fluid, an elongated three-dimensional body at an angle of attack experiences a pure couple tending to increase the angle of attack. This is shown in Fig. 49. This couple is composed of equal and opposite forces acting over the bow half and over the stern half of the body so that in an ideal fluid, there is no resultant lateral force acting on the body, only a destabilizing moment. The magnitude of this moment according to Fig. 49 is

$$(N)_i = 2lY_B$$

so that

$$(N_v)_i = 2l \frac{\partial Y_B}{\partial v}$$

where  $l$  is taken as always positive and  $Y_B$  is negative

if it is directed to port at the bow and positive if it is directed to starboard.

The relationship between this expression and that given in Equation (66) for the Munk moment derivative is as follows:

$$(N'_v)_i = -(k_2 - k_1)\Delta' = \frac{(N_v)_i}{(\rho/2)L^2TV} = \frac{2l \frac{\partial Y_B}{\partial v}}{(\rho/2)L^2TV} \quad (67)$$

The preceding development is based on ideal, potential-flow considerations. In a viscous fluid, a deeply submerged ellipsoid at an angle of attack generates vortices on the after, or downstream, side of the body which can be represented as reducing the pressures over the stern of the body as shown in Fig. 49 with little or no influence on the pressures over the bow. In spite of this representation, the usual simplifying assumption in hydrodynamics is that potential-flow effects and viscous-flow effects are independent of one another. Hence, it is assumed that the lateral force acting on the ellipsoid owing to vorticity is independent of and does not react with the force distribution in an ideal fluid. The total moment,  $N$ , acting on the submerged ellipsoid at an angle of attack in a real fluid is taken to be the sum of two independent parts, one the ideal Munk moment and the other the moment of the lateral force arising from real fluid effects. Thus, following Fig. 49:

$$N = 2Y_B l + x_p Y_L \quad (68)$$

where  $x_p$  is the distance from the origin (taken at  $\infty$ ) to the point of application of the real-fluid lateral force,  $Y_L$  (negative if  $Y_L$  is aft of  $O$ ).

According to Fig. 49, the real-fluid lateral force  $Y_L$  will always act in the same direction as  $Y_B$ . Further-

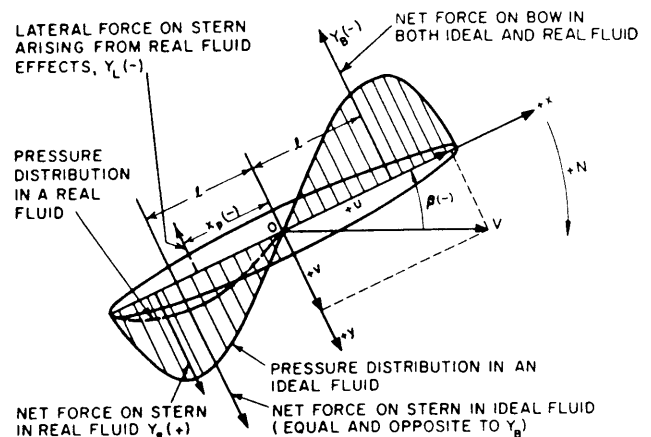


Fig. 49 Forces acting on a submerged ellipsoid at an angle of attack in an ideal and a real fluid

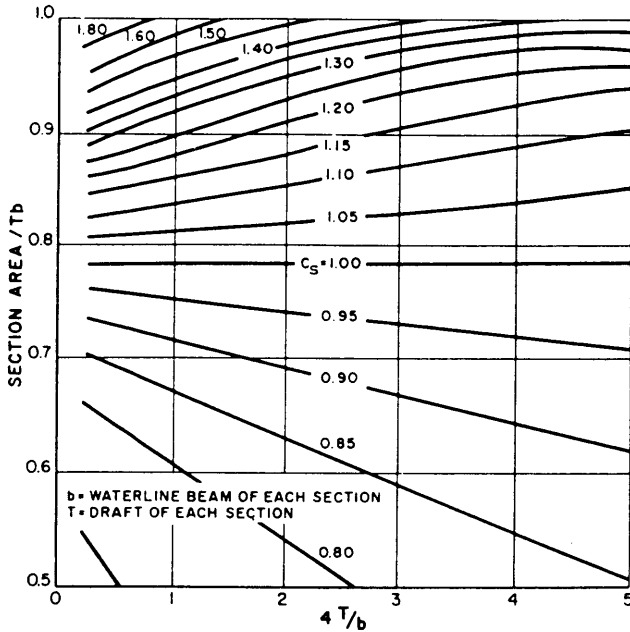


Fig. 50 Sectional inertia coefficients,  $C_s$ , as functions of local beam/draft ratio and section area coefficient (Prohaska, 1947)

more, experiments with slender bodies of revolution reported by Johnson (1951) have shown that  $x_p$  is always negative and lies between 0.2 and 0.3 of the length of the body aft of the midlength. If these signs are associated with Equation (68), it will be seen that  $N$ , the upsetting moment in a real fluid, is smaller in magnitude than the upsetting moment in an ideal fluid which is represented by the first term of (68).

For shiplike bodies at a free surface, the same basic expression shown in (68) is used but the particulars differ significantly. If the derivative is taken with respect to  $v$  and the result is nondimensionalized, the following is obtained:

$$N'_v = \frac{N_v}{(\rho/2)L^2TV} = \frac{2l}{(\rho/2)L^2TV} \left( \frac{\partial Y_B}{\partial v} \right) + \frac{x_p}{(\rho/2)L^2TV} \left( \frac{\partial Y_L}{\partial v} \right) \quad (69)$$

Substituting from Equation (67) for the first term on the right of (69), we obtain for the ellipsoid:

$$N'_v = -(k_2 - k_1)\Delta' + \frac{x_p}{L} \left( \frac{\partial Y'_L}{\partial v'} \right) \quad (70)$$

For the surface ship, Jacobs (1964) wrote an analogous expression:

$$(N'_v)_h = -(\Delta'_2 - k_1\Delta') + \frac{x_p}{L} (Y'_v)_h \quad (71)$$

where

$\Delta'$  = mass of ship,  $\Delta$ , nondimensionalized by  $(\rho/2)L^2T$

$\Delta'_2 = \Delta_2/(\rho/2)L^2T$

$$= \frac{k_2}{(\rho/2)L^2T} \int_{\text{bow}}^{\text{stern}} L/T(\rho/2)\pi C_s h^2 dx$$

$C_s$  = two-dimensional lateral added-mass coefficient (sectional-inertia coefficient) determined for each section strip of width  $dx$  along  $x$ -axis. The  $C_s$  may be determined from several sources, e.g., Fig. 16 of Prohaska (1947) reproduced in Fig. 50.

$k_1\Delta'$  = the so-called "added" mass of ship in the longitudinal  $x$ -direction;  $k_1\Delta' = -(X'_u)_h$

$\Delta'_2$  = the so-called "added" mass of ship in the transverse  $y$ -direction;  $\Delta'_2 = -(Y'_i)_h$

$h$  = local draft at each station

$k_1, k_2$  = as defined for Equation (66) and as given in Fig. 48. For surface ships, the abscissa of Fig. 48 is defined as  $2T/L$ , where  $T$  corresponds to minor axis and  $L$  to major axis

$x_p$  = as defined in Equation (68)

$(Y'_v)_h$  = as given in Equation (64a)

The results for  $C_s$  given by Prohaska (1947) are for very-high-frequency oscillations in heave. However, it is assumed by Martin (1961) and confirmed by Porter (1966) that if the scale of the abscissa of Fig. 16 of Prohaska (1947) is treated as a scale of  $4T/b$  instead of  $b/T$ , the  $C_s$  values of that figure are applicable to near-zero frequency oscillations in sway. As indicated in Section 8.5, interest in this chapter centers on near-zero frequency oscillations.

The first term on the right of Equation (71) differs from that of (70) only in the expression for  $\Delta'_2$ . The quantity under the integral sign in the expression for  $\Delta'_2$  represents the summation of the added masses of two-dimensional strips taken over the length of the ship. This first term can be estimated for any given ship form on the basis of the data given in Figs. 48 and 50.

Prediction of the second term on the right of Equation (71) depends on knowledge of  $x_p$  for shiplike bodies, since  $(Y'_v)_h$  can be readily calculated from (64a). The major difference between ellipsoids and ships insofar as  $x_p$  is concerned is that ship bows are more slender, have a constant local draft forward and, for bows that are not bulbous in shape, have section shapes forward that are relatively sharp at the keel for a short distance aft of the bow. Therefore, these ship hulls at an angle of attack generate vortices on the downstream side of both the bow and stern, whereas the ellipsoid hull was assumed to generate vortices only downstream of the stern. This change tends to move forward the point of application of the

Table 5—Hull Form and Appendage Configurations Studied by Tsakonas, Martin and Jacobs

No.	Model description	Dav. Lab. model no.	L/B	B/T	L/T	$C_p$	$C_B$	$x'_G$	$x'_{\square}$	Propeller	Rudder	Skeg(s)
1	Taylor's	843	4.36	2.92	12.74	0.54	0.50	0	-0.019	None	None	None (see Fig. 81)
2	Std. Series	845	4.36	4.62	20.13							None
3		847	6.90	1.85	12.74							None
4		842	6.90	2.92	20.13				+0.020			None and to sta 17, 18 and 20
5		846	6.90	4.62	31.9				-0.019			None and to sta 20
6		848	8.68	2.92	25.42							None and to sta 20
7		844	10.89	1.85	20.13							None
8		841	10.89	2.92	31.9							None
	Series 60 Normal form	3,0,0 & 3,1,1	6.0	3.12	18.75	0.614	0.60	0	+0.015	None(0) & with, (1)	None(0) & $A'_R = 0.016(1)$	Normal Single Screw Stern (see Fig. 83)
		6,0,0 & 6,1,1	7.0	2.07	14.50	0.614	0.60					
		5,0,0 & 5,1,1	7.0	3.28	23.00	0.614	0.60					
		2,0,0; 2,1,1;	7.0	2.68	18.75	0.614	0.60				None(0) & $A'_R = 0.016(1)$ , 0.025(2), 0.012(3)	
		2,1,2 & 2,1,3									None(0) & $A'_R = 0.016(1)$	
		7,0,0 & 7,1,1	7.0	2.68	18.75	0.713	0.70		+0.005			
		8,0,0 & 8,1,1	7.0	2.68	18.75	0.807	0.80		-0.025			
		1,0,0 & 1,1,1	7.5	2.50	18.75	0.614	0.60		+0.015			
		4,0,0 & 4,1,1	8.0	2.34	18.75	0.614	0.60		+0.015			
9	Series 60, Ext. V Model (Eda, 1965)	9,0,0 & 9,1,1	7.5	2.50	18.75	0.614	0.60	0	+0.011			
10	Mariner	...	6.84	3.10	21.19	0.620	0.61	0	+0.023	None	With (see [41])	As built (see [41])
11	Destroyer DD692	...	9.45	2.90	27.40	0.643	0.57	0	+0.022	With 2 props.	With 2 rudders	As built
12	Hopper Dredge	Heavy	6.00	2.41	14.51	0.727	0.72	0	0	None	With	Like Fig. 51(c)
13	Hopper Dredge	Light	5.78	3.46	20.00	0.840	0.82	0	+0.012	None	With	Like Fig. 51(c)

lateral force  $Y_L$ , shown in Fig. 49 for the ellipsoid. That is,  $x_p$  is less negative and may even be positive for some ship hulls, whereas it is always large and negative for ellipsoids.

On the basis of experiments with a group of eight Taylor Standard Series models of varying  $B/T$  ratio and  $L/B$  ratio (see Table 5), Martin (1961) showed that the distance  $x_p$  lay between  $\pm 0.1L$  from the center of gravity of the model which was  $0.02L$  forward of the midlength. Jacobs (1964) suggests that  $x_p$  be measured from  $G$  to the center of area of the hull profile. Thus, according to Jacobs,  $x_p$  is likely to be positive for ships without bulbous bows. Accepting the Jacobs' suggestion, it is apparent that whereas for ellipsoids the moment derivative in a real fluid is less in magnitude than the ideal moment derivative, for many ships the real moment derivative may be greater than the ideal moment derivative.

Fundamentally, since  $x_p$  is a function of external body geometry, it is more accurate to relate it to some geometric position on the body, such as its midlength rather than to  $G$ , which is a function of the location of the internal weights of the body. This was one of the reasons why the equations of motion (10) were so written that the origin could be taken at  $\mathcal{O}$  rather than at the center of gravity.

It will be noted that the second term of Equation (71) is equivalent to the expression for  $(N_v)_f$  given in (59a) with the important distinction that  $x_p$  is very small compared to  $x_f$ . Strictly, (59a) should include a term representing the Munk moment of the fin. However, because of the assumed short chord length of the fin relative to the distance  $x_f$ , the Munk moment for the fin is negligible. For the ship's hull, on the other hand, where  $x_p$  is very small, the Munk moment term is of dominant importance.

It follows from these remarks that the Munk moment is important for fins when moments are taken about an axis located in the fin. An important practical case is the prediction of rudder torques about the rudder stock shown partly in (124).

The rotary-force derivative for the bare hull,  $(Y_v)_h$ , like the velocity-dependent moment derivative  $(N_v)_h$  just discussed, also includes two terms, one arising from ideal fluid considerations and the other from real-fluid effects. For a ship in a real fluid, the expression is as follows:

$$(Y'_r)_h = \frac{(Y_r)_h}{(\rho/2)L^2TV} = -k_1\Delta' + \frac{x_p}{L}(Y'_v)_h \quad (72)$$

with symbols as defined for Equation (71).

The first term corresponds to an outward (centrifugal) force exerted by the fluid on a body in rotary motion. This force is due to the uniform rate of change of direction of the longitudinal momentum of the fluid which has been imparted to the fluid by the body moving in a circular path. The second term arises from viscous-flow effects and is identical in form to the con-

tribution of a fixed fin to the rotary-force derivative shown in Equation 59b. Since both  $k_1$  (see Fig. 48) and  $x_p/L$  are very small for slender, shiplike bodies, the rotary-force derivative for the bare hull is always small. This is in accord with Section 4.2. If  $x_p$  is positive, as suggested by Jacobs (1964)  $(Y'_r)_h$  will be negative since  $(Y'_v)_h$  is always negative.

As noted in (11), the derivative  $Y'_r$  is only one of the terms in the coefficient of  $r'$ ; the other is  $\Delta'$ . If these two terms are grouped together as they are in (11), and combined with (72), the following expression used by Jacobs (1964) is obtained:

$$(\Delta' - Y'_r)_h = (1 + k_1)\Delta' - \frac{x_p}{L}(Y'_v)_h \quad (73)$$

The first term on the right of Equation (73) is the actual mass plus the "added mass" in the  $x$ -direction. Jacobs uses the symbol  $\Delta'_x$  for the first term and refers to the second term as  $(Y'_r)_h$ . Since  $(Y'_r)_h$ , by definition, should encompass all of its hydrodynamic parts, it should be defined as in Equation (72).

Jacobs (1964) following Martin (1961) expresses the rotary-moment derivative as the sum of a potential and a viscous term although Lamb's potential-flow analysis indicates that  $N_r$  should be zero in an ideal fluid (Lamb, 1945). According to Jacobs:

$$(N'_r)_h = \frac{(N_r)_h}{(\rho/2)L^3TV} = -\Delta'_s \frac{\bar{x}}{L} + \left(\frac{x_0}{L}\right)^2 (Y'_v)_h \quad (74)$$

where  $\Delta'_s$  is the so-called rotational added-mass coefficient acting at a distance  $\bar{x}$  from  $G$ ;

$$\Delta'_s = (k'/k_2)\Delta'_2 = \Delta'_2/(\rho/2)L^2T$$

$$\bar{x} = \frac{\int_{\text{bow}}^{\text{stern}} C_s h^2 x dx}{\int_{\text{bow}}^{\text{stern}} C_s h^2 dx}$$

$x$  = distance from  $O$  to section strip of width,  $dx$ , positive if forward of  $O$ , negative if aft

$x_0/L$  = taken as half the value of the prismatic coefficient of ship and is assumed to be always positive

All other symbols are as defined for Equation (71)

While  $\bar{x}/L$  may be either positive or negative, its value is always small. On the other hand,  $x_0$  is much larger than  $\bar{x}$  and since  $(Y'_v)_h$  is always negative,  $(N'_r)_h$  will always be large and negative. This is in accord with Section 4.2.

The two cross-coupled acceleration derivatives,  $Y_r$  and  $N_v$  have very small values for the bare hull and in practice are often assumed to be zero. The linear acceleration derivative  $Y'_v$  is equivalent to the term

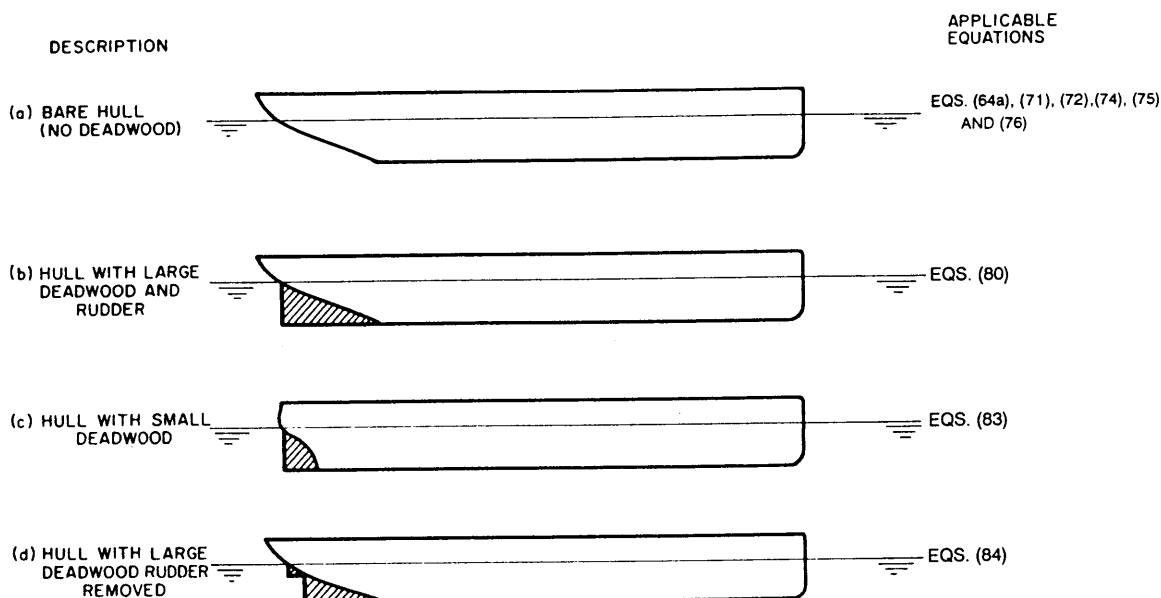


Fig. 51 Hull-deadwood configurations treated by Jacobs (1964)

$-\Delta'_2$  as defined in Equation (71). For completeness:

$$(Y'_i)_h = \frac{(Y_i)_h}{(\rho/2)L^2T} = -\Delta'_2$$

$$= -\frac{k_2}{(\rho/2)L^2T} \int_{\text{bow}}^{\text{stern}} L/T (\rho/2) \rho C_s h^2 dx \quad (75)$$

with all symbols as defined for (71).

The rotary-acceleration derivative,  $N'_r$ , is defined in similar terms as follows:

$$(N'_r)_h = \frac{(N_r)_h}{(\rho/2)L^4T}$$

$$= -\frac{k'}{(\rho/2)L^4T} \int_{\text{bow}}^{\text{stern}} L/T (\rho/2) \pi C_s h^2 x^2 dx \quad (76)$$

where  $k'$  is the Lamb coefficient for accession to inertia in rotation as given in Fig. 48 and all other symbols are as defined in (71).

It is seen that both of the acceleration derivatives,  $Y'_i$  and  $N'_r$ , are composed only of potential-flow terms and they are generally calculated without resort to empirical experimental data.

**9.5 Prediction of the Hydrodynamic Derivatives of Practical Ship-Fin Configurations.** Jacobs (1964) has shown that the hydrodynamic derivatives of the bare hull-deadwood combinations shown in Fig. 51 can be computed with reasonable accuracy by simply adding the contributions of the appropriate fixed fin to the bare hull derivatives. For the bare hull shown in Fig.

51(a), equations of the previous subsection are applicable as shown. For the kind of deadwood configurations shown in Figs. 51(b) and 51(c) Jacobs assumes that the effective span of the deadwood (fin) is equal to the height of the deadwood,  $h_f$ , at the trailing edge of the deadwood. For the case shown in Fig. 51(b),  $h_f$  is identical to the ship draft,  $T$ . The deadwood is also assumed to be of sufficiently low aspect ratio that the Jones' formula for the lift-curve slope is applicable. If the fin length along the keel is taken as  $l_f$ , the fin area is then  $h_f l_f/2$ ; the mean chord,  $\bar{c}$  is  $A_f/h_f = l_f/2$  and the fin effective aspect ratio is  $2h_f/l_f/2 = 4h_f/l_f$  since the hull provides full groundboard effect for the deadwood.

If the preceding relationships and the Jones' formula, Equation (65), are substituted in (58), the following expression for the contribution of the fin to the velocity-dependent force derivative is obtained:

$$(Y'_v)_f = \frac{-(\rho/2)(h_f)(l_f/2)V\left(\frac{\pi}{2}\right)\left(\frac{4h_f}{l_f}\right)}{(\rho/2)LTV} = -\frac{\pi h_f^2}{LT}$$

(77a)

and for  $h_f = T$

$$(Y'_v)_f = -\frac{\pi T}{L}$$

Jacobs considers the distance from the stern to the center of pressure of the deadwood to be a negligible part of the distance to the origin; hence, the distance  $x_f$ , as defined in Fig. 46 is taken as  $-L/2$ . Inserting this value of  $x_f$  and the value of  $(Y'_v)_f$  from Equation

NOTE: THE  $(Y'_i)_f$  VALUES GIVEN ON THIS FIGURE ARE RELATED TO THE  $Y'_i$  VALUES AS FOLLOWS:  $Y'_i = (Y'_i)^2 - 8$ , m' IN ACCORDANCE WITH EQUATIONS (72) AND (73) DERIVATIVES EVALUATED WITH ORIGIN AT G, WHICH IS 0.02 L AFT OF  $\bar{M}$

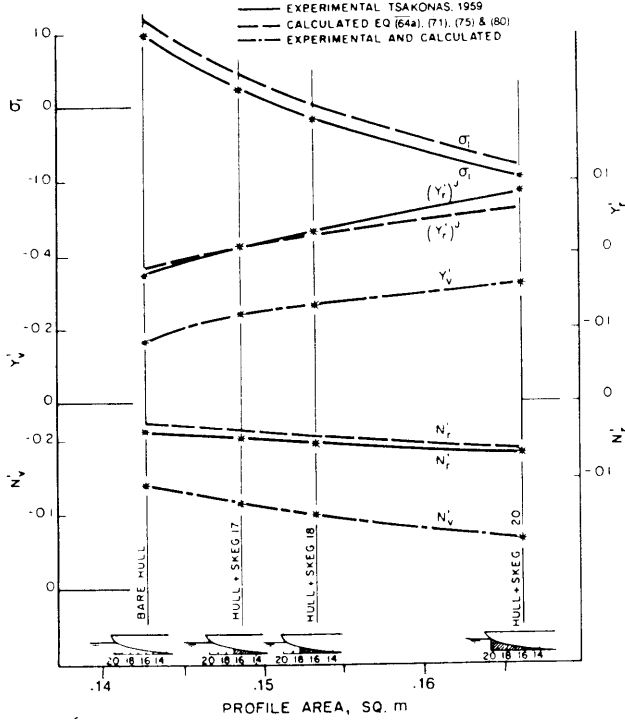


Fig. 52 Comparison of calculated and experimental stability derivatives and indexes for Taylor's Standard Series Model 842 and various skeg extensions

(77) into (59a-c), and nondimensionalizing, the following is obtained:

$$(N'_v)_f = -\frac{1}{2}(Y'_v)_f = +\frac{\pi h_f^2}{2TL}$$

$$= +\frac{\pi}{2} \frac{T}{L} \text{ for } h_f = T \quad (77b)$$

$$(Y'_r)_f = -\frac{1}{2}(Y'_v)_f = +\frac{\pi h_f^2}{2TL}$$

$$= +\frac{\pi}{2} \frac{T}{L} \text{ for } h_f = T \quad (77c)$$

$$(N'_r)_f = +\frac{1}{4}(Y'_v)_f = -\frac{\pi h_f^2}{4TL}$$

$$= -\frac{\pi}{4} \frac{T}{L} \text{ for } h_f = T \quad (77d)$$

where the signs conform to the stern location of the deadwood.

The fin acceleration derivative following (61) is:

$$(Y'_i)_f = -\frac{4\pi A'_f h'_f}{(a^2 + 1)^{1/2}} \quad (78)$$

where  $A'_f = A_f = A_f/LT$  and  $h'_f = h_f/L = T/L$  for the deadwood of Fig. 51(b). Following Equations (62a-c) and noting that  $x_f = -L/2$ :

$$(N'_i)_f = +\frac{2\pi A'_f h'_f}{(1 + a^2)^{1/2}} \quad (79a)$$

$$(Y'_i)_f = +\frac{2\pi A'_f h'_f}{(1 + a^2)^{1/2}} \quad (79b)$$

$$(N'_i)_f = -\frac{\pi A'_f h'_f}{(1 + a^2)^{1/2}} \quad (79c)$$

The total derivatives for the ship with the deadwood shown in Fig. 51(b) are as follows:

$$Y'_v = (Y'_v)_h + (Y'_v)_f \text{ Equation (64a) + (77a)}$$

$$N'_v = (N'_v)_h + (N'_v)_f \text{ Equation (71) + (77b)}$$

$$Y'_r = (Y'_r)_h + (Y'_r)_f \text{ Equation (72) + (77c)}$$

$$N'_r = (N'_r)_h + (N'_r)_f \text{ Equation (74) + (77d)} \quad (80)$$

$$Y'_i = (Y'_i)_h + (Y'_i)_f \text{ Equation (75) + (78)}$$

$$N'_i = (N'_i)_h + (N'_i)_f \text{ Equation (76) + (79c)}$$

$$Y'_i = 0 + (Y'_i)_f \text{ Equation (79b)}$$

$$N'_i = 0 + (N'_i)_f \text{ Equation (79a)}$$

Jacobs assumes that the derivatives  $(Y'_i)_f$ ,  $(N'_i)_f$ ,  $(Y'_i)_f$ ,  $(N'_i)_f$ ,  $Y'_r$ , and  $N'_i$  are zero.

Because of the high aspect ratio of the small deadwood shown in Fig. 51(c), the Jones' formula which was used in Equations (77) is not applicable. For this case, Jacobs (1964) elected to use the classical lift-curve slope relationship

$$\frac{\partial C_L}{\partial \beta} = \frac{2\pi}{1 + 2/\alpha} \text{ per radian} \quad (81)$$

This equation is plotted on Fig. 137 for comparison with the Jones' formula and with Equation (122b). It is seen that while Equation (81) is much more accurate in the high aspect-ratio range than the Jones' formula, it overpredicts for all aspect ratios in comparison to Equation (122b) and the experimental data shown in Fig. 137. Nevertheless, in order to preserve the essence of the Jacobs' work for the remainder of this section, use of Equation (81) will be retained.

If (81) is substituted into (58) and the result is non-dimensionalized on the basis of  $\rho$ ,  $T$ ,  $L$ , and  $V$ , the following is obtained:

$$(Y'_v)_f = -A'_f \left( \frac{2\pi}{1 + 2/\alpha} \right) \quad (82)$$

The total derivatives for the ship with the deadwood shown in Fig. 51(c) are then as follows:

$$Y'_v = (Y'_h) + (Y'_v)_f$$

Equation (64a) + (82)

$$N'_v = (Y'_v)_h - \frac{1}{2}(Y'_v)_f$$

Equation (71) -  $\frac{1}{2}$ (82)

$$Y'_r = (Y'_r)_h - \frac{1}{2}(Y'_v)_f$$

Equation (72) -  $\frac{1}{2}$ (82)

$$N'_r = (N'_r)_h + \frac{1}{4}(Y'_v)_f \quad (83)$$

Equation (74) +  $\frac{1}{4}$ (82)

$$Y'_\dot{v} = (Y'_\dot{v})_h + (Y'_\dot{v})_f$$

$$N'_\dot{r} = (N'_\dot{r})_h + \frac{1}{4}(Y'_\dot{v})_f \quad \text{same as Equation (80)}$$

$$Y'_\ddot{r} = 0 - \frac{1}{2}(Y'_\dot{v})_f$$

$$N'_\ddot{r} = 0 - \frac{1}{2}(Y'_\dot{v})_f$$

The hull-deadwood configuration shown in Fig. 51(d) corresponds to that shown in Fig. 51(b) with the rudder removed. For this configuration, Jacobs suggests that values of  $(Y'_v)_f$  for the rudder be computed in accordance with (82) and inserted in the second terms of (83). Obviously,  $A'_R$  in this case will correspond to the area,  $A'_R$ , of the rudder. The resulting values of the contribution of the rudder to the derivatives should then be subtracted from the values computed in (80) for the hull with the complete deadwood.

Thus the total derivatives for the configuration shown in Fig. 51(d) are as follows:

$$Y'_v = (64a) + (77a) - (82)$$

$$N'_v = (71) + (77a) + \frac{1}{2}(82) \quad (84)$$

$$Y'_r = (72) + (77b) + \frac{1}{2}(82)$$

$$N'_r = (74) + (77c) - \frac{1}{4}(82)$$

$$Y'_\dot{v} = (59) + (62) \text{ for deadwood} - (62) \text{ for rudder}$$

$$N'_\dot{r} = (60) + (63c) \text{ for deadwood} - (63c) \text{ for rudder}$$

$$Y'_\ddot{r} = (63b) \text{ for deadwood} - (63b) \text{ for rudder}$$

$$N'_\ddot{r} = (63a) \text{ for deadwood} - (63a) \text{ for rudder}$$

**9.6 Comparison Between Results of Calculation and Model Experiment.** Tsakonas (1959), Martin (1961), Jacobs (1963 and 1964), each drawing on the earlier work, have carried out a fairly extensive comparison of predicted hydrodynamic derivatives with experimental results for a wide variety of ships and models. The model experimental results used by these authors include those of Eda and Crane (1965), Suarez (1963), and Paulling (1962). With the exception of Paulling's work, all results were measured on the rotating-arm facility at the Davidson Laboratory. As noted in Section 8.5, the Paulling experimental data were based on planar motion mechanism tests at the University of California. A description of each of the hull form and appendage variations included in one or more of the

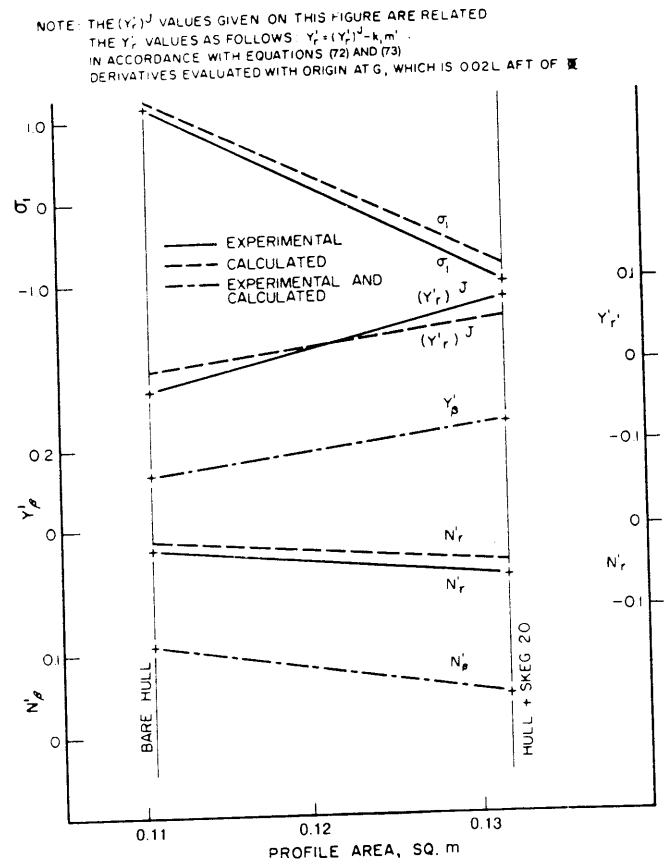


Fig. 53 Comparison of calculated and experimental stability derivatives and indexes for Taylor's Standard Series Model 848 with and without skeg

Table 6—Stability Derivatives for the Series 60 Hull

(a) Models with Rudder and Propeller

Series Model No.	$C_B$ Series			$L/B$ Series			$L/B$ Series		
	2,1,1	7,1,1	8,1,1	3,1,1	2,1,1	1,1,1	4,1,1		
$C_B$	0.60	0.70	0.80	$L/B$	6.0	7.0	8.0		
$B/T$	2.68	2.68	2.68	$B/T$	3.12	2.68	2.50	2.34	
$\Delta'$	0.171	0.200	0.229	$\Delta'$	0.200	0.171	0.160	0.150	
$LCG/L$	0.515	0.505	0.475	$LCG/L$	0.515	0.515	0.515	0.515	

(1) Estimated From Theory (80)

Derivative	Eq. (80)			Eq. (80)			Eq. (80)		
$-Y'_v = L'_\beta$	0.335	0.335	0.335	0.335	0.335	0.335	0.335	0.335	0.335
$-N'_v$	0.086	0.097	0.095	0.085	0.086	0.088	0.089	0.089	0.089
$Y'_r$	+0.076	+0.075	+0.089	+0.076	+0.076	+0.077	+0.067	+0.067	+0.067
$N'_r$	-0.066	-0.068	-0.077	-0.066	-0.066	-0.066	-0.066	-0.066	-0.066
$C' \times 10^2$	1.40	1.07	1.25	1.16	1.40	1.49	1.48	1.48	1.48
$\sigma_1$	-0.55	-0.35	-0.33	-0.41	-0.55	-0.59	-0.61	-0.61	-0.61
$Y'_\delta$	+0.038	+0.038	+0.038	+0.038	+0.038	+0.038	+0.038	+0.038	+0.038
$N'_\delta$	-0.019	-0.019	-0.019	-0.019	-0.019	-0.019	-0.019	-0.019	-0.019
$\partial r'/\partial \delta_R$	-0.68	-0.94	-0.80	-0.83	-0.68	-0.65	-0.66	-0.66	-0.66

See notes 1, 2, 3, 4 and 5 on Table 66

(2) Estimated From "Least Squares" Fit of Experimental Data

$-Y'_v$	0.305	0.324	0.354	0.308	0.305	0.270	0.283
$-N'_v$	0.095	0.104	0.086	0.089	0.095	0.108	0.091
$Y'_r$	0.090	0.083	0.085	0.089	0.090	0.088	0.088
$\Delta'_z - Y'_r$	0.081	0.127	0.125	0.111	0.081	0.040	0.062
$N'_r$	-0.070	-0.068	-0.060	-0.075	-0.070	-0.067	-0.066
$C' \times 10^2$	1.37	0.94	0.89	1.32	1.37	1.03	1.25
$\sigma_1$	-0.51	-0.31	-0.28	-0.42	-0.51	-0.39	-0.56
$N'_\delta$	-0.024	-0.025	-0.035	N.A.	-0.024	-0.022	N.A.
$Y'_\delta$	0.050	0.052	0.065	N.A.	0.050	0.046	N.A.
$\partial r'/\partial \delta_R$	-0.88	-1.44	-2.03	N.A.	-0.88	-1.06	N.A.

$L/T$ Series			Rudder Area Series					
	6,1,1	2,1,1	5,1,1		2,1,3	2,1,1	2,1,2	
$L/T$	14.5	18.75	23.0	$A'_R$	0	0.012	0.016	0.025
$B/T$	2.07	2.68	3.28	$B/T$	2.68	2.68	2.68	2.68
$\Delta'$	0.171	0.171	0.171	$\Delta'$	0.171	0.171	0.171	0.171
$LCG/L$	0.515	0.515	0.515	$LCG/L$	0.515	0.515	0.515	0.515

(1) Estimated From Theory

Eq. (80)			Eq. (84)			Eq. (82, 84)		
0.434	0.335	0.273	0.303	0.329	0.335	0.347	0.347	0.347
0.114	0.086	0.071	0.110	0.089	0.082	0.080	0.080	0.080
+0.094	+0.076	+0.061	+0.052	+0.073	+0.076	+0.082	+0.082	+0.082
-0.081	-0.066	-0.054	-0.055	-0.065	-0.066	-0.069	-0.069	-0.069
2.64	1.40	0.70	0.36	1.27	1.40	1.68	1.68	1.68
-0.76	-0.55	-0.33	-0.15	-0.49	-0.55	-0.64	-0.64	-0.64
+0.045	+0.038	+0.031	...	+0.034	+0.038	+0.041	+0.041	+0.041
-0.023	-0.019	-0.015	...	-0.017	-0.019	-0.021	-0.021	-0.021
-0.58	-0.68	-0.91	...	-0.68	-0.68	-0.63	-0.63	-0.63

(2) Estimated From "Least Squares" Fit of Experimental Data

0.349	0.305	0.260	0.245	0.293	0.305	0.311
0.133	0.095	0.075	0.114	0.100	0.095	0.081
0.099	0.090	0.094	0.070	0.082	0.090	0.096



(2) "Least Squares" Fit (continued)

0.077	0.081	0.077	0.101	0.089	0.081	0.075
-0.081	-0.070	-0.057	-0.055	-0.073	-0.070	-0.076
1.82	1.37	0.912	0.190	1.25	1.37	1.76
-0.52	-0.51	-0.45	-0.09	-0.45	-0.51	-0.62
N.A.	-0.024	N.A.	...	-0.018	-0.024	-0.031
N.A.	0.050	N.A.	...	0.037	0.050	0.060
N.A.	-0.88	N.A.	...	-0.72	-0.88	-0.825

Tsakonas, Martin, and Jacobs works is given in Table 5.

Comparisons of the velocity dependent and rotary derivatives taken from Jacobs (1963) are shown for two Taylor Standard Series models with various skeg extensions in Figs. 52 and 53. The agreement between the prediction of these derivatives using the equations and experimental results is seen to be excellent, particularly for the velocity derivatives  $N'_v$  and  $Y'_v$ . Values of the stability indexes computed in accordance with Equation (14) are also shown in this figure. For the purposes of these computations as well as those shown in Table 6, Jacobs assumed that the cross-coupled acceleration derivatives ( $Y'_r$ ) and ( $N'_r$ ) are zero along with the contributions to the acceleration derivatives of the skegs ( $Y'_{\dot{v}})_f$  and ( $N'_{\dot{v}})_f$ .

Table 6 tabulates data for the entire group of Series 60 normal-form models described in Table 5. A further description of these models is given in Table 7, (Jacobs, 1964). In Table 7 each model is designated by a sequence of three digits. The first signifies a change in hull; the second signifies presence, 1, or absence, 0, of propeller; the third signifies presence, 1, or absence, 0, of the design rudder,  $A'_R = 0.016$ . The digit 2 in the third place refers to the larger rudder,  $A'_R = 0.025$ , while the digit 3 in the third place refers to the smaller rudder  $A'_R = 0.012$ .

For the models labeled  $(-1,1)$  with rotating propeller and design rudder, Equations (80) were used for predicting the derivatives with  $C_D$  taken as zero since the propeller revolutions were adjusted to obtain zero drag. No correction was made to (80) for the effects of propeller rotation, although it is shown in Section 17.9 that this correction should not be negligible. For the models labelled  $(-0,0)$  (without propeller or rudder) Equations (84) were used. In these cases  $C_D$  is the experimentally measured drag coefficient at zero yaw angle. Models 2,1,2 and 2,1,3 with larger and smaller rudders respectively were treated by subtracting the lift due to the design rudder, Equation (82) and adding the lift due to the replacement rudder again using (82). The stern configuration of all of the Series 60 models with the design rudder is shown in Fig. 54.

Table 6 shows that while there are a few instances of poor agreement among the individual derivatives, the comparison of the cumulative effect as shown by

the stability index,  $\sigma_1$ , shows reasonably good agreement. The latter comparisons are shown in Fig. 253 for the models with rudder and propeller and in Fig. 176 for the models without rudder and propeller. It is seen that agreement in the case of the effect of the  $L/T$  ratio is very poor in both figures, although the trends are similar, and that agreement is also poor on Fig. 176 in the case of the effect of the  $L/B$  ratio. Further critical comments on the correlation achieved in the case of the models with propeller and rudder are made in Section 17.9.

Jacobs (1964) shows similar comparisons for the remainder of the hull form and appendage configurations described in Table 5. The results, tabulated in Table 8, show reasonably good agreement for a wide range of models. However, it is shown in Section 17.9 that the agreement in the case of some of these models may be fortuitous.

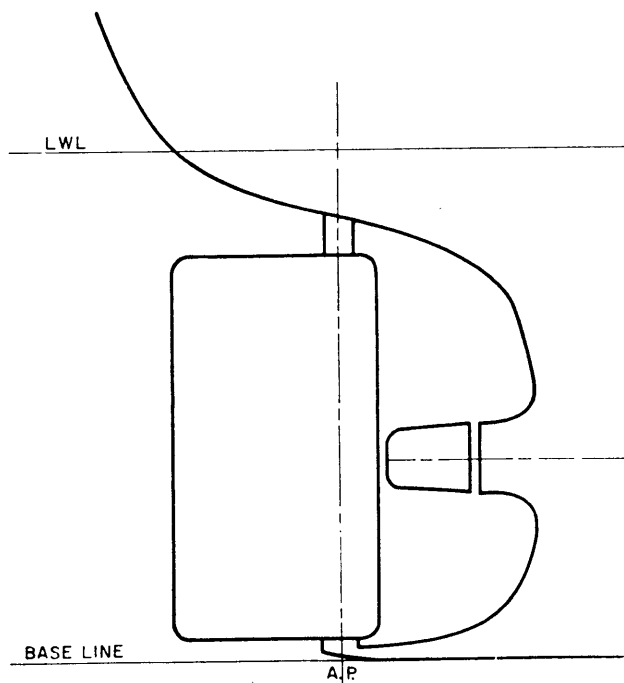


Fig. 54 Stern profile of Series 60 models with design rudder (Jacobs, 1964)

Table 6 continued

## (b) Model Without Rudder or Propeller

Series Model No.	$C_B$ Series			$L/B$ Series				$L/T$ Series			
	2,0,0 $C_B$ 0.60	7,0,0 0.70	8,0,0 0.80	3,0,0 $L/B$ 6.0	2,0,0 7.0	1,0,0 7.5	4,0,0 8.0	6,0,0 $L/T$ 14.5	2,0,0 18.75	5,0,0 23.0	
Derivative	(1) Estimated From Theory, Equation (84)										
$-Y'_v = L'_\beta + C_D$	0.303	0.306	0.309	0.305	0.303	0.303	0.302	0.395	0.303	0.247	
$-N'_v$	0.110	0.121	0.121	0.109	0.110	0.112	0.113	0.140	0.110	0.092	
$Y'_r$	0.052	0.051	0.064	0.050	0.052	0.052	0.042	0.068	0.052	0.040	
$N'_r$	-0.055	-0.056	-0.064	-0.055	-0.055	-0.055	-0.055	-0.068	-0.055	-0.043	
$\sigma_1$	-0.15	+0.032	+0.005	-0.027	-0.15	-0.20	-0.20	-0.38	-0.15	+0.075	
	(2) Estimated from "Least Squares" Fit of Experimental Data										
$-Y'_v$	0.245	0.287	0.256	0.237	0.245		0.260	0.315	0.245	0.217	
$-N'_v$	0.114	0.121	0.093	0.134	0.114		0.116	0.140	0.114	0.097	
$Y'_r$	0.070	0.051	0.075	0.066	0.070		0.069	0.068	0.070	0.071	
$N'_r$	-0.055	-0.056	-0.052	-0.054	-0.055		-0.059	-0.068	-0.055	-0.045	
$\sigma_1$	-0.09	+0.067	+0.033	+0.19	-0.09		-0.26	-0.22	-0.09	0	

## NOTES:

- 1 All derivatives nondimensionalized using  $\rho$ ,  $L$ ,  $T$  and  $V$  rather than  $\rho$ ,  $L$  and  $V$
- 2 All derivatives evaluated with origin taken at  $G$ , i.e.,  $x'_G = 0$
- 3 All experimental data for Table 6(a) obtained with propeller operating at model self-propulsion point
- 4 Experimental derivatives for Table 6(a2) taken from Eda and Crane (1965); all derivatives in Table 6(a1) and 6(b) taken from Jacobs (1964) except  $Y'_r$  and  $N'_r$  which were computed from Equations (122a), (63a), and (63c)
- 5 Values of  $\partial r / \partial \delta_R$  in Table 6(a) were computed using Equation (84)

Table 7—Pertinent Characteristics of the Series 60 Hulls

Model	1,1,1	2,1,1	2,1,2	2,1,3	3,1,1	4,1,1	5,1,1	6,1,1	7,1,1	8,1,1
Length $L$ , ft	5.0									
Beam $B$ , ft	0.667	0.714			0.833	0.625	0.714			
Draft $T$ , ft	0.267						0.2175	0.345	0.267	
Displacement $\Delta$ , lb	33.27	35.63			41.56	31.19	29.10	46.07	41.64	47.50
Prismatic coefficient, $C_p$	0.614						0.616	0.614	0.713	0.807
Block coefficient $C_B$	0.600								0.700	0.800
LCG/ $L$ from bow	0.515								0.505	0.475
$x'x$	+0.015								+0.005	-0.025
$x_G$	0									
$B/T$	2.50	2.68			3.12	2.34	3.28	2.07	2.68	2.68
$L/B$	7.5	7.0			6.0	8.0	7.0	7.0	7.0	7.0
$L/T$	18.75						23.00	14.50	18.75	
Rudder span, ft	0.200						0.164	0.258	0.200	0.200
Rudder chord, ft	0.105	0.105	0.167	0.080	0.105					
Rudder aspect ratio	1.90	1.90	1.20	2.50	1.90	1.90	1.56	2.46	1.90	1.90

Lamb's Coefficients of Accession to Inertia for Equivalent Ellipsoids

Minor axis/major axis, $2T/L$	0.1067						0.0870	0.0690	0.1067	
$K_1$ (longitudinal)	0.022						0.019	0.033	0.022	
$k_2$ (lateral)	0.957						0.968	0.940	0.957	
$k'$ (rotational)	0.875						0.903	0.820	0.875	
									1 m = 3.28 ft	
									1 kg = 2.2 lb	

Other Physical Characteristics

$\Delta'$ , mass coefficient	0.160	0.171			0.200	0.150	0.171	0.171	0.200	0.229
$k_1\Delta'$ , longitudinal added-mass coefficient	0.003	0.004			0.004	0.003	0.004	0.006	0.004	0.005
$\Delta'_2$ , lateral added-mass coefficient	0.171	0.170			0.169	0.172	0.138	0.220	0.180	0.194
$\Delta'_3$ , rotational added-mass coefficient	0.153	0.152			0.151	0.154	0.127	0.192	0.165	0.175
$I'_x - N'_x$ , virtual moment-of-inertia coefficient	0.0213	0.0219			0.0237	0.0206	0.0202	0.0239	0.0237	0.0271
$\bar{x}/L$ , CG of lateral added mass from LCG	0.048	0.049			0.048	0.049	0.048	0.049	0.039	0.005
$x_p/L$ , center of area of profile from LCG	0.028						0.033	0.028	0.026	-0.016
$C'_D$ , estimated drag coefficient at $\beta = 0$	0.015				0.017	0.014	0.017	0.015	0.019	0.021

Table 8—Comparison of Theoretically Predicted Stability Indexes With Experimentally Predicted Values

No. from Table 5	Model Description	Appendage description	Equations used for theor. derivatives	$\sigma_1$ calc. from theor. derivatives	Ref. for experimental derivatives	$\sigma_1$ calc. from exper. derivatives
9	Series 60 Ext V	with prop & rudder	(80)	-0.62	(Eda and Crane, 1965)	-0.39
9	Series 60 Ext V	w/o prop & rudder	(84)	-0.17	(Eda and Crane, 1965)	-0.17
10	Mariner	with rudder only	(80)	-0.49	(Jacobs, 1964)	-0.49
10	Mariner	with rudder only	(80)	-0.49	(Pauling and Wood, 1962)	-0.16 to -0.42
11	Destroyer DD692	with 2 prop & 2 rudders	(80)	-0.76	(Jacobs, 1964)	-0.76
12	Hopper dredge, heavy	with skeg & rudder	(83)	+0.84	(Jacobs, 1964)	+0.89
13	Hopper dredge, light	with skeg & rudder	(83)	+0.60	(Jacobs, 1964)	+0.82

**9.7 Summary and Update of Slender Body Strip Theoretical Approaches.** While the slender body and strip methods described in preceding sections have had some success in the case of aircraft where body geometry is dominated by wings and fins, results for ships have not been very accurate since there are no flat stabiliz-

ing surfaces and the flow around the hull is greatly altered by the fluid viscosity. Clarke's (1982) review of attempts assuming the hull is a low aspect ratio wing turned on its side and the Jones theory concludes the following derivatives as a function of the length to draft ratio of the ship, multiplied by certain constant

factors:

$$\begin{aligned}
 Y'_{\dot{v}} &= -\pi \left( \frac{T}{L} \right)^2 (1) \\
 Y'_{\dot{r}} &= -\pi \left( \frac{T}{L} \right)^2 (0) \\
 N'_{\dot{v}} &= -\pi \left( \frac{T}{L} \right)^2 (0) \\
 N'_{\dot{r}} &= -\pi \left( \frac{T}{L} \right)^2 \left( \frac{1}{12} \right) \\
 Y'_{\ddot{v}} &= -\pi \left( \frac{T}{L} \right)^2 (1) \\
 Y'_{\ddot{r}} &= -\pi \left( \frac{T}{L} \right)^2 \left( -\frac{1}{2} \right) \\
 N'_{\ddot{v}} &= -\pi \left( \frac{T}{L} \right)^2 \left( \frac{1}{2} \right) \\
 N'_{\ddot{r}} &= -\pi \left( \frac{T}{L} \right)^2 \left( \frac{1}{4} \right)
 \end{aligned} \tag{85}$$

By using the horizontal added mass coefficients  $C_H$  for sections along the hull, Clarke (1972) extended the slender body strip method to yield expressions for the derivatives dependent on hull shape through the longitudinal added mass distribution. These Equations (86) result when the constant factors in (85) are replaced by integral functions of the added mass distribution:

$$\begin{aligned}
 Y'_{\dot{v}} &= -\pi \left( \frac{T}{L} \right)^2 \int_{\text{Bow}}^{\text{Stern}} C_H dx' \\
 Y'_{\dot{r}} &= -\pi \left( \frac{T}{L} \right)^2 \int_{\text{Bow}}^{\text{Stern}} C_H X' dx' \\
 N'_{\dot{v}} &= -\pi \left( \frac{T}{L} \right)^2 \int_{\text{Bow}}^{\text{Stern}} C_H X' dx' \\
 N'_{\dot{r}} &= -\pi \left( \frac{T}{L} \right)^2 \int_{\text{Bow}}^{\text{Stern}} C_H X'^2 dx' \\
 Y'_{\ddot{v}} &= -\pi \left( \frac{T}{L} \right)^2 [C_H]_{\text{Stern}} \\
 Y'_{\ddot{r}} &= -\pi \left( \frac{T}{L} \right)^2 [C_H x']_{\text{Stern}} \\
 N'_{\ddot{v}} &= -\pi \left( \frac{T}{L} \right)^2 [[C_H x']_{\text{Stern}} + \int_{\text{Bow}}^{\text{Stern}} C_H dx']
 \end{aligned} \tag{86}$$

$$N'_{\ddot{r}} = -\pi \left( \frac{T}{L} \right)^2 [[C_H x'^2]_{\text{Stern}} + \int_{\text{Bow}}^{\text{Stern}} C_H x' dx']$$

where  $C_H$  is the zero frequency added mass coefficient at station  $x'$ , which is the non-dimensional ( $x/L$ ) from midships (these equations reduce to (85) if  $C_H = 1.0$  for all hull sections).

Not-well-understood viscosity effects near the stern are dominant and have made it difficult to successfully evaluate these expressions. Direct evaluation of the acceleration and velocity derivatives is thus not yet thought to be practical. The semi-empirical and theoretical approaches described in the next section are more promising practical techniques for design purposes.

**9.8 Semi-Empirical Methods, Regression Analysis, and Three-Dimensional Potential Flow Analysis.** Several attempts have been made to derive empirical expressions for the derivatives based on measured values from planar motion and rotating arm experiments, but primarily for the velocity derivatives. Smitt (1970), Norrbin (1971), and Inoue (1981) developed empirical formulas that were compared by Clarke (1982) against scatter plots of velocity derivatives available in the literature. Clarke then used multiple linear regression analysis to develop empirical formulas to explain the variation in the available data for the velocity derivatives and also the acceleration derivatives. His resulting four equations for velocity derivatives were obtained from the pooled data, and the remaining equations for acceleration derivatives from available planar motion data:

$$\begin{aligned}
 -Y'_{\dot{v}}/\pi(T/L)^2 &= 1 + 0.16 C_B B/T - 5.1 (B/L)^2 & (5.0) & (2.0) \\
 -Y'_{\dot{r}}/\pi(T/L)^2 &= 0.67 B/L - 0.0033 (B/T)^2 & (7.2) & (3.2) \\
 -N'_{\dot{v}}/\pi(T/L)^2 &= 1.1 B/L - 0.041 B/T & (2.9) & (2.1) \\
 -N'_{\dot{r}}/\pi(T/L)^2 &= 1/12 + 0.017 C_B B/T - 0.33 B/L & (4.3) & (5.6) \quad (87) \\
 -Y'_{\ddot{v}}/\pi(T/L)^2 &= 1 + 0.40 C_B B/T & (9.6) & \\
 -Y'_{\ddot{r}}/\pi(T/L)^2 &= -1/2 + 2.2 B/L - 0.080 B/T & (5.2) & (4.1) \\
 -N'_{\ddot{v}}/\pi(T/L)^2 &= 1/2 + 2.4 T/L & (0.6) & \\
 -N'_{\ddot{r}}/\pi(T/L)^2 &= 1/4 + 0.039 B/T - 0.56 B/L & (3.4) & (2.2)
 \end{aligned}$$

Results of the regression analysis are statistically significant but have not accounted for all the variations in the available derivative data and are far from satisfactory.

Mikelis and Price (1980) have found good agreement with measurements in both deep and shallow water through use of a three-dimensional potential flow analysis of the fluid using a finite element method. Accurate acceleration coefficients can thus be developed taking into account the ship's individual form.

**9.9 Systems Identification Methods.** The formal scientific approach of systems identification has also been utilized to develop hydrodynamic coefficients for mathematical modeling of ship trajectories. Primary application has been in the development of math model coefficients from full scale ship operations for use in ship handling computer simulations (see description of Ship Handling Simulators in Section 16.9).

Systems identification is the technology of developing mathematical models of vehicles from their dynamic responses to rudder movements. It is a highly mathematical technology that can be rigorously defined only in statistical terminology. The following engineering application definition is instructive (Hall, 1977): "System identification determines, from a given input/output data record of vehicle test response, an estimate of the physical model which relates to the observed data."

The actual processing of the data requires three major steps (Trankle, 1979): (a) model structure determination, (b) parameter estimation, and (c) model validation. Model structure determination is the process of selecting a mathematical form for the equations of motion. Questions addressed here include the determination of the order of the model (e.g., number of degrees of freedom) and a mathematical form (e.g., polynomial) to represent any nonlinear character in the dynamic equations. For linear dynamic systems, the determination of order is of primary importance. For nonlinear systems the determination of forms to represent nonlinearities has equal importance. For the case of ship hydrodynamics, model structure determination reduces to finding equations to represent the three terms  $N'$ ,  $Y'$ , and  $X'$  of Equation 22. For example, the curvature in the function representing yaw moment  $N'$  as a function of  $v'$  might use a cubic polynomial

$$N' = a_0 + a_1(v') + \dots + a_7(v')^3 + \dots$$

or might use a square-absolute form

$$N' = a_0 + a_1(v') + \dots + a_7 v' |v'| + \dots$$

(a) *Model structure determination* methods such as subset regression can assess the relative utility of these two models (Draper and Smith, 1966).

(b) *The estimation of unknown parameter values* follows the determination of a suitable model structure. Numerical values of unknown parameters are determined by choosing them to optimize some per-

formance index that measures how well the mathematical model represents the observed data. Two methods that have been applied to the ship hydrodynamics case are *output error* (Trankle, 1985) and *extended Kalman filter* (Abkowitz, 1980).

The output error method requires the minimization of the fit error between the measured ship trajectory and the trajectory as estimated by a simulation. Let  $\underline{y}(t_i)$  be a vector of measurements taken aboard the ship during a set of maneuvers. This vector might include

$$\underline{y}(t_i) = \begin{bmatrix} u \text{ (longitudinal velocity)} \\ v \text{ (lateral velocity)} \\ r \text{ (yaw rate)} \\ \psi \text{ (yaw angle)} \\ x \text{ (position north)} \\ y \text{ (position east)} \end{bmatrix}$$

Let  $\hat{\underline{y}}(\underline{\theta}, t_i)$  be the corresponding measurements as estimated by a simulation of the same maneuver. The simulated measurements are functions of a vector of unknown parameters  $\underline{\theta}$  (hydrodynamic coefficients such as  $Y_v$ ,  $N_r$ ) as well as of time. The fit error  $\underline{\epsilon}(\underline{\theta}, t_i)$  and performance measure  $L_o$  are

$$\underline{\epsilon}(\underline{\theta}, t_i) = \hat{\underline{y}}(\underline{\theta}, t_i) - \underline{y}(t_i) \quad L_o = \sum_{i=1}^n \underline{\epsilon}(\underline{\theta}, t_i) \cdot W \underline{\epsilon}(\underline{\theta}, t_i)$$

where  $W$  is a diagonal weighting matrix.

The extended Kalman filter method is similar to the output error method except that the parameters are treated as additional differential equations to be integrated along with the six first order differential equations of the ship motion. The extended Kalman filter method has the advantage of being able to provide parameter estimates in real time, i.e., as the data are collected. Its disadvantage is that convergence to the best parameter values may be more difficult to control.

(c) *Model validation* follows the determination of model structure and estimation of parameter values. A good criterion for the validation of a model is the use of the model to predict new data. A typical procedure might be to use, say, 80 percent of the available data to determine the model structure and parameter values. Then the resulting model would be used to predict ship motion for the remaining 20 percent of the data. The degree of validation achieved can then be interpreted from the accuracy of the prediction.

Statistical performance criteria for "the accuracy of the prediction" include the magnitude of the mean square fit error  $\underline{\epsilon}(\underline{\theta}, t_i)$  in predicting the additional data and the *whiteness* or statistical independence of the fit errors. Whiteness can often be evaluated effectively by visual inspection of plots of the observed data  $\underline{y}(t_i)$  superimposed on plots of the predicted data  $\hat{\underline{y}}(\underline{\theta}, t_i)$ . Plots of the fit error history itself may also be used.

Finally, validation should include comparison of the model determined from system identification with

- "Measurement" or Identification of the Magnitude of the Hydrodynamic Coefficients from the Measurement of the Ship Response to Given Rudder Action.

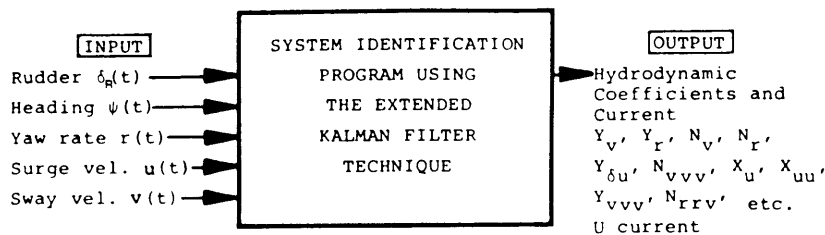


Fig. 55 System identification

models available *a priori*. Hydrodynamic coefficients of a ship as determined by identification should be compared to those for similar hull forms determined from captive model tests.

Whereas known simulation models are used to predict the output of the system to any given input to the system (ship motion response to rudder deflection or to propeller revolutions), the system identification process "identifies" the proper simulation model and its coefficients by analyzing various measured outputs in relation to the particular inputs that caused them. Abkowitz (1980) successfully applied systems identification techniques to the analysis of data from the full scale trials for the VLCC *Esso Osaka* (Crane, 1979). Fig. 55 from Abkowitz shows a schematic of the system identification procedure. Here the input to the system identification process is both the rudder deflection and the resulting motion responses, while the output is the identified parameters of the simulation model. System simulation is essentially an integration of a known differential equation; a process which is

rather exact. System identification, on the other hand, is concerned with comparing the integral (a numerical value) and the parameter (also a numerical value) and determining the differential equation involved (the integrand). The latter process is far from being exact, since several differential equations could give the same integral.

Most system identification techniques essentially go through a process whereby the predicted values of state variables (the motion variables in our case of  $u$ ,  $v$ ,  $r$ , and  $\psi$  as functions of time) are compared with the measured variables, and the differences are considered the error in the estimation. The values of the coefficients are then continuously updated, as the data are passed through, by an algorithm that tends to reduce the error, eventually seeking a set of coefficients which minimizes the error function.

Abkowitz (1980) used the *Extended Kalman filter* (EKF) technique with computer programs as developed and refined at MIT for the ship maneuvering problem. In this approach, the hydrodynamic coefficients are treated as additional variables but must be constant in time. Details of the MIT system are given in Szeto (1977) and Hwang (1980).

Experience with system identification processes shows that identifiability is enhanced by careful attention to the particular choice of trials and to achieving quality of measured data. The solution of coefficient drift and error cancellation is also a key to successful identification. The techniques of *parallel processing* and *over and under initial estimates* were developed to solve the coefficient drift problem. Parallel processing involves passing the data of two different maneuvers (a Z-maneuver with a turning circle maneuver, for instance) simultaneously through the identification process. The over and under initial estimates technique involves the automatic analysis of ratios of coefficients through the deliberate overestimation of the numerator and underestimation of the denominator. As the updating process proceeds, the minimizing of the error between estimated and measured motion parameters will result in approaching the correct ratio.

The resultant simulation equations developed

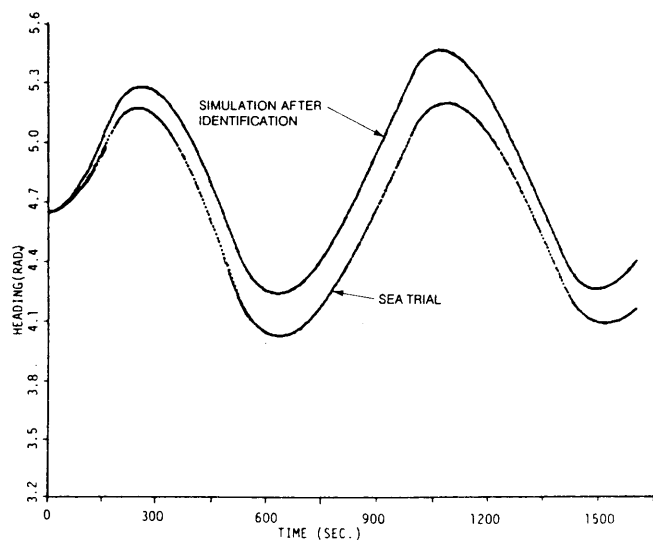


Fig. 56 Heading simulation of 20-deg-20-deg zigzag maneuver for Esso Osaka after the identification, deep water

through Abkowitz's system identification study show very good agreement with trial data. An example correlation is shown in Fig. 56. Now that the process has been refined and carefully validated with the *Esso*

*Osaka* data, the method holds great potential for easy application by using a portable instrumentation package on future ship trials to identify appropriate models and coefficients for other vessels (Trankle, 1986).

## Section 10

### Accelerating, Stopping, and Backing

**10.1 Introduction.** Accelerating, stopping, and backing are important ship maneuvers; the latter two particularly when near land, other vessels, and fixed structures. However, the interactions between hull and propeller(s) during these maneuvers are quite complex. Because of this and the transient character of maneuvering, empirical calculations of the characteristics of these maneuvers are sometimes used when adequate motion equation coefficients are not available for simulation.

*Accelerating* means increasing ship speed from rest, or from a particular ahead speed to a higher ahead speed.

*Stopping* is decelerating the ship from any given ahead speed until the ship comes to rest. When discussing stopping capabilities, at least two ahead speeds should be considered: a *crash stop* from full-ahead-sea-speed, and a "stop from harbor speed." Harbor speed may be about 12 knots for a slow ship, such as a tanker, or about 15 knots for a fast ship, such as a containership. Although in practice "emergency full astern" is almost never ordered from full-ahead-sea-speed, it is a customary machinery acceptance trial, and the results are useful as a relative measure of stopping ability.

*Coasting* refers to decelerating without using backing power. Time and distance required for a ship to decelerate to a slower speed is often of interest in ship handling. Decelerating more generally means that engine power ahead is insufficient to maintain steady forward speed. In that case, the unbalanced longitudinal force (i.e., thrust is less than resistance) then causes the ship to decelerate until resistance again equals thrust, at some slower speed. Rarely will a shiphandler coast a ship to near dead-in-the-water, because of the very long time it takes. However, decelerating at the least sustainable ahead power at which the ship will steer is very important to the ship handler. The distance required to thus decelerate is critical to getting a ship's speed down from the harbor approach velocity to a speed regime at which tugs can be effective in controlling the ship. In harbors where berthing may be located near the harbor entrance, this figures in harbor design, siting of terminals, and in the selection and use of tugs. In some places it has led to the use of braking tugs.

*Backing* a ship is a maneuver of accelerating from

rest to a given astern speed, or distance. A backing propeller, on the other hand is one in which the blades are turning with negative angle of attack, producing astern thrust.

The principal performance indexes of these maneuvers reflect the time and distance from initiation to completion. To simplify analyses, we often assume that the ship travels on a straight line during stopping. This is generally not true except in the case of some multiscrew ships with opposite rotating propellers, in the absence of appreciable wind, current, and rudder angle (and with controls-fixed straight-line stability). For the backing or stopping of ships with single-screws or unirotating multiscrews, the rotation of the propeller tends to swing the stern to port if the propellers are right-handed (positive rotation according to sign convention), and to starboard if they are left-handed (negative rotation). Other factors may cause the ship to veer in the opposite direction.

When a ship deviates from its straight path during a stopping or backing maneuver, the distance traveled is measured along its curved track. But the projections of this distance, termed head reach and side reach are generally of greater importance as performance indexes.

**10.2 Acceleration Times, Distances, and Velocities.** Acceleration ahead is important for naval ships that may have a change position rapidly in a task force, or accelerate suddenly for other tactical reasons.

A method for determining the acceleration of a ship is given by Peach (1963). The value of the accelerating force, at any given speed, is the difference between the value of the ship's net thrust,  $T_\phi$ , available at that speed, and the ship's resistance,  $R_t$ , at the same speed, Fig. 57. The acceleration may then be found from

$$R_t + T_\phi(1 - t) = (\Delta - X_u)\dot{u} \quad (88)$$

where

$R_t$  is the ship's resistance (positive for positive ahead speeds)

$T_\phi$  is the ship's net thrust (positive if thrust direction is ahead)

$t$  is the thrust deduction

$\Delta$  is the ship's mass

$X_u$  is the added mass in the  $x$ -direction (see Fig. 48).

$\dot{u}$  is the acceleration in the  $x$ -direction.

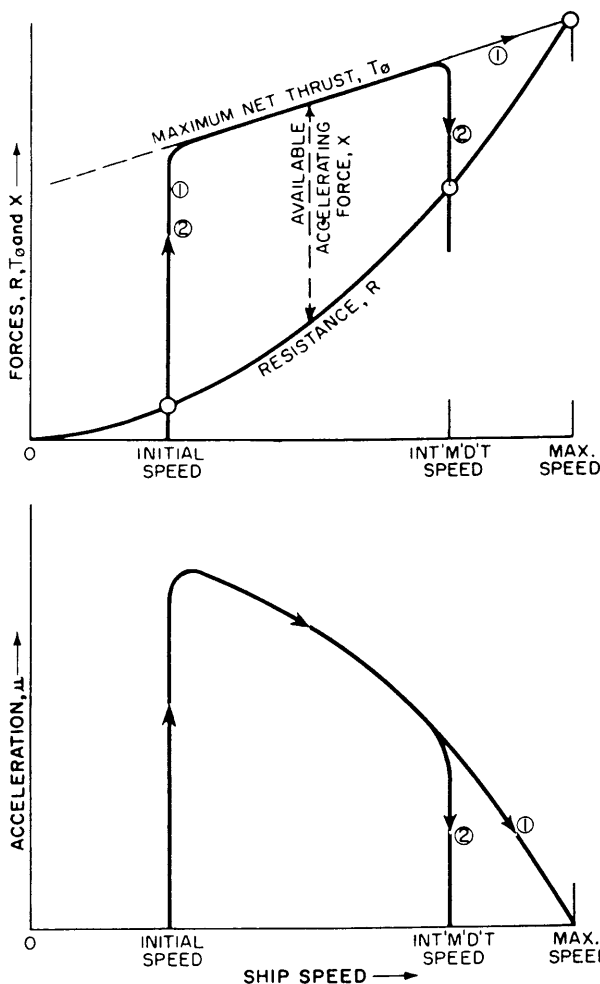


Fig. 57 Acceleration force and acceleration as functions of ship speed

Typical relationships amongst  $R$ ,  $T$ ,  $X$ , and speed for a steam turbine ship are shown in the Figure. Thrust curves 1 and 2 in Fig. 57 apply to the case where the initial speed is greater than zero. In the case shown, because thrust is greater than resistance at the initial speed, there is no equilibrium and the ship accelerates. At "execute," the thrust is increased rapidly to the amount desired. Then thrust curve 1 applies. Of course, the time to reach total equilibrium at maximum speed will be quite long. This is because resistance will very gradually approach the thrust curve as speed approaches maximum, and there is gradually diminishing unbalanced thrust remaining to cause acceleration.

If the final desired speed after acceleration is less than the maximum speed, then much less time and distance are needed. Then the maximum available thrust of curve 1 is utilized until the desired speed is reached and the thrust is appropriately reduced to equal the resistance at the desired speed, curve 2. This technique is useful in conducting maneuvering trials

to shorten the time needed to "steady up" on the approach course.

Figure 57, in the lower part, shows the relationship defined by Equation (88) between  $\dot{u}$  and ship speed,  $V$ , corresponding to thrust curves 1 and 2. The relationship between time, velocity, and distance may be computed as follows using Fig. 00:

$$\dot{u} = dV/dt$$

$$dt = \frac{1}{\dot{u}} dV$$

$$t = \int \frac{1}{\dot{u}} dV \quad (89)$$

$$S = \int V dt \quad (90)$$

where

$V$  is the ship velocity

$t$  is any time while accelerating, stopping, and so forth, also the total time.

$S$  is the distance traveled by the ship in any time  $t$ ; also total distance to accelerate, stop, and so forth.

These relationships are shown in Fig. 58. Fig. 59 shows the speed-distance diagram based on Fig. 58. The data shown on these figures were taken from Peach (1963) for a submarine with the characteristics given in Table 9.

The ship resistance,  $R$ , shown in Fig. 57 may be computed for any ship speed,  $V$ , by the methods given in Chapter V.

For a submarine or a slow surface ship (low  $F_n$ ), the following simple expression is appropriate:

$$R = kV^2$$

where  $k$  is a constant which may be obtained from data for similar submarines. For high speed surface ships, substantially higher average effective values are appropriate (see Table 10).

For a given ship and propeller configuration, and at any speed less than maximum ship speed, the maximum available thrust,  $T_\phi$  can be calculated using a diagram combining the propeller characteristics and the torque characteristics of the prime-mover, similar

Table 9

Ship	Propellers
$\Delta = 4000$ tons	$D = 2.74$ m (9 ft)
$V = 22$ knots	rpm = 315
shp = 12,600	$P/D = 1.00$
$X_b = -0.20$ m	3-bladed, NSMB, Series B50
$R = 285V^2$ ( $V$ in knots)	Twin-screw propulsion



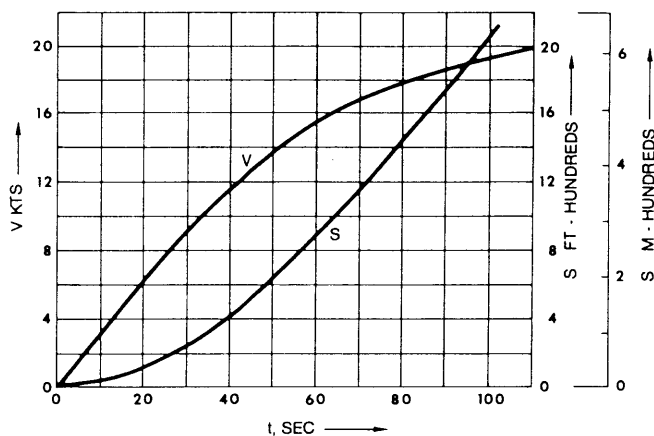


Fig. 58 Speed and distance versus time for a starting submarine

to Fig. 60. While this figure is applicable in particular only to the engine astern condition, it is also typical of ahead conditions. Since the prime-mover characteristic curves shown dashed in Fig. 60 are for a constant power steam turbine, they show increasing values of torque as the RPM is reduced. If a diesel-engine prime mover were portrayed, the dashed lines would be approximately horizontal.

Simplifying assumptions usually made in calculating the accelerating characteristics of ships are:

(a) *Instantaneous propeller acceleration*: Although in reality it takes finite time for the propeller to accelerate to a higher rotational speed, this assumption is sometimes made as in the submarine example of Peach (1963). The propeller and the value of the thrust are thus assumed to change instantaneously.

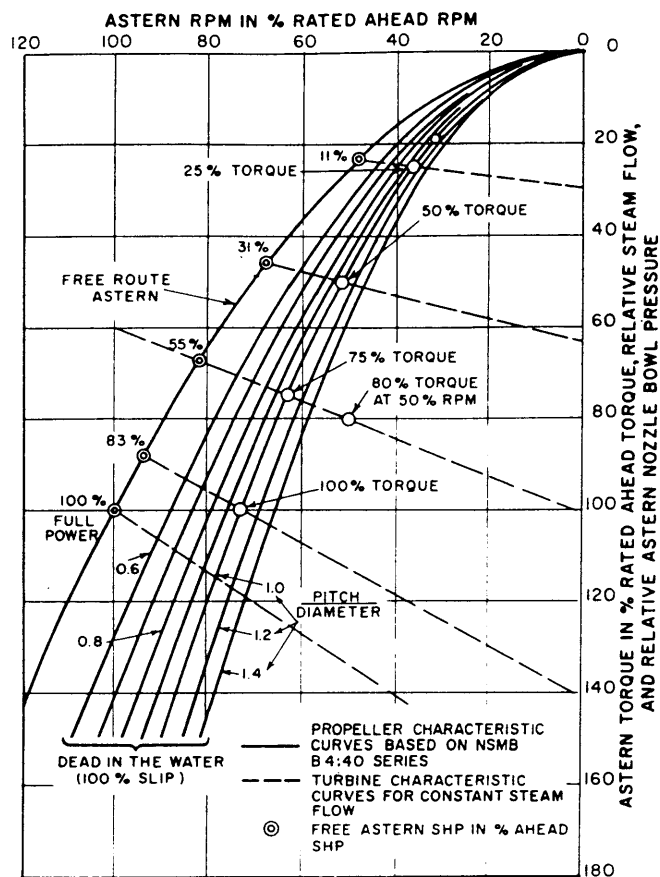


Fig. 60 Propeller-turbine characteristics

neously. Since for most ships the time to accelerate is large compared to the time to build up thrust, this assumption introduces only a small error.

(b) *Constant thrust deduction*: Thrust deduction varies with both propeller speed and ships speed. However, for most cases, these variations will not appreciably change the time to reach a given ahead speed. For the submarine example, thrust deduction was assumed to be constant throughout the starting maneuver. It is also assumed to be constant for the stopping maneuver discussed in the next section.

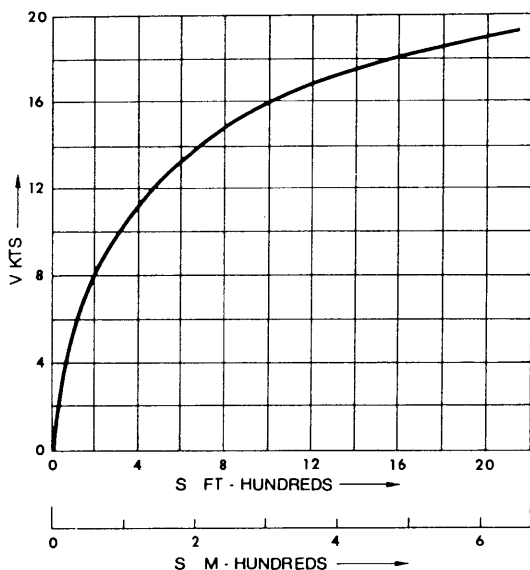


Fig. 59 Speed versus distance for a starting submarine

Table 10—Approximate Values of  $n$  in Expression  $R = kV^2$  as a Function of  $V/\sqrt{L}$  for Destroyer-Type Hulls

Approximate value of  $n$  for  $B/T = 3.0$   
and  $C_v = 2 \times 10^{-3}$

$V/\sqrt{L}$	$C_p/B$	0.60	0.65
	$L/B$	9.6	10.0
< 0.7		2.0	2.0
0.7-1.2		2.3	2.5
1.2-1.3		3.9	2.5
1.3-1.5		3.9	3.9
1.5-1.8		2.1	2.1
> 1.8		1.5	1.5

$C_v$  = Volumetric coefficient  $\nabla/L^3$

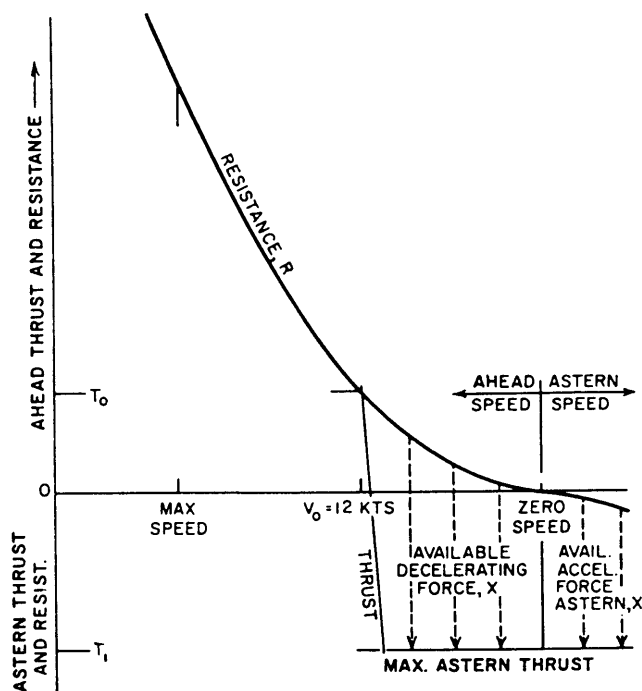


Fig. 61 Resistance, thrust and decelerating force versus speed in a stopping maneuver

**10.3 Stopping Distances.** Stopping is a maneuver of interest primarily from the point of view of avoiding collisions, rammings, and groundings. The distance in the original direction traveled by a ship in coming to a stop is called the *head reach*. Stopping tests of single-screw ships indicate that from modest maneuvering speeds, head reach is approximately the same whether the stopping path is along a straight or curved trajectory (Chase, et al 1957).

Ship operators generally consider the head reach from harbor speeds, established at 12 knots by Chase et al (1957), to be the important criterion for determining the backing power of ships. The head reach from full speed has little bearing because collision usually may be avoided more readily by turning than by stopping. As initial ship speed is reduced, the stopping maneuver does assume greater importance and the turning maneuver becomes less significant.

The two factors that are important in determining the accelerating characteristics of ships are also important for stopping. The ship's own resistance at higher initial speed will dissipate a substantial amount of the kinetic energy in the ship at the beginning of the maneuver. The resistance falls off rapidly, however, with speed decrease, Fig. 61. The other factor is the backing thrust developed by the ship's propeller. Opposing the deceleration caused by these two forces is the inertial effect of the ship's mass plus its longitudinal added mass.

A method for calculating head reach and time to

stop was developed in Chase, et al (1957), based on both theoretical and empirical considerations. This method considers the finite time for the thrust to change from steady ahead to steady astern, Fig. 62, and is applicable to any ship at any speed through use of an expression for ship's resistance

$$R = kV^n \quad (91)$$

where  $n$  may be any number, zero or greater. The method assumes that if the resistance varies as the  $n$ th power of the velocity at maximum ship speed, it will vary as the same power of the velocity at all speeds down to zero. This is approximately true only for the case of  $n = 2$ ; hence the method is strictly valid only for  $n = 2$ . Full-scale trial data have shown that it can be accurate to within a few percent for straight path stopping. The following paragraphs trace the manual calculation procedure.

Propeller thrust is shown in Fig. 62 as a linear function of the distance the ship travels until a constant astern value of  $T_1$  is reached. The thrust is then assumed to remain constant. Ship trial measurements of Hewins, Chase and Ruiz (1950) justify this approximation. The constant astern thrust,  $T_1$ , corresponds to astern thrust at dead in the water, while  $T_0$  is the initial free-running ahead thrust at the start of the maneuver. Both  $T_0$  and  $T_1$  are net thrusts; i.e., they include thrust-deduction corrections.

Chase, et al (1957) showed that good correlation between calculated and measured values of head reach and time to stop is obtained by assuming that the time

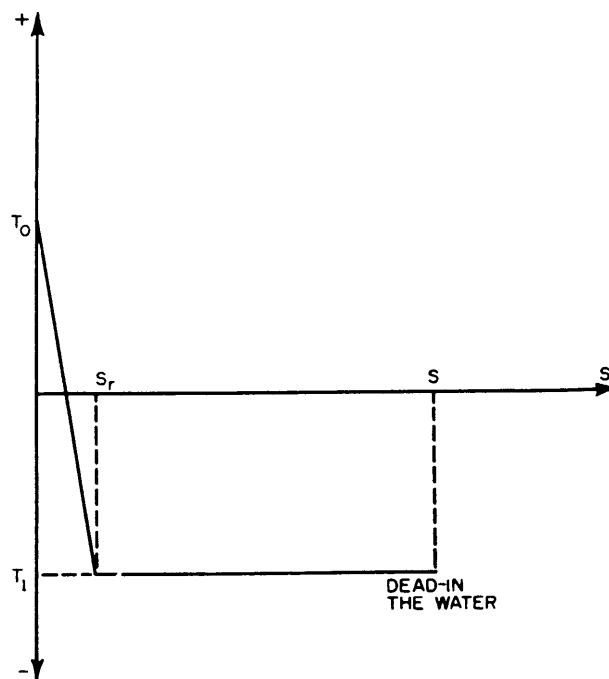


Fig. 62 Assumed thrust during crashback

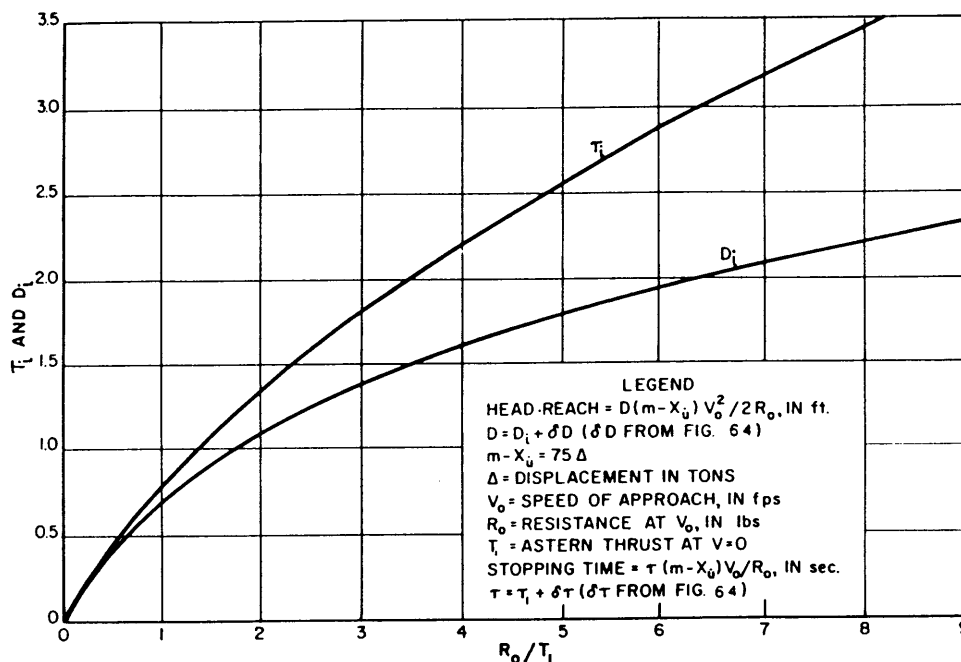


Fig. 63 Dynamic potential and dynamic impulse; astern thrust instantaneously applied

required to achieve constant astern thrust is the same as that required to close the ahead and open the astern throttle. This time,  $t$ , may be estimated from experience, or 20 seconds used for a modern vessel with automated controls.

The basic operations used in Chase, et al (1957) to compute head reach and time to stop are identical to Equations (88), (89), and (90). It was found that the variables naturally grouped themselves in three dimensionless ratios: dynamic potential, dynamic impulse, and ahead resistance to astern thrust. They were formalized with symbols as follows:

$$\text{Dynamic potential, } D = \frac{2R_0 S}{(\Delta - X_u)V_0^2} \quad (92)$$

where

$$\text{Dynamic impulse} = \tau = \frac{R_0 t}{(\Delta - X_u)V_0} \quad (93)$$

Ahead resistance to astern thrust ratio =  $R_0/T_1$

where

$V_0$  = initial steady ahead ship's speed at the start of the stopping maneuver.

$R_0$  = total resistance at  $V_0$ .

$T_1$  = constant astern thrust (dead in water)

Other symbols were defined previously.

Dynamic potential relates effective energy expended (as if the initial resistance stayed constant throughout

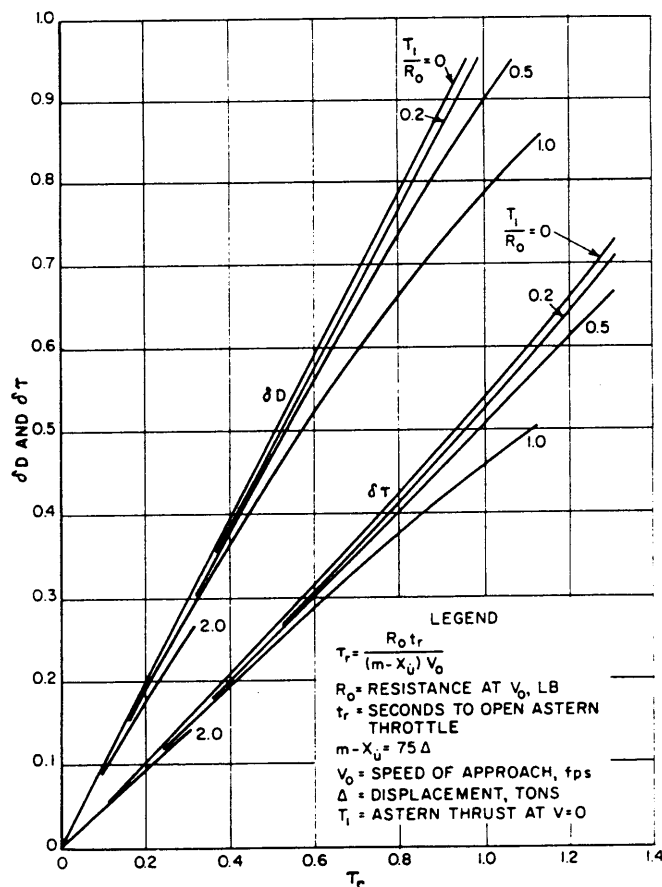


Fig. 64 Dynamic potential and dynamic impulse; astern thrust gradually applied

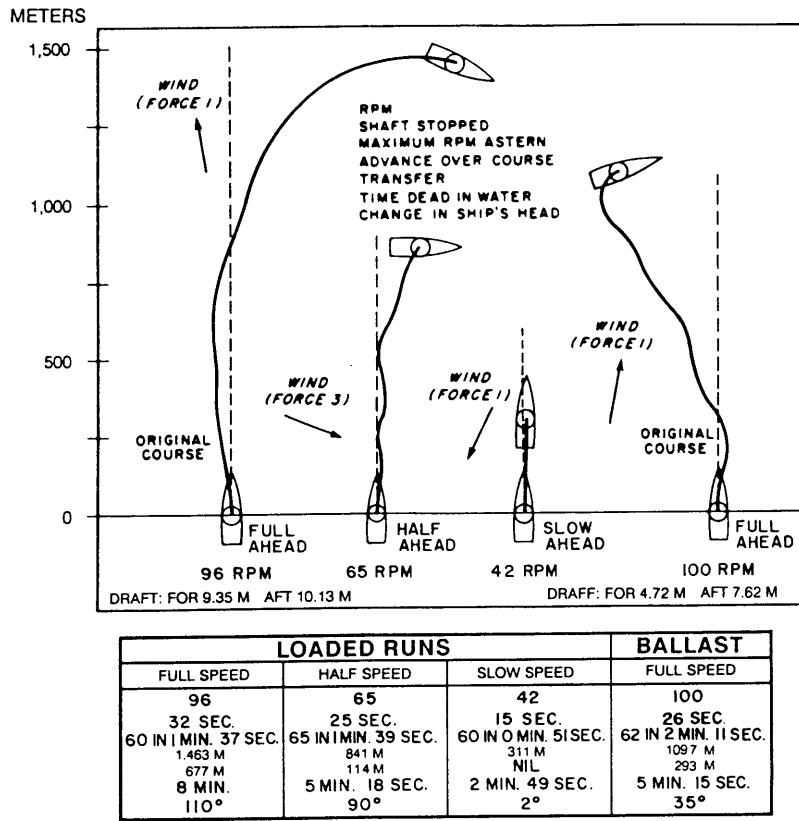


Fig. 65 Emergency stopping trials Esso Lima (26,700 dwt) (Crane, 1973)

the stopping distance) to the loss of kinetic energy of the ship. Dynamic impulse relates the impulse supplied by the ship's resistance (as if it had remained constant throughout the stopping time) until the loss of momentum of the ship. Equations (92) and (93), based on average impulse and momentum, when solved for stopping time and head reach show that time and reach vary inversely with retarding force. At slow ship speeds, propulsion is the predominant stopping force because resistance is small. Also, because at slow speed thrust varies approximately as RPM squared, head reach and stopping time show inverse square law characteristic versus RPM. From higher approach speeds the RPM squared characteristics is diluted by the initially large hull resistance.

The dynamic potential  $D$  of Equation (92), from which the head reach  $S$  may be computed, is expressed by  $D = D_i + \delta D$ , while the dynamic impulse  $\tau$ , from which the time to stop can be computed, is expressed by  $\tau = \tau_i + \delta \tau$ . Terms  $D_i$  and  $\tau_i$  are the values of the dynamic potential and the dynamic impulse for a constant astern thrust instantaneously applied, and are given in Chase, et al (1957) as functions of  $R_0/T_1$  and  $n$ . Terms  $\delta D$  and  $\delta \tau$  are corrections to  $D$  and  $\tau$  that take account of the fact that it takes finite time for the astern thrust,  $T_1$ , to develop. Values of  $\delta D$  and  $\delta \tau$  are given as functions of  $n$ ,  $R_0/T_1$  and  $\tau_r$ , where  $\tau_r$  is

the value of  $\tau$  when  $t = t_r$ . As indicated earlier,  $t_r$  is the time taken to open the astern throttle. Figs. 63 and 64 taken from Chase, et al (1957) show values of  $D_i$ ,  $\tau_i$ ,  $\delta D$ , and  $\delta \tau$  for  $n = 2$  ( $m$  = ship mass in days).

In addition to the assumption of  $n = 2$ , the following assumptions may be used in association with Figs. 63 and 64 for estimates of head reach early in the design stage:

(a) Astern thrust at dead in the water,  $T_1$ , is given by  $T_1 = 5.5 Q_1/P$ , where  $Q_1$  is the numerical value of the astern torque at dead in the water in ft-lb and  $P$  is the propeller pitch in ft.

(b)  $X_u \approx -0.08 m$ .

(c) The time to close the ahead and open the astern throttle,  $t_r$ , is 20 sec.

Values of  $Q_1$  needed in the first of these assumptions may be obtained from Fig. 60. Turbines of most merchant ships, were designed to provide an astern torque equal to 80 percent of the rated ahead torque at an astern propeller rpm of 50 percent of the rated ahead rpm. This is commonly referred to as "80-50" backing power, and many merchant-ship, steam turbines have been designed to these values. In Fig. 60, the (dashed) turbine characteristic curve passing through the "80-50" point intersects the propeller characteristic curve ( $P/D = 1.04$ ) at a torque ratio  $Q_1/Q$  of 0.755.

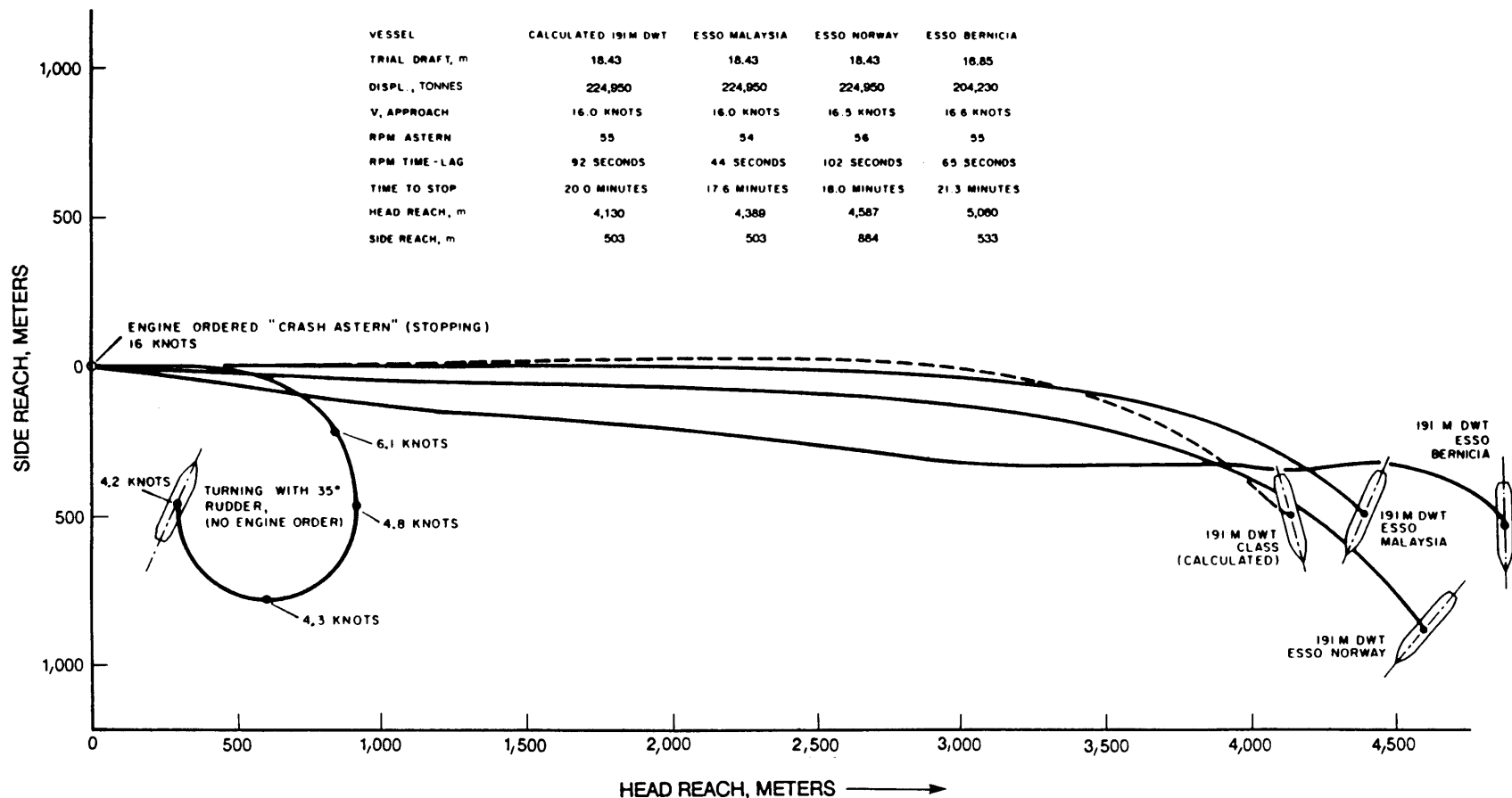


Fig. 66 Comparison of calculated "crash astern" maneuvers with full-scale trial results (Exxon 191,000-dwt tankers, load condition) (Crane, 1973)

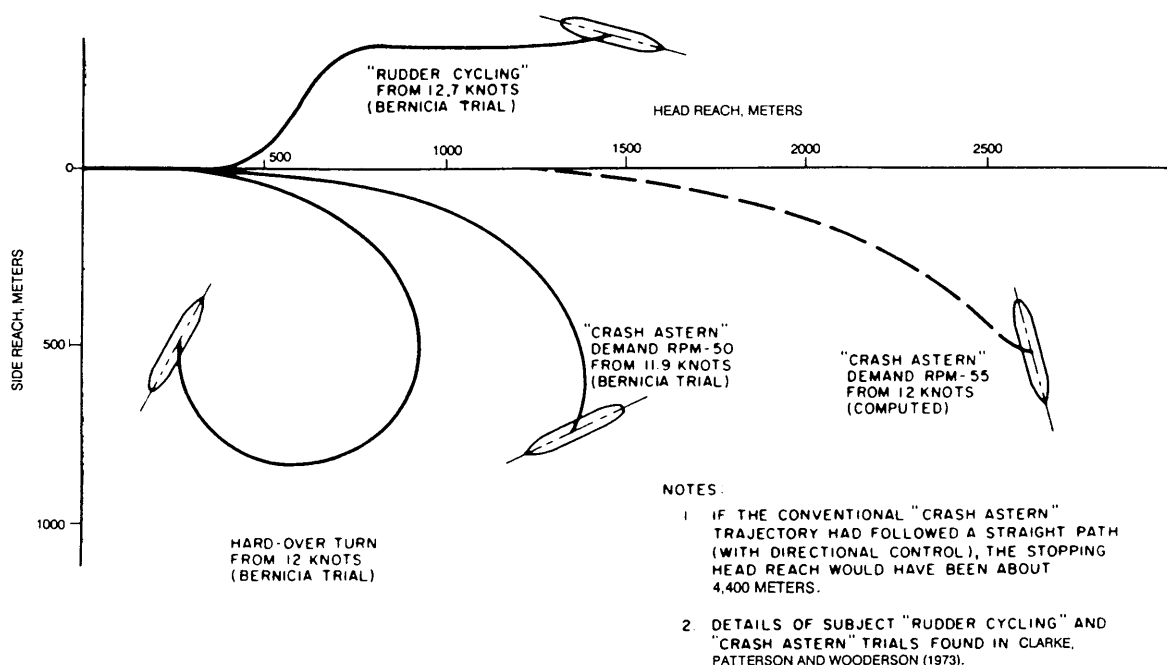


Fig. 67 "Rudder cycling" stopping maneuver versus "crash astern" and hard-over turn from *Esso Bernicia* trials (Clark, 1970). Moderate approach speeds of about 12 knots (Crane, 1973)

Chase, et al (1957) gives a detailed explanation of the construction of Fig. 60, as well as information for estimating the astern torques for types of power plants other than steam turbines.

**10.4 Stopping with Freedom to Turn.** In the "crash astern" maneuver of a single-screw ship, the trajectory is usually unpredictable due to loss of directional control. This was illustrated by the 1955 trials of the *Esso Lima* and *Esso Paterson* (Hewins, Chase, and Ruiz, 1950). See Fig. 65 for examples of *Esso Lima* results.

At high speeds and with sufficient sea room, turning of a large ship is much superior to stopping for avoiding a hazard. Advance in a turn is much less than head reach in stopping, and directional control is maintained. This is illustrated by full-scale trials and simulated stopping and turning maneuvers of the former 190,000-dwt Exxon design tanker shown in Fig. 66 for the trial full-load case.

From a slower approach speed, such as 6 knots, head reach and heading and path deflections during stopping are much less, and no general superiority for turning exists.

Full-scale trials indicate that if an auxiliary steering control force, such as a stern thruster, acts at the stern, it may be capable of controlling a ship's heading during a stopping maneuver under conditions when the ship's rudder or bow thruster cannot. However, this is not a general conclusion that a stern thruster will materially affect directional control when stopping from speeds above 6 knots.

**10.5 Rudder Cycling Maneuver.** In June 1969, maneuvering trials of the *Esso Bernicia*, a 190,000-dwt

tanker, were conducted and reported (Clarke, 1970). As part of the trials the "rudder cycling" maneuver was evaluated as a means of stopping without loss of steering control. The rudder cycling maneuver, which is illustrated in Clark (1970) is also depicted in Fig. 67. The maneuver comprises four partial turns to alternating sides about the base heading. Large speed reduction results from the hull's inertial reactions in the turns. Engine speed is reduced in steps during the maneuver until finally reversed, and engine orders are keyed to heading changes. Effectiveness of the maneuver and required lateral sea room are shown clearly in Fig. 67 (although exact comparison between *rudder cycling* and *crash astern* is not possible due to differences in wind velocity and water depth).

The general advantages of the rudder cycling stopping maneuver over the conventional crash astern are a more predictable trajectory and a reduced head reach. However, if lateral sea room permits, a simple hard-over turn is better than either and from approach speeds below about 8 knots the direct crash astern maneuver is generally best. Of course, if impact cannot be avoided, crash astern will reduce the striking vessel's speed and energy of impact.

**10.6 Effects of Machinery Characteristics and Dynamics.** The characteristics and dynamics of the propulsion machinery (engine, gears, shafting, and propellers) can have a significant effect on controllability.

Stopping ability of lighter, relatively high powered vessels is significantly dependent on maximum attainable time rates of change of propeller RPM, which

determine the time required to stop the propellers and to approach maximum astern RPM. Head reach in a crash stop will, for these ships, decrease significantly with a significant increase in time rate of change of propeller RPM. The effect will be less for very large relatively low powered vessels such as large tankers.

Controllability, and particularly stopping ability, can be seriously degraded in restricted waters for direct drive diesel-powered ships that have a limited ability to reverse engines frequently. Limited compressed air supply can severely limit the number of times the engines can be reversed in a relatively short period, and that can result in temporary loss of ability to reverse the propellers under the demands imposed by severely restricted water conditions. Such limitations should be avoided in any ship design.

**10.7 Simulation of Stopping.** The complexity of accelerating, stopping, and backing maneuvers in real life makes computer simulation useful for their study. Simulation equations contain terms selected depending on their use for design or operating studies or for training. For each of these uses, simulations must allow for the effect of transient RPM on rudder forces, and for the inclusion of other terms representing such factors as wind, current, and shallow water.

Several propeller and rudder factors affect the degree of ship response, including configurations of propeller, hull and rudder, propeller RPM, and rate of RPM change. Also, the ship's linear and angular velocities strongly influence propeller/rudder force, as does rudder angle and its rate of movement. Similarly the ship's hydrodynamic environment; i.e., the water density, depth, lateral boundaries and waves also affect propeller/rudder forces. For this reason, even with the computer's capability to handle many terms, we usually have to make simplifications, either because of

Table 11—Main particulars of tankers studied  
(Crane, 1973)

	Esso 191,000 dwt	Esso Suez 27,000 dwt
Hull		
Length between perpendiculars, $L$ , ft.	1000	612
Beam, $B$ , ft.	154.8	82.5
Draft, $H$ , ft.	60.5	31.5
Block coefficient, $C_b$	0.83	0.75
Displacement, $\Delta$ , long tons	221,400	34,100
Deadweight, long tons	191,350	27,000
Shaft horsepower, maximum		
continuous ahead	30,000	12,700
Design propeller rpm, ahead	80	112
Propeller		
Number of blades	6	4
Diameter, $d$ , ft.	29.2	20.0
Pitch, $p$ , ft.	20.7	16.83
Disk area ratio	0.585	0.550
	( $m = 3.28$ ft.)	

limited data or to avoid obscuring the central issue of the study.

Straight path stopping, with continuous application of astern power, is realistic only from modest approach speeds or when special means are provided for controlling heading; however, the assumption is useful when comparing proposals for shortening the stopping maneuver.

In this section, the effects of several ship design and operating parameters are demonstrated. Stopping of the 27,000 dwt former *Esso Suez* is shown in Fig. 68 to show how well the ship's predicted stopping time history compares with the ship's trial results. Main particulars of the two ships are given in Table 11.

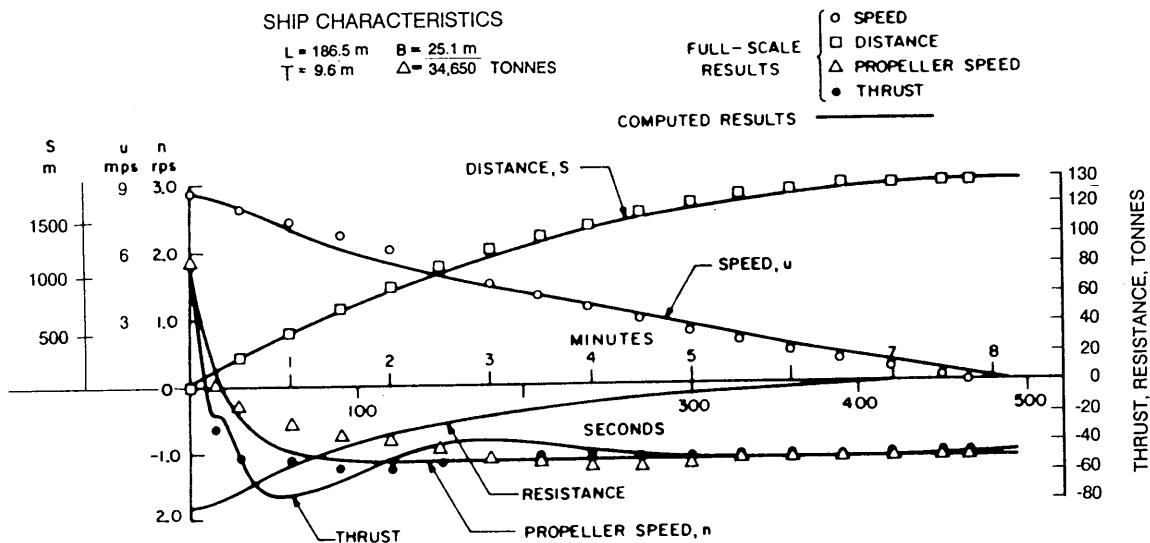


Fig. 68 Longitudinal stopping reponse of *Esso Suez* by trial and computation. Propeller speed approximated by exponential function. Run No. 3 of Hewins, Chase, and Ruiz (1950).

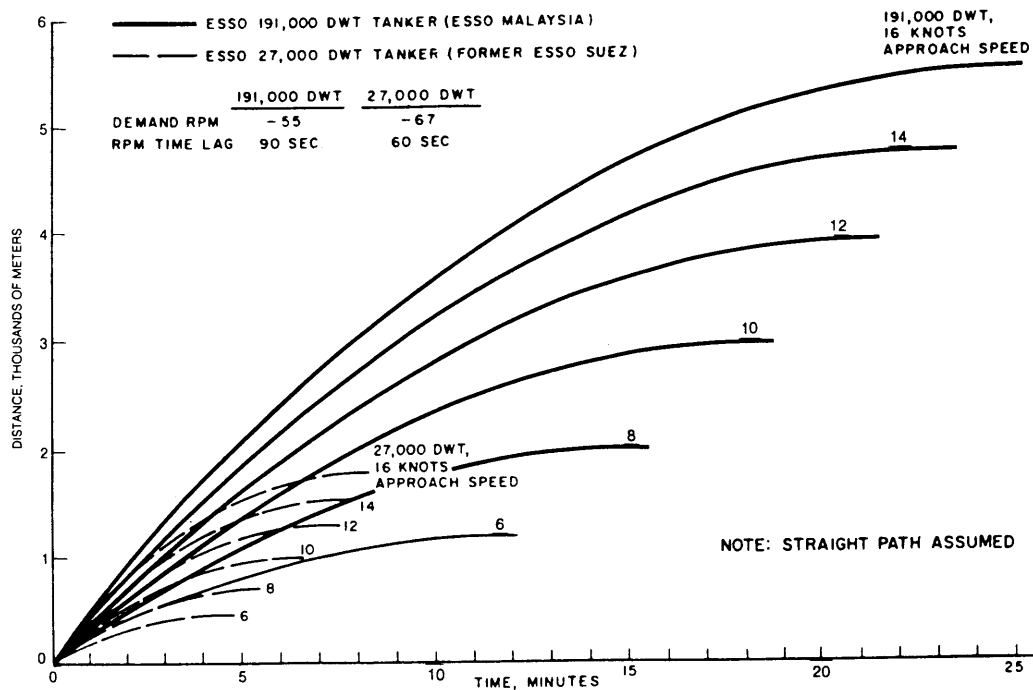
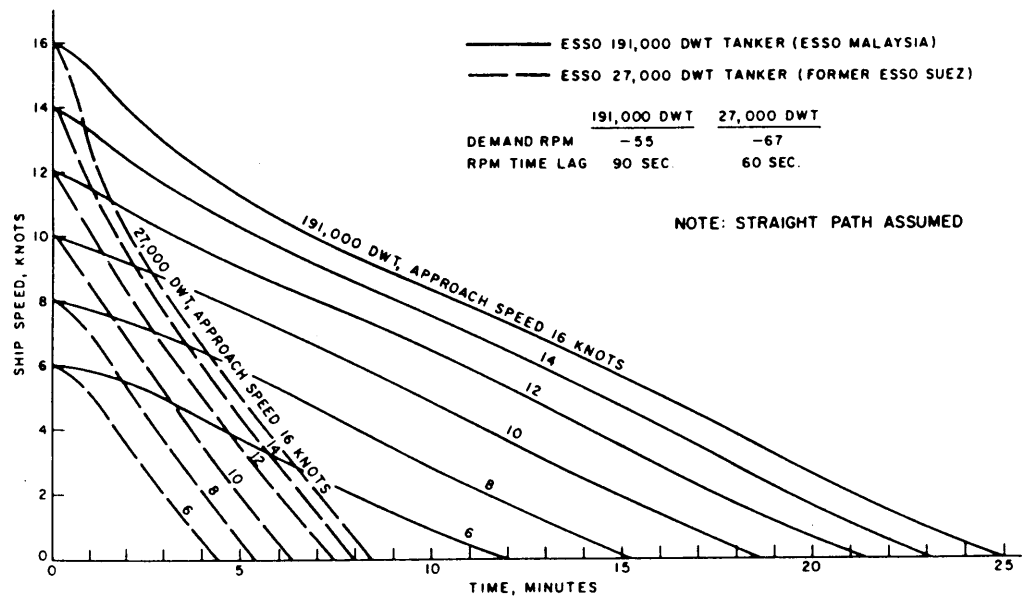


Fig. 69 Effects of ship size and speed; computed time histories of distance during stopping (Crane, 1973)

To show the effect of initial ship speed, ship speed and distance time histories during stopping maneuvers were computed for a number of approach speeds of the fully loaded 190,000-dwt tanker. These are shown in Figs. 69 and 70, together with the 27,000-dwt *Esso Suez* results. In Fig. 70 the final stopping time and head reach values of the 190,000-dwt tanker are summarized, together with results for different levels of

demand astern RPM. Astern thrust predominates when stopping a large tanker on a straight path from moderate speed. Propeller cavitation, however, could cause a significant reduction of astern thrust when RPM astern is more than about 70 percent of maximum ahead.

The important result is that there is only a decrease of about 20 to 25 percent of the original head reach



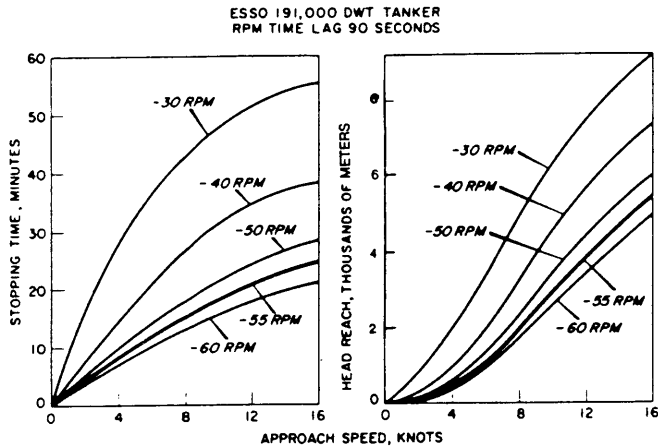


Fig. 70 Effect of approach speed on stopping time and headreach, with demand astern rpm as parameter (Crane, 1973)

by increasing the absorbed astern horsepower by as much as 100 percent (i.e., by increasing horsepower from about 30 to 60 percent of maximum ahead). This is because astern thrust increases by only about the  $2/3$  power of shp. Also, the time lag in reversing RPM tends to dilute the resulting thrust increase.

The net effect of ship size on stopping head reach is shown on Fig. 71. Trial data points for full-scale vessels are shown, together with, computed curves. All the trial data are from ships' service speeds which average around 15 knots (+1.5). Information is not available on heading and lateral deviations of these ships, so the data show only general trends. They are shortened to some extent by speed reduction effects of unintentional turning.

Stopping head reach and time to stop vary almost directly with ship's displacement, if we assume that astern thrust is affected only slightly by changes of propeller submersion. With this assumption, Fig. 72 shows the effect of loading condition on stopping a 191,000-dwt tanker from 16 knots.

Stopping results from slow speeds of up to about 6 knots are shown in Fig. 73. The independent variable is absorbed astern horsepower, with corresponding values of astern RPM and shaft torque shown. Head reach and time are normalized in the figure by dividing the results obtained at 55 RPM astern.

For large tankers, stopping is relatively insensitive to time lag in reversing the engine. On the other hand it may be important for relatively light, high speed vessels, where thrust is large compared to ship's mass.

**10.8 Coasting.** Coasting with the propeller windmilling consists of reducing the ahead power to that level necessary to cause the propeller to rotate without producing any thrust. In this case, the ship would be slowed solely by its hull resistance. When coasting with the propeller stopped, the ship would be slowed

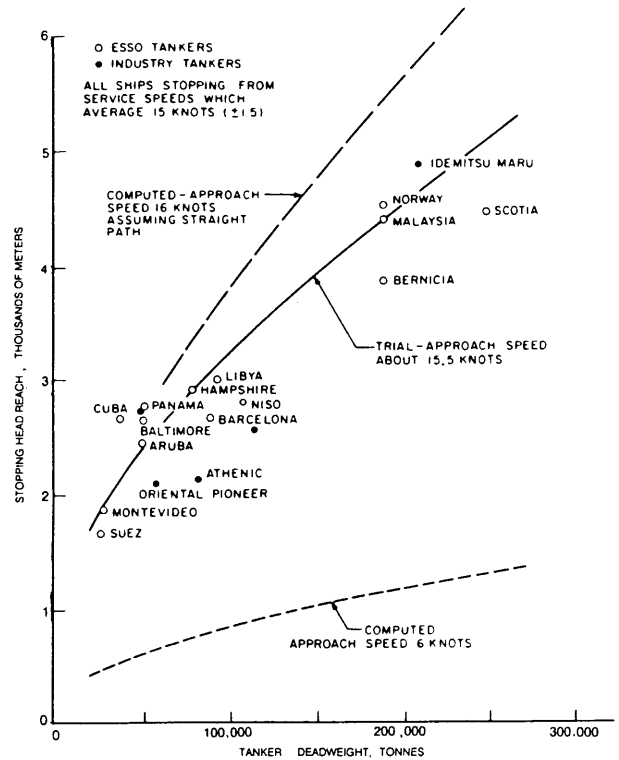


Fig. 71 General effect of ship size on stopping headreach (Crane, 1973)

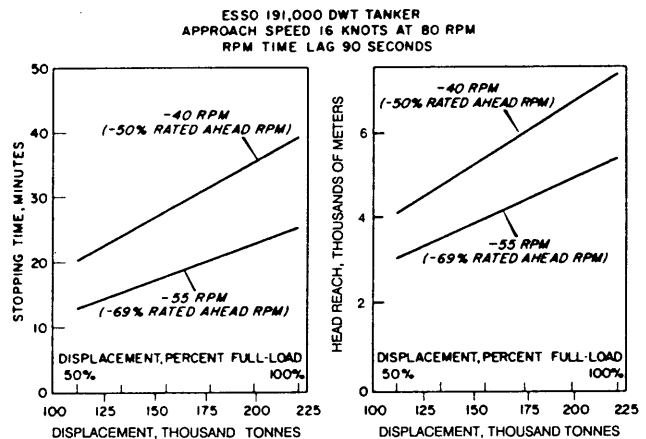


Fig. 72 Effect of ship displacement on emergency stopping time and headreach (Crane, 1973)

Table 12—Coasting Equations

Final speed	$\frac{V}{V_0} = \frac{2}{3}$	$\frac{1}{2}$	$\frac{1}{3}$
Initial speed			
Distance traveled $S$ , ft	$\frac{86 \Delta V_0^2}{R_0}$	$\frac{15 \Delta V_0^2}{R_0}$	$\frac{236 \Delta V_0^2}{R_0}$

where  $V_0$  is in knots and  $R_0$  is the total resistance at speed  $V_0$ ; i.e., with the propeller windmilling it is the hull resistance only, and with the propeller locked it is the hull resistance plus  $\delta R$ .

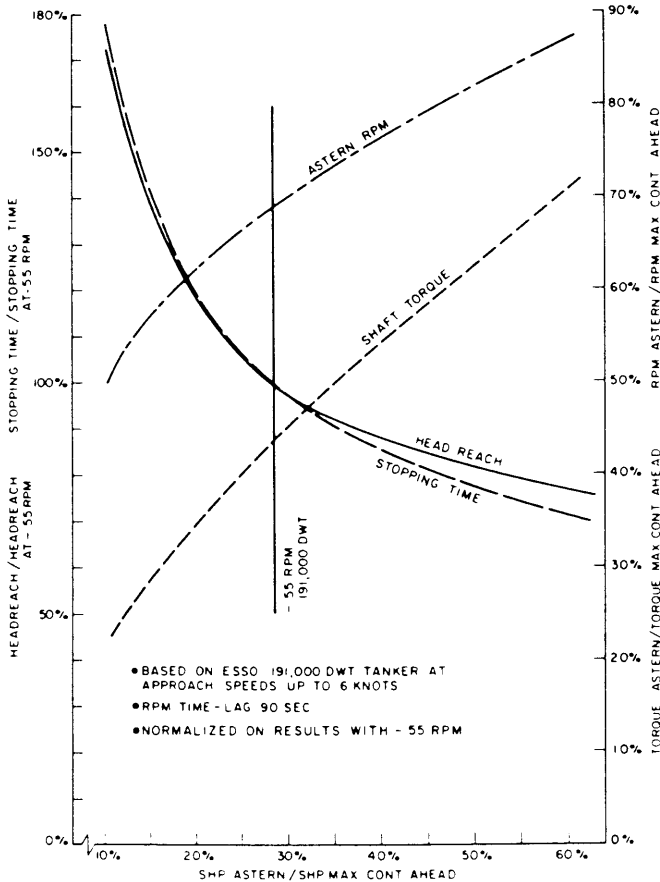


Fig. 73 Dimensionless presentation of effects of astern ship on stopping characteristics (Crane, 1973)

by its hull resistance plus the resistance of the locked propeller. In practice, the propeller's RPM is likely to be slightly less than its zero-slip value, so that it exerts some sternward thrust. With feedback engine control it may cycle between very slow ahead and astern. A workable measure of coasting behavior is the distance traveled by the ship to reach a specified fraction of the initial steady ahead speed.

Equations (92) and (93) for estimating stopping distance and time apply also to coasting with the following exceptions:

- The final speed is not zero but some specified fraction of  $V_0$ .
- With propeller windmilling, astern thrust,  $T_1$ , is zero.

- With the propeller locked,  $T_1$  is also zero but the hull resistance  $R$  is augmented by the added drag of the propeller,  $\delta R$ , so that  $R = R_h + \delta R$ .

The ahead thrust  $T_0$  is assumed to go to zero instantaneously at "execute." As a result of this assumption,  $\delta D$  and  $\delta T$  of Equations (92) and (93) are taken as zero.

Table 12 gives equations developed in Chase, et al (1957) from Equations (92) and Fig. 63 that are useful for estimating coasting distances. For this develop-

ment,  $X\dot{u}$  was taken as  $-0.08$  m, and  $n$  as 2, in accordance with earlier assumptions. An interesting result of the assumption that  $n = 2$  is that the distance traveled in coasting to a given fraction of the initial speed is independent of the magnitude of the initial speed. This of course would not be true if  $n$  were other than 2 (see Table 10).

The resistance augment,  $\delta R$ , of a locked propeller needed in connection with Table 12 may be estimated from the conventional drag formulation:

$$\delta R = C_D(\rho/2)AV^2 \quad (94)$$

where

$A$  = the developed area of the propeller in square feet.

$V$  = velocity of flow in feet per second. In this case  $V$  corresponds to the speed of advance,  $V_A = (1 - w)V_0$ .

$w$  = hull wake fraction.

$C_D$  = is a nondimensional drag coefficient. Hewins, et al (1950) estimate the value of  $C_D$  for a locked propeller as 1.0.

$\rho$  = is the mass density of sea water;  $\rho/2 = 1.0$  for sea water.

The added drag of a locked propeller computed on this basis is very large. Computations show that the ratio of  $\delta R/R_n$  in the speed range when  $n = 2$  ranges from less than 150 for very large, slow-speed ships to about 3.0 for large, fast twin-screw passenger liners. In other words, a locked propeller can constitute almost as much drag, and in some cases several times as much, as does the ship itself. These values used in association with Equation (94) and Table 12 indicate that coasting distances may be reduced by a factor of between two and four if the propellers are locked instead of allowed to windmill.

**10.9 Backing Times, Distances, and Velocities.** The survey of ship operator opinion conducted in connection with Chase, et al (1957) indicated that while there

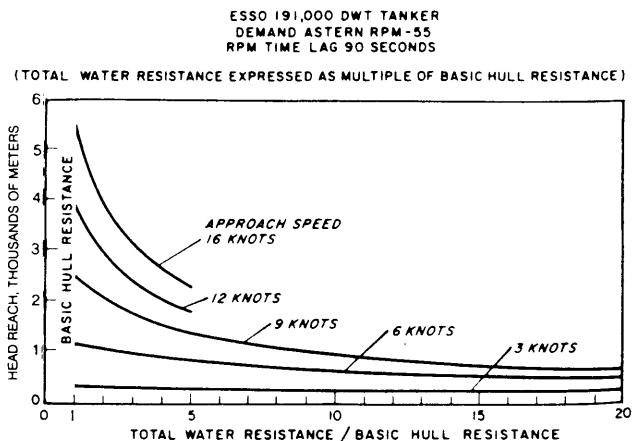


Fig. 74 Added hydrodynamic resistance effect on headreach, showing importance of approach speed; hull resistance supplemented by brake flaps, water parachutes, etc.

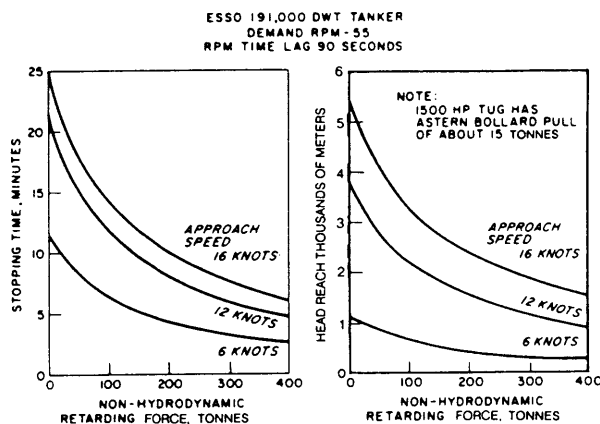


Fig. 75 Effect of nonhydrodynamic retarding force on stopping from 6, 12, 16 knots (Crane, 1973)

is agreement that ability to stop from harbor speed is important, many operators feel that backing time should be established primarily on the basis of maneuverability around docks. In the case of clearing a ship slip, the astern speed achieved after the ship has traveled one ship length may be an adequate criterion for judging backing speed. However, a poll of the operators did not suggest what that speed should be, but rather indicated that experience and the particular hydrographic conditions would dictate the desirable astern speed.

The astern speed,  $V$ , reached in differential time at starting from rest may be obtained by equating the product of the instantaneous accelerating force,  $X$ , times the distance traveled,  $S$ , to the kinetic energy of the ship at the speed  $V$ . Thus

$$SX = \frac{1}{2} (\Delta - X_w) V^2 \quad (95)$$

**10.10 Auxiliary Stopping Devices.** Resistance is a major contributor to stopping force at high ship speeds and is roughly proportional to the square of speed. For this reason, devices such as water parachutes and brake flaps which utilize hydrodynamic resistance are relatively ineffective for ship stopping from moderate speeds, and that is where unplanned stops are most likely.

In Fig. 74 the total resistance of a 190,000-dwt tanker (hull resistance plus added resistance) has been varied to represent effects of hydrodynamic stopping devices such as parachutes and brake flaps. Curves are drawn for stopping from 3, 6, 9, 12, and 16 knots. The total augmented resistance is expressed here as a multiplier of the basic hull resistance. The results show that ships moving at slow maneuvering speeds can benefit very little from added hydrodynamic resistance, even if as much as twenty times normal hull resistance (See also Clarke, 1971).

To consider effectiveness of nonhydrodynamic stop-

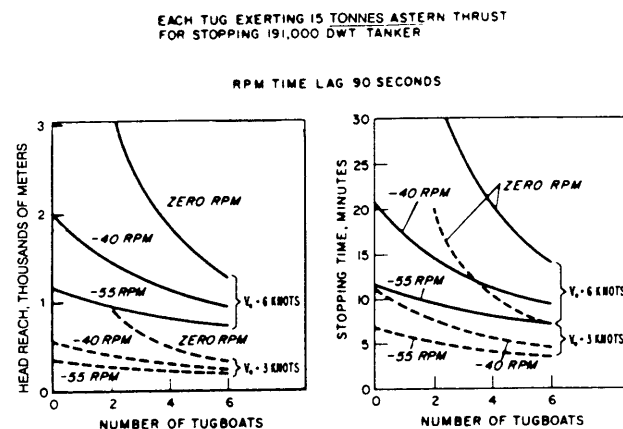


Fig. 76 Variation of head reach and stopping tie with number of 1500 hp tugboats and varied tanker approach speed and demand rpm

ping devices, a fixed retarding force, such as a rocket motor is examined by simulation. In Fig. 75, the effects of adding as much as 400 tons retarding force (equivalent to the takeoff thrust of forty Boeing 707 jet engines) is shown for the case of the 190,000-dwt tanker stopping from 6, 12, and 16 knots. The added retarding force is assumed maintained until the tanker stops. Somewhat greater effect might be obtained by increasing the amount of force at the high speed beginning of the maneuver, and shortening its duration.

Tugboats are regularly used to provide stopping forces at slow harbor speeds and are, therefore, part of the ship control system. Tugs are normally assumed fixed to the tanker in *power tie-up* so that the forward speed of the tanker and tugs is always the same. The effect of tugboats is essentially that of an added constant retarding force.

Figure 76 shows results from a simulation of the effects of tugs stopping a 190,000-dwt tanker (Crane, 1973). Tanker demand RPM is treated as a parameter. With fewer than two tugs and zero tanker RPM, stopping time and head reach are extremely long and not shown. The astern thrust of a 1,500-shp tug is represented in the simulation as a function of the tug's astern RPM and forward speed. Effects of tug hull resistance, mass, and added mass are included, but hydrodynamic interaction effects with the tanker are neglected. Each tug is assumed fully utilized for retarding the tanker making no contribution to directional control. From zero to six tugs are considered at tanker approach speeds of three and six knots. Above six knots, tugs are impractical due to the difficulties of tying up.

Figure 76 emphasizes that approach speed and tanker astern RPM have much more effect than number of tugs (provided that the tanker uses at least 40 RPM astern). Also, the case of zero tanker RPM with six tugs hauling astern yields about the same head reach as with 55 RPM astern and no tugs. With modern, more powerful tugs, of course, comparable tug

braking force can be achieved with fewer units than in this case. Kroda (1977) provides some valuable work

on the use of tugs in a braking situation. Adequate steering control is, of course, a separate consideration.

## Section 11

### Automatic Control Systems

**11.1 Introduction.** Regardless of hull and appendage characteristics and pilot/helmsman proficiency, good controllability at sea in all weather may depend greatly on the design and use of automatic control systems to perform steering and positioning functions. Ship autopilots have been in practical use since the mid 1920s being a classical application of feedback control. See Franklin, et al (1986) for a treatise on feedback control. Automatic control systems are also widely used on offshore drilling vessels and platforms for dynamic positioning. Recently, highly sophisticated "adaptive autopilots" have been developed which adapt to situations such as weather variations and attempt to minimize speed losses due to excessive rudder action and distance traveled while maintaining a desired course.

For both naval and merchant ships it is common practice to have a helmsman standing by at all times ready to take over when rough seas may reduce autopilot effectiveness. All-weather steering is thus a problem of control as well as ship design, and a system is required that will maintain desired heading under all sea conditions and ship courses. Furthermore, hull design and the control system must be *tuned* to minimize the possibility of broaching under severe following and quartering sea conditions when automatic control systems are in operation.

The elements of automatic control systems in handling basic course keeping will be discussed first followed by an approach to analyzing automatic control systems when applied to unstable vessels.

**11.2 Course-keeping With Automatic Control.** One of the functions of ship control is to maintain a ship's heading. In performing this function, a helmsman deflects the rudder in a way that will reduce the error between the actual and the desired heading, designated as  $\psi$  on Fig. 77. Since the actual heading angle can be determined by means of a compass, the magnitude of  $\psi$  can be readily displayed to the helmsman (Fig. 1). A good helmsman will not only deflect the rudder in response to the heading error,  $\psi$ , but he is also sensitive to the angular velocity of the ship,  $\dot{\psi}$  ( $\equiv r$ ), and he will ease off the rudder and apply a little opposite rudder in order to prevent overshooting the desired heading. It follows that an automatic pilot should also be responsive to control signals measuring both  $\psi$  and  $\dot{\psi}$ . (In some commercial autopilots for ocean-going ships, there is a feedback signal from the helm angle output to the heading error detector. By this means, the detector can anticipate the yawing of

the ship in response to helm already applied. Such a feedback signal is not, however, the equivalent of a sensitivity to  $\dot{\psi}$ ). Thus a rudder, under automatic control, might be deflected in accordance with the following linear expression:

$$\delta_R = k_1\psi + k_2\dot{\psi} \quad (96)$$

where  $\delta_R$ ,  $\psi$ , and  $\dot{\psi}$  are all functions of time and where  $k_1$  and  $k_2$  are the constants of proportionality of the control system.

Following the sign convention of this chapter, both  $k_1$  and  $k_2$  should be positive for proper control. Substituting Equation (96) into the equations of motion (12), the following equations are obtained:

$$\begin{aligned} Y'_v v' + (Y'_\psi - \Delta')\dot{v}' + k_1 Y'_\delta \dot{\psi} \\ + (Y'\psi - \Delta' + k_2 Y'_\delta)\dot{\psi}' + (Y'\ddot{\psi}) \ddot{\psi}' = 0 \end{aligned} \quad (97)$$

$$\begin{aligned} N'_v v' + N'_\psi \dot{v}' + k_1 N'_\delta \dot{\psi} \\ + (N'_\psi + k_2 N'_\delta)\dot{\psi}' + (N'_\psi - I'_z)\ddot{\psi} = 0 \end{aligned}$$

Equations (97) are simultaneous differential equations of the first order in  $v'$  and of the second order in  $\psi$ . The solution of these equations for  $v'$  and  $\psi$  yields a third-order differential equation which as noted in Section 3.1 leads to the concept of directional stability or instability. The solutions to Equations (97) are

$$\begin{aligned} v' &= v_2 e^{\sigma_1 t} + v_2 e^{\sigma_2 t} + v_4 e^{\sigma_1 t} \\ \psi' &= \psi_2 e^{\sigma_1 t} + \psi_8 e^{\sigma_2 t} + \psi_4 e^{\sigma_2 t} \end{aligned} \quad (98)$$

The equations of motion with automatic control, Equation (97), differ from the equations of motion with controls fixed at  $\delta_R = 0$ , Equation (11), in two major respects. Equation (97) implies a sensitivity to the orientation of the ship,  $\psi$ , which is absent in Equation (11). This is, of course, implicit in the concept of directional stability as opposed to straight-line stability. Secondly, two of the terms which appear in the criterion,  $C$ , Equation (14b), for controls-fixed, straight-line stability, are altered by the presence of the controls. The former term  $(Y'_r - \Delta')$  now appears as  $(Y'_r - \Delta' + k_2 Y'_\delta)$  and what was formerly  $(N'_r)$  now appears as  $(N'_r + k_2 N'_\delta)$ . Thus the second effort of automatic controls is to make the ship behave as if it

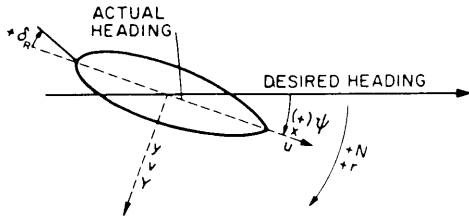


Fig. 77 Definition diagram for heading error

possessed different values of its inherent hydrodynamic derivatives.

From Equation (14c) then, when  $Y'_r(N'_r + k_2 N'_{\delta R}) > N'_r(Y'_r - \Delta' + k_2 Y'_{\delta R})$  the ship would be stable having negative stability roots ( $\sigma_1$  and  $\sigma_2$ ) and exhibiting no hysteresis loop in a plot of  $\dot{r}$  vs  $\delta_R$ .

It follows that a ship that is unstable with controls fixed can be made to be stable in terms of both straight-line and directional stability by the use of automatic controls. According to Equation (14b), stability is improved as  $(Y'_r - \Delta')$  increases in positive value, and as  $N'_r$  increases in negative value. Since  $Y'_\delta$  is always positive and  $N'_r$  is always negative for rudders at the stern and since  $k_2$  is positive, it follows that automatic controls designed in accordance with Equation (96) will improve stability.

Although not practical for a number of ship types, a desired ship characteristic is that it be stable with controls fixed so that automatic controls should not be used to overcome the inherent instability of a ship but rather to provide it with directional stability in addition to straight-line stability.

**11.3 Automatic Control of Unstable Vessels.** Eda (1971) has developed an approach for examining the effect of applying automatic control to vessels with varying degrees of inherent dynamic stability.

The following rudder control model is an example of an idealized simple autopilot expressed in a non-dimensional manner:

$$\delta_d = k_1(\psi - \psi_R) + k_2\dot{\psi}' + \delta_e = \delta_R + t'_r\dot{\delta}'_R \quad (99)$$

where

$\delta_d$  = rudder command

$\delta_R$  = actual rudder angle

$t'_r$  = time constant in rudder activation = 0.1

$k_1$  = yaw-gain constant

$k_2$  = yaw-rate gain constant

and subscript  $e$  indicates the value at the equilibrium conditions and yaw gain and yaw-rate gain constants  $k_1$  and  $k_2$  respectively, are based on nondimensional values (e.g., nondimensional time and shiplengths of travel,  $tU/l$ ).

Stability of heading angle can be examined using this rudder control model and the following set of solutions of perturbation equations, which are derived

from equations of yaw and sway motions and rudder control:

$$\psi = \sum_{n=1}^4 \psi_n e^{\sigma'_n t} \quad (\text{heading angle}) \quad (100)$$

$$v' = \sum_{n=1}^4 v'_n e^{\sigma'_n t} \quad (\text{sideslip velocity}) \quad (101)$$

$$\delta_R = \sum_{n=1}^4 \Delta_n e^{\sigma'_n t} \quad (\text{rudder angle}) \quad (102)$$

where  $\psi_n$ ,  $V'_n$  and  $\Delta_n$  are constants depending upon the initial conditions, and  $\sigma'_n$  are the eigenvalues of the system, which are determined by nontrivial solutions of the following characteristic equations:

$$\rho_0 \sigma'^4 + \rho_1 \sigma'^3 + \rho_2 \sigma'^2 + \rho_3 \sigma' + \rho_4 = 0 \quad (103)$$

If the real parts of all roots of the characteristic equation have a negative sign ( $\text{Re} \sigma'_n < 0$ ), the system is stable. In determining whether or not the system is stable, it is sufficient to know the sign of the real parts of the roots only.

On the other hand, if all the roots are determined, more detailed characteristics of the system can be obtained. Time constants and frequencies of the system can be determined from the real and imaginary parts of the roots, respectively. Furthermore, the solution vector can be determined from the initial conditions, and the actual ship dynamic response to any disturbance can be computed readily, if required. Accordingly, eigenvalues of the system can be directly determined on a digital computer for a wide range of control gain constants.

Stability roots were determined in Eda (1974) for three ships:

Ship A: Dynamically stable ship (stability index  $\sigma'_1 = -0.377$ ,  $l/B = 7$ )

Ship B: Dynamically unstable ship ( $\sigma'_2 = 0.164$ ,  $l/B = 5$ )

Ship C: Very dynamically stable ship ( $\sigma'_2 = 0.425$ ,  $l/B = 4$ )

for the following range of control systems characteristics:

Yaw gain  $k_1 = 0$  to 10

Yaw-rate gain  $k_2 = 0$  to 5

Time constant  $t' = 0$  to 2

Fig. 78 shows examples of stability roots for one gain and time constant and Fig 79 shows the resulting directionally stable regions for the three ships. The abscissa and the ordinate represent yaw-rate and yaw gain, respectively. The figure reveals the following:

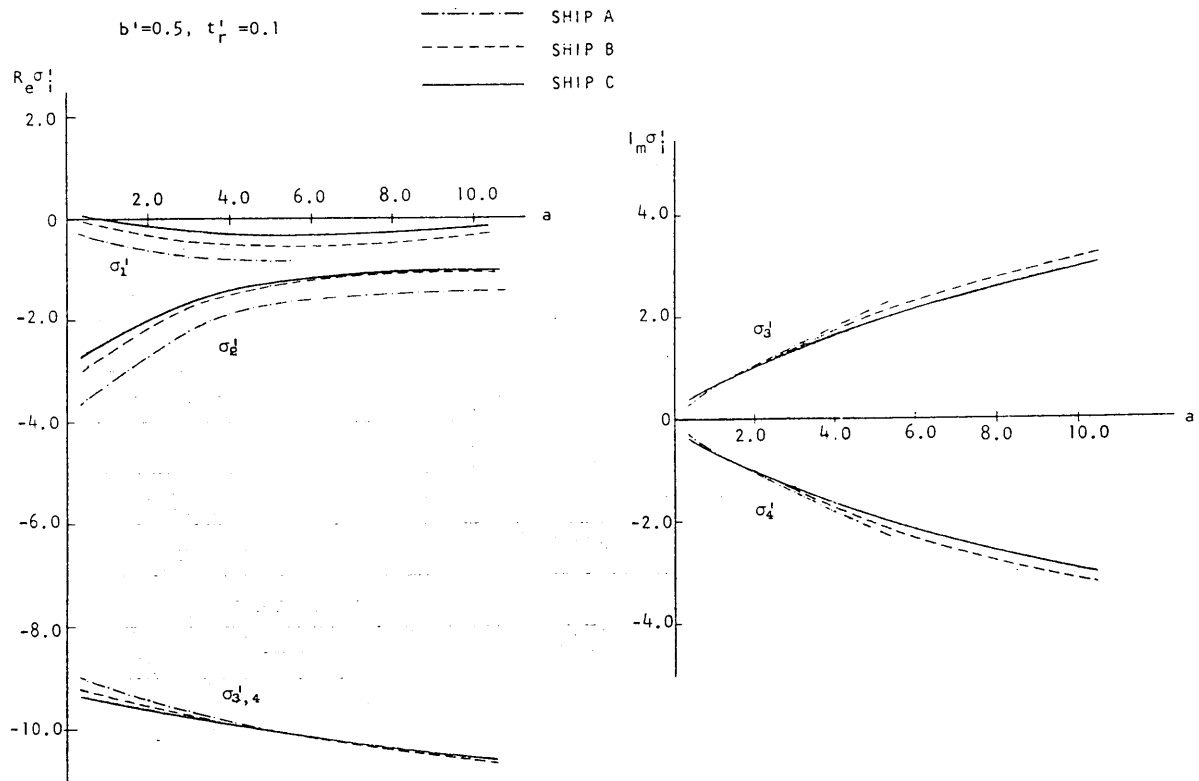


Fig. 78 Directional stability root locus

(a) Yaw gain must be positive to achieve directional stability whereas yaw-rate gain can be negative under certain conditions (i.e., when the ship has sufficient inherent dynamic stability or when sufficiently large yaw gain is simultaneously used).

(b) Three ships, having widely ranging degrees of dynamic stability, show a similar trend in stability change with changes in yaw and yaw-rate gains. Slopes of curves for neutral stability are roughly the same for these three ships; the only major difference is in the location of the intersection on the yaw-rate gain axis.

(c) Inherent dynamic instability can be eliminated by adding hydrodynamic damping through the rudder by mean of yaw-rate gain control. A ship with a greater degree of inherent instability requires a greater value of yaw-rate gain to achieve directional stability (when yaw gain is fixed).

It should be recognized that stable regions shown in Figure 79 are results of the eigenvalue analysis of the linear system so that the results are only valid for the case where deviations from the equilibrium conditions are very small. For example, a limit in available rudder angle in an actual system is not included in the analysis. When large values of gain constants are used, there exists a possibility of saturation in rudder angle which can introduce the instability into the system during actual operation.

Accordingly, results for the very unstable Ship C should be treated with caution because of the possibility of rudder angle saturation due to the large gain constants required for directional stability. Furthermore, there are certain limitations in the magnitude of gain constants in actual operations depending on the kind of maneuver. For example, a large yaw-rate gain constant (e.g.,  $k_2 > 0.75$ ) would not be acceptable for operation in a seaway because excessive rudder activity could be introduced due to yawing in waves. (Although steering gear machinery can operate continuously for hours, hunting or other high frequency movements caused by such wave induced yawing would be particularly hard on the system). These results indicate possible difficulties in handling of a very unstable ship such as Ship C.

**11.4 Input Data and Time Lag Effects.** All automatic control systems operate using certain state, or input data such as heading, yaw rate. Heading and yaw rate can be readily determined using a gyro compass and rate gyro. Position, for dynamic positioning systems, or is usually determined using sonar sending units or pingers placed at known locations on the ocean bottom or by using a satellite-based inertial navigation system.

Adaptive autopilots also use a number of additional methods to improve upon the relatively simple rudder control model, especially for use in severe bow seas,

Equation (99). These include:

- (a) Addition of an acceleration gain term,  $k_3\ddot{\psi}'$  where  $\ddot{\psi}'$  is yaw acceleration;
- (b) Addition of a track error gain term,  $k_4y'$ , where  $y'$  is distance from desired track (nondimensional).
- (c) Use of low-pass and sophisticated filters to reduce or eliminate high-frequency rudder motions due to wave forces particularly for head and bow seas.

The additional data required such as integrated position, and yaw acceleration, can be determined by integration or differentiation of measured data. The usual concerns about errors introduced by differentiation of measured data, exist, however. Ship velocity, relative to the bottom, can be determined using a two-axis Doppler system.

Wind velocity and direction, when required as for a dynamic positioning system, can be readily determined from a shipboard anemometer. This anemometer must be so placed that there is negligible interference with ship structure regardless of wind direction.

In the case of coursekeeping, although  $\psi$  and  $\dot{\psi}$  may be measured and signaled to the autopilot at time  $t$ , there are lags in any control system and it requires finite time  $\bar{t}$ , for the rudder to reach the deflection angle prescribed by Equation (96). Hence, the deflection of the rudder,  $\delta_R$  at time  $t$  is proportional to  $\psi$  and  $\dot{\psi}$  at an earlier time,  $t_1 = t - \bar{t}$ . In functional form, Equation (96) becomes:

$$\delta_R(t) = k_1\psi(t - \bar{t}) + k_2\dot{\psi}(t - \bar{t}) \quad (104)$$

where  $\bar{t}$  is the time lag of the control system.

Following Equation (7c) the linearized form of the Taylor expansion of (104) is:

$$\delta_R(t) = k_1[\psi(t) - \bar{t}\dot{\psi}(t)] + k_2[\dot{\psi}(t) - \bar{t}\ddot{\psi}(t)] \quad (105)$$

Nondimensionalizing this equation, substituting it into Equation (12a), and dropping the functional notation ( $t$ ) which is implicit, the following is obtained:

$$\begin{aligned} Y'_v v' + (Y'_\psi - \Delta')\dot{\psi}' + k_1 Y'_\delta \psi' \\ + (Y'_\dot{\psi} - \Delta' + k_2 Y'_\delta - k_1 \bar{t}' Y'_\delta)\dot{\psi}' \\ + (Y'_\ddot{\psi} - k_2 \bar{t}' Y'_\delta)\ddot{\psi}' = 0 \end{aligned} \quad (106)$$

$$N'_v v' + (N'_\psi)\dot{\psi}' + k_1 N'_\delta \psi'$$

$$\begin{aligned} + (N'_\dot{\psi} + k_2 N'_\delta - k_1 \bar{t}' N'_\delta)\dot{\psi}' \\ + (N'_\ddot{\psi} - I'_z - k_2 \bar{t}' N'_\delta)\ddot{\psi}' = 0 \end{aligned}$$

where  $\bar{t}' = (\bar{t})(V/L)$ .

Again, comparing terms of the criterion,  $C$ , Equation (13b), it is noted that the term  $(Y'_r - \Delta')$  now appears as  $(Y'_r - \Delta' + k_2 Y'_\delta - k_1 \bar{t}' Y'_\delta)$  and the term  $N'_r$  appears as  $(N'_r + k_2 N'_\delta - k_1 \bar{t}' N'_\delta)$ . Two important facts emerge from these comparisons:

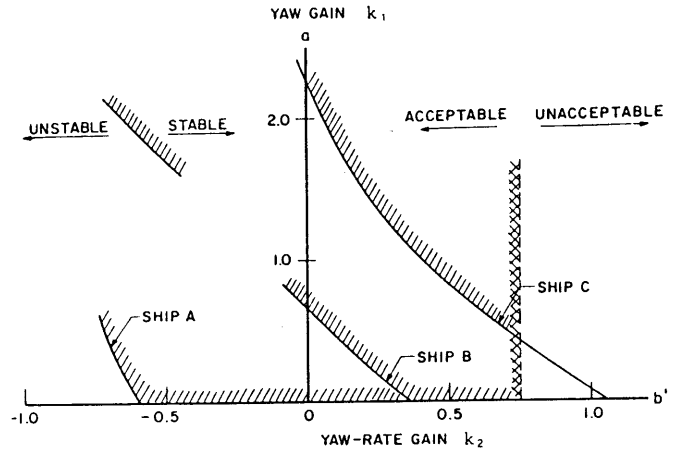


Fig. 79 Region of directional stability

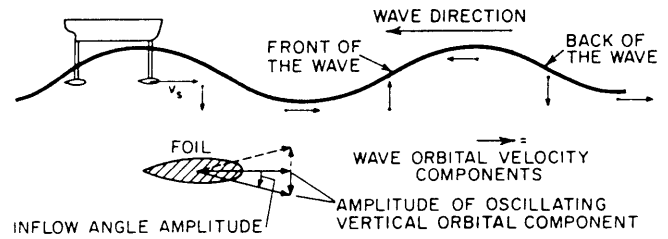


Fig. 80 Hydrofoil craft in regular ahead waves (Abkowitz, 1964)

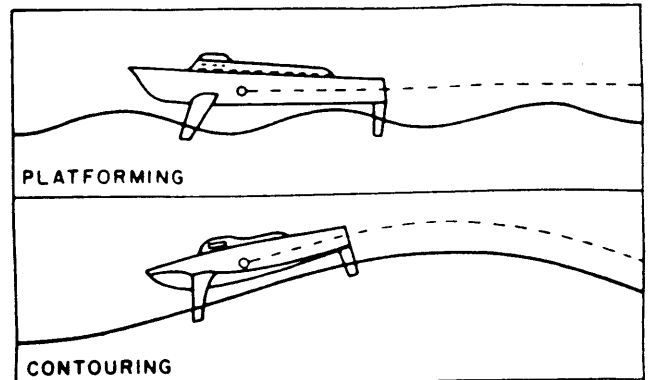


Fig. 81 Illustration of hydrofoil platforming and contouring modes

(a) The existence of a time lag,  $\bar{t}$ , detracts from the stability of the ship compared to zero time lag.

(b) If automatic controls were made sensitive only to  $\psi$ , and not to  $\dot{\psi}$ , ( $k_2 = 0$ ) and a time lag existed, the stability of the ship with controls would be less than without controls. It is conceivable that this decrease in stability could cause a ship that was stable without controls to become unstable with controls.

**11.5 Automatic Control of Hydrofoils.** It is particularly difficult, if not impossible, to manually control

a high-speed hydrofoil craft with a fully submerged foil system operating in rough water. Such craft therefore depend on an automatic control system that constantly adjusts foil angle of attack, either through changes in foil incidence or flap angle. These adjustments are made to port and starboard, as well as fore and aft foils to maintain trim and keep the hull at a given height above the mean water surface in the presence of disturbances. In order to achieve as high a lift-to-drag ratio as possible in the cruise condition, the foils are designed to operate with relatively small mean incidence or flap angles. This then provides adequate reserve to generate the required control forces. This is necessary because of the changes in foil angle of attack resulting from the orbital velocities of waves (see Fig. 80) which, if not compensated for, can produce significant craft excitations.

In general, these excitations must be compensated for by the control system if the craft is to fly straight and level and remain foilborne in large waves without excessive cresting of the hull or broaching of the foils. Broaching refers to a condition when the foil breaks through the water surface, losing its lift, possibly causing the craft to go hullborne.

There are two modes in which a hydrofoil control system operates, namely, the platforming mode and contouring mode. As the name implies, in the former mode the craft flies at given height above the mean water surface, as illustrated in Fig. 81, and is controlled automatically so that there is minimum motion. The limit on this mode is a function of wave height and foil system strut length. When wave height and steepness exceed a value where the ship can no longer "platform," the operator resorts to the contouring mode, in which the hydrofoil flies approximately parallel to the smoothed contour of the sea surface or nearly follows the wave contour.

In modern hydrofoils, such as the US Navy PHM, the time constants of the control system are sufficient

to handle both of the above modes of operation. During early developments of hydrofoils, control systems utilized input sensors for spatial anticipation of oncoming waves. These mechanical devices were known as "feelers," or a stinger projecting ahead of the craft. The modern hydrofoil control system uses either a sonic or radar height sensor, or both. These devices continually measure the distance to the water surface and input signals to the control system, which, together with other autopilot inputs, provide signals to the hydraulically actuated foil system. An improvement is currently being developed and is called a Forward Looking Radar Height Sensor. This device will determine wave height well ahead of the hydrofoil and in sufficient time, switch from one mode to the other to minimize not only ship motion, but loads imposed on the foil, hydraulic systems, and hull.

**11.6 Dynamic Positioning Systems.** Dynamic positioning (DP) systems, which are described in Section 1.7 of Chapter XII in Taggart (1980), are used to maintain a vessel within a specified watch circle, or radius from a specified location, to facilitate operations such as offshore drilling for oil or mine hunting. A typical watch circle radius is five percent of water depth, a value based on extensive operating experience.

Brink and Stuurman (1979), have provided a detailed description of a DP system for minehunters. This is termed a PID system which uses position (P), integral or cumulative time average of position (I), and differential of position or velocity away from the desired position (D). The role of model test data in tuning the system is discussed, as is the important subject of feed-forward. Feed-forward is used to anticipate future motions by sampling variables, such as wind velocity and direction, which vary slowly and thus have a direct influence on future events. To date, feed forward has been limited to wind effects, as wave and current characteristics are hard to measure, and wave elevation is highly transient.

## Section 12

### Effects of the Environment

**12.1 Introduction.** Ship controllability can be significantly affected by the immediate environment (wind, waves, and current). Environmental forces can cause reduced coursekeeping stability or complete loss of ability to maintain a desired course. They can also cause increased resistance to a ship's forward motion, with consequent demand for additional power to make good a given speed.

**12.2 Dynamic Behavior in Wind.** When the ratio of wind velocity to ship speed is large, wind has an appreciable effect on ship control. Even a moderate wind can make a ship advancing at slow speed difficult to control. To provide adequate control of ships in wind,

it is necessary to develop information concerning wind effects on ship controllability under various situations and to analyze the problem discovered to exist. A measure of control can be achieved by varying the ship characteristics, such as hull profile, rudder size, and other design variables and by adding thrust devices (See Section 17).

Effects of a given wind increase in a direct ratio to (a) above water area, (b) distance from the center of lateral area to the LCG, and (c) aerodynamic drag coefficients. Since some types of ships such as automobile carriers, container ships, and LNG ships have relatively large windage areas due to high freeboard,



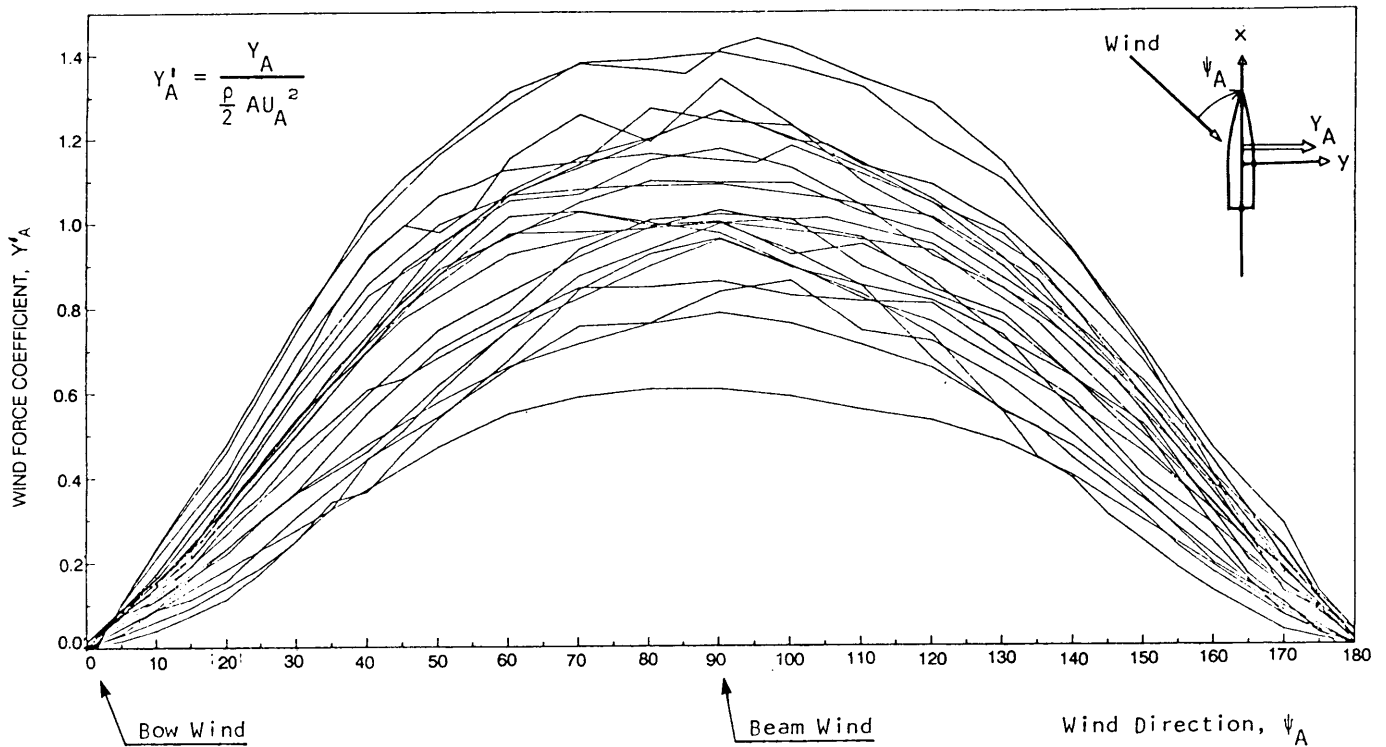


Fig. 82 Nondimensional aerodynamic side-force coefficients for many ships

the low-speed handling characteristics of such ships are critically influenced by wind.

Fig. 82 shows examples of nondimensional aerodynamic side-force coefficients for many ships plotted against wind direction. These data show a fairly even pattern of distribution with respect to a coefficient amplitude of about 1.0.

The equations of motion can be modified to include nondimensionalized aerodynamic surge and sway forces and yawing moments  $X_a$ ,  $Y_a$  and  $N_a$ , respectively. These additional forces and moments are defined by the following equations:

$$X_a = \frac{1}{2} \rho_a u_a^2 A_{ax} = X'_a \frac{1}{2} \rho u^2 L^2 \quad (107)$$

$$Y_a = \frac{1}{2} \rho_a v_a^2 A_{ay} = Y'_a \frac{1}{2} \rho u^2 L^2 \quad (108)$$

$$N_a = Y_a x_{ac} = N'_a \rho u^2 L^2 \quad (109)$$

where

$\rho_a$  is air mass density

$U_a$  and  $V_a$  are longitudinal and transverse components of relative wind velocities, resp.

$A_{ax}$  and  $A_{ay}$  are maximum longitudinal and transverse projections, respectively, of aerodynamic area.

$x_{ac}$  is the longitudinal coordinate of the center of transverse aerodynamic force relative to midships.

When the magnitude and the direction of wind velocity relative to the  $x_o$  and  $y_o$  axes fixed on the earth's

surface are given, as shown in Fig. 83 with reference to Fig. 2 the ship's  $x$  and  $y$  axis components of ship velocity relative to the air are:

$$u_a = u + U_a (\cos \psi + \psi) \quad (110)$$

$$v_a = V - U_a (\sin \psi_a + \psi) \quad (111)$$

where

$U_a$  is speed (velocity) of wind

$\psi_a$  is direction from which wind arrives relative to the earth-fixed coordinate axes.

When the wind/ship velocity ratio is moderate, operation in such wind is possible, using the rudder to maintain a desired course. But when this velocity ratio increases, stable coursekeeping may not be possible for wide ranges of wind heading angle,  $\psi_a$ .

Thus, in order to maintain a predetermined straight course in a moderate wind, some degree of rudder angle is required to counteract the aerodynamic and hydrodynamic forces and moments. When ship speed and heading, and wind velocity and direction are given, then the required rudder angle can be determined to produce the necessary sideslip of the ship for a straight course, if the following coefficient values are available:

$$\text{Sideslip, } v_e = \frac{Y'_a N'_\delta - N'_a Y'_\delta}{N'_v Y'_\delta - Y'_v N'_\delta} \quad (112)$$

$$\text{Rudder angle, } \delta_R = \frac{N'_a Y'_v - Y'_a N'_v}{N'_v Y'_\delta - Y'_v N'_\delta} \quad (113)$$

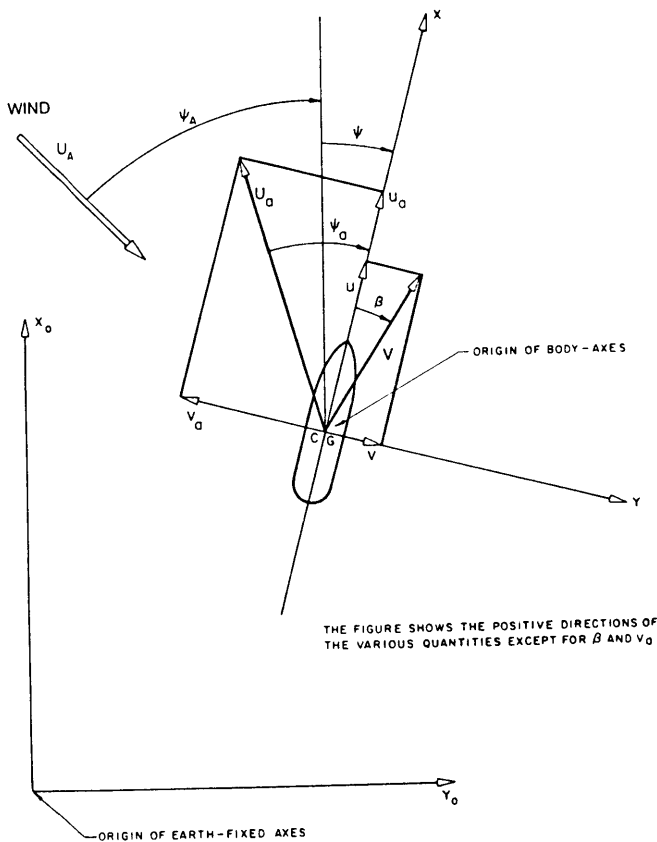


Fig. 83 Coordinates to describe ship motions in wind

Typical computed results for required rudder angle and sideslip, as functions of wind velocity, are graphed in Fig. 84 for a *Mariner* cargo ship. The figure shows that for a given wind-to-ship velocity ratio greater rudder angles are required when the wind is from the beam.

Since the maximum rudder angle of many ships is limited to 35 degrees, the ship will not be generally controllable in a wind that requires a rudder angle close to this limit. For example, Fig. 84 shows that the ship (a *mariner*-class vessel at full-load condition) will not be controllable at some headings when beam-wind velocity is relatively large ( $U_a = 10V$ ). The combined aerodynamic and hydrodynamic effects then exceed the capacity of the rudder. On the other hand, the ship may be controllable in wind of the same magnitude but from another direction. The directional stability of the system must then be examined further. Other computed results indicate that the stability requirement presents a critical wind velocity lower than that resulting from the 35-degree rudder angle for maintaining the desired course.

A stability analysis of a typical ship affirms other interesting aspects of ship behavior in wind. Eigenvalues or stability roots of an unsteered ship in wind from the bow were solved for on a computer. Real and imaginary parts of critical roots (the root with the algebraically greatest real part is called the critical root) are shown on the basis of wind velocity in Fig.

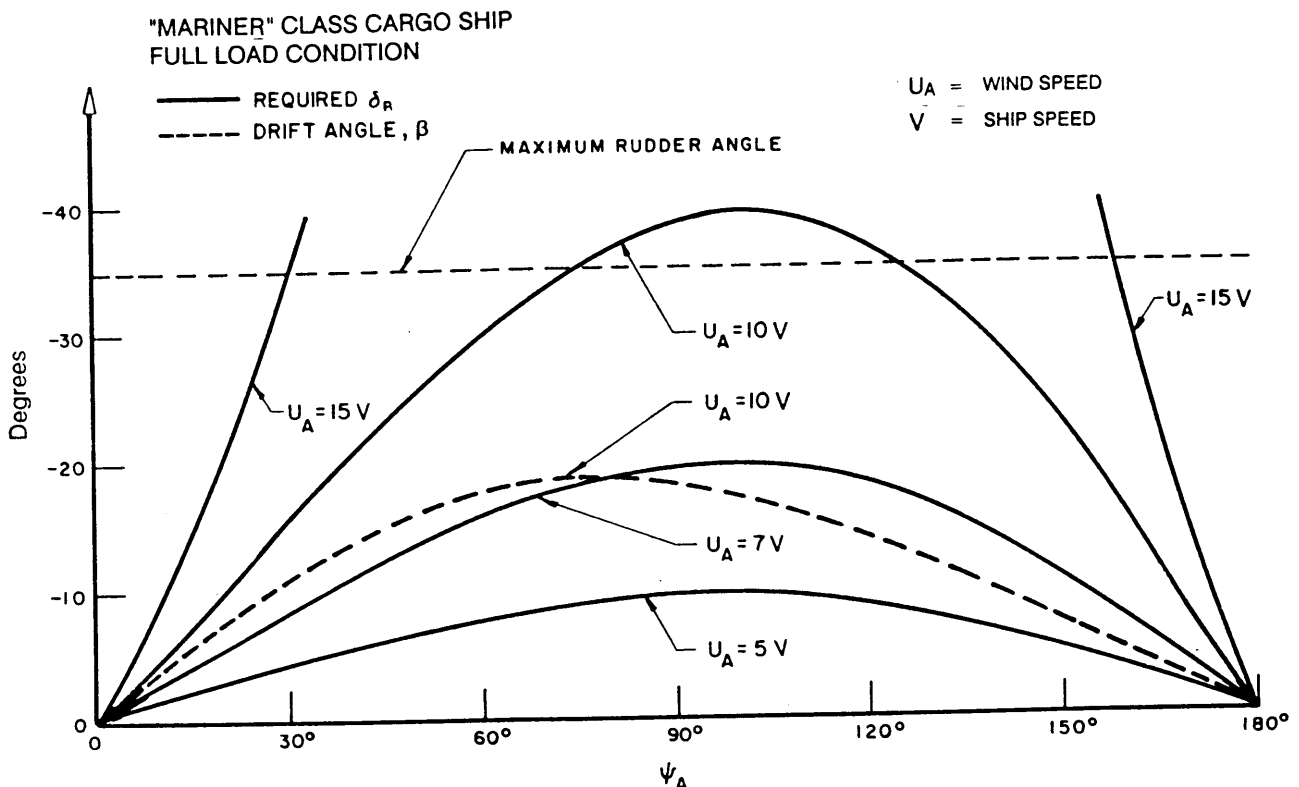


Fig. 84 Required rudder angle versus wind direction (Eda, 1966)

"MARINER" CLASS CARGO SHIP  
FULL LOAD CONDITION

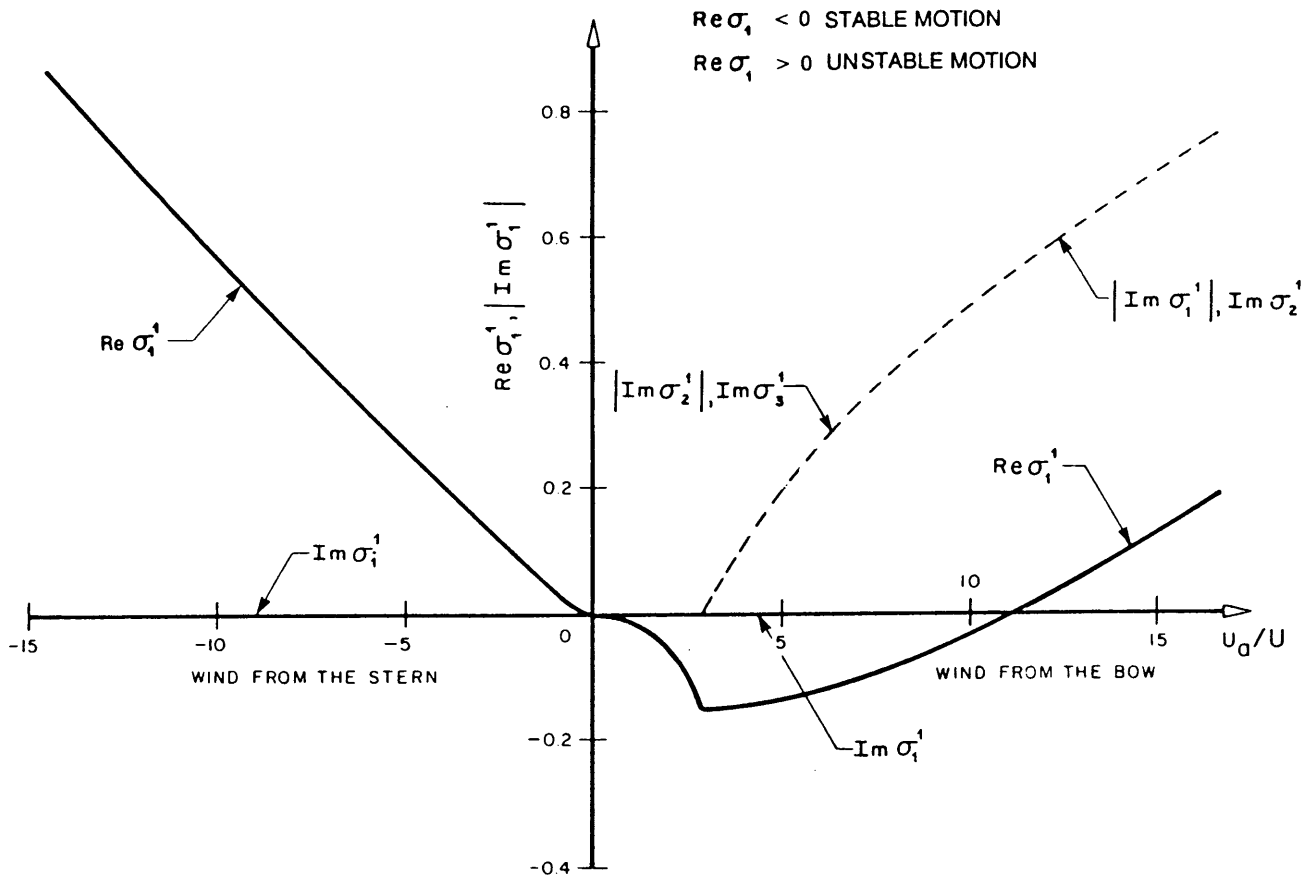


Fig. 85  $\text{Re } \sigma'$  and  $\text{Im } \sigma'$  versus wind speed (unsteered ship)

85. The horizontal axis in the figure represents relative wind speed ( $U'_a$ ). The figure shows that the ship will be neutral at  $U'_a = 0$ , implying that the ship has no preferred heading under this condition of no wind.

When the wind approaches the ship from the bow ( $U_a > 0$ ), this ship's motion may be characterized by three different properties of stability depending on the magnitude of  $U'_a$  as follows:

- (a)  $0 < U'_a < 3$  stable, nonoscillatory case
- (b)  $3 < U'_a < 11$  stable, oscillatory case
- (c)  $11 < U'_a$  unstable, oscillatory case

In cases (a) and (b), the ship tends to maintain the original course without the application of control forces. When the bow wind exceeds certain values ( $U'_{aa} = 3$ ), the imaginary parts of certain of the roots are not zero and increase with  $U'_a$  as shown in the figure. This behavior implies that the frequency of oscillatory motion increases with  $U'_a$ .

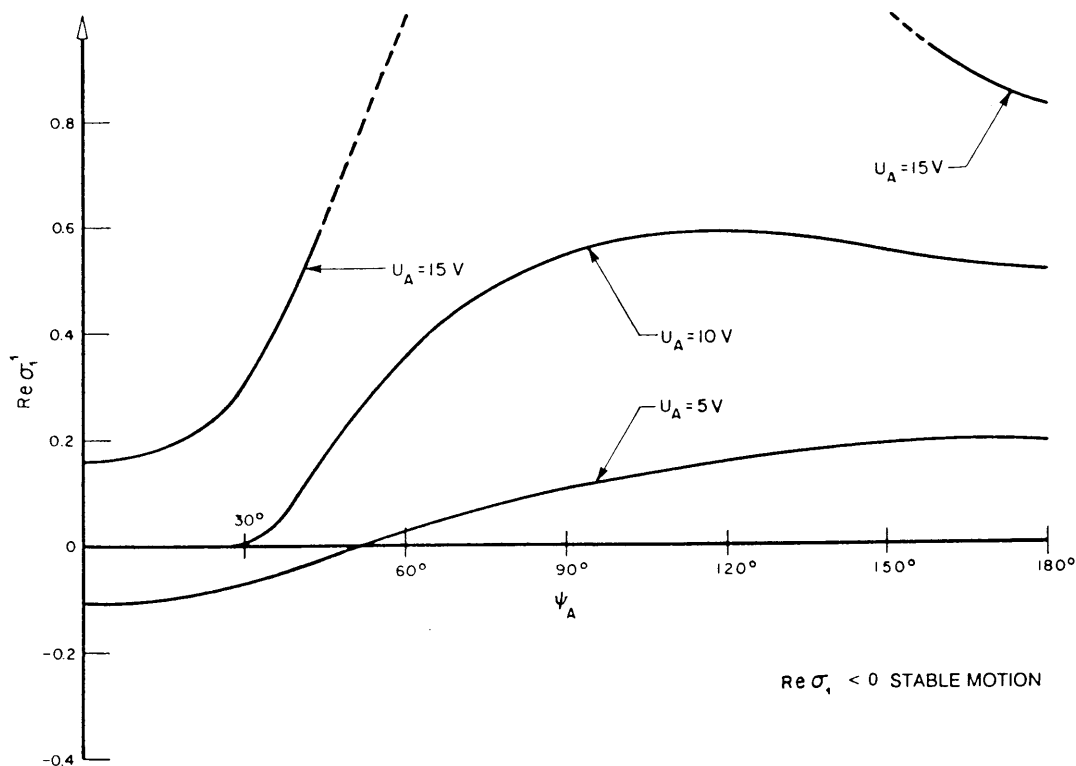
The ship is always unstable in wind from the stern, or when  $U'_a < 0$ . With an increase in wind velocity from the stern, the instability of the ship increases monotonically. Imaginary parts of the critical roots in this case are zero, implying that ship motions in wind from the stern after perturbation tend to diverge, with-

out oscillations. The rate of divergence increases with increasing values of  $U'_a$ .

Stability analysis of automatically steered ships in wind from an arbitrary direction leads to solution of a fifth-order characteristic equation. Fig. 86 shows real parts of critical roots with variations of wind velocity. The figure indicates that the ship will be stable in wind that is not strong ( $U_a \leq 5V$ ) and blows from near the bow ( $-50^\circ \leq \psi_a \leq 50$  degrees, ship lateral symmetry assumed). The ship will be unstable in the same magnitude of wind from other directions. The degree of instability is greatest in wind from the stern ( $\psi_a = 180$  degrees).

These results show that the unsteered ship will generally be more unstable as wind velocity increases. It can be shown that great improvement in stability in a wind can be achieved by using a well-designed automatic control system instead of a human helmsman, even one who is highly experienced.

**12.3 Current Effects.** Ocean or waterway current affects controllability in a manner somewhat different from that of wind. The effect of current is usually treated by using the relative velocity between the ship and the water, particularly in maneuvering simulation

Fig. 86  $\text{Re } \sigma$  versus wind direction (unsteered ship)

studies. Using a definition of current velocity vector analogous to that for wind in Fig. 83 relative velocities are defined as:

$$u = u + U_c \cos(\psi_c + \psi) \quad (114)$$

$$v = v + U_c \sin(\psi_c + \psi) \quad (115)$$

Where  $U_c$  and  $\psi_c$  are current velocity (drift) and current direction (reciprocal to set) relative to earth-fixed coordinate axes.

Local surface current velocities in the open ocean are generally modest and close to constant in the horizontal plane. Such currents do not present difficulties for open-sea controllability. Currents do, however, become important in restricted waters where ship operating speeds are often low and currents nonuniform. They are most likely to create a controllability problem for a vessel traveling downstream in a river or canal that carries significant current, particularly in bends, where significant spatial current velocity gradients tend to occur. Navigation safety often necessitates low operating speeds over the bottom and the resulting low relative speed through water,  $u-v$ , may be too small to develop adequate rudder force and force on the hull.

Ship handling simulators, Section 16.9, provide an ideal means for evaluating such effects. Miller (1978) describes a simulator study that included detailed mod-

eling of river currents and their effect on river tow safety. In fact, detailed water current studies are often a necessary input to simulator studies where a port entrance (or waterway with tributaries) has significant cross flows present from tides, etc.

**12.4 Stability and Control in Waves.** Waves can have significant effect on coursekeeping and maneuvering. A ship attempting to maintain a steady course in rough seas experiences wave-induced oscillatory motions in all six degrees of freedom. In Chapter VIII it is shown that in the linear theory of ship motions in waves the coupled transverse responses of sway, yaw, and roll can generally be considered separately from pitch, heave, and surge. However, the main interest is in roll and to some extent in sway. This chapter concerns mainly yaw and sway, which have been seen to be closely related to each other even in calm water. Roll is also involved in controllability, especially in high-speed ships. Turning can cause roll (or heel) and rolling can affect steering.

In the case of head and bow seas, where the frequency of encounter with waves causing yawing and swaying is comparatively high, and where course stability is usually large, serious difficulties seldom occur. The experienced helmsman ignores the high-frequency yawing and steers in relation to the mean ship heading. In using automatic controls, the tendency is for the system to call for high-frequency rudder movements

that produce increased resistance but have little effect on ship heading. Hence, it is desirable to select appropriate control settings, or to introduce filtering into the system, to minimize unnecessary rudder motions, as done in adaptive autopilots (Section 11).

As shown in Section 6.5, yaw-roll rudder coupling often occurs when a ship is turning. This effect is due to the rudder, which produces a heeling moment as well as a yawing moment. Fig. 87 presents a simulation of a vessel that shows yaw-roll coupling effects. Other coupling effects are often experienced when a ship proceeds at high speed in quartering or following seas. Serious rolling motions associated with steering in presence of waves are often observed in actual operations of some ships and in model testing. Anomalous behavior of rolling and steering was clearly evident, for example, in full-scale tests of a high-speed container ship during cross-Atlantic operations (Taggart, 1970).

Under seagoing conditions a number of new factors enter, particularly in the path of long overtaking waves at high speeds, because:

(a) Frequencies of wave encounter are low, so that large roll as well as yaw moments can build up.

(b) High-speed ships generally have relatively low static transverse stability (low  $GM$ ).

(c) Significant changes in static stability occur in waves, which affect roll and hence yaw (Oakley, Paulling and Wood, 1974). For example, for following seas with wave crests at the bow and stern, the middle of the ship is in a trough. This portion, therefore, develops much less righting moment; hence large roll angles occur.

(d) Since the rudder has a large effect on roll as well as on yaw, the design characteristics of the automatic control system are of critical importance (Taggart, 1970).

(e) High-speed ships have relative fore-and-aft asymmetry, which changes in rolling.

For these reasons, the possibility exists of significant coupling among yaw, sway, roll, and rudder action, as reported by de Santis and Russo (1936), especially in high-speed operations.

Figure 88 shows two sets of curves that indicate,

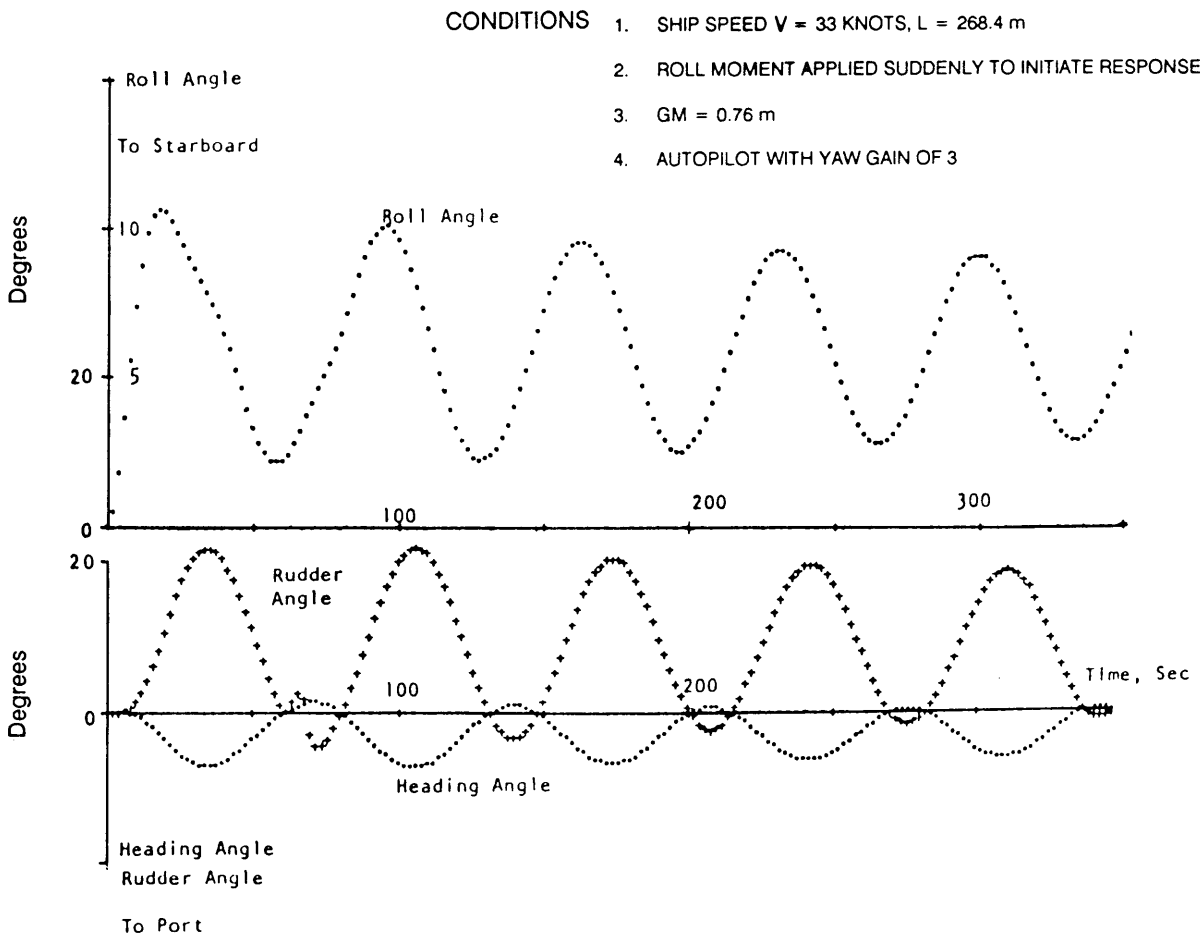


Fig. 87 Simulated roll-yaw-rudder coupled motion

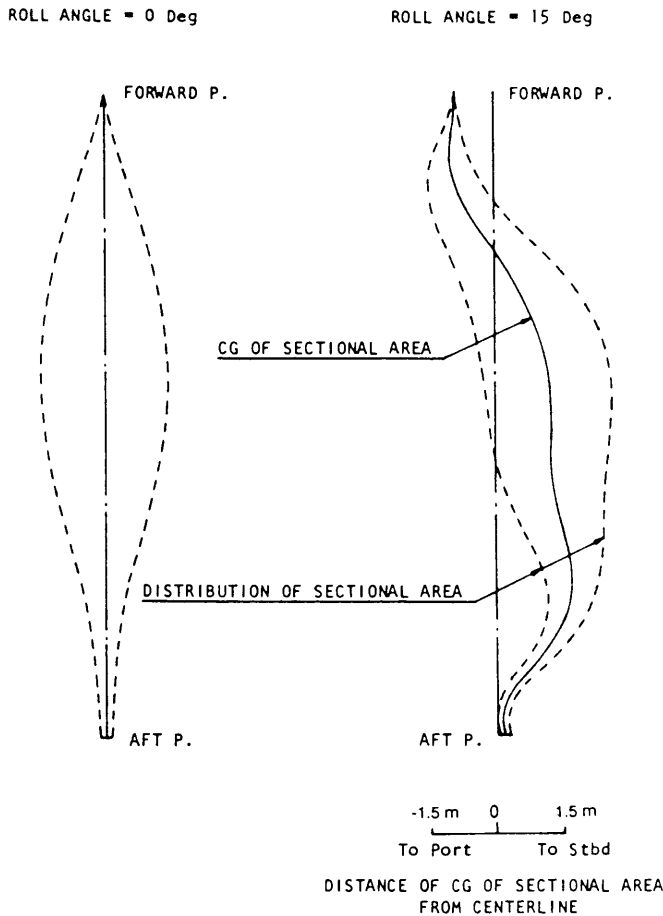


Fig. 88 Longitudinal asymmetry due to heel

for a fast containership, the transverse distance of the *CG* (centrum) of the local sectional area from the longitudinal centerline at roll angles  $\phi=0$  and  $\phi=15$  degrees in calm water. The curves can be considered equivalent to the camberlines of a wing section.

When heel angle is not zero, and ship speed is not zero, then the camberline is not a straight line (as shown in Fig. 88) and therefore introduces hydrodynamic yaw moment and side force. This trend is made more pronounced by the fore-and-aft asymmetry of the hull form, particularly during high-speed operation. Most high-speed ships have a bulbous bow for the purpose of improving resistance characteristics. The increased fore-and-aft asymmetry due to this type of bow introduces greater athwartship asymmetry of underwater hull form when the ship is heeled. Automatic control systems as discussed in Section 11 can be designed to help overcome unfavorable coupling. Figure 89 shows how the motions smooth out when an automatic control system yaw rate gain of 1.0 is applied to the simulation represented in Fig. 87.

**12.5 Coursekeeping in Astern Seas.** Much more serious steering and control difficulties are experienced by ship operators in quartering and following seas.

Du Cane and Goodrich (1962) give an overview of the problem. They report model tests in following waves that demonstrated the large range of wavelengths over which the model was carried along at the wave crest speed.

Wahab and Swaan (1964) investigated theoretically the problem of coursekeeping and broaching (turning broadside to the waves) in following seas by concentrating on the above-cited limiting condition of ship's speed equal to wave velocity (zero frequency of encounter). They assumed as self-evident that difficulty in steering—and danger of eventually broaching—is caused by dynamic course instability. They concluded that “all unsteered ships appear to be unstable somewhere on the downward slope of a wave.” Hence, they considered the characteristics of the autopilot to be very important. Nevertheless, “a reduction of the danger of broaching can be attained by increasing the course stability of the ship in smooth water.” However, no one has been able to specify exactly how much course stability is enough, or the optimal amount. In fact, some writers assert that a superior control system can overcome instability even in waves.

The definition diagram for a ship operating in regular waves is shown in Fig. 90. According to this diagram, the period and frequency of encounter between the ship and the waves are:

$$T_e = \frac{L_w}{V_w - V \cos \chi} \quad (115)$$

$$\omega_e = 2\pi \frac{(V_w - V \cos \chi)}{L_w}$$

where

- $T_e$  = period of encounter with component waves
- $\omega_e$  = angular frequency of encounter with component waves =  $2\pi/T_e$
- $L_w$  = length of wave components
- $V$  = ship velocity
- $V_w$  = component wave velocity
- $\chi$  = angle from ship velocity vector to wave direction of advance

It is evident from Fig. 90 and Equations (114) that if the seas are approaching from ahead ( $90^\circ < \chi < 270^\circ$ ),  $\cos \chi$  is negative and the frequency of encounter  $\omega_e$  is higher than if the seas were approaching from the stern ( $0^\circ < \chi < 90^\circ$  and  $270^\circ < \chi < 360^\circ$ ). In astern seas, the term  $(V_w - V \cos \chi)$  can be very small indeed and hence the frequency of encounter very low. Largely because of this reduction in frequency of encounter, coursekeeping in astern seas usually poses more difficulty than in ahead seas even though it is by no means always easy in severe ahead seas. For this reason most studies of yaw motion in rough water have been concerned with astern seas. An exception is work of Rydill (1959), who applies linear theory to the steering of ships in ahead as well as astern seas.

- CONDITIONS:
1. SHIP SPEED  $V = 33$  KNOTS,  $L = 268.4$  m
  2. ROLL MOMENT APPLIED SUDDENLY
  3.  $GM = 0.76$  m
  4. AUTOPILOT WITH YAW GAIN OF 3 AND YAW-RATE GAIN OF 1.0

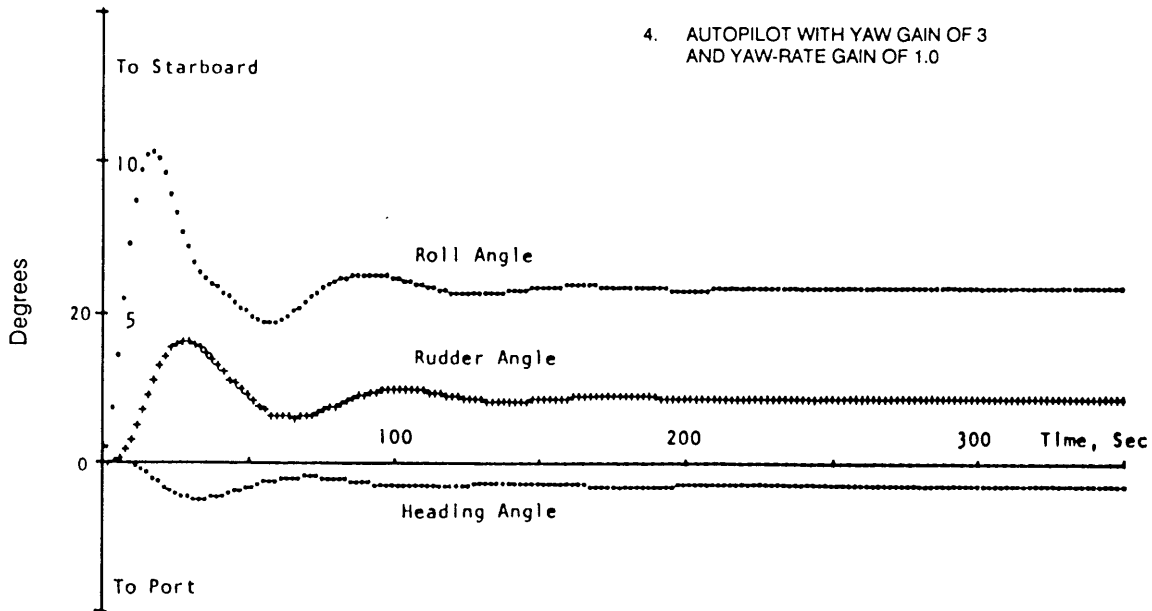


Fig. 89 Simulated roll-yaw-rudder coupled motion

It is important to distinguish the three possible situations in astern seas:

- (a)  $V \cos \chi < V_w$  (overtaking seas)
- (b)  $V \cos \chi = V_w$  (semistatic case)
- (c)  $V \cos \chi > V_w$  (following seas)

In (a), the waves are overtaking the ship and the frequency of encounter is low. These are called overtaking seas (Mandel, 1960). In (b), the frequency of encounter is zero and if the ship is poised on the down slope of a wave at time  $t = 0$  it will remain so poised at time  $t = t_1$ . In these respects, this is a steady-state, time-invariant condition. In (c), the frequency of en-

counter may also be low [but of opposite sign to that in (a)] and the ship is overtaking the waves. These are called following seas (Mandel, 1960). To an observer aboard ship, the waves in this condition appear to be falling astern even though to an observer on land they appear to move in the opposite direction.

In ahead seas (that is, seas approaching from ahead) and in situations (a) and (c), but not in situation (b), the sway exciting forces and the yaw exciting moments acting on a ship are oscillatory with time. This becomes evident from Fig. 90 if the orbital velocities of the waves are considered. When a ship is positioned as shown in Fig. 90 with its stern at a crest and its bow at a trough, the orbital velocities of the waves induce a destabilizing yaw moment on the ship unless  $\chi$  and

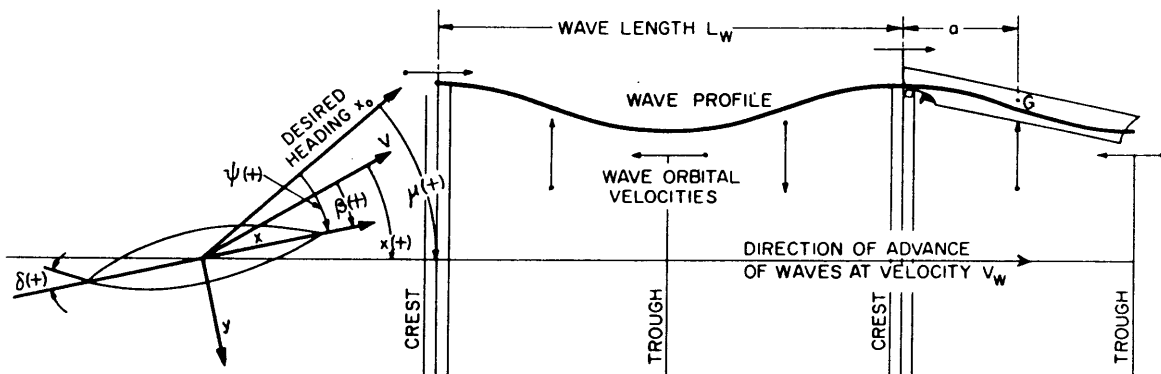


Fig. 90 Definition diagram for a ship operating in regular waves

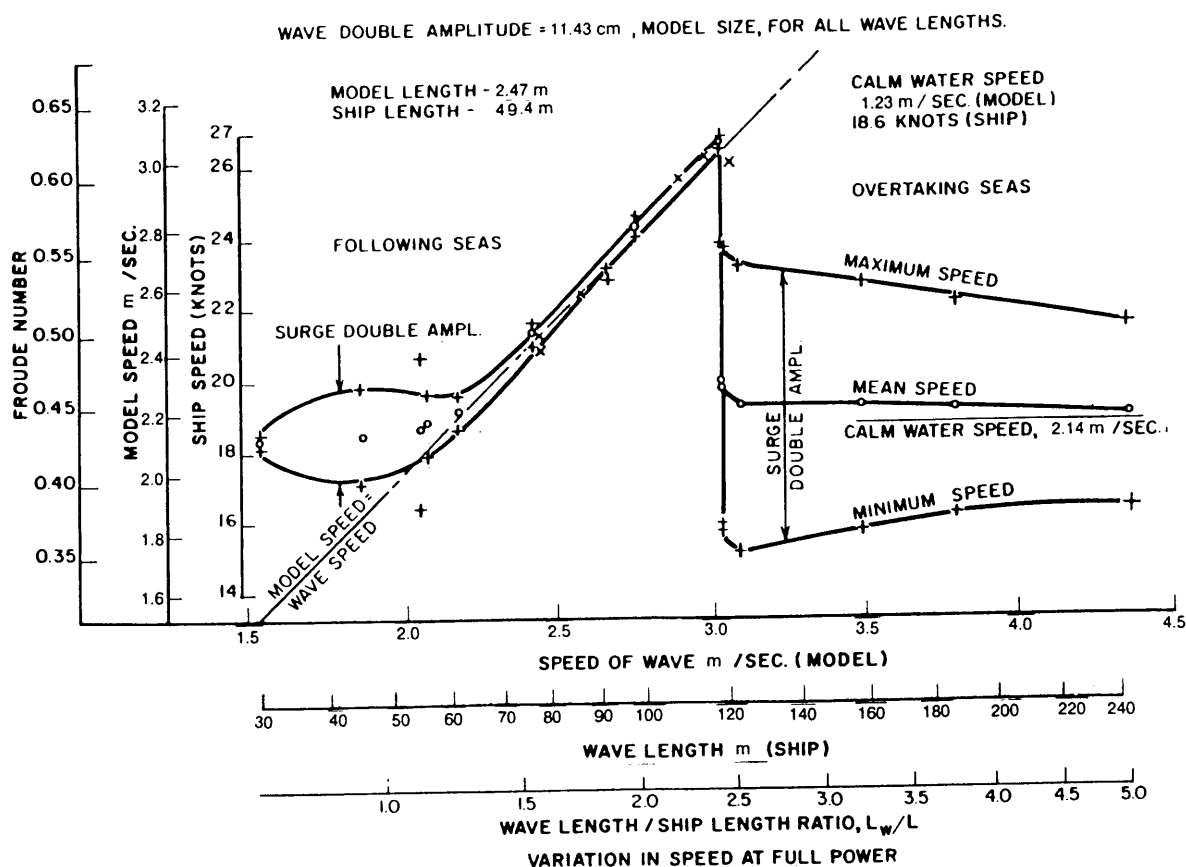


Fig. 91 Variation of speed with wavelength in uniform astern seas (DuCane and Goodrich, 1962)

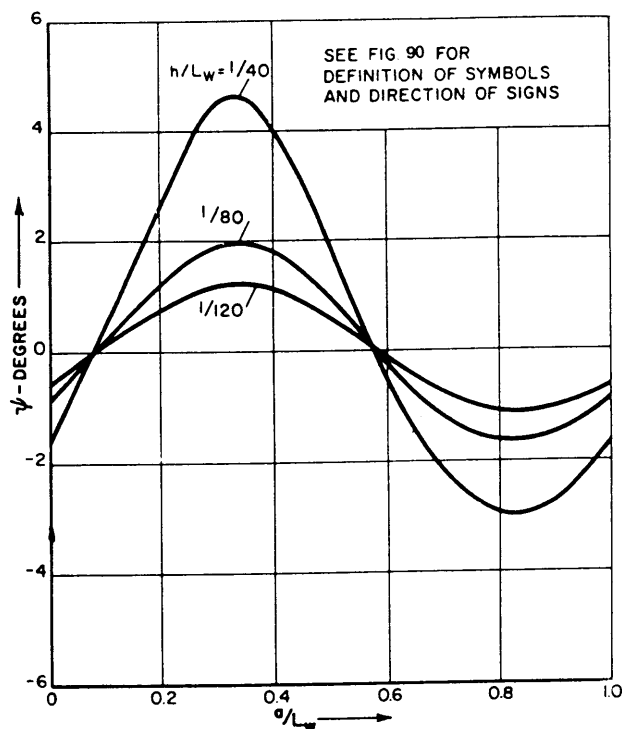


Fig. 92 Static equilibrium values of  $\psi$  for a destroyer travelling at same speed as a wave as a function of wave amplitude  $h$  and position on wave, for  $\mu = -15^\circ$ ,  $L_w/L = 2$ ,  $-\chi$ ,  $Fn = 0.565$  (Wahab and Swaan, 1964)

$\beta$  are precisely zero. When, after a time interval of half the period of the encounter, the ship is positioned with its stern at a trough and its bow at a crest, the yaw moment induced by the waves is a stabilizing moment tending to return the ship toward its original heading. In situation (b), since the ship does not change its position relative to the wave with time, the exciting forces and moments also do not vary with time.

Experimental and predicted values of yaw amplitudes, phase lags, yaw exciting moments, and sway exciting forces with controls fixed are given by Eda and Crane (1965) for a Series 60 model ( $C_B = 0.60$ ) in regular waves ( $0.5 < L_w/L < 1.5$ ) ( $\chi = 30$  and  $60^\circ$ ) at low speeds ( $Fn \leq 0.24$  or  $V = 18$  knots for a 500-ft ship), which correspond in all cases to overtaking seas; that is,  $V \cos \chi < V_w$ . The results of Eda and Crane (1965) also show that the yaw amplitudes increase with increasing ship speed (as  $\varphi_e \rightarrow 0$ ) but fall off sharply as the wave length is decreased from  $L_w/L = 1.0$ . They also decrease slightly as the wave length exceeds  $L$  ( $L_w/L > 1.0$ ). Calculated results for variations in the longitudinal radius of gyration,  $k$ , show also that yaw amplitudes decrease significantly with increase in  $k$ . While the effect of corrective rudder action in reducing yaw amplitudes in overtaking seas was not shown by Eda and Crane (1965), this effect would be very small, because in general, wave exci-



tations exert far larger forces than those that a rudder can exert.

Although, theoretically, only small, fast ships can achieve the condition  $V \cos \chi = V_w$  [condition (b)] with wave components that are of significant length compared to the ship ( $L_w/L \geq 1.0$ ), Grim (1965) indicates that ships may inadvertently be accelerated to this condition if they are operating in regular, astern seas of significant wavelength and if their initial calm-water speed exceeds a Froude number of 0.25 ( $V/\sqrt{L} = 0.84$ ). For this reason, this condition is of great interest, and it has been extensively studied not only by Grim, but also by DuCane and Goodrich (1962) and Wahab and Swaan (1964).

Results of the self-propelled model tests in astern seas reported by DuCane and Goodrich are reproduced in Fig. 91. This Figure shows model speed as a function of wave length in uniform astern seas for two levels of model power output. For both power levels, a significant surge amplitude exists with a mean speed fairly close to the calm-water speed in both the short waves corresponding to following seas and in the long waves corresponding to overtaking seas. However, in the range of wave lengths such that  $1.25 < L_w/L < 2.4$  in Fig. 91, the surge amplitude is zero and the model is accelerated by the waves above its calm-water speed to the speed of the waves. That is, in a large range of wavelengths, the waves carry the model along at speeds higher than its calm-water speed independent of the power delivered by the propellers. This phenomenon is, of course, well known to surf riders.

Grim (1965) carried out a theoretical analysis of this phenomenon and in his discussion of the work of DuCane and Goodrich (1962) shows that his analysis yields excellent agreement with the experimental results.

The equations of motion used by Wahab and Swaan (1964) with semistatic wave excitation functions can also be used to compute the static equilibrium orientations, the controls-fixed stability, and the stability

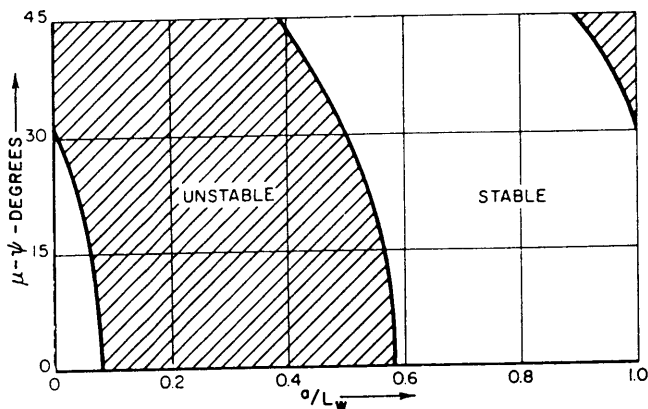


Fig. 93 Positions along wave where destroyer of Fig. 92 is stable and unstable with controls fixed (from Wahab and Swaan, 1964)

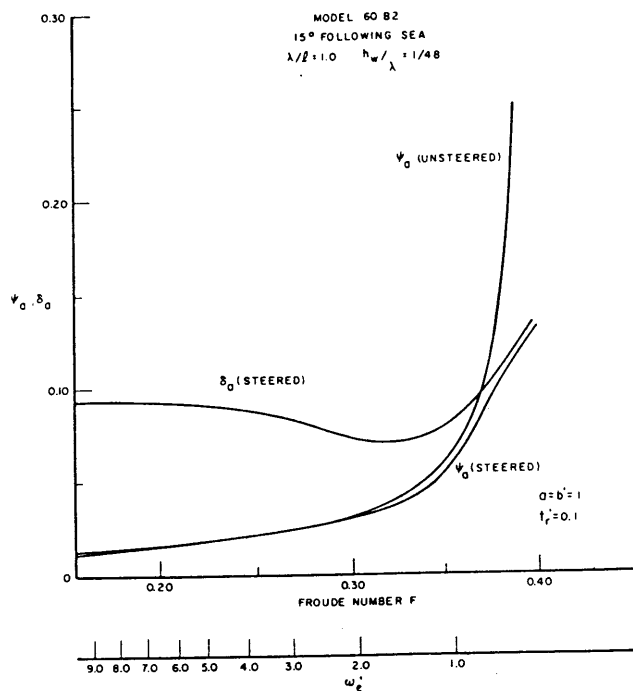


Fig. 94 Oscillatory yaw motion and rudder angle

with automatic controls working of a destroyer posed at various positions on the profile of a wave traveling at the same speed as the destroyer ( $V \cos \chi = V_w$ ). Fig. 92 shows the computed values of the heading deviation,  $\psi$ , from the prescribed course required to maintain static equilibrium, as a function of the position of the destroyer on a wave profile with  $L_w = 2L$ , if the destroyer were attempting to maintain a course angle,  $\mu = 15$  deg, to the wave direction (see Fig. 90). Fig. 92 shows that the required heading deviation is greater when the ship has its bow in a trough than when its bow is in a crest.

Whether the static equilibrium orientations corresponding to Fig. 92 are stable or unstable with controls fixed was also studied by Wahab and Swaan (1964) with the results shown in Fig. 93. These results confirm the observation made earlier in this section that the positions of a ship with its bow in the trough are unstable whereas the positions of the ship with its bow in the crest may be stable. The equations also show that no matter how much controls-fixed stability a ship may have in smooth water, it becomes unstable in long waves ( $L_w/L > 1.5$ ) at position  $a/L_w = 0.25$ , where  $a$  is the distance of ship's CG ahead of a wave crest, as shown in Fig. 90. However, ships that are unstable in smooth water may become stable in long waves when their bows are near the wave crest.

From their stability analysis of the destroyer poised on a wave with automatic controls working, Wahab and Swaan (1964) conclude the following:

(a) Even with controls working, there is a great danger of broaching (turning broadside to the waves)

for all ships when their bows are in the trough of an astern wave whose length is  $1.5L$  or more if the ship is traveling at about the same speed as the wave.

(b) The likelihood of broaching in the condition just described increases as the wave height increases.

(c) A reduction in the danger of broaching can be achieved by an increase in fin area aft improving the smooth-water controls-fixed stability.

(d) An autopilot with a large control constant,  $k_1$  (Equation 96), can reduce the regions of instability shown on Fig. 93 for the controls-fixed case.

(e) The introduction of a sensitivity to  $\dot{\psi}$  (Equation 96) does not reduce the regions of instability significantly, and an increase in the time lag,  $\bar{t}$  in the controls does not significantly increase the region of instability.

Results are presented here of a study made of ship motions in waves, on the basis of hydrodynamic data obtained in rotating-arm tests as reported by Wahab and Swaan (1964) and Eda (1972).

Ship translational motions in the horizontal plane (yaw, sway, and surge) do not have a natural frequency, except possibly a very low frequency associated with ship autopilot response. Therefore, the effects of encounter frequency on these motions are entirely different from those on pitch, heave, and roll, which do have natural frequencies.

Computed results obtained at 15 degrees and 30 degrees in following seas are shown on the basis of speed and encounter frequency in Fig. 94. In this case, with  $L = L_w$ , and when the encounter frequency is relatively high ( $\omega_e' = \omega_e L / V > 2$ ), the difference between the oscillatory motions of steered and unsteered ships is insignificant, regardless of rudder motions. This is due to a very small ratio of rudder force to wave excitation, and to the ship's inertia.

When the encounter frequency is relatively low ( $\omega_e' < 2$ ), the yaw motion of the unsteered ship becomes extremely large in this region of frequency, rudder effectiveness is greatly increased, and the advantage of steering is clearly indicated.

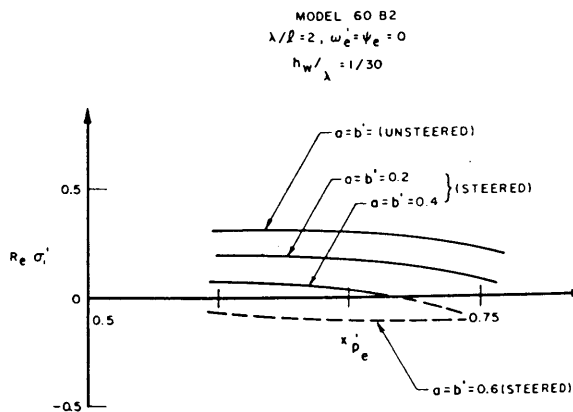


Fig. 95 Effect of control system on stability (Eda, 1972)

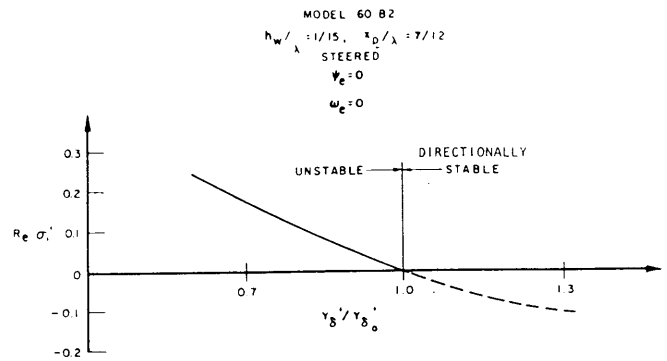


Fig. 96 Effect of rudder size in following sea (Eda, 1972)

The research also showed that when wavelength decreases to less than one ship length, yaw response decreases significantly. At an encounter angle of 30 degrees, yaw amplitude becomes almost zero when the wavelength is half the ship length.

When the encounter frequency is relatively low, the effect on ship stability is greatly improved by introduction of the control system. Fig. 95 shows that the degree of instability decreases with an increase in gain constants (yaw-gain constant =  $k_1$ , yaw-rate gain constant =  $k_2$ ) in the control system.

It was found that the choice of time constant, yaw gain constant, and yaw-rate gain constant for 60-degree quartering seas (where the encounter frequency is relatively high) had little effect on the control system, regardless of size of gain constant. Use of relatively large time constants can help to prevent the violent rudder activity often experienced in following seas.

There was a great increase in rudder motion with increased yaw-rate gain constant, indicating the advantage of small values of the constant in reducing rudder activity in waves, Section 11.3.

It is known that increasing rudder size is an effective way of achieving both greater stability and better turning ability. The effect of rudder size was examined by varying rudder-force rate ( $Y\delta$ ). Rudder-force rates for computations were varied as 0.7, 1.0, and 1.3 times the standard rudder-force rate. For a ship running in following seas at the same speed as the waves the effect of rudder size is shown in Fig. 96. Significant improvement is indicated with increasing rudder-force rate, which is proportional to rudder area.

If, however, the encounter frequency is relatively high, as in the case of running at low speed, (for example,  $Fr < 0.30$ ) in a quartering sea, the effect of rudder size is very insignificant for both steered and unsteered ships at high frequency, that is, at low speeds in following seas. This result is confirmed by solutions to the equations of motion.

Oakley, et al (1974) report on extensive model tests in astern seas and on the development of a time domain numerical simulation program for motions and capsiz-

ing (Section 5 of Chapter VIII discusses their work further). Perez and Perez (1974) and others have focused on the problem of maneuvering in waves, and general time domain models addressing the total six-

degree-of-freedom situation in waves and wind (including wave-induced motions) have been developed (see McCreight, 1985), (Hooft, 1987), and (Ankudinov and Jakobsen, 1987).

## Section 13

### Vessel Waterway Interactions

**13.1 General.** Successful operation of a ship in restricted waterways depends on the ship, its pilot, the local environment, and informational factors as indicated in Fig. 97.

Direct analysis of navigation in a restricted waterway is very complex. Decisions on maneuvering safely in waterways have been mainly based on rules of thumb, comparisons with successful practice, and "seaman's eye." However, the problems of control of ships in confined waters, particularly in narrow waterways, have been receiving a great deal of attention in recent years. Among the reasons for this heightened interest are the ever increasing size of ships—notably tankers and bulk carriers—the consequences of accidents involving hazardous cargoes, and the social costs of personal injury and property damage. In confined waters, potential hazards of collision and grounding attain their greatest concentration, and control errors may result in personal injury and costly damages to both the ship and the ruin of the environment. The accidents can have far-reaching effect.

In regard to maneuvering performance, shallow waters may be defined as water in which the ratio of

water depth to ship draft is three or less. At greater ratios, shallow-water effects on maneuvering performance become rapidly less significant as the water deepens. Restricted waters may be defined as narrow channels or canals, waterways with vertical or overhanging banks, or areas that include piers and breakwaters which introduce a substantial change in maneuvering characteristics or requirements. Obviously, most restricted waters include shallow water, and many include significant current and tide. In restricted waters, areas available for navigation are naturally limited, thus further complicating the problems of maneuvering and control of the ship.

When a ship is proceeding in very shallow or restricted waters, its dynamic behavior is much different from that of the same ship proceeding in wide stretches of deep water, because of changes in magnitude of the hydrodynamic forces and moments acting on it. Hydrodynamic effects on control can be grouped in the following general categories:

- (a) The effect of water depth relative to ship draft.
- (b) The effect of channel width and topographic character relative to ship beam.

#### WATERWAY TRANSPORTATION SYSTEM

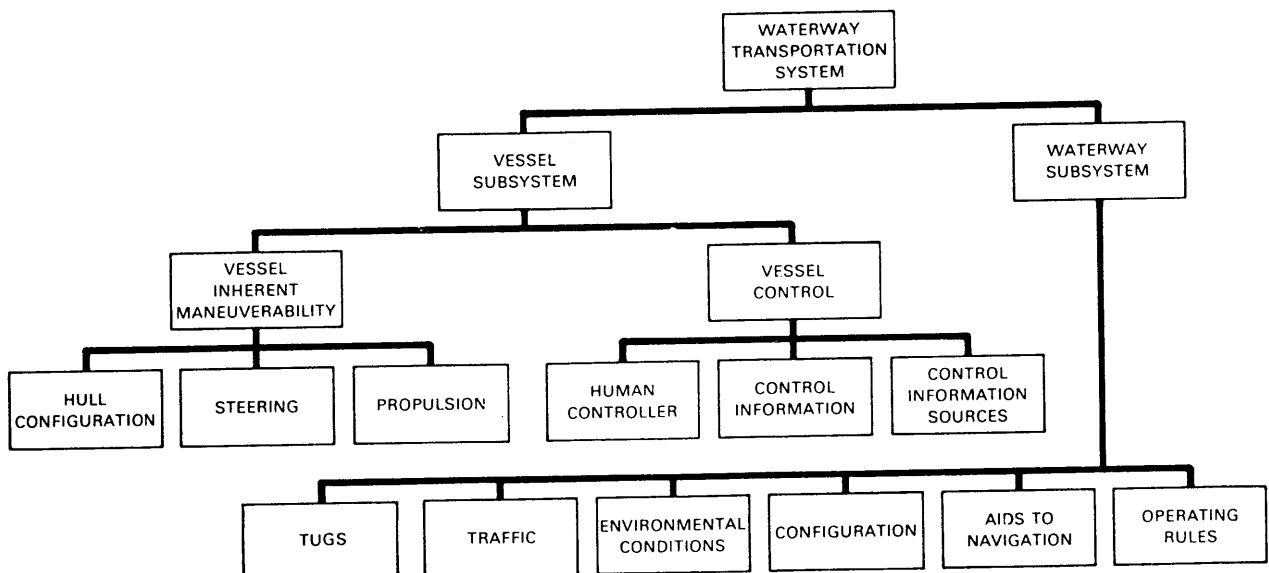


Fig. 97 Restricted waterway system factors

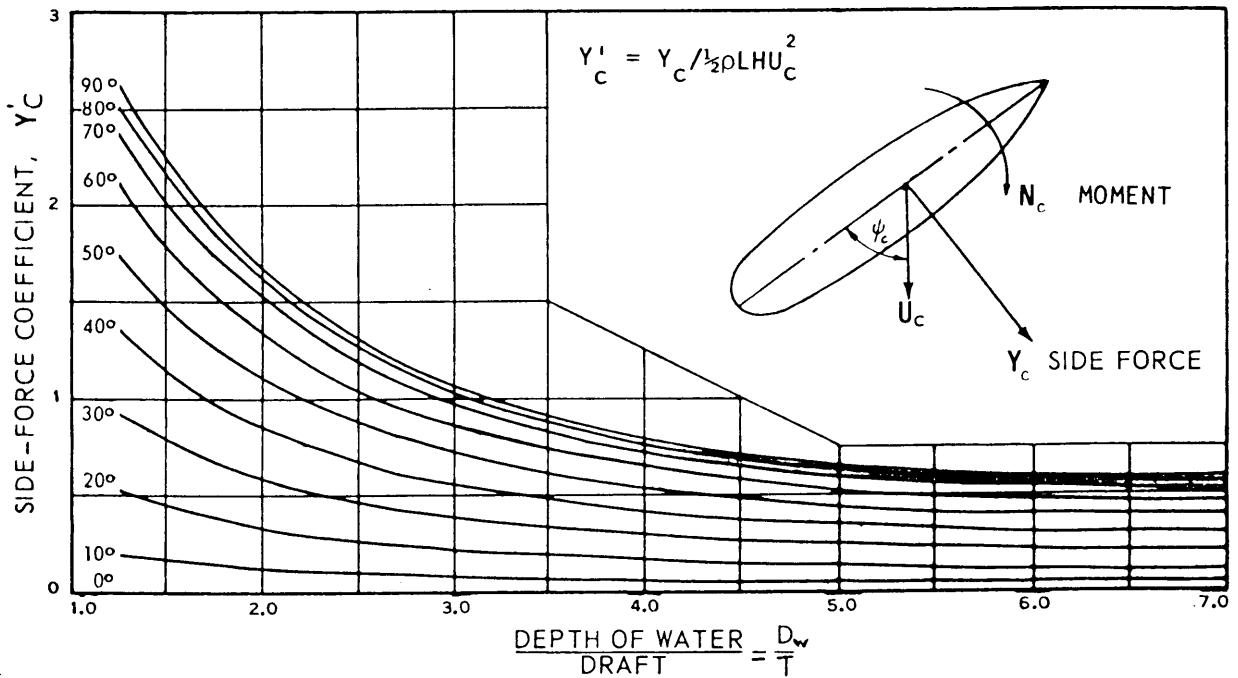


Fig. 98 Nondimensional side force coefficient as a function of depth ratio and resultant flow angle (Yeh, 1964)

(c) Significant changes in water depth or channel width relative to ship size.

(d) Interaction between two ships.

(e) Combinations of the foregoing.

These categories are discussed in the following portions of this section.

**13.2 Shallow-Water Effects.** Yeh (1964) reports the shallow-water current-induced forces at zero ship speed relative to the bottom. Model tests of seven

different hulls were carried out in varying depths of water at different current velocities, with hulls oriented at various angles to the axis of flow of the current.

Data in Yeh (1964) have been reduced to a series of curves of side force and yawing moment as a function of flow angle and depth-to-draft ratio (Figs. 98 and 99). These curves provide an indication of the effect of shallow water on hydrodynamic forces.

Figs. 100a and 100b show examples of turning trajectories obtained in computer model simulations for various ships with changes in water depth. These figures illustrate how significantly the turning trajectory can be influenced by water depth.

Fig. 101 shows results of the 278,000-dwt *Esso Osaka* full-scale trials reported by Crane (1979) and carried out under various water-depth conditions. In comparing the trajectories obtained in computer simulation runs, for example, those shown in Fig. 100 with those measured in ship trials, shown in Fig. 101, similar tendencies in shallow water effect on turning trajectory can be observed. A substantial increase in turning diameter is shown in shallow water ( $D_w/T = 1.2$ ) as opposed to deep water in Fig. 100 and 101. This change in maneuvering characteristics is very important from the viewpoint of maneuvering safety, because maneuvering ability becomes of critical importance in shallow water, as in harbors or other restricted waterways.

Experimental data on turning rate can be summarized. Taking angular velocity in deep water as 100 percent, the shallow water rates are generally:

(a) In water depth 2.5 times ship draft, 90 to 95 percent (that is, roughly 5 to 10 percent increase in

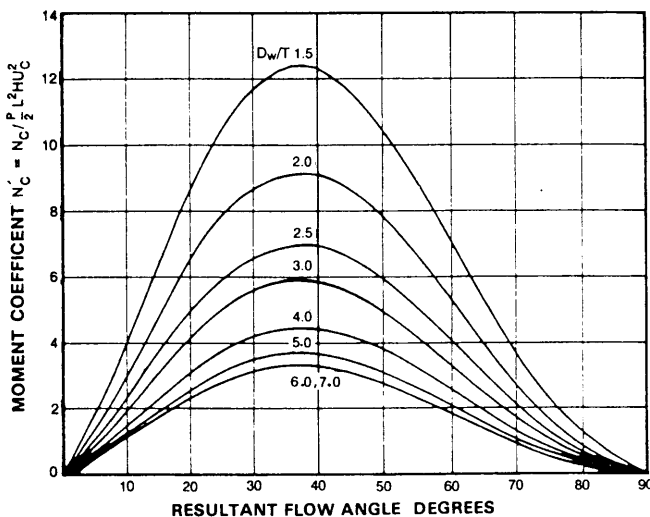


Fig. 99 Moment coefficient as a function of resultant flow angle for various depth to draft ratios (Yeh, 1964)

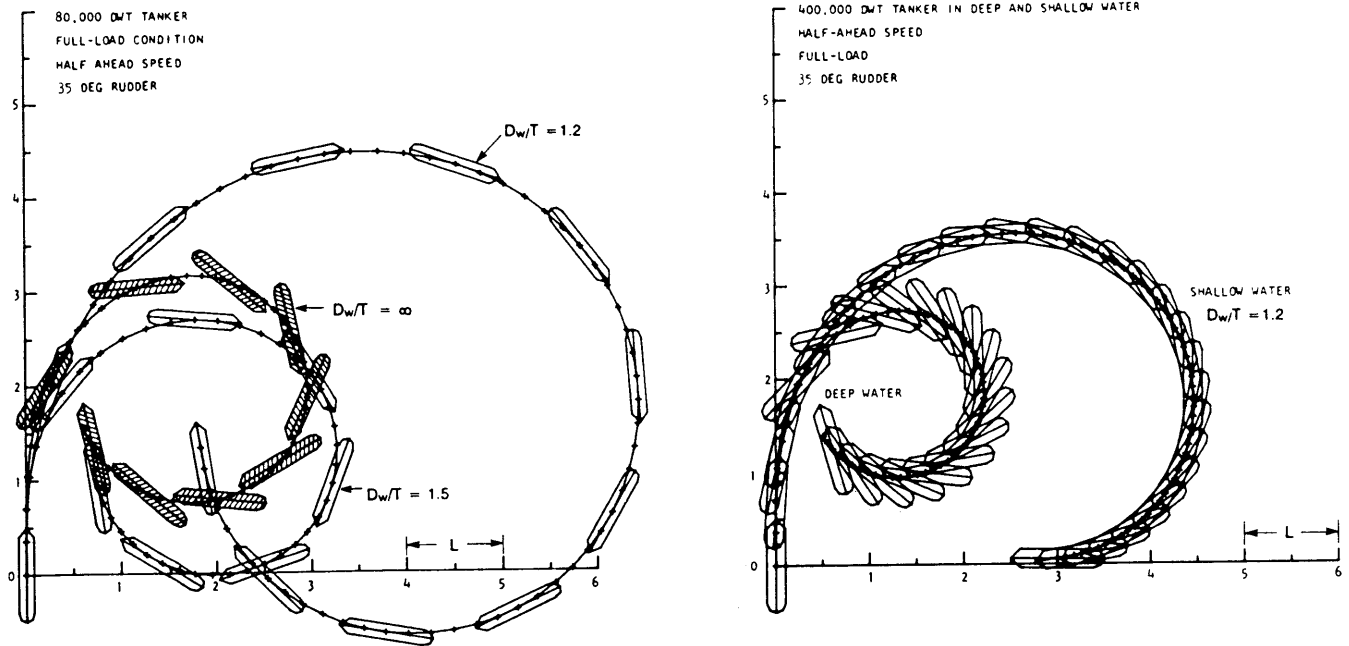


Fig. 100 (a and b) Effect of water depth on computed turning trajectory performance (Eda and Walden, 1979)

turning diameter)

(b) In water depth 1.25 times ship draft, 50 to 60 percent (that is, roughly 60 to 100 percent increase in turning diameter)

Nizerry and Page (1969) report trial data of a 213,000-dwt tanker that indicates approximately a 30-percent increase of transfer and turning diameter at a water depth 1.5 to 1.75 times ship draft. This result correlates fairly well with the above mentioned free running model test results. A similar tendency was also indicated in the captive model test reported by Fujino (1968 and 1970) for a *Mariner*-Class ship and an oil tanker.

From the *Esso Osaka* trials, checking and counter-turning ability were reduced as water depth decreased from deep to an intermediate depth (50 percent of draft as bottom clearance) and then increased at the shallower depth (20 percent of draft under keel). This phenomenon is related to an apparent reversal in controls-fixed course stability as shown in Fig. 102, where stability first decreases but then increases as water depth becomes very shallow.

Stopping distance in the *Esso Osaka* trials was largely independent of water depth, Fig. 103. Heading deviation in stopping increased from 18 to 50 and then to 88 degrees in going from deep to medium and then to shallow water. Inoue, et al (1980) have also shown that stopping distance and lateral deviations become smaller and larger respectively with an decrease in water depth.

It should be recognized that a keel clearance of 20 percent of draft (as in the trials of the *Esso Osaka*) while difficult to test is not very shallow. Ships often

operate with about 10 percent clearance in low water and with only 5 percent in berth at a pier or wharf.

With the availability of the *Esso Osaka* shallow-draft trials, theoretical and experimental work has been accomplished in the determination of hydrodynamic forces acting in shallow water. Fujino, et al

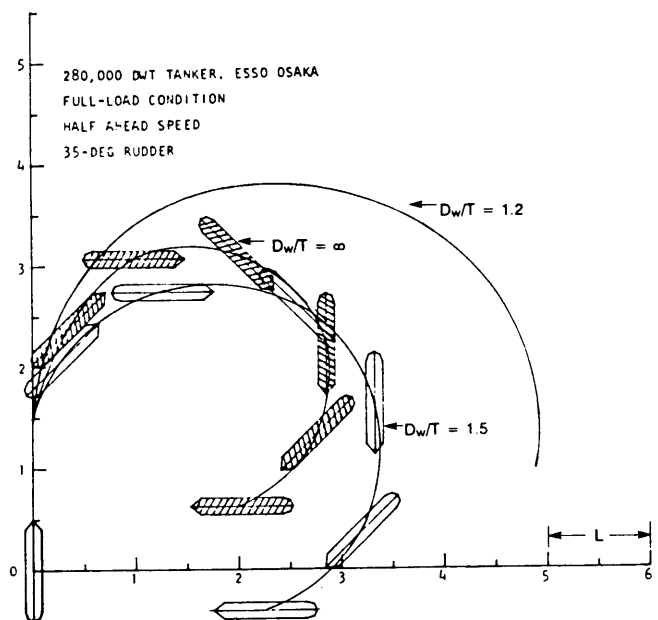


Fig. 101 Effect of water depth on turning performance (*Esso Osaka*)

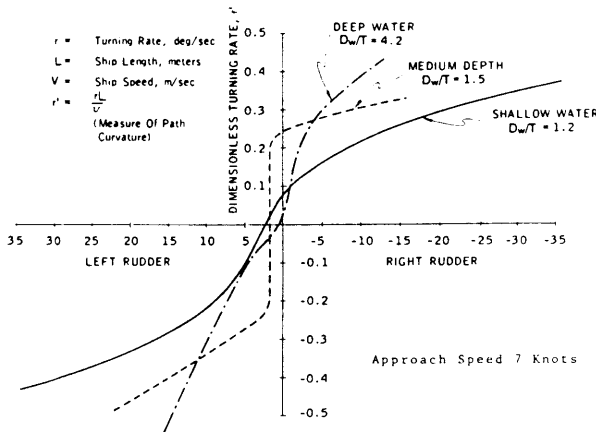


Fig. 102 Smooth spiral test results, showing dimensionless turning rate versus rudder angle, from 7 knots

(1987) report on the extension of a deep water model to predict motions in shallow water with particular attention to the shallow water effects on rudder effectiveness. A simple approach by Hirano and Takashina (1987) proposes estimating the linear derivatives in shallow water through use of an "effective ship aspect ratio,"  $K_e$ .

$$k_e = \frac{k}{\frac{T}{2D_w} k + \left( \frac{\pi T}{2D_w} \cot \frac{\pi T}{2D_w} \right) \lambda} \quad (116)$$

where

$k$  = is effective aspect ratio in deep water  
 $T$  = mean draft/mean length ship's draft

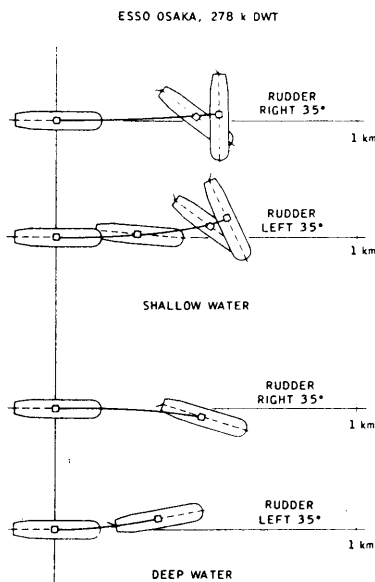


Fig. 103 Rudder angle effect on stopping in shallow water and deep water from 3.8 knots, with 45 rpm astern

$D_w$  = depth of water

$\lambda$  = an empirical parameter to be evaluated

Based on experimental results with a VLCC, a LNG carrier, and a passenger car carrier the following values for  $\lambda$  are proposed, Fig. 104:

$$\lambda = 2.3 \text{ for } Y'_v$$

$$\lambda = 1.7 \text{ for } N'_v$$

$$\delta l = 0.7 \text{ for both } Y'_r \text{ and } N'_r$$

**13.3 Effects of Narrow Channels.** When a ship moves through water that is unrestricted in depth and in width, the lines of flow go not only around the sides of the ship but also along the bottom of the ship. If the water is shallow, the flow under the hull is restricted, causing greater flow along the sides. This change in flow in turn changes the side forces and moments acting on the ship and hence the hydrodynamic derivatives of the ship such as  $Y_v$ ,  $N_v$ , and  $Y_r$  are changed.

If, in addition to being shallow, the channel is also restricted in width, as in a canal, the hydrodynamic derivatives are even more severely altered than they are in shallow water of unrestricted width. If a ship, symmetrical about its  $xz$ -plane, is restricted in its motions so that its  $x$ -axis and its velocity vector,  $V$ , are exactly collinear with the centerline of the canal, and if the canal cross section is constant and symmetrical about its vertical centerline plane, then there is flow symmetry port and starboard and the ship is subjected to no yaw moment or side force. If, however, the same ship is moving along the same canal with its  $x$ -axis parallel to the centerline of the canal but displaced a horizontal distance  $y_0$  from the canal centerline, the flow symmetry is disturbed as shown in Fig. 105. The increase in the velocity of flow between the hull and the near wall coupled with the decreased velocity of flow between the hull and the far wall creates a force that draws the ship toward the near wall and, as shown both by full-scale experience and by model experiments, at the same time sets up a moment tending to swing the bow toward the far wall; that is, the derivative  $Y_{y_0}$  is always positive and the derivative  $N_{y_0}$  is negative according to the sign convention of this chapter. The magnitude of the derivatives  $Y_{y_0}$  and  $N_{y_0}$  increases as the canal width decreases.

The derivatives  $Y_{y_0}$  and  $N_{y_0}$  imply the existence in canals of a sensitivity to position which does not exist in the open ocean. Operation in canals also leads to a heading sensitivity which does not exist in the open ocean. According to the flow diagram shown in Fig. 106, the existence of an angle  $\psi$  will create a moment  $N$  that tends to increase  $\psi$ ; that is, the derivative  $N_\psi$  is always positive. Term  $N_\psi$ , like  $Y_{y_0}$ , is therefore a destabilizing derivative. Important to note is that if the path of the ship is restricted to being parallel to the centerline of the canal, it is impossible to make a distinction between  $N_\beta$  and  $N_\psi$  and  $Y_\beta$  and  $Y_\psi$  because

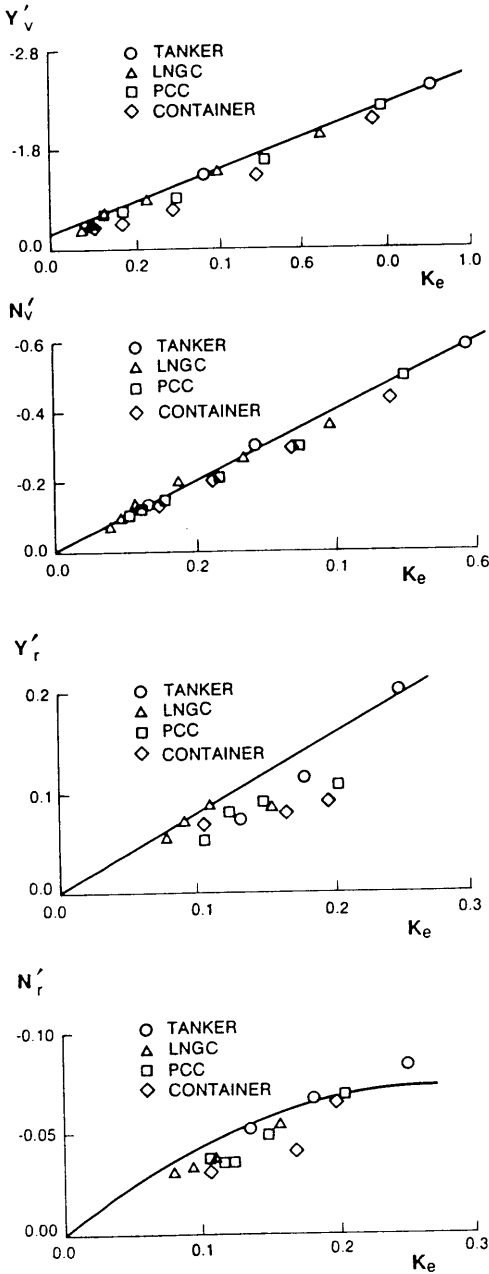


Fig. 104 Linear derivatives in shallow water as functions of effective aspect ratio

in this case  $\beta = \psi$ . However, in the general case, the path of the ship is not parallel to the centerline of the canal. For example, if the ship is steering across the canal as in Fig. 106,  $\beta$  may be zero while  $\psi$  is not zero. In this case, forces and moments may exist that correspond to  $Y_\psi\psi$ ,  $Y_{y_0}$ ,  $N_\psi\psi$ , and  $N_{y_0}y_0$ . On the other hand,  $Y_\beta\beta$  and  $N_\beta\beta$  can only be zero since  $\beta$  is zero. Noting that for small motions;

$$\dot{y}_0 = v + u_1\psi; \quad \dot{y}'_0 = v' + \psi$$

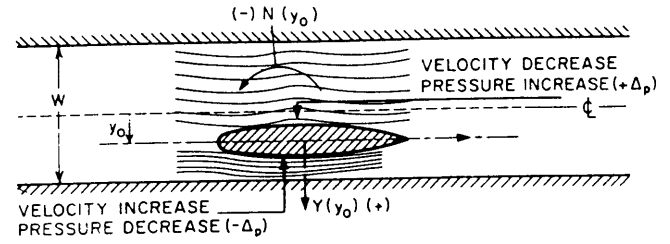


Fig. 105 Flow diagram in canal with ship and its velocity vector parallel to canal wall (Abkowitz, 1964)

$$v = \dot{y}_0 - u_1\psi; \quad v' = \dot{y}'_0 - \psi \quad (117)$$

$$\dot{v} = \dot{y}_0 - u_1\dot{\psi} \quad \dot{v}' = \dot{y}'_0 - \dot{\psi}$$

and following Equation (11), the equations of motion of a ship in restricted water are as follows:

$$\begin{aligned} Y'_{y_0}y'_0 + Y'_v\dot{y}'_0 + (Y'_v - \Delta')\dot{y}'_0 + (Y'_\psi - Y'_v)\psi \\ + (Y'_\psi - Y'_v)\dot{\psi} + Y'_\psi\ddot{\psi} = 0 \end{aligned} \quad (118)$$

$$\begin{aligned} N'_{y_0}y'_0 + N'_v\dot{y}'_0 + N'_v\dot{y}'_0 + (N'_\psi - N'_v)\psi \\ + (N'_\psi - N'_v)\dot{\psi} + (N'_\psi - I'_2)\ddot{\psi} = 0 \end{aligned}$$

Since both equations are of second order in both  $y_0$  and  $\psi$ , their simultaneous solution leads to a fourth-order differential equation. In view of the nature of  $Y_{y_0}$ ,  $N_{y_0}$ , and  $N_\psi$  as discussed earlier, no ship can possess controls-fixed positional stability with respect to the centerline of the canal and any ship operating on the canal centerline is in a position of unstable equilibrium. The only way of holding a ship's path on the canal centerline is by use of controls, either manual or automatic. If automatic controls are employed, a continuous signal measuring the distance from each bank must be provided and Equation (96) has to include an additional term that is sensitive to the distance,  $y_0$ .

Extensive model testing has been conducted at the David Taylor Research Center to evaluate narrow

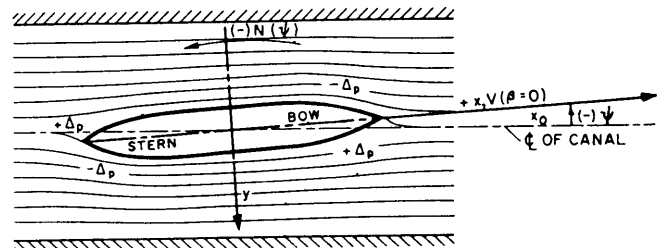


Fig. 106 Flow diagram in canal with ship and its velocity vector at angle  $\psi$  to canal wall

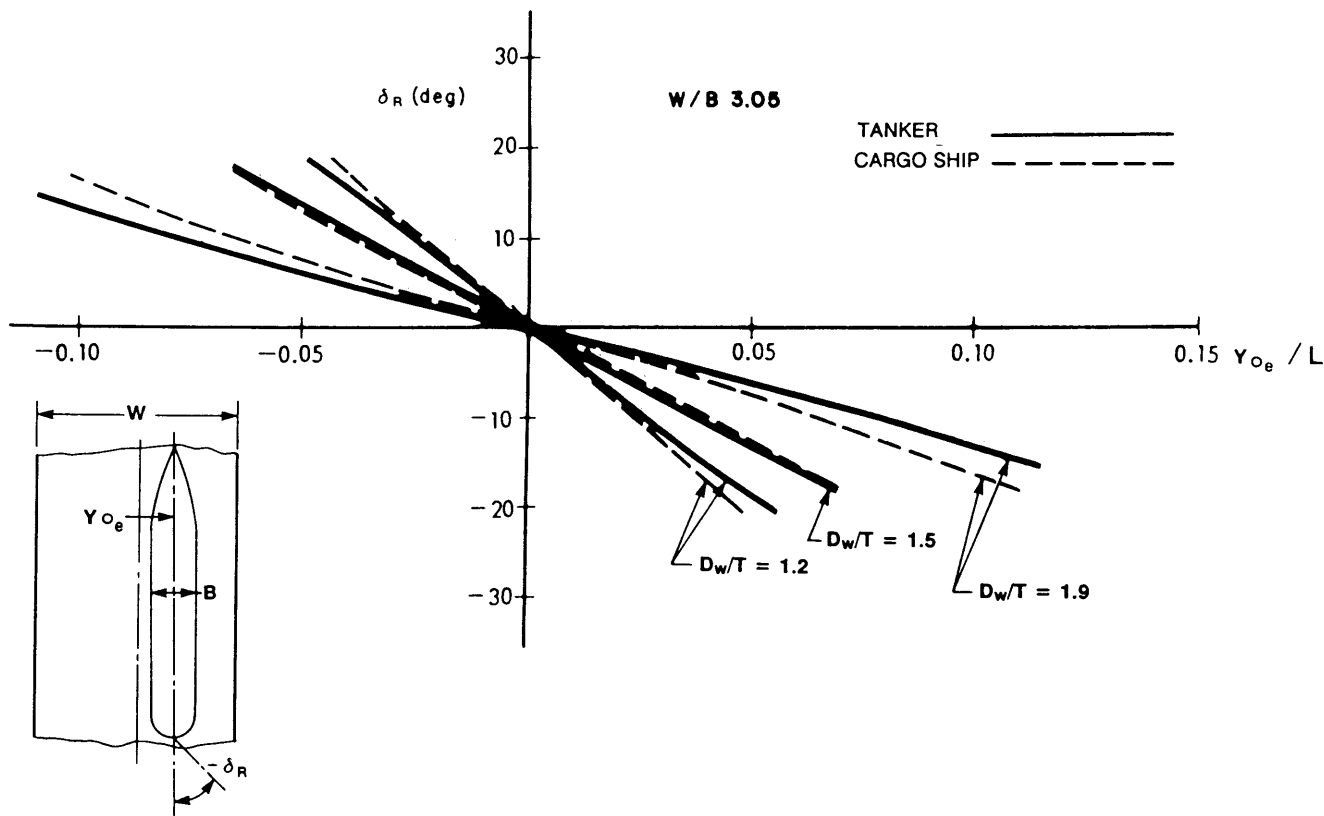


Fig. 107 Required rudder angle to maintain off-centerline course

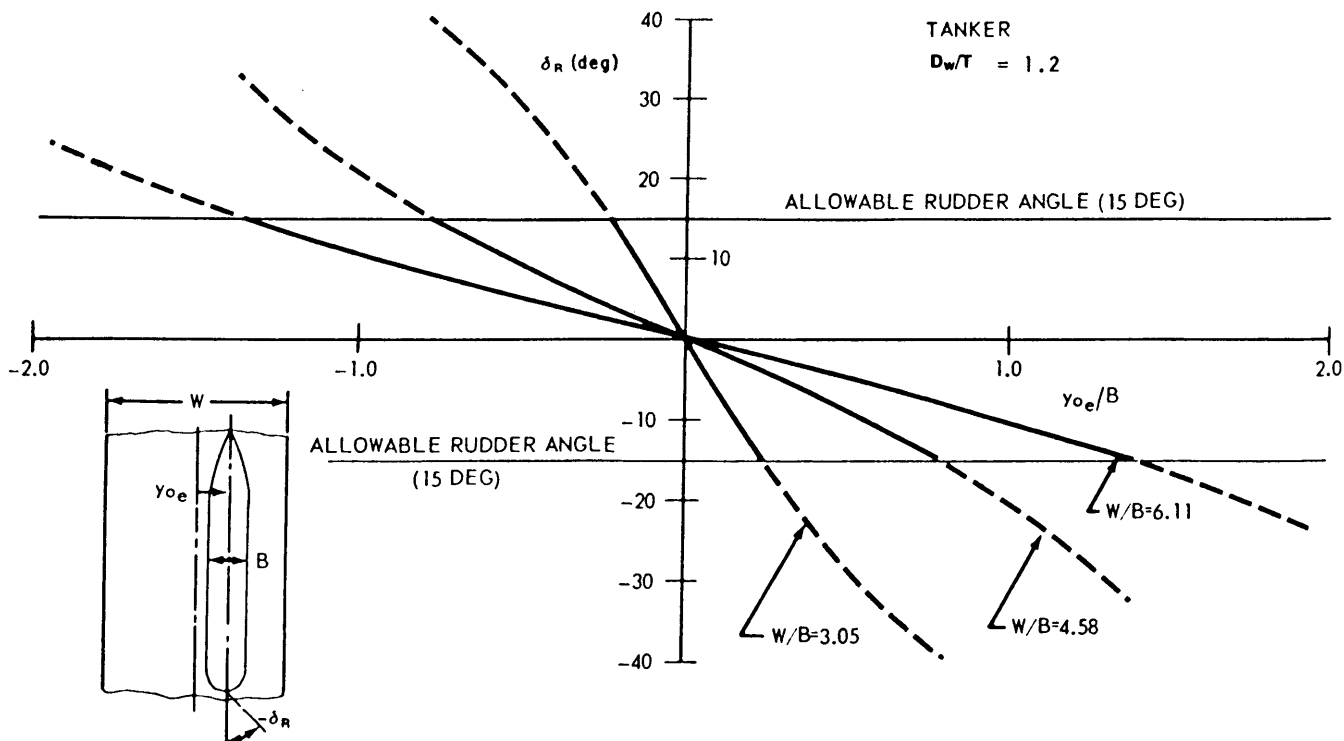


Fig. 108 Required rudder angle to maintain off-centerline course



channel effect, much of it in connection with Panama Canal improvements (Garthane, 1946). A useful reanalysis of basic results was made by Schoenherr (1960). The original tests were for distance ratios (distance to channel centerline divided by ship beam) ranging from about 0.23 to 2.6, while the ratios of channel depth to ship draft ranged from about 1.40 to 2.49. Schoenherr has faired the data, generalized, and prepared design charts covering forces and yawing moments over a wide range.

Moody (1964) presented the results of a series of model tests on the handling of deeply laden ships in a widened and asymmetrically deepened section of Gaillard Cut in the Panama Canal. His data show that widening and deepening the channel greatly reduced the interaction forces over the greater part of the channel width, and that this effect was accompanied by a marked improvement in dynamic course stability of very large ships. Also concluded from this investigation is that the asymmetrical shape of the channel and the abrupt change in depth between the old cut on one side and the new cut on the other did not have any untoward effect on ship performance.

Moody's report (1964) is of interest to ship designers because it presents forces and moments as functions of lateral position and yaw angle together with observations on control of the model.

A series of analytical and experimental studies of ship control problems in canals was conducted by Eda (1971, 1973) under the Interoceanic Canal Study project. A nonlinear mathematical model formulated on a digital computer was used to examine the dynamic behavior of two ships, namely, a large tanker of 250,000 dwt, 335 m (1085-ft) length,  $C_B$  0.83, and a cargo ship 188 m (600 ft) length,  $C_B$  0.60. Available

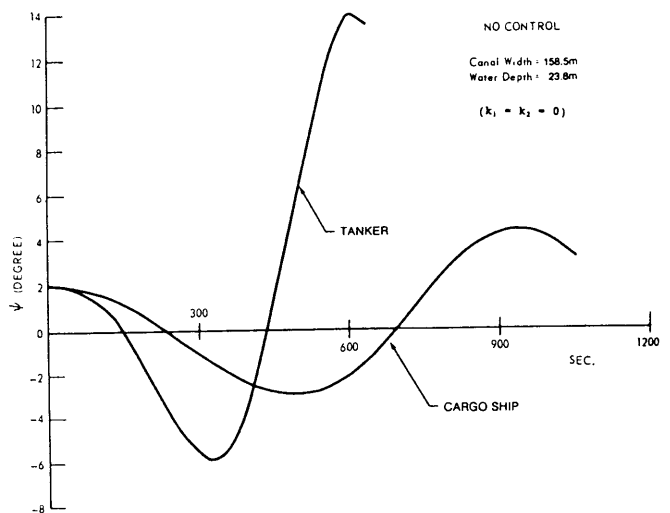


Fig. 109 Heading change after yaw disturbance of 2 deg in canal

hydrodynamic results of captive model tests were employed in order to establish realistic dynamic models.

Figs. 107 and 108 show results in the form of estimated required rudder angles to maintain off-centerline course under equilibrium conditions with changes in water depth and channel width relative to ship dimensions. The abscissas show the ratio of distance off-centerline to ship length. In all cases, equilibrium drift angle was relatively small.

Figs. 109 and 110 show calculated heading changes of the cargo ship and tanker after a yaw disturbance of 2 degrees from the initial centerline course. Both ships were run at the same speed at 6 knots in a canal 158 m (520 ft) wide with a depth of 24 m (78 ft).

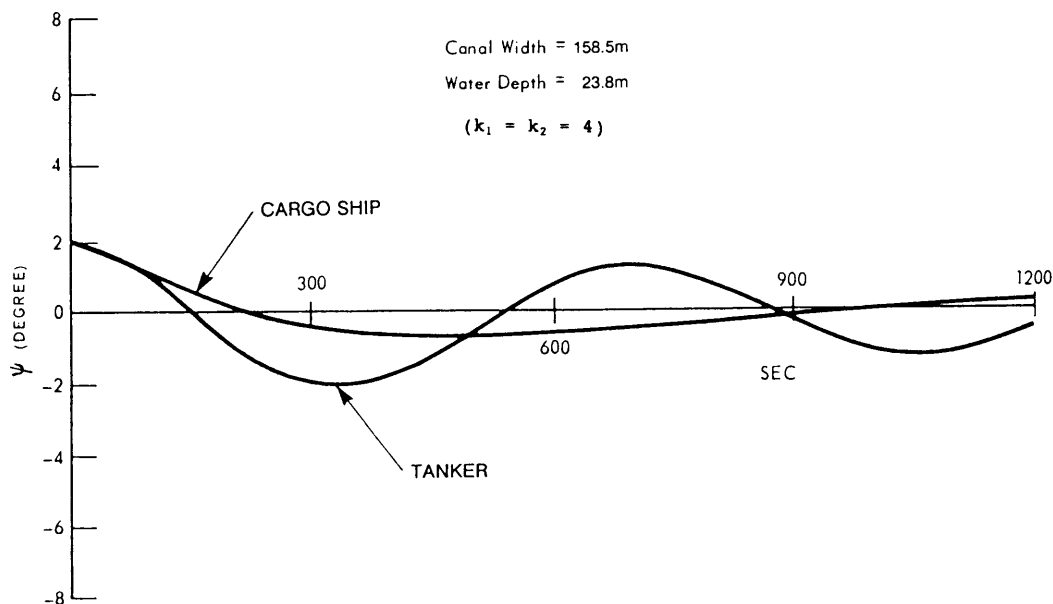


Fig. 110 Heading change after yaw disturbance of 2 deg in a canal—with control

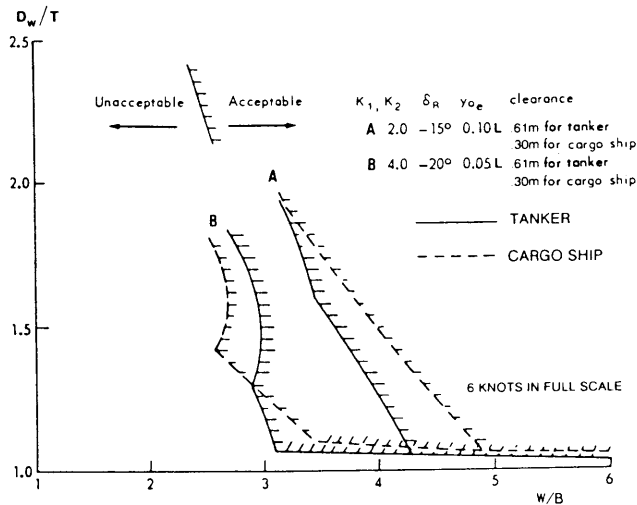


Fig. 111 Composite limiting contours for directed stability in canals

The oscillatory divergent motions shown in Fig. 109 indicate that both ships are directionally unstable and that the degree of instability is greater for the tanker than for the cargo ship when the rudder is fixed (gain constants  $K_1$  and  $K_2 = 0$ ). When yaw gain  $K_1 = 4$  and yaw-rate gain  $K_2 = 0$ , for example, a rudder of 4 degrees is ordered at the heading angle deviation of one degree. Fig. 110 shows the motions with activated rudder (gain constants  $K_1$  and  $K_2 = 4$ ). It will be seen that both ships are now directionally stable. As shown in these figures, the dynamic behavior of the cargo ship is much better than that of the tanker, mainly because of its much smaller size relative to the specified canal dimensions.

The dynamic simulations were continued for the ships in canals, with variations in canal dimensions and rudder control gain constants. Based on these results, the contours of neutral stability for various canal dimensions were obtained. Fig. 111 provides the developed guide to acceptable ship control parameters relative to ship size and canal dimensions on the basis of the following assumed study criteria (although the solution is certainly not a complete solution nor a universally applicable one):

- (a) Equilibrium rudder angle of 15 and 20 degrees at 5 percent and 10 percent ship lengths off-centerline.
- (b) Neutral stability with  $K_1 = K_2 = 2$ , and 4.
- (c) 30 cm (1-ft) and 60 cm (2-ft) bottom clearance to allow for squat at limiting ship speed of 6 knots in full scale for the cargo ship and the tanker, respectively.

The acceptable performance region of canal dimensions lies above and to the right of the contours in Fig. 111.

The importance of the operator-ship-steering system has been recognized by many investigators. For ex-

ample, Brard (1950) said, "The difficulty of keeping the model off a solid boundary is the basic criterion as to its canal-transiting qualities. Naturally this whole operation depends on the operator."

In an extension of Brard's investigations, De-Verdiere and Audren (1951) offered the following two qualitative design observations which were derived from experimental tests with models steered by a human helmsman in a simulated canal: 1. Ship forms that are full at the bow and sharp at the stern are more favorable to good handling qualities in a canal, and 2. Maneuvering qualities of a vessel with two propellers are improved when the rudder is placed abaft of the propellers."

Similar trends for ships with one propeller were noted earlier by Baker (1924) who observed that rudders that deflect into the propeller race are more effective in maneuvering, whether in a canal or in open water.

River towboat pilots indicate an interesting approach to control. In some instances, they go through bends in a river by ordering rate of turn on the autopilot rather than ordering rudder angle. Such boats are equipped with gyrocompass rate-of-swing indicators, and this mode of control is apparently useful in familiar locations with variable tows.

Bindel (1960) presents test results for three tanker models in canals. Two of the models had a single screw and single rudder, and the third had twin screws and a single rudder. Different canal configurations were used during these tests; bed width and water depth were varied while bank slopes were kept constant at a slope of 1:3. It was found that for a given ship and canal there may exist a critical speed from the point of view of ship maneuverability, that is, the speed that causes the greatest difficulty in passing through the canal. The intensity of the difficulty depends on both

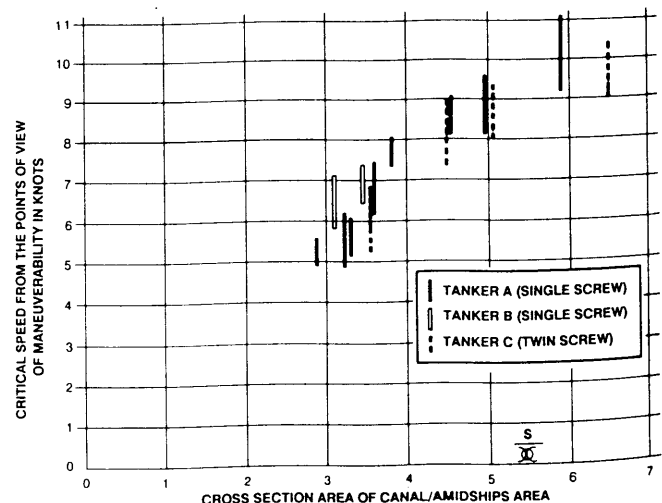


Fig. 112

the ship and the canal. For three different tankers Fig. 112 indicates bands of critical speeds in knots plotted against the ratio of the cross-sectional area of the canal to the midship section area of the ship. The graph shows that the higher this ratio, the higher the critical speed. Above and below the critical speed band, maneuverability of the single-screw models was satisfactory. The performance of the twin-screw model, which was poorer, can be ascribed to a difference in rudder effectiveness, for the single centerline rudder was not located in the propeller race.

Norrbin (1971) provides observations on a model for deep and confined waters, and Fujino (1976) offers a state-of-the-art survey of maneuverability in restricted waters with concentration on course stability.

If the handling qualities of a ship are so poor that it is impossible to negotiate restricted waterways, Moody (1964) suggests that a practical solution is to attach a tugboat to the stern of the ship by towline. With the tugboat holding back on the stern, the ship's propeller slipstream velocity is increased, thus improving rudder effectiveness. Furthermore, the towline tension at the stern of the ship improves the stability of the ship, thus reducing the rudder action needed to maintain a straight course.

**13.4 Interaction Between Two Vessels.** Just as the passage of a ship near a channel boundary causes forces and moments to act on the ship that do not exist in unrestricted waters, so too does passage by another ship close aboard. The principal difference in discussing the two cases is that the channel boundary may be assumed to be long relative to the ship length and of constant cross-sectional shape; hence the interaction forces and moments in a channel may be assumed to depend only on the transverse distance,  $y_0$ , and the ship's yaw angle,  $\psi$ . In the case of one ship passing close to another, the interaction forces are functions also of the longitudinal distance,  $x_0$ , separating the two ships as well as the lateral distance  $y_0$  and the yaw angles, plus the relative sizes of the ships.

Close passage of two ships and the resulting hydrodynamic interactions between the two are operationally important for situations such as overtaking or meeting in a restricted channel, maneuvering to avoid collision, passing a ship moored adjacent to a narrow channel, and conducting underway replenishment at sea (UNREP).

Some of the investigations of ship-to-ship interactions, including cases of overtaking, meeting (ships moving in opposite directions head on or nearly so), and a ship passing a stopped (or moored) ship are discussed in this Section.

Figs. 113 and 114 summarize the most significant results reported by Newton (1960). To obtain the data shown on the upper part of Fig. 113, two models were towed without propellers and with  $\beta = \delta_R = 0$  on parallel straight courses at different longitudinal positions relative to each other over a range of full-scale

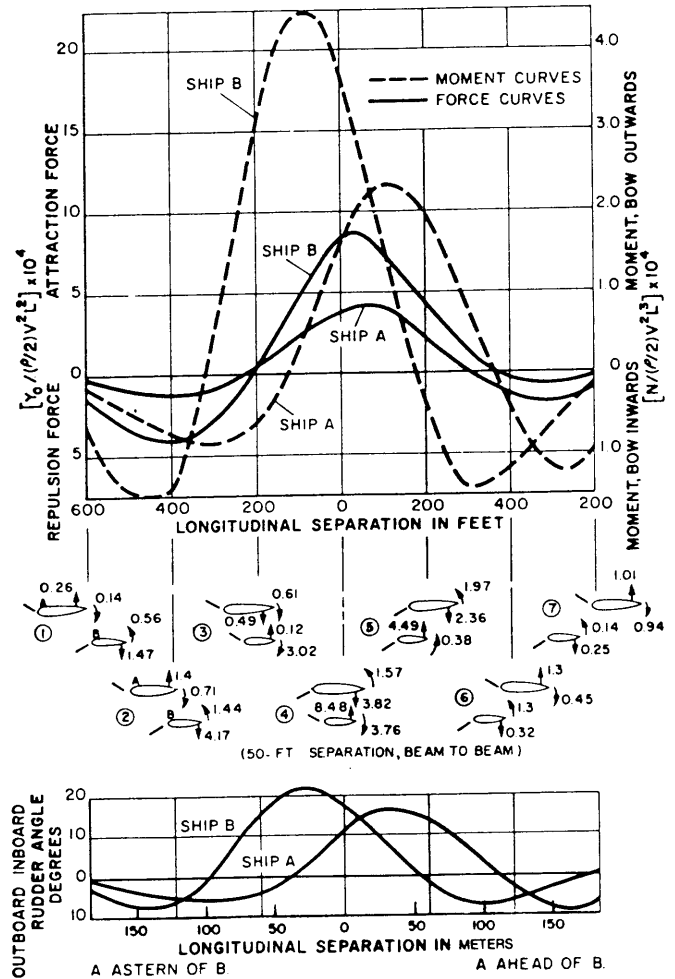


Fig. 113 Measured interaction forces and moments (and correcting rudder angles) between two ships on parallel courses as larger ship overtakes the smaller (Fig 2, Newton, 1960)

speeds from 10 to 20 knots, and the  $Y$ -force and  $N$ -moment acting on each model in each position was measured. The longitudinal separation scale shown as the abscissa on Fig. 113 is measured between the mid-length of the two ships. The rudder angle data shown in the lower part of the figure were obtained by computing the values of  $\delta_1$  and  $\beta_1$  needed to maintain equilibrium at each of the relative positions shown. The following assumptions, partly validated by free-running, piloted model tests, were made in computing  $\delta_1$  and  $\beta_1$ :

(a) That the system could be treated as one of steady motion.

(b) That interaction forces and moments are unaffected by the action of the propeller or by the small values of  $\beta$  and  $\delta_R$  needed to maintain equilibrium.

The magnitudes of the maximum forces of attraction shown on Fig. 113 are of interest. At a speed of 10

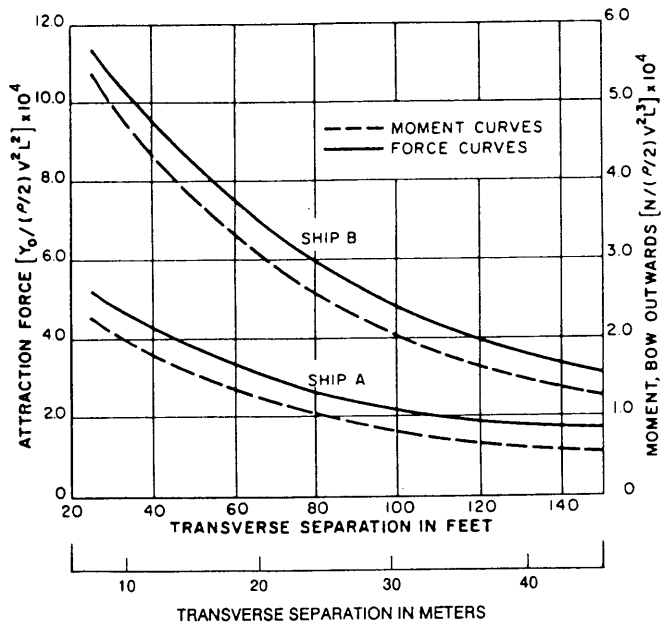


Fig. 114 Variation of interaction forces and moments with transverse separation for abreast longitudinal position

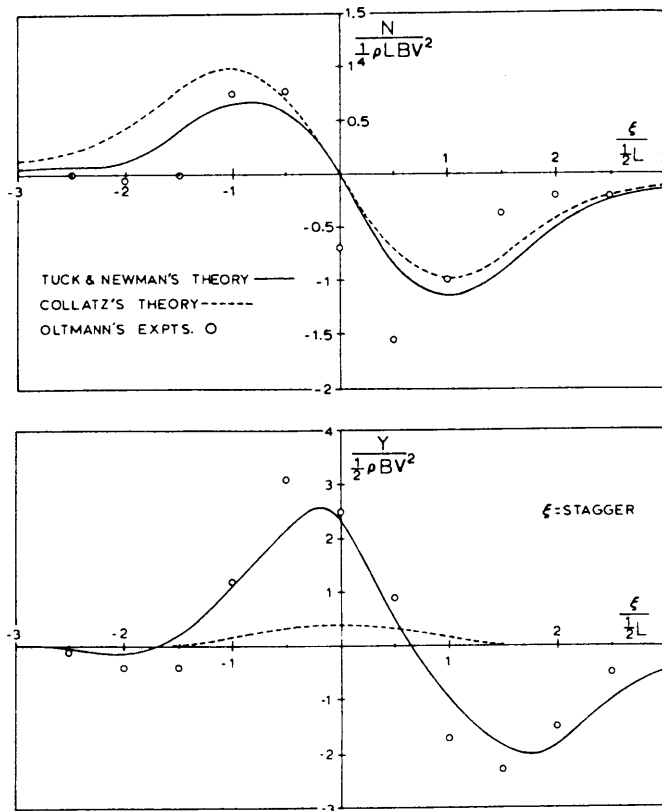


Fig. 115 Predicted and measured sway forces and yawing moments on two identical ships operating on parallel courses at equal speeds

knots the maximum attraction force is 13kN (26 tons) for ship A and 17.5 kN (35 tons) for ship B for the

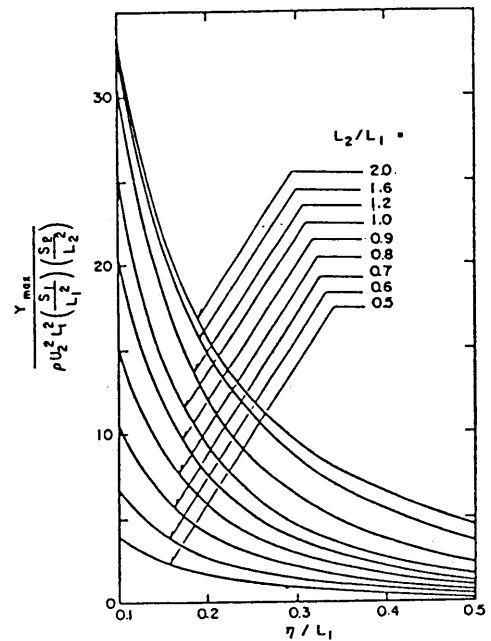


Fig. 116 Peak sway force on a fixed or moving ship as a function of its clearance from a passing ship

15.5 m (59-ft) beam-to-beam separation, and these occur when the two ships are very close to the fully abreast position 4. These forces would be quadrupled at a speed of 20 knots, and according to Fig. 114 would be decreased by about 40 per cent if the beam-to-beam separation were increased to 30 m (100 ft.)

It is evident from Fig. 113 that there are positions when both the interaction force and the interaction moment tend to draw one ship toward the other. Such positions are 3 for ship A and 5 for ship B. Fig. 113 shows that, in these positions, the rudder deflection angles are such that the rudder moments oppose the interaction moments. However, with these deflection angles, the rudder force tends to add to the force of attraction. Therefore, in these positions it is necessary to deflect the rudder sufficiently so that not only is the interaction moment overcome, but also a yaw angle,  $\beta$ , is introduced that creates an outboard force that counteracts both the attraction force and the rudder force. By this means, the two ships should be able to avoid collision in positions 3 and 5 provided that the transverse separation between the two ships is not so small that the available rudder force cannot correct the inward swing caused by the interaction moment.

It should be noted that position 3 immediately precedes and position 5 immediately follows the directly abreast position when the two ships have to apply opposite rudder to keep on parallel straight courses. Thus, in the short space of time between positions 3 and 4 for ship A and between positions 4 and 5 for ship B, the rudder has to swing from a large port deflection to a starboard deflection. Obviously, the pre-

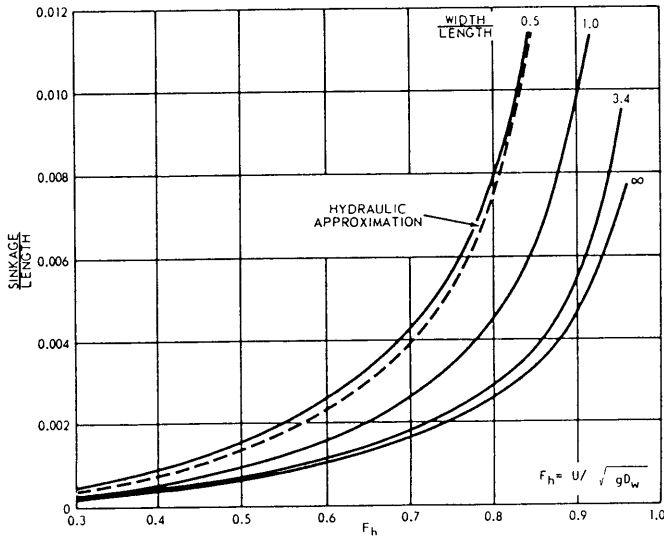


Fig. 117 Sinkage at various canal widths

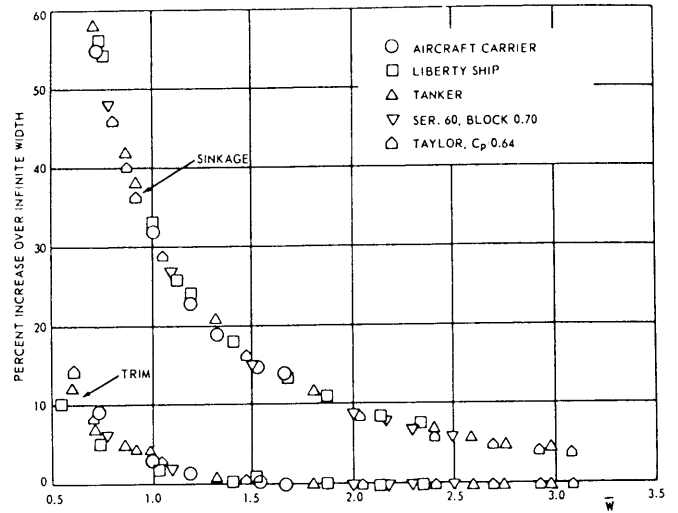
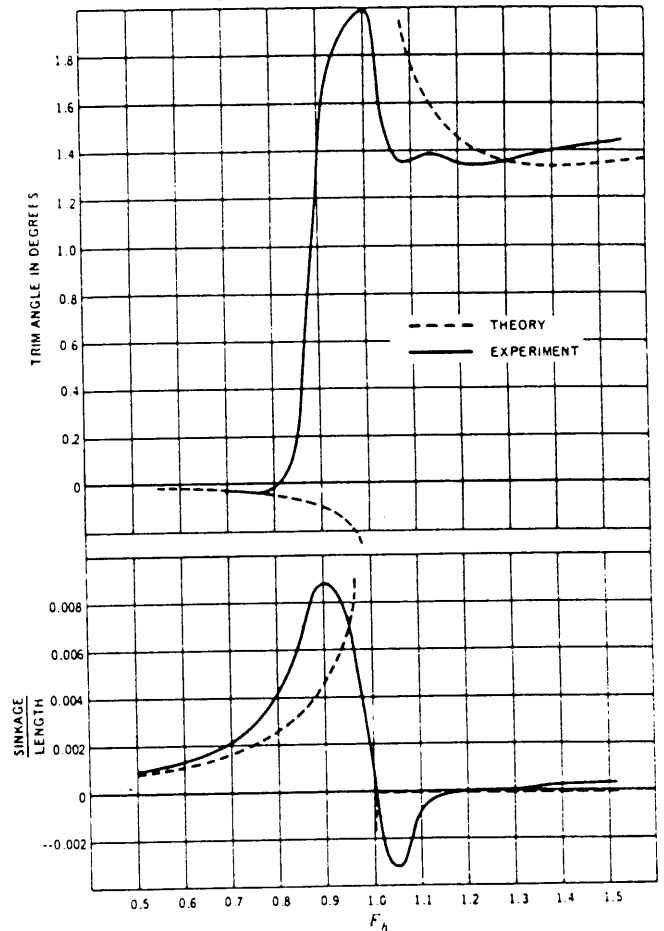


Fig. 118 Calculated sinkage and trim at finite canal width relative to infinite width

cise timing when this has to be done is not easy to choose. It is therefore true that two passing ships suffer the greatest risk of collision in positions 3 and 5, which would be augmented if the seas were rough and a heavy wind were blowing. Corrective action, if collision seemed imminent in position 3, would be for ship A to reduce speed and ship B to increase speed. If collision were imminent in position 5, Ship B should decrease speed and ship A increase speed.

A number of theoretical methods (Tuck, 1974, Wang, discussion of Tuck, Dand, 1974, and Abkowitz et al, 1970) for predicting interaction forces and moments have been developed and are in reasonable agreement with available model test data. Fig. 115 presents typical results for two ships moving at equal speed on parallel courses. Figs. 113, 114, and 115 illustrate the effect of parameters such as longitudinal and lateral separation and water depth on interaction forces and moments. Fig. 116 illustrates the variation of maximum sway force with lateral separation and relative ship length,  $L_2/L$ , for the case of a ship passing a stopped or moored ship (Wang, 1979).

Applications of theoretical methods and results have included simulation of UNREP operations, (Abkowitz, Ashe, and Fortson, 1970) and potential collision scenarios, (Dand, 1974). Kaplan and Sankaranarayanan (1987) reported an efficient numerical method for predicting lateral forces and yaw moments on ships on a parallel course at different speeds, operating at a given lateral and longitudinal separation distance in a shallow asymmetric canal. Kijima (1987) also described an approach for handling ship to ship interactions in a channel. Norrbin (1974) reports on tests of bank effects on a ship moving through a short dredged channel, and later (1985) on a tanker moving near a vertical wall and near a bank that has varying slope.

Fig. 119 Comparison between theoretical and experimental sinkage and trim at  $D/L = 0.125$

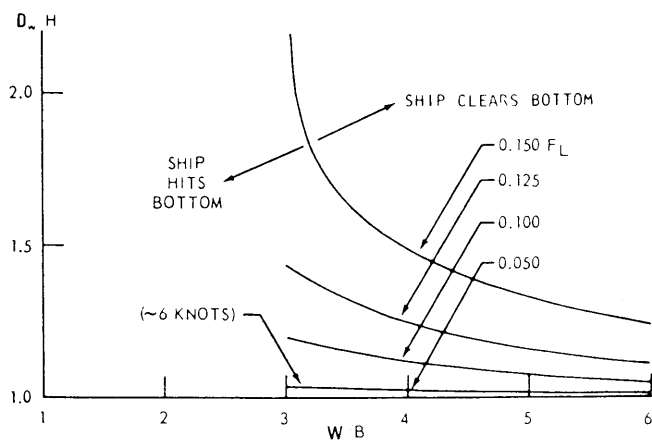


Fig. 120 Limiting speeds in canals based on squat

**13.5 Sinkage and Trim.** Tuck (1966 and 1967) presented results obtained from theoretical studies on the problem of sinkage and trim of ships in shallow and restricted waters. His calculations imply a nearly universal nondimensional curve for sinkage and trim which is almost independent of ship form. Sinkage is defined here as the downward vertical displacement of ship's center of gravity, and positive trim as the bow-up angle of rotation of the ship at its center of gravity. *Squat* is the resultant movement due to sinkage and to bow-up rotation. In many cases, trim can be negative (that is, bow down) owing to low-speed operation in shallow water.

As examples of computation of sinkage and trim, Tuck (1967) shows, as in Fig. 117, curves of sinkage against Froude number  $F_n$  for ratios of canal width to ship length ( $W/L$ ) of infinity, 3.4, 1.0, and 0.5. Froude number here is based on water depth,  $F_n = U/\sqrt{gD_w}$ . The ship form used is a Taylor Standard Series with a prismatic coefficient of 0.64. The value 3.4 for  $W/L$  corresponds to the dimensions of the towing tank in which the measurements of Graff (1964) were performed. Clearly, at  $W/L = 3.4$  and for moderate values of  $F_n$ , the departure from the result for infinite width is small, but it is already about 10 percent at  $F_n = 0.8$ , even for such a wide channel. Also shown by the broken line are the results of the hydraulic approximation at  $W/L = 0.5$  which give a slightly underestimated amount of sinkage compared to results predicted by the theory. The following formula may be used to obtain the approximate value of vertical hydraulic force acting on the ship proceeding in a relatively narrow canal:

$$F = \frac{\rho U^2}{S_0(1 - F_n^2)} \int_L S(x)B(x)dx \quad (119)$$

where

$F$  is vertical force, positive downward  
 $S_0$  cross-sectional area of the canal  
 $S(x)$  is local cross-sectional area of the ship  
 $B(x)$  is local beam of ship  
 $\rho$  is mass density of canal water

Tuck's theory predicts the points on the curve shown in Fig. 118 for ships moving along the centerline of a channel that has vertical walls. Since the calculated points cover wide ranges of practical ship forms and ship speeds, the curves may be considered as the universal curves of sinkage and trim. In the figure,  $\bar{W}$  is the *effective width* of the canal relative to ship length, that is  $\bar{W} = (W/L)\sqrt{1 - F_n^2}$ . The figure shows that the effect of finite narrow width is much greater for sinkage than it is for trim.

Fig. 119 shows the comparison between Tuck's computed sinkage and trim and the experimental results reported by Graff et al (1964) for a value of  $D_w/L = 0.125$  with sidewalls at infinity. The agreement is good for values of  $F_n < 0.7$ , but the comparison deteriorates as  $F_n$  approaches 1, that is, as the ship speed approaches the critical speed of  $U = \sqrt{gD_w}$ . (This critical speed, the reader will notice, closely approximates the celerity of waves in water that is shallow in comparison to wave length). Lea and Feldman (1972) extended the theory for the case  $F_n \approx 1$ . This figure also shows that sinkage is the dominant phenomenon at subcritical speeds ( $F_n < 1$ ), whereas trim is dominant at supercritical speeds ( $F_n > 1$ ). The figure also shows that the large subcritical sinkage is always positive (that is, downward), whereas the super-critical trim is likewise positive (that is, bow up).

Sufficient bottom clearance is one of the crucial requirements for ship operation in a canal. Fig. 120 shows contours presented by Eda (1971) of speed as limited in canals of various size to enable the ship to clear the bottom of the canal. These curves were obtained by using the following semiempirical equation, which is based on model test results (Yamaguchi, 1967, 1968):

$$F_{n_L} = \left\{ \frac{2\rho a(m-1)}{\left[ \frac{m}{q(1+me) - n} \right]^2 - 1} \right\}^{1/2}$$

where

$F_{n_L}$  = limiting Froude number,  $U/\sqrt{gL}$   
 $p$  = draft/ship length,  $h/L$   
 $q = 1/(1 + e)$ , where  $e = 0.24$  from test results  
 $m$  = water depth/ship draft,  $D_w/T$

## Section 14

### Hydrodynamics of Control Surfaces

**14.1 Geometry, Forces, and Moments.** The purpose in having a control surface on a ship is to control the motion of the ship. The control surface may be composed entirely of a single movable surface or of a combination of fixed and movable portions. It may typically be a rudder used to control the horizontal motion of a ship, a diving plane to control the vertical motion of a submarine, or an activated fin to reduce the rolling motion of a ship. A control surface has one sole function to perform in meeting its purpose, and that is to develop a control force in consequence of its orientation and movement relative to the water. The control force exerted by a rudder, for example, at the stern of a ship creates a moment,  $N_s \delta_{R_s}$ , on the ship which causes the ship to rotate and to orient itself at an angle of attack to the flow. The forces and moments generated as a result of this rotation and angle of attack then determine the maneuvering characteristics of the ship.

The simplest and most common type of control surface is the all-movable surface as diagramed in Fig. 121; other types are described in Section 14.7. The dimensions of a typical all-movable control surface are expressed as lying in three mutually orthogonal directions as indicated in Fig. 121: chord dimensions parallel to the direction of motion, span dimensions normal to the direction of motion, and thickness dimensions normal to both the span and the chord. Since most control surfaces are neither rectangular in shape nor of uniform thickness, each of these dimensions may have several values. Following aeronautical nomenclature, the edge of a control surface adjacent to the hull to which it is attached is referred to as the root and the opposite edge as the tip. Hence, there is a root chord,  $c_r$ , and a tip chord,  $c_t$ , and their average is the mean chord,  $\bar{c}$  (for straight-edged surfaces). There are similarly defined thickness dimensions as shown in Fig. 121. The mean span,  $\bar{b}$  is the average of the spans of the leading and the trailing edges of the rudder. The ratio  $\bar{b}/\bar{c}$  is the geometric aspect ratio, the ratio  $\bar{t}/\bar{c}$  is the thickness chord ratio, and the ratio  $c_t/c_r$  is the taper ratio. The profile area,  $A_p$ , may be taken as  $\bar{b} \times \bar{c}$  and  $\Delta$  is the sweepback angle of the quarter-chord line.

In contrast to an airplane wing, a control surface must usually be capable of developing lift in either of two opposed directions. Hence, the section shape shown is symmetrical about the centerplane of the control surface.

For the sake of simplicity, this section will treat the rudder principally, although most of the discussion will apply with equal validity to any control surface. The additional complicating effects of propellers on the flow over control surfaces are addressed in Section 17.

Consider a rudder as a separate body, completely immersed in a nonviscous fluid at an angle of attack,  $\alpha$ , to the uniform flow velocity unaffected by ship hull or propeller, Fig. 122. According to the two-dimensional (infinite aspect ratio) theory developed in Chapter VI, Section 2.5, Vol. II, the combination of forward velocity and angle of attack will induce a circulation about the rudder which in turn produces a lift force on the rudder. Since in the steady, two-dimensional, ideal, nonviscous, deeply-submerged flow considered in this paragraph there is no drag force, the total force due to the angle of attack will act normal to the direction of the free-stream velocity.

However, because rudders have a finite aspect ratio, two-dimensional theory does not accurately predict the forces acting on them. When the rudder is at an angle of attack, vortices are shed over the root of the rudder (unless the hull is close enough to the root to prevent the formation of vortices) and over the tip of the rudder, which induce velocities in the plane determined by the span and thickness. These velocities when added to the stream velocity cause, among other effects, an induced-drag force in the direction of motion.

In addition to the preceding two- and three-dimensional effects which can be predicted by frictionless flow theory, there exist friction and separation forces that arise because water is a viscous fluid. While the frictional force acts tangentially to the surface of the

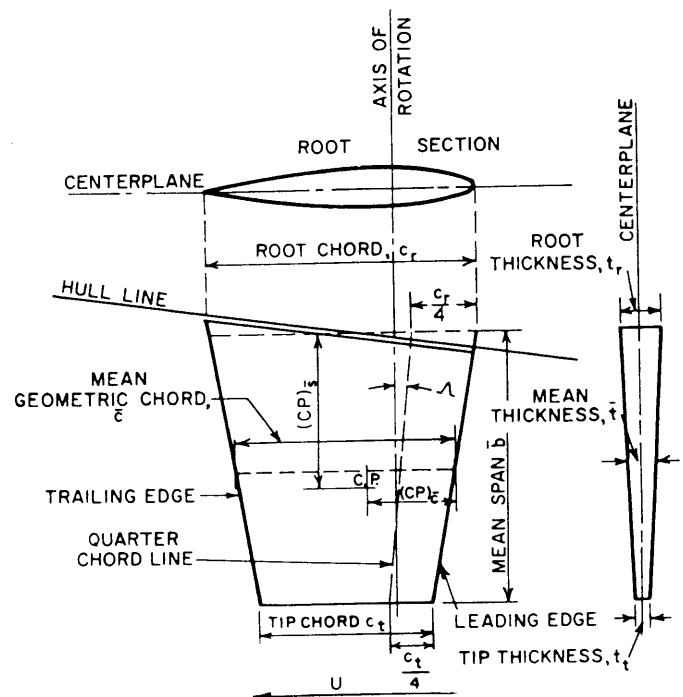


Fig. 121 Dimensions of a typical all-movable control surface

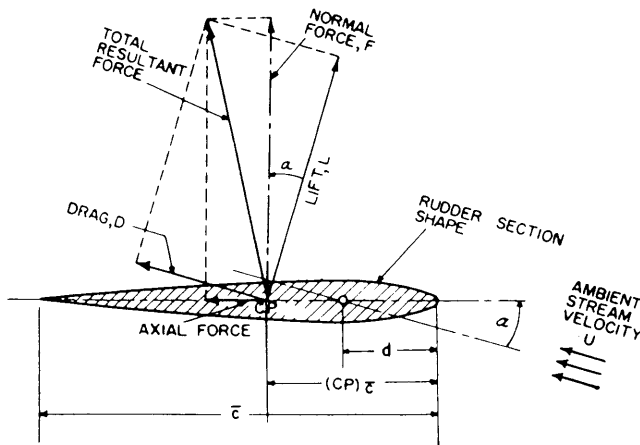


Fig. 122 Rudder force components

rudder, the direction of the force caused by separation of the viscous boundary layer cannot be predicted precisely. One effect of viscosity is to prevent the achievement of any positive incremental pressures at the tail of the control surface, thus introducing a so-called form or eddy drag into the force system acting on the control surface.

The total resultant hydrodynamic force in a real fluid arising from the effects described in the preceding paragraphs is shown in Fig. 122 as acting at a single point called the center of pressure, CP. In contrast to the resultant force in ideal, two-dimensional flow which would be normal to the direction of motion, the total resultant force in a real fluid is more nearly normal to the centerplane of the rudder. This force may be variously resolved into any number of components. Three components of interest in ship control are a lift component,  $L$ , normal to the direction of motion, a drag component,  $D$ , parallel to the direction of motion, and a  $y$ -component normal to the axis of the ship. This latter component is the reason for having a rudder. If there were no interaction between the pressure field around the rudder and the adjacent ship and its appendages, this  $y$ -component would be the control force,  $Y_{\delta R}$ , introduced in Section 3.5, and the moment of this component about the  $z$ -axis of the ship would be the control moment,  $N_{\delta R}$ . According to Figs. 122 and 22, the  $y$ -component of the total rudder force, assuming no interaction between the ship and the rudder, is:

$$Y_{\delta} \delta_R = Y_{\text{rudder}} = \pm (L \cos \beta_R + D \sin \beta_R) \quad (121a)$$

and

$$N_{\delta} \delta_R = N_{\text{rudder}} = (Y_{\text{rudder}}) (x_R) \quad (121b)$$

where  $\beta_R$  is the drift angle at the rudder (see Fig. 22),  $x_R$  is the distance from the origin of the ship to the CP of the rudder, and  $L$  and  $D$  are the lift and drag of the rudder. The  $x$ -component of the resultant rudder force is:

$$X_{\text{rudder}} = L \sin \beta_R - D \cos \beta_R \quad (121c)$$

For the purposes of Equations (121a-c), the signs of  $L$ ,  $D$ , and  $\beta_R$  must always be taken as positive, whereas  $x_R$  should be negative if the rudder is aft of the origin and positive if it is forward. With these assumptions, the sign of  $Y_{\text{rudder}}$  in Equation (121a) will depend on the sign of  $\delta_R$ . If  $\delta_R$  is negative,  $Y_{\text{rudder}}$  is negative; if  $\delta_R$  is positive,  $Y_{\text{rudder}}$  is positive. It is for this reason that the expression for  $Y_{\text{rudder}}$  is preceded by a  $\pm$  sign. Since in Equation (121c)  $D \cos \beta_R$  is always larger than  $L \sin \beta$ ,  $X$  is always negative; that is, directed aft.

Equations (121) are valid only for the special case of a rudder that is well isolated from the ship to which it is attached. In most practical cases, significant interaction takes place between the rudder and the ship so that the total  $Y$ -force created by rudder deflection acting on the combined ship-rudder system, is larger than that indicated by the equation and its center of action is forward of the center of pressure of the rudder itself. In fact its center of action may not be on the rudder at all.

For purposes of rudder design, the component of the total rudder force, excluding interaction effects, which is normal to the center plane of the rudder and designated,  $F$ , in Fig. 122 is of importance. The product of this component times the distance of the center of pressure from the centerline of the rudder stock yields the hydrodynamic torque experienced by the stock. Using the nomenclature of Figs. 121 and 122:

$$Q_H = F(d - \overline{CP}_s) \quad (121d)$$

where  $d$  is the mean distance between the leading edge of the rudder and the centerline of the rudder stock. The sign of moments about the rudder stock should be determined on the basis of whether  $d$  is greater or less than  $(\overline{CP})_s$  and not on the basis of the right-hand rule.

Similarly, the bending moment on the rudder stock about the root section is

$$(L^2 + D^2)^{1/2} \times (\overline{CP})_s$$

where  $\bar{s}$  denotes spanwise. The maximum anticipated values of these moments are used in the design of the rudder stock, the rudder bearings, and the steering engine. The rudder stock diameter, in turn, determines the root thickness of the rudder itself (see Section 17.8).

To permit ready comparison of rudder forces and moments among similar rudders of different size and operating at different speeds, it is convenient to express the rudder forces and moments in nondimensional form as was done in Section 3 for the hull forces and moments. The parameters used for nondimensionalization in this case are  $\rho$ ,  $U$ ,  $A_R$  and  $\bar{c}$  or  $\bar{b}$  in lieu of  $\rho$ ,  $V$ , and  $L$ . The following are the nondimensional forms of the most commonly used rudder forces and



moments:

$$\begin{aligned} \text{Lift coefficient} \quad C_L &= \frac{L}{(\rho/2)A_R U^2} \\ \text{Drag coefficient} \quad C_D &= \frac{D}{(\rho/2)A_R U^2} \\ \text{Normal force coefficient} \quad C_N &= \frac{F}{(\rho/2)A_R U^2} = \\ &C_L \cos \alpha + C_D \sin \alpha \end{aligned}$$

$$\begin{aligned} \text{Moment (torque) coefficient about the rudder stock} \quad (C_M)_H &= \frac{F(d - CP_{\bar{c}})}{(\rho/2)A_R U^2 \bar{c}} = \\ &\frac{Q_H}{(\rho/2)A_R U^2 \bar{c}} \end{aligned}$$

$$\begin{aligned} \text{Moment coefficient about the quarter chord, } C_{m_{\bar{c}/4}} &= \\ &\frac{F(0.25\bar{c} - CP_{\bar{c}})}{(\rho/2)A_R U^2 \bar{c}} \end{aligned}$$

$$\begin{aligned} \text{Bending moment coefficient about the root section} &= \\ &\frac{(L^2 + D^2)^{1/2} CP_s}{(\rho/2)A_R U^2 \bar{b}} \end{aligned}$$

**14.2 Flow Around a Ship's Rudder.** A rudder on a ship performs its function in a highly complicated medium. Hydrodynamic flow phenomena such as stall, cavitation, and aeration exist which place definite limits on maximum achievable rudder performance. These are very involved phenomena, which are discussed only briefly in this chapter. For a fuller discussion of stall and cavitation the reader is referred to Thwaites (1960) and Breslin and Landweber (1961).

Stall is defined as a more or less abrupt discontinuity in the lift versus angle-of-attack curve. As the angle of attack on a rudder is increased, the point where the flow separates on the downstream side of the rudder moves forward along the chord of the rudder. As the extent of the region of flow separation increases, the slope of the lift curve with respect to the angle of attack begins to decrease. Finally, if the angle of attack is further increased to a certain critical (stall) angle, there is an abrupt discontinuity in the growth of the lift (or normal force) with angle of attack, and the lift begins to decrease with increased angle of attack. Typical curves of normal force coefficient versus angle of attack, carried through the stall point, for a rudder in the free stream as well as in the propeller race are shown in Figure 248.

Cavitation and aeration are governed by the magnitude of the reduction of pressure on the downstream side of the rudder. Inception of cavitation is critically dependent on nuclei in the water and on roughnesses on the rudder surface. As described in Chapter VI, cavitation occurs when the sum of the maximum negative pressure (below ambient) on the downstream

side of the rudder, plus atmospheric pressure and hydrostatic pressure, is less than the vapor pressure of the fluid. The effect of cavitation is shown in Fig. 123. The shaded area I shows for a particular section shape the extent of negative pressure that would not be achievable because of cavitation at any angle of attack of 10 deg at a speed of 20 knots and a depth of submergence of 3 m (10 ft). The shaded area II shows similar data for an angle of attack of 15 deg, a speed of 15 knots, and a submergence of 10 ft. It is clear from Fig. 123 that by limiting the growth of the negative-pressure region around a rudder, cavitation reduces the rate of increase of lift as the angle of attack is increased at any given speed, but cavitation alone does not stop the growth of the lift curve with angle of attack; it only slows growth. Thus at moderate speeds, cavitation is not as restrictive of rudder performance as stall is. However, Fig. 123 shows that as speed is increased, the inhibiting effect of cavitation on lift becomes greater. Furthermore, at any speed, cavitation can cause erosion of the surface of the rudder. Some authorities have also ascribed a serious case of rudder-induced vibration on a ship to cavitation around the rudder (Macovsky, Duerr, and Jewell, 1959).

As its name implies, aeration (also called ventilation) involves the drawing of air from the atmosphere into

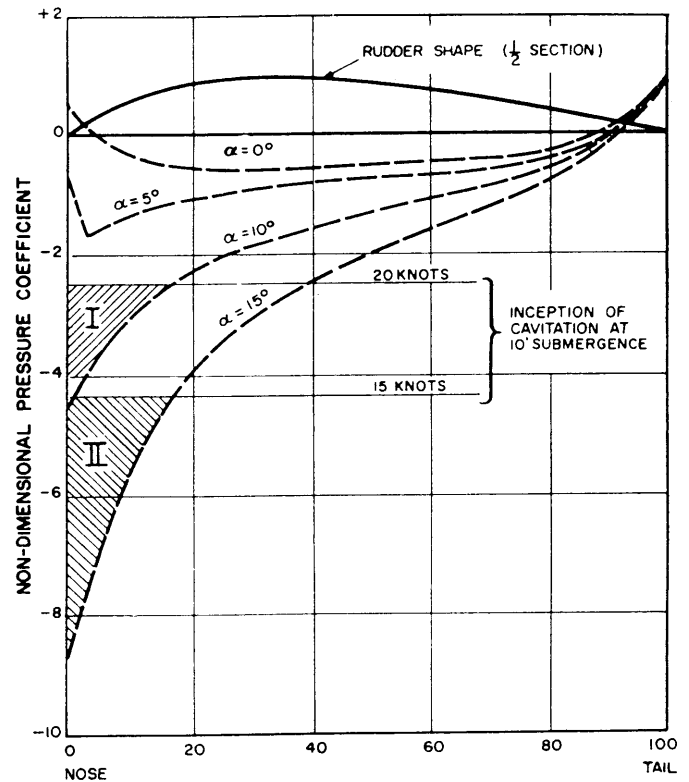


Fig. 123 Pressure distributions on downstream side of a rudder (Mandel, 1953)

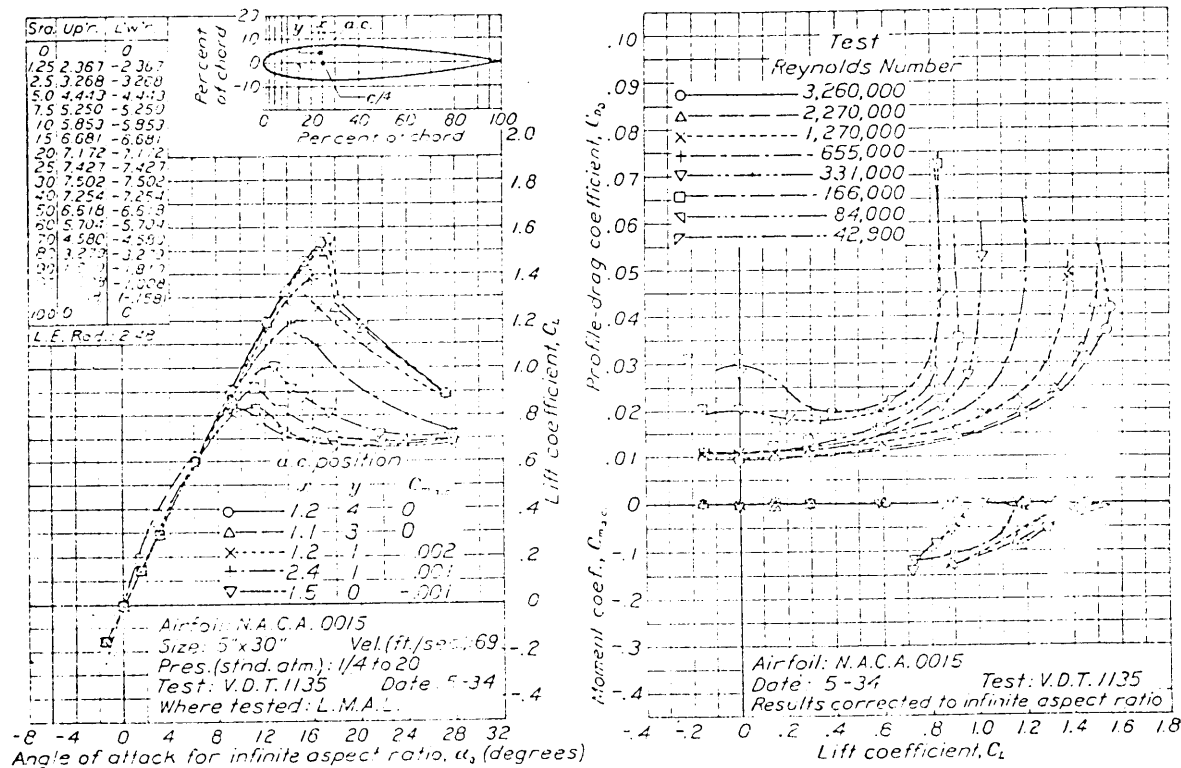


Fig. 124 NACA 0015

the suction (downstream) side of the rudder. It usually occurs when the rudder is at or near the surface of the water and when the difference in pressure between the atmosphere and the suction side of the rudder exceeds the resistance to air drawing from the surface. Thus if the resistance to air drawing is low, aeration will occur at lesser angles of attack or at lower speeds

than will cavitation. Rudder aeration occurs frequently in model turning tests and is immediately recognizable at the rudder. In some tests the very bottom of a model rudder has been seen to be clear of water, that is, the air bubble is carried all the way down the suction side of the rudder.

The occurrence of stall, cavitation, and aeration is

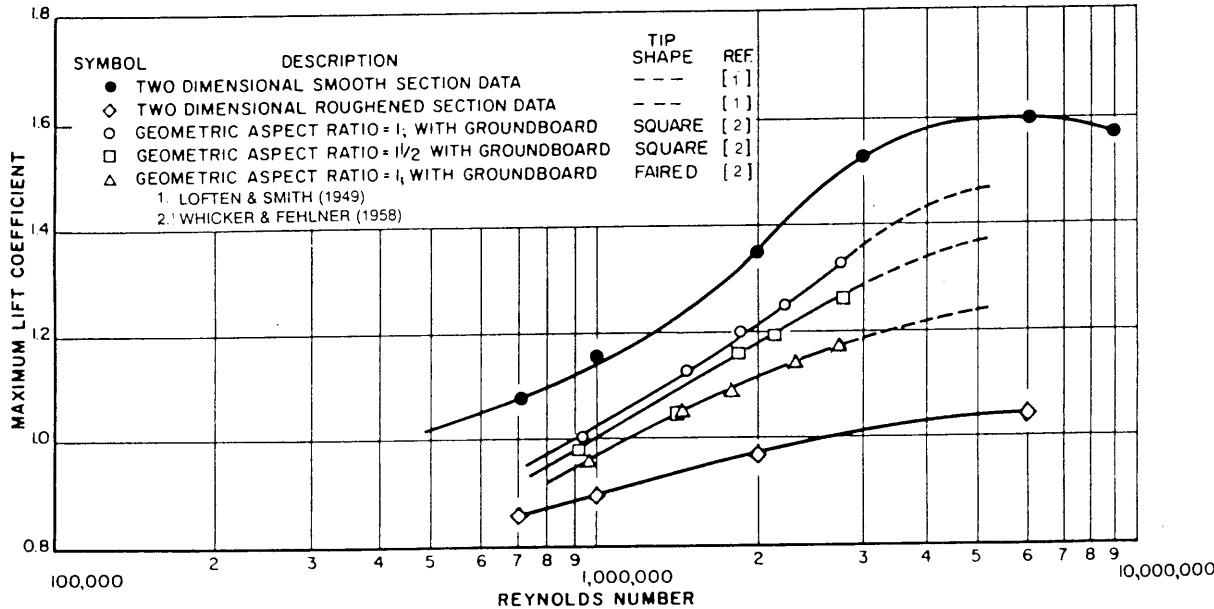


Fig. 125 Effect of Reynolds number on maximum lift coefficient

difficult enough to predict for a rudder in a free stream where the velocity and angle of attack are precisely known. When the rudder is located under the stern of a ship, these fundamental quantities are not known with accuracy unless very special instrumentation is used, because the ship's hull and appendages ahead of the rudder influence both the direction and speed of the flow to the rudder. This altered flow is part of the interference effect mentioned in Section 14.1. This interference effect for a ship in a turn is shown in Fig. 22 by use of a straightening influence, angle  $\epsilon$ , which tends to increase the angle of attack on the rudder beyond that which it would have if there were no interference effects. The velocity at the rudder is also generally different from the ship's velocity because the presence of the ship slows the flow to the rudder; on the other hand, if the rudder is located abaft a propeller and nearly in line with it, the flow velocity is increased by the race of the propeller. Furthermore, since the wake field is usually nonuniform at the stern, the rudder undergoes different magnitudes and directions of velocity vector throughout its span. Thus the rudder passes through a complicated flow environment at the stern of a ship that is similar to that undergone by a propeller. In addition, the complicated flow environment at the stern of a model of a ship may be quite different from that at the stern of the ship itself.

**14.3 Scale Effects.** Each of the phenomena discussed in the previous subsection is governed by different laws of similitude. These laws are discussed in Chapters V and VI of Vol. II.

Very important scale effects on rudder performance occur with the typical small-scale free running models run in compliance with Froude's Law. Neither full-scale Reynolds number nor Weber number (defined later in this section) can be simulated, and the effect of Reynolds number on maximum lift and stall angle is serious.

For actual ships, Reynolds number for the rudder is roughly of the order of  $10^7$ . Since model tests are usually conducted at the speed determined by Froude's Law, Reynolds number for the model rudder is much smaller than that for the actual rudder, that is:

Reynolds number for model =  $\alpha^{3/2} \times$  Reynolds number for ship where  $\alpha$  is the scale ratio of the model to the ship.

Wind tunnel test results as reported by Shiba (1960) for the NACA sections as shown in Figs. 124 and 125 illustrate the important trends affecting the correlation of model test results to full scale ships:

(a) Maximum lift coefficient increases with Reynolds number because of the delay of stall angle.

(b) Lift curve slope varies little with Reynolds number (also with section shape).

(c) Drag coefficient decreases with increase of Reynolds number.

Surface roughness must also be reviewed, because it has an important effect on maximum lift coefficient

(Lofton and Smith, 1949, and Whicker and Fehlner, 1958).

Free stream rudder tests, where compliance with Froude's Law is not necessary, also indicate qualitatively that the higher the Reynolds number, the greater the angle of attack at which stall occurs. Fig. 126 shows this relationship for foils of various aspect ratio. (Dieudonné, 1953). Concurrent with this delay of the stall angle of attack is an increase in the maximum lift coefficient developed by the rudder. This effect is shown in Fig. 125, which also shows the important effect of surface roughness on maximum lift coefficient.

The preceding deals with the effect of Reynolds number on stall in fully turbulent flow. At low Reynolds numbers, the flow about a model rudder may be laminar rather than turbulent. Since laminar flow is much more susceptible to separation than is turbulent flow, laminar flow may be a factor in inducing premature stall in model tests of rudders.

As a result of the foregoing considerations, model test results at low Reynolds numbers may be conservative in predicting the magnitudes of maximum lift coefficients for actual ships, which operate at comparatively high Reynolds numbers.

In addition to scale effect on stall because of different Reynolds numbers, there is the possibility of scale effect because of dissimilar cavitation indexes between model and full scale. However, in contrast to stall scale effect, cavitation occurs at lower rudder angles or

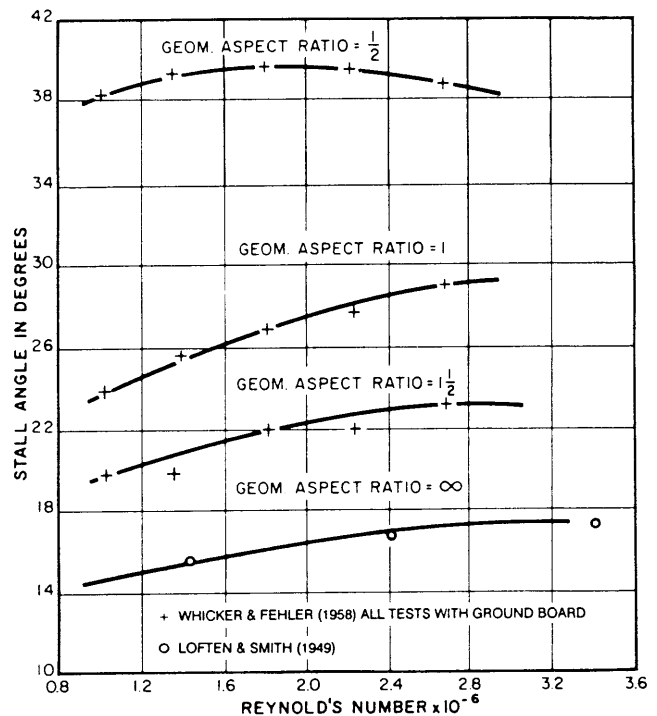


Fig. 126 Effect of Reynolds number on stall angle

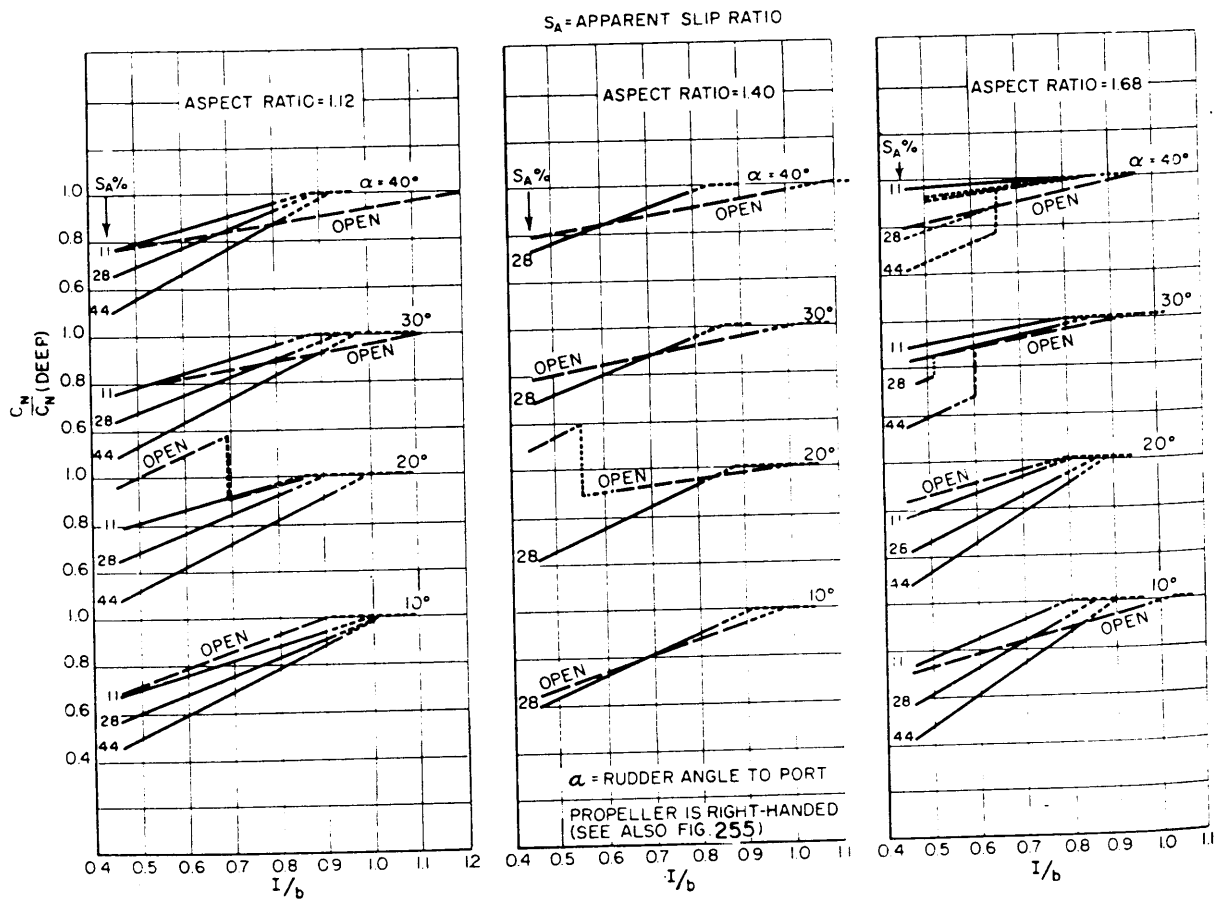


Fig. 127 Effect of rudder submergence ratio  $I/b$  on rudder normal force coefficient (Shiba, 1960)

speeds on ships than on models run in accordance with Froude's Law.

Froude's Law dictates that the model speed be less than the ship speed, with the model speed equal to ship speed times the square root of the scale ratio. As long as geometric similitude is adhered to, the negative pressure on the downstream side of the rudder in coefficient form,  $-p/(\rho/2)V^2$  will be identical between model and ship. This will also be true of the hydrostatic pressure  $\rho gh/(\rho/2)V^2$ . However, atmospheric pressure and vapor pressure have the same absolute value for both model and ship, hence in coefficient form they will be much larger for the model than for the ship. Since atmospheric pressure is usually the larger of these pressures, it delays the onset of cavitation to a higher Froude number on the model than that corresponding to the speed of the full-scale ship. In any case, as noted earlier, the scale effect due to cavitation is not likely to be as severe as the scale effect due to stalling.

If the rudder penetrates the free surface, as it does in the light condition for some ships, the occurrence of air drawing is a function of the Reynolds number

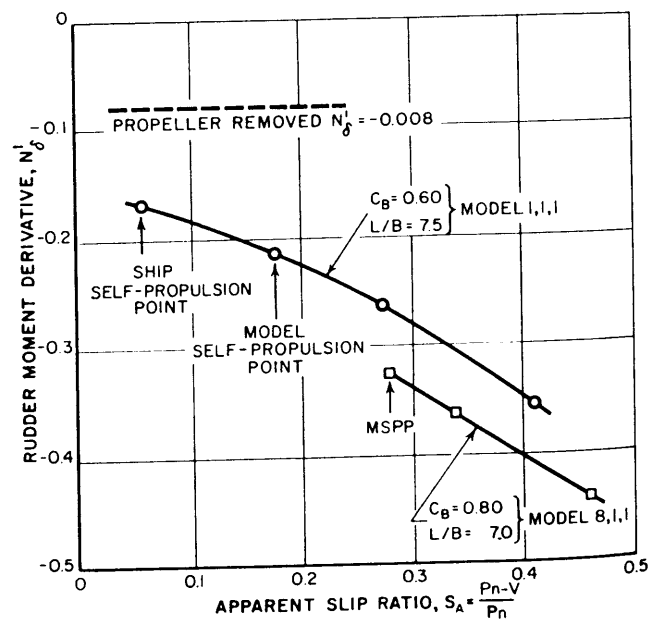


Fig. 128 Effect of propeller slip ratio on rudder moment derivative

and Weber number of the experiment, as well as of the angle of, the attack and the geometric properties of the rudder. Shiba (1960) states that separation is a necessary but not sufficient condition for the occurrence of air drawing; that its occurrence in the model range also depends on the Weber number,  $W$ , defined here as

$$W = V \left( \frac{\rho}{S} R \right)^{1/2}$$

where

$R$  is radius of leading edge of rudder

$S$  is surface tension of water (force/unit length)

$\rho$  is mass density of water

$V$  is velocity

Shiba states that if  $W \geq 0.15 \times 10^{-2}$ , the occurrence of air drawing ceases to be a function of the Weber number. Thus if this condition is met and separation (stall) is not occurring (Fig. 126) then presumably air drawing will not occur even if the rudder penetrates the free surface.

Meijer (1964), however, indicates that no satisfactory criteria have been established that relate the various factors that influence aeration. Gertler (1965) further indicates that there have been several high-speed naval vessels for which the full-scale turning diameters are much larger than those obtained from free-turning model tests and that the cause is believed to be aeration occurring on the full scale but not on the model.

Fortunately, when aeration does occur it is usually readily visible and can be remedied by installing a physical barrier between the water surface and the top of the rudder. Discussion by G. R. Hagen of Mandel (1953) indicates that aeration rarely, if ever, occurs on single-rudder ships if the top of the rudder is well submerged and is shielded from direct access to the free surface by the ship's hull.

Even if aeration does not occur, proximity to the free surface can cause a degradation in rudder performance because of wave generation. Quantitative data on this effect are shown in Fig. 127. In the ordinary free-running model test, this effect is properly scaled provided the model speeds are determined in accordance with Froude scaling laws.

Usually, the ship's turning path or *tactical diameter* is practically independent of speed at Froude numbers less than about 0.30, but at higher ship speeds, the tactical diameter begins to increase, primarily because of the consequences of wavemaking. This increase for the full-scale ship could also be partly attributable to rudder cavitation. As the tactical diameter increases, the inflow angle at the rudder,  $\beta_R$ , Fig. 122 decreases, with a consequent increase in the angle of attack of the rudder, which is being held at a constant deflection angle. The cause of severe rudder stall in free-turning tests is, then, very likely the increased angle of attack

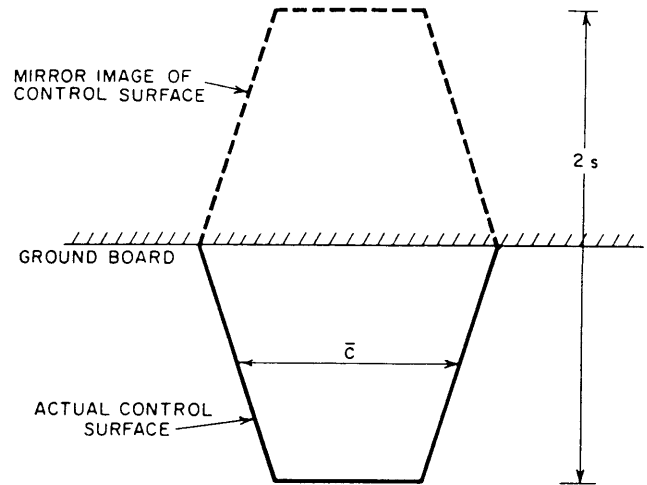


Fig. 129 Control surface against groundboard

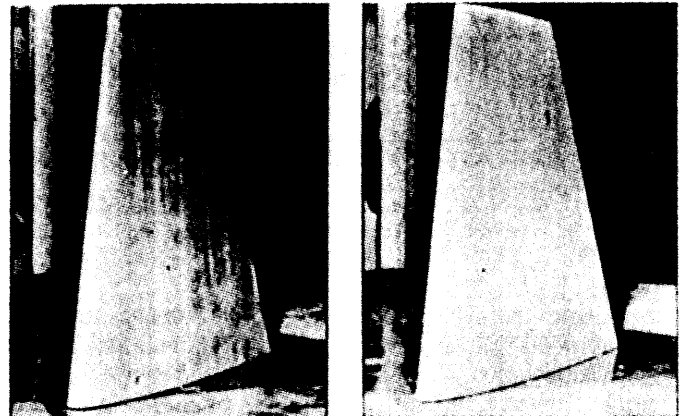


Fig. 130 Control-surface model mounted over ground board in wind tunnel

(a) With faired tip (b) Without faired tip

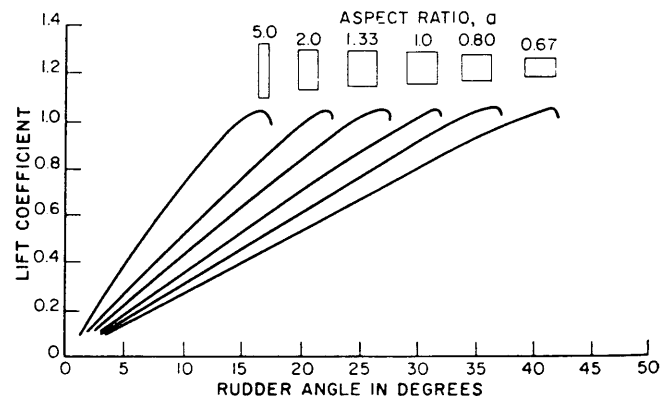


Fig. 131 Effect of rudder aspect ratio on lift coefficient (VanLammeren, Troost, and Koning, 1948)

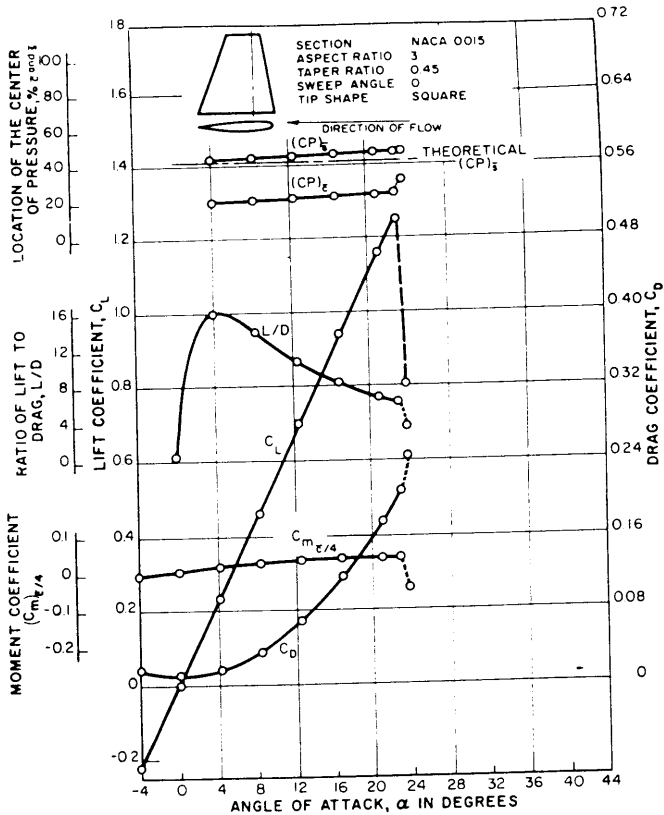


Fig. 132 Free-stream characteristics of an NACA 0015 section in ahead condition at a Reynolds number of  $2.70 \times 10^6$  (Whicker and Fehlner, 1958)

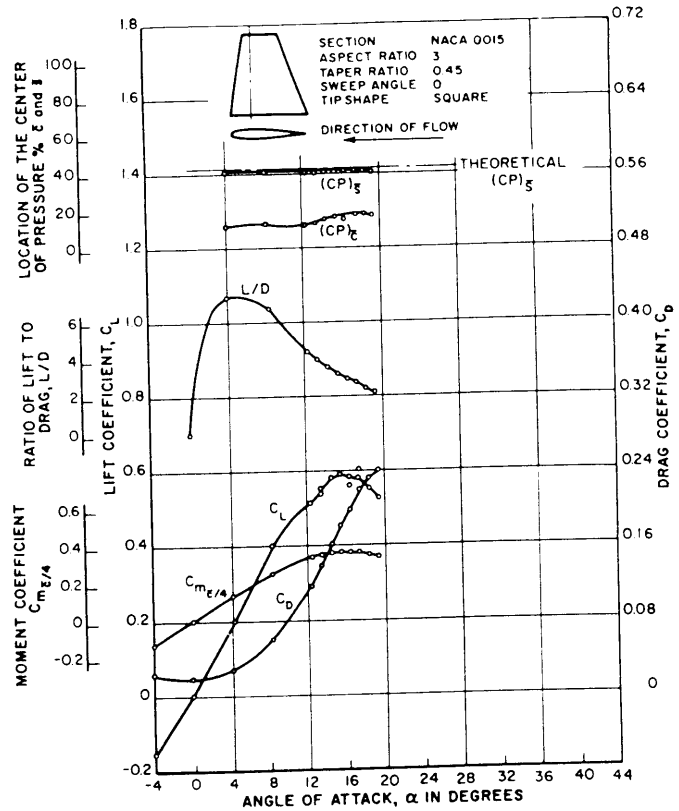


Fig. 133 Free-stream characteristics of an NACA 0015 section in astern condition at a Reynolds number of  $3.00 \times 10^6$  (Whicker and Fehlner, 1958)

resulting from higher speed and not necessarily the high speed in itself.

In addition to these kinds of scale effects, free-running maneuvering tests of models of multiple rudder, multiple-propeller ships where the rudders are located in the propellers' slip streams are subject to additional scale effects because the velocity of the model propeller race relative to the free-stream velocity is larger than that of the ship propeller race. This is a Reynolds number effect; the much smaller Reynolds number of the model compared to that of the ship causes the model to have a larger drag coefficient, which in turn requires that the model propeller operate at a larger slip ratio than does the ship propeller, Fig. 128. For such ships, it might be expected that free-running model tests would underpredict the maneuvering characteristics of the full-scale ship.

This scale effect applies also to single-propeller, single-rudder ships. However, these ships have a compensatory scale effect, because the rudder (and propeller) of these ships operate in flow heavily influenced by the hull ahead of the rudder. Again as a result of the lower Reynolds number of the model, its frictional boundary layer and its stern separation zone are relatively thicker on the model than on the ship. This greater relative thickness reduces the velocity of the flow to the propeller and to the rudder relative to

the free-stream velocity more on the model than on the ship. Since this change in velocity is opposite to the one caused by the difference in propeller slip ratio, these two scale effects tend to cancel each other in free-running maneuvering tests of models of single screw, single-rudder ships (Shiba, 1960).

However, in free-running maneuvering tests of models where the flow to the rudder is not influenced by the hull ahead of it but the rudder is not abaft a propeller this cancelling effect would not take place. This lack of cancelling is shown by many commercial multiple-screw, single-rudder ships. Brard (1951) states that model tests of these ships will overpredict the tactical diameter (for example) of the full-scale ship, possibly by as much as 10 to 15 percent, because of the failure of the hull wake to scale properly.

**14.4 Effect of Aspect Ratio.** A control surface of infinite aspect ratio has the same flow pattern in all planes perpendicular to the span. In other words, there is no flow component along the span and the flow over any section of the control surface is strictly two dimensional. However, as noted in Section 14.1, in the case of a finite aspect-ratio, cross flow does occur over the root and over the tip from the high-pressure side to the low-pressure side, thus causing the flow over all sections to be three dimensional. This cross flow increases with decreasing span, and causes a concom-

itant decrease in the lift generated by the rudder for any given angle of attack.

The preceding physical picture leads to the concept of *effective aspect ratio*. If the root section of a control surface is sufficiently close to the hull that all cross flow over the root is prevented, the lift coefficient developed by that control surface for any given angle of attack is identical to that of a control surface of twice its geometric aspect ratio. Fig. 129 shows this doubling effect by projecting a "mirror image" of a control surface flush against a "groundboard." In computing the lift generated, the area of control surface to use is that bounded by the solid lines, but its effective aspect ratio,  $a$ , is  $2s/\bar{c}$  rather than  $s/\bar{c}$ .

On the basis of this discussion, the control surface in Fig. 125, for example, described as "geometric aspect ratio = 1; with groundboard," has an effective aspect ratio,  $a$ , of 2. Photographs of two control surfaces like those reported on in Fig. 125, mounted against a groundboard in a wind tunnel are shown in Fig. 130 (Fig. 137, presented in the next section, also shows directly the effect of aspect ratio on lift-curve slope).

In the middle 1920's, Prandtl of Germany developed a reasonably accurate theory for predicting the effect of aspect ratio on lift and drag. This theory applies to control surfaces whose spanwise load-distribution curve is elliptical in shape. The theory shows that for such control surfaces, the following simple expressions relate the drag coefficient and the angle of attack in

radians to aspect ratio for any constant lift coefficient:

$$C'_D = C_D + \frac{C_L^2}{\pi} \left[ \frac{1}{a'} - \frac{1}{a} \right] \quad (122a)$$

$$\alpha' = \alpha + \frac{C_L}{\pi} \left( \frac{1}{a'} - \frac{1}{a} \right) \quad (122b)$$

where  $C_D$  and  $\alpha$  correspond to an aspect ratio  $a$ , and  $C'_D$  and  $\alpha'$  correspond to an aspect ratio  $a'$ . Fig. 131 shows the relationship between lift coefficient and aspect ratio (down to  $\frac{2}{3}$ ) as computed from Equation (122b) based on experimental data for an aspect ratio of 5.0. Fig. 131 shows clearly that the slope of the lift-coefficient curve versus angle of attack decreases sharply with decreasing aspect ratio. This relationship is consistent with theoretical formulations of lift-curve slope (Weinig, 1947) as well as experimental data (Lof-ten and Smith, 1949, and Larson, 1946). The latter is shown in Fig. 18 of Mandel (1953).

As computed from Equation (122b), Fig. 131 shows the maximum lift coefficient to be independent of aspect ratio. This independence is not borne out by experiment. For example, Fig. 125 shows that a control surface with an effective aspect ratio (twice the "geometric" aspect ratio) of 2 achieves a larger maximum lift coefficient than does an effective aspect ratio of 3. However, Fig. 125 also shows that the effect of Reynolds number and of surface roughness are much more

(Continued on page 302)

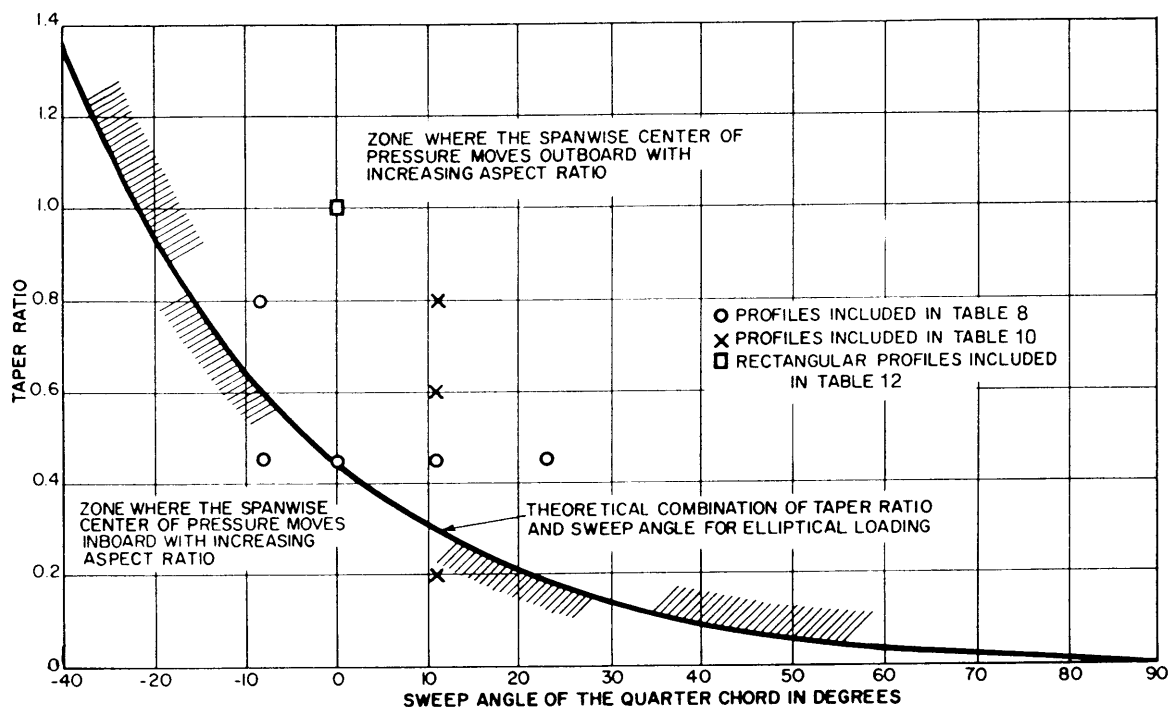


Fig. 134 Theoretical relationship between taper ratio and sweep angle to achieve an elliptical spanwise load distribution (Whicker and Fehlner, 1958)

Table 13—Effect of Aspect Ratio, Sweep Angle and Tip Shape on the Free-Stream  
(all control surfaces tested against

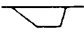
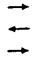

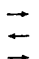
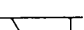
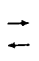
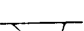


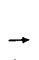



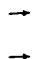
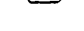
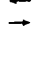
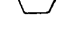
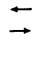



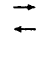


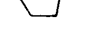

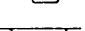



Item No.	Profile	$\xi$ , ft	$a$	$\Lambda$ , deg	$\lambda$	$t/c$	Section Shape	Tip Shape	$Rn \times 10^{-4}$ of test	Direction	$(\frac{\partial C_L}{\partial \alpha})_{\alpha=0}$ per degree
1			2.0	1	-8	0.45	NACA 0015	Square	2.25	Ahead	0.023
								Square	3.00	Astern	0.023
								Faired	2.28	Ahead	0.021
2			2.0	2	-8	0.45	NACA 0015	Square	2.72	Ahead	0.04
								Square	3.00	Astern	0.012
								Faired	2.72	Ahead	0.039
3			2.0	3	-8	0.45	NACA 0015	Square	2.26	Ahead	0.056
								Square	3.00	Astern	0.047
								Faired	2.26	Ahead	0.049
4			2.0	1	0	0.45	NACA 0015	Square	2.70	Ahead	0.023
								Square	3.00	Astern	0.023
								Faired	2.29	Ahead	0.020
5			2.0	2	0	0.45	NACA 0015	Square	2.72	Ahead	0.04
								Square	3.00	Astern	0.039
								Faired	2.72	Ahead	0.04
6			2.0	3	0	0.45	NACA 0015	Square	2.70	Ahead	0.054
								Square	3.00	Astern	0.042
								Faired	2.26	Ahead	0.052
7			2.0	1	11	0.45	NACA 0015	Square	2.28	Ahead	0.024
								Square	3.00	Astern	0.023
								Faired	2.28	Ahead	0.021
8			2.0	2	11	0.45	NACA 0015	Square	2.72	Ahead	0.042
								Square	3.00	Astern	0.026
								Faired	2.72	Ahead	0.043
9			2.0	3	11	0.45	NACA 0015	Square	2.26	Ahead	0.050
								Square	3.00	Astern	0.046
								Faired	2.26	Ahead	0.054
10			3.0	2	22.5	0.45	NACA 0015	Square	3.00	Ahead	0.045

Table 14—Effect of Section Shape on Free-Stream Characteristics of  
(all control surfaces tested against

Item No.	Profile	$\xi$ , ft	$a$	$\Lambda$	$\lambda$	$t/c$	Tip Shape	Section Shape	Direction	$Rn \times 10^{-4}$ of test	$(\frac{\partial C_L}{\partial \alpha})_{\alpha=0}$ per degree
1			2.0	2	0	0.45	Square	NACA 0015	Ahead	2.72	0.0412
								NACA 0015	Astern	3.00	0.0388
2			2.0	2	0	0.45	Square	TMB EHP	Ahead	2.70	0.0382
								TMB EHP	Astern	3.00	0.0325
3			2.0	2	0	0.45	Square	NSS	Ahead	2.70	0.0332
								NSS	Astern	3.00	0.0362
4			2.0	2	0	0.45	Square	TMB Fairing No. 7	Ahead	2.77	0.04
								TMB Fairing No. 7	Astern	3.00	0.046
5			2.0	2	0	0.45	Square	TMB 07507515	Ahead	2.77	0.0481
								TMB 07507515	Astern	3.00	0.0487



## Characteristics of All-Movable Control Surfaces (Whicker and Fehlner, 1958)

groundboard with gap = 0.005c

$C_L$ @ 10°	$C_L$ @ 20°	$C_{L_{max}}$	Stall Angle, deg	$\alpha$ for ( $L/D$ ) <sub>max</sub> deg	$L/D_{max}$	$L/D$ @ $\alpha = 10^\circ$	$L/D$ @ $\alpha = 20^\circ$	$L/D$ @ Stall Angle	$(CP)'_z$ @ $\alpha =$		$(CP)'_z$ @ $\alpha =$	
									10°	Stall	10°	Stall
0.25	0.59	1.24	39.4	8	8.0	7.45	4.24	2.0	0.14	0.30	0.48	0.51
0.30	0.67	0.96	31.2	8	5.4	5.36	2.85	1.7	0.20	0.27	0.45	0.42
0.23	0.53	1.03	36.3	8	8.2	7.66	4.27	1.8	0.10	0.32	0.46	0.49
0.42	0.91	1.33	28.7	6	12.2	10.1	5.9	4.0	0.18	0.25	0.45	0.48
0.40	0.64	0.64	21.0	7	6.8	5.89	2.4	2.3	0.18	0.20	0.40	0.39
0.41	0.86	1.24	28.8	5	13.0	10.9	5.9	4.0	0.18	0.24	0.44	0.47
0.56	1.09	1.13	21.0	4.6	15.8	12.05	6.95	6.8	0.19	0.22	0.44	0.45
0.46		0.62	17.4	5	8.1	5.75		2.7	0.13	0.17	0.38	0.40
0.51	1.02	1.21	24.0	4.4	15.4	12.15	6.8	5.4	0.195	0.24	0.44	0.47
0.27	0.60	1.26	38.5	7.0	8.0	7.16	4.25	2.2	0.16	0.31	0.48	0.50
0.30	0.68	0.93	29.2	7.8	5.5	5.1	2.9	1.9	0.19	0.26	0.42	0.41
0.24	0.54	1.11	36.4	8	8.2	7.35	4.31	2.0	0.11	0.31	0.46	0.49
0.44	0.93	1.33	28.7	5.5	12.4	10.35	5.79	4.0	0.19	0.25	0.45	0.48
0.40	0.62	0.63	19.2	6.8	6.8	5.41	2.54	2.7	0.15	0.18	0.41	0.41
0.42	0.87	1.17	26.8	5	13.0	10.61	5.88	4.2				
0.55	1.10	1.25	23.0	4.5	16.0	12.4	7.05	6.0	0.18	0.23	0.45	0.48
0.46		0.59	15.5	5.2	7.5	6.05		3.3	0.11	0.16	0.42	0.42
0.53	1.05	1.14	22.0	4.6	16.2	12.6	7.1	6.4	0.20	0.22	0.44	0.46
0.26	0.60	1.40	43.4	7.0	8.2	7.42	4.22	1.7	0.17	0.34	0.46	0.49
0.29	0.67	0.84	28.2	8.0	5.7	5.00	2.92	1.8	0.17	0.26	0.42	0.40
0.25	0.55	1.21	39.4	7.0	8.3	8.80	4.44	2.0	0.12	0.32	0.45	0.50
0.45	0.94	1.33	28.8	4.0	13.2	10.20	5.73	4.0	0.19	0.25	0.46	0.48
0.39	0.61	0.65	18.2	8.0	6.8	6.21	2.52	3.1	0.12	0.19	0.42	0.44
0.44	0.90	1.18	26.8	4.6	14.0	10.50	5.70	4.4	0.18	0.23	0.44	0.47
0.52	10.5	1.25	24.2	5.0	15.5	12.85	7.00	5.6	0.20	0.24	0.44	0.47
0.48		0.57	13.4	5.6	7.4	5.22		3.6	0.10	0.16	0.42	0.44
0.54	10.55	1.08	20.9	4.0	16.8	12.72	7.03	5.6	0.185	0.21	0.44	0.45
0.46	0.96	1.46	31.8	5.2	10.6	9.10	5.45	3.3	0.22	0.26	0.44	0.49

## All-Movable Control Surfaces (Whicker and Fehlner, 1958)

groundboard with gap = 0.005c

$C_L$ @ 10°	$C_L$ @ 20°	$C_{L_{max}}$	Stall angle, deg	$\alpha$ for ( $L/D$ ) <sub>max</sub> deg	$L/D_{max}$	$L/D$ @ $\alpha = 10^\circ$	$L/D$ @ $\alpha = 20^\circ$	$L/D$ @ stall angle	$(CP)'_z$ @ $\alpha =$		$(CP)'_z$ @ $\alpha =$	
									10°	Stall Pt.	10°	Stall Pt.
0.435	0.93	1.32	28.3	5.5	12.3	10.35	5.81	4	0.195	0.25	0.425	0.48
0.39	0.63	0.63	20.0	6.8	6.8	5.42	2.58	2.5	0.15	0.19	0.41	0.41
0.392	0.85	1.18	27.8	6.4	12	10.9	5.99	4.4	0.15	0.21	0.45	0.48
0.395	0.61	0.61	23.3	8	7.3	6.37	2.6	2.5	0.16	0.19	0.41	0.40
0.375	0.842	1.24	29.7	6.6	12.2	10.7	5.93	4.0	0.12	0.22	0.45	0.48
0.4	0.635	0.66	18.0	8	9.7	8.9	2.87	3.5	0.14	0.15	0.43	0.41
0.42	0.885	1.13	24.5	7	10.2	9.55	5.82	4.8	0.13	0.20	0.45	0.48
0.44	0.865	0.89	21.5	10	6.7	6.66	3.23	2.7	0.21	0.26	0.41	0.41
0.51	1.65	1.45	26.9	6	10.9	8.8	5.60	4.1	0.20	0.24	0.46	0.49
0.505	0.886	0.89	20.0	8	4.8	4.43	2.59	2.6	0.13	0.29	0.42	0.41

Table 15—Effect of Taper Ratio and Tip Shape on the  
(all control surfaces tested against

Item No.	Profile		$\bar{c}$ , ft	$\alpha$	$\Lambda$ , deg	$t/c$	$\lambda$	Section Shape	Tip Shape	$Rn \times 10^{-4}$ of test	Direction	Ref. Fig. No.
1		→ →	3.0	2	11	0.15	0.80	NACA 0015	Square Faired	3.0 3.0	Ahead Ahead	7(a-d) 22(a-f) *
2		→ →	3.0	2	11	0.15	0.60	NACA 0015	Square Faired	3.0 3.0	Ahead Ahead	7(a-d) 22(a-d) *
3		→ → ← ←	2.0	2	11	0.15	0.45	NACA 0015	Square Square Faired	2.72 3.00 2.72	Ahead Astern Ahead	60 94 85 † † †
4		→ →	3.0	2	11	0.15	0.20	NACA 0015	Square Faired	3.0 3.0	Ahead Ahead	7(a-d) 29(a-d) *

(Continued from page 299)

significant than the effect of aspect ratio on maximum lift coefficient. Since the magnitude of the roughness on a ship's rudder is not known with precision, and since test data at full-scale Reynolds number are not usually available, the precise effect of aspect ratio on maximum lift is not of practical importance.

**14.5 Free-Stream Characteristics of All-Movable Low Aspect-Ratio Control Surfaces.** The decade 1950–1960 saw considerable wind tunnel, free-stream testing of all-movable, low aspect-ratio control surfaces suitable for ship application. As a result of this effort, reliance on the Joessel formulas (Equations 44 and 45 of Van Lammeren et al, (1948)), which, in spite of their known inadequacy, had been extensively used in practical design work since their publication in 1892, has become unnecessary.

The most important of the works of the decade is reported by Whicker and Fehlner (1958). As will be seen in Tables 12 and 13, it includes a large variety of control-surface profile shapes (projections on the plane of the chord and the span) as well as section shapes.

Results include almost all of the hydrodynamic data necessary for rudder design, namely, lift coefficient  $C_L$ , drag coefficient  $C_D$ , moment coefficient about the quarter-chord point ( $C_m$ )  $c/4$ , distance of center of pressure from the leading edge  $CP_c$  and distance of the center of pressure from the root section  $CP_r$  for rudders operating in both the ahead and astern directions. The maximum test Reynolds numbers vary from about two million to three million. Samples of the data available showing results in both the ahead and astern condition are shown in Figs. 132 and 133.

One of the effects of geometric properties thoroughly studied by Whicker and Fehlner (1958) is the effect of tip shape. All profiles were tested with tips squared off or faired with circular arcs, Fig. 130. Fig. 125 shows that the sections with squared-off tips achieve a substantially larger maximum lift than the sections with faired tips. This result is consistent with an increase in the stall angle with squared-off tips. In most cases, however, the faired tips reduced the drag by a small amount at all angles of attack, as shown in Tables 13 and 15 from Whicker and Fehlner (1958) and Windsor (1962).

It has been shown theoretically that there is a re-

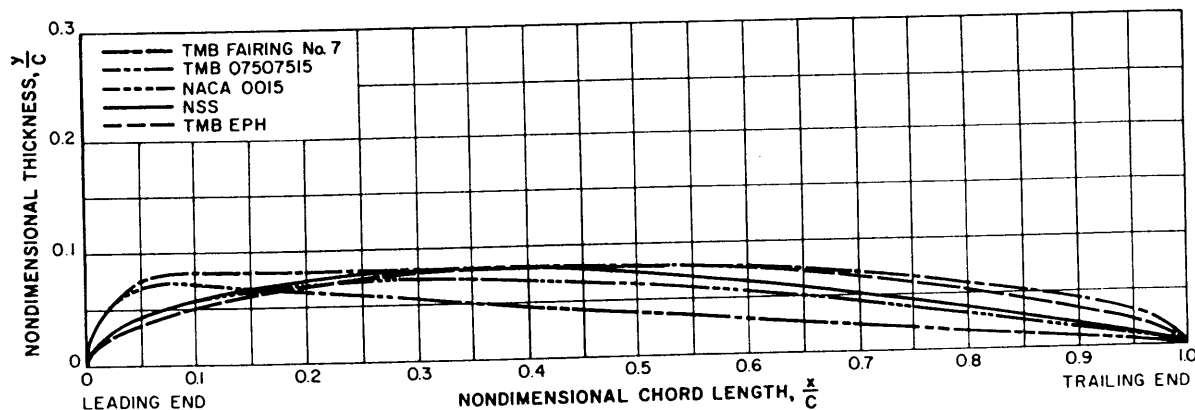


Fig. 135 Section shapes of control surfaces (Whicker and Fehlner, 1958)

Free Stream Characteristics of All-Movable Control Surfaces (Windsor, 1962)  
groundboard with gap = 0.005c)

$\left(\frac{\partial C_L}{\partial \alpha}\right)_{\alpha=0}$ per degree	$C_L$ @ 10°	$C_L$ @ 20°	$C_{L_{max}}$	Stall Angle, deg	$(L/D)_{max}$	$L/D$ @ $\alpha =$ 10°	$L/D$ @ $\alpha =$ 20°	$L/D$ @ Stall Angle	$(CP')$ $\alpha =$ 10°	$(CP')$ $\alpha =$ Stall	$(CP')$ $\alpha =$ 10°	$(CP')$ $\alpha =$ Stall	$\alpha$ for $(L/D)_{max}$ deg
0.046	0.47	1.0	1.53	31.6	11.1	9.05	5.41	3.5	0.215	0.26	0.45	0.52	6
0.046	0.47	0.97	1.30	28.4	11.0	9.4	5.61	3.61	0.19	0.235	0.455	0.51	4
0.046	0.46	0.99	1.45	30.2	10.81	9.2	5.6	3.7	0.206	0.26	0.445	0.51	6
0.046	0.45	0.93	1.26	27.7	10.51	9.39	5.07	4.0	0.19	0.255	0.438	0.50	6
0.042	0.45	0.95	1.33	28.8	13.2	10.2	5.73	4.0	0.19	0.25	0.46	0.48	4
0.026	0.39	0.61	0.65	18.2	6.8	6.21	2.52	3.1	0.12	0.19	0.42	0.44	8
0.043	0.44	0.90	1.18	26.8	14.0	10.5	5.7	4.4	0.18	0.23	0.44	0.47	4.6
0.040	0.42	0.89	1.24	27.6	11.9	9.55	5.85	4.2	0.175	0.23	0.415	0.475	6
0.040	0.42	0.84	1.25	27.5		13.6	6	4.3	0.155	0.23	0.42	0.474	

\* Windsor, 1962.

† Whicker and Fehlner, 1958.

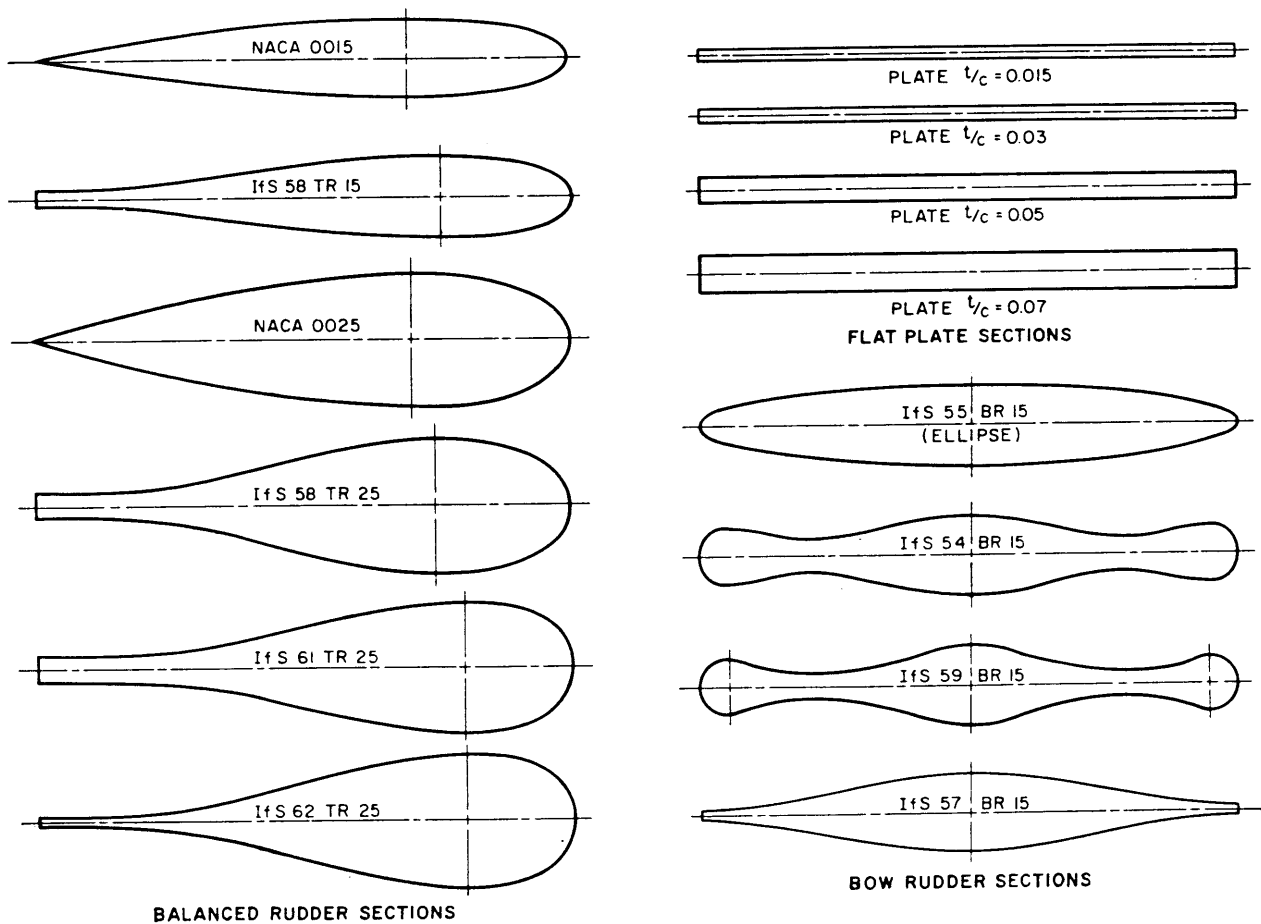


Fig. 136 Section shapes of Table 16 (Thieme, 1965)

Table 16—Effect of Section Shape and Thickness-Chord Ratio on the Free-Stream Characteristics of Square (Aspect Ratio = 1, Square Tips), All-Movable Control Surfaces Without Groundboard (Thieme, 1965)

Item No.	Section Shape	$t/c$	Direction	$Rn \times 10^{-4}$	Ref. Fig. No.	$\left(\frac{\partial C_L}{\partial \alpha}\right)_{\alpha=0}$ per degree	$C_L$ @ $10^\circ$	$C_L$ @ $20^\circ$	$C_{L_{max}}$	Stall angle	Approx. $\alpha$ for $(L/D)_{max}$	$L/D_{max}$	$L/D$ @ $10^\circ$	$L/D$ @ $20^\circ$	$L/D$ @ stall	— (CP') — @ $10^\circ$	@ stall
1	Flat plate	?	Either	?	6 <sup>1</sup>	0.028	0.38	0.89	...	38	...	...	...	...	...	0.272	0.411
2	Flat plate	0.015	Either	0.71	36	0.028	0.35	0.75	1.20	39	5	4.4	4.4	2.8	1.3	0.264	0.400
3	Flat plate	0.030	Either	0.71	37	0.0305	0.34	0.72	1.14	40	5	4.0	3.8	2.5	1.3	0.275	0.414
4	Flat plate	0.050	Either	0.67	38	0.029	0.34	0.70	1.12	40	10	2.9	2.8	2.2	1.2	0.311	0.432
5	Flat plate	0.070	Either	0.71	39	0.0325	0.32	0.65	1.00	38.5	9	2.6	2.5	2.1	1.2	0.303	0.429
6	TMB 075-075-15	0.15	Ahead	0.69	18	0.0275	0.29	0.58	0.88	37.5	9	2.7	2.6	2.2	1.3	0.347	0.413
			Astern	0.56	19	0.0364	0.34	0.70	1.12	37	8	2.9	2.8	2.2	1.3		
7	NACA 0015	0.15	Ahead	0.79	20	0.028	0.29	0.62	1.06	33.8	9	7.2	7.2	4.4	2.3	0.178	0.353
			Astern	0.56	21	0.048	0.38	0.64	1.06	40	8	3.9	3.8	2.5	1.2		
8	NACA 0025	0.25	Ahead	0.78	22	0.0275	0.27	0.59	1.34	46	10	5.4	5.4	4.2	1.7	0.196	0.352
			Astern	0.56	23	0.0534	0.41	0.67	0.93	38.3	8	3.0	2.9	2.3	1.2		
9	IFS 58 TR 15	0.15	Ahead	0.78	24	0.030	0.32	0.67	1.18	33.5	10	6.4	6.4	3.9	2.4	0.247	0.330
			Astern	0.56	25	0.0264	0.27	0.65	1.11	40	9	3.0	3.0	2.2	1.3		
10	IFS 58 TR 25	0.25	Ahead	0.78	26	0.031	0.31	0.66	1.45	48	8	4.0	3.9	3.5	1.5	0.294	0.375
			Astern	0.56	27	0.0302	0.29	0.67	0.98	40	10	2.1	2.1	1.9	1.1		
11	IFS 61 TR 25	0.25	Ahead	0.79	28	0.030	0.32	0.69	1.34	41	9	4.0	4.0	3.6	1.8	0.256	0.353
			Astern	0.56	29	0.0284	0.30	0.66	1.00	41	10	2.0	2.0	1.7	1.1		
12	IFS 62 TR 25	0.25	Ahead	0.78	30	0.032	0.33	0.71	1.48	46	10	4.8	4.7	3.6	1.5	0.265	0.359
			Astern	0.56	31	0.0294	0.42	0.70	1.05	38	9	2.5	2.5	2.1	1.2		
13	IFS 55 BR 15	0.15	Either	0.71	32	0.040	0.34	0.60	0.72	30	10	5.7	5.7	3.3	1.6	0.300	0.366
14	IFS 54 BR 15	0.15	Either	0.78	33	0.030	0.34	0.63	0.99	37.2	9	2.9	2.8	2.2	1.3	0.337	0.422
15	IFS 59 BR 15	0.15	Either	0.78	34	0.033	0.34	0.65	1.03	38	10	2.5	2.4	2.2	1.2	0.370	0.425
16	IFS 57 BR 15	0.15	Either	0.72	35	0.0295	0.29	0.67	1.04	40	5	6.6	4.1	2.6	1.2	0.364	0.407

<sup>1</sup> Original Edition of Principles of Naval Architecture, Vol. II, Chapter 4, Figures 6, 7, and 8 (1939)

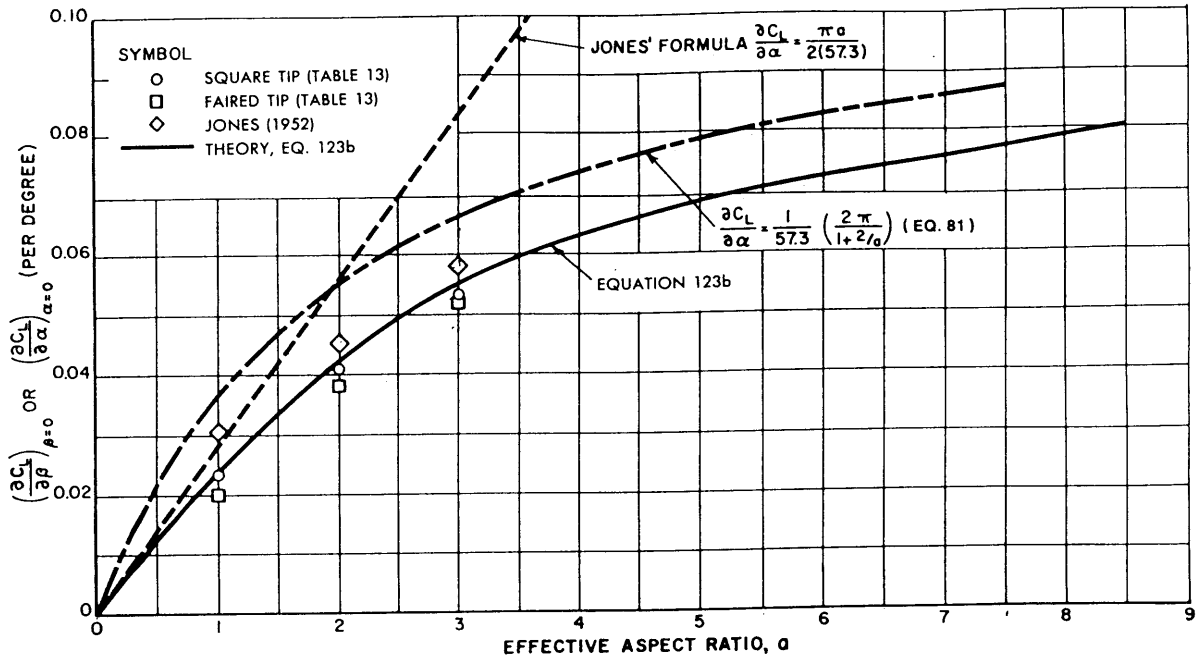


Fig. 137 Effect of aspect ratio on lift-curve slope

relationship, shown in Fig. 134, between sweep angle and taper ratio for which the spanwise center-of-pressure location is independent of aspect ratio. Profiles conforming to this relationship should also have minimum drag, increased cavitation resistance, and improved lift-curve slopes. However, experimental data shown in Tables 13 and 15 for profiles not conforming to this relationship do not in all cases confirm these theoretical advantages. In general, Table 13 shows that variations of sweep angle from +22.5 to -8 deg for a constant taper ratio of 0.45 do not significantly affect the free-stream characteristics. However, Table 15 shows that as the taper ratio is increased from 0.2 to 0.8 for a constant sweep angle of +11 deg, the maximum lift coefficient and the stall angle are increased.

Tables 14 and 16 summarize the effect of section shape on free-stream characteristics from Whicker and Fehlner (1958) and Thieme (1965). The section shapes tested are shown in Figs. 135 and 136. These data indicate that a wide selection of section shapes have reasonably good characteristics, as shown by large values of  $\partial C_L/\partial \alpha$ ,  $C_{L_{max}}$ , and low center-of-pressure travel. In the United States the NACA symmetrical sections have been widely used.

Quite apart from section shape, the effect of thickness-to-chord ratio on control-surface characteristics is also of importance. This effect is shown in Table 16 (after Thieme, 1965, and *Principles of Naval Architecture*, 1939, Figs. 6, 7, and 8) and Table 17 (after Windsor, 1962, and *Principles of Naval Architecture*, 1939, Figs. 6, 7, and 8) for rectangular-shaped control surfaces tested without groundboards. It is seen that

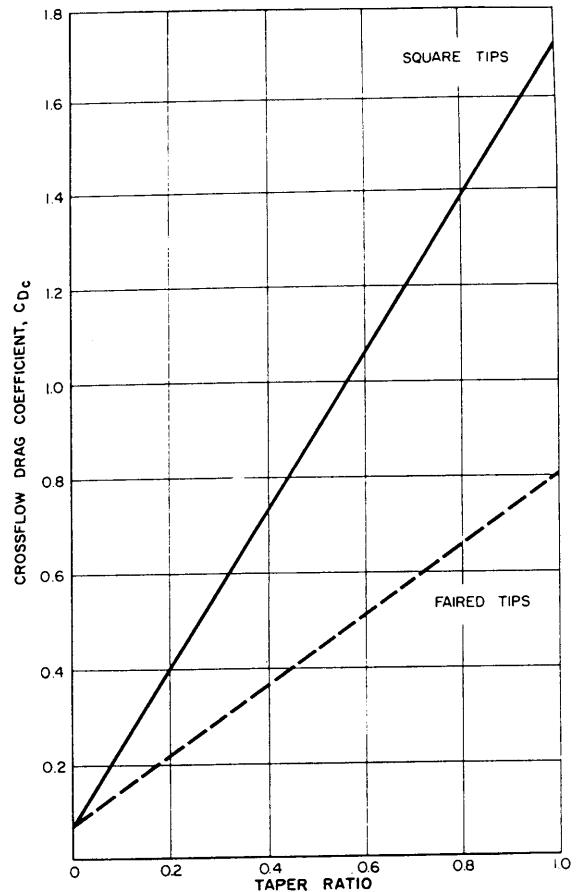
Fig. 138 Effect of tip shape and taper ratio,  $\lambda$ , on crossflow drag coefficient (Whicker and Fehlner, 1958)

Table 17—Effect of Thickness-Chord Ratio and Aspect Ratio on the Free-Stream Characteristics of Rectangular

Item No.	Profile*	$\alpha$	$\Lambda$ , deg	$\lambda$	$t/c$	Section Shape	Tip Shape	Direction	$Rn \times 10^{-4}$ of test	Ref.	Fig. No.
1	$\rightleftharpoons$	5.0	0	1.0	0	Plate	Square	Either	?	PNA	6
2	$\rightleftharpoons$	1.0	0	1.0	0	Plate	Square	Either	?	PNA	6
3	$\rightleftharpoons$	0.2	0	1.0	0	Plate	?	Either	?	PNA	6
4	$\rightarrow$	6.0	0	1.0	0.06	NACA 0006	?	Ahead	?	PNA	7, 8
5	$\rightarrow$	6.0	0	1.0	0.12	NACA 0012	?	Ahead	?	PNA	7, 8
6	$\rightarrow$	6.0	0	1.0	0.18	NACA 0018	?	Ahead	?	PNA	7, 8
7	$\rightarrow$	6.0	0	1.0	0.25	NACA 0025	?	Ahead	?	PNA	7, 8
8	$\rightarrow$	6.0	0	1.0	0.12	NACA 0012	Square	Ahead	0.6	Windsor	33-33(d)
9	$\rightarrow$	6.0	0	1.0	0.15	NACA 0015	Square	Ahead	0.6	Windsor	8(a-d)
10	$\rightarrow$	3.0	0	1.0	0.12	NACA 0012	Square	Ahead	0.6	Windsor	33-33(d)
11	$\rightarrow$	3.0	0	1.0	0.15	NACA 0015	Square	Ahead	0.6	Windsor	8(a-d)
12	$\rightarrow$	1.34	0	1.0	0.12	NACA 0012	Faired	Ahead	1.58	Windsor	37-37(d)
13	$\rightarrow$	2.61	0	1.0	0.12	NACA 0012	Faired	Ahead	1.1	Windsor	37-37(d)
14	$\rightarrow$	5.16	0	1.0	0.12	NACA 0012	Faired	Ahead	0.99	Windsor	37-37(d)
15	$\rightarrow$	1.13	0	1.0	0.10	64A010	Faired	Ahead	4.4	Windsor	50-50(d)
16	$\rightarrow$	2.13	0	1.0	0.10	64A010	Faired	Ahead	3.1	Windsor	50-50(d)
17	$\rightarrow$	4.13	0	1.0	0.10	64A010	Faired	Ahead	2.2	Windsor	50-50(d)

flat-plate sections have the poorest free-stream characteristics, whereas sections with thickness-to-chord ratios of about 0.12 to 0.18 have the best. Table 15 also shows this result.

In addition to containing extensive experimental data, [Whicker and Fehlner (1958)] show that reasonable correlation exists between existing experimental data and the following theoretical and semi-empirical equations for estimating free-stream, low-aspect-ratio, all-movable-control-surface characteristics:

$$\text{Lift coefficient: } C_L = \left( \frac{\partial C_L}{\partial \alpha} \right) \alpha + \frac{C_{D_c}}{a} \left( \frac{\alpha}{57.3} \right)^2 \quad (123a)$$

$$\left( \frac{\partial C_L}{\partial \alpha} \right)_{\alpha=0} = \frac{(0.9)(2\pi)a}{57.3 \left[ \left( \cos \Lambda \sqrt{\frac{a^2}{\cos^4 \Lambda} + 4} \right) + 1.8 \right]} \quad (\text{per degree}) \quad (123b)$$

where

$$\left( \frac{\partial C_L}{\partial \alpha} \right)_{\alpha=0} = \text{slope of lift coefficient with respect to angle of attack } \alpha \text{ at } \alpha = 0$$

$\alpha$  = effective aspect ratio

$\Lambda$  = sweep angle of the quarter-chord line

$\alpha$  = angle of attack in degrees

$C_{D_c}$  = crossflow drag coefficient dependent on both tip shape and taper ratio (see Fig. 138)

Drag coefficient:<sup>4</sup>

$$C_D = C_{d_0} + \frac{C_L^2}{\pi a e} \quad (124)$$

where

$C_{d_0}$  = minimum section drag coefficient;  $C_{d_0} = 0.0065$  for NACA 0015 section

$e$  = so-called "Oswald" efficiency factor;  $e = 0.90$  from Whicker and Fuhlner (1958)

Moment coefficient about the quarter chord:

$$C_{m_{z/4}} = \left[ 0.25 - \left( \frac{\partial C_m}{\partial C_L} \right)_{C_L=0} \right] \left( \frac{\partial C_L}{\partial \alpha} \right)_{\alpha=0}$$

<sup>4</sup> A comparison between theory as given by Equation (123b) and experimental data given in Table 13 is shown in Fig. 137 from Whicker and Fehlner (1958) and Jones (1952).

## All-Movable Control Surfaces Without Groundboard (Windsor, 1962 and PNA, 1939)

$\left(\frac{\partial C_L}{\partial \alpha}\right)_{\alpha=0}$ per degree	$C_L$ @ 10°	$C_L$ @ 20°	$C_{L_{max}}$	Stall Angle, deg	$\alpha$ for $L/D_{max}$ , deg	$(L/D)_{max}$	$L/D$ @ $\alpha = 10^\circ$	$L/D$ @ $\alpha = 20^\circ$	$L/D$ @ Stall Angle	$(CP)_c$ $\alpha = 10^\circ$	$(CP)_c$ $\alpha = \text{Stall}$
0.08	0.76	0.87	...	10	...	...	...	...	...	0.313	0.411
0.028	0.38	0.89	...	38.3	...	...	...	...	...	0.272	0.411
0.011	0.16	0.50	...	52.5	...	...	...	...	...	0.272	0.38
0.083	0.72	...	0.88	16.7	3.26	27.8	10.3	...	3.26	0.26	0.358
0.076	0.76	1.43	1.52	22.5	8.96	25.3	18	10.15	8.96	0.241	0.29
0.075	0.74	1.40	1.48	22.5	4	25	17.7	10.2	8.8	0.235	0.23
0.067	0.68	1.20	1.20	20.59	8	16.7	16.2	8.06	8.3	0.226	0.247
0.068	0.70	...	0.955	14.2	4	18	15.5	...	12.7	0.25	0.25
0.056	0.61	...	0.90	16	8	8.74	8.75	...	7.6	0.226	0.24
0.069	0.44	...	0.80	16	8	12	10.85	...	8.9	0.23	0.36
0.033	0.45	0.83	0.87	20.2	10	5.24	5.24	4.05	4.2	0.25	0.25
0.025	0.30	0.71	0.82	21.4	10	8.56	8.58	5.68	6.56	0.143	0.245
0.05	0.50	...	0.70	14	10	12.20	12.20	...	9.98	0.17	...
0.07	0.71	...	0.83	12	6	16.70	7.40	...	13.80	0.235	...
0.028	0.28	...	0.53	18	8	8.80	8.00	...	4.40	0.185	0.27
0.04	0.51	...	0.64	16	6	14.30	10.20	...	2.69	0.24	0.365
0.067	0.65	...	0.72	14	6	16.20	10.81	...	1.65	0.235	0.36

\* All profiles are rectangles.

$$-\frac{1}{2} \frac{C_{Dc}}{a} \left( \frac{\alpha}{57.3} \right)^2 \quad (125)$$

where

$$\left( \frac{\partial C_m}{\partial C_L} \right)_{C_L=0} = \text{slope of the moment coefficient, } C_{m\bar{c}/4} \text{ with respect to lift coefficient } C_L \text{ at } C_L = 0$$

$$= \frac{1}{2} - \frac{1.11 [(a^2 + 4)^{1/2}] + 2}{4(a + 2)}$$

$$\left( \frac{\partial C_L}{\partial \alpha} \right)_{\alpha=0} \text{ is given by Equation (123b)}$$

Center-of-pressure chordwise distance from the leading edge:

$$(CP)_c = \left( 0.25 - \frac{(C_m)_{c/4}}{C_N} \right) \bar{c} \quad (126)$$

where

$C_N$  = normal force coefficient =  $C_L \cos \alpha + C_D \sin \alpha$

Center-of-pressure spanwise distance from the root section:

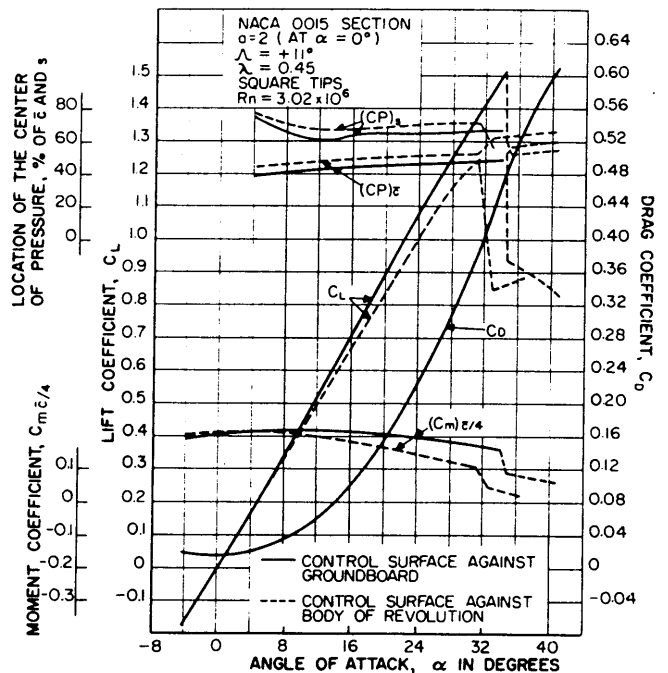


Fig. 139 Effect of type of bounding surface on characteristics of an all-movable control surface (Harper and Sinites, 1959)

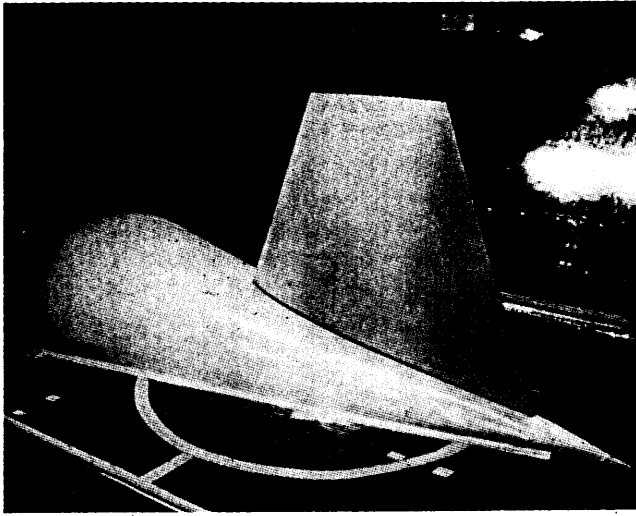


Fig. 140 Control-surface model mounted against simulated body of revolution (Harper and Sinites 1959)

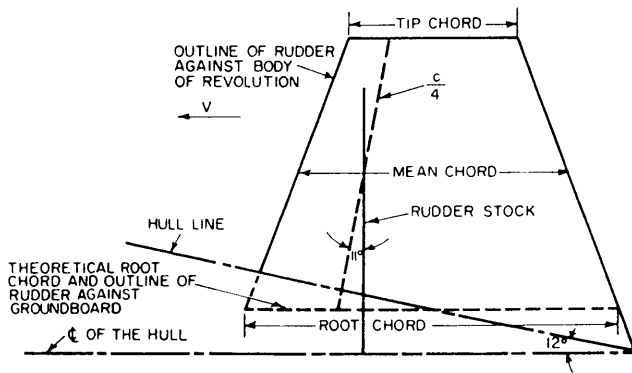


Fig. 141 Outline of rudders used

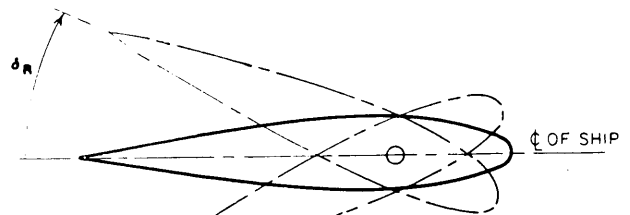
$$(CP)_s = \left(\frac{4}{3\pi}\right) \bar{b} \quad (127)$$

for profiles with taper ratios and sweep angles conforming to the relationship shown in Fig. 134 for an elliptical spanwise loading distribution.

**14.6 Influence of Hull Shape on Effective Aspect Ratio of All-Movable Control Surfaces.** Generally, the idealization achieved when a rudder is tested against a groundboard is not realized when the rudder is located adjacent to a ship's hull. While it may be possible to achieve a very small gap between the root section of the rudder and the adjacent ship hull at zero rudder angle, the gap will increase in size as the rudder is laid over because the ship's hull immediately over the rudder is rarely a plane surface normal to the rudder stock. Hence, while the effective aspect ratio of a rudder may be twice its geometric aspect ratio at zero deflection angle, this ratio will decrease as the rudder is laid over.

Fig. 139 taken from Harper and Sinites (1959) shows wind tunnel test results of a control surface

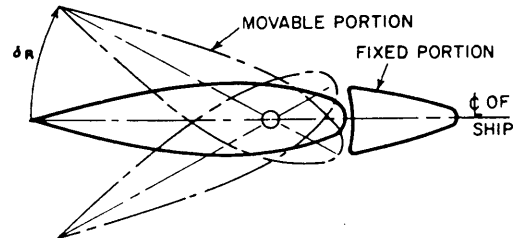
with a geometric aspect ratio of 1.0 tested against both a groundboard in the conventional manner and against a conical half-body of revolution. A photograph of the test setup is shown in Fig. 140, and the necessary modifications to the rudder profile for the two tests are shown in Fig. 141. The conical-shaped body of revolution has a body diameter at the quarter-chord of the rudder of 0.3 times the mean geometric chord of the rudder and a half-angle of closure of 12 deg. Fig. 139 shows that the rudder against the body of revolution has the same lift-curve slope at the origin as



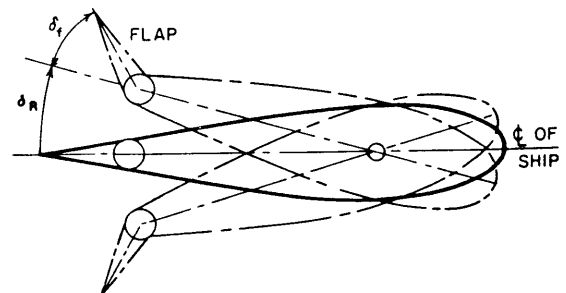
LIFT DEVELOPED BY ANGLE OF ATTACK  
(a) ALL-MOVABLE RUDDER



LIFT DEVELOPED BY FIXED CAMBER  
(b) AIRPLANE WING



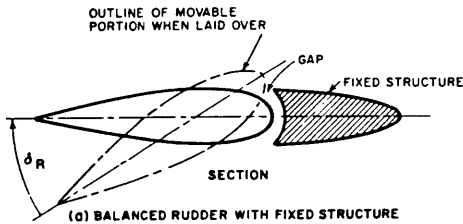
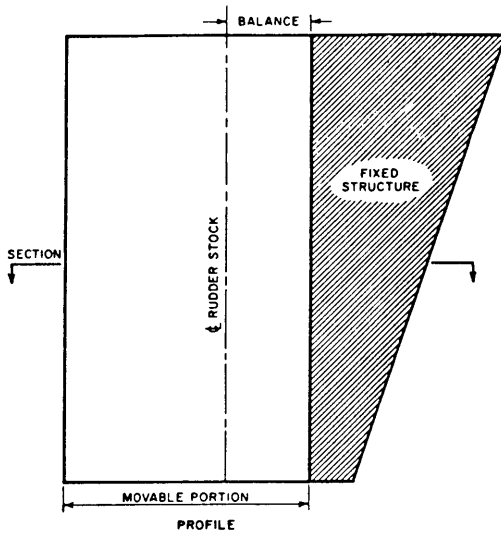
LIFT DEVELOPED BY VARIABLE CAMBER  
(c) RUDDER BEHIND FIXED STRUCTURE



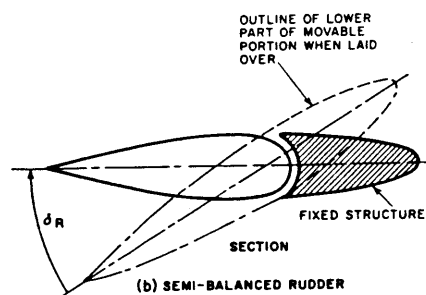
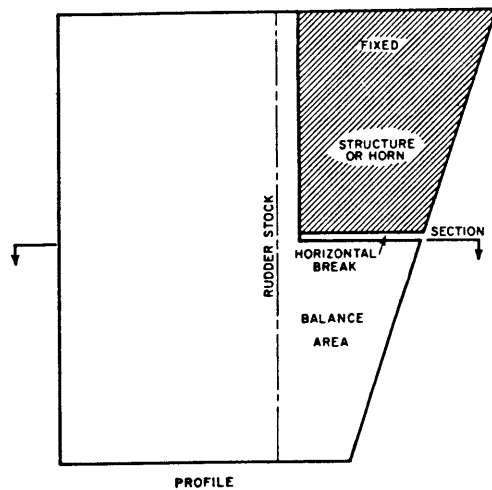
LIFT DEVELOPED BY ANGLE OF ATTACK + VARIABLE CAMBER  
(d) ALL-MOVABLE RUDDER WITH TAIL FLAP

Fig. 142 Four variations of lifting surfaces





(a) BALANCED RUDDER WITH FIXED STRUCTURE



(b) SEMI-BALANCED RUDDER

Fig. 143 Typical balanced and semi-balanced rudders with fixed structure

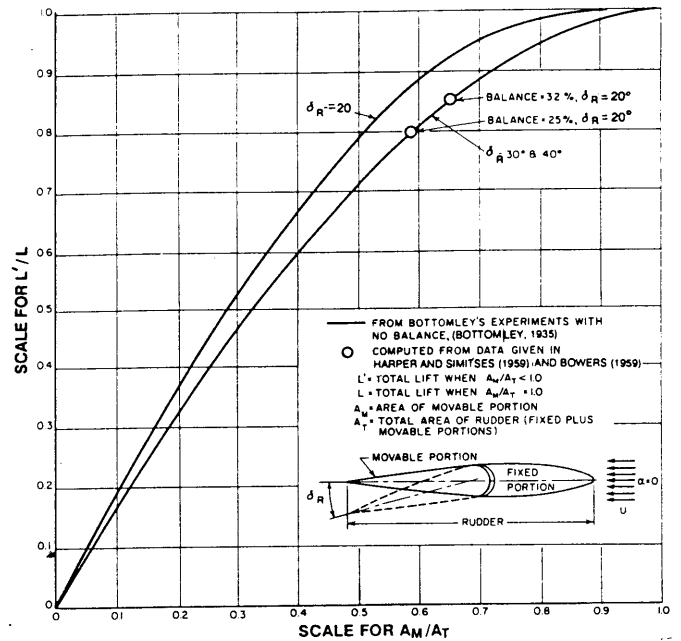


Fig. 144

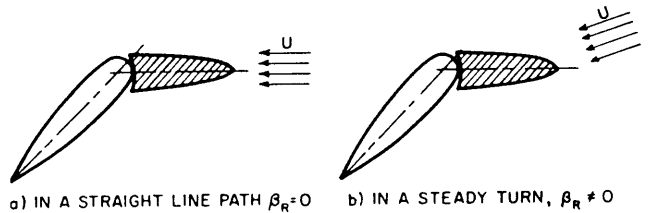


Fig. 145 Inflow velocity to a rudder with fixed structure

the rudder against the groundboard. Thus the effective aspect ratio of the rudder at zero deflection angle with both boundary conditions is two. However, at angles of attack greater than about 6 deg, the lift curves for the two boundary conditions begin to diverge, and the maximum lift of the rudder against the body of revolution is only about 80 percent of the lift against the groundboard. Applying Equation (122b) to the data given in Fig. 139, the effective aspect ratio of the rudder against the body of revolution is essentially a linear function of rudder angle varying from two at zero rudder angle to 1.7 at 27 deg. Beyond 27 deg the effective aspect ratio drops off more rapidly to a value of about 1.5 at the stall angle of 31 deg. While this is an isolated experiment its implications are important, for it shows that even at large angles of attack a hull that is only moderately close to a rudder serves to increase its effective aspect ratio well beyond its geometric value.

**14.7 Influence of Fixed Structure and Flapped Control Surfaces.** The all-movable rudder has several important variants. If a fixed structure is placed just ahead of the rudder in a manner similar to that shown in Fig. 142(c), the forces and moments acting on the rudder

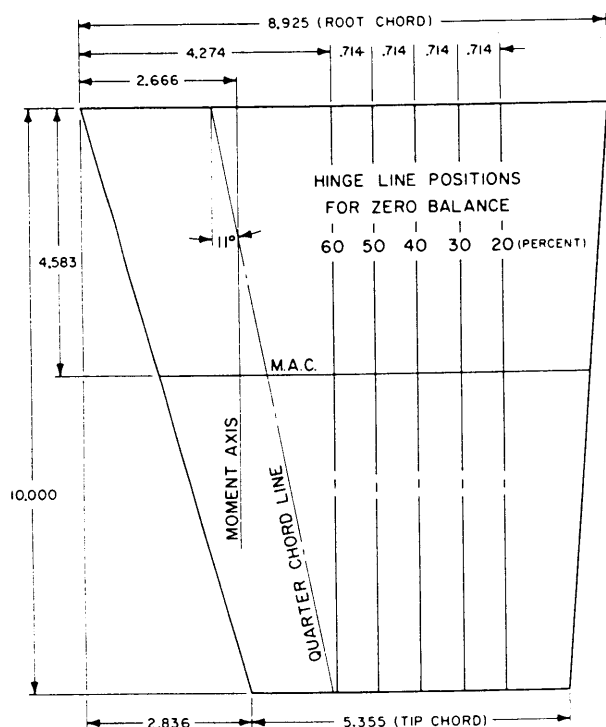
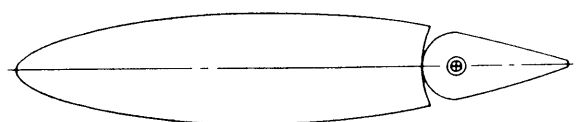
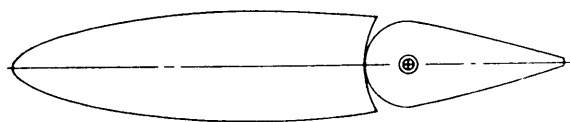


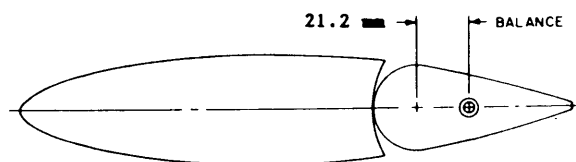
Fig. 146



NO. 1      20% FLAP      0% BALANCE



NO. 2      30% FLAP      0% BALANCE



NO. 3      30% FLAP      39.05% BALANCE

Fig. 147 Root sections of each of the models tested showing flap proportions and location of flap hinge point

as well as the forces and moments acting on the ship, due to rudder deflection, will be different from what they would be if the fixed structure were absent. A rudder consisting of both a fixed and a movable portion as shown in Fig. 142(c) will generally produce a larger control force (with the ship moving in the ahead direction) than if the fixed portion were missing. Such a rudder is sometimes called a flapped or hinged rudder (Bowers, 1959). If the fixed portion of the rudder is clearly definable as part of the rudder, as it is for example in Figs. 143(a) and 143(b), then all of the geometric properties of the rudder such as aspect ratio, thickness-to-chord ratio, taper ratio, and so on should be computed as if the fixed portion were in fact an integral part of the rudder. By analogy with the airplane wing shown in Fig. 142(b), a rudder consisting of a combination of movable and fixed portions develops its lift by means of varying its camber as well as by varying the angle of attack. This distinction is emphasized in Fig. 142.

The favorable effect of the fixed structure ahead of a rudder on lift in the ahead condition with zero inflow angle to the fixed structure was developed in a set of experiments conducted by Bottomley (1935) and shown in Fig. 144. That figure shows, for example, that at rudder angles of 30 to 40 deg, a 25-percent fixed 75-percent movable rudder combination produced more than 90 percent of the lift produced by an all-movable rudder of the same *total* area. In Bottomley's experiments, there was no gap between the leading edge of the movable portion and the trailing edge of the fixed structure for any angular deflection of the rudder. Generally in the practical case, the movable portion incorporates some balance area forward of the centerline of the stock as shown in Fig. 143, in order to reduce the torque on the rudder. With balance, some gap is inevitable between the fixed structure and the movable portion at large deflection angles. Fig. 144 shows the results of computations comparing experimental data from Bowers (1959) for a control surface abaft a fixed structure with two values of balance to similar data from Harper and Simitses (1959) for an all-movable control surface, both sets of data being corrected to a common aspect ratio. Both sets of data were taken with the control surfaces mounted against a conical half-body of revolution in a wind tunnel. For both values of balance the lift developed is about 8 percent less than if there were no balance and no resulting gap.

The favorable effect of a fixed structure ahead of a rudder shown by the Bottomley experiments should be reflected in improved course keeping where the inflow angle to the fixed structure is essentially zero, Fig. 145(a). However, the inflow angle to the fixed structure in a steady turn can have a decidedly nonzero value as shown in Fig. 145(b). This angle of attack in turns will detract from the favorable coursekeeping effect of the fixed structure shown in Fig. 144, which applies only if  $\beta_R = 0$ .

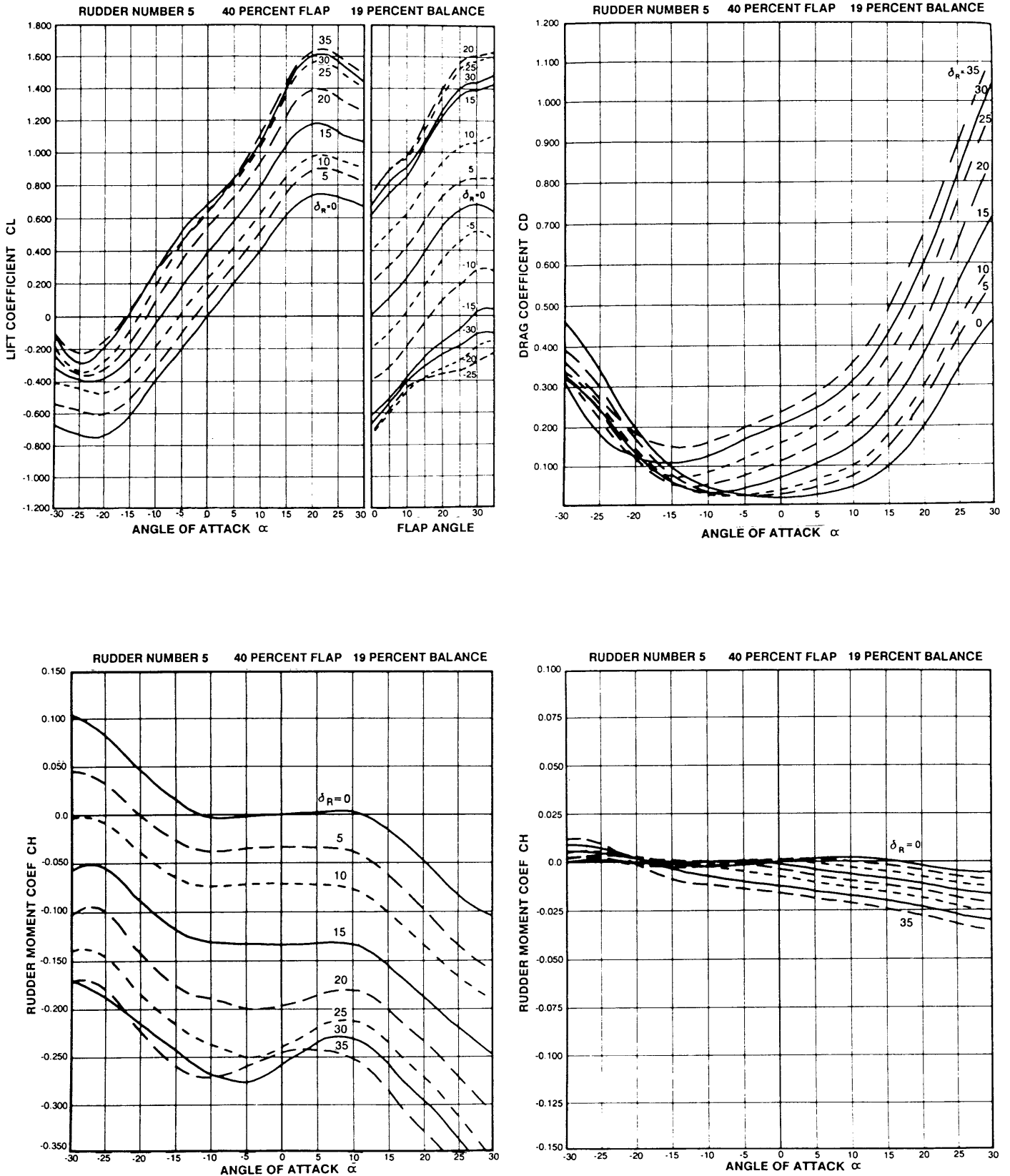


Fig. 148 Rudder series hydrodynamic data

Table 18—Principal Hydrodynamic Characteristics of Rudder Series

Rudder	% Flap	% Balance	$(C_L)_{\max}$	$(C_L)_{\max}$ ( $\alpha = 0$ )	$C_D \left\{ \begin{array}{l} \delta = 0 \\ C_L = 0.6 \end{array} \right\}$	$C_D @$ $(C_L)_{\max}$	$(C_D)_{\min}$	$\frac{(C_L)_{\max}}{(C_D)_{\min}}$	$(C_{MF})_{\max}$ (Pos. $C_L$ )	$\frac{(C_L)_{\max}}{(C_D)_{\min}}$ ( $\alpha = 0$ )
1	20	0	1.40	0.47	0.07	0.47	0.013	108	-0.017	36
2	30	0	1.24	0.60	0.08	0.39	0.016	78	-0.042	38
3	30	39	1.18	0.29	0.11	0.58	0.018	66	-0.007	16
4	40	0	1.36	0.66	0.10	0.53	0.015	91	-0.080	44
5	40	19	1.63	0.69	0.09	0.69	0.016	102	-0.037	44
6	40	38	1.29	0.51	0.11	0.70	0.017	76	-0.010	30
7	50	0	1.35	0.70	0.11	0.54	0.017	80	-0.135	41
8	50	18	1.29	0.64	0.12	0.66	0.018	72	-0.067	35
9	50	36	1.26	0.61	0.13	0.93	0.020	63	-0.025	31
11	60	18	1.20	0.86	0.17	0.67	0.016	75	-0.105	54
12	60	36	1.17	0.76	0.18	0.83	0.025	47	-0.045	30
32	0 <sup>a</sup>	0 <sup>a</sup>	0.88	0	0.07	0.19	0.013	68	(-0.120) <sup>a</sup>	..

<sup>a</sup> Rudder 32 has no flap.

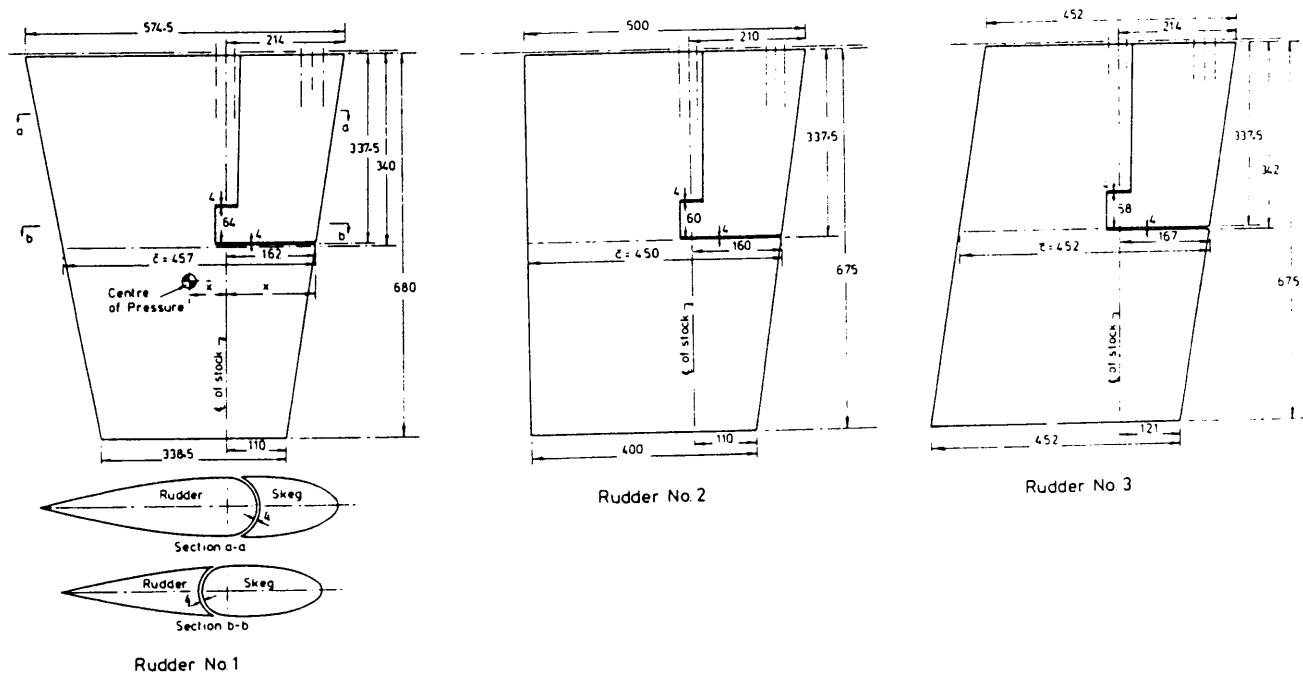


Fig. 149 Dimensions of model rudders (all dimensions in mm)

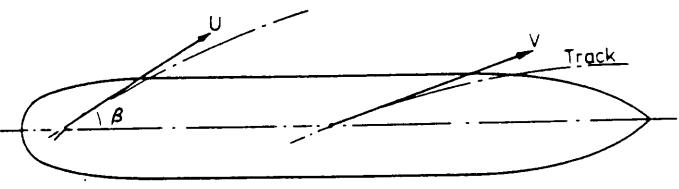


Fig. 150 Cross flow at stern of ship when in a turn

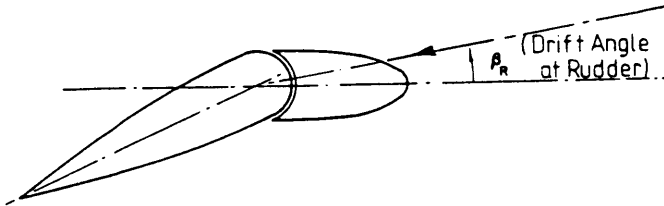


Fig. 151 Development of negative inflow angle on skag due to drift

Kerwin, et al (1972) tested a series of 12 flapped control surfaces in a water tunnel while varying the amount of flap area and balance. The outline for the rudder model tested is shown in Fig. 146.

Principal hydrodynamic characteristics of the series are given in Table 18. Fig. 147 illustrates typical properties and the achievement of 39.05-percent balance in the 30-percent flapped rudder No. 3. The experiments were run at a Reynolds number of about  $1.2 \times 10^6$  and there was no evidence that the results should not apply at much higher Reynolds numbers.

Results typical of those presented for each rudder are shown in Fig. 148 for Rudder No. 5. This rudder developed the greatest lift coefficient of those tested, nearly doubling the 0.88 maximum lift coefficient of

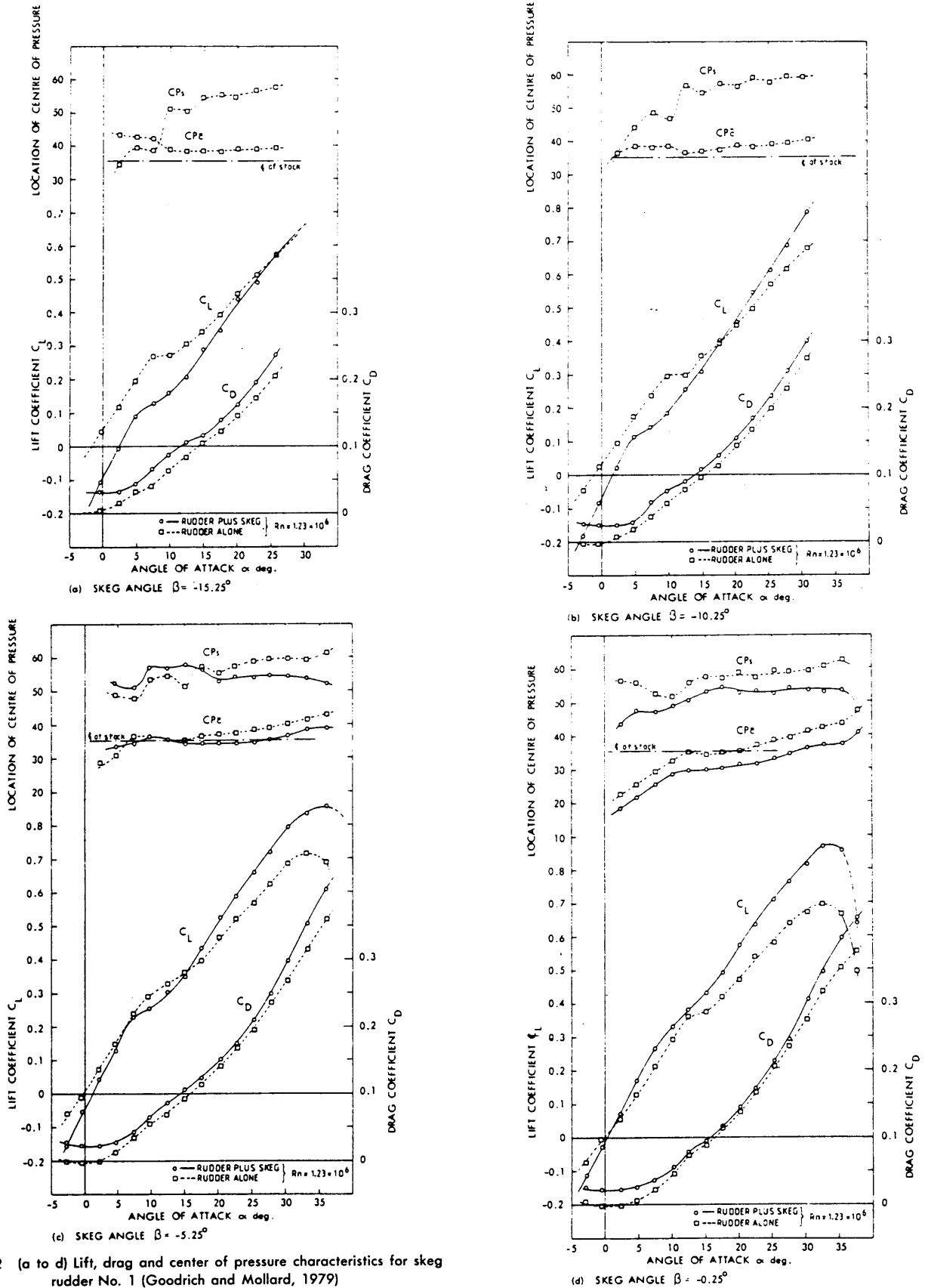


Fig. 152 (a to d) Lift, drag and center of pressure characteristics for skeg rudder No. 1 (Goodrich and Mollard, 1979)

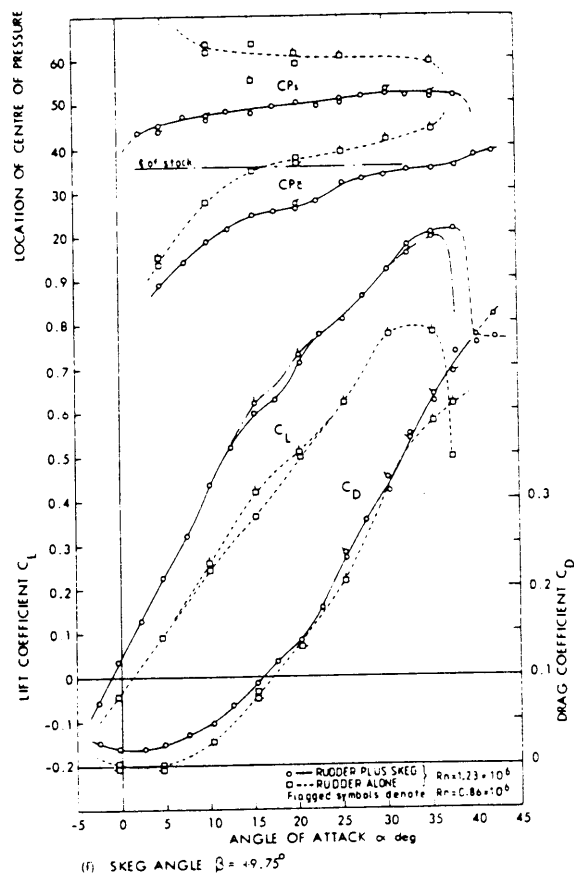
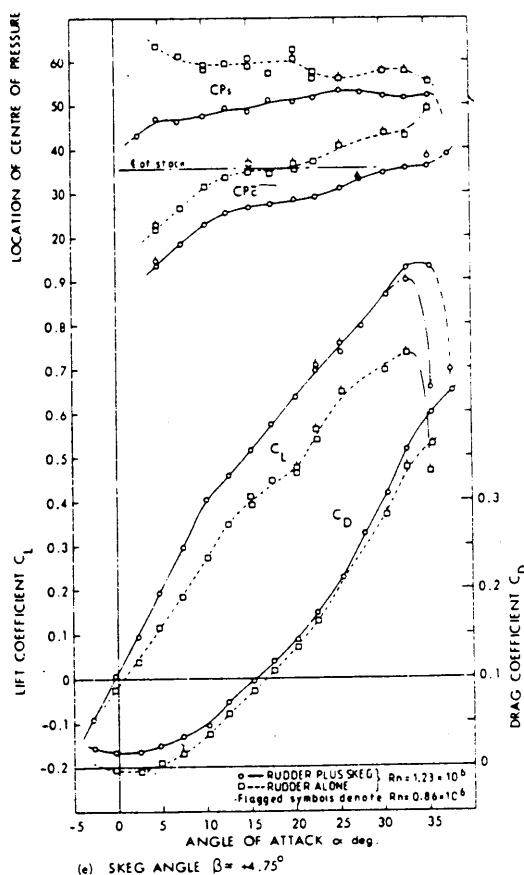


Fig. 152 (cont) (e and f)

the parent unflapped Rudder No. 32. Columns headed  $C_{L_{\max}}/C_{D_{\min}}$  and  $(C_{L_{\max}})/C_{D_{\min}} (\alpha = 0)$  in Table 18 indicate the relative drag penalty when the rudder is not in use for steering.

The doubly all-movable rudder with even a small (unbalanced) flap has much larger maximum lift coefficient than an all-movable rudder with no flap. Increasing the flap size to more than 20 percent has little influence on maximum lift. The lift increases are achieved at the expense of large increases in rudder hinge moments and somewhat increased drag. Flap hinge moments are, however, substantially less than the maximum rudder moments of the zero-flap rudder.

Comparisons at fixed values of the lift coefficient, also tabulated by Kerwin et al (1972), indicate that the doubly all-movable rudder with a 20-percent flap has less drag than a zero-flap rudder at lift coefficients greater than 0.6, and comparable drag at lower lift coefficients. The disadvantages of the all-movable rudder are its increased hinge moments, mechanical complexity, and possible maintenance difficulties.

In practice, the fixed structure, if used, may involve either a faired sternpost, a *horn* (whether full

depth as in Fig. 143(a) or partial depth as in Fig. 143(b)), or even the *deadwood* or skeg of the ship itself. In the latter case, the movable-rudder area is small indeed compared to that of the fixed structure ahead of it. From a hydrodynamic point of view the performance of such a rudder can be predicted only if the entire ship ahead of the rudder is treated as the fixed portion of the rudder. This mode of treatment would apply both to experimental testing with models and to analytical prediction of rudder performance by theory. In the analytical approach the really important parameters would be the ratio of the chord length of the movable rudder to the length of the ship, the aspect ratio of the movable part of the rudder, and the aspect ratio of the ship as a whole, that is, its draft-to-length ratio. Such a rudder would develop far more lift on the ship as a whole in the ahead condition than would an isolated rudder of identical area. In the astern condition, however, such a rudder would be only a small flap on the leading edge of the ship and as such would be almost completely ineffective in turning the ship (see articles 37.10 and 37.11 of Saunders (1957)). An important variety of rudder in common use on many

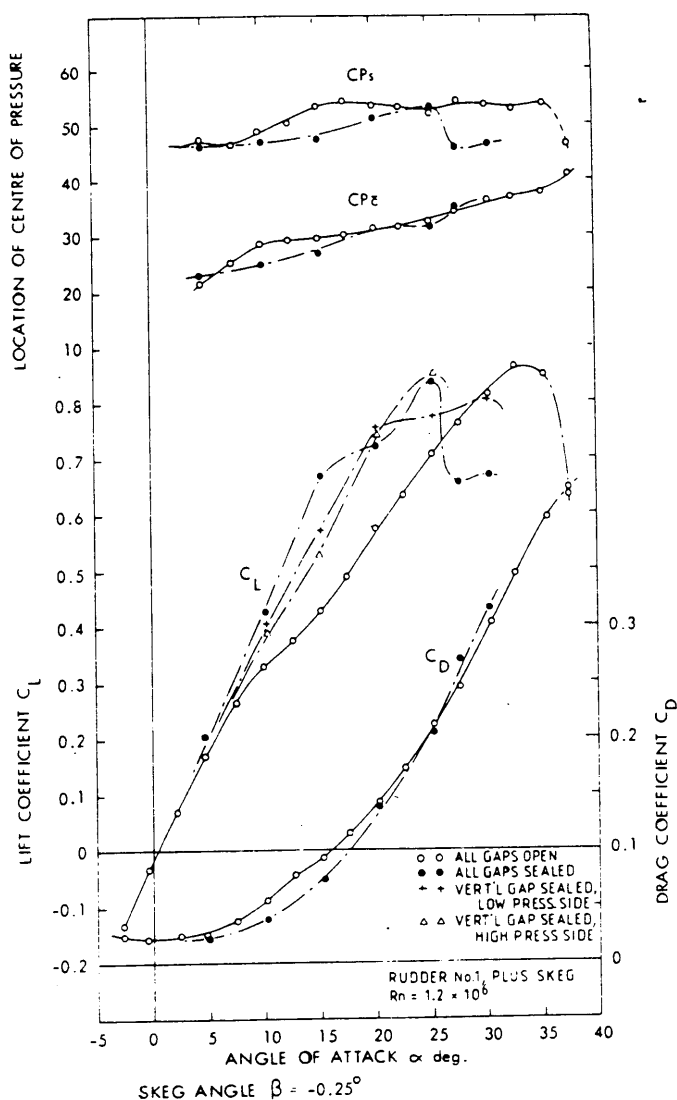


Fig. 153 Influence of sealed gaps

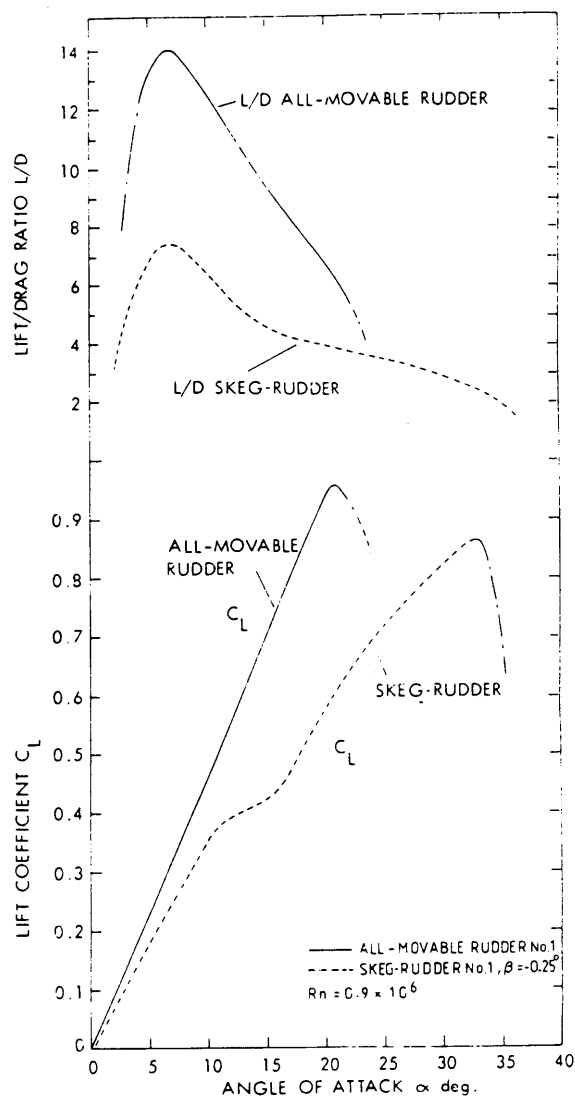


Fig. 154 Comparison between skeg rudder No. 1 and its all-movable equivalent (Goodrich and Mollard, 1979)

ships is a rudder equipped with a partial depth fixed horn, such as the semibalanced rudder in Fig. 143(b). This rudder incorporates balance area without introducing a gap when the rudder is laid over. However, this type of rudder necessarily incorporates a horizontal break between the top of the balance area and the lower side of the fixed portion, and this break has unfavorable influence on its characteristics.

Free-stream wind tunnel experiments on semibalanced skeg rudders were presented by Goodrich and Mollard (1979). Tests were performed on three rudders having differing taper ratios of 0.59, 0.80, and 1.00, each rudder with a skeg and with NACA 0020 sections. Overall characteristics are typical of the rudders fitted to many ships, and are shown in Fig. 149.

One of the variables in the tests was drift angle at

the rudder from crossflow at the stern of the ship in turning, as diagramed in Fig. 150. The effective influence of the drift angle on the all-movable rudder is simply to increase its angle of attack. In the case of the skeg rudder, it also leads to inflow angles on the skeg as shown in Fig. 151. Alternatively, if the rudder is shifted while the ship is in a turn, a positive angle of attack is developed by the skeg, which assists the desired motion. Skeg test angles of  $\pm 15$  degrees were used to represent realistic limits of drift angle at the rudder. Results for rudder No. 1 are presented in Fig. 152. The discontinuities in the lift and drag curves are presumably due to early separation downstream of the skeg, and this was confirmed by the visual flow studies. While this separation on the skeg starts at relatively low rudder angles, separation on the all-movable part

does not start until somewhat higher angles are reached.

A general finding for aircraft flaps is that gaps precipitate stalling of the flap. Fig. 153 shows results for various sealing of vertical gaps in rudders. In each case, the lift developed with either the high or the low pressure side of the gap sealed is only slightly lower than with all gaps sealed, but is much higher than for all gaps open.

As shown in Fig. 154, the rudder-plus-skeg combination has less lift increase for increasing angles of attack than has the all-movable rudder. The stall angle,

however, is delayed by about 12 degrees, and the maximum lift coefficient achieved is only 10 percent less. For the same lift the skeg rudder does have a much higher drag. For zero and negative skeg angles the maximum lift coefficient developed by the skeg rudder is a little less than for the all-movable rudder. A reversal of the rudder while the ship is in a turn, however, results in the adding of the angles and a higher maximum lift coefficient produced by the skeg rudder.

The differences among the three skeg rudders of Fig. 149 as tested were not large. Increasing the taper ratio improved the lift at the larger angles of attack.

## Section 15

### Maneuvering Trials and Performance Requirements

**15.1 Introduction.** Every ship must have at least some inherent control qualities that enable it to maintain its intended course in the open sea, to maneuver safely in ports and restricted waterways, and to stop within a reasonable distance. These minimum capabilities are needed under all conditions of loading, at both high speeds and the moderate speeds associated with restricted water, and in wind and waves as well as in calms.

With reference to the material introduced in Sections 4 and 5, good coursekeeping means ability to maintain a steady course or heading without excessive rudder activity, whether in manual or automatic control, particularly under adverse weather conditions. Continuous helm corrections lead to unnecessary wear and tear on steering gear, add to hull drag, and may create an undesirable and potentially dangerous work load for the helmsman in restricted waters where the risk is greatest. Dynamic stability is a desirable but not always a necessary ship characteristic for good coursekeeping. The requirement varies according to a ship's geometry, size, and speed. This relationship has much to do with the relative reaction times of ship and controllers. For example, the heading of a very large tanker at slow speed tends to change quite slowly because of the ship's great inertia and slow forward speed. The tanker can, therefore, tolerate moderate levels of dynamic instability, because it will diverge course only slightly in the time required for corrective rudder action. This response is consistent with the slow reaction times of rudder and steering machinery, equipments which are massive and not highly powered in large vessels. Conversely, a small, fast vessel like a high-speed patrol boat cannot tolerate much, if any, instability.

Maneuverability requires reliable and prompt changes of heading on demand, which implies predictable turning response to rudder movement and correspondingly prompt checking of the turn when rudder

position is reversed. Although a small steady-turning diameter (Section 6) may be an indication of good maneuverability, it does not define a ship's ability to make the short and frequent transient course changes that are so often required in restricted channels.

Finally, a ship's ability to stop reliably, particularly in an emergency, is obviously desirable. However, it is difficult to specify what is a "reasonable" or safe distance for stopping, except to match usual practice. In unrestricted water, turning is often a better way to avoid trouble than attempting to stop. A rudder cycling maneuver in which the rudder is alternated between left and right (see section 10.5) may also be more effective in slowing a vessel than the reversing of engines in restricted waterways.

**15.2 Controllability Performance Requirements.** Although the desirable qualities of controllability are well known, it is difficult to specify adequately the required or minimum coursekeeping and maneuvering capabilities. Still, as discussed in Sections 4 through 6, certain guidelines have been available to aid the designer, and several definitive trial maneuvers have been adopted to various extents. Sometimes the criteria may be qualitative and require only that the ship be able to hold course without excessive attention to the helm, and that the ship have turning and stopping ability comparable to that of other ships of like size and type.

For most conventional displacement ships some quantitative performance criteria are required. The most frequently specified criterion is the maximum allowable tactical diameter in a full-rudder turn. Sometimes, allowable head reach in a crash stop from full speed is specified, and other performance criteria (described subsequently) are used, especially for high-speed merchant and naval vessels, and for submarines. Other concerns are the potential danger associated with machinery malfunctions, and the need to demonstrate ability for timely recovery from an emer-



Table 19—Principal Maneuvering Trial Codes in 1988

Maneuvering Trial	BMT	SNAME	DnV	ITTC
Crash stop (ahead) at full speed	•	•	•	•
Stopping trial at low speed				•
Coasting stop test			•	
Crash-stop (astern)		•		
Stopping by use of rudder (cycling)			•	
Turning test at full speed	•	•	•	•
Turning test at medium speed				•
Turning test at slow speed	•		•	•
Turning test with propulsion stopped			•	
Turning test from zero speed	•			•
Pullout (from turn)	•			•
Weave maneuver	•			
Z maneuver	•	•	•	•
Direct spiral	•			•
Reverse spiral	•		•	•
Statistical method	•			
Change of heading				•
Lateral thruster:				
• Turning test			•	•
• Turning test			•	•
• Turning test			•	•
• Coursekeeping test, astern			•	

gency. A typical emergency to be anticipated is sudden and unplanned excursion of the rudder hard over, or other failure of the steering gear system such as that which caused the catastrophic 1972 *Seawitch* collision and fire in New York Harbor.

Fortunately the problem of quantifying criteria for acceptable controllability has been clarified in recent years by application of the analyses, model tests, full-scale trials, and computer simulations described in the previous sections. Work by groups such as the U.S. Coast Guard, International Maritime Organization (IMO), and SNAME Panel H-10 (Ship Controllability) has led to tentative national and international criteria as summarized by Panel H-10 (1975) and Landsburg, et al (1983). Such developments are discussed in this section, first for conventional displacement ships and then for high-speed craft.

**15.3 Maneuvering Trial Codes and Guidelines.** Ship controllability continues to be evaluated by means of full-scale trials and analyses, involving either a few definitive maneuvers or a complete set of tests. Ideally, this assessment of adequacy should be based on numerical measures or indexes that are derived from these maneuvers and those that can be calculated during design.

At least four authoritative organizations have developed maneuvering trials codes, but these codes do not agree in details. Table 19 shows the proposed coverage of maneuvering trials codes of British Maritime

Technology (BMT), SNAME, Det norske Veritas (DnV), and the International Towing Tank Conference (ITTC). All four organizations agree on the need to conduct three specific types of maneuvers, and so these three are included in a great many trials:

- (a) Turning maneuver from full speed.
- (b) Zigzag or Z-maneuver.
- (c) Crash stop from full ahead speed.

Two or three organizations also agree on the need to conduct three additional trials:

- (d) Direct or reversed spiral tests.
- (e) Pullout (from turn).
- (f) Turning maneuver at low speed.

With the purpose of developing an approach to determining a ship's trials program, Glansdorp (1976) provided a very instructive survey of the various trials, and rated their general value for scientific, nautical, and experience-gained purposes. He has also developed a general rating system with weighting factors for use in deciding which trials would be useful to run for various types and sizes of vessels, with concern given to their intended cargo, voyage itinerary, and environment.

In 1985 as a preliminary action to enable the collection of standardized data and the development of criteria and minimum standards, the International Maritime Organization (IMO) published MSC/Circ. 389, "Interim Guidelines for Estimating Maneuvering Performance in Ship Design." These guidelines provide that the maneuvering performance of all new ships of 100 meters in length and over, are to be estimated, tested, and verified. The guidelines state that all ships should have maneuvering qualities which permit them to keep course, to turn, to check turns, to operate at acceptably slow speeds and to stop, all in a satisfactory manner. Definitive trials were specified and the following characteristics were called out for estimation and verification for both fully loaded and trial conditions:

(a) *Turning circle characteristics.* These can be determined from the turning circle tests using a rudder angle of 35 degrees.

(b) *Yaw checking ability.* This can be determined by the first overshoot angle and the time to check the yaw in a zigzag maneuver.

(c) *Initial turning ability.* This can be determined at the beginning of the zigzag maneuver from the change of ship's heading angle per unit rudder angle and the distances traveled ahead and to the side after a rudder command is executed.

(d) *Coursekeeping ability.* While no single measure of coursekeeping ability has yet been developed, this quality may be evaluated for ships of comparable type, size, and speed by comparison of Z-maneuver, direct or reverse spiral, and pullout (from turn) tests. If the ship is expected to be dynamically unstable, the degree of human (or automatic) control needed to steer the ship should be considered in the design stage. Con-

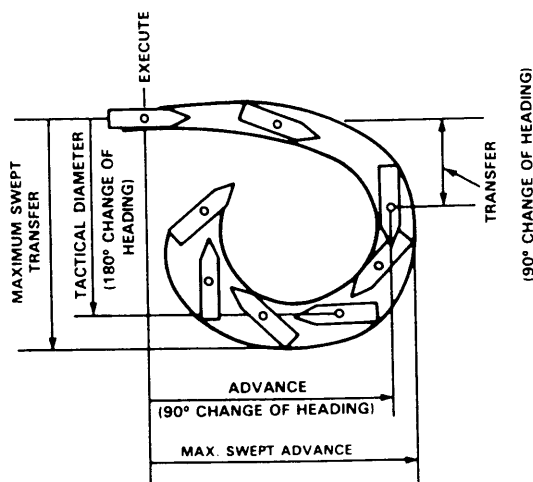


Fig. 155 Definition diagram—turning circle maneuver

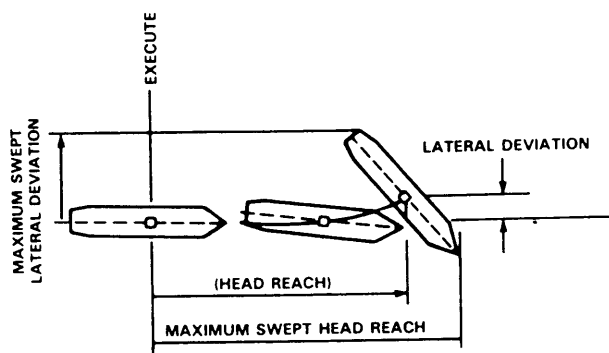


Fig. 157 Definition diagram—stopping maneuver

sideration should also be given during design to the *neutral rudder angle* necessary for proceeding on a straight course.

(e) *Slow steaming ability.* The ability to proceed at steady slow speed is a desirable quality. It is usually determined only from the ship's speed associated with the lowest possible engine RPM.

(f) *Stopping ability.* This can be determined from the distance the ship travels along its track once a crash-astern order is given. Turning while stopping from higher speeds is also of concern, and should be measured and recorded.

The adoption of such a code will be welcomed by ship designers both as a guide to the specification of trials and as a future source of statistical performance data.

**15.4 Basic Trial Considerations.** Although the indexes from the definitive maneuvers may offer suitable measures to use in developing criteria and standards for different ships, they give little information on how much space a ship requires. Figs. 155, 156, and 157 show the turning circle, zigzag, and stopping maneuvers with the ship outline plotted. This *swept path*

presentation is most useful for ship handlers when estimating potential clearance with respect to waterways, other vessels, obstructions, etc.

In developing standards, the relationships between swept path and movement of a reference point must be appreciated. For example, a tanker has a small turning circle relative to its length, but it requires substantially more turning area than indicated by the path of its reference point. This requirement for greater area is due to the tanker's great length and drift angle, which together cause the tanker to sweep a considerably larger swath of water area when turning than when going straight ahead.

Nevertheless, statistical analyses of results of swept path extremities may not show smooth functions of control settings or ship design parameters. For this reason, the traditional measures using the measured path of the ship's center-of-gravity or midships reference point are used for comparative purposes, and they provide useful information when related to the ship type and size.

Different parameters have been used in the definitive maneuvers for various purposes. In the turning maneuver, maximum rudder angle capability is sometimes greater than the 35 degrees required. While it is helpful to know turning characteristics at the maximum angle, characteristics at 35 degrees provide consistent parameters for comparison. Similarly, variations in the zigzag maneuver have proved useful. The alternate 10 - 10 zigzag and other variants (20-degree rudder, 10-degree change of heading, for example) are sometimes used; either to keep the maneuver in the hydrodynamically linear range, or to enable a free-running model test to take place between the walls of a straight-line towing tank. A variation using only 5-degree rudder angles and 1-degree course changes has also been suggested and tried by simulation. However, as a ship trial this may be impractical because of the difficulty in achieving sufficiently precise settings. The 20 - 20 zigzag maneuver is generally preferred because:

- It has been used for many years, so that a considerable body of statistical data now exists.
- Ship handlers often use 20 degrees of rudder when initiating and checking turns.
- With some ships, 10 degrees of rudder may not suffice for checking turns; that is, no data will be obtained.
- Inexact setting of the rudder angle in a trial is less harmful in a 20-20 than in a 10-10 degree zigzag maneuver.

The crash stop maneuver is a good test for trying out extremes for the machinery and as an index to relative stopping ability. For ship handlers' information, a stopping trial from a more likely maneuvering speed would be more useful. That speed depends on a ship's size and power. For traditional "full ahead" maneuvering the engine order corresponding to about

12 knots may be reasonable for bulk carriers and 16 knots for higher speed cargo vessels.

The direct or reversed spiral test has not been traditionally specified. It does not provide a test of the machinery extremes can require significant trials time. The data gathered, however, are critical to determining the controls-fixed dynamic stability of the ship.

Practical considerations usually limit maneuvering trials to the fewest number that can reliably show a ship to have adequate controllability.

Maneuvering trials for oil tankers should be made at summer full load draft. Experience and trial data show that maneuvering and coursekeeping at other drafts is generally superior. This is because trim by the stern and reduced mass in lighter operating conditions result in greater dynamic stability and quicker response. These conclusions may not be true in strong wind, but such conditions are not covered in basic trials.

For uniformity in selecting ballast drafts, consideration should be given drafts specified by the IMO 1973 Marine Pollution Convention (MARPOL).

Except for tankers, ore-bulk-oil carriers, and other vessels with large tankage it is generally impractical to ballast to summer full-load draft before delivery from the construction yard. Therefore, some other standard draft is needed. For containerhips and other ship types with relatively light draft and high freeboard, trials should be conducted at a draft where the greatest maneuvering problems are experienced. It may be necessary instead, however, to compare trial performance at light draft with that of similar ships of known merit.

The most demanding maneuvering requirements for many ships are those for operations in shallow water during coastal and port navigation. The practical difficulties of finding a broad testing area of nearly constant shallow depth are usually insuperable. Ship trials are thus usually run in deep water. Therefore, the adequacy of a ship's maneuvering capability in shallow water must usually be inferred from its success in deep water and its capabilities relative to other known vessels. The full scale trials of the 278,000-dwt *Esso Osaka* in shallow water as reported by Crane (1979)

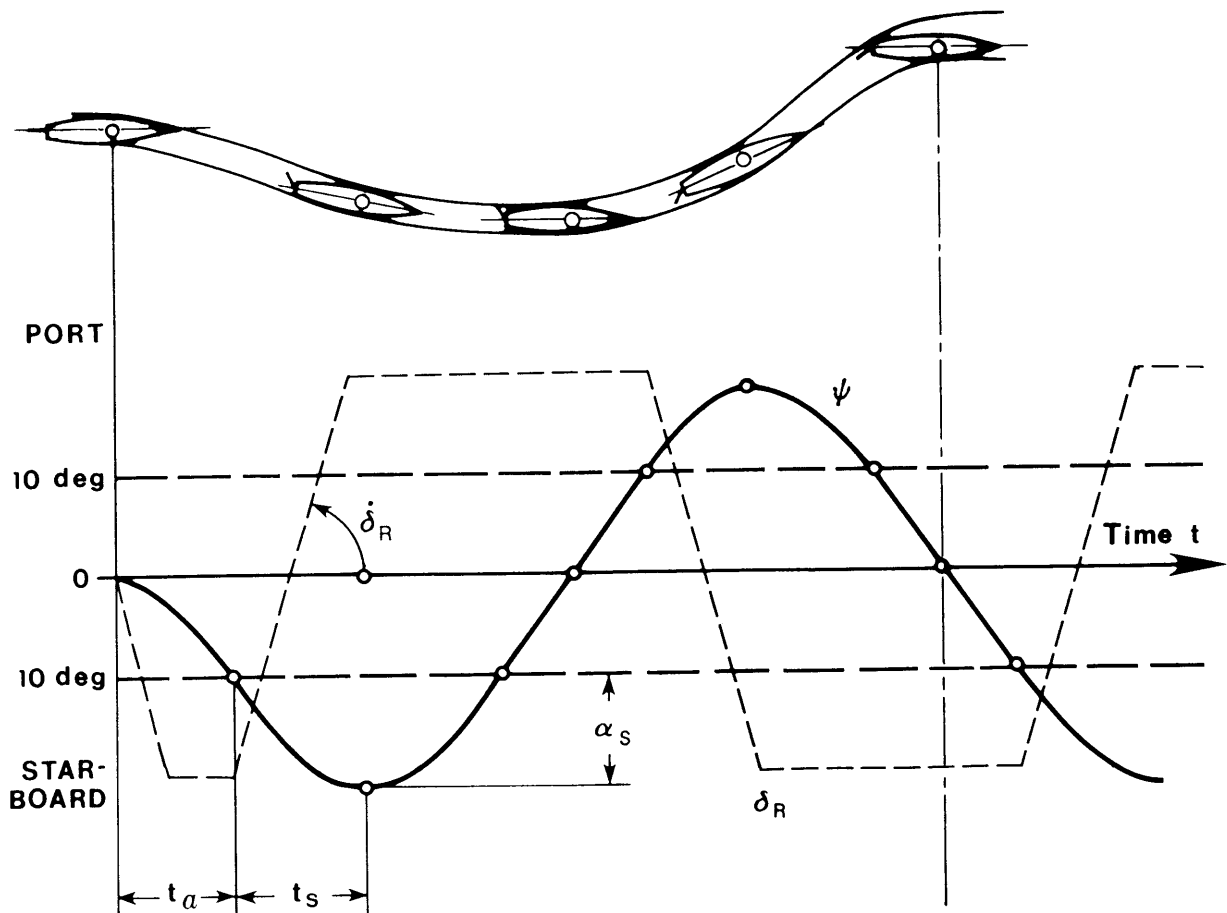


Fig. 156 Definition diagram—Z-manuever (20 deg rudder 10 deg heading change)

Table 20—Trial Indexes of Basic Controllability Qualities

	Required Quality	Trial Maneuver	Indexes
Coursekeeping	Course stability	Spiral	1. Loop width and height
		Pullout*	1. Convergence small; turning rate same from each side.
	Turn Checking	Zigzag Maneuver	1. First overshoot angle 2. Time to check yaw
	Turn initiation	Initial turning	1. Time
Maneuvering	Turning	Minimum turning Circle	1. Advance 2. Transfer 3. Tactical diameter
	Turn Checking	Zigzag maneuver	1. First overshoot angle 2. Time to check yaw 3. Maximum width of path 4. Overshoot width of path
	Stopping	Crash astern from a standard maneuvering speed	1. Headreach 2. Lateral deviation

\* Obtainable from zigzag maneuver for a particular rudder angle.

provide valuable data on the prediction of tanker capabilities in shallow water.

**15.5 Relating Controllability Indexes to Tests.** Basic performance criteria for ship controllability together with the appropriate tests for evaluating each criteria are summarized in Table 20. Coursekeeping ability depends on the ship's dynamic stability, its rudder effectiveness in turning its control system characteristics, and its size and speed. Thus, coursekeeping ability is not indicated directly by any one definitive trial. However, a ship's dynamic stability can be directly demonstrated by the pullout or spiral test, as discussed previously.

The zigzag maneuver is the traditional maneuvering trial that provides the greatest amount of directly useful information on the combined effect of hull form parameters (including draft and trim), rudder performance, and control system. Yaw-checking ability, which is important for both coursekeeping and maneuvering, is indicated directly by the first overshoot angle  $\alpha_s$  and by the time to check yaw,  $t_s$  (See Figs. 156 and 18). Although the test does not indicate coursekeeping capability directly, the Nomoto-Norrbin parameter  $T'$  which is indicative of dynamic stability can be calculated from the zigzag maneuver, along with  $K'$  which is indicative of turning ability. As discussed in Section 5.4, the  $K'$  and  $T'$  parameters should be used as rough comparative measures because of their

linear development. The ratio of  $K'/T'$  is an indicator of overall controllability.

A ship's turning ability is indicated in general by the characteristics of the simple turning circle (advance, transfer, and tactical diameter). However, most maneuvers involve only transient phases of turning. Hence, quantities such as quickness of initiating a turn may be more important for maneuvering in waterways than the overall turning circle dimensions. Quickness of response is indicated in the zigzag maneuver by the time,  $t_a$ , required for the ship's heading to reach the first rudder shift angle (20 deg in Fig. 156). Similarly, yaw-checking ability is directly signified by the time to check yaw,  $t_s$ , and indirectly by the overshoot angle magnitudes (mainly the first yaw overshoot angle  $\alpha_s$ , as noted above).

Ship motions during large maneuvers cannot be described accurately by linear functions; hence values of  $K'$  and  $T'$  are not constant but are functions of amplitudes of motion. Therefore, it is essential to estimate the values of both of these indexes for the same operating conditions.

Stopping capability, head reach, and lateral deviation in stopping are easy to measure, but are much harder to improve after construction, even with significant changes in propulsion power. In practice, ample stopping capability is achieved by the operator's careful management of ship speed.

**15.6 Status on Development of Minimum Inherent Controllability Standards.** In response to "The Presidential Initiative to Reduce Maritime Oil Pollution of March 1977," the U.S. Coast Guard began an intensive evaluation of means for improving the maneuvering and stopping ability of large tankers (Card, Cojeen, et al 1979). Their main conclusion was that all vessels of more than 1,000 gross tons intended for the normal transport of cargo or passengers should meet reasonable minimal standards of maneuvering performance in normal turns, crash stops, and zigzag maneuvers. They also concluded that minimum continuous maneuvering speed capability and the controllability of ships with high freeboard in wind are worthy of standards development, although controllability in wind is more difficult to set and to predict during design.

At the same time, SNAME Panel H-10 (Ship Controllability) addressed the subject, including aspects of piloted controllability in Crane, et al (1975), Landsburg, et al (1978), Notes, (1983), and Landsburg, et al (1983). As previously noted, the IMO is working on international standards, having already provided maneuvering test guidelines and recommendations.

The U.S. Coast Guard approach assumes that most oceangoing ships do perform adequately in the hands of trained and experienced shiphandlers. Nonetheless, even poor performers should not be tolerated. Shiphandlers should not have to stretch their "windows of adaptability" to accommodate unnecessarily poor-performing vessels.

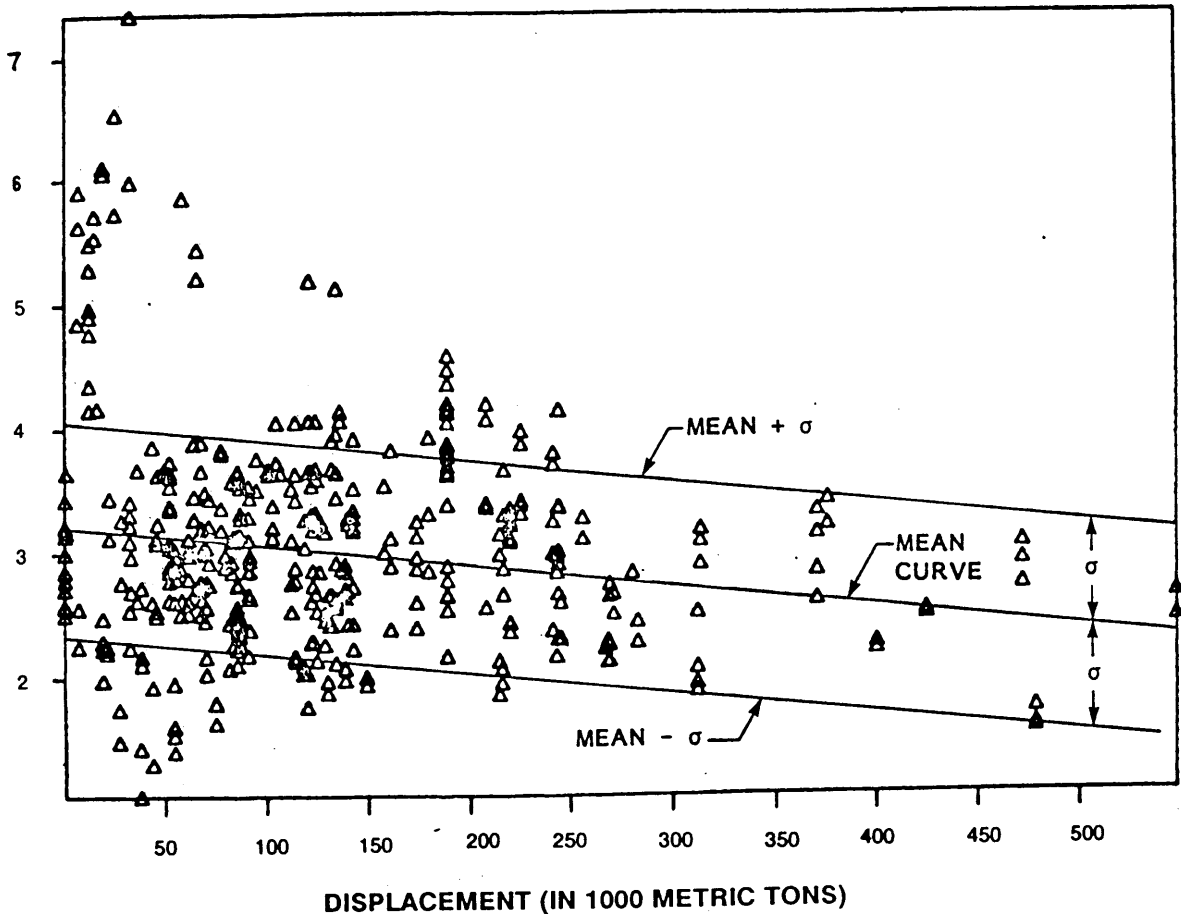
NON-DIMENSIONAL TACTICAL DIAMETER  $DT|\delta_R|/35 \text{ LBP}$ 

Fig. 158 Tactical diameter data and analysis for all ships (Barr, 1981)

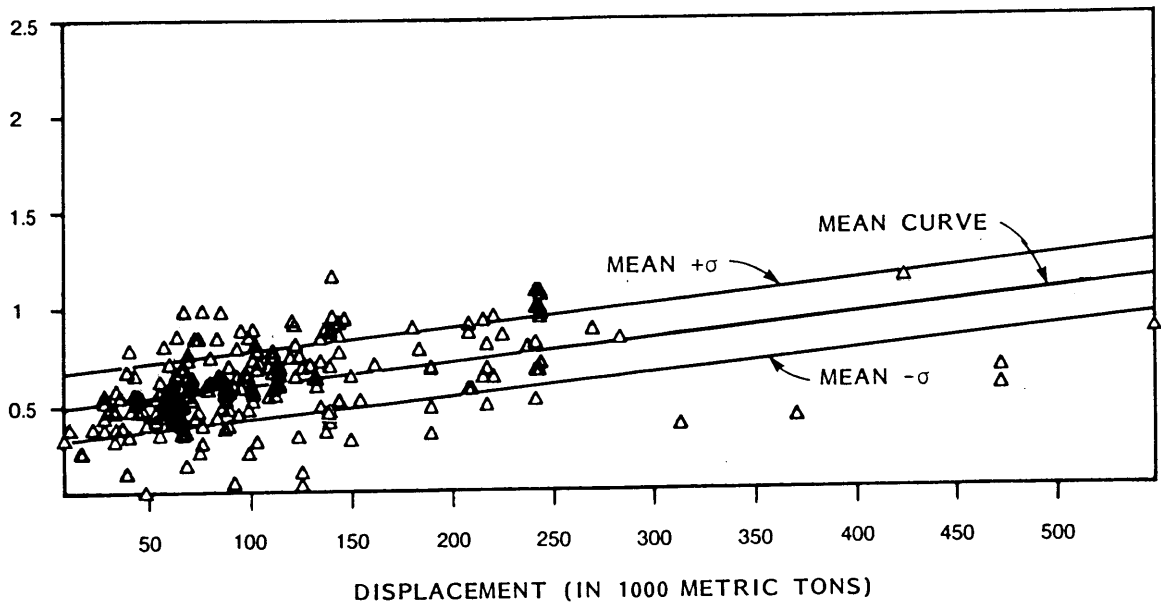
NON-DIMENSIONAL HEAD REACH  $R_H / F \times \text{LBP}$ 

Fig. 159 Stopping head reach data and analysis for all ships (Barr, 1981)

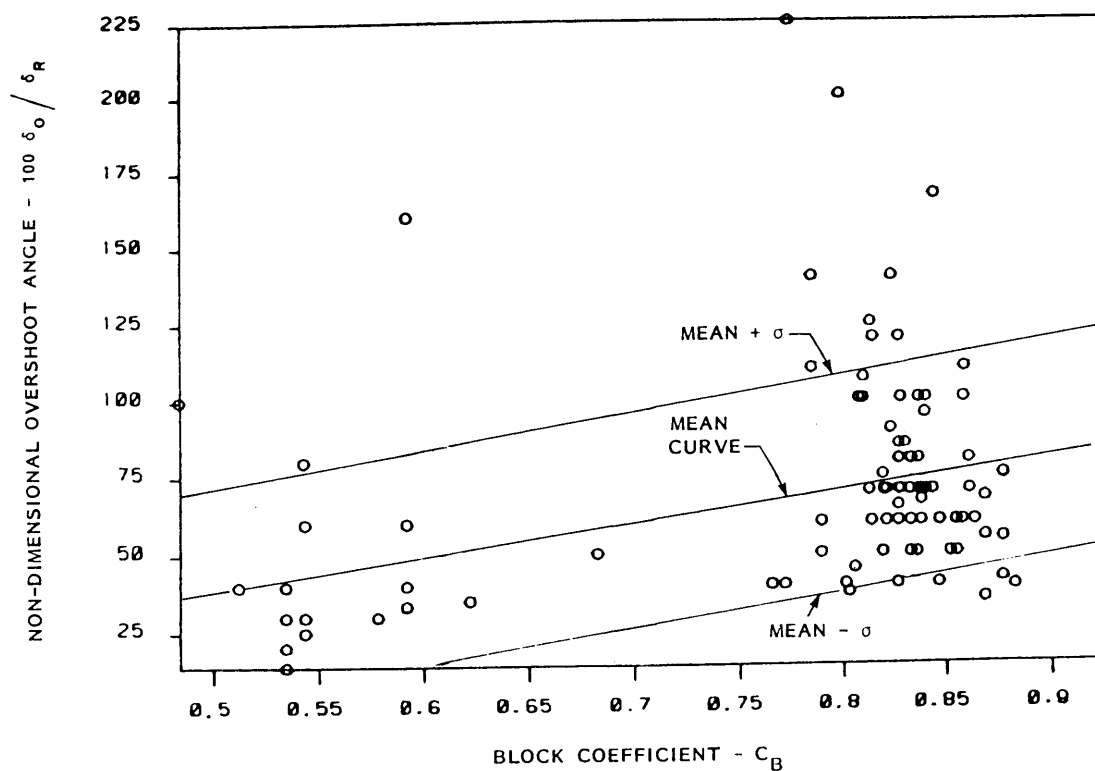
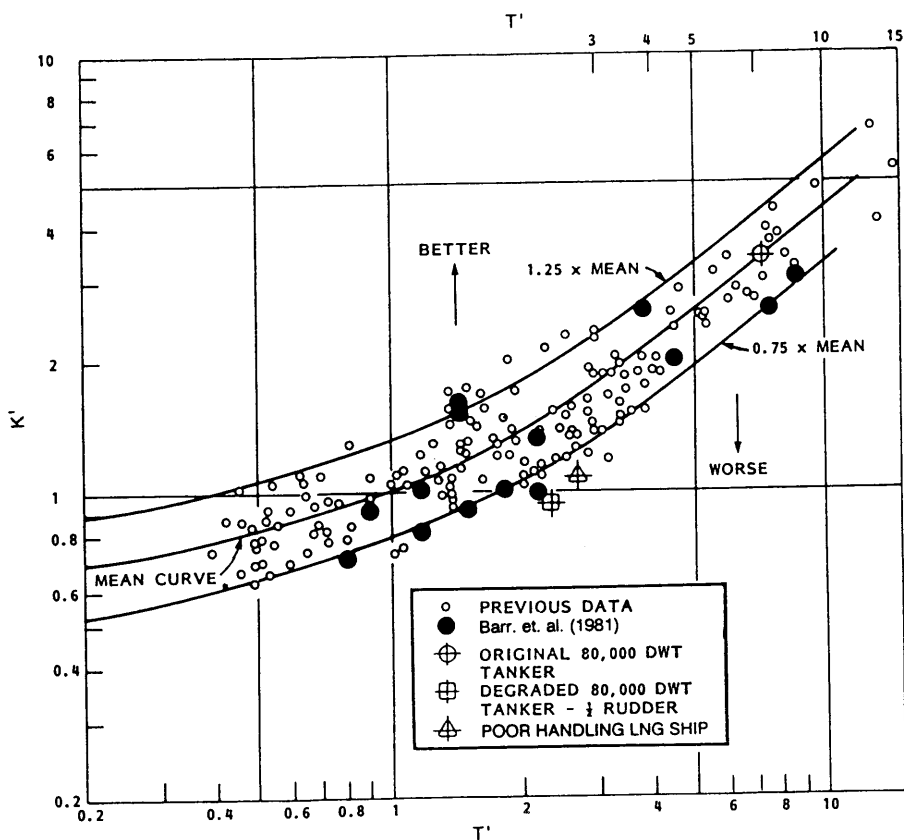


Fig. 160 Statistical analysis of all zigzag overshoot angle data

Fig. 161 Comparison of various data for zigzag parameters  $K'$  and  $T'$

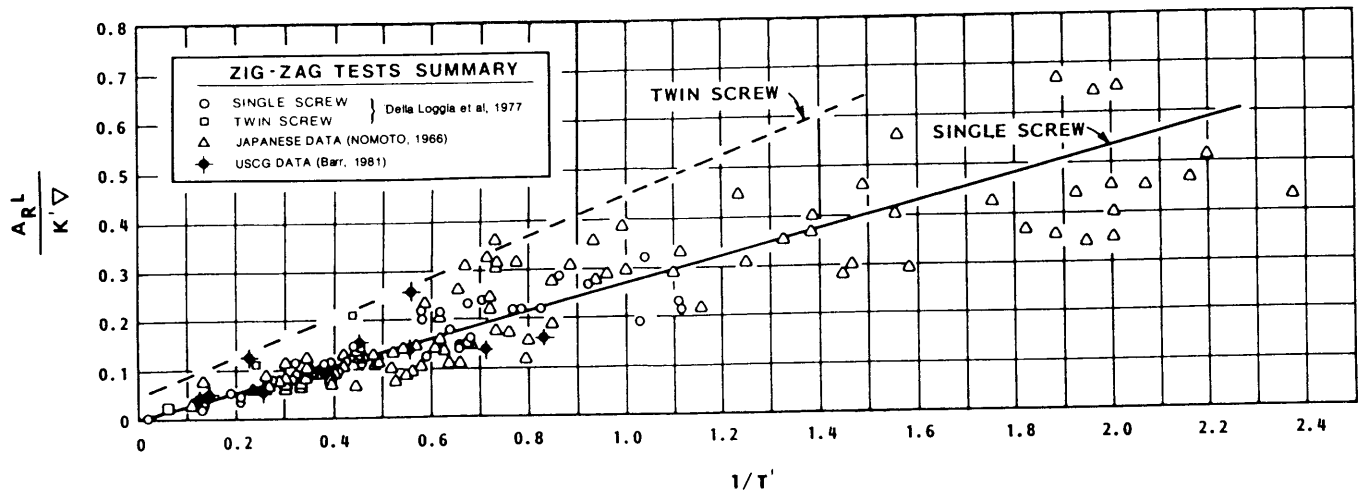


Fig. 162 Correlation of zigzag maneuver performance parameters  $K'$  and  $T'$

At the outset of its work, the USCG established a data base of performance measures for various ships (Barr, et al 1981). Values of the various controllability indexes were collected from trade journals and publications, shipowners, shipyards, and IMO reports. Tankers are by far the largest group of ships in the data base, followed by other bulk carriers. Few other ship types are found. In Barr, et al (1981), ships are identified only by ship number, because some of the data are proprietary. A complete discussion of the USCG data base and the approach to analyses is also given. Although the data base is limited, the maneuvering responses are useful as guides to levels of performance for the general ship classes.

To illustrate the variability of the results, four plots are presented showing:

- Non-dimensional ratio of tactical diameter to length, plotted against displacement, for 35-degree rudder turns (Fig. 158). Note that this ratio is roughly proportional to  $1/K'$  (Equation 77).
- Head reach divided by the product of ship length times Froude number, plotted against displacement, for crash stop (Fig. 159).
- Ratio of overshoot angle to rudder angle, plotted against block coefficient, for 20-20 zigzag maneuvers (Fig. 160).
- Relationship of steering quality indices,  $T'$  and  $K'$  (Fig. 161).

Figs. 158 through 160 illustrate the variability of the data. Shown are the data points, mean curves, and standard deviation of the mean. Fig. 161 shows a somewhat similar array of data, but with the upper and lower curves set at 1.25 times the mean and 0.75 times the mean. One approach to setting standards might be to assign ratings ranging from superior to marginal.

Rating curves paralleling the mean curve could be developed from statistically assessments of certain vessels that were commonly referred to as being particularly good or bad.

The scatter of data for overshoot angle in Fig. 160 makes performance ratings based on such data highly suspect. Nomoto (1966) has shown, as pointed out in Section 5.4, that overshoot angle is nearly proportional to  $K'/T'$  with rudder angle  $\delta_R$  fixed. Fig. 161 confirms his suggestion that the parameters  $K'$  and  $T'$  probably provide a more useful basis for analyzing results of zigzag maneuvers than does overshoot angle. Parameters  $K'$ ,  $T'$ , and rudder area,  $A_R$ , are related as shown in Fig. 162. This relationship may also be useful as a design tool in selecting rudder area. Fig. 162 indicates that  $K'$ - $T'$  data available for ships in the USCG data base are generally in good agreement with data from other sources.

**15.7 Submarines and Submersibles.** Submarines and submersibles must have adequate depth keeping and vertical plane maneuvering ability, in addition to stopping, coursekeeping and horizontal plane maneuvering ability. Fig. 163 shows some of the design considerations. Stern diving planes provide major control forces and moments in the vertical plane. For additional control, forward fairwater or bow planes are often installed. When the submarine operates close to the ocean surface or ocean floor, forces of attraction come into play that are similar to those that cause surface ship bank effects.

The height of the fairwater (sail) is an important design element. First, the problem to settle is how high should the periscope sight line be above mean wave height. After that, the taller the sail the less the disturbing force on the hull. However, a tall sail has large

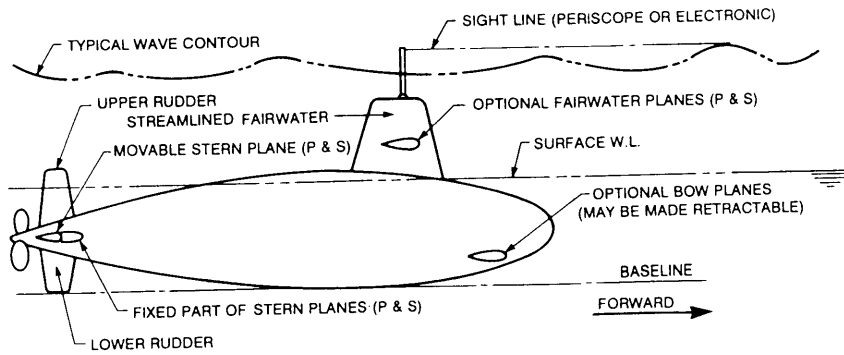


Fig. 163 Schematic submarine control surfaces elevation view

drag and induces larger snap roll when the submarine turns. A large snap roll can be highly undesirable for submarine maneuvers and depthkeeping. A snap roll occurs when the transverse velocity from yawing in a turn combines vectorially with the fore-and-aft velocity to create a lift force on the fairwater, thus producing a rolling moment. The snap roll also affects submarine depth, because with the submarine at a heel angle, the rudder acts as a diving plane. The diving planes similarly provide a partial yawing effect.

The vertical overshoot maneuver, is much like a zigzag maneuver but is terminated after the first overshoot (Fig. 164). The maneuver is similar to that in the horizontal plane except that a submerged submarine also has some metacentric stability. For the vertical overshoot maneuver, the maximum depth change is analagous to about one-half the swept path in a horizontal zigzag maneuver. This depth change and the pitch overshoot angle are important measures of the submarine's controllability and safety.

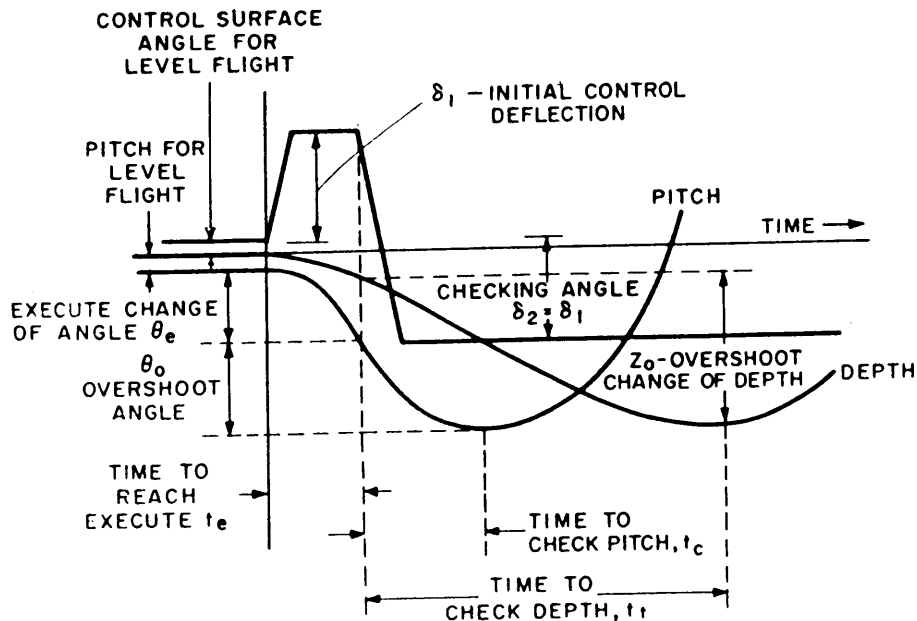


Fig. 164 Definition diagram for overshoot maneuver in vertical plane (Arentzen and Mandel, 1960)



The *meander maneuver* provides a measure of how well the submarine's depth stabilizes following execution of a depth-changing maneuver. The depth overshoot distance, and time required for depth to become constant, provide a measure of depth checking ability. In the meander as well as in the overshoot maneuver, metacentric stability helps to maintain level flight, particularly at low speeds.

Ability to recover from a stern plane jam, without exceeding allowable maximum operating depth, is crucial. The submarine should be able to recover from a stern plane jam that occurs at a typical operating speed and depth. The maneuver is complex because it may include control of propellers, rudders, bow planes, and ballasting system. For this reason, stern plane jam recoveries are usually investigated through mathematical simulations as shown, for example, by Giddings and Louis (1966).

For these reasons, requirements for submarine controllability are not only more extensive but also generally more stringent than those for surface ship controllability.

**15.8 High-Speed Vessels.** High-speed ships usually experience large roll motions or heel in turns. This roll or heel is of particular concern because in extreme cases it can lead to roll instability and capsizing. Therefore, high-speed vessels usually roll into a turn. That is, they heel toward the center of a turn to assure roll stability and keep the resultant forces perpendicular to the deck.

Controllability can be adequately characterized by the same four basic maneuvers as used for conventional ships, that is, the turn, spiral, zigzag, and crash stop. Because performance is so sensitive to speed, it is desirable to conduct turns, spirals, and zigzags at several speeds. In the case of hydrofoil craft, it is important to characterize controllability in both the hull and foil-borne modes.

Hydrofoil craft and surface effect vessels have specialized control requirements. These vessels are not displacement type ships in their underway modes. Rather, the hull of a hydrofoil craft is supported by dynamic lift from its submerged hydrofoils and a surface effect vessel is supported by an air cushion restrained by fixed and/or flexible walls or skirts.

A fundamental control problem for hydrofoil craft concerns vertical plane operations in waves. A decision has to be made whether the craft is to follow the contour of waves or try to fly level through them, and whether active lift control or passive (ladder foils) will be used. Hydrofoil craft with automatically controlled foils can generally operate in rougher seas than the area-stabilized type. Loss of height or hull clearance during maneuvering is another problem unique to hydrofoil craft. Loss of foil lift during turning can lead to undesirable turning characteristics or, in extreme cases, to hull impact. It is important to insure that no significant loss of hull clearance or change of trim

occurs during turning of a hydrofoil craft. No quantitative criteria exists in this area.

**15.9 Piloted Controllability.** Little mention has yet been made in this section of performance in real operating circumstances. The emphasis has been on providing a hull with good basic coursekeeping characteristics. Many additional factors also affect navigational safety. Expected traffic situations, environmental conditions (primarily wind, current, waves, and visibility), vessel-waterway geometry, the placement of navigational aids, and, of course, human variability have profound influences on what amount of controllability is prudent for a given design. The most important element of ship control is the human controller, who must be considered seriously during ship design and operations.

Panel H-10 (Ship Controllability) of SNAME (1975) proposed a "Design, or ABC harbor" as a standard scenario approach for examining the combined effects of ship design and piloting factors in realistic waterway settings. An ABC harbor can incorporate many of the critical components of a variety of real world ports where the particular ship is to be handled. Study of the ship's ability to transit the ABC harbor through simulations using the controllability characteristics of the vessel design in "fast-time" or "manned real-time" situations can then show acceptability of operations (Section 16.9).

Reviewing the various interactions further, Veldhuyzen and Strassen (1977) and Glansdorp (1977) have schematically traced the main interactions among ship, environment, and human controller in a manner similar to that illustrated in Fig. 165. We may conclude that a shiphandler's functions may be separated into an estimator, an internal prediction model, and a decision-making element. This division of functions provides a framework for studying and understanding human control in shiphandling simulations. However, it does not provide information on mean response or the variability of human functions which are best studied by using a research shiphandling simulator (as described in Section 16.9).

A maneuvering emergency is an urgent immediate need for control action. In such a case, a pilot would prefer to have the ability to turn or stop instantly. These preferences are unrealistic, as are many other arbitrary suggestions for large increases in inherent controllability for use only in emergencies. Even if they could be provided and were provided, shiphandlers might be tempted to take greater risks, and still be unprepared to use the extra forces. The correct alternative is to provide a good design and properly train the operator so that he knows the ship's capabilities and will exercise prudence.

Miller, et al (1981) considered various types of maneuvering emergencies extracted from U.S. Coast Guard casualty reports. Crane (1973) demonstrated the relative benefits of alternate control equipment and

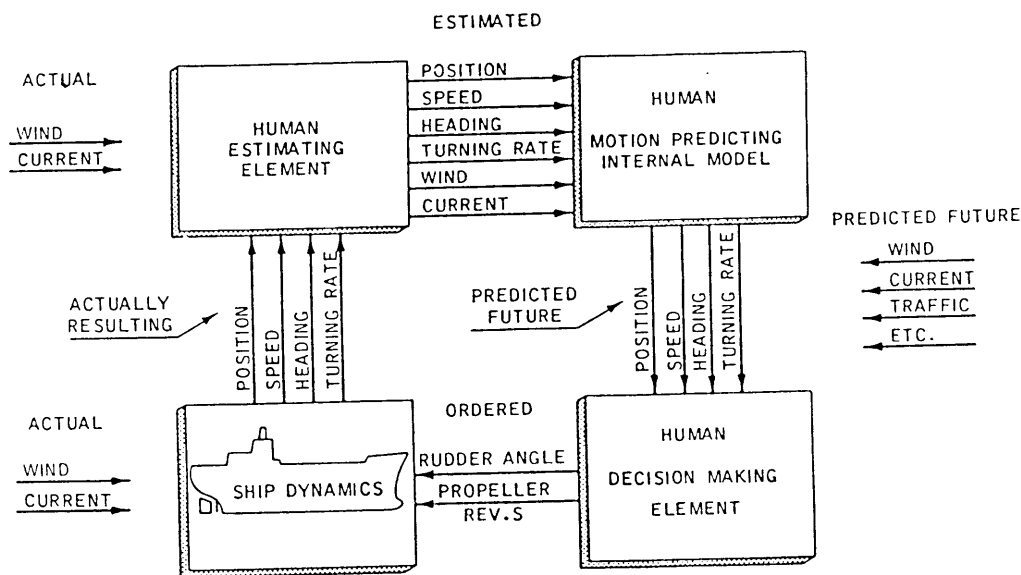


Fig. 165 Man-ship control loop (Crane, 1983)

actions in possible emergencies of large tankers. Other studies by Clarke (1971) have shown similar results.

For lack of data, emergency maneuvering requirements are difficult to analyze realistically. A large variety of singular emergencies can be speculated upon, and these will vary from port to port. System safety studies, however, can be performed on a port-specific basis. Attempting to do so is discussed by Crane (1983), and Grose (1980).

Conventional maneuvering trial indexes are generally not useful for rating piloted controllability performance in realistic waterways. Several additional indexes have been developed for statistical analyses of channel navigation. Included are the "clearance distance," "safe speed margin," and "rudder use" indexes suggested by Panel H-10 (1975), and a channel based grid system for ranking track-keeping performance described by Keith, et al (1977). Similar criteria are regularly used at the Computer Aided Operations Research Facility (CAORF) and other shiphandling simulation research facilities.

Among the thousands of existing research studies on ship control, few relate ship control design parameters to performance in real waterways. Some exceptions are discussed here. Atkins and Gaffney (1980) describe a shiphandling simulator investigation of a

proposed increase in maximum ship size for an existing "tight but manageable" port. In this study, harbor pilots accustomed to the particular port piloted the simulated ships. The buoys, lighted ranges, and other visual cues were simulated, and water current velocity was varied between runs. This type of study is now common for analyzing port approaches or modifications. Only recently have applications to specific ship design characteristics been undertaken. In one CAORF research project (Aranow, 1983), the size of a tanker's rudder was halved to determine the extent to which experienced pilots could adapt and compensate for this drastic reduction of inherent controllability. The finding was that, by using larger rudder angles and more anticipation, the expected reduction in performance did not occur. Of course, the maneuvering margins decreased somewhat and the pilot's stress level must have increased greatly.

A study of optimum spacing and configurations of buoy placements was made for the U.S. Coast Guard (Bertsche, 1982). This study assigned relative risk factors to channels according to configurations of turns, channel widths, ship size, currents, buoy placement, and visibility. Although not intended for assessing ship design changes, the study may prove useful in that application.

## Section 16

### Application to Design

**16.1 Controllability in the Ship Design Spiral.** As stricter performance standards are developed and greater emphasis is placed on having a ship that maneuvers well, it becomes increasingly important to pay attention to controllability throughout design. Traditionally, analysis of controllability has been performed late in a design, to check acceptability. Controllability now, however, has become an important item in the ship design spiral, requiring analysis and review at each successive stage (Landsburg, et al 1983). This section reviews procedures and analysis tools that can be used at various stages of design to help ensure development of an adequately controllable vessel. Section 17 will provide further information on design of the rudder and other control surfaces, and on the application of auxiliary maneuvering devices. The introduction to control systems given in Section 9 also needs to be conscientiously applied in developing a good design.

Clarke (1987) put the design process into perspective as shown in Fig. 166. As noted in Section 5.4, the more maneuverable ships have lower  $T'$  and higher  $K'$  values, with tankers tending to be found in the upper

right part of the scatter diagram, and cargo vessels in the lower left (see also Section 15.6). Clarke has used systematic experimental data from the Technical Research Center of Finland (1984) to show the trends caused by  $C_B B/L$  and  $A_R/LT$  ( $A_R$  = rudder area). The figure shows that the "obesity" coefficient,  $C_B B/L$ , is responsible for most of the diagonal spread of the data, whereas the relative rudder area,  $A_R/LT$ , causes little shift by comparison. (This obesity coefficient should not be confused with the volumetric coefficients, also known as fatness ratio, which is defined as  $\nabla/(L/10)^3$ ; see Section 3.2 of Vol I).

The major controllability criterion to be considered, even at the earliest design stage when selecting basic dimensions, is thus the measure of dynamic course stability,  $\sigma_1$ . To emphasize the effect of dynamic stability on vessel performance, an example of three vessels is taken from Eda (1983). Characteristics of the three hulls are given in Table 21, and their steady turning rates are plotted against rudder angles in Fig. 167. Basic concepts relating to controllability were introduced in Sections 3 and 4.

Digital simulations were performed for these three

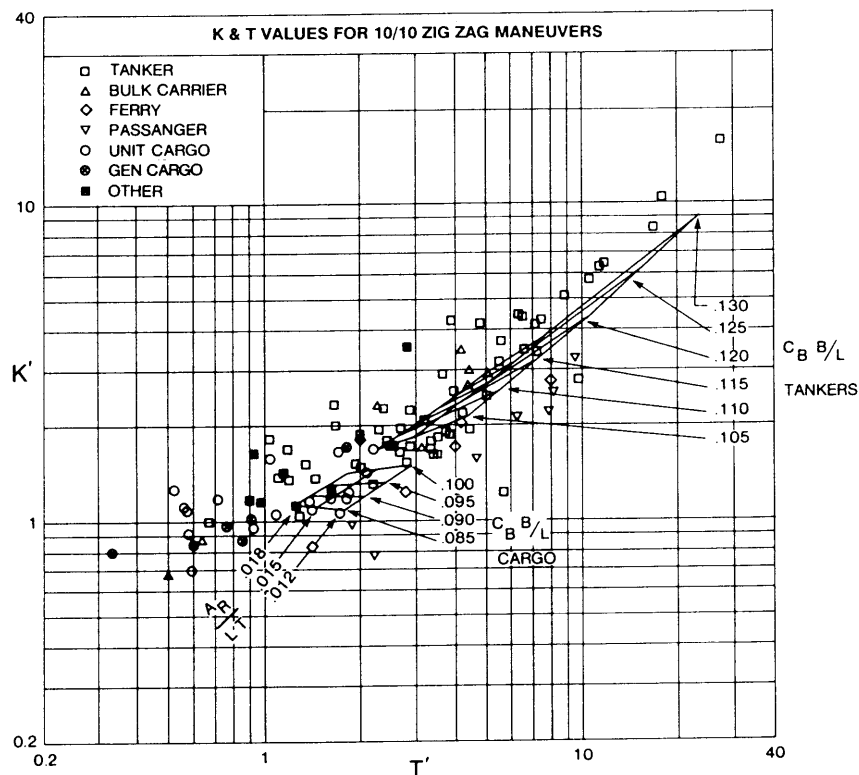


Fig. 166 Nomoto  $K'$  and  $T'$  for tankers and cargo ships (Clarke, 1987)

Table 21—Principal Model Particulars

Design Stability Hull Form	A Stable Slender, Fine	B Unstable Wide, Full	B Very Unstable Very Wide, Full
$LBP/B$	6.95	5	4
$LBP/T$	19.56	16.2	16.2
$B/T$	2.81	3.24	4.03
$C_B$	0.613	0.820	0.810
$C_P$	0.625	0.823	0.813
LCG fwd $\infty/LBP$	-0.015	0.026	0.019
$A_R/LBP \times T$	0.022	0.019	0.021

ships to examine the effect of various degrees of inherent course stability on ship maneuvering performance. The analyses are based on the hydrodynamic data of yaw moment and lateral force that were obtained in a series of captive model tests on a rotating arm. The mathematical model used in this study was a fairly realistic representation of ship dynamic motions and similar to that developed in Section 8.1.

The solid-line curves in Fig. 167 show steady-turning rates ( $r'$ ) predicted for ships A, B, and C. Arrows along the curves show the sequence of results predicted for the spiral tests. Dotted lines indicate the jump in steady-turning rate during spiral tests of dynamically unstable ships B and C.

To show the operational effects of excess instability, zigzag maneuver trajectories were computed for the three ships at an approach speed of 14.5 knots ( $\psi$  = heading angle). Results of a series of digital simula-

tions indicated dynamic behavior of these ships during the zigzag maneuvers as follows: The dynamically stable ship A has a small overshoot angle and can quickly finish a zigzag maneuver. The unstable ship B has a larger overshoot angle and it takes more time to finish the test than does ship A. While ship B finished the 15 to 15 deg zigzag test in a stable fashion, it could not finish zigzag tests of 7.5-7.5 and 5-5 deg (Fig. 168) in a stable manner (the heading angle was oscillatory, divergent in unstable patterns). For the very unstable ship C, for which heading angle is divergent after the first execution of rudder angle, recovery cannot be achieved by the use of the opposing rudder angle at the second execution. Ship C did finish the 15-15 deg zigzag maneuver test in stable fashion because of the significant contribution of the nonlinear terms.

Since unstable ships cannot finish ordinary zigzag tests in a stable manner when contributions of nonlinear terms are relatively small, as in the case of 5-5 deg zigzag shown in Fig. 168, the modified zigzag can be used to obtain test results in a stable manner for better comparison of capability. Fig. 169 shows predictions of heading angle response during a modified zigzag maneuver in which the rudder angle of 5 deg is shifted to the opposite direction when heading angle deviations reach only 1 deg instead of a heading change equal to the rudder angle. Both ships A and B may thus be acceptable performers in full-scale operations, but ship C remains problematical.

One useful design technique for simultaneously assessing both turning ability and dynamic stability of the hull-propeller-rudder arrangement is to make use of the *Diagram of Steering*. This diagram, based on the design's steady turning motion characteristics, plots rate of turn ( $r'$ ) drift angle ( $\beta$ ), residual speed ratio in the turn ( $V'$ ), and turning diameter ( $STD/L$ ) all against steady rudder angle ( $\delta_R$ ) as shown in Fig. 170.

The diagram of steering is convenient to use in design tradeoff studies since it reflects any significant change in hull configuration or rudder parameters. Tracing the change of the diagram of steering form and principal characteristics ( $\delta_{op}$ , slope of branches, minimum  $STD/L$  ratio, maximum drift angle, maximum angular velocity) the designer can investigate

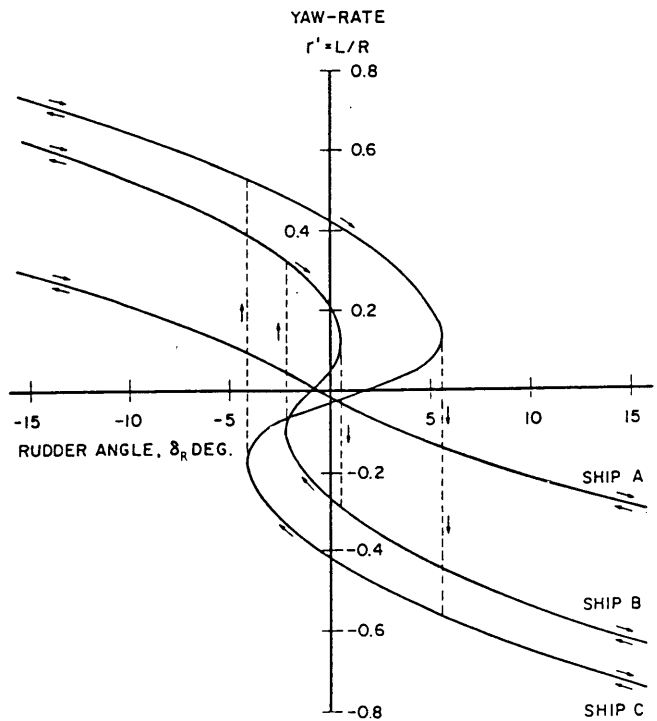


Fig. 167 Steady turning rate versus rudder angle

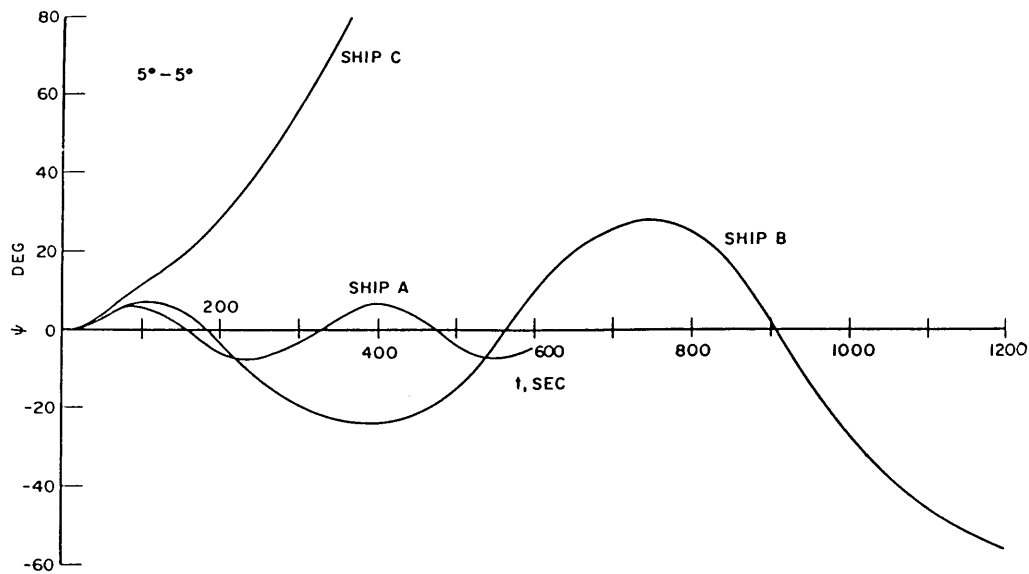


Fig. 168 Zigzag maneuver response: 5-deg/5-deg

the impacts of hull appendages, skeg stabilizers, propeller modifications, and variations in rudder efficiency. For example, Fig. 171 shows several typical situations. In Curve 1, where the zone of instability is large and slope of the branches is small, the ship is slow in response to a rudder angle change when the "meeting rudder" maneuver (opposite rudder ordered to counter turn) is executed. When the zone is smaller (Curve 2) the meeting rudder characteristics are better, as well as all of the other maneuverability parameters. Curve 4 is a design that has more than minimum stability and offers degraded performance over the ship of Curve 3 which also has adequate stability.

The diagram of steering is useful throughout the design cycle for evaluating performance options and can be effectively used in retrofit situations after a vessel has been in service. In the early phases of design, maneuvering prediction models such as those described in Section 16.7, based only on major characteristics, can be used to predict elements of the diagram of steering. As the design is refined, more sophisticated prediction models based on coefficients developed from theory or from model testing can be used. Finally, spiral and turning trials can provide data from the full-scale ship for direct comparison with design predictions.

While greatest attention needs to be placed on the hull-propeller-rudder arrangement in ensuring that the ship shall have the inherent capabilities necessary for a good handling vessel, many other variables are also important. Fig. 172 notes many of the major design variables that have impact on controllability. Variables such as house location and bridge layout with attention to details affecting visibility and ease of operation can

have major affect on the piloted controllability of the vessel. Not all these aspects of design are covered here, but Vantine (1976) provides guidelines on bridge layout to ensure conning effectiveness. Marino and Cooper, (1982), Van Donselaar, et al (1979) and Draft Guidelines (1985) also address the bridge design problem.

Only approximate rules are provided for reader awareness in Fig. 172. Each design presents its own peculiar problems requiring earlier or later detailed analysis of capabilities. The appropriate strategy for solving them will vary depending on ship type, size, cargo route, port situation, and other considerations.

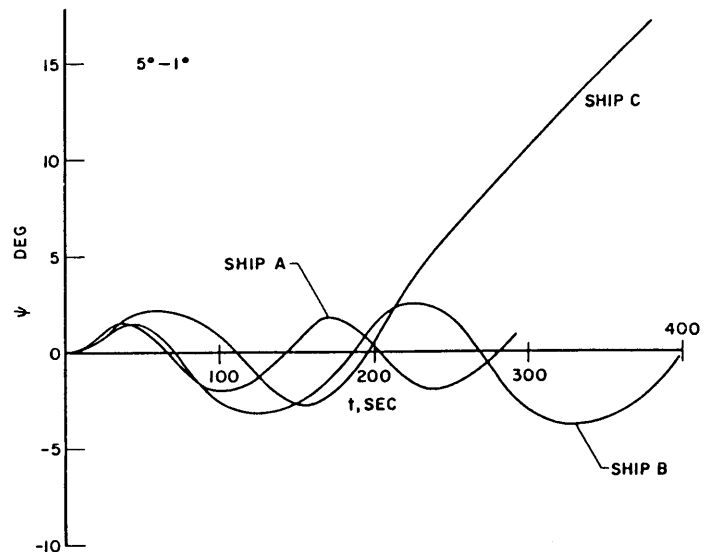


Fig. 169 Zigzag maneuver response: 5-deg/1-deg

Table 22—Controllability

	Level of Design Where Normally Used			
	Concept	Preliminary	Contract	Detail
• <i>Rules of thumb</i> —Rough guides based on individual experience or other commonsense “truisms”	X	X		
• <i>Design guides</i> —Formulas, tables, or figures recommending sizes or desirable parameter ratios and warning of potential problem areas (based on experience of existing vessels, series model tests, or simulation studies). These may be merely somebody else’s published rules of thumb, but at least rules that have been satisfactory for years	X	X	X	
• <i>Design data sheets and engineering principles</i> —Detailed procedures (available generally only for machinery items) and equations for predicting performance, as prepared by groups or recognized experts with technical backgrounds		X	X	X
• <i>Digital computer predictions</i> —Mathematical models (simple or sophisticated) based on similar ship model coefficients used to predict maneuvering trajectory performance		X	X	X
• <i>Free-running self-propelled models</i> —Small models of the new design run in basins with trajectories scaled up to predict at-sea performance		X	X	
• <i>Captive model tests and digital computer simulation</i> —Series of captive model tests [rotating arm and planar motion mechanism (PMM)] using the hull form result in coefficients that are then used in mathematical models to predict maneuvering trajectory performance		X	X	X
• <i>Hydraulic waterway model with self-propelled ship models</i> —Ship models run in accurately modeled waterways to gain knowledge of bank and constrained water effects			X	X
• <i>Man-in-the-loop simulation</i> —Bridge simulations using sophisticated digital computer ship maneuvering models to show trajectory performance when operator variability and performance under stress are included		X	X	X

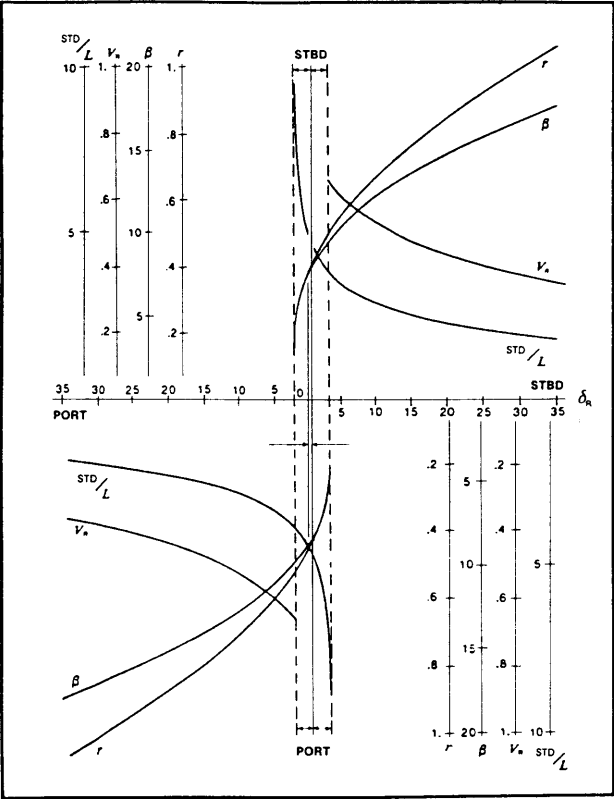


Fig. 170 Diagram of Steering of an unstable ship (Asinovsky, 1989)

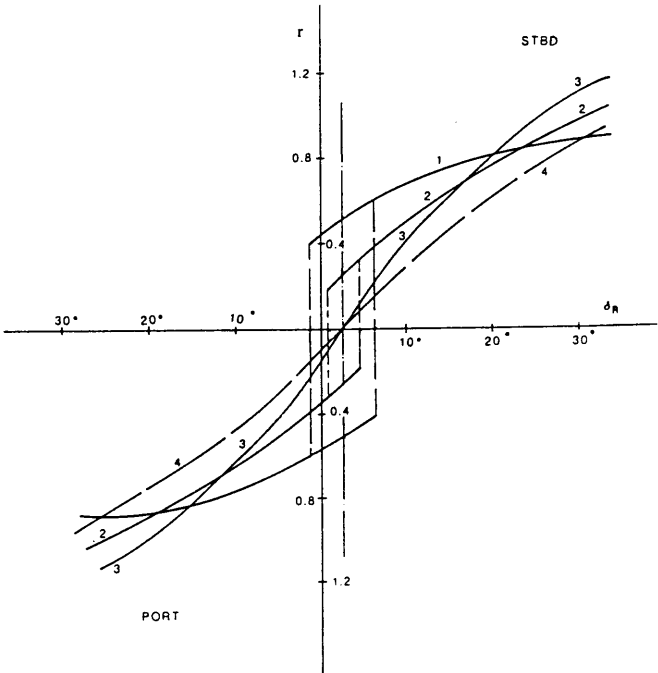


Fig. 171 Transformation of the diagram of steering (Asinovsky, 1989)

Types of design analysis tools may be classified as shown in Table 22. The level of design at which the tools are normally utilized is indicated in the table, but

Table 23—Effect of Increasing Fin Area, Holding Aspect Ratio Constant, or of Increasing Aspect Ratio, Holding Fin Area Constant, on the Hydrodynamic Derivatives, on Controls-Fixed Stability, and on Steady Turning Radius

(a) For Fixed Fins Located Forward of $\overline{XX}$			
Derivative	Effect on the derivative	Effect on stability	Effect on steady turning radius
$Y_v$	more negative (58)	favorable	unfavorable
$N_r$	more negative (59c)	favorable	unfavorable
$N_v$	more negative (less positive) (59a)	unfavorable	favorable
$Y_r$	less positive (59b)	unfavorable	favorable
(b) For Fixed Fins Located Aft of $\overline{XX}$			
$Y_v$	more negative (58)	favorable	unfavorable
$N_r$	more negative (59c)	favorable	unfavorable
$N_v$	less negative (more positive) (59a)	favorable	unfavorable
$Y_r$	more positive (59b)	favorable	unfavorable
(c) For Movable Fins (Rudders) Aft of $\overline{XX}$			
$Y_v$	more negative (58)	favorable	unfavorable
$Y_\delta$	more positive	...	favorable
$N_r$	more negative (59c)	favorable	unfavorable
$N_v$	less negative (more positive) (59a)	favorable	unfavorable
$Y_r$	more positive (59b)	favorable	unfavorable

their actual application may need to be earlier or later in any particular case.

If the design is based on a previous class, the naval architect should review the historic controllability characteristics of that class. These characteristics will be affected by changes in ship geometry, control surfaces provided, propulsion type installed, and the arrangements of the vessel. Because alterations can have large effects, they require thorough analysis.

An evaluation of trade routes and ports of call, to include restrictions present in harbors and approach waters, will help establish the operating environment of the vessel and identify whatever special capabilities may be needed in meeting design operational goals. Various historical and comparative ratios may be useful. Glansdorp (1976) suggested the use of three of these service ratios:

Slow-Speed Service Ratio

$$= \frac{\text{Voyage time in difficult areas at maneuvering speed}}{\text{Total voyage sailing time}}$$

Dense-Traffic-Service Ratio

$$= \frac{\text{Voyage time in areas of dense traffic flows}}{\text{Total voyage sailing time}}$$

Difficult-Geography Service Ratio

$$= \frac{\text{Voyage time in geographically difficult areas}}{\text{Total voyage sailing time}}$$

He also proposed that use of a ship's *risk factor* (or potential for serious difficulties) be considered during design. The factor could incorporate the nature of the cargo and quantity, crew capability, vessel protection, nature of prime mover (nuclear for example), and other items that might affect risk.

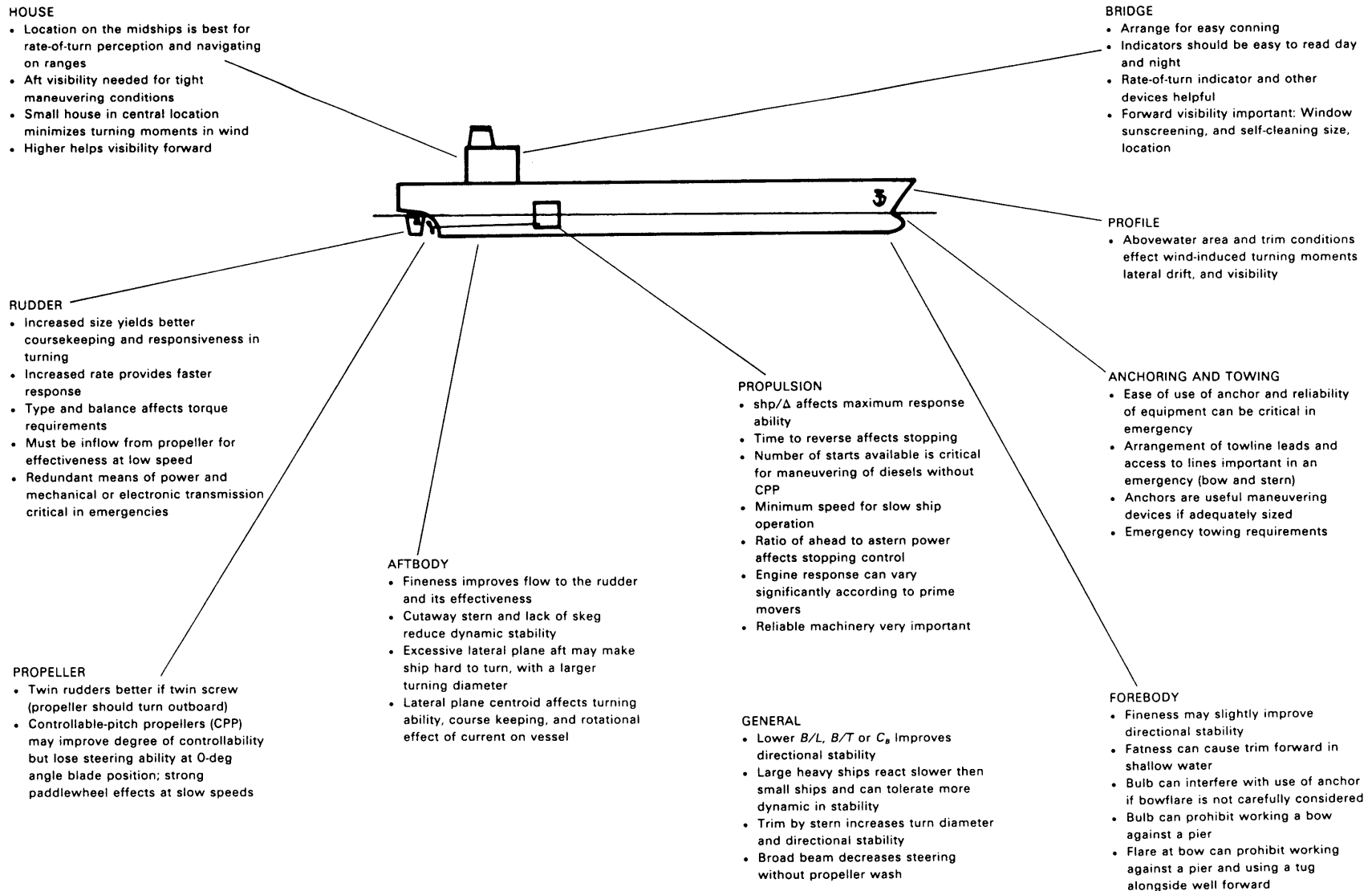


Fig. 172 Some controllability design notes



A particular waterway or special mission such as cable laying may force consideration of a bow or stern thruster for positive control of a vessel at low speeds without tug assistance. For some vessels careful consideration of harbor maneuvering requirements is important at the very beginning of a ship design. Knowing of potential vessel handling difficulties can help the naval architect and owner select a propulsion plant, propeller, and rudder arrangement to improve the handling characteristics of the vessel where difficult maneuvering situations are anticipated. With this knowledge in mind, the owner and designer should list the required vessel handling capabilities, considering items such as:

(a) *Harbor environment:*

- special maneuvering requirements
- location of dock, etc.
- currents or winds
- water depth
- maneuvering speeds
- traffic lane or passage width
- tug assistance and mode of tug use

(b) *Maneuvering devices:*

- bow or stern thruster
- number of propellers
- controllable-pitch propeller
- rudder type and arrangement
- rudder or steering augments
- maximum rudder angle
- rudder rate
- Kort nozzle
- anchors

(c) *Navigating devices:*

- echo sounder
- Doppler sonar
- radar
- SAT NAV (satellite navigator)
- rate of turn indicator

(d) *Manning requirements:*

- deck personnel
- machinery personnel

(e) *Degree of bridge system integration and ease of navigation and controllability related operations*

(f) *Owner experience or preferences in manning, equipment, and maintenance policies.*

Although a guide to analyzing performance of a design is presented here, specific requirements and standards to be met using the criteria described in the previous section are currently few. Generally the standard for performance will be that the vessel operate in a fashion similar to that of a previous design.

With the recent proliferation of special-purpose ships and with the increased concern for safety and environmental protection, careful attention must be paid to controllability design. This attention often needs to start in the early stages of design, and it may lead to performing model tests to establish acceptability. Even before a hull shape is defined, decisions

made about principal dimensions can have serious effects on controllability.

The next three parts of this section (16.2, 16.3, and 16.4) will describe the effects of major design parameters on controllability. The process of comparing with an existing design and using basic characteristics to predict performance capability will be addressed in Part 16.5. An example prediction method for determining dynamic stability will be presented in Part 16.6. Use of trajectory prediction models based on major characteristics, and the more advanced approaches using model testing and design-oriented modular models will follow in Parts 16.7 and 16.8. Finally, in Part 16.9, shiphandling simulation involving man-in-the-loop considerations will be addressed as a design tool for both ships and waterways.

**16.2 Effect of Fixed and Movable Fins on Controls-Fixed Stability and on Turning** Equations (58), (59a-c) permit evaluation of the effect of fin area, aspect ratio, and location on the major stability derivatives. This information, in conjunction with that in Table 1, can be used to determine the qualitative effect on controls-fixed stability and on the radius of the steady turn within the range where linear theory is applicable.

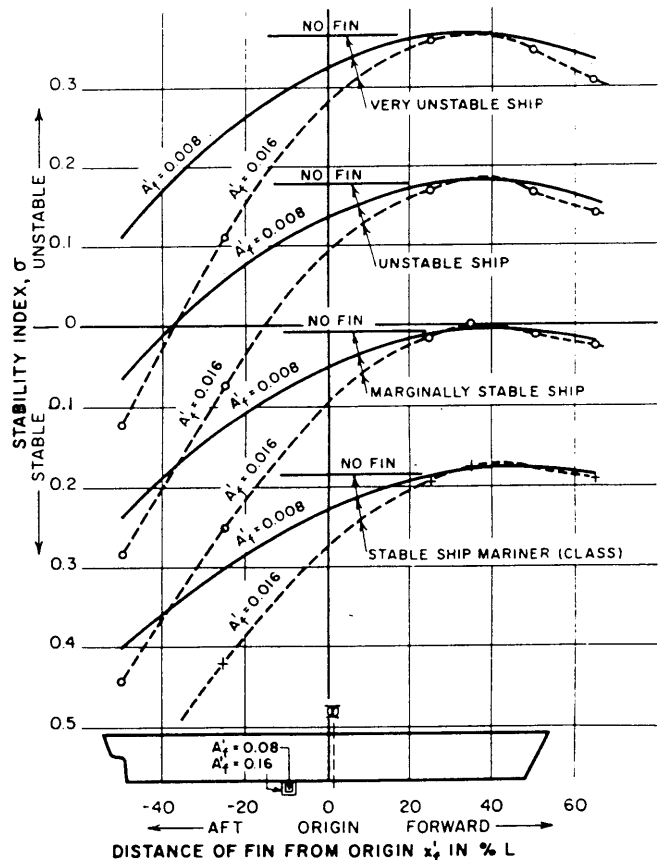


Fig. 173 Effect of fin area and fin location on controls-fixed stability for typical ships

This information is summarized in Table 23 for three common situations:

- Fixed fins located forward of the midlength.
- Fixed fins located aft of the midlength.
- Movable fins (rudder) located aft of the midlength.

In all three of these situations, the qualitative effects on the hydrodynamic derivatives (not on stability and turning) of increasing fin area or fin aspect ratio at a fixed location or of moving a fin of constant area and aspect ratio toward the extremities of the ship are the same, except for the effect of  $Y_r$  and  $Y_\delta$ . While these two derivatives increase negatively (decrease algebraically) with increased fin area and aspect ratio, they are independent of fin location. Thus while (a) and (b) of Table 23 show that adding fin area anywhere along the ship length may improve stability, they also show that moving a fin of constant area and aspect ratio forward may impair stability because the favorable effect of a negative increase in  $Y_v$  is lost.

These effects are illustrated by the computed results shown in Fig. 173 for the stable *Mariner* Class, the marginally stable, the unstable, and the very unstable hull forms described in Section 8.7 and Fig. 45. The effect of added fin area and changes in fin location were computed from Equations (14a), (122b), (58), (59a-c), (62a-c), and (78). The two fin areas,  $A'_f = 0.008$  and  $0.016$ , were in both cases assumed to have a square profile as shown in Fig. 173; that is, both have an effective aspect ratio of 2.0. It is seen in Fig. 173 that, for these hull forms, adding fin area anywhere along the model length except in the region of the bow improves stability compared to the no-fin case but with much diminished effect as the fin is moved forward. Furthermore, the stability is diminished as a fin of constant area is moved forward until a location close to the bow is reached corresponding to the pivot point discussed in Section 6.1. At this point, adding fin area tends to impair stability very slightly.

Fig. 174 shows corresponding information for the linear turning parameter  $\partial r' / \partial \delta_R$  whose most meaningful physical interpretation in the current context is degrees change of heading per ship length of travel per degree rudder deflection.

As explained in Section 6.4, a negative  $\partial r' / \partial \delta_R$  is associated with stable ships, and a positive  $\partial r' / \partial \delta_R$  with unstable ships. The following equation developed from Equation (26a) was used to compute  $\partial r' / \partial \delta_R$ :

$$\frac{\partial r'}{\partial \delta_R} = \frac{N'_v Y_\delta - Y'_v N'_\delta}{C} \quad (127)$$

Figure 169 like Fig 173, confirms the trends noted in Table 23(a, b). It also shows that locating the fin anywhere between the bow and forward quarter point of the stable and marginally stable ships improves turning relative to the no-fin case. Furthermore, increasing fin area in this vicinity has a small favorable

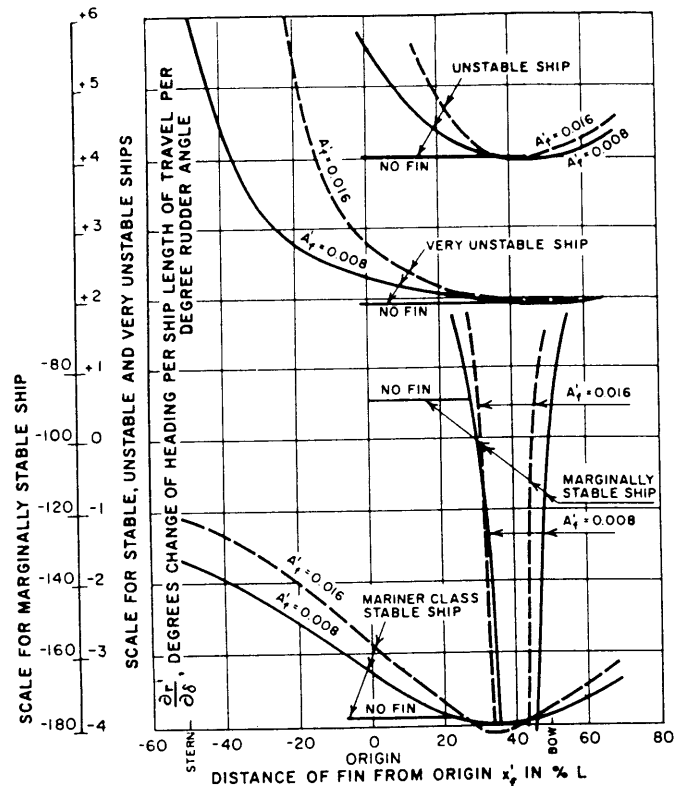


Fig. 174 Effect of fin area and fin location on  $\partial r' / \partial \delta$  for typical ships

effect on turning. These effects are not, however, displayed by the unstable and very unstable ships of Fig. 174, which shows that they are not universally applicable.

The effect of fin location on  $\partial r' / \partial \delta_R$  for the marginally stable ship in Fig. 174 is extraordinarily pronounced near the bow. This relationship arises from the fact that according to the figure the stability index and hence the stability criterion  $C$  hovers near zero for fins located in this region. Since in (127) the expression for  $\partial r' / \partial \delta_R$  contains only  $C$  in the denominator, it increases without limit as  $C$  approaches zero. This pronounced effect on  $\partial r' / \partial \delta_R$  predicted by linear theory is not observed in practice, for strong nonlinear effects take effect as the angular velocity departs substantially from zero. Thus, according to the nonlinear results shown in Fig. 45, the angular velocity at  $\delta_R = 10$  deg is not significantly different for the marginally stable ship as compared to the stable ship.

A practical example of the effect of adding forward profile area in the form of "filling" in the forefoot of a ship is shown in the comparison between Models 60P2 and 60P1 in Table 24 taken from Eda and Crane (1965). The experimental values of the derivatives follow precisely the trends indicated in Table 23. In this case the stability is slightly improved by the additional forefoot area and presumably the turning would be impaired

slightly. This result is in accord with those shown in Table 23. The slight improvement in stability is due entirely to the very large increase in  $Y_r$ . If the value of  $Y_r$  for Model 60P1 were assumed to be intermediate between those of Models 60P2 and 2,1,1, its stability would be almost identical to that of Model 60P2.

Another practical example is noted by Arontzen and Mandel (1960). There the effect of a fairwater (sail) on the controls-fixed stability in the horizontal plane of a submarine in the submerged condition is also shown to be favorable. In this case, the centroid of the fairwater profile area was located about 15 percent of the length of the submarine forward of its midlength.

Table 23(b) shows that the effects on all of the derivatives of increasing the area of a fixed fin aft or of

increasing its aspect ratio are decidedly favorable to controls-fixed stability and unfavorable to the radius of the steady turn. Figs. 173 and 174, show similar effects for moving a fin of constant area and aspect ratio aft. All of these effects, except that on  $Y_r$ , are confirmed for practical changes in ship profiles aft by the comparison between Model 2,1,1 and Model 60P1 in Table 24. Figs. 52 and 53 also show quantitative evidence of the favorable effect on the stability index of fixed fin area aft added in the form of skeg area. Fig. 175 shows similar evidence for fin area added in the form of rudder area (see Fig. 54) rather than skeg area.

Bilge keels are another example of additional fixed fin area. These usually improve stability, but their effect on turning depends on their fore-and-aft location and on their longitudinal extent.

The effect of changes in trim of a ship may be predicted on the basis of fin area considerations. Trim by the stern results in additional profile area aft, which is favorable to stability and unfavorable to turning, and in reduced profile area forward, which has little effect on either stability or turning. On the other hand, trim by the bow decreases profile area aft which has a decidedly unfavorable effect on stability and a favorable effect on turning, while the increased profile area forward has little effect on either.

The fact that the addition of fixed fin area of constant aspect ratio aft has the universal effect of improving stability but impairing turning and the fact that increasing the stability criterion  $C$  impairs turning according to linear theory have led to the generally held belief concerning ships—that good stability and good turning are mutually incompatible qualities; that changes made to improve one of these qualities inevitably impair the other. Table 23(c) shows however, that if the increase in aft fin area or aspect ratio is due to a change in movable rudder characteristics rather than to a change in fixed fin characteristics, the additional area or aspect ratio not only has a decidedly favorable effect on stability but may also have a favorable effect on turning. This possibility is shown in Fig. 213.

However, the trends determined from the linear theory displayed in Table 23(c) show that the effect of increasing rudder area, holding aspect ratio constant, on each of the derivatives, is not universally favorable as far as turning is concerned; only the effects of  $Y_s$  and  $N_s$  are favorable. Hence, it is entirely possible that in some cases increasing the rudder area and holding aspect ratio constant will not improve turning.

To summarize, four important conclusions based on linear theory but also borne out in practice have been reached in this subsection:

(a) Adding fixed fin area and holding aspect ratio constant, either aft or forward, has a favorable effect on stability but with vanishing effect as the fin location approaches the pivot point.

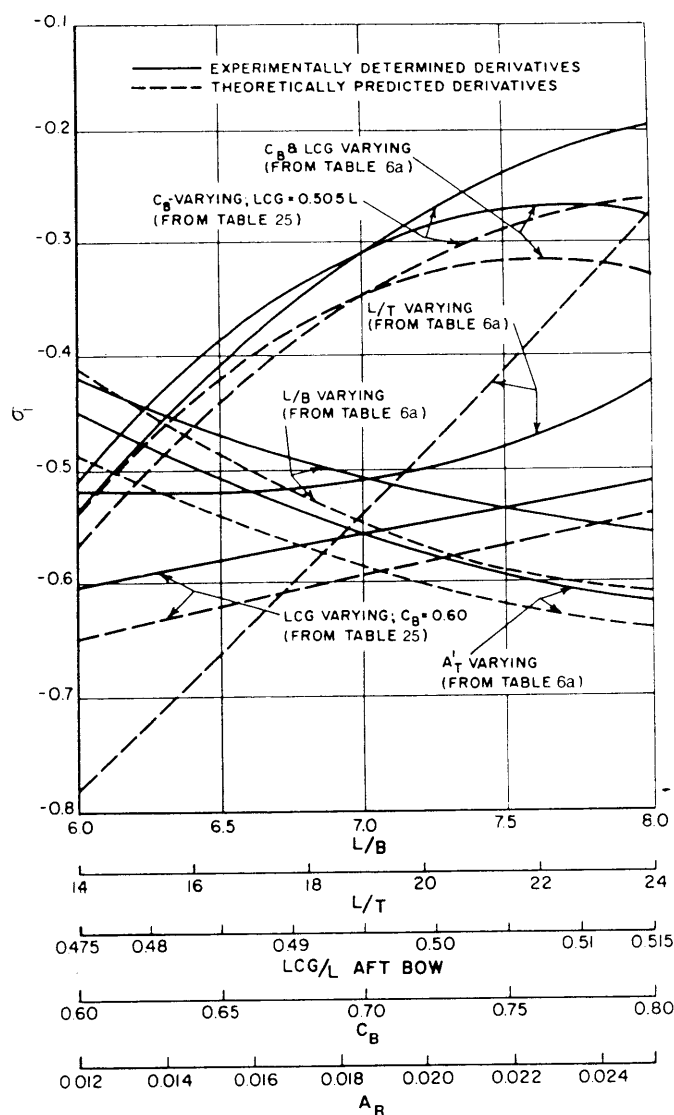


Fig. 175 Effect of hull-form parameters and rudder area on stability index  $\sigma_1$ ; Series 60 with propeller and rudder

(b) Adding fixed fin area aft or increasing fixed fin aspect ratio aft has a decidedly unfavorable effect on turning. Adding fixed fin area or increasing fixed fin aspect ratio in the vicinity of the pivot point may improve turning.

(c) The qualities of controls-fixed stability and small turning radius are not necessarily incompatible either in theory or in practice, and a ship may in fact possess both qualities in superior measure.

(d) Increasing rudder area does not in all cases reduce the turning radius of a ship.

The preceding are the important direct effects of fixed and movable fins on stability and turning. Fixed fins can also exert important indirect effects on stability and turning. For example, fixed fins in the form of skegs like those shown in Fig. 52 strongly influence the magnitude of the straightening effect,  $\epsilon$ , (see Fig. 22) and hence influence the rudder force and moment exerted during steady turns. Experimental data reported by Eskigian (1956) for Model 842 of Table 5, fitted with twin screws, show that for rudders located on the centerline with their midchord about  $0.45L$  aft of  $\bar{X}$ , the straightening effect,  $\epsilon$ , amounts to:

(a) 20 percent of the geometric drift angle at the rudder for the ease of no skeg.

(b) 55 percent of the geometric drift angle for the case of a skeg extending to within  $0.08L$  of the leading edge of the rudder.

(c) 70 percent of the geometric drift angle for a skeg extending to within  $0.03L$  of the rudder.

**16.3 Effect of Hull Configuration on Controls-Fixed Stability.** Jacobs (1964) and Eda and Crane (1965) describe an extensive study of the effect of hull shape and proportions on controls-fixed stability, based on systematic variations of the Series 60 form. Results are given in Tables 6, 24, and 26, and some of the data are plotted in Figs. 175 and 176. Three general trends concerning hull shape and proportions are displayed in these figures, both by theoretical predictions and by experimental results using models without rudder and propeller and models with rudder and propeller.




(a) Stability is in general impaired as the block coefficient is increased.

(b) In almost all cases, the stability index is improved by increasing the  $L/B$  ratio.

(c) In almost all cases, stability is impaired by increasing the  $L/T$  ratio, i.e., by decreasing the draft. Theory seriously overpredicts this effect compared to experiment, but the trends are the same.

The block coefficient ( $C_B$ ) series shown in Table 6 includes a substantial variation in LCG ( $0.475L$  to  $0.515L$  aft of the bow) associated with the primary variation in block coefficient. The more forward location of LCG is associated with the large  $C_B$  while the aft location is associated with the low  $C_B$ . These LCG locations stem from minimum resistance consideration and are in accord with usual ship design practice. In order to show the separate effects of these two variations on the stability index, use was made of Equations (14) and (14a) which permit evaluation of the effect of LCG location on the stability index. The results of these calculations showing the stability index as a function of LCG location for a constant block coefficient ( $C_B = 0.60$ ) and showing the stability index as a function of  $C_B$  value for a fixed LCG position ( $0.505L$  aft) are tabulated in Table 25 and plotted in Figs. 175 and 176. These figures show that the generally unfavorable effect on the stability index of increasing the block coefficient, evident in Table 6, is accentuated if the LCG location is held compared to the case where the LCG location is moved forward. In Table 25 the origin location remains unchanged for each of the three models, but the physical characteristics of the three models, but the physical characteristics of the three models are assumed to be changed by the change in the location of the center of gravity. Hence the results show, as they should, that the stability index is affected by the change in LCG location. However, as long as the location of the origin is not changed, the values of the hydrodynamic derivatives

Table 24—Experimentally Determined Effects of Changes in Profile Area and in Profile Area Distribution on the Hydrodynamic Derivatives

Model	60P2	60P1	2.1.1
Description			
Bow cutaway <sup>a</sup> per cent $L \times T$	1.12	0.15	0.15
Stern cutaway <sup>a</sup> per cent $L \times T$	1.88	1.88	0.97
$Y'_v$	-0.284	-0.315	-0.305
$N'_v$	-0.108	-0.126	-0.0954
$Y'_r$	+0.0542	+0.577	+0.0896
$N'_r$	-0.0621	-0.0718	-0.0701
$\sigma_1$	-0.19	-0.25	-0.51

<sup>a</sup> Relative to a rectangle of length  $L$  and width  $T$ .

Table 25—Stability Index and Turning Parameter  $\partial r'/\partial \delta$  as a Function of LCG Location and Block Coefficient—Series 60

Model		2,1,1 0.60			7,1,1 0.70		8,1,1 0.80	
$C_B$		0.515			0.505		0.475	
LCG/L from Table (7)		0.475	0.505	0.515	0.505		0.475	0.505
Selected variation of LCG/L		+0.040	+0.010	0	0		0	-0.030
Corresponding $x'_G$		+0.015	+0.015	+0.015	+0.005		-0.025	-0.025
Corresponding $x'_R$		-0.65	-0.57	-0.54	-0.35		-0.33	-0.26
$\sigma_1$ with rudder and propeller	Theory	-0.60	-0.53	-0.51	-0.31		-0.28	-0.20
	Exper.	-0.60	-0.53	-0.51	-0.31		-0.28	-0.20
$\sigma_1$ without rudder and propeller	Theory	-0.25	-0.17	-0.15	+0.03		+0.005	+0.06
	Exper.	-0.07	-0.10	-0.08	+0.07		+0.03	+0.09
$\partial r'/\partial \delta$ with rudder and propeller	Theory	-0.60	-0.66	-0.68	-0.94		-0.80	-1.03
	Exper.	-0.77	-0.85	-0.88	-1.44		-2.03	-2.99

given in Table 6 apply without change, regardless of LCG location.

To gain insight into the effect of hull parameters on the stability index, it is useful also to examine their effect on the hydrodynamic derivatives. Table 6 shows, for example, that an increase in the length-beam ratio causes hardly any change in the theoretical values of the hydrodynamic derivatives but does cause a substantial decrease in the mass coefficient,  $\Delta'$ .

With a fixed-length model, changes in the  $L/B$  ratio must be accompanied by either changes in the  $B/T$  ratio or in the  $L/T$  ratio. The latter ratio is, however, considered to be of far greater importance insofar as the effect on the stability derivatives in the horizontal plane is concerned. Therefore, the  $L/T$  ratio appears as a separate series in Table 6, but both it and the  $L/B$  series also involve changes in the  $B/T$  ratio.

In accord with Table 1, the decrease in mass coefficient improves stability as the  $L/B$  ratio is increased. In view of the scatter in the experimental values of the hydrodynamic derivatives of Table 6, they cannot be said to confirm the theoretical results; but neither do the experimental data exhibit any consistent trend with the  $L/B$  ratio that disagrees with the theoretical results. It is therefore concluded that the major effect of increasing the  $L/B$  ratio is to decrease the mass coefficient, which in turn improves stability.

The theoretical and experimental values of the derivatives of Table 6 show that the effects of increasing the length-draft,  $L/T$ , ratio are:

- $Y'_v$  is less negative (destabilizing)
- $N'_v$  is less negative (stabilizing)
- $N'_r$  is less negative (destabilizing)

The theoretical values of  $Y'_r$  becomes less positive (also destabilizing according to Table 1) with increasing  $L/T$  ratio, but the experimental values exhibit a very small opposite trend. The value of  $\Delta' = \Delta/(\rho/2)L^2T$  did not change with the  $L/T$  ratio in Table 6 because  $\Delta$  was changed in direct proportion to  $T$ . Since the changes in at least two of the derivatives are destabilizing and the change in only one derivative is stabilizing, the stability is impaired as the length-draft ratio is increased. Thus, a ship at light draft will have less controls-fixed stability than the same ship at

deep draft, provided the trim by the stern in the light draft condition is not greater than in full load condition.

The experimental data of Fig. 175 show the interesting fact that the change in relative rudder area  $A'_R$

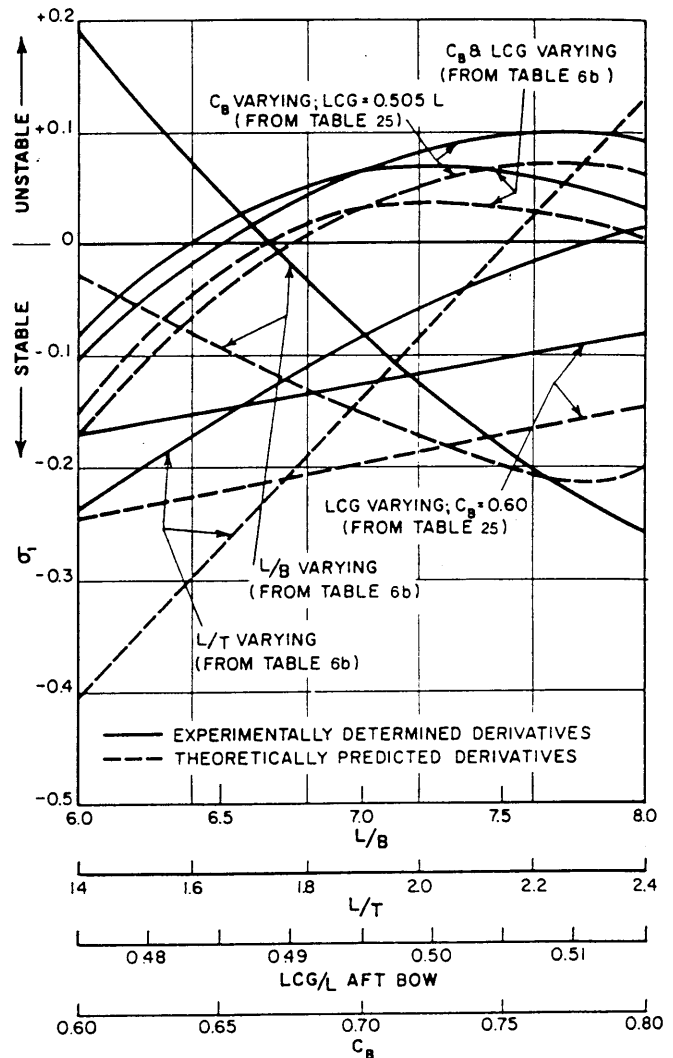


Fig. 176 Effect of hull-form parameters on stability index  $\sigma_1$ ; Series 60 bare hull

Table 26—Effect of Ship Section Shape on the Hydrodynamic Derivatives and on the Stability Index

Model No. from Table 10 Section Shape How Determined Condition Reference No.	1,1,1 Normal Experiment —(Eda and Crane, 1965)—	9,1,1 Vee Theory	1,1,1 Normal Theory	9,1,1 Vee Theory	1,0,0 Normal Experiment —Without Propeller and Rudder— (Jacobs, 1964)	9,0,0 Vee Theory	1,0,0 Normal Theory	9,0,0 Vee Theory
$Y'_v$	-0.270	-0.266	-0.335	N.A.	N.A.	N.A.	-0.303	N.A.
$N'_v$	-0.108	-0.117	-0.088	N.A.	N.A.	N.A.	-0.112	N.A.
$Y'_r$	+0.088	+0.081	+0.077	N.A.	N.A.	N.A.	+0.052	N.A.
$N'_r$	-0.067	-0.075	-0.066	N.A.	N.A.	N.A.	-0.055	N.A.
$\sigma_1$	-0.41	-0.39	-0.59	-0.62	N.A.	-0.17	-0.20	-0.17

from 0.012 to 0.024 exerts greater influence on the stability index than do the displayed changes in the  $L/B$  and  $L/T$  ratios. From a practical design point of view, it is therefore usually preferable to attempt to alter controls-fixed stability by adjusting rudder area or fin area rather than by changing the basic dimensions of a ship.

Table 26 shows that a change in the section shape from normal Series 60 shape to an extreme Vee shape, in ships of normal proportions ( $L/B = 7.5$ ,  $L/T = 18.75$ ,  $C_B = 0.60$ ), has little effect on the hydrodynamic derivatives or on the stability index. This result is obtained whether the derivatives are determined experimentally or calculated theoretically and whether the model is equipped with rudder and propeller or not.

To show the effect of block coefficient on the hydrodynamic derivatives, it is necessary to correct the latter values given in Table 6 so that they apply to a

common origin. The common origin selected for all three block coefficients was the  $0.505L$  position of the LCG of Model 7. The values of the derivatives about this origin were computed by the following equations, which can be derived from Equations (14a-c):

$$(Y'_v)_{0.505} = (Y'_v)_{0.475, 0.515}$$

$$(N'_v)_{0.505} = (N'_v)_{0.475, 0.515} - (Y'_v)x'$$

$$(Y'_r)_{0.505} = (Y'_r)_{0.475, 0.515} - (Y'_v)x'$$

$$(N'_r)_{0.505} = (N'_r)_{0.475, 0.515} - (Y'_v)x'^2 - (Y'_r)_{0.505}x' - (N'_v)_{0.505}x'$$

where

(a) The numerical subscripts refer to the origin location as function of the ship length.

Table 27—Stability Derivatives, Stability Indexes, and Turning Parameter  $\partial r'/\partial \delta_r$  as a Function of Block Coefficients—Series 60

(Fixed Origin and LCG;  $x'_G = 0$ ;  $x'_{CG} = +0.005$ )

(a) Model With Propeller and Rudder

Model $C_B$ $\Delta'$	2 0.60 0.171	7 0.70 0.200	8 0.80 0.229
	Theory	Theory	Theory
$Y'_v$	-0.335	-0.335	-0.335
$N'_v$	-0.083	-0.097	-0.105
$Y'_r$	+0.079	+0.075	+0.079
$N'_r$	-0.066	-0.068	-0.077
$\sigma_1$	-0.57	-0.35	-0.26
$C'_1 \times 10^2$	+1.45	+1.07	+1.00
$Y'_\delta$	+0.038	+0.038	+0.038
$N'_\delta$	-0.019	-0.019	-0.019
$\partial r'/\partial \delta$	-0.67	-0.94	-1.03
	Exper.	Exper.	Exper.
$Y'_v$	-0.305	-0.324	-0.354
$N'_v$	-0.092	-0.104	-0.097
$Y'_r$	+0.093	+0.083	+0.075
$N'_r$	-0.070	-0.066	-0.060
$\sigma_1$	-0.53	-0.31	-0.20
$C'_1 \times 10^2$	+1.41	+0.92	+0.63
$Y'_\delta$	+0.050	+0.052	+0.065
$N'_\delta$	-0.024	-0.025	-0.035
$\partial r'/\partial \delta$	-0.85	-1.44	-2.99

(b) Model Without Propeller or Rudder

$Y'_v$	-0.303	-0.245	-0.306	-0.287	-0.309	-0.256
$N'_v$	-0.107	-0.112	-0.121	-0.121	-0.130	-0.101
$Y'_r$	+0.055	+0.072	+0.051	+0.051	+0.055	+0.067
$N'_r$	-0.054	-0.055	-0.056	-0.056	-0.066	-0.053
$\sigma_1$	-0.17	-0.10	+0.03	+0.07	+0.06	+0.09

(b)  $x' = +0.010$  in the case of Model 2 ( $C_B = 0.60$ ) where the origin initially is at  $0.515L$  aft of the bow.

(c)  $x' = -0.030$  in the case of Model 8 ( $C_B = 0.80$ ) where the origin initially is at  $0.475L$  aft of the bow.

The results of these computations are shown in Table 27. The values of the stability indexes shown in Table 27 are of course identical to the values shown in Table 25.

Table 27 reveals the following trends:

(a)  $Y'_v$ —Theory indicates no significant change with  $C_B$ . Experimental results with propeller and rudder show that  $Y'_v$  increases negatively with increasing  $C_B$ . This is a stabilizing trend.

(b)  $N'_v$ —Theory indicates that it should increase negatively (destabilizing), but experimental values do not in some cases confirm this trend.

(c)  $Y'_r$ —Theory indicates no consistent trend, but the experimental data for the model with propeller and rudder show a decrease in the positive value of this derivative with increasing  $C_B$ . This is a destabilizing trend.

(d)  $N'_r$ —Theory indicates that it should increase slightly in negative value (stabilizing), but the experimental values show a slight opposite trend.

The preceding trends indicate that the reduction in stability associated with an increase in block coefficient, as shown in Figs. 175 and 176, results largely from the increase in the mass coefficient  $\Delta'$  associated with increased  $C_B$  and not from changes in the hydrodynamics derivatives. This same conclusion was reached in evaluating the effect of the  $L/B$  ratio. On

this basis Jacobs (1964) merged the effects of  $C_B$  and  $L/B$  and chose to display  $\sigma$  as a function of  $\Delta'$  with the  $L/T$  ratio as a parameter. The pertinent data are tabulated in Table 28 and plotted in Fig. 177.

Jacobs fitted the following empirical expression to the data shown in Fig. 177(b) which she suggested was appropriate for stable ships with large skegs at the stern:

$$\sigma_1 \approx -\left(\frac{5}{\Delta' - Y'_v L/T}\right)^{2.5} \quad (128)$$

This relationship is also plotted in Fig. 177 where it agrees reasonably well with the  $\sigma$ -values computed from the theoretically calculated derivatives.

Equation (128) has three major weaknesses that seriously limit its applicability:

(a) Although it ostensibly depends only on  $\Delta'$ ,  $Y'_v$ , and the  $L/T$  ratio, it also includes the spurious effect of a variation in  $LCG/L$  as discussed in this section.

(b) It fails to include the effects of differences of fin area, rudder area, and propeller influences, which are important even in stable ships.

(c) It applies only to stable ships; it cannot, therefore, predict whether a given design will be stable or unstable, which is often the important question in design.

Hence, the equations of Section 9 are preferable for use in predicting the controls-fixed stability of a new design.

**16.4 Effect of Hull Configuration on Nonlinear and Linear Maneuvers.** Because of the high cost of the experiments needed to predict nonlinear maneuvers and because of the lack of universality of the results of those experiments, the effect of hull configuration on nonlinear maneuvers has not been extensively studied. Two of the available studies, Shiba (1960) and Davidson Lab (1965), report results of free-running model tests. Eda and Crane (1965) employ a simplified version of the nonlinear equations of motion [(36), (37), and (38)] along with results of rotating-arm experiments. The limited number of terms included in the nonlinear equations are shown in Table 4.

Steady turning diameters as a function of hull configuration taken from these sources (at a constant rudder angle of 30 deg) are compared in Table 29 with two results predicted from linear theory Equation (26a). The first linear theory result uses the experimental derivative values given in Tables 6(a)2 and 27. The second linear theory result uses the theoretical derivative values given in Table 6(a)1 and 27. [The partial derivative  $\partial r'/\partial \delta_R$  of Table 6(a) is related to  $D/L$  at  $\delta_R = 30$  deg in Table 29 by the expression,

$$D/L = \frac{2}{\frac{\partial r'}{\partial \delta_R} \times \frac{30}{57.3}}]$$

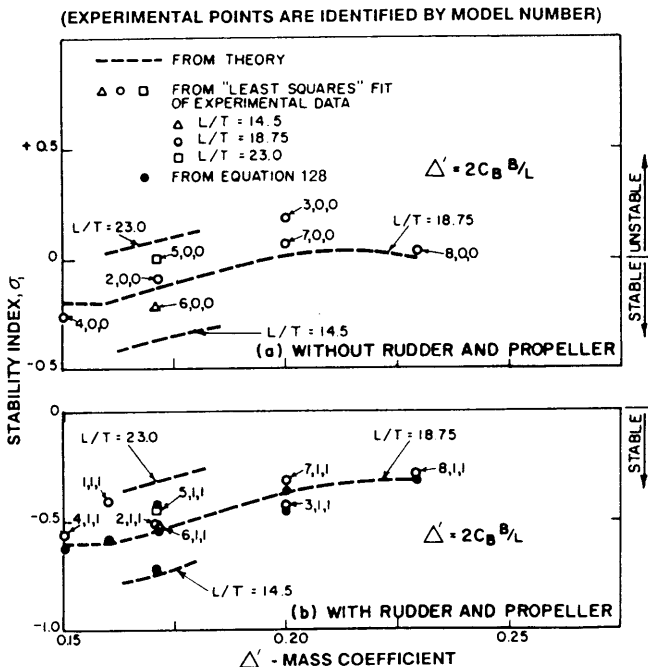


Fig. 177 Stability index  $\sigma$ , as a function of mass coefficient  $\Delta'$ , Series 60

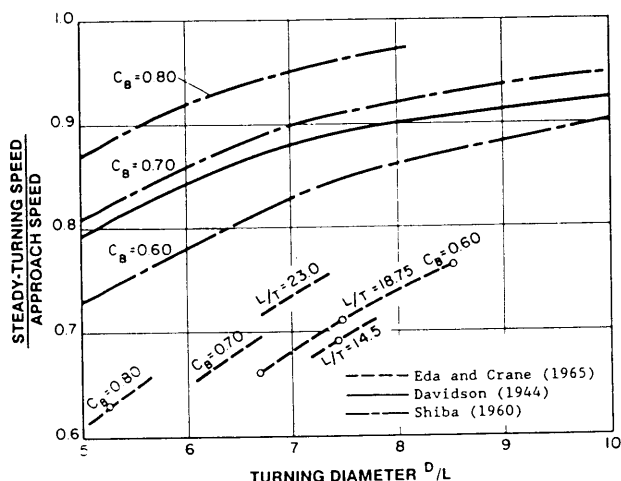


Fig. 178 Speed reduction in a turn as a function of turning diameter and hull configuration

In the case of the block-coefficient variation, all sources except the second linear theory agree that an increase in block coefficient significantly improves turning. Examination of Equation 26(a) and of the experimental derivative values in Table 6(a)2 shows that the decrease in turning diameter with increasing  $C_B$  is associated with two factors:

- 1 The reduction in the stability criterion  $C$ .
- 2 The large increase in  $N'_s$  and  $Y'_s$ .

Of these two factors, the first is the more important. The second factor is caused by the more highly loaded propeller on a single-screw ( $C_B = 0.80$ ) ship compared to a single-screw ( $C_B = 0.60$ ) ship as shown in Fig. 128. Because the theoretical method developed in Section 9 ignores propeller interaction, the results of the second linear theory shown in Table 29 do not confirm the general trend. Interesting to note is that this effect of block coefficient on turning would not be duplicated on multiple-screw ships if the rudders were not located in the propeller race.

While there is some disagreement in Table 29(a) concerning the effect of  $L/B$  ratio on turning, both the trends and the magnitudes shown by the free-turning tests of Davidson Lab (1965) agree remarkably with results from the second linear theory. The opposite trend exhibited by the linear predictions based on the experimental derivatives of Table 6(a)2 is caused by the exceptionally poor stability of the ( $L/B = 7.5$ ) model compared to that of the ( $L/B = 7.0$ ) and ( $L/B = 8.0$ ) models shown in Table 6(a)2 [see also Table 28 and Fig. 177(b)]. This trend may be delusive, for it is not confirmed by the theoretical derivatives of Table 6(a)1. It is concluded from Table 29(a) that while low values of  $L/B$  are favorable for turning, the effect of increasing the  $L/B$  ratio to very high values is also somewhat favorable.

As for the effect of  $L/T$  ratio, Table 29(a) again

shows remarkable agreement between the free-turning results of Davidson Lab (1965) and the second linear theory. The improvement in turning caused by increasing the  $L/T$  ratio as well as by moving the LCG aft is associated with the impairment of stability caused by these two changes as shown in Fig. 175.

As far as the effect of profile shape is concerned, Table 6(a) shows that the linear theory based on the experimental derivatives of Table 24 exaggerates the favorable effect of cutting away stern area compared to the results from Davidson Lab (1965).

The data shown in Table 29(b) taken from several sources and the data shown in Fig. 219 taken from Shiba (1960) display clearly the saturation effect reached as rudder area is increased. Shiba (1960) associates this anomaly entirely with the decrease in rudder aspect ratio as rudder area is increased, and Table 29(c) shows that the magnitudes of  $Y'_s$  and  $N'_s$  do decrease for the largest rudder area. As noted in Section 16.2, however, this is not a necessary condition for the existence of the anomaly, and in principle it can be encountered even when rudders of constant aspect ratio are increased in area. Further discussion of the important information shown in Fig. 219 is contained in Sections 17.4 and 17.5.

Fig. 178 shows data on speed loss in a turn. The data from Eda and Crane (1965) disagree quantitatively with the data from the other sources largely because of the very limited number of terms included in their  $X$ -equation [see Table 4(a)]. The trends, however, from all three references do agree. For example,

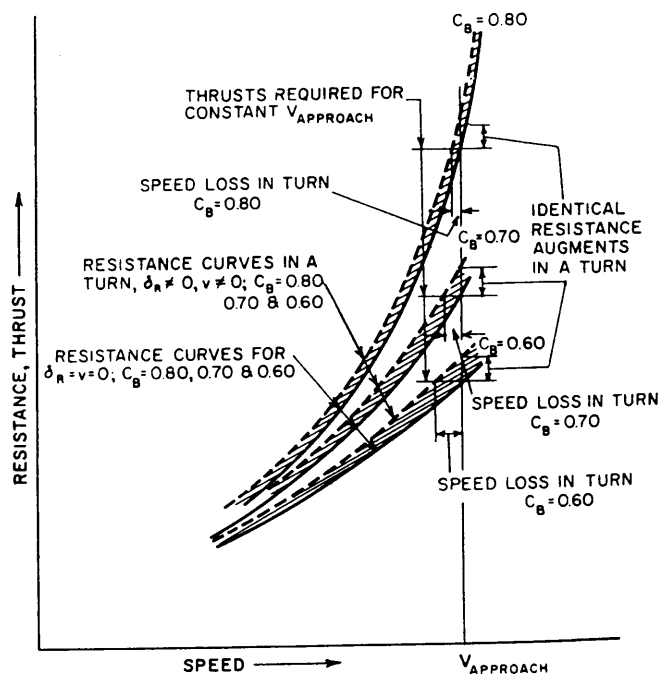


Fig. 179 Effect of block coefficient on speed loss in a turn



Table 28—Stability Index as a Function of Mass Coefficient and  $L/T$  Ratio

$\Delta'$	$C_B$	$L/B$	$L/T$	$A'_R$	$LCG/L$	With propeller and rudder				Without propeller and rudder		
						Davidson Laboratory Model No.	Stability index, $\sigma_1$			Davidson Laboratory Model No.	Stability index $\sigma_1$	
							Theory Table 6(a)1	Equation (128)	Exper. Table 6(a)2		Theory Table 6(b)1	Exper. Table 6(b)2
0.150	0.60	8.0	18.75	0.016	0.515	4,1,1	-0.61	-0.63	-0.56	4,0,0	-0.20	-0.26
0.160	0.60	7.5	18.75	0.016	0.515	1,1,1	-0.59	-0.58	-0.41	1,0,0	-0.20	N.A.
0.171	0.60	7.0	14.50	0.016	0.515	6,1,1	-0.76	-0.73	-0.52	6,0,0	-0.38	-0.22
0.171	0.60	7.0	18.75	0.016	0.515	2,1,1	-0.55	-0.54	-0.51	2,0,0	-0.15	-0.09
0.171	0.60	7.0	23.00	0.016	0.515	5,1,1	-0.33	-0.42	-0.45	5,0,0	+0.075	-0.045
0.200	0.60	6.0	18.75	0.016	0.515	3,1,1	-0.41	-0.45	-0.42	3,0,0	-0.03	+0.19
0.200	0.70	7.0	18.75	0.016	0.505	7,1,1	-0.35	-0.41	-0.31	7,0,0	+0.03	+0.07
0.229	0.80	7.0	18.75	0.016	0.475	8,1,1	-0.33	-0.32	-0.28	8,0,0	+0.005	+0.03

Table 30—Computed ZigZag Maneuver Responses as Functions of Ship Configuration [from Eda and Crane (1965)]  
( $L = 152$  m (500 ft),  $V = 14.8$  kts,  $\delta_R = 20$  deg)

Series	Davidson Laboratory Model	Variation	Stability Index $\sigma_1$	$\frac{N'_s}{I'_s - N'_r}$	Time to 1st Exec sec	Yaw-Angle Overshoot,			Over- shoot Width of Path, $Y_0/L$	—Reach—		Period sec
						1st	deg 2nd	3rd		Time sec	Dist $x_R/L$	
Rudder Area, $A'_R$	2, 1, 3	0.012	-0.45	-0.82	60	5.89	5.88	6.31	1.46	160	7.30	305
	2, 1, 1	0.016	-0.51	-1.09	50	6.97	5.86	6.27	1.33	139	6.30	267
	2, 1, 2	.025	-0.62	-1.41	47	6.03	5.69	5.15	1.11	127	5.70	251
Block coefficient, $C_B$	2, 1, 1	0.60	-0.51	-1.09	50	6.97	5.86	6.27	1.33	139	6.30	267
	7, 1, 1	0.70	-0.31	-1.05	46	9.55	8.80	9.23	1.53	139	6.18	268
	8, 1, 1	0.80	-0.28	-1.29	39	10.22	10.36	10.70	1.34	120	5.34	243
Draft, $L/T$	5, 1, 1	23.00	-0.45	—	45	6.40	6.50	6.80	1.20	126	5.68	249
	2, 1, 1	18.75	-0.51	-1.09	50	6.97	5.86	6.27	1.33	139	6.30	267
	6, 1, 1	14.50	-0.51	—	53	6.28	5.65	6.50	1.31	143	6.52	277
Profile Shape	2, 1, 1	Standard	-0.51	-1.09	50	6.97	5.86	6.27	1.33	139	6.30	267
	60P1	Stern	-0.29	-1.00	44	10.04	9.00	8.74	1.52	135	5.98	262
cutaway	60P2	Stern and	-0.19	—	44	8.85	9.35	8.69	1.42	131	5.82	263
bow cutaway	(See Table 24)											
Section Shape	1, 1, 1	Unmodified	-0.41	-1.03	51	8.10	8.32	7.52	1.42	142	6.36	276
	60V1	Vee	-0.39	—	49	7.51	7.48	7.19	1.406	140	6.30	274

Table 29(a)—Values of Steady Turning Diameter as a Function of Hull Configuration for Single-Screw Ships From Four Different Sources ( $A'_R = 0.016$  and  $\delta_R = +30$  deg)

Hull Configuration							Turning Diameter/Ship Length				
$C_B$	$L/B$	$L/T$	$LCG/L$	Profile Shape		Section Shape note 2	Free-Turning Tests		Nonlinear Theory note 5	Linear Theory Equation (26a)	
				Bow cutaway, Pct note 1	Stern cutaway, Pct note 1		note 3	note 4		note 6	note 3
0.60	7.0	18.75	0.515	0.15	0.97	Normal	5.1	5.3	7.5	4.3	5.6
0.70	7.0	18.75	0.505	0.15	0.97	Normal	4.2	3.7	6.3	2.6	4.1
0.80	7.0	18.75	0.475	0.15	0.97	Normal	3.3	2.75	5.25	1.9	4.8
0.60	7.0	18.75	0.505	0.15	0.97	Normal	—	—	—	4.5	5.8
0.70	7.0	18.75	0.505	0.15	0.97	Normal	4.2	3.7	6.3	2.6	4.1
0.80	7.0	18.75	0.505	0.15	0.97	Normal	—	—	—	1.35	3.9
0.60	6.0	18.75	0.515	0.15	0.97	Normal	4.7	—	—	—	4.7
0.60	7.0	18.75	0.515	0.15	0.97	Normal	5.1	—	—	4.3	5.6
0.60	7.5	18.75	0.515	0.15	0.97	Normal	6.3	—	—	3.6	5.9
0.60	8.0	18.75	0.515	0.15	0.97	Normal	5.8	—	—	—	5.8
0.60	7.0	14.50	0.515	0.15	0.97	Normal	6.9	—	7.4	—	6.7
0.60	7.0	18.75	0.515	0.15	0.97	Normal	5.1	—	7.5	4.3	5.6
0.60	7.0	23.00	0.515	0.15	0.97	Normal	4.4	—	7.0	—	4.2
0.60	7.0	18.75	0.515	0.15	0.97	Normal	—	—	—	4.3	5.6
0.60	7.0	18.75	0.505	0.15	0.97	Normal	—	—	—	4.5	5.8
0.60	7.0	18.75	0.475	0.15	0.97	Normal	—	—	—	5.25	6.4
0.60	7.0	18.75	0.515	1.12	1.88	Normal	4.9	—	—	—	—
0.60	7.0	18.75	0.515	0.15	1.88	Normal	4.8	—	—	2.1	—
0.60	7.0	18.75	0.515	0.15	0.97	Normal	5.1	—	—	4.3	—
0.60	7.5	18.75	0.515	0.15	0.97	Normal	6.3	—	—	3.6	—
0.60	7.5	18.75	0.515	0.15	0.97	Vee	6.3	—	—	—	—

NOTE 1 See Table 23 for more complete description of profile shapes.

NOTE 2 Normal section shapes are those corresponding approximately to the Series 60. Vee-shaped sections are those of Davidson Laboratory Model No. 9,1,1 of Table 5.

NOTE 3 Davidson Lab (1965).

NOTE 4 The  $C_B$  and  $A'_R$  series of Shiba (1960) have the following characteristics:  $L/B = 7.3$ ,  $L/T = 18.25$ , LCG not specified, normal section shapes, stern cutaway = 1.25 percent  $LxT$ , and bow cutaway = 2.0 percent for  $C_B = 0.60$ , 1.3 percent for  $C_B = 0.70$  and 0.7 percent for  $C_B = 0.80$  (Shiba, 1960).

NOTE 5 Eda and Crane (1965).

NOTE 6 This is really a pseudo-linear theory because it utilizes experimentally determined derivatives [Tables 6(a)2 and 27] in conjunction with the linear equation (26a).

NOTE 7 This linear theory utilizes the theoretically determined derivatives of Table 6(a)1 and Table 27.

the lesser speed loss in a turn resulting from increased  $C_B$ , as shown by Shiba (1960), is confirmed by the simplified nonlinear prediction of Eda and Crane (1965). As shown in Fig. 179, this favorable effect can be explained by the much steeper resistance-as-a-function-of-speed curve of high-block-coefficient ships, on the assumption that the added drag in a turn does not change with increase in block coefficient.

On the other hand, the lesser speed loss in a turn resulting from a decrease in draft (increase in  $L/T$  ratio) as shown by the data of Eda and Crane (1965) in Fig. 178 is directly associated with the decrease in drag in a turn caused by the decreased draft.

Computed values of  $\psi$ , and  $\dot{\psi}$ , and other parameters during the transient phase of a turn as a function of hull configuration are shown in Fig. 180, taken from Eda and Crane (1965). These curves show that the

higher the turning ability of a ship, the greater is the reduction in the turning rate after a peak value is achieved early in the turn. According to Fig. 180, the first phase of a turn ( $\dot{\psi} \neq 0$  and  $\dot{\psi} = 0$ ) described in Section 6.2 is over in a very few seconds, whereas the second phase of a turn ( $\dot{\psi} \neq 0$ ,  $\dot{\psi} \neq 0$ ) lasts for more than three minutes for ships of this length and speed. In general, the trends with changes in hull configuration exhibited in Fig. 180 confirm those of Table 29.

The predictions in Fig. 180 were made for a 152-m (500-ft) ship running at an approach speed of 14.8 knots. The response for ships of other lengths and speeds can be readily estimated from the results shown in the figure, in this manner:

$$\text{Time, } t, \text{ sec} \quad t_B = t_A \times \left( \frac{L_B V_A}{L_A V_B} \right)$$

Table 29(b)—Values of Steady Turning Diameter as a Function of Block Coefficient, Rudder Area, and Rudder Aspect Ratio for Single-Screw Ships From Four Different Sources [ $\delta_R = +30^\circ$ ]

$C_B$	$A'_R$	Rudder Aspect Ratio		Turning Diameter/Ship Length		Nonlinear Theory note 5	Linear Theory equation (26a) note 6	Theory equation (26a) note 7
		note 8	note 8	Free-Turning Tests note 3	note 4			
0.60	0.012	2.50	2.33	6.9	6.8	8.5	5.3	5.6
0.60	0.016	1.90	1.75	5.1	5.3	7.5	4.3	5.6
0.60	0.020	—	1.40	—	4.5	—	—	—
0.60	0.025	1.20	1.12	4.9	4.25	6.7	4.6	6.1
0.60	0.0285	—	0.98	—	4.35	—	—	—
0.70	0.012	—	2.33	—	5.0	—	—	—
0.70	0.016	1.90	1.75	4.2	3.7	6.3	2.6	4.1
0.70	0.020	—	1.40	—	3.2	—	—	—
0.70	0.025	—	1.12	—	3.1	—	—	—
0.70	0.0285	—	0.98	—	3.15	—	—	—
0.80	0.012	—	2.33	—	3.9	—	—	—
0.80	0.016	1.90	1.75	3.3	2.75	5.3	1.9	4.8
0.80	0.020	—	1.40	—	2.4	—	—	—
0.80	0.025	—	1.12	—	2.45	—	—	—
0.80	0.0285	—	0.98	—	2.65	—	—	—

NOTE 8 The effective aspect ratio and the geometric aspect ratio of the rudders reported on by Eda and Crane (1965) and Shiba (1960) are identical because, as shown in Fig. 54, the rudders are not close enough to the hull for it to form a groundboard (see Section 14.6).

$$\text{Angular rates, deg/sec} \quad \begin{bmatrix} \dot{\psi} \\ \dot{\delta}_R \end{bmatrix}_B = \begin{bmatrix} \dot{\psi} \\ \dot{\delta}_R \end{bmatrix}_A \times \left( \frac{L_A U_B}{L_B U_A} \right)$$

where  $L$  and  $U$  are length and speed, and subscripts  $A$  and  $B$  designate the original ship and the proposed ship, respectively; e.g.,  $L_A = 152$  m and  $V_A = 14.8$  knots.

Path characteristics of the ship (longitudinal and lateral position in multiples of ship length,  $x/L$  and  $y/L$ ) remain identical for the same Froude number and remain generally the same regardless of changes in ship length and speed (on both of which Froude number depends). For example, advance and transfer,  $AD/L$  and  $TR/L$ , remain unchanged. Angles, such as ship's heading and drift angle do not change when results are scaled. The ratios,  $x/L$  and  $y/L$ , depend weakly on Froude number as shown in the development of nonlinear equations of motions.

The increase in turning ability with an increase in rudder size is clear in Fig. 180. It should be noted that transient turning rate behavior depends upon final turning ability. For a ship that has the ability to turn quickly, the turning rate increases rapidly to a peak and then gradually decreases to a final steady value, with the greatest rates of turn taking place during the transient phase of the turn. Section 17 will address this area further. The curves for advance and transfer indicate a trend showing saturation of improvement in turning quality for relatively large rudder sizes. The same saturation of turning quality for large rudder size is also demonstrated in computation of zigzag maneuvers. Additional rudder area is almost always useful in turning.

Predicted results show that turning quality is sensitive to the fullness of a ship's hull and increases appreciably with increasing block coefficient. For ordinary ship forms, an increase of ship mass should be expected to improve turning quality, because of the destabilizing eccentricity of centrifugal force and lateral hydrodynamic force. The changes in both inertial and hydrodynamic terms with block coefficient tend to give greater turning ability. Also, quickness of response with large rudder angles as indicated by the time at which peak turning occurs is little affected by an increase in block coefficient or ship mass.

Hydrodynamic terms vary significantly with ship's draft, as expected in view of the relation of draft to the important aspect-ratio variable in wing theory. According to response predictions, these terms, together with corresponding mass and inertia changes, produce good turning qualities for vessels that have large

Table 29—(c) Theoretical Values of  $Y'_s$  and  $N'_s$  for the Models of Shiba (1960)

$A'_t$	$a$	$\frac{\partial C_L}{\partial \alpha}$ (1/deg)	$Y'_s$ Equation 47(a)	$N'_s$ Equation 47(c)
(Shiba, 1960)		Fig. 41		
0.012	2.33	0.0475	0.0326	−0.0163
0.016	1.75	0.038	0.0349	−0.0175
0.020	1.40	0.0315	0.0361	−0.018
0.025	1.12	0.0265	0.0380	−0.019
0.0285	0.98	0.0225	0.0368	−0.0184

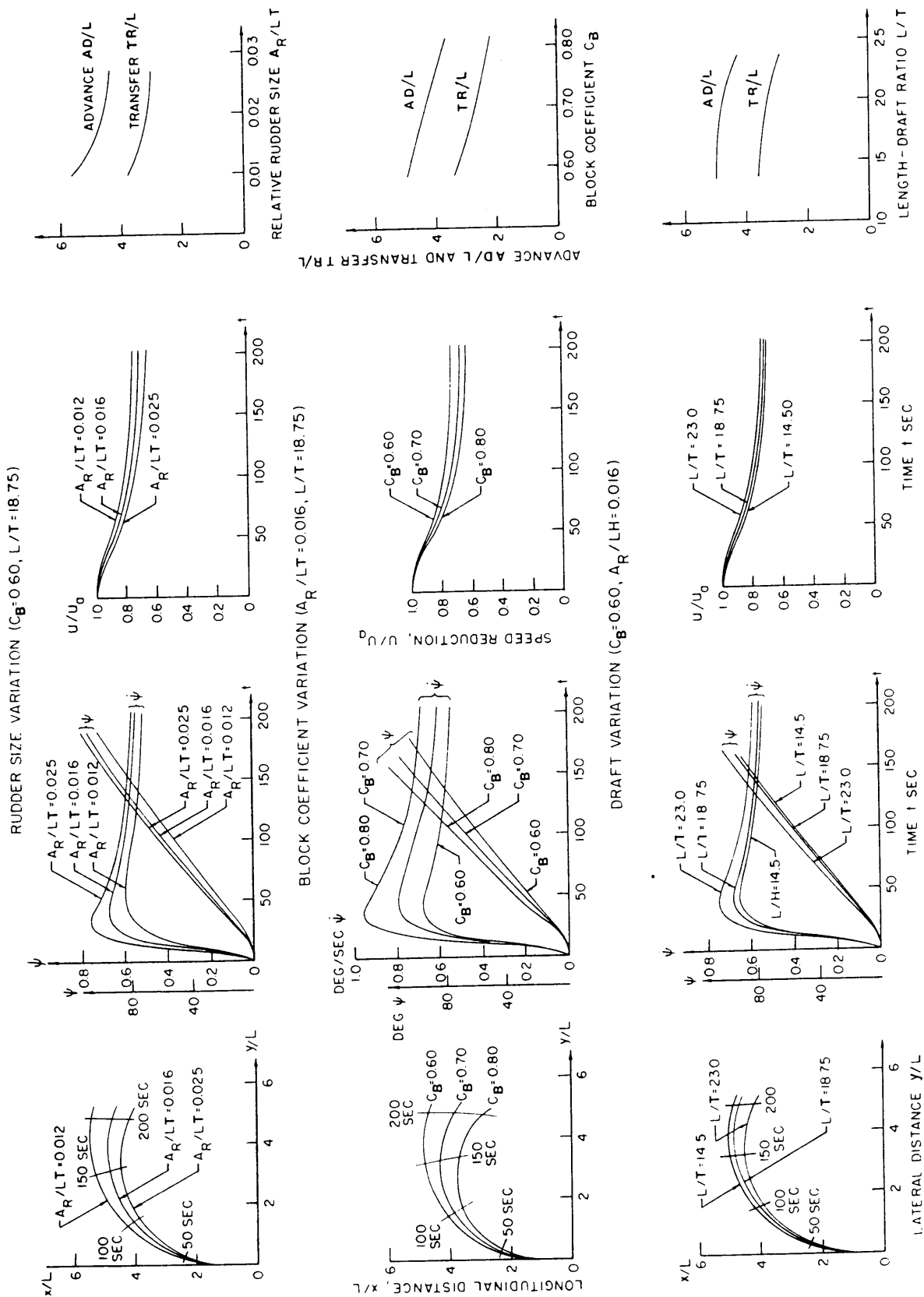


Fig. 180 Computed transient turning characteristics for various ship configurations ( $L = 500$  ft.,  $V = 14.8$  knots,  $A = 30$  deg) (Eda and Crane, 1965)

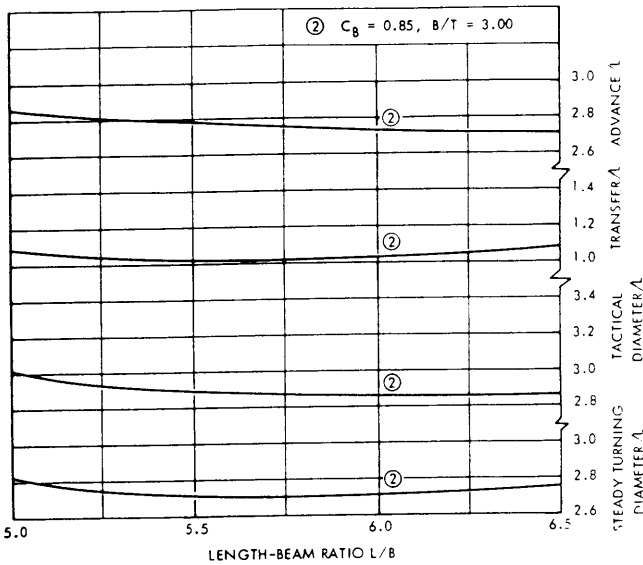


Fig. 181 Effect of length-beam ratio variation on nondimensional measures associated with a 35-degree-rudder starboard turn

length-draft ratio. There is little change in response, however, for length-draft ratios less than about 18.

Figs. 181 and 182 show predicted variations of turning performance with beam-draft and length-beam ratios for a systematic series of full form, restricted draft hulls as reported by Roseman (1987). These hulls are much more representative of current full-form ( $C_B > 0.80$ ) hulls than are the  $C_B = 0.80$  Series 60 hulls. The curves indicate rather small variations of turning performance with length-beam ratio. Variation of turning performance with beam-draft ratio for these forms is larger, with the best turning performance occurring for beam-draft ratios near 3.5. The worst turning performance occurs for the maximum (and extreme) beam-draft ratio of 4.5.

Table 30 shows computed zigzag maneuver responses as functions of hull configuration, from Eda and Crane (1965). Parameter,  $N'_s/(I'_z - N'_s)$ , used by Arentzen and Mandel (1960) is introduced in this table. It is a convenient index of rudder effectiveness related to the inertia of the ship and its hydrodynamic added inertia. The rudder area and the profile-shape series of Table 30 show that both stability and rudder effectiveness improve with increased rudder area and with decreased stern cutaway. According to the findings of Arentzen and Mandel (1960) as reported in Section 5.3, these attributes conflict as far as their influence on time to execute and yaw-angle overshoot is concerned, but the overshoot width of path should decrease as both of these attributes increase. The results shown in Table 30 are entirely consistent with these findings.

In the block-coefficient series, the stability is decreased with increased  $C_B$ , but the control effectiveness of the ( $C_B = 0.80$ ) is much better than the

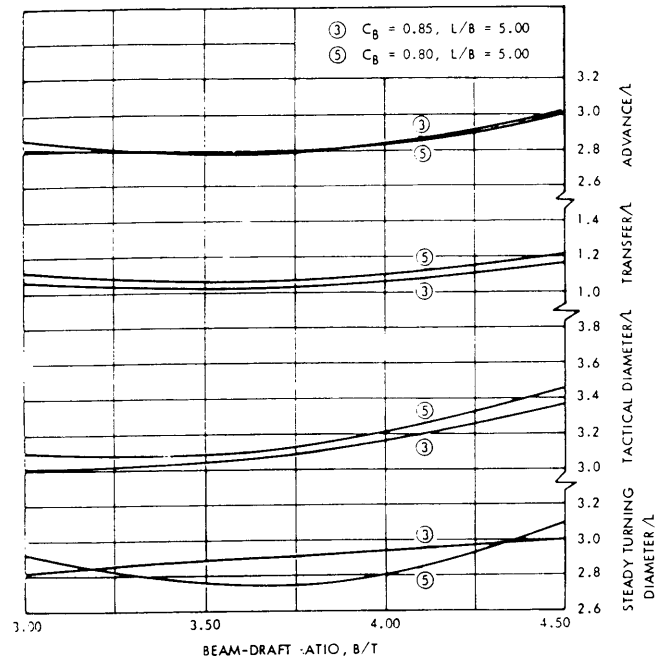


Fig. 182 Effect of beam-draft ratio variation on nondimensional measures associated with a 35-degree-rudder starboard turn

( $C_B = 0.70$ ) or the ( $C_B = 0.60$ ) models. According to Arentzen and Mandel (1960), both of these features should decrease time to execute and increase the overshoot yaw angle but they conflict as far as the overshoot width of path is concerned. Again, these findings are confirmed in Table 30.

In summary, it is concluded from this section and from Section 16.3 that for single-screw merchant ships:

(a) Increasing the block coefficient,  $L/T$  ratio, or stern cutaway area, or decreasing the  $L/B$  ratio impairs stability, improves turning, and decreases the time to change heading a specified number of degrees.

(b) Increasing the block coefficient or increasing the stern cutaway area increases the yaw-angle overshoot.

(c) Increasing the stern cutaway area increases the overshoot width of path.

(d) Changing block coefficient or the  $L/T$  ratio has an indecisive effect on overshoot path width, and changing the latter ratio also has an indecisive effect on the over-shoot yaw angle.

(e) Changes in section shape from normal to extreme V exert a very minor influence on all maneuvering characteristics.

(f) If the initial rudder area is small, increasing the rudder area will improve stability, reduce turning diameter, decrease the time to change heading, decrease the overshoot width of path, and have an indecisive effect on overshoot yaw angle; but if the initial rudder area is large, some of the preceding effects may be reversed with a further increase in rudder area.

**16.5 Comparison with Existing Vessels and Simple Prediction Equations.** Early in concept design, poten-

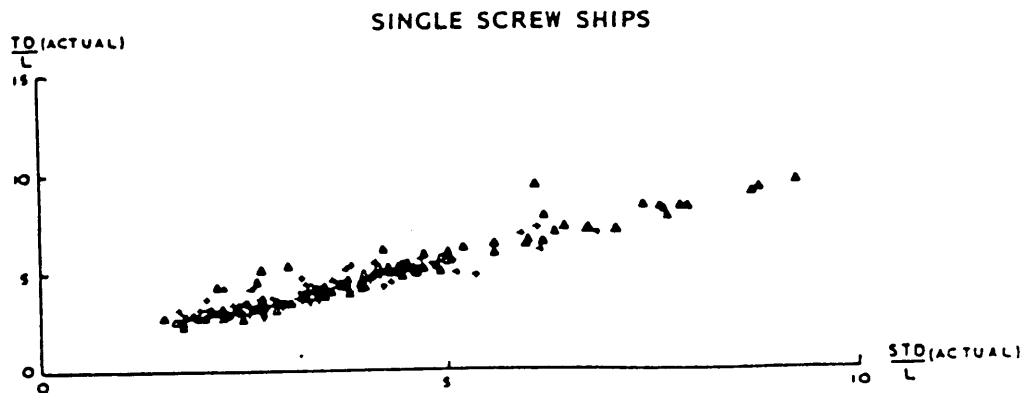


Fig. 183 Nondimensional values of steady turning diameter (STD) and tactical diameter (TD) for single-screw ships (Lyster, 1979)

tial controllability faults should be investigated by reviewing the capabilities of similar vessels. Available trials or model test data for maneuvers such as turns, zigzags, spirals, and crash stops for an existing ship that geometrically resembles very closely a proposed design can be used to estimate maneuvering performance. The data must be for the correct speed-length ratio or Froude number, and the existing ship must closely approximate the proposed design in all important geometric characteristics, including:

- Block coefficient

- Length-to-beam and beam-to-draft ratios
- Longitudinal center of submerged lateral plane area as percent of length from the forward perpendicular
- Rudder area divided submerged lateral area
- Same number of propellers and rudders, same types of rudders, and very nearly the same relative placement of propellers and rudders.

Even with all the foregoing characteristics identical, variations in the stern lines or amount of cutaway at the stern can result in markedly different performance.

Table 31—General vessel hull form coefficients

Vessel Type	Typical Form Coefficients and Ratios			Speed $V$ , knots	Froude No. $V/\sqrt{gL}$	Number of Propellers/ Rudders	Rudder Area Ratios <sup>a</sup>	Dynamic Course Stability <sup>b</sup>
	$C_B$	$L/B$	$B/T$					
Harbor tug	0.50	3.3	2.1	10	0.25	1/1	0.025	S
Tuna seiner	0.50	5.5	2.4	16	0.31	1/1	0.025	S
Car ferry	0.55	5.1	4.5	20	0.34	2/2	0.020	S <sup>c</sup>
Container high speed	0.55	8.3	3.0	28.5	0.53	2/2	0.015	S
Container high speed	0.55	8.3	3.0	28.5	0.53	2/1	0.025	S <sup>c</sup>
Cargo liners	0.58	6.9	2.4	21	0.29	1/1	0.015	S
RO/RO	0.59	6.9	3.0	22	0.26	1/1	0.015	S
Barge carrier	0.64	7.5	2.9	19	0.20	1/1	0.015	S
Container Med. Speed	0.70	7.1	2.8	22	0.25	1/1	0.015	S <sup>d,e</sup>
Offshore supply	0.71	4.7	2.75	13	0.28	2/2	0.016	S
General cargo low speed	0.73	6.7	2.4	15	0.20	1/1	0.015	S
Lumber low speed	0.77	6.7	2.6	15	0.20	1/1	0.025	S
LNG (125 000 m <sup>3</sup> )	0.78	6.8	3.7	20	0.20	1/1	0.015	U
OBO (Panamax)	0.82	7.5	2.4	16	0.17	1/1	0.018	U
OBO (150 000 dwt)	0.85	6.4	2.4	15	0.15	1/1	0.017	U
OBO (300 000 dwt)	0.84	6.0	2.5	15	0.14	1/1	0.015	U
Tanker (Panamax)	0.83	7.1	2.4	15	0.16	1/1	0.015	U
Tanker 100 000 to 350 000 dwt	0.84	6.2	2.4	16	0.15	1/1	0.015	U
Tanker 350 000 dwt	0.86	5.7	2.8	16	0.13	1/1	0.015	U
U.S. river towboat	0.65	3.5	4.5	10	0.25	2/2	...	U <sup>d,e</sup>

<sup>a</sup> Not for design guidance.

<sup>b</sup> U = unstable course stability; S = stable course stability.

<sup>c</sup> Although the vessel is directionally stable, maneuvering is difficult at low speeds when the propeller wash is not effective over the rudder.

<sup>d</sup> Maneuverability is good owing to installation of Kort nozzles, flanking rudders, and other capabilities.

<sup>e</sup> Twin screw because of restricted draft.

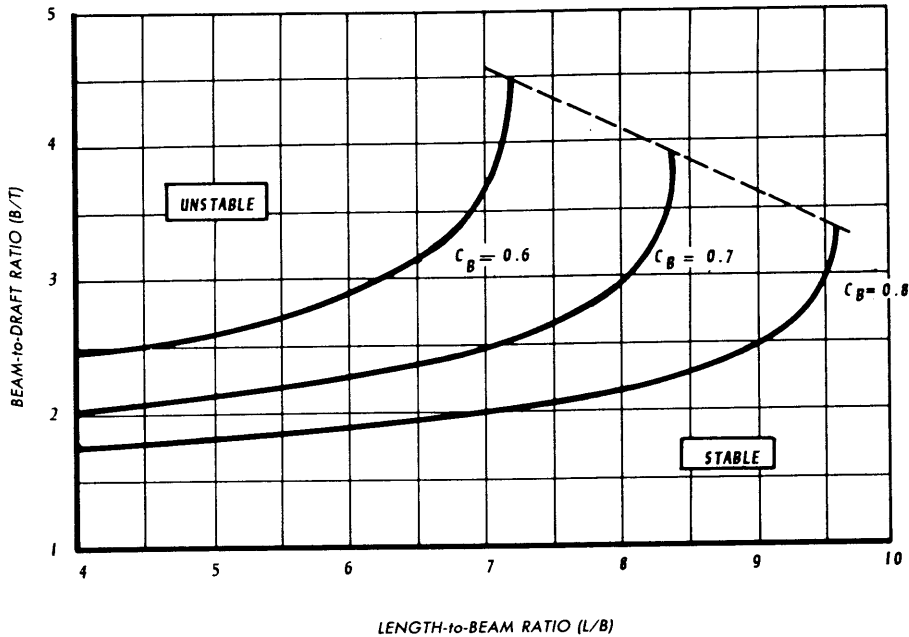


Fig. 184 Dynamic stability boundaries for various hull geometries (Clarke, 1977)

Table 31 summarizes various vessel types and presents a guide for “nominal” hull form coefficients and geometric proportions. As a rule of thumb, a variation from the norms of 10 percent either way would not vitiate the proportions. If the contemplated design has proportions or characteristics outside the range of those vessels considered normal, the designer should immediately plan to undertake additional studies to assure adequate maneuverability.

For normal ships the designer can also make preliminary estimates of maneuvering characteristics through a number of approximation methods and thus see if his design presents the likelihood of meeting desired needs. Lyster (1979) developed some empirical estimating equations for ship turning characteristics based on regression of statistical data for both twin- and single-screw ships. The equations are useful in the early design process since they require the nondimensional parameters of only major characteristics, which are estimated early on. In developing the relationships, characteristic data from a number of ships are plotted, and coefficients for the equations are obtained through regression techniques. A typical plot of relationships is shown in Fig. 183. The corresponding predictor equations for steady turning diameter (STD) along with predictor equations for advance, transfer, and reduced velocity ratio (sometimes called speed loss, although “speed remainder” would be more accurate) determined as linear functions of STD are as follows:

(a) Single-Screw Vessels

$$\frac{STD}{L} = 4.19 - \frac{203C_B}{\delta_R} + 47.4 \frac{Trim}{L} - \frac{13.0B}{L} + \frac{194}{\delta_R}$$

$$\begin{aligned} & - 35.8 \frac{SpCh}{LT} (ST - 1) \\ & + 3.82 \frac{SpCh}{LT} (ST - 2) + 7.79 \frac{A_B}{LT} \\ & + 0.70 \left( \frac{T}{T_L} - 1 \right) \left( \frac{\delta_R}{|\delta_R|} \right) (ST - 1) \end{aligned}$$

$$\frac{AD}{L} = 0.519 \frac{TD}{L} + 1.33$$

$$\frac{TR}{L} = 0.497 \frac{TD}{L} - 0.065$$

$$\frac{V_T}{V_A} = 0.074 \frac{TD}{L} + 0.149$$

(b) Twin-Screw Vessels

$$\frac{STD}{L} = 0.727 - 197 \frac{C_B}{|\delta_R|} + 4.65 \frac{B}{L} + 41.0 \frac{Trim}{L} + 188 \frac{1}{|\delta_R|}$$

$$- 218 \frac{SpCh}{LT} (NR - 1) + 3.20 \frac{V_A}{\sqrt{L}} + 25.56 \frac{A_B}{LT}$$

$$\frac{TD}{L} = 0.140 + 1.000 \frac{STD}{L}$$

$$\frac{AD}{L} = 1.100 + 0.514 \frac{TD}{L}$$

$$\frac{TR}{L} = -0.357 + 0.531 \frac{TD}{L}$$

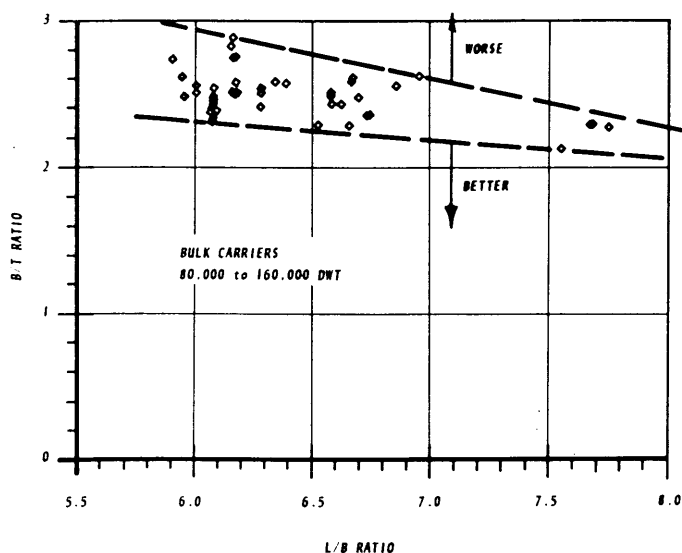


Fig. 185 Example B/T versus L/B dynamic course stability guide

$$\frac{V_T}{V_A} = 0.543 + 0.28 \frac{TD}{L}$$

Where in English units:

$ST$  is Stern type ( $ST=1$  for closed stern;  $ST=2$  for open water stern)

$NR$  is Number of rudders

$L$  is Length between perpendiculars, ft

$C_B$  is Block coefficient

$\pm \delta_R$  is Rudder angle, degrees (negative if to starboard)

$B$  is Beam molded

$A_B$  is Submerged bow profile area considered positive if projecting forward of the forward perpendicular and negative if corresponding to 'cutaway' as in the case of a conventional raked stem

$T$  is Draft on trial

$T_L$  is Design load draft

$V_A$  is Velocity of approach, knots

$V_T$  is Velocity on steady turn, knots

$S_p$  is Span of rudder

$Ch$  is Chord of rudder

Circle

$STD$  is Steady turning diameter

$TD$  is Tactical diameter

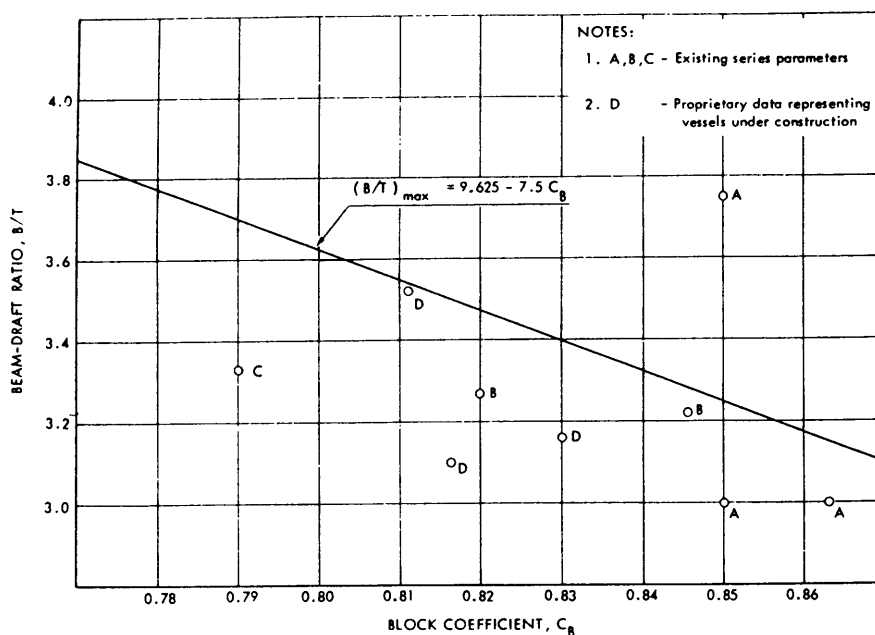
$AD$  is Advance at 90 deg of turn

$TR$  is Transfer at 90 deg of turn

$V_T/V_A$  is Reduced velocity ratio on steady turn

The weighted factor  $\left(\frac{T}{T_L} - 1\right) \left(\frac{\delta_R}{\delta_{R1}}\right) (ST - 1)$

is included to take account of the difference in size that was found to exist between circles to port and circles to starboard in single-screw vessels with open water sterns. The difference was found to depend not only on the direction of rotation of the propeller, but also on the fractional draft,  $T/T_L$ , and to be markedly greater at light drafts than at deep ones (see Section 13.2). The circle to port tends to be smaller in ships with right-handed propellers. The single-screw ships from which the data were obtained all had right-

Fig. 186 Maximum beam-draft ratio vs. block coefficient for  $L/B = 5.0$  (Roseman, Gertler, and Kuhl, 1974)



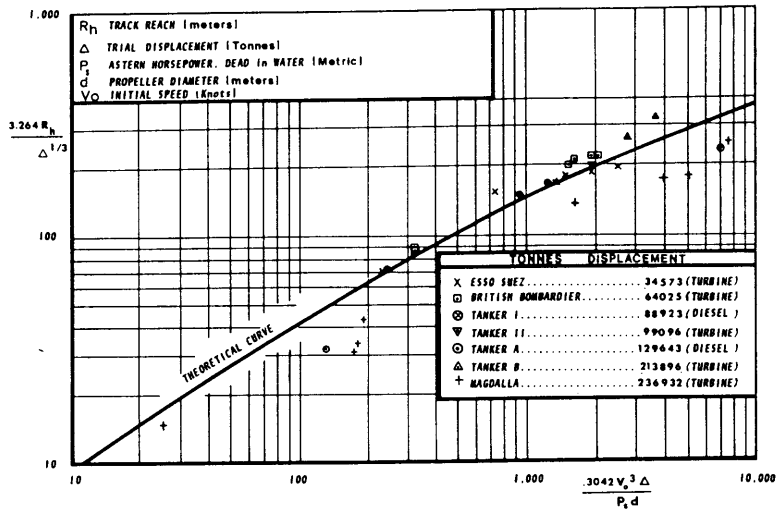


Fig. 187 Universal stopping curve for tankers (Clarke, 1977)

handed propellers, except for a possible few in which the direction of rotation was not known.

Eda (1974) and Fedyayevskly (1964) also have methods for calculating approximate turning diameters early in design. These turning circle characteristics are useful in obtaining limiting values and comparisons of what may be possible. Further studies are necessary to assure that these capabilities can be obtained and to assure good coursekeeping and turning abilities.

Use of a fullness criterion during early design can provide a guide to potential acceptability of the basic hull proportions. Fig. 184 from Clarke (1977) shows boundaries of stability of a particular hull and appendage configuration for  $C_B$  varying from 0.6 to 0.8. From this figure the degree of stability of a proposed vessel design can be approximated if basic dimensions are known. The diagram applies only to the one hull form but indicates general trends. Stability is sensitive to many properties such as hull shape, rudder effectiveness, and speed. Based on these trends, designers can use as a guide plots such as Fig. 185 showing  $B/T$  versus  $L/B$  of existing vessels for particular ship type and size groups. When the shape of the curves for Fig. 184 are applied to Fig. 185, one can conclude, for instance, that existing bulk carriers of  $L/B = 6$ , while adequate in real piloted conditions, are most likely inherently unstable. Those existing with  $L/B = 7.5$ , on the other hand, can probably tolerate a larger  $B/T$  than indicated to have an equivalent capability. With existing vessel data, the designer can thus surmise at an early stage whether a design can attain a reasonable range of course stability without the addition of skegs or special attention to the design of the lateral plane area. A similar fullness criterion was proposed by Roseman, et al (1974) in their study of restricted draft bulk carriers. Fig. 186 adapted from

their paper, illustrates how candidate designs can be compared with known models or ships. Falling above the trend indicates a potential for controllability trouble. Such an indication by itself does not mean that with proper attention to design of hull form and rudder an acceptable design cannot be achieved. It merely forewarns that special attention may become necessary.

Figs. 187 and 188, adapted from Clarke (1977) are useful in estimating tanker stopping distances. Fig. 188 can be derived from Fig. 187, and indicates the relationship of stopping distance to approach speed and reverse power. The time contours on Fig. 188 indicate the number of minutes required for each stopping maneuver. Information such as that provided on

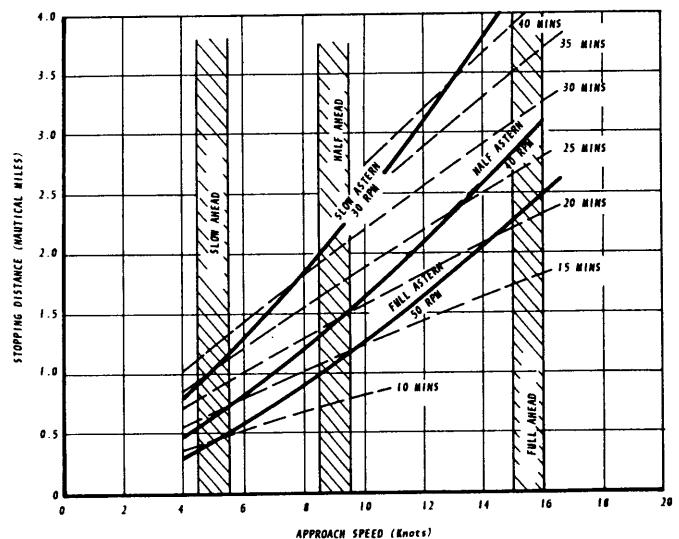


Fig. 188 Stopping curves for 210,000-dwt tanker (Clarke, 1977)

Table 32—Principal Particulars of Series 60 Models

Model designator	60	60R1	60R2	(metric)
Length (BP), $L$ , ft	5.00	5.00	5.00	1.52 m
Breadth, $B$ , ft	0.714	0.714	0.714	0.217 m
Draft, $T_m$ , ft	0.267	0.267	0.267	8.1 cm
Block coefficient, $C_B$	0.60	0.60	0.60	0.60
$L/T$	18.75	18.75	18.75	18.75
$L/B$	7.00	7.00	7.00	7.00
$B/T$	2.68	2.68	2.68	2.68
Displacement (FW) $\Delta$ , lb	35.63	35.63	35.63	16kg
$L \times T$ , ft <sup>2</sup>	1.335	1.335	1.335	0.123 m <sup>2</sup>
Lateral area of hull, ft <sup>2</sup>	1.320	1.320	1.320	0.1226 m <sup>2</sup>
Area of rudder, $A_R$ , ft <sup>2</sup>	0.021	0.033	0.016	
$C_m^2/LH$	0.195	0.306	0.148	
$A_R/LH$	0.016	0.025	0.012	—
Aspect ratio of rudder	1.90	1.20	2.50	—
LCG/ $L$ from FP	0.515	0.515	0.515	0.515
Radius of gyration in air	0.25 $L$	0.25 $L$	0.25 $L$	0.25 $L$
Prismatic coefficient	0.614	0.614	0.614	0.614

the graphs of both figures is especially useful in comparing contemplated vessels with existing vessels.

**16.6 An Example Prediction Method for Dynamic Stability.** The extent of the lateral plane (underwater profile of the vessel) and the position of the center of effort have major effects on the course stability and turning ability of the hull form. The equations of Jacobs (1964) and others for estimating bare hull hydrodynamic derivatives based on variations in underwater profile (See Section 9.5) are useful for showing trends of dynamic stability and maneuvering performance even though they ignore important propeller-rudder effects.

While hull resistance to motion and flow of water to the propeller must be considered, additions to lateral plane area such as those caused by rudder, deadwood, skegs, fins, and other appurtenances must also be evaluated for their effect on stability. Skegs and fins may actually be added late in a design to reduce a dynamic stability deficiency of the hull form. Increasing the rudder size also helps improve the stability situation while, of course, helping turning ability.

To illustrate the elements involved in a practical analysis, a somewhat simplified theoretical procedure for calculating dynamic straight-line stability developed by Eda (1974) is presented here. It is based on the linear theory of Section 2 and is believed to be sufficiently accurate for design use, as in the selection of rudder size for a ship outside the range of empirical data.

This method involves predicting the hydrodynamic

derivatives using a combination of theoretical and empirical inputs. First the ship's hull is viewed as a fin of large area but very low aspect ratio. With the hull considered as a fin, its geometric aspect ratio is its draft-to-length ratio, its thickness-to-chord ratio is its beam-to-length ratio, its taper ratio is usually close to 1.0, its sweepback angle is usually slightly negative, and its mean section shape corresponds to the shape of its water plane at half draft. At speeds ( $F_n < 0.25$ ) for which the influence of wavemaking may be neglected and the current approaches are few, it was shown by Tsakonas (1959) that the free water surface serves as a groundboard for the ship's hull. Hence, the effective aspect ratio of the hull may be taken as twice the geometric aspect ratio, that is, as  $2T/L$ . Because of the hull's poor section shape as a lifting surface and because of its very low aspect ratio, a ship's hull might be expected to generate very small hydrodynamic forces and moments compared to its rudder; but because of its very large profile area, a ship's hull does in fact generate forces and moments that are far larger than the control forces and moments generated by its rudder (see also Section 3.5).

One of the many assumptions made in linear theory is that the mutual interference effects between the ship's hull and its appendages such as fixed fins and rudders are negligible. This assumption is hard to justify on physical grounds, and it is obviously not justified for tight maneuvers. Nevertheless it and the other assumptions made in the linear prediction do lead to reasonable correlation with experimental data for

small motions within the linear range, for example, predicting straight-line stability (Eda and Crane, 1965).

As developed by linear theory in Section 4.2, the criterion for stability is  $\sigma_{1,2} < 0$  where from Equations (14) and (14a),

$$\sigma_{1,2} = \frac{-(-n_z' Y_v' - \Delta_y' N_r') \pm \sqrt{(-n_z' Y_v' - \Delta_y' N_r')^2 + 4\Delta_y' n_z' [-Y_v' N_r' - (\Delta' - Y_r') N_v']}}{2\Delta_y' n_z'} \quad (129)$$

These coefficients can be estimated as follows:

(a) Inertial Coefficients

$$\Delta' = \frac{\Delta}{\rho/2L^2T} = \text{coefficient of added mass of the ship} \\ = \left( \frac{pLBTC_B}{\rho/2L^2T} \right) \quad (130)$$

$$n_z' = I_z' - N_r', \quad I_z' = \frac{k'}{L^4T} \int_{x_s}^{x_b} C_s(x) \pi t^2 x^2 dx$$

$$\Delta_y' = \Delta' - Y_v', \quad -Y_v' = \frac{k_2}{L^2T} \int_{x_s}^{x_b} C_s(x) \pi t^2 dx$$

$$\Delta_x' = (1 + k_1)\Delta' = \Delta' - X_{\dot{u}}'$$

where  $t$  = draft of local section (constant at even-keel conditions)

$b$  = breadth of local section

$x_s, x_b$  = respective distances of stern and bow from LCG (positive if forward from LCG)

$C_s$  = two-dimensional lateral added-mass coefficient (section inertia coefficient) (see Fig. 50)

$k_1, k_2, k'$  = three-dimensional correction factor (see Fig. 48)

$I_z'/\rho/2L^4\pi$  = moment-of-inertia coefficient of added mass of the ship  $\cong \Delta'/16$

$L, T$  = length and mean draft of the ship, respectively

(b) Linear Hydrodynamic Coefficients with rudder (Barehull),

$$(Y_v')_{BH} = -\frac{2\pi T}{L}$$

$$(N_v')_{BH} = -(\Delta_y' - \Delta_x') - (x_p' + x_s') \frac{\pi T}{L} \quad (131)$$

$$(Y_r')_{BH} - \Delta' = -(x_p' + x_s') \frac{\pi T}{L} - \Delta'$$

$$(N_r')_{BH} = -\frac{k'\pi \int_{x_s}^{x_b} C_s(x) t^2 dx}{L^2T} \bar{x}' - \left[ \left( \frac{c_p}{2} \right)^2 + x_s'^2 \right] \frac{\pi T}{L}$$

and

$$\bar{x}' = \frac{1}{L} \int_{x_s}^{x_b} C_s(x) t^2 x dx / \int_{x_s}^{x_b} C_s(x) t^2 dx$$

where

$x_p'$  = distance of center of pressure from LCG, as fraction of ship length (positive if forward from LCG)

$x_s'$  = distance of skeg (or rudder) location from LCG, as fraction of ship length (negative if aft from LCG, as is usual)

$c_p$  = prismatic coefficient

The relationships between these hydrodynamic coefficients and rudder force coefficients are given by,

$$\begin{aligned} Y_v' &= (Y_v')_{BH} - Y_\delta' \\ N_v' &= (N_v')_{BH} - Y_\delta' x_r' \\ Y_r' &= (Y_r')_{BH} - Y_\delta' x_r' \\ N_r' &= (N_r')_{BH} - Y_\delta' x_r'^2 \end{aligned} \quad (132)$$

As assumed in the foregoing equations, each linear hydrodynamic coefficient for the ship equals the al-

Table 33—Inertial Coefficients for Models 60, 60R1, and 60R2

Minor axis/major axis, $2T/L$	0.1067
$k_1$ (longitudinal)	0.022 (From Fig. 48)
$k_2$ (lateral)	0.957 (From Fig. 48)
$k'$ (rotational)	0.875 (From Fig. 48)
$\Delta'$ , mass coefficient	0.171
$\Delta_x'$ , longitudinal virtual-mass coefficient	0.175
$\Delta_y'$ , lateral virtual-mass coefficient	0.341
$n_z'$ , virtual moment-of-inertia coefficient	0.0219
$\bar{x}/L$ , CG of lateral added mass from LCG	0.049
$x_p'/L$ , center of area of profile from LCG	0.028

Table 34—Hydrodynamic Coefficients and Stability Indexes Estimated

Model	60	60R1	60R2
$Y'_v$	-0.335	-0.347	-0.329
$N'_v$	-0.086	-0.080	-0.089
$Y'_r - \Delta_m'$	-0.095	-0.089	-0.098
$N'_r$	-0.066	-0.069	-0.065
$\sigma_1$	-0.55	-0.64	-0.49

gebraic sum of those for the bare hull and the rudder. The rudder force coefficient can be estimated for rudder in propeller race by Equation (133). This equation allows for effects of wake and propeller slip ratio on rudder forces by incorporating terms in  $w$  and  $s$ , respectively,

$$Y'_s = (1 - w)^2 \frac{6.13\lambda}{\lambda + 2.25} (1 + ks^{1.3}) \frac{A_R}{LT} \quad (133)$$

where

- $w$  = mean effective wave fraction of the propeller
- $\lambda$  = rudder aspect ratio
- $s = 1 - \frac{U}{Pn}$
- $P$  = propeller pitch
- $n$  = propeller revolutions per unit time
- $k = 3.36$

An example is shown for the case of the Series 60 hull form with block coefficient 0.60,  $L/B = 7.0$ , and  $B/T = 2.68$ . The principal characteristics of three models (M-60, M-60R1, and M-60R2) are shown in Table 32. These models have the same hull form but different rudders of varying chord length. Table 33 gives the estimated inertial coefficients obtained in Equation (130).

Linear hydrodynamic coefficients for M-60 are determined by Equation (131). Then rudder coefficients  $Y'_s$  for the three rudders can be estimated by Equation (132). Hydrodynamic coefficients for Models 60R1 and 60R2 are determined by subtracting  $Y'_s$  terms due to the original rudder for M-60 and adding those due to rudders of different size for M-60R1 and M-60R2, in Equation (132).

Finally, stability indexes for the three models are estimated by substituting all inertial and hydrodynamic terms in Equation (129). Table 34 shows the estimated hydrodynamic coefficients and the stability indexes as finally determined; these are negative for all three models with rudders of different size. Thus, it is shown that all three models are dynamically stable.

Calculated and experimental values of stability indexes and hydrodynamic terms are compared in Figure 189, which shows fairly good agreement between calculated and experimental results.

**16.7 Prediction Models Using Basic Ship Characteristics.** Recently, reasonably good analytical approaches have been developed for estimating mathematical model hydrodynamic coefficients based

on basic ship characteristics alone. The mathematical models can be used to quickly simulate ship capabilities to evaluate the effects of change in a ship's physical character.

Inoue, et al (1981) provided the basis for practical realistic simulations at the early stages of design with their collection and parametric analysis of nonlinear model test data. In their development they assumed that the nondimensional lateral force  $Y'$  and yaw moment  $N'$  about an axis at midship can be represented as,

$$\begin{aligned} Y'(\beta, r') &= Y'_\beta \beta + Y'_r r' + f_y(\beta, r') \\ N'(\beta, r') &= N'_\beta \beta - N'_r r' + f_N(\beta, r') \end{aligned} \quad (134)$$

where  $f_y(\beta, r')$  and  $f_N(\beta, r')$  represent the nonlinear terms. Model tests measuring  $Y$  and  $N$  were performed at a Froude number of approximately 0.06 for three oil tankers, three dry cargo ships, a containership, an LNG carrier, a RO/RO ship, and a car carrier. Approximate formulas for estimating the linear deriva-

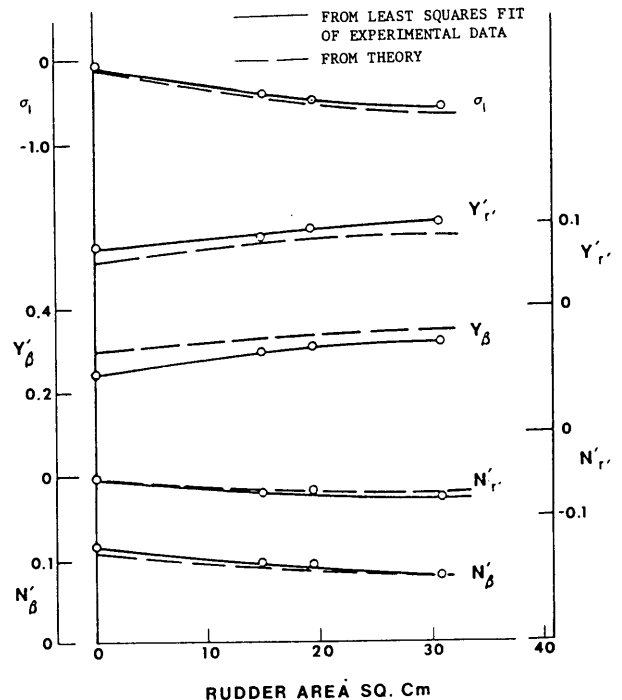


Fig. 189 Comparison of calculated and experimental model stability derivatives and indexes for Series 60, Models 60, 60R1, and 60R2

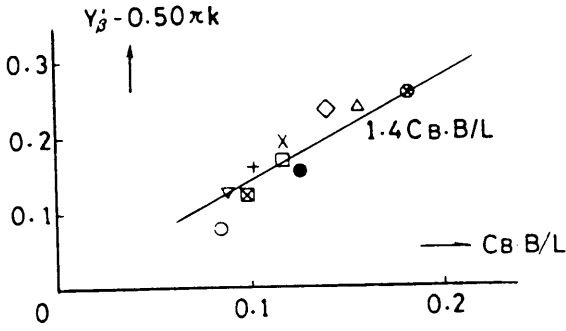
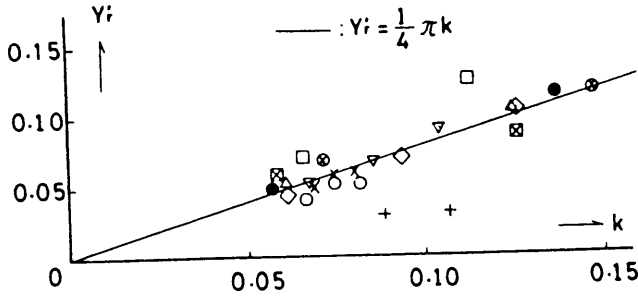

 Fig. 190 The function  $f$  in equation


Fig. 191 Derivative of lateral force in even keel condition for turning motion

tives on the bare hull for full load and even keel were developed by applying lifting surface theory:

$$\begin{aligned} Y'_\beta &= \frac{1}{2} \pi k + f(C_B B/L) \\ Y'_r &= \frac{1}{4} \pi k \\ N'_\beta &= k \\ N'_r &= 0.54k - k^2 \end{aligned} \quad (135)$$

where function  $f(C_B B/L)$  as shown in Fig. 190 was necessary to account for the different hull types. Fig. 191 is typical of the test results and shows the relatively good agreement in the relationships for the variety of models tested.

The nonlinear terms  $f_y(\beta, r')$  and  $f_N(\beta, r')$  were assumed to depend on  $\beta^2$ ,  $\beta r'$  and  $r'^2$  in application of cross-flow theory or Newtonian law. With additional review of the data the following formulation was used:

$$\begin{aligned} f_Y &= Y_{\beta\beta}\beta|\beta| + Y_{\beta r}\beta|r'| + Y_{rr}r'|r'| \\ f_N &= N_{rr}r'|r'| + (N_{r\beta}r' + N_{\beta\beta}\beta)\beta r' \end{aligned} \quad (136)$$

Fig. 192 shows the resultant fit for  $Y_{\beta\beta}$ ,  $Y_{\beta r}$ , and  $Y_{rr}$ . Thus, hydrodynamic forces acting on a bare hull can be estimated by using Equations (135) and (136).

Further model tests were performed with stern trim

conditions at fixed displacement. Results were compared to a theoretical approach developed using the slender-body theory or low-aspect-ratio lifting surface theory. The basic theoretical approach uses the methods of Inoue and Kijima (1978) and Fuwa (1973) based on the slender body theory of Newman (1977). The following relationships show close agreement with the measured results:

$$\begin{aligned} Y'_\beta(\tau) &= Y'_\beta(0) \left[ 1.0 + \frac{2\tau}{3T_m} \right] \\ N'_\beta(\tau) &= N'_\beta(0) \left[ 1.0 - \frac{0.27\tau}{l_\beta T_m} \right] \\ Y'_r(\tau) &= Y'_r(0) \left[ 1.0 + 0.80 \frac{\tau}{T_m} \right] \\ N'_r(\tau) &= N'_r(0) \left[ 1.0 + 0.30 \frac{\tau}{T_m} \right] \end{aligned} \quad (137)$$

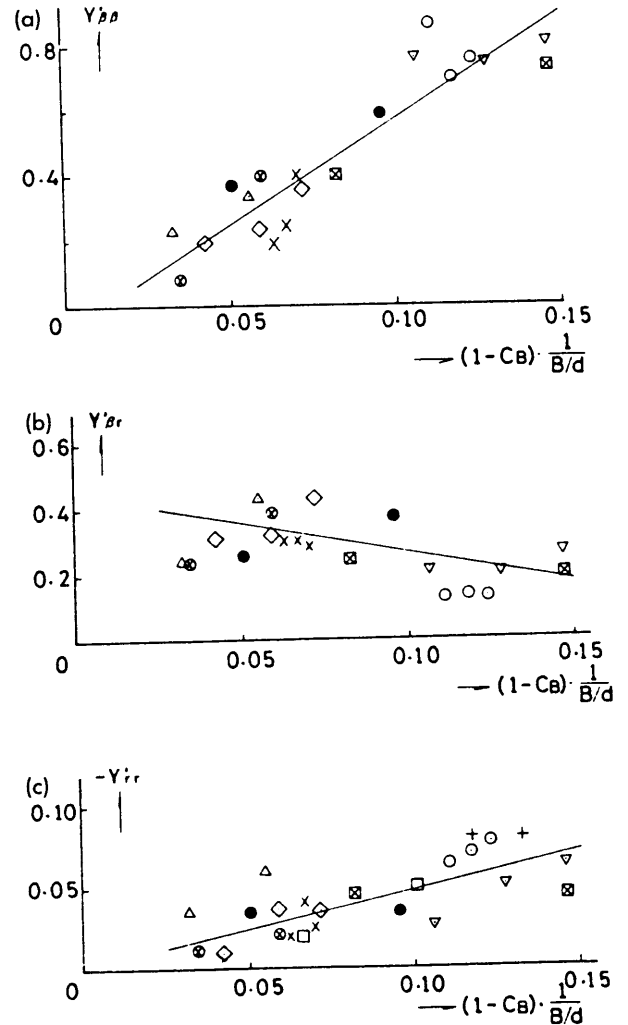


Fig. 192 Nonlinear derivatives of lateral force

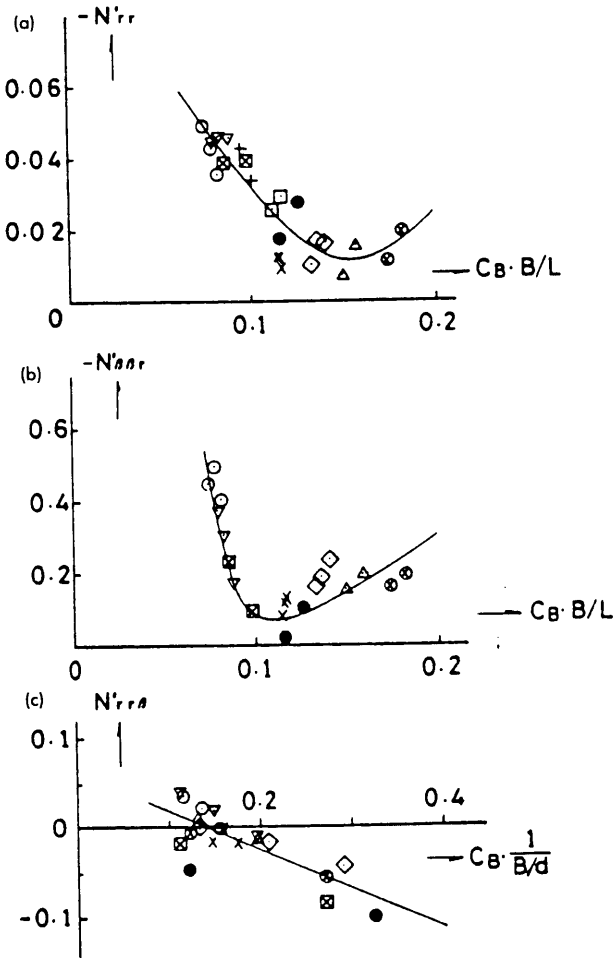


Fig. 193 Nonlinear derivatives of yaw moment

where  $T_m$  is mean draft of the ship,  $\tau$  is the trim quantity (positive by stern), and  $l_p = N_\beta(0)/Y'_\beta(0)$ .

The formulas resulting from combining Equations 137, 136, and 135 into 134 provide a method of estimating hydrodynamic forces acting on a given ship form as a function of its draft, trim, and aspect ratio:

$$\begin{aligned}
 Y' &= \left[ \frac{1}{2} \pi k + f(C_B B/L) \right] \left( 1 + \frac{2\tau}{3T_m} \right) \beta \\
 &\quad + \frac{\pi k}{4} \left( 1 + 0.8 \frac{\tau}{T_m} \right) r' \\
 &\quad + Y'_{\beta\beta} \beta |\beta| + Y'_{\beta r} \beta |r'| + Y'_{rr} r' |r'| \\
 N' &= k \left( 1 - \frac{0.27}{l_\beta} \frac{\tau}{T_m} \right) \beta \\
 &\quad - (0.54k - k^2) \left( 1 + 0.30 \frac{\tau}{T_m} \right) r' \\
 &\quad + N'_{rr} r' |r'| + (N'_{rr\beta} r' + N'_{\beta\beta r} \beta) \beta r'
 \end{aligned} \tag{138}$$

$$\text{where } l_\beta = k / \left[ \frac{1}{2} \pi k + f(C_B B/L) \right]$$

The nonlinear terms are derived from Fig. 193.

Inoue et al (1981) presented a complete practical calculation method based on the foregoing and on other works. Their method allows calculation of maneuvering motions using only the principal particulars of the ship hull, propeller, and rudder as known at the initial design stage. The basic equations used are

$$\text{Surge force: } \Delta(\dot{u} - vr) = X_H + X_P + X_R$$

$$\text{Sway force: } \Delta(\dot{v} + ur) = Y_H + Y_R$$

$$\text{Yaw torque: } I_{zz} \dot{r} = N_H + N_R \tag{139}$$

$$\text{Roll torque: } I_{xx} \ddot{\varphi} = K_H + K_R$$

$$\text{Propulsion torque: } 2\pi I_{pp} \dot{n} = Q_E + Q_p$$

where the subscripts  $H$ ,  $P$ , and  $R$  refer to the hull, propeller, and rudder, respectively, and  $X_P$ ,  $Q_P$ , and  $Q_E$  represent propeller thrust, propeller torque, and engine torque, respectively. The coupling effects due to roll are included and considered important for high-speed container carriers and others.

Longitudinal forces acting on the ship are written,

$$X_H = -\Delta_x \dot{u} + (\Delta_y + X_{vr})vr + X(u). \tag{140}$$

Added inertia terms  $\Delta_x$  and  $\Delta_y$  (and  $J_{zz}$  in Equation (140) can be estimated from the charts proposed by Motora (1960). When the quantity  $(\Delta_y + X_{vr})$  is rewritten as  $c_m \Delta_y$ , then  $c_m$  may have an approximate value in the interval 0.50 to 0.75 (Yoshimura and Nomoto, 1978), to provide a good estimation for the entire second term. The third term represents ship resistance as a function of speed (see Chapter VI, Vol II).

The propeller thrust  $X_P$  and the propeller torque  $Q_P$  can be written

$$X_P = (1 - t_{p0}) \cdot p n^2 D^4 K_T(J_P) \tag{141}$$

$$Q_P = -2\pi J_{pp} \dot{n} - p n^2 D^5 K_Q(J_P)$$

The thrust coefficient  $K_T(J_P)$  and the torque coefficient  $K_Q(J_P)$  can be computed from the propeller characteristic curves as functions of the advance constant,  $J_P = u(1 - w_p)/(nD)$ . The effective propeller wake fraction  $w_p$ , which is defined with the concept of the propeller thrust identity, may vary from that in the straight running condition. Hirano (1980) proposed the following estimating formula,

$$w_p = w_{p0} \exp(K_1 \beta_P^2), \tag{142}$$

where  $K_1 = -4.0$ , and  $\beta_P = \beta - x_P' r'$ .

The lateral force and the yaw moment,  $Y_H$  and  $N_H$  can be written as,

$$\begin{aligned}
Y_H &= -\Delta_y \dot{v} - \Delta_x u r + Y_{H0}(v, r) + Y_{H1}(v, r, \varphi) \\
N_H &= -J_{zz} \dot{r} + N_{H0}(v, r) + N_{H1}(v, r, \varphi) \\
&\quad + [Y_{H0}(v, r) + Y_{H1}(v, r, \varphi)]x_s.
\end{aligned} \tag{143}$$

Where the terms  $Y_{H0}(v, r)$  and  $N_{H0}(v, r)$  represent the fundamental force and moment, each of which play an important part in the ship maneuvering motion. Inoue et al (1981) express these terms as.

$$\begin{aligned}
Y_{H0}(v, r) &= \frac{1}{2} \rho L d V^2 [Y'_v v' + Y'_r r' + Y'_{vv} v' |Zv'|] \\
&= Y'_{v|v} v' |r'| + Y'_{r|v} r' |r'| \\
N_{H0}(v, r) &= \frac{1}{2} \rho L^2 d V^2 [N'_v v' + N'_r r' + N'_{vvr} v'^2 r' \\
&\quad + N'_{vrr} v' r'^2 + N'_{r|v} r' |r'|].
\end{aligned} \tag{144}$$

where

$$\begin{aligned}
Y'_v &= [a_1 k + f(C_B B/L)](1 + b_1 \tau') \\
Y'_r &= a_2 k(1 + b_2 \tau') \\
N'_v &= a_3 k(1 + b_3 \tau') \\
N'_r &= (a_4 k + a_5 k^2)(1 + b_4 \tau') \\
k &= 2d/L \\
\tau' &= \tau/d
\end{aligned} \tag{100}$$

and  $a_1, a_2, \dots, b_1, b_2, \dots$  etc. are constants. Estimate charts, as functions of the principal dimensions of ship hull, are given by Inoue et al. (1981).

The terms  $Y_{H1}(v, r, \varphi)$  and  $N_{H1}(v, r, \varphi)$  represent the added terms due to inclusion of the roll effect and can be estimated as shown by Hirano and Takashina (1980).

The roll moment acting on ship hull can be written

$$\begin{aligned}
K_H &= -J_{xx} \ddot{\varphi} - N(\dot{\varphi}) \\
&\quad - W \cdot GZ(\varphi) - Y_H \cdot z_H.
\end{aligned} \tag{145}$$

The coupling effect due to the horizontal motions on the motion of roll is reflected in the form of  $Y_H \cdot z_H$ . The vertical distance  $z_H$  (from  $G$  to the point on which  $Y_H$  acts) can be estimated, following Inoue (1979), as a function of  $C_b$ .

Rudder forces and moments, including the hydrodynamic forces and moments induced on ship hull by rudder action, can be written in the following form,

$$\begin{aligned}
X_R &= -F_N \sin \delta \\
Y_R &= -(1 + a_H) F_N \cos \delta \\
N_R &= -(1 + a_H) x_R F_N \cos \delta \\
K_R &= (1 + a_H) z_R F_N \cos \delta.
\end{aligned} \tag{146}$$

The hydrodynamic force induced on ship hull by rudder action is described in the form of  $a_H F_N \cos \delta$ . The coefficient  $a_H$  can be estimated based on some model experimental results, which suggest that  $a_H$  may be expressed as a function of  $C_B$  after Hirano (1980). The rudder normal force  $F_N$  can be written in the form

$$F_N = \frac{1}{2} \rho \frac{6.13 \lambda}{\lambda + 2.25} A_R V_R^2 \sin a_R. \tag{147}$$

where the effective rudder inflow speed and angle,  $V_R$  and  $a_R$ , are calculated as follows,

$$V_R = V(1 - w_R)[1 + K_2 g(s)]^{1/2} \tag{148}$$

with  $K_2 = 1.065$  for the port rudder and  $K_2 = 0.935$  for the starboard rudder and  $w_R$  is the effective rudder wake fraction. The term  $K_2 g(s)$  represents the effect of the propeller slipstream on  $V_R$ , and

$$g(s) = \eta \kappa [2 - (2 - \kappa)s]/(1 - s)^2 \tag{149}$$

where

$$s = 1 - u(1 - w_p)/(nP)$$

$$\eta = D/H$$

$$\kappa = 0.6(1 - w_p)/(1 - w_R)$$

Estimation of the effective rudder wake fraction is made on the assumption that

$$w_R/w_{R0} = w_p/w_{p0} = \exp(K_1 \beta_p^2). \tag{150}$$

The effective rudder wake fraction  $w_{R0}$  of full-scale ships may be obtained from the results of the model experiments in the same manner as for the effective propeller wake fraction  $w_{p0}$  in ship propulsion, that is, by making use of the technique of estimating the full-scale value from the model experimental results while applying the concept of wake ratio.

The effective rudder inflow angle, with the flow-rectifying effect taken into consideration, can be expressed in the form

$$\alpha_R = \delta_R + \delta_0 - \gamma \beta'_R \tag{151}$$

where  $\beta'_R$  is defined as  $\beta'_R = \beta - 2x'_R r'$ . The flow-rectifying effect may be considered to be developed from separate hull and propeller effects with the flow-rectification coefficient  $\gamma$  written as

$$\gamma = C_P \cdot C_S. \tag{152}$$

where

$$C_P = 1/[1 + 0.6\eta(2 - 1.4s)/(1 - s)^2]^{1/2}$$

and

$$C_S = K_3 \beta'_R \quad \text{for } \beta'_R < C_{S0}/K_3$$

$$C_S = C_{S0} \quad \text{for } \beta'_R > C_{S0}/K_3$$

$$\text{with } K_3 = 0.45, \quad \text{and } C_{S0} = 0.5.$$

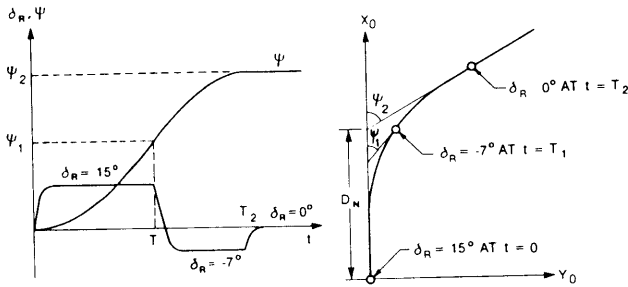


Fig. 194 Illustration of course changing maneuver with rudder angle of  $15^\circ/7^\circ$

The following torque characteristics are used for the main engines:

Slow speed diesel engine

$$Q_E = |Q_P| \quad \text{for } |Q_P| \leq Q_{E\text{MAX}} \quad (153)$$

$$Q_E = Q_{E\text{MAX}} \quad \text{for } |Q_P| > Q_{E\text{MAX}}$$

Steam turbine

$$Q_E = \text{SHP}/(2\pi n).$$

Computed results by Inoue et al (1981) for seven typical ships of different types were developed to verify the accuracy of the method through comparisons with full-scale trial results. The available data were for ships under ballast conditions except for one ULCC at full load and one VLCC at both full load and ballast. The computed results show satisfactory agreement

with all of the full-scale trials in regard both to turning trajectory and to time history of heading angle, ship speed, and propeller rotational speed.

This model, and models of many others using the same basic concepts, for example, those of Mikelis (1985) and NSMB (1984) can be applied in the earliest stages of design, with good results to be expected. Predicted maneuvering performance can then be simulated for comparison with other vessels of known design needs or of demonstrated performance.

Beyond predictions of the standard definitive maneuvers in deep water, mathematical models can be used for many other tasks. Inoue et al (1981) extended their model, for instance, to providing estimates of turning circle and course changing abilities at different drafts and trim. Their formulae become especially useful when one needs estimates of capabilities under loading conditions different from those of actual trials or physical model tests. Course changing abilities were also analyzed by evaluating the effect of applying rudder angle and then corrective rudder (angles 15 and 17 deg) as in Fig. 194. The course changing ability is generally described with the indices of  $\psi_2$  and  $D_N$  with computed results for the container vessel and tanker shown in Fig. 195. Estimation formulae derived to show the effect of loading are as follows:

$$\begin{aligned} \psi_2(\text{Ballast}) &= (1 - A_5 d^*)(1 - B_5 \tau^*) \\ &\quad (1 + C_5 a^*) \cdot \psi_2(\text{Full}) \end{aligned} \quad (154)$$

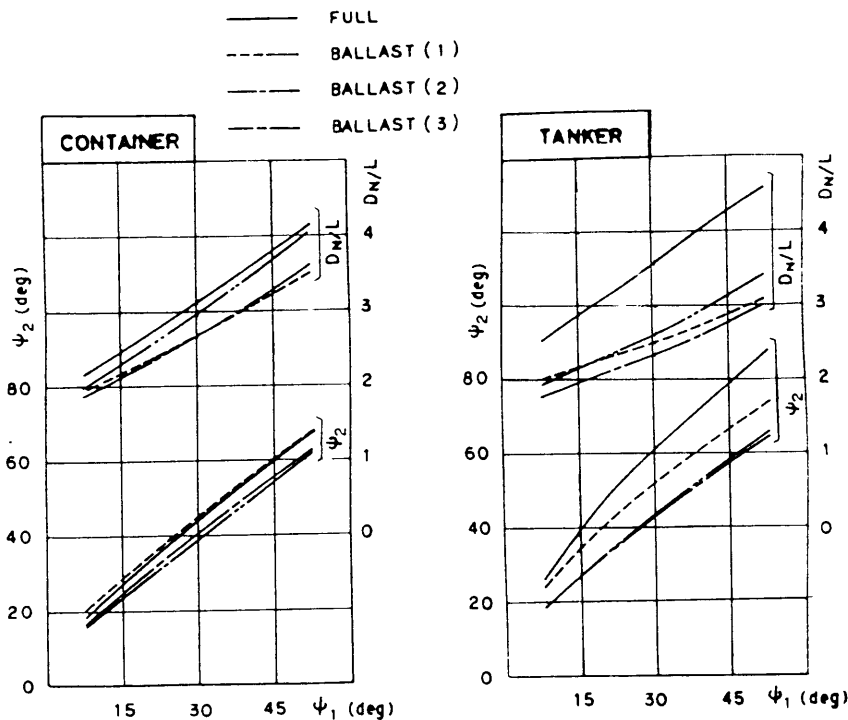


Fig. 195 Computed results of new course distance and new course angle for a containership and a tanker (Inoue et al., 1981)



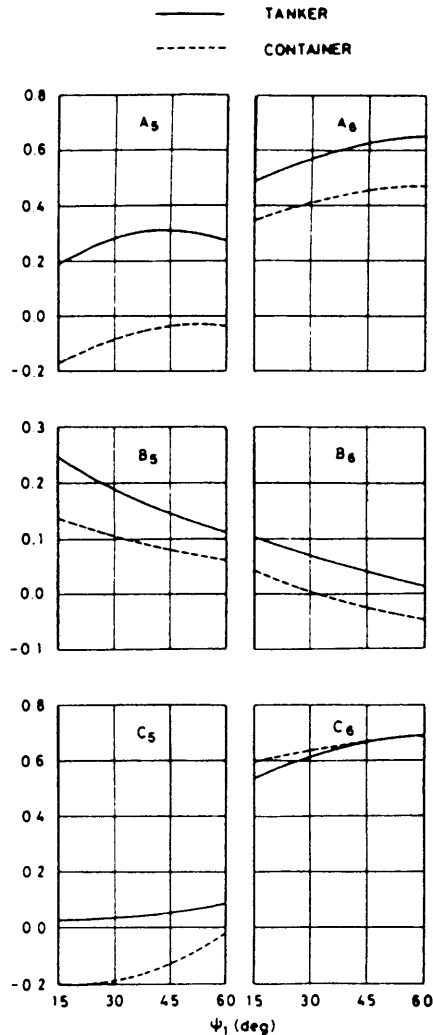


Fig. 196 Coefficients  $A_5$ ,  $A_6$  etc. for indices of course changing ability

$$D_N(\text{Ballast}) = (1 - A_6 d^*)(1 - B_6 \tau^*) \\ (1 + C_6 a^*) \cdot D_N(\text{Full})$$

where the coefficients  $A_5$ ,  $A_6$ , etc. can be determined from Fig. 196. These approximation formulae may have practical utility at sea as well as in design analysis.

Hirano et al (1987) further extended this model to account for lateral thruster forces, wind forces, wave drifting forces, and other forces such as those from tugs or mooring lines. Shallow water and bank effects are also addressed by applying correction factors to various coefficients. The resulting model with graphical output can generate plots useful in meeting IMO requirements for publishing maneuvering booklets and posting information, as well as in design comparison studies. Other derivable information, such as helm angles to check course (see Fig. 197) under specified wind conditions, can be of practical help to the mariner.

**16.8 Model Testing and Advanced Mathematical Models.** Given only the principal characteristics of the ship design, the mathematical models described in the previous section can produce a usable prediction of maneuverability. Once the hull form shape is defined, however, it is desirable to refine the analysis in order to predict maneuvering capability with greater assurance.

If the design uses the hull form, appendages, and rudder(s) from an existing maneuvering model test series, coefficients are available from the series without further testing. The Series 60 data of Todd (1963) and the wide-beam, shallow-draft, high-block-coefficient bulk carrier of Roseman (1987) provide two such series. Further refinements to the hull form, particularly the afterbody, will require additional model tests to verify performance.

Traditionally, model tests of the refined hull form using the rotating arm or planar motion mechanism (PMM) have been performed to develop coefficients for mathematical models such as those described in Section 8). Since model testing is expensive, only the fully appended model is usually tested. Definitive maneuvers are then predicted, with the model used to determine adequacy of the design through application of criteria, direct comparison with existing ships, use of the diagram of steering, and other techniques. Full scale free running model tests as described in Section 7 are also used to a limited degree to demonstrate the adequacy of a design.

The fully appended tests and the perturbation model

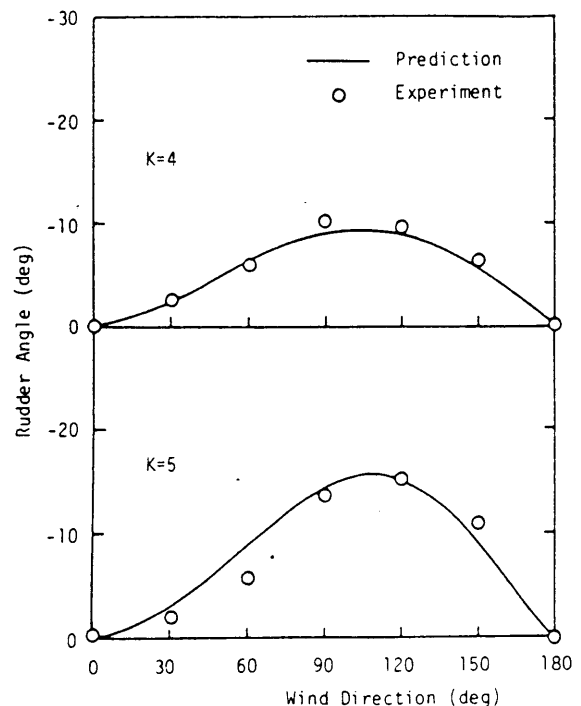


Fig. 197 Maneuvering motion in wind (LNGC model) (Hirano, et al 1987)

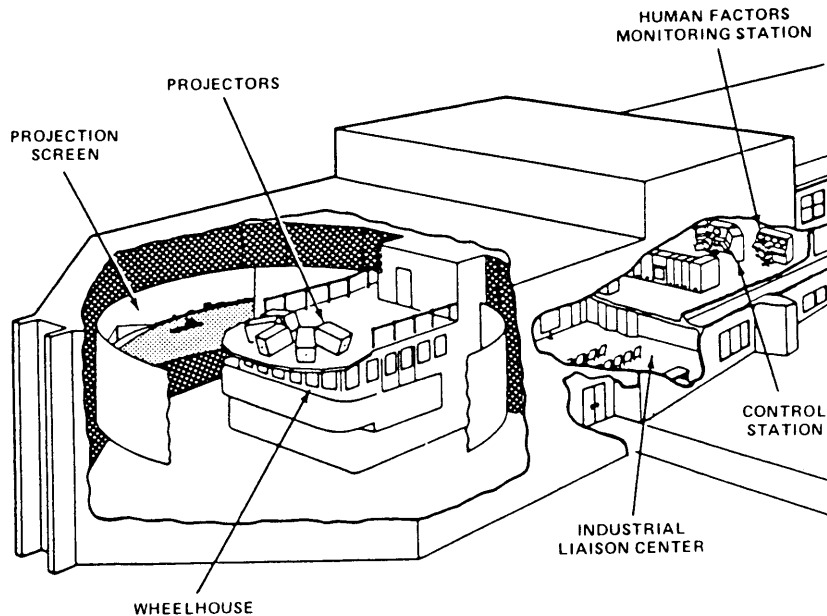


Fig. 198 Cutaway showing CAORF shiphandling simulator system

such as that of Abkowitz (1964) work well as a final check of capabilities but do not practically assist with the alterations that may need to be made to improve capabilities of the hull form. The main reasons for this shortcoming are the cost and time required for testing. Changing the rudder to a more efficient form, for instance, would require a complete retesting since the properties of a new rudder and the complex interaction effects with the hull are not separately identifiable in these models.

Fediaevsky and Sobolov (1964), Asinovsky, et al (1987), the Japanese Mathematical Modeling Group (MMG) through Kose (1982), Dand (1987), Ankudinov (1987), Mikelis (1985), and others recommend using mathematical models that are more physically oriented. Authors of these reports attempt to separate the effects of hull, rudder(s), and propeller(s) in an approach much like that taken with the simplified equations used in the prediction models described in Section 16.7. Some combination of series model tests and theoretical coefficient prediction methods, along with proof-tested interaction relationships between hull, rudder, and propeller, will be necessary to make these models a practical reality for the ship designer. Their utility, however, will be tremendous, allowing easy, quick, and inexpensive tradeoffs among rudder, hull-form, and propeller alternatives in improving ship design.

**16.9 Shiphandling Simulation.** Accident studies such as Special Study (1981) have concluded that the primary cause of maneuvering accidents is operator error. The consideration of the human as part of the control loop of Fig. 1 (Section 2.1) is necessary if the vessel is to have adequate controllability for the op-

erational scenario and the conditions anticipated.

Under most conditions, a pilot or shiphandler will deliberately use less of the controllability of a ship than it inherently possesses. The shiphandler must allow for his inability consistently to anticipate exact vessel response under changing conditions, and his inability always to make perfect judgments. He must also allow for time lags in machinery and other human controlled responses. Accordingly, a ship may be justly assumed to have less "piloted" controllability than "inherent" controllability. The difference is called the "piloting margin" or margin of error, which is a prudent consideration in all forms of transportation used by man.

Shiphandling simulators use a highly realistic theater- or stage-like setting to allow the study of ship controllability with direct inclusion of human responses and with allowances and reruns to accommodate variations from man to man and from passage to passage. For realism the entire bridge arrangement is usually duplicated as shown by example in Fig. 198. Often the "real world" outside the conning station is displayed by projection on a screen away from the bridge. Experienced pilots are normally chosen to handle the "vessel," and they may be provided with familiar navigational aids such as conventional bridge instruments, a usable radar display, and a collision avoidance system. Leading lights (range marks), buoys, shorelines, and key visual cues, along with other vessels, can also be portrayed visually on the screen.

Historically, simulation has been associated with training instead of research as such. A familiar example is the aircraft cockpit simulator known as the

Link trainer, which has seen service at least since World War II. First-generation maritime simulators were in operation by 1968 (Puglisi, 1987).

In the early 1970's, it became apparent that research-oriented shiphandling simulators were needed to investigate problems associated with marine transportation. Such simulators would have the flexibility necessary to investigate various aspects of the real-world problems that concern the human control of ships.

In the broader picture, the approach to studying problems related to the human control of vessels in restricted waterways is largely fragmented, that is, naval architects address vessel design; civil engineers, channel design; the U.S. Coast Guard, aids to navigation; psychologists, the decision-making processes of the mariner on the bridge; etc. A complete examination of a marine transportation system requires inclusion and integration of all relevant factors in the complex interactions of man, ship, and environment. Some of the important factors are:

- Channel geometry
- Vessel hydrodynamics and aerodynamics including shallow-water, bank and passing-ship effects
- Prevailing current and wind forces
- Formal aids to navigation, such as lights, ranges (leading marks), and buoys
- Informal aids to navigation, such as land features and buildings
- Visibility, ambient lighting, and other environment effects
- Human operator control and decision processes
- Availability of direct assistance, as by tugs

In considering the need to include these interrelationships, a logical approach might seem to be to study the operating system in its natural environment—in situ, so to speak. Costs and risks make such studies impractical to do properly. To help ensure that accidents should not occur, the customary procedure has been to overdesign the channel, that is, to provide more channel than is necessary or optimal to permit adequate safety in the face of unknown factors. Such an approach is not cost effective in view of modern dredging costs; nor is it cost effective in view of the paradoxical circumstance, now well established, that providing greater searoom does not necessarily provide greater safety but may provide less.

A number of methods of analysis are available, but each method differs in the degree to which it can address the entire navigational process and in the time and cost that it entails. Hydraulic models as discussed in Section 7.3 provide a good representation of bank and bottom irregularities and their effects on hydraulic forces. The approach, however, has high cost and time requirements, and does not usually address the navigation process or accurately model the vessel trajectories because of the small ship models involved and the time-scaling difficulties in using moving models.

The shiphandling simulator provides the ability to operate in real time and allows accurate use of the human being. The approach is limited only by the accuracy of its mathematical models of ship and waterway (including current), and by the physical and visual resemblance of the arrangement to reality. Real-time operations, however, are time consuming and costly, even though only parts of any one voyage usually need to be simulated, whether for research or training.

Shiphandling simulators are controlled by computers employing mathematical models of varying complexity to predict ship trajectories. Effects of shallow water, banks, currents, wind, waves, and even tugs are often included in the mathematical model. To allow use of these effects, the data base must provide definition of the waterway's physical and environmental conditions in addition to a thorough mathematical description of the behavior of the ship. McIlroy and Carpenter (1979) summarize the technical aspects of fast time simulation at CAORF.

While the computer generated visual display has become the most popular approach, early simulators utilized a point light source and shadow projection arrangement to effectively simulate night operations (Hoof, 1975). There is also a "model board" approach, in which a miniature camera probe moves over a model harbor as the ship is steered, and pictures of the surroundings are projected on the screen. The use of simulators to deal realistically with maneuvering problems has become fairly well accepted (Keith, 1977). Table 35 lists representative shiphandling simulator installations existing in 1986 (Puglisi, 1987).

The shiphandling simulator is used for a wide variety of purposes including design of the ship (determination of required inherent maneuvering capabilities, bridge arrangement and equipment layout, and determining operational procedures, among other applications), training of the mariner, design of harbors and waterways, the placement of navigational aids, and others. Puglisi (1987) provides an overview of the history and predicted future development of marine simulators.

One of the most extensive research projects to use the shiphandling simulator was a study at the CAORF simulator on the widening of the Panama Canal (Puglisi et al., 1987). In addition to real-time simulations with experienced pilots on the full-scale bridge, many off-line or "fast time analysis" runs were made to investigate alternative layouts.

Representation of pilot control characteristics is necessary on a fast-time study of trajectories. Basically, a rudder command is generated if the ship track shows deviations in heading and distance of the ship from the desired trajectory, indicated as follows:

$$\delta_R = a(\psi - \psi_c) + b'\dot{r}' + c'l'_p \quad (155)$$

where

(Continued on page 362)

Table 35—Full Bridge Simulators (Puglisi, 1987)  
(IMSF Correspondence, & Various MARSIM Conference Papers)

Operator	Location	Start Date	Manufacturer	Image Generator Source	Image Display Type
Japan Radio Communications, Ltd.	Tokyo, Japan	1965	Japan Radio Communications, Ltd.	4	3
Swedish State Shipbuilding Experimental Tank Simulator (SSPA)	Gothenberg, Sweden	06/67	SSPA	Unique	3
TNO/IWECO Institute of Mechanical Engineering	The Netherlands	04/68	TNO/IWECO, Delft, Holland TNO/IZF, Soesterberg, Holland (Advisors)	3	1
Maritime Research Institute Netherlands, Wageningen	The Netherlands	11/70	TNO/Delft, Holland TNO/IZF, Soesterberg, Holland (Advisors)	3	1
Hiroshima University	Hiroshima, Japan	06/71	Ship Motion Laboratory	Unique	1
Bremen Nautical Academy Simulator No. 1	Bremen, W. Germany	03/75	Messerschmitt-Bolkow-Blohm, GMBH (MBB)	Unique	2
Simulator No. 2	Bremen, W. Germany	1978	Messerschmitt-Bolkow-Blohm, GMBH (MBB)	2	1
TNO Institute for Perception Soesterberg, The Netherlands	The Netherlands	06/75	TNO-IZF, Soesterberg, Holland	4	1
Ishikawajima Harima Heavy Industries Co., Ltd. (IHI)	Tokyo, Japan	06/75	Ishikawajima Harima Heavy Industries	Unique	1
University of Osaka	Osaka, Japan	09/75	Hitachi Electric Co. (Visual) Furuno Electric (Radar)	Unique	1
Computer Aided Operations Research Facility, U.S. Maritime Administration	New York, USA	01/76	Sperry Systems, USA	1	1
Royal Netherlands Naval College, Den Helder	The Netherlands	10/76	Royal Netherlands Naval College, Netherlands	Unique	1
Tokyo Univ. of Mercantile Marine	Tokyo, Japan	10/76	Tokyo Univ. of Mercantile Marine	Unique	1
Marine Safety International	New York, USA	11/76	Sperry Systems, USA	4	1
College of Maritime Studies Simulator No. 1	Warsash, England	03/77	Racal-Decca Systems & Simulator, Ltd.	2	2
Simulator No. 2	Warsash, England	02/81	Racal-Decca Systems & Simulator, Ltd.	2	2
LMT Simulator & Electronics Div.	Trappes, France	06/78	LMT	1	4
South Shields College of Nautical Studies	South Shields, U.K.	1980	Racal/Decca, U.K.	2	2
Glasgow College of Nautical Studies	Glasgow, U.K.	1980	Racal/Decca, U.K.	2	2

**Table 35—Full Bridge Simulators (Continued)**  
(IMSF Correspondence, & Various MARSIM Conference Papers)

Operator	Location	Start Date	Manufacturer	Image Generator Source	Image Display Type
Ship Maneuvering Simulator	Trondheim, Norway	01/80 06/83	Messerschmitt-Bolkow-Blohm Second Visual System	2 Unique	1 1
Ship Analytics, Inc.	Connecticut, USA	03/80	Ship Analytics, Inc., USA	1	2
Maritime Institute of Technology and Graduate Studies (2 Bridges)	Maryland, USA	1982	MBB/Singer Link	2	1
SUSAN Schiffsuhrungs-Simulator Hamburg	Hamburg, W. Germany	03/83	Krupp Atlas Electronics Bremen, W. Germany	1	2
CASSIM—Dept. of Maritime Studies Univ. of Wales Institute of Science & Technology	Cardiff, U.K.	07/82	Racal/Decca/Marconi	1	2
CNHMF					
Simulator No. 1	Leningrad, USSR	1983	Seagull, Norway	2	1
Simulator No. 2	Leningrad, USSR	1985	Seagull, Norway	2	1
Maritime Training and Research Center	Ohio, USA	09/83	Ship Analytics, Inc., USA	1	2
Quindao Maritime College	Quindao, China	1985	Seagull	2	1
Finsim Technical Research Center of Finland, Ship Laboratory	Helsinki, Finland	03/85	Racal/Decca/Marconi	1	2
Australian Maritime College	Tasmania, Australia	04/85	Krupp Atlas Electronics, W. Germany	1	2
Australian Navy	Tasmania, Australia	06/85	Krupp/Atlas Electronics, W. Germany	1	2
Maritime Technical College	Achiya, Japan	1986	Tokyo Keiko Co., Ltd Japan Radio Co., Ltd.	1	2
National College of Marine Science Technology	Kee Lung, Taiwan	1986	Krupp Atlas Electronics, W. Germany	1	2
United States Coast Guard Academy	Connecticut, USA	03/86	Ship Analytics, Inc., USA	1	2
Harry Lundberg's School of Seamanship (SIU)	Maryland, USA	04/86	Ship Analytics, Inc., USA	1	2
Kobe Mercantile Marine University	Kobe, Japan	1986	Furuno Electric Co., Ltd.	2	1
West German Navy	Muewick, Germany	11/86	Krupp Atlas Electronics, W. Germany	1	2

Note: This table includes all simulators known in 1986.

(Continued from page 359)

- $\sigma_R$  = rudder command  
 $\psi$  = ship heading angle  
 $\psi_c$  = channel direction  
 $l_p$  = distance between the ship and the desired trajectory relative to the ship length  
 $a, b, c'$  = gain constants  
 $\dot{\gamma}'$  = nondimensional rate of change of ship heading

Anticipatory control in negotiating turns in the waterway can be included. For this situation, rudder action starts in advance of reaching the actual location of the turn in the waterway.

Criteria for acceptability under piloted control can include those addressed in Section 15. In the harbor and restricted waterway or channel situation, additional criteria may be applied in shiphandling simulation studies. Panel H-10 (1975) proposed a series of controllability indices to give realistic measures of capability:

- Clearance distance of ship's swept path to channel bank and other obstacles along the path
- Preferred speed relative to upper and lower safe limits
- Rudder deflections required and used en route
- Wind and current effects
- Margin of bottom clearance along path

The Panel also proposed the concept of the "ABC" harbor wherein a test harbor or waterway situation could consist of a series of elemental maneuvers linked

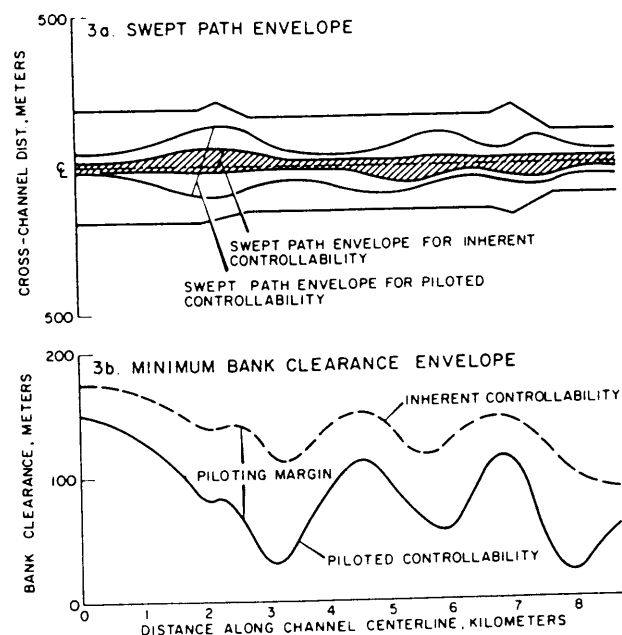


Fig. 199 Expected characteristics of swept path and bank clearance during ABC port entry

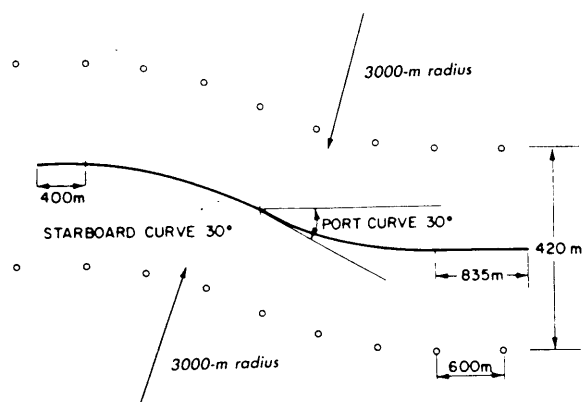


Fig. 200 Sketch of maneuver used during "S-shaped" channel experiments. Total length of maneuver is 4500 meters

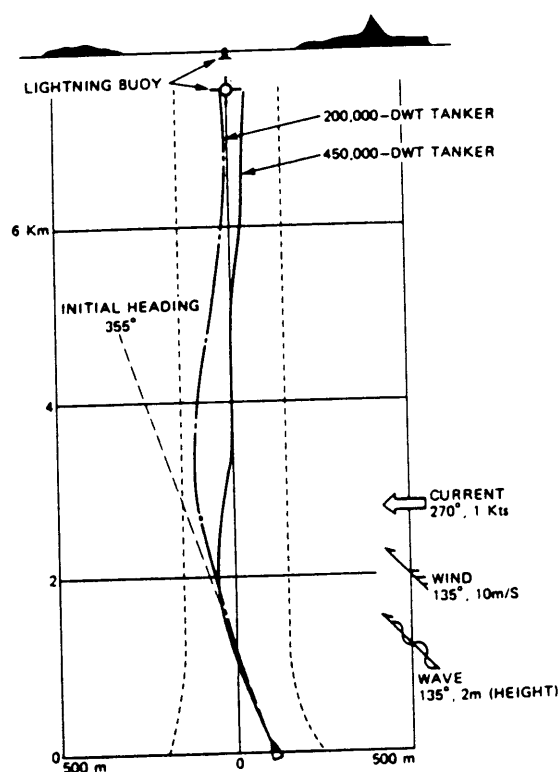


Fig. 201 Example of records from coursekeeping tests

together. The elemental maneuvers could be drawn from difficult or representative passages from a number of different real-life situations the design ship would be expected to encounter. Fig. 199 shows an application of the swept path or bank clearance criteria after a number of runs were made through the test situation. Within the path envelope fall the trajectories of the trial runs, and an idea of how well the vessel-human system can perform is derivable from the plot.

Research utilizing the human must be with great care and with proper understanding if correct results are to be obtained. As an example, in an experiment

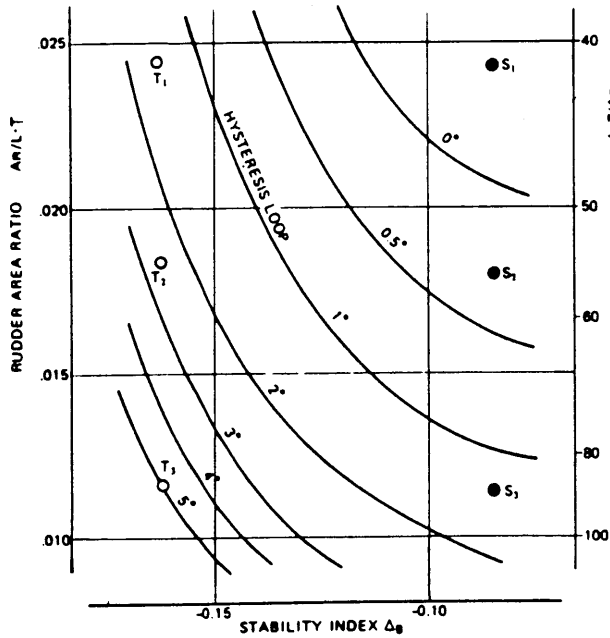


Fig. 202 Dynamic variations of spiral loop half-width with changes in hull stability index

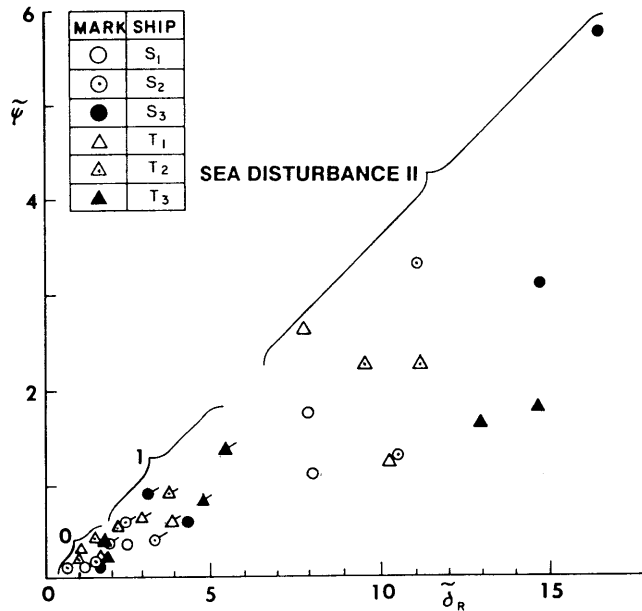


Fig. 203 Manual coursekeeping performance

for Exxon, investigators using the MARIN simulator at Wageningen (Panel H-10, 1975) attempted to determine the necessary width for an S-shaped channel to safely accommodate a 400,000-dwt vessel (see Fig. 200). The intuitive belief is that the wider the channel, the better the seafarer will do. The narrowest channel simulated did result in the worst performance (largest excursions from channel centerline). It was found, however, that there is an optimal width. A marked hypothetical channel of moderate width provided a bet-

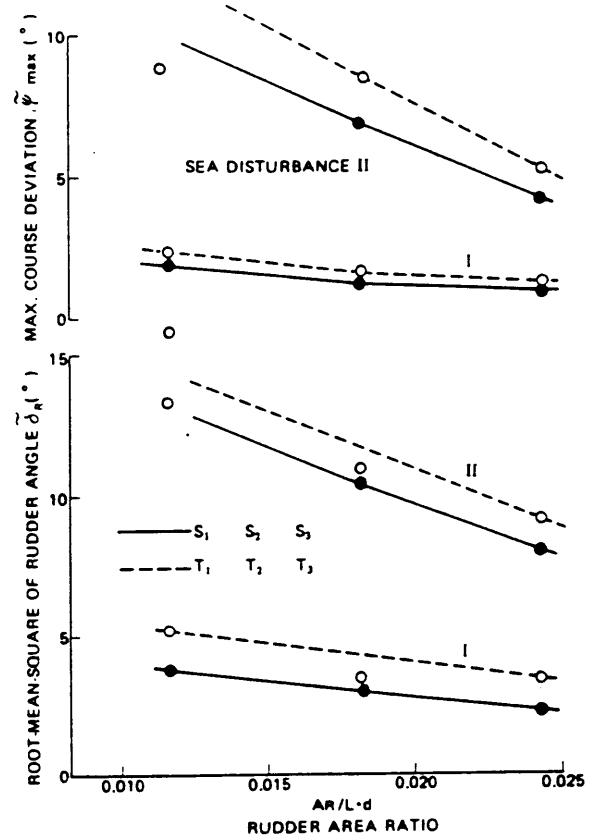


Fig. 204 Maximum course deviation and rudder angle vs. rudder area ratio

ter guide for the pilot than did a very wide channel. Apparently, the narrowness helped him anticipate the needed maneuvers and kept him moderately stressed, (i.e., alert) so that he did a better job.

Ohtagaki and Tanaka (1984) report use of the IHI Ship Maneuvering Simulator to determine the controllability adequacy of a 450,000-dwt ULCC. Piloted operations of the design were compared with those of an existing 200,000-dwt vessel (see Fig. 201 for an example of test records). Results indicated that the new design would be controllable by the bang-bang rudder control with ease comparable to that of the existing smaller design.

In another study, runs of a 20,000-dwt wide-beam, full-form, small- $L/B$  vessel were performed to study the level of directional instability allowable. Fig. 202 shows the dynamic stability index,

$$\Delta_B = \frac{N'_r}{Y'_r - (\Delta'_x + \Delta'_y)} - \frac{N'_B}{Y'_B}$$

plotted against rudder area ratio. The vacant circles marked  $T_1$ ,  $T_2$ , and  $T_3$  and the filled circles  $S_1$ ,  $S_2$ , and  $S_3$  represent the combinations of  $C_B/(L/B)$  and rudder area ratio adopted for the test ships. The manual coursekeeping simulations were performed at three levels of sea disturbance:

Sea disturbance relative to ship	Wind		Wave	
	Direction (deg)	Speed (m/s)	Direction (deg)	Height (m)
0	—	0	—	0.0
I	150	10	150	1.5
II	150	20	150	3.0

To evaluate the coursekeeping performance of these ships, root-mean-square values of course deviation  $\psi$  and rudder angle,  $\bar{\delta}_R$ , were plotted on a graph as in Fig. 203 and 204. The results suggest that coursekeeping performance was impaired, as shown by increases in both course deviation and applied rudder angle due to reduction of either rudder area ratio or bare-hull dynamic stability, but rudder area was the more important. Also suggested is that a hysteresis loop width of 4 deg should cause no appreciable difficulty for manual coursekeeping, provided that the rudder is of adequate size. The loop width could thus serve as a practical stability design criterion for this class of ship.

Ohtagaki and Tanaka (1984) looked at the effects of wind on LNG vessels of differing tank concepts. Rudder angles necessary to maintain course in straight

and bent channels were evaluated with rudder angle margin defined as

$$\delta_R = 35 \text{ deg} - (\bar{\delta} + \delta_{SD}) \quad (118)$$

where  $\bar{\delta}_R$  and  $\delta_{SD}$  are the mean value and standard deviation of rudder angles applied for keeping the initial course.

For vessels having a variety of controllability needs, such as oceanographic vessels and salvage ships, the simulator can be used in studying maneuvering capability and operational procedures to determine vessel adequacy. One such study was reported by Miller, et al (1984). Comparative measures such as the time to carry out a 360-degree standing turn can be evaluated by trying different machinery and propeller arrangements and bow thruster options.

## Section 17

### Design of Rudder and Other Control Devices

"The rudder serves the twofold function of stabilizing a straight motion by fin effect and controlling the ship in steering and maneuvering," (Norrbin, 1960)

**17.1 Rudder and Control Device Design Process.** The rudder, other control surfaces, and control devices such as bow thrusters are critically important features in achieving vessel controllability goals. Although other control devices can assist in achieving controllability, the rudder is nearly always the most prominent. Accordingly, the rudder receives the greatest attention in this section, which outlines the design process.

At the concept design stage, the naval architect has little on which to base decisions. In sketching the vessel profile, what may temporarily suffice is to allow room for what merely looks right: a reasonably shaped rudder of the size and type commonly seen for ships of the anticipated class and service. Thrusters should be sketched in if they are commonly used. If possible, mission requirements should be defined by this stage, and tradeoffs brought under consideration.

During the preliminary design development of the hull form, decisions must be made regarding the shape of the underbody, distribution of buoyancy, shapes of sections, and the underwater profile. Propeller, rudder,

and thruster sizes and placement can then be defined. All of these items affect the controllability of the ship and are coupled as noted in earlier sections. Therefore the type of stern, the shafting supports, the type of rudder, its hydrodynamic efficiency, its structural supports, and clearances between propeller and rudder should be evaluated.

Toward the end of the preliminary design stage, the rudderstock location should be examined to see whether structural supports can be provided and whether steering gear can be arranged as normal in past practice. If not, special arrangements should be considered. (For example, the steering gear rams may be located a deck below the pumps and motors that drive them.)

The contract design stage generally includes an early review of the previous design work. This review is to check whether typical "last-minute refinements," particularly of the hull form, require changes in the rudder shape, efficiency, or location. These changes are made along with the usual effects of continuing design developments (for example, changes in the pro-



pellor location). The results of tests ordered earlier are also used, and there may still be time to order additional maneuvering design studies.

The designer is limited in design of the rudder and other control surfaces by four major constraints:

(a) In profile, the rudder should fit within the dimensions dictated by the shape of the hull. Its maximum span should fit within the vertical distance measured from the bottom of the deepest projection below the baseline of the ship permitted by draft or docking restrictions upward to the bottom of the hull immediately over the rudder or to the minimum prescribed depth below the water surface (see Section 17.2), whichever is lower. If the rudder is abaft the propeller, its chord should fit within the horizontal distance from the extremity of the ship to a line corresponding to a prescribed clearance from the propeller. (Control surfaces that extend significantly beyond the block dimensions of a ship, such as fin stabilizers, or the bow planes on some submarines, are almost always designed to be retractable.)

(b) The rudders, in maintaining a straight course, should minimize speed loss at every level of ship powerplant output.

(c) The rudder, the rudder stock, the rudder support, and the steering engine, considered together, should be of minimum size, weight, complexity, and initial cost, consistent with needed effectiveness and accepted standards of reliability and low upkeep costs.

(d) Undesirable effects of the rudder on the ship such as rudder-induced vibration should be kept to a tolerable level.

Speed loss and angle of heel during limit maneuvers are excluded from the last constraint since for conventional ships fitted with the usual appendages both of these items are mainly functions of the severity of the maneuver. They should be considered when the limiting design maneuvers are selected. Speed loss during maneuvers is a function of the type of propulsion plant and of the ship configuration; it is not a direct function of the rudder design. Angle of heel during maneuvers is a function of hull configuration and the mass distribution of the hull, and only secondarily of rudder design.

Violation of any of the four listed constraints constitutes a misjudgment in rudder design. Because of the influence of the rudder on ship power [constraint (b)] adherence to a minimum total ship cost [constraint (c)] requires consideration of the entire ship design process.

From a hydrodynamic point of view, the basic considerations of rudder design are summarized as follows:

(a) *Type of Rudder:* All-movable rudders are desirable for their ability to produce large turning forces for their size (Section 12). The following ranges of numerical values can be used as a rough first guide in selecting a balance ratio according to block coefficient

(by "balance ratio" is meant the rudder area forward of the rudder stock divided by the total rudder area):

Block coefficient, $C_B$	Balance ratio range
0.60	0.250 to 0.255
0.70	0.256 to 0.260
0.80	0.265 to 0.270

Structural considerations, cost, the need for additional stabilizing side forces provided by a horn, and the considerations may require use of other types of rudders such as the semisuspended (or horn) rudder. The horn type is also favored for operations in ice.

(b) *Location:* Every effort should be made to place the rudder abaft of the propeller at the stern. Combinations such as twin rudders with single screw or single rudder with twin screws should be avoided. At zero or low ship speed, the propeller ship stream increases rudder effectiveness to a great extent. The stern rudder is far more effective than the bow rudder for maneuvering ahead. The main reason for this difference in effectiveness is the direction of drift angle, which makes a substantial contribution to the turning of the ship when the rudder is located at the stern. The contribution of drift angle is in the opposite direction if the bow rudder is used, reducing ahead maneuvering performance. For astern maneuvering, the bow rudder becomes the more effective, for the same reason.

(c) *Area:* A suitable rudder area for a given hull form can be selected to satisfy desired degrees of dynamic stability and maneuvering performance in calm water. Since full-form ships are generally less stable, relatively more rudder area for these ships is helpful for meeting stability requirements. The final determination of rudder area should reflect the fact that relatively large rudders provide superior performance under adverse conditions of wind and wave.

(d) *Height:* Although rudder height is generally limited by the stern shape and draft, rudder height should be increased as much as possible, to obtain the more efficient higher aspect ratio. The bottom of the rudder is kept above the bottom of the keel for protection, with high clearances in cases where there is frequent operation with trim by the stern.

(e) *Section Shape:* Relatively thick streamlined sections (e.g., NACA 0018 and 0021) are desirable, because these sections have a relatively constant center of pressure. Thick sections are also superior from a structural point of view, and they offer reasonable drag characteristics.

(f) *Rate of Swing:* In addition to the size and hydrodynamic efficiency of the rudder design, the rate of swing should be considered. The effect of an increase over the  $2\frac{1}{2}$  deg/sec standard rate is greatest on fast and responsive vessels.

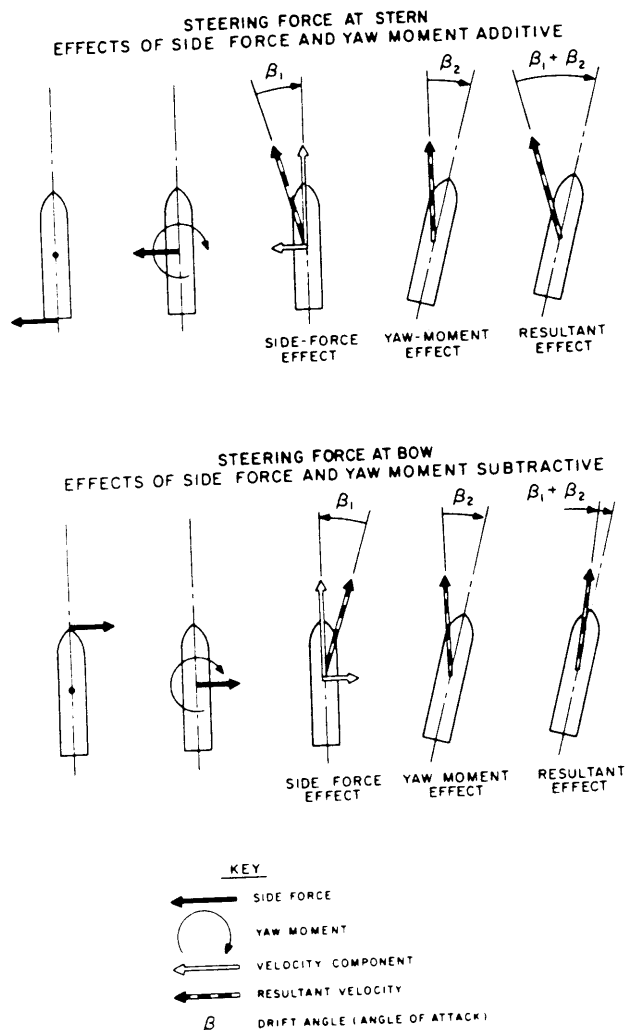


Fig. 205 Effect of location of steering force (Crane, 1973)

Large full-form ships benefit more from having large-area rudders than from an increase in rate of swing.

The following sections address these basic items in more detail and review other control devices that can be used to improve the controllability of the basic vessel.

**17.2 Rudder Types and Location.** The type of rudder and its location and placement relative to the propeller have significant influence on rudder effectiveness and ship controllability. Rudders should be located near the stern and should be located in the propeller stream for good controllability.

Both experience and theory show that for a dynamically stable forward-moving ship at all speeds except dead slow, lateral control forces should be exerted at the stern and not at the bow. This assertion can be demonstrated as follows:

The formula for a ship's dimensionless turning rate (ignoring nonlinear effects) as derived from the linear

equations of ship motion for dynamically stable ships (Section 6.4) is:

$$\text{Turning rate} = \frac{L}{R} = \delta_R \left[ \frac{Y'_v N'_\delta - N'_v Y'_\delta}{Y'_v N'_r - N'_v (Y'_r - \Delta')} \right] \quad (26b)$$

where  $L$  is ship length,  $R$  is turning radius, and  $\delta_R$  is rudder angle. Although Equation 26b relates properly only to dynamically stable ships, it illustrates the point for any vessel.

With conventional rudder location at the stern, the dimensionless turning rate is proportional to the sum of the magnitudes of the two numerator terms (as a result of canceling signs, etc.). But if the rudder is located at the bow, the sign of the factor  $N'_\delta$  is reversed, and turning rate is then proportional to the difference in the magnitudes of the two terms.

Physically this relationship is explained as follows: A lateral control force at the *stern* produces two actions—rotation of the hull in one direction and trans-

lation to the opposite side (Fig. 205). When combined with forward ship motion these actions generate drift angle in the same direction, and drift angle brings into play the large hydrodynamic side force and consequent yaw moment that actually causes the turning. If, instead, the lateral control force acts at the bow, the contributions to drift angle due to yaw rotation and lateral translation are in opposite directions and tend to cancel each other. Because both contributions are large, their difference is small, and turning rate is much smaller than in the rudder-aft case.

Locating rudders at the stern in the propeller race takes advantage of the added velocity of the race both at normal ahead speeds and at zero ship speed. This advantage is significant and may not require any increase in propulsion power over what would be required if the rudder were not in the race. The reason for this fortunate circumstance is that a properly shaped rudder in the race can recover some of the rotating energy of the race which would otherwise be lost. There are, however, some negative aspects associated with locating a rudder in the propeller race. One is the possibility of rudder-induced ship vibration. For this reason, clearances of one propeller radius or more are common between the propellers and rudders of high-powered ships. Weinig (1947) further cautions against locating a rudder directly behind the centerline of the propeller shaft on high-speed ships, because at high speeds the propeller hub sheds a vortex or cavitation cone which tends to erode a rudder located directly abaft the hub. Because of this effect, twin rudders of high-speed ships are sometimes displaced a short distance athwartships from the centerline of the propeller shaft, but are nevertheless still substantially in the propeller race. Locating twin rudders off the shaft centerline may also be desirable to permit shaft withdrawal during repair or overhaul of the ship.

Some kinds of ships with specialized functions have bow control surfaces as well as stern control surfaces. For example, double-ended ferry boats, which do not turn around at their terminals, have a bow rudder as well as a stern rudder so that no matter which way the ferry goes, it has a rudder at its "stern."

Submarines have horizontal bow planes and stern planes to control their motion in the vertical plane. Bow planes are moderately effective in this case because they either extend beyond the hull lines or are located on a superstructure above the main hull and hence do not interact too unfavorably with the hull. Bow planes extending beyond the hull lines are usually made retractable. The primary function of bow planes is to improve control at low speed at periscope depth under a rough sea. In the case of submarines that are very unsymmetrical about the  $xy$ -plane, bow planes are also useful to control depth at very low speeds deeply submerged; in this case the stern planes can cause ambiguous effects for reasons associated with the existence of the hydrostatic moment,  $M_\theta$ . This

topic is more fully discussed by Arentzen and Mandel (1960).

If possible, surface-ship rudders should be located so that the hull of the ship at the waterline covers the top of the rudder throughout its arc of swing. Keeping the rudder covered acts to prevent aeration even if the depth of submergence of the top of the rudder is small. On some ships this covering is easily achieved.

The trend towards wide stern and transom-stern merchant ships, initiated primarily to increase propeller-hull clearance as ship speed increases (Hadler and Cheng, 1965), facilitates permitting the hull to completely cover the rudder.

On some merchant ships, the top of the rudder should be kept as far below the water surface as possible. Shiba (1960) indicates that the depth of submergence ( $I$ ) to the midspan of the rudder should be not less than about 0.9 of the span ( $b$ ) to avoid the deleterious effects of the free surface on rudder lift. If the submergence ratio is less than 0.9, the effect on the rudder normal force coefficient is reduced as was shown in Fig. 127 (See also Section 14.3).

Usually the shape of a ship's hull is developed without particular regard to the rudder. In that event the rudder location should conform to the shape of the hull.

With few exceptions, the axes of ships' rudders are vertical and the axes of submarines' bow and stern planes are horizontal. Exceptions are the canted rudders used on a few large tankers and the "X-stern" used on certain submarines with the four control surface axes located at 45 deg to the horizontal and vertical.

Fig. 206 shows the major rudder types available to the designer. The performance characteristics of some have been discussed in Section 14. The following four rudder types will be examined in the light of the four constraints of Section 17.1:

- (a) All-movable rudder [c, g, h of Fig. 206, see also Figs. 54, 121, 142(a), 207, and 149]
- (b) Horn rudder [e and f, see also Figs. 143(b) and 208]
- (c) Balanced rudder with fixed structure [d, see also Fig. 143(a)]
- (d) All-movable rudder with tail flap [see Fig. 142(d)]

Each of these types has been used as a single or multiple rudder on single and multiple-screw ships. As noted in Section 14 the fourth type is most commonly used as stabilizer fins on ships and only rarely as a rudder, even though any specified level of course-changing ability (but not controls-fixed stability) can be achieved with less rudder area with this than with any of the other types. The main disadvantages of this type of rudder are the complexity and cost of its construction and maintenance, and its being less effective astern than the simpler, all-movable rudder.

With the possible exception of the large, fast ships

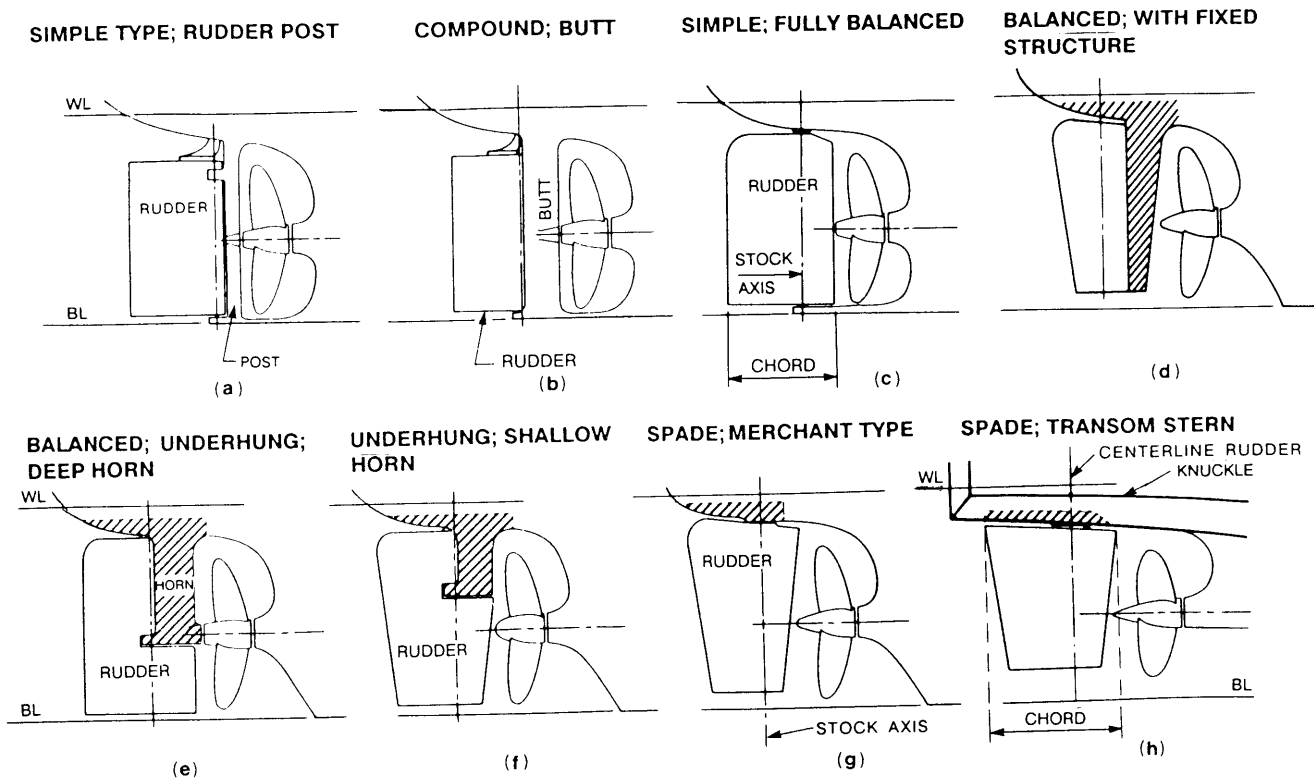


Fig. 206 Various rudder-fin arrangements (Saunders, 1965)

discussed in the next paragraph, the all-movable rudder is preferable for ships that possess controls-fixed stability without a rudder. For ships that are unstable without a rudder, the rudder area needed to achieve controls-fixed stability may be larger than that necessary to provide the specified course-changing ability. If so, the horn rudder or balanced-with-fixed-structure rudder may be an attractive alternative to the all-movable rudder because the total (fixed plus movable) area of either of these rudders can be adjusted to provide the necessary controls-fixed stability while the movable area can be adjusted independently to provide the required limit-maneuver characteristic. Minimum total area generally satisfies the second but not necessarily the third constraint of Section 17.1, while minimum movable area should satisfy the third constraint.

The principal disadvantage of an all-movable rudder is that unless structural support is provided to the bottom of the rudder (see Figs. 54 and 207) the rudder stock must withstand a substantial bending moment as well as the torque moment. The bottom-supported type of rudder was common on slow- and medium-speed single-screw merchant ships, but its use is avoided on high-speed ships because the cantilevered support is a potential source of vibration. Also, its contribution to the support of the rudder may be structurally complicated.

While the required rudder stock size is not excessive for most ships, it tends to become excessive on large,

fast ships. On these ships, a reduction in required rudder stock size can be achieved by extending the lower support bearing down into the horn rudder as far as practical, or by using either the horn rudder or the balanced rudder with fixed structure. With these rudders, the bending moment on the stock is substantially reduced because bearing support is provided close to the spanwise location of the center of pressure of the rudder.

**17.3 Number of Rudders.** The use of more than one rudder can increase controllability. Consider twin rudders athwartship of each other in the free stream. The total lift and drag produced should be identical to that of a single rudder, provided that each of the twin rudders is geometrically similar to the single rudder and that the area of the single rudder is twice the area of one of the twin rudders. As the spacing between the twin rudders is reduced, they become less effective because of the interference (cascade) effect between them. In practice, however, two rudders can usually have a much higher aspect ratio than that of a single rudder of equal total area. Hence, at any given angle of attack below the stall angle, twin rudders may have a higher total lift coefficient and therefore larger values of  $Y'_s$  and  $N'_s$  than a single rudder in spite of the interference effect. Furthermore, on multiple-screw ships, twin rudders can each be located in a propeller race, whereas a single centerline rudder ordinarily cannot.

Another, subtle difference between twin and single

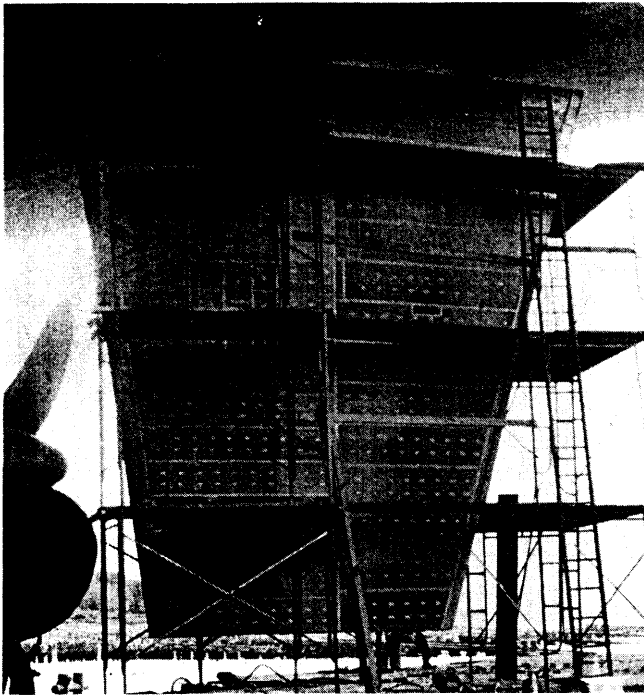


Fig. 207 All-movable rudder without bottom support

rudders has more important influence than the preceding on both course-keeping and course-changing ability. Figs. 47(a) and 47(b) show that for a single rudder in the free stream,  $Y'_s$  and  $N'_s$  are equivalent to  $(Y'_\beta)_f$  and  $(N'_\beta)_f$  the situation of a fixed fin at an angle of attack. Comparison of Fig. 209(a) with Fig. 209(b) shows that this is not true for twin rudders even if only free-stream effects are considered. Because of the location of the twin rudders relative to the flow in Fig. 209(b) the interference effects between them is larger than it is in Fig. 209(a). To keep interference effects to a minimum, the location relative to the flow shown on Fig. 209(e) would be best. (This is the conventional location of the two wings of a biplane.) Since in Fig. 209(b) the two rudders are in just the opposite positions, the lift developed by the flow conditions corresponding to that figure is less than that of Fig. 209(a).

When the straightening effect of the hull and propeller,  $\epsilon$ , (see Fig. 209(b) on the flow to twin rudders is considered, the lift developed by the flow conditions of Fig. 209(b) is even less than in the free stream. Fig. 3 of Surber (1955) shows that the value of  $\epsilon$  at the athwartship location of the rudder on the inside of a turn is larger than at the location of the outside rudder over the lower half of the rudder span. This inequality arises because the flow to the inside rudder is somewhat straightened by the intervening propeller and hull, whereas at least the lower half of the outside rudder is subjected to the full geometric drift angle. As a result of this effect, and the effect described in the previous paragraph, the  $(Y'_\beta)_f$  and  $(N'_\beta)_f$  values of

the rudder on the inside of the turn are substantially less than its  $Y'_s$  and  $N'_s$  values.

As a result of this distinction between twin and single rudders, the effect of increasing rudder area or rudder aspect ratio on the stability index and on the steady turning diameter is also different. Results of linear computations are shown in Fig. 210 for the twin-screw model of Gertler and Bradley (1948). For simplicity, the effect of rudder area in the race was neglected.

The experimental data of Shiba (1960) and Gertler and Bradley (1948) indicate that the relative improvement in steady turning diameter attributable to twin rudders compared to a single rudder shown Fig. 210 for a rudder deflection angle of 15 deg also exists at the maximum deflection angle of 35 deg. Hence, the trends observed in Fig. 210 are true for severe limit maneuvers. It follows that twin rudders are likely to be preferable to a single rudder for ships that have very stringent limit-maneuver requirements. For example, the fourth and fifth scales show that twin rudders with a total area of 2.5 percent of  $L \times T$  and a span of 17.3 percent of  $(L \times T)^{1/2}$  have a STD/L value 26 percent less than that of a single rudder of identical area and span. Furthermore, Fig. 210 shows that this reduction is achieved with no sacrifice in stability index. Conversely, if the turning diameter associated with a single rudder is adequate, the figure shows that the same turning diameter might be achieved with far less total rudder area with twin rudders. However, in

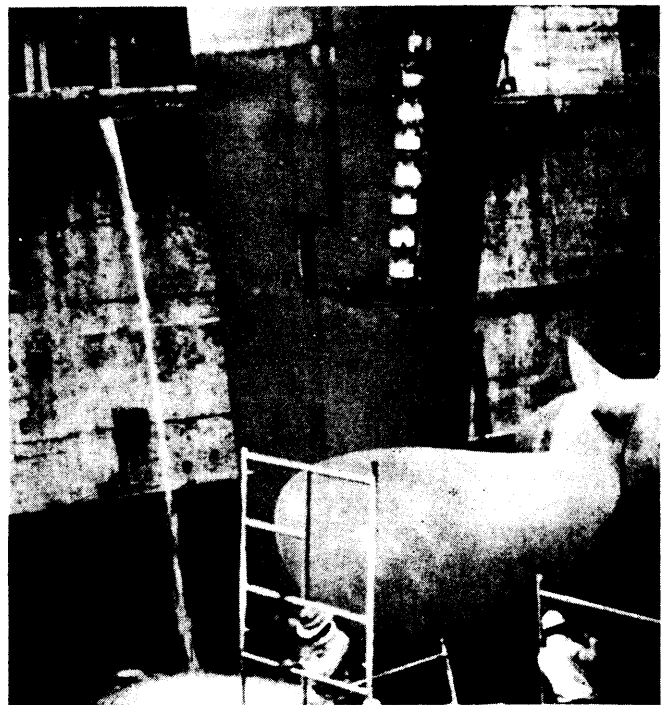


Fig. 208 Horn rudder

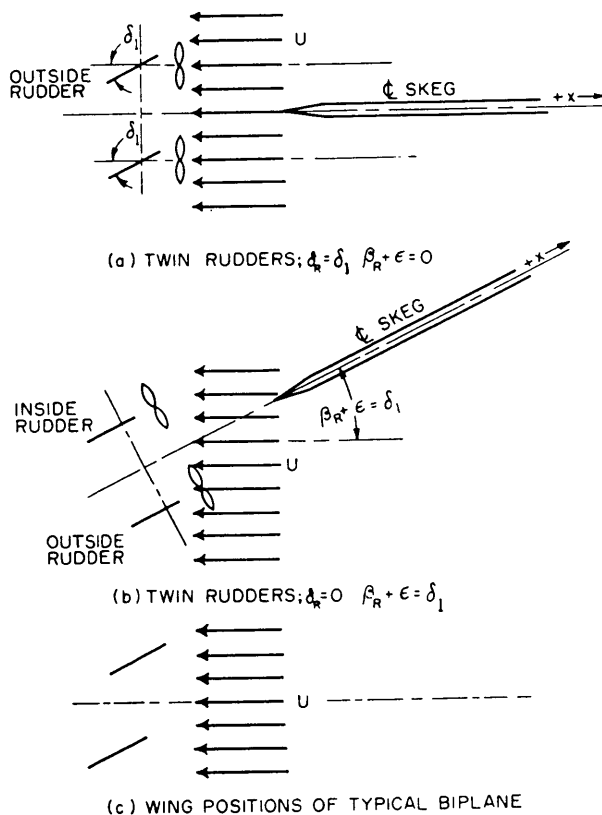


Fig. 209 Single and twin lifting surfaces relative to flow velocity (side view)

this case, the twin-rudder ship would exhibit a marked reduction in controls-fixed stability compared to the single-rudder ship.

For most ships, constraints (b) and (c) of Section 17.1 dictate the selection of a single rudder. An exception is the case where the specified course-changing ability cannot be achieved with a rudder that fits within the dimensional constraint (a). However, no single-screw merchant ship is in this category, nor are most multiple-screw merchant ships. Thus some multiple-screw ships do have single centerline rudders, but with the consequent penalty in turning characteristics shown in Fig. 210, along with the significant penalty in low-speed maneuvering ability associated with not having a rudder in the propeller race.

Vessels of low to moderate draft often require multiple rudders to provide adequate maneuverability, since a reasonable aspect ratio cannot be obtained with only one rudder. For example, multiple rudders are utilized on river towboats that must maneuver a large flotilla of barges, many times their own size, in a narrow river channel. Some of these rudders, forward of the propellers, are called "flanking" rudders. Also, because of the first constraint of Section 17.1 and because of the requirements for outstanding maneuvering performance, the majority of naval combatant ships have two or more rudders.

Fig. 211 shows an unusual triple-rudder arrangement, that achieves most of the maneuvering advantages of twin rudders but at less cost. While the horizontal struts needed to support the wing blades add to the drag of this installation, only a single steering engine is required, and by properly choosing the fore-and-aft location of the wing blades the torque required to deflect the rudder can be kept to modest levels. This arrangement has been used on a twin screw ship built with a single centerline rudder.

**17.4 Rudder Size.** The rudder area should be calculated and verified during the initial ship arrangement study. A good first step is to use the Det norske Veritas (DnV) value for minimum rudder area (Rules, 1975):

$$A_R = \frac{T \times LBP}{100} \left[ 1 + 25 \left( \frac{B}{LBP} \right)^2 \right] \quad (156)$$

where

$A_R$  = area of rudder

$T$  = draft

$LBP$  = length between perpendiculars

$B$  = beam

The formula applies only to rudder arrangements in which the rudder is located directly behind the propeller. For any other rudder arrangement, DnV requires an increase in the rudder area of at least 30 percent. A twin-screw (or more) arrangement should be combined with rudders located directly behind the propellers for maximum low-speed maneuverability. A single rudder placed between two propellers may be inadequate because the rudder blade does not swing sufficiently into the flow of a propeller to generate the needed turning moment.

The bracketed quantity in the preceding formula is essentially a rudder area coefficient. The value of this quantity should be compared with an independent estimate made by:

(a) Selecting a tentative value from design experience such as in Tables 31 and 36 or similar tables prepared by Lamb and Cook (1961) or others. Fig. 212 may also be used which shows a plot of rudder areas against the underwater profile areas for vessels in the USCG maneuvering data base (Barr, Miller, Ankudinov and Lee, 1981). The mean lines indicate average rudder area by vessel type and underwater profile. Rudder areas lying much below the mean line should be avoided.

(b) Modifying the tentative value in light of published sources and other historical experience.

Many potential maneuvering troubles can be avoided early in the design stage by providing a margin of extra rudder area. For some vessel types, however, the benefits may diminish after the rudder profile has reached 2 percent of the lateral underwater area. The designer must realize that the effectiveness of extra rudder areas is directly dependent on the inherent dynamic course stability of the vessel class. Vessels with

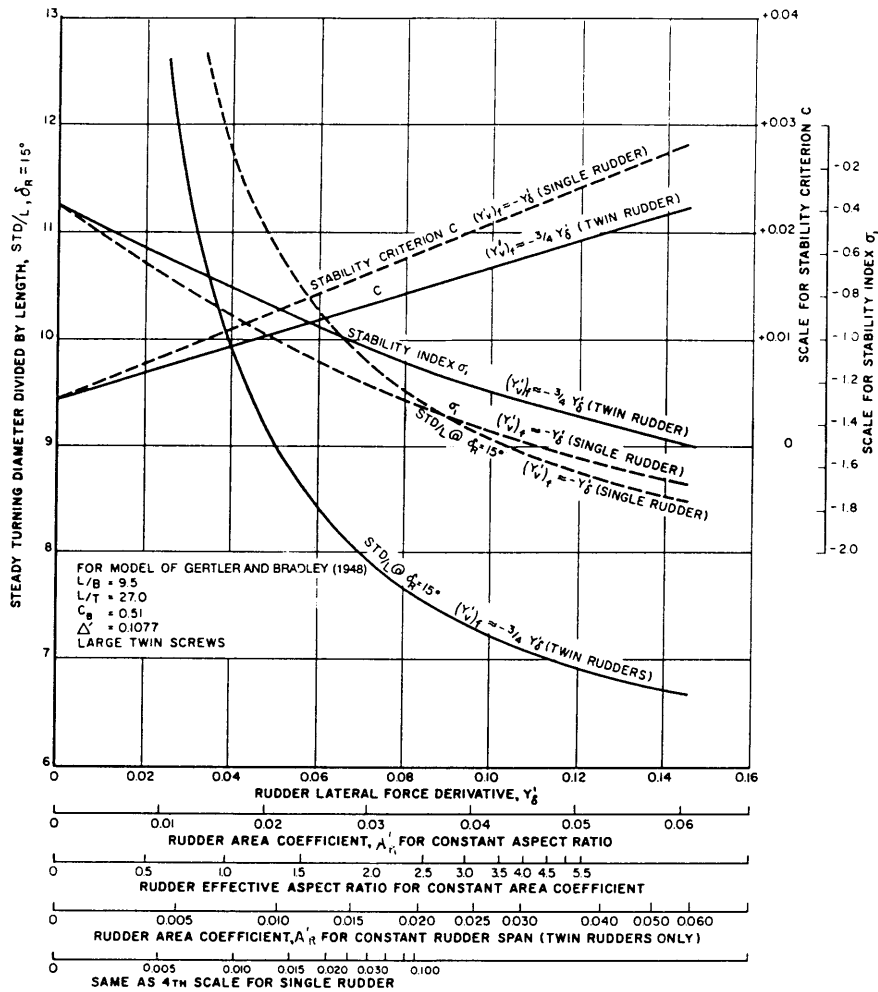


Fig. 210 Effect of rudder area and aspect ratio on the calculated steady-turning diameter, stability criterion, and stability index for single and twin rudders for twin-screw model (Gertler and Bradley, 1948)

Table 36—Rudder area coefficients

Vessel Type	Percent of $L \times T$
Single-screw vessels	1.6 to 1.9
Twin-screw vessels	1.5 to 2.1
Twin-screw vessels with two rudders (total area)	2.1
Tankers	1.3 to 1.9
Large passenger vessels	1.2 to 1.7
Fast passenger vessels for canals	1.8 to 2.0
Coastal vessels	2.3 to 3.3
Vessels with increased maneuverability	2.0 to 4.0
Fishing trawlers and vessels with limited sailing area	2.5 to 5.5
Seagoing tugs	3.0 to 6.0
Sailing vessels	2.0 to 3.0
Pilot vessels and farries	2.5 to 4.0
Motorboats	4.0 to 5.0
Keel launches and yachts	5.0 to 12.0
Centerboard boats	30 or more

marked stability will benefit least, while vessels with instability will benefit most.

These values should be compared and the selected rudder area drawn to scale on the stern outline, using the lines, propeller, and rudderstock location.

Table 29(b) and Fig. 180 in Section 16, along with Fig. 212, show the effects of rudder size in relationship to turning diameter and rudder area for models that have different block coefficients. Table 29(b) lists results from Shiba (1960) which were obtained in free-running model tests of models 2.5 m long ( $L/B = 7.30$ ,  $B/T = 2.5$ ). As shown in the test results, the effects of speed on turning diameters are very small in a speed range corresponding to Froude numbers as high as 0.25. Fig. 212 shows that the best turning performance for the Series 60 design is obtained when rudder area is roughly 1/50 to 1/40 the product of length times draft (LT). Since the standard size of the rudder for the Series models is 1/62 of LT, the maneuvering per-

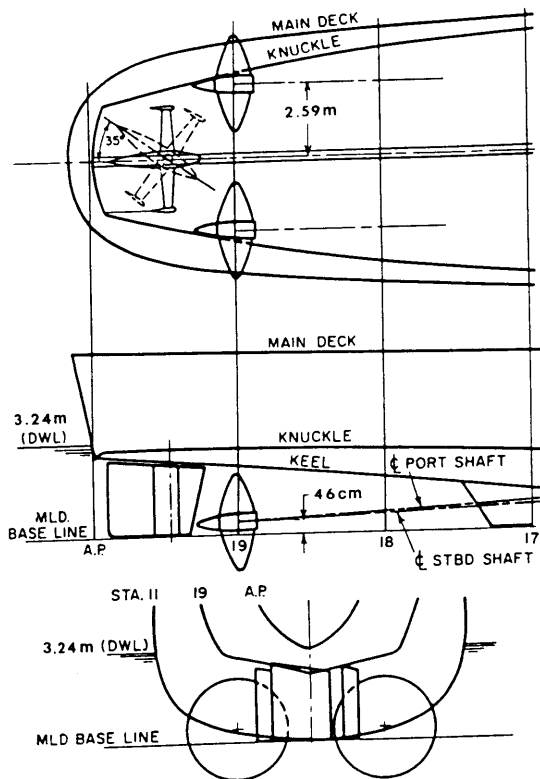


Fig. 211 Triple-bladed rudder on a twin-screw ship (Fig. 10 of Gertler and Bradley, 1948)

formance can be further improved by increasing rudder area up to  $1/50$  to  $1/40$  of  $L \times T$ . As discussed in Section 14.4, however, rudder effectiveness may not increase significantly if only rudder chord is increased, for rudder effectiveness depends more heavily on rudder span length than on chord length. The data in Table 29(b) show this anomalous saturation effect as rudder area is increased. Shiba (1960) associates this anomaly entirely with the decrease in rudder aspect ratio as rudder area is increased, but decreasing aspect ratio is not a necessary condition for the existence of the anomaly and in principle it can be encountered even when rudders of constant aspect ratio are increased in area. Table 37 provides further examples of geometry on several existing ships. Rudder size versus effectiveness was studied relative to the importance of rudder deflection rate and is discussed in Section 17.6. Depending on hull form and powering, a larger rudder with slower deflection rate may be as effective as a smaller rudder with faster rate.

Previous analyses of directional stability and control under adverse conditions in wind and waves indicate that performance with a relatively larger rudder is superior. Such a rudder may also be effective in extreme maneuvers such as those required to avoid a collision in an emergency. These important factors

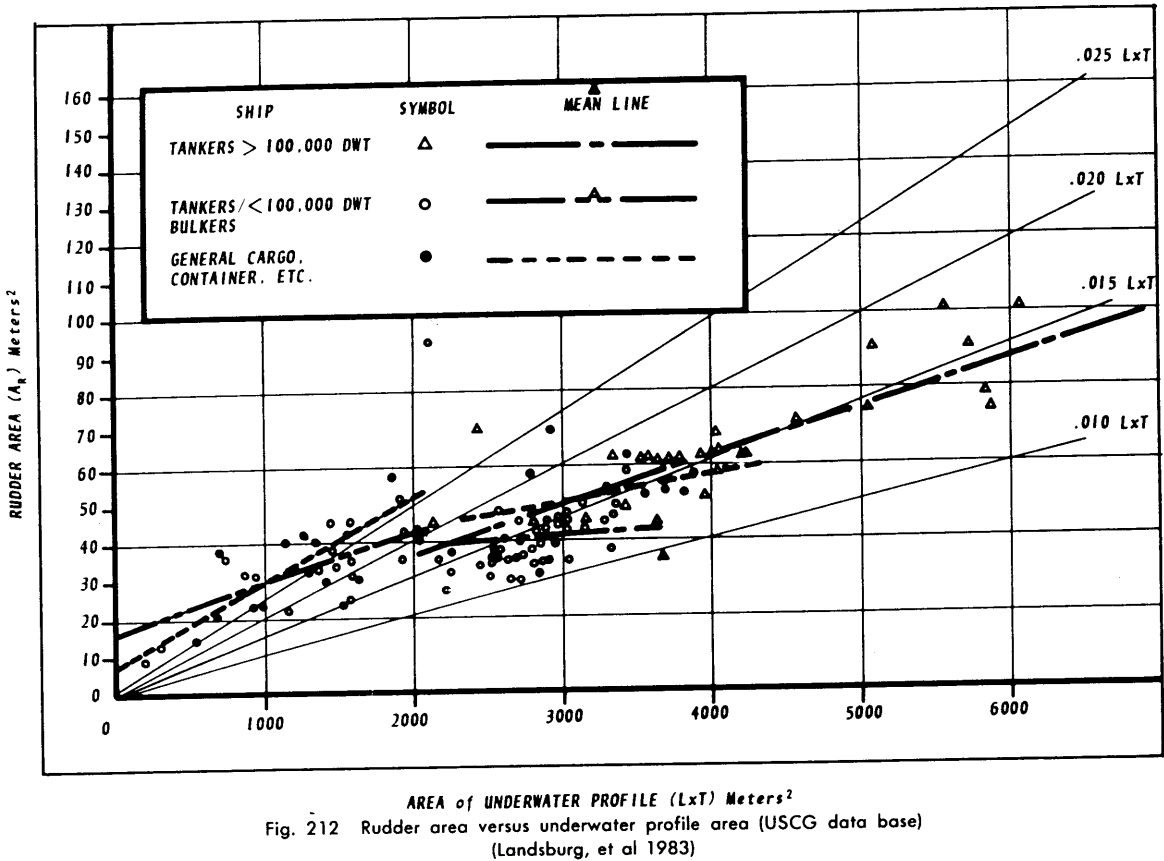


Fig. 212 Rudder area versus underwater profile area (USCG data base) (Landsburg, et al 1983)



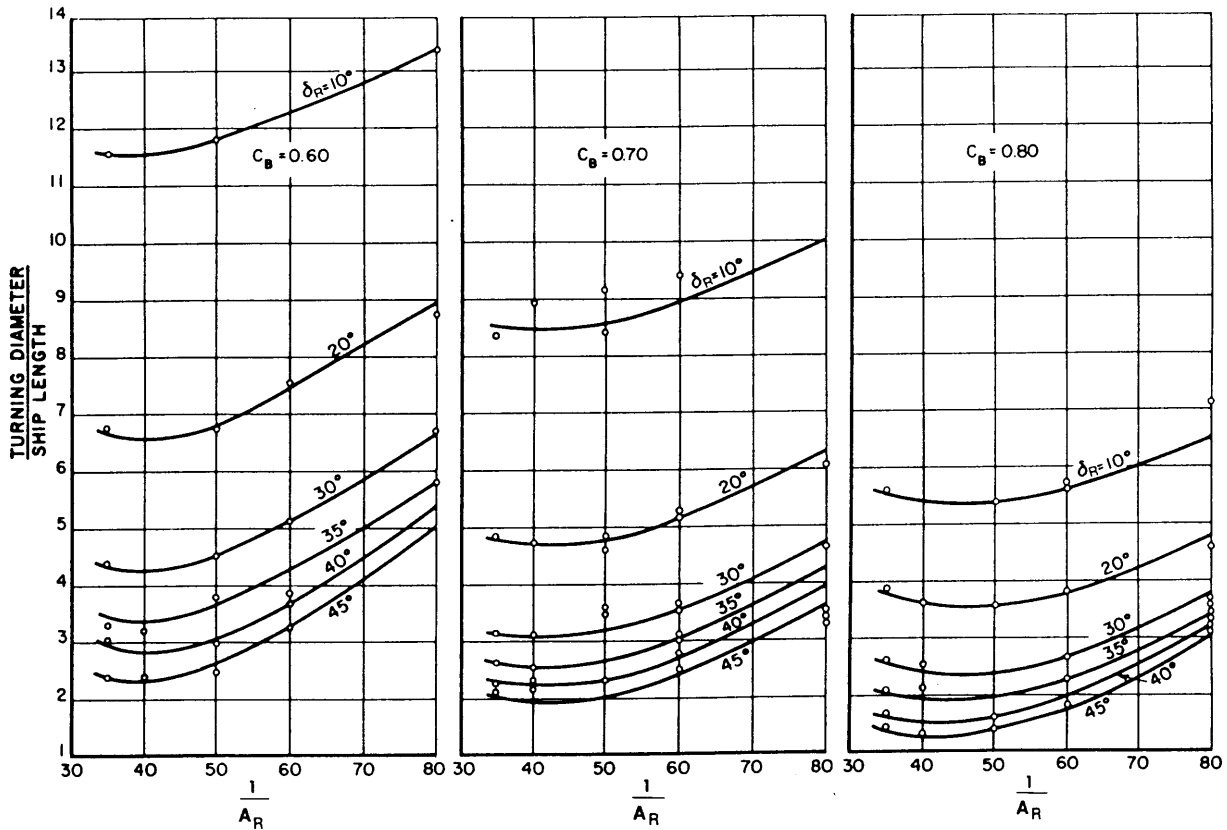


Fig. 213 Effect of rudder area and deflection angle on turning diameter (Shiba, 1960)

should be reflected in the final determination of rudder size in conjunction with constraint (c) of Section 17.1, which urges economy.

One approach to determining the needed rudder area and aspect ratio is to start with a value of the stability index thought necessary and use linear methods to determine areas and aspect ratios that will meet the requirement (See Section 16.6). Also, if the most severe limit-maneuver characteristic is required, such as the rate of change of heading or the steady turning diameter, a similar approach can be taken in meeting those requirements. For a more limited group of hull forms, available series model test data can be used such as those reported by Eda and Crane (1965), Taylor's Standard Series (using Jacobs, 1962), and Roseman (1987). The all-movable rudder area needed in association with a fixed span to achieve specified nonlinear limit-maneuver characteristics for single-screw merchant forms may also be approximated from the experimental data of Figs. 180 and 213. Empirical guidance for selecting the rudder area of single-screw merchant ships to provide controls-fixed dynamic stability and specified turning characteristics is given in Figs. 1 and 2 of Thieme (1965).

The vital effect of changes in hull form on the rudder

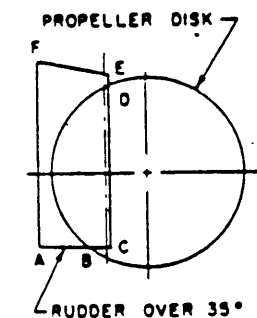
area needed to achieve a specified turning diameter is shown in Fig. 213. For example, this figure indicates that 40 percent more rudder area is required to achieve a turning diameter of three ship lengths at  $\delta_R = 45^\circ$  deg with the ( $C_B = 0.60$ ) model than with the ( $C_B = 0.80$ ) model. If a turning diameter of two ship lengths were required, it could not be achieved on the ( $C_B = 0.60$ ) model with a single rudder, regardless of area. Increase in rudder effectiveness through using an improved section or adding fins or mounting twin rudders may be required.

For most single-rudder ships, the limit on rudder span imposed by the first constraint of Section 17.1 is much more severe than the restriction on rudder chord. As a result, the rudder span permitted by the first constraint is usually chosen. For any given rudder area this span determines the aspect ratio. Increasing the rudder chord, particularly the part in the propeller race, may solve the problem. As area is increased, the aspect ratio is decreased. Only on some twin-rudder ships is there any real freedom to alter rudder area and rudder aspect ratio independently of each other.

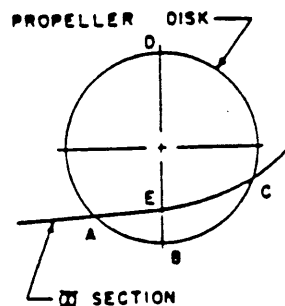
Where this freedom does exist, the designer must note that the rudder area that is in the propeller race may change with aspect ratio. If the restriction on

Table 37—Parameters of Hull and Appendage Geometry of Several Existing Ships (Mandel, 1953)

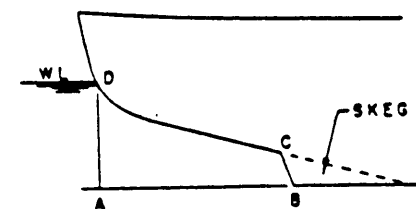
1	2	3	4	5	6	7	8	9	10	11	12
Tactical diam/ $L$ , at low $V/\sqrt{L}$	Type of rudder	No. of rudders	No. of screws	Length/beam	Length/draft	<sup>1</sup> Average rudder overlap, percent	<sup>2</sup> Propeller outside of Hull	<sup>3</sup> Cut-away area/ $L \times T$ , percent	Length of cut-away $L$ , percent	Skegs	Movable rudder area/ $L \times T$ , percent
2.4	All movable	2	2	6.2	26.1	54.4	Low	7.3	8.1	Single	3.2
2.5	All movable	2	2	5.5	20.9	83.3	Low	6.5	10.8	Single	2.3
2.6	All movable	2	2	6.7	29.9	67.9	Low	7.8	17.5	Single	2.6
2.7	Horn	1	4	8.8	29.7	11.1	Low	7.5	13.1	Single	1.9
2.8	Horn	2	4	6.6	21.9	72.3	Low	5.5	8.0	Twin inb'd	2.6
2.8	Horn	2	4	8.0	24.1	62.1	Low	6.6	9.0	Twin inb'd	2.3
2.9	Horn	1	4	9.5	29.2	24.2	Low	7.1	12.6	Single	1.9
3.0	Horn	1	4	9.1	25.0	13.7	Low	7.1	15.7	Single	1.9
3.0	Horn	1	4	9.2	28.3	15.4	Low	6.9	14.9	Single	2.0
3.0	Horn	1	2	7.1	22.6	0	Low	4.6	7.6	Single	2.2
3.0	Horn	2	4	6.2	19.6	72.2	Low	8.2	9.9	Twin outb'd	2.4
3.0	Horn	1	4	10.1	26.6	20.0	Low	7.4	15.3	Single	2.1
3.1	All movable	2	2	4.9	15.6	58.4	Medium	9.2	13.6	Single	3.6
3.2	Horn	1	4	8.4	25.8	13.7	Low	7.4	15.7	Single	2.0
3.2	Horn	1	4	9.4	27.4	10.1	Low	8.2	15.4	Single	2.0
3.3	Horn	1	4	8.7	27.8	6.5	Low	6.8	14.2	Single	1.9
3.3	Horn	2	4	8.0	27.7	58.3	Low	7.1	8.5	Twin inb'd	2.4
3.4	Horn	1	4	9.3	28.4	6.5	Low	7.0	14.2	Single	1.9
3.4	Horn	2	4	6.7	25.1	50.0	Low	5.7	10.8	Single	1.5
3.4	Horn	1	4	8.8	25.6	13.9	Low	6.7	10.6	Single	2.0
3.5	Horn	1	2	10.0	25.9	26.8	Medium	7.6	13.9	Single	1.9
3.5	All movable	2	2	9.5	31.8	62.3	High	9.6	16.0	Single	3.1
3.6	All movable	2	2	8.2	25.2	58.8	Medium	6.9	14.9	Single	2.0
3.7	All movable	1	2	9.1	30.2	4.4	Medium	7.2	17.3	Single	2.1
3.7	All movable	1	2	9.3	31.7	5.0	Medium	7.5	17.0	Single	2.1
3.8	All movable	2	2	9.2	29.7	64.9	High	7.7	16.0	Single	3.3
4.0	Horn	2	2	9.0	27.9	77.7	High	8.5	15.1	Single	2.4
4.2	Horn	1	2	9.4	27.9	5.2	High	8.0	15.1	Single	3.0
4.3	All movable	1	2	10.2	29.0	28.0	High	10.3	16.7	Single	3.0
4.3	Horn	2	2	9.4	28.1	73.8	High	8.4	14.5	Single	2.3
4.7	Flap	1	2	7.2	17.5	19.2	Low	2.7	3.2	Single	1.9
4.9	All movable	1	2	9.5	26.7	6.8	High	7.6	13.7	Single	2.0
5.1	Horn	1	2	9.4	29.3	5.2	High	8.8	15.1	Single	2.2
5.2	Horn	1	4	8.3	27.8	7.7	Low	2.4	5.0	Single	2.4



① RUDDER OVERLAP =  $\frac{BCDB \times 100}{ABCDEFA}$



② PROPELLER OUTSIDE OF HULL =  $\frac{ABCEA}{ABCDFA}$

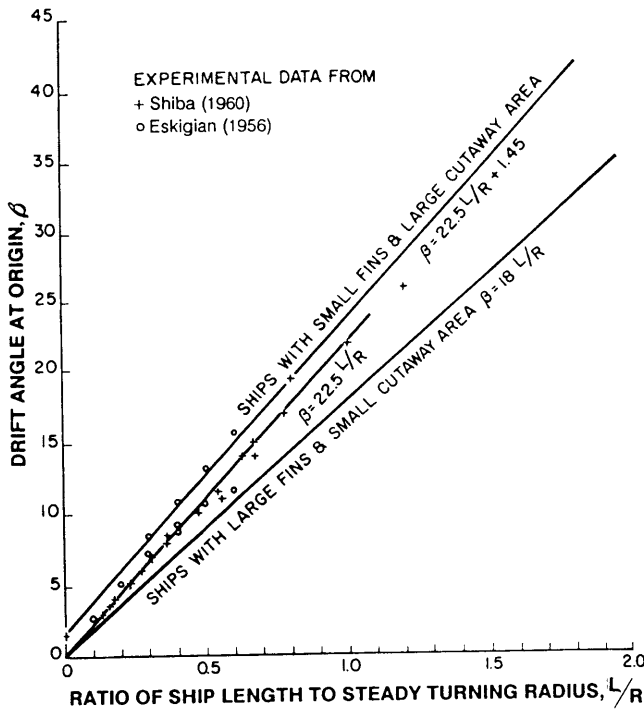


③ CUTAWAY AREA = ABCDA  
LENGTH OF CUTAWAY = AB

rudder span is imposed by proximity to the free sea surface, then a study of the relative advantages of conserving aspect ratio and increasing submergence may be desirable. These can be evaluated for all-movable rudders within the range of geometric aspect ra-

tios of 1.1 to 1.7 by reference to Figs. 26.1, 26.2, and 26.3 of Shiba (1960) from which Fig. 127 was constructed.

If, within the limits of a fixed span, the rudder area necessary to achieve controls-fixed stability is larger


 Fig. 214 Drift angle,  $\beta$ , as a function of  $L/R$ 

than the all-movable rudder area required to achieve the most severe specified limit maneuver, then, as indicated in Section 17.2, a horn rudder or a balanced rudder with fixed structure should be employed. Fig. 144 may be used to determine the area of the movable part of a zero-balance rudder with fixed structure for equal effectiveness with an all-movable rudder at  $\beta = 0$ . Calculation of the required movable area of balanced rudders with fixed structure for the general case of  $\beta \neq 0$  and nonzero balance, and of the required movable area of horn rudders, is not yet possible for the reason noted in the previous section.

Free-stream information useful in the selection of rudder profile shape (sweep angle and taper ratio), section shape, tip shape, and thickness-chord ratio for all-movable rudders is contained in Section 14.5 and Tables 13 through 17. While this information is useful, it is not necessarily decisive. For example, consideration of rudder area in the propeller race should also influence selection of rudder profile shape. For all-movable rudders, structural rather than hydrodynamic considerations may dictate the selection of the root-thickness/chord ratio because the thickness is determined by the diameter of the rudder stock. Structural considerations are treated in Section 17.8. In practice, root-thickness/chord ratios greater than about 0.25 are avoided, to prevent flow separation and the possibility of vortex-excited vibration.

**17.5 Maximum Rudder Deflection Angle** At least three meanings of "maximum" rudder deflection angle are important to distinguish from one another:

(a) Design maximum. The maximum angle to which the steering engine can turn the rudder.

(b) Maneuver maximum. The maximum angle that is specified to be used in any particular maneuver.

(c) Maximum useful. For certain operationally important maneuvers such as the steady turn (Section 6.1) or the depth-changing maneuver for a submarine, there exists a deflection angle which if exceeded yields no significant improvement in the characteristics of the maneuver. This is the maximum useful deflection angle. Deciding of both (a) and (b) depends on (c); hence, most of the discussion of this subsection concerns the maximum useful rudder deflection angle. For rudders that experience an abrupt decrease in lift at the stall angle, maximum useful deflection angles are likely to approximate the stall angle, but as shown in this subsection, a maximum useful rudder deflection angle may exist at angles of attack less than that of stall.

The possibility of the rudder's achieving an angle of attack exceeding the stall angle is far more likely during transient maneuvers such as the overshoot maneuver than during a steady turn. For example, when the rudder is laid over in the opposite direction to check an overshoot maneuver (see Fig. 18), the angle of attack on the rudder may be larger than the deflection angle if the rudder deflection rate is fast enough. On the other hand, Fig. 22 shows that in a steady turn, the angle of attack on the rudder is far less than the deflection angle. For this reason, deflection angles that are useful in a steady turn are likely to be far greater than those that are useful in an overshoot maneuver. Thus, consideration of the steady turn will, in almost all cases, determine the magnitude of the design maximum rudder deflection angle.

The angle of attack at the rudder in a steady turn is

$$\alpha = \delta_R - \beta_R \quad (157)$$

with symbols as defined on Fig. 22. The value of the geometric drift angle at the rudder,  $\beta_R + \epsilon$  is a function of the radius of the turning circle. For a rudder located a distance  $L/2$  aft of the origin,  $\beta_R + \epsilon$  is related to the drift angle at the origin of the ship,  $\beta$ , by

$$\tan(\beta_R + \epsilon) = \tan \beta + \frac{L}{2R \cos \beta} \quad (158)$$

Measurements of  $\beta$  made during the turning experiments of the single-screw merchant ship models reported in Fig. 213 indicate that

$$\beta \approx 22.5 L/R \quad (\beta \text{ in degrees}) \quad (159)$$

which as shown in Fig. 214 is intermediate between

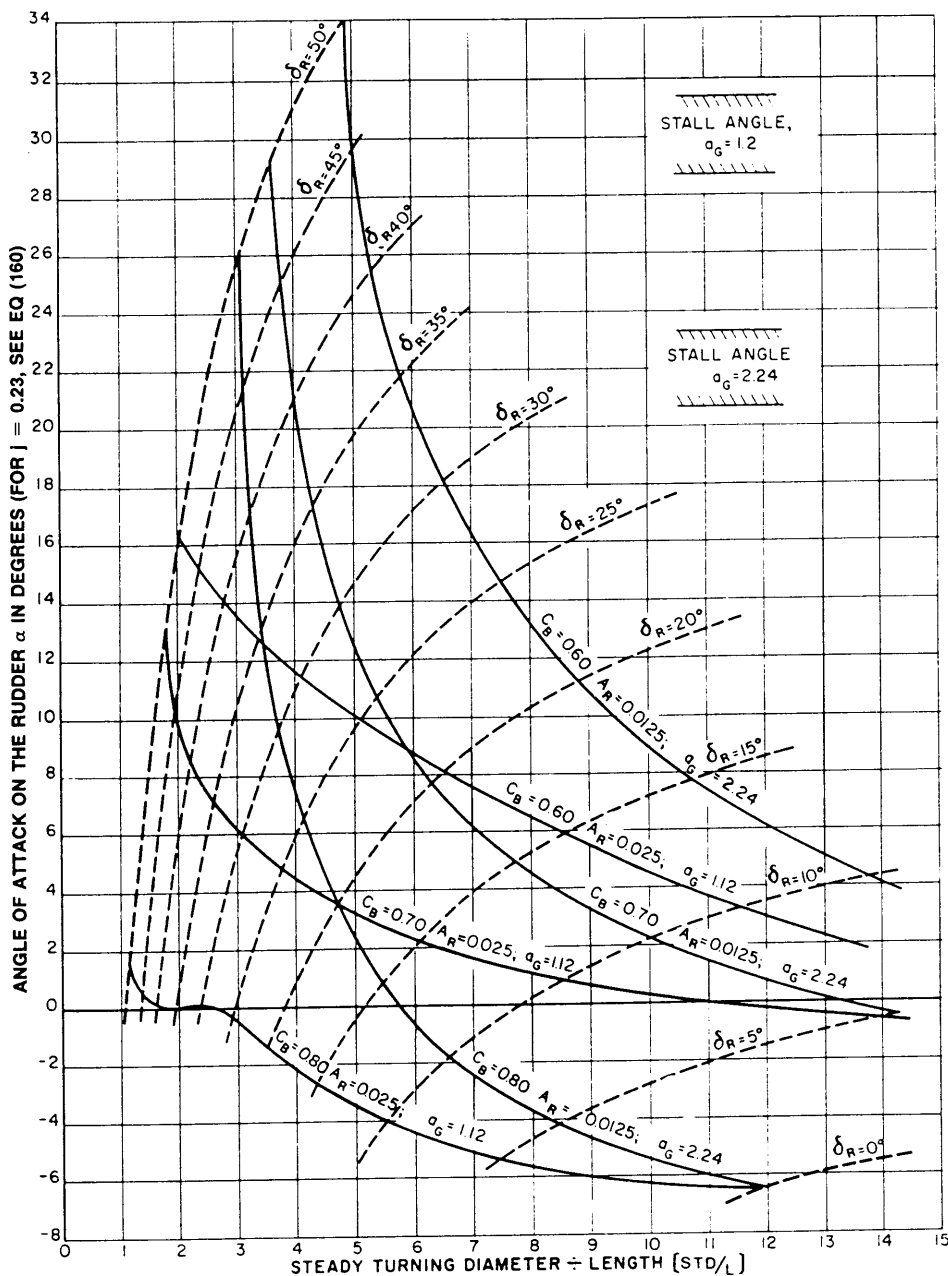


Fig. 215 Angle of attack at rudder as a function of  $D/L$  and  $\delta_R$  for the particular single-screw merchant ship hull forms (Shiba, 1960)

the two empirical expressions for  $\beta$  given in Section 6.1.

Results reported by Shiba (1960) and Surber (1955) indicate that the straightening effect of the hull and the propeller on the rudder is approximately a linear function of the geometric drift angle at the rudder:

$$\epsilon \approx j(\beta_R + \epsilon) \quad 0 \leq j < 1.0$$

$$\epsilon \approx \frac{j}{1-j} \beta_R \quad (160)$$

Combining Equations (157-160), the following expression for the angle of attack on the rudder of the models of Shiba (1960) in a steady turn is obtained:

$$\alpha = \delta_R - \left\{ \tan^{-1} \left[ \tan (22.5 L/R) + \frac{L}{2R \cos (22.5 L/R)} \right] \right\} (1-j) \quad (161)$$

The dashed contours plotted in Fig. 215 show  $\alpha$  as

a function of  $\delta_R$  and  $STD/L$  as computed from Equation (161) for a  $j$ -value of 0.23.

This is the approximate value of  $j$  for the single-screw, single rudder models of Shiba (1960) as computed from Table 5 of the same author. The  $j$ -values computed from Eskigian (1956) and Surber (1955) are considerably larger. Equation 161 can be used to compute values of  $\alpha$  for any value of  $j$  for the models of Shiba (1960).

Some results of the turning tests with the ( $C_B = 0.60$ , 0.70, and 0.80) models from Fig. 219 are superimposed on these dashed contours and displayed on Fig. 215 as solid curves. These curves show, for example, that the ( $C_B = 0.60$ ) ( $A'_R = 0.0125$ ) model has a steady turning diameter of  $6\frac{1}{2}$  ship lengths at a rudder deflection angle of 30 deg, which corresponds to an angle of attack of 18 deg on the rudder.

One of the most striking features of Fig. 215 is that with the assumption of  $j = 0.23$ , the angle of attack on the rudder is zero or negative for  $STD/L$  values as low as 1.5 for the ( $C_B = 0.80$ ) model. In other words, this model turns in a very small diameter with the rudder exerting little or no control force. This, in conjunction with the fact that the ( $C_B = 0.80$ ) model of Shiba (1960) turns with zero rudder, suggests that this model may be unstable. To a lesser extent, the same comment applies to the ( $C_B = 0.70$ ) model.

The approximate rudder stall angles as measured in the propeller race for the two rudders included in Fig. 215 are also shown in that figure. The effect of stall which otherwise should be discernible on Fig. 215 for the ( $C_B = 0.60$ ) ( $A'_R = 0.0125$ ) model is not perceptible.

In general, Fig. 215 shows that stall does not play a dominant role in determining the maximum useful rudder deflection angle in a steady turn for the models of Shiba (1960). For example, the ( $C_B = 0.80$ ) ( $A'_R = 0.0125$ ) model shows almost no reduction in steady turning diameter as a result of increasing the rudder deflection angle from 35 to 45 deg. Yet the angle of attack on the rudder even at  $\delta_R = 45$  deg is below stall. Clearly then, on some of the models, the nature of the hull forces and moments and not the occurrence of stall is what limits the maximum useful rudder deflection angle.

It is seen from Fig. 215 that for the three models with the larger rudders, rudder deflection angles larger than the common design maximum of 35 deg result in smaller diameter steady turns with no increase in rudder area. For some of the models, deflection angles larger than 50 deg result in significant reductions in turning diameter. Information shown in Fig. 19 of Mandel (1953) indicates that deflection angles as large as 65 deg may be useful for some ships. Thus, it is not possible to generalize concerning the maximum rudder deflection angles that are likely to be useful.

As a result, considering the state of the art of rudder design, it is preferable during development of a new ship design for which maneuvering performance is of

utmost importance, to determine the adequacy of any proposed rudder, including its design maximum deflection angle, by means of model tests. This general preference for model tests prevails even though scaling difficulties will arise as noted in Section 14.3. The maneuvering performance of any proposed ship design and guidance for design modification to improve maneuvering performance can be accurately determined during the design stage by means of the experimental and semi-theoretical techniques described in Section, 8, 9, 16.6 and 16.7.

Constraint (c) of Section 17.1 tends to impose an upper limit on rudder deflection angle which is independent of turning considerations. For example, certain types of otherwise efficient and suitable steering

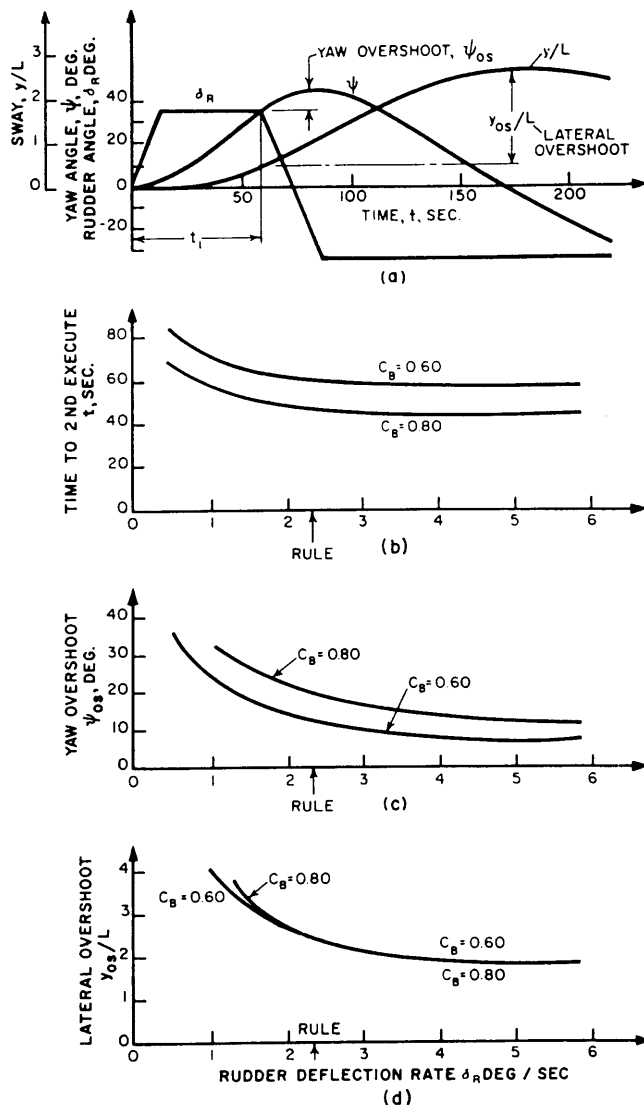


Fig. 216 Effect of rudder deflection rate on ship response for two Series 60 ships,  $L = 152.4$  m and (500 ft) and  $V = 14.8$  knots (Eda and Crane, 1965)

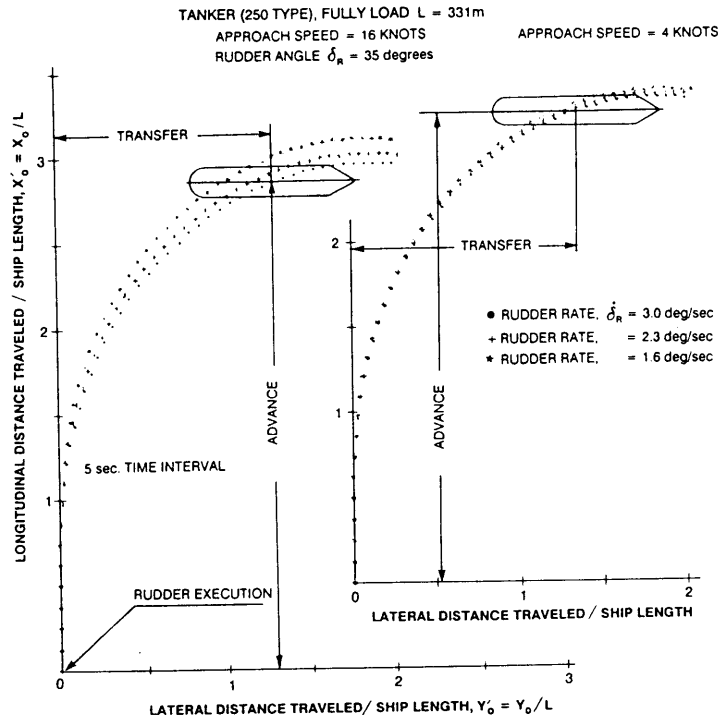


Fig. 217 Enter-a-turn trajectory (Eda, 1983)

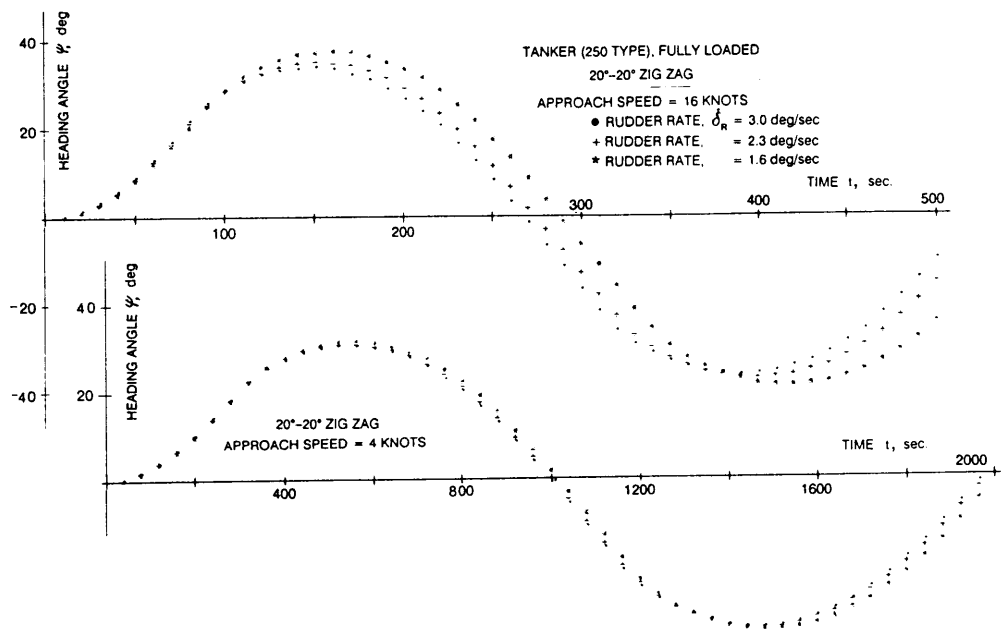


Fig. 218 Zigzag maneuver response (Eda, 1983)

engines may not be suitable for mechanical reasons for deflection angles larger than about 35 deg. Since other relatively inexpensive means of achieving a specified turning diameter may be available, such as increasing rudder area, the problem of selecting the design maximum rudder deflection angle may require detailed cost studies of alternative means for its ultimate resolution. Interesting to note is that most Great Lakes ships and many naval vessels are built with design maximum rudder deflection angles up to 45 deg.

**17.6 Rudder Deflection Rate.** Whereas desired steady turning characteristics are a guide to the choice of the design rudder deflection angle, transient maneuvers (in which the period of time that the rudder is in motion is relatively long compared to total maneuver time) are the major ingredients in determining needed rudder deflection rate. Such limit-maneuver abilities as zigzag overshoot characteristics and time to change heading a small number of degrees are influenced by rudder deflection rate. The rate, however, has no influence on the diameter of the steady turn, although it may have a very minor effect on the tactical diameter.

Mandel (1953) explored quantitative relationships between rudder deflection rate and pertinent maneuvering characteristics using full-scale turning trajectory data. Subsequently, predictions of nonlinear ship maneuvers were made by Eda and Crane (1965) to evaluate the effect of rudder rate on maneuvering performance for two ship designs (Series 60 hull forms with block coefficients 0.60 and 0.80). Zigzag maneuver trajectories at 35 deg-35 deg were computed for the 152m long ship at approach speed of 14.8 knots. Figure 216 shows variations in time to reach 35 deg heading change from the original course, yaw angle overshoot, and lateral overshoot as functions of rudder rate, together with a sample time history of ship response as a definition diagram. It can be seen that quickness of response, an overshoot in yaw and sway, improve with increased rudder rate, but at the higher rudder rates, further improvements are insignificant. The pattern of behavior is almost identical for the two ships of different block coefficients despite their quite different steering qualities.

At present, a minimum rudder rate of  $2\frac{1}{3}$  deg/sec, which is independent of ship parameters, is required by regulatory agencies and classification societies. As shown in Fig. 216 the rudder rate of  $2\frac{1}{3}$  deg/sec provides zigzag-maneuver response reasonably close to what might be achieved if the rudder rate were made arbitrarily high, at least for vessels of 152 m (500-ft) length at 14.8-knot approach speed. The law of diminishing returns tends to apply at rates beyond this prescribed rudder rate.

Dimensional analysis leads to the expectation that the rudder rate should be directly related to ship size and speed. Effort has been made to evaluate the effect

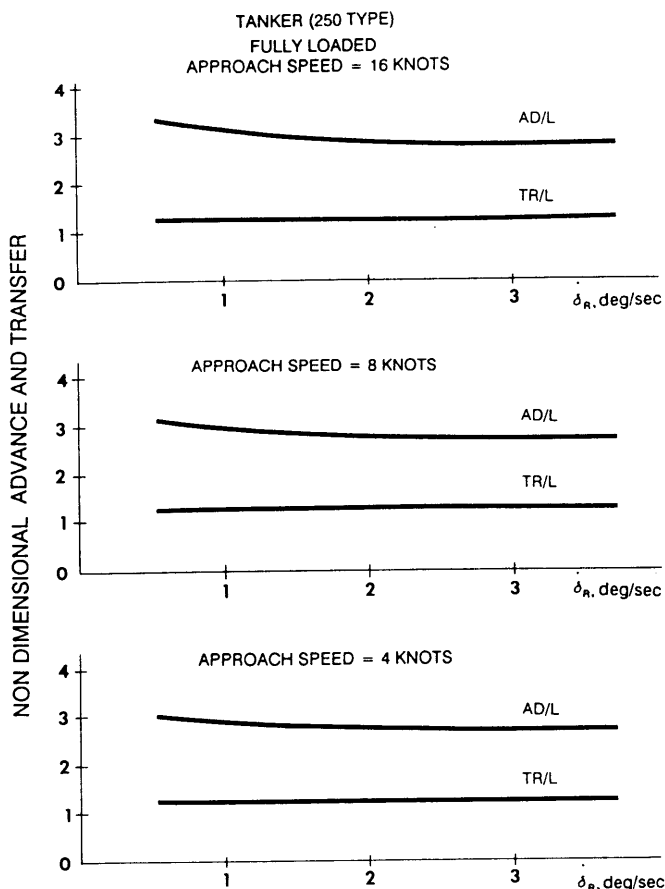


Fig. 219 Effect of rudder rate on turning trajectory (Eda, 1983)

of rudder rate as well as rudder size on the performance of a large tanker (250,000 dwt) in a series of digital computer simulations (Eda, 1976). Available captive model data were utilized to formulate a realistic mathematical model.

Fig. 217, for example, shows turning trajectories with application of 35-deg rudder angle at approach speeds of 16 knots and 4 knots. These trajectories show that the effect of rudder angular rate is much less at the lower speed (4 knots) than at the higher speed (16 knots). Fig. 218 shows 20 deg-20 deg zigzag maneuver response at approach speeds of 16 and 4 knots. These figures also indicate an effect of rudder angular rate that is much like that shown for turning.

A summary chart is shown in Fig. 219 as a result of a series of entering-turn maneuvers. Advance and transfer in units of ship length are shown on the basis of rudder angular rate for three different approach

TANKER (250,000 DWT), FULLY LOADED

L = 331m

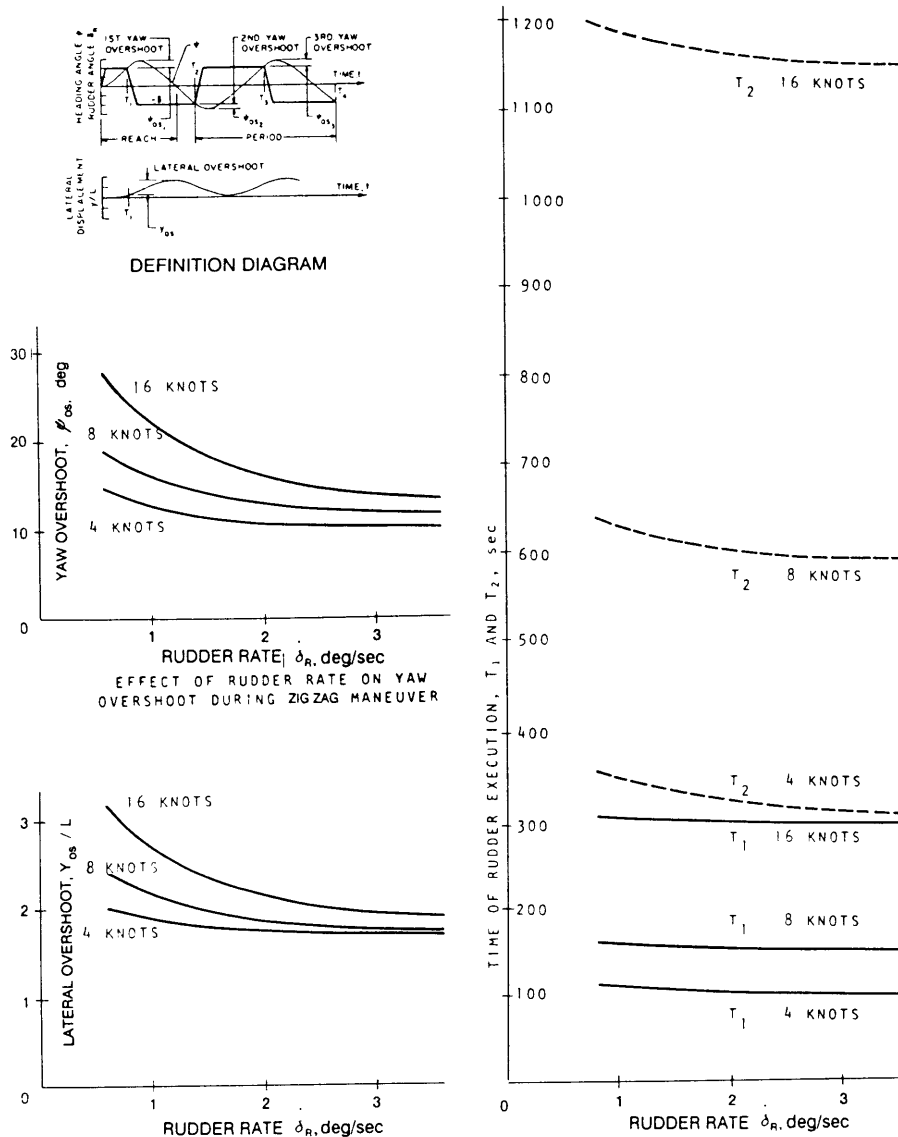


Fig. 220 Effect of rudder rate during zigzag maneuver (Eda, 1983)

speeds (16, 8 and 4 knots). Advance and transfer are longitudinal and lateral distances traveled from the time of rudder command to the time of 90 deg heading change, as shown in Fig. 217.

The figures show that the advance is reduced with an increase of rudder angular rate but that the rate of reduction becomes insignificant in the higher range of rudder rates, and that the effect of rudder rate on advance becomes insignificant at low speeds. At all speeds examined, transfer is influenced very little by the rudder angular rate.

Fig. 220 shows summary charts from a series of 20 deg-20 deg Z-maneuvers at speeds of 16, 8, and 4 knots.

Time to the second and third rudder executions, yaw overshoot, and lateral path overshoot are shown on the basis of rudder angular rate in these charts. It is seen that quickness of response and overshoots in yaw and sway are all improved with an increase of rudder rate, but that these improvements become unimportant at rudder rates greater than approximately 2 deg/sec. This tendency is like that shown in Fig. 216 except that the tendencies appear at lower rudder rates owing of course, to longer ship length without much difference in speed. In addition the large full-form tanker loses more speed in turning than does the cargo ship (16 to 6 knots, versus 14.8 to 9 knots).



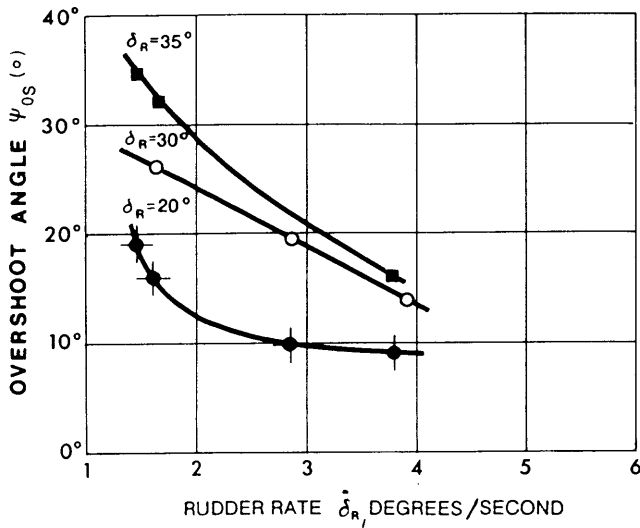


Fig. 221 Zigzag tests at 14 knots comparison for 20, 30, and 35 degree rudder angle at varying rudder rate (Taplin and Atkinson, 1987)

Taplin and Atkinson (1987) performed some full-scale tests on the effect of rudder rate on the highly maneuverable U.S. Coast Guard cutter *Gallatin*. Many test variations were tried, and the effectiveness of higher rudder rates in correcting a "helmsman error" was studied. Fig. 221 shows overshoot angles in a zigzag maneuver for various rudder angle commands (overshoot was measured after a 20-deg change of heading was achieved). When larger rudder angles are applied, it is seen that increased rudder rate is even more advantageous. Effectiveness in checking swings was studied further with angles and times required to check steady turns as shown in Fig. 222.

"Helmsman's error" tests were also developed and performed to measure the effects of turning the rudder in the wrong direction. From a steady base course, an initial rudder execute is made followed by corrective opposite helm after a delay representing the time to discover the helm error and commence corrective action. Results show that for this highly maneuverable ship, a higher rudder rate results quickly in a higher rate of swing that is difficult to check in the "shifted rudder" phase. With the prudent application of moderate rudder angles, however, early detection of error and higher rudder rates can result in smaller excursions. Future trials with other vessel types should yield further information in this area.

If an acceptable rudder rate for a given vessel design can be decided on, then the rudder rate for similar vessels of different size and speed may be estimated by use of the relationship,

$$\dot{\delta}_{RA} \frac{L_A}{V_A} = \dot{\delta}_{RB} \frac{L_B}{V_B} \quad (162)$$

where

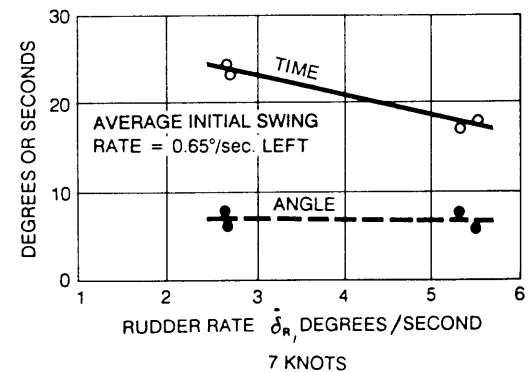
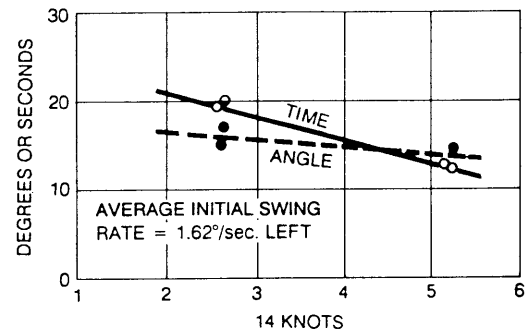
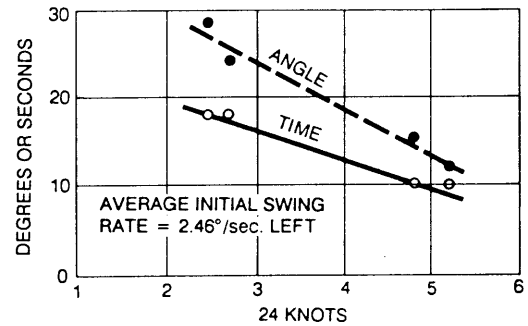
$\dot{\delta}_R$  = rudder turning rate

$L$  = ship length

$V$  = ship speed

Subscripts A and B refer to the separate vessels.

The results for the cargo ship and large tanker discussed in this section might therefore be applied to other similar vessels. However, vessel with different propulsion and rudder arrangements might merit separate attention—possibly based on earlier full-scale trial results with different rudder rates. Acquiring such trial results is not difficult if more than one steering unit is provided, as is the usual case.



- — TIME REQUIRED TO STOP LEFT SWING (SECONDS)
- — ANGLE REQUIRED TO STOP LEFT SWING (DEGREES)

Fig. 222 Checking steady left swings by use of right 35 deg. rudder data for 7, 14, and 24 knots (Taplin and Atkinson, 1987)

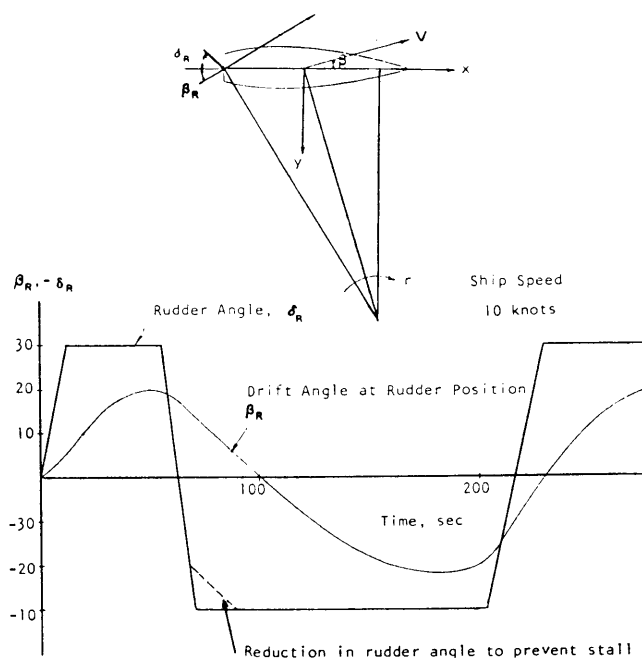


Fig. 223 Rudder angle and drift angle at rudder position during zigzag maneuver (Eda, 1983)

When the rudder is not located abaft a propeller or integral skeg, the effective rudder angle can be considered as an algebraic sum of actual rudder angle and drift angle at the location of rudder.

(This simple summation is not applicable to the rudder abaft a propeller because of the predominant effect of the propeller stream onto the rudder, making the local drift angle effect insignificant).

Fig. 223 shows the relationship between actual rudder angle  $\delta_R$  and geometric drift angle at the rudder stock; the data are from full-scale zigzag maneuvers. Possible in this maneuver is to have a situation in which the effective rudder angle exceeds the stall angle, thereby introducing the possibility of substantial loss in rudder force.

The ideal rate of rudder deflection is one that allows the rudder to generate its maximum possible lift when required, that is, fully utilizing the rudder without exceeding the stall angle. The rudder should be deflected at the maximum rate to just below the stall angle to initiate or check a maneuver. Then the rudder angular rate should be reduced to the rate of change of  $\beta_R$  as indicated by a dotted line in Fig. 223. This deliberate variation in rudder rate pertains especially to vessels constructed to allow very large rudder angles, say 45 deg or greater. As with the rudder deflection angle, constraint (c) of Section 17.1 imposes

an upper limit on the rudder deflection rate. Increased rate not only increases the power demand on the steering engine, but it also increases rudder torque slightly. Except for high-speed ships with special response requirements, few ships exceed the regulatory  $2\frac{1}{3}$  deg/sec rate. On high-speed container ships with concern for cargo damage from tight turns at high speed, a rate limiting mechanism is sometimes installed to reduce the rate when the ship is travelling fast.

**17.7 Selection of Section Shape.** The selection of chordwise section shape, given rudder location and size, among other concerns, is governed by the following ideal considerations:

- Highest possible maximum lift,
- maximum slope of the lift curve with respect to angle of attack,
- maximum resistance to cavitation,
- minimum drag and shaft power,
- favorable torque characteristics,
- ease of fabrication

The comparison of wind-tunnel test results reveals that the NACA symmetrical section shape (OOXX Series where XX represents a two-digit number indicating thickness as a percent of chord length) is one of the most desirable sections for rudders (See also Thieme, 1965, for other desirable choices).

Table 38 shows the results of free-stream wind-tunnel tests of the NACA symmetrical section. A section shape is shown in Fig. 224. Results are given for the highest test Reynolds number of  $2.7 \times 10^6$  for all-movable foils having a thickness ratio of 6.7 and an effective aspect ratio of 2.0.

The trailing edge of the rudder is deliberately intended to have noticeable thickness rather than to taper to a knife or feather edge. The bluntness of the trailing edge allows increased ruggedness of construction, which is especially useful for astern operation. The bluntness is also believed, in some cases, to cause appreciably greater lift with little penalty in increased drag, although the slope of the curve of lift versus angle of attack is but slightly affected.

Fig. 225 shows the basic rudder foil chord-wise cross section with a table of ordinates, for a rudder with a thickness of 20 percent of the chord. (Points obtained from the Göttingen 398 and the Clark Y sections are also plotted on the figure, for comparison.)

The ordinate of the profile is given by an equation of the form

$$\pm y = a_0 \sqrt{x} + a_1 x + a_2 x^2 + a_3 x^3 + a_4 x^4 \quad (163)$$

where the chord is expressed in fractions of chord length along the  $x$ -axis from 0 to 1. The constants were determined from imposed conditions; e.g., the maximum ordinate was set at 0.1 chord length at abscissa 0.3 chord length. NACA sections having any desired maximum thickness,  $t$ , can be obtained by multiplying the basic ordinates by the proper factor, as follows:

Table 38—Wind Tunnel Test Results of NACA Rudder Section

$\ast \left( \frac{\partial C_L}{\partial \alpha} \right)_{\alpha=0}$	Maximum Lift Coefficient	Stall angle, deg	Drag Coefficient $\alpha = 0$
0.041	1.32	28.7	0.009

$\ast (\partial C_L / \partial \alpha)_{\alpha=0}$  = Slope of the lift coefficient curve with respect to angle of attack ( $\alpha$ ) in degrees at  $\alpha = 0$ .

$$\pm y_t = \frac{t}{0.20} (0.29690 \sqrt{x} - 0.12600x - 0.35160x^2 + 0.28430x^3 - 0.10150x^4) \quad (164)$$

The profiles derived are shown in Fig. 226. What appear as threadlike leading and trailing edges in these profiles are merely remnants of centerlines used in drafting. The leading edge has theoretically zero thickness at the tangent to the curve of cross section, but the trailing edge has finite thickness as a consequence of the sum of the  $\alpha$ -coefficients being greater than zero (at  $x$  equal to unity, that is, full chord length).

The characteristics of symmetric profiles having various thickness ratio are shown in Fig. 227a and b and in Table 39. These characteristics are based on infinite span. Characteristics of the rudder of small aspect ratio are different. Figs. 228 and 229 show comparisons of characteristics for thickness variations.

Sections with greater thickness (0018 through 0025) have hydrodynamic advantages, namely (1) greater stall angle (larger maximum lift coefficient) and (2) relatively constant location of center of pressure. The drag increase with thickness is relatively small. Thick sections are also superior from a structural point of view. A limit on thickness is imposed by root-thickness chord ratio considerations as discussed near the end of Section 17.4.

**17.8 Steering Gear Torque and Rudder Balance.** The process of rudder design is usually conducted in two parts: (a) selection of the geometric

parameters and turning rate necessary to develop the desired ship turning characteristics, and (b) calculation of the force and torque loadings on the arrangement including the steering gear that must control the rudder movements. As has been noted by Harrington (1981), Hagen (1972), Asinovsky (1985), and others, prediction of full-scale torque loadings is a problem that has not been satisfactorily solved in spite of many years of effort in perfecting design methods.

Determination of hydrodynamic forces and torque requires accurate assessment of hull wake, propeller race, hull drift angle, and change in rudder angle of attack as the hull turns, in addition to the effects of the arrangement of the particular rudder under analysis. Another component of importance derives from frictional losses in the rudderstock bearings and steering gear driving mechanisms.

Empirical formulas for estimating rudder forces and moments are given by Jaeger (1955) and Attwood et al. (1953). All have shortcomings, but the method of Joessel, based on experiments with a flat rectangular plate (See "Steering" by Schoenherr as cited by Rossell and Chapman, 1939), has gained wide acceptance despite its own shortcomings, which include some physical ones:

$$Q = 0.811 A v^2 \omega \sin \alpha \quad (165)$$

and

$$\frac{x}{\omega} = (0.195 + 0.305 \sin \alpha) \quad (166)$$

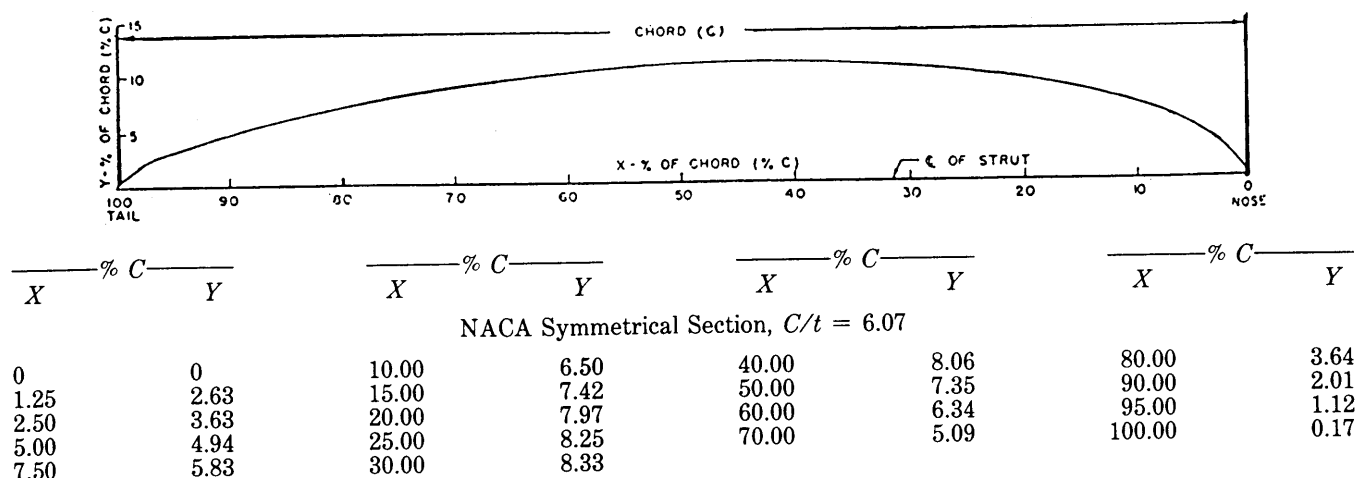
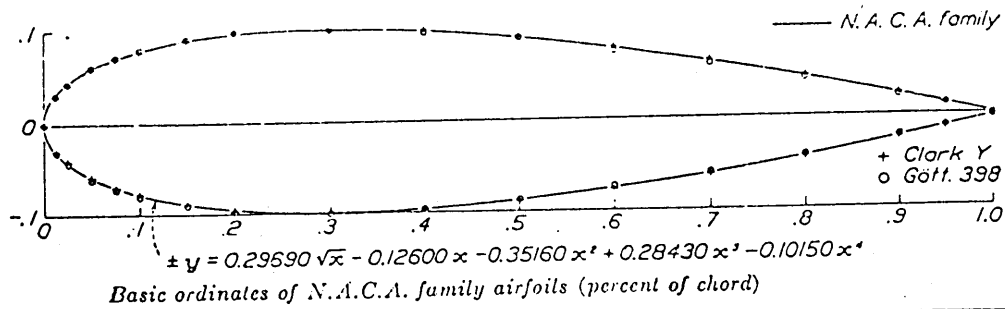


Fig. 224 NACA section shape with ordinates



Sta.....	0	1.25	2.5	5.0	7.5	10	15	20	25	30	40	50	60	70	80	90	95	100
Ord.....	0	3.157	4.358	5.925	7.000	7.805	8.909	9.563	9.902	10.003	9.072	8.823	7.000	6.107	4.372	2.413	1.314	0.210

L.E. radius, 4.40.

Fig. 225 Thickness variation

Table 39—Characteristics of NACA Sections Having Various Thickness  
(Aspect Ratio Unlimited. Test Reynolds Number =  $3.2 \times 10^6$ )

Chord/ Thickness	NACA Series Designation	$\left(\frac{\partial C_L}{\partial \alpha}\right)_{\alpha=0}$	Maximum Lift Coefficient	Drag Coefficient at $\alpha = 0$
4.0	0025	0.089	1.20	0.014
4.8	0021	0.094	1.38	0.012
5.6	0018	0.098	1.40	0.011
6.7	0015	0.100	1.53	0.009
8.3	0012	0.101	1.53	0.008
11.1	0009	0.101	1.27	0.007
16.7	0006	0.102	0.88	0.006

where

- $Q$  = rudder torque about leading edge of plate, ft-lb
- $A$  = area of plate,  $\text{ft}^2$
- $v$  = water velocity, fps
- $\omega$  = plate width, ft
- $\alpha$  = angle of attack, deg
- $x$  = distance from leading edge to center of pressure, ft

By combining Equations (165) and (166) to find  $Q/x$ , the resultant force on a plate is determined to be

$$F = \frac{Q}{x} = \frac{0.811 A v^2 \sin \alpha}{0.195 + 0.305 \sin \alpha} \quad (167)$$

where  $F$  is the resultant force on the plate in lb. The equations were used in conjunction with Joessel coefficients ( $K_{\text{ahead}}$  and  $K_{\text{astern}}$ ) developed for various ship types, and many influences such as rudderstock bearing friction were considered to be included. Harrington (1981) describes the use of the Joessel method as applied in Fig. 237 to a horn-type rudder. The rudder is broken into two rectangles, and expressions for the ahead and astern rudder torques become as follows upon application of Equations (165), (166), and (167), and the suitable Joessel coefficient:

$$Q_{\text{ahead}} = K_{\text{ahead}} 0.811 v^2 \sin \alpha \quad (168)$$

$$\begin{aligned} & \times \left[ \left( \frac{w_1 (0.195 + 0.305 \sin \alpha) - b}{0.195 + 0.305 \sin \alpha} \right) w_1 h_1 + w_2^2 h_2 \right] \\ Q_{\text{astern}} &= K_{\text{astern}} \frac{0.811 v^2 \sin \alpha}{0.195 + 0.305 \sin \alpha} \\ & \times [(\alpha - w_1 (0.195 + 0.305 \sin \alpha)) w_1 h_1 \\ & + w_2^2 h_2 (0.805 - 0.305 \sin \alpha)] \end{aligned}$$

Whicker and Fehlner (1958) provide a logical design theory for calculating rudder forces and their spanwise and chordwise locations. Also included are wind-tunnel

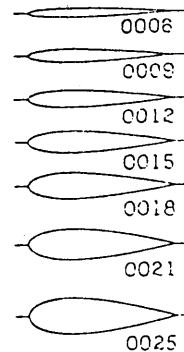


Fig. 226 NACA Symmetrical airfoils

## CHARACTERISTICS OF AIRFOIL SECTIONS FROM TESTS IN VARIABLE-DENSITY WIND TUNNEL

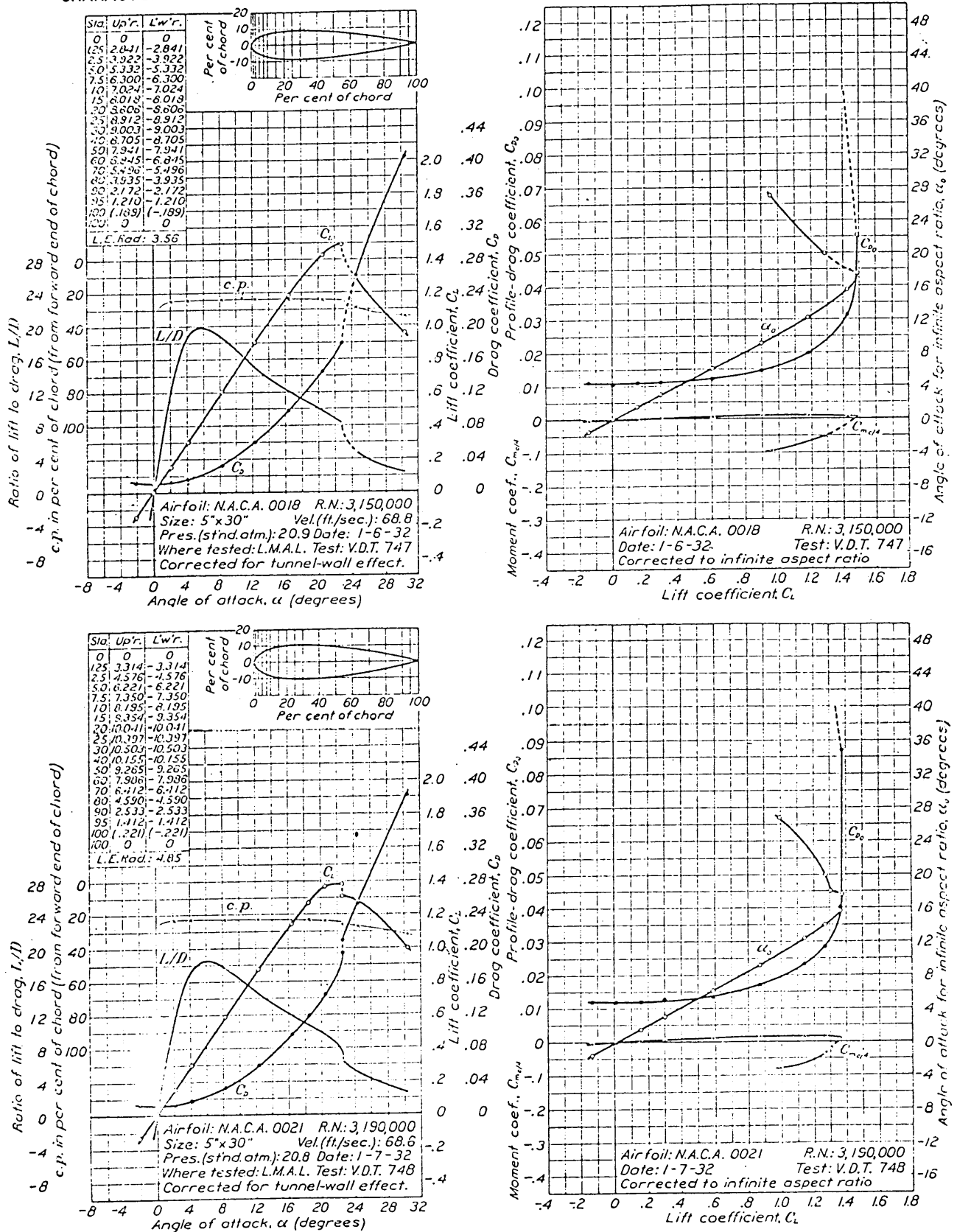


Fig. 227(a) and (b) NACA 0018 and 0021 airfoils

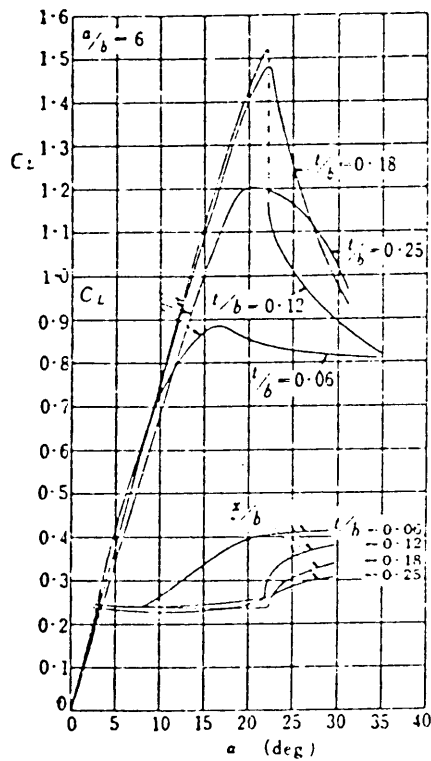


Fig. 228 Lift coefficients of NACA symmetrical airfoils

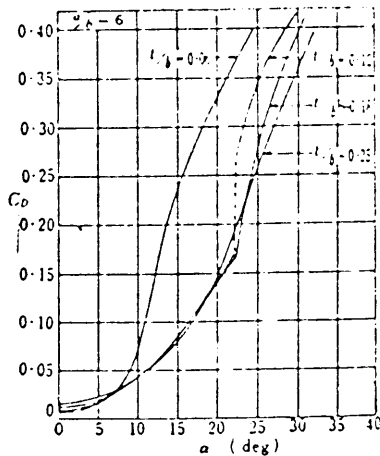


Fig. 229 Drag coefficients of NACA symmetrical airfoils

test results at Reynolds numbers up to about 3 million, for a systematic family of all-movable control surfaces including some astern data.

The computation of rudderstock size requires knowledge of:

- The maximum design value of the resultant force on the rudder.
- The location of the spanwise center of pressure (CP)<sub>s</sub> corresponding to the maximum resultant force.
- The location of the rudder bearings.

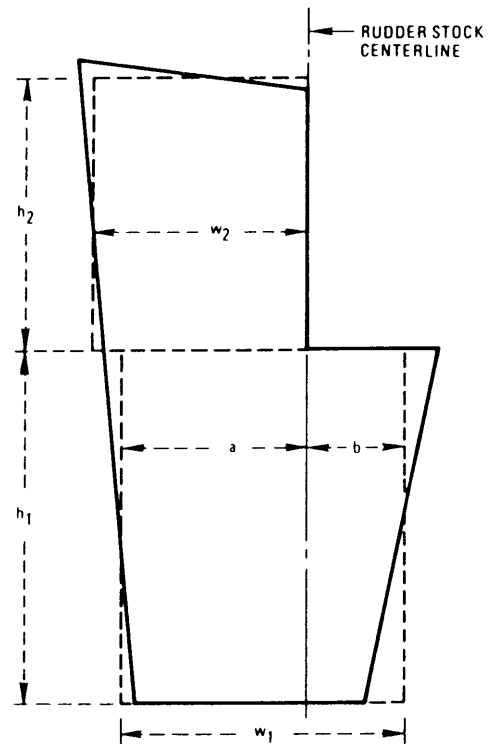


Fig. 230 Model of a horn-type rudder used with the Joessel method

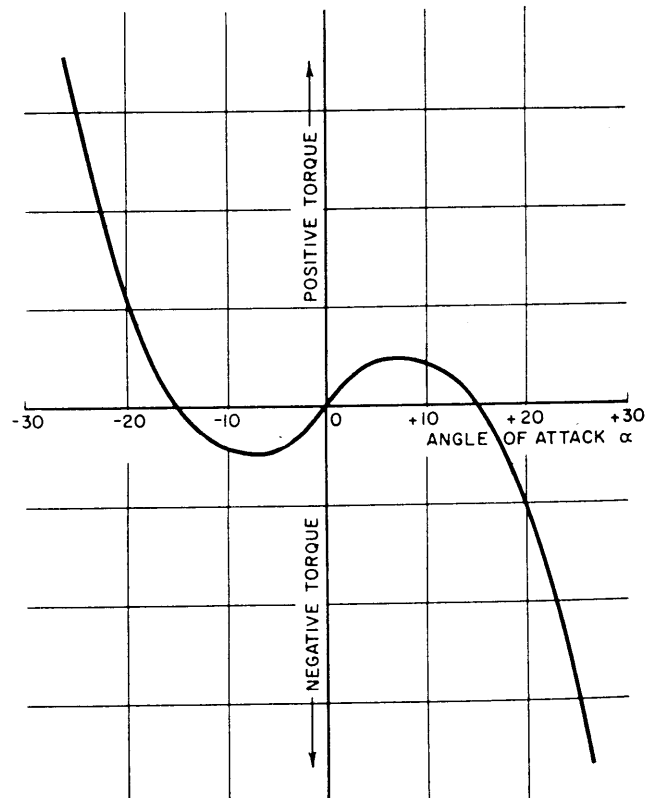


Fig. 231 Typical torque versus angle of attack relationship

The computation of rudder-stock location and steering-gear torque for all rudders requires knowledge of:

(d) The rudder normal force  $F$  and the location of the chordwise center of pressure ( $CP$ )<sub>c</sub> as a function of rudder angle of attack at the maximum ship speed.

(e) Bearing radii and coefficients of friction.

On ships that have no restrictions on use of the rudder in going astern, items  $a$ ,  $b$ , and  $d$  have to be known for both maximum ahead and maximum astern speeds. On recent naval ships, there has been recognition of the following:

(a) Typical naval combatant ships have large astern power and hence are capable of correspondingly high astern speed.

(b) Adequate design for that astern speed would require large, heavy steering gear.

(c) It seems reasonable to allow use of full astern power for crash stops, but there is no need to go astern at high speed after stopping.

(d) Accordingly, instruction plates are provided limiting the sustained astern shaft rotational speed to that which permits steering gear operation within the ahead limits.

(e) The acceptance trials include demonstration of the workability of the Instruction Plate limit.

Thus, design practice for naval combatant ships (Taplin, 1960) bases the calculation of rudder-stock size, stock location, and steering-gear torque on the ahead condition.

Appendixes A and B of Taplin (1960) detail the com-

putation of items 1 and 4 for all-movable rudders using the free-stream data of Whicker and Fehlner (1958). However, in order to use the free-stream data to compute the maximum design value of the normal force, assumptions have to be made concerning

(a) The maximum angle of attack that the rudder is likely to encounter,  $\alpha_{\max}$ .

(b) The maximum flow velocity averaged over the rudder,  $(V_R)_{\max}$ .

(c) Rudder effective aspect ratio,  $a$ .

Taplin (1960) takes the angle of attack to be  $5/7$  of the rudder deflection angle for all rudders. For rudders suffering a loss of lift at stall, Mandel (1953) suggests that the normal force at stall be taken as the maximum design value.

For the flow velocity averaged over the rudder,  $V_R$ , Taplin (1960) uses the assumption that for rudders in the propeller race:

$$V_R = k(1 + S_a)V \quad (169)$$

where  $k$  has a value between 0.8 and 1.0, depending on how much of the rudder area is located in the propeller race, and  $S_a$  is the propeller apparent slip ratio. Fig. 250 contains somewhat more refined data than what is implied by Equation (169).

In Section 14.6, the effective aspect ratio of a control surface tested against a body of revolution hull was compared to the effective aspect ratio of the same control surface tested against a groundboard. It was shown that in the former case

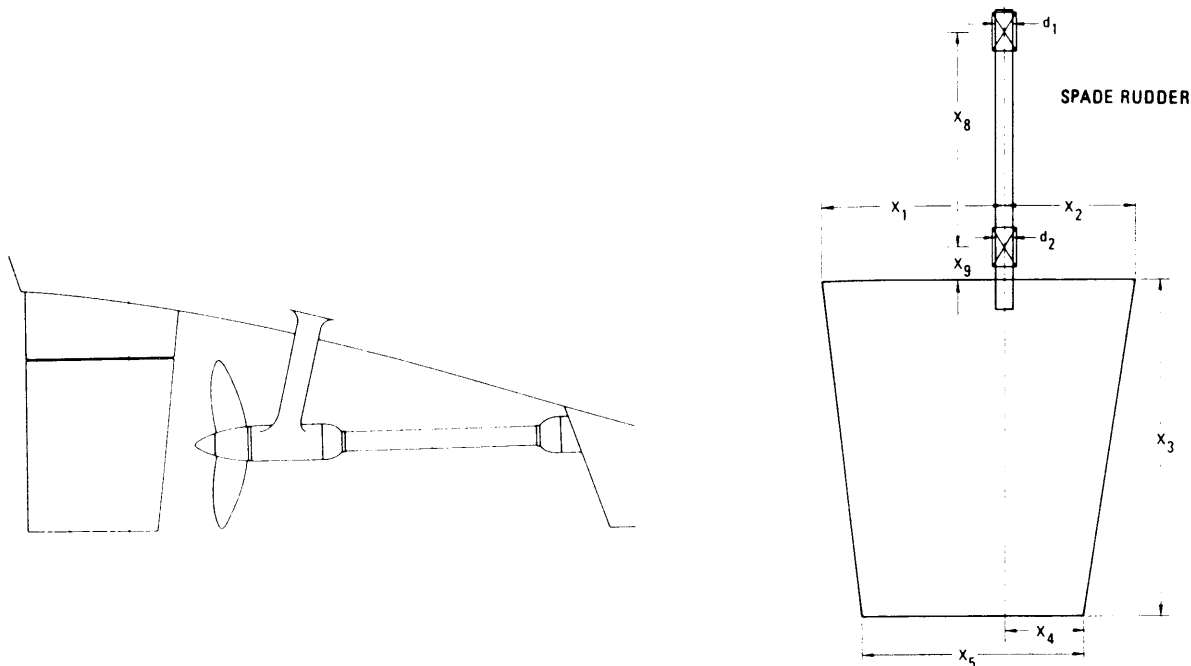


Fig. 232 Ship A stern arrangement and support details

Table 40—Ahead Rudder Torque Calculations for a Typical Spade Rudder Using Cross-faired Test Data (Whicker and Fuhlner, 1958) (Harrington, 1981)

NOTE: These calculations are for 20-deg rudder angle-of-attack position for Ship A, as defined by Figs. 232 and Table 41			
Propeller thrust = $326 Pe/V(1 - t)$	$T$	251 900 lb	114,262 Kg
Speed of advance = $1.69 V(I - w)$	$v$	33.61 fps	10.24 m/s
Dynamic pressure = $0.994 v^2 + \frac{4T}{\pi D^2}$	$p$	1924.7 psf	1.943 MPa
Taper ratio = $X_5/(X_1 + X_2)$	$\lambda$	0.875	
Mean chord = $0.5(X_1 + X_2 + X_5)$	$\bar{c}$	16.875 ft	5.143 m
Sweep angle = $\tan^{-1} \left[ \frac{0.25(X_5 - X_1 - X_2) + X_2 - X_4}{X_3} \right]$	$\Omega$	4.82 deg	
Rudder angle	$\alpha$	20 deg	
Effective aspect ratio = $\frac{X_3}{\bar{c}} \left( 2 - \frac{\alpha}{75} \right)$	$\alpha$	2.054	
Data uncorrected for taper ratio:			
lift coefficient (see Figs. 240 and 241)	$C_{L1}$	0.942	
drag coefficient (see Figs. 242 and 243)	$C_{D1}$	0.163	
center of pressure (see Figs. 244 and 245)	$CP_{\bar{c}_1}$	0.220	
Lift coeff. corr. = $\frac{1.63\lambda - 0.73}{\alpha} \left( \frac{\alpha}{57.3} \right)^2$	$\Delta C_L$	0.041	
Corrected lift coeff. = $C_{L1} + \Delta C_L$	$C_{L2}$	0.983	
Drag coeff. correction = $\frac{C_{L2}^2 - C_{L1}^2}{2.83a}$	$\Delta C_D$	0.014	
Corrected drag coeff. = $C_{D1} + \Delta C_D$	$C_{D2}$	0.177	
$C_{L1} \cos \alpha + C_{D1} \sin \alpha$	$C_{N1}$	0.941	
$C_{L2} \cos \alpha + C_{D2} \sin \alpha$	$C_{N2}$	0.984	
$(0.25 - CP_{\bar{c}_1})C_{N1} - \frac{1}{2} \Delta C_L$	$C_{Mc}/4_2$	0.00773	
Corr. center of pressure = $0.25 - \frac{C_{Mc}/4_2}{C_{N2}}$	$CP_{\bar{c}_2}$	0.242	
Normal force = $p\bar{c}X_3C_{N2}$	$F$	639 200 lb	315,000 kg
Hydrodynamic torque = $12F \left( \bar{c} CP_{\bar{c}_2} - \frac{X_2 + X_4}{2} \right)$	$Q_H$	$-3.84 \times 10^6$ in.-lb	$43.4 \times 10^4$ N·m
Rudderstock bearing friction			
$= \mu_1 \frac{d_1}{2} F \left( \frac{0.42X_3 + X_9}{X_8} \right) + \mu_2 \frac{d_2}{2} F \left( \frac{0.42X_3 + X_8 + X_9}{X_8} \right)$	$Q_F$	$2.32 \times 10^6$ in.-lb	$26.45 \times 10^4$ N·m
Rudder torque displacing = $Q_F + Q_H$	$Q_D$	$-1.52 \times 10^6$ in.-lb	$17.32 \times 10^4$ N·m
Rudder torque restoring = $Q_F - Q_H$	$Q_R$	$6.16 \times 10^6$ in.-lb	$70.24 \times 10^4$ N·m

$$a = (2 - 0.0111\alpha) a_G \quad 0 < \alpha < 27 \text{ deg} \quad (170)$$

$$a = 1.5 a_G \quad \alpha = 31 \text{ deg (stall angle)}$$

In contrast to these data, Taplin (1960) suggests for rudders where the gap is considered small at  $\alpha = 0$  and large at  $\alpha = \alpha_{\max}$  that the effective aspect ratio be taken as:

$$a = \left( 2 - \frac{\alpha}{\alpha_{\max}} \right) a_G \quad (171)$$

It is clear that the use of Equation (170) would result

in a larger maximum resultant force than Equation (171). However, if the other assumptions are used, use of Equation (171) is recommended.

By using the preceding three assumptions and the freestream data, the maximum bending moment,  $(Q_{BM})_{\max}$  and the maximum hydrodynamic torque,  $(Q_H)_{\max}$  acting on the rudder stock may be computed as follows:

$$(Q_H)_{\max} = F(d - CP_{\bar{c}}) \quad (120d)$$

$$(Q_{BM})_{\max} = (L^2 + D^2)^{1/2} (CP_{\bar{c}} + b) \quad (172)$$



where  $F$ ,  $L$ ,  $D$ ,  $CP_c$ , and  $CP_s$  are determined at  $\alpha = \alpha_{\max}$  and  $V_r = (V_r)_{\max}$  and  $b$  is the distance from the root chord of the rudder to the center of the lower bearing supporting the rudder.

If the chordwise center of pressure on a rudder remained in a fixed location as the angle of attack on the rudder increased, it would be desirable always to locate the rudder stock just forward of the center of pressure. This would insure a low maximum torque value and in the event that the rudder were inadvertently freed, the rudder would tend to trail at  $\delta_R = 0$  deg as long as  $\alpha = 0$  deg. Unfortunately, on most rudders the center of pressure moves aft as the angle of attack increases. Therefore, in order to reduce the maximum torque value, most ship rudders are not designed as trailing rudders; rather, the practice, according to Taplin (1960) and Comstock (discussion of Mandel (1953)), is to determine the location of the stock on the basis that the hydrodynamic torque should be zero at an angle of attack of about 10 to 15 deg. Thus, a typical torque versus angle of attack curve takes the form shown in Fig. 231. It is clear from this Figure that if the zero torque point were taken at a larger angle of attack, the maximum torque at  $\alpha = \pm \alpha_{\max}$  could be significantly reduced. Nevertheless, the 10 to 15-deg zero torque point is used in the interests of minimizing the power required for routine steering and coursekeeping, which on most ships seldom requires more than 10 to 15 degree of rudder angle.

As is shown in Fig. 231, such a rudder is unstable at  $\alpha = 0$ ; if it were freed, the rudder would flop over to either plus or minus 15 deg. Romahn and Thieme (1957) have pointed out that this instability may produce rattling, shock, and excessive wear in geared steering mechanisms. Their recommendation is that rudders should be at least neutrally stable at  $\alpha = 0$  deg; that is, the rudder stock should be located at the ( $\alpha = 0$  deg) position of the center of pressure. But unless means are discovered for reducing the center-of-pressure travel as  $\alpha$  is increased, this recommendation leads to the requirement for larger steering-gear capacity.

Harrington (1981) presented extensive trial results and comparative analyses using improvements on the Whicker and Fehlner (1958) methods for predicting torque. The calculation method is presented in Table 40. Figs. 233-238 provide cross-plots of lift coefficient, drag coefficient, and chordwise center of pressure for zero and +11-deg sweep angles. These figures were adapted from Whicker and Fehlner (1958) to simplify the calculations. In order to permit projections beyond the stall angle indicated by the model test data, extrapolations of the original data are shown on these figures as dashed lines for rudder angles of attack that exceed the predicted stall angle. These extrapolations provide insight into the risk involved if stall does not occur as predicted.

In the calculations given in Table 40, the velocity of

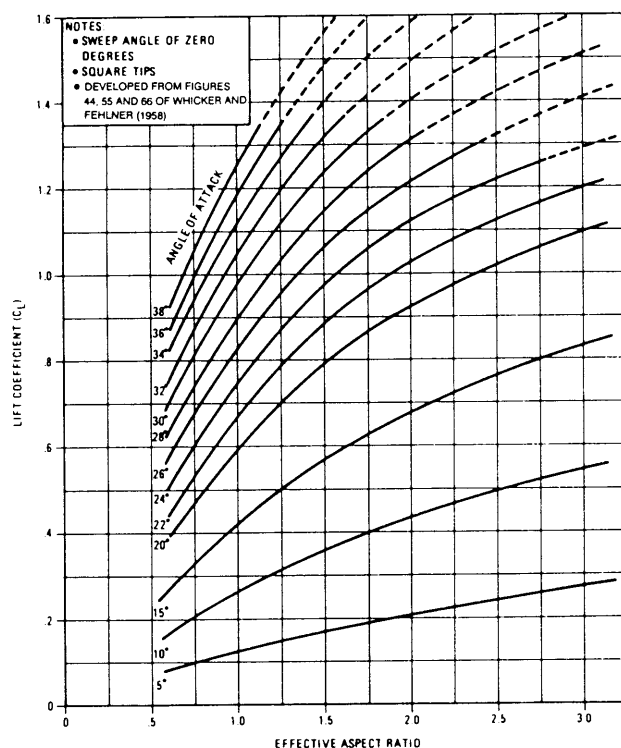


Fig. 233 Lift coefficient, sweep angle of 0 deg (Harrington, 1981)

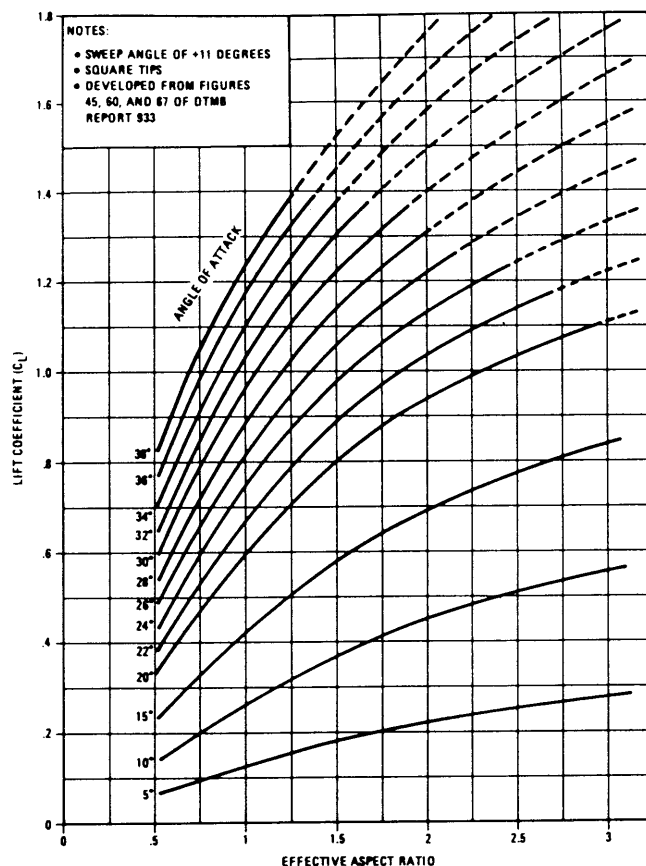


Fig. 234 Lift coefficient, sweep angle of +11 deg (Harrington, 1981)

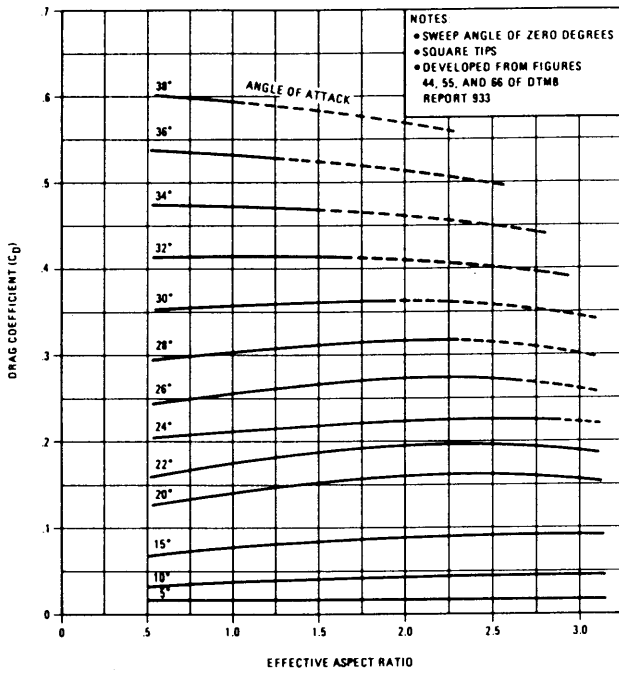


Fig. 235 Drag coefficient sweep angle of 0 deg (Harrington, 1981)

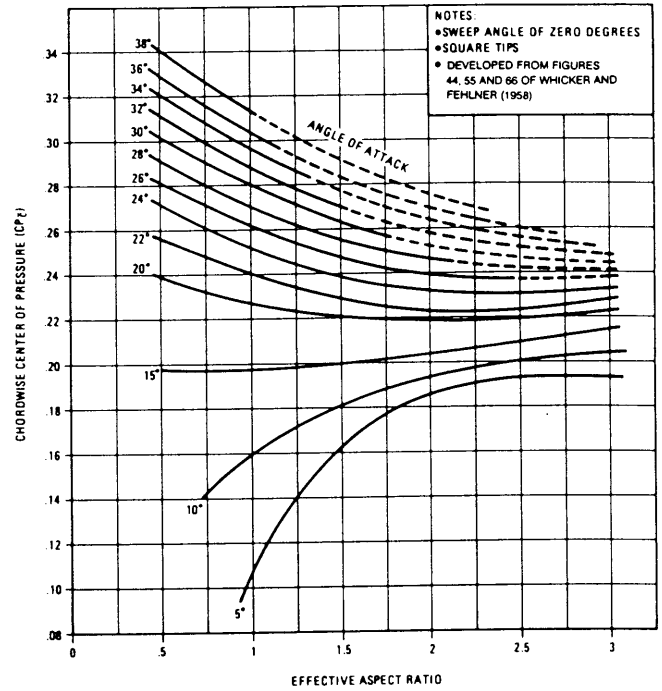


Fig. 237 Chordwise center of pressure, sweep angle of 0 deg (Harrington, 1981)

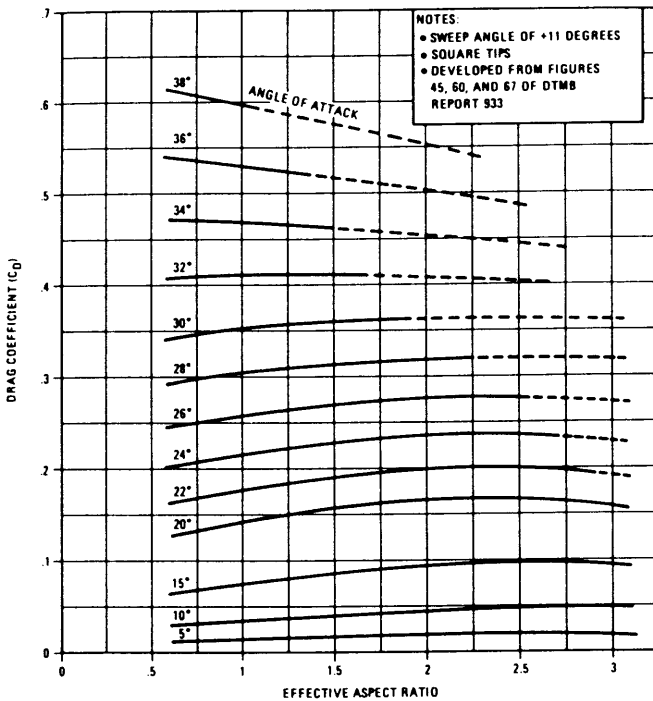


Fig. 236 Drag coefficient sweep angle of +11 deg (Harrington, 1981)

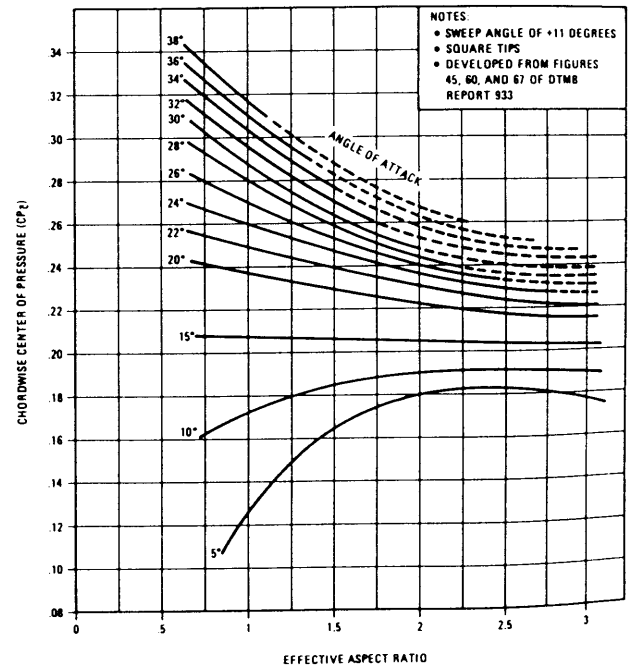


Fig. 238 Chordwise center of pressure, sweep angle of +11 deg (Harrington, 1981)

the water over the rudder is assumed to be uniform, and a correction is made for the average wake effects and the augmented water velocity due to the effects of the propeller race. The speed-of-advance calculation (wake effect) is familiar, but the dynamic pressure calculation (propeller race effect) may be unfamiliar. Here it is assumed that the propeller actuator-disk

theory, as described by Rossell and Chapman (1958, Schonherr) applies, and the propeller thrust is expressed as

$$T = \rho A \left( v + \frac{z}{2} \right) z \quad (173)$$

Table 41—Descriptive Data for Three of the Six Ships Instrumented During Steering Trials (Harrington, 1981. Also see Figs. 232 and 240.)

Ship			A	B	C
Hull: length	ft		550	1143	916
beam	ft		82	228	135
draft	ft		19.9	74	36
displacement (trial)	tons		13 800	450 600	97 098
Rudder type	...		spade	shoe	horn
Steering gear: type	...		Rapson	Rapson	Rapson
number of rams	$Z$	...	2	2	1
ram diameter	$d$	in.	10	18.625	16.25
crosshead radius	$R$	in.	28	55.5	37
Ship ahead speed (trial)	$V$	knots	22.6	15.5	19.5
shaft horsepower	$P$	hp	22 000	45 000	40 000
performance coefficient	$e$	...	0.697	0.676	0.635
thrust deduction factor	$t$	...	0.122	0.267	0.12
wake fraction	$w$	...	0.12	0.668	0.13
propeller diameter	$D$	ft	20	31.5	25
Ship astern speed (trial)	$U$	knots	10	4.6	9.5
Rudder dimensions:	$X_1$	ft	12.29	25.25	12.34
	$X_2$	ft	5.71	10.75	7.5
	$X_3$	ft	20	41.75	17.17
	$X_4$	ft	3.46	10.75	5.75
	$X_5$	ft	15.75	36	14.92
	$X_6$	ft	...	25.25	14.87
	$X_7$	ft	...	6.25	14
Rudder support details:	$X_8$	ft	12.1	34.9	18.42
	$X_9$	ft	3.8	...	6.3
	$X_{10}$	ft	...	44.64	10.43
	$X_{11}$	ft	...	...	2.2
	$X_{12}$	ft	...	...	1.1
Upper stock OD	$d_1$	in.	22	43	25.75
Upper stock brg. type	...	...	roller	bronze	bronze
Upper stock brg. frict. coeff.	$\mu_1$	...	0.01	0.10	0.05
Lower stock OD	$d_2$	in.	35	32	25.5
Lower stock brg. type	...	...	phenolic	phenolic	phenolic
Lower stock brg. frict. coeff.	$\mu_2$	...	0.10	0.20	0.10
Rudder pintle OD	$d_3$	in.	...	32	24
Rudder pintle brg. type	...	...	...	phenolic	phenolic
Rudder pintle frict. coeff.	$\mu_3$	...	...	0.20	0.10

1 ft = 0.304 m

1m = 0.326 ft

where

$T$  = propeller thrust  
 $A$  = propeller disk area  
 $\rho$  = water density  
 $v$  = propeller speed of advance  
 $z$  = velocity imparted to the water by the propeller

This equation can be combined with the usual expression for dynamic pressure to eliminate  $z$  and form the following expression for the dynamic pressure,  $p$ :

$$p = \frac{\rho}{2} (z + v)^2 = \frac{\rho}{2} v^2 + \frac{T}{A} \quad (174)$$

This is the basic form of the expression used in Table 40.

The effective aspect ratio (slenderness ratio or span-to-width ratio) of most rudders does not lend itself to

an exact evaluation, and this inexactitude introduces unavoidable inaccuracies into the calculations. As can be imagined, a very high aspect ratio would suggest a long, continuous lifting surface where the breakdown of lift due to end effects is minimal and the flow conditions are ideally suited to development of lift at low angles of attack.

One means of effectively increasing the aspect ratio of a rudder is to develop an arrangement in which the rudder is bounded on one end by a surface that is in the plane of the flow. If the bounding surface completely seals the end of the rudder, thereby eliminating cross-flows and end losses, a mirror-image effect is achieved and the "effective" aspect ratio is equal to twice the geometric aspect ratio. This condition may exist in the case of the fairwater diving planes on some submarines where the fairwater diving planes abut the sail, which is nearly plane-sided, thereby providing mirror-image conditions. However, the opportunity to

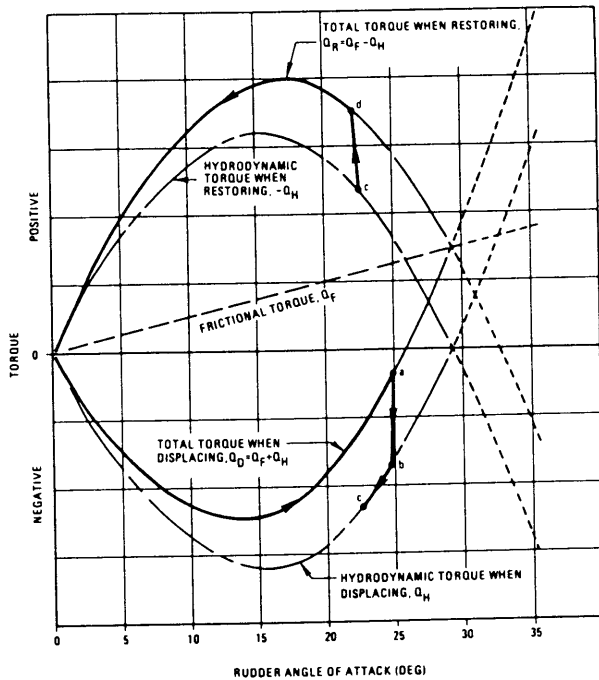


Fig. 239 Rudder torque elements during a simple maneuver (Harrington, 1981)

provide a mirror effect at all angles of attack seldom arises in the design of rudders, because the hull surface in way of the rudder is rarely flat.

Harrington (1981) notes that the frictional torque can be predicted by assuming that the position of the spanwise center of pressure is located 42 percent of the span distance from the root chord and assuming that the rudder normal force is equal to the rudder resultant force. On these assumptions, which are sufficiently accurate for the purpose, the loads carried by the upper and lower rudderstock bearings are readily determined. Then, with the bearing loads and stock diameter known, the bearing frictional torque can be computed if the friction coefficient is known. Selecting reasonable values for coefficients of friction presents no serious difficulty, given the materials and lubricants normally used. Based on the information provided by Taplin (1960), Smith (1967), standard handbooks, a friction coefficient of 0.2 for reinforced laminated phenolic (such as Micarta) bearings appears reasonable.

The frictional torque is significant as shown in Fig. 239, which graphs typical torque elements during a simple maneuver. The  $Q_D$  curve represents the sum of the frictional and hydrodynamic components. Movement of the rudder from centerline would entail torques following the curve until the ordered angle is

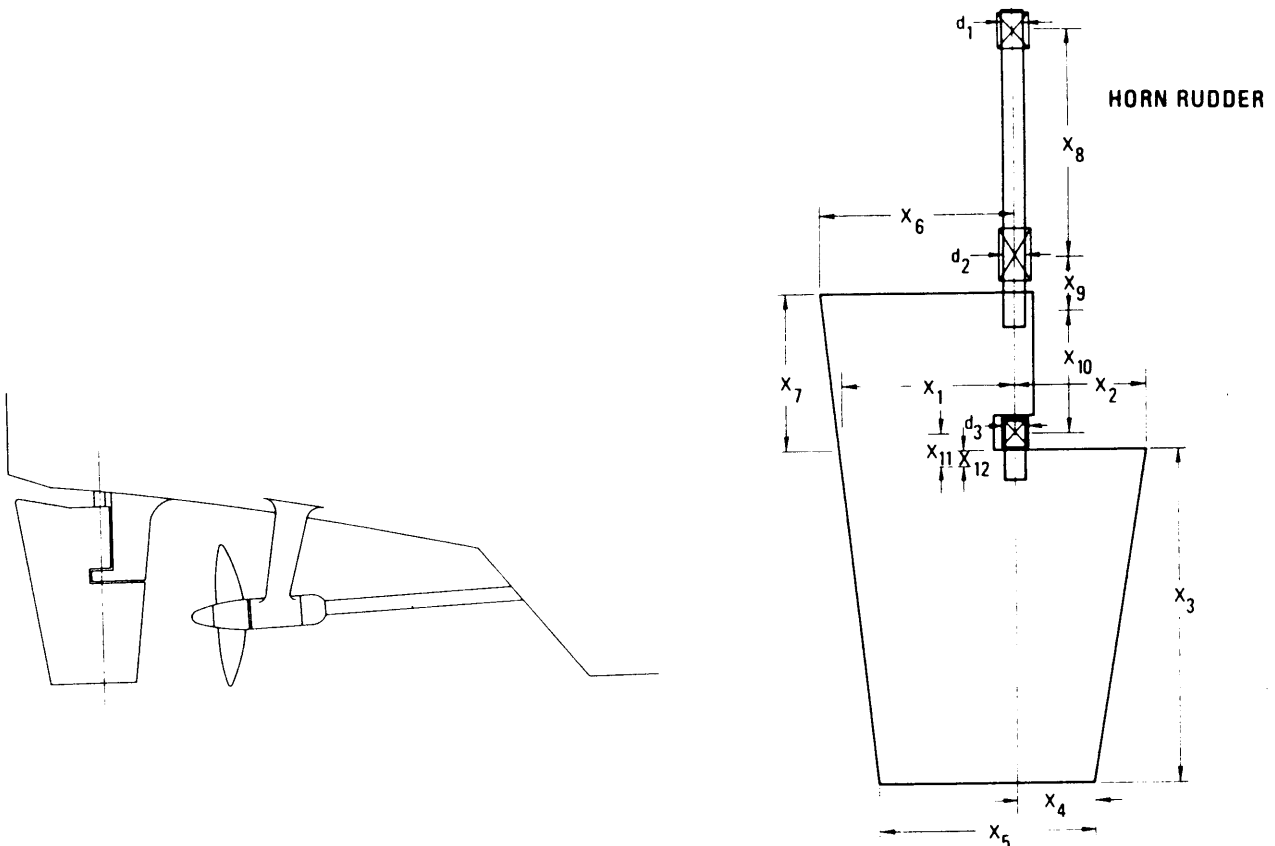


Fig. 240 Ship C stern arrangement and support details

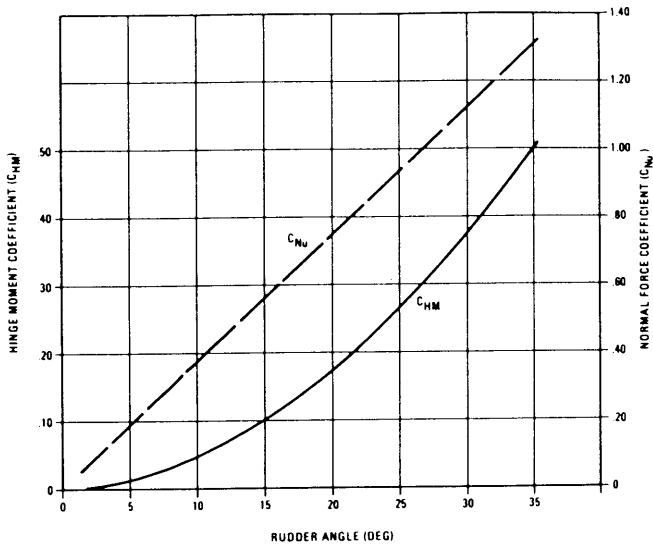


Fig. 241 Hinge moment and normal force coefficients of rudder area abaft horn (Harrington, 1981)

reached at Point a. The rudder is then held in position by the hydraulic ram pressure, and small movements tend to dissipate the effects of friction in making the transition to Point b on the  $Q_H$  curve. A drift angle is assumed by the vessel, causing movement to point c. If the rudder is then ordered to centerline, the process works in reverse from the  $-Q_H$  curve moving to the  $Q_R$  curve.

Harrington (1981) provides Table 42 as a procedure for the calculation of torque requirements for a horn rudder. As with the spade rudder, the velocity of the water onto the rudder is assumed to be uniform and equal to the velocity in the propeller race. In some calculation procedures, only that portion of the rudder within the projected outline of the propeller disk is considered subject to uniform velocity in the propeller race, and parts of the rudder not within projection of the propeller disk area are considered subject to a water velocity equal to the speed of the ship. This approach may be logical and consistent with other approaches that have been taken, but parts of most horn rudders are outside a projection of the propeller and a correlation of results obtained with this procedure against trial data will not support the assumption. Wind tunnel test data from Bowers (1959) for a series of flapped control surfaces were adjusted to be applicable to horn rudders. Paired into the relationship of Fig. 241, these data permit a simple and straightforward prediction for the hydrodynamic characteristics of that part of the rudder that trails the horn in customary rudder configurations. Reviews of trial data suggest that over-capacity is a prudent objective.

In a discussion of Harrington (1981), R. Taggart provided Fig. 242, which shows torques as developed from ram pressures and strain gages on the rudder

stock for the DE1040 during zigzag maneuvers. A very comprehensive analysis was described which predicted the two values quite well. Harrington noted that the figure helps illustrate the accuracies required in design. Maximum torque based on ram pressure data is shown at about  $0.994 \times 10^6$  N·m ( $8.8 \times 10^6$  in.-lb) with the strain gage torque at  $0.768 \times 10^6$  N·m ( $6.8 \times 10^6$  in.-lb). Normal force on the DE-1040 rudder at stall is estimated to be about 320,000 kg (700,000 lb); therefore, if the rudderstock had been moved aft in the rudder just about 8 cm (3 in.), the design rating would not have been exceeded. If it had been moved aft 18 cm, however, the steering engine may have been considered to be overrated. With the mean chord at 3.5 m (11 ft), considerable accuracy in locating the stock is thus required.

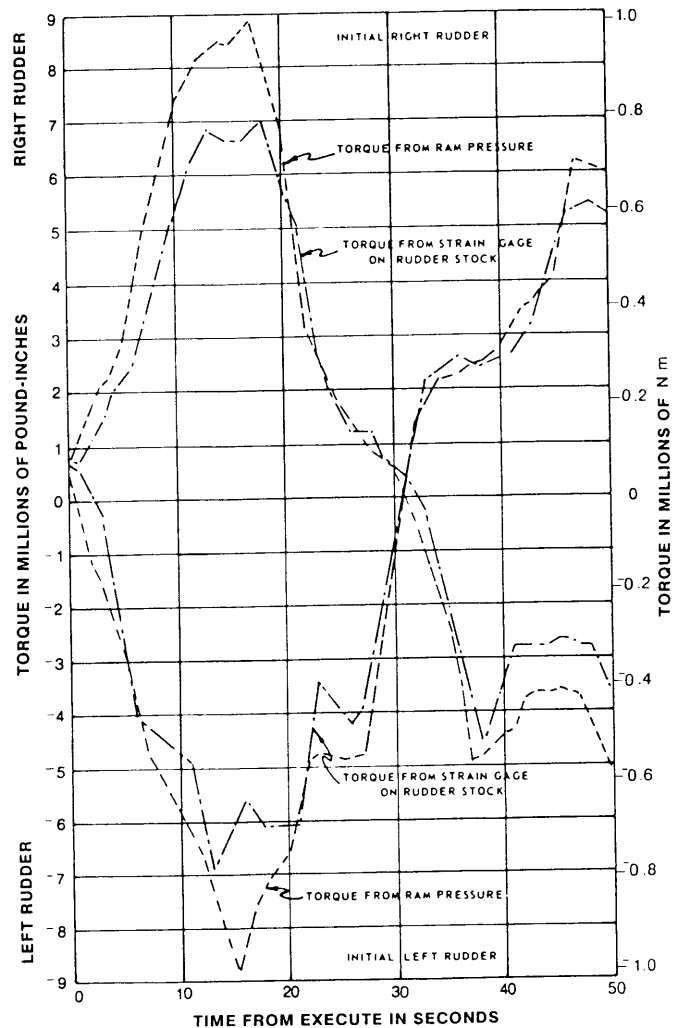


Fig. 242 Trial data: DE 1040 Z-manuevers at maximum approach speed

Table 42—Ahead Rudder Torque Calculations for a Typical Horn-type Rudder (Harrington, 1981)

NOTE: These calculations are for the 20-deg rudder angle-of-attack position for Ship C, as defined by Fig. 240 and Table 41.

Propeller thrust = $326 Pe/V(1 - t)$	$T$	482 500 lb	220,000 kg
Speed of advance = $1.69V(1 - w)$	$v$	28.67 fps	11.8 m/s
Dynamic pressure = $0.994v^2 + \frac{4T}{\pi D^2}$	$p$	1800 psf	1.8 MPa
Rudder angle	$\alpha$	20 deg	
Lower Rudder Section:			
Taper ratio = $X_5/(X_1 + X_2)$	$\lambda$	0.752 ...	
Mean chord = $0.5(X_1 + X_2 + X_5)$	$\bar{c}$	17.38 ft	7.2 m
Sweep angle = $\tan^{-1} \left[ \frac{0.25(X_5 - X_1 - X_2) + X_2 - X_4}{X_3} \right]$	$\Omega$	1.73 deg	
Aspect ratio = $\frac{X_3}{\bar{c}} \left( 2 - \frac{X_2}{X_1 + X_2} \frac{\alpha}{75} \right)$	$a_l$	1.88 ...	
Data uncorrected for taper ratio:			
lift coefficient (see Figs. 240 and 241)	$C_{L1}$	0.901 ...	
drag coefficient (see Figs. 242 and 243)	$C_{D1}$	0.16 ...	
center of pressure (see Figs. 244 and 245)	$CP_{\bar{c}_1}$	0.219 ...	
Lift coeff. correction = $\frac{1.63\lambda - 0.73}{a_l} \left( \frac{\alpha}{57.3} \right)^2$	$\Delta C_L$	0.032 ...	
Corrected lift coefficient = $C_{L1} + \Delta C_L$	$C_{L2}$	0.933 ...	
Drag coefficient correction = $\frac{C_{L1}^2 - C_{L2}^2}{2.83a_l}$	$\Delta C_D$	0.011 ...	
Corrected drag coefficient = $C_{D1} + \Delta C_D$	$C_{D2}$	0.171 ...	
$C_{N1} = C_{L1} \cos \alpha + C_{D1} \sin \alpha$	$C_{N1}$	0.902 ...	
$C_{N2} = C_{L2} \cos \alpha + C_{D2} \sin \alpha$	$C_{N2}$	0.936 ...	
$C_{M_{\bar{c}}/4_2} = (0.25 - CP_{\bar{c}_1})C_{N1} - \frac{1}{2} \Delta C_L$	$C_{M_{\bar{c}}/4_2}$	0.012 ...	
Corrected center of pressure = $0.25 - \frac{C_{M_{\bar{c}}/4_2}}{C_{N2}}$	$CP_{\bar{c}_2}$	0.237 ...	
Normal force = $p\bar{c}X_3C_{N2}$	$F_l$	503 000 lb	240 000 kg
Hydrodynamic torque = $12F_l(\bar{c}CP_{\bar{c}_2} - \frac{X_2 + X_4}{2})$	$Q_{H_l}$	$-15.1 \times 10^6$ in.-lb	$-170 \times 10^4$ N·m
Bearing friction			
$= \mu_3 \frac{d_3}{2} F_l \left( 1 + \frac{0.42X_3 - X_{12}}{X_{10} + X_{11}} \right)$			
$+ \frac{F_l}{2X_8} \left( \frac{0.42X_3 - X_{12}}{X_{10} + X_{11}} \right) [\mu_2 d_2(X_8 + X_9) + \mu_1 d_1 X_9]$	$Q_{F_l}$	$1.4 \times 10^6$ in.-lb	$16 \times 10^4$ N·m
Upper Rudder Section:			
Mean chord = $0.5(X_1 + X_5)$	$C_u$	13.605 ft	5.6 m
Normal force coeff. (see Fig. 248)	$C_{Nu}$	0.75 ...	

$C_{HM}$	0.174 ...	122 000 kg
$F_u$	257 000 lb	$110 \times 10^4$ N·m
$Q_{Hu}$	$9.7 \times 10^6$ in.-lb	
$Q_{Fu}$	$0.4 \times 10^6$ in.-lb	$4.5 \times 10^4$ N·m
$Q_H$	$-5.4 \times 10^6$ in.-lb	$-59 \times 10^4$ N·m
$Q_F$	$1.8 \times 10^6$ in.-lb	$20 \times 10^4$ N·m
$r$	0.018 ...	
$Q_D$	$-3.5 \times 10^6$ in.-lb	$39 \times 10^4$ N·m
$Q_R$	$7.3 \times 10^6$ in.-lb	$8 \times 10^4$ N·m

Hinge moment coeff. (see Fig. 241)  
 Normal force =  $p c_u X_7 C_{Nu}$   
 Hydro. torque =  $12 p c_u^2 X_7 C_{HM}$   
 Bearing friction  

$$= \mu_3 \frac{d_3}{2} F_u \left[ 1 - \frac{0.42 X_7 + X_{12}}{X_{10} + X_{11}} \right]$$
  

$$+ \frac{F_u}{2 X_8} \frac{0.42 X_7 + X_{12}}{X_{10} + X_{11}} [\mu_2 d_2 (X_8 + X_9) + \mu_1 d_1 X_9]$$

Total Rudder:

$$\text{Hydrodynamic torque} = Q_{Hl} + Q_{Hu}$$

$$\text{Bearing friction} = Q_{Fl} + Q_{Fu}$$

$$\text{Single-ram correction} = \frac{\mu_1 d_1 \cos \alpha}{2R}$$

$$\text{Rudder torque displacing}$$

$$= Q_F + Q_H + r|Q_F + Q_H|$$

$$\text{Rudder torque restoring}$$

$$= Q_F - Q_H + r|Q_F - Q_H|$$

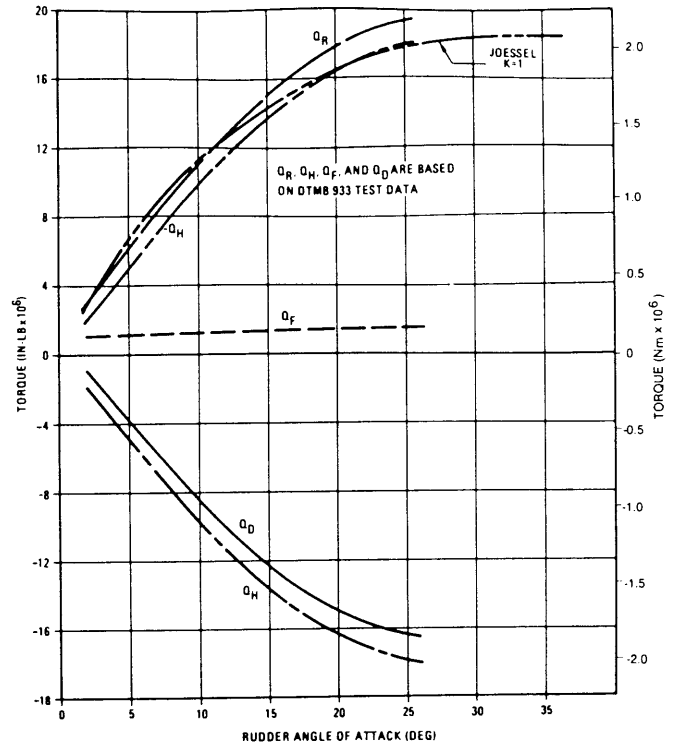


Fig. 243 Astern torque curves for Ship B (See Table 41): ship speed of 4.6 knots (Harrington, 1981)

The test data and analytical procedures available for use in making astern torque predictions are very limited. Accuracy is not as important in making astern torque predictions, because rudder balance is not in consideration. The entire astern torque curve has a negative sense and reaches a maximum numerical value near the maximum (or stall) angle of attack.

For this reason, use of the Joessel method is often advocated; it being further argued that the rudder sections have no aerodynamic shape in the astern direction and thus are, in effect, the same as the flat plate used by Joessel in conducting his experiments.

The velocity of the water flowing onto the rudder is considered to be uniform and equal to the astern speed of the ship. Considerable difficulty may be encountered in establishing an estimate of the astern speed. A rule of thumb that may provide useful results is to assume that the power required astern is twice the power required going ahead at the same speed, and that the power-RPM relationship is the same going ahead or astern. However, this approximation can be considerably in error for some types of ships. In some cases the astern power may be more than three times the ahead power required at the same ship speed.

Horn rudders are divided into two sections for analysis purposes: the upper section abaft the horn, and the lower section below the horn. The results obtained for the two sections are then added.

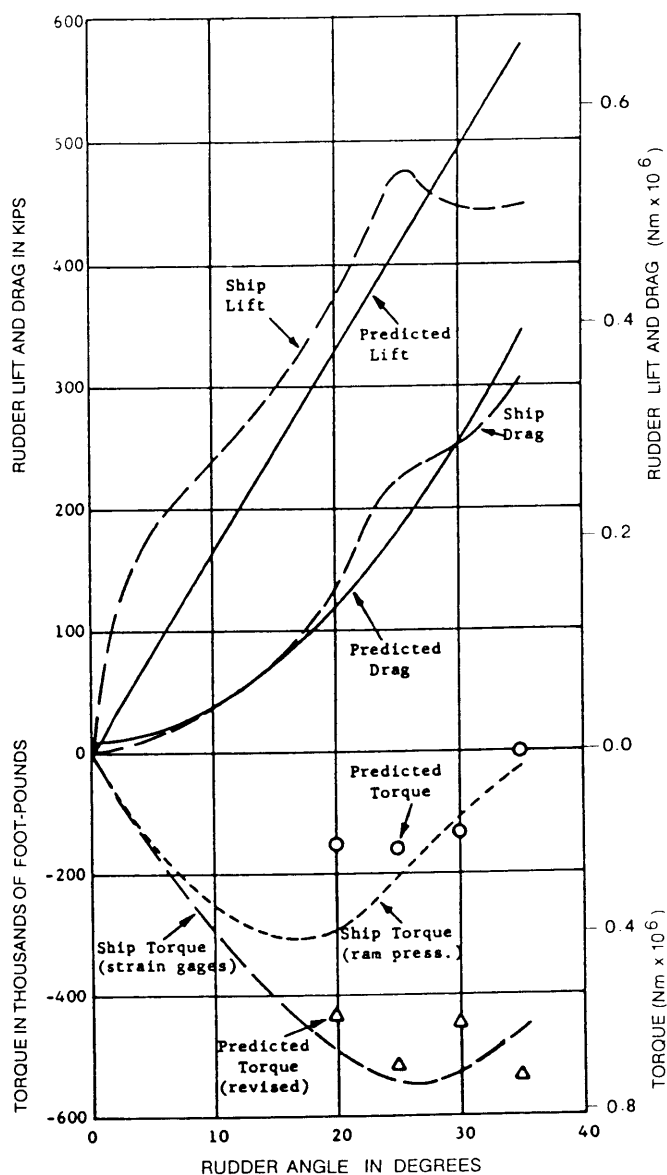


Fig. 244 Comparison of measured and computed rudder loads for USS Norfolk in 30-knot turn

Aspect-ratio considerations must again be dealt with in making astern predictions. In the case of spade rudders such as that for Ship A (see Fig. 232), the effective aspect ratio is taken to be twice the geometric aspect ratio at all rudder angles, for two reasons: One is that at low angles of attack the close proximity of the adjoining hull structure would support that assumption. The other reason is that stall conditions are reached at a relatively low angle of attack in going astern, so that allowances for a reducing aspect ratio

with increasing rudder angles would not be of practical importance. For horn rudders, both the upper and lower rudder sections are considered to have effective aspect ratios equal to twice the geometric aspect ratios at all rudder angles, owing to the sealing effect that each section provides the other and the effect of the horn on the lower section; no allowance is made for the increasing gap between the horn and lower rudder section at larger rudder angles.

Predictions for the frictional components of the astern rudder torque are made as outlined in Tables 40 and 42, for spade and horn rudders, respectively, for the ahead case.

Figure 243 shows plots of astern torque predictions using both the Joessel method and cross-faired Whicker and Fuhlner (1958) test data, such as illustrated by Figs. 233 through 238 for the ahead case. As with the ahead predictions, estimates are made for the rudder being both displaced (frictional torque plus hydrodynamic torque) and restored (frictional torque minus hydrodynamic torque).

The analysis of forces and torque should be done simultaneously with maneuverability analysis to attain dynamically correct results. Asinovsky (1985) has argued that sufficient accuracy can be attained if the calculations cover the range of the angles of attack. Attempts at correlating the rudder angle with the angle of attack of the rudder do not all seem consistent with physical principles. When the value of the maximum angle of attack is being determined, the increase of the stall angle behind the hull and propeller must be taken into account. If the results of model tests of a rudder under these conditions are not available to assist in evaluation, the value of the maximum angle of attack,  $\alpha_{max}$ , can be accepted as equal to 25 deg for aspect ratios in the interval of 1.0 to 2.0. The experimental hydrodynamic characteristics of the rudder obtained under open-water conditions should be extrapolated, and the value of the speed of the incoming wake taken as the ship speed on a straight course.

Hagen (1972) showed that the unsteady lift coefficient and chordwise center-of-pressure location are functionally related to two simple rudder-shape parameters. He proposed using these relationships in estimating rudder loads for ships having generally similar rudder-hull configurations. Comparison of measured rudder loads with values computed by his method is shown in Fig. 244. Agreement is very good except for torque. Comparisons of rudder stock torque for several ships indicated that the estimated center-of-pressure locations are too far aft. Reliable corrections are thought possible by assuming the relationship of center-of-pressure location and the shape parameter  $P$  shown in Fig. 245, but shifting the curves based on measured full-scale rudder torques.

**17.9 Effects of Propulsion Plant and Propellers.** The type of propulsion and propellers has various effects on not only the basic acceleration responsiveness of



the vessel but also on the directional stability characteristics.

The power-to-displacement ratio ( $\text{shp}/\Delta$ ) affects the responsiveness potential of the vessel. The type of power plant, propeller, and control systems can also have very important effects on controllability that should be reviewed during design. A closer examination of the two power plants most commonly used in commercial ships reveals the following:

Astern propulsion characteristics relative to ahead, percent

TYPE OF POWER PLANT	TORQUE	RPM	THRUST
Steam turbine	75	65	32
Diesel	100	100	32

The steam turbine power plant typically provides less than 50 percent thrust astern depending on turbine design. In addition, the reversing time on trials from ahead to astern averages 20 sec. In the case of the diesel power plant which can deliver 100 percent torque astern, the non-controllable-pitch (non-CP) propeller can absorb only about 80 percent of ahead thrust and perhaps even less for modern highly skewed propellers, owing to strength limitations. The reversing time averages 20 sec if the engine is a reversible diesel and ship speed is not high. In the case of the nonreversible diesel, where separate engines drive the propeller through a hydraulic clutch, the reversing time averages 35 to 40 sec.

Neither power plant is currently able to meet all the needs for good slow-speed maneuverability unless coupled with CP propellers. CP propellers, however, have some drawbacks at slow speed because they tend to blanket the rudder and because they have a continuous paddle wheel effect. Tradeoffs must, therefore be accepted. Further, the pitch distribution of the blades is designed for ahead and not astern operation. The steam turbine-powered ship (without an auxiliary astern turbine) is able also to develop and maintain the "slow ahead" speed, but generally delivers less astern power for backing or stopping. The diesel power plant can deliver 80 percent astern thrust, but many diesels have difficulty maintaining the 4 to 5 knots slow-ahead speed (for extended periods) because of the tendency toward carbon buildup in the engine at low engine speed. The nonreversible diesel has the additional disadvantage of the longer reversing time. Attention must be given to the number of possible starts (for reversing the screw) in the case of the reversing diesel. During channel and harbor maneuvering, the pilot may need to stop and start the engine a number of times to achieve controllability.

Crash stopping performance is highly dependent on propeller diameter as well as on astern power. Since propeller diameter is generally already maximized to limiting hull geometry for efficiency purposes, its size does not provide a useful variable in design for astern

operation. Increasing the machinery responsiveness, or time rate of change of shaft rotational speed, is another possible way of improving performance. The CP propeller does improve stopping performance from 6 knots, but only by about 5 percent. That this performance is not greater is attributed to the adverse propeller pitch distribution for astern thrust. At 16 knots, however, the CP propeller realizes the advantages of optimum mean pitch, maximum available ahead shaft power, and quick thrust reversal. Head reach is reduced by about 30 percent. Table 43 summarizes the chief propulsion changes that would reduce stopping head reach for large tankers, and shows the relative gains to expect from each change for approach speeds of 6 and 16 knots. The relative importance is put in perspective by listing the reduced alternative approach speed that would be necessary to achieve the same effect, without any propulsion change. Some of the alternative propulsion systems will have additive effects when combined. One example is the use of a ducted propeller combined with increased steam turbine astern power. Another is the CP propeller for improved high speed stopping, combined with the slow speed diesel for improved slow speed stopping, the latter done by reversing the engine and adjusting the propeller pitch to provide maximum

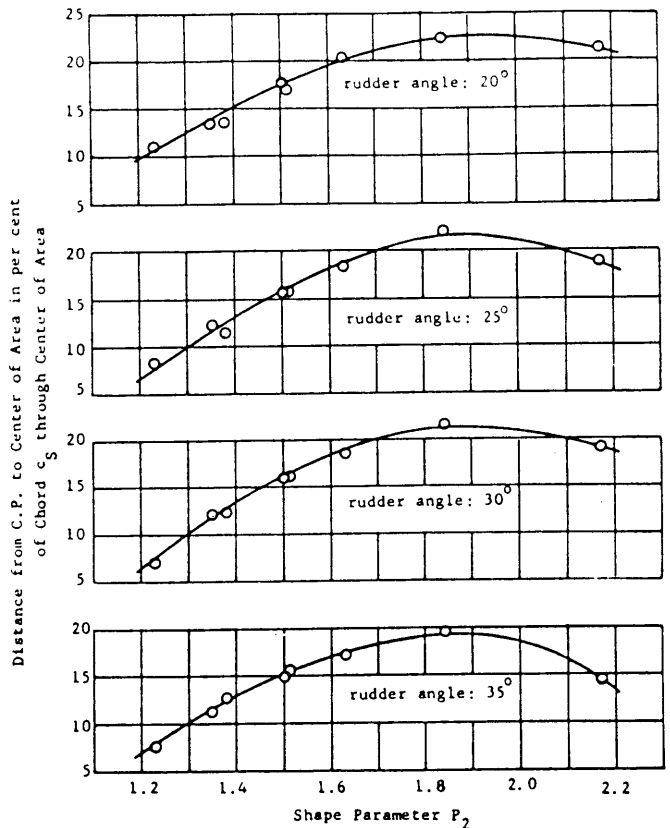


Fig. 245 Center-of-pressure locations from tests on a turning model

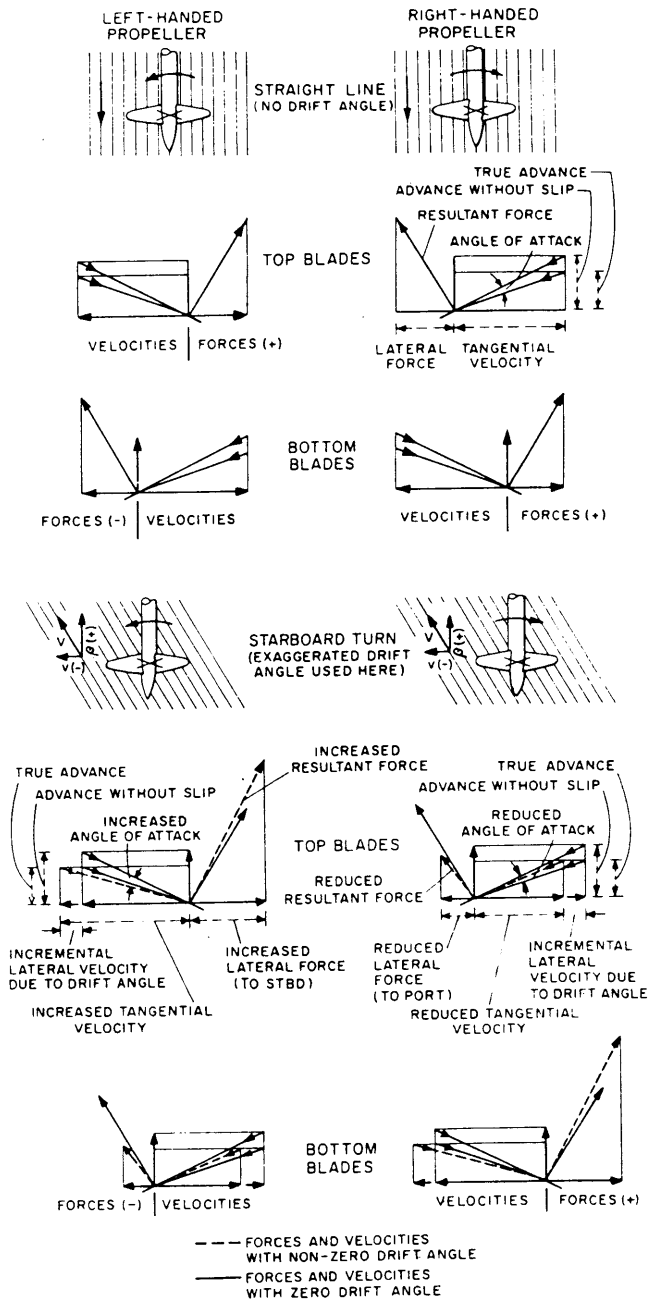
astern thrust. (The practical opportunities for confusion of terminology in direction of pitch, thrust, and engine and shaft rotation are rife.)

The effect of doubling absorbed astern power as shown in Table 43 is based on the 191,000-dwt design and on results obtained within one project. As mentioned previously, other arrangements have been evaluated or their effects derived from results presented by Goddard (1973). This latter work was aimed mainly at stopping from initially high speeds, but the calculated time histories of speed and distance during deceleration permitted adaptation of lower speed segments to the larger 191,000-dwt vessel by correcting for changes in ship mass and power. The other ship is a 100,000-dwt tanker having 28,000 shp available at 85 rpm ahead. This adaptation of results appears to be valid for slow speeds because mass and propulsion thrust are then the predominant factors that affect stopping (straight path assumed). But from a speed of 16 knots, hull resistance also becomes a major factor, and in conjunction with the two other factors, mass and thrust, it renders difficult making the corrections needed to apply the results to other vessels. For this reason the use of results from Goddard (1973) to stopping from 16 knots is only roughly approximate.

Pilothouse control of main propulsion machinery provides for rapid shaft reversal and optimum buildup of astern power. It also avoids the possibility of unnecessary time delay while the engine room watch answers unexpected emergency engine orders. The effects of varying the engine acceleration response time were shown and discussed in Section 10.6 and 10.7. In other studies a prompt response time of 90 sec (to achieve  $\frac{1}{10}$  of ordered engine speed change) has been customary.

Propeller effects deserve special attention. A propeller, or propellers, rotating behind a ship's hull to provide thrust for a constant ahead speed influence both directly and indirectly the sway forces and yawing moments that act on the ship. The direct forces and moments are those produced by the propeller and not by the action of the propeller on the hull and rudder. The indirect influences of the propeller are those that result from the modification of the flow conditions around the stern of a ship induced by the propeller. These changes in flow speed and direction cause changes both in the rudder forces and moments and in the hull forces and moments as compared to the situation in the absence of propellers.

The sway forces and yawing moments induced by the propeller influence the stability and control derivatives of almost all ships. In addition, on ships with an odd number of propellers or with any number of unrotating propellers, the propellers introduce substantial forces and moments even with  $v$ ,  $\delta_R$ , and  $r$  all equal to zero. That is, even though such ships may possess controls-fixed, straight-line stability, they can-



FOUR-BLADED PROPELLER ASSUMED FOR CONVENIENCE. EFFECT OF DRIFT ON HORIZONTAL BLADES IS NEGLIGIBLE, SO ONLY TOP AND BOTTOM BLADES ARE CONSIDERED HERE

Fig. 246 Effect of drift angle on propeller forces

not sail a straight course with the rudder angle held at zero. In order to sail a straight course, such ships must carry a small fixed rudder angle,  $\delta_1$ , and a small drift angle,  $\beta_1 \propto v$ . Angles  $\delta$ , and  $\beta$ , are the so-called neutral angles introduced in Section 4.3.

The most important direct influence of the propeller on stability and turning arises from the fact that when

a ship is turning, the propeller is subjected to a horizontal inflow velocity that is not parallel to the plane of symmetry of the ship (see also Section 17.3). Assumed initially is that the propellers are exposed to the full geometric drift angle at the propeller location. This geometric drift angle corresponds to the angle  $\beta_R + \epsilon$  shown in Fig. 245, measured at the longitudinal position of the propeller. The straightening influence of the hull on the horizontal inflow velocity to the propeller which corresponds roughly to the angle  $\epsilon$  in Fig. 245 can be substantial. This influence is discussed later in this section.

The effect of an inflow angle on a rotating propeller is diagramed in Fig. 246 (taken from Davidson (1945)). In the case of a single, right-handed propeller, the two diagrams in the lower right-hand corner show that a positive inflow velocity angle at the propeller (negative  $v$ ), corresponding to the geometric drift angle at the propeller for a ship turning to starboard, results in the top blades developing a small lateral force directed to port (negative  $Y$ ) and in the bottom blades developing a much larger lateral force directed to starboard (positive  $Y$ ). Thus, a substantial net  $Y$ -force to starboard results. Similarly, a left-handed propeller would also develop a substantial net force to starboard, although the top blades rather than the bottom blades would be responsible for the direction of the net force. Thus, regardless of the direction of rotation of the propeller or of how many propellers there are, they develop a

lateral force to starboard in a starboard turn and to port in a port turn, provided they are subjected at least partially to the geometric drift angles associated with those turns. Since a ship's propellers are aft, this lateral force introduces a moment acting on the ship's hull tending to reduce the magnitude of the drift angle of the ship. That is, the direct contribution of the propeller to the  $N_v$ -derivative of the ship is positive and stabilizing.

From the preceding, and recollecting that a positive rotation  $r$  of the ship introduces a negative  $y$  at the propeller location, one may conclude that the direct effects of a rotating propeller, subjected to a horizontal inflow velocity angle, on the principal hydrodynamic derivatives of a ship are as follows:

$Y_v$ —increase negative magnitude  
 $N_v$ —decrease negative magnitude  
 $Y_r$ —increase positive magnitude  
 $N_r$ —increase negative magnitude

Since these effects are identical to those for a fixed fin abaft the midlength of a ship, the effects of a rotating propeller subjected to a horizontal inflow velocity angle on stability and turning are identical to those of a fixed fin aft, that is, favorable to stability and unfavorable to turning.

However, the straightening influence of the hull ameliorates the preceding effect considerably if the bottom as well as the top of the propeller disk is located

Table 43—Effect of Possible Propulsion Changes of Large Tankers on Emergency Stopping

Propulsion arrangement	Percent Reduction of headreach	Percent Reduction of approach speed for equal effect (alternative)	Reduced approach speed for equal effect, knots
Approach speed, 6 knots			
Base-case steam turbine	...	...	6.0
Double astern power	20–25	11	5.3
Double astern power with increased propeller diameter	roughly 30	15	5.1
Controllable-pitch propeller	20	10	5.4
Slow-speed diesel	about 20	10	5.4
Ducted propeller	15–20	9	5.5
Approach speed 16 knots			
Controllable-pitch propeller	about 30	25	12
Base-case steam turbine	...	...	16
Double astern power	about 20	18–20	13
Double astern power with increased propeller diameter	roughly 25	20	12.8
Ducted propeller	about 5	5–7	15
Slow-speed diesel	about 20 increase	n.a.	n.a.



pellers, the detrimental influence of the geometric drift angle at the propellers on turning was considerably alleviated by the cruiser hull but not by the destroyer hull.

This direct influence of the propeller on stability and turning is important principally for certain military ships. The other direct influences of the propeller which primarily affect the magnitude of the neutral angles,  $\delta_1$  and  $\beta_1$ , are important principally on single-screw ships since most multiple-screw ships have opposite-rotating propellers. The wake field of a single-screw ship has an upward component throughout the propeller disk. As a result, a blade in the three o'clock position (seen from aft) of a right-handed propeller develops a larger thrust than does a blade in the nine o'clock position. Therefore, the center of thrust of a propeller in this flow field is not at the shaft center but is displaced to starboard. This direct influence of the propeller tends to cause the ship to turn to port.

Another feature of the flow field of a single-screw ship is the high wake velocity near the twelve o'clock position on the propeller disk in contrast to the lesser velocity near the six o'clock position. By analogy with Fig. 246, this velocity difference causes a blade of a right-handed propeller to receive a large lateral reaction force to port in the twelve o'clock position, while a blade in the six o'clock position receives a much smaller reaction force to starboard. This force difference results in a net reaction force to port which tends to cause the ship to turn to starboard. Thus, the two direct influences of the propeller discussed in this and in the preceding paragraph produce opposing yawing moments on a single-screw ship. Shiba (1960) has shown that the yawing moment induced by the difference in wake between the top and bottom of the propeller disk is much the stronger of the two effects and that free-running models of single-screw ships with right-handed propellers and with rudder removed turn strongly to starboard. However, as shown later in this section, this tendency is more than offset by other factors when the rudder is in place.

The proximity of the propeller to the free surface with the concomitant possibility of aeration or the actual emergence of the propeller also causes the propeller to produce lateral forces and yawing moments when  $v$ ,  $r$ , and  $\delta_R$  all equal zero in addition to those described in the preceding. Most of these effects are of particular importance in the starting, stopping, and backing of ships and are discussed in Section 10. Consideration in this section is limited to the constant-speed-ahead situation.

The net direct effect of a right-handed propeller in applying a starboard turning moment to a single-screw ship is opposed by two indirect effects of the propeller, one on the rudder and the other on the hull. The latter effect is called the "Hovgaard effect" by Saunders (1957, Section 33.17), and arises from the stronger negative pressure field around the starboard side of the

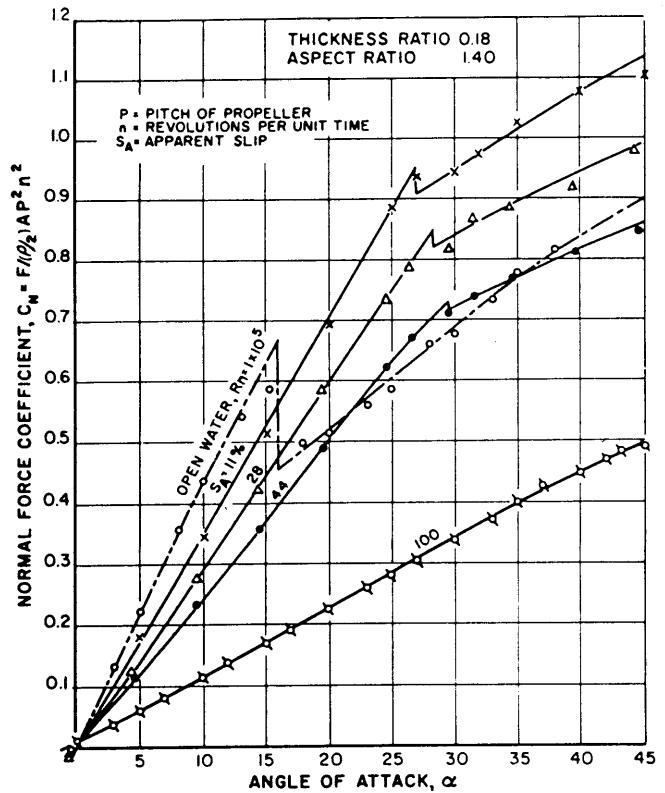


Fig. 248 Results of open-water testing of three rudders of differing aspect ratios

hull developed by a right-handed propeller compared to the port side. This difference in pressure is also caused by the upward component of the flow into the propeller disk resulting in larger angles of attack on the propeller blades in the three o'clock position compared to the nine o'clock position. The difference in pressure at the stern of the ship results in a net force to starboard at the stern which produces a port yawing moment. Shiba's experiments, however, with free-running models with their rudders removed, mentioned previously, tend to discount the strength of the Hovgaard effect.

Of greater importance, one of the indirect influences of a right-handed propeller on a rudder in its race causes a strong port yawing moment to be applied to the ship. In Saunders' words, "The greater tangential component of the velocity (induced by the propeller) in the upper part of the outflow jet, because of the increased wake and increased thrust of the propeller blades in that region, produces a greater (lateral) force acting to starboard when the rotating outflow jet impinges obliquely on the upper part of the rudder." This lateral force acting to starboard at the stern applies a port yawing moment to the ship.

The net effect of all the preceding direct and indirect influences of a single propeller rotating to produce thrust for uniform straight-ahead motion, on all single-

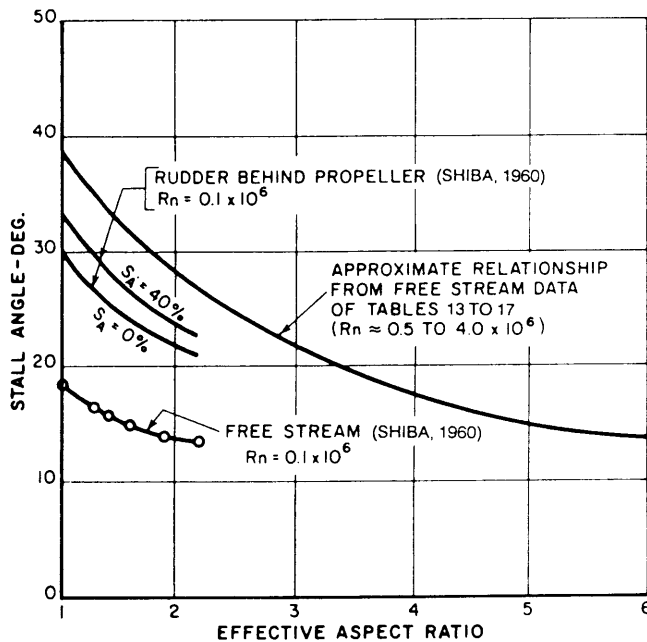


Fig. 249 Stall angle as a function of aspect ratio for rudders behind propellers as well as in free stream

screw merchant ships, is to tend to turn the ship to port if the propeller is right-handed and to starboard if the propeller is left-handed.

The neutral angles  $\delta_1$  and  $\beta_1$  needed to maintain a straight course, that is,  $r = 0$ , under the action of all the preceding direct and indirect effects of asymmetry arising from single-propeller rotation may be determined from results of captive model tests such as those described in Section 8.3. The following equations apply:

$$\begin{aligned} -Y_v v_1 - Y_\delta \delta_1 &= Y^* \\ -N_v v_1 - N_\delta \delta_1 &= N^* \end{aligned} \quad (175)$$

where  $Y^*$  = net sway force measured in a captive model test with the model restrained to move in a straight line, with  $\delta_R$  and  $v = 0$ , and with propeller operating at ship propulsion point; and

$N^*$  = corresponding net yawing moment

Some of the components of  $Y^*$  and  $N^*$  may be isolated by conducting captive model tests with (a) propeller and rudder removed, (b) propeller rotating and rudder removed, and (c) propeller rotating and rudder set at zero. However, these tests are not necessary to determine  $\delta_1$  and  $v_1$ .

For a submerged submarine, the neutral angles needed to maintain horizontal flight are highly speed-dependent, whereas the values of  $v_1$  and  $\delta_1$  determined from Equation (175) are not highly speed-dependent. The speed-dependency in the vertical plane arises because the moment equation in the vertical plane must

include the longitudinal hydrostatic trimming moment  $M_\theta \theta$  which in coefficient form is highly speed-dependent. This relationship is more thoroughly discussed by Arentzen and Mandel (1960).

The indirect effect of a rotating propeller on a rudder located in its race has an even more important influence on stability and turning than on the moments due to asymmetry. Fig. 248 shows an example of results for three rudders of differing aspect ratios tested in open water as well as in the race of a propeller with their leading edges a distance of 0.2 propeller diameter abaft the propeller. As noted in the figure the normal force coefficients are nondimensionalized in the case of the rudder operating in the propeller race on the basis of  $P_n$ , the theoretical velocity existing immediately abaft the propeller. Fig. 248 displays two important influences of the propeller on the rudder:

(a) Rudder stall point is delayed until larger angles of attack are reached than in open water. This effect is displayed in Fig. 249 which shows stall angle as a function of aspect ratio. The very low stall angle of the freestream data of Shiba (1960) is due to the low Reynolds number of the experiments.

(b) The effect of stall is much less pronounced than in open water. Rather than exhibiting an abrupt decrease in normal force at stall, the rudder in the propeller race shows only a slight discontinuity in the slope of the normal force curve at stall.

Using a lift identity method, similar in principle to the thrust identity method described in Chapter VII, Vol. II to determine wake velocities in self-propulsion tests, the data reported by Shiba (1960) including those shown in Fig. 248 have been used to compute the velocity increase, averaged over the entire area of the rudder, as a function of the propeller slip ratio. These results, in the form of the velocity ratio  $V_r/V$ , are shown in Fig. 250. Within the band of values shown,  $V_r/V$  is independent of rudder aspect ratio, rudder area, and rudder angle of attack. For all the variations of these three quantities, 100 percent of the area of all the rudders was located entirely within the propeller race.

The velocity increases due to propeller slip shown in Fig. 250 are of great significance to the stability and turning of ships because the magnitude of both  $(Y')_f$  and  $Y'_\delta$  increases directly with the velocity increase as do  $(Y'_v)_f$  and  $Y'_\delta$  which are defined in terms of the ship's velocity and not of the velocity of flow past the rudder. The expressions for  $(Y'_v)_f$  and  $Y'_\delta$  [(58) and 63a] will be modified as follows if a portion or all of the rudder is located in the propeller race:

$$\begin{aligned} Y'_\delta &= -(Y'_v)_f \\ &= A'_R \frac{\partial C_L}{\partial \alpha} \left\{ 1 + p \left[ \left( \frac{V_r}{V} \right)^2 - 1 \right] \right\} \end{aligned} \quad (176)$$

where  $p$  is the fraction of rudder area located within the propeller race and  $V_r/V$  may be determined from Fig. 250.

The expression within the brackets of Equation (176) is plotted in the insert of Fig. 250 as a function of the fraction,  $p$ , and the apparent propeller slip ratio,  $S_A$ .

Following the Figure and Equation (176) the effect of the propeller on the rudder influences the ship's derivatives as follows:

- (a) Increases negative magnitude of  $Y'_v$ ,  $N'_v$ , and  $N'_\delta$ .
- (b) Increases positive magnitude of  $Y'_r$  and  $Y'_\delta$ .
- (c) Decreases negative magnitude of  $N'_v$ .

The effect of the propeller race on  $N_\delta$  has been measured directly and reported by Eda and Crane (1965). Results are shown in Fig. 128, with the stern configuration shown in Fig. 54. Also shown in Fig. 128 are the slip ratios corresponding to the model and ship self-propulsion points for the two models. The figure shows the magnitude of the scale effect in free-running model tests where the propeller must operate at the model self-propulsion point rather than at the ship propulsion point. Since the same propeller was used on both models, and since the ( $C_B = 0.80$ ) model has much the larger drag of the two, the slip ratio corresponding to its self-propulsion point is much larger than that of the ( $C_B = 0.60$ ) model. This difference

accounts for the larger rudder force and moment derivatives shown for the ( $C_B = 0.60$ ) model. This difference accounts for the large rudder force and moment derivatives shown for the ( $C_B = 0.80$ ) model.

The propeller race also exerts an important influence on the straightening effect,  $\epsilon$ , for rudders located in the race. Data presented by Surber (1955) show that for a cruiser model with skeg and propeller locations as shown in Fig. 247,  $\epsilon$  averages about 50 percent of the geometric drift angle at a distance  $0.0125L$  abaft the inboard propeller disks. Interestingly,  $\epsilon$  is reported to be essentially zero on the centerline of the ship, indicating that a single centerline rudder derives little benefit from straightening effect on a twin- or quadruple-screw ship. However, this result conflicts with that of Eskigian (1956), who reported an  $\epsilon$ -value of 55 percent of the geometric drift angle on the centerline of a twin-screw model with a skeg extending to Station 17. The results did indicate, however, that a centerline rudder on a multiple-screw ship with no centerline propeller does not derive any change in speed of flow as a result of the propeller race.

A secondary indirect influence of the propeller is on the hull stability derivatives. An isolated experimental

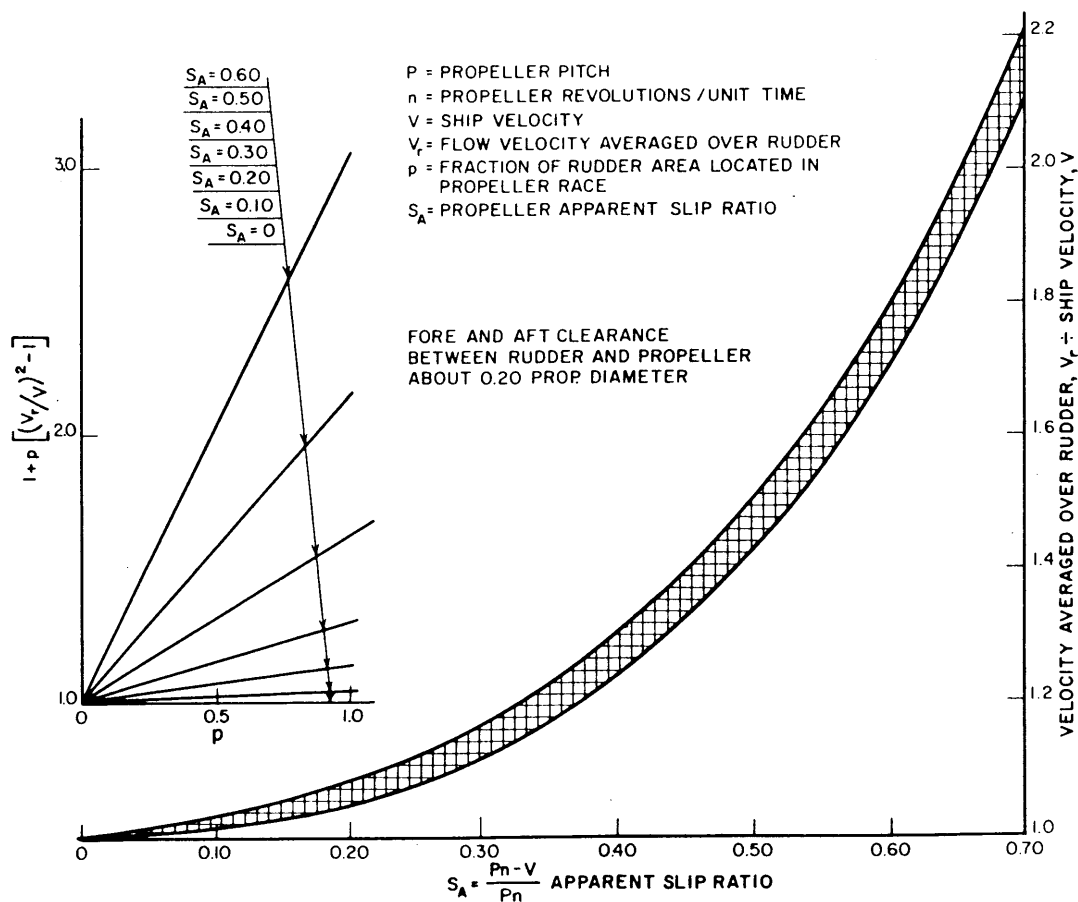


Fig. 250 Effect of propeller slip on velocity over rudder in propeller race (Shiba, 1960)

result shown in Fig. 9 of Eda and Crane (1965) shows that this influence is likely to:

- (a) Increase negative magnitude of  $Y'_{\nu}$ .
- (b) Slightly increase positive magnitude of  $Y'_{\nu}$ .
- (c) Decrease negative magnitude of  $N'_{\nu}$ .
- (d) Increase negative magnitude of  $N'_{\nu}$ .

These are the same effects as those of a fixed fin aft.

To summarize, the following direct and indirect effects of a rotating propeller are all favorable to stability but unfavorable to turning:

- (a) The direct influence of a rotating propeller due to a horizontal inflow angle,
- (b) the indirect effect of a rotating propeller on a rudder in its race treated as a fixed fin, and
- (c) the indirect effect of a rotating propeller on the hull derivatives.

In contrast, the indirect effect of a propeller on a rudder treated as a movable control surface is favorable to turning.

**17.10 Use of Other Control Devices.** While the hull-propeller-rudder design approach provides the basic parameters available to the designer through which to develop an adequately maneuverable ship, additional control devices and operational techniques may be applied to complement and provide a greater degree of maneuverability than would otherwise be attainable. Use of additional control devices may become a necessity in meeting special purposes that require control in a seaway at virtually zero ship speed. Cable layers, drill rigs, and oceanographic research ships, for instance, often face this need. Other control devices are frequently installed because they provide maneuverability at slow speeds, especially in restricted harbor situations, where the vessel's hull-propeller-rudder capabilities are not as effective as at higher speeds in deeper water. The other devices can facilitate mooring and getting underway without use of tugs, and they can provide good maneuverability astern and good maneuverability under unfavorable harbor and wind conditions. The types and characteristics of a number of these devices, and general information on their limitations and applications, are briefly outlined in this section, comprehensively by Wilson, et al (1979).

In reviewing devices and operational techniques that are available to improve maneuvering and stopping ability, Card, et al (1979) made an extensive listing as shown in Table 44. They then subjectively rated each with regard to improvement in maneuverability, cost and effect on vessel design, practicality and reliability, and experience with the installation on large tankers.

Under rudder augmentation, a number of the items listed in the table have already been covered in this chapter in some detail. Rudder area, angle, rate, location, and number are basic to a design. The advantages in using balanced rudders with fixed structure have also been addressed. Special rudder designs, however, provide higher efficiency of operations through hydrodynamic design or use of flow controlling plates.

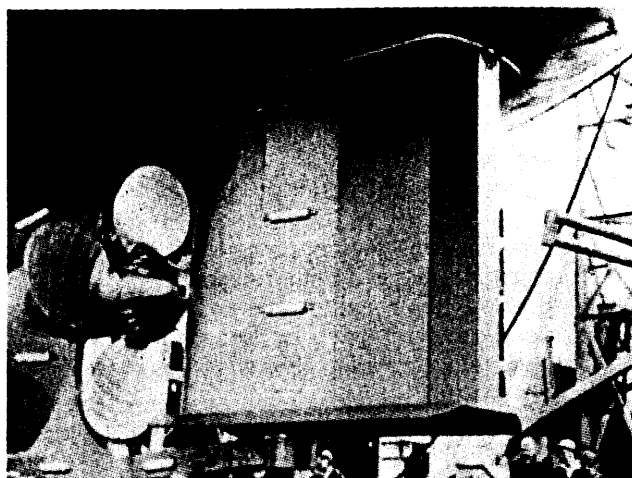


Fig. 251 Schilling Rudder shown on a 1000 DWT coastal tanker

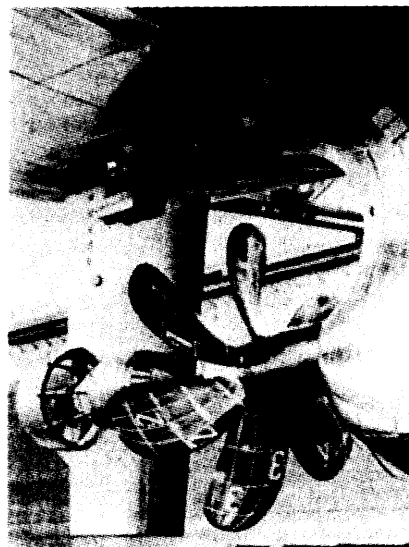


Fig. 252 The Pleuger active rudder in tandem abaft the main propeller

The Schilling rudder shown in Fig. 251 is a good example of use of large horizontal plates to reduce flow losses and a special highly effective section with flared trailing edge. Installations on smaller vessels have shown high effectiveness.

An *active rudder* as shown in Fig. 252 has a submerged motor and propeller as an integral part of the trailing edge of a standard rudder. It is particularly useful at low speeds where flow across the rudder from the main propeller is low.

The *shutter rudder* consists of three or more rudders which are mechanically linked as shown in Fig. 253. Although the maximum amount of the propeller race is utilized, this arrangement is most suitable for tugs and work boats fitted with ducted propellers. For



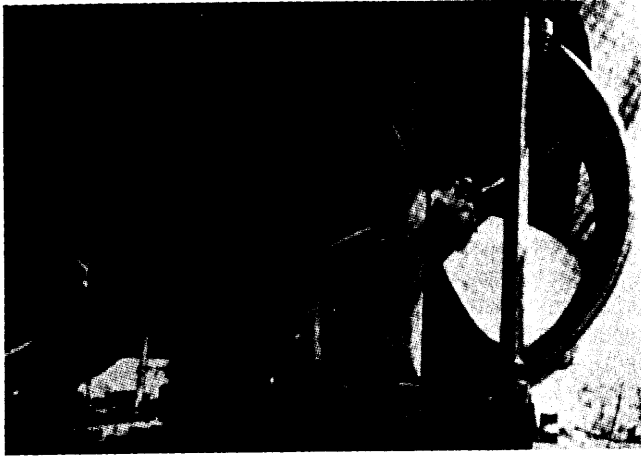


Fig. 253 A Shutter Rudder installation on the 40-m tug *Salimi*



Fig. 254 Rotating cylinder rudder fitted to a radio-controlled maneuvering model

related reasons flanking rudders are best suited to restricted-draft craft with Kort Nozzles.

The *rotating cylinder rudder* incorporates a vertical rotatable cylinder on the forward edge of the rudder or before a flap as shown in Fig. 254. When the cylinder is rotated, circulation is generated and a lift force produced which is normal to the stream and the cylinder. The lift coefficient is a function primarily of the ratio  $u/V$ , where  $u$  is the peripheral speed of the cylinder. The lift also depends on the aspect ratio of the cylinder and on its end conditions. Fig. 255, after Steele and Harding (1970), shows the lift coefficient rising steeply until the speed ratio approximates 3. Further increases in speed ratio have been found to cause little rise in the coefficient. As shown by the

curves and their labels, Betz obtained twice the lift (comparing favorably against the curve of much higher aspect ratio from Reid) by simply adding end plates.

As suggested by the nearly linear parts of the curves on Fig. 255, the lift coefficient can be expressed approximately as:

$$C_L = Mu/V - N \quad (177)$$

where  $M$  and  $N$  are constants. Thus the lift,

$$\begin{aligned} L &= \frac{1}{2} \rho A V^2 (Mu/V - N) \\ &= \frac{1}{2} \rho A (MuV - NV^2) \end{aligned} \quad (178)$$

If, at the speeds of interest, lift is obtained, then  $MuV > NV^2$ . As the speed is reduced the numerical value of  $V^2$  will decrease faster than that of  $V$ . Thus,

at low speed  $MuV \gg NV^2$  and  $L$

$$= \frac{1}{2} \rho A MuV \text{ approximately.}$$

This last equation shows the advantage in using the rotating cylinder at low ship speeds. Rather than falling off as the square of forward speed, the side force of the rotating cylinder falls off only as the forward speed.

Located along a leading edge of the rudder, the rotating cylinder can be used to control the boundary layer, energizing it with fluid of increased velocity. Rotated slowly, the cylinder permits larger angles of incidence before stall. The control available is a function of the rotational speed of the cylinder.

The so-called *Kitchen* or *clam shell rudders* are similar to the thrust reversing devices on jet aircraft, where clam shell deflectors are moved to turn astern thrust from the jets (corresponding to propeller race on ships) to other directions. Proposals to use this device or the rotating-cylinder rudder introduce addi-

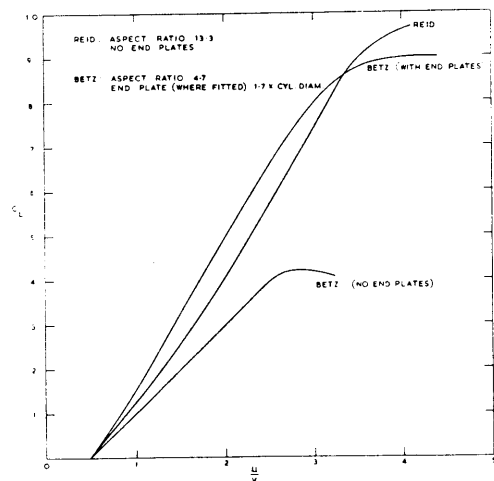


Fig. 255 Lift on rotating cylinders

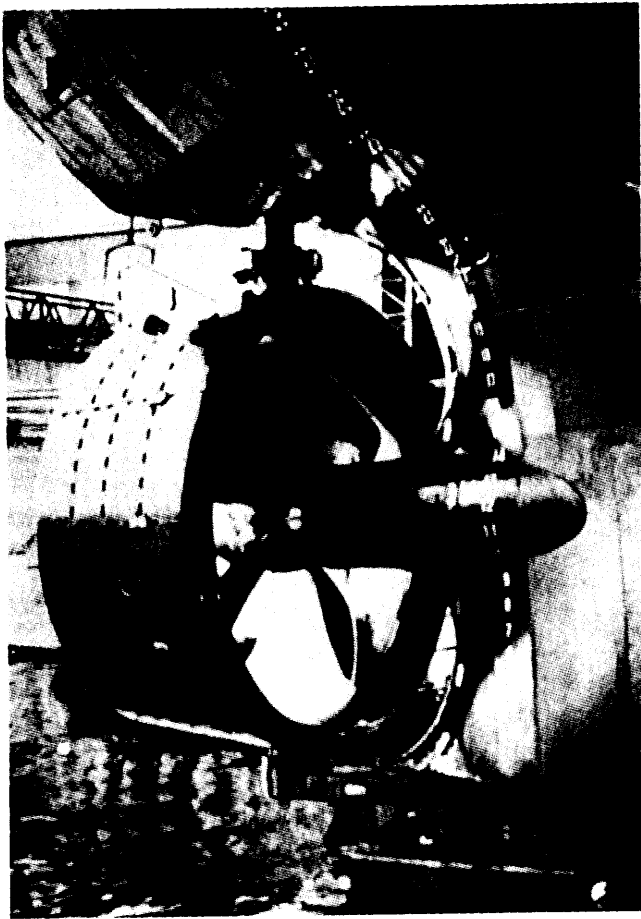


Fig. 256 Bulk carrier *Ralph Misener* (25,000 DWT) with steerable Kort nozzle

tional mechanical problems that must be addressed during design of the ship.

The basics of propulsion augmentation and rudder augmentation have been covered in the previous section. These approaches increase maneuverability by increasing the flow across the rudder. The steerable nozzle is a special topic that has received detailed attention by Asinovsky (1985) and others. Fig. 256 shows a steerable Kort nozzle installed on a 25,000-DWT Great Lakes bulk carrier.

The Voith Schneider vertical-axis propeller system is a special form of propulsion that provides extraordinary maneuverability for a vessel. Fig. 257 shows a typical unit. By controlling the angle of attack of the blades as they orbit, thrust can be applied in any direction. These units have proved very effective on tugs, workboats, and ferries.

The effect of drag augmentation devices has been covered in Section 10.10, and operational techniques and methods as listed in Table 44 are available to the mariner for use as needed, provided, of course, that the necessary equipment is available and in working condition.

Aside from rudders, thrusting devices are the most popular control device. The tunnel thruster (Fig. 258) is most common and consists of a transverse duct with an impeller in the middle. The power offered by manufacturers in standard sizes ranges from 10 to several thousand hp.

The thrust required for a given application of a maneuvering device depends on the particular operating needs. For oceanographic or offshore drilling and mining vessels and other special-purpose craft, the thrust requirement must be met if the mission is to succeed. Accordingly, within limits, the initial cost, added resistance at ahead speeds, and other factors are of secondary importance to performance. The influence of economic factors is much greater, however, in considering the use of maneuvering devices on merchant ships. An installation that would always eliminate the need for tugs or always meet maneuvering needs in the face of very high wind and current forces would probably be prohibitively expensive and space consuming. Therefore, maneuvering devices for merchant vessels are usually sized to achieve the greatest increase in maneuverability consistent with limits of economic, space, and resistance considerations as prescribed by the ship owner.

Gurovich et al. (1967) suggest that statistical data be used in the first stages of design to estimate thruster power needed. To determine needed thrust analytically, they recommend using computations for solving specific problems when maneuvering is to be assured. The authors examine the following problems and provide computational approaches for solving them:

- (a) Determining thrust necessary to clear the vessel from a wall, such as a quay face, with wind pressing the vessel toward it,
- (b) determining the angular velocity of a turn in place at a given thrust of the thruster,

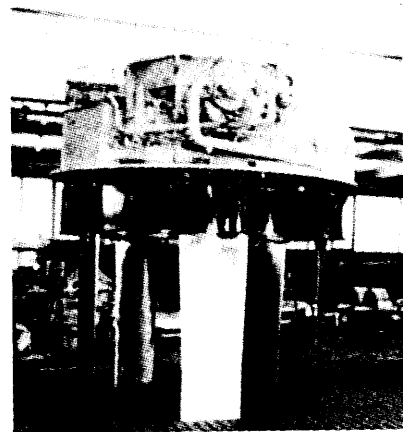


Fig. 257 A Voith-Schneider unit with blades 1.6m long

**Table 44—Devices and Operational Techniques to Improve the Maneuvering and Stopping Ability of Vessels**

Rudder Augmentation	Propulsion/Rudder Augmentation
Increased Rudder Area	Steerable (Kort) Nozzle
Increased Rudder Angle	Voith Schneider (Vertical Axis) Steerable Propeller
Increased Rudder Rate	Thrusting Devices
Twin Rudders	Fixed (bow, stern) Thruster
Schilling Rudder	Trainable Thruster
Balanced Rudder with Fixed Structure (BRWFS)	Jet Engine Thruster
Steerable BRWFS	Rockets
Active Rudder	Drag Augmentation Devices
Shutter Rudder	Stern Anchor
Rotating Cylinder Rudder	Stern Flap (abaft screw)
Rotating Cylinder with Flap	Twin (splayed) Rudders
Kitchen Rudder	Brake Flaps
Clam Shell Rudder	Bow Opening
Jet Flap (Fluidic)	Parachute
Bow Rudder	
Propulsion Augmentation	
Twin Screw (and Rudder)	
Increased Astern Power	
Controllable Pitch Propeller	
Contra-Rotating Propeller	
Operational Techniques and Methods	
Slower Approach Speed	
Hard-over Turn	
Propeller Kick	
Rudder Cycling	
Tug Assistance:	
Rudder Tug	
Braking Tug	
Alongside Tug	
Traditional Tug	

(Card, et al 1979)

(c) evaluating the possibility of mooring or moving broadside against the wind, and

(d) Determining the thrust necessary to keep a vessel moving on steady heading at low speed under the influence of wind.

Unfortunately, full-scale trial results are available for only a few maneuvering-device installations. Most of the available data on the thrust-producing capabilities of these devices are based on design estimates. Further, these are estimates of the thrust delivered at the propeller and do not take other important hydrodynamic effects into consideration. Nevertheless, the published data are of value. Fig. 259 shows a plot of thrust to power ratio versus power loading or shaft horsepower to swept area ratio. In plots such as these,

the different types of devices can be segregated and a line of proportionality more readily defined for each. The factor of proportionality is the nondimensional parameter

$$"C" = 2(T/P)^{3/2} \sqrt{P/\rho A} \quad (179)$$

where  $T$  is thrust

$P$  is power

$A$  is disk area of the propeller

$\rho$  is the mass density of water

The thruster devices discussed here are essentially dead-pull propulsion devices, but this is not to say that they are of no value when the ship is moving. Although their value changes and usually decreases dramatically as speed increases, maneuvering propulsion devices have some effect at ahead and astern speeds, particularly those ship speeds at which the rudder is least effective. A tunnel thruster at the bow is generally effective at ahead ship speeds as high as about 4 knots. At higher ship speeds, the flow around the hull distorts the thruster outflow, and it becomes practically ineffective (Chislett and Bjorheden, 1966). To indicate such changes in the bow thruster effectiveness with ship speed, turning trajectories in Fig. 260 were computed by Eda for a 250,000-dwt tanker with bow thruster, using captive model test data.

A tunnel thruster at the stern, however, is in boundary layer flow, and is effective at higher ship speeds. For a 250-m (806-ft) Great Lakes ore carrier, the stern tunnel thruster was reported effective at ship speeds up to 10 miles per hour (9.7 knots) by Nielson and Kendall (1974).

Various limitations or other considerations concern the application of maneuvering devices. A few of the more important ones are mentioned here. Maneuvering devices should be located to achieve the greatest possible turning moment. This concern implies a position well forward or aft, but space and hydrodynamic considerations often necessitate locating the device closer to the center of gravity. A bow thruster usually has a slightly greater lever arm to the ship center of grav-

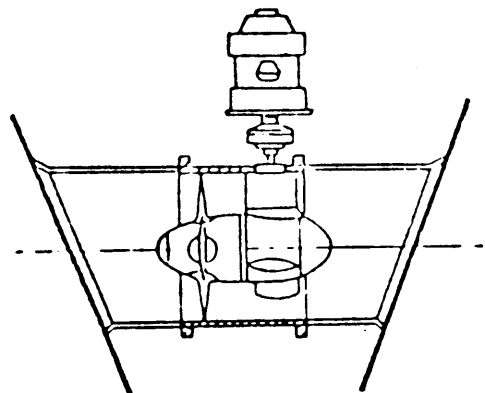


Fig. 258 Bow thruster

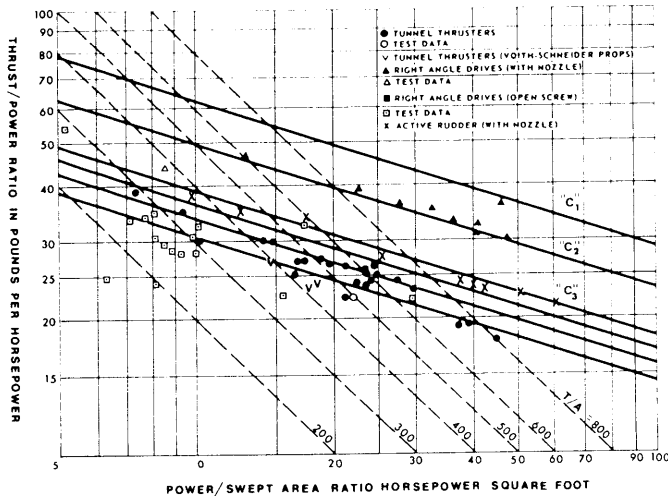


Fig. 259 Thrust/Power Ratio versus Power/Swept Area Ratio for Various Special Maneuvering Devices (Aucher, 1972)

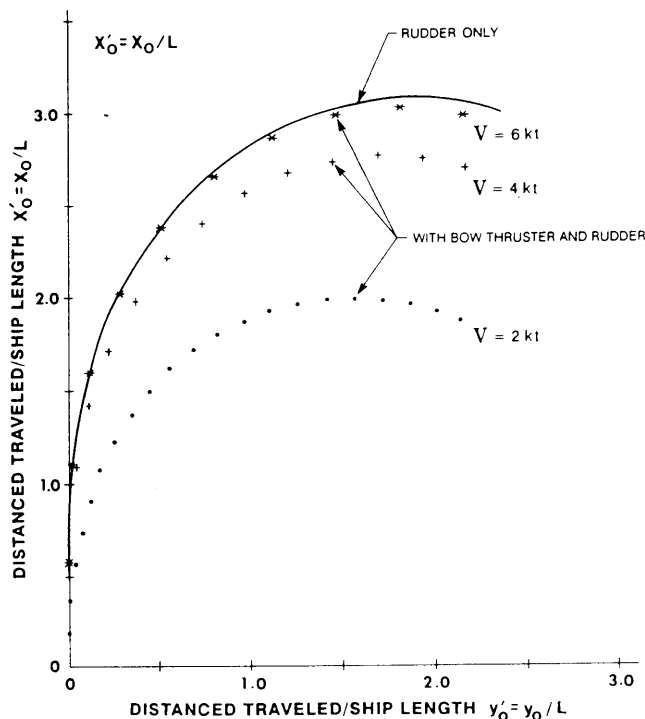


Fig. 260 Enter-a-turn trajectory

ity than has a stern thruster. This difference is significant for moments at virtually zero ship speed. If, however, the thruster is intended to operate at a few knots of ship speed, advantages may begin to favor a stern location. This shift is pointed out by Crane (1973). Essentially, hull forces come into action as a result of the low forward speed and the hull drift angle. For the stern thruster these forces combine favorably,

whereas for the bow thruster there is some cancellation of effectiveness.

Maneuvering devices require a degree of submergence to operate effectively. Often this requirement necessitates the use of two units side by side to avoid excessive vertical dimensions, as is the case with some oil tankers and passenger ships. For ships with wide ranges of draft variation, the minimum submergence is an important consideration. The consensus is that the centerline of the maneuvering device propeller should be at least one diameter below the waterline and that it should be as low in the hull as space permits.

For merchant vessels and certain other types, draft limitations may eliminate from consideration devices that extend below the hull baseline.

The added resistance that may result from installation of a maneuvering device will depend on the type and location of the device. For tunnel thrusters, model test experiments indicate that a carefully designed tunnel entrance will keep the added resistance to roughly 1 to 5 percent of the effective propulsion power, depending on the size of the ship. Actual experience with full-scale ships on the Great Lakes has revealed that in most instances, the speed loss due to the added resistance of the tunnel openings is small and difficult to determine precisely, because of the presence of other influencing factors.

Very little information is available on the added resistance characteristics of other types of maneuvering devices such as active rudders and fixed right-angle drives. Presumably, a drag coefficient can be assumed and the added resistance estimated.

The selection of maneuvering propulsive devices requires consideration of many technical, operational, and economic factors, some of which have been covered briefly here (see also Hawkins, 1965; English, Rowe, and Bain, 1972; Stuntz and Taylor, 1964; English, 1963; and Taniguchi, 1966). The hydrodynamic features of tunnel thrusters are covered by Beveridge (1972). A total ship performance analysis under thruster control is shown by Wise and English (1975) and by Eda (1975).

## REFERENCES

- Abbott, I.H., and Von Doenhoff, A.E., *Theory of Wing Sections*, Dover Publications, Inc., 1958.
- Abkowitz, M.A., Ashe, G.M., and Fortson, R.M., "International Effects on Ships Operating in Proximity in Deep and Shallow Water," Proceedings of the Eleventh Symposium on Naval Hydrodynamics, ONR Publication, 1970.
- Abkowitz, M.A., "Lectures on Ship Hydrodynamics—Steering and Maneuverability," Hydro-Og Aerodynamisk Laboratorium, Report Hy-5, Lyngby, Denmark, 1964, pp. 113.
- Abkowitz, M.A., "Measurement of Hydrodynamic

Characteristics from Ship Maneuvering Trials by Systems Identification," *SNAME Transactions*, Vol. 88.

Alman, P.R., Bertsche, W.R., Boylston, J.W., Card, J.C., Crane Jr., J.L., Eda, H., Keith, V.F., Landsburg, A.C., McCallum, I.R., Miller, Jr., E.R., and Taplin, A., "Design and Verification for Adequate Ship Maneuverability, etc." *SNAME Transactions*, Vol. 91.

Ames, M.B. and Sears, R.I., "Determination of Control-Surface Characteristics from NACA Plain-Flap and Tab Data," NACA Report 721, National Advisory Committee for Aeronautics, 1940.

Ankudinov, V.R., Miller, E.R., Alman, P.R., Jacobson, B.K. and Conrad, R.E., "Ship Maneuverability Assessment in Ship Design-Simulation Concept," *Proceedings*, International Conference on Ship Maneuverability Prediction and Achievement, RINA, London, April/May 1987.

Aukudinov, V.K., and Jakobson, B.K., "Mathematical Modeling for Naval Ship Handling Simulators," *Proceedings* MARSIM '87 Conference on Marine Simulation, Trondheim, Norway, 1987.

Aranow, P.I., "Maneuvering Response Supplemental Experiments (Collier and Containerships)," National Maritime Research Center, New York, CAORF Technical Report 42-8218-01, 1983.

Arentzen, E.S., and Mandel, P., "Naval Architecture Aspects of Submarine Design." *SNAME Transactions*, Vol. 68.

Asinovsky, V., "Consideration of Maneuverability Characteristics in the Rudder Design Process," *SNAME Los Angeles Section*, March 1985, pp. 43.

Asinovsky, V., "Simplified Approaches for the Evaluation of Maneuverability of Ships," *Naval Engineers Journal*, March 1986.

Asinovsky, V., Landsburg, A.C., and Hagen, G.R., "Ship Maneuverability Analysis Using the Differential Approach," *Proceedings*, International Conference on Ship Maneuverability Prediction and Achievement, RINA London, April/May 1987.

Asinovsky, V., "Review and Analysis of Ship Maneuverability Criteria," *Naval Engineers Journal*, May 1989.

Atkins, D., and Gaffney, M., "Relationship of Ship Size to Transit Performance in a Channel Section Containing Cross Current," Fourth CAORF Symposium, U.S. Maritime Administration, Kings Point, NY, 1980.

Attwood, E.L., Pengelly, H.S., and Sims, A.J., *Theoretical Naval Architecture*, Longmans, Green and Co., London, 1953.

Aucher, M., "Unconventional Maneuvering Devices," The 13th ITTC Proceedings, 1972.

Baker, G.S., "Steering of Ships in Shallow Water and Canals," *Trans. INA*, 1924.

Barr, R.A., Miller, E.R., Ankudinov, V., Lee, F.C. "Technical Basis for Maneuvering Performance Standards," U.S. Coast Guard Report CG-M-8-81, NTIS AD A 114471, Dec. 1981.

Bech, M., "The Reversed Spiral Test as Applied to

Large Ships," *Shipping World and Shipbuilder*, November 1968.

Bertsche, W.R., Smith, M.W., Marino, K.L., Cooper, R.B., "Draft SRA/RA Systems Design Manual, Restricted Waterways," Eclectech Associates, Inc., for U.S. Coast Guard, 1982.

Beveridge, J.L., "Design and Performance of Bow Thrusters," *Marine Technology*, October 1972.

Bhattacharyya, R., *Dynamics of Marine Vehicles*, John Wiley & Sons, New York, 1978, Pg. 408.

Bindel, S.G., "Experiments on Ship Maneuverability in Canals as Carried Out in the Paris Model Basin," First Symposium on Ship Maneuverability, DTRC Report 1461.

Bindel, S.G., "Turning Characteristic Coefficients for a Cargo Ship and Destroyer," First Symposium on Ship Maneuverability, DTRC Report 1461.

Bishop, R., Burcher, R.K., and Price, W.G., "The Determination of Ship Maneuvering Characteristics from Model Tests," *Trans. RINA* 1975.

Bottomley, G.H., "Maneuvering of Single-Screw Ships," Institute of Civil Engineers, 1935.

Bowers, A.A., "Wind Tunnel Investigation of the Characteristics of a Flapped Control Surface Mounted on a Simulated Submarine Hull," University of Maryland Report 259, June 1959.

Boylston, J.W., "Is Port Study Model Testing Really Worthwhile?" *Marine Technology*, January 1974.

Brard, R., "Essais en modele de canal le modeles de Navires autopropulses," Assn. Technique Maritime et Aeronautique, 1950.

Brard, R., "Maneuvering of Ships in Deep Water, Shallow Water and in Canals," *SNAME Transactions*, Vol. 59.

Breslin, J.P., and Landweber, L., "A Manual for Calculation of Inception of Cavitation on Two- and Three-Dimensional Forms," *SNAME Bulletin* 1-21, October 1961.

Brink, A.W., and Stuurman, A.M., "Automatic and Manual Control of the Tripartite Minehunter in the Hover and Trackkeeping Modes—A Preliminary Design Study," *International Shipbuilding Progress*, Vol. 26, No. 300, 1979.

Burcher, R.K., "Developments in Ship Maneuverability," *Trans. RINA*, 1972.

Burcher, R.K., "Studies into the Validity of Quasi Steady Prediction Techniques," *Proceedings*, Vol. 2, International Towing Tank Conference, 1975, pp. 404-407.

Cahill, J.F., "Summary of Section Data on Trailing-Edge High-List Devices," NACA Report 938, National Advisory Committee for Aeronautics, 1949.

Card, J.C., Cojeen, H.P., Spencer, J.S., and Harmon, J.P., "Report to the President on an Evaluation of Devices and Techniques to Improve Maneuvering and Stopping Abilities of Large Tank Vessels," U.S. Coast Guard, Washington, DC, Sept. 1979.

Chase, H.J., and Ad Hoc Panel Members, "Guide to

the Selection of Backing Power," T. and R. Bulletin No. 3-5, SNAME, 1957.

Chislett, M.S., and Bjorheden, O., "Influence of Ship Speed on the Effectiveness of Lateral Thruster Unit," Hydro-Og Aerodynamisk Laboratorium, Lyngby, Denmark, Report Hy-8, 1966.

Chislett, M.S., and Strom-Tejsen, J., "Planar Motion Mechanism Tests and Full Scale Steering Maneuvering Predictions for a *Mariner* Class Vessel," Hydro-Og Aerodynamisk Laboratorium, Report HyA 6, Lyngby, Denmark, April 1965.

Clarke, D., "Considerations of Shiphhandling in Hull Design," *Nautical Institute Conference*, 1977.

Clarke, D., "Assessment of Maneuvering Performance," *Ship Maneuverability Prediction and Achievement*, RINA, London, 1989.

Clarke, D., Gedling, P., and Hine, G., "The Application of Maneuvering Criteria in Hull Design Using Linear Theory," *Trans. RINA*, 1982.

Clarke, D., Patterson, D.R., and Wooderson, R.K., "Maneuvering Trials with the 193,000 Tonne Deadweight Tanker *Esso Bernicia*," *Trans. RINA*, 1973.

Clarke, D., "A Two-Dimensional Strip Method for Surface Ship Hull Derivatives: Comparison of Theory with Experiments on a Segmented Tanker Model," *Journal of Mechanical Engineering Science*, Proceedings of an International Symposium on Direction Stability and Control of Bodies Moving in Water, Vol. 14, No. 7, 1972.

Clarke, D. and Wellman, F., "The Stopping of Large Tankers and Feasibility of Using Auxiliary Braking Devices," *Trans. RINA*, Vol. 113, 1971.

"Code of Recommended Standards for the Prevention of Pollution in Terminal Systems," Canadian Coast Guard, February 1977.

Cojeen, H.P., Landsburg, A.C., and MacFarlane, A.A., "One Approach to the Development and Achievement of Maneuvering Standards," *Proceedings, International Conference on Ship Maneuverability Prediction and Achievement*, RINA London, April/May 1987.

Constantine, T., "On the Movement of Ships in Restricted Waterways," *Journal of Fluid Mechanics*, Vol. 9, October 1960.

Crane, Jr., C.L., "Maneuvering Safety of Large Tankers: Stopping, Turning, and Speed Selection," *SNAME Transactions*, Vol. 81.

Crane, C.L., "Maneuvering Trials of 278,000 DWT Tanker in Shallow and Deep Waters," *SNAME Transactions*, Vol. 87.

Crane, Jr., C.L., "Response of Slowly Moving Ship to Propeller and Rudder Actions," First Ship Control Symposium, Annapolis, MD, 1966 (and Davidson Laboratory Report No. 1169, 1966).

Crane, C.L., "State of the Art on How to Include Human Control into the Method of Investigation," General Lecture No. 3, Symposium on Aspect of Navigability, Delft, Holland, April 1978.

Crane, C.L., "Navigation in Ship Maneuvering in

Channels," Hydraulic Design of Deep-Draft Navigation Channels, U.S. Army Corps of Engineers Waterways Experiment Station, Vicksburg, Miss., 1983.

Dand, I.W., "On Modular Maneuvering Models," *Proceedings, International Conference on Ship Maneuverability Prediction and Achievement*, RINA London, April/May 1987.

Dand, I.W., "Some Aspects of Maneuvering in Collision Situations in Shallow Water," Proceedings of the Tenth Symposium on Naval Hydrodynamics, ONR Publication ACR-204, 1974.

Dand, I.W., and Hood, D.B., "Maneuvering Experiments Using Two Geosims of the *Esso Osaka*," National Maritime Institute, Feltham, England, May 1983.

Davidson, K.S.M., "Concerning the Differences in Minimum Turning Diameters of Cruisers and Destroyers," ETT Technical Memo 73, July 1945.

Davidson, K.S.M., "On the Turning and Steering of Ships," *SNAME Transactions*, Vol. 52.

Davidson, K.S.M., and Schiff, L., "Turning and Course Keeping Qualities of Ships," *SNAME Transactions*, Vol. 54.

Davidson Lab, "Free-Running Tests," unpublished report, 1965.

"Deep Draft Navigation Project Hydraulic Design—DRAFT," Engineer Manual EM 1110-2, Office of the Chief of Engineers Corps of Engineers, Dept. of the Army, 1982.

Demenet, P.F., Lewis, G., Mikelis, N.E., Hollocou, Y., "Results from Maneuverability Tests with Models at the Port Revel Centre and Some Comparisons with Mathematical Predictions," *Ship Maneuverability Prediction and Achievement*, RINA, London, April-May, 1987.

Detchmendy, D.M. and Sridhar, R., "Segmental Estimation of States and Parameters in Noisy Nonlinear Filtering Theory," *Journal of Basic Engineering*, ASME, June 1966.

DeSantis, R. and Russo, M., "Rolling Experiments" *SNAME Transactions*, Vol. 44, 1936.

"Design Manual—Harbor and Coastal Facilities," U.S. Navy, NAVDOCKS DM-26, Government Printing Office Publication D209/14:26.

DeVerdiere, G., and Andren, V., "Influence des formes de navires et de gouvernails sur la navigation en canal," *Assn. Technique Maritime et Aeronautique*, 1951, p. 491.

DeVris, W.A., "Determination of Hydrodynamic Coefficients by Force Excitation on Free Sailing Ships, *MARSIM 84, Proceedings*, of the Third International Conference on Marine Simulation, Rotterdam, The Netherlands, June, 1984.

Dieudonne, J., "Collected French Papers on Stability of Route of Ships at Sea, 1949-1950," DTRC Translation 246, 1953.

"Draft Guidelines on Navigation Bridge Visibility," International Maritime Organization, MSC/Circ. 403, June, 1985.

- Drager H., "Cause Relationship of Collisions and Groundings," *Proceedings First International Bridge Design and Operations Forum*, National Maritime Research Center, Kings Point, New York, October 1979, pp. 26-36.
- Draper, N.R., Smith, H., "Selecting the 'Best' Regression Equation," Chapter 6 of *Applied Regression Analysis*, Wiley, New York, 1966.
- Ducane, P., and Goodrich, G.J., "The Following Sea, Broaching and Surging," *Trans. RINA*, 1962.
- Eda, H., "Applications of Digital Simulation Analysis to Ship Control-Dynamic Positioning Control of Drilling Ships," *Proceedings, Fourth Ship Control Systems Symposium*, Royal Netherlands Naval College, Rotterdam, Netherlands, Vol. 4.
- Eda, H., "Directional Stability and Control of Ships in Restricted Channels" *SNAME Transactions*, Vol. 79.
- Eda, H., "Directional Stability and Control of Ships in Waves," *Journal of Ship Research*, SNAME, September 1972.
- Eda, H., "Dynamic Behavior of Tankers During Two-Way Traffic in Channels," *Marine Technology*, Vol. 10, July 1973.
- Eda, H., "Dynamic Positioning Control of Drilling Ships," *Proceedings, The Fourth Ship Control Systems Symposium*, Rotterdam, 1975.
- Eda, H., "Effect of Rudder Rate on Maneuvering Performance of a Large Tanker," *SNAME T & R Report R-22*, 1976.
- Eda, H., Falls, R., Walden, D., "Ship Maneuvering Safety Studies," *SNAME Transactions*, Vol. 87.
- Eda, H., "Maneuvering Characteristics of Large Tankers," *The Million Ton Carrier*, Super Ocean Carrier Conference, San Pedro, California, 1974, pp. 379-400.
- Eda, H., "Notes on Ship Controllability," *SNAME Bulletin* No. 1-41, April 1983.
- Eda, H., "Shiphhandling Simulation Study During Preliminary Ship Design," *Proceedings, Fifth CAORF Symposium*, Kings Point, N.Y., May 1983.
- Eda, H., "Ship Control Bibliography," *SNAME Bulletin* No. 1-40, April 1982, pp. 185.
- Eda, H., "The *Mariner* Model Cooperative Test Program—Correlations and Applications," *Proceedings*, Vol. 2, International Towing Tank Conference, 1975.
- Eda, H., "Tracking an Oil Tanker from New York Harbor Narrows to Arthur Kill," *SNAME Transactions*, Vol. 85.
- Eda, Haruzo, and Crane, Jr., C.L., "Steering Characteristics of Ships in Calm Water and in Waves," *SNAME Transactions*, Vol. 73.
- English, J.W., Rowe, S.J., and Bain, D.C., "Some Maneuvering Devices for Use at Zero and Low Ship Speed," *National Physical Laboratory Report* No. 163, 1972.
- English, J.W., "The Design and Performance of Lateral Thrust Units for Ships," *Royal Institute of Naval Architects*, January 1963.
- Eskigian, N.M., "A Model Study of the Fluid Flow at the Rudder Stock of a Surface Ship," *ETT Report* 600, September 1956.
- Fediaevsky, K.K., and Sobolev, G.V., *Control and Stability in Ship Design*, U.S. Department of Commerce Translation, Washington, DC, 1964, pp. 423.
- Franklin, G.F., Powel, J.D., and Emami-Naeini, A., *Feedback Control of Dynamic Systems*, Addison-Wesley, 1986.
- "Free-Turning Test Results of Series 60 Models," Unpublished Data, Davidson Laboratory, June 1965.
- Fujino, M., "Experimental Studies of Ship Maneuverability in Restricted Waters," *International Shipbuilding Progress*, Part I, Vol. 15, No. 168, 1968 and Part II, Vol. 17, No. 186, 1970.
- Fujino, M., *Maneuverability in Restricted Waters: State of the Art*, University of Michigan, No. 184, August 1976, pp. 141.
- Fujino, M. and Fukasawa, T., Ishiguro, T., and Watanabe, K., "Rudder Force and Maneuvering Motions in Shallow Water," *Proceedings, International Conference on Ship Maneuverability Prediction and Achievement*, RIMA, London, April/May 1987.
- Fuwa, T., "Hydrodynamic Force Acting on Ship in Oblique Towing," *Journal of the Society of Naval Architects of Japan*, Vol. 134, 1973.
- Garthune, R.L., et al, "The Performance of Model Ships in Restricted Channels in Relation to the Design of a Ship Canal," *DTRC Report* 601, August 1946.
- Gertler, M., and Bradley, F.D., "The Effects of Various Types of Rudders on the Turning Characteristics of a Destroyer Model," *DTRC Restricted Report* R-270, 1948.
- Gertler, M., and Gover, S.C., "Handling Quality Criteria for Surface Ships," *Chesapeake Section, SNAME*, 1959.
- Gertler, M., "Steering and Maneuvering; the State of the Art," 14th *ATTC Conference*, September 1965.
- Gertler, M., "The DTMB Planar Motion Mechanism System," *Symposium of Towing Tank Facilities*, Zagreb, Yugoslavia, September 1959.
- Giddings, A.J. and Louis, W.L., "Overcoming Submarine Control Surface Jams and Flooding Casualties," *Naval Engineers Journal*, December 1966.
- Glansdorp, C.C., "Research on Steering, Maneuvering and Controllability of Surface Shps—Part I: Ships Maneuvering Trials and Some New Concepts in Ship Controllability," *Netherlands Maritime Institute, Rotterdam*, 1977.
- Glansdorp, C.C., "Research on Steering, Maneuvering and Controllability of Surface Ships—Part I," *SNAME Chesapeake Section*, 1977.
- Glansdorp, C.C., "Maneuvering Trials—An Evaluation of Existing Codes, Trials, and Measuring Techniques and Recommendations for Future Performance of Maneuvering Trials" *Report* No. 11, *Navigation Research Center, Netherlands Maritime Institute, Rotterdam*, 1976, pp. 52.



Goddard, T.A., "Maneuvering of Large Tankers," SNAME Transactions, 1972.

Goodman, A., "Experimental Techniques and Methods of Analysis Used in Submerged Body Research," Third Symposium on Naval Hydrodynamics, Scheveningen, The Netherlands, September 1960.

Goodman, A., Gertler, M., and Kohl, R., "Experimental Techniques and Methods of Analysis Used at Hydronautics for Surface-Ship Maneuvering Predictions," Eleventh ONR Symposium on Naval Hydrodynamics, London, 1976.

Goodman, T.R., "System Identification and Prediction—An Algorithm Using a Newtonian Iteration Procedure," Quarterly of Applied Math., Vol. XXIV, No. 3, Oct. 1966.

Goodrich, G.J., and Mollard, A.F., "Wind Tunnel Investigations of Semi-Balanced Ship Skeg-Rudders," Trans. RINA, 1979, pp. 285-307.

Graff, W., et al, "Some Extensions of D.W. Taylor's Standard Series," SNAME Transactions, Vol. 72.

Grim, O., "The Ship in a Following Sea," DTRC Translation. No. 313, by E.N. Labouvie, February 1965.

Grose, Vernon L., "Converting Health Hazard Control from Moralism to Management," Professional Safety, American Society of Safety Engineers, March 1980.

Gurovich, A.N., Rodionob, A.A., Asinovsky, V.I., and Grinberg, D.A., *Hull Equipment Handbook for Designers and Builders*, Chapter I "Steering Gear," Sudostroyeniye, (NAVSEA Translation No. 2021), 1967.

Hadler, J.B., and Cheng, H.M., "Analysis of Wake Data of Single and Twin-Screw Ships," SNAME Transactions, Vol. 73.

Hagen, Grant R., "A Catalog of Existing Mathematical Models for Maneuvering," Twentieth American Towing Tank Conference, August, 1983.

Hagen, Grant R., "A Contribution to the Hydrodynamic Design of Rudders," Trans. Third Ship Control Systems Symposium, Ministry of Defence, Bath, United Kingdom, 1972.

Hall, Jr., W.E., "System Identification—An Overview," *Naval Research Reviews*, Arlington, Va., Vol. XXX, No. 4, April 1977.

Harper, J.J., and Simitses, G.J., "Effect of a Simulated Submarine Hull on the Characteristics of All-Movable Control Surfaces," Georgia Institute of Technology Report 439, August 1959.

Harrington, R.L., "Rudder Torque Prediction," SNAME Transactions, 1981.

Hawkins, S., Taggart, R., and Hoyt, E.D., "The Use of Maneuvering Propulsion Devices on Merchant Ships," Report RT-8518 for the Office of R&D Division of Power Research, U.S. Maritime Administration, January 1965.

Hawkins, S., "The Selection of Maneuvering Devices," Chesapeake Section SNAME, September 1965.

Henschke, W., *Schiffbautechnisches Handbuch* (Shipbuilders Handbook), 2nd ed., VEB Verlag Technik, Vol. 1, 1957.

Hewins, E.F., Chase, H.J., and Ruiz, A.L., "The Backing Power of Geared-Turbine-Driven Vessels," SNAME Transactions, Vol. 58.

Hirano, M., "A Practical Calculation Method of Ship Maneuvering Motion at Initial Design Stage," *Journal of Society of Naval Architects of Japan*, Vol. 147, June 1980.

Hirano, M., Takashina, N., and Moriya, S., "A Practical Prediction Method of Ship Maneuvering Motions and Its Application," *Proceedings*, International Conference on Ship Maneuverability Prediction and Achievement, RINA London, April/May 1987.

Hirano, M., Takashina, J., Moriya, S. and Nakamusa, Y., "An Experimental Study on Maneuvering Hydrodynamic Forces in Shallow Water," *Trans. of the West-Japan Society of Naval Architect*, No. 69 (1985).

Hirano, M., and Takashina, J., "A Calculation of Ship Turning Motion Taking Coupling Effect due to Heel into Consideration," *Trans.*, Society of Naval Architects of West Japan, No. 59, 1980.

Hirano, M., and Takashina, J., "Estimation of Linear Derivatives in Shallow Water," International Towing Tank Conference *Proceedings*, Session on Maneuverability, 1987.

Hooft, J.P., and Paymans, P.J., "Four Years Operation Experience with the Ship Control Simulator," *Proceedings*, First Ship Technology and Research (STAR) Symposium, SNAME, August 1975.

Hooft, J.P., and Pieffers, J.B.M., "Maneuverability of Frigates in Waves," Chesapeake Section Paper, Society of Naval Architects and Marine Engineers, New York, October, 1987.

Hoyt, E.D. and Imlay, R.F., "The Influence of Metacentric Stability on the Dynamic Longitudinal Stability of a Submarine," DTRC Report C-158, October 1948.

Hwang, W.Y., "Hydrodynamic Interactions Between Ships in Shallow Waters," Masters Thesis, Massachusetts Institute of Technology, September 1976.

Hwang, W.Y., "Application of System Identification to Ship Maneuvering," Ph.D. Thesis, Department of Ocean Engineering, M.I.T., Cambridge, Mass., 1980.

Iijima, Y., and Honda, K., "On a Lane Width of a Harbor Passage," Doctoral Thesis, Kobe University of Mercantile Marine, 1977.

Inoue, S., Hirano, M., Kijima, K., and Takashina, J., "A Practical Calculation Method of Ship Maneuvering Motion," *International Shipbuilding Progress*, Rotterdam, Netherlands, Vol. 28, No. 325, September 1981.

Inoue, S., Hirano, M., and Kijima, K., "Hydrodynamic Derivatives on Ship Maneuvering," *International Shipbuilding Progress*, Rotterdam, Netherlands, Vol. 28, No. 321, May 1981.

Inoue, S., and Kijima, K., "The Hydrodynamic Derivatives of Ship Maneuverability in Trimmed Condition," *15th ITTC Proceedings*, Part 2, 1978.

Inoue, S., Kijima, K., Tanaka, S., and Eto, T., "Simulation of Stopping Maneuvers of Ship in Restricted



Waters," *Journal*, Society of Naval Architects of West Japan, No. 60, 1980.

Inoue, S., "On the Point in Vertical Direction on which Lateral Force Acts." (In Japanese), Technical Report Sp 82, West Japan Society of Naval Architects, 1979.

ITTC "Ship Maneuvering Committee Report," *Proceedings*, 16th International Towing Tank Conference, 1981.

ITTC Report of the Maneuverability Committee, 17th International Towing Tank Conference, Goteborg, 1984.

Jacobs, W.R., "Estimation of Stability Derivatives and Indices of Various Ship Forms and Comparison with Experimental Results," Davidson Laboratory R-1035, September 1964.

Jacobs, W.R., "Method of Predicting Course Stability and Turning Qualities of Ships," Davidson Laboratory Report 945, March 1963.

Jaeger, H.E., and Jourdain, M., *Le Freinage de Grands Navires*, Bulletin de L' Association Technique Maritime et Aeronautique, Paris, December 1962.

Jaeger, H.E., "Approximate Calculation of Rudder Torque and Rudder Pressures," *International Shipbuilding Progress*, Vol. 2, No. 10, 1955.

Jaeger, H.E., "Le Freinage de Grands Navires (11) Influence des Freins Hydrodynamiques Escamotables sur La Estabilite de Route," Bulletin de L' Association Technique Maritime et Aeronautique, Paris, May 1963.

Johnson, J.L., "The Static Stability Derivatives of a Series of Related Bodies of Revolution," DTRC Report C-383, 1951.

Jones, Jr., W., "Aerodynamic Characteristics of Three Low Aspect Ratio Symmetrical Wings with Rectangular Plan Forms at Reynolds Numbers between  $0.4 \times 10^6$  and  $3.0 \times 10^6$ " NACA RM L52G18, 1952.

Kaplan, P., Sargent, T.P., and Goodman, T.R., "The Application of System Identification to Dynamics of Naval Craft," *Proceedings*, Ninth Symposium on Naval Hydrodynamics, Paris, August 1972.

Kaplan, P. and Sankaranarayanan, K., "Hydrodynamic Interaction of Ships in Shallow Channels, Including Effects of Asymmetry," *Proceedings*, International Conference on Ship Maneuverability Prediction and Achievement, RINA, London, April/May 1987.

Keith, V.T., Porricelli, J.D., Hooft, J.P., Paymans, J.P., and Witt, F.C.J., "Real Time Simulation of Tanker Operations for the Trans-Alaska Pipeline System," *SNAME Transactions*, Vol. 85.

Kempf, G., "Maneuvering Standards of Ships," *Deutsche Schiffahrts Zeitschrift*, Hansa No. 27/28, 1944.

Kerwin, Justin E., Mandel, Philip, and Lewis, S. Dean, "An Experimental Study of a Series of Flapped Rudders," *Journal of Ship Research*, December 1972, pp. 221-239.

Kijima, K., "Maneuverability of a Ship in Confined Water," *Proceedings*, International Conference on

Ship Maneuverability Prediction and Achievement, RINA, London, April/May, 1987.

Koning, *Resistance, Propulsion and Steering of Ships*, Technical Publishing Company, Holland, 1948.

Kose, K., "On a New Mathematical Model of Maneuvering Motions of a Ship and its Applications," *International Shipbuilding Progress*, Rotterdam, Netherlands, Vol. 29, No. 336, August 1982.

Koseki, Yamonouchi, Matsuoka, and Yamazaki, "Some Model Experiments on Shallow Water Effects Upon Turning Ability," *Journal Society of Naval Architects of Japan*, Vol. 117, June 1965.

Kroda, S., "Research and Survey on the Braking Tugboat for Very Large Vessels," Japan Work Vessel Association, Tokyo, 1977, pp. 130.

Lamb, G. and Cook, S., "A Practical Approach to Rudder Design," *Shipbuilding and Shipping Record*, No. 11, 1961.

Lamb, H., *Hydrodynamics*, Sixth Edition, Dover Publications, New York, 1945.

Landsburg, A.C., Card, J.C., Crane, Jr., C.L., Alman, P.R., Bertsche, W.R., Boyleston, J.W., Eda, H., Keith, V.F., McCallum, I.R., Miller, Jr., E.R., and Taplin, A., "Design and Verification for Adequate Ship Maneuverability," *SNAME Transactions*, Vol. 91.

Landsburg, A.C., Card, J.C., Knierim, T., Von-Breitenfeld, H.C., and Eda, H., "Proposed Shipboard Maneuvering Data," *SNAME STAR Proceedings*, 1980.

Larsen, K., "Review of Previously Published Rudder Studies," ETT TM 79, 1946.

Lea, G.K., Feldman, J.T., "Transcritical Flow Past Slender Ships," Ninth Symposium a Naval Hydrodynamics, Paris, Government Printing Office, Washington, D.C., Edited by R. Brard and A. Castera, 1972.

Loften, K., Jr., and Smith, H.A., "Aerodynamic Characteristics of NACA Airfoils at Varying Reynolds Numbers," NACA TN 1945, October 1949.

Lyster, C.A., "Prediction Equations for Ships' Turning Circles," *Trans. RINA*, Vol. 121, 1979.

Macovsky, M.S., Duerr, R.J., and Jewell, D.A., "An Investigation of a Flow-Excited Vibration of the USS *Forrest Sherman* DD931," DTRC Report 1168, August 1959.

Mandel, P., "Some Hydrodynamic Aspects of Appendage Design," *SNAME Transactions*, Vol. 61.

Mandel, P., "Subcritical and Supercritical Operation of Ships in Waves," *Journal of Ship Research*, Vol. 4, June 1960.

"Maneuvering Devices in Ships," *Naval Architect*, RINA, April 1974.

Mannola, K., "New Technology and Channel Design," *Navigator Z-3/75*, Helsinki, Finland.

Marino, K.L., Cooper, R.B., *U.S. Merchant Ship Bridge Design Standards*, Maritime Administration, Washington, DC, October 1982.

Martin, L.L., "Ship Maneuvering and Control in Wind," *SNAME Transactions*, Vol. 88.

Martin, M., "Analysis of Lateral Force and Moment

Caused by Yaw during Ship Turning," Davidson Laboratory Report 792, March 1961.

Martinusen, K., and Linnerud, I., "Techniques for Predicting Maneuvering Characteristics of Ships at the Design Stage," *Ship Maneuverability Prediction and Achievement*, RINA, London, April 1987.

McCreight, W.R., "Ship Maneuvering in Waves," Symposium *Proceedings*, Office of Naval Research, Berkeley California, 1985.

McGoldrick, R.T., "Rudder-Excited Hull Vibration on the USS *Forrest Sherman* DD931," *SNAME Transactions*, Vol. 67.

McIlroy, W. and Carpenter, G., "Technical Aspects of Fast-Time Simulation at CAORF," *Proceedings*, Third CAORF Symposium, Maritime Administration, October 1979.

Meijer, M.C., "An Experiment Concerning Party Closed Cavities Behind a Surface-Piercing Rod," California Institute of Technology, Hydrodynamics Laboratory Report E-110-1, January 1964.

Mikelis, N.E., and Price, W.G., "Two Dimensional Sway Added Mass Coefficients for Vessels Maneuvering in Restricted Waters," *RINA Supplementary Papers*, No. 121, July 1979.

Mikelis, N.E., "A Procedure for the Prediction of Ship Maneuvering Response for Initial Design, International Conference on Computer Application . . . etc.," ICCAS '85, North Holland Publishing Co., Trieste 1985.

Mikelis, N.E., and Price, W.G., "Comparisons of Acceleration Coefficients and Correction Factors Associated Between Theory and Experiments," *Trans. RINA*, 1980.

Miller, E.R., Van Dyke, P., Lord, R.S., and Conrad, R.E., "The Use of Real-Time Maneuvering Simulations in the Contract Design Evaluation of a Salvage Ship," *Naval Engineers Journal*, January 1984.

Miller, E.R., Ankudinov, V., and Termes, T., "Evaluation of Concepts for Improved Controllability of Tank Vessels," *Marine Technology*, Vol. 18, No. 4, Oct. 1981.

Miller, E.R., "Model Test and Simulation Study Based on the Full Scale *Esso Osaka* Maneuvering Data," U.S. Maritime Administration Report, October 1980.

Miller, E.R., "The Performance of River Tow Maneuvering Performance," U.S. Coast Guard Report D-32-78, Washington, DC, May 1978.

"Model Test and Simulation Correlation Study Based on the Full Scale *Esso Osaka* Maneuvering Data," Hydronautics, Inc., Maritime Administration, Washington, D.C., October 1980.

Moody, C.G., "The Handling of Ships through a Widened and Asymmetrically Deepened Section of Gaillard Cut in the Panama Canal," DTRC Report 1705, August 1964.

Moody C.G., "The Handling of Ships in the Panama Canal," DTRC Report 1705, August 1964.

Morse, R.V., and Price, D., "Maneuvering Characteristics of the Mariner Class Ship in Calm Seas,"

Sperry Gyroscope Company Report GJ-2233-1019, December 1961.

Motora, S., and Couch, R., "Maneuverability of Full Bodied Ships in Restricted Waters," University of Michigan, 1961.

Motora, S., "Maneuverability at Slow Speed," Contribution to the 11th ITTC (Tokyo), pp. 1-4.

Motora, S., "On the Measurement of Added Mass and Added Moment of Inertia of Ships in Steering Motion," *Proceedings*, First Symposium on Ship Maneuverability, David Taylor Research Center, Report 1461, 1960.

Motora, S., "Proposed Maneuverability Indices as a Measure of the Steering Qualities of Ships," 9th IPPC.

Munk, M.M., *Aerodynamic Theory of Airships*, W.F. Durand, Editor, Julius Springer, 1934.

Newman, J.N., *Marine Hydrodynamics*, MIT Press, 1977.

Newton, R.N., "Interaction Effects Between Ships Close Aboard in Deep Water," DTMB Report 1461, October 1960.

Nichols, W.O., Ruben, M.L., Danielson, R.V., "Some Aspects of Large Tanker Design," *SNAME Transactions*, Vol. 68.

Nielsen, R.A., and Kendall, H.K., "Stern Thruster Installation on the SS *John Sherwin*," *Marine Technology*, Jan. 1974.

Nikolaev, E., and Lebedeva, M., "On the Nature of Scale Effect in Maneuvering Tests with Full-Bodied Ship Models," *Proceedings*, 13th Symposium on Naval Hydrodynamics, Tokyo, 1980.

Nizerry, B., and Page, J.P., "Maneuvering Tests on the 213,000-ton Tanker (in French)," Assn. Technique Maritime et Aeronautique, 1969.

"Nomenclature for Treating the Motion of a Submerged Body through a Fluid," *SNAME Technical and Research Bulletin* 1-5, 1952.

Nomoto, K., "Analysis of Kempf's Standard Maneuver Test and Proposed Steering Quality Indices," First Symposium in Ship Maneuverability, DTRC Report 1461, October 1960.

Nomoto, K., and Norrbin, N.H., "A Review of Methods of Defining and Measuring the Maneuverability of Ships," International Towing Tank Conference, Appendix I, Report of Maneuverability Committee, Rome, 1969.

Nomoto, K., et. al., "On the Steering Qualities of Ships," *International Shipbuilding Progress*, Vol. 4, No. 35, 1957.

Nomoto, K., "Response Analysis of Maneuverability and its Application to Ship Design, Researches on the Maneuverability of Ships in Japan," Society of Naval Architects of Japan, Tokyo, 1966.

Nomoto, K., "Ship Response in Directional Control Taking Account of Frequency Dependent Hydrodynamic Derivatives," *Proceedings*, Vol. 2, International Towing Tank Conference, 1975.

Nomoto, K., "Some Aspects of Simulator Studies on

Ship Handling," International Symposium on Practical Design in Shipbuilding, 1977.

Norrbin, N.H., "Theory and Observation on the Use of a Mathematical Model for Ship Maneuvering in Deep and Confined Waters," Swedish State Shipbuilding Experimental Towing Tank, Publication 68, 1971.

Norrbin, N.H., and Williams, A., "The SSPA Steering and Maneuvering Simulator," Report No. 40 (2nd Ed.), The Swedish State Shipbuilding Experimental Tank, March 1974.

Norrbin, N.H., "Bank Effects on a Ship Moving Through a Short Dredged Channel," *Proceedings*, Tenth Symposium on Naval Hydrodynamics, Cambridge, Massachusetts, 1974.

NTSB, "Marine Collisions . . .," MSS-81-1, Washington, D.C., 1981.

Oakley, Jr., O.H., Pauling, J.R., and Wood, P.D., "Ship Motions and Capsizing in Astern Seas," *Proceedings*, Tenth Symposium on Naval Hydrodynamics, Cambridge, Massachusetts, 1974.

Ohtagaki, Y., and Tanaka, M., "Application of Real-Time Ship Maneuvering Simulator in the Past Ten Years," *Proceedings* MARSIM '84, June 1984.

Okamoto, H., Tamai, H., and Oniki, H., "Correlation Studies of Maneuverability of Full Ships," 13th International Towing Tank Conference, Berlin/Hamburg, 1972.

Olson, C.R., "Effect of Linkage Ratio and Flap Area on the Free Stream Characteristics of an All-Movable Flapped Rudder," DTRC Report 991, September 1955.

Oltmann, P., and Sharma, S.D., "Simulation of Combined Engine and Rudder Maneuvers Using an Improved Model of Hull-Propeller-Rudder Interactions," *Proceedings*, 15th ONR Symposium on Naval Hydrodynamics, Hamburg, 1984.

Panel H-10, "Proposed Procedures for Determining Ship Controllability Requirements and Capabilities," *Proceedings*, First Ship Technology and Research (STAR) Symposium, SNAME, August 1975.

Pauling, J.R., Sibul, O.I., "New Experiment and Techniques for the Experimental Evaluation of Ship's Lateral Stability," University of California, Berkeley, August 1962.

Pauling, J.R., and Wood, L.W., "The Dynamic Problem of Two Ships Operating on Parallel Courses in Close Proximity," University of California Series 189, July 1962.

Peach, R.W., "A Method for Determining Acceleration of a Ships," *International Shipbuilding Progress*, June 1963.

Perez y Perez, L., "A Time-Domain Solution to the Motions of a Steered Ship in Waves," *Journal of Ship Research*, SNAME, March 1974.

PIANC International Commission for the Reception of Large Ships (ICORELS), Working Group No. 4: "III. Recommendations Concerning Approach Channels and Maneuvering Areas for Large Ships" November 1977.

Porter, W.R., "Added Mass, Damping and Wave-

Ratio Coefficients for Swaying Ship-Like Cylinders," *Journal of Ship Research*, Dec. 1966. SNAME *Principles of Naval Architecture*, Vol. II, Chapter 4, Figs. 6, 7, and 8, 1939.

Prohaska, C.W., "The Vertical Vibration of Ships," *Shipbuilding and Marine Engine Builder*, October-November 1947.

Puglisi, J.J., "History and Future Developments in the Application of Marine Simulators, Tomorrow's Challenge Role for the International Marine Simulator Forum (IMSF)," *Proceedings*, MARSIM '87, Trondheim, Norway, June 22-24, 1987.

Puglisi, J.J., VanHoorde, G., Kaufman, E., and Eda, H., "The Proposed Plan for Widening of the Panama Canal and Application of Simulator Techniques for the Development and Validation of the Proposed Solution," *Proceedings*, MARSIM '84, Rotterdam, Netherlands.

Ribadeau Dumas, L.R., "Ports and Navigation Aids," *Trans. First International Symposium on Ship Approach and Berthing Maneuvers*, Grenoble, France, 1977.

Ribadeau Dumas, L.R., "Problems Arising from the Navigation of Large and Very Large Ships in Narrow Channels and Port Entrances," IX International Conference on Lighthouses and Other Aids to Navigation, IALA/AISM Ottawa, 1975.

Ridley, V.W., and Henkin, Y., "Upgrading Steering Gear Systems from Inception to Operation," SNAME *Transactions*, 1982.

Riek, J., Tenenbaum, S., McIlroy, W., "An Investigation into the Safety of Passage of Large Tankers in the Puget Sound Area, Vol. 1," U.S. Maritime Administration NMRC, Kings Point, 1978.

Romahn, K., and Thieme, H., "On the Selection of Balance Area for Rudders Working in the Slip Stream," *Schiffstechnik* No. 21, 1957.

Roseman, D.P., *The MARAD Systematic Series of Full-Form Ship Models*, SNAME, 1987.

Roseman, D.P., Gertler, M., and Kohl, R.E., "Characteristics of Bulk Products Carriers for Restricted-Draft Service," SNAME *Transactions*, 1974.

Rossell, H.E. and Chapman, L.B., "*Principles of Naval Architecture*," (Schoenherr, K.E., "Propulsion and Propellers") Vol. 2, SNAME, 1939.

*Rules for the Construction and Classification of Steel Ships*, Det norske Veritas, Oslo, 1975, pg. 102.

Rydfill, L.J., "A Linear Theory for the Steered Motion of Ships in Waves," *Trans. INA*, 1959.

Sargent, T.P., and Kaplan, P., "System Identification of Surface Ship Dynamics," Oceanics Inc., NTIS (AD-712448), 1970.

Sato, S., Takagi, Hikino, et. al., "On A Study of Ship-Controllability of a Wide-Beam Tanker," *Journal*, Society of Naval Architects, Japan, Vol. 134, Dec. 1973.

Saunders, H.E., "*Hydrodynamics in Ship Design*," SNAME, 1957.

Schoenherr, K.E., "A Program for the Investigation

of the Rudder Torque Problem," *Marine Technology*, SNAME, July 1965.

Schoenherr, K.E., "Bank Suction Effects on Merchant Ship Hulls in Restricted Waters," First Symposium on Ship Maneuverability, DTRC Report 1461, October 1960.

Schoenherr, K.E., "Data for Estimating Bank Suction Effects in Restricted Water on Merchant Ship Hulls," First Symposium on Ship Maneuverability, DTRC Report 1461, October 1960.

Segel, Leonard, "Ship Maneuverability as Influenced by Transient Response to the Helm," First Symposium on Ship Maneuverability, DTRC Report 1461, October 1960.

Shiba, H., "Model Experiments about the Maneuverability of Turning of Ships," First Symposium on Ship Maneuverability, DTRC Report 1461, October 1960.

Silverstein, B.L., "Linearized Theory of the Interaction of Ships," University of California, Institute of Engineering Research, May 1957.

Smitt, L.W., "Comparative Results from Different Captive Model Test Techniques," *Proceedings*, International Towing Tank Conference, 1975.

Smitt, L.W., and Chislett, M.S., "Course—Stability While Stopping," *Journal of Engineering Science*, Vol. 14, No. 7, 1972.

Smitt, L.W., "Steering and Maneuvering of Ships—Full Scale and Model Tests," *European Shipbuilding*, Parts I and II, No. 6, 1970, and No. 1, 1971.

Smitt, L.W. and Chislett, M.S., "Large Amplitude PMM Tests and Maneuvering Predictions for a Mariner Class Vessel," *Proceedings of the Tenth Symposium on Naval Hydrodynamics*, ONR Publication ACR-204, 1974.

SNAME Panel H-10 (Ship Controllability), "Procedures for Determining Ship Controllability Requirements and Capabilities," *Proceedings* SNAME STAR Symposium, Washington, DC, 1975.

"Special Study—Marine Collisions and Effects of Preventive Recommendations," National Transportation Safety Board, NTSB-MSS-81-1, September 1981.

Steele, B.N., and Harding, M.H., "The Application of Rotating Cylinders to Ship Maneuvering," National Physical Laboratory, Ship Division, London, Report No. 148, 1970.

Stilwell, J.J., Nelson, P.W., and Porter, W.R., "Hydrofoils at the Crossroads," IAS Paper 61-44, 1961.

Strandhagen, A.G., Schoenherr, K.E., and Kobayashi, F.M., "The Dynamic Stability on Course of Towed Ships," *SNAME Transaction*, Vol. 58.

Strom-Tejsen, J., "A Digital Computer Technique for the Prediction of Standard Maneuvers of Surface Ships," DTRC Report 2130, December 1965.

Strom-Tejsen, J., and Chislett, M.S., "A Model Testing Technique and Method of Analysis for the Prediction of Steering and Maneuvering Qualities of Surface Ships," *Hydro-Og Aerodynamisk Laboratorium Report No. HyA 7*, Lyngby, Denmark, June 1964.

Strumpf, A., "Calculation of Hydrodynamic Side

Forces and Yaw Moments of Merchant Ships," Maritime Administration, Washington, D.C., July 1983.

Stuntz, G., and Taylor, R., "Some Aspects of Bow Thruster Design," *SNAME Transactions*, Vol. 72.

Suarez, A., "Rotating Arm Experimental Study of a Mariner Class Vessel," Davidson Laboratory Note 696, June 1963.

Sukselainen, J., "On Ship Maneuvering and Waterway Width" Helsinki University of Technology, Finland, 1975.

Surber, Jr., W.C., "An Investigation of the Flow in the Region of the Rudder of a Free-Turning Model of a Multiple-Screw Ship," DTRC Report 998, 1955.

Szeto, F.F., "Systems Identification from Ship Maneuver in Currents," Masters Thesis, Massachusetts Institute of Technology, May 1977.

Taggart, R., *Ship Design and Construction*, SNAME, New York, 1980.

Taggart, R., Kobayashi, S., "Anomalous Behavior of Merchant Ship Steering Systems," *Marine Technology*, April, 1970.

Taniguchi, K., et al, "Investigations into the Fundamental Characteristics and Operating Performance of Side Thrusters," Mitsubishi Technical Bulletin No. 35, 1966.

Taplin, A. and Atkinson, J.A., "Rudder Rate Tests on the U.S. Coast Guard Cutter *Gallatin* (WHEC 721)," *SNAME T & R Bulletin* 1-43, 1987.

Taplin, A., "Sea Trials for Measuring Rudder Torque and Force," *Trans.*, Fourth Ship Control Systems Symposium, Den Helder, Holland, 1975.

Taplin, A., "Note on Rudder Design Practice," First Symposium on Ship Maneuverability, DTRC Report 1461, 1960.

Technical Research Center of Finland, "Zigzag Maneuvering Data Analysis," COST 301/SF/VTT/T1. 01 OP 5, October 1984.

Thieme, H., "Design of Ship Rudders," DTRC Translation No. 321, by E. N. LaBouvie, November 1965.

Thwaites, B., *Incompressible Aerodynamics*, Oxford University Press, England, 1960.

Todd, F.H., "Propeller Action in a Single Screw Ships," DTRC June 1951.

Todd, F.H., "Some Further Experiments on Single Screw Merchant Ship Forms—Series 60," *SNAME Transactions*, 1953.

Trankle, T.L., "Practical Aspects of System Identification," ASME paper 79-WA/DSC-23, presented at Winter Annual Meeting, December 1979.

Trankle, T.L., "Identification of Ship Steering Dynamics Using Inertial Sensors," Seventh IFAC symposium on Identification and Parameter Estimation, New York, July 1985.

Trankle, T.L., "Status of MARCIS: The Marine Coefficient Identification System," American Towing Tank Conference, Washington, D.C., 1986.

Tsakonas, S., "Effect of Appendage and Hull Form on the Hydrodynamic Coefficients of Surface Ships," Davidson Laboratory Report 740, May 1959.

Tuck, E.O., and Newman, J.N., "Hydrodynamic In-

teraction Between Ships," Proceedings of the Tenth Symposium on Naval Hydrodynamics, ONR, 1974.

Tuck, E.O., "Shallow Water Flows Past Slender Bodies," *Journal of Fluid Mechanics*, 1966.

Tuck, E.O., "Sinkage and Trim in Shallow Water of Finite Width," *Schiffstechnik*, Bd. 14, 1967.

Van Donselaar, H., Lazet A., Schuffel, H., and Wepster, A., *Merchant Vessel Bridge Lay-Out*, Netherlands Maritime Institute, Rotterdam, Netherlands, 1979.

Van Lammeren, W.P.A., Troost, L., and Koning, J.G., *Resistance, Propulsion and Steering of Ships*, Technical Publishing Company, Holland, 1948.

Van Leeuwen, G., "The Lateral Damping and Added Mass of a Horizontally Oscillating Ship Model," Netherlands Research Center Report 65S, December 1964.

Vantine, W.H., "Good Ship Bridge Design from a Master Mariner's Point of View," *Ship Operation Automation, Proceedings*, IFAC/IFIP Symposium, Washington, DC, 1976.

Veldhuyzen, W., and Stassen, H.G., "Internal Model Concept: An Application to Modelling Human Control of Large Ships," *Human Factors*, Vol. 19, Aug. 1977.

Wahab, R., and Swaan, W.A., "Course Keeping and Broaching of Ships in Following Waves," *Journal of Ship Research*, April 1964.

Wang, S., Discussion of Reference. (Tuck, 1979).

Weinig, F., "Lift and Drag of Wings with Small Span," NACA TM 1151, 1947.

Whicker, L.F., and Fehlner, L.F., "Free Stream

Characteristics of a Family of Low Aspect Ratio Control Surfaces for Application to Ship Design," DTRC Report 933, 1958.

Wilson, M.B., and Von Kerczek, C., "An Inventory of Some Force Producers for Use In Marine Vehicle Control," David Taylor Research Center, No. 79/097, November 1979.

Windsor, R.I., "Survey of Low Aspect Ratio Characteristics Useful in the Design of Control Surfaces," University of Maryland Wind Tunnel Report 62-1, 1962.

Wise, D.A., and English, J.W., "Tank and Wind Tunnel Tests for a Drill Ship with Dynamic Position Control," Paper No. OTC 2345, Offshore Technology Conference, 1975.

Wride, A.T.A., Wills, A.E., and Leckenby, "Behavior of Large Ships in Shallow and Confined Waters (Southampton)," NPL Report Mar Sci R121, 1975.

Yamaguchi, A., et al, "Full Scale Tests on Sinkage of Super-Tankers Through Shallow Water," Kobe University of Mercantile Marine, *Memoirs*, 1968.

Yamaguchi, A., et al, "Model Tests on Sinkage of Vessels Underway in Restricted Channels," Kobe University of Mercantile Marine, *Memoirs*, 1967.

Yeh, H., "NS Savannah Shallow Water Mooring Test," DTRC Report 1883, August 1964.

Yoshimura, Y., and Nomoto, K., "Modeling of Maneuvering Behavior of Ships with a Propeller Idling, Boosting, and Reversing," (In Japanese), *Journal of Society of Naval Architects of Japan*, Vol. 144, 1978.

# Nomenclature

## Controllability

The following symbols apply to Chapter IX only. The phrase "stands for" is understood between the symbol and its definition.

### Arranged Functionally

#### Control-Surface Geometry

$A_F$	area of flap of control surface
$A_M$	movable area of control surface
$A_T$	total area of control surface
$A_R$	rudder area
$a$	effective aspect ratio
$a_G$	geometric aspect ratio
$\bar{b}$	mean span
$\bar{c}$	mean chord
$c_r$	root chord
$c_t$	tip chord
$d$	chordwise distance from leading edge at mean geometric chord to axis of rotation

CP	center of pressure
$(CP)_c$	chordwise distance from leading edge at mean geometric chord to center of pressure; usually given as a percentage of mean chord $\bar{c}$
$(CP)_b$	spanwise distance from root chord to center of pressure; usually given as a percentage of mean span $\bar{b}$
$\bar{t}$	mean thickness
$\lambda$ (lambda)	taper ratio, $c_t/c_r$
$\Lambda$ (Lambda)	sweepback angle of the quarter-chord line

#### Axes and Distances

$a_0$	amplitude of transverse linear oscillation in planar motion tests
$G$	position of center of gravity of a ship
$O$	origin of reference axes fixed in the ship ( $O$ may, but need not, coincide with $G$ or $\infty$ )
$\infty$	position of midlength of ship
$x, y, z$	system of reference axes through $O$

	whose directions remain fixed in the ship
$x_0, y_0, z_0$	system of reference axes whose origin and direction remains fixed in the earth
$x_G, y_G, z_G$	components of distances from $O$ to $G$ , measured along $x, y$ , and $z$ -axes, respectively
$x_{0G}, y_{0G}, z_{0G}$	components of distance from origin of earth axes to $G$ , measured along $x_0, y_0$ , and $z_0$ -axes, respectively
$x_R$	distance from $O$ to center of pressure of control surface, measured along $x$ -axis
$x_f$	distance from $O$ to center of pressure of fin, measured along $x$ -axis
$x_{\infty}$	distance from $O$ to $\infty$ , measured along $x$ -axis

#### Inertia Characteristics

$k_1$	Lamb's coefficient of accession to mass in the longitudinal ( $x$ ) direction, for an ellipsoid; $k_1 m = -X_u$
$k_2$	Lamb's coefficient of accession to mass in the lateral ( $y$ ) direction, for an ellipsoid
$k'$	Lamb's coefficient of accession to inertia in rotation about the $z$ -axis, for an ellipsoid
$I_x, I_y, I_z$	mass moments of inertia of a ship about the $x, y$ , and $z$ -axes, respectively
$\Delta'_2$	lateral "added" mass, nondimensionalized by $\frac{1}{2}\rho L^2 T$ ; $\Delta'_2 = -Y'_v$
$\Delta'_x$	actual plus "added" mass in the longitudinal direction, $\Delta'_x = \Delta'_x(1 + k_1)$ ; nondimensionalized by $\frac{1}{2}\rho L^2 T$
$\Delta'_s$	rotational "added" mass; $\Delta'_s = (k'/k_2)\Delta'_2$ ; nondimensionalized by $\frac{1}{2}\rho L^2 T$

**Angles**

$\phi$ (phi)	roll angle, measured from the vertical $XZ_0$ plane to the $z$ -axis of the ship; positive in the positive sense of rotation about the $x$ -axis
$\theta$ (theta)	pitch angle, measured from the horizontal $x_0y_0$ plane to the $x$ -axis of the ship; positive in the positive sense of rotation about the $y_0$ -axis
$\psi$ (psi)	yaw angle, measured from the vertical $x_0z_0$ plane to the $x$ -axis of the ship; positive in the positive sense of rotation about the $z_0$ -axis
$\psi_0$ (psi)	amplitude of yaw oscillation in planar motion tests
$\alpha$ (alpha)	angle of attack on a control surface
$\alpha$ (alpha)	angle of attack in pitch on the hull, measured from the resultant ship velocity $V$ to the $xy_0$ -plane
$\beta$ (beta)	angle of attack in yaw on the hull (or drift angle), measured from the resultant ship velocity $V$ to the $xz_0$ -plane
$\beta_R$	inflow angle at the rudder (see Fig. 22)
$\delta_R$ (delta)	angular displacement of the rudder, measured from the $xz$ -plane of the ship to the plane of the rudder
$\delta_F$ (delta)	angular deflection of the control-surface flap, measured from the plane of the control surface to the plane of the flap
$\epsilon$ (epsilon)	phase angle
$\epsilon$ (epsilon)	straightening influence of hull and propeller on the flow to the rudder

**Translational and Angular Velocities and Accelerations**

$U$	resultant velocity of the fluid relative to a control surface or a fixed fin
$V_0$	resultant velocity, relative to the earth, of the origin $O$ . (In general, except for fluid motions induced either by movement of the ship or by waves, the fluid in which the ship is moving is assumed to be stationary relative to the earth.)†
$\left. \begin{matrix} p, q, r \\ (\dot{\phi}, \dot{\theta}, \dot{\psi}) \end{matrix} \right\}$	components of resultant angular velocity of the ship about the $x, y$ , and $z$ -axes, respectively
$u, v, w$	components of $V$ along the $x, y$ , and $z$ -axes, respectively
$\left. \begin{matrix} \dot{p}, \dot{q}, \dot{r} \\ (\ddot{\phi}, \ddot{\theta}, \ddot{\psi}) \end{matrix} \right\}$	components of resultant angular acceleration of the ship about the ship axes
$\ddot{u}, \ddot{v}, \ddot{w}$	components of resultant linear acceleration of the ship, $\dot{V}$ along the ship axes

$u_1$	initial equilibrium value of $u$
$v_1$	initial equilibrium value of $v$
$u_0$	component of $V$ along the $x_0$ -axis
$\dot{\delta}_R$ (delta)	rate of deflection of rudder or other control surface

**Forces**

$D$	drag force; component of a resultant total force parallel to the direction of motion, developed as a result of an angle of attack ( $C_D$ , drag coefficient, $= D / \frac{1}{2} \rho A U^2$ )
$F$	component of the total force on a control surface normal to the center-plane of the surface ( $C_N$ , normal force coefficient, $= F / \frac{1}{2} \rho A U^2$ )
$L$	lift force; component of a resultant total force normal to the direction of motion, developed as a result of an angle of attack ( $C_L$ , lift coefficient, $= L / \frac{1}{2} \rho A U^2$ )
$\left. \begin{matrix} X_0, Y_0, Z_0, \\ X, Y, Z \end{matrix} \right\}$	components of a resultant total force acting at the origin $O$ directed along the $x_0, y_0, z_0$ and $x, y, z$ -axes, respectively
$X^0, Y^0, Z^0$	values of $X, Y$ , and $Z$ at $v = r = w = q = \dot{v} = \dot{r} = \dot{w} = \dot{q} = 0$ and $V = u_1$

**Force Derivatives**

$Y_v$	partial derivative of $Y$ with respect to $v$
$Y_{\dot{v}}$	partial derivative of $Y$ with respect to $\dot{v}$
$Y_r$	partial derivative of $Y$ with respect to $r$
$Y_{\dot{r}}$	partial derivative of $Y$ with respect to $\dot{r}$
$Y_{\delta_R}$	partial derivative of $Y$ with respect to $\delta_R$
$Y_u^0$	partial derivative of $Y^0$ with respect to the ahead velocity component $u$
$Z_w$	partial derivative of $z$ with respect to $w$
$Z_{\dot{w}}$	partial derivative of $z$ with respect to $\dot{w}$
	etc.

**Linearized Force Components**

$Y_v v$	linearized $Y$ -component developed as a result of a drift angle, $\beta \approx -v/V$
$Y_{\dot{v}} \dot{v}$	linearized $Y$ -component developed as a result of an acceleration, $\dot{v}$
$Y_r r$	linearized $Y$ -component developed as a result of an angular velocity, $r$

$Y_{\dot{r}}$	linearized $Y$ -component developed as a result of an angular acceleration, $\dot{r}$
$Y_{\delta_R}$	linearized $Y$ -component developed as a result of a rudder angle, $\delta_R$
$Z_w$	linearized $z$ -component developed as a result of an angle of attack, $\alpha \approx \frac{w}{V}$
$z_w \dot{w}$	linearized $z$ -component developed as a result of an acceleration, $\dot{w}$ etc.

### Moments

$K, M, N$	components of a resultant total moment acting on a ship about the $x, y$ , and $z$ -axes, respectively; referred to as the rolling, pitching, and yawing moments, respectively
$M^0, N^0$	values of $M$ and $N$ at $v = r = w = q = \dot{v} = \dot{r} = \dot{w} = \dot{q} = 0$ and $V = u_1$
$Q_{\bar{c}/4}$	moment of normal force on a control surface about quarter chord; $C_{m\bar{c}/4} = \frac{Q_{\bar{c}/4}}{(\rho/2)AU^2\bar{c}}$
$Q_H$	moment of hydrodynamic normal force about rudder stock; $C_m = \frac{Q_H}{(\rho/2)AU^2\bar{c}}$

### Moment Derivatives

$N_v$	partial derivative of $N$ with respect to $v$
$N_r$	partial derivative of $N$ with respect to $r$
$N_{\dot{v}}$	partial derivative of $N$ with respect to $\dot{v}$
$N_{\dot{r}}$	partial derivative of $N$ with respect to $\dot{r}$
$N_{\delta_R}$	partial derivative of $N$ with respect to $\delta_R$
$M_w$	partial derivative of $M$ with respect to $w$
$M_q$	partial derivative of $M$ with respect to $q$
$M_{\theta}$	partial derivative of $M$ with respect to $\theta$
$K_v$	partial derivative of $K$ with respect to $v$

### Linearized Moment Components

$N_v v$	linearized $N$ -component developed as a result of a drift angle, $\beta \approx -\frac{v}{V}$
---------	--

$N_r r$	linearized $N$ -component developed as a result of an angular velocity, $r$
$N_{\dot{v}}$	linearized $N$ component developed as a result of an acceleration, $\dot{v}$
$N_{\dot{r}}$	linearized $N$ -component developed as a result of an angular acceleration, $\dot{r}$
$N_{\delta_R}$	linearized $N$ -component developed as a result of a deflection angle, $\delta_R$
$M_v w$	linearized $N$ -component developed as a result of an angle of attack, $\alpha \approx \frac{w}{V}$
$M_q q$	linearized $M$ -component developed as a result of an angular velocity, $q$
$M_{\theta} \theta$	linearized $M$ -component developed as a result of a pitch angle, $\theta$
$K_v v$	linearized $K$ -component developed as a result of a drift angle, $\beta \approx -\frac{v}{V}$

### Notes

1. Signs of all directions, forces, distances, velocities, and accelerations are positive downward along the  $z$ -axis, positive to starboard along the  $y$ -axis, and positive forward along the  $x$ -axis, and similarly along the  $x_0, y_0$ , and  $z_0$ -axes

2. Signs of all signs, angular velocities, angular accelerations and moments (except control-surface torques and bending moments) are positive if clockwise when facing in the positive direction of the appropriate axis. Rudder torques are positive if the center of pressure is forward of the point about which the torques are taken.

3. All inertia and mass characteristics are assumed as positive.

4. The prime superscript ( $'$ ), except where otherwise stated, indicates the value of an item nondimensionalized on the basis of a combination of  $\rho, L$  (or  $T$ ), and  $V$  or powers thereof.

5. The subscript (1), except where otherwise stated, indicates the initial equilibrium value of a distance, velocity, or angle.

6. The superscript (0), except where otherwise stated, indicates force, distance, velocity, and acceleration components along the earth's ( $x_0, y_0, z_0$ ) axes rather than along the ship's ( $x, y, z$ ) axes.

### Arranged Alphabetically

$A_F$	area of flap of a control surface
$A_M$	movable area of a control surface
$A_T$	total area of a control surface
$A_R$	rudder area
$a$	effective aspect ratio
$a_G$	geometric aspect ratio
$b$	span of a control surface (see Fig. 27)
$\bar{b}$	mean span of a control surface



$c$	chord of a control surface (see Fig. 27)
$\bar{c}$	mean chord of a control surface
$c_r$	root chord
$c_t$	tip chord
$C_D$	drag coefficient = $D/(\rho/2)AU^2$
$C_L$	lift coefficient = $L/(\rho/2)AU^2$
$C_N$	normal force coefficient = $F/(\rho/2)AU^2$
CP	center of pressure
$D$	drag force, parallel to direction of flow
$d$	distance from leading edge of a control surface at $\bar{c}$ to axis of rotation
$F$	component of total force normal to centerplane of control surface
$I$	mass moment of inertia of the ship
$K$	component about the $x$ -axis of the total moment acting on the ship (rolling moment)
$k$	Lamb's coefficients of accession
$L$	lift force, normal to the direction of flow
$M$	component about the $y$ -axis of the total moment acting on the ship (pitching moment)
$N$	component about the $z$ -axis of the total moment acting on the ship (yawing moment)
$m$	mass per unit length
$O$	origin of reference axes, fixed in the ship
$p$	component of angular velocity about the $x$ -axis (rolling)
$q$	component of angular velocity about the $y$ -axis (pitching)
$R$	turning radius
$r$	component of angular velocity about the $z$ -axis (yawing)
$u$	component of $V$ along the $x$ -axis
$v$	component of $V$ along the $y$ -axis
$U$	resultant velocity of the fluid relative to a control surface or a fixed fin.
$V$	resultant velocity of $O$ , relative to the earth
$w$	component of $V$ along the $z$ -axis
$X$	component of total resultant force along the $x$ -axis
$x$	longitudinal axis through $O$
$Y$	component of total resultant force along the $y$ -axis
$y$	transverse axis through $O$
$Z$	component of total resultant force along the $z$ -axis
$z$	vertical axis through $O$
$\alpha$ (alpha)	angle of attack in pitch; angle of attack on a control surface
$\beta$ (beta)	angle of attack in yaw (drift angle)
$\beta_R$	inflow angle at the rudder

$\Delta$ (Delta)	mass displacement
$\delta$ (delta)	angle of deflection of a control surface; increment
$\delta_f$ (delta)	angle of flap relative to control surface
$\epsilon$ (epsilon)	straightening influence of hull and propeller on flow to rudder;
	phase angle
$\theta$ (theta)	angle of pitch
$\Lambda$ (lambda)	sweepback angle
$\lambda$ (lambda)	taper ratio
$\sigma$ (sigma)	stability index
$\phi$ (phi)	angle of roll
$\psi$ (psi)	angle of yaw

### Special Symbols

$\mathbf{l}$	denotes baseline
$\mathbf{e}$	centerline
$\overline{\mathbf{X}}$	midlength, in general
$\nabla$	vol volume of displacement

### Mathematical Symbols

$\partial$	is a partial derivative sign
$i$	is $\sqrt{-1}$
$\approx$	approximately equal to
$<$	less than
$>$	greater than
$\dot{x}$	(one dot over a variable) is the first derivative of the variable
$\ddot{x}$	(two dots over a variable) is the second derivative of the variable
$\propto$	proportional to
$\infty$	infinity
$\delta$ (delta)	a finite increment
$\Sigma$ (Sigma)	summation of
$\pi$ (pi)	ratio of circumference of circle to diameter
$\int$	integral of
$f$	some function of
$\rightarrow$	approaches as a limit
$\equiv$	is identical to
$=$	equal to
$\neq$	not equal to
$\geq$	equal to or greater than
$\leq$	equal to or less than
$\oint$	integration around a closed curve

### Acronyms Used in References

ABS	American Bureau of Shipping
ATMA	Association Maritime Technique et Aeronautique, Paris
ASME	American Society of Mechanical Engineers

ASNE	American Society of Naval Engineers	MARIN	Maritime Research Institute Netherlands (formerly NSMB)
ASCE	American Society of Civil Engineers	NASA	U.S. Space Administration (formerly NACA)
ATTC	American Towing Tank Conference	NAVSEA	U.S. Naval Ship Systems Command
BMT	British Maritime Technology (formerly BSRA)	NECI	Northeast Coast Institute of Engineers and Shipbuilders
DTNSRDC	David Taylor Naval Ship Research and Development Center (formerly EMB DTMB) (now DTRC, David Taylor Research Center)	NMI	National Maritime Institute (formerly NPL), London
IESS	Institute of Engineers and Shipbuilders in Scotland	NTSB	National Transportation Safety Board
IME	Institute of Marine Engineers	ONR	Office of Naval Research, U.S. Navy Dept.
IMO	International Maritime Organization (formerly IMCO)	OTC	Offshore Technology Conference
ISSC	International Ship Structures Congress	RINA	Royal Institute of Naval Architects, formerly (INA)
ITTC	International Towing Tank Conference	RSE	Royal Society of Edinburgh
JSR	SNAME <i>Journal of Ship Research</i>	SSC	Ship Structures Committee
JSTG	<i>Jahrbuch des Schiffbautechnischen Gesellschaft</i>	SNAME	Society of Naval Architects and Marine Engineers
		SSPA	Swedish State Shipbuilding Experimental Tank
		WEBB	Webb Institute of Naval Architecture

---

**International System of Units (Système International d'Unités, or SI) Useful quantities for Naval Architecture**

---

Quantity	SI Unit	Definition	Conversions	
			English to SI	SI to English
<u>Base Units</u>				
Length	meter, m		1 ft = 0.305m	1m = 3.28 ft
Mass	kilogram, kg		1 lb = 0.454 kg	1 kg = 2.20 lb
Time	second, s			
<u>Supplementary Units</u>				
Angle, plane	radian, rad	1 rad = 180°/π		
Density of solids of liquids		kg/cm³ or t/m³ kg/L		
Distance	nautical mile, knot	1.852 km		1 knot = 6,080 ft
Force	newton, N kilonewton, kN	1 kg-m/s² 103 kg-m/s²	1 lb (force) = 4.45N	1 N = 0.225 lb
Frequency	hertz, Hz	cycle/sec, cps		
Mass	metric ton, t	10³ kg	1 long ton (weight) = 1.016 t	1t = 0.98 long tons
Power	watt, W kilowatt, kW	1 N-m/s 1 kN-m/s	1 hp = 0.746 kW	1kW = 1.34 hp
Pressure	kilopascal, kPa	10³ N/m²	1 lb/in² = 6.895 kPa	1kPa = 0.15 lb/in²
Specific vol.	1/density	m³/t		
Stress	megapascal, MPa	MN/m² = N/mm²	1 long ton/in² = 15.44 MPa	1MPa = 0.065 long tons/in²
Volume of solids of liquids	m³ liter, L	10 <sup>-3</sup> m³ = d³		
Velocity	meters/sec knot	m/s 1 nmi/hr = 1.852 km/kr.	1ft/sec = 0.305 m/s	1m/s = 3.28 ft/sec

# Index

- ABC Harbor, 325
- Acceleration
  - effect of propeller on, 397
  - instantaneous propeller, 253
  - fin derivatives, 235
  - time and distance required, 251
- Accelerations
  - amplitudes of, 125
  - due to rolling, 73
  - forces due to, 125
  - heaving, 99
- Added Mass
  - hydrodynamic, 51
  - coefficient of, 53, 57
  - coefficients, 238, 248
  - concept, 198
  - of a fin, 235
  - on a turning ship, 194
  - forces, 194
  - (vertical acceleration), 42
- Added resistance
  - effects of, 119
  - spectrum of, 119
- Advance, turning definition, 209
- Aeration of rudders, 293, 367
- Airfoil sections
  - control surfaces, 291
  - rudders, 382
- Amplitudes
  - exciting, 58
  - forces and moments, 124
- Angle of attack
  - control surface, 236
  - fixed fin, 234
- Anti-pitching devices, 136
- Anti-rolling devices, active, 133
  - control of, 133
  - fin stabilizers, 134
  - gyroscopic stabilizers, 133, 135
  - tanks, 136
- Anti-rolling devices, passive, 79, 127
  - bilge keels, 170
  - sails, 127
  - tanks, 127
- Appendages
  - effect of, 234, 333
- Aspect ratio (control surface)
  - effective, 235, 299
  - effect of, 298
  - of a fin, 235
  - of a bare hull, 236
- Astern seas
  - effect of, 274
- Augmentation (control)
  - drag, 404, 408
  - operational techniques, 404
  - propulsion, 404
  - rudders, 404
  - thrusting devices, 404, 407
- Automatic control; see control automatic
- Auto pilots, 264
  - adaptive, 266
  - tuning, 264
- Auxiliary stopping devices, 263
- Backing maneuvers, 251
  - times, distances, velocities, 262
- Balance of rudders, 383
- Bech spiral maneuver, 204
- Bending moment
  - in waves, hull, 102, 109
  - rudder stock, 292
- Bernoulli's Theorem
  - applied to waves, 7
  - equation, 48
- Bilge keels, 79, 127, 170
- Bow
  - effect of flare, 115
  - impact on, 116
  - planes (submersible), 323, 367
  - rudders, 366
- Bow motions
  - influence of shape on, 115
  - kinematic solution, 112
  - relative, 112
  - shipping water, 112
- Braking flaps, 262
- Bretschneider wave spectrum, 37
- Bridge simulators, 360
- Broaching
  - definition, 274
  - danger of, 277
- Canals
  - course-keeping in, 282, 326
  - interaction with, 279
- Canted rudders, 367
- CAORF Simulator, 359
- Capsizing, 83
- Cavitation, rudder, 293
- Celerity, wave, 4, 6
- Center of pressure (control surface), 221, 292
- Climatology, wave, 34
- Coasting (to a stop), 251, 261
- Coefficients
  - added mass, 53, 57
  - damping, 53, 57
  - diffraction, 53
  - equations of motion, 53, 57, 65
  - Ogilvie & Tuck, 53
- Coefficient (control surface)
  - drag, 234, 295
  - lift, 234, 295
- Coefficients (nonlinear)
  - added mass, 238, 248
  - equations of motion, 227, 228, 264
- Coefficients (model), 249
  - drift, 250
  - error cancellation, 250
- Computations, response, 92
- Compound gravity waves, 11
- Computers
  - simulation of stopping, 259
- Computer programs, motion
  - Frank's method, 60
  - Lewis-forms, 60
  - hybrid method, 63
  - 3-dimensional methods, 65
  - seakeeping data base, 109
- Confidence level, 91
- Conformal mapping, 61
- Constant pressure, 7
- Contours, wave, 7
- Control, automatic, 264
  - unstable vessels, 265
  - hydrofoils, 267

- Control considerations, 317
  - device design, 364
  - requirements, 320
- Controls-fixed motion stability, 195, 199, 265
- Control forces and moments
  - derivatives, 198
  - experimental determination, 221
- Control loops (the), 192
- Control, ship motions, 126
  - roll, 127
  - pitch, 136
- Control surface (also see rudder), 292
  - center of pressure, 221
  - design of, 221, 364
  - effect of, 221
    - aspect ratio, 236, 299
    - fixed structure, 310
    - profile shape, 305
    - thickness, 305
  - experimental techniques, 221
  - forces and moments on, 221, 292
  - free-stream characteristics, 302
  - geometry of, 291
  - hydrodynamics of, 291
  - planar-motion mechanism, 221
  - rotating-arm technique, 222
  - section shapes, 303
  - stall, 227, 293, 375
- Control surface coefficients; see coefficients
- Control systems
  - automatic, 192, 264
  - input data, 266
  - time-lag effects, 266
- Controllability
  - application to design, 327
  - piloted, 325
  - of submarines, 323
  - of high-speed craft, 325
  - standards
    - relation to tests, 320
    - status of development, 320
- Correlation
  - maneuvering prediction of, 232
- Course (ship's)
  - changing ability, 191, 317
  - keeping ability
    - in astern seas, 274
    - evaluation of, 317
    - in proximity to another ship, 287
    - in restricted waters, 279
- Crash astern maneuver (stop), 251, 258, 317, 318, 397
- Criteria
  - stability, 200, 317
  - discussion, prescribed values, 142, 144
  - governing, 144
  - limiting valves, 142
  - seakeeping performance, 3, 137, 223
  - maneuvering, 200, 317
  - swept path, 318
- Cross spectral analysis, 103
- Currents
  - effect of local, 271
- Damping
  - coefficients, motion, 53, 57, 60
  - dynamic, 118
  - estimation of roll, 81
  - hydrodynamic, 43, 51
  - of roll, 100
  - wave system, 24
  - wave radiation, 101
- d'Alembert forces, 122, 194
- Deadwood (fixed fin)
  - derivatives of, 242
  - effect of, 241, 314
- Decrement of roll, 82
- Definitive maneuvers, 206
- Degrees of freedom, 45
- Derivatives, control
  - prediction of, 236
- Derivatives, hydrodynamic
  - comparison prediction, 243
  - control force, 198
  - full-scale tests, 231
  - model tests, 243
  - contribution, fixed fin 241
  - determination of, 236
    - bare hull, 236
    - ship-fin configuration, 241
  - of stability, 200
- Derived responses, 2
- Design for seakeeping, 109, 160
- Det norske Veritas, 370
- Diagram of Steering, 328
- Diameter, tactical, 209, 297, 348
- Dieudonne spiral maneuver, 202
- Diffraction problem, 49
  - coefficients of, 53
- Directional stability, see stability, motion
- Doppler shift, 22, 24
- Drag
  - coefficient, 234
  - control surface, 234
  - locked propeller, 262
- Drift
  - angle of, 193
  - effect, 398
- Dutch roll, 83
- Dynamic behavior
  - in wind, 268
  - in shallow water, 280
  - in narrow channels, 282
- Dynamic impulse, 255, 256
- Dynamic positioning, 268
- Dynamic potential, 255, 256
- Dynamic stability
  - discriminant, 201
  - prediction of, 350
- Effective wave length, 105
- Encounter frequency, 22, 41, 80, 104
- Energy
  - of waves, 8
  - dissipation by rolling, 82
- Environmental operability, 137
- Environmental effects
  - currents, 271
  - wind, 268
- Environmental effects (*continued*)
  - waves, 272
- Equations of motion, 2, 41
  - coefficients of, 53, 57, 65
  - controls fixed, 198, 193, 264
  - linear, 196
  - linearized, 51
  - maneuvering, 196, 217
  - Newton's, 193
  - nonlinear, 217
  - pitching and heaving, 42
  - with automatic control
  - with six degrees of freedom, 45
- Eso Osaka* tests, 319
- Exciting forces, wave, 67
- "Feelers", hydrofoil, 268
- Fetch, 5, 24
- Fins, fixed
  - added mass of, 235
  - aspect ratio, 235
  - contribution of, 234
  - effect on
    - stability in turning, 235, 333, 350
    - maneuvering, 235
- Fins, moveable; see rudders, planes
- Flanking rudders, 370
- Flaps
  - braking, 262, 263
- Following seas
  - effect of, 274
- Forces
  - components, 196
  - control and moments, 198
  - d'Alembert, 194
  - derivatives, 197
  - during maneuvers, 194
  - wind and wave, 194
  - hydrodynamics, 194
  - inertial reaction, 194
- Forces, ship motions, 124
  - exciting, 42, 50, 58, 67, 123
  - d'Alembert, 122, 194
  - fluid, 46
  - hydrostatic, 47
  - hydrodynamic, 49, 194
  - radiating, 42, 51
  - restoring, 42
- Forces and moments, rudder, 292
- Fourier technique, 4, 14
- Frank's method, 60
- Freeboard
  - bow, 113
  - nominal, 114
  - ratio, 167
- Frequency, also see Period
  - natural, 103
  - of pitch and heave, 69, 103
  - of roll, 78, 103
  - of encounter, 22, 41, 104
- Froude number, 202
- Froude number (synchronism), 104
- Froude's law, 295
- Froude-Krylov
  - approximation, 50

- Froude-Krylov (*continued*)  
 exciting forces, 50, 58  
 sectional amplitude, 58
- Full-scale measurement  
 pitch-heave, 70  
 rolling, 82
- Gallatin* tests, 380
- Gaussian process, 84
- Gyroscopic stabilizers, 133, 135
- "Harbor" speed, 251
- Haskind relations, 51, 58
- Head reach, 254
- Head seas  
 motions in, 42  
 exciting forces in, 67
- Heave  
 acceleration variance, 99  
 in irregular waves, 95
- Heaving  
 coupled with pitching, 65  
 forces due to, 124  
 general considerations, 65  
 natural period of, 103
- Heel  
 angle in a turn, 212  
 during maneuvers, 228
- Helmsman error tests, 381
- High-speed vessels  
 control requirements, 325
- Horn rudder, 314, 367, 393
- Hovgaard effect, 401
- Human factor, 325
- Hydrofoils, control of, 267, 325
- Indexes  
 $K'$  and  $T'$  coursekeeping and turning, 207, 327  
 stability, 207  
 controllability, 320  
 trial, 320  
 motion stability, 199, 337
- Instability  
 in turning, 199  
 in waves, 272  
 transverse, 203
- Interactions  
 between two vessels, 287  
 hull and rudder, 292  
 vessel and waterway, 279, 326
- Irregular waves  
 heave acceleration in, 99  
 heave in, 95  
 motions in, 92  
 pitch in, 96  
 rolling in, 100  
 speed reduction in, 105
- Joessel's formula, 302, 384
- Jones' formula, 236
- JONSWAP wave spectrum, 38
- Kalman filter, 249
- Kempf overshoot maneuver, 206
- Lateral motions, 285
- Leeway angle, 83, 193
- Lewis-forms, 60
- Lift coefficient, control surface, 234, 295
- Linear random theory  
 validity for ships, 102  
 validity for other than normal ship forms, 103
- Linear superposition theory, 84
- Loads, wave, 122
- Longitudinal Center of Buoyancy (LCB), 164
- Machinery characteristics  
 effects of maneuvering, 258, 397
- Magnification factor, 78
- Mass transport, 9
- Maneuvers, definitive, 206  
 crash astern, 258  
 Dieudonne spiral, 202  
 rudder cycling, 258  
 thrust during, 228  
 turning test, 209  
 overshoot (zigzag), 206  
 pullout spiral, 204  
 submersible, 324
- Maneuvering model techniques  
 oscillator, 224  
 planar motion mechanism, 221  
 rotating-arm tests, 221, 224, 243  
 straight-line tests, 222
- Maneuvers, nonlinear  
 captive model tests, 221  
 effect of hull configuration, 339, 342  
 free-running model tests, 215  
 nonlinear equations of motion, 217, 229
- Maneuvers, prediction of  
 bare hull derivatives, 236  
 control derivatives, 236
- Maneuverability  
 high-speed vessels, 325  
 submersibles, 323  
 trial codes, 317, 318
- Maneuvering  
 characteristics, 317  
 criteria, 317  
 devices, 333  
 effect of  
 fixed fins, 235  
 block coefficient, 327  
 hull configuration, 333, 336  
 moveable fins, 333  
 propellers, 397  
 propulsion plants, 397  
 full-scale tests in, 258, 317  
 wind, 269  
 current, 271  
 astern seas, 274  
 restricted waters, 279  
 standards, 318  
 test code, 318  
 trials, 318
- Meander maneuver, 324
- Measurements, full-scale  
 pitch, heave, 70
- Measurements, full-scale (*continued*)  
 roll, 82
- Metacentric height  
 effect on roll, 78, 80, 170  
 variation in, 83
- Mission effectiveness, 3, 152, 138
- Model coefficients; see coefficients
- Model tests  
 bending movement in waves, 102  
 pitching and heaving, 69, 70  
 speed loss in waves, 120  
 seakeeping, 69
- Model tests, maneuvering  
 captive, 217, 221, 243  
 comparison of results, 243  
 free-running, 215  
 full-scale data comparison, 232  
 hydraulic, 217  
 in astern seas, 277  
 in restricted waters, 280, 283  
 nonlinear prediction from, 229  
 rudders, 315  
 Series 60 tests, 245
- Model testing (perturbation), 357
- Moment, bending; see Bending Moment
- Moments, motion  
 exciting, 42, 58  
 radiating, 42  
 restoring, 42
- Motion stability; see Stability, Motion
- Motion, equations of; see Equations of Motion
- Motions of ships in regular waves, 2  
 control of, 126  
 linear theory of, 41  
 local and relative, 109  
 longitudinal, 65  
 sinusoidal, 42  
 with six degrees of freedom, 45, 109  
 yawing and broaching, 116
- Munk moment, 237
- Natural period; see Period, natural
- Newton's Law, 46
- Norrbin parameter, 208
- Observations, maneuvering, 232, 258, 280
- Ochi wave spectrum, 40
- Oscillator technique (pmm), 224
- Operability index, 151
- Overshoot (zigzag) maneuver, 206, 317  
 angle of, 208
- Path, ship's  
 changing ability, 317  
 keeping ability, 317
- Performance prediction, 108
- Performance requirements, 316
- Period/length ratio, 105
- Period, natural  
 effect of  $\overline{GM}$ ,  $\overline{GZ}$ , 78, 170  
 heaving, 103  
 pitching, 103  
 rolling, 103  
 magnitude of, 105  
 of waves, 8

- Pitch
  - radius of gyration, 69
- Pitching
  - effect on controllability, 195
- Pitching (motion)
  - coupled with heaving, 65
  - effect of speed and hydrostatic coefficient, 66
  - effect of wavelength, 105
  - effect on resistance, 118
  - forces due to, 124
  - full-scale measurements, 105
  - in irregular waves, 97
  - in oblique seas, 109
  - subcritical, 105
  - supercritical, 108
  - synchronous, 105
- Pitching, natural period, 105
  - means of shortening, 106
- Pitching and heaving
  - control of, 136
  - coupled, 67
  - guidance for design, 160, 166
- Pivot point (turning), 209
- Planar motion mechanism, 224, 221
- Powering in waves, 120
- Prandtl's theory, 299
- Pressure, fluid, 48
- Profiles, wave, 7
- Propellers
  - effects of, 397
  - effect on
    - maneuvers, 228, 397
    - stability, 397
    - turning, 348
    - turning moment, 400
  - thrust, 228
  - transverse forces, 400
  - vertical-axis, 407
- Properties, wave, 8
- Propulsion efficiency
  - reduced in waves, 118
- Pullout spiral maneuver, 204
- Radiation problem, 54
- Radius, turning circle, 209, 210
- Resistance, added, 118
  - effect on
    - pitching and heaving, 118
    - rolling, 120
    - yawing, 120
- Response Amplitude Operator (RAO), 85
  - heaving, 96
  - pitching, 96
  - rolling, 100
- Response, ship
  - components of, 41
  - derived, 2, 109
  - in irregular waves, 95
  - in a seaway, 84
  - synthesis
    - heave, pitch, 95, 97
    - rolling, 100
  - theory of, 92
- Response theory
  - computations, 92
  - long-crested waves
    - zero speed, 86
    - forward speed, 87
  - short-crested seas
    - statistics of maxima, 89, 90
- Reynolds number, rudders, 295
- Righting arm curve, 79
- Risk factor, 331
- Roll
  - behavior at resonance, 78
  - center of, 77
  - control of, 127
  - curve of, 82
  - extinction test, 80, 82
  - instability, 83
  - damping, 76, 79
    - artificial, 170
    - devices, 127
    - estimation of, 81
    - mechanism involved, 82
    - moments, 83
    - non-linearity of, 102
  - resonant period of, 78
  - righting arm, 79
- Rolling
  - decrement, 82
  - effect on
    - resistance, 120
    - personnel, 73
  - factors affecting, 170
  - forces due to, 73, 124
  - in irregular waves, 100
  - natural period of, 101
  - in oblique seas
    - reduction of, by, 101
  - tanks, 127
  - bilge keels, 79, 127
  - fin stabilizers, 134
  - gyroscopic stabilizers, 135
  - synchronous, 101, 104
- Rotating-arm tests
  - facilities, 222
  - turning, 221
- Rudder cycling maneuver, 258
- Rudders (see also control surfaces)
  - aeration, 293, 367
  - all-moveable, 367
  - area, 365, 369
  - augmentation of, 404
  - aspect ratio, 291, 298, 306
  - balance, 383
  - balanced, 367
  - bow, 366
  - canted, 367
  - cavitation, 293
  - center of pressure, 292
  - deflection angle, 199, 375
  - deflection, maximum, 375
  - deflection rate, 218, 379
  - design, 364
  - flanking, 370
  - flapped, 310
  - flow around, 310
- Rudders (*continued*)
  - forces and moments, 199, 292
  - height, 365
  - horn, 314, 367, 393
  - interaction with hull, 292
  - location, 364, 366
  - model test, 302
  - multiple, 298, 368
  - number of, 368
  - scale effects, 295
  - section shape selection, 375
  - size, 278, 370
  - skeg, 316
  - stall, 293, 375
  - torque curve, 386
  - twin, 368
  - types of, 365, 370
  - vibration induced by, 365
  - spade, 387
- Rudder stock
  - bending moment, 292
  - calculations, 292
  - location, 364
  - size, 365
  - torque prediction, 240, 383
- Scale effect
  - control surface, 295
  - rudders, 295
  - model tests, 227
- Sea data, typical, 2, 26, 28
- Seakeeping
  - above water form, 167
  - database, 109
  - design guidance, 166
  - for rolling, 170
  - high performance ships, 171
  - operating envelope, 151
  - pitching and heaving, 160
  - procedures evaluation for, 174
  - merchant ships, 175
  - U.S. Navy, 176
- Seakeeping Performance Index, 3, 127, 138, 140
  - criteria, 137, 141, 144
  - limiting value, 142
  - steps in obtaining, 150, 160
- Sea-kindliness, 2
- Sea states
  - real, 27
  - statistical representation, 5, 27, 28
- Seawitch collision, 317
- Sensors, wave height, 268
- Shallow water effects on
  - turning circle, 280
  - maneuvering, 279
  - stopping distance, 281
  - sinkage and trim, 290
- Shipping water
  - forward, 112
  - aft, 115
- Simulation
  - bridge, 360
  - harbor and canal, 359
  - ship handling, 358

- Sinkage and trim, 290
- Slamming
  - probability of, 115
  - stresses, 116
- Slender Body theory, 53, 55, 64
- Slope
  - spectrum, 22
  - wave surface, 7, 22
- Slow steaming ability, 318
- Smith effect, 7, 44, 122
- Snap roll, 213, 323
- Spade rudder, 387
- Spectra, wave
  - development and decay, 24
  - point, 30
  - directional, 34
- Spectrum
  - Bretschneider, 37
  - broadness, parameter of, 18
  - concept, 2, 18
  - directional, 121
  - JONSWAP, 38
  - narrow band, 19
  - Ochi, 40
  - Pierson-Moskowitz, 36
  - simple-point, 14, 22
  - slope, 22
  - frequency of encounter, 22
  - energy, 14
- Spectrum of
  - added resistance, 119
  - energy, 14
  - encounter, 22
  - slope (wave), 22
- Speed
  - distance diagram, 252
  - maneuvering, 252
  - reduction or loss
    - in a turn, 214
  - “harbor”, 251
  - supercritical, 108
  - reduction in seas, 118, 138
  - transit, 3, 138, 151
  - polar plot, 150
- Spiral maneuvers
  - Bech, 204
  - Dieudonne, 202
  - pullout, 204
  - reverse, 319
- Spreading function, 90
- Springing, 123
- Squat, ships, 290
- Stability, dynamic
  - prediction of, 350
- Stability, motion
  - criteria, 317, 200
  - definition, 195
  - derivatives, 200
  - directional, 195
    - criterion, 200, 317
  - effects of
    - fin, 333
    - appendages, 333
    - propellers, 397
- Stability, motion (*continued*)
  - in waves, 272
  - indexes, 199, 337
- Stabilizers (roll)
  - active, 133
  - fin, 134
  - gyroscope, 133, 135
  - moving weight, 127, 128
  - passive, 127, 132
  - rudder, 135
  - sails, 127
  - tanks, 127, 128, 136
- Stabilization of roll, 127
- Standard ship motion program, 54
- Standards
  - controllability, 320
  - maneuvering, 317
  - status of development, 320
- Standing waves, 11
- Stall, control surface, 227, 293, 375
- Starting of ships, 251
- Station “India”, 27
- Statistics
  - of maxima, 90
  - wave, 5
- Statistical analysis (sea state), 5
- Steady turning radius, 210
- Steering (see also maneuvering)
  - diagram of, 328
  - in astern seas, 274
  - in canals, 282
  - in proximity to other ships, 288
  - in shallow water, 279
- “Stingers,” hydrofoil, 268
- Stokes equation, 9
- Stopping of ships
  - ability, 254, 318
  - auxiliary devices, 251, 263
  - distances required, 254
  - Esso Suez* trial, 259
  - in shallow water, 281
  - emergency, 316
  - simulation of, 259
  - with freedom to turn, 258
- Strip theory, 2, 41, 53
- Supercritical
  - speed, 108
  - operation factors, 108
  - heave response, 97
- Superposition, 2
  - theory of linear, 84
  - of bending moments, 102
  - extension, short crested seas, 2
  - principle of, 119
- Surge, 54, 56, 66
- Sway, 73, 77, 83
- Swell, 5
- Swell-up
  - static, 114
  - dynamic, 114
- Swept-path criterion, 318
- Synchronism
  - heave and pitch, 69
  - rolling, 78, 101, 103
  - Froude number for, 104
- Systems identification methods
  - output error, 249
  - extended Kalman filter, 249
- Tactical diameter
  - definition, 209, 297
  - variation in, 348
- Tanks, anti-roll
  - active, 133, 136
  - passive, 127
- Taylor expansion, 196, 218
- Thrust
  - astern, 251
  - constant deduction, 253
  - in a maneuver, 228
  - maximum available, 252
  - propeller, 254
- Torque
  - astern value, 256
  - curve, rudder, 386
  - prime movers, 253
  - ratio, 256
  - on rudder stock, 240, 383
  - steering gear, 383
  - calculation, 388, 394
- Trajectories
  - mathematical modeling, 249
  - systems identification method, 249
- Transfer, turning
  - definition, 209
- Transit speed, 3, 138, 151
- Trials, full-scale
  - basic considerations, 318
  - codes, 317
  - Esso Bernicia*, 258
  - Esso Lima*, 258
  - Esso Osaka*, 231, 281, 319
  - mariner*, 230
  - maneuvering, 316
  - indexes of, 320
- Trochoidal wave, 9
- Tuck's theory, 290
- Tucker meter, 30
- Tugboats
  - use in maneuvering, 263, 287
  - power tie-up, 263
- Tuning factor, 69, 104
- Turning, model
  - planar motion mechanism, 221
  - rotating arm, 221, 223
  - straight-line, 222
- Turning, ship
  - ability, 209, 318, 343
  - analysis, 209
  - angle of heel, 212
  - characteristics, 209
  - circle
    - maneuver, 209
    - test, 209, 291, 317
    - prediction, 343
  - heel during, 212
  - path, 209, 297
  - pivot point, 209
  - speed reduction during, 214
  - steady radius of, 210



Unstable ships' maneuvers  
 prediction, nonlinear theory, 217, 227  
 prediction, vs full scale trials, 229

Variance, wave, 8

Velocity  
 orbital, 7  
 wave, 6

Vertical-axis propellers, 407

Vertical overshoot maneuver, 324

Velocity potential, 6, 8

Wave bending moments, 102, 122, 123

Wave effect on  
 course keeping, 272  
 directional stability, 272

Wave height sensors, 268

Wave loads  
 bending moments, 122  
 shearing forces, 122

Waves, ocean  
 amplitude, 20  
 celerity, 4, 6, 8  
 compound gravity, 11  
 climatology, 34

Waves, ocean (*continued*)  
 data, 26  
 deep water, 3  
 diffraction theory, 65  
 effect on  
   bending moment, 102, 122  
   resistance, 120  
 energy of, 8  
 excitation of, 123  
 finite height, 9  
 group velocity, 6, 7  
 generational theory of, 15  
 harmonic (sinusoidal), 8  
 height, 8 observation of  
   length, 8  
   period, 8  
 properties, 3, 8  
 "significant" height, 30  
   amplitudes, 20  
   records analysis, 3  
 simple gravity, 2  
 slope, 22  
   spectra, 2, 4, 12, 14, 22  
   moments, 17  
   point, 14, 22  
   directional

Waves, ocean (*continued*)  
 observations, 26, 27  
 standing, 11  
 statistical representation, 4, 20  
 Stoke's, 9  
 surface profile, 7  
 Trochoidal, 9  
 variance, 8  
 velocity of, 6, 7

Wave systems  
 damping of, 24  
 generation and decay of, 24  
 stationary, 3  
 stochastic, 3  
 "Whiteness", 249  
 Wind effects on control, 268

Yaw  
 angle of, 193, 272  
 checking ability, 317

Yawing  
 prediction of, 73, 77, 116  
 in extreme high waves, 83

Zigzag (overshoot) or "Z" maneuver,  
 206, 320, 329, 395